VOLUME 10, 1959

BRITISH JOURNAL OF

Applied Physics

733

EDITOR: H. R. LANG, A.R.C.S., PH.D., F.INST.P.
Secretary of The Institute of Physics

THE INSTITUTE OF PHYSICS
LONDON

RESEARCH LIBRARY
KODAK PARK

THE INSTITUTE'S JOURNALS

ADVISORY COMMITTEE

for year ending 30 September, 1959

J. M. A. LENIHAN, M.SC., PH.D., A.M.I.E.E., F.INST.P., *Chairman*
N. F. ASTBURY, M.A., SC.D., M.I.E.E., F.INST.P.
J. BLEARS, B.SC., A.M.I.E.E.
H. J. J. BRADDICK, B.A., PH.D.
E. H. S. BURHOP, B.A., M.SC., PH.D., *Representing The Physical Society*
R. E. BURNETT, M.A., A.M.I.E.E., A.INST.P.
A. B. D. CASSIE, C.B.E., M.A., PH.D., D.SC., F.INST.P.
W. D. CORNER, B.SC., PH.D., F.INST.P., *Representing the North Eastern Branch*
A. J. DALLADAY, A.INST.P.
A. FELTON, B.SC., A.M.I.E.E., *Representing the National Physical Laboratory*
C. G. GARTON, M.I.E.E., F.INST.P.
J. E. GEAKE, M.SC., PH.D., F.INST.P., *Representing the Manchester and District Branch*
K. E. GREW, PH.D., D.SC., F.INST.P., F.R.S.E., *Representing the South Western Branch*
K. J. HABELL, A.R.C.S., M.SC., F.INST.P., *Representing the National Physical Laboratory*
M. E. HAINE, D.SC., A.M.I.E.E., F.INST.P.
N. L. HARRIS, B.SC., F.INST.P.
C. A. HOGARTH, B.SC., PH.D., F.INST.P.
E. J. IRONS, PH.D., D.SC., A.M.I.E.E., F.INST.P., *Representing the Education Group*
R. V. JONES, C.B., C.B.E., M.A., D.PHIL., F.INST.P., F.R.S.E.
O. P. T. KANTOROWICZ, D.PHIL., F.INST.P.
R. KING, B.SC., A.INST.P.
H. LIPSON, M.A., D.SC., F.INST.P., F.R.S.
M. MCCAIG, M.SC., PH.D., F.INST.P., *Representing the Yorkshire Branch*
J. D. MCGEE, O.B.E., M.SC., PH.D., F.INST.P.
J. W. MENTER, M.A., PH.D., F.INST.P., *Representing the Electron Microscopy Group*
G. MORRIS, B.SC., PH.D., F.INST.P.
F. OLDHAM, J.P., M.A., B.SC., F.INST.P.
E. A. OWEN, M.A., SC.D., D.SC., F.INST.P., *Representing the Liverpool and North Wales Branch*
E. R. PONSFORD
F. Y. POYNTON, M.SC., F.INST.P.
H. O. PULS, B.SC., PH.D., F.INST.P., *Representing the South Wales Branch*
H. PURSEY, B.SC., *Representing the National Physical Laboratory*
T. LL. RICHARDS, B.SC., PH.D., F.I.M., F.INST.P., *Representing the Midland Branch*
L. ROTHERHAM, M.SC., F.I.M., F.INST.P.
L. A. SAYCE, C.B.E., M.SC., PH.D., F.R.I.C., F.INST.P.
W. E. SCHALL, B.SC., F.INST.P., *Representing the Non-Destructive Testing Group*
R. M. SILLITTO, B.SC., F.INST.P.
H. SPOONER, B.SC., A.INST.P.
E. G. STANFORD, M.SC., PH.D., F.INST.P.
J. R. STANSFIELD, M.A., F.INST.P., *Representing the Applied Spectroscopy Group*
W. STECKELMACHER, B.SC.
E. G. STEWARD, B.SC., PH.D., F.INST.P., *Representing the X-Ray Analysis Group*
A. M. TAYLOR, M.A., PH.D., F.INST.P., *Representing the London and Home Counties Branch*
D. TAYLOR, M.SC., PH.D., M.I.E.E., F.INST.P.
J. TAYLOR, M.B.E., PH.D., D.SC., F.R.I.C., F.INST.P., *Honorary Treasurer, The Institute of Physics*
J. THEWLIS, D.SC., F.INST.P.
SIR GEORGE THOMSON, M.A., SC.D., LL.D., HON.F.INST.P., F.R.S., NOBEL LAUREATE, *President, The Institute of Physics*
J. THOMSON, M.A., D.SC., F.R.I.C., M.I.E.E., F.INST.P., *Representing the British Scientific Instrument Research Association*
S. TOLANSKY, PH.D., D.SC., F.INST.P., F.R.S., *Representing The Physical Society*
F. A. VICK, O.B.E., B.SC., PH.D., A.M.I.E.E., F.INST.P., *Honorary Secretary, The Institute of Physics*

CONTENTS OF VOLUME 10

PAGE

JANUARY 1959

SPECIAL ARTICLE

Solid and liquid state research with cold neutrons. By P. A. EGELSTAFF 1

ORIGINAL CONTRIBUTIONS

Papers

Evaporation of thorium from carburized thoriated tungsten cathodes. By R. O. JENKINS and W. G. TRODDEN 10

On the creep, recovery, relaxation and elastic "memory" of some renneted milk gels. By G. W. SCOTT BLAIR and J. BURNETT 15

Electromagnetic fields in ferrite ellipsoids. By R. A. WALDRON 20

Thermal conductivities of fused and crystalline quartz. By E. H. RATCLIFFE 22

Collection of gas-borne dust particles by means of an aspirated sampling nozzle. By S. BADZIOCH 26

Theorem concerning anisotropic dielectrics. By G. POWER 32

Preparation of metal film resistors on laminated plastics. By G. SIDDALL and G. SMITH 35

Cooling of a spinning thread-line. By E. H. ANDREWS 39

Interaction between two equal-sized equal-settling spheres moving through a viscous liquid. By G. F. EVESON, E. W. HALL and S. G. WARD 43

Approximate solution of a non-linear differential equation giving the temperature distribution in the positive column of a static arc. By H. GOLDENBERG 47

Torsional vibrational experiments on rectangular concrete beams. By R. JONES 51

Correspondence

S-band ferrite isolator for use with a linear accelerator. From C. S. GASKELL and D. WALSH 53

Radiofrequency method for the measurement of conductive liquid saturation in a porous medium. From R. W. SNELL 54

Centripetal air-pump operated electromagnetically. From B. POPPER and M. REINER 54

NOTES AND NEWS

Notes and comments 56

FEBRUARY 1959

ORIGINAL CONTRIBUTIONS

Papers

Counter diffractometer—The theory of the use of centroids of diffraction profiles for high accuracy in the measurement of diffraction angles. By E. R. PIKE and A. J. C. WILSON 57

Effect of temperature and moisture content on the orientation produced by the drawing of Nylon 66. By C. G. CANNON and F. P. CHAPPEL 68

Thermionic properties of thorium deposits on control grid materials. By J. A. CHAMPION 71

NEW BOOKS SECTION

Reviews 75

ORIGINAL CONTRIBUTIONS (*continued*)

Method for measuring the complex dielectric constant of a high-loss liquid at 8 mm wavelength. By E. H. GRANT 87

Linear photomultiplier bridge circuit for the measurement of small changes in absorption. By P. HARIHARAN and M. S. BHALLA 89

Deposition by thermal evaporation of thin films of titanium and zirconium for tritium targets. By V. D. SCOTT and L. W. OWEN 91

Experimental determination of the atomising efficiency of a high-speed spinning disk atomiser. By D. J. RYLEY . 93

Distribution of relaxation times in a symmetrically stressed renneted milk gel. By G. W. SCOTT BLAIR and J. BURNETT 97

Volume of drops of aqueous solutions transferred to a slide by a "micro-rod." By A. E. HAWKINS 99

Correspondence

The problem of exo-electron emission phenomena. From B. SUJAK; L. GRUNBERG 102

NOTES AND NEWS

Notes and comments 104

MARCH 1959

CONFERENCE REPORTS

Summarized proceedings of a colloquium on X-ray fluorescence analysis—London, February and April 1958. By F. W. J. GARTON and H. M. DAVIS . . . 105

Summarized proceedings of a conference on X-ray analysis—Manchester, April 1958. By A. HARGREAVES and E. STANLEY 116

ORIGINAL CONTRIBUTIONS

Papers

Evaluation of approximate methods of applying binary scale factors in pulse-counting systems of measurement. By W. T. BANE and M. P. ATKINSON. 124

Some experimental results on the impact sensitivity of mercury fulminate. By M. P. MURGAI and A. K. RAY 132

Alternative method of correlating forced convection heat transfer data. By P. H. PRICE 135

Method for size-distribution determinations of non-volatile droplets by electron microscopy. By W. J. HARRIS 139

New method for increasing the X-ray reflection power of lithium fluoride crystals. By E. F. PRIESTLEY . . 141

Ferromagnetic after-effect in mumetal. By L. CASTELLIZ and W. W. H. CLARKE 142

Production of X-rays during a low-pressure gas discharge. By R. F. THUMWOOD 147

NOTES AND NEWS

Notes and comments 152

PAGE

APRIL 1959

CONFERENCE REPORT

Summarized proceedings of a conference on solid state memory and switching devices—London, September 1958. By T. B. RYMER 153

ORIGINAL CONTRIBUTIONS

Papers

Investigation of the ignition of a gas by an electric spark. By D. R. LINTIN and E. R. WOODING 159
Unifying design principle for the resistance network analogue. By F. C. GAIR 166
Effect of deformation of the surface texture on rolling resistance. By J. HALLING 172
Use of an electronic analogue computer with resistance network analogues. By J. PH. KORTHALS ALTES . 176
Analysis of a polydisperse aqueous spray from a high-speed spinning disk atomizer. By D. J. RYLEY . . 180
Excitation and ionization rates of mercury in discharge plasmas. By M. A. CAYLESS 186
Analysis of the lighter elements by total reflexion of their characteristic X-ray wavelengths. By A. FRANKS and R. F. BRAYBROOK 190

Correspondence

On the use of coarse gratings in ultrasonics. From G. M. SREEKANTATH 191
Comments on the A.S.T.M. Powder Data File—4. From J. W. HUGHES, ISABEL E. LEWIS and A. J. C. WILSON . 192

MAY 1959

SPECIAL ARTICLE

Superconducting computer elements. By E. H. RHODERICK 193

ORIGINAL CONTRIBUTIONS

Papers

High-resolution shadow-casting technique for the electron microscope using the simultaneous evaporation of platinum and carbon. By D. E. BRADLEY . . . 198
Flow of heat in a composite solid. By T. P. NEWCOMB . 204
Deposition of unipolar charged aerosol particles by mutual repulsion. By W. W. FOSTER 206
Viscous properties of thixotropic materials. By D. G. OSBORNE and S. THORNTON 214
Amplitude corrections for vibroscope measurements. By IAN M. STUART 219
Investigation of Nylon "texture" by X-ray diffraction. By K. LITTLE 225
Inductance of an eccentric tubular conducting system. By E. E. JONES 230
Image fluctuations in cascade intensifiers. By L. MANDEL 233

Correspondence

Electrical determination of the thermal parameters of semiconducting thermoelements. From C. HERINCKX and A. MONFILS 235

JUNE 1959

CONFERENCE REPORT

Summarized proceedings of a conference on nuclear fuel cycles—London, January 1959. By W. A. COOPER . 237

PAGE

ORIGINAL CONTRIBUTIONS

Papers

Determination of the size of defects by the ultrasonic impulse echo method. By J. KRAUTKRÄMER . . . 240
Energy variation with pressure and temperature in a sonic stationary wave. By A. R. INGLES 246
Effect of sound intensity on dispersion and coagulation in ultrasonic emulsification. By R. S. KRISHNAN, V. S. VENKATASUBRAMANIAN and E. S. RAJAGOPAL . . . 250
Temperature errors introduced by temperature-measuring probes. By I. G. DONALDSON 252
Technique for preparing thin films of α-iron. By D. G. BRANDON and J. NUTTING 255

NEW BOOKS SECTION

Reviews 257

ORIGINAL CONTRIBUTIONS (*continued*)

Measurement of the tensile strength of brittle materials. By R. BERENBAUM and I. BRODIE 281
Relationship between strength and porosity for coal compacts. By D. J. MILLARD 287
Measurement of high intensity stress pulses. By J. S. BUCHANAN and H. J. JAMES 290
Absorption of sodium and argon by glass. By J. W. WHEELDON 295

Correspondence

Cadmium sulphide photoconductive layers. From R. LAWRANCE 298

NOTES AND NEWS

Notes and comments 300

JULY 1959

ORIGINAL CONTRIBUTIONS

Papers

First ionization coefficients in hydrogen, neon and argon. By D. E. DAVIES and J. G. C. MILNE 301
Permittivity of mixtures of zinc oxide and rubber. By N. H. LANGTON and D. MATTHEWS 306
Theory of operation and constructional principles of a high-precision spectroscopic spark source. By Á. BARDÓCZ 310
Transient temperature rise due to a line source in a semi-infinite medium, with a radiation boundary condition at the interface. By H. GOLDENBERG 314
Studies of the viscosity and sedimentation of suspensions. Part 5.—The viscosity of settling suspensions of spherical particles. By D. R. OLIVER and S. G. WARD . . 317
New method for the determination of grain or crystallite size from spotty diffraction rings. By K. W. ANDREWS and W. JOHNSON 321
Transient response of direct current amplifier systems. By R. D. STUART 326
Measurement of fibre diameter variation by optical diffraction. By W. J. ONIONS and B. ELLINGHAM . 328
Methods of cleaning glass by vapour degreasing and ultrasonically agitated solvents. By T. PUTNER . . 332
Technique for determining the orientation of single crystals of bismuth. By D. T. J. HURLE and S. WEINTROUB 336
Transient temperatures attained in disk brakes. By T. P. NEWCOMB 339

PAGE

AUGUST 1959

ORIGINAL CONTRIBUTIONS

Papers

Differential scattering cross-section of atoms to medium energy electrons at small angles. By M. E. HAINE and A. W. AGAR 341
Electric stress and heat transfer. By P. H. G. ALLEN . 347
Spectrum display comparator. By W. J. PRICE . . 352
Microwave method of investigating the afterglows of pulsed gaseous discharges. By M. C. SEXTON, J. J. LENNON and M. J. MULCAHY 356
Reversible poisoning by sulphur, oxygen and other gases of oxide-coated cathodes at high temperatures. By N. A. SURPLICE 359
Bistable behaviour of the Bayard–Alpert ionization gauge. By G. CARTER and J. H. LECK 364
Pick-up of copper and duralumin on bonded tungsten carbide. By J. GOLDEN and G. W. ROWE . . . 367
Theoretical evaluation of capillary viscometers for the measurement of the viscosity of suspensions of spheres. By A. D. MAUDE 371
Measurement of the quantum efficiency of a proportional counter using X-rays. By A. E. KISS and N. PATLA . 376

Correspondence

Reaction of indium solder with mercury telluride. From S. NIELSEN 380

NOTES AND NEWS

Notes and comments 381

SEPTEMBER 1959

CONFERENCE REPORT

Summarized proceedings of a symposium on current developments in the production of high vacua—London, April 1959. By J. YARWOOD 383

SPECIAL ARTICLE

Dense electron beams. By B. MELTZER 391

ORIGINAL CONTRIBUTIONS

Papers

Bulb breaking correction for heats of wetting determinations. By R. C. GALLAVAN 398
Application of delayed feedback in electronic circuits. By Zs. NÁRAY 400
Dielectric properties of water/alumina. By J. L. WOOD . 404
Powder technique for the empirical determination of absorption corrections. By H. A. RICHARD WEGENER 406
Cathode emission measurements in low pressure discharges. By A. D. FORSTER-BROWN and M. A. CAYLESS 409
Use of an integrating sphere to distinguish between absorption and scattering in solids. By J. A. BASTIN, E. W. J. MITCHELL and J. WHITEHOUSE 412
Attenuation of light by wood smoke. By W. W. FOSTER 416
The X-ray scanning microanalyser. By P. DUNCUMB . 420

Correspondence

Dimensions of microscope eyepiece graticules. From R. J. HAMILTON 428
Absolute measurement of light intensities. From M. E. HAINE and J. S. PRESTON 428

PAGE

Controlling the habit of potassium cobalticyanide crystals. From A. E. RENNIE and S. NIELSEN 429

NOTES AND NEWS

Notes and comments 430

OCTOBER 1959

SPECIAL ARTICLE

Nuclear magnetic resonance in solids. By E. R. ANDREW 431

CONFERENCE REPORT

Summarized proceedings of a conference on precipitation in alloys and on metal structures—London, November 1958. By A. FRANKS and R. S. M. REVELL . . 438

ORIGINAL CONTRIBUTIONS

Papers

Interferometric measurement of small angular displacements. By P. HARIHARAN and D. SEN 445
Refrigeration of a superconducting memory for a computer. By A. C. ROSE-INNES 452
Study of gas-lubricated, hydrodynamic, full journal bearings. By S. WHITLEY and C. BETTS 455
Estimation of trace water content in a halogenated oil by means of tritiated water. By J. F. CAMERON, I. S. BOYCE and R. M. GLAISTER 463
Experimental method of investigating stresses in buttress dams. By J. R. RYDZEWSKI 465

Correspondence

Improved semiconductor-to-copper soldered contact. From G. REICHENBAUM 469

NOVEMBER 1959

ORIGINAL CONTRIBUTIONS

Papers

Some aspects of the design of large permanent magnets. By J. E. COUSINS and W. F. NASH 471
Some aspects of the rheology of milk gel. By C. S. LANDAU 476
Correction for size of cross-section of the secondary windings of mutual inductance standards of the Campbell type. By P. VIGOUREUX 481

NEW BOOKS SECTION

Reviews 484

ORIGINAL CONTRIBUTIONS *(continued)*

Cathode work function, sparking potentials and secondary ionization coefficients for oxide-coated cathodes in hydrogen. By D. E. DAVIES and B. J. HOPKINS . . 498
Influence of the cathode work function on the sparking potential in hydrogen. By D. E. DAVIES and R. K. FITCH 502
Efficiency of characteristic K_α X-ray production in copper between 9 and 15 kV. By N. A. DYSON . . . 505
Electrical conductivity of vitrain during carbonization. M. I. POPE and S. J. GREGG 507

DECEMBER 1959

PAGE

ORIGINAL CONTRIBUTIONS

Papers

Effect of crystallographic twins on the d.c. and a.c. properties of nickel-iron alloys. By J. E. THOMPSON . 511

Thermal transients in graphite-copper contacts. By W. DAVIES 516

Glow discharge characteristics of helium-neon mixtures. By G. F. WESTON 523

Method for photographic identification of microscopic radioactive particles. By J. SISEFSKY 526

Study of cadmium sulphide crystals grown from the vapour phase in a stream of argon. By J. WOODS . 529

PAGE

Torsion balance measurements with molecular beams. By D. W. BASSETT and A. J. B. ROBERTSON . . 534

Steady-state temperature distribution in solids undergoing certain change of property. By T. J. MIRSEPASSI . 538

Correspondence

Use of an electronic analogue computer with resistance network analogues. From I. C. HUTCHEON, J. PH. KORTHALS ALTES, L. DEKKER and H. P. J. GILISSEN . 542

Single-etch extraction replica method adapted for carbon films. From G. R. BOOKER and J. NORBURY . . 543

NOTES AND NEWS

Notes and comments 544

SUBJECT INDEX TO VOLUME 10 545

AUTHOR INDEX TO VOLUME 10 553

INDEX TO VOLUME 10

SUBJECTS

(SA) denotes special article, (CR) conference report, (C) correspondence, and (NC) notes and comments.

Absorption
and scattering in solids, Use of an integrating sphere to distinguish between 412
corrections, Powder technique for the empirical determination of 406
of sodium and argon by glass 295
, small changes in, Linear photomultiplier bridge circuit for the measurement of 89
Aerosol particles, Deposition of unipolar charged, by mutual repulsion 206
After-effect, Ferromagnetic, in mumetal 142
Afterglows of pulsed gaseous discharges, Microwave method of investigating the 356
Air-pump, Centripetal, operated electromagnetically 54 (C)
Alloys, nickel–iron, Effect of crystallographic twins on the d.c. and a.c. properties of 511
Alloys, Summarized proceedings of a conference on precipitation in, and on metal structures—London, November 1958 438 (CR)
Alpha-iron, Technique for preparing thin films of 255
Alternating loss, Effect of twins on 511
Alumina, water/, Dielectric properties of 404
Analogue
computer, electronic, Use of an, with resistance network analogues 176, 542 (C)
resistance network, Unifying design principle for the 166
Argon
Absorption of sodium and, by glass 295
hydrogen, neon, and, First ionization coefficients in 301
stream of, Study of cadmium sulphide crystals grown from the vapour phase in a 529
Amplifier systems, direct current, Transient response of 326
Analogues, resistance network, Use of an electronic analogue computer with 542 (C)
Analysis, X-ray fluorescence, Summarized proceedings of a colloquium on,—London, February and April 1958 105 (CR)
Analysis, X-ray, Summarized proceedings of a conference on,—Manchester, April 1958 116 (CR)
Angles, diffraction, Counter diffractometer—The theory of the use of centroids of diffraction profiles for high accuracy in the measurement of 57
Anisotropic dielectrics, Theorem concerning 32
Annals of occupational hygiene, The 544 (NC)
Aqueous solutions, Volume of drops of, transferred to a slide by a "micro-rod" 99
Aqueous spray, polydisperse, Analysis of a, from a high-speed spinning disk atomizer 180
Arc, static, Approximate solution of a non-linear differential equation giving the temperature distribution in the positive column of a 47
A.S.T.M. Powder Data File—4, Comments on the 192 (C)
Atomizer, high-speed spinning disk, Analysis of a polydisperse aqueous spray from a 180
Atomizer, high-speed spinning disk, Experimental determination of the atomizing efficiency of a 93
Atoms, Differential scattering cross-section of, to medium energy electrons at small angles 341

Balance measurements, Torsion, with molecular beams 534
Bayard–Alpert ionization gauge, Bistable behaviour of the 364
Beams, Dense electron 391 (SA)
Beams, molecular, Torsion balance measurements with 534
Beams, rectangular concrete, Torsional vibrational experiments on 51
Bearings, Study of gas-lubricated, hydrodynamic, full journal 455
Binary scale factors, Evaluation of approximate methods of applying, in pulse-counting systems of measurement 124
Bismuth, orientation of single crystals of, Technique for determining the 336

Books, New
Acoustics, noise and buildings 75
Aerodynamik des Flugzeuges 259
Analog simulation: solution of field problems 269
Annual international conference on high energy physics at CERN, 1958 271
Approximate methods of higher analysis 492
Atmospheric explorations. Papers of the Benjamin Franklin memorial symposium of the American Academy of Arts and Sciences 77
Automatic control. Principles and practice 75
Automatic measurement of quality in process plants 76
Automatic process control 261
Axial flow compressors 260
BEAMA catalogue, The 276
Bibliography on industrial radiology, 1956–1959 497
Bone and radiostrontium 271
British coal mining explosives 269
British instruments, directory and buyers' guide 277
Calculateurs analogiques répétitifs 492
Čerenkov radiation and its applications 271
Chambers's technical dictionary 83
Chemical engineering practice. Vol. 5, *Fluid systems I.* Vol. 6, *Fluid systems II* 277
Chemische Reaktionen ionisierender Strahlen (Radiation chemistry) 262
Computability and unsolvability 78
Conductance design of active circuits 489
Conduction of heat in solids 267
Conference on extremely high temperatures, Boston, Massachusetts, 18–19 *March*, 1958 266
Conference on hyperconjugation 492
Conversion factors and tables. Part 1, *Basis of tables conversion factors* (B.S. 350: Part 1: 1959) 497
Cryogenic engineering 488
Design of physics research laboratories, The 78
Determination of molecular structure, The 485
Dictionary of named effects and laws in chemistry, physics and mathematics, A 83
Dislocations and mechanical properties of crystals 85
Dispersion of carbon black in rubber and its role in vulcanizate properties, The 268
Dynamical analogies 492
Effect of surface on the behaviour of metals 77
Effects of radiation on materials 271
Einführung in der Wärme—und Stoffuastausch 489
Electric conduction in semiconductors and metals 85
Electrolyte solutions 485
Electromagnetic phenomena in cosmical physics. International astronomical union symposium No. 6 272
Electromagnetic radiation from cylindrical structures 489
Electrophoresis: Theory, methods and application 486
Encyclopedia of chemistry (supplement), The 278
Experimental designs in industry 78
Extensive air showers 272
Fast reactions in solids 262
Field studies of the movement of soil moisture 261

Books, New—*continued*
Fifteen years of semiconducting materials and transistors 268
Fluctuation phenomena in semi-conductors 490
Forschung und Entwicklung auf dem Gebiete des chemischen Apparatewesens in Einzelabhandlungen. Dechema-Monographien Band 30*: Kern-wissenschaft und-technik, Band* 31*: Laboratoriums-technik* 486
Free radicals as studied by electron spin resonance 272
Frottement et échanges thermiques dans les gaz raréfiés 86
Fundamental constants of physics, The 78
Fundamentals of advanced missiles 270
Glass-melting tank furnaces 79
Glossary of terms used in vacuum technology 497
Glove boxes and shielded cells for handling radioactive materials 272
Group theory and its applications to the quantum mechanics of atomic spectra 493
Growth and perfection of crystals 279
Growth of crystals 496
Grundriss der Photographie und ihrer Anwendungen besonders in der Atomphysik 82
Halbleiterprobleme IV 264
Halbleiter und Phosphore. Vorträge des Internationalen Kolloquiums 1956 "*Halbleiter und Phosphore*" *in Garmisch-Partenkirchen* 86
Handbook of chemistry and physics 278
Handbook of physics 278
Handbook of supersonic aerodynamics: NAVORD Report 1488. Vol. 3. Section 6 83
Handbook of supersonic aerodynamics. Section 7: *Three-dimensional airfoils* (NAVORD Report 1488, Vol. 3) 485
Handbook on torsional vibration, A 261
Handbuch der Physik. Vol. 26 83
Handbuch der Physik. Vol. VII/2 497
Heat exchangers. Applications to gas turbines 267
High speed aerodynamics and jet propulsion, Vol. III. *Fundamentals of gas dynamics* 260
Internal conversion coefficients 269
Introduction to monopulse 490
Introduction to the theory of compressible flow 485
Introduction to the theory of sound transmission, with application to the ocean 259
Ionosphere, The 268
Irreducible tensorial sets 269
Jahrbuch der wissenschaftlichen gesellschaft für luftfahrt E.V. (W.G.L.) 270
Kernverfahrenstechnik. Eine Einführung für Ingenieure 80
Leybold Vakuum-Taschenbuch 84
Lichtelektrische Effekt und seine Andwendungen, Der 276
Liquids and liquid mixtures 486
Low temperature physics and chemistry. Proceedings of the fifth international conference on low temperature physics and chemistry 266
Magneto-ionic theory and its applications to the ionosphere, The 268
Matrix calculus 493
Max Planck: Physikalische Abhandlungen und Vortrage, Vols. I, II and III 79
Mechanical properties of non-metallic brittle materials 263
Mesure précise du temps en fonction des exigences nouvelles de la science, La 495
Metal fatigue 487
Methods based on the Wiener–Hopf technique for the solution of partial differential equations 494
Modern geometrical optics 82
Modern materials. Advances in development and applications. Vol. 1 263
Molecular science and molecular engineering 487
New chemistry 262
Noble metal thermocouples 268
Noise in electron devices 490
Nomenclature of organic chemistry 1957 262
Nonlinear problems in random theory 494

Books, New—*continued*
Nuclear electronics 495
Nuclear handbook, The 273
Nuclear moments 273
Nuclear reactions. Vol. 1 273
Nuclear reactor experiments 81
Nuclear scattering 81
Nuclear spectroscopy tables 274
Nuclear structure 81
Optical properties of semi-conductors 276
Papers presented to the section on mineral chemistry. 16th International Congress of Pure and Applied Chemistry, Paris, 1957 262
Physical acoustics and the properties of solids 259
Physical metallurgy of magnesium and its alloys, The 487
Physical theory of neutron chain reactors, The 275
Physics and heat technology of reactors 495
Physics of rubber elasticity, The 76
Physikalisches Praktikum 495
Physik der Halbleiter 491
Physik und Technik der Atomreaktoren 81
Plasma in a magnetic field. A symposium on magneto-hydrodynamics, The 265
Platinum in the glass industry 268
Practical microscopy 82
Premier colloque international de photographie corpusculaire 496
Preparation of single crystals 279
Principes de la théorie électromagnétique et de la relativité, Les 493
Principles and applications of random noise theory 265
Principles of electrophoresis, The 266
Principles of quantum electrodynamics 274
Principles of quantum mechanics, The 80
Proceedings of conference on magnetism and magnetic materials 491
Proceedings of the second conference on ultrasonics. 18–28 *VI,* 1956 259
Proceedings of the third conference on carbon 488
Programming for digital computers 494
Progress in biophysics. Vol. 8 79
Progress in dielectrics. Vol. 1 491
Progress in non-destructive testing. Vol. 1 270
Progress in nuclear energy. Series 1, Vol. 3. *Physics and mathematics* 496
Progress in nuclear energy. Series 1. Vol. 2. *Physics and mathematics* 274
Progress in nuclear energy. Series VII, *Medical sciences* 496
Progress in nuclear energy. Series IX, Vol. 1. *Analytical chemistry* 496
Progress in nuclear physics. Vol. 7 496
Properties and characteristics of aluminium casting alloys, The 268
Propriétés et applications des transistors 264
Quecksilber-niederdruckgasentladungen 265
Questions and answers on electron microscopes 268
Reflex klystrons 77
Registrierinstrumente 261
Rohrhydraulik: Ein Handbuch zur praktischen Strömungs-berechnung 84
Reports on progress in physics, Vol. XXI 80
Reports on progress in physics. Vol. XXII 495
Reports of the United Nations Scientific Committee on the effects of atomic radiation. General Assembly. Official Records; Thirteenth Session, Supplement No. 17 (*A*/3838) 274
Rheology of disperse systems 488
Safe handling of radioisotopes 275
Sampled-data control systems 494
Second symposium on coal preparation 266
Semiconductors 491
Seventh symposium (*international*) *on combustion* 489

Books, New—*continued*
Solid state physical electronics 280
Solid state physics. Advances in research and applications. Vol. 6 86
Solid state physics: Advances in research and applications. Vol. 7 280
Solid state physics. Advances in research and applications. Vol. 8 497
Sourcebook on atomic energy 82
Spectrum of atomic hydrogen 275
Story of temperature measurement, A 268
Structure and properties of porous materials, The 263
Structure of electrolytic solutions, The 488
Structure reports. Vol. 14. *Supplementary volume and cumulative index for* 1940–1950 497
Tables of interatomic distances and configuration in molecules and ions 275
Tables of thermodynamic functions of air 269
Technical writer, The 278
Techniques of polymer characterization 488
Technische Hydro-und Aeromechanik 260
Theory and design of magnetic amplifiers, The 266
Thermische Turbomaschinen 267
Torsionstheorie 76
Transformation characteristics of direct-hardening nickel-alloy steels 77
Transient response from frequency response 77
Transistor era, The 491
Transistor technology. Vols. 2 and 3 264
Vacancies and other point defects in metals and alloys 263
Van Nostrand's scientific encyclopedia 85
Wiggin nickel alloys v. caustic alkalies 268
Zone melting 77
Boundary condition, radiation, Transient temperature rise due to a line source in a semi-infinite medium, with a, at the interface 314
Breakdown
potential and normal cathode fall 523
potentials in hydrogen 502
potentials, thermionic cathodes 498
British Standards Yearbook 1959 544 (NC)
Brittle materials, Measurement of the tensile strength of 281
Bulb-breaking correction for heats of wetting determinations 398

Cadmium sulphide crystals grown from the vapour phase in a stream of argon, Study of 529
Cadmium sulphide photoconductive layers 298 (C)
Campbell type, mutual inductance standards of the, Correction for size of cross-section of the secondary windings of 481
Capillary viscometers, Theoretical evaluation of, for the measurement of the viscosity of suspensions of spheres 371
Carbon films, Single-etch extraction replica method adapted for 543 (C)
Carbon, platinum and, High-resolution shadow-casting technique for the electron microscope using the simultaneous evaporation of 198
Carbonization, Electrical conductivity of vitrain during 507
Cascade intensifiers, Image fluctuations in 233
Cathode
emission measurements in low pressure discharges 409
work function, Influence of the, on the sparking potential in hydrogen 502
work function, sparking potentials and secondary ionization coefficients for oxide-coated cathodes in hydrogen 498
Cathodes
carburized thoriated tungsten, Evaporation of thorium from 10 in hydrogen, oxide-coated, Cathode work function, sparking potentials and secondary ionization coefficients for 498
, oxide-coated, Reversible poisoning by sulphur, oxygen and other gases of, at high temperatures 359
Centripetal air-pump operated electromagnetically 54 (C)
Centroids of diffraction profiles, Counter diffractometer—The theory of the use of, for high accuracy in the measurement of diffraction angles 57
Characteristic K_α X-ray production in copper, Efficiency of, between 9 and 15 kV 505
Circuit, Linear photomultiplier bridge, for the measurement of small changes in absorption 89
Circuits, electronic, Application of delayed feedback in 400
Cleaning glass, Methods of, by vapour degreasing and ultrasonically agitated solvents 332
Coagulation, dispersion and, Effect of sound intensity on, in ultrasonic emulsification 250
Coal compacts, Relationship between strength and porosity for 287
Coercive force, Effect of twins on 511
Cold neutrons, Solid and liquid state research with 1 (SA)
Colloquium on X-ray fluorescence analysis—London, February and April 1958, Summarized proceedings of a 105 (CR)
Comité Consultatif de Thermométrie, Proceedings of 544 (NC)
Compacts, coal, Relationship between strength and porosity for 287
Comparator, Spectrum display 352
Computer
, electronic analogue, Use of an, with resistance network analogues 176
elements, Superconducting 193 (SA)
Refrigeration of a superconducting memory for a 452
Use of an electronic analogue, with resistance network analogues 542 (C)
Concrete beams, rectangular, Torsional vibrational experiments on 51
Conducting system, eccentric tubular, Inductance of an 230
Conductive liquid saturation in a porous medium, Radiofrequency method for the measurement of 54 (C)
Conductivities, Thermal, of fused and crystalline quartz 22
Conductivity, electrical, of vitrain, during carbonization 507
Conference
, Australian, on solid state physics 104 (NC)
, Geneva, Review of the Proceedings of the 382 (NC)
on nuclear fuel cycles, Summarized proceedings of a,—London, January 1959 237 (CR)
on precipitation in alloys and on metal structures, Summarized proceedings of a,—London, November 1958 438 (CR)
on solid state memory and switching devices, Summarized proceedings of a,—London, September 1958 153 (CR)
on some aspects of magnetism 56 (NC)
on X-ray analysis, Summarized proceedings of a—Manchester, April 1958 116 (CR)
Contact, Improved semiconductor-to-copper soldered 469 (C)
Contacts, graphite-copper, Thermal transients in 516
Control 152 (NC)
Convection heat transfer data, correlating forced, Alternative method of 135
Convention, International, and exhibition on transistors 56 (NC)
Convention on thermonuclear processes 56 (NC)
Cooling of a spinning thread-line 39 (*erratum*) 104
Copper
and duralumin, Pick-up of, on bonded tungsten carbide 367
, Efficiency of characteristic K_α X-ray production in, between 9 and 15 kV 505
soldered contact, semi-conductor-to-, Improved 469 (C)
Correction, Bulb-breaking, for heats of wetting determinations 398
Correction for size of cross-section of the secondary windings of mutual inductance standards of the Campbell type 481
Corrections, absorption, Powder technique for the empirical determination of 406
Corrections, Amplitude, for vibroscope measurements 219
Correlating forced convection heat transfer data, Alternative method of 135
Cosmic ray studies, Large permanent magnets for 471
Counter diffractometer—The theory of the use of centroids of diffraction profiles for high accuracy in the measurement of diffraction angles 57

Counter, proportional, Measurement of the quantum efficiency of a, using X-rays 376
Creep, recovery, relaxation and elastic "memory" of some renneted milk gels, On the 15
Crystallite size, New method for the determination of grain or, from spotty diffraction rings 321
Crystallographic twins, Effect of, on the d.c. and a.c. properties of nickel–iron alloys 511
Crystals
  lithium flouride, New method for increasing the X-ray reflexion power of 141
  , potassium cobalticyanide, Controlling the habit of 429 (C)
  , single, of bismuth, Technique for determining the orientation of 336
  , Study of cadmium sulphide, grown from the vapour phase in a stream of argon 529
Cycles, nuclear fuel, Summarized proceedings of a conference on,—London, January 1959 237 (CR)

Dams, buttress, Experimental method of investigating stresses in 465
Data, correlating forced convection heat transfer, Alternative method of 135
Defects, size of, Determination of the, by the ultrasonic impulse echo method 240
Deformation, Effect of, of the surface texture on rolling resistance 172
Degreasing, vapour, Methods of cleaning glass by, and ultrasonically agitated solvents 332
Deposition by thermal evaporation of thin films of titanium and zirconium for tritium targets 91
Deposition of unipolar charged aerosol particles by mutual repulsion 206
Diameter variation, fibre, Measurement of, by optical diffraction 328
Diamond, Absorption and scattering in 412
Dielectric constant of a high-loss liquid, Method for measuring the complex, at 8 mm wavelength 87
Dielectric properties of water/alumina 404
Dielectrics, anisotropic, Theorem concerning 32
Differential equation, Approximate solution of a non-linear, giving the temperature distribution in the positive column of a static arc 47
Diffraction
  , optical, Measurement of fibre diameter variation by 328
  profiles, Counter diffractometer—The theory of the use of centroids of, for high accuracy in the measurement of diffraction angles 57
  rings, spotty, New method for the determination of grain or crystallite size from 321
Diffractometer, Counter,—The theory of the use of centroids of diffraction profiles for high accuracy in the measurement of diffraction angles 57
Discharge, Glow, characteristics of helium-neon mixtures 523
Discharge, low pressure gas, Production of X-rays during a 147
Discharge plasmas, Excitation and ionization rates of mercury in 186
Discharges, low pressure, Cathode emission measurements in 409
Discharges, pulsed gaseous, Microwave method of investigating the afterglows of 356
Disk
  atomizer, high-speed spinning, Analysis of a polydisperse aqueous spray from a 180
  atomizer, high-speed spinning, Experimental determination of the atomizing efficiency of a 93
  brakes, Transient temperatures attained in 339
Dispersion and coagulation, Effect of sound intensity on, in ultrasonic emulsification 250
Displacements, Interferometric measurement of small angular 445
Display comparator, Spectrum 352
Drawing of Nylon 66, Effect of temperature and moisture content on the orientation produced by the 68
Droplets, non-volatile, Method for size-distribution determinations of, by electron microscopy 139
Drops of aqueous solutions, Volume of, transferred to a slide by a "micro-rod" 99
Duralumin, Pick-up of copper and, on bonded tungsten carbide 367
Dust particles, Collection of gas-borne, by means of an aspirated sampling nozzle 26

Eccentric tubular conducting system, Inductance of an 230
Echo method, ultrasonic impulse, Determination of the size of defects by the 240
Efficiency, Experimental determination of the atomizing, of a high-speed spinning disk atomizer 93
Electric spark, Investigation of the ignition of a gas by an 159 (*erratum*) 382
Electrical determination of the thermal parameters of semiconducting thermoelements 235 (C)
Electrical instrument test service 300 (NC)
Electromagnetic fields in ferrite ellipsoids 20
Electron
  beams, Dense 391 (SA)
  microscope, High-resolution shadow-casting technique for the, using the simultaneous evaporation of platinum and carbon 198
  microscopy, Method for size-distribution determinations of non-volatile droplets by 139
Electronic analogue computer, Use of an, with resistance network analogues 176
Electronic circuits, Application of delayed feedback in 400
Electrons, medium energy, at small angles, Differential scattering cross-section of atoms to 341
Elements, Analysis of the lighter, by total reflexion of the characteristic X-ray wavelengths 190
Elements, Superconducting computer 193 (SA)
Ellipsoids, ferrite, Electromagnetic fields in 20
Emission measurements, Cathode, in low pressure discharges 409
Emission phenomena, exo-electron, The problem of 102 (C)
Emulsification, ultrasonic, Effect of sound intensity on dispersion and coagulation in 250
Energy variation with pressure and temperature in a sonic stationary wave 246
Errors, Temperature, introduced by temperature-measuring probes 252
Evaluation of approximate methods of applying binary scale factors in pulse-counting systems of measurement 124
Evaporation
  , Deposition by thermal, of thin films of titanium and zirconium for tritium targets 91
  of platinum and carbon, High resolution shadow-casting technique for the electron microscope using the simultaneous 198
  of thorium from carburized thoriated tungsten cathodes 10
Excitation and ionization rates of mercury in discharge plasmas 186
Exhibition of scientific instruments and apparatus, The Physical Society's annual 544 (NC)
Exhibition on transistors, International convention and 56 (NC)
Exo-electron emission phenomena, The problem of 102 (C)
Extraction replica method, Single-etch, adapted for carbon films 543 (C)
Eyepiece graticules, microscope, Dimensions of 428 (C)

Fallout, Identification of radioactive particles from 526
Feedback, Application of delayed, in electronic circuits 400
Ferrite ellipsoids, Electromagnetic fields in 20
Ferrite isolator, S-band, for use with a linear accelerator 53 (C)
Ferromagnetic after-effect in mumetal 142
Fibre diameter variation, Measurement of, by optical diffraction 328
Fields, Electromagnetic, in ferrite ellipsoids 20
Film resistors, Preparation of metal, on laminated plastics 35

Films
, carbon, Single-etch extraction replica method adapted for 543 (C)
, thin, Deposition by thermal evaporation of, of titanium and zirconium for tritium targets 91
, thin, of α-iron, Technique for preparing 255
Flow of heat in a composite solid 204
Fluorescence analysis, X-ray, Summarized proceedings of a colloquium on,—London, February and April 1958 105 (CR)
Forces, Measurement of very small 534
Fuel cycles, nuclear, Summarized proceedings of a conference on,—London, January 1959 237 (CR)

Gas
-borne dust particles, Collection of, by means of an aspirated sampling nozzle 26
discharge, low pressure, Production of X-rays during a 147
, Investigation of the ignition of a, by an electric spark 159 (*erratum*) 382
-lubricated, hydrodynamic, full journal bearings, Study of 455
Gases, Reversible poisoning by sulphur, oxygen and other, of oxide-coated cathodes, at high temperatures 359
Gauge, Bayard–Alpert ionization, Bistable behaviour of the 364
Gel, milk, Some aspects of the rheology of 476
Gel, symmetrically stressed renneted milk, Distribution of relaxation times in a 97
Gels, milk, On the creep, recovery, relaxation and elastic "memory" of some renneted 15
Geneva Conference, Review of the Proceedings of the 382 (NC)
Germanium, Contacts to 469 (C)
Glass, Absorption of sodium and argon by 295
Glass, Methods of cleaning, by vapour degreasing and ultrasonically agitated solvents 332
Grain or crystallite size, New method for the determination of, from spotty diffraction rings 321
Graphite-copper contacts, Thermal transients in 516
Graticules, microscope eyepiece, Dimensions of 428 (C)
Gratings, On the use of coarse, in ultrasonics 191 (C)
Grid materials, control, Thermionic properties of thorium deposits on 71

Health physics 152 (NC)
Heat
, Flow of, in a composite solid 204
transfer data, correlating forced convection, Alternative method of 135
transfer, Electric stress and 347
Heats of wetting determinations, Bulb breaking correction for 398
Helium-neon mixtures, Glow discharge characteristics of 523
Hydrodynamic, full journal bearings, Study of gas-lubricated 455
Hydrogen
, Influence of the cathode work function on the sparking potential in 502
, neon, and argon, First ionization coefficients in 301
, oxide-coated cathodes in, Cathode work function, sparking potentials and secondary ionization coefficients for 498

ICSU review (International Council of Scientific Unions) 382 (NC)
Identification, photographic, of microscopic radioactive particles, Method for 526
Ignition of a gas, Investigation of the, by an electric spark 159 (*erratum*) 382
Image fluctuations in cascade intensifiers 233
Impact sensitivity of mercury fulminate, Some experimental results on the 132
Impulse echo method, ultrasonic, Determination of the size of defects by the 240
Indium solder, Reaction of, with mercury telluride 380 (C)
Inductance of an eccentric tubular conducting system 230
Inductance standards of the Campbell type, mutual, Correction for size of cross-section of the secondary windings of 481
Institute of Physics, Elections to The 104 (NC), 382 (NC), 430 (NC)
Instrument test service, Electrical 300 (NC)
Integrating sphere, Use of an, to distinguish between absorption and scattering in solids 412
Intensifiers, cascade, Image fluctuations in 233
Intensities, light, Absolute measurement of 428 (C)
Interface, Transient temperature rise due to a line source in a semi-infinite medium with a radiation boundary condition at the 314
Interferometric measurement of small angular displacements 445
Interferometry, Symposium on 104 (NC)
Ionization
coefficients, First, in hydrogen, neon, and argon 301
coefficients, secondary, Cathode work function, sparking potentials and, for oxide-coated cathodes in hydrogen 498
gauge, Bayard–Alpert, Bistable behaviour of the 364
rates of mercury, Excitation and, in discharge plasmas 186
Isolator, S-band ferrite, for use with a linear accelerator 53 (C)

Journal of Mechanical Engineering Science, The 430 (NC)

K_α X-ray production in copper, Efficiency of characteristic, between 9 and 15 kV 505

Laminated plastics, Preparation of metal film resistors on 35
Lapis 104 (NC)
Layers, Cadmium sulphide photoconductive 298 (C)
Light, Attenuation of, by wood smoke 416
Light intensities, Absolute measurement of 428 (C)
Linear accelerator, S-band ferrite isolator for use with a 53 (C)
Line source, Transient temperature rise due to a, in a semi-infinite medium with a radiation boundary condition at the interface 314
Liquid
, Method for measuring the complex dielectric constant of a high-loss, at 8 mm wavelength 87
saturation, conductive, in a porous medium, Radiofrequency method for the measurement of 54 (C)
state research, Solid and, with cold neutrons 1 (SA)
, viscous, Interaction between two equal-sized equal-settling spheres moving through a 43 (*erratum*) 104
Lithium fluoride crystals, New method for increasing the X-ray reflexion power of 141
Low-pressure gas discharge, Production of X-rays during a 147
Low temperature memory store 452

Magnetic resonance, Nuclear, in solids 431 (SA)
Magnetism, Conference on some aspects of 56 (NC)
Magnets, Some aspects of the design of large permanent 471
Manufacturers, British, F.B.I. Register of 152 (NC)
Measurement, pulse-counting systems of, Evaluation of approximate methods of applying binary scale factors in 124
"Memory," On the creep, recovery, relaxation and elastic, of some renneted milk gels 15
Memory, Refrigeration of a superconducting, for a computer 452
Memory, solid state, Summarized proceedings of a conference on, and switching devices—London, September 1958 153 (CR)
Mercury
fulminate, Some experimental results on the impact sensitivity of 132
in discharge plasmas, Excitation and ionization rates of 186
telluride, Reaction of indium solder with 380 (C)
Metal film resistors, Preparation of, on laminated plastics 35
Metal structures, Summarized proceedings of a conference on precipitation in alloys and on,—London, November 1958 438 (CR)

Metallurgy, Powder 430 (NC)
Microanalyser, The X-ray scanning 420
"Micro-rod," Volume of drops of aqueous solutions transferred to a slide by a 99
Microscope eyepiece graticules, Dimensions of 428 (C)
Microscopic radioactive particles, Method for photographic identification of 526
Microwave method of investigating the afterglows of pulsed gaseous discharges 356
Milk
  gel, Some aspects of the rheology of 476
  gel, symmetrically stressed renneted, Distribution of relaxation times in a 97
  gels, some renneted, On the creep, recovery, relaxation and elastic "memory" of 15
Moisture content, Effect of temperature and, on the orientation produced by the drawing of Nylon 66 68
Molecular beams, Torsion balance measurements with 534
Mumetal, Ferromagnetic after-effect in 142
Mutual inductance standards of the Campbell type, Correction for size of cross-section of the secondary windings of 481

Neon, and argon, hydrogen, First ionization coefficients in 301
Neon mixtures, Helium-, Glow discharge characteristics of 523
Neutrons, cold, Solid and liquid state research with 1 (SA)
Nickel-iron alloys, d.c. and a.c. properties of, Effect of crystallographic twins on the 511
Nozzle, an aspirated sampling, Collection of gas-borne dust particles by means of 26
Nuclear fuel cycles, Summarized proceedings of a conference on,—London, January 1959 237 (CR)
Nuclear magnetic resonance in solids 431 (SA)
Nylon 66, drawing of, Effect of temperature and moisture content on the orientation produced by the 68
Nylon "texture," Investigation of, by X-ray diffraction 225 (*erratum*) 382

Oil, Estimation of trace water content in a halogenated, by means of tritiated water 463
Optical diffraction, Measurement of fibre diameter variation by 328
Orientation of single crystals of bismuth, Technique for determining the 336
Orientation produced by the drawing of Nylon 66, Effect of temperature and moisture content on the 68
Oxide-coated cathodes in hydrogen, Cathode work function, sparking potentials and secondary ionization coefficients for 498
, Oxygen, Reversible poisoning by sulphur, and other gases of oxide-coated cathodes at high temperatures 359

Particles
  , aerosol, Deposition of unipolar charged, by mutual repulsion 206
  , Collection of gas-borne dust, by means of an aspirated sampling nozzle 26
  , microscopic radioactive, Method for photographic identification of 526
  , spherical, Studies of the viscosity of sedimentation of suspensions. Part 5—The viscosity of settling suspensions of 317 (*erratum*) 430
  , wood smoke, Properties of 416
Permittivity of mixtures of zinc oxide and rubber 306
Photoconductive layers, Cadmium sulphide 298 (C)
Photographic identification, Method for, of microscopic radioactive particles 526
Photomultiplier bridge circuit, Linear, for the measurement of small changes in absorption 89
Physical Society's annual exhibition of scientific instruments and apparatus, The 544 (NC)
Pick-up of copper and duralumin on bonded tungsten carbide 367
Planetary and space science 544 (NC)
Plasmas, discharge, Excitation and ionization rates of mercury in 186
Plastics, laminated, Preparation of metal film resistors on 35
Platinum and carbon, High resolution shadow-casting technique for the electron microscope using the simultaneous evaporation of 198
Poisoning, Reversible, by sulphur, oxygen and other gases of oxide-coated cathodes at high temperatures 359
Polydisperse aqueous spray, Analysis of a, from a high-speed spinning disk atomizer 180
Porosity, strength and, Relationship between, for coal compacts 287
Porous medium, Radiofrequency method for the measurement of conductive liquid saturation in a 54 (C)
Potassium cobalticyanide crystals, Controlling the habit of 429 (C)
Potential distribution in regions having potential-dependent dielectric constants 538
Potential, sparking, in hydrogen, Influence of the cathode work function on the 502
Potentials, sparking, and secondary ionization coefficients for oxide-coated cathodes in hydrogen, Cathode work function 498
Powder Data File—4, A.S.T.M., Comments on the 192 (C)
Powder metallurgy 430 (NC)
Powder technique for the empirical determination of absorption corrections 406
Precipitation in alloys, Summarized proceedings of a conference on, and on metal structures—London, November 1958 438 (CR)
Pressure and temperature, Energy variation with, in a sonic stationary wave 246
Probes, temperature-measuring, Temperature errors introduced by 252
Proceedings of Comité Consultatif de Thermométrie 544 (NC)
Profiles, diffraction, Counter diffractometer—The theory of the use of centroids of, for high accuracy in the measurement of diffraction angles 57
Pulse-counting systems of measurement, Evaluation of approximate methods of applying binary scale factors in 124
Pulses, high intensity stress, Measurement of 290

Quantum efficiency, Measurement of the, of a proportional counter using X-rays 376
Quartz, absorption and scattering in, Use of an integrating sphere to distinguish between 412
Quartz, fused and crystalline, Thermal conductivities of 22

Radioactive particles, microscopic, Method for photographic identification of 526
Radioactive trace, Method for 463
Radio-frequency method for the measurement of conductive liquid saturation in a porous medium 54 (C)
Radio-frequency spectroscopy 431 (SA)
Reactor technology 544 (NC)
Recovery, relaxation and elastic "memory", On the creep, of some renneted milk gels 15
Reflexion of their characteristic X-ray wavelengths, Analysis of the lighter elements by total 190
Reflexion power, X-ray, New method for increasing the, of lithium fluoride crystals 141
Refrigeration of a superconducting memory for a computer 452
Register of British Manufacturers, F.B.I. 152 (NC)
Relaxation and elastic "memory", On the creep, recovery, of some renneted milk gels 15
Relaxation times, Distribution of, in a symmetrically stressed renneted milk gel 97
Replica method, Single-etch extraction, adapted for carbon films 543 (C)

Resistance
network analogue, Unifying design principle for the 166
network analogues, Use of an electronic analogue computer with 176, 542 (C)
, rolling, Effect of the determination of the surface texture on 172
Resistors, Preparation of metal film, on laminated plastics 35
Resonance, Nuclear magnetic, in solids 431 (SA)
Response, Transient, of direct current amplifier systems 326
Rheology of milk gel, Some aspects of the 476
Rolling resistance, Effect of the determination of the surface texture on 172
Rubber, zinc oxide and, Permittivity of mixtures of 306

Sampling nozzle, an aspirated, Collection of gas-borne dust particles by means of 26
Saturation, conductive liquid, Radiofrequency method for the measurement of, in a porous medium 54 (C)
S-band ferrite isolator for use with a linear accelerator 53 (C)
Scale factors, binary, Evaluation of approximate methods of applying, in pulse counting systems of measurement 124
Scanning microanalyser, The X-ray 420
Scattering, absorption and, in solids, Use of an integrating sphere to distinguish between 412
Scattering cross-section of atoms, Differential, to medium energy electrons at small angles 341
Sedimentation, Studies of the viscosity and, of suspensions. Part 5—The viscosity of settling suspensions of spherical particles 317 (*erratum*) 430
Semiconducting thermoelements, Electrical determination of the thermal parameters of 235
Semiconductor-to-copper soldered contact, Improved 469 (C)
Sensitivity, impact, of mercury fulminate,. Some experimental results on the 132
Service, Electrical instrument test 300 (NC)
Settling suspensions of spherical particles, The viscosity of, Studies of the viscosity and sedimentation of suspensions., Part 5—317
Shadow-casting technique, High-resolution, for the electron microscope using the simultaneous evaporation of platinum and carbon 198
Silicon, Contacts to 469 (C)
Single crystals of bismuth, orientation of, Technique for determining the 336
Size
-distribution determinations, Method for, of non-volatile droplets by electron microscopy 139
, grain or crystallite, New method for the determination of, from spotty diffraction rings 321
of defects, Determination of the, by the ultrasonic impulse echo method 240
Smoke, wood, Attenuation of light by 416
Sodium and argon, Absorption of, by glass 295
Solder, indium, Reaction of, with mercury telluride 380 (C)
Soldered contact, Improved semiconductor-to-copper 469 (C)
Solid
and liquid state research with cold neutrons 1 (SA)
, composite, Flow of heat in a 204
state memory and switching devices, Summarized proceedings of a conference on,—London, September 1958 153 (CR)
state physics, Australian conference on 104 (NC)
Solids
, absorption and scattering in, Use of an integrating sphere to distinguish between 412
, Nuclear magnetic resonance in 431 (SA)
Steady-state temperature distribution in, undergoing certain change of property 538
Solutions, aqueous, Volume of drops of, transferred to a slide by a "micro-rod" 99
Sonic stationary wave, Energy variation with pressure and temperature in a 246
Sound intensity, Effect of, on dispersion and coagulation in ultrasonic emulsification 250
Source, high-precision spectroscopic spark, Theory of operation and constructional principles of a 310
Source, line, Transient temperature rise due to a, in a semi-infinite medium with a radiation boundary condition at the interface 314
Spark, electric, Investigation of the ignition of a gas by an 159 (*erratum*) 382
Spark source, high-precision spectroscopic, Theory of operational and constructional principles of a 310
Sparking potential in hydrogen, Influence of the cathode work function on the 502
Sparking potentials and secondary ionization coefficients, Cathode work function, for oxide-coated cathodes in hydrogen 498
Spectrographs, μ-meson, Large permanent magnets for 471
Spectroscopic spark source, high-precision, Theory of operation and constructional principles of a 310
Spectroscopy, Radio-frequency 431 (SA)
Spectrum display comparator 352
Spheres, Interaction between two equal-sized equal-settling, moving through a viscous liquid 43 (*erratum*) 104
Spheres, suspensions of, Theoretical evaluation of capillary viscometers for the measurement of the viscosity of 371
Spherical particles, Studies of the viscosity and sedimentation of suspensions. Part 5.—The viscosity of settling the suspensions of 317 (*erratum*) 430
Spinning
disk atomizer, high-speed, Analysis of a polydisperse aqueous spray from a 180
disk atomizer, high-speed, Experimental determination of the atomizing efficiency of a 93
thread-line, Cooling of a 39 (*erratum*) 104
Spray, polydisperse aqueous, Analysis of a, from a high-speed spinning disk atomizer 180
Steady-state diffusion through certain composite solids 538
Steady-state temperature distribution in solids undergoing certain change of property 538
Strength and porosity, Relationship between, for coal compacts 287
Strength, tensile, Measurement of the, of brittle materials 281
Stress, Electric, and heat transfer 347
Stress pulses, high intensity, Measurement of 290
Stresses, Experimental method of investigating, in buttress dams 465
Structures, metal, Summarized proceedings of a conference on precipitation in alloys and on,—London, November 1958 438 (CR)
Sulphur oxygen and other gases, Reversible poisoning by, of oxide-coated cathodes at high temperatures 359
Superconducting computer elements 193 (SA)
Superconducting memory, Refrigeration of a, for a computer 452
Surface texture, Effect of deformation of the, on rolling resistance 172
Suspensions of spheres, viscosity of, Theoretical evaluation of capillary viscometers for the measurement of the 371
Suspensions of spherical particles, The viscosity of settling, Studies of the viscosity and sedimentation of suspensions. Part 5—317
Switching devices, Summarized proceedings of a conference on solid state memory and,—London, September 1958 153 (CR)
Symposium
on current developments in the production of high vacua 56 (NC)
on current developments in the production of high vacua—London, April 1959, Summarized proceedings of a 383 (CR)
on interferometry 104 (NC)

Targets, tritium, Deposition by thermal evaporation of thin films of titanium and zirconium for 91
Temperature
and moisture content, Effect of, on the orientation produced by the drawing of Nylon 66 68

Temperature—*continued*
distribution, Approximate solution of a non-linear differential equation giving the, in the positive column of a static arc 47
distribution, Steady-state, in solids undergoing certain change of property 538
, Energy variation with pressure and, in a sonic stationary wave 246
errors introduced by temperature-measuring probes 252
, Low, memory store 452
rise, Transient, due to a line source in a semi-infinite medium with a radiation boundary condition at the interface 314
Temperatures, high, Reversible poisoning by sulphur oxygen and other gases of oxide-coated cathodes at 359
Temperatures, Transient, attained in disk brakes 339
Tensile strength, Measurement of the, of brittle materials 281
Test service, Electrical instrument 300 (NC)
"Texture," Nylon, Investigation of, by X-ray diffraction 225 (*erratum*) 382
Texture, surface, Effect of deformation of the, on rolling resistance 172
Theorem concerning anisotropic dielectrics 32
Thermal
conductivities of fused and crystalline quartz 22
evaporation, Deposition by, of thin films of titanium and zirconium for tritium targets 91
transients in graphite-copper contacts 516
Thermionic properties of thorium deposits on control grid materials 71
Thermoelements, semiconducting, Electrical determination of the thermal parameters of 235
Thermonuclear processes, Convention on 56 (NC)
Thixotropic materials, Viscous properties of 214
Thorium deposits, Thermionic properties of, on control grid materials 71
Thorium, Evaporation of, from carburized thoriated tungsten cathodes 10
Thread-line, spinning, Cooling of a 39 (*erratum*) 104
Titanium and zirconium, Deposition by thermal evaporation of thin films of, for tritium targets 91
Torsion balance measurements with molecular beams 534
Torsional vibrational experiments on rectangular concrete beams 51
Trace water content in a halogenated oil, by means of tritiated water, Estimation of 463
Transient
response of direct current amplifier systems 326
temperature rise due to a line source in a semi-infinite medium, with a radiation boundary condition at the interface 314
temperatures attained in disk brakes 339
Transients, Thermal, in graphite-copper contacts 516
Transistors, International convention and exhibition on 56 (NC)
Tritiated water, Estimation of trace water content in a halogenated oil by means of 463
Tritium targets, Deposition by thermal evaporation of thin films of titanium and zirconium for 91
Tubular conducting system, eccentric, Inductance of an 230
Tungsten carbide, bonded, Pick-up of copper and duralumin on 367
Tungsten cathodes, carburized thoriated, Evaporation of thorium from 10
Twins, crystallographic, Effect of, on the d.c. and a.c. properties of nickel-iron alloys 511

Ultrasonic emulsification, Effects of sound intensity on dispersion and coagulation in 250
Ultrasonic impulse method, Determination of the size of defects by the 240
Ultrasonically agitated solvents, vapour degreasing and, Methods of cleaning glass by 332
Ultrasonics, On the use of coarse gratings in 191 (C)

Vacua, high, Summarized proceedings of a symposium on current developments in the production of,—London, April 1959 383 (CR)
Vacua, high, Symposium on current developments in the production of 56 (NC)
Vapour phase, Study of cadmium sulphide crystals grown from the, in a stream of argon 529
Vibrational experiments, Torsional, on rectangular concrete beams 51
Vibroscope measurements, Amplitude corrections for 219
Viscometers, capillary, Theoretical evaluation of, for the measurement of the viscosity of suspensions of spheres 371
Viscosity and sedimentation of suspensions, Studies of the, Part 5—The viscosity of settling suspensions of spherical particles 317 (*erratum*) 430
Viscosity of suspensions of spheres, Theoretical evaluation of capillary viscometers for the measurement of the 371
Viscous liquid, Interaction between two equal-sized equal-settling spheres moving through a 43 (*erratum*) 104
Viscous properties of thixotropic materials 214
Vitrain, Electrical conductivity of, during carbonization 507
Volume of drops of aqueous solutions transferred to a slide by a "micro-rod" 99

Water/alumina, Dielectric properties of 404
Water content, trace, Estimation of, in a halogenated oil by means of tritiated water 463
Wave, sonic stationary, Energy variation with pressure and temperature in a 246
Wetting determinations, heats of, Bulb breaking correction for 398
Wood smoke, Attenuation of light by 416
Work function, cathode, Influence of the, on the sparking potential in hydrogen 502
Work function, Cathode, sparking potentials and secondary ionization coefficients for oxide-coated cathodes in hydrogen 498

X-ray
analysis, Summarized proceedings of a conference on,—Manchester, April 1958 116 (CR)
diffraction, Investigation of Nylon "texture" by 225 (*erratum*) 382
fluorescence analysis, Summarized proceedings of a colloquium on,—London, February and April 1958 105 (CR)
production in copper, Efficiency of characteristic K_α, between 9 and 15 kV 505
reflexion power, New method for increasing the, of lithium fluoride crystals 141
scanning microanalyser, The 420
wavelengths, Analysis of the lighter elements by total reflexion of their characteristic 190
X-rays, Measurement of the quantum efficiency of a proportional counter using 376
X-rays, Production of, during a low-pressure gas discharge 147

Zinc oxide and rubber, Permittivity of mixtures of 306
Zirconium, titanium and, Deposition by thermal evaporation of thin films of, for tritium targets 91

AUTHORS

(SA) denotes special article, (CR) conference report and (C) correspondence.

Agar, A. W., *see under* Haine, M. E.
Allen, P. H. G., Electric stress and heat transfer 347
Andrews, E. H., Cooling a spinning thread-line 39
Andrew, E. R., Nuclear magnetic resonance in solids 431 (SA)
Andrews, K. W., and W. Johnson, New method for the determination of grain or crystallite size from spotty diffraction rings 321
Atkinson, M. P., *see under* Bane, W. T.

Badzioch, S., Collection of gas-borne dust particles by means of an aspirated sampling nozzle 26
Bane, W. T., and M. P. Atkinson, Evaluation of approximate methods of applying binary scale factors in pulse-counting systems of measurement 124
Bardócz, Á., Theory of operation and constructional principles of a high-precision spectroscopic spark source 310
Bassett, D. W., and A. J. B. Robertson, Torsion balance measurements with molecular beams 534
Bastin, J. A., E. W. J. Mitchell and J. Whitehouse, Use of an integrating sphere to distinguish between absorption and scattering in solids 412
Berenbaum, R., and I. Brodie, Measurement of the tensile strength of brittle materials 281
Betts, C., *see under* Whitley, S.
Bhalla, M. S., *see under* Hariharan, P.
Booker, G. R., and J. Norbury, Single-etch extraction replica method adapted for carbon films 543 (C)
Boyce, I. S., *see under* Cameron, J. F.
Bradley, D. E., High-resolution shadow-casting technique for the electron microscope using the simultaneous evaporation of platinum and carbon 198
Brandon, D. G., and J. Nutting, Technique for preparing thin films of α-iron 255
Braybrook, R. F., *see under* Franks, A.
Brodie, I., *see under* Berenbaum, R.
Buchanan, J. S., and H. J. James, Measurement of high intensity stress pulses 290
Burnett, J., *see under* Scott Blair, G. W.

Cameron, J. F., I. S. Boyce and R. M. Glaister, Estimation of trace water content in a halogenated oil by means of tritiated water 463
Cannon, C. G., and F. P. Chappel, Effect of temperature and moisture content on the orientation produced by the drawing of Nylon 66 68
Carter, G., and J. H. Leck, Bistable behaviour of the Bayard–Alpert ionization gauge 364
Castelliz, L., and W. W. H. Clarke, Ferromagnetic after-effect in mumetal 142
Cayless, M. A., Excitation and ionization rates of mercury in discharge plasmas 186
Cayless, M. A., *see under* Forster-Brown, A. D.
Champion, J. A., Thermionic properties of thorium deposits on control grid materials 71
Chappel, F. P., *see under* Cannon, C. G.
Clarke, W. W. H., *see under* Castelliz, L.
Cooper, W. A., Summarized proceedings of a conference on nuclear fuel cycles—London, January 1959 237 (CR)
Cousins, J. E., and W. F. Nash, Some aspects of the design of large permanent magnets 471

Davies, D. E., and B. J. Hopkins, Cathode work function, sparking potentials and secondary ionization coefficients for oxide-coated cathodes in hydrogen 498
Davies, D. E., and J. G. C. Milne, First ionization coefficients in hydrogen, neon, and argon 301
Davies, D. E., and R. K. Fitch, Influence of the cathode work function on the sparking potential in hydrogen 502
Davies, W., Thermal transients in graphite-copper contacts 516
Davis, H. M., *see under* Garton, F. W. J.
Dekker, L., *see under* Korthals Altes, J. Ph.
Donaldson, I. G., Temperature errors introduced by temperature-measuring probes 252
Duncumb, P., The X-ray scanning microanalyser 420
Dyson, N. A., Efficiency of characteristic K_α X-ray production in copper between 9 and 15 kV 505

Egelstaff, P. A., Solid and liquid state research with cold neutrons 1 (SA)
Ellingham, B., *see under* Onions, W. J.
Eveson, G. F., E. W. Hall and S. G. Ward, Interaction between two equal-sized equal-settling spheres moving through a viscous liquid 43

Fitch, R. K., *see under* Davies, D. E.
Forster-Brown, A. D., and M. A. Cayless, Cathode emission measurement in low pressure discharges 409
Foster, W. W., Deposition of unipolar charged aerosol particles by mutual repulsion 206
Attenuation of light by wood smoke 416
Franks, A., and R. F. Braybrook, Analysis of the lighter elements by total reflexion of their characteristic X-ray wavelengths 190
Franks, A., and R. S. M. Revell, Summarized proceedings of a conference on precipitation in alloys and on metal structures—London, November 1958 438 (CR)

Gair, F. C., Unifying design principle for the resistance network analogue 166
Gallavan, R. C., Bulb breaking correction for heats of wetting determinations 398
Garton, F. W. J., and H. M. Davis, Summarized proceedings of a colloquium on X-ray fluorescence analysis—London, February and April 1958 105 (CR)
Gaskell, C. S., and D. Walsh, S-band ferrite isolator for use with a linear accelerator 53 (C)
Gilissen, H. P. J., *see under* Korthals Altes, J. Ph.
Glaister, R. M., *see under* Cameron, J. F.
Golden, J., and G. W. Rowe, Pick-up of copper and duralumin on bonded tungsten carbide 367
Goldenberg, H., Approximate solution of a non-linear differential equation giving the temperature distribution in the positive column of a static arc 47
Transient temperature rise due to a line source in a semi-infinite medium, with a radiation boundary condition at the interface 314
Grant, E. H., Method for measuring the complex dielectric constant of a high-loss liquid at 8 mm wavelength 87
Gregg, S. J., *see under* Haine, M. E.
Grunberg, L., The theory of exo-electron emission phenomena 103 (C)

Haine, M. E., Absolute measurement of light intensities 428 (C)
Haine, M. E., and A. W. Agar, Differential scattering cross-section of atoms to medium energy electrons at small angles 341
Hall, E. W., *see under* Eveson, G. F.
Halling, J., Effect of deformation of the surface texture on rolling resistance 172

Hamilton, R. J., Dimensions of microscope eyepiece graticules 428 (C)
Hargreaves, A., and E. Stanley, Summarized proceedings of a conference on X-ray analysis—Manchester, April 1958 116 (CR)
Hariharan, P., and D. Sen, Interferometric measurement of small angular displacements 445
Hariharan, P., and M. S. Bhalla, Linear photomultiplier bridge circuits for the measurement of small changes in absorption 89
Harris, W. J., Method for size-distribution determinations of non-volatile droplets by electron microscopy 139
Hawkins, A. E., Volume of drops of aqueous solutions transferred to a slide by a "micro-rod" 99
Herinckx, C., and A. Monfils, Electrical determination of the thermal parameters of semiconducting thermoelements 235 (C)
Hopkins, B. J., *see under* Davies, D. E.
Hughes, J. W., Isabel E. Lewis and A. J. C. Wilson, Comments on the A.S.T.M. Powder Data File—4 192 (C)
Hurle, D. T. J., and S. Weintroub, Technique for determining the orientation of single crystals of bismuth 336
Hutcheon, I. C., Use of an electronic analogue computer with resistance network analogues 542 (C)

Ingles, A. R., Energy variation with pressure and temperature in a sonic stationary wave 246

James, H. J., *see under* Buchanan, J. S.
Jenkins, R. O., and W. G. Trodden, Evaporation of thorium from carburized thoriated tungsten cathodes 10
Johnson, W., *see under* Andrews, K. W.
Jones, E. E., Inductance of an eccentric tubular conducting system 230
Jones, R., Torsional vibrational experiments on rectangular concrete beams 51

Kiss, A. E., and N. Patla, Measurement of the quantum efficiency of a proportional counter using X-rays 376
Korthals Altes, J. Ph., Use of an electronic analogue computer with resistance network analogues 176
Korthals Altes, J. Ph., L. Dekker and H. P. J. Gilissen, Use of an electronic analogue computer with resistance network analogues 542 (C)
Krautkrämer, J., Determination of the size of defects by the ultrasonic impulse echo method 240
Krishnan, R. S., V. S. Venkatasubramanian and E. S. Rajagopal, Effect of sound intensity on dispersion and coagulation in ultrasonic emulsification 250

Landau, C. S., Some aspects of the rheology of milk gel 476
Langton, N. H., and D. Matthews, Permittivity of mixtures of zinc oxide and rubber 306
Lawrance, R., Cadmium sulphide photoconductive layers 298
Leck, J. H., *see under* Carter, G.
Lennon, J. J., *see under* Sexton, M. C.
Lewis, Isabel E., *see under* Hughes, J. W.
Lintin, D. R., and E. R. Wooding, Investigation of the ignition of a gas by an electric spark 159
Little, K., Investigation of Nylon "texture" by X-ray diffraction 225

Mandel, L., Image fluctuations in cascade intensifiers 233
Matthews, D., *see under* Langton, N. H.
Maude, A. D., Theoretical evaluation of capillary viscometers for the measurement of the viscosity of suspensions of spheres 371
Meltzer, B., Dense electron beams 391 (SA)
Millard, D. J., Relationship between strength and porosity for coal compacts 287
Milne, J. G. C., *see under* Davies, D. E.
Mirsepassi, T. J., Steady-state temperature distribution in solids undergoing certain change of property 538
Mitchell, E. W. J., *see under* Bastin, J. A.
Monfils, A., *see under* Herinckx, C.
Mulcahy, M. J., *see under* Sexton, M. C.
Murgai, M. P., and A. K. Ray, Some experimental results on the impact sensitivity of mercury fulminate 132

Náray, Zs., Application of delayed feedback in electronic circuits 400
Nash, W. F., *see under* Cousins, J. E.
Newcomb, T. P., Flow of heat in a composite solid 204
Transient temperatures attained in disk brakes 339
Nielsen, S., Reaction of indium solder with mercury telluride 380 (C)
Nielsen, S., *see under* Rennie, A. E.
Norbury, J., *see under* Booker, G. R.
Nutting, J., *see under* Brandon, D. G.

Oliver, D. R., and S. G. Ward, Studies of the viscosity and sedimentation of suspensions. Part 5.—The viscosity of settling suspensions of spherical particles 317
Onions, W. J., and B. Ellingham, Measurement of fibre diameter variation by optical diffraction 328
Osborne, D. G., and S. Thornton, Viscous properties of thixotropic materials 214
Owen, L. W., *see under* Scott, V. D.

Patla, N., *see under* Kiss, A. E.
Pike, E. R., and A. J. C. Wilson, Counter diffractometer—The theory of the use of centroids of diffraction profiles for high accuracy in the measurement of diffraction angles 57
Pope, M. I., and S. J. Gregg, Electrical conductivity of vitrain during carbonization 507
Popper, B., and M. Reiner, Centripetal air-pump operated electromagnetically 54 (C)
Power, G., Theorem concerning anisotropic dielectrics 32
Preston, J. S., Absolute measurement of light intensities 428 (C)
Price, P. H., Alternative method of correlating forced convection heat transfer data 135
Price, W. J., Spectrum display comparator 352
Priestley, E. F., New method for increasing the X-ray reflexion power of lithium fluoride crystals 141
Putner, T., Methods of cleaning glass by vapour degreasing and ultrasonically agitated solvents 332

Rajagopal, E. S., *see under* Krishnan, R. S.
Ratcliffe, E. H., Thermal conductivities of fused and crystalline quartz 22
Ray, A. K., *see under* Murgai, M. P.
Reichenbaum, G., Improved semiconductor-to-copper soldered contact 469 (C)
Reiner, M., *see under* Popper, B.
Rennie, A. E., and S. Nielsen, Controlling the habit of potassium cobalticyanide crystals 429 (C)
Revell, R. S. M., *see under* Franks, A.
Rhoderick, E. H., Superconducting computer elements 193 (SA)
Richard Wegener, H. A., Powder technique for the empirical determination of absorption corrections 406
Robertson, A. J. B., *see under* Bassett, D. W.
Rose-Innes, A. C., Refrigeration of a superconducting memory for a computer 452
Rowe, G. W., *see under* Golden, J.

Rydzewski, J. R., Experimental method of investigating stresses in buttress dams 465
Ryley, D. J., Experimental determination of the atomizing efficiency of a high-speed spinning disk atomizer 93
Analysis of a polydisperse aqueous spray from a high-speed spinning disk atomizer 180
Rymer, T. B., Summarized proceedings of a conference on solid state memory and switching devices—London, September 1958 153 (CR)

Scott Blair, G. W., and J. Burnett, On the creep, recovery, relaxation and elastic "memory" of some renneted milk gels 15
Distribution of relaxation times in a symmetrically stressed renneted milk gel 97
Scott, V. D., and L. W. Owen, Deposition by thermal evaporation of thin films of titanium and zirconium for tritium targets 91
Sen, D., *see under* Hariharan, P.
Sexton, M. C., J. J. Lennon and M. J. Mulcahy, Microwave method of investigating the afterglows of pulsed gaseous discharges 356
Siddall, G., and G. Smith, Preparation of metal film resistors on laminated plastics 35
Sisefsky, J., Method for photographic identification of microscopic radioactive particles 526
Smith, G., *see under* Siddall, G.
Snell, R. W., Radiofrequency method for the measurement of conductive liquid saturation in a porous medium 54 (C)
Sreekantath, G. M., On the use of coarse gratings in ultrasonics 191 (C)
Stanley, E., *see under* Hargreaves, A.
Stuart, Ian M., Amplitude corrections for vibroscope measurements 219
Stuart, R. D., Transient response of direct current amplifier systems 326
Sujak, B., The problem of exo-electron emission phenomena 102 (C)
Surplice, N. A., Reversible poisoning by sulphur, oxygen and other gases of oxide-coated cathodes at high temperatures 359

Thompson, J. E., Effect of crystallographic twins on the d.c. and a.c. properties of nickel-iron alloys 511
Thornton, S., *see under* Osborne, D. G.
Thumwood, R. F., Production of X-rays during a low-pressure gas discharge 147
Trodden, W. G., *see under* Jenkins, R. O.

Venkatasubramanian, V. S., *see under* Krishnan, R. S.
Vigoureux, P., Correction for size of cross-section of the secondary windings of mutual inductance standards of the Campbell type 481

Waldron, R. A., Electromagnetic fields in ferrite ellipsoids 20
Walsh, D., *see under* Gaskell, C. S.
Ward, S. G., *see under* Eveson, G. F.
Ward, S. G., *see under* Oliver, D. R.
Weintroub, S., *see under* Hurle, D. T. J.
Weston, G. F., Glow discharge characteristics of helium-neon mixtures 523
Wheeldon, J. W., Absorption of sodium and argon by glass 295
Whitehouse, J., *see under* Bastin, J. A.
Whitley, S., and C. Betts, Study of gas-lubricated, hydrodynamic, full journal bearings 455
Wilson, A. J. C., *see under* Hughes, J. W.
Wilson, A. J. C., *see under* Pike, E. R.
Wood, J. L., Dielectric properties of water/alumina 404
Wooding, E. R., *see under* Lintin, D. R.
Woods, J., Study of cadmium sulphide crystals grown from the vapour phase in a stream of argon 529

Yarwood, J., Summarized proceedings of a symposium on current developments in the production of high vacua—London, April 1959 383 (CR)

PRINTED IN GREAT BRITAIN BY UNWIN BROTHERS LIMITED, WOKING AND LONDON

SPECIAL ARTICLE

Solid and liquid state research with cold neutrons

By P. A. EGELSTAFF, B.Sc., Ph.D., United Kingdom Atomic Energy Authority*

The basic physical information which can be obtained from studies of the scattering of cold neutrons by matter is reviewed in this paper. The theoretical background is covered in a general way only, but the properties of the energy transfer processes and the information they yield concerning the thermal behaviour of matter are emphasized. Experimental work is discussed historically where appropriate and numerous recent experiments are mentioned (without considering any one in detail) to illustrate the many branches of these fields into which cold neutron research is moving. With the current improvements in experimental neutron fluxes and techniques, cold neutron methods will be used extensively during the next decade for solid and liquid state research.

1. INTRODUCTION

Cold neutron scattering experiments have become, over the past ten years, a new and powerful tool in the hands of the solid or liquid state physicist. By this means he is now in a position to measure many properties which have been hitherto inaccessible to direct experiment. For example, in the case of solids the spectrum of the normal modes of vibration of a crystal lattice and the scattering of phonons can be studied. While in the case of liquids the microscopic behaviour can be studied through a determination of the space-time correlation function.

Cold neutrons have two properties of particular value in this research. First their low energy means that in many cases the energy transferred in the interaction with the solid or liquid is equal to or greater than the initial neutron energy. And this in turn means that the important measurements of the energy transfer are relatively easy to make. Secondly, their long wavelength (3 to 10 Å) makes cold neutrons suitable for the study of long range effects, such as fluctuation phenomena, which is of particular interest near the critical point of a phase transition. Also neutrons of sufficiently long wavelength do not suffer Bragg reflection by crystals, and this property may be used both in the production of pure cold neutron beams of high intensity (see section 3) and for experiments where Bragg reflections might produce a large unwanted background.

These properties should be compared with those of shorter wavelength neutrons (~1 Å) and X-rays. Such radiation is most useful for crystal structure studies because many Bragg reflections can be seen with these wavelengths and also for pair-distribution studies of liquids. However, X-ray energies are many orders of magnitude greater than the energy transfer and therefore much of the work to be discussed here cannot be done with X-rays. On the other hand, the energy transfer in the scattering of (approx.) 1 Å neutrons can often be measured and yields information which is either similar or complementary to that obtained with cold neutrons. The distinction between the shorter and longer wavelength neutrons is one of experimental convenience only, and results obtained with 1 to 2 Å neutrons will be referred to in the course of the discussion.

The development of cold neutron research from a curiosity to a powerful tool has taken place during the past decade. This period has seen the foundation of the theory and techniques of the subject and experiments have been done which verify the basic ideas. Now a number of powerful neutron sources are coming into use which, with the period of development over, can be employed in large-scale research with this new tool. Thus the next few years should be a period of rapid growth in the knowledge of, particularly, the thermal behaviour of solids and liquids.

In sections 2 and 3 the theory and the techniques respectively will be reviewed. These sections serve as an introduction to the discussion of recent measurements of some properties of solids and liquids given in sections 4 to 7. For the full understanding of any physical phenomenon the combination of the results of many types of experiment is necessary, and the way in which cold neutron research can add new light to existing problems is illustrated by the work reviewed in those sections.

2. THEORY OF COLD NEUTRON INTERACTIONS

2.1 *General.* The type of interaction which a neutron may have with nuclei or with matter is governed by its velocity. The cold neutrons discussed here have velocities less than about 1200 m/s, which if the neutrons had a Maxwellian distribution would correspond to temperatures less than 100° absolute (−173° C).

On the other hand, the de Broglie wavelength of these neutrons is greater than 3 Å, which is somewhat greater than the average spacing between atoms in many solids and liquids. Consequently, although the well-known interference effects, giving rise to Bragg reflections for example, may be observed with cold neutrons very little cold neutron work involves the study of these effects. Rather the interaction of cold neutrons with thermal vibrations is the chief interest, and as might be expected this is the main interaction in many cases.

Cold neutrons interact with atomic nuclei in two ways. First they may be absorbed with the emission of γ-rays and secondly they may be elastically scattered (that is the quantum state of the nucleus is unchanged). If the magnitude of the first interaction greatly exceeds the second—as for ^{113}Cd—the scattering effects of interest here are very difficult to observe. Fortunately, in many cases the second process is of equal or greater magnitude than the first; in the following discussion the absorption will be ignored since its effect may be readily calculated and experimental results suitably corrected.

The scattering of cold neutrons by individual nuclei is isotropic since the neutron wavelength is many orders of magnitude greater than the size of a nucleus. But the scattering by an assembly of nuclei may be anisotropic and involve an exchange of energy with the internal motions of

* At present attached to Atomic Energy of Canada, Ltd., Chalk River, Ontario, Canada.

the assembly, since the neutrons can "see" the assembly as a whole.

Now the magnitude of the scattering of neutrons by nuclei is denoted by a scattering amplitude, a, which may be positive or negative depending on whether the scattered wave is 180° out of phase or is in phase with the incident wave. (This convention was adopted since the scattering by most nuclei involves a 180° phase shift.) The values of a for various nuclei cannot be calculated from nuclear theory and have to be determined experimentally. They vary in an irregular way throughout the periodic table, the largest is about 2×10^{-12} cm while the smallest is about -1×10^{-12} cm. The mean value is about $+0{\cdot}6 \times 10^{-12}$ cm.

Because of this spread in values of the scattering amplitude, the scattering by an assembly of nuclei of several isotopes exhibits both coherent and incoherent effects. However, incoherent effects are also observed in monisotopic specimens. This is because the neutron is a spin 1/2 particle and when it interacts with a non-zero spin nucleus two scattering amplitudes have to be considered, one for the neutrons and nuclear spins parallel and one for them antiparallel. The amount of scattering observed from each of these states depends on the product of the probability of forming that state and its scattering amplitude.

Hence it is convenient to discuss the scattering of cold neutrons in terms of two cross-sections, a coherent and an incoherent cross-section. These cross-sections cannot be observed as to magnitude in the same sense as the absorption cross-section can be, rather they are used as parameters in expressions which give the amount of coherent and incoherent scattering to be seen in any situation. They are defined for an element by the relations

$$\text{coherent cross-section } S = 4\pi(\sum_{n,m} p_{nm}a_{nm})^2 \tag{1}$$

$$\text{incoherent cross-section } s = 4\pi[\sum_{n,m} p_{nm}a_{nm}^2 - (\sum_{n,m} p_{nm}a_{nm})^2] \tag{2}$$

where p_{nm} is the abundance of the n^{th} isotope multiplied by the probability of forming the m^{th} spin state ($m = 1$ or 2) and a_{nm} is the scattering amplitude of the n^{th} isotope in the same spin state.

In addition to the above nuclear properties neutrons are scattered through the interaction of the magnetic moments of the neutron and atoms or molecules. In this case, the scattering is no longer isotropic because the size of the distribution of electrons around an atom is of the same order as the neutron wavelength. Thus a form factor similar to that for X-rays enters the cross-section formulae for magnetic scattering, but unlike the X-ray form factor it arises solely from the distribution of unpaired electrons. The magnitude of the magnetic scattering is of the same order as the nuclear scattering in many magnetic materials.

2.2 *Interaction with crystals.* The discussion of the previous section dealt with the general aspects of neutron scattering. In this section the relation between cold neutron scattering and the crystal lattice vibrations will be considered. The theory of this interaction has been covered in many papers notably those of Waller and Froman[1] and Placzek and Van Hove[2] (earlier work is quoted therein).

The energy quantum of an elastic wave in the crystal is represented by its frequency ω and its wave number q. One of the fundamental results to be obtained from the scattering experiments is the relation between ω and q (i.e. the dispersion law) and how this law depends upon the mode of vibration and the direction in which the wave is travelling. Another important factor is the frequency spectrum of lattice vibrations often approximated by the Debye frequency spectrum. It will be seen below how these two properties are obtained from the neutron scattering data.

It has been shown theoretically and confirmed experimentally that the scattering process involving the excitation or de-excitation of one phonon is the most important: in a typical case of a crystal at room temperature it may represent 90% of the scattering. Since this process contains the most easily analysible information the observations are usually corrected for multiphonon processes and then interpreted as the one phonon cross-section.

For scattering by a single crystal the conservation laws impose certain geometrical conditions upon the scattering. First the energy conservation law is

$$k^2 - k'^2 = \frac{2m}{\hbar}\omega \tag{3}$$

where k and k' are the wave numbers of the incident and scattered neutrons respectively, and m is the neutron mass. Secondly, when the neutron is scattered coherently interference between the scattered waves requires

$$k - k' = 2\pi\boldsymbol{\tau} - q \tag{4}$$

where $\boldsymbol{\tau}$ is any vector of the reciprocal lattice. Now all the quantities in equation (4) are proportional to momentum and therefore this equation represents the conservation of momentum; the left-hand side is the momentum lost (or gained) by the neutron and the right-hand side the momentum gained (or lost) by the crystal. The part $2\pi\boldsymbol{\tau}$ is taken up by the crystal as a whole and the part $\boldsymbol{q}$ by the wave involved.

It is usual in current experiments to keep $\boldsymbol{k}$ and $\boldsymbol{\tau}$ fixed by a suitable choice of experimental conditions as explained later. The direction of $\boldsymbol{k}'$ is also fixed and the intensity of the scattered neutrons as a function of the magnitude of $\boldsymbol{k}'$ is measured. Because, in general, there is a one to one correspondence between ω and q (and the polarization) equations (3) and (4) can be satisfied under these conditions for discrete values of k' only. Consequently the distribution of scattered intensity as a function of k' shows a number of well defined maxima whose positions give corresponding values of ω and q by application of equations (3) and (4). Fig. 1, an example of the scattering of cold neutrons by aluminium, illustrates this type of data.

For a perfect crystal in which the oscillation of the atoms about their mean position is harmonic the analysis of the vibrations yields unique values for the phonon energies. This means that the peaks in the experimental data of Fig. 1 should be of negligible width. However, crystals are not perfect and the vibrations not exactly harmonic consequently the phonon energies are not unique, so that the observed lines should have a finite width. This width is related to the mean free path of a phonon which in turn is related to several physical properties (e.g. thermal conductivity).

The intensity (integrated over both angular and energy variations) under each of the peaks of Fig. 1 is proportional to the frequency spectrum $g(\omega)$ of normal modes of vibration of the lattice. Thus from the variation of integrated intensity with ω, the frequency spectrum may be obtained after several complicated geometrical factors, the Boltzman and other factors have been taken out.

However, the frequency spectrum may be obtained in a much simpler manner if the incoherent scattering can be observed. In this case the energy conservation equation (3) holds, but equation (4) is invalid since it rests upon the

interference of the scattered waves, for incoherent scattering momentum conservation does not impose geometrical restrictions. It can be shown (Placzek and Van Hove[2]) that the energy spectrum of the incoherently scattered neutrons is proportional to $g(\omega)$, and thus after certain elementary factors are removed from the observed spectrum, $g(\omega)$ vs. ω is obtained directly.

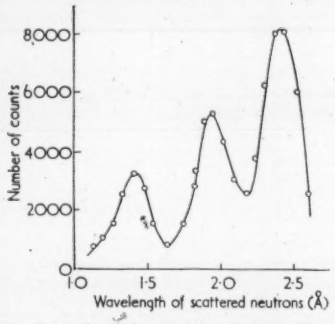

Fig. 1. Example of the neutron spectrum observed in the inelastic scattering of 4·5 Å neutrons by a single crystal of aluminium. (From Carter and his co-workers.[19])

Finally, consider the magnetic scattering. For ferro- or antiferro-magnetic crystals at low temperatures the thermal disordering is usually described in terms of excitations called "spin waves." The neutron scattering by spin waves is similar to the lattice vibration scattering discussed earlier, in particular, energy and momentum conservation equations analogous to (3) and (4) govern the geometrical conditions under which scattering may take place. Thus the dispersion law, frequency spectrum and mean free path of spin waves may in principle be obtained from the neutron scattering data. The theory of this scattering process has been given by Elliot and Lowde.[3]

At temperatures near the Curie point the spin wave theory is invalid and the neutron scattering has quite a different form. The main effect comes from the fluctuations in the regions of spin order, which lead to a type of critical scattering. The theory is given by Van Hove[4] and Elliot and Marshall.[5] Determinations of the size of the regions of spin order from the critical scattering will be discussed at section 6.

The cold neutron magnetic scattering by samples both at low temperatures and near the Curie point have been discussed in the papers cited above in relation to the Heisenberg or collective electron theories of magnetism. The limitations of these theories can be shown from a comparison of complete cold neutron scattering data with their predictions, and thus this work could lead to an improved theory of magnetism.

2.3 *Interaction with liquids.* Because of the complicated motions of the atoms or molecules composing a liquid a simple interpretation (such as that given for crystals) of the cold neutron inelastic scattering by liquids is not possible. Instead it is interpreted in terms of the "space time correlation function" $G(r, t)$. A particle is considered to be at the spacial origin at a given time, then $G(r, t)$ is the number density of particles at a distance r from the origin at time t later on. This function may be divided into two parts, one part $G_s(r, t)$ due to the motion of the original particle and the other part $G_d(r, t)$ due to the motion of all the other particles.

Van Hove[6] has shown that the coherent and incoherent scattering by a liquid are given in terms of these functions as

$$\text{coherent} - \frac{S}{4\pi} \cdot \frac{Nk'}{2\pi\hbar k} \cdot \int \exp\left[i(\boldsymbol{Q} \cdot \boldsymbol{r} - \omega t)\right] G(r, t) dr dt \quad (5)$$

$$\text{incoherent} - \frac{s}{4\pi} \cdot \frac{Nk'}{2\pi\hbar k} \cdot \int \exp\left[i(\boldsymbol{Q} \cdot \boldsymbol{r} - \omega t)\right] G_s(r, t) dr dt \quad (6)$$

where N is the number of particles in the liquid, $\boldsymbol{Q} = \boldsymbol{k} - \boldsymbol{k}'$ and $\hbar\omega$ is the energy transfered in the interaction. Thus $G(r, t)$ is obtained from a two dimensional Fourier transformation of the scattering data expressed as a function of energy and momentum transfer variables ω and $\boldsymbol{Q}$.

The quantity $G(r, t)$ can clearly tell us a great deal about the local behaviour of the particles in a liquid and physical properties on a microscopic scale. Unfortunately, its proper determination in any one case has not yet been carried out. Up to the present time the experimental work has had fairly limited objectives as will be described in section 7.

In some cases the neutron scattering by a liquid can be related directly to a macroscopic physical property. An example of this is the relationship between the isothermal compressibility and the scattering near the critical point of a liquid. It has been shown by Van Hove[6] that near the critical point the scattering is determined almost entirely by the instantaneous correlation function $G_d(r, o)$. This function is the familiar pair-distribution obtained from an analysis of X-ray or fast neutron scattering by liquids. Thus in this special case both cold neutrons and X-rays give the same diffraction pattern. The long range part of $G_d(r, o)$ gives the density fluctuations of the liquid and hence is related to the isothermal compressibility (χ_T). At very small angles of scattering the cross section is given by

$$\frac{S}{4\pi} \cdot NKT\chi_T \quad (7)$$

where N is the number of atoms per unit volume, and KT is the absolute temperature multiplied by Boltzman's constant.

The example given above has been familiar for a long time in X-ray scattering theory. However, because of the easily observable energy transfers in the scattering of cold neutrons, the relationships between the scattering of radiation and the usual physical properties are more important in the latter case. In particular the dependence of cold neutron scattering upon viscosity and diffusion coefficient are under study.

Liquid helium II is an unusual case of a liquid (in this case a quantum liquid) in its ground state. Consequently, the neutron scattering by liquid helium II is a special case and can be discussed without reference to the concepts of the previous paragraphs. Cohen and Feynmann[7] have shown that excitations in this liquid have long mean free paths at temperatures below 1° K, and that the possible interaction of a cold neutron with the liquid resulting in the creation of an excitation is governed by the laws of conservation of momentum and energy in just the same way as for the crystal [i.e. equations (3) and (4)]. For helium these laws are

$$k^2 - k'^2 = \frac{2m}{\hbar}\omega \quad (3a)$$

$$\boldsymbol{k} - \boldsymbol{k}' = \boldsymbol{q} \quad (4a)$$

The energy conservation equations (3) and (3*a*) are identical but the momentum conservation equations (4) and (4*a*) differ

by the momentum $2\pi\tau$ which is taken up by the crystal as a whole. For liquid helium the whole momentum transfer is equal to the momentum q of the excitation created.

The analysis of cold neutron scattering data using equations (3*a*) and (4*a*) has recently been employed to determine the important dispersion relationship for the excitations of liquid helium II.

3. SOURCES AND TECHNIQUES

Although some of the earliest cold neutron experiments were carried out using the cyclotron as a neutron source, reactor neutron sources are at present the only sources employed in this field. Nevertheless the reactor source is far from ideal because its neutrons are maintained at temperatures greater than room temperature. The most widely used method of obtaining cold neutrons is to place across a beam of reactor neutrons a filter which transmits only the very low energy part of the spectrum. Anderson, Fermi and Marshall[8] were the first to use this method. Subsequently the technique was developed by Egelstaff and Pease[9] who obtained beams of reasonable intensity containing less than 1% contamination by the main part of the reactor neutron spectrum. The cold neutron filters consist simply of blocks of polycrystalline material having a low absorption cross-section, and the neutrons passed by such filters are those whose wavelengths are too great for Bragg reflexion. In Fig. 2 an example of the filter technique is given. As can be seen from the figure the disadvantage of this technique lies in the broad wavelength spectrum transmitted.

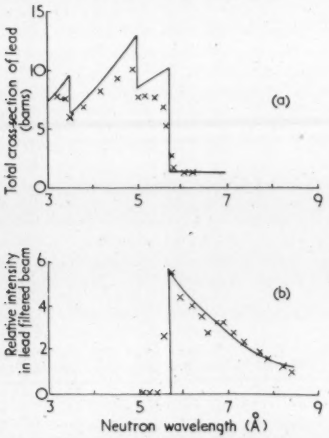

Fig. 2. Example of cold neutron filter technique; the solid lines are calculated values and the crosses represent experimental points (Egelstaff and Pease[9]). Figure (*a*) shows the large cross section for Bragg scattering in lead at wavelengths less than 5·7 Å, while figure (*b*) shows the type of neutron spectrum transmitted by a lead filter.

In many of the experiments carried out up to the present time the scattering of the whole spectrum of filtered neutrons is observed. For some measurements only the total cross-section of a sample or the number of neutrons scattered into a given angle are required. But in other cases (such as the crystal studies discussed in section 2.2) the spectral distribution of the scattered neutrons is required, and this is usually* obtained by the time-of-flight technique employing a device called a "chopper." The chopper is placed in the beam of scattered neutrons and its purpose is to "chop" the beam into short pulses. The neutron detector is placed several metres from the chopper and the distribution of the times-of-flight of the scattered neutrons from the chopper to detector is measured (see Fig. 5).

Fermi, Marshall and Marshall[10] built the first chopper for this range of neutron velocities, and subsequently there have been many developments of their device. One of the most recent is illustrated in Fig. 3, which shows a 10 in. diam.

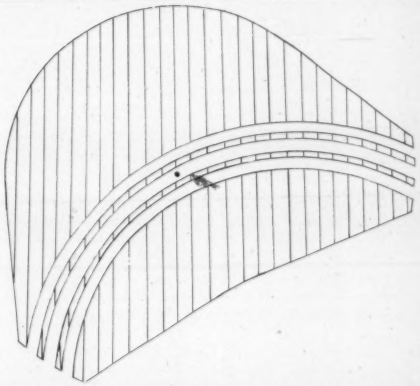

Fig. 3. A cross-sectional diagram of the new Harwell cold neutron chopper. The material is magnesium containing 10% cadmium, and this chopper has been tested at speeds up to 45 000 rev/min. (The dot indicates the centre of rotation.) The assymetrical plan form assists in the attainment of high rotational speeds, while the curved channels permit the passage of neutrons travelling within a limited velocity range only.

chopper made of Mg/Cd alloy. This chopper has $\frac{1}{4}$ in. wide channels, and can be spun at rotational speeds up to 45 000 rev/min. The effect of the curvature of the channels is to limit the width of the velocity band passed by the chopper: in contrast the channels of the type of chopper employed in the experimental arrangement of Fig. 5 are either straight or slightly curved so allowing a wide velocity band to be passed.

Returning to the point made at the commencement of this section, namely, that only a small fraction of the reactor neutron spectrum is passed by the cold neutron filter, recent work by Butterworth and his co-workers[11] has changed this situation. They employed a cell containing 200 c.c. of liquid hydrogen to moderate neutrons at the centre of a reactor to low energies. The beam of neutrons coming from this moderator is greatly enriched in cold neutrons—a factor of 30 at 10 Å wavelength.

With the greater intensity obtained with this type of cold

* Note, however, that crystal spectrometers were used for the experiments with 1 to 2 Å neutrons referred to in sections 4 to 7.

neutron moderator, especially when it is used with the high flux reactors now coming into use, multiple spectrometer arrangements can be employed in cold neutron experiments. A narrow band of wavelengths will be selected from the reactor cold neutron spectrum by means of the time-of-flight method or crystal reflexion techniques. This monokinetic beam will fall upon the sample, and the spectrum of the scattered neutrons will be measured with a second spectrometer (which again may be of the time-of-flight or crystal reflexion types).

The chopper of Fig. 3 both produces bursts of neutrons and by means of the curved slits defines their velocity. For example, at 36000 rev/min, 940 m/s (4·2 Å) neutrons are transmitted. Thus, if unlike the arrangement at Fig. 5, this chopper is placed in the filtered neutron beam it will act as the first section of a multiple spectrometer arrangement. The second section is then provided by an electronic system which measures the time-of-flight of the scattered neutrons.

Another multiple spectrometer technique recently developed by Brockhouse[12] is that of the rotating crystal. The beam of filtered neutrons falls on to a rotating crystal, suitably oriented in the plane of rotation, so that pulses of neutrons of a given wavelength are Bragg reflected. These pulses fall upon the sample under study and, as before, the distribution of times-of-flight of the scattered neutrons from sample to a detector is measured. This technique is likely to be of great value in the future.

Multiple spectrometer instruments are now being used in several laboratories, and will provide the data called for in the theoretical discussion of the previous section. The data which has been obtained to date will be reviewed in the remainder of this paper, and in the general sense it must be looked on as providing an introduction both to the application of these techniques and to the results which will shortly be obtained. (See, however, the recent work on germanium by Brockhouse and Iyengar.*)

4. EXPERIMENTS ON THE SCATTERING OF COLD NEUTRONS BY CRYSTALS

4.1 *General studies.* The first studies of the scattering of cold neutrons by phonons were of necessity rather crude. They consisted of measurements of the attenuation of cold neutrons by polycrystalline samples as a function of the temperature of the sample. The attenuation is related to the total scattering cross-section (i.e. the sum of the probabilities for scattering at all possible angles with all possible energy transfers). The earliest experiments of this kind were made by Cassels and Latham[13] and Cassels.[14]

These total cross-section measurements are similar to specific heat measurements in that the quantity studied contains a sum over all possible lattice vibrations. Thus for the theoretical calculation of the total cross-section the Debye approximation to the lattice vibration spectrum is employed and reasonable agreement with experiment is obtained. This is illustrated in Fig. 4, where the results and calculation of Squires[15] for polycrystalline magnesium are given. Exact agreement between theory and experiment cannot be expected always until the proper lattice dynamics is used. The same type of measurement was made subsequently by Palevsky and his co-workers[16] for a wider range of materials and with similar results.

The next step was to study the average energy transfers and the angular distribution of the neutrons scattered by polycrystals. Measurements of this sort were made by Egelstaff,[17] who determined the Debye temperature of the materials studied from such data. The results are given in Table 1 compared with the Debye temperatures determined from specific heat data; agreement between the two sets of data is good. Jacrot[18] has extended this type of work.

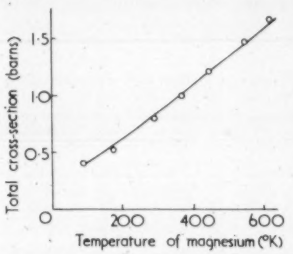

Fig. 4. The total cross-section of magnesium for 6·25 Å neutrons as a function of sample temperature The circles are experimental values and the solid line is a theoretical curve (after Squires[15])

Table 1. *Values of the Debye temperature of Be, Mg and Pb obtained from the scattering of* 20° *K neutrons*

Material (used at room temp.)	*Temperature of scattered neutrons (K)*	*Value of Debye temp. deduced from energy transfer (K)*	*Value of Debye temp. from specific heat measurements (K)*
Be	420 ± 50	930 ± 100	925
Mg	220 ± 50	350 ± 50	300
Pb	40 ± 4	65 ± 12	88

Up to this stage the neutron experiments had provided no new information about solids: rather the experiments served to verify that the theoretical ideas on the scattering process were satisfactory.

4.2 *Dispersion law for phonons in aluminium.* Since 1955 experiments have been carried out which have determined the dispersion law or the frequency spectrum for certain crystals, in the manner explained in section 2. The material most extensively studied is aluminium, for which three similar experiments have been carried out. (Carter and his co-workers,[19] Brockhouse and Stewart[20], Larsson.[21]) A typical experimental arrangement used in this work is shown in Fig. 5. The beam of neutrons from a reactor is filtered through berylium (see section 3) and most of those neutrons transmitted by the filter have wavelengths in the 4 to 6 Å range. The filtered beam falls on a single crystal of aluminium oriented in a pre-determined manner, and those neutrons which are scattered at an angle of 90° (chosen for experimental convenience) fall on the neutron chopper. Bursts of neutrons transmitted by the chopper are timed over a 3 to 6 m flight path between the chopper and a bank of neutron detectors. The sort of spectrum observed is shown in Fig. 1. The sharpness of the peaks in this spectrum is a good test of the reality of phonons (mean free path much greater than wavelength), and the relation between frequency and wavelength is determined immediately from the experimental geometry and the positions of the peaks in the observed spectra [as shown by equations (3) and (4)].

Combining the results of the several experiments the dispersion law for phonons travelling in the 100 direction is

* Shortly to be published in *The Physical Review.*

given in Fig. 6. Also presented is a theoretical curve and similar results obtained from X-ray scattering data. The agreement is seen to be fairly good. However, unlike the X-ray work the neutron experiments can yield similar information for directions of propagation which do not have a high degree of symmetry, and such results have also been obtained for aluminium.

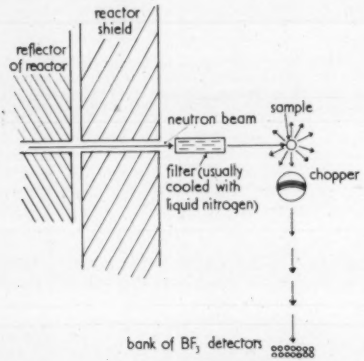

Fig. 5. Typical experimental arrangement used for the cold neutron scattering experiments described in section 4. Shielding around the filter, chopper and detector is not shown

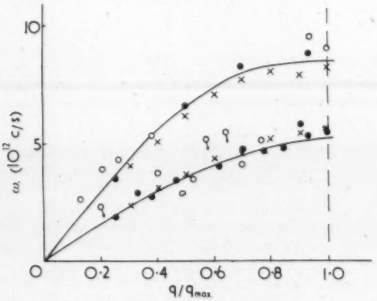

Fig. 6. The dispersion law for phonons travelling in the 100 direction in aluminium

——— calculation (Squires)[43]
○ cold neutron experimental data (Carter and co-workers)[19]
● cold neutron experimental data (Brockhouse and Stewart)[20]
× X-ray data (Walker)[45]

4.3 *Phonon frequency distribution for vanadium.* The frequency distribution (i.e. the numbers of modes at each value of ω) can be obtained in principle from the absolute intensity of the peaks of Fig. 1 and similar spectra. However, at present the difficulties inherent to this method have prevented its use. But as pointed out in section 2 there is an alternative method of obtaining the frequency distribution based on the inelastic scattering related to spin and isotope incoherence. For this study vanadium is the obvious choice since it is almost unique in having an incoherent cross-section which is 99% of the bound atom cross-section. The spectrum of neutrons scattered inelastically by vanadium thus shows no discrete peaks of the type seen in Fig. 1, but has the general shape of the frequency distribution.

Two experiments have been carried out on vanadium (Eisenhauer and his co-workers,[22] Stewart and Brockhouse[23]) and the results are shown in Fig. 7. It can be seen that the distribution is double-peaked and shows qualitatively the departures from the Debye frequency distribution which are expected theoretically. However, the experimental discrepancies require further investigation.

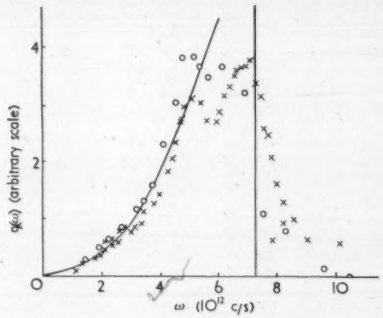

Fig. 7. The frequency distribution of the normal modes of vibration in vanadium

○ experimental values (Stewart and Brockhouse)[23]
× experimental values (Eisenhauer and co-workers)[22]
——— Debye spectrum for comparison

4.4 *Phonon mean free path.* As was stated above the absolute widths of the lines in the spectra of inelastically scattered neutrons are related to the mean free path of phonons. Since the experimentally observed widths (see Fig. 1) are usually equal to the revolution width of the instrument, the true width must be small confirming that the mean free path is long. Now the mean free path of phonons is determined by anharmonic forces between atoms, phonon-electron scattering, crystalline defects and similar factors. Often only one of these factors is of major importance in determining the mean free path in a given situation, and thus this factor can be studied alone.

The first experiment of this kind has been conducted by McCallum and Egelstaff[24] who measured the width of the scattered neutron lines corresponding to transverse phonons travelling near to the 111 direction in lead (at room temperature). The results showed a mean free path of 110 Å. This is of the order expected from phonon-phonon scattering, which is believed to be the main effect contributing to the mean free path in this case.

5. EFFECT OF LATTICE DEFECTS ON SCATTERING COLD NEUTRONS

If the de Broglie wavelength of a beam of cold neutrons is too great for Bragg reflection to take place in crystalline samples, and further the samples are cooled to a low temperature so that scattering by lattice vibrations is very small, then the cold neutrons will have a very small chance of suffering any interaction involving scattering (there will be,

in addition, the nuclear absorption discussed in section 2). Under these special conditions lattice defects caused by cold work, irradiation or similar factors, produce detectable amounts of neutron scattering—because the conditions for the complete cancellation of the scattered waves are not then satisfied. The amount of scattering can be related to the number of defects (assuming that the type of defect is known) and so provides a very powerful tool for the absolute determination of the concentration of defects.

Observations of scattering by dislocations in cold worked copper have been made by Lowde and Atkinson[25] who have determined dislocation densities of the order of $10^{11}/cm^3$. Irradiation damage in graphite has been studied by Antal, Weiss and Dienes,[26] and in silica by Mitchell and Wedepohl.[27] In both experiments the density of point defects measured was about $10^{21}/cm^3$.

6. EXPERIMENTAL STUDIES OF MAGNETIC SCATTERING

6.1 *Spin waves.* The magnetic scattering of neutrons of 1 to 2 Å wavelength has been employed frequently for studies of magnetic structures. However, the importance of the magnetic scattering of cold neutrons lies in the field of the thermal behaviour of magnetic materials rather than with their structures. At the end of section 2 the similarity between the phonon and spin wave scattering was noted. Again the relation between frequency and wave number of the waves, and their mean free path, can in principle be determined from the inelastic scattering, but cold neutron experiments of the type described in section 4 have not yet been attempted with magnetic materials. However, two inelastic scattering experiments have been done with shorter wavelength neutrons.

Lowde[28] studied the diffuse Laue reflections from a single crystal of iron and showed that magnetic inelastic scattering occurred and its magnitude was consistent with theory. Brockhouse[29] measured the spectrum of inelastically scattered neutrons when a magnetite crystal at room temperature was irradiated with 1·5 Å neutrons. Several crystal orientations were studied. Unfortunately, his results are not sufficiently precise to give the frequency wave number relationship properly, but they do confirm, in a direct manner, the existance of spin waves.

6.2 *Fluctuations of regions of spin order.* A large increase in the cold neutron total cross-section of iron near the Curie temperature has been noted by Palevsky and Hughes[30] and by Squires.[31] This effect has been interpreted by Van Hove[4] as a form of "critical scattering" due to the size fluctuations of the regions of magnetic order. [i.e. A phenomenon analogous to the scattering at the liquid-gas critical point discussed in section 2.3. The parameter K_1 introduced below plays the same role as X_T in equation (7)].

Near the Curie point and for small scattering angles, the the effect is predominantly elastic scattering. The cross-section for small scattering angles (θ)* and for temperatures slightly greater than the Curie temperature is given by Elliot and Marshall[5]

$$\left(\frac{e^2\gamma}{mc^2}\right)^2 \frac{f^2}{\hbar r_1^2(K_1^2 + \theta^2 k^2)} \qquad (8)$$

where f is the magnetic form factor, r_1 is a parameter which depends upon crystal structure and temperature and K_1 is the effective range of the correlation in the spin system (i.e. the size in the regions of order).

Several experiments (Gersh, Wilkinson and Shull,[32] Lowde,[33] Galula Jacrot and Mangin[34]) have been carried out in which the variation of the cross-section with θ or k [equation (8)] was measured for iron at various temperatures. From this variation the value of K_1 is deduced. A summary of these results is given in Fig. 8, compared with the Heisenberg theory for spin 1. The agreement is seen to be poor, and further experimental work is needed.

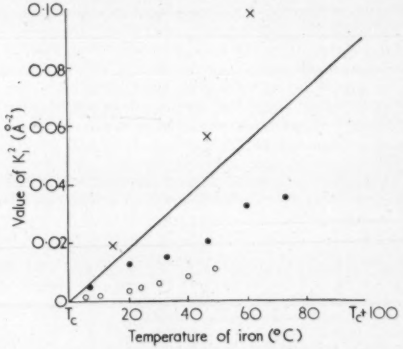

Fig. 8. The range K_1 of the correlation in the spin system for iron just above the Curie temperautre

× experimental values (Gersh and co-workers)[32]
• mean experimental values (Lowde)[33]
○ experimental values (Galula and co-workers)[34]
—— Heisenberg theory for spin 1, calculated by Elliot and Marshall[5]

7. COLD NEUTRON SCATTERING EXPERIMENTS WITH LIQUIDS

7.1 *Classical liquids.* The study of cold neutron scattering by liquids is one of the most recent branches of the subject to receive experimental attention. Consequently proper determinations of the space-time correlation function $G(r, t)$ have not been undertaken as yet. Rather the type of experiments carried out have been aimed at understanding the general features of liquid scattering, for example the experiments of Squires,[35] Egelstaff[36] and Brockhouse.[37]

Egelstaff compared the inelastic scattering of 14° K neutrons from solid and liquid lead. Measurements were made of the average energy transferred in the scattering process, and the results are summarized at Table 2.

Table 2. *Average energy transferred in the scattering of 14° K neutrons by solid and liquid lead*

Sample temperature °K	*State*	*Average energy transfer— K*
293		55 ± 14
430	Solid	65 ± 8
590		60 ± 6
620		60 ± 6
685	Liquid	50 ± 6
775		50 ± 10

The independence of the energy transfer upon either the state or temperature of the sample confirms the similarity of

* For the case being considered scattering angle means a deviation from a Bragg reflection position. Cold neutrons suffer critical scattering about the 000 (forward) direction and give the most favourable conditions for studying this effect.

interatomic energies for solid and liquid lead near the melting point, frequently deduced (e.g. Frenkel[38]) from the near continuity of specific heat and similar properties at the melting point.

A more elaborate set of measurements was carried out by Brockhouse[37] on light and heavy water, with the aim of understanding the basic features of liquid scattering. His measurements covered a wide range of incident neutron energies and angles of scatter, and in most cases the spectrum of the scattered neutrons was obtained. An example of this work is given in Fig. 9 which shows the spectra of scattered neutrons obtained from the bombardment of a sample of H_2O with 1·62 Å neutrons. The solid curves indicate the instrumental resolution function.

It can be seen that the spectra consist of an apparently elastic peak superimposed on a broad inelastic component. Brockhouse[37] has shown that the latter component may be represented quite well as the scattering by a gas of particles of mass 18. In this respect the water molecules are behaving as free particles. Further the apparent elastic peak is ascribed to the fact that each molecule occupies the same point in space for a short period; then the width of the peak will be related to the rate of diffusion of the molecule. The variation of the width of this peak with sample temperature (seen in Fig. 9), is

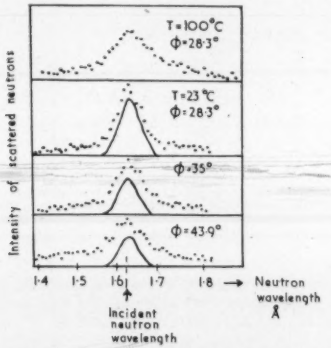

Fig. 9. The neutron spectra obtained from the scattering of 1·62 Å neutrons by H_2O at various angles (ϕ) and temperatures (T) (Brockhouse[37])

very similar to the variation of the diffusion coefficient of water with temperature. Similar measurements on H_2O at other incident neutron energies may be interpreted in the same way.

The work described above has confirmed that the scattering of cold neutrons by liquids could be a useful tool for the study of the problem of liquid dynamics. However, proper measurements of the space-time correlation functions and their interpretation are needed before the potential of the technique is realized, and such measurements are now in hand at several laboratories.

7.2 *Dispersion law for excitations in liquid helium II.* The main interest in liquid helium centres on the fact that it is a quantum liquid and exhibits unusual properties at temperatures below 2·2° K. The understanding of the properties has concerned physicists since 1911, and various theories had suggested that many of them could be explained in terms of the disperion law for excitations in liquid helium II. Consequently the direct determination of this law by cold neutron

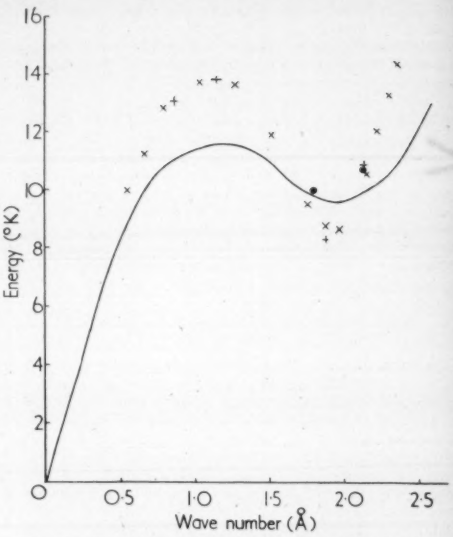

Fig. 10. Experimental values for the dispersion law for excitations in liquid helium II

× points deduced from cold neutron experiments (Yarnell and co-workers)[41]

+ points deduced from cold neutron experiments (Henshaw)[40]

• points deduced from cold neutron experiments (Palevsky and co-workers)[39]

—— theory predicted by Landau[44]

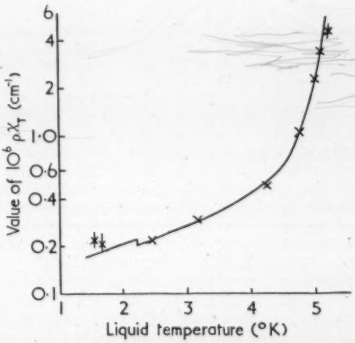

Fig. 11. The isothermal compressibility of liquid helium I (for convenience the product of density (ρ) and compressibility is plotted)

× values obtained from cold neutron scattering measurements (Egelstaff and London).[42] The vertical bar indicates the size of the experimental error on the extreme points; on the other points the error is smaller than the cross.

—— mean values obtained from compressibility experiments.

scattering experiments is of great importance to these theories.

Three experiments (Palevsky and his co-workers,[39] Henshaw,[40] Yarnell and his co-workers[41]) employing the principles discussed in relation to equations (3*a*) and (4*a*), have been carried out and the results are summarized in Fig. 10. The experiments are in good agreement, and the curve through the points has the shape required by theory to explain the unusual properties of liquid helium II. More detailed measurements by these workers are in progress, but there is no doubt that the data of Fig. 10 represents one of the major triumphs for this new tool. The accurate determination of the dispersion law will be a major factor in the quantitative solution of the problem of liquid helium II.

7.3 *Isothermal compressibility of liquid helium.* At temperatures above 2·2° K liquid helium behaves in a fashion similar to that of a classical liquid. The small angle scattering technique (discussed earlier) to measure the isothermal compressibility for liquid helium I was employed by Egelstaff and London.[42] Their results are shown in Fig. 11 compared with those deduced from measurements of density as a function of pressure and temperature. The excellent agreement verifies the usefulness of this technique.

8. CONCLUSIONS

Many fields of solid and liquid state research have been touched on briefly in this review, but in each cold neutron techniques are making an important contribution now or will do so in the near future. In some cases, as with liquid helium, this contribution is a major one, and in others, such as the study of defects in solids, its value lies in the greater accuracy and reliability achieved compared with conventional methods.

Even though these techniques are not as yet employed widely it has been impossible to review all the research properly, but enough has been said to show the manner in which the technique is used and the type of information which can be obtained. It is clear that many years of fruitful study in the solid and liquid state fields lie ahead for neutron techniques in general and cold neutrons in particular.

With the initial application of a new technique a flood of new knowledge, hitherto unobtainable, is rapidly released but then the technique takes its place in a complementary fashion to well used ones. Cold neutron techniques will be no exception to this rule.

9. REFERENCES

(1) WALLER, I., and FROMAN, P. O. *Ark. Fys.*, **4**, p. 183 (1952).

(2) PLACZEK, G., and VAN HOVE, L. *Phys. Rev.*, **93**, p. 1207 (1954).

(3) ELLIOT, R. J., and LOWDE, R. D. *Proc. Roy. Soc. A*, **230** p. 73 (1955).

(4) VAN HOVE, L. *Phys. Rev.*, **93**, p. 268 (1954).

(5) ELLIOT, R. J., and MARSHALL, W. *Rev. mod. Phys.*, **30**, p. 75 (1958).

(6) VAN HOVE, L. *Phys. Rev.*, **95**, p. 249 (1954).

(7) COHEN, M., and FEYNMANN, R. P. *Phys. Rev.*, **107**, p. 13 (1957).

(8) ANDERSON, H. L., FERMI, E., MARSHALL, L. *Phys. Rev.*, **70**, p. 815 (1946).

(9) EGELSTAFF, P. A., and PEASE, R. S. *J. Sci. Instrum.*, **31**, p. 207 (1954).

(10) FERMI, E., MARSHALL, L., and MARSHALL, J. *Phys. Rev.*, **72**, p. 193 (1947).

(11) BUTTERWORTH, I., EGELSTAFF, P. A., LONDON, H., and WEBB, J. *Phil. Mag.*, **2–19**, p. 917 (1957).

(12) BROCKHOUSE, B. N., *Bull. Amer. Phys. Soc.*, 111, **3**, p. 233 (1958).

(13) CASSELS, J. M., and LATHAM, R. *Phys. Rev.*, **74**, p. 103 (1948).

(14) CASSELS, J. M. *Proc. Roy. Soc. A*, **208**, p. 527 (1951).

(15) SQUIRES, G. L. *Proc. Roy. Soc. A*, **212**, p. 192 (1952).

(16) PALEVSKY, H., ZIMMERMAN, R. L., and HUGHES, D. J. *Phys. Rev.*, **99**, p. 611 (1955).

(17) EGELSTAFF, P. A. *Nature* [*London*], **168**, p. 290 (1951), and

(18) JACROT, B. *Comptes Rendus* (*Paris*), **240**, p. 745 (1955).

(19) CARTER, R. S., HUGHES, D. J., and PALEVSKY, H. *Phys. Rev.*, **106**, p. 1168 (1957).

(20) BROCKHOUSE, B. N., and STEWART, A. T. *Rev. mod. Phys.*, **30**, p. 236 (1958).

(21) LARSSON, K. E. Proc. of meeting on use of slow neutrons to investigate solid state (Stockholm: Swedish Atomic Energy Company, 1958).

(22) EISENHAUER, C. M., PELAH, I., HUGHES, D. J., and PALEVSKY, H. *Phys. Rev.*, **109**, p. 1046 (1958).

(23) STEWART, A. T., and BROCKHOUSE, B. N. *Rev. mod. Phys.*, **30**, p. 250 (1958).

(24) MCCALLUM, G., and EGELSTAFF, P. A., *Nature* [*London*], **181**, 643 (1958).

(25) LOWDE, R. D., and ATKINSON, H. H. *Acta Cryst.*, **10**, p. 824 (1957).

(26) ANTAL, J. S., WEISS, R. J., and DIENES, J. J. *Phys. Rev.*, **99**, p. 1081 (1955).

(27) MITCHELL, W., and WEDEPOHL, P. Private communication (1957).

(28) LOWDE, R. D. *Proc. Roy. Soc. A*, **235**, p. 305 (1956).

(29) BROCKHOUSE, B. N. *Phys. Rev.*, **106**, p. 859 (1957).

(30) PALEVSKY, H., and HUGHES, D. J. *Phys. Rev.*, **92**, p. 202 (1953).

(31) SQUIRES, G. L. *Proc. Phys. Soc.* (*London*) *A*, **67**, p. 248 (1954).

(32) WILKINSON, M. K., and SHULL, C. G. *Phys. Rev.*, **103**, p. 516 (1956)

GERSH, H. A., SHULL, C. G., and WILKINSON, M. K. *Phys. Rev.*, **103**, p. 525 (1956).

(33) LOWDE, R. D. *Rev. mod. Phys.*, **30**, 69 (1958).

(34) GALULA, M., JACROT, B., and MANGIN, J. P. Proc. of meeting on use of slow neutrons to investigate solid state (Stockholm: Swedish Atomic Energy Company, 1958).

(35) SQUIRES, G. L. *Acta Cryst.*, **7**, p. 673 (1954).

(36) EGELSTAFF, P. A. *Acta Cryst.*, **7**, p. 674 (1954).

(37) BROCKHOUSE, B. N. *Phys. Rev.*, **98**, p. 1171 (1955), and *Acta Cryst.*, **10**, p. 827 (1957).

(38) FRENKEL, J. *Kinetic Theory of Liquids* (London: Oxford University Press, 1946).

(39) PALEVSKY, H., OTNES, K., LARSSON, K. E., PAULI, R., STEDMAN, R. *Phys. Rev.*, **108**, p. 1346 (1957).

(40) HENSHAW, D. G. *Phys. Rev.* To be published (1958).

(41) YARNELL, J. L., ARNOLD, G. P., BENDT, P. J., and KERR, E. C. *Phys. Rev.* To be published (1958).

(42) EGELSTAFF, P. A., and LONDON, H. *Proc. Roy. Soc. A*, **242**, p. 374 (1957).

(43) SQUIRES, G. L. *Phys. Rev.*, **103**, p. 304 (1956).

(44) LANDAU, L. *J. Phys.* (*U.S.S.R.*), **5**, p. 7 (1941); **11**, p. 91 (1947).

(45) WALKER, C. B. *Phys. Rev.*, **103**, p. 597 (1956).

Evaporation of thorium from carburized thoriated tungsten cathodes*

By R. O. Jenkins, A.R.C.S., Ph.D., F.Inst.P., and W. G. Trodden, B.Sc., The Research Laboratories of The General Electric Co. Ltd., Wembley, England

[*Paper received* 13 *June*, 1958]

The evaporation of thorium from carburized thoriated tungsten cathodes is shown experimentally to be approximately the same as that from similar uncarburized cathodes at the same temperature. The thorium in a carburized cathode is, however, produced continuously at an adequate rate at the operating temperature of 2000° K by reduction of the thoria by the tungsten carbide. The uncarburized cathode operates on a reserve of thorium built up by flashing at 2800° K at which temperature the tungsten reduces some of the thoria. These reactions have been examined by thermochemistry and it is shown that thorium diffuses to the surface of both types of cathode by a mechanism relatively insensitive to temperature.

The thoriated tungsten cathode has increased in importance in recent years having largely replaced pure tungsten in high-power transmitting valves. This has become possible as a result of better vacuum techniques and the use of zirconium as a getter. Prior to this it was found that the monolayer of thorium activating the cathode surface would be removed by ion bombardment or poisoned by gas under the very onerous conditions met in such valves. The original thoriated tungsten cathode studied by Langmuir[1] consisted of tungsten containing about 1% thoria (ThO_2) and was activated by a high-temperature flash at about 2800° K, followed by a period at about 2200° K before operating at 2000° K. Extensive studies of this cathode indicated that thorium was formed during the high-temperature flash. It subsequently diffused to the surface mainly along grain boundaries,[2] during the activating period and migrated over the surface, covering it with a monatomic layer which had a lower work function than clean tungsten.

These cathodes were very susceptible to poisoning, and it was subsequently found that by carburizing the surface layer a cathode was obtained with similar thermionic properties, but which was less sensitive to poisoning. Activation of such carburized cathodes was also possible at the normal operating temperature of 2000° K. The carburizing process consisted of turning the surface layer of the tungsten wire to tungsten carbide (W_2C) by heating it in an atmosphere containing a hydrocarbon vapour till a depth of carbide corresponding to about 10% of the radius was formed. The immediate surface layer was often subsequently decarburized before use by heating in hydrogen.

Most of the fundamental work on thoriated tungsten cathodes was carried out on the original tungsten type. A paper by Andrews,[3] however, showed that the rate of evaporation of thorium, from a layer of thorium deposited from an external source on to the tungsten carbide surface, was only about a sixth of that from a similar layer on a pure tungsten surface. This experiment has been subsequently misinterpreted as indicating that the rate of evaporation of thorium from an operating cathode is lower if the cathode is of the carburized type,[4] and this misinterpretation has been largely accepted as true. In fact, direct measurements of the thorium evaporated from similar cathodes in the carburized and uncarburized state do not appear to have been published, and the experiments described in this paper have therefore been carried out.

The rate of evaporation of thorium throws some light on processes taking place in the cathode and is also of practical importance in that the evaporated thorium causes unwanted thermionic emission (grid emission) from other electrodes in a valve.

THE EXPERIMENTAL METHOD

The filaments examined contained 0·7% of thorium oxide in a wire of diameter 0·3 mm. They were in the form of helices of length 15 mm having twenty turns of outside diameter 1 mm. These filaments have a fibrous structure initially, but recrystallize at about 2000° K giving approximately equi-axed crystals about 10 μ in size.

The carburized filaments were prepared by operating at a temperature of 2300° K in an atmosphere made by bubbling a 90% nitrogen, 10% hydrogen mixture through xylene, until the resistance at this temperature had increased by 9% of its initial value. Then the temperature was maintained at 2300° K in an atmosphere of the nitrogen and hydrogen mixture until the resistance had fallen to 7% above its initial value at 2300° K. This resulted in the filament having an inner tungsten carbide (W_2C) layer of thickness about 10% of the wire radius, and a thin outer sheath of pure tungsten.

In one filament decarburizing of the outer layer was not carried out, to see if this affected the rate of evaporation of thorium, in view of the fact that some users omit the decarburizing process.

The experimental valves shown in Fig. 1 had a 0·1 mm diameter pure tungsten receptor wire mounted parallel to the axis of the thoriated tungsten filament. The distance of the axis of the coil to the filament was varied from valve to valve in a range of 1–5·5 mm. Situated behind the wire, so that it did not interrupt the stream of evaporating thorium between the filament and the wire, was a molybdenum plate 0·2 mm thick. This was used as the anode when measuring thermionic emission from the filament or from the wire. A barium getter was mounted adjacent to the lead glass foot tube, and the valves also had lead glass envelopes. Initial processing was as follows. The valves were evacuated on a mercury diffusion pump with liquid air trap, and were subsequently baked for one hour at 400° C. The molybdenum plate was thoroughly outgassed by eddy-current heating, and the tungsten wire outgassed by flashing for a few seconds at

* G.E.C. communication No. 799.

a temperature of 2600° K. In the valves with uncarburized filaments the filament was flashed at the usual 2800° K for three minutes to produce some free thorium necessary for activation. In the valves with carburized filaments the filament was run at 2200° K for fifteen minutes. The getter was outgassed by eddy-current heating, and some barium evaporated into the base of the bulb, before sealing off from the pump. The temperatures of both the thoriated tungsten coil and the receptor wire were calibrated in terms of heating current using a disappearing filament optical pyrometer, and a correction was made for absorption in the glass bulb. True temperature was obtained from the corrected brightness temperature assuming that the spectral emissivity of the surface was that of tungsten. In both types of cathode, activation was then carried out for about an hour at a temperature of 2100° K, until the thermionic emission had stabilized, the emission during this time being observed at intervals. The saturated emission was measured at 1500° K during the subsequent evaporation experiments.

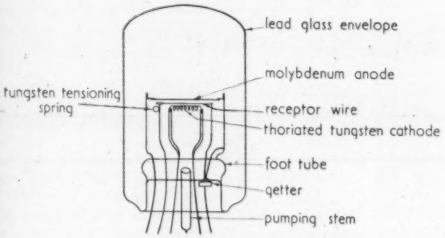

Fig. 1. Experimental measurement tube

Evaporation rates for both types of thoriated cathode were determined at temperatures 2000, 2100 and 2200° K. The method was to evaporate thorium from the cathode on to the tungsten receptor wire, measuring the thermionic emission from the wire at a fixed temperature of about 1200° K at intervals. The thermionic emission measured in this way goes through a maximum value, which occurs when one monolayer has been deposited on the wire.[5] This is related to the number of monolayers evaporated from the thoriated filament by a factor depending on the geometry of the valve. This factor, the ratio of the number of monolayers evaporated by the cathode to that received by the filament, was evaluated approximately as follows. The cathode was considered as a helix of tape, the width of which was equal to the wire diameter, wound on a cylinder of radius 0·35 mm (the radius of the coil at the wire centre) and evaporating uniformly in a radial direction. A complete cylinder would result in a ratio of $d/0{\cdot}35$ where d is the distance in millimetres between the axis and the receptor wire. A further factor corresponding to the ratio of the area of the cylinder and the area of the tape must also be included. With a wire diameter of 0·3 mm and a pitch of 0·75 mm this factor is $0{\cdot}75/0{\cdot}6$. Hence the required correction factor is the product of these two ratios which is $3{\cdot}57d$.

THE EXPERIMENTAL RESULTS

The curves of rise in thermionic emission from the receptor wire as a function of the time of exposure of the wire to the stream of evaporant were similar to that shown by Brattain and Becker,[5] which was obtained by evaporating thorium on to a tungsten ribbon. In the authors' experiments it was found that the uncarburized cathodes became partially deactivated during determinations of the evaporation rates at 2100 and 2200° K. As it was desirable to measure the rates of evaporation with the cathode fully activated initially, the cathode was flashed at 2800° K and activated at 2100° K before each determination of evaporation rate. With the carburized cathodes no appreciable deactivation occurred during a determination of evaporation rate at any of the temperatures studied. The evaporation rates for the uncarburized and the carburized cathodes are given as a function of $10^4/T$ in Figs. 2 and 3 respectively. Fig. 2 is based on

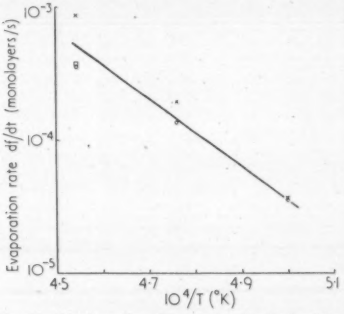

Fig. 2. Evaporation from uncarburized cathodes
× = valve *a*. □ = valve *b*. ○ = valve *c*.

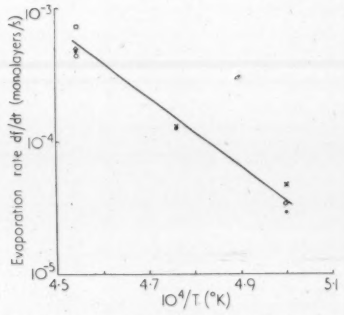

Fig. 3. Evaporation from carburized cathodes
× = valve *e*. ● = valve *g*. □ = valve *d*. △ = valve *f*. ○ = valve *h*.

results from three valves, *a*, *b* and *c*. The correction factors for these were respectively 12·5, 3·6 and 6·5. For Fig. 3 five valves were used, *d*, *e*, *f*, *g* and *h*. The appropriate correction factors were 19·7, 14·3, 4·3, 3·6 and 5·4. The differences in evaporation rate at a given temperature from valve to valve could be due to small errors in cathode temperature. The greatest differences are at 2200° K with the uncarburized cathodes. Here the greatest departure of an experimental point from the line drawn corresponds to an error in temperature of about 50° K.

Another possible reason for the differences in evaporation rates, particularly at the higher temperatures, is that the

receptor wire might have become sufficiently hot, by radiation from the cathode, to give appreciable migration or incomplete adsorption of the evaporant. This would be more serious in the valves with small spacing. In such a valve the resistance of the receptor wire was measured with the cathode cold and at 2200° K. On the assumption that the heating of the wire took place over a length of 1 cm at its centre, the temperature at the centre of the receptor wire when the cathode was at 2200° K was estimated to be about 1130° K in a valve in which d was 1 mm. The receptor wire in a valve with a larger spacing was then operated at 1130° K by heating it electrically. It was found that there was no significant difference in the rate of thorium evaporation observed with or without the extra heating. Such a result is in line with an observation by Brattain and Becker[5] that the shape of the activation curve of their tungsten ribbon was the same whether the ribbon was heated continuously at 1274° K, or heated at this temperature only while measuring the ribbon activity.

The observed rates of evaporation may be represented by equations of the form

$$\log (df/dt) = A - (b/T) \qquad (1)$$

where df/dt is the evaporation rate in monolayers per second and A and b are constants. In this paper a monolayer ($f = 1$) is considered to be 5×10^{14} atoms/cm^2 which, from the work of Brattain and Becker[5] and Langmuir,[6] gives the optimum thermionic emission.

The experimental values for the uncarburized cathodes shown in Fig. 2 may be represented by the equation

$$\log_{10} (df/dt) = 8{\cdot}30 - 2{\cdot}55\,(10^4/T) \qquad (2)$$

Those for the carburized cathodes shown in Fig. 3 may be represented by the equation

$$\log_{10} (df/dt) = 8{\cdot}56 - 2{\cdot}60\,(10^4/T) \qquad (3)$$

There was no significant difference between the rates of evaporation from the cathode which had not been decarburized and the rates at corresponding temperatures from cathodes which had been decarburized.

During determinations of the evaporation rates at 2100 and at 2200° K from uncarburized cathodes, the thermionic emission of the cathode decayed. Fig. 4 shows typical curves of the thermionic emission measured at 1500° K as a function of the total amount of thorium evaporated. At 2000° K there was no decay in thermionic emission during a determination of evaporation rate. For comparison, a curve for the emission from the carburized type of cathode at 2200° K is also shown; this emission shows no deterioration, in contrast to that of the uncarburized cathode.

Repeated evaporation runs were made with both types of cathode at 2200° K and the results are shown in Fig. 5. It may be seen that the supply of thorium in the uncarburized cathode is depleted exponentially while that of the carburized cathode is well maintained.

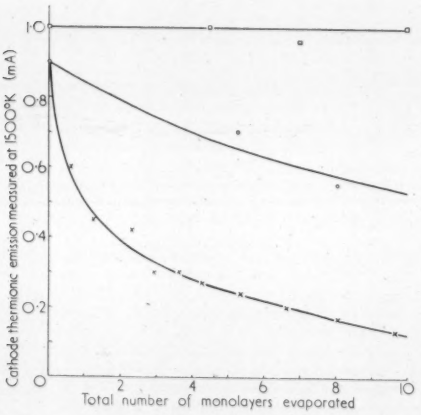

Fig. 4. Decay of thermionic emission of cathodes operated at 2200 and at 2100° K

× = 2200° K, uncarburized cathode. ○ = 2100° K, uncarburized cathode. □ = 2200° K, carburized cathode.

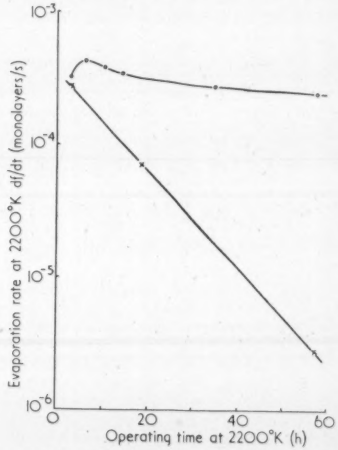

Fig. 5. Rate of evaporation at 2200° K for carburized and uncarburized cathodes with time

× = uncarburized cathode (curve 1).
○ = carburized cathode (curve 2).

DISCUSSION

Comparison with previous data. The experimental results can be compared with those of previous workers and also considered thermochemically. Direct comparison with the previously observed evaporation rates can only be made for the uncarburized cathode. In making comparisons, misinterpretation of the data must be avoided by considering the various mechanisms involved. The rate of evaporation from a particular area of the cathode surface depends on its temperature and on the coverage by thorium, and much of the published work has been concerned with this dependence. During the operation of a cathode, however, when once equilibrium is reached, the rate of evaporation of thorium is the rate at which it reaches the surface. If this latter rate is less than that from a monolayer, the surface will be only partially covered. If, however, the rate is greater, most of the surface will be covered by a monolayer, with local patches having greater than monolayer coverage adjacent to points

where the rate of arrival of thorium to the surface is greatest. The evaporation from these points is considerably greater than from the monolayer.

Brattain and Becker[5] show curves of the rate of evaporation of thorium at 2200° K plotted against f, the coverage in fractions of a monolayer. From the initial decay of emission observed at 2200° K from the present authors' uncarburized cathodes, the coverage, using Brattain and Becker's emission results, is about 0·6 at that temperature. From their results the corresponding evaporation rate df/dt should be 10^{-3} monolayers/s, which is in fairly good agreement with the authors' figure of $0{\cdot}5 \times 10^{-3}$ monolayers/s. Brattain and Becker's results were comparable with those of Langmuir[1] but higher than those of Andrews.[3]

Values of the rate of arrival of thorium to the cathode surface are given by Smithells[7] for various temperatures and should be directly comparable with the present authors' figures. In fact they show the same variation with temperature and differ in magnitude by a factor of only about 1·2.

A point worth discussing is the comparative behaviour of emission from the two types of cathode at 2200° K. It is clear from the curves of Fig. 4 that a monolayer coverage is maintained on the carburized cathode but not on the uncarburized type, in spite of the fact that the rates of supply of thorium to their surfaces are not very different. This would be expected for the cathode with the carburized surface, as Andrews's[3] results indicated that thorium is more strongly adsorbed on tungsten carbide than on tungsten. For the cathodes with decarburized surfaces an alternative explanation must be sought. It seems probable that the carburizing and decarburizing processes break up the surface layer and thus give more grain boundaries along which diffusion takes place. Surface migration distances to maintain a uniform coverage are thus less for this type of cathode and it is possible for a much more uniform coverage to be maintained. A possible alternative is that the physical nature of the surface on an atomic scale has been altered and more sites for strong adsorption are available.

Formation of thorium in the uncarburized cathode. The formation of free thorium within the cathode may be considered thermochemically. Langmuir's[1] results for the uncarburized cathode showed that thorium could be produced by heating at 2800° K, and that the thorium so formed would subsequently diffuse to the surface and activate it thermionically. He showed that the rate at which thorium was produced at the activating temperature of 2150° K and the operating temperature of 2000° K was quite inadequate to form the activating monolayer on the surface. An approximate estimate of the maximum possible rate of production of thorium by various reactions can be made using thermochemical data. The Gibbs–Helmholz free energy equation may be applied to evaluate the equilibrium pressures of gaseous reaction products. This equation may be written in the form

$$\log_{10}(p) = \frac{0{\cdot}2185}{n}\left(-\frac{\Delta H}{T} + \Delta S\right) + 2{\cdot}88 \qquad (4)$$

where n is the number of gaseous molecules in the reaction product
ΔH is the change in enthalpy (cal)
ΔS is the change in entropy (cal/°K)
T is the absolute temperature (°K), and
p is the required equilibrium reaction pressure (mm of mercury).

In the case of the present reactions, the thoria occupies only about 1% of the total volume and the approximate maximum rate of evaporation of the gaseous products, assuming their free removal can be calculated from the relationship

$$m = \frac{1{\cdot}36 \times 981}{100}\sqrt{\left(\frac{M}{2\pi RT}\right)}p \qquad (5)$$

where m is in g cm^{-2} s^{-1}
M is molecular weight
R is the gas constant.

If the appropriate values for thorium are used together with the value of 5×10^{14} atoms/cm^2 for a monolayer ($f = 1$), the maximum evaporation rate possible from a reaction is

$$\log_{10}(df/dt) = \log_{10} p + 4{\cdot}56 - \tfrac{1}{2}\log_{10}(T) \qquad (6)$$

The following reactions may now be considered and their maximum rates of thorium production estimated. All the products on the right-hand side may be considered gaseous at the cathode temperature.

$$ThO_2 + \frac{2}{3}W \rightleftarrows Th + \frac{2}{3}WO_3 \qquad (7)$$

$$ThO_2 + W \rightleftarrows Th + WO_2 \qquad (8)$$

$$ThO_2 \rightleftarrows Th + O_2 \qquad (9)$$

$$ThO_2 \rightleftarrows Th + O + O \qquad (10)$$

When evaluating ΔH and ΔS, the contribution of the specific heat has been neglected as it is relatively small. The values of enthalpy and entropy are derived mainly from data tabulated by Kubaschewski and Evans[8] and are shown in the Appendix. Applying this data to the reaction equations (7), (8), (9) and (10) the following values are obtained for $\log_{10} p$.

Reaction (7) $\log_{10} p = 12{\cdot}32 - 4{\cdot}86\,(10^4/T)$ (11)

Reaction (8) $\log_{10} p = 13{\cdot}37 - 4{\cdot}49\,(10^4/T)$ (12)

Reaction (9) $\log_{10} p = 10{\cdot}65 - 4{\cdot}62\,(10^4/T)$ (13)

Reaction (10) $\log_{10} p = 10{\cdot}10 - 3{\cdot}94\,(10^4/T)$ (14)

Considering the reactions at 2000° K and using equation (6), reactions (8) and (10) are most productive of thorium, giving maximum values for (df/dt) of $1{\cdot}2 \times 10^{-6}$ and 4×10^{-7} monolayers/s respectively.

These are smaller than the authors' observed value of $3{\cdot}6 \times 10^{-5}$ monolayer/s. This indicates that these reactions would be completely unable to maintain the thorium supply at this temperature. Calculating the rates for reactions (8) and (10) at 2800° K they are 1·8 and 0·1 monolayers/s respectively. The extrapolation of the experimental evaporation curve to 2800° K gives a value of 0·15 monolayers/s. This suggests that reaction (8) might thus be able to build up the thorium reserve during the flash at 2800° K.

An alternative explanation has been proposed by Hoch and Johnson.[9] They assume that during the flash at 2800° K the ThO_2 partially dissociates to ThO and $\frac{1}{2}O_2$, the latter diffusing away and leaving some free ThO. The latter is unstable below about 2150° K, so that when the temperature is dropped below this point the ThO disproportionates to Th and ThO_2. In their experiments on the effusion of the reaction products from a hole in a closed vessel they obtained about 5–10% of free thorium in the evaporation product when it was allowed to disproportionate. It should be possible to distinguish whether this is the operative mechanism in a cathode or whether reaction (8) produces

the thorium as follows. If Hoch and Johnson's mechanism produces thorium it should be necessary to lower the cathode temperature to about 2150° K before there is a supply of free thorium. On the other hand, if reaction (8) produces the thorium it should be present in the tungsten directly after the flash at 2800° K. The following experiment was therefore carried out.

An uncarburized cathode was flashed at the usual 2800° K and its temperature then lowered to 2400° K. The evaporation rate was measured in the usual way after a short ageing period at this temperature which should have evaporated about the same quantity of thorium as the usual ageing period of one hour at 2100° K. It was found that thorium evaporation did take place, thus suggesting that some thorium must have been produced by reaction (8). The cathode temperature was then lowered to 2100° K for an hour and the evaporation rate at 2400° K re-measured. It was found that the rate was, in fact, just slightly less than that originally recorded. This result suggests that all the thorium must have been produced by reaction (8) and not by the mechanism suggested by Hoch and Johnson. The thorium produced by reaction (8) would be retained mainly in the grain boundaries and dislocations. The decay of evaporation shown in Fig. 5, curve (1), shows that the thorium reserve held in this way corresponds to a total of about fifteen monolayers on the outer wire surface. In view of the grain size of the wire this appears to be a reasonable quantity to be retained in this manner.

Formation of thorium in the carburized cathode. The carburized cathode may now be considered thermochemically. The two possible effective reactions which would produce thorium at rates significantly different from those already considered are as follows:

$$ThO_2 + W_2C \rightleftarrows Th + 2W + CO_2 \qquad (15)$$

$$ThO_2 + 2W_2C \rightleftarrows Th + 4W + 2CO \qquad (16)$$

Applying the thermochemical data to these reactions the following are the approximate reaction vapour pressures of thorium.

$$\text{Reaction (15)} \quad \log_{10} p = 10{\cdot}75 - 3{\cdot}77\,(10^4/T) \qquad (17)$$

$$\text{Reaction (16)} \quad \log_{10} p = 11{\cdot}26 - 2{\cdot}88\,(10^4/T) \qquad (18)$$

This indicates that reaction (16) will be the most effective. Considering this reaction at 2000° K by applying equations (6) and (18), the maximum rate of production of thorium will be 1 monolayer/s which is large compared with the observed value of 5×10^{-5} monolayers/s. This means, in fact, that the escape of thorium is limited by the diffusion process and that reaction (16) should be fully adequate to activate the cathode at its normal operating temperature.

The diffusion mechanism. At this point the diffusion mechanism may be examined more closely, considering first the uncarburized cathode. Previous workers have obtained evidence that most of the thorium diffuses to the surface along grain boundaries[2] although some also diffuses through the crystals, probably along dislocations.[10, 11] The difference in pressure causing diffusion will be the saturated vapour pressure of the free thorium produced during the flash. This vapour pressure may be represented approximately from data given by Hampel[12] by the equation

$$\log_{10} p = 8{\cdot}6 - 2{\cdot}63\,(10^4/T) \qquad (19)$$

Applying equation (6) for a temperature in the neighbourhood of 2100° K, the maximum rate of evaporation of thorium should be

$$\log\,(df/dt) = 11{\cdot}6 - 2{\cdot}63\,(10^4/T) \qquad (20)$$

Comparing this with the experimental results represented by equation (2) it will be seen that the variation with T is almost identical. This fact indicates that the diffusion process does not vary rapidly with temperature and is therefore analogous to molecular or viscous flow. The process which appears to satisfy this requirement would be migration of layers of thorium atoms over other thorium atoms adsorbed on the tungsten in the grain boundaries or dislocations. As bulk thorium is liquid at the cathode temperature this process should not be very temperature dependent.

The carburized cathode may now be considered in a similar manner. Equation (18) for the carbide reaction combined with equation (6) for T in the neighbourhood of 2100° K results in a maximum rate of evaporation given by

$$\log_{10}\,(df/dt) = 14{\cdot}25 - 2{\cdot}88\,(10^4/T) \qquad (21)$$

Comparing this with the experimental relationship of equation (3), and allowing for experimental errors and the approximations used to derive equation (21), the terms giving the variation with temperature are in fair agreement. This suggests that the same diffusion mechanism is also operating in the carburized cathodes.

The fact that there was no significant difference in evaporation rate between cathodes with decarburized surface layers and that with the carbide surface, suggests that the decarburized layer is so broken up as a result of carburizing and decarburizing that it presents little impedance to the diffusion of thorium.

CONCLUSIONS

The main conclusions which may be drawn from the work are that the rate of evaporation of thorium from a carburized filament is, within experimental error, the same as that from a similar uncarburized type in the 200°–2200° K temperature range. In spite of this, the carburized type is able to maintain a fully activated surface to a higher temperature than the uncarburized type. The thorium in the carburized type is produced continuously at a rate adequate for activation at the operating temperature by reduction of the thoria by the carbon in the tungsten carbide. In the uncarburized cathode the rate of production of thorium at the operating temperature is insufficient for activation, and a reserve of thorium must be built up in the grain boundaries and dislocations by flashing at 2800° K. At this temperature the rate of reduction of thorium by tungsten has increased sufficiently to build up this concentration, in spite of the increased rate of evaporation.

The thorium reaches the surface of each type of cathode by diffusion along the grain boundaries and dislocations in the crystals, and this process is shown not to be very temperature sensitive.

ACKNOWLEDGEMENT

The authors wish to thank the M.-O. Valve Co. Ltd. for permission to publish this paper.

REFERENCES

(1) LANGMUIR, I. *Phys. Rev.*, **22**, p. 357 (1923).
(2) CLAUSING, P. *Physica*, **7**, p. 193 (1927).
(3) ANDREWS, M. R. *Phys. Rev.*, **33**, p. 454 (1929).

(4) AYER, R. B. *Proc. Inst. Radio Engrs*, **40**, p. 591 (1952).
(5) BRATTAIN, W. H., and BECKER, J. A. *Phys. Rev.*, **43**, p. 428 (1933).
(6) LANGMUIR, I. *J. Franklin Inst.*, **217**, p. 543 (1934).
(7) SMITHELLS, C. J. *Tungsten*, 3rd Ed., p. 216 (London: Chapman and Hall, 1952).
(8) KUBASCHEWSKI, O., and EVANS, E. L. *Metallurgical Thermochemistry* (London: Butterworths Scientific Publications for Springer-Verlag, 1951).
(9) HOCH, M., and JOHNSON, H. L. *J. Amer. Chem. Soc.*, **76**, p. 4833 (1954).
(10) FONDA, G. R., YOUNG, A. H., and WALKER, A. *Physics*, **4**, p. 1 (1933).
(11) AHEARN, A. J., and BECKER, J. A. *Phys. Rev.*, **54**, p. 448 (1938).
(12) HAMPEL, C. A. *Rare Metals Handbook* (New York: Reinhold Publishing Corp., 1954).

APPENDIX

The following are the values at 298° K used in the thermochemical calculations.

Enthalpy values		
Heat of formation (kcal/mol)	*Heat of vaporization* (kcal/mol)	*Entropy values* (cal °K^{-1} mol^{-1})
ThO_2 solid 293	WO_3 — 122	W (solid) 8
WO_2 solid 134	WO_2 — 122*	WO_2 (gas) 82
WO_3 solid 200	Th — 130	WO_3 (gas) 83
W_2C solid 12		Th (gas) 42
CO_2 (gas) 94		CO (gas) 47·5
CO (gas) 26		CO_2 (gas) 51
O (gas) —59		W_2C (solid) 17
		ThO_2 (solid) 20
		O (gas) 38·5
		O_2 (gas) 49

* Assumed value.

On the creep, recovery, relaxation and elastic "memory" of some renneted milk gels

By G. W. SCOTT BLAIR, M.A., D.Sc., F.R.I.C., F.Inst.P., and J. BURNETT, National Institute for Research in Dairying, University of Reading

[*Paper received 5 June*, 1958]

Small pressures are applied to one end of a column of renneted milk gel ("curd") in a U-tube and the displacements at the other end are magnified a hundredfold. As a first approximation, the curd behaves as a "Burgers body", except that the creep curve shows a much greater "rapid" strain than does the recovery curve. Relaxation at constant strain follows a power relation between stress and time with an exponent of 0·40. The time taken for the stress to halve itself is proportional to the initial (rapid) rate of straining. Under selected conditions, creep and relaxation curves during ageing approximate to Boltzmann's Superposition Principle. Hysteresis curves, obtained by repeated loading and unloading, show marked stiffening, followed by a (Bauschinger) softening when the direction of loading is reversed. Following suitable stressing in alternate directions, curd shows "elastic memory," i.e. the recovery curves change direction. Such behaviour necessitates additions to the Burgers model. A modification of Boltzmann's Superposition equation is discussed and Graham's equation, which includes an Andrade term, has been applied to some of the data. The relative significance of the analytical and integrative approaches to these problems is considered.

In an earlier paper[1] the present authors have described in detail a method for measuring the increasing shear moduli and viscosities of milk gels as they set under the action of rennet.* In principle, the method is very simple. Some 50 ml. of acidified and renneted milk are set in a U-tube in a constant temperature water-bath, normally at 32° C and, after setting has started, small pressures are applied by means of compressed air to one side of the column of gel for a period of 1 min. The displacements of the meniscus on the opposite side are measured, with a magnification of about a hundred-fold, by the movement of an index of coloured alcohol along a narrow horizontal tube. (If the recorder tube is too narrow, the viscosity of the air causes a time lag.) The pressure is then reduced to zero, and the elastic recovery is followed for 2 min, by which time it is nearly, but not quite, complete. The test is usually repeated, applying stresses in alternate directions by means of a 4-way tap, every 4 min during the course of the setting of the gel. The stresses are normally progressively increased to produce approximately the same strains throughout.

With some milk samples, syneresis causes the plug of curd to become partly detached, in course of time, from the walls of the U-tube. This effect is prevented, or at least minimized by: (*a*) Using reconstituted fat-free dried milk; but since dried milks are apt to be deficient in soluble calcium, a standard quantity of calcium chloride solution is added; (*b*) etching the walls of the U-tube with hydrofluoric acid; and (*c*) pouring the milk directly into the "bend" of the tube by means of a suitably designed pipette (for details see Scott Blair and Burnett[2, 3]).

The calculation of the overall shear modulus G follows the treatment of Saunders and Ward[4] who used a similar method (but with a straight cylindrical test-piece) for gelatin gels. Curvature of the test-piece has no appreciable effect on the treatment. The shear modulus G is calculated from the movement of the alcohol index on recovery h, ignoring the small amount of recovery still incomplete after 2 min; the manometer reading P; the density of the manometer liquid (kerosene) ρ; the radius of the U-tube R; the length

* Analogous to "gelatine" and "gelatin," "rennet" is the commercial product and "rennin" the pure enzyme.

of the column of gel L; and the radius of the recorder capillary a, by means of an equation, exactly analogous to that of Poiseuille

$$G = \frac{R^4 \rho g}{8La^2} \cdot \frac{P}{h} \qquad (1)$$

It is shown in the first paper[1] that, if readings are taken throughout the 2 min of recovery, a linear curve is obtained during the greater part of this period, when the logarithm of the proportion of unrecovered displacement at time t is plotted against t. If such straight lines are extrapolated back to the time-zero, a value is obtained for the proportion of the elastic recovery which is delayed. (This gives, of course, only a formal division of the strain and not a true measure of the experimental acoustic elasticity.)

Since there is always some displacement which is never recovered during the course of the test, four independent parameters can be calculated: the immediate modulus G_1; the delayed modulus G_2; the internal (damping) viscosity η_2, calculated from the retardation time t_{ret}; and the external viscosity η_1 from the finally unrecovered displacement. In these simple experiments, curd behaves approximately as a "Burgers body," i.e. a dashpot N_M and spring H_M in series (Maxwell body) attached to a dashpot N_K and spring H_K in parallel (Kelvin body). This may conveniently be written as $(H_M - N_M) - (H_K|N_K)$ (see Reiner[5]). It has been shown[3, 6] that the rate of increase of the Burgers parameters and their ratios ($t_{ret} = \eta_2/G_2$; $t_{rel} = \eta_1/G_1$) where t_{rel} is relaxation time; and $N = t_{rel}/t_{ret}$, known as the "springiness number" (Scott Blair[7]) gives useful measures of the quantitative effects of various industrial treatments of liquid milk, e.g. homogenization, pasteurization, separation. Moreover, graphs plotting G_1 or any of the Burgers parameters, against logarithmic time give remarkably straight lines, except in the earliest stages of setting, so that their rates of increase are best expressed as increases on doubling the time t.

This logarithmic plot, though useful, is entirely empirical. It probably reflects a more interesting relation. If the log time straight line is extrapolated to find a value of $G(G_\infty)$ corresponding to a long time, say twice the duration of the experiment, it may be assumed that by this time most of the casein molecules will be in the gel form. If values of $\log (G_\infty - G)/G_\infty$ are now plotted against t, fairly good straight lines are obtained. The determination of G_∞ by this method is arbitrary, but it seems likely that, once setting is well established, the rate of increase of G is proportional to the amount of still unset casein. If this is so, the conveniently linear part of the $G/\log t$ curves corresponds to the central portion of what is really a sigmoid curve.

The U-tube gelometer, however, with a few quite simple modifications, can be used for much more far-reaching and fundamental studies of the rheological properties of these gels, and it is such experiments which will be described in the present paper.

To this end, the compressed air reservoir was attached to a long rubber tube which passed between two rollers in the form of a "mangle." The pressure is increased or decreased by turning this mangle by hand. If a constant rate of change of pressure is required, a suitably geared motor, fitted with a reversing mechanism, can be fitted.

EXPERIMENTAL PART

The simplest experiment consists in applying a constant load to the curd for some considerable time and measuring the displacement before and after removing the load. A typical creep and recovery curve is shown in Fig. 1. Without first applying some equation to linearize such curves, it is notoriously difficult to extrapolate them so as to determine the amount of instantaneous (acoustic) elasticity. Nevertheless, one thing is quite clear merely from inspection: the immediate elastic strain under stress is very much greater than that which is immediately recovered after unloading.

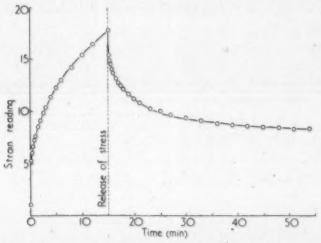

Fig. 1. Creep and recovery curve for milk curd

This is somewhat unusual. Compare, for example, the data of Schofield and Scott Blair (Ref. 8, Fig. 2) for flour doughs, in which no such difference is observed. There are many other instances in the literature. This phenomenon is not due to any unrecoverable deformation, since, if the pressure is released after a few seconds loading, almost the whole of the instantaneous deformation is recovered in due course.

It is convenient to discuss such phenomena in terms of dashpot and spring models, without prejudice as to their fundamental nature. All models of this kind are known to be reduceable to two canonical types. The simplest illustration of one type is the Burgers body: the other type is represented by the Kuhn body: $(H - N)|(H - N)$ and these two models are equivalent (see Leaderman[9]). Either canonical type may be used, but it is felt that the working of the former is rather easier to envisage and it will therefore be used throughout this paper.

In terms of the Burgers body, then, this feature of the creep curve means that the spring H_M does not maintain a constant strain under constant load but relaxes, presumably due to a fall in the viscosity η_1 of the dashpot N_M as straining proceeds. It is, of course, possible, but less easy to envisage, that G_1 increases with straining so that the strain of H_M corresponding to the constant stress diminishes. Either way, it is clear that $t_{rel} = \eta_1/G_1$ must fall with straining and whether this is to be regarded as a type of thixotropy, or of strain-stiffening* or both, it is to be expected that there will be some reversal, i.e. an increase in t_{rel}, if the strain is held constant.

Many experiments have shown that this is the case. If a fairly large strain is set up rather quickly, in say 5 s, and maintained constant by progressively lowering the stress, it is found that a linear relation is obtained by plotting log stress, not against time, which would be the case if t_{rel} were constant, but against log time, showing that the Maxwellian relaxation time is increasing. Two typical curves are shown in Fig. 2.

* Most rheologists use the term "work-hardening" to describe any such increase in consistency, shear modulus or viscosity. The use of this term as applied to metals is more restricted and it is suggested that "strain-stiffening" would be a less controversial term for general use.

The question always arises, in plotting logarithmic time for relaxation data, whether to take the zero of time at the start of the loading or at the moment where the constant strain is just reached. Although this may involve a difference of only 5 s, it will markedly affect the linearity of the first part of the curves. It seems more logical to use the former zero, since relaxation has, of course, started before the final

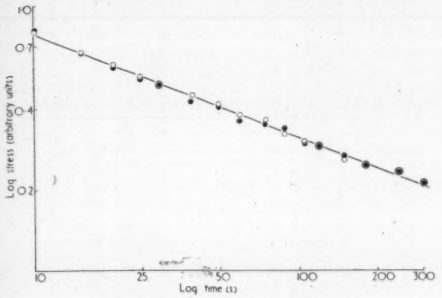

Fig. 2. Relaxation curves (milk curd)
○; ●, duplicate runs.

strain is reached. With the present data, moreover, better straight lines were obtained in this way than when the latter zero was tried and the former method was therefore used throughout. The relaxation phenomena will be described in detail later. We will now return to the creep curves.

In order to study further the progressive fall in "quick" elastic displacement during loading (where "quick" arbitrarily refers to the strain after 5 s, since such strains can be accurately measured, whereas acoustic strains are not easy to determine) experiments were done in which the loads were applied and removed after various intervals of time. For such experiments it was found best to age and "condition" the gels (see Leaderman[9, 10]). After ageing for about an hour, a stress was applied for 2 min and allowed to recover for 10 min. After this conditioning, in one experiment

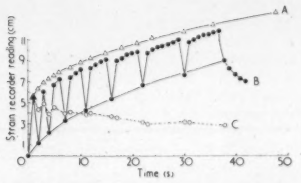

Fig. 3. Continuous and interrupted creep curves
A, first experiment; *B*, second experiment; *C*, intermittent experiment.

(curve *A* in Fig. 3) the same stress was continuously maintained to give a typical creep curve. In a second experiment (curve *B*), the stressing was interrupted by 5 s recovery periods, at first very frequently and later less often. It will be seen that the curves *A* and *B* do not coincide. This may be due partly to the fact of permanent N_M flow, the stress being applied for a shorter total time in the case of curve *B*; but, from the way in which the continuous portions of loading curve tend upwards, it seems likely that much of the discrepancy is due simply to lack of time, with such short recoveries and loadings.

Curve *C* shows the fall in quick-elasticity during the intermittent experiment. At the start, there is seen to be a marked difference between the modulus in loading and unloading (alternate points). This suggests that the thixotropy (or its equivalent) is most marked during the first few seconds of straining and recovery.*

These experiments immediately raise the question as to how far these gels may be said to approximate to Boltzmann's superposition principle. It has already been found that there is some permanent N_M flow. Recovery curves have been followed over very long periods and even fairly drastic vibrations have failed to release any more elastic strain ("redress"). The permanent flow is evidently not linear, since a linear correction for it has not proved effective; but it is not difficult to "correct" for the much more serious thixotropic effect described above.

Several experiments were done following the method proposed by McHenry[11] for concrete, a material which ages over a period of months but which does not show permanent "flow." McHenry also used this method for phenolic resins.

Our experiments were done with drastic, with moderate and with no pre-conditioning of the gel, the most satisfactory being that with the same moderate pretreatment as was used for the experiment shown in Fig. 3.

An experiment following McHenry is shown in Fig. 4. *A* is an experimental creep curve for a gel aged for 80 min, *B* for a

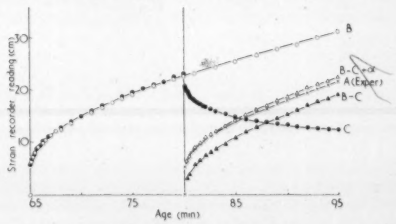

Fig. 4. McHenry's experiment

gel at 65 min and *C* duplicates *B* except that at 80 min stress is removed and recovery is followed. Following simple superposition, the calculated curve $B - C$ should coincide with *A*. However, since we know from the experiment shown in Fig. 3 that the H_M strain is falling during loading, we should add to the calculated curve a quantity α equal to the difference between the 5 s displacement on loading at 60 min and that on recovery at 85 min. It will be seen that the calculated curve marked $B - C + \alpha$ shows remarkably good agreement with the experimental curve *A* at small strains, nor is the divergence very great even at large strains. The strains are given in arbitrary units (recorder readings—cm) since there is no constant strain radially across the U-tube. To give some idea of absolute magnitudes, however, it may be said that the maximum strain at the wall corresponding to a reading of $h = 10$ cm on the recorder, is about 0·5. Even half this value would be a very large strain for superposition to hold, even approximately, and it should be

* *Note added to proof:* An alternative explanation for this phenomenon is offered in a later communication.

emphasized that good agreement has been obtained only under empirically favourable conditions of pre-stressing, ageing, etc. Nevertheless, the result is rather remarkable.

The importance of pre-conditioning of the gel depends on the fact that, like many other materials, the curd shows much strain-stiffening, especially in the first cycle of loading and recovery. This must be due to increase in consistency corresponding to parts of the model other than the Maxwell element. (We shall see later that a second Kelvin element is needed to account for more complex behaviour.)

The "firming" is well seen in the data from an experiment in which a gel, unconditioned except by the determination of a single modulus, was progressively loaded and unloaded, to give the series of hysteresis loops shown in Fig. 5. These curves are very similar to those found by Schofield and Scott Blair for flour doughs (Ref. 8, Fig. 5).

The rate of firming is given by the relation between the strain readings at zero stress and the cycle number. Plotted on log/log paper, this gives a straight line of slope 0·58. If the direction of loading is reversed, the strain associated with the first loading cycle in the new direction is at least as great as that produced in the first cycle of the original loading. The material softens when the direction of loading is reversed.

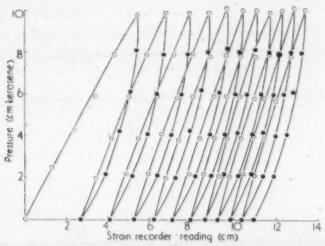

Fig. 5. Hysteresis curves

Following the study of superposition from these gels, one is naturally led to ask whether they show the phenomena of elastic "memory" well known for wires and threads of metals, silk, rubber and various high-polymers. We are not aware that the phenomenon has ever previously been found with gels.

To test this, an aged gel was first loaded for half an hour at a fairly large stress (20 cm kerosene). At the end of this time, the direction of stress was reversed and a slightly smaller stress was immediately applied for one or two minutes. After release, the whole recovery curve was followed. Curves from two such experiments are shown in Fig. 6.

The "memory effect" is striking. The (negative) strain first diminishes, then, after a short period of approximate balance, the recovery from the earlier loading is resumed, until a final equilibrium is reached.

In terms of models, such behaviour requires the addition in series to the Burgers body of another Kelvin body. Describing the viscous and elastic elements of these Kelvin groups as $N_{K1} : H_{K1}$ and $N_{K2} : H_{K2}$, if we postulate $N_{K1} \gg N_{K2}$ and stretch the model for a relatively long period, $N_{K2} : H_{K_2}$ will be stretched to its utmost and $N_{K1} : H_{K1}$ very considerably. On reversing the direction and compressing for a short time, whereas $N_{K2} : H_{K2}$ will be considerably compressed, the higher viscosity of N_{K1} will prevent much change in length. On release, $N_{K2} : H_{K2}$ will quickly expand, after which the slower contraction of $N_{K1} : H_{K1}$ will become evident.

It remains only to describe in more detail some further experiments on stress relaxation at constant strain. Returning to Fig. 2, the use of power equations to describe relaxation

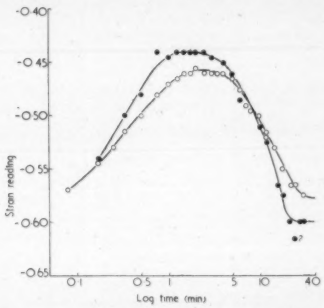

Fig. 6. Elastic "memory" of milk gels
(Two ages and loading times.)

has a long history, which is described by Leaderman.[9] More recently, Scott Blair and Caffyn[12] have shown that many and diverse materials obey a power equation of relaxation and have proposed extensions of the simple equation where it does not suffice. Before considering the development of these ideas, the results of our recent experiments will be described.

We have seen that repeated loading in one direction stiffens the gel, whereas change of direction softens it. It was found that, if relaxation data are plotted $\log (P/P_0)$ against $\log t$ where P is the pressure at time t and P_0 is the maximum (original) pressure, the straight lines so obtained, after the first run or two, coincide independently of stiffening and softening and may therefore be taken as characteristic of the gel itself.

In a series of relaxation experiments loading always in the same direction, the slopes of the $\log (P/P_0)$ against $\log t$ curves seldom differ much from 0·4. Since these curves are power curves, there is no point in defining a "relaxation time" in terms of the base of natural logarithms. The best measure of relaxation rate would seem to be the "half relaxation period" (τ), defined as the time taken for the pressure to fall to half its initial value. Its reciprocal may be called "the generalized* relaxation rate" and it has been found that, when the initial straining is effected at different speeds ($\dot{\epsilon}$) the value of $\tau\dot{\epsilon}$ is remarkably independent of the magnitude of $\dot{\epsilon}$.

The experiments were done in all cases with pre-selected values of P_0. In some cases the time of increasing strain at constant load θ was pre-selected and the strain for subsequent relaxation was measured; in other cases the time needed to reach the pre-selected strain was measured. Either way, the only function of P_0, strain and θ which was found to bear any regular relation to τ was the average rate of straining, got by dividing the strain by θ. The reason for this is not known. It is not unreasonable to suppose, however, that when the strain is built up slowly, some of the rapidly

* "Generalized" because it does not depend on any postulated relation between stress and time.

relaxing elements will not survive to contribute to the maximum stress. With a rapid straining, a higher value of P_0 will be reached, other things being equal. This will tend to give a shorter half-relaxation period in the latter case. But it is far from obvious why the product of $\tau\dot{\epsilon}$ should become so remarkably constant. This product has the advantage of being dimensionless. It may be regarded as a strain and is doubtless an important constant of the gel. Fig. 7 shows a plot of $1/\tau$ against $\dot{\epsilon}$ for relaxation of a series of stresses in the same direction. Only the first one or two points, which represent conditioning, lie seriously off the straight line. The numbers refer to the order in which the experiments were done. The strain was pre-selected in experiments 1–4 and the time θ in experiments 5–9.

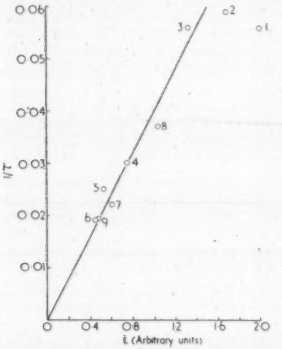

Fig. 7. Relationship between "generalized relaxation rate" ($1/\tau$) and average rate of straining ($\dot{\epsilon}$) for standard dried milk

When the direction of loading is alternated with each experiment, the slopes of the power-equation relaxation curves remain unchanged at almost exactly 0·40. The value of τ may increase very slightly. These results are quite unlike those obtained when the direction of loading remained unchanged.

DISCUSSION

In the previous section it has been convenient to describe our experiments mainly in terms of models of dashpots and springs but the results, especially of the relaxation experiments, clearly indicate the limitations of this type of description. For example, how is the principle of superposition to be reconciled with the power equation relating dissipating stress to time?

This question has been ably discussed by Graham,[13] who suggests that the well-known Boltzmann equation should be modified to allow for the non-linearity inherent in such phenomena as memory effects. The linearity of a plot of $\log \sigma$ against $\log t$, where σ is a relaxing stress, is a special case (constant strain) of the Nutting[14] equation

$$\epsilon = \psi^{-1}\sigma^{\beta}t^{k} \qquad (2)$$

in which β/k represents the slope of the relaxation curve. But the Nutting equation expresses a unique relation between its variables, inconsistent with such phenomena as elastic memory.

Graham suggests that equation (2) is obeyed only for incremental changes while relationships between finite quantities are calculated by a linear superposition of Nutting elements. He proposes, then, to modify the Boltzmann equation to read:

$$\psi\epsilon = k\int_0^{t'}(t' - t)^{k-1}\sigma^{\beta}dt \qquad (3)$$

in which t', the current time, is any particular value of the variable t.

Scott Blair and Caffyn, in the paper already cited,[12] and Scott Blair, Veinoglou and Caffyn in an earlier work[15] suggested that equation (2) is a limiting case of a much more general relationship involving the fractional, differential equation (the symbols have been changed from those used in Refs. (12) and (15) to conform to modern usage):

$$\frac{d^{\mu+\omega}\epsilon}{dt^{\mu}\,.\,d\sigma^{\omega}} = \text{const} \qquad (4)$$

(μ and ω are fractions). Graham pointed out that there is a very close connexion between these two treatments; in certain special cases the equations become identical, to give:

$$\epsilon = (At^{k} + Bt^{k-1} + \ldots)(A'\sigma^{\beta} + B'\sigma^{\beta-1} + \ldots) \qquad (5)$$

Graham has modified this equation so that the successive powers of t no longer differ by unity. For creep curves for metal alloys, Graham and Walles[16] fit a three-term equation with time exponents of $\frac{1}{3}$, 1 and 3 and we are indebted to Mr. A. Graham and his colleague Mr. C. S. Landau for applying this equation to some of our data on curd. Our data are found to be entirely consistent with this interpretation but they are insufficient in extent to make it possible to establish definite proof. Further co-operation in this connexion is planned.

In conclusion, it should be pointed out that there is a fundamental difference between the "analytical" treatment of rheological data in terms of models of dashpots and springs and the "integrative" method associated with such equations as (3) and (4) (see Scott Blair[17]). The former may be regarded as a method of successive approximations. Starting with the Burgers model to explain the simpler types of behaviour, we have been led to add more and more elements to account for additional complications. However complex the behaviour, it is always possible to use this method, even if continuous spectra of relaxation and retardation times have to be introduced. Alternatively, we may retain a small number of dashpots and springs but ascribe to them complex behaviour, such as thixotropy and shear-stiffening. Such treatments are by no means new. As a temporary expedient, they help to provide some sort of visual representation for the kind of creep behaviour found for milk gels. But the use of complex elements in models has only a limited value. The point of the model is to describe complex behaviour in terms of the interaction of simple linear elements. If the elements of the model are themselves complex, comparatively little is gained. A very similar criticism applies to the use of models containing an infinite number of linear elements. A model simply represents an equation and equations of continuous spectra of retardation and relaxation times are no simpler and certainly no more meaningful than are equations such as (3) and (4).

The integrative method is, as Graham[13] puts it, "primarily a method to be used when basic principles are in doubt, and it is one of successive guess-correction, by which discrepant elements of the argument are discarded,

rather than of successive approximation by which these elements are inevitably retained." For the kind of gels studied in the present work, it is felt that both treatments should play their parts in elucidating the phenomena observed.

ACKNOWLEDGEMENT

We are much indebted to Messrs. A. Graham and C. S. Landau, of the National Gas Turbine Establishment, for many helpful suggestions.

REFERENCES

(1) Scott Blair, G. W., and Burnett, J. *Lab. Practice*, **6**, p. 570 (1957).
(2) Scott Blair, G. W., and Burnett, J. *J. Dairy Res.*, **25**, p. 297 (1958).
(3) Scott Blair, G. W., and Burnett, J. *J. Dairy Res.*, **25**, p. 457 (1958).
(4) Saunders, P. R., and Ward, A. G. *Proc. II Internat. Congr. Rheology*, p. 284 (London: Butterworths Scientific Publications, 1953).
(5) Reiner, M. *Deformation and Flow* (London: H. K. Lewis and Co. Ltd., 1949).
(6) Scott Blair, G. W., Burnett, J., and Lilley, H. *Dairy Inds.*, **23**, p. 182 (1958).
(7) Scott Blair, G. W. *Research*, **11**, p. 123 (1958).
(8) Schofield, R. K., and Scott Blair, G. W. *Proc. Roy. Soc. A*, **141**, p. 72 (1933).
(9) Leaderman, H. *Creep of Filamentous Materials* (Washington: Textile Foundation, 1943).
(10) Leaderman, H. *Rheology*, Ed. F. R. Eirich, Chap. 1, Vol. 2 (New York: Academic Press Inc., 1958).
(11) McHenry, D. *Bull. Amer. Soc. Test. Mater.*, **43**, p. 1069 (1943).
(12) Scott Blair, G. W., and Caffyn, J. E. *Phil. Mag.* (ser. VII), **40**, p. 80 (1949).
(13) Graham, A. *Research*, **6**, p. 92 (1953).
(14) Nutting, P. G. *J. Franklin Inst.*, **191**, p. 679; and *Proc. Amer. Soc. Test. Mater.*, **21**, p. 1162 (1921).
(15) Scott Blair, G. W., Veinoglou, B. C., and Caffyn, J. E. *Proc. Roy. Soc. A*, **189**, p. 69 (1947).
(16) Graham, A., and Walles, K. F. A. *J. Iron Steel Inst.*, **179**, p. 105 (1955).
(17) Scott Blair, G. W. *A Survey of General and Applied Rheology*, 2nd Ed. (London: Sir Isaac Pitman and Sons Ltd., 1949).

Electromagnetic fields in ferrite ellipsoids

By R. A. Waldron, B.A., A.Inst.P., Marconi's Wireless Telegraph Co. Ltd., Research Department, Great Baddow, Essex

[*Paper first received* 7 *August, and in final form* 28 *August*, 1958]

It is pointed out that the derivation of the field in a ferrite, when immersed in a uniform field, from a knowledge of the demagnetizing factors is logically unjustifiable, since these quantities depend on a knowledge of the internal fields. The internal fields should logically be calculated from the magnetic potential equation by the application of suitable boundary conditions. Results of such calculations are given for spheres, rods of circular or elliptical cross-section, longitudinally or transversely polarized, and disks polarized perpendicularly or parallel to their planes. Some of these results have been previously reported, but are included here for the sake of completeness; the majority, however, are believed to be original. The demagnetizing factors are also deduced from the fields.

It is frequently necessary to know the internal dielectric or magnetic field in a non-conducting body when it is immersed in a uniform electric or magnetic field. The need arises, for example, in perturbation calculations with waveguides and cavities. Shapes of body amenable to exact calculation are special cases of the general triaxial ellipsoid. The forms which are of most interest, and for which results are given here, are the sphere, the infinitely long rod of circular or elliptical cross-section, and the infinite disk.

The formulae have been derived for the case of a ferrite, characterized by the tensor permeability

$$\mu_0[\mu] = \mu_0 \begin{bmatrix} \mu & -j\alpha & 0 \\ j\alpha & \mu & 0 \\ 0 & 0 & 1 \end{bmatrix} \qquad (1)$$

and immersed in a uniform field $\boldsymbol{H}$. The polarizing field is taken always to be in the z direction, and the microwave fields, both internal and external, are supposed to lie in the $(x–y)$ plane. Actually, if the external fields lie in the $(x–y)$ plane, calculation shows that in all cases so do the internal fields. Electric fields for a scalar dielectric are easily obtained from the formulae for magnetic fields, by replacing α by zero, μ by ϵ, and choosing the formula for a ferrite which has the polarizing field perpendicular to the actual external electric field.

METHOD OF CALCULATION

Formulae for internal fields have usually been calculated in the past by starting with the equation

$$\mu_0 \boldsymbol{h} = \mu_0 \boldsymbol{H} - [N]\boldsymbol{M} \qquad (2)$$

where $[N]$ is a tensor having only diagonal elements N_x, N_y, N_z, $\boldsymbol{H}$ denotes the uniform field which existed before the introduction of the ferrite, and $\boldsymbol{h}$ is the field in the ferrite due to $\boldsymbol{H}$. This procedure is unsatisfactory, however, for two reasons. In the first place, $\boldsymbol{M}$ is not a directly measurable quantity, and in the second the assumption that $[N]$ does not contain off-diagonal elements requires justification in the case of a substance having a tensor permeability.

On the other hand, the permeability tensor elements, μ and α, are directly measurable, and a treatment in terms of these quantities is unexceptionable. The method followed

by the present author is to start from the magnetic potential equation[1,2]

$$\frac{\mu\partial^2\psi}{\partial x^2}+\frac{\mu\partial^2\psi}{\partial y^2}+\frac{\partial^2\psi}{\partial z^2}=0 \tag{3}$$

This is solved in an appropriate co-ordinate system for the interior of the ferrite. Laplace's equation is solved for the space outside the ferrite. The boundary conditions are then applied, and an unambiguous expression for the potential in the ferrite is obtained. The gradient of this gives the internal field $\boldsymbol{h}$.

From the results of this treatment, equation (2) can be derived and hence the form of $[N]$ is obtained. It is only in this way that $[N]$ can be determined; in the scalar case the result is, of course, well known, but there is no justification for the normal practice of taking $[N]$ as derived for the scalar case and using this value for the tensor case.

INTERNAL FIELDS

Sphere

The result for a sphere has been given previously by Berk and Lengyel[1] and by the present author[2]; the latter gives the derivation from the magnetic potential equation. The results are

$$\left.\begin{aligned} h_x &= 3\left[\frac{(\mu+2)H_x+j\alpha H_y}{(\mu+2)^2-\alpha^2}\right] \\ h_y &= 3\left[\frac{(\mu+2)H_y-j\alpha H_x}{(\mu+2)^2-\alpha^2}\right] \end{aligned}\right\} \tag{4}$$

Rod of circular cross-section

(*a*) *Longitudinally polarized* (*z parallel to axis of rod*). The result for this case has also been given by Berk and Lengyel,[1] and the derivation from the magnetic potential equation is given by the present author.[3] The results are

$$\left.\begin{aligned} h_x &= 2\left[\frac{(\mu+1)H_x+j\alpha H_y}{(\mu+1)^2-\alpha^2}\right] \\ h_y &= 2\left[\frac{(\mu+1)H_y-j\alpha H_x}{(\mu+1)^2-\alpha^2}\right] \end{aligned}\right\} \tag{5}$$

(*b*) *Transversely Polarized* (*x, z, perpendicular to axis of rod, y parallel to axis*). These formulae are obtained from those given below for the transversely magnetized rod of elliptical cross-section by putting $b=a$.

$$\left.\begin{aligned} h_x &= \frac{2H_x+j\alpha H_y}{\mu+1} \\ h_y &= H_y \end{aligned}\right\} \tag{6}$$

Rod of elliptical cross-section

(*a*) *Longitudinally Polarized* (*z parallel to axis of rod*). Without loss of generality, we take the x-axis to be the major axis, ($2a$), and the y-axis to be the minor axis, ($2b$), of the cross-section. The results are

$$\left.\begin{aligned} h_x &= 2\left\{\frac{A[(\mu+1)H_x+j\alpha H_y]+[(\mu-1)H_x-j\alpha H_y]}{A[(\mu+1)^2-\alpha^2]-(1/A)[(\mu-1)^2-\alpha^2]}\right\} \\ h_y &= 2\left\{\frac{A[(\mu+1)H_y-j\alpha H_x]-[(\mu-1)H_y+j\alpha H_x]}{A[(\mu+1)^2-\alpha^2]-(1/A)[(\mu-1)^2-\alpha^2]}\right\} \end{aligned}\right\} \tag{7}$$

where $A=(a+b)/(a-b)$. Equations (7) reduce to equation (5) on putting $a=b$, and to equations (10) and (12) in the limit as $a\to\infty$.

(*b*) *Transversely polarized* (*z parallel to one or other axis of the cross-section*). We take y to be parallel to the axis of the rod, z parallel to the axis $2a$, x parallel to the axis $2b$. It is not necessary to stipulate which of a and b is the greater. There is loss of generality in taking the polarizing field to be parallel to one of the axis of the cross-section, but as this is most likely to be the case in practice, the lack of generality is not important. The results are

$$\left.\begin{aligned} h_x &= \frac{(a+b)H_x+j\alpha aH_y}{\mu a+b} \\ h_y &= H_y \end{aligned}\right\} \tag{8}$$

Equations (8) reduces to equations (9) on letting b approach infinity, and to equations (6) on putting $b=a$.

Disk

An exact treatment can only be given of a disk which is of infinite extent in two dimensions. In practice, disks are used in which the thickness is small compared with the other two dimensions, when the following are approximately true.

(*a*) *Magnetized normally to its plane* (*x and y in plane of disk*). This case is trivial; as Rowen and von Aulock have pointed out,[4] the results are obviously

$$\left.\begin{aligned} h_x &= H_x \\ h_y &= H_y \end{aligned}\right\} \tag{9}$$

(*b*) *Magnetized parallel to its plane* (*z in plane of disk*). We take x also to lie in the plane of the disk, y perpendicular to the plane, and have immediately

$$h_x = H_x \tag{10}$$

In equation (3), $\dfrac{\partial^2\psi}{\partial x^2}=\dfrac{\partial^2\psi}{\partial z^2}=0$. Hence $h_y=$ constant. To satisfy the boundary condition that the normal component of magnetic induction is continuous at the surface of the disk, we thus require.

$$\mu h_y = j\alpha h_x = H_y \tag{11}$$

Eliminating h_x between equations (10) and (11), we obtain

$$h_y=\frac{1}{\mu}(H_y-j\alpha H_x) \tag{12}$$

DEMAGNETIZING FACTORS

From equation (2), we write

$$\begin{bmatrix} N_x & n_x & 0 \\ n_y & N_y & 0 \\ 0 & 0 & N_z \end{bmatrix}\boldsymbol{M}=\mu_0(\boldsymbol{H}-\boldsymbol{h}) \tag{13}$$

where the form of $[N]$ is determined by symmetry requirements and M_z refers only to a microwave component and so is zero. We can also relate $\boldsymbol{M}$ to $\boldsymbol{h}$ by

$$\boldsymbol{M}=\mu_0\begin{bmatrix} (\mu-1) & -j\alpha & 0 \\ j\alpha & (\mu-1) & 0 \\ 0 & 0 & 0 \end{bmatrix}\boldsymbol{h} \tag{14}$$

Eliminating $\boldsymbol{M}$ from equations (13) and (14), we obtain

$$\left.\begin{aligned} N_x[(\mu-1)h_x-j\alpha h_y]+{} & \\ +n_x[(\mu-1)h_y+j\alpha h_x] &= H_x-h_x \\ -n_y[(\mu-1)h_x-j\alpha h_y]+{} & \\ +N_y[(\mu-1)h_y+j\alpha h_x] &= H_y-h_y \end{aligned}\right\} \tag{15}$$

n_x and n_y are in all cases found to be zero; this follows in each case from the fact that they are independent of the fields. Since $M_z = 0$, N_z has to be determined from the fact that, after n_x and n_y have been found to be zero, it is possible to put $N_x + N_y + N_z = 1$. For ellipsoids of various shapes, the right-hand sides of equations (15) can be obtained from equations (4), (5), (6), (7), (8), (10), and (12), and hence the N_i and n_i can be determined. The results are:

Sphere
$$N_x = N_y = N_z = 1/3, \; n_x = n_y = 0 \tag{16}$$

This result is well known in the isotropic case.

Rod of circular section, longitudinally polarized
$$N_x = N_y = \tfrac{1}{2}, \; N_z = n_x = n_y = 0 \tag{17}$$

This result is also well known for the isotropic case.

Rod of circular section, transversely polarized
$$N_y = n_x = n_y = 0, \; N_z = N_x = \tfrac{1}{2} \tag{18}$$

Rod of elliptical section, longitudinally polarized
$$N_x = \frac{b}{a+b}; \; N_y = \frac{a}{a+b}; \; N_z = n_x = n_y = 0 \tag{19}$$

Rod of elliptical section, transversely polarized
$$N_x = \frac{b}{a+b}; \; N_z = \frac{a}{a+b}; \; N_y = n_x = n_y = 0 \tag{20}$$

Disk normally polarized
$$N_z = 1; \; N_x = N_y = n_x = n_y = 0 \tag{21}$$

Disk polarized parallel to its plane
$$N_x = N_z = n_x = n_y = 0; \; N_y = 1 \tag{22}$$

Equations (16) to (22) demonstrate the fact, which is well known for the isotropic case, that the demagnetizing factors in the anisotropic case are functions of shape alone, i.e. regardless of the properties of the substance, the off-diagonal elements of the demagnetizing factor tensor are zero.

ACKNOWLEDGEMENT

The author wishes to express his gratitude to the Engineer-in-Chief of Marconi's Wireless Telegraph Company Ltd. for permission to publish this paper.

REFERENCES

(1) BERK, A. D., and LENGYEL, B. A. *Proc. Inst. Radio Engrs*, **43**, p. 1587 (1955).
(2) WALDRON, R. A. *Proc. Instn Elect. Engrs*, Suppl. No. 6, p. 307 (1957).
(3) WALDRON, R. A. *Brit. J. Appl. Phys.* (to be published).
(4) VON AULOCK, W., and ROWEN, J. H. *Bell Syst. Tech. J.*, **36**, p. 427 (1957).

Thermal conductivities of fused and crystalline quartz

By E. H. RATCLIFFE, National Physical Laboratory, Teddington, Middlesex

[*Paper first received* 7 *May, and in final form* 16 *June*, 1958]

The thermal conductivities of fused quartz and of crystalline quartz (heat-flow at 90° to the optic axis) have been measured by steady-state plate methods; the former over the range −150 to 50° C, and the latter at 28° C. The most probable thermal conductivity values of these two materials have been formulated as functions of temperature, having in mind their use as calibration specimens for apparatus measuring the thermal conductivities of rocks, important in the calculation of terrestrial heat-flow. Detailed description is given of apparatus and measurement methods, and the results of other observers are listed and briefly discussed.

The thermal conductivities of fused quartz and of crystalline quartz (heat flow perpendicular to the optic axis), have been measured by many observers, or have been used to calibrate apparatus for measuring the thermal conductivities of rock specimens.[1–25] Based on values previously published by this Laboratory,[1, 2] Benfield[13] proposed the lines $k = 0{\cdot}00320 + 0{\cdot}00000183t$, for fused quartz, and $k = 0{\cdot}0157 - 0{\cdot}000039t$ for crystalline quartz, where k is the thermal conductivity in cal cm/cm^2 s deg C,* and t is the temperature in °C.

PRESENT MEASUREMENTS

(i) *Small disk apparatus* (*Apparatus A*)

In 1952, the South African National Physical Research Laboratory sent to this Laboratory, for thermal conductivity measurements, three fused quartz disks and three crystalline quartz disks intended as calibration specimens for their divided-bar apparatus: the opportunity was taken to arrange for these to be measured together with the same disks used by Bullard,[12] and by Bullard and Niblett.[15] Some new crystalline quartz disks had also been obtained by this Laboratory from the Quartz Crystal Co. of New Malden, Surrey (as well as some new fused quartz ("transparent Vitreosil") disks from the Thermal Syndicate Ltd. of Wallsend-on-Tyne): these new disks were manufactured in thicknesses matching Bullard's disks. All the above-mentioned disk specimens were used in the present measurements, totalling eight of crystalline quartz (faces cut parallel to the optic axis), and twelve of fused quartz; for each material the disk thicknesses varied between about 0·2 and 1·2 cm, and the disk diameters were approximately $1\frac{3}{8}$ in.

The apparatus consisted fundamentally of a flat, circular metal hot-plate containing an electrical heater, and a pair of water-cooled cylindrical cold-plates (Fig. 1). The plate faces were plated and lapped: glycerine films were applied between these surfaces and the quartz test specimens. Plate

* For convenience in comparing past results, calorie units have been used throughout this paper. To obtain conductivities in J cm/cm^2 s deg C units, which are more logical for electrically-measured heat-inputs, multiply the values quoted by 4·187 (see Brit. Stand. 874 : 1956).

temperatures were measured by 40 s.w.g. copper/constantan thermocouples. A 120 V battery was used as energy source, and current and voltage were measured potentiometrically. A guard heater and insulation, as shown, reduced heat-losses. A vertical load equivalent to $3\frac{1}{2}$ lb/in.^{2} on the disks was applied. Results were also obtained using either a single fused or crystalline quartz specimen on one side of the hot-plate, and a disk of heat-insulating material of known conductivity on the opposite side. The results for measurements

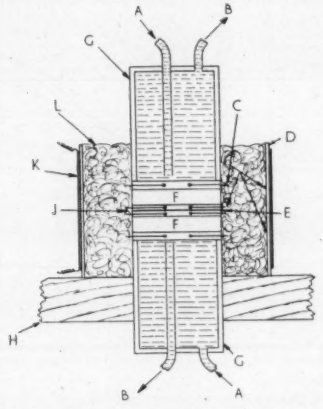

Fig. 1. Guarded disk apparatus (schematic). Thermocouple and heater leads not shown

A, water inflow; *B*, water outflow; *C*, thermocouples; *D*, metal tube; *E*, electrical heater; *F*, test disks; *G*, cold-plates; *H*, wooden shelf; *J*, hot-plate; *K*, cylindrical guard heater; *L*, lagging.

in pairs were used for the final values. The measurements on single disks showed that any small measured differences between the thermal conductivities of disks of fused or crystalline quartz were within the overall experimental error, which was assessed as $\pm 1\frac{1}{2}\%$. As far as can be seen, however, the conductivity differences were real and not entirely random in the case of fused quartz, and a tendency towards differences of about 1%, based on several repeat measurements, was noticed. All measurements were carried out at a specimen mean temperature of about 28° C, the hot and cold face temperatures being about 32 and 24° C respectively.

A check that the crystalline quartz disks had been cut correctly was carried out by the Metallurgy Division of this Laboratory, by X-ray examination. The average angle between the optic axes of the disks and their flat surfaces was found to be about 0° 45′; in the worst case the angle was about 2°, and from consideration of the conductivity ellipsoid even this was unlikely to introduce a departure of more than 0·1% from the conductivity obtainable when the optic axis lay exactly in the surface. Regarding the transparent Vitreosil disks, the makers stated that the principal impurity was aluminium at less than fifty parts per million, and that other impurities were only present in traces.

The glycerine films. Ideally, there should be perfect thermal contact between plates and specimens. In fact, liquid films are necessary to secure a reproducible contact, and their thermal resistances cannot be neglected. Assuming that these films are reasonably reproducible from experiment to experiment, and that the sum of the thicknesses of the films on either side of the disk is very small in comparison with the disk thickness, it is possible to eliminate their effect by making use of the linear relationship

$$\frac{1}{k_a} = \frac{c}{t} + \frac{1}{k}$$

where k_a and k are the apparent and real conductivities of a material of thickness t, and c is the thickness of the two glycerine films divided by their thermal conductivity. To test the reproducibility of the films and this method of correction when a high conductivity material was being measured, four disks of different thicknesses of "Macloy *G*" high alloy steel (0·49% carbon, 1·9% silicon, 0·58% manganese, 16·75% chromium, 36·5% nickel, with a conductivity about 75% greater than the crystalline quartz) were tested. The result (0·0265 cal cm/cm^2 s deg C at 28° C) was within 3% of a value obtained by Dr. R. W. Powell and Mr. R. P. Tye of this Laboratory, using an absolute longitudinal heat-flow method. For the thinnest of the steel disks, the temperature drop across both films was 25% of the temperature difference across the plates. In the case of fused quartz, this drop had varied between 1 and 5% of the overall temperature difference, and between $2\frac{1}{2}$ and 13%, for crystalline quartz, depending on the thicknesses of the disks.

Heat losses. Preliminary trials with the guard not heated indicated that, for the specimen temperature conditions required, thermal losses from the apparatus would be from less than 1% up to about $1\frac{1}{2}$% of the total heat input to the hot-plate for crystalline quartz, and from about 1 to 6% for fused quartz, depending on the thicknesses of the disks. Further trials, using disks of other materials and of known low conductivity, showed that a condition of near-zero loss was common within small limits if the temperature of the guard was maintained about 6° C above that of the hot-plate. When fused quartz disks were measured under this empirically found "no-loss' condition, the results obtained were the same as those when the guard was left unheated and a loss correction applied.

Other corrections. These involved the calibration of shunts associated with current and voltage tappings, and the potential drop correction for short lengths of heater wire projecting from the hot-plate and soldered to copper wires just outside it, all of which were not thought likely to introduce an experimental error greater than about $\pm\frac{1}{4}$% in the results.

(ii) *Large disk apparatus* (*Apparatus B*)

This was similar to the smaller $1\frac{1}{8}$ in. diameter apparatus except in size, the plates being 3 in. in diameter. The applied load was about $5\frac{1}{2}$ lb/in.^{2} The thermocouples were 36 s.w.g. nickel–chromium/constantan. Measurements were made on two pairs of fused quartz disks supplied by the Thermal Syndicate, Ltd., the disks of each pair being 0·5 and 1·5 cm thick. Glycerine films were mainly used, but some measurements were carried out with air films between plates and specimens. The guard cylinder was maintained at about 10 deg C above the hot-plate temperature to reduce heat losses, this condition being found as described for Apparatus *A*. Thermal conductivities were measured at specimen mean temperatures of 28 and 50° C. The overall experimental error was assessed as $\pm 1\frac{1}{2}\%$.

(iii) *Low temperature disk apparatus* (*Apparatus C*)

This apparatus is shown in Fig. 2, and was used to measure the thermal conductivities of 3 in. diameter disks when the

cold-plates were cooled by a solid carbon dioxide/acetone mix, or by liquid nitrogen, the upper "plate" *D* being a hollow cylindrical metal vessel, and the lower *I* a cylindrical metal block. Thermocouples used were 40 s.w.g. copper/constantan; a load equivalent to 15 lb/in.^{2} was applied through the ebonite plunger *C*. An isothermal low-temperature guard surface surrounded the test specimens.

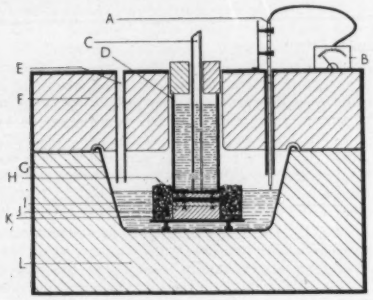

Fig. 2. Low temperature disk apparatus (schematic). Thermocouple and heater leads not shown

× = thermocouples.

A, thermocouple level indicator; *B*, millivoltmeter; *C*, ebonite loading tube; *D*, top "cold-plate" containing liquid nitrogen or solid carbon dioxide/acetone mix; *E*, ebonite filling tube; *F*, cellular plastic insulation inside wooden lid; *G*, basin containing liquid nitrogen or solid carbon dioxide acetone mix; *H*, test specimens on either side of hot-plate; *I*, bottom "cold-plate"; *J*, fibrous thermal insulation; *K*, guard cylinder; *L*, cellular plastic insulation inside wooden box.

Four pairs of fused quartz disks, 3 in. in diameter, which included the two pairs measured in Apparatus *B*, were measured. Normally, identical specimens were placed one on each side of the hot-plate, but in order to obtain a conductivity figure for specimens at higher mean temperatures and the normal temperature differences, it was necessary to interpose, on each side of the hot-plate, between the disk to be measured and the cold-plate, another disk, not necessarily of quartz. In this case, a $\frac{1}{8}$ in. thick flat brass disk, with thermocouples in drill-holes, was placed between the two disks referred to, to measure the cold-side temperature of the quartz.

Ethyl alcohol films were used between plates and specimens when the film temperature was between about −80 and −40° C: above this temperature range, turpentine was used; below it, no liquid films were used. As an additional check, all conductivity measurements carried out using liquid films were repeated without liquid films. The conductivity/temperature curve obtained using turpentine films extrapolated upwards to within 1% of the 28° C results from Apparatus *A* and *B*. Near −40° C, a temperature suitable for measurements with air, turpentine and alcohol films, the air films and alcohol films gave approximately parallel curves, with a spread of conductivities of ±3% from the median turpentine curve. Measurements were carried out at many specimen mean temperatures between −150 and −20° C.

Final results were obtained graphically as described for Apparatus *A* and *B*, after correcting for edge losses. The overall experimental error was assessed as ±5% at −150° C, scaling down to ±2% at −20° C.

RESULTS AND CONCLUSIONS

(i) *Fused quartz.* The smoothed fused quartz results for all apparatus are shown in Fig. 3, together with the results of other observers. Over the temperature range −150 to

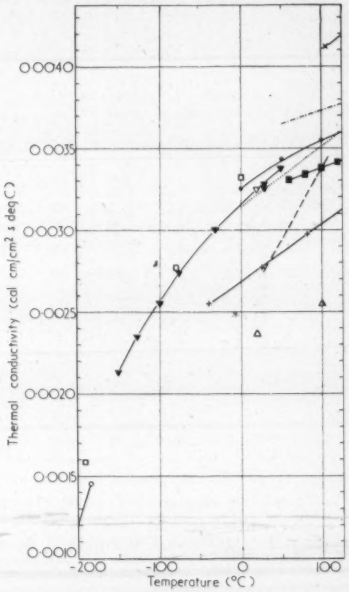

Fig. 3. The variation in the thermal conductivity of fused quartz with temperature

□ = Eucken[7]
△ = Barratt[8]
■ = Kaye and Higgins[2]
+ = Seemann[9]
• = Birch and Clark[11]
× = Knapp[18]
▽ = Butler[19]
○ = Berman[25]
▼ = present measurements
..... = Ito[10] after Birch and Clark
— — — = Colosky[20]
—·—·— = Kingery and Norton[21]

50° C, the variation found in the thermal conductivity (k), in cal cm/cm^2 s deg C units, with temperature (t) can be closely expressed by the following quadratic equation:

$$10^7k = 31\,600 + 46t - 0{\cdot}16t^2$$

(ii) *Crystalline quartz.* Results, including the present value of $k = 0{\cdot}0151$ cal cm/cm^2 s deg C at 28° C, are shown in Fig. 4. Over the temperature range 0 to 100° C, the most probable values would seem to be obtainable more realistically from the curve $1/k = 60{\cdot}7 + 0{\cdot}242\,t$. Conductivity values derived from this equation agree closely with values obtained by Griffiths and Kaye,[1] Kaye and Higgins,[2] Birch and Clark,[11] and the author, and are shown as a dotted line in Fig. 4.

Two monographs were to hand at the time of the present measurements: these were R. B. Sosman's *Properties of Silica*,[26] and G. W. Morey's *The Properties of Glass*,[27]

and the conductivity values given by the former are naturally based mainly on the early work of Eucken. Surprisingly, however, Morey's book again quotes Eucken's values for fused quartz and other glasses, including his clearly doubtful result of 0·004 57 cal cm/cm² s deg C for fused quartz at 100° C: only passing reference is given to Birch and Clark's work, and no mention made of any other work on the conductivity of fused quartz after 1911. Other volumes consulted, including standard reference works, were badly out of date: a current handbook of the American Institute of Physics,[28]

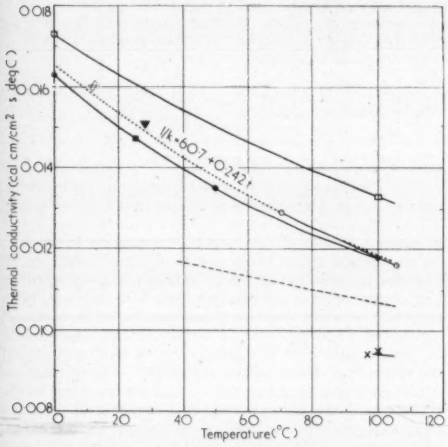

Fig. 4. The variation in the thermal conductivity of crystalline quartz with temperature. (Heat flow at 90° to the optic axis)

▽ = Tuchschmid[5] △ = Lees[4] + = Weber[6]
□ = Eucken[7] ■ = Griffiths and Kaye[1]
○ = Kaye and Higgins[2] ● = Birch and Clark[11]
× = Knapp[18] ▼ = present work
— — — = Colosky[20]
- - - - - = most probable values

quoted fused quartz conductivities between −270 and 240° C, apparently following close to Berman's figures at the low end of the scale, and using the Kaye and Higgins values above 60° C, but, for intermediate temperatures, the values given were inconsistent—a value of 0·003 52 at 0° C, for example, was not acceptable, if only from the fact that the quoted value of 180° C was 0·003 53. For crystalline quartz the same book quoted only Eucken's 1911 values up to 100° C, and Knapp's results from 260° C upwards—a combination which must be inconclusive, for referring to Fig. 4, there is a very wide difference between values by these observers at 100° C.

ACKNOWLEDGEMENT

The work described above has been carried out as part of the research programme of the National Physical Laboratory, and this paper is published by permission of the Director.

REFERENCES

(1) GRIFFITHS, E., and KAYE, G. W. C. *Proc. Roy. Soc. A*, **104**, p. 71 (1923).
(2) KAYE, G. W. C., and HIGGINS, W. F. *Proc. Roy. Soc. A*, **113**, p. 335 (1926).
(3) LODGE, O. J. *Phil. Mag.*, **5**, p. 110 (1878).
(4) LEES, C. H. *Phil. Trans A*, **183**, p. 481; **191**, p. 399 (1892).
(5) TUCHSCHMID, A. *Diss. Zurich* (1883); *Beiblatter, Ann. Phys. Chem.*, **8**, p. 490 (1884).
(6) WEBER, R. *Arch. Sci. Phys.*, **33** p. 590 (1895).
(7) EUCKEN, A. *Ann. Phys. (Leipzig)*, **34**, p. 185 (1911); *Ver. Deut. Phys., Ges.*, **13**, p. 829 (1911).
(8) BARRATT, T. *Proc. Phys. Soc. (London)*, **27**, p. 81 (1914).
(9) SEEMANN, H. E. *Phys. Rev.*, **31**, p. 119 (1928).
(10) ITO, S. *Mazda Res. Rep.*, **4**, p. 188 (1929).
(11) BIRCH, F., and CLARK, H. *Amer. J. Sci.*, **238**, pp. 529, 613 (1940).
(12) BULLARD, E. C. *Proc. Roy. Soc. A*, **173**, p. 474 (1939).
(13) BENFIELD, A. E. *Proc. Roy. Soc. A*, **173**, p. 428 (1939).
(14) COSTER, H. P. *Roy. Astron. Soc. Geophys. Suppl.*, **5**, p. 131 (1947).
(15) BULLARD, E. C., and NIBLETT, E. R. *Roy. Astron. Soc. Geophys. Suppl.*, **6**, p. 222 (1951).
(16) MOSSOP, S. C., and GAFNER, G. *J. Chem. Soc. S. Africa*, **52**, p. 61 (1951).
(17) CARTE, A. E. *Proc. Phys. Soc. (London) B*, **67**, p. 664 (1954).
(18) KNAPP, W. J. *J. Amer. Ceram. Soc.*, **26**, p. 48 (1943).
(19) BUTLER, D. W. Unpublished data (National Physical Laboratory, 1950).
(20) COLOSKY, B. P. *Bull. Amer. Ceram. Soc.*, **31**, p. 465 (1952).
(21) KINGERY, W. D., and NORTON, F. H. *U.S. Atomic Energy Comm. NYO-6444* (1954).
(22) BECK, A. E. *Ph.D. Thesis* (Australian National University, 1956).
(23) GAFNER, G. *Brit. J. Appl. Phys.*, **8**, p. 393 (1957).
(24) RATCLIFFE, E. H. Private communication to the National Physical Research Laboratory, S. Africa (1955).
(25) BERMAN, R. *Proc. Roy. Soc. A*, **208**, p. 90 (1951).
(26) SOSMAN, R. B. *The Properties of Silica* (New York: The Chemical Catalog. Co., 1927).
(27) MOREY, G. W. *The Properties of Glass*, 2nd Ed. (New York: Reinhold Pub. Corp., 1954).
(28) *American Institute of Physics Handbook* (New York: McGraw-Hill Book Co. Inc., 1957).

Collection of gas-borne dust particles by means of an aspirated sampling nozzle

By S. BADZIOCH, B.Sc., Grad.Inst.P., British Coal Utilisation Research Association, Leatherhead, Surrey

[*Paper first received* 23 *June, and in final form* 28 *July*, 1958]

The efficiency of collection of gas-borne particles by an aspirated sampling nozzle is investigated theoretically and experimentally. The efficiency is shown theoretically to depend on (*a*) the ratio of the velocity of aspiration into the sampling nozzle to the velocity of the undisturbed gas stream, and (*b*) the ratio of a length representing the distance of disturbance upstream of the nozzle to the "range" of a particle. The "range" is defined as the distance a particle would travel, before coming to rest, if projected into still gas with a velocity equal to that of the gas stream. In the range of conditions investigated experimentally, which included nozzles of 0·65 to 1·90cm diameter aspirating from *turbulent* gas streams, it is found that the length representing the upstream disturbance is a function of the diameter of the nozzle.

1. INTRODUCTION

The concentration of dust present in flowing gas streams is commonly measured by extracting a sample of dusty gas by means of an open-ended nozzle facing upstream and determining the mass of dust in the sampled volume, the dust being removed from the gas sample by means of a suitable dust-extracting device. The dust concentration, i.e. the mass of dust per unit volume of gas, is normally calculated from the ratio of the mass of dust collected to the volume of gas sampled.

The dust concentration calculated from the sample will be correct provided the gas sample is drawn into the nozzle at the same velocity as that of the gas stream. This is known as isokinetic sampling. Only such under conditions will the gas stream remain undisturbed. When the velocity of aspiration of gas into the nozzle (sampling velocity) is lower than that of the gas stream, some of the gas will be diverted around the sampling nozzle, whereas some of the dust particles originally present in this deflected gas stream will, by virtue of their inertia, enter the nozzle. Thus the dust concentration in the sample will be higher than that in the gas stream. Similarly, if the sampling velocity is too high, the gas converges into the nozzle, but the inertia of the particles may prevent them from being deflected into the nozzle. Thus the dust concentration will be underestimated. Only when the particles are very fine, so that they follow the gas streamlines closely, will there be little error in the measured dust concentration when the sampling velocity differs from the gas velocity. It is equally easy to visualize what happens when very coarse dust is sampled. This will, by virtue of its momentum, persist in its direction of travel, and, whatever the sampling velocity relative to the stream velocity, the *mass* of dust that will enter the nozzle will be equal to the *mass* of dust flowing in the undisturbed gas stream through the projected area of the nozzle. Thus the mass flow rate of coarse dust is measured correctly whatever the sampling velocity.

Although the mechanism of collection of particles by a nozzle is easy to envisage when sampling either very fine or very coarse dusts, these two extreme cases seldom occur in practice. The errors arising from a difference between the gas velocity, and the sampling velocity (anisokinetic sampling) cannot be calculated exactly in a general case because the flow pattern at an aspirating sampling nozzle is not known. A simple theoretical treatment, given in Section 2, yields an expression into which empirical constants can be inserted on the basis of experimental data. The published data[1–5] are inadequate for the purpose and therefore an experimental investigation has been carried out using a dust tunnel. These experiments are described in Section 3.

Application of the results to the problem of dust sampling will be considered elsewhere.[6]

2. THEORETICAL

(2.1) *Elementary theory of the process of collection of gas-borne particles by means of an aspirated sampling nozzle.* The problem of the motion of particles at an aspirated nozzle is basically similar to the process of impaction of particles on an obstacle situated in a stream of fluid. Impaction of particles on obstacles has been extensively investigated by various authors (see, for example, Ref. 7) in connexion with collection of water droplets or ice particles on the wings of aeroplanes. The procedure is first to establish theoretically or experimentally the flow pattern of the fluid upstream of the obstacle, such as a sphere or cylinder. The efficiency of collection is then found by step-by-step computations of the trajectories of the particles, and hence deducing the projected cross-sectional area from which the particles reach the surface of the obstacle. The ratio of this area to the projected area of the obstacle is the efficiency of collection of particles. The efficiency of collection (α_0) of an obstacle is a function of a dimensionless parameter K given by

$$K = [(\sigma - \rho)d^2V]/18\eta D \qquad (1)$$

where
σ = density of particles,
ρ = density of fluid,
d = diameter of particles,
V = undisturbed velocity of fluid,
η = viscosity of fluid, and
D = size of obstacle (e.g. diameter of sphere)

Since the free-falling velocity v of a particle is, by Stokes' law, given by

$$v = [(\sigma - \rho)d^2g]/18\eta \qquad (2)$$

where g is the acceleration due to gravity, K can be conveniently expressed as

$$K = vV/gD \qquad (3)$$

The pattern of flow, for a given shape of obstacle, is characterized by its Reynolds number $R_D = VD/\mu$ (μ being the kinematic viscosity of the fluid), and the efficiency of collection for a given obstacle is therefore determined by K and R_D. The functional relation is different for different obstacle shapes. Fig. 1 shows the results of computations by Langmuir[7] of the collection efficiencies of a sphere in viscous ($R_D \to 0$) and ideal ($R_D \to \infty$) flow of fluid together with the theoretical forms of the curves derived later. The efficiency is lower in the case of viscous flow because the disturbance extends further upstream than in the case of

ideal flow, and the particles are subjected to a deflecting drag for a longer time.

The flow pattern at an aspirated sampling nozzle is not known and therefore no exact calculations can be carried out in this case. A theoretical treatment has therefore been attempted into which empirical constants can be inserted on the basis of the experimental data given in Section 3.

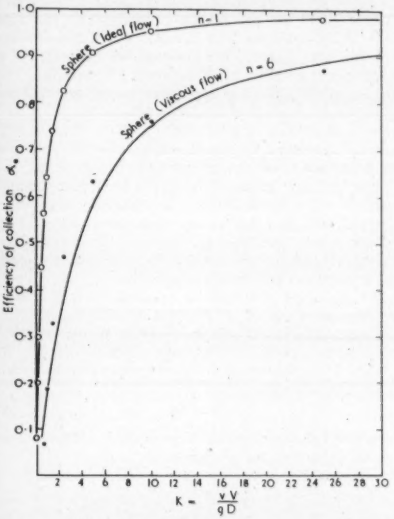

Fig. 1. Comparison of Langmuir's computations[7] for impaction with form of the curves derived in Section 2.2

Equations of curves $\alpha_0 = [1 - \exp(-n/K)]/(n/K)$.
Langmuir's computations: ○ = ideal flow. ● = viscous flow.

Let us consider the case when the sampling velocity V_s is lower than the undisturbed gas velocity V (Fig. 2). If a is the cross-sectional area of the nozzle facing upstream, the volume of gas approaching the nozzle per unit time is aV. The volume of gas drawn into the nozzle is aV_s and the volume $(aV - aV_s)$ by-passes it. It is evident that all the particles contained in the volume aV_s will enter the nozzle. Owing to the inertia of the particles, a fraction α of the particles present in the deflected volume $(aV - aV_s)$ will enter the sampling nozzle. Henceforth α will be referred to as the inertial parameter. Therefore, if C is the true dust concentration, the dust concentration C_s of the sample is

$$C_s = [aV_sC + (aV - aV_s)\alpha C]/aV_s \qquad (4)$$

That is

$$C_s/C = \alpha(V/V_s) + (1 - \alpha) \qquad (5)$$

An identical expression can be derived for the case when the sampling velocity is higher than the gas velocity.

Multiplying equation (5) by aV_s/aV we obtain the collection efficiency of the sampling nozzle in terms of the mass of particles

$$M_s/M = (1 - \alpha)(V_s/V) + \alpha \qquad (6)$$

where M_s = mass rate of collection of particles by a nozzle,
and M = mass flow rate of particles through an area in the undisturbed gas stream equal to the projected area of the nozzle.

The value of α depends on the inertia of the particles and tends to unity for very coarse particles. For this extreme case the mass of dust entering the sampling nozzle will be independent of the sampling velocity, i.e. a correct mass flow rate of dust will be measured whatever the sampling velocity relative to the gas velocity. For very fine particles α tends to zero and the mass of dust entering the sampling nozzle is directly proportional to the sampling velocity. When the sampling velocity V_s is equal to the gas velocity V (isokinetic sampling), $M_s = M$, that is, a correct sample is obtained no matter what is the value of α.

It is not known whether α is constant and independent of the sampling velocity. It is, however, evident that as the sampling velocity tends to zero, equation (6) must reduce to the case of impaction and α will then have the value of α'_0, which is the efficiency of impaction of particles into the sampling nozzle. (A nozzle without suction is a "soft" obstacle, the stationary air in it forming a cushion, and it may therefore differ in behaviour from a solid obstacle, i.e. α'_0 is not necessarily equal to α_0.) The discussion below shows, in a general way, why the value of α is not equal to α'_0.

When the sampling velocity tends to zero, then by analogy with impaction, the length of upstream disturbance at the nozzle will be determined by the nozzle size but the flow pattern (for a given Reynolds number) will be geometrically similar for nozzles of different sizes. Hence the efficiency of

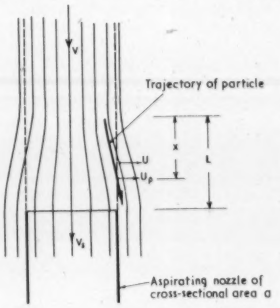

Fig. 2

impaction of particles into the nozzle, α'_0, can be expressed as a function of K. Conditions, however, are considerably different when suction is applied to the nozzle. In the extreme case of isokinetic sampling the nozzle becomes effectively non-existent. When the sampling velocity differs from isokinetic the nozzle is equivalent not to a disk but to a ring-like obstacle. If the diameter of a nozzle is large, the parts of the ring on opposite sides of a diameter behave as independent obstacles and the length of disturbance upstream of the nozzle is small. As the nozzle becomes smaller the "independent" disturbances at the edge of the nozzle begin to interact more and more and the effective disturbance extends further upstream. For sampling velocities not greatly different from isokinetic the "ring" will be located close to the edge of the nozzle and the effective length of disturbance

due to the nozzle will remain substantially constant. However, when the sampling velocity is reduced further, the "ring" will gradually close in and the length of disturbance due to the nozzle will increase. Eventually, when the sampling velocity is zero, the nozzle is equivalent to a disk-like obstacle.

The value of the inertial parameter depends on the length of the upstream disturbance and therefore it can be expected to remain substantially constant over a range of sampling velocities not greatly different from isokinetic, but it will decrease as the sampling velocity is reduced. It is also evident that the inertial parameter α cannot be satisfactorily expressed as a function of K, since the upstream flow pattern is geometrically different for nozzles of different sizes.

We shall now attempt to find an approximate functional form for α. Consider again the case when the sampling velocity is lower than the gas velocity (Fig. 2). Let U be the lateral component of velocity (perpendicular to the axis of the nozzle) of the streamlines by-passing the nozzle. The viscous drag of this component of velocity will displace the particles laterally from the original direction of motion parallel to the axis of the nozzle. As a criterion for the dilution of the concentration of particles in the volume of gas by-passing the nozzle, we shall take the ratio of the lateral component U_p of the velocity of particles to the lateral component of the streamlines U at the dotted cylinder in Fig. 2. This ratio can be found by considering a simplified form of the flow pattern at the sampling nozzle. Assume that the streamlines begin to diverge at a distance L from the plane of the nozzle entrance and that the lateral component of the gas velocity U is constant over the whole length L. It can be easily shown by Stokes' law that a particle, originally at rest, subjected to a uniform gas velocity U will in time t acquire a velocity U_p given by

$$\frac{U_p}{U} = \left\{1 - \exp\left[-\frac{18\eta t}{(\sigma - \rho)d^2}\right]\right\} \tag{7}$$

Particles will reach the dotted cylinder over the whole length L according to their original position with respect to it. The component of velocity parallel to the axis of the nozzle with which a particle travels is approximately V, and therefore the time during which the particle is accelerated laterally before reaching the cylinder is given by

$$t = x/V \tag{8}$$

where x is the distance travelled by the particle in the direction parallel to the axis of the nozzle.

From equations (7) and (8), the average concentration of particles relative to the true concentration for all the particles passing through the dotted cylinder over the whole length L is given by

$$\frac{1}{L}\int_0^L \left[1 - \exp\left(-\frac{x}{\lambda}\right)\right]dx \tag{9}$$

where
$$\lambda = [(\sigma - \rho)d^2V]/18\eta \tag{10a}$$

or
$$\lambda = vV/g \tag{10b}$$

λ is known as the "range" of a particle; it is defined as the distance a particle would travel, before coming to rest, if projected with velocity V into a still fluid.

By definition of the inertial parameter α, given earlier, the concentration of particles (relative to the true concentration) in the volume of gas deflected around the nozzle is $(1 - \alpha)$. Equating this to the value of the integral (9) we obtain

$$\alpha = [1 - \exp(-L/\lambda)]/(L/\lambda) \tag{11}$$

As discussed earlier the length of disturbance L upstream of the sampling nozzle is expected to decrease as the diameter of the nozzle increases. This is confirmed by experiments described in Section 3; an approximate empirical equation for L is:

$$L = 6{\cdot}0 - 1{\cdot}6D \tag{12}$$

where L and D are in centimetres.

Owing to the scatter of observations the constant and the coefficient of D are not known precisely, and the experimental results obtained are unsuitable for considering a curvilinear relationship. The constant lies between 5·2 and 6·8 and the coefficient of D between 1·0 and 2·2. (The limits stated are the 95% confidence limits, the regression analysis involving seventy-nine observations.)

It is unlikely that the assumption of a simplified flow pattern at the sampling nozzle will greatly affect the form of the function α. In reality the disturbance at the nozzle will develop very gradually and the drift component of velocity U will not be constant as assumed; however, the discrepancy will probably be absorbed merely by modifying the value of L. The value of L deduced from experiments will probably indicate the length over which the disturbance to the streamlines is fairly pronounced.

(2.2) *Application of the theory to the process of impaction of particles on obstacles.* In the case of solid obstacles (or a nozzle without suction), the geometry of the upstream disturbance is independent of the size of the obstacle. Thus the length of the disturbance L can be described in terms of the size of the obstacle:

$$L = nD \tag{13}$$

where n is a constant depending on the flow pattern (namely R_D and the shape of the obstacle).

Substituting this value into equation (11), we obtain

$$\alpha_0 = [1 - \exp(-n/K)]/(n/K) \tag{14}$$

where
$$K = \lambda/D \tag{15}$$

Langmuir's computations[7] for the efficiencies of collection of particles by a sphere in viscous and ideal flow of fluid are plotted in Fig. 1 together with the curves calculated from equation (14) for two assumed values of n. It will be seen that for ideal flow of fluid there is a very good agreement, for $K > 0{\cdot}1$, between Langmuir's curve and a plot of equation (14) with n taken to be 1·0. In the case of viscous flow, the agreement is reasonable, for $K > 1$, when n is taken to be 6·0. The values of n have been chosen to give the best fit but they indicate the distances (nD) of upstream disturbance that seem reasonable, for the two types of flow of fluid round a sphere.

It should be noted that Langmuir defined K in terms of the radii (not diameters) of the particles and obstacles. Therefore the values of K given by Langmuir should be divided by 2 to comply with the definition given by equation (1).

3. EXPERIMENTAL

(3.1) *Dust tunnel and apparatus.* Experimental investigation of the collection of particles by a sampling nozzle has been carried out in a dust tunnel forming a closed circuit in which a quantity of test dust was continuously circulated. The dust tunnel (Fig. 3) was constructed of 8 in. diameter steel pipe. Air in the tunnel was circulated by means of an 8 h.p. fan A, the air velocity being adjustable by means of a Saunder's diaphragm valve B. The sampling position was in a long vertical section of the tunnel 24 in. (three pipe

diameters) before a bend. The gas velocity at the sampling point (centre of the pipe) was measured with an ellipsoidal head pitot-static tube of $\frac{5}{16}$ in. diameter.

Samples of dusty air were extracted by means of a suction fan *C*. The dusty air enters the sampling nozzle *D*, the dust being extracted by means of a glass wool filter *E*. Clean air passes *via* an orifice flowmeter *F* and fan *C* back to the tunnel to avoid bleeding of air into the system.

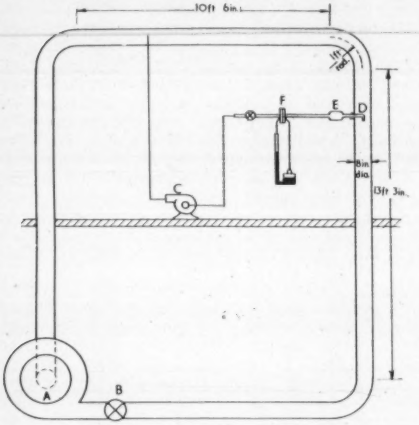

Fig. 3. Diagram of dust tunnel

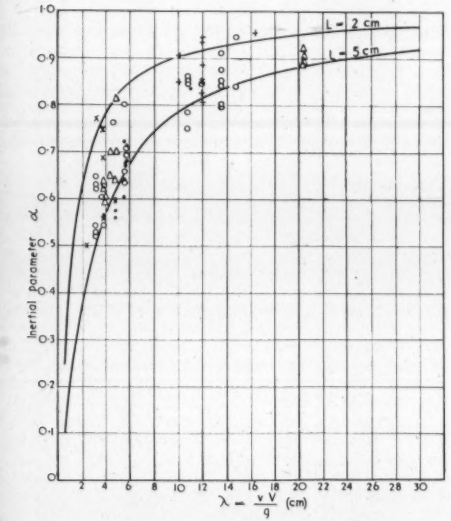

Fig. 4. Inertial parameter α as a function of particle "range" λ

Diameters of nozzles (cm).
● = 0·653
△ = 0·962
○ = 1·275
× = 1·536
+ = 1·896

The nominal internal diameters of the nozzles used were $\frac{1}{4}$, $\frac{3}{8}$, $\frac{1}{2}$, $\frac{5}{8}$, and $\frac{3}{4}$ in. (Actual diameters, which were slightly different, are listed in Fig. 4.) The nozzles used were blunt-edged of edge thickness about 0·6 mm. The area of the largest nozzle amounted to 0·87% of the cross-section of the tunnel.

(3.2) *Test dusts.* Two materials were used in the tests, Aerocat and commercially available zinc spheres—produced by condensation of zinc vapour.

Aerocat is a synthetic material manufactured for the catalytic cracking process used in the petroleum industry (by Cyanamid of Great Britain Ltd.) and consisting of amorphous silica with a small percentage of alumina. The particles are hard, smooth and almost spherical in shape and have a density of approximately 1·4 g/cm^3. Mutual attraction between the particles is very low so that they do not form stable aggregates and do not stick appreciably to the walls of the tunnel.

Both materials, as supplied, covered a wide range of sizes. They were separated into narrow size grades by means of a centrifugal separator developed by this Laboratory.

The particles of zinc test dust were sized under the microscope by Fairs' method[8] and since they were spherical their free-falling velocities could be calculated from Stokes' law. In the case of Aerocat particles, owing to imperfect sphericity and some uncertainty regarding the density, the free-falling velocities in air were determined directly by observing the times of fall of particles through a long tube on to the top face of a 45° prism where their arrivals could be viewed with a low-power microscope. Some corrections were necessary and these were found from observations with three different heights of fall. The results were finally expressed in terms of the free-falling velocity distributions by weight and their average size expressed by the median free-falling velocity.

The test dusts were sufficiently monodisperse to display diffraction rings when spread on a microscope slide. The average particle size was deduced from the observed angular diameters of the diffraction rings seen in sodium light. This served as a useful check of the reliability of sizing by the other methods. The essential characteristics of the test dusts are summarized in Table 1.

Table 1. *Characteristics of the test dusts*

Test dust	*Density particle of material* (g/cm^3)	*Median free-falling velocity at room temperature* (23° C) (cm/s)	*Median Stokes' diameter* (μ)	*Average size deduced from diffraction rings* (μ)
		Aerocat dusts (*Free-falling velocities in air determined directly*)		
A1	≃1·4	1·95	21	—
A2	≃1·4	2·3	22	19
A4	≃1·4	4·1	30	27
		Zinc dust (*sized under the microscope*)		
Zn3	6·9	14·0	26	23

The median free-falling velocity of the zinc dust, calculated from Stokes' law, is overestimated by about 3%. A correction could be applied but this was not considered justifiable.

(3.3) *Experimental procedure.* In a continuously circulating dust tunnel, the dust concentration decreases on

sampling. To take account of the fall of the dust concentration alternate isokinetic and anisokinetic samples were taken. In calculating the value of the inertial parameter (see Section 3.4) from the apparent dust concentration of an anisokinetic test, the mean of two "isokinetic" concentrations before and after the test was taken as the true dust concentration. This procedure compensated adequately not only for the drop in the dust concentration due to the removal of some dust on sampling, but also for the "losses" of dust due to sticking to the walls.

There was no danger of breakage of the zinc spheres in the dust tunnel. As a safeguard against errors due to breakage of Aerocat particles the samples collected were examined under the microscope. These particles could be circulated without breakage up to some air velocity the magnitude of which depends upon particle size; the coarser the particles the lower the "safe" velocity.

The duration of the tests ranged from 1 to 5 min according to the dust concentration, nozzle size and air velocity. The dust concentrations in the various tests ranged from 0·1 to 10 mg/l (0·044 to 4·4 grains per ft^3).

The mass of dust collected in a test was found by weighing the filter before and after the test. To avoid weighing errors due to absorption of moisture, each filter was dried by passing through it hot (160° C) filtered air for a few minutes and then placed in a desiccator to cool. The cold filter was weighed at a definite time (1 min) after removal from the desiccator, there being a continuous pick-up of moisture. After use the filters were dried and weighed in the same way.

When tests with a particular dust grade were completed,

Table 2. *Results of experiments*

D (cm)	V (cm)	v^* (cm/s)	V/V_s	C_s/C
		Aerocat—A1		
0·653	2440	1·75	0·355	0·61
0·962	2440	1·75	0·715	0·80
			0·375	0·595
1·275	2430	1·75	0·575	0·675
1·596	1310	1·8	0·78	0·89
		Areocat—A2		
0·653	2270	2·1	0·66	0·805
			0·37	0·625
			0·305	0·61
			0·55	0·73
	2720	2·05	0·435	0·63
			0·355	0·54
0·962	2270	2·1	0·625	0·695
			0·555	0·715
			0·37	0·56
1·275	1510	2·1	0·78	0·88
			0·72	0·855
			0·57	0·73
			0·43	0·63
			0·38	0·675
			0·52	0·70
1·596	1520	2·1	0·565	0·665
		Zinc–Zn 3		
0·653	820	13·2	0·275	0·395
0·962	1540	13·0	0·25	0·335
			4·62	4·28
			3·26	3·09
			0·375	0·445
1·275	800	13·2	0·385	0·475
			0·26	0·37
			3·49	2·95
			2·50	2·27
			0·56	0·67
			0·38	0·47
			0·285	0·385
	900	13·1	0·285	0·395
	1000	13·2	0·555	0·61
			4·11	3·49
			0·375	0·43
			2·87	2·59
0·653	1000	3·8	1·72	1·42
			2·34	1·76
	1440	3·75	0·38	0·555
			0·20	0·515
		3·8	0·275	0·515
			0·31	0·535
0·962	1000	3·85	0·365	0·595
			0·32	0·595
			0·44	0·66
			0·275	0·55
1·275	1000	3·85	0·555	0·72
			0·495	0·68
			0·365	0·655
			0·435	0·645
			0·265	0·555
			0·295	0·56
	1440	3·8	0·75	0·80
			2·50	1·95
			0·545	0·70
			0·36	0·545
			0·415	0·595
1·596	1000	3·85	0·38	0·535
			0·55	0·69
			0·42	0·675
		Zinc–Zn 3		
1·275	1000	13·2	2·50	2·26
			0·22	0·38
			0·185	0·31
	1100	13·1	2·19	2·00
			0·265	0·305
1·896	750	13·2	0·38	0·44
			0·275	0·385
	900	13·1	2·54	2·32
			0·565	0·615
			0·39	0·425
			0·33	0·41
			0·625	0·65
			2·37	2·10
			0·595	0·665
			0·52	0·55
			0·415	0·485
	1220	13·1	0·555	0·575

* The free-falling velocities are corrected for the temperature of the air in the tunnel.

the remaining dust was removed from the tunnel by boosting the air velocity to a high value and "sampling" with a large nozzle at a high suction rate. After some half-an-hour only minute traces of dust remained in circulation.

(3.4) *Analysis of the experimental data.* The results of experiments are given in Table 2. The median free-falling velocities of the test dusts (column 3) are corrected for the change in the viscosity of air with temperature, the air in the tunnel being heated by friction. Column 4 shows the ratios of the air velocity to the sampling velocity (velocity ratios) and column 5 the corresponding ratios of the apparent to the true dust concentration. No attempt was made to set the velocity ratios to any particular values; they ranged from about 0·2 to 4. In most tests the sampling velocity was higher than the air velocity.

The experimental values of the inertial parameter α are calculated from equation (5), namely

$$\alpha = \frac{1 - (C_s/C)}{1 - (V/V_s)} \tag{16}$$

In Fig. 4 the experimental values of the inertial parameter α are plotted against the "range" λ (calculated from the median free-falling velocities); the different nozzles used are indicated. Owing to the scatter of the observations the change of α with the nozzle size is not very apparent. Two theoretical curves (equation 11) with arbitrary values of $L = 2$ and 5 cm are also plotted in Fig. 4, to provide a rough visual comparison between the experimental and theoretical form of the function α; the agreement appears to be fairly satisfactory.

The theoretical form of α (see equation 11) is unfortunately too awkward to be applied directly to the analysis of the experimental data. The analysis of the data has been carried out as follows. By plotting a family of α against λ curves, given by equation (11), with the different values of L and superimposing on them the experimental values of α (elaborated version of Fig. 4), the values of L corresponding to each test have been estimated.

The first step of the analysis was to examine whether the experimental values of α agree with the theoretical curves. If the experimental values of α, for a given nozzle size, did not follow the theoretical curve, then different values of L would correspond to points at different values of λ and a plot of L against λ would have some trend. Regression analyses of L on λ for different nozzle sizes did not reveal slopes of the lines significantly different from zero. This implies that the experimental values of α do not differ significantly from the theoretical form of α given by equation (11). It is possible that there is some slight discrepancy but it is not detectable owing to the scatter of observations. This discrepancy, however, as in the case of the application of the theory to impaction (Section 2.2), is unlikely to be serious.

The next step of the analysis was the investigation of the variation of the disturbance length L with the diameter of the sampling nozzle. The nature of this function is not easily established. It is, however, apparent (see Section 2.1) that for very large nozzles L will tend to some small steady value. As the size of the nozzle decreases L will increase. The regression analysis of L upon D, taken as a straight line, yields equation (12) which was given earlier.

The results of the analysis are plotted in Fig. 5 in a form suitable for application to the problems of dust sampling. The α against λ curves are plotted for nozzles of $\frac{1}{4}$, $\frac{1}{2}$, $\frac{3}{4}$ and 1 in. diameter.

(3.5) *Calculation of the effective value of the inertial parameter for a given dust.* The values of the inertial parameter shown in Fig. 5 refer to particles of one size only. When the dust covers a range of sizes, the effective value $\bar{\alpha}$ of the inertial parameter is given by

$$\bar{\alpha} = \frac{1}{100}\sum \alpha_i(\Delta W_i) \tag{17}$$

where the summation extends over all the size grades; α_i is the value of the inertial parameter for the mean size of grade i and (ΔW_i) is the weight percentage of dust in the grade. For the purpose of this calculation the dust should be classified in terms of the Stokes' diameters.

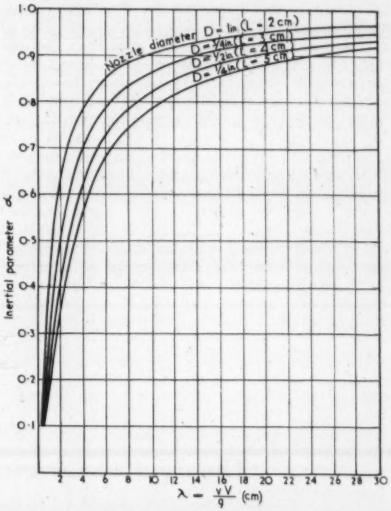

Fig. 5. Values of the inertial parameter α for nozzles of various diameters

(3.6) *Miscellaneous comments.* The investigations presented here cannot be regarded as complete. Several aspects need further consideration.

(*a*) As discussed in Section (2.1) the value of inertial parameter can be expected to remain substantially constant over some restricted range of velocity ratios (V/V_s); only in this range will equation (5) be linear. The range over which equation (5) holds has not been investigated, but both the experiments described here and the published data (with the exception of Watson's experiments[5]) indicate that the equation holds over a range of velocity ratios (V/V_s) from about $\frac{1}{4}$ to at least 2.

(*b*) The linearity of equation (5) over a considerable range of the velocity ratios implies that the function α is probably only negligibly affected by the use of blunt-edged nozzles. As discussed in Section (2.1) an obstacle equivalent to a sampling nozzle has the form of a ring of width depending upon the velocity ratio. The blunt edge will simply increase the width of the "ring" a little. But the inertial parameter is not very sensitive to the width of the "ring," since it is constant over a fairly wide range of velocity ratios. This implies that the data obtained with blunt-edged nozzles are unlikely to differ appreciably from those that would be

obtained with sharp-edged nozzles. Nevertheless, some direct evidence would be desirable.

(*c*) The results obtained may be slightly biased because the "range" λ has been calculated from the median diameters of the test dusts. The effect due to spread of sizes of particles present in the test dusts could have been accounted for by regarding the curves in Fig. 5 as a first approximation. These could then have been used to calculate, for each set of conditions, an effective value of the inertial parameter weighted according to the size distribution by the method given in Section 3.5, and hence to obtain a better estimate of λ. However, the corrections calculated in a few cases have been found to be very small since the test dusts were reasonably monodisperse.

(*d*) The efficiency of collection by impaction, discussed in Section (2.1), may convey an erroneous idea about the effect of the Reynolds number of the obstacle. The difference between the efficiency of collection of particles by an obstacle in viscous or ideal flow is considerable (see Fig. 1), but this is due to an enormous change in the Reynolds number. The Reynolds numbers of the sampling nozzles in the practice of dust sampling will cover a relatively narrow range, and variations due to Reynolds number need not be considered.

(*e*) The "range" of particles λ can be expressed in two ways (equations 10*a* and *b*). In the Stokes' range the two values are identical, but outside this range it is appropriate to use equation (10*b*) since the motion of a particle is characterized by the actual value of its free-falling velocity.

ACKNOWLEDGEMENTS

The author wishes to express thanks to Mr. P. G. W. Hawksley for his help and encouragement; to Dr. R. Jackson for his assistance in the preparation of this paper, and to Messrs. J. A. Esilman, S. W. Feegrade, N. Bowles and A. France (vacation student) who assisted in various stages of the experiments. The paper is published by permission of the Director General of the British Coal Utilisation Research Association.

REFERENCES

(1) HEMEON, W. C. L., and HAINES, G. F. *Air Repair*, **4**, p. 159 (1954).
(2) FAHRENBACH, W. *Forsch. Ing. Wes.*, **2**, p. 395 (1931).
(3) ZIMMERMAN, E. *Z. Verein. Disch. Ingen.* [*VDI*], **75**, p. 481 (1931).
(4) GRIFFITHS, J. H., and JONES, T. D. *Trans Inst. Min. Engrs*, **99**, p. 150 (1939–40).
(5) WATSON, H. H. *Amer. Ind. Hyg. Assoc. Quart.*, **15**, p. 1 (1954).
(6) BADZIOCH, S. *Correction for Anisokinetic Sampling*. Private communication, B.C.U.R.A. Information Circular No. 174—Part III, 1957 (June).
(7) LANGMUIR, I. *J. Meteorol.*, **5**, p. 175 (1948).
(8) FAIRS, G. L. *J. Roy. Microscopical Soc.*, **71**, p. 209 (1951).

Theorem concerning anisotropic dielectrics

By G. POWER, M.A., Ph.D., A.Inst.P., University of Nottingham

[*Paper received* 18 *July*, 1958]

A theorem is enunciated which enables the perturbation effects of an anisotropic dielectric cylinder set in a general two-dimensional electric field to be written down. The results are extended to allow for certain other finite conducting or insulated boundaries, thus providing simple solutions for some apparently difficult problems.

GENERAL RESULTS

The circle theorem is widely used in many branches of mathematical physics to facilitate the solution of two-dimensional problems which previously had to be treated by *ad hoc* methods. Unfortunately the application of this theorem in electrical theory is confined to dielectrics which are homogeneous and isotropic. It is therefore of importance to attempt to formulate a general result of this type when an anisotropic dielectric is placed in a given two-dimensional electric field. Let us therefore consider such an anisotropic dielectric cylinder, having an uncharged cross-section bounded by a closed curve C, and let it be set in an infinite homogeneous isotropic dielectric of constant k_0. We will not yet specify the shape of the boundary C, but it is to be expected that it will be a curve which will become a circle for the special case when both dielectrics are isotropic. There are no other finite boundaries.

Let us assume that the known unperturbed complex potential of the field in the dielectric k_0 be $f(z)$ which can be expanded in the form

$$f_0[pz + qg(z)] = \Sigma a_n[pz + qg(z)]^n, \; z = x + iy, \qquad (1)$$

such that $f_0[pz + qg(z)] \to f(z)$ as $z \to \infty$, where p, q are constants and $g(z)$ a function of z as yet all undefined. The axes of x and y are taken to coincide with the electrical axes of the homogeneous anisotropic dielectric. This means that inside C the field is derivable from an electric potential ϕ_i which satisfies the differential equation

$$k_1(\partial^2\phi_i/\partial x^2) + k_2(\partial^2\phi_i/\partial y^2) = 0, \qquad (2)$$

k_1, k_2 being known constants. The dielectric is isotropic if $k_1 = k_2$.

If we set $X\sqrt{k_1} = x$, $Y\sqrt{k_2} = y$, then we see that ϕ_i is a harmonic function of X, Y, that is to say ϕ_i may be regarded

as the real part of a function of $pz + q\bar{z}$, with the usual notation for complex conjugates, where $p + q = 1/\sqrt{k_1}$, $p - q = 1/\sqrt{k_2}$. We will regard these two equations as defining p, q in equation (1).

We must next consider the conditions that have to be satisfied at a point on the boundary. Since C is uncharged, these are well known to be:

(i) the potential is continuous, i.e. $\phi_0 = \phi_i$;

(ii) the normal components of polarization are the same, i.e.

$$lk_0\frac{\partial\phi_0}{\partial x} + mk_0\frac{\partial\phi_0}{\partial y} = lk_1\frac{\partial\phi_i}{\partial x} + mk_2\frac{\partial\phi_i}{\partial y},$$

the suffixes $_{0,\ i}$ referring respectively to the fields outside and inside C, and l, m being the direction-cosines of the normal to the boundary. Since ϕ_i is a harmonic function of $x/\sqrt{k_1}$, $y/\sqrt{k_2}$, it is easy to see by considering the Cauchy–Riemann differential equations that the second boundary condition reduces to

$$k_0(\partial\psi_0/\partial s) = \sqrt{(k_1k_2)}(\partial\psi_i/\partial s),$$

where ψ is the current function corresponding to ϕ, and δs represents an element of arc length of the boundary C.

The perturbed complex potentials of the fields may thus be taken to be

$$\left.\begin{aligned} w_0 &= f_0[pz + qg(z)] + \Sigma\frac{b_n}{[pz + qg(z)]^n} \\ w_i &= \Sigma c_n(pz + q\bar{z})^n \end{aligned}\right\} \quad (3)$$

with the conditions that

$$\left.\begin{aligned} &\mathrm{Re}(w_0) = \mathrm{Re}(w_i) \\ &k_0\mathrm{Im}(w_0) = \sqrt{(k_1k_2)}\mathrm{Im}(w_i) \end{aligned}\right\} \text{ on the boundary } C. \quad (4)$$

Let us now take the boundary C to be given by

$$(pz + q\bar{z})(p\bar{z} + qz) = a^2, \quad (5)$$

from which

$$\bar{z} = \left\{-z(p^2 + q^2) \pm \sqrt{[z^2(p^2 - q^2)^2 + 4a^2pq]}\right\}\Big/ 2pq. \quad (6)$$

The function of z on the right-hand side of equation (6) is used to define $g(z)$, and since $qg(z)$ must tend to zero with q, the positive square root is taken, that is to say

$$g(z) \equiv \left\{-z(p^2 + q^2) + \sqrt{[z^2(p^2 - q^2)^2 + 4a^2pq]}\right\}\Big/ 2pq, \quad (7)$$

where $p + q = 1/\sqrt{k_1}$, $p - q = 1/\sqrt{k_2}$. It is easily seen that the boundary C given by equation (5) is the ellipse

$$(x^2/k_1) + (y^2/k_2) = a^2. \quad (8)$$

On these assumptions, the conditions (4) show that on expanding $f_0[pz + qg(z)]$ as in equation (1), and comparing coefficients of $(pz + q\bar{z})^n$ on the boundary, the coefficients b_n, c_n in equations (3) are given by

$$b_n = \left[\frac{k_0 - \sqrt{(k_1k_2)}}{k_0 + \sqrt{(k_1k_2)}}\right]a^{2n}\bar{a}_n$$

$$c_n = \frac{2k_0}{k_0 + \sqrt{(k_1k_2)}}a_n.$$

Logarithmic terms can easily be incorporated.

This immediately yields

$$\left.\begin{aligned} w_0 &= f_0[pz + qg(z)] + \\ &\quad + \left[\frac{k_0 - \sqrt{(k_1k_2)}}{k_0 + \sqrt{(k_1k_2)}}\right]f_0\left[\frac{a^2}{pz + qg(z)}\right] \\ w_i &= \frac{2k_0}{k_0 + \sqrt{(k_1k_2)}}f_0(pz + q\bar{z}). \end{aligned}\right\} \quad (9)$$

The form of $f_0[pz + qg(z)]$ is usually found by considering what happens at a great distance from C. The results for fields caused entirely by singularities inside C may be obtained similarly.

We can now state the theorem in its general form as follows.

Let $f_0[pz + qg(z)]$ be a representation of the unperturbed complex potential of an electrical distribution in an isotropic dielectric, constant k_0, lying entirely outside the ellipse $(x^2/k_1) + (y^2/k_2) = a^2$, and $f_i(pz + q\bar{z})$ represent the unperturbed complex potential of a distribution in an anisotropic medium, constants k_1, k_2, lying entirely within the ellipse, where $p + q = 1/\sqrt{k_1}$, $p - q = 1/\sqrt{k_2}$, and $g(z)$ is given by equation (7). There are no other finite boundaries. The perturbed fields outside and inside the ellipse are then given by

$$\left.\begin{aligned} w_0 &= f_0[pz + qg(z)] + Af_0'\left[\frac{a^2}{pz + qg(z)}\right] + \\ &\quad + Bf_i[pz + qg(z)] \\ w_i &= f_i(pz + q\bar{z}) + Df_i'\left(\frac{a^2}{pz + q\bar{z}}\right) + Ef_0(pz + q\bar{z}) \end{aligned}\right\} \quad (10)$$

where $D = -A = 1 - 2\alpha$, $B = 2(1 - \alpha)$,

$$E = 2\alpha,\ \alpha = k_0/[k_0 + \sqrt{(k_1k_2)}].$$

With results in so general a form it is natural that the boundary shape should be linked to the ratio of permittivities, but as usual, the use of conformal transformations enables these results to solve problems involving other types of boundary profiles.

Similar results can be obtained if the region outside C is also anisotropic, but the formulae will be somewhat complicated. In this case the boundary C will also be a closed curve, but different from the ellipse (8).

It is to be noted that if we set $k_1 = k_2 = k_i$ in our results, the dielectric inside C becomes isotropic, $p = 1/\sqrt{k_i}$, $q = 0$, and $qg(z) = 0$. The elliptical boundary C becomes circular, and equation (10) then becomes simply the general statement of the circle theorem for two homogeneous isotropic dielectrics,* with a surface of separation which is a circular cylinder of radius $a\sqrt{k_i}$.

For electrode systems with the boundary either insulated or conducting we set $k_0 = 0$ or $k_0 = \infty$ in equation (10) for w_i and ignore the functions w_0, f_0.

Application. Let the cylinder of anisotropic dielectric with cross-section $(x^2/k_1) + (y^2/k_2) = a^2$, be placed in a uniform electric field of strength E in air, making an angle θ with the x-axis. At great distance from the cylinder $w_0 \to E\exp(-i\theta)z$, so that

$$f_0[pz + qg(z)] = \frac{Ep\exp(-i\theta)}{(p^2 - q^2)}[pz + qg(z)],$$

* POWER, G., and JACKSON, H. L. W. *Appl. Sci. Res.*, *B*, **6**, p. 456 (1957).

yielding immediately

$$w_0 = \left(\frac{Ep}{p^2 - q^2}\right)\left\{\exp(-i\theta)[pz + qg(z)] + \right.$$
$$\left. + \left[\frac{1 - \sqrt{(k_1k_2)}}{1 + \sqrt{(k_1k_2)}}\right]\left[\frac{a^2 \exp(i\theta)}{pz + qg(z)}\right]\right\}$$
$$w_i = \frac{2Ep \exp(-i\theta)(pz + q\bar{z})}{[1 + \sqrt{(k_1k_2)}](p^2 - q^2)}.$$

This shows, amongst other things, that the lines of force in the anisotropic medium are straight, making an angle $\tan^{-1}[\sqrt{(k_1/k_2)} \tan\theta]$ with the x-axis.

EXTENSION OF THEOREM

The introduction of further finite boundaries will, in general, violate the above results, and the problem then proves to be complicated. We shall now investigate what other conducting or insulated boundaries may be inserted in order that the theorem may still hold. This makes possible a simple solution to apparently difficult problems.

Let L be a boundary which is introduced into the original field, and to be specific we shall assume that it is a conductor. In the first instance we suppose that f_i does not exist, so that from equation (10)

$$2\phi_0 = w_0 + \bar{w}_0 = f_0[pz + qg(z)] + f_0'[p\bar{z} + qg(\bar{z})] +$$
$$+ Af_0'\left[\frac{a^2}{pz + qg(z)}\right] + Af_0\left[\frac{a^2}{p\bar{z} + qg(\bar{z})}\right]. \quad (11)$$

Strictly speaking, if

$$f_0[pz + qg(z)] = f\left[\frac{pz + qg(z)}{\gamma}\right],$$

where $\gamma = (p^2 - q^2)/p$,

and if $z = z_0$ is a point on the conductor L, then since L is a curve of constant electric potential in the original field, the sum of the first two terms of the right-hand side of equation (11) is constant, say, when $Z = Z_0 = \gamma z_0$. The sum of the remaining terms must also be constant, that is to say, points such that

$$[p\bar{z} + qg(\bar{z})]_0[pz + qg(z)]_1 = a^2 \quad (12)$$

must also define an equipotential. This may be written

$$\bar{Z}_0 Z_1 = a^2. \quad (13)$$

Let L project into the curve M in the Z-plane ($Z = \gamma z$). Equation (13) means that the inverse curve of M with regard to the circle $|Z| = a$ must project into an equipotential in the z-plane. Clearly the condition that the projection of inverse curves must be equipotentials imposes a strict limit on the field $f(z)$. But if it so happens that M inverts into itself with regard to $|Z| = a$, then the results can hold for all fields $f(z)$ having a conducting boundary coincident with L. As w_i is simply a multiple of the original field, it will not matter if L extends into the region inside C.

The same argument will hold when the field f_i is also present. The same result will also be obtained if L is an insulated boundary, but in this case we should consider the current function ψ instead of the potential ϕ.

We can therefore say that the theorem (10) will still be true if there are conducting or insulated boundaries present, provided the projections of these boundaries on to the Z-plane invert into themselves with regard to the circle $|Z| = a$.

Examples of curves that invert into themselves are easy to obtain. We may take any arc of a circle orthogonal to $|Z| = a$ between points P and Q provided P, Q are inverse points; and in particular the straight line joining PQ is a possible curve.

Application. The straight line joining the points $z = \beta$, $z = a^2/\gamma^2\beta$, where β is real can easily be seen to be a curve, the projection of which inverts into itself. If this is made into a conducting plate and placed in a uniform electric field of strength E in air, making an angle θ with the x-axis, then apart from a constant term

$$f(z) = E\{\cos\theta[(z - \beta)(z - a^2/\gamma^2\beta)]^{\frac{1}{2}} - i\sin\theta z\}. \quad (14)$$

From equation (14) we see that we may take

$$f_0[pz + qg(z)] = E\left(\cos\theta\left\{\left[\frac{pz + qg(z)}{\gamma} - \beta\right]\right.\right.$$
$$\left.\left.\left[\frac{pz + qg(z)}{\gamma} - a^2/\gamma^2\beta\right]\right\}^{\frac{1}{2}} - \frac{i\sin\theta}{\gamma}[pz + qg(z)]\right)$$

where $\gamma = (p^2 - q^2)/p$, so that from equation (10) the perturbed fields can be immediately put in the form

$$w_0 = E\left(\cos\theta\left\{1 + \frac{a[1 - \sqrt{(k_1k_2)}]}{[pz + qg(z)][1 + \sqrt{(k_1k_2)}]}\right\}\right.$$
$$\left\{\left[\frac{pz + qg(z)}{\gamma} - \beta\right]\left[\frac{pz + qg(z)}{\gamma} - a^2/\gamma^2\beta\right]\right\}^{\frac{1}{2}}$$
$$\left. - \frac{i\sin\theta\{[pz + qg(z)]^2[1 + \sqrt{(k_1k_2)}] - a^2[1 - \sqrt{(k_1k_2)}]\}}{\gamma[1 + \sqrt{(k_1k_2)}][pz + qg(z)]}\right)$$

$$w_i = \frac{2E}{[1 + \sqrt{(k_1k_2)}]}\left\{\cos\theta\left[\left(\frac{pz + q\bar{z}}{\gamma} - \beta\right)\right.\right.$$
$$\left.\left.\left(\frac{pz + q\bar{z}}{\gamma} - a^2/\gamma^2\beta\right)\right]^{\frac{1}{2}} - \frac{i\sin\theta(pz + q\bar{z})}{\gamma}\right\}.$$

These represent the disturbed flow when an anisotropic elliptic dielectric cylinder with an inset conducting plate is placed in a field uniform at infinity.

If we put $k_1 = k_2 = k$, the internal dielectric becomes isotropic, and the above agrees with results previously given,* remembering that the boundary C has now become a circle of radius $a\sqrt{k}$.

* POWER, G. *Brit J. Appl. Phys.*, 7, p. 218 (1956).

Preparation of metal film resistors on laminated plastics

By G. Siddall and G. Smith, Edwards High Vacuum Ltd., Crawley, Sussex

Some properties of metal resistance films on resin-bonded glass cloth have been investigated. Plastics laminates bonded with different polymers were coated with films of nickel–chromium alloy by vacuum evaporation and with sandwich films of gold between bismuth oxide layers deposited by sputtering. Glow discharge cleaning was essential before evaporation to make adherent films. Silicone resin bonded laminates were unsuitable for preparing stable resistors, because they had a large number of surface defects produced by strains arising during the curing process. Melamine bonded laminates were decomposed by ion bombardment during discharge cleaning or sputtering. The resistors were tested under a load of 1 W/in.^{2} of film area over a period of 3 months. Resistors which became non-conducting during the test were found to break down invariably along surface scratches in the base material. The most stable resistors on plastics bases were produced with epoxy or polyester resin bonded laminates, and with the metal films protected by a melamine lacquer. Nickel–chromium films up to 800 Ω/square and gold films up to 50 Ω/square reached a stable resistance value after an ageing period of about eight weeks.

INTRODUCTION

Work has already been carried out on the properties of conducting films on glass substrates. Alderson and Ashworth have described the preparation and properties of stable nickel-chromium films on glass.[1] They found that it was possible to obtain a predetermined resistance value up to about 300 Ω/square with an accuracy of ±0·1% and long-term stability to within ±½%. They recommended induction heating for evaporating thick films of nickel chromium alloy on to boro-silicate glasses, because nickel-chromium alloys readily dissolve the tungsten filaments, normally used for heating.

Gillham and others[2] have carried out work on the deposition of thin metal films sandwiched between metal oxide layers on glass. The conductivity of certain metal films is higher when deposited upon an oxide substrate, because the metal structure is less aggregated than when deposited directly on a glass surface. Thin gold films deposited on bismuth oxide have a conductivity almost approaching the bulk value. Ennos[3] has shown that similar results may be obtained using evaporation rather than sputtering for the deposition of the composite layers of oxide and metal. Some of the metal film resistance elements prepared by the foregoing techniques were stable up to about 200° C when using fused silica or glass substrates. The stability and conductivity were improved by heating the film to 300–350° C either during or after deposition to reduce disorder in the crystal lattice.

Evaporated film resistors on flexible base materials made from synthetic resins are being used in the United States, but their stability and temperature coefficient of resistance have not been given. Such resistors are of interest because they can be cut to different shapes for use as microwave attenuators, potentiometers, etc.

The aim of our investigation was the preparation of stable metal film resistors covering a wide range of resistance values using both evaporated and sputtered films on different resin bonded glass laminates. Many of the new laminated materials now becoming available have a high resistance to decomposition at temperatures approaching 250° C and a low outgassing rate in vacuum.

In the experiments to be described reactive sputtering was used for preparing the metal oxide films, and one of the first tests was carried out to determine whether a series of different laminated materials would decompose in the glow discharge, where they would be subjected to electron and positive ion bombardment. Nickel–chromium films were deposited by evaporation to make films with resistance values from about 50–800 Ω/square, and bismuth oxide–gold films were deposited by sputtering to give resistance values from about 10–100 Ω/square. Gold was chosen to give the very low values of resistance, in order to avoid using thick layers of nickel–chromium and the consequent danger of the film peeling from the base.

EXPERIMENTAL METHOD

Deposition plant. The deposition plant used for preparing the nickel–chromium films and the oxide–gold films was fitted with vapour sources and sputtering electrodes. The rotating workholder was used in conjunction with a special jig for holding specimen plates size 3 × 1 in. The sputtering system used was that described by Holland[4] in which the material to be deposited is sputtered from a pair of sector-shaped electrodes, each connected to the output of an h.t. transformer having a high leakage reactance. In operation, each electrode becomes negative during each cycle, and sputters on to the rotary workholder. By using two pairs of such electrodes, films of gold could be sputtered on previously sputtered bismuth oxide films without breaking the vacuum.

Bombardment of substrate materials. The substrate materials consisted of layers of woven fibre glass fabric bonded with synthetic resins under heat and pressure. At present such materials are used mainly for insulation purposes in electrical apparatus, because amongst other reasons they can be readily machined. Four different types of laminates bonded with polyester, melamine, epoxy, and silicone synthetic resins were obtained for experimental use in $\frac{1}{16}$ in. thick sheets. They can be obtained in sizes up to about 40 in.^{2}. A thin laminated sheet $\frac{1}{64}$ in. thick which could be cut to shape with scissors was obtained to determine whether resistors could be made with a flexible base. The sheets were cut into convenient slides of size 3 × 1 in. for experimental use.

The surfaces of the four different types of laminate were examined under an optical microscope at about 50× magnification. The melamine bonded laminate had a smooth surface with a few slight imperfections due to dust [Fig. 2(*a*)] but the surface of the polyester laminate was smoother. The epoxy-bonded laminate had a fairly smooth surface with a few defects which were probably caused by strains set up during the curing of the resin. The weave of the glass cloth was less visible in this sample, probably because the resin was more opaque. Strains were apparent in the silicone-bonded laminate. The board itself was not perfectly flat, and the surface was covered with imperfections set up during the curing of the resin. The appearance suggested that strain

was due to shrinkage, and the imperfections corresponded with the weave of the glass cloth. A metal film deposited on this surface would have either a high resistance, or be completely non-conducting. Fig. 1(*a*) is a micrograph of a typical uncoated surface at 29× magnification.

The four laminates were tested for breakdown under ionic bombardment during the sputtering of bismuth oxide films. A slide of size 3 × 1 in. of each material was mounted on a jig, so that the effect of ion bombardment on each could be compared under identical conditions. After only 2 min bombardment (3 kV, 1 mA/cm^2) the surface of the melamine had started to change colour, and after 5 min the laminate had become black. Cracks were apparent in the surface. After 15 min the melamine was completely disintegrated. There was little change in the colour of the other laminates and an oxide film of interference thickness was deposited on their surfaces.

(*a*)

(*b*)

Fig. 1. The surface of a silicone laminate (*a*) before and (*b*) after positive ion bombardment (×29)

Microscopic examination of the bombarded surfaces at about 50× magnification showed that the cracks in the silicone-bonded laminate were much deeper and wider [Fig. 1(*b*)]. The epoxy resin was found to have many irregular hair lines in the surface in addition to the few defects initially observed. The polyester laminate had some small pits and irregular lines. The surface of the melamine laminate was broken by deep cracks following the weave of the cloth. It was also covered with finer pitted lines suggesting further damage to the resin. The melamine surfaces before and after bombardment are shown in Fig. 2(*a*) and 2(*b*) respectively. The surface of all four samples showed some small metallic deposits, probably of unoxidized bismuth metal.

Protective lacquers. A small oven capable of operation at 400° C was used for annealing the films after deposition, and for curing the protective lacquers. Silicone and melamine lacquers were used for protection. The silicone lacquer required curing at such a high temperature (2 h at 250° C) that the substrate was damaged. The melamine resin was used in preference, because of its lower curing temperature (30 min at 140° C). The slides were placed in the oven after lacquering and cured under the appropriate conditions. They were then taken out and allowed to cool to room temperature before measuring the resistance again.

(*a*)

(*b*)

Fig. 2. The surface of a melamine laminate (*a*) before and (*b*) after positive ion bombardment (×29)

SPUTTERED GOLD FILMS

Preparation. Each slide was vapour degreased in isopropyl alcohol and transferred immediately to the coating chamber. The slides were divided into numbered batches of four containing one of each type of laminate to be tested. The four slides were placed in a jig on the rotary workholder. Bismuth oxide was sputtered for one minute before the deposition of gold and one minute after at the rate of 200 Å/min. Resistances were required in the range up to about 100 Ω/square so that the sputtering time of gold was varied between about 15 and 80 s. The rate of deposition was 4 Å/s.

The sputtering was carried out at 3 kV, and a maximum current of 250 mA was available, giving an effective current density of 1 mA/cm^2 of work area. The plant had two needle valves, one of which was used for the admission of oxygen or air for the sputtering of bismuth oxide and the other to admit argon for the sputtering of gold. After the deposition of bismuth oxide the chamber was pumped to 0·1 micron mercury to remove most of the residual oxygen before the admission of argon. When the chamber pressure reached 0·1 micron mercury, the diffusion pump was baffled down to give a pressure differential across the valve. The h.t. was switched to the required pair of electrodes and the rotary drive was switched on. Gas was admitted to the chamber until the discharge appeared. The needle valve was adjusted until the cathode dark space extended about two-thirds of the distance from the cathode to the work. The above procedure was used for sputtering both gold and bismuth oxide.

After a batch had been coated the slides were taken out and contacts were sprayed on to the ends using a compressed air atomizer which was made for spraying a 50/50 indium–tin alloy. The centre portion of the slide was masked to give end contacts about $\frac{1}{4}$ in. wide.

Results. Slides sputtered with bismuth oxide–gold–bismuth oxide were examined with the optical microscope at a magnification of about 100×. The defects in the surface of the silicone laminate were so extensive that the films of gold 300 Å thick remained discontinuous. The melamine slides showed a breakdown in the laminate which was most apparent for thick gold films. The formation of the cracks was similar to the piece which was broken down by ion bombardment. The epoxy and polyester laminates remained free from defects.

The initial resistance measurement on the whole series of gold and bismuth oxide films showed that:

(i) The surface of the silicone laminate was so irregular that conducting films were almost impossible to obtain. Treatment with a base coating of lacquer might solve this problem.
(ii) The melamine resins also gave high values of resistance; this was to be expected from the microscopic tests.
(iii) The film resistance could not be related directly to gold sputtering time. It was assumed that the surfaces were variable in smoothness, or that gold deposition was affected by outgassing from the resin surface.
(iv) Some glass slides were introduced for comparison purposes; lower values of resistance were obtained for the same film thickness, probably because the glass surface was more uniform than a resin surface. Films on the epoxy resins showed the lowest values of resistance. Films on the polyester and the melamine laminates were more disordered.
(v) Baking the films to 140° C increased the conductivity.

EVAPORATED NICKEL–CHROMIUM FILMS

Preparation. The same cleaning method was used. Four slides were coated in each cycle, using the same jig as in the sputtering experiments. The silicone laminate was not included in this series of tests, because of its discontinuous surface. The silicone slide in each batch was replaced by glass to obtain a comparison of the resistance values of the deposits. The gold cathodes were replaced by cathodes of super-pure aluminium for ionic cleaning. Air was admitted to carry out the ion bombardment under the same conditions of voltage and current as were used for sputtering. Some of the slides were not discharge cleaned for the purpose of comparison.

Nickel–chromium alloy (80 : 20) wire 20 s.w.g. was evaporated from helical tungsten filaments made from three strands of 0·5 mm diameter using an l.t. supply of 60 A at 12 V. Several filaments were required to evaporate enough metal to obtain the lowest film resistance and a rotating turret head of sources was fitted to the plant. Four filaments could be evaporated during each processing cycle. The evaporation was carried out at a pressure of less than 0·3 micron mercury. Care was taken to ensure that, after evaporation, air was not admitted to the chamber too quickly otherwise the filaments were oxidized, and the next run contaminated. The slides were sprayed with indium alloy contacts after evaporation as before and the resistances were measured and tabulated. Thirteen batches of resistors were prepared in this manner together with twelve batches which were not discharge cleaned. They were divided into two groups having similar resistance values. One group was protected with melamine lacquer. The resistances were again measured and tabulated after lacquering.

Results. The slides which had not been discharge cleaned had a very poor film adhesion, and it was difficult to obtain thick films without peeling. It was concluded that discharge cleaning was essential. The slides which had not been so treated were considered unsuitable for further experiments.

The measurements of resistance made on glow discharge cleaned glass and resin surfaces showed that in general:

(i) Conducting films on glass were less disordered than on the resin. In most cases the resistance value of a film on glass was at least 50% less than the corresponding film on a laminated resin.
(ii) The polyester and epoxy resins gave about the same results, whereas the melamine laminate was unsatisfactory.
(iii) Lacquering and baking the slides at 140° C had no effect on the films on glass. Films on the laminated resins showed an increase in resistance after this treatment. This was probably because the latter films had a less dense structure into which the lacquer could penetrate.

STABILITY TESTS ON BOTH SPUTTERED AND EVAPORATED FILMS

Of the 150 resistors produced by different methods only 60 were considered suitable for stability test. Slides which had not been discharge cleaned were rejected because of their poor film adhesion. Slides made from the silicone laminate were also excluded because most of them were already non-conducting. The melamine laminates were rejected because of their poor resistance to heat, and because of their breakdown under ionic bombardment.

The resistors were tested for stability over a period of three months. During this time they were under continuous electrical and thermal stress, dissipating about 1 W/in.^{2} of film area. These conditions were obtained by connecting each resistor to a suitable tapping on an auto-transformer, which was arranged to give an output variable in 1 V steps up to 250 V (50 c/s). When dissipating 1 W/in.^{2}, the slides were running at a temperature 40°–50° C above ambient. The resistors were mounted for convenience on an insulated board, and held in position by spring clips, which also served to make contact to the sprayed electrodes of each slide. The measurements of resistance were made at room tempera-

ture using a Wheatstone bridge capable of giving an accuracy of $\pm 0{\cdot}1\%$ but variable contact resistance prevented this from being realized. Slight day-to-day variations showed that $\pm \frac{1}{2}\%$ would be a nearer estimate of the accuracy of measurement.

During the first two weeks of the life test the resistors were measured every day because resistance changes were greater during the initial life. Measurements were then made at intervals of one week for the remainder of the test period. Gold films not protected by lacquer were found to be very unstable and have not been shown in the results.

The percentage change in resistance was calculated for each measurement. Average values of resistance change were then obtained for all resistors of the same type, and the results have been plotted in Fig. 3.

In Fig. 3(*a*) the results have been given for the first three weeks of test, during which the significant changes in resistance had taken place. Some results have not been shown, for the sake of clarity, because they lie so close to the abscissa. Fig. 3(*b*) shows the results over the full twelve-week period, but the scale of the ordinate has been increased to show the resistance changes of the more stable resistors.

Averaging the percentage changes of at least six resistors of the same type was found to be a fairly reasonable way of presenting the results, because there was no apparent relationship between resistance change and resistance value within the ranges considered (10–800 Ω/square) except in the case of unprotected nickel–chromium films on the epoxy and polyester resin bonded laminates. Unprotected films of nickel–chromium on the epoxy resin (*A*) with resistance less than about 40 Ω/square increased in resistance by an average of 100% compared with only 12% for films higher than

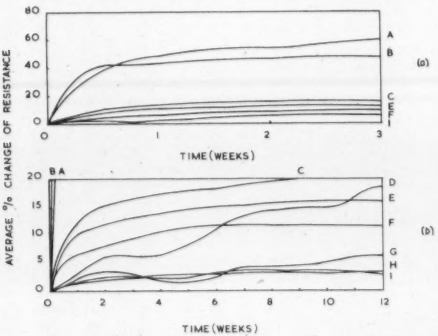

Fig. 3. The percentage change in resistance of the following types of resistor is shown against time. The scales in (*a*) and (*b*) have been changed to show different parts of the curves more clearly. Average values have been obtained from at least six resistors of each type: *A*, unprotected nickel-chromium films up to 40 Ω/square (epoxy base); *B*, unprotected nickel–chromium films up to 800 Ω/square (polyester base); *C*, Melamine protected nickel–chromium films of up to 800 Ω/square (polyester base); *D*, Melamine protected gold–bismuth oxide films up to 50 Ω/square (epoxy base); *E*, Melamine protected nickel–chromium films up to 800 Ω/square (epoxy base); *F*, Unprotected nickel–chromium films from 40–800 Ω/square (epoxy base); *G*, Melamine protected gold–bismuth oxide films up to 50 Ω/square (polyester base); *H*, Melamine protected nickel–chromium films up to 150 Ω/square (glass base); *I*, Unprotected nickel–chromium films up to 150 Ω/square (glass base).

40 Ω/square (*F*). Unprotected films of nickel–chromium on the polyester resin (*B*) showed a similar effect, the percentage resistance change decreased for the higher resistance values. These results may have been obtained because the thicker films were produced by the evaporation from four filaments fired in sequence on to a comparatively rough surface, giving a modified grain structure, or because of strains set up in the formation of the film. Films deposited on glass slides during the same evaporation showed no such effects. Unprotected films above about 1000 Ω/square were very unstable; some became non-conducting during the first day.

Fig. 3 shows that most of the resistance change occurs during the first few days, representing the initial ageing of the film. Then there is a gradual increase. After a period of three months the resistance has reached a steady value for films which have been protected with lacquer. This is also true for unprotected nickel–chromium films on glass (*I*). Unprotected nickel–chromium films on the polyester laminate (*B*) appear to be slowly increasing, as also are the unprotected films under 40 Ω/square on the epoxy resin base (*A*). Unprotected films of nickel–chromium over 40 Ω/square on the epoxy resin (*F*) are rather more stable and are reaching a constant resistance value. Gold films less than about 50 Ω/square protected by lacquer (*D*) and (*G*) are very slowly increasing.

Measurements of temperature coefficient of resistance were made on several of the completely aged resistors, but no relationship to substrate surface or resistance value could be found as in earlier work.[5] Within the temperature range 20–110° C, the order of value of temperature coefficient was found to be $0{\cdot}15\%/°$ C for gold and $0{\cdot}02\%/°$ C for nickel–chromium.

Analysis of resistance failures. Seven of the resistors failed during the period of stability test. These were examined under the microscope in order to discover the cause of failure. It appeared that failure could in all cases be attributed to excessive current density.

The current flowing for a dissipation of 1 W/in.^{2} is an order less than the observed breakdown current density of about 10^6 A/cm^2 and it was necessary for the film or base to be scratched before breakdown occurred. Most films which broke down in the tests were found to be scratched. When the scratches were almost completely overlapping, leaving a very short conducting path, then breakdown was immediate and could be attributed to excessive current density. This effect is shown in the micrograph. Fig. 4 at $22{\cdot}5\times$ magnification.

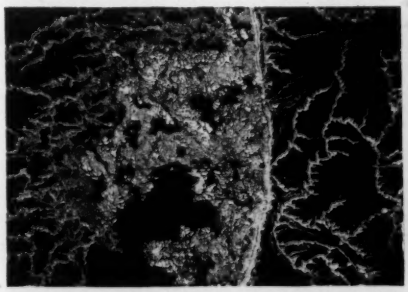

Fig. 4. Film breakdown caused by excessive current ($\times 22{\cdot}5$)

The scratch can be seen as a continuous line, and the region of breakdown is marked by the starred lines where the film has burned away.

Where a much wider conducting path occurred between the scratches, the base became overheated, which was revealed by the discoloration of the resin to a darker colour on the back of the slide. Microscopic examination showed a regular breakdown pattern due to rupture of the film, possibly caused by the differential expansion of the base and the film. This was found to be characteristic of the type of breakdown caused by slow overheating. Fig. 5 is a micrograph showing this effect at 38× magnification.

Fig. 5. Film breakdown caused by overheating the base (×38)

CONCLUSIONS

The results show that melamine protected films of nickel–chromium alloy up to about 800 Ω/square and sandwich films of gold between bismuth oxide up to about 50 Ω/square, deposited on to certain epoxy and polyester resin bonded laminates can be stabilized by ageing. The stable value may be as high as 20% above the initial resistance, but further serious change is unlikely if the films are kept within the rating of 1 W/in.^{2} Tropical tests have not been carried out, but the results so far obtained indicate that there should be many uses for this material.

ACKNOWLEDGEMENTS

Acknowledgements are made to Mr. A. S. D. Barrett, Technical Director, Edwards High Vacuum for permission to publish this report, to Mr. L. Holland, Head of the Vacuum Coating Laboratory for his guidance throughout this work, and to Mr. A. W. Agar of Aeon Laboratories for producing the micrographs.

REFERENCES

(1) Alderson, R. H., and Ashworth, F. *Brit. J. Appl. Phys.*, **8**, p. 205 (1957).
(2) Gillham, E. J., Preston, J. S., and Williams, B. E. *Phil. Mag.*, **46**, p. 1051 (1955).
(3) Ennos, A. E. *Brit. J. Appl. Phys.*, **8**, p. 113 (1957).
(4) Holland, L. *Nature [London]*, **177**, p. 1229 (1956).
(5) Holland, L., and Siddall, G. *Vacuum*, **3**, p. 375 (1953).

Cooling of a spinning thread-line

By E. H. Andrews, B.Sc., A.Inst.P.,* Imperial Chemical Industries Ltd., Fibres Division, Harrogate, Yorks.

[*Paper received* 1 *September*, 1958]

The cooling of an extruded stream of molten polymer is considered for the case in which the solidified thread-line is "wound up" some distance from the spinneret. The heat flow equations are set up and solved approximately with the aid of empirical data. The predicted temperature-distance relations appear to be substantially correct, though the predicted radial temperature distribution in the thread-line is only accurate to within 20%.

In the process of "melt spinning" a molten material is forced through an orifice (or spinneret) to form a fine thread, which then cools and solidifies. In the manufacture of polymer fibres the cooling is accompanied by a stretching process, induced by winding up the solidified fibre at high speed some way below the spinneret. It has been recognized that the rapid cooling of the spinning thread-line must affect the properties of the spun fibre, and it is desirable to study the manner in which it occurs.

The cooling of melt spun glass fibres has been recently discussed by Anderson,(1) and various problems solved in terms of the velocity of the thread-line, its radius R and the flow rate $Q = \pi R^2 v$. The case of polymer spinning is one stage more complicated, in that the high wind-up speed applied at the end of the thread-line causes both v and R to be functions of time (or distance x below the spinneret).

This paper is an attempt to solve, with the use of certain empirical data obtained with Terylene, the cooling problem for a "wound-up" thread-line.

* Now at The British Rubber Producers' Research Association, Welwyn Garden City, Herts.

STATEMENT OF THE PROBLEM

The spinning conditions are defined by the following known parameters:

the extrusion velocity	V_0	
the final velocity	V	
the extrusion temperature	T_0	abs.
the environmental temperature	T_e	abs.
the flow rate (volume extruded per unit time)	Q	

The following properties of the polymer are assumed known:

thermal conductivity	K_p
density	ρ
surface emissivity	ξ
thermal capacity	C

It is necessary to have further empirical information on two important matters. Firstly, the thread-line diameter, and thence its velocity, must be known as a function of distance x below the spinneret. A method for obtaining such data has been successfully used by the author.(2) Secondly, the

form of the function F, relating the forced convective heat loss to the Reynolds' number for the moving thread-line, must be known (see next section). This has been determined empirically for thin wires (Ref. 3, p. 250) and we shall assume these data to be valid for our own case.

Given this information we wish to find the temperature at any point P within the spinning thread-line, the co-ordinates of P being given as r, the radial distance from the thread-line axis, and x, the distance measured down the thread-line from the spinneret. We shall find that, with certain approximations, it is possible to obtain a solution which gives good agreement with an experimental check.

GENERAL OUTLINE OF THE SOLUTION

We consider initially an element of the thread-line, of length δx and radius $R(x)$, fixed in space (Fig. 1). If the

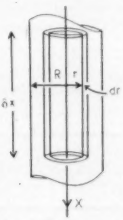

Fig. 1. Thread-line element

absolute temperature at any point is T, we define the excess temperature

$$\theta = T - T_e \tag{1}$$

Instead of using the radial distance r of a point from the axis of the thread-line, we use the dimensionless quantity

$$u(x) = r/R(x) \tag{2}$$

With the variables in this form it is a simple matter to set up the heat flow equation

$$Z\frac{\partial\theta}{\partial x} = \frac{1}{u}\frac{\partial}{\partial u}\left(u\frac{\partial\theta}{\partial u}\right) + R^2\frac{\partial^2\theta}{\partial x^2} \tag{3}$$

where $Z = Q\rho C/\pi K_p$ and is constant. The term $R^2(\partial^2\theta/\partial x^2)$ represents diffusion of heat along the thread-line axis. Because of the magnitude of R

$$R^2\frac{\partial^2\theta}{\partial x^2} \ll \frac{1}{u}\frac{\partial}{\partial u}\left(u\frac{\partial\theta}{\partial u}\right)$$

and may thus be neglected.

The boundary conditions for this equation are

$$\theta = \theta_0 \text{ for all } u \text{ at } x = 0 \tag{4}$$

and heat loss from surface per unit length, per second, per degree excess temperature

$$-H(x) = 2\pi K_p(u/\theta)(\partial\theta/\partial u) \text{ at } u = 1 \tag{5}$$

It is at this point that difficulties arise, for we see that the radial boundary condition (5) is dependent upon x. It follows that equation (3) is not separable in x and u.

HEAT LOSS FROM THE SURFACE

The heat H_1 lost from the surface of the thread-line per unit length, per second, per degree excess temperature by forced convection in air is given[3] by dimensional analysis

$$H_1/K = F(vd/\nu) \tag{6}$$

where K is the thermal conductivity of air, $v(x)$ the velocity of the thread-line, $d(x)$ the diameter of the thread-line, ν the kinematic viscosity of air, and F a function which must be found empirically. From the data given by Roberts (Ref. 3, p. 251) we can express equation (6) by

$$H_1/K = [\alpha(vd/\nu)]^q \tag{7}$$

where α, q are constant over quite a wide range of Reynolds number vd/ν. Their value will depend upon the range of Reynolds' number encountered in an actual case.

Now the continuity equation of the thread-line is

$$Q = (\pi d^2/4)v \tag{8}$$

so that
$$H_1/K = [(\alpha/\nu)v^{\frac{1}{2}}(4Q/\pi)^{\frac{1}{2}}]^q$$
or
$$\left.\begin{aligned} H_1 &= G_1 v^{q/2} \\ G_1 &= K[(2\alpha/\nu)(Q/\pi)^{\frac{1}{2}}]^q \end{aligned}\right\} \tag{9}$$

The radiation losses may be calculated separately and are found to be negligible except for low values of x. The heat radiated per second from the thread-line surface per unit length is

$$P = 2\pi R\sigma\xi(T^4 - T_e^4)$$

where σ is Stefan's constant. Since $R = (Q/\pi v)^{\frac{1}{2}}$ we have

$$P = 2\sigma\xi(\pi Q/v)^{\frac{1}{2}}(T^2 + T_e^2)(T + T_e)(T - T_e)$$

and designating

$$(T^2 + T_e^2)(T + T_e) \equiv NT_e^3$$

where N will vary from 4 to 15 as T varies from T_e to $2T_e$, we obtain the heat lost per unit length, per second, per degree excess temperature as

$$\left.\begin{aligned} H_2 &= G_2 v^{-\frac{1}{2}} \\ G_2 &= 2\sigma\xi NT_e^3(\pi Q)^{\frac{1}{2}} \end{aligned}\right\} \tag{10}$$

Since the conduction along the thread-line can be shown to be negligible, we have

$$H = (H_1 + H_2) = (G_1 v^{q/2} + G_2 v^{-\frac{1}{2}}) \tag{11}$$

Or, more simply, since v is given as an empirical function of x,

$$H = H(x) \text{ known empirically.}$$

This is our second boundary condition to equation (3).

APPROXIMATING THE HEAT FLOW EQUATION

Since equation (3) is not fully separable, we put

$$\theta(x, u) \equiv S(x, u)\tau(x) \tag{12}$$

This gives
$$\frac{Z}{\tau}\frac{\partial\tau}{\partial x} = \frac{1}{S}\left(\frac{1}{u}\frac{\partial S}{\partial u} - Z\frac{\partial S}{\partial x} + \frac{\partial^2 S}{\partial u^2}\right) \tag{13}$$

If we equate both sides of equation (13) to a quantity $-p^2$, this quantity must be a function of x only.

$$\left.\begin{aligned} \frac{Z}{\tau}\frac{\partial\tau}{\partial x} &= -p^2(x) \\ \tau(x) &= a\exp\left[-\int_0^x (p^2/Z)dx\right] \end{aligned}\right\} \tag{14}$$

And
$$\frac{\partial^2 S}{\partial u^2} + \frac{1}{u}\frac{\partial S}{\partial u} + S\left(p^2 - \frac{Z}{S}\frac{\partial S}{\partial x}\right) = 0 \tag{15}$$

We now assume
$$\frac{Z}{S}\frac{\partial S}{\partial x} \ll p^2 \tag{16}$$

So that equation (15) reverts to Bessel's equation of zero order with the solution

$$S(\rho, x) = b(x)J_0(\rho) \tag{17}$$

where the substitution $\rho = pu$ has been made. The assumption (16) will be examined later. The general approximate solution is then,

$$\theta(x, \rho) = B(x)J_0(\rho) \exp\left[-\int_0^x (p^2/Z)dx\right] \qquad (18)$$

where $B = ab$. The value of B must be found from the boundary conditions, and it will be seen presently that it possesses an infinity of discrete values B_i over which the solution must be summed.

APPLYING THE BOUNDARY CONDITIONS

The radial boundary condition is

$$H(x) = -2\pi K_p \frac{u}{\theta} \frac{\partial\theta}{\partial u}\bigg|_{u=1} \qquad (5)$$

Substituting the value of θ given by equation (18)

$$\frac{H(x)}{2\pi K_p} = -\frac{J_0'(\rho)}{J_0(\rho)}$$

where J_0' is the derivative with regard to u of J_0. Using the property.

$$J_0'(ax) = -aJ_1(ax)$$

and since $\rho \equiv up$, and $u = 1$ we obtain

$$\frac{H(x)}{2\pi K_p} = p\frac{J_1(p)}{J_0(p)} \qquad (19)$$

For any value of $H(x)$, and therefore of x, this equation will possess an infinite number of roots p_j, the complete solution for θ being the summation over j.

The remaining boundary condition, that $\theta = \theta_0$ for all values of u at $x = 0$ gives, from equation (18),

$$\theta_0 = \Sigma B_j J(p_j u)$$

By multiplying both sides by $uJ_0(p_j u)$, integrating over u and using the orthogonal properties of the Bessel function, we finally obtain

$$B_j = \frac{2\theta_0}{p_j} \frac{J_1(p_j)}{J_0^2(p_j) + J_1^2(p_j)} \qquad (20)$$

Giving

$$\theta = 2\theta_0 \Sigma \frac{J_1(p_j)J_0(p_j u)}{p_j[J_0^2(p_j) + J_1^2(p_j)]} \exp\left(-\int_0^x \frac{p_j^2}{Z}dx\right) \qquad (21)$$

where the values of p_j are the roots of equation (19).

THE SOLUTION IN AN ACTUAL CASE

The problem of applying the solution to an actual case consists of evaluating the function $H(x)$, and of justifying the approximation of equation (16).

Evaluation of $H(x)$. We require to know the values of G_1, G_2, q and $v(x)$, which then define $H(x)$ from equation (11). The function $v(x)$ may be derived numerically from the empirical diameter—distance curve, which takes the form shown in Fig. 2 for a particular thread-line of known flow rate Q, and initial and final velocities V_0 and V. The Reynolds number range is readily found from the same data, and the values, $\alpha = 10$, $q = 0{\cdot}38$, chosen for equation (7). Using known thermal properties of this material we find eventually,

$$G_1 = 1{\cdot}40 \times 10^{-4} \text{ c.g.s. (cal)}$$
$$G_2 \simeq 1{\cdot}60 \times 10^{-4} \text{ c.g.s. (cal)}$$

Since G_1 and G_2 are nearly equal, the relative importance of the convection and radiation terms $H_1(x)$ and $H_2(x)$ is governed by their dependence upon v [see equation (11)]. With $V_0 = 17{\cdot}1$ cm/s and $V = 2030$ cm/s the radiation term evidently decreases rapidly with increasing values of x, soon becoming negligible. Table 1 gives $v(x)$, $H_1(x)$, $H_2(x)$ and $H(x)$ as functions of x for the particular thread-line chosen. In the table the radiation term $H_2(x)$ has been corrected for varying values of N [see equation (10)].

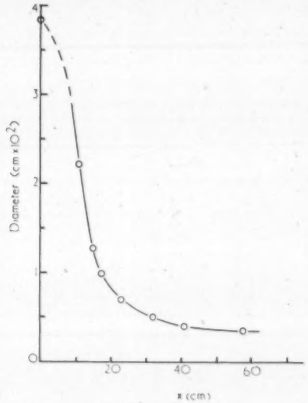

Fig. 2. Empirical diameter-distance curve for a chosen thread-line with flow rate $Q = 1{\cdot}95$ cm³/s

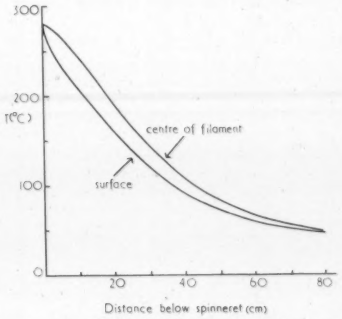

Fig. 3. Calculated temperature-distance curves for centre ($u = 0$) and surface ($u = 1$) of a spinning thread-line

The excess temperature. The function $H(x)$ was plotted out graphically and used to obtain the roots p_j of equation (19) at intervals of x of 5 cm. These roots are tabulated as functions of the left-hand side of equation (19) by Carlslaw and Jaeger.[4]

Table 2 shows the numerical calculation of θ from equation (21), for the two special cases $u = 0$ (thread-line axis) and $u = 1$ (thread-line surface). Only the first term in the summation of equation (21) is shown, but correction has been applied at $x = 5$ cm for higher terms in the summation. For $x > 5$ cm all higher terms are negligible.

Fig. 3 is a graph of temperature (θ + room temperature) against x for an extrusion temperature of 280° C ($\theta_0 = 240°$ C, room temperature = 40° C. "Room temperature" here

Table 1. *Heat loss from the thread-line surface*

v (ft/min)	v (cm/s)	x (cm)	$\gamma^{0\cdot19}$	$e^{-0\cdot5}$	$H_1(x)$	$H_2(x)$	Adjusted* $H_2(x)$	$H(x)$
33·6	17·1	0	1·17	0·242	0·280	0·044	0·044	0·324
100	51	11	2·11	0·140	0·346	0·025	0·022	0·368
300	153	15	2·60	0·081	0·427	0·015	0·012	0·439
500	254	17·5	2·86	0·063	0·469	0·011	0·009	0·478
1000	508	23	3·27	0·044	0·536	0·008	0·006	0·542
2000	1015	32	3·72	0·031	0·610	0·006	0·004	0·614
3000	1525	41	4·03	0·026	0·662	0·005	0·002	0·664
4000	2030	58	4·25	0·022	0·697	0·004	0·001	0·698

* Adjustment is for variation of N as T falls from its maximum value to room temperature. See equation (10).

Table 2. *Calculation of temperature distribution*

x(cm)	p_1	$\int_0^x p_1^2 dx$	Exponential term	$\frac{J_1}{2p_1(J_0^2+J_1^2)}$	$\frac{J_1J_0}{2p_1(J_0^2+J_1^2)}$	θ/θ_0 core	θ/θ_0 surface	T (°C) core	T (°C) surface
0	0·77	0	1	1·07	0·92	1*	1*	280	280
5	0·79	3·1	0·884	1·08	0·92	0·940*	0·805*	269	235
10	0·81	6·2	0·780	1·09	0·91	0·850	0·710	244	210
15	0·89	9·8	0·672	1·10	0·90	0·740	0·598	218	184
20	0·95	14·1	0·569	1·11	0·89	0·632	0·506	192	161
25	0·99	18·8	0·472	1·12	0·88	0·528	0·415	167	140
30	1·02	23·9	0·385	1·13	0·87	0·435	0·331	144	119
35	1·04	29·2	0·310	1·14	0·86	0·353	0·267	125	104
40	1·06	34·7	0·249	1·15	0·85	0·286	0·212	109	91
45	1·07	40·4	0·198	1·15	0·84	0·228	0·166	95	80
50	1·08	47·1	0·151	1·15	0·84	0·174	0·127	82	73
55	1·087	52·1	0·122	1·16	0·84	0·142	0·103	74	64
60	1·087	59·0	0·094	1·16	0·84	0·109	0·079	66	59
65	1·087	65·9	0·072	1·16	0·84	0·084	0·061	60	55
70	1·087	72·8	0·055	1·16	0·84	0·064	0·046	55	51
75	1·087	79·7	0·045	1·16	0·84	0·052	0·038	52	49
80	1·087	86·6	0·031	1·16	0·84	0·036	0·026	48	46

* Corrected for higher terms in summation.

means that of the air surrounding the thread-line. This air is drawn down by the filaments from the region of the spinning "head" and is very warm). The Bessel function variation of temperature across the radius of the thread-line is indicated in Fig. 4 for several values of x.

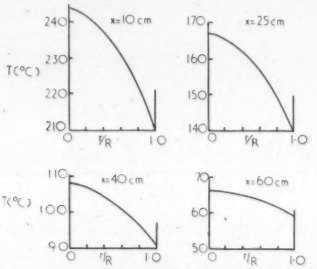

Fig. 4. Calculated temperature distributions across the thread-line at various distances from the spinneret

Errors due to approximation. The approximation

$$\frac{Z}{S}\frac{\partial S}{\partial x} \ll p^2 \qquad (16)$$

may now be tested, remembering that

$$aS = B(x)J_0(\rho)$$

so that

$$\frac{Z}{S}\frac{\partial S}{\partial x} \simeq \frac{Z}{BJ_0}\frac{\Delta(JB_0)}{\Delta x} \equiv \psi$$

Using the particular value of $Z = 25$ cm for this thread-line and taking the first root p_1 for p, we find from Table 2

$$\psi|_{u=0} \simeq 0{\cdot}05$$

$$\psi|_{u=1} \simeq -0{\cdot}05$$

for x from 0 to 40 cm and smaller elsewhere, compared with values of 0·5 to 1·2 in p_1^2. The approximation error is thus 10% or less. The effect of this error can be seen from equation (15).

If p_j' is the value obtained from the boundary equation, and hitherto considered to equal the real p_j, we have

$$p_j^2 = p_j'^2 + \psi \qquad (22)$$

Since it is p_j and not p_j' which appears in the exponential term (14), our approximation predicts too slow a fall of this term at the filament core ($u = 0$) where ψ is positive, and too fast a fall at the filament surface ($u = 1$) where ψ is negative. A correction may clearly be applied from equation (22) to improve the approximation.

At core and surface the error is appreciable, though because of the factor $1/Z$ the 10% error shifts the temperature-distance curve along the x axis by only about 2·5 cm. More important, however, is the fact that at some value of u close to 0·5, ψ must be zero, and our assumption exact.

It may be concluded then that whilst the radial temperature distribution as calculated shows too large a temperature differential between surface and core (by up to 20%), the mean temperature-distance curve is substantially accurate.

GENERAL COMMENTS

The apparent success of the approximate methods outlined above is fortunate because of the difficulty of attempting a *numerical* solution of equation (3). This difficulty arises because of the great difference in magnitude between the radial and axial distance scales. (The thread-line is at most points only some 20–100 μ in diameter, compared with a length of more than 100 cm.) Convergent difference equations seem to demand that increments in r and in x be of similar magnitude, which would require thousands of increments along the length of the thread-line.

The empirical data for diameter as a function of x show fairly clearly the point at which the diameter becomes constant. This almost certainly occurs when the temperature in the thread-line approaches the glass transition temperature, which for amorphous Terylene is about 80° C. For the thread-line treated, this "freezing" occurred at $x = 58$ cm, whilst our calculated temperature curve predicts a temperature of 80° C at $x = 51$ cm (centre of filament).

This provides an agreeable indication of the theoretical treatment's validity. It would be interesting to examine the possibility of a more exact mathematical treatment which would give the true radial temperature distribution in the thread-line, for the severity of the radial gradient (e.g. more than 4000° C/cm at $x = 25$ cm), is likely to play an important role in the spinning process.

ACKNOWLEDGEMENT

The author is indebted to the Board of Imperial Chemical Industries Ltd., Fibres Division, for permission to publish this work.

REFERENCES

(1) ANDERSON, O. L. *J. Appl. Phys.*, **9**, p. 29 (1958).
(2) ANDREWS, E. H. Unpublished work.
(3) ROBERTS, J. K. *Heat and Thermodynamics* (London: Blackie and Son, Ltd., 1940).
(4) CARSLAW, H. S., and JAEGER, J. C. *Conduction of Heat in Solids*, p. 379 (London: Oxford University Press, 1947).

Interaction between two equal-sized equal-settling spheres moving through a viscous liquid

By G. F. EVESON, Ph.D., E. W. HALL, Ph.D., Grad. Inst.P.,* and S. G. WARD, Ph.D., M.Sc., D.I.C.,
Department of Mining, The University, Edgbaston, Birmingham

[*Paper first received* 16 *October*, 1957, *and in final form* 25 *July*, 1958]

Details are given of an experimental investigation of the interaction between two equal spheres settling through a viscous liquid in the presence of each other at various distances between sphere centres and with the line of centres at various angles to the horizontal. The results are represented by simple empirical equations. These results are discussed in relation to the theoretical predictions of other workers.

The nature of particle-particle interactions which affect the properties of suspensions is not well understood. Theoretical approaches to the simplest problem of this type, namely the interaction between two identical spheres moving in a viscous medium, have been made by Smoluchowski,(1) Stimson and Jeffery(2) and Burgers(3) but it appears that no experimental investigation of such a system has been made.

In this paper is described that part of an experimental investigation of the interaction between two equi-settling spheres, which are also equi-sized, settling under conditions of laminar flow. It is hoped in a second paper to describe similar work on the interaction of two equal-settling spheres which are not equi-sized.

THE INTERACTING SYSTEM

To ensure that a single sphere falls under conditions of laminar flow in an infinite expanse of liquid the Reynolds number should not exceed 0·05 and should preferably be below 0·02. To obtain such low Reynolds numbers a liquid medium of high viscosity is required together with small spheres of density only slightly greater than that of the fluid.

The fluid used was castor oil having a viscosity of about 10 poises and a density of about 0·96 g/ml. at 20° C. Pairs of spheres of Perspex and of cellulose nitrate were prepared in compressed air mills similar in design to those used by Whitmore.(4) Table 1 contains a summary of the details of the pairs of spheres used in the investigation.

The density of each sphere was obtained by suspending the sphere in a liquid the density of which was adjusted until the sphere remained in suspension; the density of the liquid was then determined by means of a pyknometer. The diameters of the spheres were determined from micrometer measurements across fifty different diameters of each sphere.

Table 1. *Details of spheres used*

Material	*Code*	*Density* (g/ml.)	*Mean diameter* (cm)*	*Standard deviation* (10^{-3} cm)
Perspex	P.1	1·192	0·327	2·0
		1·193	0·326	1·0
Perspex	P.2	1·190	0·344	6·9
		1·191	0·345	2·4
Perspex	P.3	1·192	0·418	1·0
		1·192	0·419	1·0
Perspex	P.4	1·191	0·449	1·3
		1·192	0·451	1·3
Perspex	P.5	1·192	0·471	2·2
		1·192	0·477	2·8
Cellulose nitrate	C.N.1	1·389	0·277	1·3
		1·388	0·278	1·4

* Mean of 50 observations for each sphere.

* Now at Armstrong Siddeley Motors Ltd., Coventry.

APPARATUS

A vacuum release system, in which a sphere is held on to the end of a tube by suction provided by a filter pump and released by breaking the vacuum and applying a small positive pressure, was found to be suitable for controlled release of a sphere. By using two tubes connected to a single vacuum line it was found possible to release two spheres simultaneously causing virtually no disturbance of the fluid at release. Provision was made to ensure that no moisture entered the system when the positive pressure was applied. A photograph of the release tubes and their mounting is shown in Fig. 1. This release device was suitable for

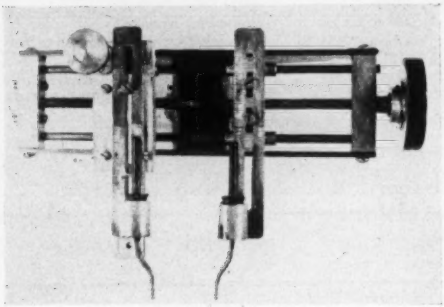

Fig. 1. The sphere-release device

all initial positions of the spheres except for that where one sphere was to fall vertically behind another. For this condition the release mechanism was a vertical tube of bore slightly greater than the diameter of the spheres; one end dipped beneath the surface of the liquid whilst the other was connected to the vacuum system. A small quantity of liquid was sucked into the tube and the spheres were retained in this liquid. On release the spheres and trapped liquid passed into the bulk of the fluid. Each release mechanism could be attached centrally to a cylindrical wooden lid which fitted rigidly on a cylindrical Pyrex glass vessel 10·25 in. diameter and 15·5 in. high.

The cylindrical vessel containing castor oil was placed in a thermostatically-controlled bath filled with water to about 1 in. above the level of the castor oil in the vessel and maintained within $\pm 0{\cdot}1^\circ$ C at either 20° C or 25° C. Resistors placed around the underside of the lid and connected to the d.c. mains through a rheostat enabled the air beneath the lid to be maintained at the same temperature as the castor oil. The motion of the spheres was followed by means of a short focus cathetometer with vernier attachments.

EXPERIMENTAL METHODS

Experimental techniques differed slightly according to the spheres used and the angles at which they fell, but the following details were common to all experiments.

The time of fall of the spheres over known distances was determined by means of stop watches reading to 0·1 s. The spheres were released about 3 cm beneath the surface of the castor oil after a few seconds had elapsed to allow them to attain temperature equilibrium with the castor oil. The spheres travelled a distance of at least 6 cm from the point of release before the timing of their motion was commenced. Such timing ceased at a distance of at least 6 cm from the base of the vessel; in this way it was ensured that the observed motion was always uniform and that initial acceleration and final deceleration did not influence the observed motion.

1. *Spheres falling at an angle of* 0° *between line of centres and horizontal*

The positions of the release tubes were adjusted so that the spheres under test were in the same horizontal line and just touching. The spheres were released together and timed in their fall over 20 cm. The time of fall of one member of the pair of spheres traversing the same path alone was then determined. These two operations were then repeated until three sets of consistent timings were obtained. The experiments were then repeated with the spheres at various distances apart, the distances being increased until the spheres, when falling together, fell with velocities comparable with those when the spheres were falling alone. The velocities were determined from the times and distance of fall.

The distance between the sphere centres was determined by two methods; firstly from the number of revolutions turned through by the threaded spindle to which the release tubes were attached and secondly by means of eyepiece graticule readings of the positions of the spheres as they passed the fiducial marks. The eyepiece graticule had previously been calibrated by means of a scale placed in the plane of fall of the spheres. The positions of the spheres when falling individually were also noted in a similar way; hence it was possible to detect any deviation from the vertical in the alignment of the cathetometer.

In addition to the experiments carried out at 20° $\pm 0{\cdot}1^\circ$ C employing all the pairs of spheres, the spheres P.3 were used for experiments at 25° $\pm 0{\cdot}1^\circ$ C. In all cases the spheres were observed to travel vertically with uniform velocities.

2. *Spheres falling at an angle of* (i) 30°; (ii) 45°; *and* (iii) 60° *between line of centres and the horizontal*

All experiments were carried out at 20° $\pm 0{\cdot}1^\circ$ C.

(i) 30° *angle*. Spheres P.3 were used. The positions of the release tubes were adjusted such that the lines of centres of the spheres were inclined at an angle of 30° to the horizontal with the desired distance D between sphere centres. The left-hand tube (Fig. 1) was provided with a rack and pinion device for vertical adjustment, the distance being measured with a Mercer dial gauge (calibrated in 0·01 mm divisions and with a total traverse of 25 mm).

Each of the spheres was timed in its fall of 19 cm by employing two stop watches. The spheres were observed to move in straight lines with equal uniform velocities higher than when falling individually but the paths were deflected from the vertical by a small angle ϵ in the direction of the leading sphere. To determine this angle the positions of the spheres were observed at the initial and final fiducial marks. By means of a previous calibration the distance each sphere had moved horizontally from the vertical was determined. Experiments were carried out, as before, at various distances between sphere centres.

(ii) 45° *angle*. Spheres P.3 and C.N.1 were used; the experimental technique was as for the 30° angle.

(iii) 60° *angle*. Spheres P.2 and P.3 were used. The motions of the spheres were followed throughout their complete fall, excluding the initial period of acceleration, instead of timing over a fixed distance. Distance-time graphs were plotted which were linear and this confirmed

previous qualitative experiments that the spheres always fell with uniform velocity, and that their trajectories, although displaced from the vertical, were always linear.

3. *Spheres falling at an angle of 90° between line of centres and the horizontal*

The glass release tube discussed earlier was employed. Two pairs of spheres P.3 and C.N.1 were used, and experiments were carried out at temperatures of 20° ±0·1° C and 25° ±0·1° C.

Two methods were used to determine the distance between sphere centres according to the proximity of the spheres. In the first the telescope was moved manually at a similar speed to that of the fall of the spheres so that the spheres appeared stationary relative to the moving observer. From the calibrated eye-piece graticule the distance between sphere centres was determined. The second method was to determine the time interval which elapsed between the passage of the spheres past a fixed fiducial mark. From a knowledge of the velocity of the spheres the distance between centres could be determined.

To obtain the velocities, each of the spheres was timed over a known distance. The spheres were then released individually and timed in their fall over the same distance.

EXPERIMENTAL RESULTS

d = diameter of either sphere (cm)
D = distance between sphere centres (cm)
v = velocity of either of the spheres, when falling in the presence of each other (cm/s)
v_∞ = velocity of a sphere when falling alone (cm/s)
β = angle between line of centres and the horizontal
ϵ = angle from the vertical of the path of the spheres

Results were plotted in the form of graphs of v_x/v against d/D. The term v_∞ is the measured velocity of the sphere when in the presence of each other were comparable with their speeds when falling alone.

The equation of the relationship was determined using a linear regression technique and is given in Table 2 together with the number of observations. The graph with the experimental results is shown plotted in Fig. 2.

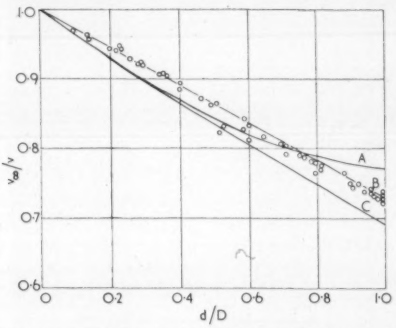

Fig. 2. Comparison of experimental results with theoretical predictions of other workers for an angle of 0° between line of centres and the horizontal
A, Smoluchowski; *B*, experimental; *C*, Burgers.

For the cases where the spheres fell with their line of centres making angles of (i) 30°, (ii) 45°, (iii) 60° and (iv) 90° with the horizontal the experimental plots consist of curves (see Figs. 3, 4, 5 and 6). The equations of the curves were determined in each case by means of a non-linear regression technique and are given in Table 2. It may be seen from Table 2 that, at least for the range of conditions investigated,

Table 2. *Regression equations for two equal spheres falling at various angles between line of centres and horizontal*

Angle between line of centres and horizontal	*Number of observations*	*Equation*	*Equation number*
0°	70	$v_x/v = 1{\cdot}001 - 0{\cdot}314d/D$	(1)
30°	10	$v_x/v = 1{\cdot}008 - 0{\cdot}352(d/D) + 0{\cdot}066(d/D)^2$	(2)
45°	20	$v_x/v = 1{\cdot}003 - 0{\cdot}443(d/D) + 0{\cdot}129(d/D)^2$	(3)
60°	20	$v_x/v = 0{\cdot}998 - 0{\cdot}475(d/D) + 0{\cdot}160(d/D)^2$	(4)
90°	43	$v_x/v = 1{\cdot}006 - 0{\cdot}614(d/D) + 0{\cdot}268(d/D)^2$	(5)

falling alone through the castor oil and as such is not the true Stokes' velocity. To obtain Stokes' velocity it would be necessary to apply a wall correction as the fluid is not infinite in extent. Such wall effects would be small as the ratio of diameter of sphere to vessel was large. In addition, the influence of surrounding walls on the motion of a sphere which is not falling along the central axis of a cylindrical vessel is not known.

Such effects were compensated for as far as possible by releasing the spheres individually in exactly the same positions as when they were released together and ensuring that the spheres when released together, were released at equal distances from the central axis of the vessel.

When the spheres fell with their line of centres inclined at an angle of 0° to the horizontal all the experimental points obeyed a linear relationship over the complete range of values of d/D, i.e. from $d/D = 0$ to $d/D = 1{\cdot}0$. The smallest value of d/D at which an experimental observation was made was 0·097; at smaller values the speeds of fall of the spheres

the equations can be represented without the inclusion of the density of the spheres, and of the viscosity and density of the liquid.

The spheres traversed vertical paths when falling with their line of centres either horizontal or vertical; in all other cases the paths of the spheres were deflected from the vertical by a small angle ϵ which was dependent upon the distance between the spheres (see next section). In all cases the spheres were observed to travel without rotation. The Reynolds number for an individual sphere did not exceed 0·018 and in most cases was less than 0·010.

COMPARISON WITH THE RESULTS OF OTHER WORKERS

Burgers[3] derived an equation for the resultant downward velocity of either of two equal spheres falling together under gravity in terms of the external force, the radius of sphere, the distance between centres and the angle between the

vertical and line of centres of the spheres. By means of Stokes' law it is possible to express the external force in terms of the system parameters.

By carrying out the necessary substitutions, Burgers' equations may be reduced to the form

$$\frac{v_\infty}{v} = \left[1 + \frac{3}{8}(1 + \sin^2\beta)\left(\frac{d}{D}\right) + \frac{1}{16}(1 - 3\sin^2\beta)\left(\frac{d}{D}\right)^3 - \frac{15}{64}\sin^2\beta\left(\frac{d}{D}\right)^4\right]^{-1} \quad (6)$$

where β is the angle between the line of centres of the spheres and the horizontal.

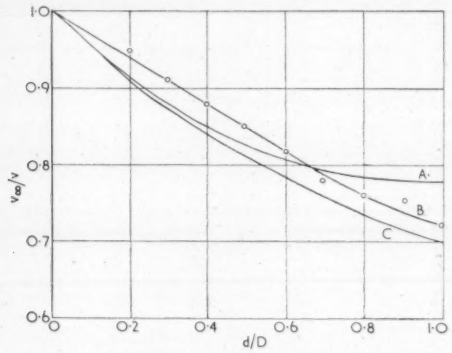

Fig. 3. Comparison of experimental results with theoretical predictions of other workers for an angle of 30° between line of centres and the horizontal

A, Smoluchowski; *B*, experimental; *C*, Burgers.

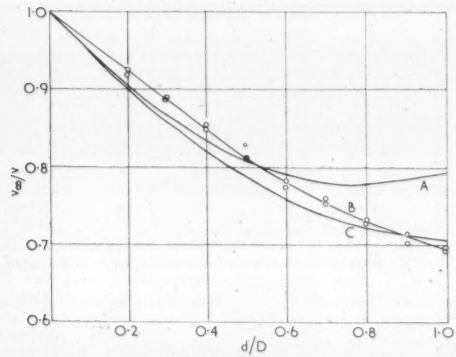

Fig. 4. Comparison of experimental results with theoretical predictions of other workers for an angle of 45° between line of centres and the horizontal

A, Smoluchowski; *B*, experimental; *C*, Burgers.

Burgers gave no expression for the angle the path of the spheres makes with the vertical throughout their fall, but he states that the two spheres also acquired velocities in directions perpendicular to the vertical axis and that it appears that these velocities are likewise the same for both bodies, so that their distance and positions relative to each other are not changed.

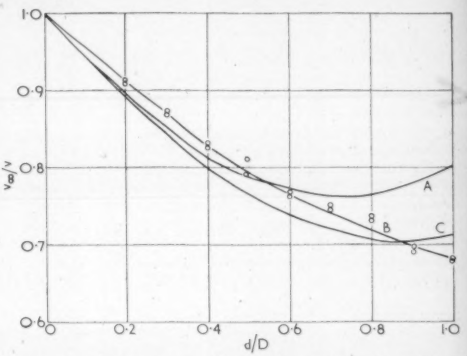

Fig. 5. Comparison of experimental results with theoretical predictions of other workers for an angle of 60° between line of centres and the horizontal

A, Smoluchowski; *B*, experimental; *C*, Burgers.

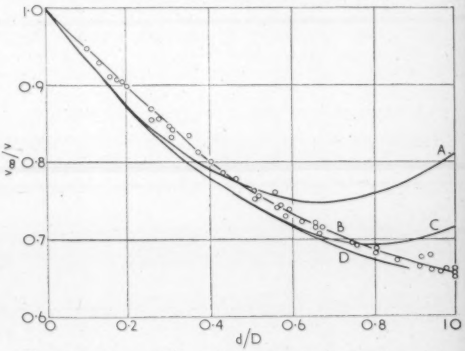

Fig. 6. Comparison of experimental results with theoretical predictions of other workers for an angle of 90° between line of centres and the horizontal

A, Smoluchowski; *B*, experimental; *C*, Burgers; *D*, Stimson and Jeffery.

Smoluchowski[1, 5] derived expressions for the components of force tending to diminish the resistance in the direction of motion along the line of centres. These may be combined with the normal Stokes' resistance to give the following equation

$$\frac{v_\infty}{v} = \left[1 - \frac{3}{8}(1 + \sin^2\beta)\left(\frac{d}{D}\right) + \frac{9}{64}(1 + 3\sin^2\beta)\left(\frac{d}{D}\right)^2\right] \quad (7)$$

Smoluchowski also gave the relationship

$$\sin\epsilon = \frac{3}{8}\left(\frac{d}{D}\right)\left[1 - \frac{3}{4}\left(\frac{d}{D}\right)\right]\cos\beta\sin\beta \quad (8)$$

for the angle ϵ through which the spheres would be deflected from the vertical towards the line of centres.

Stimson and Jeffery[2] used a different technique from that employed by either Burgers or Smoluchowski for the solution of the problem of two spheres moving with equal small constant velocities parallel to their line of centres. Their solution is based on the determination of Stokes' stream function for the motion of the fluid and from this the forces necessary to maintain the motion of the sphere are calculated.

By utilizing Stokes' equation their relationship may be reduced to the form

$$\frac{v_\infty}{v} = \frac{2}{3}\sinh\sum_{n=1}^{\infty}\frac{n(n+1)}{(2n-1)(2n+3)}\gamma \qquad (9)$$

where $\gamma = \left[1 - \frac{4\sinh^2(n+\frac{1}{2})\alpha - (2n+1)^2\sinh^2\alpha}{2\sinh(2n+1)\alpha + (2n+1)\sinh 2\alpha}\right]$

where $\cosh\alpha = D/d$

A comparison of the experimental results with the work of Burgers, Smoluchowski, and Stimson and Jeffery may be made by means of equations (6), (7), (8) and (9), respectively. This has been done for values of β equal to 0°, 30°, 45°, 60° and 90°. Values are shown plotted in Figs. 2 to 6 for easy comparison.

It can be seen that neither Burgers' nor Smoluchowski's equations give good agreement with experiment over the complete range of d/D values. Divergence between theory and experiment is particularly pronounced in the regions of d/D close to unity. It is suggested that there are two probable reasons for this. It may be that inertial effects, which are ignored in the derivation of the theoretical equations, become of increasing importance as the spheres approach close to one another and fall much faster than when falling individually. The other reason is that by considering interactions of higher order than have been taken into account, closer agreement of theory and experiment may result.

The curve plotted from Stimson and Jeffery's equation ($\beta = 90°$) follows the experimentally determined curve very closely in the regions near $d/D = 0$ and $d/D = 1{\cdot}0$; values of v_∞/v determined from Stimson and Jeffery's curve are in all cases low, although the maximum deviation from the experimentally determined curve is only $3\frac{1}{2}\%$.

Values of the angle ϵ, as determined experimentally (to the nearest half degree), are in good agreement with those calculated from Smoluchowski's equation.

CONCLUSIONS

When two equal spheres are falling in the presence of each other through a viscous liquid with various angles between the lines of centres and the horizontal, there is a mutual interaction causing an increase in the uniform velocity above the normal Stokes' velocity obtaining when such spheres are falling individually. Relationships have been determined between the parameters involved [see equations (1–5)].

In all cases, apart from when the line of centres is horizontal or vertical, the paths of the spheres are deflected from the vertical by a small angle the experimental values of which are in agreement with Smoluchowski's relationship [equation (8)].

The spheres maintain their positions relative to one another throughout the whole of their fall; there is no rotation of the spheres.

ACKNOWLEDGEMENTS

The authors wish to acknowledge the assistance of the workshop staff of the Mining Department, who constructed part of the apparatus; of Messrs. H. A. Stanley and P. G. Robinson, who made some of the experimental measurements, and of Mr. W. A. Dooley who was responsible for part of the photography.

E. W. Hall wishes to thank the University of Birmingham and the Royal Society respectively for a Research Scholarship and a Tyndall Research Award for 1955 to 1956.

REFERENCES

(1) Smoluchowski, M. S. Von. *Bull. Acad. Sci. Cracovie*, **1A**, p. 28 (1911).
(2) Stimson, M., and Jeffery, G. B. *Proc. Roy. Soc. A*, **111**, p. 110 (1926).
(3) Burgers, J. M. *Proc. K. Ned. Akad. V. Wetensch.*, **44**, pp. 1045, 1177 (1942); **45**, pp. 9, 126 (1942).
(4) Whitmore, R. L. *J. Sci. Instrum.*, **31**, p. 223 (1954).
(5) Smoluchowski, M. S. Von. *Proc. 5th Intern. Congr. of Math.* (Cambridge 1912), **2**, p. 192 (London: Cambridge University Press, 1913).

Approximate solution of a non-linear differential equation giving the temperature distribution in the positive column of a static arc

By H. Goldenberg, M.Sc., The Electrical Research Association Laboratory, Leatherhead, Surrey

[*Paper received* 31 *July*, 1958]

An approximate method is presented for the solution of the differential equation giving the temperature profile of the positive column of a static arc, when heat conduction only is taken into account. The method of Eyres, Hartree and others[3] is first used to change the dependent variable in order to replace the two non-linear functions of temperature present in the differential equation, namely the electrical and thermal conductivities, by a single non-linear function. When this non-linear function is approximated by a piecewise linear function, the basic differential equation can be integrated directly, and the temperature profile obtained. An example shows close agreement with King's results.[1]

INTRODUCTION

In a recent paper by King,[1] and in earlier work by Brinkman,[2] the temperature profile of the positive column of a static arc has been calculated numerically or graphically as the solution of Elenbaas's energy balance differential equation, taking heat conduction only into account. This differential equation contains two non-linear functions of temperature, namely the thermal and electrical conductivities, and its solution is extremely tedious by each of the previously adopted methods. The present paper shows how the initial differential equation can be simplified so as to contain only one non-linearity, and presents a direct method of solution

when this single non-linearity can be approximated piecewise by straight lines.

2. BASIC THEORY

Elenbaas's differential equation, giving the steady-state temperature T at a radius r measured from the axis of a cylindrical positive column of a static arc, is

$$\sigma E^2 = -\frac{1}{r}\frac{d}{dr}\left(rK\frac{dT}{dr}\right) \tag{1}$$

where σ and K are the electrical and thermal conductivities respectively of the gas, and E is the axial electric field. In the derivation of this energy balance differential equation, the radiation and convection contributions have been assumed negligible compared to that due to conduction.

In general σ and K are non-linear functions of temperature, while the electric field is constant. Following Eyres, Hartree and others,[3] we introduce a new variable

$$\phi = \int_{T_c}^{T} K(T)dT \tag{2}$$

where T_c is an arbitrary temperature. If, in addition, we denote $x = rE$, then

$$\frac{d\phi}{dx} = K\frac{dT}{dx}$$

and equation (1) assumes the form

$$\frac{d^2\phi}{dx^2} + \frac{1}{x}\frac{d\phi}{dx} + \sigma = 0 \tag{3}$$

Now $K(T)$ is a known function of temperature only, so that for any assumed lower limit of temperature T_c, $\phi(T)$ can be obtained as a function of temperature by numerical integration. The electrical conductivity σ is also a known function of temperature, so that to each temperature there corresponds a pair of values σ and ϕ. A graph of σ against ϕ can then be drawn, based on corresponding values of σ and ϕ at different temperatures. The $\sigma - \phi$ characteristic, which can be prepared before any solution of the differential equation (3) is attempted, is then the only non-linear element present in the differential equation. Finally, after obtaining ϕ as a function of x, the temperatures corresponding to different values of ϕ can be taken from a $T - \phi$ characteristic, and the temperature T can be plotted directly against x.

In practice the temperature profile is required for a number of assumed central temperatures, so that finally the temperature profile will be known for a number of values of electrical power dissipated per unit length of the positive column. Further the temperature profile need only be calculated until the temperature drops to a value below which the electrical conductivity and current are negligible. The boundary conditions for equation (1) are therefore

$$T = T_0,\ dT/dr = 0 \quad \text{when } r = 0,$$

the latter condition arising from the symmetry about $r = 0$. The corresponding conditions for equation (3) are therefore

$$\phi = \phi(T_0) = \phi_0,\ d\phi/dx = 0 \text{ when } x = 0 \tag{4}$$

as $K(T_0)$ is non-zero.

It will be observed that the term $(1/x)(d\phi/dx)$ occurs in equation (3), and that this term appears indefinite at $x = 0$, but an application of L'hopital's rule gives a limiting value of $(d^2\phi/dx^2)_{x=0}$ as $x \to 0$. Hence a derived boundary condition of equation (3) is $(d^2\phi/dx^2)_{x=0} = -[\sigma(T_0)]/2 = -\sigma_0/2$. This boundary condition is necessary for a numerical solution of equation (3).

Let us suppose for the moment that the $\sigma - \phi$ characteristic is a straight line of the form

$$\sigma = A\phi + B \tag{5}$$

The differential equation (3) is then immediately integrable, and has the general solution

$$\phi = -(B/A) + C_1J_0(x\sqrt{A}) + C_2Y_0(x\sqrt{A}) \quad \text{for } A > 0 \tag{6a}$$

$$\phi = -(Bx^2/4) + C_1 lnx + C_2 \quad \text{for } A = 0 \tag{6b}$$

$$\phi = -(B/A) + C_1I_0(x\sqrt{-A}) + C_2K_0(x\sqrt{-A}) \text{ for } A < 0 \tag{6c}$$

where $J_0(X)$ and $Y_0(X)$ are Bessel functions of the first and second kind respectively, $I_0(X)$ and $K_0(X)$ are modified Bessel functions of the first and second kind respectively, and C_1 and C_2 are arbitrary constants. Further $\phi = \phi_0$ and $(d\phi/dx) = 0$ at $x = 0$, so that

$$\phi = -(B/A) + [\phi_0 + (B/A)]J_0(x\sqrt{A}) \quad \text{for } A > 0 \tag{7a}$$

$$\phi = -(Bx^2/4) + \phi_0 \quad \text{for } A = 0 \tag{7b}$$

$$\phi = -(B/A) + [\phi_0 + (B/A)]I_0(x\sqrt{-A}) \quad \text{for } A < 0 \tag{7c}$$

In general the $\sigma - \phi$ characteristic can be assumed linear for a small range of values in the neighbourhood of $\phi = \phi_0$, so that equations (7*a*, *b* and *c*) can be used as starting formulae for a limited range of values of x.

It is frequently the case that a piecewise-linear representation of a non-linear characteristic in a differential equation yields a solution that is a very good approximation to the correct one. Let us therefore assume that the $\sigma - \phi$ relation can be represented in this way, and that

$$\left.\begin{aligned} &\sigma = A\phi + B \text{ for } \phi_0 \geqslant \phi \geqslant \phi_1 \\ &\sigma = A_r\phi + B_r \text{ for } \phi_r \geqslant \phi \geqslant \phi_{r+1},\ r = 1, 2, 3, \ldots N \end{aligned}\right\} \tag{8}$$

where, for the purposes of ease of illustration only, all the A's are assumed positive. Then ϕ is given by equation (7*a*) for $\phi_0 \geqslant \phi \geqslant \phi_1$, and the range of values of x over which equation (7*a*) is valid is $0 \leqslant x \leqslant x_1$, where x_1 is the minimum positive solution of

$$J_0(x_1\sqrt{A}) = [\phi_1 + (B/A)]/[\phi_0 + (B/A)] \tag{9}$$

such that $\phi(x_1) = \phi_1$.

We can therefore calculate values of ϕ valid for $0 \leqslant x \leqslant x_1$ from equation (7*a*), and, with the aid of the $\phi - T$ characteristic, we then have the temperature profile for $0 \leqslant x \leqslant x_1$.

The solution over the second interval $\phi_1 \geqslant \phi \geqslant \phi_2$ is of the form

$$\phi = -(B_1/A_1) + C_1J_0(x\sqrt{A_1}) + C_2Y_0(x\sqrt{A_1}) \tag{10}$$

where C_1 and C_2 are constants that can be obtained by making ϕ and $d\phi/dx$ continuous at $x = x_1$. C_1 and C_2 are therefore the solutions of the two linear equations

$$\left.\begin{aligned} &\phi_1 = -(B_1/A_1) + C_1J_0(x_1\sqrt{A_1}) + C_2Y_0(x_1\sqrt{A_1}) \\ &[\phi_0 + (B/A)]A^{\frac{1}{2}}J_1(x_1\sqrt{A}) = \\ &\quad = A_1^{\frac{1}{2}}[C_1J_1(x_1\sqrt{A_1}) + C_2Y_1(x_1\sqrt{A_1})] \end{aligned}\right\} \tag{11}$$

where, at this stage, all the quantities in the equations except C_1 and C_2 are known numerically. The range of validity of this second solution is $x_1 \leqslant x \leqslant x_2$, where x_2 is a solution of

$$\phi_2 = -(B_1/A_1) + C_1J_0(x_2\sqrt{A_1}) + C_2Y_0(x_2\sqrt{A_1})$$

This equation can be solved for x_2 (by Newton's method for example), or, more simply, from a graph of ϕ against x in the interval $\phi_1 \geqslant \phi \geqslant \phi_2$. With the aid of the $\phi - T$ characteristic we then have the temperature profile for $x_1 \leqslant x \leqslant x_2$, and hence for $0 \leqslant x \leqslant x_2$.

This general procedure can be continued, but it will obviously entail a good deal of work if the number of different lines representing the $\sigma - \phi$ relation is large. In the example in Section 4 it will be seen that even a rough piecewise-linear approximation can give very good results, while, if a large number of lines are to be considered, the present method appears adaptable for solution with the aid of an analogue computer of the electronic differential analyser type, with a non-linear function generator to simulate the piecewise-linear characteristic.

3. ELECTRICAL POWER DISSIPATED

The electrical power W_r dissipated per unit length of the positive column from the centre of the arc up to any radius r is given by

$$W_r = 2\pi E^2 \int_0^r r\sigma dr = 2\pi \int_0^{rE} x\sigma dx$$

Now equation (3) can be written in the form

$$x\sigma = -\frac{d}{dx}\left(\frac{xd\phi}{dx}\right)$$

so that W_r is given by

$$W_r = -2\pi rE\left(\frac{d\phi}{dx}\right)_{x=rE} \qquad (12)$$

as $(d\phi/dx) = 0$ when $x = 0$. Further ϕ can be obtained approximately as an analytic function of x for each linear portion of the $\sigma - \phi$ characteristic, so that approximate values for $d\phi/dx$ and hence W_r can be readily obtained. In particular if the behaviour of ϕ at $x = rE$ is given by equation (6*a*), then

$$W_r = 2\pi rE(\sqrt{A})[C_1 J_1(rE\sqrt{A}) + C_2 Y_1(rE\sqrt{A})] \qquad (13)$$

and W_r can be graphed as a function of r.

The total electrical power W dissipated per unit length of the positive column is obtained by replacing the upper limit of the integral defining W_r by infinity. In practice, however, a finite upper limit can be assumed for r or x as the electrical conductivity σ falls very rapidly with the decreasing temperatures found at distances sufficiently far from the centre of the arc. If a suitable assumed finite upper limit for x is X, then the total electrical power W dissipated per unit length of the positive column is

$$W = -2\pi X\left(\frac{d\phi}{dx}\right)_{x=X}$$

4. EXAMPLE

Let us consider the radial temperature distribution in arcs in nitrogen, as dealt with in some detail by King,[1] whose curves for the dependence of the electrical and thermal conductivities on temperature are reproduced as Figs. 1 and 2 of this paper. It can be observed from Fig. 1 that the electrical conductivity rapidly diminishes in the neighbourhood of 5000° K, with the result that T_c, the lower limit of integration in the definition of ϕ given by equation 2, has been assumed as 4000° K. With this assumed lower limit of integration, ϕ has been obtained by the numerical integration of $K(T)$, where $K(T)$ is given in Fig. 2, and the resultant curve of $\phi(T)$ against T is presented in Fig. 3. From the graphs of Figs. 1 and 3 corresponding pairs of values of σ and ϕ can be read off for different temperatures T, and a graph of σ against ϕ prepared. The resultant $\sigma - \phi$ characteristic for the present example is given in Fig. 4.

A central core temperature of 18 000° K has been assumed, and the $\sigma - \phi$ characteristic has been approximated by three straight lines, as shown in Fig. 4. The initial straight line passes through the point $\phi = 896{\cdot}5$, $\sigma = 79{\cdot}0$, corresponding to a central temperature of 18 000° K, and through the point $\phi = 235$, $\sigma = 37{\cdot}3$, and is

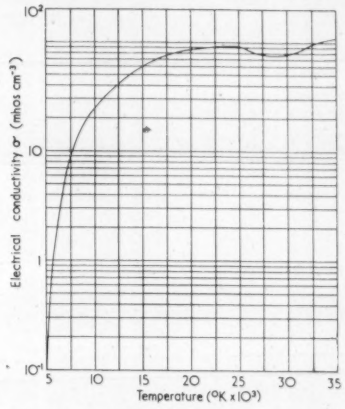

Fig. 1. Electrical conductivity of nitrogen

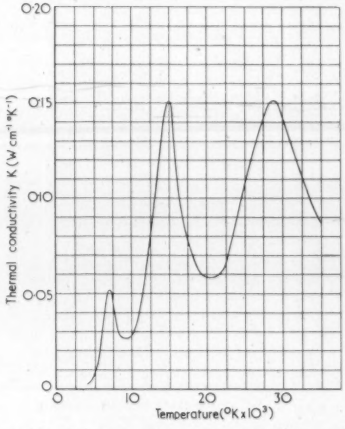

Fig. 2. Thermal conductivity of nitrogen

$$\sigma = 0{\cdot}0630\,\phi + 22{\cdot}5 \quad \text{for } 896{\cdot}5 \geqslant \phi \geqslant 235 \qquad (14a)$$

The second straight line passes through the points $\phi = 235$, $\sigma = 37{\cdot}3$ and $\phi = 77$, $\sigma = 7{\cdot}1$ and is

$$\sigma = 0{\cdot}1911\,\phi - 7{\cdot}6 \quad \text{for } 235 \geqslant \phi \geqslant 77 \qquad (14b)$$

The final straight line passes through the points $\phi = 77$, $\sigma = 7{\cdot}1$ and $\phi = 8$, $\sigma = 0$, and is

$$\sigma = 0{\cdot}1029\,\phi - 0{\cdot}82 \quad \text{for } 77 \geqslant \phi \geqslant 0 \qquad (14c)$$

The slope of each of these straight lines is positive, and the detailed method of solution is as presented in Section 2. The dependence of ϕ on x in the initial region starting at $x = 0$ is given by equation (7*a*), and is

$$\phi = -356{\cdot}7 + 1253{\cdot}2\,J_0(0{\cdot}2511x) \text{ for } 896{\cdot}5 \geqslant \phi \geqslant 235 \qquad (15a)$$

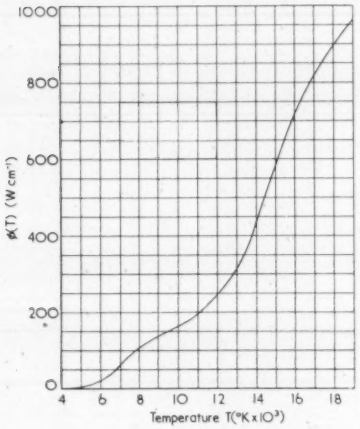

Fig. 3. Graph of $\phi(T) = \int_{4000}^{T} K(T)dT$

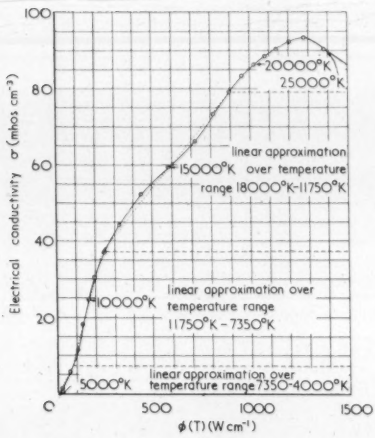

Fig. 4. The $\sigma - \phi$ characteristic

This equation is valid until ϕ drops to a value of 235, which takes place when $x = 6{\cdot}255$. (Extensive tables of Bessel functions[4] are useful at this and subsequent stages.) The value of $\phi = 235$ corresponds to a temperature of 11 750° K, so that from equation (15*a*) and Fig. 3 the temperature profile has been calculated for the range $0 \leqslant x \leqslant 6{\cdot}255$, while the temperature drops from 18 000° K to 11 750° K. The resultant temperature profile is given in Fig. 5, which also gives the complete temperature profile obtained by King.

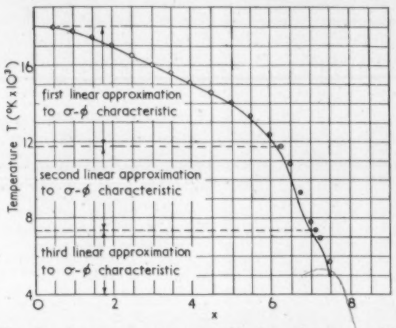

Fig. 5. Arc temperature profile for nitrogen, with a central temperature of 18 000° K

——— curve obtained by King.
○ values obtained by present method.

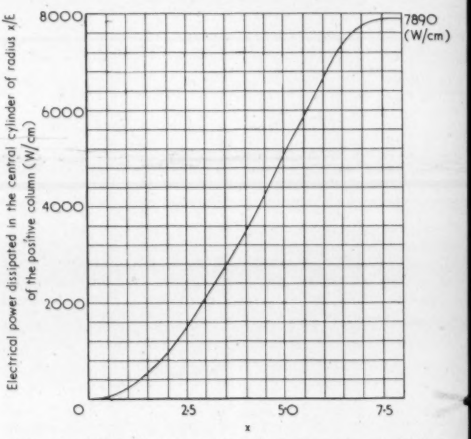

Fig. 6. Watts dissipated within a central cylinder of the positive column, for a central arc temperature of 18 000° K (E = electric field.)

The behaviour of ϕ in terms of x when ϕ lies within the range $235 \geqslant \phi \geqslant 77$ is given by equations (10), (11) and (14*b*), and is

$$\phi = 39{\cdot}8 + 590{\cdot}6\,J_0(0{\cdot}4372x) + 637{\cdot}5\,Y_0(0{\cdot}4372x) \text{ for } 235 \geqslant \phi \geqslant 77 \qquad (15b)$$

which is valid within the temperature range $11\,750° \text{ K} \geqslant T \geqslant 7350°$ K, and within the range $6{\cdot}255 \leqslant x \leqslant 7{\cdot}142$. The corresponding section of the temperature profile is given in Fig. 5.

The behaviour of ϕ in terms of x when $77 \geqslant \phi \geqslant 0$ can

be found in a manner similar to that of equation (15*b*), and is

$$\phi = 8{\cdot}0 + 1002{\cdot}0\,J_0(0{\cdot}3208x) + \\ + 16{\cdot}6\,Y_0(0{\cdot}3208x) \text{ for } 77 \geqslant \phi \geqslant 0 \quad (15c)$$

The remaining part of the temperature profile for the temperature range 7350° K $\geqslant T \geqslant$ 4000° K, is given in Fig. 5, and it will be seen that the overall agreement with King's results is quite close.

The electrical power W_r dissipated per unit length of the positive column from the centre of the arc up to a radius $r = (x/E)$ can be found from equations (12), (15*a*), (15*b*) and (15*c*), and is presented in graphical form in Fig. 6. As the electrical conductivity of nitrogen is negligible for temperatures less than 5000° K, which is the temperature at $x = 7{\cdot}6$, the total electrical power dissipated per unit length of the positive column has the value of 7890 W/cm, which compares with the figure of 8070 W/cm, obtained by King.

ACKNOWLEDGEMENTS

The author wishes to express his thanks to Mr. L. King, of the Electrical Research Association, for bringing the present problem to his notice, and to the Director of the Electrical Research Association for permission to publish this paper.

REFERENCES

(1) KING, L. A. *Theoretical Calculation of Arc Temperatures in Gases, Colloquium Spectroscopicum Internationale VI* (Amsterdam, 1956) p. 152 (London: Pergamon Press, 1957). (Based on E.R.A. Report Ref. G/XT155).
(2) BRINKMAN, H. Thesis (Utrecht, 1934).
(3) EYRES, N. R., HARTREE, D. R., INGHAM, J., JACKSON, R., SARJANT, R. J., and WAGSTAFF, J. B. *Phil. Trans*, Series A, **240**, p. 1 (1946).
(4) *British Association Mathematical Tables*, Vol. 6, *Bessel Functions, Part* 1, *Functions of Orders Zero and Unity* (London: Cambridge University Press, 1937).

Torsional vibrational experiments on rectangular concrete beams

By R. JONES, B.Sc., Ph.D., Road Research Laboratory, Harmondsworth, Middlesex

[*Paper received* 23 *May*, 1958]

Earlier anomolous results obtained in measuring the dynamic shear modulus of specimens of concrete by a torsional resonance technique are now explained satisfactorily. A theory, given by Davies in 1938, predicts discrepancies in the apparent shear modulus obtained at higher harmonic resonances due to warping of the rectangular section during vibration. The experimental results are in extremely good agreement with Davies's theory, and it is found that the corrected shear modulus is not significantly influenced by the frequency at which it is measured. This conclusion agrees with the results obtained from torsional resonances on a concrete beam of circular cross-section for which no correction is required.

Experiments have been made to determine the dynamic shear modulus of concrete from torsional resonance experiments on beams and rectangular cross-section to find whether the dynamic shear modulus of concrete varied with frequency. A range of frequency of 500 to 10 000 c/s was obtained by observing resonances up to the 19th harmonic on beam *A*, 5 ft long × 6 in. × 3 in., and up to the 14th harmonic on beam *B*, 7 ft 6 in. × 6 in. × 3 in. For comparison, resonances up to the 13th harmonic were observed on a beam of circular cross-section (beam *C*, 6 ft long and 4 in. in diameter).

The dynamic shear modulus was calculated at each harmonic from the following relations.(1)

Rectangular beams

$$\frac{G}{d} = \frac{4l^2}{g}\left(\frac{f_t}{i}\right)^2\left[\frac{a/b + b/a}{4a/b - 2{\cdot}5(a/b)^2 + 0{\cdot}21(a/b)^6}\right] \quad (1)$$

Circular beam

$$\frac{G}{d} = \frac{4l^2}{g}\left(\frac{f_t}{i}\right)^2 \quad (2)$$

where G is the dynamic shear modulus, d is the density of the concrete, l is the length of the beam, a and b are the lengths of the sides of the cross-section, $b > a$, and f_t is the resonant frequency at the ith harmonic.

For the beam of circular section the dynamic shear modulus, or, for reasons of convenience, the factor G/d, as calculated from equation (2), was not significantly influenced by frequency.(2) However, in the case of the rectangular beams, the dynamic shear modulus, calculated from equation (1), increased with increase in frequency or, more specifically, with increase in the order of harmonic. The differences were relatively small for the first few harmonics but showed increasing divergence as the order of the harmonic increased; the discrepancies were also more marked for the shorter beam. Torsional experiments by Giebe and Blechschmidt(3) on rectangular beams of quartz were cited as giving similar anomolies.

This paper gives an explanation of the anomolous results obtained with the rectangular beams using a theory by Davies(4) which appears to have been overlooked in References (1) and (3).

CORRECTIONS FOR BEAMS OF FINITE LATERAL DIMENSIONS

When the wavelength of the torsional vibrations in a beam becomes comparable with the cross-sectional dimensions, the torsional displacement of points off the axis of the beam is accompanied by a longitudinal displacement. Davies(4)

calculated the effect of this warping of the cross-section upon the resonant frequency and, in the case of a beam free from restraint at its ends, showed that the value of G derived from equation (1) is related to the true shear modulus (G_c) by the equation:

$$G = G_c[1 + (i^2\pi^2\mu^2/l^2)] \quad (3)$$

where μ is a constant depending on the shape and dimensions of the cross-section.

For a beam of circular cross-section, Davies showed that μ was zero, and thus no correction is required to equation (2).

For a rectangular beam in which $1 < S < 3$, where $S = b/a$, μ is obtainable from:

$$\frac{\mu^2}{a^2} = \frac{1}{3(1+S^2)}\left(S^2 + 4{\cdot}577\tanh\frac{\pi S}{2} + \right.$$
$$\left. + 2{\cdot}397\tanh^2\frac{\pi S}{2} - 7{\cdot}190\right) \quad (4)$$

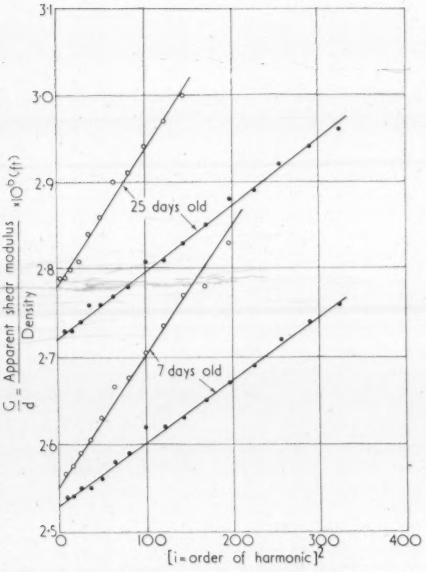

Results from torsional resonance experiments on rectangular concrete beams in comparison with theoretical lines given by Davies's analysis

○ = beam A, 60 × 5·98 × 3·10 in.
● = beam B, 90·1 × 6·12 × 3·25 in.

ANALYSIS OF RESULTS FROM RECTANGULAR CONCRETE BEAMS

Equation (3) indicates that when the apparent shear modulus given by equation (1) is plotted against the square of the order of the harmonic, the points should fall on a straight line, the slope of which depends solely on the dimensions of the specimen.

The value of μ has been calculated for the two rectangular beams for which the accurate value of S was 1·93 for beam A and 1·88 for beam B. The calculations indicated that theoretical lines should be as follows:

beam A $\quad G = G_c(1 + 0{\cdot}000\,59\,i^2)$ (5)

beam B $\quad G = G_c(1 + 0{\cdot}000\,284\,i^2)$ (6)

The experimental results obtained from each beam at ages of seven and twenty-five days are given in Fig. 1, and the theoretical lines corresponding to equations (5) and (6) have also been drawn: there is remarkably good agreement between experiment and theory from which it may be concluded that the dynamic shear modulus of the concrete was not significantly affected by the frequency at which it was measured. This conclusion substantiates the conclusion reached from the experiments on the circular beam.

CORRECTIONS FOR BEAMS OF SQUARE SECTION

Most experimenters are interested in the vibrational testing of beams of square section which conform to standard specifications. The correction to be applied to the torsional results in these cases is generally quite small and, for a perfectly square cross-section, Davies's correction is:

$$G = G_c\left(1 + 0{\cdot}003\,45\frac{a^2}{l^2}i^2\right) \quad (7)$$

Thus, for a standard beam of dimensions 20 × 4 × 4 in., the correction to be applied at the 5th harmonic is only of the order of $\frac{1}{3}$%. For the 15th harmonic, however, the correction is 3·1%.

ACKNOWLEDGEMENT

The work described in this paper was carried out as part of the programme of the Road Research Board of the Department of Scientific and Industrial Research. The paper is published by permission of the Director of Road Research.

REFERENCES

(1) PICKETT, G. *Proc. Amer. Soc. Test. Mater.*, **45**, pp. 846–63 (1945).

(2) JONES, R. *Mag. Concrete Res.*, **9**, pp. 69–72 (1957).

(3) GIEBE, E., and BLECHSCHMIDT, E. *Hochfrequenztech. u. Elektroakust.*, **56**, pp. 65–87 (1940).

(4) DAVIES, R. M. *Phil. Mag.*, **25**, pp. 379–86 (1938).

Correspondence

S-band ferrite isolator for use with a linear accelerator

Although ferrite isolators have been extensively described in the literature during the past five years[1] there are two points of interest in the present development. Firstly, an S-band isolator is not commercially available in England, although isolators for X- and Q-bands are. This is mainly because special material has to be designed with low saturation magnetization so that the ferrite is not inherently lossy at the comparatively low field corresponding to resonance. Secondly, the use of an isolator to couple a magnetron to a narrow band circuit like an accelerator has not previously been reported to our knowledge. The tendency has been to use high-power klystrons, which have an output less sensitive to loading than that of a magnetron. With an isolator, stable operation can be obtained from a magnetron.

The present isolator has been made for an S-band linear accelerator driven by a 1 MW magnetron. Several materials were tried, the final choice being a manganese magnesium aluminized ferrite supplied by Dr. R. J. Benzie of Marconi's Wireless Telegraph Co. Laboratory.

The isolator was made by cementing two pieces of this ferrite on to opposite broad faces of a 10 in. length of waveguide of No. 10 size. They were fixed in the position where the magnetic field vector was circularly polarized, which by calculation is $0{\cdot}74a$ from the narrow face where a is the broad dimension of the waveguide. Since the material was in the form of flat slabs this position was not critical. At first sparking occurred at peak powers of around 1 MW. This was prevented by rounding and tapering edges, and staggering the two pieces of ferrite by $\lambda g/4$ so that reflected power would be partially attenuated before reaching the guide narrowed by both ferrite slabs (Fig. 1). With these

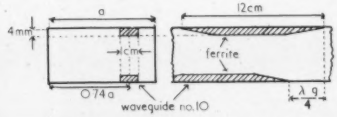

Fig. 1. Position and shape of ferrite in waveguide

modifications the isolator did not spark at 1 MW peak power with a voltage standing wave ratio of 7 : 1 at any phase, at atmospheric pressure.

The bandwidth of the accelerator corresponds to a Q of about 1000. Without the isolator the output spectrum of the magnetron is given in Fig. 2(*a*), whereas the matched spectrum, which is attained with the isolator between magnetron and accelerator, is shown in Fig. 2(*b*). The low level characteristics of the isolator are shown in Fig. 3. No high power measurements were made, the mode suppression shown in Fig. 2 being a sufficient criterion. The field of 1400 oersted could be achieved with two Eclipse Major horse-shoe magnets (by James Neill and Co.), and mild steel rectangular pole-pieces. Fine adjustments to the field were made by decreasing the gap with steel shims.

There is a possible future application of isolators for electron acceleration. The fact that a magnetron can now operate into a high Q circuit could lead to a reassessment of the possibilities of achieving a few megavolts with a single cavity. Medium energy electron accelerators employing a single microwave cavity were suggested and demonstrated some years ago.[2] The main difficulty was that between the

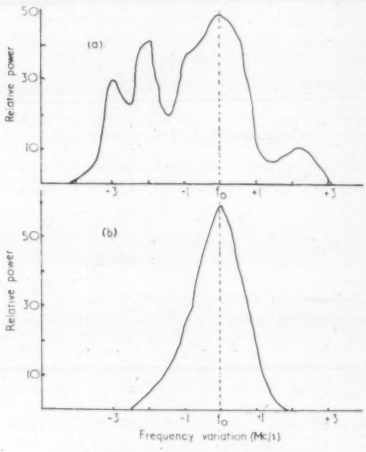

Fig. 2. Magnetron spectrum

(*a*) without isolator; (*b*) with isolator. Frequency f_0 = 2840 Mc/s

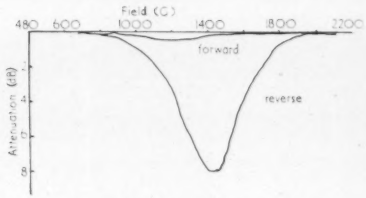

Fig. 3. Low level characteristics of the isolator measured at a frequency of 2840 Mc/s

magnetron and the cavity there had to be loss of power so that the oscillator would work stably. In fact, it seemed that a practical device would have to compromise between power loss and Q. The advent of ferrite isolators should change this state of affairs. Both an isolator that will work at a peak power of a few megawatts and a high Q cavity can be achieved in the few thousand megacycles range.

An isolator could also enable designs of accelerator having a very high Q, or an impedance that varies during the current build-up, to be envisaged. A promising example having these characteristics is the dielectric loaded accelerator.[3]

The work, of which this development is a part, is being assisted financially by a United States Air Force contract

and by the Associated Electrical Industries Research Laboratory.

Engineering Laboratory, Oxford University.

C. S. GASKELL
D. WALSH

[1 *July*, 1958]

REFERENCES

(1) HOGAN, C. L. *Bell Syst. Tech. J.*, **31**, p. 1 (1952).
(2) MILLS, B. Y. *Proc. Instn Elect. Engrs*, **97** (III), p. 425 (1950).
(3) WALKER, G. B., and WEST, N. D. *Proc. Instn Elect. Engrs, C*, **104**, p. 381 (1957).

Radiofrequency method for the measurement of conductive liquid saturation in a porous medium

An electrodeless method for measuring the saturation of a conductive liquid held in the pores of a porous medium has been developed as part of a research project to study the relative permeability behaviour of oil, water and gas mixtures. The porous medium consists of an unconsolidated sand-pack contained in a Perspex tube, and the method facilitates spot measurements of saturation without resorting to the usual conductivity measurements between electrodes in the "core."

An LRC series-resonant circuit is tuned to its resonant frequency at 100% water saturation and the voltage across the capacitance is measured with a valve voltmeter, the inductance being in the form of a pair of search coils, connected in parallel, mounted on either side and at right angles to the core. A plot of voltage against water saturation is obtained over the range 0 to 100% saturation at the fixed 100% saturation frequency.

The method depends on the small change in resonant frequency as the coil impedance changes with change in water saturation, the circuit response being plotted against saturation instead of actually measuring changes in resonant frequency (which is less than 1% for a change of 0–100% in saturation).

To minimize the effects of adjacent conducting bodies the outer turns of each coil are earthed. The search coils had to be some twelve feet from the oscillator and voltmeter and it was found that a length of coaxial cable was suitable as transmission line although it introduced some parallel capacitance into the circuit. Response is improved by earthing the conducting liquid.

Using a weak salt solution it was found that the best results were obtained between 700 kc/s and 1·5 Mc/s. The results shown in the figure were obtained at 1·2 Mc/s and are compared with conductivity measurements between electrodes in the core, the results being plotted as voltage and conductivity ratios against saturation as percentage of available pore space filled by salt solution. The saturation range of interest in the projected research is from 20 to 80%.

It will be appreciated that most commercial Q-meters work on a similar principle, the circuit response at resonance being indicated as a voltage across a standard capacitance, and such instruments afford ready availability of a suitable variable oscillator, variable capacitance and valve voltmeter.

Two books,* containing numerous references, have covered the field of radiofrequency conductivity measurements adequately although it is believed that the use of the response/frequency curve, using a search coil in this manner, has not previously been recorded.

The writer is indebted to Prof. F. H. Garner for his kindness in providing facilities for this work to be carried out.

Dept. of Chemical Engineering,
University of Birmingham.

R. W. SNELL

[7 *May*, 1958]

* BLAKE, G. G. *Conductimetric analysis at Radio Frequency* (London: Chapman and Hall Ltd., 1950). DELAHAY, P. *New Instrumental Methods in Electrochemistry* (New York: Interscience Publishers, 1954).

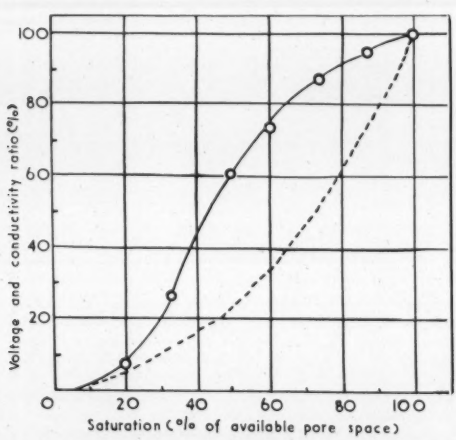

Results obtained using radiofrequency method on a weak salt solution at 1·2 Mc/s

Voltage ratio $= [(S_x - S_0)/(S_{100} - S_0)] \times 100\%$ at resonance frequency at 100% saturation where S indicates the signal strength and the suffixes the saturation conditions.

Centripetal air-pump operated electromagnetically

In previous issues of this *Journal*[1] we have described an instrument which works as a centripetal air-pump, and thus demonstrates the existence of cross-forces in the laminar flow of gases. While one of us[2] attributes these cross-forces to cross-stresses such as exist in non-Newtonian flow, Taylor and Saffman[3] have shown that a small error in the perpendicularity of either the rotor or stator to the axis of rotation may produce such effects in a Newtonian fluid such as a gas, if it is compressible. In order to check whether one or other of the theories, or both, are applicable, a modified instrument has been built which is illustrated in the figure.

The main elements of the instrument are, as before, the rotor R and the stator S. An electromotor revolves the rotor R up 9000 rev/min. Bearings of the rotor at B are preloaded by a spring so as to diminish their clearance. The stator S is supported by three small balls T. Each ball is free to perform slight displacements in its seat. Since these balls touch a spherical sector of the stator, the stator can perform slight turns around any axis passing through the centre O of the sphere. However, pin P, which has a ball-shaped head within a slot, prevents the stator from turning around its axis of symmetry. The three springs G hold the stator in its seat and the tension of these springs is individually adjustable. This makes a more or less self-alining stator in accordance with the pre-adjusted tension of the springs.

The stator seat is fixed to pillars *L*, but is electrically isolated from them. The pillars can tilt about the centre point *C* of the cross-spring pivot which, for small angular displacements, provides a bearing without clearance or backlash. In addition, the cross-springs tend to open the gap between stator and rotor.

The armature of an electromagnet *M* is attached to the pillars *L* by means of two flat springs *F*. When the magnet *M* is energized it draws the armature on to the core of the magnet, and then armature and core are held tightly together. The armature thus stresses the flat springs *F*, which pull the stator assembly against the traction of the cross-springs and the gap between rotor and stator is closed. By displacing the magnet with the set screw *W*, the stress of the flat spring is varied and the pressure of the stator against the rotor can be adjusted. A speed sensitive switch is attached to the motor. This switch prevents the current from energizing the magnet *M* as long as the speed is less than 6000 rev/min.

The instrument can work both as a centrifugal and a centripetal pump. For the first, the electromotor is energized by closing the electrical circuit to the motor by means of a manual switch. The rotor then revolves with a speed which gradually increases to about 9000 rev/min. The gap between rotor and stator is about 2·5 mm, and centrifugal suction in the stator centre can be observed on a manometer. When a speed of about 6000 rev/min is reached, an automatic speed switch contacts a second circuit. When this is closed by means of another manual switch, the electromagnet *M* is energized. The gap between rotor and stator is then reduced to about 8 μ. The air sheared in the gap prevents the plates from coming into contact, a cross-pressure is developed which balances the pre-set force of spring *F*, and the air moves centripetally towards the centre causing the manometer to show a pressure.

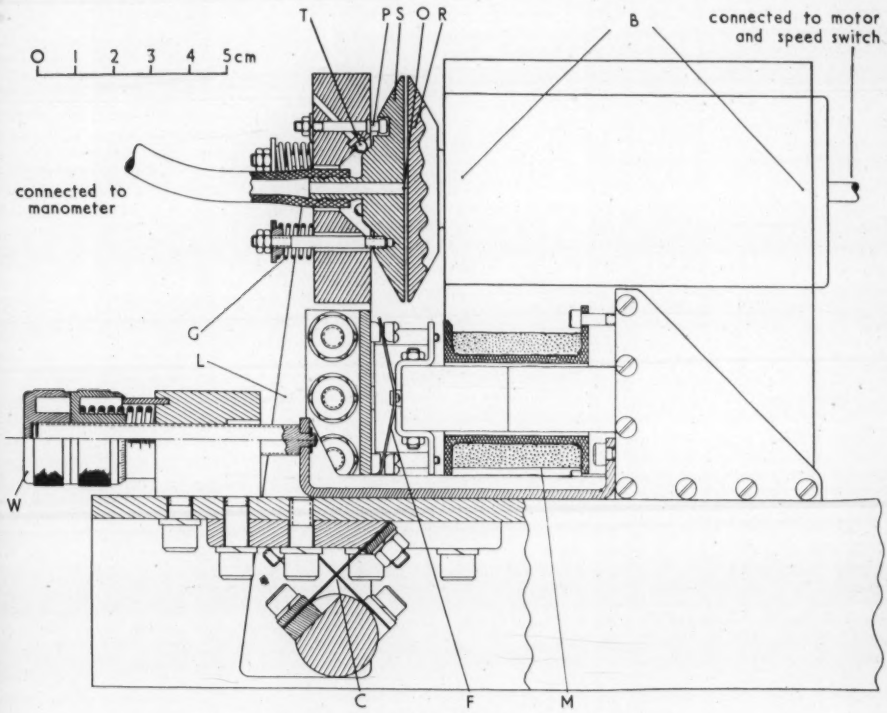

Automatic instrument showing centripetal pumping action

The instrument is at present on display in the Science Pavilion of the Brussels Exhibition. This research has been sponsored in part by the Air Research and Development Command of the United States Air Force.

Israel Institute of Technology,
Haifa,
Israel.

B. Popper
M. Reiner

[24 *July*, 1958]

REFERENCES

(1) Popper, B., and Reiner, M. *Brit. J. Appl. Phys.*, **7**, pp. 452–3 (1956); **8**, pp. 493–4 (1957).
(2) Reiner, M. *Proc. Roy. Soc. A*, **240**, pp. 173–89 (1957).
(3) Taylor, G., and Saffman, P. G.. *J. Aeronaut. Soc.*, **24**, pp. 553–62 (1957).

Notes and comments

Convention on thermonuclear processes

The Institution of Electrical Engineers has arranged a convention on thermonuclear processes to be held in London on 29 and 30 April, 1959. Details of the programme have not yet been finalized, but the probable range of topics to be covered is as follows: basic physics of thermonuclear processes; prototype British thermonuclear experiments—Zeta 1, Sceptre 111 and the linear pinch; constructional features of Zeta 1; design problems in future Zeta type systems; possibilities of direct conversion from nuclear to electrical energy.

Reviews of related work in the U.S.A. and the U.S.S.R. will also be included in the programme. Further details can be obtained from The Secretary, The Institution of Electrical Engineers, Savoy Place, London, W.C.2.

Conference on some aspects of magnetism

The Institute of Physics announces that it is arranging a conference on some aspects of magnetism to take place in Sheffield from 22–24 September, 1959. The subjects to be covered by the conference are:

(*a*) Fundamental theories to ferro-, ferri- and antiferromagnetism, including magnetic structure.
(*b*) Theories of technical magnetization processes, including hysteresis, coercivity, anisotropy and directional effects.
(*c*) Theoretical and experimental studies of domain phenomena in bulk materials and thin films.
(*d*) Experimental and theoretical studies of antiferromagnetism in metals and non-metals.

Each session will be opened by an invited speaker and offers of other contributions should be submitted to the Conference Secretary at The Institute of Physics, 47 Belgrave Square, London, S.W.1, before 31 January next. The conference is intended mainly for persons working in the field. Abstracts (but not preprints) will be circulated before the conference, the proceedings of which will not be published in full.

Further particulars will be available in due course from the Secretary, The Institute of Physics, at the above address.

Symposium on current developments in the production of high vacua

The Institute of Physics is arranging a one-day symposium, entitled Current developments in the production of high vacua, to take place in London on 17 April, 1959. There will be three sessions:

(*a*) Chemical and ionic pumping in kinetic vacuum systems.
(*b*) Problems in the production of high vacua in large equipment.
(*c*) Analysis of residual gases in kinetic vacuum systems.

Each of the first two sessions will be opened by invited speakers, and offers of short contributions, especially for the third session, will be considered by the Organizing Committee if outlines are submitted forthwith.

The symposium is intended mainly for persons working with high vacua. Abstracts (but not preprints) will be circulated before the symposium, the proceedings of which will not be published in full.

All communications regarding the symposium should be sent to the Secretary, The Institute of Physics, 47 Belgrave Square, London, S.W.1.

International convention and exhibition on transistors

The Institution of Electrical Engineers has arranged an international convention on transistors and associated semiconductor devices, to be held at Earl's Court, London, 21–27 May, 1959, which, it is hoped, will be the most comprehensive ever held on the subject. Associated with the convention will be an international scientific exhibition. Further details can be obtained from the Secretary, The Institution of Electrical Engineers, Savoy Place, London, W.C.2.

Journal of Scientific Instruments

Contents of the January issue

ORIGINAL CONTRIBUTIONS

Papers

High-temperature rotor bore dilatometer unit. By J. Wise.
Impaction sampler for size grading air-borne bacteria-carrying particles. By O. M. Lidwell.
Electrolytic potentiometer as a general purpose physiological transducer. By W. G. Whittlestone.
Improved Lyman-continuum flash-source of large aperture. By W. R. S. Garton.
X-ray analysis technique for very high temperatures. By E. Aruja, J. H. Welch and W. Gutt.
Calorimeter with automatic control. By G. Bullock.
Simple apparatus for measuring dielectric constants and losses from 10 c/s to 50 kc/s. By J. C. S. Richards.
Radiosonde measurement of vertical electrical field and polar conductivity. By O. C. Jones, R. S. Maddever and J. H. Sanders.
Measurement of the temperature of a running threadline. By M. F. Culpin and D. Madoc Jones.
Simple, high-sweep-speed, single stroke oscilloscope. By W. P. Baker.
Isotopic analysis of lithium by mass spectrometry. By P. G. Bentley, J. Bishop, D. F. Davidson and P. B. F. Evans.
Measurement of the falling velocity of particles in opaque fluids. By V. Fidleris and R. L. Whitmore.
Special type of grating, possessing the properties of a neutral filter for use in homochromatic photometry. By G. M. Sreekantath and C. A. Verghese.
Surface ionization source for mass spectrometry. By R. D. Craig.
Low background gas flow-counter. By G. H. Bergold and G. R. Haney.
Transmission specimen holder for electron diffraction. By R. I. Garrod and R. K. Hart.

Laboratory and workshop notes

Method for filling capillary pipettes with mercury for calibration purposes. By P. H. Bigg.
Valve for pressures of 10 kilobars. By E. Whalley and A. Lavergne.
Labyrinth radiation trap for use with standard X-ray diffraction equipment. By O. Kennard, A. J. P. Martin and L. Woodget.
Method for breaking open sealed electronic devices in vacuo. By M. G. Charlton and G. M. C. Perkin.
Experimental determination of effective bandwidth of monochromators. By I. Dayet.
Automatic protecting switch for water-cooled compressors. By J. K. N. Sharma.
An oscillating-plate differentiator for spectrophotometry. By I. G. McWilliam.

Correspondence

Counter diffractometer—the effect of vertical divergence on the displacement and breadth of powder diffraction lines. From E. R. Pike.
Gas circulating pump for enclosed systems. From H.-J. Pagel, W. Schwarz and W. Simon.

NOTES AND NEWS

New instruments — New books — Notes and comments

THIS JOURNAL is produced monthly by The Institute of Physics, in London. It deals with all branches of applied physics (including theory and technique).
All rights reserved. Responsibility for the statements contained herein attaches only to the writers.
EDITORIAL MATTER. Communications concerning editorial matter should be addressed to the Editor, The Institute of Physics, 47 Belgrave Square, London, S.W.1. (*Telephone:* Belgravia 6111.) Prospective authors are invited to prepare their scripts in accordance with the *Notes on the preparation of contributions*. (Price 2*s*. 6*d*. including postage.)
REPRODUCTION. The Institute of Physics is a signatory to The Royal Society's Fair Copying Declaration. Details may be obtained upon application from The Royal Society, London, W.1.
ADVERTISEMENTS. Communications concerning advertisements should be addressed to the agents, Messrs. Walter Judd Ltd., 47 Gresham Street, London, E.C.2. (*Telephone:* Monarch 7644.)
CLAIMS FOR MISSING JOURNALS. Claims from regular subscribers to this *Journal* for missing numbers will only be considered if received within 60 days of the date of mailing plus normal outward time of transit and time for lodging the claim. Losses attributable to failure to notify a change of address or to similar omissions will not be considered.
SUBSCRIPTION RATES. A new volume commences each January. The charge is £6 per volume ($17 U.S.A.), including index (post paid), payable in advance. Single parts, so far as available, may be purchased at 12*s*. 6*d*. each ($1.75 U.S.A.), post paid, cash with order. Orders should be sent to The Institute of Physics, 47 Belgrave Square, London, S.W.1, or to any bookseller.

Counter diffractometer—The theory of the use of centroids of diffraction profiles for high accuracy in the measurement of diffraction angles

By E. R. PIKE, B.Sc., Ph.D., A.Inst.P., and A. J. C. WILSON, M.Sc., Ph.D., A.I.M., F.Inst.P., Department of Physics University College, Cardiff

[*Paper received* 28 *July*, 1958]

The high resolution of the diffractometer, together with its ability to measure intensities accurately, allows the whole profiles of the diffraction lines to be studied. The width of the profiles is dependent on the spectral width of the characteristic radiation and on the geometry of the instrument. It is shown theoretically that the true Bragg angles can only be found, for work of the highest accuracy, from the centroids (first moments) of the profiles, the mathematics required to correct the peak positions being prohibitive. Experimental procedures required to put this theoretical advantage of the centroid into practice are explained, and difficulties due to the slow decay of the tails of the lines, and the uncertainty of background level are circumvented. An expression for the uncertainty in the centroid, found by step-by-step scanning by the fixed-time technique, due to counting statistics, is derived. This is plotted for the case of a single Cauchy profile. It is found that this uncertainty depends greatly on the peak-to-background ratio, and hence that scintillation or proportional counters have a marked advantage over Geiger counters for this type of work. It is concluded that, when the maximum accuracy in lattice-spacing measurements is desired, the centroid must be used instead of the peak, and that this does not involve excessive inconvenience in practice.

1. INTRODUCTION

The present-day counter diffractometer is an instrument capable of high resolution and high absolute angular accuracy. The diffraction lines from a well-crystallized specimen are sharp; the CuKα doublet begins to appear at a Bragg angle of about $\theta = 15°$, and angles may be measured accurately to the order of $0{\cdot}001° 2\theta$. The distortions and systematic errors are small compared with those of the powder camera. Thus for routine work the sharp line-peaks are convenient and accurate measures of line position. For work of higher accuracy the instrument can be used to give very accurate measurements of intensity, by step-by-step scanning over the reflexions, and the whole line-profile of each diffraction maximum can be studied. In this Introduction the factors which contribute to the form of the observed profiles will be reviewed briefly, from the physical rather than the mathematical point of view.

The target of an X-ray tube emits continuous "white" radiation over a considerable range of wavelengths, from the short-wave upper-energy limit down to very soft long-wavelength components. Superimposed upon this continuum are the characteristic sharp spectral lines of the target material. A "spectrum" of this radiation would consist of intensity emitted per unit time plotted against wavelength. This spectrum is dependent upon the angle at which the target is viewed, and will differ inside and outside the tube, as some parts of the spectrum will be absorbed more than others in the tube window. The spectrum at a given angle of view and through a given window cannot be measured without using some sort of instrument, such as a crystal spectrometer or grating spectrograph, and the spectrum observed will further depend on instrumental factors such as beam divergences, absorption in an analyser crystal, air paths if present, and, finally, upon the type of detector used. This latter factor in particular has a great influence on the spectrum observed; photographic film, Geiger counters, proportional counters, and scintillation counters each respond differently to different wavelengths, and the spectrum recorded by each will be quite different from that recorded by any of the others. If used in conjunction with filters, still more variations are possible.

A complete powder diffraction pattern consists of one such spectrum of coherently scattered radiation for each lattice spacing, superimposed upon the incoherent radiation from the specimen, and other sources of "background" such as air scatter, cosmic radiation, etc. Thus the coherently scattered "white" radiation for one interplanar spacing will form part of the "background" of the coherently scattered characteristic radiation for other spacings.

The purpose of explaining these differences in the way spectra may be recorded is to emphasize that the "background" upon which the "lines" of a diffraction pattern are imposed, and even the shape and position of the lines themselves, depend to a large extent upon the instrument used and the conditions under which the pattern is obtained.

The spectrum recorded by a Geiger counter with nickel filter, analysed by a silicon 111 analyser crystal mounted in a Norelco 17 cm. radius air-path goniometer, from a copper-target X-ray tube operated at 40 kVP on a full-wave rectified supply, with take-off angle 3°, is given in Fig. 1.[1] The distortions introduced by the instrument vary with the Bragg angle, and if this same spectrum were recorded at a higher angle, the apparent width of the characteristic lines (in terms of wavelength) would decrease. In fact, a large proportion of the line width shown in Fig. 1 is due to instrumental broadening, and this cannot be avoided if reasonable intensities are required without unduly long counting times.

The superposition of three such spectra on an incoherent background can be seen in the portion of the powder pattern of aluminium shown in Fig. 2. The pattern is simple and illustrates the general features of the formation of any powder diffraction pattern by the process of each plane "analysing" the incident radiation with varying degrees of dispersion. The form of one such spectrum may be studied

in detail before problems due to superposition of several are discussed. As a starting point the form of the spectrum emerging from the window of a given X-ray tube, operating under given conditions, will be assumed known (in a later section dealing with wavelengths this point will be discussed more fully). This spectrum will be modified by instrumental factors, and factors depending upon the condition of the specimen, before being measured as the output of the detector. These factors cause a broadening and displacement of the characteristic lines.

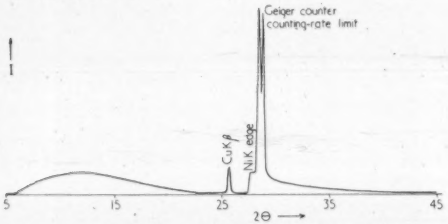

Fig. 1. Copper target (40 kVp) spectrum, analysed by silicon 111, recorded with Geiger counter with nickel filter

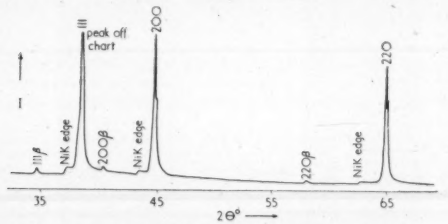

Fig. 2. Portion of the powder pattern of aluminium recorded with Geiger counter and nickel filter

If the source (S in Figs. 4 and 5), specimen P, and receiving slit R were negligibly small (and if the specimen contains a sufficiently large number of atoms and has no intrinsic defects), the spectrum emitted from the tube window would suffer only the distortion caused by the variation with wavelength of the response of the detector. There would be no broadening or displacement of the characteristic lines, and we can define the spectrum which would be obtained under such ideal conditions as the ideal spectrum for the given detector. This ideal observed spectrum would be generated on the angular scale by a given lattice spacing d by analysing the spectrum emerging at the tube window according to the Bragg law

$$\lambda = 2d \sin\theta \qquad (1)$$

A single correction would be necessary for the slight departure from unity of the refractive index of the material for the radiation employed.[2] The conditions of diffraction may be visualized graphically in Fig. 3.

The angular distribution will differ slightly from the wavelength distribution because of the sine term. This phenomenon is called dispersion. This distortion is negligible over the regions of the characteristic lines for d values diffracting them at low Bragg angles, but at high Bragg angles the dispersion must be considered as an appreciable distorting factor. An allied distortion arises from the Lorentz-plus-polarization factor, which is again negligible at low angles, but appreciable at high angles. At high Bragg angles the combined effect of these two factors is apparent as a "stretching" of the profile along the horizontal axis, more at the high-angle end than the low-angle end, with the ordinates remaining unaffected.[3-5]

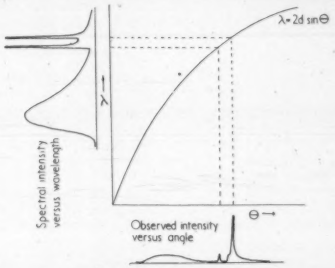

Fig. 3. The transformation from wavelength to angle by the Bragg law. Observed spectrum recorded with Geiger counter and nickel filter

The physical effects of the instrumental broadening factors may be clearly understood by considering in detail the effect on the line profiles of a typical one only. Consider, for example, the effect of extension of the specimen. A crystallite displaced from the ideal position at a point inside a finite specimen will reflect the spectrum at slightly different angles from the ideal observed spectrum defined above. This contribution will not be as strong as the ideal one, due to absorption, and the resultant observed profile due to the two contributions will be the sum of the two. The effect is shown in Fig. 4 for a resolved doublet of the spectrum. There is

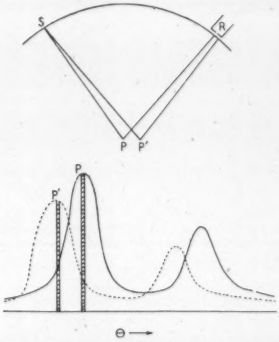

Fig. 4. Contribution to the observed spectrum of a second crystallite P' displaced from the ideal position P

now no longer one angle θ corresponding to one value of λ, but in this case there are two diffractometer settings that satisfy the Bragg equation for each value of λ. The two angular elements shaded in the figure correspond to the same wavelength element. If all the crystallites in a flat specimen are considered, this single wavelength element will be diffracted over a range of angles by the various parts of the specimen

as shown in Fig. 5. The original wavelength element is "smeared out" by the so-called aberration function $g(\theta)$. The origin of the aberration function corresponds to diffraction at the ideal position. The observed profile will be made up of the sum of the elements of the ideal profile, each "smeared out" by $g(\theta)$, as illustrated in Fig. 6. This is called

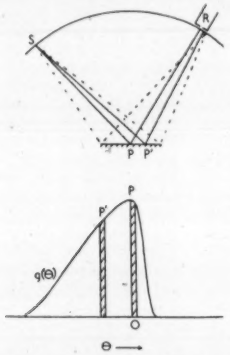

Fig. 5. The formation of the aberration function, $g(\theta)$, by the diffraction of a single wavelength element over a range of angles by the various parts of the specimen

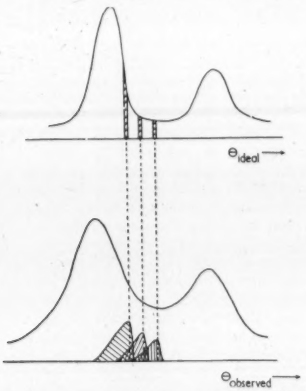

Fig. 6. Generation of the observed profile by the summation of the ideal wavelength elements each "smeared out" by the aberration function. In this figure and Fig. 7 the origin of the aberration function is shown near the peak. In the general case the origin can occur in any position

the fold or convolution of the ideal profile, which we shall call $f(\theta)$, with the aberration profile $g(\theta)$.

The form of the observed profile depends in a critical and complicated way on the form of the aberration function. If appreciable aberrations are present, the original profile may be almost unrecognizable in the observed one, as, for example, in most low-angle lines, where even the doublet form of the original is not apparent. Here, the aberration function dominates the convolution, and quite different profiles will be obtained by varying geometrical factors such as beam divergences.

2. THE THEORETICAL ADVANTAGE OF THE CENTROID OVER THE PEAK

The position of the peaks of the ideal spectrum will not, of course, correspond to the peaks of the observed profile. To find the ideal peak positions from the observed profile, the profile of the aberration function would have to be known, and this and the observed profile would have to be "unfolded" to remove the effect of the aberration. There is no simple method of carrying out this process and no "short-cut" by which the shift of the peak may be otherwise determined. The process is impracticable in most cases, as the profiles of the aberration functions are not known with sufficient accuracy. The observed peak positions cannot therefore be easily corrected for the effects of the various instrumental distortions of the spectrum, or distortions due to absorption in the specimen, etc., and accurate results from the use of peak positions can only be obtained if all aberrations are very small. Even if this is the case, it is difficult to estimate the final accuracy of the angles obtained.

An alternative process which is being studied at Cardiff and at Philips Laboratories, Irvington, involves the use of the centroids or centres of gravity (first moments) of the profiles rather than the peaks. The theoretical basis for this method may be explained by using the conception of the observed profile as being made up of the sum of the elements of the ideal profile, each "smeared out" by the aberration function. As far as the centres of gravity of the profiles are concerned, the contributions of the smeared-out elements can be thought of as "masses" at their centres of gravity, as shown in Fig. 7. Each mass (m_1, m_2 or m_3) of the ideal profile can be seen to be shifted by the constant amount G, which is the distance from the origin to the centre of gravity of the aberration

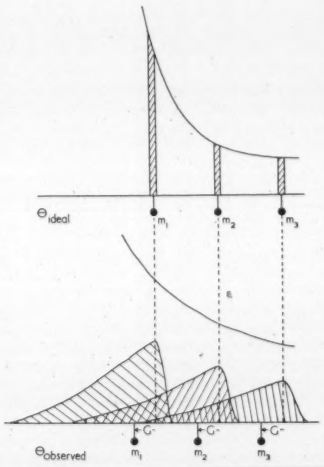

Fig. 7. Contributions of ideal and smeared-out elements to the centres of gravity of the ideal and observed profiles

function. The centre of gravity of the whole profile will therefore be displaced by this same amount. To find the true angular position of the centre of gravity of the ideal profile with the effect of the aberration removed, the process of simple subtraction is substituted for the "unfolding" process needed for the peaks. Furthermore, the entire profile of the aberration function does not need to be known, but only the value of G, which is its first moment. The effects of several aberrations are combined by folding their separate aberration functions together in the same manner as described above, and, by the same argument, the effect on the observed profile is to shift the centre of gravity (henceforth abbreviated to c.g.) by the sum of the first moments of the individual aberration functions. The first moments of all the major aberrations of the diffractometer, i.e. specimen-surface displacement, flat-specimen error, transparency error and axial ("vertical") divergence, have been worked out in the last decade.[6-8] They are much easier to calculate than the actual profiles, and have been reasonably confirmed experimentally. Subtraction of the appropriate values of G for each of the aberrations from the observed c.g. gives the position of the c.g. of the ideal angular profile defined above. Before this angle can be used in the Bragg equation as the equivalent value of θ in Fig. 3 to the c.g. of the wavelength spectrum it must be corrected for dispersion, Lorentz and polarization factors, where these are appreciable. This correction again takes the form of simple subtraction. The correction for refraction may be made to the final value of d obtained.

The above considerations indicate that it is worthwhile investigating the possibilities of using the centroid, rather than the peak, as the measure of position of an X-ray diffraction maximum, in virtue of the ease with which such a measure can be corrected for the effects of instrumental distortions of the profiles, in contrast to the difficulties involved in determining these effects on the peaks.

3. THEORETICAL DISADVANTAGES

In spite of the above very weighty advantage of the c.g. as a measure of line position, there are many factors to consider before a decision can be made upon the relative merits of peak and c.g. There is firstly the obvious question of convenience from the practical point of view. The relative ease with which peak or c.g. may be found in practice must be balanced against the relative accuracy obtainable by making use of one or the other method. A full discussion of this point must be postponed until the concluding section of this paper when some assessment of the relevant factors has been made, but a few points may be made here.

A review of methods which have been used to find line peaks has been given by Ladell, Parrish and Taylor;[9] most of them involve plotting the profile and drawing a median line. Techniques for obtaining the c.g. have been developed[10,11] which are no more time consuming than plotting the profile and constructing the median, or fitting a parabola to the peaks. Furthermore, a statistical analysis to be given in Section 7 of this paper shows that accurate c.g.'s may be obtained with relatively fast scanning speeds, and hence, although rather more points are required than to construct a median, the counting time at each point may be reduced and, on balance, little disadvantage results, particularly if a line has a high peak-to-background ratio. For work of routine accuracy, where no such trouble is taken to locate the peak, and no corrections are to be applied for instrumental distortions, the c.g. is obviously more complicated to determine and would not be of great value, but this practical disadvantage is not pronounced when work of the highest accuracy is contemplated.

Rather more serious disadvantages of the c.g. are the errors involved in determining the "background" upon which the given spectrum is superimposed, and errors which arise due to the fact that it is impracticable to use the c.g. of the whole spectrum, to which the theory strictly applies, but only a "truncated" portion of it in the neighbourhood of a characteristic line. These errors will be discussed in detail below.

A further disadvantage of the c.g. as compared with the peak is that for certain distortions the c.g. is more sensitive than the peak. In the extreme case of the Lorentz-plus-dispersion correction the error in our knowledge of the shift of c.g. due to this effect is greater than the corresponding shift of the peak, the latter being negligibly small, while the former, at angles above $2\theta \simeq 145°$, can be the largest correction required.

This list of disadvantages must also include at the present time the lack of knowledge of the wavelength spectrum to the accuracy required to find a sufficiently precise value of c.g. to use in the Bragg equation. The peak wavelengths are not known with the accuracy desired, but even less is known about the c.g.'s.

We now proceed to investigate these disadvantages in order to find ways in which they may be minimized, and to obtain some indication of the magnitude of errors they may introduce.

4. CHOICE OF LIMITS AND TRUNCATION ERROR

For the purposes of this section the lack of knowledge of the background upon which the spectrum for a given lattice plane is superposed will be ignored, this background including coherent radiation from other planes. The way in which this lack of knowledge will modify our results will be discussed in Section 5. It is assumed, then, that we have an observed spectrum, generated in the way outlined above, by transforming the wavelength spectrum to the angular scale as in Fig. 3, and then folding this ideal spectrum with the aberration function. The theory of the use of the c.g., as illustrated in Fig. 7, strictly requires the use of the whole spectrum (Fig. 1), since the overlapping smeared-out elements of the observed profile cannot be sorted out and identified with the elements of the ideal profile over any particular section of the spectrum. In practice, however, the characteristic lines only must be used because of overlapping and other obvious difficulties, and the problem now has to be faced of applying the principles of Fig. 7 to "truncated" sections of the spectrum in the region of the characteristic lines. The question of choice of limits on the observed profile now arises and proves to be rather complicated. Since wavelength peaks do not correspond to observed peaks, nor backgrounds to backgrounds, there are no recognizable corresponding points to locate the limits. Ladell, Parrish and Taylor[9] have treated this problem in detail, from a standpoint rather different from ours.

Our approach will now be discussed in detail. An appropriate range of the wavelength spectrum from spectroscopic measurements is taken by defining limits λ_A and λ_B on either side of the characteristic line being used. The c.g. between these limits is calculated and used as the value of λ in the Bragg equation. The variation in the response of the

detector over this short wavelength range is neglected, and also the variation of absorption in the air path and specimen. The value of d, if known, would then give the equivalent points, say θ_A and θ_B, on the spectrum on the angular scale, from the wavelength limits λ_A and λ_B; the c.g. of the ideal profile between these limits, when corrected for dispersion and Lorentz factor, would correspond in the Bragg equation to the wavelength c.g. defined above. Even without aberrations, however, d is not known (for it is to be found), and hence θ_A and θ_B are not known to find the ideal c.g., to find d, to find θ_A and θ_B. This vicious circle does not, of course, arise when using peaks, as only one point is involved. The problem is not insuperable, however, because an estimate of d can be made, to give trial limits, and the ideal c.g. found by successive approximations. The c.g. found by using the trial limits is used to find a better value of d, which is, in turn, used to find new trial limits, and so on. The process can be shown to converge rapidly for cases of practical interest where the limits lie in the Cauchy-like "tails" of singlet or doublet profiles.

This successive-approximation method of finding equivalent limits, ranges, and c.g.'s, and λ and θ scales can be much simplified in practice if the original spectroscopic limits are chosen in such a way that they are symmetrical about the c.g. of the portion between them. This can easily be done by successive approximations as above. If this is the case, then, apart from the second-order effect which dispersion will have on the process, the ideal c.g. will also lie mid-way between the final limits. In practice also, the variation of angular range during the successive-approximation process will have a negligible effect on the c.g., and hence the trial range need not be altered. The above two assumptions allow the c.g. to be found by calculating roughly the angular range required and, by successive approximations, finding a c.g. over this range which is symmetrical with respect to the range. Further steps which simplify the method will be discussed in Section 6.

As yet we have not considered the effect of aberrations on the method. The observed profile will be shifted by G, and broadened with respect to the ideal profile used in the above arguments. The shifting can easily be dealt with by applying appropriate reverse shifts when necessary. The trial value of d for instance, gives values of θ_A and θ_B which must be shifted by G (to say θ'_A and θ'_B) before they apply to the observed profile; similarly, when the c.g. between θ'_A and θ'_B is found G must be added before the new value of d is calculated. If the simplications mentioned above are used, the original process is unaltered, since the observed c.g. must still lie mid-way between θ'_A and θ'_B. The addition of G is made to the final value of the observed c.g. to find the corresponding ideal position.

The broadening introduced by the aberrations is more troublesome and gives rise to an error implicit in the method of using c.g.'s, which may be called the truncation error. [This is not quite the same as the error called by the same name by Ladell, Parrish and Taylor.[9]] The situation is illustrated in Fig. 8. We require to find the c.g. of the observed profile corresponding to the c.g. of the portion of the ideal profile between θ_A and θ_B. All elements between θ_A and θ_B are effectively shifted by the aberration to points between θ'_A and θ'_B on the observed profile, but due to the broadening the elements at θ_A and θ_B are spread out with equal moments about the limits θ'_A and θ'_B and half of their contributions to the observed c.g. will lie outside the limits. Similarly elements near A and B will contribute smaller fractions overlapping the limits. The total effect is to make the difference between the c.g. of the observed profile between limits θ'_A and θ'_B, and the c.g. of the ideal profile between limits A and B, slightly different from G, the first moment of the aberration function. The error has been treated theoretically by Pike and Rogers[12] (see also Ladell, Parrish and Taylor[9]) by assuming Cauchy-like tails for the spectral lines and a triangular-shaped aberration function. The conclusions are that, providing a range can be used which is large compared with the width of the aberration function, the truncation errors can be reduced so that d is in error by less than few parts in 10^6. If the broadening aberration

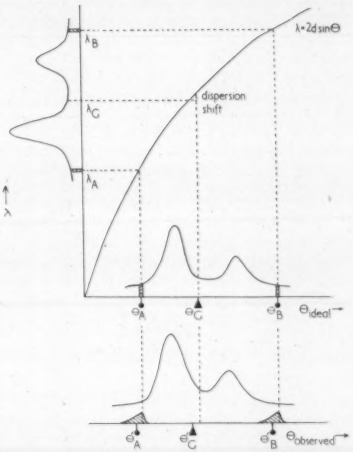

Fig. 8. Contributions of elements at the truncation limits

function is assumed triangular, and this will be approximately the case for transparency, flat-specimen and axial-divergence errors, the range taken must be more than about four times its half-width, when the symmetric-limit method is used. If ranges which are too short are used, appreciable errors may occur.

We conclude, therefore, that a truncated section of the spectrum can be used for the c.g. method by calculating the c.g. of the spectral profile between two fixed wavelength limits for the value of λ to use in the Bragg equation, and locating the equivalent limits and c.g. on the observed profile by making successive approximations to the true value of d. The effect of aberrations is to shift the limits and c.g. by a constant amount G, but an exact equivalence cannot be defined when broadening effects are present, as each value of wavelength on the spectral scale now corresponds to a range of wavelengths on the angular scale. Provided, however, that the centroids of the broadened elements are taken as their effective angular positions, the errors due to truncation will be as small as possible, and, in fact, will not be troublesome unless some factor prohibits the use of a sufficiently large range about the line. The range used in most cases will be dictated by other considerations to be discussed later (Section 6), because, except at very low angles, the factor of four times the broadening-aberration half-width can easily be achieved.

5. DETERMINATION OF BACKGROUND

In the previous section it was assumed that the spectrum from a given plane had been separated by some means from the coherent radiation from other planes, incoherent scatter and the other sources of background. Reference even to the simple pattern of Fig. 2 will show that the difficulties involved in attempting to perform such a separation are such as to render the task practically impossible.

To get around this difficulty we will again assume, as above, no instrumental aberrations, for the purpose of developing a method, and later investigate the modifications necessary when they are taken into account. In the previous section the problems were due to overlapping in the "horizontal" direction of the observed profile, and "vertical" truncation was used to avoid the difficulties. We find that in a similar way the difficulty of the superposition of the spectrum on an unknown background in a "vertical" direction can be overcome by "horizontal" truncation.

The value of λ for use in the Bragg equation is now found by truncating the spectroscopic profile in both directions, as shown in Fig. 9. The "horizontal" truncation is made by joining the points on the profile at the positions of the limits and is not necessarily quite "horizontal." The c.g. of the portion cut off, which we may now call the "line," is the value of λ required. When this is transformed, as in Fig. 3, to the angular scale, the identity of the "line" is maintained, since each point of the spectral profile has a one-to-one correspondence with a point on the ideal angular profile

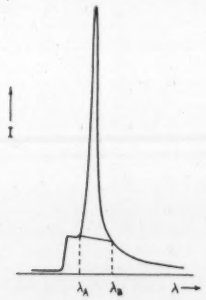

Fig. 9. The definition of a line by "horizontal" truncation

and the same two truncations may be made unambiguously. Moreover, apart from the Lorentz and dispersion corrections, the c.g.'s of the truncated portions will still be equivalent, in the sense that they are related in the Bragg equation by the true value of d. The successive-approximation method of finding d will still work for the truncated portions, and, in fact, the convergence will be even more rapid than with the "vertical" truncation only.

Now the superposition of this ideal spectrum upon a slowly varying background will not affect the c.g. of the truncated portion. This may be seen simply in Fig. 10. The shaded elements are displaced relative to one another in the vertical direction, but otherwise exert the same moments in the horizontal direction as before. The unknown slowly varying background can therefore be neglected by performing the horizontal truncation described above. The background does not affect the successive approximation method for the truncated "line" in any way, as only "horizontal" moments are involved.

It remains to discuss the modifying effect of the aberration function. This will have the effect of shifting the profile bodily by G and distorting it according to the relative widths of the aberration function and the line. The shift again will have no effect on the method, but the distortion will introduce

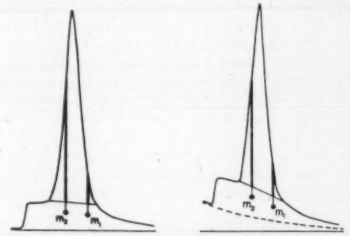

Fig. 10. Illustrating that background displaces elements by different "vertical" amounts but does not alter their "horizontal" moments

an error similar to the truncation error described above. The magnitude of this error will again depend on the exact profiles of both line and aberration function and will similarly become negligible if a sufficiently large range is taken on either side of the line. This truncation error has not been investigated theoretically, but if the range is sufficiently large for the error due to the vertical truncation to be neglected, simple considerations show that the corresponding horizontal truncation introduces no greater error. The original line can be split into the portion above the horizontal truncation and the portion below. The portion below is merely shifted bodily by the folding process without change of ordinates, and the error comes from the distortion of the portion above. This distortion causes a change in the line-minus-"background" intensity at the limits, from zero in the ideal profile to finite values in the observed one. The horizontal truncation on the observed profile, however, restores these values to zero and thus acts in the opposite direction to the original truncation error.

Experimental measurements to verify the magnitudes of these truncation errors cannot be made without a knowledge of the variation of wavelength with range to be discussed below.

6. WAVELENGTH VALUES

The method of using c.g.'s described above requires a knowledge of the distribution of intensity *versus* wavelength emerging from the tube window, and also how this is modified by the response of the detector; i.e. a knowledge of the ideal spectrum defined in Section 1. If we can neglect the variation of response of the detector over the range of wavelength of the truncated distribution used, the spectrum observed by any ideal spectroscopic instrument will suffice. When filters are used, however, the c.g. even of the truncated distribution will be altered, and if the range extends to the absorption edge, as it will with low-angle lines, then appreciable differences will occur. As an incidental point, the filter will have an effect on the peak positions very similar to the effect of sloping background on the peaks pointed out by Nigam.[13] With such knowledge of the spectral profile, any two points

on either side of the characteristic line can be used as limits, the c.g. of the doubly truncated portion calculated, and, provided that the equivalent range on the angular scale for a given reflexion satisfies the requirements of length imposed by the aberration effects, these three points are then used in the successive-approximation method for finding the value of $\hat{d}$. The simplified method mentioned above requires that these original three points, that is, the c.g. and corresponding limits, be chosen so that the limits are symmetrical about the c.g. In this case only two quantities need be specified, the symmetric range in Ångstrøm units and the wavelength of the c.g. For the region near the line there is only one c.g. for a given symmetric range. If we call the symmetric wavelength range λ_g^* and the corresponding c.g. λ_g^*, then the relation between them may be plotted on a graph; any symmetric range can then be used on the angular scale (provided dispersion is allowed for if necessary), and the corresponding value of λ for the Bragg equation is read off from the graph as the value of λ_g^* corresponding to the range used. A further simplification is again possible in practice. The wavelength distribution near the line falls off monotonically into the continuous band, approximately as the inverse square of the distance from the line. The horizontal truncation procedure, with the symmetric limit method, allows the slope of the continuous band to be neglected and gives a graph of λ_g^* against λ^* which tends asymptotically to a constant value as the range is increased, until the discontinuity at the absorption edge of the filter is reached. This fact allows the two quantities required above to be reduced to one, that is the asymptotic value of λ_g^*, say $G(\lambda^*)$, if a sufficiently long symmetric angular range is used. The actual length is immaterial, provided that the aberration limitations are complied with and that the absorption edge is not reached.

7. STATISTICAL ACCURACY OF C.G. MEASUREMENTS

It is of interest to make some estimate of the expected error of a c.g. determination due to counting statistics. This knowledge will allow the counting time to be chosen for optimum working. The c.g. will be assumed to have been found by the methods outlined above; it will therefore be at the centre of the range and this point will be taken as origin. The background will have then been taken between two points on the profile symmetrically placed about the origin.

We consider specifically the case where the profile is observed by counting quanta for a fixed time with a local detector at a series of equidistant steps along the profile. Each reading will therefore have a random value having a Poisson distribution about its mean. The mean value at θ_i will be called t_i, signifying the total intensity, line plus background, at the ith step. The respective values of line and background intensity will be called l_i and b_i. For greater generality it will be assumed that there is an additional random error in the sample taken at each step, in order to include the case when a monitoring technique is used. The monitoring count will be called M. For greater accuracy in the c.g. the values of intensity at the limits may sometimes be found more accurately than the rest by drawing a smooth line through several adjacent points on a plotted diagram or by counting for a longer time than at a normal step. This case will be included by assuming that an effective counting time p times as long as normal is used. The values of intensity at the limits will be called a and z. (They might be called t_0 and t_n, were it not for their possibly greater statistical accuracy.) The standard deviation of t_i will thus be given by

$$\sigma(t_i) = [t_i + t_i^2/M]^{\frac{1}{2}}, \tag{3}$$

and the standard deviations of a and z are similarly

$$\sigma(a) = [(a + a^2/M)/p]^{\frac{1}{2}} \tag{4}$$

and

$$\sigma(z) = [(z + z^2/M)/p]^{\frac{1}{2}} \tag{5}$$

The determined centre of gravity of the line is

$$G(l) = \sum_i (t_i - b_i)\theta_i / \sum_i (t_i - b_i), \tag{6}$$

where the background intensity at θ_i is given by

$$b_i = a + i(z - a)/n, \tag{7}$$

and $n + 1$ is the number of steps (numbered from 0 to n).

If Δ is the step length and θ_0 is taken as origin, then

$$i = \theta_i/\Delta. \tag{8}$$

G is thus a function of the random variables t_i, a and z, and is therefore a random variable itself. If a reasonable number of counts is recorded at each step the standard deviation of G will be given by

$$\sigma^2(G) = \sum_i \left(\frac{\partial G}{\partial t_i}\right)^2 \sigma^2(t_i) + \left(\frac{\partial G}{\partial a}\right)^2 \sigma^2(a) + \left(\frac{\partial G}{\partial z}\right)^2 \sigma^2(z) \tag{9}$$

From equation 6

$$\frac{\partial G}{\partial t_i} = \frac{\theta_i}{\sum_i (t_i - b_i)} - \frac{\sum_i (t_i - b_i)\theta_i}{\left[\sum_i (t_i - b_i)\right]^2} = \frac{\theta_i - G}{\sum_i (t_i - b_i)} \tag{10}$$

The integrated intensity of the line is

$$L = \sum_i (t_i - b_i) \tag{11}$$

so that

$$\frac{\partial G}{\partial t_i} = (\theta_i - G)/L. \tag{12}$$

Similarly

$$\frac{\partial G}{\partial a} = \frac{-\sum_i \theta_i(1 - i/n)}{\sum_i (t_i - b_i)} + \frac{\sum_i (t_i - b_i)\theta_i \times \sum_i (1 - i/n)}{\left[\sum_i (t_i - b_i)\right]^2} = \frac{n + 1}{6L}[3G - (n - 1)\Delta], \tag{13}$$

and

$$\frac{\partial G}{\partial z} = \frac{-\sum_i \theta_i i/n}{\sum_i (t_i - b_i)} + \frac{\sum_i (t_i - b_i)\theta_i \times \sum_i i/n}{\left[\sum_i (t_i - b_i)\right]^2} = \frac{n + 1}{6L}[3G - (2n + 1)\Delta] \tag{14}$$

Substitution in equation 8 gives

$$\sigma^2(G) = \frac{1}{L^2}\left\{\sum_i (\theta_i - G)^2\left(t_i + \frac{t_i^2}{M}\right) + \frac{(n + 1)^2}{36p}[3G - (n - 1)\Delta]^2\left(a + \frac{a^2}{M}\right) + \frac{(n + 1)^2}{36p}[3G - 2(n + 1)\Delta]^2\left(z + \frac{z^2}{M}\right)\right\} \tag{15}$$

Equation (15) is quite general and a full discussion would occupy considerable space. A simplified expression will be

found for the common practical case where the c.g. is at or near the centre of the range,

$$G \simeq \frac{n\Delta}{2}, \tag{16}$$

and where the X-ray tube is fully stabilized or M is large,

$$M \gg I_t, \tag{17}$$

In this case

$$\frac{\partial G}{\partial a} = -\frac{\partial G}{\partial z} \simeq (n+1)(n+2)\Delta/12L \simeq n^2\Delta/12L, \tag{18}$$

and also the terms divided by M may be neglected in discussing the order of magnitude of $\sigma^2(G)$. Using equations (8) and (18) and writing

$$b = (a+z)/2, \tag{19}$$

equation (15) now reduces to

$$\sigma^2(G) = [TV(t)/\Delta + n^4\Delta^2 b/72p]/L^2, \tag{20}$$

where T is the total intensity of (line plus background) and $V(t)$ is the variance of this profile. The ratio of the second to the first term in this expression may be written

$$\frac{n^4\Delta^3 b}{72pTV(t)} = \frac{n}{72} \times \frac{(\text{range})^2}{V(t)} \times \frac{r}{p} \tag{21}$$

where the range is $n\Delta$ and r is the ratio of the integrated background intensity $[=(n+1)\Delta b \simeq n\Delta b]$ to the integrated total intensity T. The ratio of equation (21) would normally be greater than unity with $p = 1$, but can be reduced by counting for a sufficiently long time at the limits. In the practical cases we have met so far, $n/72 \simeq 1$, $(\text{range})^2/V(t)$ can be 50 or more, and r is usually $< 0{\cdot}3$. Thus, to make the above ratio of the order unity, p must be roughly about 10, but if any of the factors depart radically from the above values p may be adjusted accordingly. If scintillation or proportional counters can be used with pulse-height discrimination, the value of r may be sufficiently low to allow the second term of equation (20) to be neglected when a reasonable value of p is used. The statistical error would then simplify to

$$\sigma^2(G) \simeq TV(t)/L^2\Delta \tag{22}$$

The considerations in the preceding paragraphs are quite general, and independent of any assumption about the line profile. For illustration, and to obtain an indication of orders of magnitude, we may use, as an approximation, the Cauchy or witch-type distribution superimposed upon a constant background I_B, which is of the form

$$I = I_0/(1 + k^2\theta^2) + I_B \tag{23}$$

The peak height is I_0 and the half-width is $2/k$. If the step length is Δ and the number of quanta collected at the peak is I_0, then from equation (22),

$$\sigma^2(G) = \int_{-A}^{+A} \theta^2 \left[\frac{I_0}{\Delta(1+k^2\theta^2)} + \frac{I_B}{\Delta}\right] d\theta \Bigg/ \left[\int_{-A}^{+A} \frac{I_0}{\Delta(1+k^2\theta^2)} d\theta\right]^2 \tag{24}$$

The quantities σ, Δ, and A may be expressed in terms of the half width of the profile, and we will denote them thus by primes:

$$\sigma' = \sigma k/2,\ \Delta' = \Delta k/2,\ A' = Ak/2. \tag{25}$$

The integration then gives

$$\sigma'(G) = \left[2A' - \arctan 2A' + \frac{8(A')^3}{3}\frac{I_B}{I_0}\right]^{\frac{1}{2}} \Big/ 2(I_0/\Delta')^{\frac{1}{2}} \arctan 2A' \tag{26}$$

I_0/Δ' is equal to the number of quanta counted at the peak multiplied by the number of steps in the half-width; this quantity thus gives a measure of the integrated intensity. The value of $\sigma'(G)$ is plotted as a function of I_0/Δ', $2A'$, the range of integration, and I_B/I_0, in Figs. 11 and 12. The

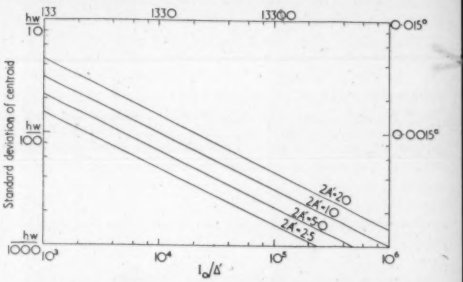

Fig. 11. The standard deviation of the centroid of a Cauchy profile due to counting statistics when step-by-step scanning by the fixed-time method is used. Variation with range of integration for $B = 0$, $M = \infty$. I_0 = number of counts at the peak, $1/\Delta'$ = number of steps in profile half width, $2A'$ = number of half widths in range of integration. The scales at the top and right are the peak intensity and standard deviation in degrees 2θ, respectively, for a profile with half width $0{\cdot}15°2\theta$, and a step length of $0{\cdot}02°2\theta$

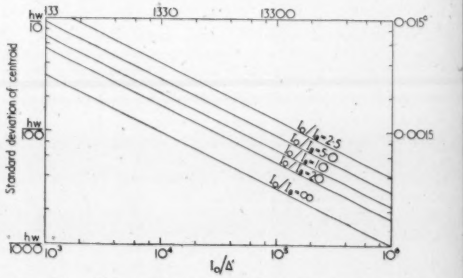

Fig. 12. As for Fig. 11. Variation with peak-to-background ratio I_0/I_B for $2A' = 10$, $M = \infty$

scales at the top and right of the figures are peak intensities, and σ in degrees 2θ, respectively, for a typical practical case where $\Delta = 0{\cdot}02°2\theta$ and the half width is $0{\cdot}15°2\theta$. As an example, for a line with peak-to-background ratio of 4 : 1 with its c.g. found over a range of 6 times the half-width, a standard deviation of $0{\cdot}001°2\theta$ will be obtained by counting, for a fixed time at each step, at such a rate that approximately 7 500 quanta are collected at the peak. For a standard deviation of $0{\cdot}01°2\theta$, approximately 75 counts at the peak will suffice. For 99% confidence limits for the same values, the corresponding numbers of quanta needed would be approximately 48 000 and 480 respectively.

The variation of $\sigma(G)$ with range of integration is of interest. The higher the value of intensity I_t at a given step, the larger will be the statistical uncertainty of the moment of this intensity about the c.g., since the standard deviation is

proportional to $t_f^{\frac{1}{2}}$. The high intensities occur nearer the c.g. than the low intensities in the tails, however, and the increase in uncertainty of intensity is compensated by the shorter moment arm. The resultant uncertainty in the c.g. as a function of integration range does not, therefore, necessarily increase appreciably as the range is extended. The "tails" fall off as the range increases, and the product of the uncertainty in intensity, which decreases, and the length of the moment arm, which increases, depends to a large extent on the background intensity. If the background is high, the decrease of the uncertainty of intensity as the range is increased is very slow and very much more than made up by the increasing length of the moment arm; if the background is low the one effect almost balances the other, and large ranges can be used without appreciably increasing the uncertainty of the c.g. Fig. 13 shows the variation of σ

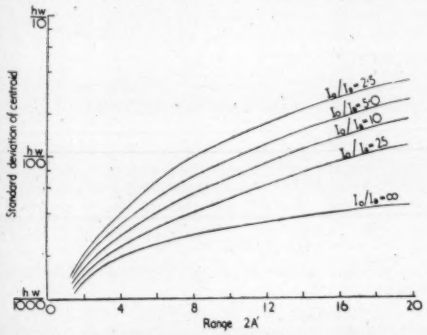

Fig. 13. The standard deviation of the centroid of a Cauchy profile due to counting statistics, when step-by-step scanning by the fixed-time method is used. Variation with range for various values of peak-to-background for $I_0/\Delta' = 10^5$, $M = \infty$

with range for different peak-to-background ratios. The limits, of course, must be accurately located, in either case, or large errors will be introduced by adding moments on one side of the c.g. which are not balanced by the corresponding ones on the other side. The successive-approximation method, however, will give limits which are as accurate as required.

The background encountered with spectroscopic instruments may be sufficiently low for c.g.'s to be almost unaffected by statistical uncertainty in the "tails." The scintillation or proportional counter has a marked advantage over the Geiger counter for measuring c.g.'s, because of the better peak-to-background ratio obtainable with these detectors. With the Geiger-counter diffractometer, except for very strong lines, the ranges must be kept as short as possible, to avoid increasing the statistical error in the c.g. unduly, but this requirement must be balanced against the advantages to be gained by increasing the range, in decreasing truncation and wavelength errors.

8. EXPERIMENTAL TECHNIQUE

The theory of the use of the centre of gravity, as described in the preceding sections, requires the following steps and conditions in practice.

(*a*) *The unsimplified procedure*

(i) Two limits λ_A and λ_B are chosen on a spectroscopically obtained profile on either side of the characteristic line to be used.

(ii) The points on the profile at λ_A and λ_B are joined, thus truncating a portion which is called, for the purpose of this paper, the "line." (The line is thus only defined in relation to two arbitrarily chosen limits; there is no exact physical quantity which can be defined as the emission line, as distinct from the rest of the coherent spectrum, since the characteristic and white components merge imperceptibly into one another. Physically, an X-ray quantum generated by the transition of an electron from an outer shell into an inner one, which is the characteristic emission process, will be diffracted in an indistinguishable manner from an X-ray quantum of the same wavelength, generated by the transition of an unbound electron into an outer shell, which is the white emission process. The spectrum must therefore be treated as a whole, and not split into "line" and "background" without careful definition.)

(iii) The centroid of the line, defined as above, is calculated and called the wavelength of the line λ_g, for use in the Bragg equation.

(iv) An approximate value of d, say d_1, is calculated for the observed reflexion, using either an estimated c.g. or the peak positions.

(v) The value of d_1 is used in the Bragg equation with λ_A, λ_B and λ_g, respectively, to find equivalent angles θ_{A1}, θ_{B1} and θ_{g1}.

(vi) The value of G for the broadening aberrations is found by reference to the published data. The angular range $2\theta_{B1} - 2\theta_{A1}$ must now be checked to see that it is more than about six times this value of G. If not, the original values of λ_A and λ_B must be chosen further apart, or the aberrations reduced.

(vii) The total value of G for all aberrations is found and subtracted from the values of $2\theta_{A1}$ and $2\theta_{B1}$ to give trial limits $2\theta'_{A1}$ and $2\theta'_{B1}$.

(viii) The points on the observed profile at $2\theta'_{A1}$ and $2\theta'_{B1}$ are joined, and the c.g. of the "line" so formed is calculated. This trial value of c.g. will be called $2\theta'_{t1}$. The corresponding value $2\theta_{t1}$ is obtained by adding G and subtracting the dispersion and Lorentz-factor corrections found from published data.

(ix) The value of $2\theta_{t1}$ is compared with the expected value $2\theta_{g1}$. The difference $2\theta_{t1} - 2\theta_{g1}$ is called the asymmetry of the trial.

(x) $2\theta_{t1}$ is used in the Bragg equation with λ_g to find a better value of d, say d_2.

(xi) Steps (v) to (x) are repeated until the asymmetry $(2\theta_{tn} - 2\theta_{gn})$ is zero, when the true value of d, (d_n), will have been obtained.

This full procedure will be required when circumstances invalidate the simplified method to be described below. One such circumstance would be the inability to include a sufficient range to reduce truncation errors to the required degree before reaching the proximity of the filter absorption edge; this will be the case with low-angle lines, say below 60° 2θ on a reasonable diffractometer. Another such circumstance would be the inability to neglect the effects of dispersion and Lorentz factor on the symmetry of the observed range required for the simplified procedure; this will be the case with high-angle lines, say above 140° 2θ.

(*b*) *The simplified procedure*

(i) Limits λ_{A1} and λ_{B1} are chosen on a spectroscopically obtained profile on either side of the characteristic line to be used.

(ii) The points on the profile at λ_{A1} and λ_{B1} are joined, thus defining a "line."

(iii) The centroid of this line is calculated, say λ_{g1}.

(iv) The mid-point of the range is compared with λ_{g1}; the difference, $\frac{1}{2}(\lambda_{A1} + \lambda_{B1}) - \lambda_{g1}$, is called the asymmetry of λ_{g1}.

(v) The range λ_{A1} to λ_{B1} is changed to a new range λ_{A1} to λ_{B2} by subtraction of twice the asymmetry of λ_{g1} from λ_{B1}. λ_{g1} is now at the mid-point of the new range.

(vi) The steps (ii), (iii) and (iv) are repeated with new limits until the asymmetry is zero, when λ_g^* will have been obtained corresponding to the final range $\lambda_{Bn} - \lambda_{A1} = \lambda^*$.

(vii) The steps (i) to (vi) are repeated for enough values of final range, λ^*, to plot a graph of λ_g^* against λ^*.

(viii) The asymptotic value of λ_g^* as the range is increased, before the filter absorption edge is reached, is found and called $G(\lambda^*)$; this is the value of λ for use in the Bragg equation.

(ix) Steps (i) to (vi) are performed on the observed profile, replacing values of λ by values of θ, taking care that the final range is sufficiently long for the asymptotic value of λ_g^* to apply, and for the truncation errors to be neglected.

(x) The value of θ_g^* so obtained is corrected for aberrations by the addition of the sum of the appropriate values of G taken from the literature. The Lorentz and dispersion factors may be subtracted if they are sufficiently small for the simplified method to be used.

(xi) The corrected value of θ_g^* is used in the Bragg equation with $G(\lambda^*)$, to obtain the true value of d.

The first eight steps of this simplified procedure need only be performed once, and the appropriate values of $G(\lambda^*)$ for various radiations can be tabulated when sufficiently accurate spectral profiles are available. The method may then be used without knowledge of the spectral distribution and reduced merely to finding a symmetric c.g. over a sufficiently long range on the observed profile.

A method developed at Cardiff for the experimental determination of such a c.g. will now be described. (See also Pike.[11]) A preliminary fast chart recording is made to locate the lines to be used. A starting point for the step-scanning process is chosen for each line according to the conditions described above. This point will be in the tail of the line, sufficiently far out to use the asymptotic value of λ_g^*, and to avoid truncation errors, but not so far that the filter absorption edge is approached or unnecessarily large statistical errors are introduced. The limiting condition with fairly high-angle lines will be the first-mentioned; a range of angle corresponding to 0·0125 Å for the copper Kα doublet has been estimated. The statistical accuracy desired is achieved by estimating the peak-to-background ratio and range, and using the graphs of Figs. 11, 12 or 13, to find the number of counts required at the peak. The counting time for the fixed-time step scan is then determined by reference to the counting rate at the peak on the chart record.

The starting point, θ_a, and counting time having been determined, the diffractometer is set and several counts are made at the initial limit. Ten times the normal counting time is usually used here, as this is a built-in facility of our equipment[14] with scale-of-ten dekatron counters. The step-scan is now started and the *accumulated* total of counts is recorded at each step. These are obtained from a scaler which is not zeroed between each step; the scaler is zeroed initially and the successive readings are denoted $S_1, S_2, \ldots, S_n, \ldots$.

As the run proceeds, the values of S are summed. The successive-approximation procedure is avoided by determining the correct step on which to end the scan in the following manner. As the estimated far limit θ_z is approached, at the end of each step, before adding the new value of S to the total ΣS, the quotient $\sum_1^n S/S_{(n+1)}$ is found (a slide-rule is sufficiently accurate). This quotient will approach $\frac{1}{2}n$ in discrete steps, and the step at which it reaches $\frac{1}{2}n$ is the correct second limit. The intensity at this limit is also determined over a longer time in a similar manner to the initial limit.

The following quantities are defined.

Δ = step length
θ_a = initial limit, step 0
θ_z = final limit, step n
$n = (\theta_z - \theta_a)/\Delta$
$S_{(n+1)} = T$ = integrated total intensity
$\sum_{i=1}^{n} S_i = \Sigma S$ = sum of partial sums of intensity
a = intensity at θ_a
z = intensity at θ_z
$b = \frac{1}{2}(a + z)$ = average background intensity
$B = (n + 1)b$ = integrated background intensity
$\delta = z - a$ = rise in background over the range
$r = B/T$ = ratio of integrated background to integrated total intensity.

The centre of gravity of the line θ_g^* is found by inserting the above quantities in the formula

$$\theta_g^* = \theta_z - \left\{\frac{\Sigma S}{T} + \frac{r}{1-r}\left[\frac{\Sigma S}{T} - \frac{n}{2} + (n+2)\frac{\delta}{12b}\right]\right\}\Delta\theta \quad (27)$$

A similar formula was originally given in equation (10) of Ref. 11, but since this was published an error has been pointed out by J. Taylor of Philips Laboratories, Irvington. The correction involves replacing the term $+\frac{1}{2n}$ by $-\frac{1}{2n}\frac{(\delta)}{3b}$, to give the above. C.g.'s found with the old formula will be very slightly affected by the correction.

If a chart recorder is used with a step-by-step scanning method, as suggested by Ladell, Parrish and Taylor,[9] the intensities t_i are read off the chart; the value of ΣS in this case may be found on an adding machine by the procedure described by Pike.[11]

The method for locating the second limit described above will ensure that the c.g. found is very close to the centre of the range. If excessive background slopes are present, however, the asymmetry may amount to a few hundredths of a degree, in which case the appropriate amount could be added to or subtracted from the range for a second approximation. The magnitude of errors arising from lack of exact symmetry are of interest. As explained in Section 6, the effect is that of using radiation, to determine the observed c.g., of wavelengths that have not been taken into account in determining the corresponding spectral c.g. The c.g. of the silicon 533 line with CuKα radiation has been determined for a given range, 135·840° to 138·400°, by the symmetric-limit method. The line may be slightly high for the simplified procedure to be used, but this will not greatly affect the conclusions to be drawn. The readings of intensity were taken from a chart recording obtained by Ladell, Parrish, and

Taylor, and kindly made available to us for the purposes of this study. A scintillation counter was employed with the standard Norelco diffraction equipment. The c.g. is not corrected for any aberrations. The effect of adding moments to one side of the line and not the other, was investigated by plotting the error in c.g., ΔG, against the asymmetry of the range, defined above as the difference between the c.g. and the mid point, $(G - m)$. The result is shown in Fig. 14.

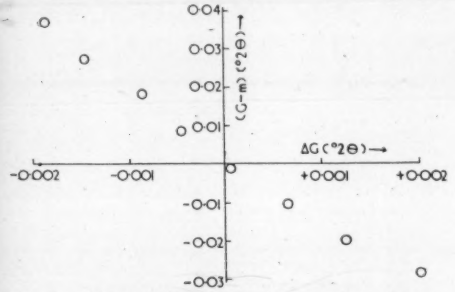

Fig. 14. Effect of errors in locating the limits of integration. The shift of the centroid, ΔG, is plotted against the difference between the centroid G and the mid-point of the range, m. Silicon 533 Cu$K\alpha$ (135·840–138·400)

The effect will, of course, vary from line to line, but, in general, the errors arising from this cause will be quite negligible if the method of finding the limits described above is adopted.

Another experimental point of interest is the variation of c.g. with range. The estimated minimum range of 0·0125 Å for Cu$K\alpha$ was derived from a study of the same silicon line. The symmetric c.g., θ_g^*, was found for a series of angular ranges corresponding to symmetric ranges of wavelength λ^*. The result is shown in Fig. 15. The effect of counting

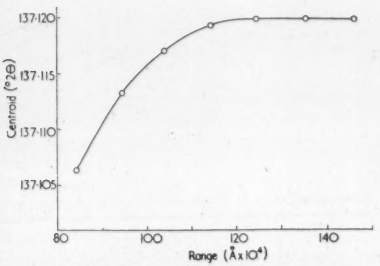

Fig. 15. Effect of increasing the range of integration on the c.g. found by the symmetric-limit method. Silicon 533 Cu$K\alpha$

statistics was minimized by drawing a smooth curve through the experimental points near the limits as described in Section 7. The asymptotic trend may be partly due to decreasing truncation errors, but is mainly due to the asymmetry of the $K\alpha$ doublet giving way to a negligible effect of lack of symmetry in the tails. This trend can be seen clearly in Fig. 16, where the points on the profile given by the symmetric-limit method are joined to show the effect of increasing range on the "line," defined, as above, by the truncated portion of the profile. The ranges in this figure correspond to the points plotted in the previous figure and the two may be studied together as an interesting demonstration of the likely effects of taking too short a range. It was hoped at one stage in our investigation that such a curve could be used to predict the effect of enforced shortening of ranges due to proximity of neighbouring lines in a complicated pattern, but the aberrations encountered in normal practice seem to cause a sufficiently large truncation error to vitiate this process. In the high-angle region where the absorption edge of the filter is not approached, and where the coherent contributions from other planes vary very slowly over the region of the line due to the high dispersion (or where a detector with pulse-height discrimination is used which will not respond to

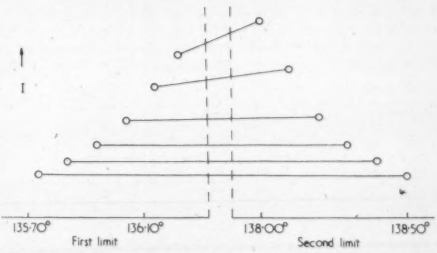

Fig. 16. The truncation line as a function of range of integration for the symmetric-limit method. The lines correspond to the points of Fig. 15. Silicon 533 Cu$K\alpha$

this coherent radiation), the levelling off of the truncation line to the slope of the "general" background at a large distance from the line can be used to find suitable limits of integration for the c.g. This method has been developed by Ladell, Parrish and Taylor,[9] who have found that, within the present limits of experimental error, the c.g.'s of the back-reflexion lines of silicon above $2\theta = 100°$ (Cu$K\alpha$) can be found to give a single lattice parameter, free of systematic variation, by using this property. The method consists essentially of determining a truncation line which is level with the "general" background and which cuts off approximately ten per cent of the intensity of the line above this background. The figure of 10% has been found empirically to give the best results, giving a range which is not so long that errors in the limits appreciably affect the c.g. and not so short that truncation errors are excessive. The "line" in this method is defined in a slightly different manner from that developed in this paper. It consists of the portion above the truncation line plus the portion, equal in range, between the truncation line and the estimated general background.

The wavelength c.g. is also slightly different, the limits of integration being found by cutting off 10% of the spectral profile above the general background in the same way.

A particular use of these methods of finding accurate d values, which is of interest in connexion with work on the A.S.T.M. X-ray Powder Data File being carried out at Cardiff, is the extreme usefulness of accurate low-angle line positions for indexing powder patterns. Extrapolation methods can be used for accurate lattice-parameter measurements, but for work where the unit cell is unknown these are of no avail; each line must instead be freed of systematic errors, before indexing procedures are tried, if success is to be achieved on a routine scale. Preliminary results of work on the value of c.g.'s compared with peaks for this purpose

are promising and it is hoped that these will be published shortly.

9. CONCLUSIONS

Sufficient experimental work is not yet available to show that the theoretical advantage of the c.g. as a measure of line position can yet be fully realized in practice over the whole range of Bragg angles, but preliminary results from Irvington and Cardiff show a distinct advantage to be gained by using c.g.'s instead of peaks. It is hoped that experimental work at present in progress will increase our understanding of the magnitudes of remaining errors, and that, as a result, considerable advances may be made over the present techniques using peak values.

This theoretical investigation leads us to conclude that there is a strong possibility that the disadvantages discussed will prove to be of small account compared with the increase in objective accuracy to be gained. The most pressing need at the present is for more accurate knowledge of the characteristic spectral distributions, and until such knowledge is available the theory cannot be used to its full potentialities in practice.

10. ACKNOWLEDGEMENTS

We wish to record our indebtedness to Dr. J. Ladell, Dr. W. Parrish and Mrs. J. Taylor, of Philips Laboratories, Irvington, New York, for most valuable co-operation during the course of this work, both in providing experimental data for mutual study, and in theoretical criticism of many points arising. Our thanks are also due to Mr. B. W. Delf, of this department, for computational work. The work has been carried out in connection with a programme supported by the [British] Institute of Physics for investigating possibilities for improving the A.S.T.M. X-ray Powder Data File.

REFERENCES

(1) PARRISH, W., and KOHLER, T. R. *Rev. Sci. Instrum.*, **27**, p. 795 (1956).
(2) WILSON, A. J. C. *Proc. Camb. Phil. Soc.*, **36**, p. 485 (1941).
(3) LANG, A. R. *J. Appl. Phys.*, **27**, p. 485 (1956).
(4) PIKE, E. R. *Acta Crystallogr.* (To be published.)
(5) PIKE, E. R., and WILSON, A. J. C. *Proc Phys. Soc. [London]*, **72**, p. 908 (1958).
(6) WILSON, A. J. C. *J. Sci. Instrum.*, **27**, p. 321 (1950).
(7) WILSON, A. J. C., and PARRISH, W. *Acta Crystallogr.*, **7**, p. 627 (1954). (Abstract only.)
(8) PIKE, E. R. *J. Sci. Instrum.*, **34**, p. 355 (1957).
(9) LADELL, J., PARRISH, W., and TAYLOR, J. (In preparation.) Brief abstract *Acta Crystallogr.*, **10**, p. 741 (1957).
(10) PIKE, E. R., WILSON, A. J. C., and HUGHES, J. W. *Acta Crystallogr.*, **10**, p. 852 (1957). (Abstract only.)
(11) PIKE, E. R. *J. Sci. Instrum.*, **35**, p. 34 (1958).
(12) PIKE, E. R., and ROGERS, D. (In preparation.)
(13) NIGAM, A. N. *Science and Culture (India)*, **20**, p. 445 (1955).
(14) HUGHES, J. W., and PIKE, E. R. *J. Sci. Instrum.*, **33**, p. 204 (1956).

Effect of temperature and moisture content on the orientation produced by the drawing of nylon 66

By C. G. CANNON, B.Sc., F.Inst.P., and F. P. CHAPPEL, M.Sc., Ph.D., A.Inst.P., British Nylon Spinners Ltd., Pontypool, Monmouthshire

[*Paper first received* 30 *May, and in final form* 30 *October*, 1958]

Increase in moisture content or ambient temperature up to about 165° C, increases the maximum extension obtained by drawing nylon 66 filaments and the resulting orientation of the molecules due to their increased mobility. Above 160° C disorientation due to thermal energy offsets this, and lower birefringences were observed for a given extension. The results are consistent with adiabatic drawing at a neck up to a natural draw ratio determined by the ambient temperature, combined with isothermal drawing uniform along the length of the specimen.

Nylon extruded in the form of filaments can be relatively unoriented, the degree of orientation increasing as the extrusion speed increases. The orientation is further increased by drawing the filament beyond the yield point to several times its original length. The degree of extension is commonly measured by a parameter known as the draw ratio, this being here defined as the ratio of the final length of the filament to its original length.

The degree of orientation may be measured by such means as birefringence, X-ray diffraction, dichroism and swelling. The authors have investigated the change of orientation of nylon 66 (polyhexamethylene adipamide) with slow drawing by hand over a temperature range of 20–250° C at normal humidity, and over a temperature range of 20–100° C when wet. They have used birefringence as the orientation parameter which, since it is a molecular property, indicates the average orientation of both ordered (crystalline) and disordered material. Preliminary results for hand drawing at room temperature have already been reported.(1) The important effect of rate of extension, particularly much higher rates, will be treated in a subsequent paper.(7)

EXPERIMENTAL

Drawing. The filaments were taken from two different extruded samples, both being of low spun birefringence (0·0015) and of initial diameter 94 μ. The samples contained some spherulites.

All the drawing was done by hand, the rate of extension being about 6 cm/s. For drawing at normal humidity a cotton thread was attached at each end of a filament 2 in. long. It was then suspended inside a tubular furnace, the temperature of which was measured with a thermocouple. Before drawing, a filament was allowed to condition in the furnace for ten minutes. After being drawn the filament was held in the furnace for two minutes at the final extension. It was then removed from the furnace and stored for twenty-four hours at 20° C and 60% r.h. This procedure was adopted to ensure uniformity of treatment and to ensure that the filaments had all reached equilibrium. At any particular temperature a number of filaments were drawn to varying lengths up to the breaking extension. For temperatures of 150° C and above an atmosphere of nitrogen replaced air to prevent thermal oxidation. In one experiment

at 175° C, the filaments were drawn and held for various times up to ten minutes at the final extension to determine the effect of holding time.

Filaments were also drawn at 22, 60 and 100° C in water and in steam. The filaments were held for ten minutes before drawing and for two minutes after drawing in the water or in the steam. After removal they were stored for twenty-four hours as before.

Measurement of birefringence and draw ratio. The birefringence measurements were made with a polarizing microscope. The filaments were mounted in cedar-wood oil and the optical path difference p, between the ordinary and extraordinary wavefronts, measured with a Berek compensator. The filament diameter d was measured at the same place on the filament. The filaments were, at all stages of drawing, taken as circular in cross-section. Any appreciable deviation from circularity would have been apparent from the non-symmetry of the birefringence fringes.

The birefringence, $\Delta\mu$, was then calculated as

$$\Delta\mu = P/d$$

The draw ratio was calculated as

$$D = d_0^2/d^2$$

where d_0 is the diameter of the undrawn filament. The draw ratio thus defined only will be equal to the draw ratio defined on the basis of extension in length (as given above) for a constant volume system. The small increase in density on drawing of about 0·4%[2] would make D greater than the extension draw ratio; but D will be less than the equivalent machine draw ratio because in these experiments the yarn was allowed to relax after drawing.

RESULTS

The birefringence was plotted as a function of filament diameter d for all the temperatures employed. In Fig. 1 the results for experiments at 22 and 155° C are plotted.

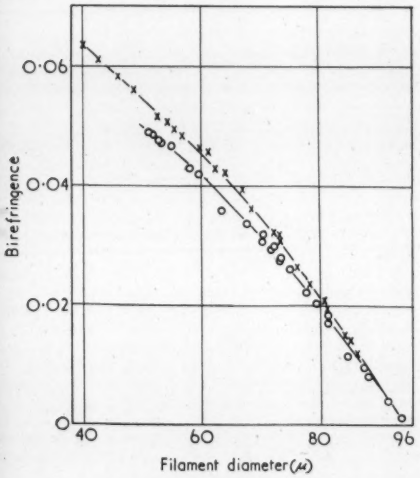

Fig. 1. Variation of birefringence with filament diameter

—○—○ = 22° C. —×—× = 155° C.

Smoothed curves were drawn through the values at each temperature and graphs of birefringence *versus* draw ratio D were plotted. In Fig. 2 the curves obtained at 22, 105 and 155° C are shown.

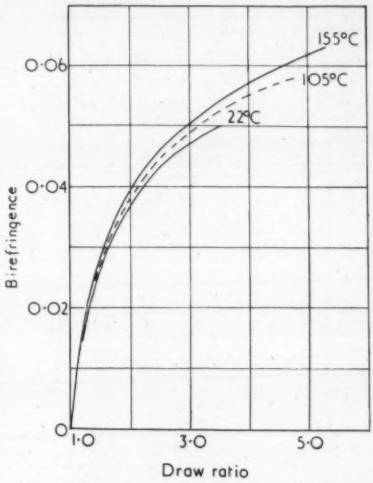

Fig. 2. Variation of birefringence with draw ratio

As the temperature was increased up to approximately 170° C, and also when drawn wet, the extent to which the filaments could be drawn also increased. For example, at a temperature of 22° C, the maximum draw ratio that could be obtained was 3·5 whilst at 155° C it had increased to 5·5.

In Fig. 3 the birefringence attained at any draw ratio is plotted as a function of temperature for a series of draw ratios between 2·0 and 5·0. For the lower temperatures, the experimentally obtained curves of birefringence *versus* draw ratio were extrapolated to a draw ratio of 5·0. The extrapolated points refer therefore to a region which was not experimentally realizable.

Filaments from the first sample could not be drawn above 200° C. At 225° C, for example, they drew down at a very abrupt neck, with little orientation, and broke. The second sample was successfully drawn up to 255° C. The birefringence temperature curves for the two samples deviate above 180° C in line with their different behaviour.

Temperature has an annealing effect on nylon 66, producing an increase in crystalline order.[3] It is possible that the annealing, and not the actual temperature of drawing, might be responsible for the increased birefringence observed up to 165° C. Filaments were accordingly annealed in the furnace at 150° C for ten minutes, removed and allowed to cool. They were then drawn at room temperature in the usual manner. The birefringence-draw ratio relationship so obtained was very similar to that for unannealed filaments drawn at room temperatures, the only difference being that the filaments ruptured internally at draw ratios above 2·5, producing internal cavitation. This was presumably due to the increased or improved perfection of crystallinity on annealing.

The effect of holding time after drawing on birefringence

was very small. At 175° C and a draw ratio of 5·0, the birefringence increased from 0·061 to 0·063 after ten minutes, probably owing to the relaxation of stress while the filament was held at constant extension.

The results for filaments drawn wet lie above those for filaments drawn at normal humidity. The two curves in the region below 100° C are nearly parallel.

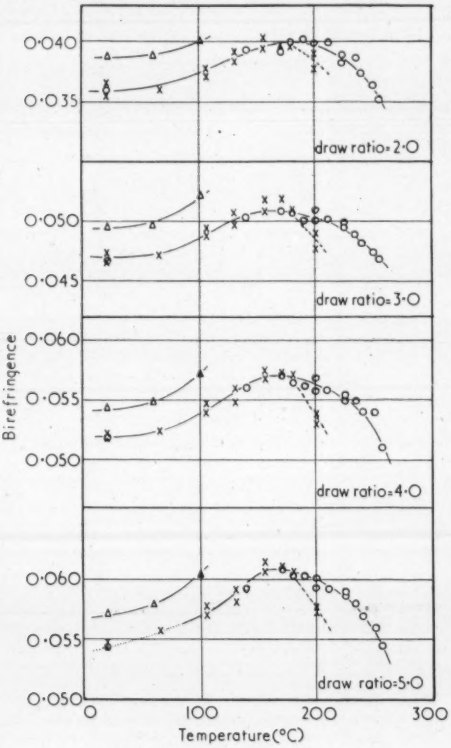

Fig. 3. Variation of birefringence with temperature

—×—× = 1st sample.
—○—○ = 2nd sample.
···· × ···· × = extrapolated region.
—△—△ = 1st sample in water.

DISCUSSION

Birefringence and temperature of drawing. The birefringence is very nearly a linear function of filament diameter under all experimental conditions. This is in good agreement with the theory of Culpin and Kemp.[1]

The present results show (Fig. 3) that especially at the lower draw ratios the birefringence increases very slowly as the temperature of the surroundings is raised to approximately 90° C. A more marked increase occurs for a further rise in temperature to approximately 165° C, above which the birefringence drops. The drop is more rapid for the first sample which would not draw above 200° C. This disorientation of the second sample increased more and more rapidly up to 255° C above which this sample could not be drawn. White[4] has shown by differential thermal analysis that disorientation begins in drawn yarns at about 200° C and becomes very rapid at 255° C in agreement with the present authors' results.

Marshall and Thompson[5] have discussed the drawing of high polymers. They show that if a polymer is drawn under adiabatic conditions, the filament will draw at a neck if the load-extension curve falls to lower loads at higher temperatures. The temperature in the neck will then rise until the adiabatic stress-strain curve becomes horizontal. In drawing, work is done which is converted into heat, this heat producing the rise in temperature. The draw ratio defined by the neck is known as the natural draw ratio (n.d.r.). This decreases with increasing temperature of the surroundings. Above a certain temperature—the "critical" temperature—the filament will cease to draw at a neck. If the material is uniform in properties along its length it will then draw down uniformly. Hookway[6] has shown that this temperature is approximately 90° C for nylon 66, and that, for unrelaxed machine drawn yarns, the n.d.r. decreases from about 5 at room temperature to 3 at 80° C and to 1 at 90–100° C.

Even for low rates of extension, as in hand drawing (approximately 6 cm/s) unoriented nylon will draw at a neck when the temperature of the surroundings is below the critical temperature. The heat is then developed under almost adiabatic conditions, and so the material will draw in the neck at a temperature of around 90° C up to the n.d.r. corresponding to the temperature of the surroundings. When the filaments are extended beyond the n.d.r., or if the temperature of the surroundings is above the critical temperature, the extension will take place uniformly. The heat will then be developed uniformly along the total length of the filament instead of just within the short length of the neck, as when drawing up to the n.d.r. This drawing is therefore taking place under nearly isothermal conditions, because the rate of development of heat per unit length will be small at low drawing speeds.

Hence a marked change of birefringence with temperature would not be expected when drawing to low draw ratios at temperatures below approximately 90° C, i.e. in the region of drawing at a neck. Beyond the neck, the drawing will be taking place at the temperature of the surroundings, i.e. at less than the critical temperature, so that only the later stages of drawing will be temperature dependent. The birefringence does change slightly more with temperature in this range for higher draw ratios. Above approximately 90° C, where the drawing is isothermal throughout the entire drawing range, a more marked temperature sensitivity is to be expected.

The effect of increase of temperature up to around 160° C and of moisture content (up to at least 100° C) is thus to increase the orientation as measured by birefringence and, at least in hand drawing, to increase the maximum obtainable extension. This is probably due to the increasing mobility of the molecular units, which are therefore able to adjust themselves more readily to the applied tension. Above 160° C, however, the thermal energy of the molecular units becomes sufficiently large for disorientation to occur, even under an applied tension, resulting in lower birefringences for a given extension.

Effect of increase of drawing speed. As the speed of drawing increases, the heat due to the work of drawing is developed within a filament more rapidly. Therefore the

conditions in the range of draw ratios above the n.d.r. will cease to be isothermal and will become more adiabatic. The temperature of the filament during drawing beyond the n.d.r. will then rise above that of the surroundings. Now at high drawing speeds (e.g. 500 cm/s), values of birefringence above 0·06 for fully drawn filaments are commonly found compared with the present work, with values up to 0·06. The present work shows that increase of temperature up to 165° C increases the birefringence obtained at any given draw ratio. The authors suggest that the high values of birefringences (about 0·060–0·065) found for filaments drawn at high speeds may be partly due to the increase in the effective temperature of drawing at these speeds.

ACKNOWLEDGEMENTS

The authors wish to thank Miss J. Tidmarsh for her assistance in the experimental measurements and the Directors of British Nylon Spinners Ltd., for permission to publish this paper.

REFERENCES

(1) CULPIN, M. F., and KEMP, K. W. *Proc. Phys. Soc.* [*London*] *B*, **69**, p. 1301 (1956).
(2) BLACK, C. E., and DOLE, M. *J. Polymer Sci.*, **3**, p. 358 (1948).
(3) FORWARD, M. F., and PALMER, H. J. *J. Text. Inst.*, **45**, p. 510*T* (1954).
(4) WHITE, T. R. *Private communication*; *Nature* [*London*], **175**, p. 895 (1955).
(5) MARSHALL, I., and THOMPSON, A. B. *Proc. Roy. Soc. A*, **221**, p. 541 (1954).
(6) HOOKWAY, D. C. *J. Text. Inst.*, **49**, p. 292*P* (1958).
(7) BADAMI, D. V., CHAPPEL, F. P., CULPIN, M. F., MADOC-JONES, D., and TRANTER, T. C. *Rheologica Acta* (in press). (Paper presented at 3rd International Conf. Rheology, Germany, September 1958.)

Thermionic properties of thorium deposits on control grid materials*

By J. A. CHAMPION, M.Sc., A.Inst.P., Research Laboratories, The General Electric Co. Ltd., Wembley, England

[*Paper first received* 23 *October, and in final form* 10 *November*, 1958]

Experiments are described in which the emission is measured from thin films of thorium deposited on different platinum–molybdenum phases of approximate composition Pt, Pt_3Mo, Pt_2Mo, Pt_3Mo_2 and Mo. The emission from all the platinum phases is considerably lower than that from pure molybdenum. The lowest emission was observed with the Pt_3Mo phase. The emission from thorium deposited on to the Pt_3Mo_2 phase decays rapidly at temperatures of 1300° C and above, whereas that from similar deposits on molybdenum does not.

The emission from thin films of thorium deposited on to titanium and tungsten has also been studied. The emission from a layer on titanium that had been thoroughly pre-cleaned was found to be much less than that from a similar layer on tungsten.

The application of these results to the suppression of grid emission in the presence of thoriated tungsten cathodes in transmitting valves is discussed.

1. INTRODUCTION

Thoriated tungsten filaments have been used in transmitting valves for a number of years. These filaments have the considerable advantage that they operate at a much lower temperature than pure tungsten thus saving a considerable amount of power, but have the disadvantage that the thorium which is evaporated from their surface may settle on the grid wires and give rise to unwanted grid emission. Various methods have been described in the literature for suppressing this unwanted grid emission. In particular the use of platinum-clad molybdenum has been mentioned, for example by Ayer[1] and by Espersen and Rogers.[2] Some previous unpublished work by Wright[3] in these laboratories indicated that the emission from thin films of thorium deposited on to platinum-coated molybdenum wire depended on the heat treatment given to the wire. A complete study of the platinum-molybdenum system was not made at that time, however, and up till now no account of the effect of the nature of the surface of the platinum-molybdenum wire on the emission seems to have been published. Rooksby[4] has shown that if a molybdenum wire coated with platinum is heated in vacuo then the molybdenum diffuses into the platinum. As the temperature is increased a number of successive phase changes occur at the surface due to the increasing proportion of molybdenum in the platinum. First the face-centred cubic platinum structure (α) is distorted to a tetragonal phase (β) of approximate composition Pt_3Mo and then to an orthorhombic phase (γ) of approximate composition Pt_2Mo and finally to a hexagonal phase (δ) of approximate composition Pt_3Mo_2. The temperatures and times required to produce these different phases depend on the thickness of the original platinum coating. In the present work the emission has been studied from each of the platinum–molybdenum phases when contaminated with a thin layer of thorium.

Espersen and Rogers[2] have examined the grid emission from titanium in the presence of a thoriated-tungsten cathode, and their results indicated that the emission was very low compared with that from tungsten under similar conditions. It was considered that titanium merited further study and the experiments carried out are also included in this paper.

2. EXPERIMENTAL VALVES

The experimental valves were similar in design to those used in earlier grid emission work.[5] Fig. 1(*a*) shows the design used for experiments concerning thorium on platinum–molybdenum and Fig. 1(*b*) shows that used for thorium on titanium. In both cases the valve consisted of a thorium source mounted on a foot tube and equidistant from the two or more wires to be tested. The thorium source comprised a globule of thorium metal supported on a tungsten wire. This was prepared by spot welding a small piece of thorium metal to the wire and premelting in vacuo before mounting in the valve. The source and wires to be tested could be heated independently electrically and were surrounded by a rectangular nickel anode. Slots were cut in the anode so that the temperature of the source and wires could be observed with an optical pyrometer. All temperatures quoted include a correction for the spectral emissivity of the material concerned. A barium getter was fixed to the bottom of the assembly.

After sealing into a glass envelope the valve was exhausted and baked on a mercury diffusion pump with liquid air trap.

* Communication No. 831 from the Staff of the Laboratories.

The anode and getter were outgassed by eddy current heating and the source and wires by electrical resistance heating. Following this the barium was released from the getter and the valve sealed off from the pump.

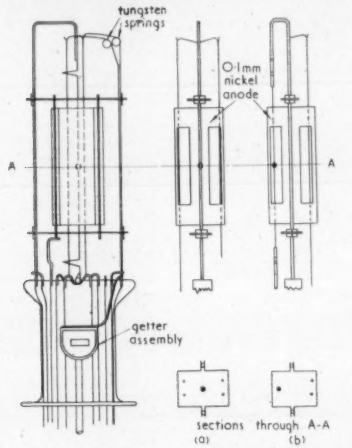

Fig. 1. Valve assemblies used for deposition experiments

It is estimated from the results of Jenkins and Trodden[6] that in a typical transmitting valve thorium is evaporated from the thoriated-tungsten filament at a rate of about 1 monolayer in 10 hours at the normal operating temperature of 1730° C and up to 4 monolayers per hour at 1930° C is reached during normal processing. In a valve with typical geometry the rate of deposition of thorium on to the control grid is likely to be about one-third of the rate of evaporation from the cathode. Deposition rates used in the experiments to be described corresponded to about 4–6 monolayers per hour and so represent the worst case which might occur if valves were aged about 100° C hotter than usual. To produce this rate of evaporation the temperature of the thorium source was maintained at about 1500° C.

3. PLATINUM–MOLYBDENUM

The first experiment was performed with a valve containing three platinum–molybdenum wires having surface structures α, β, γ respectively, prepared according to Table 1, and one molybdenum wire (μ) also 0·1 mm in diameter. The area of each thorium deposit was estimated to be 0·015 cm^2. During processing the wires were outgassed by electrical heating but care was taken to limit the temperature so that no further change in structure took place. After processing the valve the thorium source was heated to a temperature of about 1500° C with the receptors cold and at intervals of a minute, each of the four wires was heated to 1000° C and the saturated emission measured with a potential of 50 V applied to the anode. The emission corresponding to 1 monolayer and 5 monolayers on the various wires are given in Table 2, 1 monolayer being taken as the amount of thorium giving maximum emission from the molybdenum. A similar experiment was performed with another valve containing samples of β, γ, δ and μ, the results of which are also given in Table 2.

In a further experiment deposition of thorium was continued until 2 monolayers had been deposited on to the receptors. Wires δ and μ were heated to 1300° C and the change in emission with time was observed. Similar experiments were performed for temperatures of 1400° C and 1500° C. The results are shown in Fig. 2. In another

Table 1. *Heat treatments employed to produce different single phases at surface of platinum-clad molybdenum wire 0·1 mm diameter, the initial thickness of platinum being about 0·003 mm*

Surface structure	*Heat treatment (in vacuo)*
α: face-centred cubic (Pt)	none
β: tetragonal (approx. Pt_3Mo)	1000° C for 6 h
γ: orthorhombic (approx. Pt_2Mo)	1100° C for 24 h
δ: hexagonal (approx. Pt_3Mo_2)	1300° C for 1 h

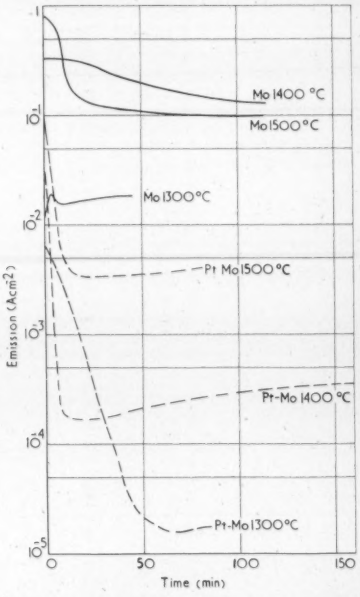

Fig. 2. Change of emission with time from molybdenum and platinum-clad molybdenum when maintained at different temperatures while thorium was deposited on to them at a rate of 1 monolayer in about 10 min

Table 2. *Emission from molybdenum and platinum-clad molybdenum wires after 1 monolayer (a) and after 5 monolayers (b) of thorium had been deposited (A cm^{-2} measured at 1000° C)*

	Molybdenum		*Platinum-clad molybdenum*									
	μ		α		β		γ		δ	
	(a)	*(b)*	*(a)*	*(b)*	*(a)*	*(b)*	*(a)*	*(b)*	*(a)*	*(b)*
1st valve	$6·0\times10^{-4}$	$3·5\times10^{-4}$	$3·0\times10^{-7}$	$2·0\times10^{-7}$	$<0·7\times10^{-7}$	$<0·7\times10^{-7}$	$0·9\times10^{-6}$	$1·2\times10^{-6}$	—	—
2nd valve	$3·2\times10^{-4}$	$1·33\times10^{-4}$	—	—	$2·0\times10^{-7}$	$0·7\times10^{-7}$	$0·7\times10^{-6}$	$1·6\times10^{-6}$	$1·1\times10^{-6}$	$1·1\times10^{-6}$

experiment about 2 monolayers of thorium were deposited on to surfaces δ and μ with the receptors cold. The temperatures of δ and μ were then raised to 1000° C and the emission measured quickly. The temperatures were then raised to 1100° C and the emission again measured quickly. This procedure was repeated for 1200° C, 1300° C, 1400° C and 1500° C. The emission at 1000° C was re-checked to confirm that no appreciable change had taken place. The results are shown in Fig. 3. Also shown in the same figure for comparison is the plot for the platinum-clad molybdenum grid wires of a high power transmitting valve type ACT101 after processing but before commencement of life. The emission indicated by this latter set of points includes a certain amount of electrical leakage current which causes the lower points to be above the extrapolated straight line. A Richardson plot of these results gave a work function of 2·74 eV for thorium on molybdenum and 3·23 eV for the thorium on δ–Pt–Mo (Pt_3Mo_2). The results are discussed later.

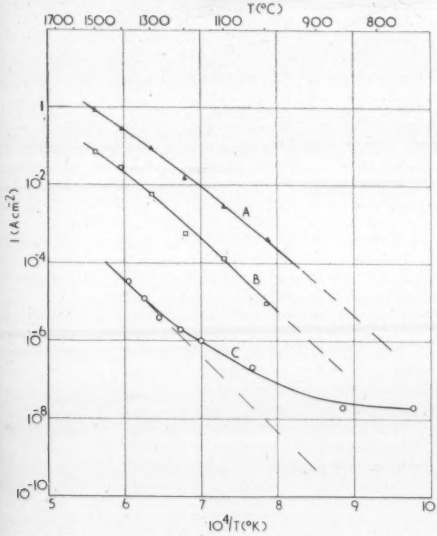

Fig. 3. Variation of emission with temperature for thorium deposited on various substrates

A, 2 monolayers of thorium on molybdenum; *B*, 2 monolayers of thorium on δ–Pt–Mo; *C*, material evaporated from thoriated tungsten filament on to Pt–Mo grid of ACT 101 valve.

4. TITANIUM

Experiments were performed in which the emission from thorium deposited on to a titanium wire was compared with that from similar deposits on a tungsten wire. Both wires were 0·1 mm in diameter and the area of each thorium deposit was in this case estimated to be 0·025 cm². The thermionic properties of this film of thorium on tungsten are well known (see, for example, the account given by Reimann[7]).

The valve used was assembled and processed as described in Section 2. Whilst the valve was still on the pump the tungsten wire was cleaned by flashing at 2300° C for 2 min and the titanium wire at 1100° C for 2 min.

As the temperature of a grid in a typical transmitting valve is known to reach 1000° C with a moderate power dissipation, in the first experiment the temperatures of the wires were kept at 1000° C while thorium was deposited on to them. The emission from each of the wires was measured at intervals and the results are shown in Fig. 4. One monolayer was

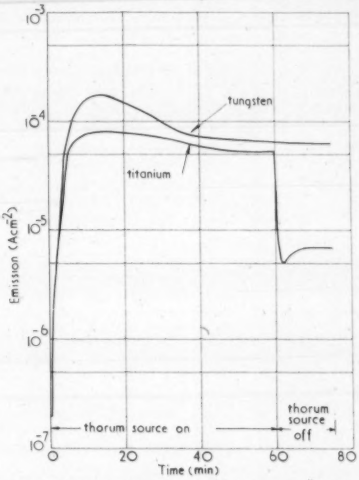

Fig. 4. Change of emission with time from thorium on tungsten and titanium wires maintained at 1000° C

taken to be that thickness of thorium giving maximum emission from the tungsten. After about 4 monolayers of thorium had been deposited on the wires the source was switched off but the temperatures of the titanium and tungsten wires were maintained at 1000° C. The emission from each of the wires was observed for the next 15 min and the results are also shown in Fig. 4.

As it was thought that the titanium wire might have been incompletely cleaned by flashing at 1100° C the titanium was heated to 1150° C for 20 min before carrying out a further series of experiments. In this further series thorium was deposited continuously at a rate of about 1 monolayer in 10 min during which the tungsten and titanium wires were maintained at 900 and 1000° C, the wires being cleaned between each experiment. The values of the maximum and final steady emission are recorded in Table 3.

Table 3. *Emission from heated tungsten and titanium wires when thorium deposited on them at a rate of about 1 monolayer in 10 min*

Temperature of tungsten and titanium (°C)	*Emission from tungsten* ($A\,cm^{-2}$)		*Emission from titanium* ($A\,cm^{-2}$)	
	Maximum value	*Final steady value*	*Maximum value*	*Final steady value*
900	$1{\cdot}1\times10^{-5}$	$0{\cdot}9\times10^{-5}$	$3{\cdot}2\times10^{-6}$	$3{\cdot}2\times10^{-6}$
950	$4{\cdot}2\times10^{-5}$	$2{\cdot}6\times10^{-5}$	$8{\cdot}0\times10^{-6}$	$5{\cdot}2\times10^{-6}$
1000	$1{\cdot}5\times10^{-4}$	$1{\cdot}4\times10^{-4}$	$2{\cdot}3\times10^{-6}$	$2{\cdot}0\times10^{-6}$

Since the above experiments indicated that the emission from thorium deposits on heated titanium rapidly decays, a further experiment was performed in which thorium was deposited with the receptors cold. The wires were first

cleaned, the titanium by heating to 1150° C for 20 min and the tungsten by flashing at 2300° C for 2 min. The thorium source was switched on for discrete intervals of time between which the emission from the tungsten wire was measured at 1000° C.

The emission from the tungsten wire was very similar to that shown in Fig. 4 when the receptors were maintained at 1000° C. The deposition of thorium was stopped when the emission from the tungsten wire reached a maximum. At this point the emission from the tungsten wire was measured at several temperatures in the range 750 to 1150° C and the results are shown in Fig. 5. A Richardson plot made from the results gave a value for the work function (2·60 eV) in close agreement with previously published values for a monolayer of thorium on tungsten.[7] The emission from the titanium was also measured, as quickly as possible, over the temperature range 800 to 950° C, and the results are shown in Fig. 5. After making these observations the emission was re-measured at 800° C. It was found that the emission had

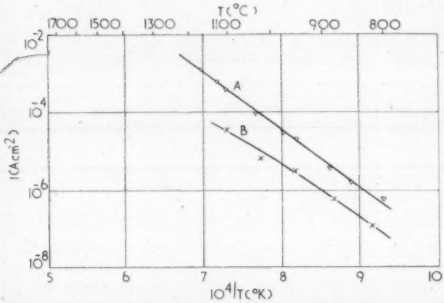

Fig. 5. Variation of emission with temperature for thorium deposited on tungsten and titanium wires

A, 1 monolayer of thorium on tungsten; *B*, 1 monolayer of thorium on titanium.

decayed by a factor of about 2·5, which accounts for the curvature of the emission plot at the higher temperature. The emission at 900 and 950° C were found to be very close to the values given in Table 3 for the maximum emission when thorium was deposited at a rate of about 1 monolayer in 10 min on to heated titanium. A Richardson plot gave the work function for a monolayer of thorium on titanium as 3·0 eV approximately.

5. DISCUSSION

5.1 *Platinum–molybdenum.* The results for platinum–molybdenum show that the emission at 1000° C from thorium deposited on any of the Pt–Mo phases is two or more orders of magnitude lower than that from similar deposits on molybdenum. This appears to be due to an appreciable difference in work function. If the temperature of the Pt_3Mo_2 phase on to which thorium has been deposited while cold is raised to 1300° C or above, the emission falls with time. This further decrease in emission is probably due to the solution of thorium in the platinum–molybdenum; but at such temperatures evaporation of platinum may begin to be appreciable and this would also cause a drop in emission by removing thorium from the surface.

The reason why the β-phase (Pt_3Mo) gives the lowest emission of all has not been established but it is no doubt associated with the lattice arrangement. One possibility is that thorium ions on the surface of this β-phase have a smaller dipole moment than in the other cases, and this would result in a higher effective work function. Consideration of Table 1 showing the temperature at which the further phases γ and δ are formed makes it seem unlikely that the extremely low grid emission from the β-phase can be utilized in high power transmitting valves, but it might be used with advantage in lower powered valves.

From the results it appears that in high power transmitting valves platinum-coated molybdenum inhibits grid emission by two mechanisms. Firstly it has a higher work function than molybdenum when covered with a layer of thorium, and secondly at temperatures above 1200 to 1300° C the thorium is removed from the wire surface either by solution into the Pt–Mo or by being carried off with evaporating platinum.

5.2 *Titanium.* The results show that if titanium is first cleaned by heating to 1150° C for 20 min then the emission from thorium deposited on to it is about a hundred times less than that from similar deposits on tungsten. This seems to be due to titanium having an appreciably higher work function than tungsten when covered with a monolayer of thorium. If thorium is deposited at a rate of about 1 monolayer in 10 min on to heated titanium the emission is higher at 950° C than at either 900 or 1000° C, whereas that from tungsten under similar conditions increases steadily with temperature. It thus appears that up to about 950° C a covering of thorium at least 1 monolayer thick can be maintained. These results are in qualitative agreement with those of Espersen and Rogers.[2]

The mechanism by which the emission from titanium contaminated with thorium falls if the temperature is raised above about 950° C is not clear from the experiments so far performed. It is known from previous work on titanium[5] that at about 950° C evaporation of the underlying titanium would begin to be appreciable and this might have the effect of removing the deposited thorium. Another possibility is that at such a temperature the titanium might dissolve the deposited thorium as suggested above in the case of platinum–molybdenum at 1300° C. A further possibility is that migration of the thorium over the surface of the titanium may cause an appreciable fall in emission if the initial layer of thorium is equal to or less than 1 monolayer.

If thorium is deposited on to titanium which has not been thoroughly cleaned then the subsequent emission may approach that from thorium deposited on to clean tungsten. Consideration of heats of formation shows that any titanium oxides present on the surface of the titanium wire would tend to be reduced by the thorium with the formation of some thorium oxide. The presence of thorium oxide with thorium on the surface of titanium would give a higher emission than from thorium on clean titanium. This would explain the magnitude and shape of the emission curve from thorium on titanium shown in Fig. 4.

Because of appreciable evaporation and excessive crystal growth, it seems unlikely that titanium would be useful at temperatures above 1000° C so that its use in transmitting valves would be confined to low power types.

REFERENCES

(1) Ayer, R. B. *Proc. Inst. Radio Engrs*, **40**, p. 591 (1952).
(2) Espersen, G. A., and Rogers, J. W. *I.R.E. Trans Electron Devices*, ED-3, p. 100 (1956).
(3) Wright, D. A. Private communication.
(4) Rooksby, H. P. Private communication.
(5) Champion, J. A. *Brit. J. Appl. Phys.*, **9**, p. 491 (1958).
(6) Jenkins, R. O., and Trodden, W. G. *Brit. J. Appl. Phys.*, **10**, p. 10 (1959).
(7) Reimann, A. L. *Thermionic Emission* (London: Chapman and Hall Ltd., 1934).

NEW BOOKS SECTION

Contents

PAGE

Acoustics

Acoustics, noise and buildings 75

Automatic control

Automatic control. Principles and practice 75
Automatic measurement of quality in process plants . . 76

Elasticity

The physics of rubber elasticity 76
Torsionstheorie 76

Electrical and electronic devices and properties

Reflex klystrons 77
Transient response from frequency response 77

Metals and metallurgy

Effect of surface on the behaviour of metals 77
Transformation characteristics of direct-hardening nickel-alloy steels 77
Zone melting 77

Meteorology

Atmospheric explorations. Papers of the Benjamin Franklin memorial symposium of the American Academy of Arts and Sciences 77

Miscellaneous and general physics

Computability and unsolvability 78
The design of physics research laboratories 78
Experimental designs in industry 78
The fundamental constants of physics 78
Glass-melting tank furnaces 79
Max Planck: Physikalische Abhandlungen und Vortrage. Vols. I, II and III 79
Progress in biophysics. Vol. 8 79
The principles of quantum mechanics 80
Reports on progress in physics 80

PAGE

Nuclear apparatus and techniques

Kernverfahrenstechnik. Eine Einführung für Ingenieure . 80
Nuclear reactor experiments 81
Nuclear scattering 81
Nuclear structure 81
Physik und technik der atomreaktoren 81
Sourcebook on atomic energy 82

Optics and photography

Grundriss der Photographie und ihrer Anwendungen besonders in der Atomphysik 82
Modern geometrical optics 82
Practical microscopy 82

Reference books

Chambers's technical dictionary 83
A dictionary of named effects and laws in chemistry, physics and mathematics 83
Handbook of supersonic aerodynamics: NAVORD Report 1488. Vol. 3. Section 6 83
Handbuch der physik. Vol. 26 83
Leybold Vakuum-Taschenbuch 84
Rohrhydraulik: Ein Handbuch zur praktischen Strömungsberechnung 84
Van Nostrand's scientific encyclopedia 85

Solid state physics and crystallography

Dislocations and mechanical properties of crystals . . . 85
Electric conduction in semiconductors and metals . . . 85
Halbleiter und Phosphore. Vorträge des Internationalen Kolloquiums 1956 "Halbleiter und Phosphore" in Garmisch-Partenkirchen 86
Solid state physics. Advances in research and applications. Vol. 6 86

Vacuum

Frottement et échanges thermiques dans les gaz raréfiés . . 86

Acoustics

Acoustics, noise and buildings. By P. H. PARKIN and H. R. HUMPHREYS. (London: Faber and Faber Ltd., 1958.) Pp. 331. Price 70*s*.

The authors of this handsome volume are respectively a physicist at the Building Research Station and a consultant architect. The collaboration has resulted in a comprehensive book, which should appeal to those seeking specialized information on the features of various types of auditorium designed for good listening.

The book is written without the use of mathematics, and with the minimum of architectural terminology so that the authors' hope that it can be understood by the layman is justified. The exposition is, in fact, "popular" in type and yet sufficiently detailed to make the book of use to the serious student of architectural acoustics. The illustrations are good, the interest maintained throughout, while tables of data and specimen calculations at the end help the reader who wishes to apply the information given in the text.

E. G. RICHARDSON

Automatic control

Automatic control. Principles and practice. By W. G. HOLZBOCK. (New York: Reinhold Publishing Corporation; London: Chapman and Hall Ltd., 1958.) Pp. vii + 285. Price 60*s*.

This book is recommended to those seeking a simple and general introduction to the subject. The treatment is descriptive and the mathematics used are elementary. Chapters 1 and 2 define the elements of the control loop and describe their static characteristics. In chapters 3 and 4, step function response is discussed and empirical formulae are given for adjusting controller settings to obtain the best performance. However, the author fails to point out that in many control systems the amplitude of the step change which can be tolerated is small with a result that the record of the process response curve is difficult to interpret. A brief introduction to frequency response methods is given in chapter 5.

In the last eight chapters mechanical and electrical components of control instruments, including measuring elements

and control valves are described and some typical industrial control applications are discussed.

The book is written in a lucid style and well illustrated with diagrams and simple numerical examples. It is a pity that a bibliography is not included to assist the student in choosing material for further reading. J. A. ORR

Automatic measurement of quality in process plants. (London: Butterworths Scientific Publications, 1958.) Pp. xi + 320. Price 50*s*.

Although automatic control finds wide application in the plants of the process industries, the method usually employed is to hold the plant under operating conditions which have been selected to give an acceptable quantity and quality of product. It would obviously be a more logical proceeding to control the output of the plant directly in terms of the product material, but this has so far proved impractical except in a few instances.

The very common practice of drawing samples from a plant and sending these to a laboratory for conventional testing by skilled analysts requires so much time that the results when obtained are too old for anything but the coarsest plant control.

The methods described to the conference sponsored by the Society of Instrument Technology in September 1957 and which form the contents of this book, may be divided into two classes: methods in which samples drawn from the plant can be analysed by unskilled workers on the plant premises, and methods of analysis which can be applied to plant streams, either using discrete samples automatically collected or by measurements made by immersing a transducer in the actual plant stream. The instruments present their result either on a scale or graph, which has to be interpreted by a human operator, or, in the more sophisticated instruments, as a signal, usually electrical or pneumatic, which can be employed to adjust the plant operating conditions. The methods suggested cover nearly the whole gamut of physical measurements from density to nuclear resonance spectroscopy, in addition to the more usual titration and pH measurements.

The quality of the papers varies widely as does their aim. Some describe techniques which it would be interesting to apply, or apparatus which could be applied widely in plant control if only the necessary spade work were done. The papers which will appeal most strongly to instrument engineers and physicists are those which detail plant experience with the apparatus described, quoting performance and reliability and describing the inevitable snags which have been encountered and overcome. The book is also recommended to the attention of senior physics students to illustrate to them the wide range over which their subject finds application in industry.

The book has been very well produced. It is to be regretted that the estimated small circulation has resulted in a price which will be unattractive to many instrument workers.

G. MORRIS

Elasticity

The physics of rubber elasticity. 2nd ed. By L. R. G. TRELOAR. (London: Oxford University Press, 1958.) Pp. 342. Price 40*s*.

This book retains the character of the earlier edition and sets out the remarkable development of the understanding of the elastic properties of rubber and rubber-like materials which has taken place in recent years.

The subject-matter of the book divides naturally into two parts. The first of these describes the development of the statistical or kinetic theory of rubber-like elasticity and shows how it provides a very satisfactory description of the basic mechanical and photoelastic properties of rubber. Dr. Treloar has been intimately associated with this field for many years and this part is written supremely well. The material is thoroughly digested and is presented in simple and forthright language as a clear and logical story. This part includes an important new chapter on swelling which shows how the essential processes of swelling may also be related to configurational changes of rubber molecules, and a new chapter on the experimental determination of the molecular network structure of vulcanized rubber. In addition the chapters on photoelastic properties and on the phenomenological theory of large elastic deformations have been rewritten and expanded considerably to deal with recent developments.

The second part, which is comprised of the last three chapters, deals with problems of breaking and non-equilibrium elastic properties of rubber. Here, neither experimental nor theoretical aspects of the subject are so well developed, and, in contrast to the first part of the book, the treatment is not so masterly. For example, in the chapter on dynamic properties, a field which is expanding rapidly, the last reference given is to work in 1952. Here much of the discussion in terms of springs and dash pots and relaxation times, which is primarily of historical interest, could have been more profitably allotted to a fuller description of the use and power of concepts of real and imaginary compliance. These comments do not detract from the high value of the book which, like its predecessor, is beautifully produced and singularly free from misprints. L. MULLINS

Torsionstheorie. By C. WEBER and W. GÜNTHER. (Braunschweig: Friedr. Vieweg and Son, 1958.) Pp. 306. Price DM. 38.

The torsion of a prism is one of the problems of elasticity which reduces analytically to two dimensions. The state in all sections perpendicular to the axis of the prism is essentially the same, and the functions of interest are functions of the x, y co-ordinates in the section.

It is with this problem that the present book is concerned. In the first chapter it is shown that the solution of the torsion problem depends on finding a pair of conjugate harmonic functions, the real and imaginary parts of an analytic function of $x + iy$, satisfying appropriate conditions on the boundaries of the section.

The rest of the book discusses this purely mathematical problem, for different shapes of cross-section, by a variety of exact and approximate methods. Prandtl's membrane analogy is described and some approximate formulae are based on it, but in the main the authors rely on conformal transformations and Fourier series.

Only elementary functions are used. Although in Chapter 13, which discusses the general case of a polygonal section, the Schwarz-Christoffel transformation is established, the functions which arise in the examples are expanded in power series.

Appendices derive briefly the relevant equations of elasticity, and the relations between two dimensional potential functions, analytic functions and conformal transformations.

The subject is treated with clarity and Teutonic thoroughness, and the book will be invaluable to those concerned with this type of mathematical problem. A. W. GILLIES

Electrical and electronic devices and properties

Reflex klystrons. By J. J. HAMILTON. (London: Chapman and Hall Ltd., 1958.) Pp. xi + 260. Price 45*s*.

The author ranges from the fundamental mathematical analysis of the electron dynamics of reflex klystrons to practical details of the many and varied processes of their manufacture and finally examines future trends in this field. In such a comprehensive undertaking brevity is inevitable and occasionally results in slight obscurity but on the whole the author has been very successful in achieving his declared object "to integrate and present the principal facets of knowledge of these oscillators." References at the end of each chapter are numerous but sometimes include what appear to be reports not available to the general reader.

G. L. HUNT

Transient response from frequency response. By V. V. SOLODOVNIKOV, YU. I. TOPCHEEV and G. V. KRUTIKOVA. (London: Infosearch Ltd., 1958.) Pp. 193. Price 42*s*.

This book describes a method whereby the response of a linear system to a step function, or Dirac delta function impulse, may be derived from a knowledge of the frequency response of the system.

There are three chapters, the first of which gives an outline of Laplace transform theory for ordinary differential equations and applies this to the analysis of the transfer functions of servo-mechanisms. The second chapter contains five practical examples, and the third "chapter" consists of tables of the function:

$$h_k(t) = \frac{2}{\pi}\left\{Si(kt) + \frac{1}{1-k}\left[Si(t) - Si(kt) + \frac{\cos t - \cos kt}{t}\right]\right\}$$

for $t = 0(\cdot 2)\ 50{\cdot}0$, $k = 0(\cdot 01)\ 1{\cdot}00$. There is also a short table of

$$Si(x) = \int_0^x \frac{\sin y}{y}\, dy$$

for $x = 0(\cdot 1)\ 50$, and a set of nomograms.

The translation is good but careless in the mathematics, for example on page 19 and in the headings of the tables on page 91 *et seq.* we find the quantity k (in $h_k(t)$) written as the Russian Ж and this may confuse the inexperienced reader. No check was made of the values of $h_k(t)$ but a comparison of some values of $S_1(x)$ with AMS (32) showed numerous errors in the fourth decimal place due, no doubt, to careless round-off.

Despite these minor blemishes the book may be recommended as a useful addition to the literature for engineers not interested in high accuracy.

A. D. BOOTH

Metals and metallurgy

Effect of surface on the behaviour of metals. (London: Iliffe and Sons Ltd., for The Institution of Metallurgists, 1958.) Pp. vii + 100. Price 21*s*.

The surfaces of metals affect to a considerable degree the properties of the bulk material and are, of course, the only parts to which our natural senses respond. The subject was, therefore, well chosen for one of the annual week-end refresher courses of the Institution of Metallurgists; the volume under review records the four lectures given to this course. They deal with method of preparation and examination of surfaces, and with their influence on the chemical, frictional and physical properties of the materials. It is, perhaps, surprising that a further lecture covering the effect on mechanical properties was not included since metals and alloys are principally used as constructional materials on account of their strength characteristics and the surface condition influences these markedly, especially under conditions of fatigue loading. The four lectures, each by an acknowledged expert in the particular subject, form excellent reviews of the present state of knowledge in the fields covered.

W. BETTERIDGE

Transformation characteristics of direct-hardening nickel-alloy steels. (London: The Mond Nickel Co. Ltd., 1958.) Pp. 91. Free of charge.

This booklet is not merely a presentation of the transformation characteristics of a number of nickel alloy steels; for the reasonably scientifically minded reader with some elementary metallurgical knowledge it forms a very useful general introduction to the heat treatment of steel. The continuous cooling diagrams are relatively new and should give a useful guide for the hardening of the steels.

F. W. JONES

Zone melting. By W. G. PFANN. (New York: John Wiley and Sons Inc.; London: Chapman and Hall Ltd., 1958.) Pp. xvi + 236. Price 60*s*.

Although it has been known for a very long time that segregation of impurities in a material frequently takes place during solidification, it is only in recent years that this phenomenon has been fully exploited for the preparation of material of very high purity. Since Pfann published his first paper on zone melting in 1952, the subject has developed sufficiently rapidly to justify the preparation of this book devoted specifically to zone melting and zone refining.

After a short introduction, the author considers in some detail the theoretical aspects of zone refining and the usefulness of this section is enhanced by the inclusion (as an appendix) of a series of calculated curves relating the distribution of impurities along a bar to the distribution coefficient and the number of passes employed. The experimental arrangements which have been used in practice are then fully described and a brief summary is presented of most of the published work on the application of zone refining to particular materials. More details of specific investigations can readily be obtained from the comprehensive bibliography. Less established techniques such as continuous zone refining, zone levelling and temperature gradient zone melting are also discussed in some detail, although the distinction between actual experimental results and, as yet, untried processes is not always sufficiently emphasized.

The author's presentation of his subject is straightforward and this first book on zone melting will be of particular value to workers considering the use of zone refining for the first time.

D. A. ROBINS

Meteorology

Atmospheric explorations. Papers of the Benjamin Franklin memorial symposium of the American Academy of Arts and Sciences. Edited by H. G. HOUGHTON. (New York: John Wiley and Sons Inc., and The Technology

Press of Massachusetts Institute of Technology; London: Chapman and Hall Ltd., 1958.) Pp. x + 125. Price 52*s*.

This book, containing two lectures on atmospheric electricity by Ross Gunn and Joachin Kuettner and two on the upper atmosphere by Harry Wexler and Henry Booker, is the product of a symposium held in 1956 to celebrate the two hundred and fiftieth anniversary of the birth of Benjamin Franklin. The subjects reflect two of Franklin's main interests in meteorology and are treated in a modern context.

Ross Gunn writes on the electrification of cloud and rain drops, a field he has much explored experimentally and theoretically, and here are his findings over recent years. Kuettner considers present evidence and views on the separation of charge in thunderclouds and shows that we still await a coherent picture of the mechanisms involved.

Wexler writes on the vertical propagation of "storms," particularly in relation to the explosive warmings that are observed in late winter in the high arctic stratosphere, and favours the view that they are essentially dynamical rather than directly induced by solar radiation. Finally Booker describes and discusses the origin of some nine distinct kinds of radio scattering in the ionosphere and suggests that they are all turbulence phenomena, though why there should be turbulence in all cases is not yet explained.

An interesting little book, this, particularly, I think, to those not expert in the disciplines discussed, but why so high a price?

P. A. SHEPPARD

Miscellaneous and general physics

Computability and unsolvability. By M. DAVIS. (New York: McGraw-Hill Book Co. Inc.; London: McGraw-Hill Publishing Co. Ltd., 1958.) Pp. xxv + 210. Price 58*s*.

The two classical papers on "computable numbers" by the late A. M. Turing have often been described as marking the invention of modern automatic digital computers. The difficulty of these pioneer writings is notorious and it is the claim of the author that the present book is designed to bring the theory within the grasp of scientists who are not mathematical specialists.

Whilst it is true that the early part of the book is considerably less obscure than Turing's original papers, it still cannot be said that the author has succeeded in doing much more than including background material in the same place as the theory which is being developed. For those physicists with a taste for axiomatics, however, the book will serve a useful purpose in bringing together a range of topics which are otherwise scattered throughout rather inaccessible literature. After an introduction dealing with notation and the elements of symbolic logic, the first part of the book contains five chapters which discuss the general theory of computability and the various operations which can and cannot be performed on Turing machines. The second part, and the most interesting, contains three chapters on combinatorial problems, diophantine equations, and unsolvability theorems of mathematical logic respectively. The third part is for specialists and describes, amongst other things, some of the author's own researches. There is a short appendix on number theory, an excellent bibliography, and an index.

A. D. BOOTH

The design of physics research laboratories. (London: Chapman and Hall Ltd., on behalf of The Institute of Physics, 1959.) Pp. 108. Price 21*s*. (Available to members of the Institute at 15*s*.)

This book contains the proceedings of the symposium organized by the London and Home Counties Branch of The Institute of Physics at the Royal Institution on 27 November, 1957. The symposium was primarily devoted to the design of physics research laboratories but much of the information has a wider application, and it is hoped that the book will be of value to all concerned with the design of science laboratories in general.

The full proceedings of the symposium are given together with many of the diagrams and photographs which were presented as lantern slides. The chapter headings give some idea of the subjects covered in the volume: The architect and physics; Some problems in the planning of research laboratories; Recent trends in the design of American industrial research facilities; Services and facilities from the user's point of view; Buildings and services from the viewpoint of the laboratory maintenance engineer; Research on the design of laboratories.

Experimental designs in industry. Edited by V. CHEW. (New York: John Wiley and Sons Inc.; London: Chapman and Hall Ltd., 1958.) Pp. xi + 268. Price 48*s*.

Experimenters in all sciences whether working in laboratory or field are realizing the value of design. In industry, especially, the haphazard exploration of effects accidentally discovered is replaced by planned searches over the fields of controllable conditions. The value of design lies not only in the reduction of errors of comparison, making experiments more sensitive but in the possibility of calculated guidance of the path of search by lines of steepest slope to the target peaks of optimum conditions.

This book contains all but five (which five have been published elsewhere) of the papers read at a symposium held at the North Carolina Institute of Statistics whose object was to review the present statistical techniques available to the research worker, to present new developments, and to discuss some of the ideas which are presenting difficulty at the moment such as sequential multiple decision procedures. A valuable further aim, one to which the whole of Part II (pp. 193–253) is devoted, was to present the result of experiences of using these techniques in industrial problems.

Although one might expect that at a symposium such as this, for a limited number of participants, much would be taken as known, the expressed purpose was partly expository and the result is an admirable account of the nature and purpose of various designs which can be understood almost without reference to other texts. The papers of Part I are: (i) Review of experimental designs useful in industrial research; (ii) Basic experimental designs; (iii) Complete factorials, fractional factorials and compounding; (iv) Simple and multiple regression analyses; (v) Experimental designs for exploring response surfaces. Part II has five papers on experiences of the use of these designs in industry including ordnance experimentation. Besides the references given in each paper there is a sectionalized bibliography of 354 selected papers.

E. D. VAN REST

The fundamental constants of physics. By E. R. COHEN, K. M. CROWE and J. W. M. DUMOND. (New York: Interscience Publishers Inc.; London: Interscience Publishers Ltd., 1957.) Pp. xii + 287. Price 58*s*.

In many ways this book is unusually refreshing. It is perhaps unlikely that the detailed information given in all the chapters will be of interest to any one person, nevertheless most physicists would benefit from reading some parts carefully.

There are eight chapters of widely varying length. The first is extremely short and serves as an introduction, while the second is a brief outline of the basic system of physical units commonly used, and includes details of the standardization procedures. The third chapter is a rather short account of measurements made on the classical constants, such as the acceleration due to gravity, the gas constant, the Faraday, etc.

The fourth, and one of the longer chapters contains a review of methods for the measurement of atomic and meson constants. The first section, on atomic masses, is very brief and does not include mass spectrometry. The rest of the chapter is devoted to masses and other properties, particularly lifetimes, of the π- and μ-mesons, the K-meson and the hyperons. Very accurate data are now available for the π- and μ-mesons but the situation is still in considerable flux for the strange particles. This chapter is probably the most concise account of the data available in the early part of 1957 and includes an excellent bibliography.

Chapter 5 is a long account of the history of the atomic constants, particularly e, m and h and the various combinations of those quantities which can be accurately measured. A considerable wealth of detail is included in this chapter but it avoids being boring. The chapter concludes with the Birge-Bond diagram and several isometric consistency charts which are not very well produced. Chapter 6 contains an account of some selected postwar high-precision measurements, mostly in the field of microwave techniques.

Chapter 7 contains a theoretical treatment of least-squares methods and the last chapter contains a detailed least-squares evaluation of the best values for the principal atomic and nuclear constants, based on data available in 1955.

The book is mainly well produced and all the chapters have extensive bibliographies. C. C. BUTLER

Glass-melting tank furnaces. By R. GÜNTHER. Translated from the German by J. Currie. (Sheffield: Society of Glass Technology, 1958.) Pp. xiv + 232. Price 60*s*.

The appearance of this book might well prompt the reader to ask why no similar book has appeared previously in England. This becomes the more surprising when the index of authors is consulted and it is noted how many important papers have been published in England by men having long practical experience, many of them past students from Sheffield where the first Chair in Glass Technology in the world was founded during World War I.

The author's preface and the explanatory foreword, written by Emeritus Professor Turner, should be read as they provide good evidence of the high standard of its contents. The committee, under Turner's chairmanship, which supervised the English version of Günther's admirable book considerably increased its value by enlarging the number of references to original papers given at the end of each chapter. The designers and operational supervisors of tank furnaces are strongly recommended to study Chapter X describing fundamental thermal calculations and to do the arithmetic necessary to obtain a general appreciation of the factors affecting thermal efficiency. The numerical example provides a basis for calculations and should stimulate critical enquiries and discussion. The continued improvement in refractories demands a review of many established practices.

The subject index is scanty, but its deficiencies are somewhat ameliorated by the very detailed "Contents" and "Author Index." However, unless the author is known, some important references could not readily be traced. For example, important contributions by Chesters, Thring and colleagues describing studies of the flow of gases are given on p. 78, but these could not be found by use of the subject index for "Flow, gaseous" or "Gases, the movement of."

It has also been noted that data are sometimes given to a much higher order of accuracy than is warranted, for examples: Fig. 20, "Temperature distribution in a tank" (the isothermals can only be estimated to about 10°), and Table 12, B.Th.U./hr./sq. ft.

These criticisms are of relatively little importance and detract nothing from the value of this book to all concerned with raising the efficiency of glass production. For the technological student, the book will serve both as a textbook and a guide to further studies. B. P. DUDDING

Max Planck: Physikalische Abhandlungen und Vortrage. Vols. I, II and III. (Braunschweig: Friedr. Vieweg and Sohn; London: K. G. Heyden and Co. Ltd., 1958); Vol. I. Pp. xv + 776. Vol. II. Pp. xi + 716. Vol. III. Pp. xii + 426. Price DM. 150.

This collection of M. Planck's scientific papers and lectures is a reproduction by a photographic process of the original publications, with an index and a foreword by M. v. Laue. It is edited by the union of German physical societies and the Max Planck Society as a memorial to the great theoretical physicist whose 100th birthday was celebrated in April of this year.

The first two volumes contain Planck's doctorate thesis, his "Habilitationsschrift" as Privatdozent in Munich and 119 papers published in various journals. The most important of these are the classical papers on the second law of thermodynamics, which was given its first precise formulation by Planck, and the notion of entropy, as well as the famous series of investigations on the theory of heat radiation which led to the discovery of the elementary quantum of action h, the notion of zero-point energy, the cell structure of the phase space, and the general statement of Boltzmann's entropy-probability relation in the form $S = k \log W$, first introducing the universal constant k (gas constant per atom), usually known as "Boltzmann's constant". There are further papers on various aspects of electromagnetic theory, on the theory of relativity, of which Planck was one of the first supporters, and on the theory of electrolytes.

The third volume contains public lectures and publications meant for a broader public, shedding light on Planck's scientific personality, his life and his philosophical ideas. Amongst these are his Nobel lecture and a wonderful short auto-biography which ought to be translated into English and widely read by young physicists. There are also a number of essays devoted to the life and work of contemporary great physicists and appreciations of Planck's own work by M. v. Laue, Otto Hahn and others.

For those physicists who are interested in studying the original works of this great master in order to learn about his way of thinking and his art of writing these three volumes will be invaluable. R. FÜRTH

Progress in biophysics. Vol. 8. Edited by J. A. V. BUTLER and B. KATZ. Pp. 410. (London: Pergamon Press, 1957.) Price 105*s*.

When the first volume of *Progress in Biophysics and Biophysical Chemistry* appeared in 1950, one wondered firstly whether the Editors would be able to maintain the high standard they appeared to have set themselves, and secondly how long it would be before suitable topics for these reviews

would be exhausted. Such reflexions were misguided. The standard has been maintained, and the momentum of the impact of physics on the biological sciences is increasing so rapidly that it is not topics which are lacking but space in which to do them all justice. The present volume is as good and as interesting as its predecessors, and contains a variety of material to please many tastes. For those engaged in teaching, there are reviews of the physiology of hearing and of human colour vision; for the radiation biologist, of the effect of radiation on DNA synthesis in mammalian cells; for those interested in the micro-structure of living matter, of the electrochemistry of the bacterial surface, of the axon surface, and of the ionic permeability of the red cell membrane; and for the more chemically minded there are articles on the biosynthesis of some connective tissue components, on the physical chemistry of deoxyribosenucleic acid, and on the biosynthesis of protein. Each contribution covers a large number of original papers and by no means the least part of their value lies in the bibliographies. Biophysicists and physicists working in the borderline region of physics and medicine need no advice to read these volumes. Perhaps one might remind physicists generally that biophysics is not new but is one of the oldest branches of physics. In recent years it has been overshadowed by the more spectacular advances elsewhere; but the same technical progress which has made those advances possible has also strengthened the armoury of those investigating the mechanism of natural processes. There is much to be learnt and to interest in the reading of these books; and it is conceivable that in the long run they may even be found to have contained knowledge more important to the human race than will be found in the depths of the atomic nucleus or in the heights of outer space.

C. B. ALLSOPP

The principles of quantum mechanics. 4th ed. By P. A. M. DIRAC. (Oxford: Clarendon Press; London: Oxford University Press, 1958.) Pp. xii + 312. Price 35*s*.

This book has been one of the classics of quantum mechanics ever since the publication of the first edition. The expansion of the later editions has covered applications rather than modifications of the fundamental principles, and there are purists who commend the austere exposition of the original version, rather than the recent more conversational tone, for the serious student.

"Dirac" is a suitable introductory textbook only for the most mathematically able undergraduates. In most physics courses, it is appropriately studied in the first post-graduate year, when the student should have already learned the elements of wave mechanics and have read Heisenberg's *Physical principles of quantum mechanics*.

The only important change in the new edition is the replacement of the former discussion of second quantization by a chapter on quantization of wave fields which serves as a lucid preparation for modern developments.

There continues to be rather little emphasis on the statistical operator (density matrix). Recent developments of operator calculus have made it a more manageable tool for the problems of statistical mechanics and kinetic theory in which its power is most useful, but there are still few books other than von Neumann's classic in which the fundamental principles are clearly set out.

That apart, Dirac's book is a very complete text on fundamental quantum theory, and one which no theoretical physicist can afford to miss. The price continues to be very moderate.

G. WYLLIE

Reports on progress in physics. Vol. 21. Edited by A. C. STICKLAND. (London: The Physical Society, 1958.) Pp. 383. Price 63*s*.

This well-produced volume contains nine reports. They are on average energy expenditure per ion pair in gases and gas mixtures (Valentine and Curran); absorption and fluorescence spectra of ions in crystals (Runciman); electromagnetic excitation of nuclei by nuclear projectiles and electrons (Huby); physics of nerve processes (Fatt); the theory of collective excitations in nuclei (Brink); Fourier methods in structure analysis by electron diffraction (Cowley and Rees); the specific heats of metals at low temperatures (Parkinson); mesonic atoms (West); the production and measurement of high temperatures (Lochte-Holtgreven, Schall and Wecken).

The final report fills nearly one-fifth of the book, the nuclear reports together nearly one-third. These contributions represent extremes in subject and treatment. The one on high temperatures should be readable with profit and pleasure by any physicist; while the others appear almost unreadable except by those familiar with modern atomic theory and practice. Fatt's abstruse but valuable paper shows a welcome widening of the scope of the Reports. Cowley and Rees, and Parkinson, have written good reviews on subjects of more general interest. It is difficult to judge how adequately recent progress has been surveyed in some of these very specialized fields, but it is not difficult to judge that the average physicist (if such exists) will find much of the book very hard to read. No doubt the obscurity of the nuclear papers is partly unavoidable, but in many articles the necessary introductions into unfamiliar fields are too brief or non-existent. In the reviewer's opinion these reports should meet the need for conveying the accepted results and future prospects in a particular type of work to those outside it. Regrettably, there is a tendency to ignore this need, and the book is the poorer for it.

S. T. HENDERSON

Nuclear apparatus and techniques

Kernverfahrenstechnik. Eine Einführung für Ingenieure. By W. MIALKI. (Berlin: Springer-Verlag, 1958.) Pp. xi + 472. Price DM. 78.60.

This book has been written to acquaint engineers with the underlying principles on which reactor technology is based. It is a "readable" book, and although it gives no great depth of information, it adequately covers the very wide field of reactor theory and technology.

In its ten chapters it covers nuclear physics, reactor physics, counting techniques, isotope production, and health physics, as well as the technology of various reactor materials. There is a most useful collection of information given in the three appendices. There are, however, certain notable omissions. Wigner growth in graphite is not mentioned, nor are any of the many deformation processes suffered by uranium during irradiation or thermal cycling. Although the temperature coefficient of reactivity is mentioned, there is no explanation of the causes of the effect, nor reference to the various partial coefficients.

There are a number of small errors and mis-statements. For example, on p. 398 the large void above the uranium in the radiograph is attributed, in the caption, to shrinkage of the uranium, whereas in fact it is caused primarily by the extension of the can. In another section, the thermal shield (usually massive) is described as being made of sheet metal.

This book is well bound, and well printed on good quality paper. An English translation should prove popular.

K. J. BOBIN

Nuclear reactor experiments. Edited by J. BARTON HOAG. (London: D. Van Nostrand Company Ltd., 1958.) Pp. xv + 480. Price 51*s*.

This book describes a collection of experiments which are performed at the International Reactor School of the Argonne National Laboratory. Just over half the book is devoted to reactor physics, the remainder consisting of experiments in the associated sciences including metallurgy, chemistry and engineering. The chapter headings include:—Radiation detection; Moderator assemblies; Subcritical assemblies; Cross sections; Operating reactors; Heat removal; Fuel preparation; Corrosion and radiation; Hot laboratory, and Separation processes.

As is inevitable in a book having contributions from over 40 people there are differences in style, but the Editor has ensured that too much overlapping does not occur. Some of the experiments are described in great detail, and are obviously applicable only to the particular apparatus at Argonne. Others are more general in character and could be performed wherever facilities are available. A short introduction is given to each of the experiments, outlining the theoretical background, but for a detailed treatment the reader is referred to the appropriate textbook.

The book would have been improved by the inclusion of typical sets of results for many of the experiments. This would have enabled the authors to include discussion of these results. The value of the book to those attending the International School at Argonne is obvious, while it is also of great value to those planning or teaching in similar courses.

D. NEWBY

Nuclear scattering. By K. B. MATHER and P. SWAN. (London: Cambridge University Press, 1958.) Pp. viii + 469. Price 80*s*.

Rutherford may have said that science was either physics or stamp collecting, but since the war unsympathetic observers have wondered whether nuclear physics was degenerating into a rather costly branch of philately. This excellent book will do a good deal to correct this attitude. The authors have imposed coherence on their material by discussing mainly those aspects of nuclear scattering which are directly relevant to finding the forces of interaction between nuclear particles. Apart from the last chapter, which, though interesting, could have gone into another book, everything hangs together except the results, which present a rich crop of conundrums for future research.

The book discusses both experiment and theory, with no more detail than is necessary to ensure comprehension. Even so, it runs to 469 pages! Full references are given, and the coverage of the literature is very thorough into 1956. I found only a few misprints, and only one, a μ omitted in what should be $\mu\mu$F on page 70, which was more than trivial. The price and content are both beyond undergraduate level, but the book can be strongly recommended for research students in nuclear physics, and for their seniors.

It is a little saddening to see what began as a cheap series of monographs reach £4 a volume!

G. WYLLIE

Nuclear structure. By L. EISENBUD and E. P. WIGNER. (London: Oxford University Press, 1958.) Pp. viii + 128. Price 25*s*.

After three chapters on binding energies and regularities in the pattern of isotopes, now fairly standard, the authors describe nuclear reactions and the concept of isotopic spin in general terms. This is all an introduction to the discussion of the various models of nuclear structure. The largest and most useful part of the book concerns the several forms of the shell model. The ranges of validity of the other models are sharply distinguished. This is a short book, only 111 pages apart from the comprehensive list of references, and consequently explanations are so much condensed that it would be difficult to gain any understanding of nuclear structure by reading this book alone. However, when it appears, as is intended, as part of a "Handbook of Physics," this shortcoming will disappear. In its present form it is most useful where compactness is a virtue, as an *aide memoire* to the practising nuclear physicist.

W. A. COOPER

Physik und technik der atomreaktoren. By F. CAP. (Wien: Springer-Verlag, 1957.) Pp. xxix + 487. Price £5 9*s*.

In 1950, Professor Cap started the first series in Europe of lecture courses on reactor physics at Innsbruck University and it is fitting that he should produce the first comprehensive book in German on reactor physics and technology.

Much of the treatment of reactor physics, which occupies the first half of this book, inevitably follows the pattern of American authors (Glasstone and Edlund). Great attention is paid to detail and clarity of definition with liberal use of qualifying sub- and super-scripts to the symbols, and the excellent practice is followed of enclosing principal formulae in line frames. The assumptions and limitations of diffusion and Fermi age approximations are clearly defined but in some cases unnecessary repetition occurs in dealing with simplifications separately rather than as approximations of more exact treatment.

The book is intended both as a course textbook on atomic energy—with well selected problems after each section—and as a reference book for the specialist. Brief surveys are given, in a chapter entitled "Reactor construction," of reactor materials, shielding and heat transfer; further chapters cover reactor operation, control, safety and health problems, production of isotopes, classification and descriptions of particular reactors and the use of reactors for research, medicine, isotope production and power production. Finally, there is a short summary of the legal aspects of reactor technology and national and international organizations dealing with atomic energy.

It is clearly no longer possible in a single volume adequately to cover such a wide field, and the specialist in each subject will find omissions. The discussion of perturbation theory could well have been extended since a firm grasp of the physical significance of the importance function (adjoint flux) is of great value to both reactor designer and experimentalist. Of value, too, would have been more detailed consideration of long term reactivity changes and their bearing on design and economics, more than a bare reference to the heterogeneous method of reactor calculation and some mention of the effects of neutron streaming. In the section on heat transfer, no mention occurs of extended surface.

These shortcomings are partially compensated by an unusually thorough and extensive selection of references to the end of 1956, lists of the more important journals, textbooks and sources. Again, unfortunate omissions occur; there is, for example, no reference to the *Journal of the British Nuclear Energy Conference*.

In spite of a large list of corrigenda issued with the book many errors remain, some serious, such as the incorrect normalizing constant in the final approximation for the

energy spectrum of fission neutrons (Eq. 6.8), erroneous values of k in Table 19, a factor of 10^6 in the tolerance level of beryllium in air quoted in Table 89.

However, these are minor shortcomings in a first edition and Professor Cap is to be congratulated on an excellent methodical survey of reactor physics and technology, backed up by a wealth of numerical data and reference material.

M. HARTNELL-BEAVIS

Sourcebook on atomic energy. 2nd ed. By S. GLASSTONE. (New York: D. Van Nostrand Co. Inc.; London: D. Van Nostrand Co. Ltd., 1958.) Pp. 641. Price 34*s*.

The first edition of this book was deservedly popular amongst both students and research workers. Unlike so many text-books, it was clear and well written, in addition to being comprehensive. At the time it appeared it was one of the few satisfactory introductions to nuclear physics, though this situation has since been remedied to some extent.

The second edition leans heavily on the material of the first, but there are important additions, reflecting both the progress of nuclear science and the increasing declassification of material. The most important of these is a complete new chapter on nuclear reactors, in which research, production, and power types are described. In the discussion of power reactors, attention is naturally concentrated on American experience with the P.W.R. and B.W.R., but the book is commendably free from any suggestion that these types are necessarily the best, and a clear and fair account is given of Calder Hall. Indeed, one wishes that all writers on nuclear energy would concentrate in the same way on technical factors and forget about questions of national prestige. Among other important additions are a much extended discussion of mesons, going as far as a definition of the strangeness number, and a section on controlled fusion: this was written before the joint U.S./U.K. release of information, and only discusses the pinch effect in general terms.

The book has all the virtues of the first edition. It is clear, readable and (by American standards at least) very cheap, though many readers will dislike the two-column presentation. There are inevitably some minor criticisms. For example, there is no mention of the role of rocketsondes in analysing primary cosmic radiation, and Dr. Willis Lamb would presumably not care much for the statement that second-order effects in quantum electrodynamics can be neglected. The rigid insistence on the necessity for true breeding (a conversion factor greater than 1) will surprise British readers, though this apparently represents the official policy of the A.E.C.

In general, the book can be strongly recommended to all classes of readers.

D. C. LESLIE

Optics and photography

Grundriss der Photographie und ihrer Anwendungen besonders in der Atomphysik. By G. JOOS and E. SCHOPPER. (Frankfurt: Akademische Verlagsgesellschaft m.b.H., 1958.) Pp. xii + 408. Price DM. 48.

The purpose of this book is to present a thorough treatment of photography as a whole to those who use it in scientific applications. The authors have been successful in discussing the basic empirical fundamentals, the theories of photographic phenomena, optical and mechanical apparatus, light sources, illumination and filters. Half of the book is devoted to these items which are discussed at a fairly high level of up-to-date knowledge of the processes with good illustrations and helpful references.

The second part of the book deals with applications of photographic materials used for recording optical images, X-ray images and nuclear tracks. The chapter on nuclear track recording is excellent, which is not surprising, as one of the authors was concerned in the early development of the subject. This chapter occupies nearly one-quarter of the book.

On the other hand the applications of photography to spectroscopy, astrophysics, light and electron microscopy and subjects such as radiography, autoradiography and high-speed photography are rather superficially treated, so that the assistance offered to readers requiring information on these topics is barely worth while.

It is to be hoped that these latter chapters will be expanded in any further edition in order to widen the scope of a very useful book.

R. H. HERZ

Modern geometrical optics. By M. HERZBERGER. (New York: Interscience Publishers Inc.; London: Interscience Publishers Ltd., 1958.) Pp. xii + 504. Price £5 8*s*.

Many new optical materials and designs have appeared in recent years, and infra-red and ultra-violet applications are increasing; anamorphotic and other aspheric surfaces can now be made sufficiently well for some applications (though not yet for all). Large-scale computers can now apply elaborate and rigorous methods which would be quite unsuitable for human computers and desk machines. This book collects theoretical investigations which are highly relevant in all these fields so long as geometrical optics suffice, without diffraction refinements. Admitted deficiencies of final completeness and full integration are rightly excused by the advantages of earlier circulation of the collected material.

The main topic is the general theory of geometrical-optics imagery, as deriving in particular from Gauss, Hamilton, Gullstrand and the author himself, with proper emphasis on implicit fundamental limitations. For centred spherical surfaces this leads finally to a design technique with a minimum of ray-tracing, where skew rays play a vital part. Formulae for tracing skew rays are derived, for polynomial fitting of ray-trace data with analysis of spot diagrams in terms of component effects. Fifth-order aberrations are considered as well as third-order (Seidel), and this is claimed to give a basis for design ordinarily effective up to apertures $f/1{\cdot}8$. Chromatic correction is well treated, and universal dispersion functions promise assistance in estimation of refractive indices for unrecorded wavelengths.

What is claimed as a minimum of mathematical technique still uses matrices and Gauss brackets, also vector algebra (where the reviewer would prefer Clarendon type to superior-arrowed italic); adequate introductions are provided in a 40-page appendix which also deals with the polynomial approximations involved. Historical references are ample, and acknowledgements conscientious; the bibliography has over 150 entries.

T. H. O'BEIRNE

Practical microscopy. 3rd ed. By L. C. MARTIN and B. K. JOHNSON. (London: Blackie and Son Ltd., 1958.) Pp. 138. Price 12*s*. 6*d*.

This third edition of a well-known work, published nine years after the second edition, has been only slightly altered. Brief sections have been added on trends in microscope design,

reflecting objectives, Köhler illumination, and microspectrophotometry, and the new edition has useful appendices giving a routine procedure for photomicrography and data regarding light-sources. In addition, the sections on phase contrast and interference microscopy have been rewritten and expanded and the chapters on binocular microscopes and on image interpretation enlarged. These several alterations have increased the length of the book from 124 to 138 pages. The chapter that, with the passage of time, might perhaps have had first claim to rewriting, is that on electron microscopy; this is, however, virtually unchanged. Modest in size, this book is well balanced and surprisingly comprehensive. H. W. EMERTON

Reference books

Chambers's technical dictionary. Revised ed. (Edinburgh: W. and R. Chambers Ltd., 1958.) Pp. 1028. Price 35*s*.

This useful dictionary containing some 60000 terms was first published in 1940 and has been revised and reissued with supplements several times since then. The present (third) edition has been "heavily revised" and the "greatly enlarged supplement contains a wealth of new terms relating to the latest advances in science and technology." English-speaking scientists, engineers and indeed "all those who wish to understand what they have to say to each other" have, for the last 18 years, been indebted to the compilers of this valuable work and will continue to be so as long as it is kept up to date in these days of rapid progress. Tables in the field of chemistry, geology, botany and zoology are included. A helpful feature is the inclusion of an observation after each term showing to which branch of science or engineering the term relates; although some might disagree with the classifications given, especially as the boundaries between subjects are so very uncertain. The noble attempt to distinguish trade names accurately when so many have almost become, if not have actually reached, the status of generic terms, will be appreciated by all technical writers and editors. In such a work it is not difficult to find points which one might disagree, and as the editors explained in their preface, many of these are matters of opinion on which experts differ. Rightly they have chosen to use the forms and definitions preferred by those who are actively engaged in the practice and teaching of their respective subjects rather than any more academic and pedantic definitions.

The productions and format is adequate for the comparatively low price of such a valuable work, but there might be a sale for a de luxe edition perhaps in two or more volumes.

H. R. LANG

A dictionary of named effects and laws in chemistry, physics and mathematics. By D. W. G. BALLENTYNE and L. E. Q. WALKER. (London: Chapman and Hall Ltd., 1958.) Pp. vi + 205. Price 30*s*.

The intention of the authors of this book is to enable a reader to find out, with a minimum of interruption to his studies, what *X*'s effect or law is; in this they have succeeded within a limited scope. There are some 800 entries ranging from Abbe's sine condition to the Zeeman effect, each of 50–100 words or so, and "pruned free from historical and other background matter."

It is not clear what terminology has been used in regard to such words as "law," "equation" and "theorem." Thus we find "Bragg equation" for what is often known as "Bragg's law" among crystallographers, and "Joule's law" for the heating effect of a current, often referred to as the "Joule effect." The latter, however, is stated to be the "mechanical change in length when subjected to a magnetic field" which might be regarded as the opposite of the Villari effect. Cross references would be a useful addition.

Although some of the well known numbers like Reynolds and Mach's are included there are many other which might be considered for future editions, for example, those bearing the names of Graetz, Grashof, Lewis, Margoulis, Nusselt, Peclet, Prandtl, Schmidt and Stantion.

In an appendix, definitions of 18 units, mostly electrical, are given; why these few should have been selected is not at all clear.

It is a pity that so promising a book should have to be sold at such a high price. H. R. LANG

Handbook of supersonic aerodynamics: NAVORD Report 1488. Vol. 3. Section 6. (Washington: U.S. Government Printing Office, 1957.) Pp. ix + 91. Price $1.50.

This *Handbook* uses as its primary criterion in selecting its material "its expected usefulness to designers of supersonic vehicles. Thus a collection of data directly useful in the design of supersonic vehicles, results of the more significant experiments, and outlines of the basic theory are included."

The material under review is that *part* of volume 3 of the *Handbook* (although the format of the covers might lead one to expect the whole of the volume inside) which is concerned with "two dimensional airfoils." The remaining sections of volume 3 on three-dimensional airfoils and bodies of revolution will be published later.

The main body of the work presented on two-dimensional airfoils is based on shock-expansion theory, the leading edges of the aerofoils considered being sharp and the Mach numbers limited to the ranges where the shock waves are attached. Useful comparisons are made between the shock-expansion theory and the first three approximations to it for double-symmetrical aerofoil sections of the double wedge, flattened double wedge and biconvex types. Modifications produced by camber and position of maximum thickness are also considered and viscous effects are briefly reviewed. Available experimental data are presented for comparison with the theoretical results.

Your reviewer has some reservations about the detailed usefulness to the designer of the results presented, but if a quick overall picture is all that is required the book has much to offer. Two of the figures are incompletely labelled.

L. HOWARTH

Handbuch der physik. Vol. 26. Edited by S. FLÜGGE. (Berlin: Springer-Verlag, 1958.) Pp. vii + 965. Price DM. 168.

This volume, one of 54 in the complete Encyclopaedia, contains three articles in English and a final one in French. It begins with Prof. Garlick's survey of luminescence, which roughly follows the plan of his well-known book, although it has now been brought more up-to-date. It emphasises subjects like trapping and thermoluminescence to which the author has himself made many contributions; however, it is not long enough (128 pp.) to allow all branches of luminescence to be discussed. Little will be found, for example, on infra-red effects, on excitation spectra, or on the more

complicated inorganic phosphors, but none of the important theoretical aspects of luminescence is neglected.

Dr. Rutgers' contribution on temperature radiation of solids (42 pp.) is a formal and concentrated treatment of the theory, with collected experimental data on the emissivity of metals, oxides, etc. This is a most valuable summary. Photometrists will regret that it does not give more than a brief section on colour temperature, or refer to luminous efficiencies of black bodies and the candela standard. The author's views on those dubious cases of non-Planckian radiation from heated oxides, where luminescence seems to be involved, would also have been welcome.

Next, Prof. Mizushima writes on the Raman effect (71 pp.). Molecular vibrations, rotations, and their combinations are treated by classical mechanics, and where this is inadequate to explain experimental results, brief additions of quantum mechanical theory are made. It is shown how the experimental data are applied in the calculation of thermodynamic functions, and in structure determination of simpler molecules, chiefly hydrocarbons. This article contains very little on experimental techniques.

The final article, by Prof. Lecomte, is on infra-red spectroscopy. It fills 700 pages, beginning with 100 pages on practical methods and equipment, followed by a review of the infra-red absorption data (and Raman data where required) for organic compounds, and their interpretation in structural terms. This includes a great number of types of compound from the simplest up to sterols and proteins. Similarly a section on inorganic materials covers many types, with lengthy discussion of important compounds like water and ammonia. Ionic crystals and minerals are also considered. Finally, there are brief sections on analytical applications with particular reference to hydrocarbons and biological substances, and on the measurement of band and line intensities and refractive indices in the infra-red. The article is based on the literature to the end of 1956. One source of confusion, which, of course, is not the fault of Prof. Lecomte, is that the figures of infra-red spectra include some with the wavelength scale increasing numerically from left to right, some with the reverse; some have a wave number scale increasing to the right, some have the reverse; others have both scales on them, and here again both possibilities occur. Literature references are given throughout the book at the foot of the appropriate page, with more general lists at the end of each article. Better use of this facility in the first article would have avoided many needless repetitions of details of the author's other publications.

As an example of book production one can only admire the quality of the text, its 754 figures and good indexes, with a slight reservation on the ruthless chopping up of words to fill the ends of lines, whereby both English and French suffer many incorrect divisions. For its authoritative contents, and chiefly for the comprehensive infra-red article, the book can be recommended to those who can afford it, though at £14 it must be one of the most expensive, both absolutely and in price per page, ever reviewed in this Journal.

S. T. HENDERSON

Leybold Vakuum-Taschenbuch. By K. DIELS and R. JAECKEL. (Berlin: Springer-Verlag, 1958.) Pp. viii + 268. Price DM. 39.

The rapid progress of vacuum techniques together with their widening applications make it increasingly difficult for the designer of vacuum plant and installations to absorb all the detailed knowledge required.

There is, therefore, room for a reference book to bridge the gap between: (i) those books dealing with vacuum techniques as a whole and related subjects, and (ii) the catalogue data of equipment manufacturers who are forced to include a considerable amount of detail concerning the correct use and application of the information they contain. It is, therefore, not surprising that the German firm Leybold have found it expedient to compile this book. In parts it consists of a useful collection of formulae and tables on such topics as the kinetic theory of gases, gas flow in vacuum systems and the properties of materials including a fairly detailed discussion of degassing and gettering properties.

In other parts the book is purely a summary of catalogue data of Leybold products; with seven pages on pumps and twenty-one pages on accessories such as seals and valves, all amply illustrated. The emphasis in the drawings generally is on physical dimensions rather than working principles or techniques. Useful sections discuss the principles to be followed in the selection of pumps and in the performance of gas ballast pumps and condensers for pumping condensible vapours. Vacuum gauges are very briefly summarized while leak detection in half a page is treated quite inadequately. Similarly, the application of vacuum techniques is treated very sketchily concluding with a table listing Leybold plants available for certain applications. Illustrations here are very variable; a drawing of a plant for the evaporation of thin film deposits is shown with a glass tap and a low speed pumping connexion, and the text on this topic is less than half a page, while on the opposite page a very industrial-looking vacuum metallurgical furnace is shown. The important technique of thin film deposition by sputtering is not mentioned at all. The concluding chapter, very unexpectedly contains a detailed collection of formulae and results concerning the thermodynamics of jets and supersonic flow which seems rather out of place in a book of this type. Finally, there are fifty pages of bibliography roughly classified but by no means complete, There is no indication of subject-matter (no titles are quoted) or of the importance of the particular references selected and such lists must be of questionable value to the reader.

One of the authors of this "pocket-book" (measuring $6\frac{1}{2} \times 9\frac{1}{2}$ in.) is well known for his fundamental treatise on the production and measurement of vacuum and by comparison the present book is rather disappointing. It was felt, in particular, that there was here a vast collection of data, some of which (particularly the purely catalogue material) was rather irrelevant with no guidance at all on methods or techniques. A start has been made, but the really useful vacuum reference book is still awaiting publication.

W. STECKELMACHER

Rohrhydraulik: Ein Handbuch zur praktischen Strömungsberechnung. 3rd ed. By H. RICHTER. (Berlin: Springer-Verlag, 1958.) Pp. xii + 354. Price DM. 37.50.

This third edition of *Rohrhydraulik* differs very little from the second edition published in 1954. The text has been revised, but alterations are limited to minor changes of wording and an expansion of the section dealing with pipe roughness.

The first half of the book remains an excellent and up-to-date account of the fluid mechanics of pipe flow, and reference must again be made to the very clear presentation and diagrams, and to the extensive lists of references. This part of the book is in the form of a textbook suitable for students, and begins from first principles.

The second half of the book is in effect a piping designers'

handbook, containing numerous graphs, nomograms and tables of data relating to the losses in pipe systems, together with tables of the relevant properties of a wide range of fluids.

H. C. WILKINSON

Van Nostrand's scientific encyclopedia. 3rd ed. (London: D. Van Nostrand Co. Ltd., 1958.) Pp. 1839. Price £11.

For those who are able to spend £11 on nearly 10 lb of printed paper containing 2×10^6 words in one volume, I recommend this work without hesitation. An earlier edition has been a *vade mecum* for me over a long period and rarely has it let me down. The compilers of this third edition have had to wrestle with the remarkable advances in science, engineering and medicine; the responsibility for the compilation of the data for each of the fields was left largely in the hands of a single contributor in order "to obtain a unity impossible when many men contribute."

There are 100000 definitions, 14000 separate articles, 1400 illustrations and 12 pages of beautiful coloured illustrations. An extensive system of cross-indexing is of great help in getting the best out of this tome. Articles dealing with simple concepts are treated generally in simple terms. Others begin with a simple definition and develop the subject, concluding with "a final reflection of the more detailed aspects of the topic treated." The information, so far as casual tests can show, is accurate and up to date, although, of course, not exhaustive in the limited space available. Sampling succeeded in finding most of the topics which have recently made scientific news, including, for example, the transuranic elements; but I did not manage to find xerography, exo-electron emission or X-ray fluoroscopic spectroscopy. In the preface, the publishers, contributors and editors ask for "the indulgence of the reader in the case of any significant omissions and in the case of errors" and surely they are entitled to it in such a monumental work. The necessity to make a discriminating selection in order to confine the material within the bounds of even so large a volume must have been very trying and will, I hope, not be necessary in future editions. Two or more volumes of a more manageable size would, in my view, have many advantages—perhaps one for the physical sciences and engineering and another for biology and medicine; this would then enable me, if I were invited to review the next but one edition, to suggest that it should be in four volumes. One cannot have too much of a good thing.

H. R. LANG

Solid state physics and crystallography

Dislocations and mechanical properties of crystals. By J. C. FISHER, W. G. JOHNSTON, R. THOMSON and T. VREELAND, Jr. (New York: John Wiley & Sons Inc.; London: Chapman and Hall Ltd., 1957.) Pp. xiv + 634. Price 120*s*.

In September 1956 a small international conference on dislocations and mechanical properties of crystals was held at Lake Placid, New York, under the sponsorship of the U.S.A.F. Office of Scientific Research and with the support of the General Electric Company. Attendance was limited to about 40 acknowledged experts in the subject of the conference and the present volume forms a complete record of the proceedings. The contributions range from lengthy reviews, such as Seeger's 87-page account of the dislocation theory of work-hardening, to single-page comments on particular aspects of experimental observations. Edited accounts of the discussion following each formal contribution are included and these provide valuable indications of the extent to which agreement was reached. In many instances, of course, the discussion performs the valuable function of pointing the direction in which further studies are required.

The book is divided into eight sections dealing with the principal practical and theoretical aspects of the study of dislocations in crystals, and perhaps the most interesting of these is the first, describing the direct observation of dislocations. The progress in the elegant experimental techniques of "decoration" of dislocations in transparent crystals by deposition of colloids, of etching and of electron microscopic observations on thin metal foils has led to the experimentalist first confirming, and now outstripping, the theoretician in a most impressive manner. In spite of this success it is to be noted that ". . . as yet no one has devised a reliable way of measuring the dislocation density and arrangement in a metal" (p. 599). This remains perhaps the most outstanding problem to be solved before a truly quantitative picture of the influence of dislocations on the mechanical properties of metals can be established.

The book forms a most interesting account of what must have been a very stimulating and informative conference, and the only criticism (apart from the cost) is that the photograph of the conferees is far too small. It is just possible to recognize familiar faces, but not to form any appreciation of the unknown ones.

W. BETTERIDGE

Electric conduction in semiconductors and metals. By W. EHRENBERG. (Oxford: Clarendon Press; London: Oxford University Press, 1958.) Pp. x + 389. Price 63*s*.

Dr. Ehrenberg devotes a little over half of his very useful textbook to a thoughtful exposition of the theory of electronic conduction; covering electron statistics in solids, scattering, mobility, relaxation times, conductivity, galvanomagnetic effects and thermoelectric effects; taking the "billiard ball" approach as far as it will go and then covering the wave mechanical derivations at greater length. In this part the author assumes a knowledge of physics and mathematics (including some wave mechanics) which most physics graduates and some engineering graduates will possess or acquire, and he reaches well beyond elementary theories; but he accompanies each calculation with lucid verbal statements of what it is about, what approximations and assumptions are made and the limitations which these impose. He takes care to anticipate the difficulties (for example, the details of contacts between metals, or the fact of electronic conduction in liquids) which often puzzle the student new to the theory, and interpolates sufficient numerical and experimental data to keep one's feet on the ground.

Some 50 pages are then given to a concise summary of the properties of many semiconductors (oxide, sulphide, elementary and intermetallic) mentioning nearly every substance which has received serious study, but giving most attention, naturally, to germanium.

Another chapter covers the simple theory of the space-charge barrier at a contact between metal and semi-conductor and summarizes the characteristics of the various contact rectifiers. Here one might desire more and earlier emphasis on surface states and inversion layers at free surfaces, as qualitatively explaining important features which the simpler model cannot account for.

The rest of the book deals in roughly historical sequence with point transistors, carrier injection, p–n junctions, carrier lifetime measurement and junction transistors, and gives a

clear account of the principles involved, illustrated by data from germanium devices.

There is a good index but a list (even a partial one) of symbols would have been helpful, also some means of quickly locating back-references to equations in earlier chapters.

Adequate references to major theoretical and experimental publications extend up to 1954 (a few later ones are quoted in the Preface) but the book will be mainly valued for its illuminating and unifying treatment of its subject, leaving the reader well equipped to study the most recent literature.

R. W. SILLARS

Halbleiter und Phosphore. Vorträge des Internationalen Kolloquiums 1956 "Halbleiter und Phosphore" in Garmisch-Partenkirchen. Edited by M. SCHÖN and H. WELKER. (Braunschweig: F. Vieweg und Sohn, 1958.) Pp. viii + 684. Price DM. 68.

A short review cannot discuss the detail of this impressive collection of papers from the Garmisch meeting of 1956, but the proceedings have been described at length elsewhere [*Nature*, **178**, p. 1156 (1956)]. The book will interest all specialists in the semiconductor field, and there are besides about a dozen papers on aspects of luminescence. No discussions are included. Nearly half the 99 papers are in English, a few in French and the rest in German; a few from Russian authors were either not preprinted or not presented at the meeting. About 16 contributions are merely abstracts, while about one-third of the papers now appear in full for the first time. For many of their authors it must have been discouraging to wait nearly two years for the publication of original work, and then in this expensive format. However, this seems difficult to avoid with the increasing size of conferences, which tend to become occasions for personal contacts rather than for the public discussion of new work. The time delay in the appearance of conference proceedings is apparently being circumvented in some cases by more rapid publication elsewhere of the same material, which unfortunately adds to the excessive bulk of scientific literature. The printing of the book is excellent, the paper is of moderate quality, and few errors have been noticed. It would have been an advantage to standardize the method of presenting paper summaries, but a more serious defect, and one difficult to excuse, is the omission of any index apart from a contents list.

S. T. HENDERSON

Solid state physics. Advances in research and applications. Vol. 6. Edited by F. SEITZ and D. TURNBULL. (New York: Academic Press Inc.; London: Academic Books Ltd., 1958.) Pp. xiv + 429. Price 86*s*.

The articles in this issue continue the high standard of the series. Rice, McQueen and Walsh discuss the work on properties of materials compressed by explosive shock waves which has been carried on since 1945 at Los Alamos. Accurate static compressibilities are known to about 100 kilobars. This work, if it is correctly interpreted, extends the range of measurement to 1000 kilobars—with the technical difficulty of recording the measurement before the sample disappears across the Californian desert.

Prof. Borelius studies the melting of metals on the basis of a rather arbitrary division of energy and entropy into vibrational and structural parts. The model brings a satisfactory degree of order into the experimental information and seems valuable both as a heuristic picture and for suggesting further research.

The articles by Pipe and Williams on electroluminescence, Dekker on secondary electron emission, and Givens on optical properties of metals give up-to-date cover of their respective fields. The remaining two articles are more concerned with the exposition of theory. C. S. Smith, on the macroscopic symmetry and properties of crystals, covers much the same essential topics as Nye in his book on *Physical properties of crystals*; Smith's article is naturally less comprehensive but discusses at least one topic, piezoresistivity, which Nye does not. Dexter gives a critical summary of the present theory of the optical properties of defects in non-metals; it seems not uncommon in this field that incomplete theories work remarkably well, and it should be profitable to try to understand why.

This series of volumes has already become an indispensable reference work for solid state physics, and all libraries serving workers with a possible interest in the field should possess them all.

G. WYLLIE

Vacuum

Frottement et échanges thermiques dans les gaz raréfiés. By F. MARCEL DEVIENNE. (Paris: Gauthier-Villars, 1958.) Pp. viii + 135. Price 2000 F.

A study of the dynamical and thermal interaction of fast moving solid bodies in a rarefied gas has become fundamental in recent research on the upper atmosphere. As pressures are reduced gas molecules can, on the average, travel further through the gas without colliding with other molecules and the degree of rarefaction is best described in terms of the Knudsen parameter (the ratio of mean free path to dimension of body). In this respect there is great similarity between the interactions of fast moving bodies in a rarefied gas and the flow of gases in a pipe. When the Knudsen parameter is larger than unity (the region of "free" molecular flow) the results of the kinetic theory of gases are applied; with small values of the Knudsen parameter, however, the gas may be treated as a continuous fluid of the classical aerodynamic type. The intermediate region presents the greatest difficulty and the theory has to be based largely on experiment. Mr. Devienne's book follows this course starting with a survey of gas flow in a pipe as applied to high vacuum systems. He goes on to review the theoretical and experimental work carried out in the last few years with a brief reference to upper atmosphere applications. He is very critical of a great deal of the experimental work and particularly recommends that much more experimental work is required to determine the various exchange and accommodation coefficients involved on a more rigorous basis. The book gives a concise, useful and critical summary of the present position and should prove useful to anyone concerned with this subject. It is in pamphlet form with a soft paper cover, printed on slightly grey paper and seems relatively expensive.

W. STECKELMACHER

Method for measuring the complex dielectric constant of a high-loss liquid at 8 mm wavelength

By E. H. GRANT, Ph.D.,* Barnato Joel Laboratories, Middlesex Hospital, London, W.1

[*Paper received* 24 *September*, 1958]

A method specifically suited to the investigation of liquids exhibiting high dielectric constant and high loss at 8 mm wavelength is described. Conventional techniques for measuring wavelength in the liquid and attenuation coefficient have been adapted for this purpose, and a feature of the method is the use of the same experimental cell for both reflexion and absorption measurements. The measured value for the complex dielectric constant of water at 25° C is in close agreement with theory.

Previous published data on high-loss liquids at 8 mm consists of the work of Kiely[1] and Poley,[2] both of whom made measurements on water and, in Poley's case, on some low- to medium-loss liquids. Kiely employed a free-space wave method and measured the reflexions from a large tank of water but, although this was an interesting pioneer study in this field, the resulting accuracy was low. Thus, the errors in ϵ' and ϵ'' were $\pm 20\%$ and $\pm 8\%$, where ϵ' and ϵ'' are the real and imaginary parts respectively of the complex dielectric constant. Poley, on the other hand, used a reflexion method with guided waves, but as mentioned previously,[3, 4] did not succeed in obtaining the same high accuracy for water as was achieved for the many medium- to low-loss liquids which were investigated. This was almost certainly due to the use of an experimental technique which was unsuitable for liquids of high dielectric constant and high loss.

The purpose of the present paper is to describe an apparatus and a technique of measurement specifically suited to the study of high-loss liquids in the 8 mm or *Q*-band wavelength region, with special reference to water.

METHOD AND APPARATUS

In order to determine completely the complex dielectric constant of a liquid it is necessary to measure two independent parameters, and for high-loss liquids the two usually chosen are the attenuation coefficient (α) and the wavelength in the liquid (λ_m). In the present case a slightly differing experimental arrangement is used for the measurement of each of these parameters.

Measurement of the wavelength in the liquid (λ_m). The general arrangement of the apparatus used for measuring λ_m is shown in Fig. 1. The source of millimetre waves used was a standard reflex klystron square wave modulated at 2 kc/s, the output of which was fed *via* an attenuative pad and directive feed into the main circuit. The H_{01} mode was used.

The use of a directive feed together with a matched load in the input circuit is somewhat unconventional, but was employed in order to minimize the reflexion coefficient presented to waves travelling from right to left, while at the same time buffering the klystron from the main circuit.

The experimental cell (Fig. 2) consists essentially of two interfaces with the liquid contained between them. The top interface, which is movable, is driven by a screw thread of small pitch, the position of which is measured by a large drum micrometer reading to one micron. In order to minimize reflexions, the matching blocks had to be chosen of a material having a dielectric constant roughly equal to the square root

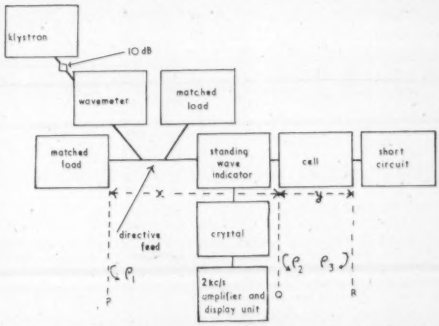

Fig. 1. Block diagram of the apparatus for measuring wavelength in liquid

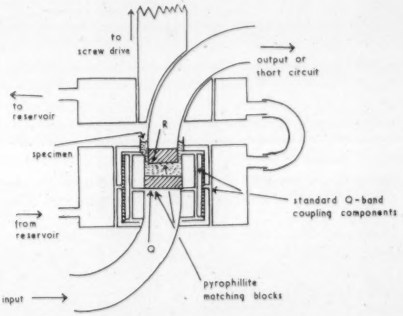

Fig. 2. Experimental cell

of that of the liquid in the cell.[5, 6] Since most of the work envisaged was on specimens of aqueous nature, pyrophillite was chosen. Pyrophillite is a ceramic of dielectric constant 5·2, while the modulus of the dielectric constant of water is

* Now at King's College Hospital, London, S.E.5.

about 30 at 8 mm wavelength. The width of the matching blocks was slightly less than the quarter-wavelength usually employed for matching into lossless dielectrics, owing to the small phase change introduced by the finite loss of the specimen. As a result of these precautions the resultant reflexion coefficient of each interface was reduced to about 0·07. The upper interface was backed by a short circuit, thereby giving sufficient signal from the first reflexion, higher reflexions being damped out by the small reflexion coefficient of the bottom of the cell and by the use of high-loss liquids. Temperature control of the specimen was effected by circulating water pumped from a thermostatically-controlled reservoir.

The method consists of maintaining the standing wave indicator probe in a fixed position, and observing the maxima and minima at the probe as the interface R is moved. The movement of R between one minimum and one maximum is then equal to a quarter of a wavelength, as will be derived below.

Consider a waveguide containing two adjacent sections, filled with air and liquid respectively, and enclosed by three interfaces P, Q, and R, of which R is movable (Figs. 1 and 2).

Radiation is incident on Q and, after suffering multiple reflexions, is collected at the probe of the standing wave indicator. The resultant electric vector at the probe may be written

$$E \propto F_1(\rho_1, \rho_2, \beta_0, x, d) + \exp(-2\gamma y)\, F_2(\rho_1, \rho_2, x, d) + \\ + \ldots + \exp[(-2n + 2)\gamma y] F_n(\rho_1, \rho_2, \beta_0, x, d) \quad (1)$$

where $F_1, F_2, \ldots F_n$ are complex functions. The relevant reflexion coefficients and dimensions are as indicated in Fig. 1, and d is the distance of the probe from Q. The complex propagation constant of the liquid is defined by $\gamma = \alpha + j\beta$ where α is the attenuation coefficient and β the phase constant. The propagation constant of the air-filled guide is simply $j\beta_0$, the attenuation coefficient being assumed negligible.

If high-loss liquids are used and ρ_1 and ρ_2 are made as small as possible, the high terms in series (1) can be neglected to give the result

$$E \propto A \exp(j\theta) + B \exp(j\phi) \exp(-2\alpha y) \exp(-2j\beta y) \quad (2)$$

where A, B, θ and ϕ are all constant real quantities. Hence

$$|E|^2 \propto A^2 + 2AB \exp(-2\alpha y) \cos(\phi - \theta - 2\beta y) \quad (3)$$

where the terms in $\exp(-4\alpha y)$ have again been neglected.

The positions of R to give maxima and minima at the probe are obtained by differentiating equation (3) and equating to zero, to give the result

$$y = n(\lambda_m/4) + C \quad (4)$$

where C is a constant, λ_m is the wavelength in the liquid and n is an integer. Thus the distance between one minimum and one maximum is exactly a quarter of a wavelength. This method of measuring $\frac{1}{4}\lambda_m$ is somewhat similar to that described by Cooper[7] based on Drude's[8] original method, but in the present case equation (4) is shown to hold for any value which the reflexion coefficients may assume, provided that the loss of the liquid is high enough to damp out multiple reflexions. The reason for making ρ_1 and ρ_2 as small as possible was to extend the range of liquids which could be examined, and also so that the same experimental cell could be used for absorption studies.

Method of measurement of the attenuation coefficient (α). Suppose that Q and R are separated sufficiently to damp out all reflexions in the water, with the experimental layout modified so that the short circuit is interchanged with the detecting system (Fig. 1) and a standard calibrated attenuator is connected between the cell and the crystal. If the interface separation is now increased by a distance y the amplitude of the output signal from the cell will be decreased by a factor $\exp(-\alpha y)$. This change in power can be compensated by decreasing the attenuation of the standard by a known amount, and thus restoring the output power from the crystal to the receiver to its original intensity. The procedure is, in fact, a simple direct substitution null method, and has been previously referred to in standard microwave text books,[5, 6] the practical difficulty lying in the elimination of reflected waves. This has been solved in the present case by employing pyrophillite matching blocks, as mentioned previously.

EXPERIMENTAL RESULT AND CONCLUSION

The above method was used to measure the dielectric constant of water at 25° C. In the reflexion method it was possible to obtain the positions of one minimum and one maximum quite sharply, the next minimum being too flat to use except as a rough check. The estimated accuracy in $\frac{1}{4}\lambda_m$ was about $\pm 1{\cdot}5\%$, this error being random. The overall error in α was estimated to be of the order of $\pm 1\%$ and the free-space wavelength λ_a was measured by the cavity wavemeter to $\pm 0{\cdot}1\%$.

The complex dielectric constant of water may be written

$$\varepsilon = \varepsilon' - j\varepsilon'' \quad (5)$$

where ε' and ε'' are the real and imaginary parts. Two further equations can then be derived[3] giving ϵ' and ϵ'' in terms of the measured experimental quantities.

$$\varepsilon' = (\lambda_a/\lambda_m)^2 - (\lambda^2\alpha^2/4\pi^2) + (\lambda_a/\lambda_c)^2 \quad (6)$$

$$\varepsilon'' = \lambda_a^2\alpha/\lambda_m\pi \quad (7)$$

where λ_c is the cut-off wavelength for the particular mode used, which in the case of the H_{01} mode is equal to twice the lateral dimension of the waveguide.

For water at 25° C the values of ε' and ε'' were found to be $20{\cdot}5 \pm 0{\cdot}7$ and $29{\cdot}4 \pm 0{\cdot}6$ respectively, these results being close to what would be expected on either of the two suggested dielectric theories.[9, 10] It should be noted, in contrast to previous work at lower frequencies, that ε'' can be measured more accurately than ε'. This is due to the greater difficulty in measuring λ_m, and to the fact that at millimetre wavelengths ε' for water is a difference of two large quantities, both of which are subject to experimental error.

In conclusion, it may be mentioned that the main features of the method are the use of the same cell for both reflexion and travelling wave methods, and the fact that the standing wave indicator is not used as a measuring instrument. The latter is an important advantage, since very large errors are involved if the conventional type of reflexion method (e.g. as described by von Hippel[11]) is used to measure substances of high dielectric constant and loss. Furthermore, highly accurate standing wave indicators for use at Q-band wavelengths are very expensive and difficult to construct.

The main error in the method lies in the measurement of $\frac{1}{4}\lambda_m$, since this is less than half a millimetre in the case of water. The accuracy could be improved here, however, by providing more solid supports for the cell and by decreasing the pitch of the screw drive mechanism still further. For high-loss liquids with lower values of ε', for example methyl

and ethyl alcohol, the method would be more accurate owing to a longer wavelength in the liquid.

ACKNOWLEDGEMENTS

Thanks are due to Dr. H. F. Cook and other colleagues for assistance and advice given. Acknowledgement is also due to Mr. D. Leegood for his careful construction of the experimental cell.

The author is particularly grateful to Mr. M. Hillier of the Services Electronics Research Laboratory, Baldock, for arranging the loan of the majority of the apparatus and for his interest at all times.

REFERENCES

(1) KIELY, D. G. *Proc. Phys. Soc.* [*London*] *B*, **63**, p. 46 p. 46 (1950).
(2) POLEY, J. PH. *Appl. Sci. Res. B*, **4**, p. 337 (1955).
(3) GRANT, E. H. *Ph.D. Thesis* (University of London, 1956).
(4) GRANT, E. H. *Proc. Phys. Soc.* [*London*] *B*, **70**, p. 937 (1957).
(5) MONTGOMERY, C. *Technique of Microwave Measurements* (New York: McGraw Hill Book Co. Inc., 1947).
(6) HUXLEY, L. G. H. *Wave Guides* (London: Cambridge University Press, 1947).
(7) COOPER, R. J. *J. Instn Elect. Engrs*, **93** (III), p. 69 (1946).
(8) DRUDE, P. *Z. Phys. Chem.* [*Leipzig*], **23**, p. 267 (1897).
(9) HASTED, J. B., and EL-SABEH, S. H. M. *Trans Faraday Soc.*, **49**, p. 1003 (1953).
(10) GRANT, E. H., BUCHANAN, T. J., and COOK, H. F. *J. Chem. Phys.*, **26**, p. 156 (1956).
(11) VON HIPPEL, A. R. *Dielectric and Waves* (New York: John Wiley and Sons Inc., 1954).

Linear photomultiplier bridge circuit for the measurement of small changes in absorption

By P. HARIHARAN, M.Sc., A.Inst.P., and M. S. BHALLA, M.Sc., National Physical Laboratory of India, New Delhi, India

[*Paper received* 11 *July*, 1958]

In the circuit described, the voltage applied to the two photomultipliers is controlled by means of a negative feedback loop so that the anode current of the monitor photomultiplier is held approximately constant. The ratio of the anode currents of the two photomultipliers is then linearly proportional to the transmission of the sample and is unaffected by fluctuations in the luminous output of the source and variations in the mains voltage. In addition, the sensitivity of the bridge remains constant, so that it is possible to estimate small changes in absorption directly from readings of the out of balance current.

Since it is impossible to operate a light source with absolutely constant intensity, it is customary, in measurements of small changes in absorption, to use a bridge circuit in which one photomultiplier views the source directly while the other receives light through the sample.[1] With such a circuit, the ratio of the output currents of the two photomultipliers is linearly proportional to the transmission of the sample, and the effects of fluctuations in the brightness of the source are considerably reduced.

In the circuit described in the present paper, the basic bridge circuit has been further refined by stabilizing the output current in the monitor photomultiplier by means of a negative feedback amplifier.[2] This results in a constant output sensitivity for the bridge, so that it is possible to measure small changes in absorption directly from readings of the out of balance current. The use of this circuit also has the advantage that it permits the employment of an unstabilized high voltage supply and completely eliminates the risk of accidentally overloading the photomultipliers.

CIRCUIT DETAILS

A diagram of the circuit is shown in the figure. Apart from the power supplies, it can be divided into two distinct sections, the negative feedback amplifier and the measuring bridge.

The negative feedback amplifier.—The individual dynode voltages for the two photomultipliers PM_1, PM_2 are taken from a chain of equal bleeder resistors R_{20}–R_{28}. The current in this bleeder and, thereby, the voltage applied to the two photomultipliers, is controlled by the series regulator tube V_7 and the difference amplifier V_8, so that the anode current of the monitor photomultiplier PM_1 is always held constant at approximately 1 μA.

Since the same voltage is also applied to the measuring photomultiplier, the ratio of the anode currents of the two tubes will remain unaffected by fluctuations in the intensity of the source, provided that if the multiplication varies as V^{β} the exponent β is the same for the two photomultipliers.[3] In practice, it is not difficult to select two photomultipliers having very nearly the same values of β, and any residual difference can be eliminated by applying a suitable negative bias by means of the potentiometer RV_2 to the last dynode of the monitor photomultiplier PM_1, thereby increasing the negative feedback to this tube.

The measuring bridge. In the measuring circuit, the signal voltages developed across the plate resistors R_{11}, R_{19} of the two photomultipliers are applied to the grids of two linear cathode followers V_9 V_{10}, which provide low impedance outputs across R_{13}, RV_3 and R_{16}, R_{17} respectively. The ratio of the current in the measuring photomultiplier PM_2 to that in the monitor PM_1 can then be easily determined by balancing the voltage across R_{16} against a suitable fraction of the voltage across the precision, decade voltage divider RV_2. The dark current of the photomultipliers as well as the grid to cathode potential difference in the cathode followers

are eliminated by applying a suitable bucking voltage from the potentiometer RV_1, while random fluctuations are reduced by the condensers C_8, C_9.

Since the anode current of the monitor photomultiplier PM_1 is held constant, it is easily seen that a given change in the setting of RV_3 will always give rise to the same galvanometer deflexion. Thus, it is possible to make the set up directly read small changes in transmission.

INITIAL ADJUSTMENT

The initial adjustment of the circuit comprises four steps.

Dark current balance. With the voltage divider RV_3 set to read zero transmission, the measuring photomultiplier PM_2 is darkened and RV_1 is adjusted until the galvanometer shows no deflexion.

Adjustment of the negative bias on the monitor. The lamp is connected to a rheostat and with PM_2 also illuminated, RV_2 is adjusted until a change of ± 10 V in the lamp supply voltage results in no change in the galvanometer reading. If the application of the bias voltage makes the fluctuations more noticeable, the photomultipliers should be interchanged, when satisfactory compensation can usually be obtained. Best results are secured when the photomultipliers are chosen so that compensation is obtained with as small a bias voltage as possible.

Adjustment of the galvanometer sensitivity. The shunt RV_4 is adjusted so that when the tapping on RV_3 is shifted by one step on the second decade (1%) the change in the galvanometer deflexion is equal to 10 scale divisions.

Full-scale adjustment. The illumination incident on the measuring photomultiplier is adjusted by means of neutral filters and an iris diaphragm until balance is obtained with RV_3 at the setting corresponding to 100% transmission.

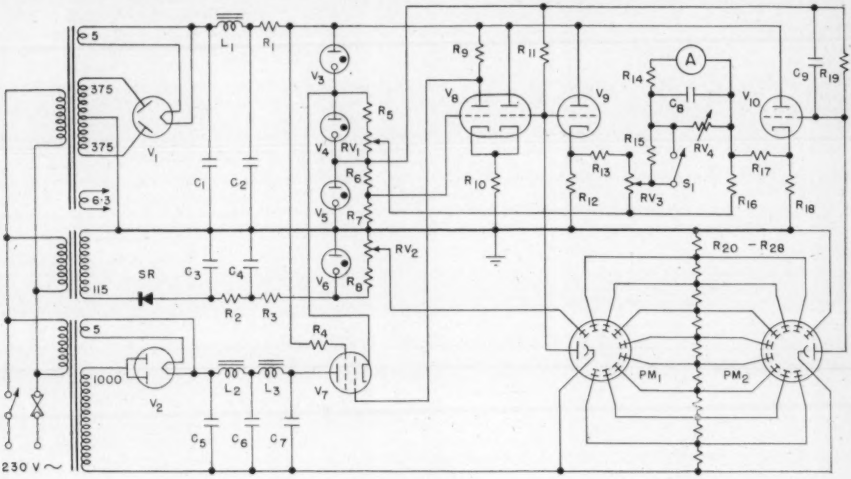

Circuit diagram

All resistors are $\pm 5\%$, 1 W carbon, except where otherwise specified.

R_1 = 5 kΩ, 10 W
R_2, R_3 = 3·3 kΩ
R_4 = 1 kΩ
R_5, R_8 = 15 kΩ, w.w.
R_6 = 33 kΩ
R_7 = 240 kΩ
R_9 = 1 MΩ
R_{10} = 150 kΩ
R_{11}, R_{19} = 20 MΩ
R_{12}, R_{18} = 330 kΩ
R_{13}, R_{17} = 2 MΩ, w.w.
R_{14} = 50 kΩ
R_{15} = 1 MΩ
R_{16} = 100 kΩ, w.w.
R_{20}–R_{28} = 15 kΩ, w.w.
RV_1 = 1 kΩ
RV_2 = 10 kΩ
RV_3 = decade voltage divider. Total resistance 100 kΩ. Smallest step 1 kΩ
C_1 = 8 μF
C_2, C_4 = 32 μF
C_3 = 16 μF
C_5, C_6, C_7 = 4 μF, oil filled
C_8 = 8 μF, paper
C_9 = 0·01 μF mica
V_1 = 5Y3 GT
V_2 = 5R4 GY
V_3, V_4 = VR 75
V_5 = VR 150
V_6 = VR 75
V_7 = 807
V_8 = 6SL7 GT
V_9, V_{10} = 6SF5
PM_1, PM_2 = 931 A
L_1–L_3 = 8 H
A = galvanometer, 500 mm/μA

After this, the circuit is ready for measurements of transmission.

PERFORMANCE

Actual measurements with this circuit showed that it was extremely stable and free from fatigue effects, and that the drift, after a very short warm up time, was negligible. In practice, it was found that even when the entire set up was operated off an unstabilized a.c. supply, changes in absorption of the order of 0·02% could be detected without much difficulty.

ACKNOWLEDGEMENTS

The authors wish to thank the Director, National Physical Laboratory of India for permission to publish this paper.

REFERENCES

(1) Oldenberg, O., and Broida, H. P. *J. Opt. Soc. Amer.*, **40**, p. 381 (1950).
(2) Sweet, M. H. *J. Opt. Soc. Amer.*, **37**, p. 432 (1947).
(3) Rodda, S. *Photo-electric Multipliers*, pp. 48, 70 (London: Macdonald and Co., Ltd., 1953).

Deposition by thermal evaporation of thin films of titanium and zirconium for tritium targets

By V. D. Scott, B.Sc., and L. W. Owen, B.Sc., Atomic Weapons Research Establishment, Aldermaston, Berks.

[*Paper first received* 28 *May, and in final form* 19 *September*, 1958]

Equipment and procedure are described for applying thin films of titanium and zirconium as tritium carriers to backings of copper, gold and platinum. A large proportion of the coatings prepared absorbed high atom ratios of tritium, titanium being more satisfactory in this respect than zirconium. It is suggested that defects in the coating arise mainly from the undesirable reaction of the metals with residual gases, particularly oxygen, during evaporation in the vacuum chamber. Firstly, this causes stress, brittleness, and owing to lack of adhesion, blistering of the deposit; secondly absorption of tritium is inhibited by the oxide film on the metal surface, and the total amount absorbed reduced as a result of there being fewer lattice sites available for the tritium. An electron diffraction examination showed that although the deposits appeared bright and metallic, a thin protective oxide film was present on the evaporated titanium and zirconium.

When tritium is bombarded with protons or deuterons a source of neutrons is obtained. In order to achieve a compact source of tritium, it is preferably absorbed in a metal which has a high affinity for the gas, such as titanium or zirconium. Ways in which such targets may be prepared have been described by Graves, Roderigues, Goldblatt and Meyer.[1] Since the bombarding particles can penetrate only a very limited thickness of the target material, tritium absorbed to a greater depth is ineffective. Thus thin films of metals with a high affinity for tritium deposited on some other non-absorbent metal achieve the object with the maximum of economy of tritium. The production of targets by the thermal evaporation of thin films of zirconium has been described by Arrol, Wilson and Evans,[2] and by Lillie and Conner.[3]

The apparatus and method is extended here, with certain modifications, to include titanium as well as zirconium. The principal causes for failure of the targets is discussed in detail.

EXPERIMENTAL DETAILS

Conventional high-vacuum evaporation equipment was used, provision being made to allow the entry of hydrogen, or another gas, into the work chamber (Fig. 1). The tungsten filament on to which the metal charge was bound with fine tungsten wire, was reduced in diameter either side of the source to produce hotter regions during the passage of current. Thus, the titanium or zirconium was prevented when molten from flowing to cooler regions nearer the electrodes. For the production of thicker deposits, two identical evaporation sources were included. In addition to the use of the metal radiation shields shown in the diagram, heating of the bell-jar was further reduced by coating the interior with a reflecting layer of aluminium, which at the high temperatures involved in the evaporation did not restrict visual observation during the deposition. Formerly, outgassing of components and metal deposition were accomplished with a single evacuation using moveable shields operated by rotary seals. However, in order to obtain the best possible vacuum with this equipment the shields were omitted. The procedure was therefore performed in stages, the apparatus being allowed to cool each time before opening the chamber to the atmosphere.

Target blanks, 1¼ in. in diameter were prepared by abrasive treatment on 000 emery paper followed by degreasing in benzene vapour, and given prolonged outgassing treatment before commencing deposition. The thickness of metal deposited was determined by weight. Electron diffraction studies of the deposits were carried out using target blanks of 1 cm diameter, reducing rings being fitted into the target support to accommodate them.

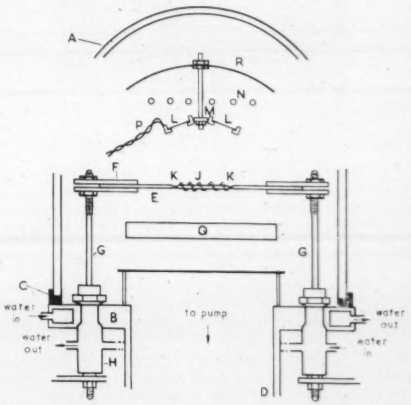

Fig. 1. Arrangement of components inside work chamber

A, bell-jar; *B*, water-cooled baseplate; *C*, rubber *L*-gasket; *D*, metal chamber; *E*, tungsten evaporator filament for supporting and heating charge; *F*, heavy copper connexions; *G*, copper upright; *H*, water-cooled electrode; *J*, metal charge; *K*, thinned portions; *L*, targets; *M*, target support; *N*, heating element for targets; *P*, thermocouple; *Q*, lower radiation shield; *R*, upper radiation shield.

RESULTS

(*a*) *Assessment of targets.* Bright metallic-looking films of titanium and zirconium were obtained on copper, gold, nickel and platinum backings by the above method. Roughening of the surface and prolonged outgassing treatment appeared to have beneficial effects on adhesion of the film.

Over 95% of titanium targets were accepted for impregnation, the coating thicknesses ranging from the equivalent of 50 to 2500 $\mu g/cm^2$, and giving Brehmstrahlung counts from 100 to over 1000 counts/s. Atom ratios of titanium:

tritium better than 1 : 1 were frequently obtained without obvious flaking of the deposit, and exceptionally up to a ratio of 1 : 2.

With zirconium, approximately 20% of the targets were of poor appearance and were lacking in adhesion. Thicknesses produced ranged from the equivalent of 50 to 500 $\mu g/cm^2$, according to requirements. In general, blistering of the deposits usually occurred when impregnation had reached an atom ratio of nearly 1 : 1.

(*b*) *Electron diffraction study.* A reflection electron diffraction pattern from the evaporated titanium deposit (Fig. 2) indicates a face-centred cubic structure with a lattice parameter of 4·28 Å (calibration with graphite powder, $d_{110} = 1{\cdot}230$ Å). Arcing of the diffraction rings (Fig. 1) shows (111) and (100) one-degree orientation.

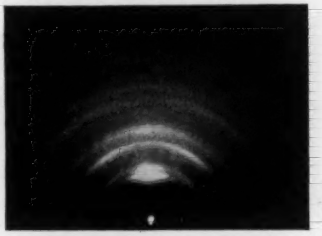

Fig. 2. Titanium monoxide on evaporated titanium film, showing (111) and (100) orientation

Available thermodynamical data[4] indicates that this thin surface film on the titanium deposits is the monoxide, with little, if any, nitride present; also the occurrence of nitride surface films appears only to have been reported after heating the specimens to above about 800° C.[5, 6] The experimental conditions in the oxidation work of Conjeaud[7] can perhaps be usefully compared with the present work. His electron diffraction study of thin single-crystal films of α-titanium, oxidized in air at a pressure of $2 \cdot 10^{-2}$ mm of mercury, showed the formation of titanium monoxide at 300° C, a mixture of anatase and rutile above 400° C, and only rutile above 550° C.

The presence of other oxide forms was not observed at this stage of the operation. Introduction of hydrogen into the system immediately after evaporation did not appear to affect this film, nor did heat treatment up to 300° C in hydrogen gas at a pressure of a few millimetres of mercury.

Fig. 3. Zirconium dioxide on evaporated zirconium film

A zirconium deposit showed either the face-centred cubic ($a = 5{\cdot}08$ Å), or the tetragonal ($c/a = 1{\cdot}015$) dioxide (see Fig. 3). It was not possible to distinguish which of these zirconium dioxide modifications occurred owing to ring broadening. A blue-coloured deposit, obtained when air was admitted too soon after evaporation onto the hot specimen, also gave this pattern. Zirconium nitride was not observed.

DISCUSSION

Two principle causes for failure of the coating were flaking of the deposit from the backing and low absorption of tritium. These defects are considered to arise mainly from the reaction of the evaporated metal with residual oxygen, and probably nitrogen, in the evacuated space of the bell jar.

At the commencement of evaporation there is an appreciable drop in pressure suggesting gettering action and it seems fairly certain that initially a film is deposited relatively rich in oxide. This film may be lacking in cohesion, but is almost certainly of poor mechanical properties and constitutes a barrier to obtaining sound adhesion. Continued deposition of titanium and zirconium would occur with less reaction with residual gases however, depending upon the leak rate and the pumping speed of the system, etc. The total gas absorbed during evaporation is considered to determine the efficiency with which tritium is absorbed since the oxygen would take up lattice sites otherwise available for tritium. Since very small amounts of oxygen rendered titanium and zirconium brittle, the extent of gas reactions occurring throughout the deposition would clearly affect the brittleness of the coating. As adhesion is likely to be poor, brittleness becomes a more important factor since cracking of the film would lead to spalling. Cracking and spalling of the film could be initiated by stress induced as a result of the different thermal expansion coefficient of the substrate. Stress in the film should be minimized by keeping evaporation and impregnation temperatures fairly low, the target temperature during evaporation being preferably about one half of that employed for impregnation.

It is clearly desirable to restrict the time of deposition since there would be less reaction with the residual gases in the chamber, but in practice the rate of evaporation is limited to that which does not endanger filament burn-out.

The oriented patterns of titanium monoxide observed in the electron diffraction examination of the films indicated that the oxide was formed while it was hot, i.e. immediately after evaporation in the vacuum system, and not later during cooling in vacuum or when air was introduced onto the cooled targets. Exposure of the titanium target to air for several weeks did not change the nature of this oxide film, neither was the oxide film upon zirconium affected by a similar time interval between evaporation and impregnation. These observations indicate that special storage precautions are unnecessary for the freshly-evaporated targets awaiting impregnation.

Electron diffraction studies on evaporated zirconium films revealed the presence of zirconium dioxide but not the monoclinic form observed by Hickman and Gulbransen[8] when heating zirconium and some alloys.

ACKNOWLEDGEMENTS

The authors wish to thank Mr. W. B. H. Lord, Senior Superintendent of Metallurgy, Atomic Weapons Research Establishment, Aldermaston, Berkshire, who directed the work, for his advice and suggestions.

REFERENCES

(1) GRAVES, E. R., RODERIGUES, A. A., GOLDBLATT, M., and MEYER, D. T. *Rev. Sci. Instrum.*, **20** (1948).

(2) ARROL, W. J., WILSON, E. J., and EVANS, C. Atomic Energy Research Establishment Internal Report 1135 (1955).

(3) LILLIE, A. B., and CONNER, J. P. *Rev. Sci. Instrum.*, **22**, p. 210 (1951).

(4) HUMPHREY, G. L. *J. Amer. Chem. Soc.*, **73**, p. 1587 (1951); **73**, p. 2261 (1951).

(5) RICHARDSON, L. S., and GRANT, N. J. *Trans. Amer. Inst. Min. (Metall.) Engrs*, **200**, p. 69 (1954).

(6) WASILEWSKI, R. J., and KEHL, G. L. *Metallurgia* **50**, p. 225 (1954).

(7) CONJEAUD, P. *J. Recherches du C.N.R.S.*, **32**, p. 273 (1955).

(8) HICKMAN, J. W., and GULBRANSEN, E. A. *J. Analyt. Chem.*, **20**, p. 158 (1948).

Experimental determination of the atomising efficiency of a high-speed spinning disk atomiser

By D. J. RYLEY, M.Sc.(Eng.), A.M.I.Mech.E., Department of Mechanical Engineering, University of Liverpool

[*Paper first received* 3 *July, and in final form* 17 *August*, 1958]

Electrically driven disks of 3 and 5 cm diameter were rotated at speeds 20 000–60 000 rev/min, and samples of an aqueous spray were analysed for flow rates of 0·12, 0·42 and 0·77 cm³/s. The reduction in disk speed during atomising was determined experimentally using an electronic pulse counter and a miniature dynamometer was devised to simulate this reduction and measure the power consumed. Atomising efficiencies for the electrically driven disk thus obtained are compared briefly with the efficiency employing air drive and also with that of a simple pressure atomiser. In all cases efficiencies are less than 0·5%.

LIST OF SYMBOLS

σ = surface tension (dyn/cm)
d = Sauter mean diameter of droplet (cm)
g = gravitational constant (cm/s²)
D = disk diameter (cm)
r = radius of disk shank (cm)
$N = \omega/2\pi$ = disk speed (rev/s)
W, w = tension in brake band (g)
E = Young's modulus (g/cm²)
I = second moment of area (cm⁴)
l, L = cantilever free length (cm)
y, Y = cantilever deflexion (cm)
Q = flow rate of test liquid (cm³/s)
ρ = density (g/cm³)
p = pressure (g/cm²)
μ = viscosity (poise)
η = nozzle efficiency
γ = isentropic index for air
n = number of droplets

Subscripts

1 = Reservoir conditions of air
2 = Expanded conditions of air

INTRODUCTION

In any atomising device the energy usefully employed is that which reappears as new surface created. Neglecting, therefore, any energy associated with the production of electrostatic charges, the useful energy may be regarded as the product of the surface tension and the extension in area, i.e.

$$\text{Useful energy} = 6\sigma/d \text{ ergs/cm}^3 \qquad (1)$$

The efficiency of an atomisation process may be defined in several ways, but fundamentally should be considered to be the ratio of the energy in the newly created surface to the energy imparted to the liquid by the atomising device employed to accomplish subdivision. In the spinning disk atomiser the latter is difficult to assess by an analytical method. The test liquid is normally fed vertically on to the centre of the disk and spreads evenly outwards being finally disrupted on leaving the edge. It is not possible to analyse hydrodynamically the motion of the water across the disk as the distributions of radial and circumferential velocities are unknown. The vertical velocity profile will also be a function of the liquid velocity, of the air drag on the free surface and probably of the disk surface texture inasmuch as slipping may occur. It would seem, however, a fair first assumption that for low flow rates the liquid is flung with a velocity equal to the circumferential velocity of the disk rim. If this be allowed

$$\text{Liquid energy} = \tfrac{1}{2}(\pi DN)^2 \text{ ergs/g} \qquad (2)$$

and the efficiency of atomisation might be defined as

$$\text{Efficiency} = 12\sigma/(\pi DN)^2 d \qquad (3)$$

The uncertainty associated with the assumption underlying equation (2) could be avoided if it were possible to measure directly the power absorbed by the disk as it assumes its liquid load. Attempts have been made by other workers to estimate the atomising efficiency by measuring the total power input to an electric motor driving the atomiser, but this is clearly unsatisfactory as the power measured includes the normal friction and motor losses. The power required for atomisation is small and may be only a minor fraction of the total; and it is not possible to separate the effects with any accuracy.

To measure the atomising power directly the method which suggests itself as most promising is to observe the speed reduction consequent upon application of the atomising load and then to employ a suitable brake on the disk when dry to accomplish the same speed reduction; the brake being capable of measuring at the same time the power required. There are, however, two major difficulties to be overcome, (*a*) the speed reduction is extremely small for normal atomising loads and has to be measured accurately for subsequent

reproduction, (*b*) the power to be absorbed by the brake is far below the capacity of any orthodox instrument.

EXPERIMENTAL WORK

In the experiments to be described these difficulties have been largely overcome. The work was conducted using an electrically-driven disk atomiser fully described elsewhere[1] together with an electronic pulse counter of standard type and a miniature rope brake.

The brake as finally designed consisted of two spring steel strips supported as cantilevers as shown in Fig. 1. A length of ordinary cotton was passed round the shank of the disk and rigidly fixed to the end of the right hand cantilever. Tension adjustment was provided by rotation of a screw mounted on the end of the left hand cantilever. Nearly the whole range of loading was accomplished using strips of spring steel $\frac{1}{2} \times 0{\cdot}015 \times 3\frac{1}{4}$ in. long. For a few tests, strips of thickness 0·020 in. were substituted and light string used instead of cotton. A suitable wood platform above the strips provided mounting for a micrometer microscope. To perform a test, the undeflected positions of the respective free ends were observed relative to a taut wire mounted on the platform. A second set of observations of these positions were taken under load. Using the notation of Fig. 1, the energy consumed is given to sufficient accuracy by

$$\text{Energy} = 2\pi r(W - w)N \text{ (g.cm/s)} \tag{4}$$

N may be taken as the nominal value of the speed.

The appropriate values of the loads W, w are obtained from the standard expression for the deflexion of a cantilever with an end load,

$$\left.\begin{aligned} W &= 3EIY/L^3 \text{ (g)} \\ w &= 3Ely/l^3 \text{ (g)} \end{aligned}\right\} \tag{5}$$

Alternatively, the cantilevers may be mounted horizontally and a load/deflexion calibration obtained by loading with small weights.

The operation of the brake exceeded expectations and it was found to be accurate and stable provided it was insulated from vibrations originating from the atomiser compressor. The horse-power absorbed ranged from approximately 1×10^{-3} to 10×10^{-3} and by employing thinner strips, and/or increasing l and L, smaller powers could be measured. It should be noticed that the load bears directly on the strips and frictional losses associated with pulleys for hanging weights have been avoided. The taking of deflexion readings would have been expedited by providing a micrometer screw behind each strip and an electric tell-tale lamp to indicate contact with the strip. A loop of cotton was found to have a life of several hours, but caused a groove to be worn in the duralumin shank of the disk. Such a groove tended to hasten fracture of the cotton and to introduce a small error into the measurement of r.

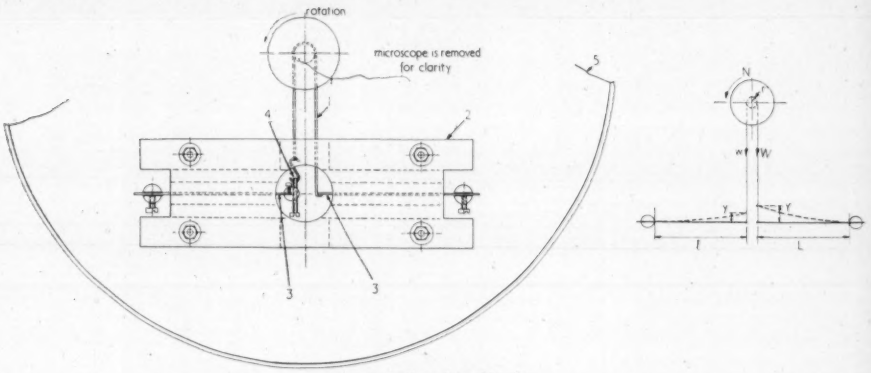

Fig. 1. Plan view of brake

1, brake band; 2, wooden supporting platform; 3, cantilevers; 4, tension adjustment; 5, drain tray.
——— stationary unloaded position. – – – deflected position under tension and rotation.

Two disks of respective diameters 5 cm and 3 cm were employed for the tests. Water was used as a test liquid and three rates of flow were available: 0·121, 0·421 and 0·771 cm^3/s. Before an atomisation test the working surface of the disk was ground using water and No. 60 carborundum powder to provide a reproducible coarse matt surface. Speeds of 20 000–50 000 rev/min were employed using the 5 cm disk and 20 000–60 000 using the 3 cm disk.

A series of separate experiments were conducted to assess the fall in speed as the atomising load is applied. Difficulties were experienced due to a small random drift in speed about the mean value. This drift, insignificant in any other context, was of absolute magnitude commensurate with the speed reduction under measurement. Accordingly, the experimental procedure was to measure alternately the speed with and without the atomising load in a consecutive series of readings for some 12 pairs.

The method of speed measurement is described in detail in Ref. 1. Briefly it consisted of a diametral hole in the disk shaft which during each revolution twice admitted light from a source to a photocell. The signal from the photocell was supplied to an Airmec frequency meter which gave a visual indication of the speed. In addition the pulse counter was connected to the photocell and arranged so as to accept some 250 impulses and to present the time therefor in microseconds. It was thus possible to accomplish a series of readings expeditiously. The direct indication of speed given by the tachometer enabled any drift of mean speed to be observed

and arrested and the counter was used to give the measurements on which the results are based. Curves of percentage speed reduction for given conditions are shown in Fig. 2.

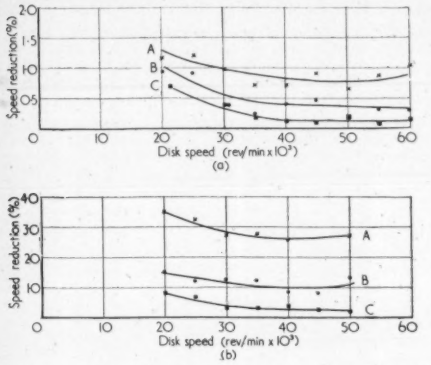

Fig. 2. Percentage reduction in speed with atomising load

(*a*) 3 cm disk; (*b*) 5 cm, disk.
(Flow rate: *A*, 0·771 cm³/s; *B*, 0·421 cm³/s; *C*, 0·121 cm³/s.)

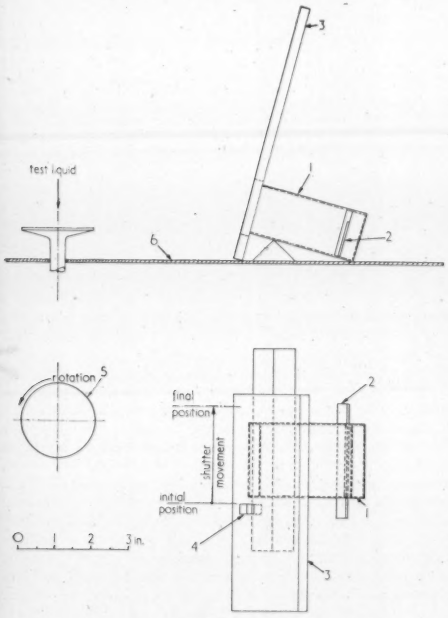

Fig. 3. Method of sampling droplets

1, open-ended receiver; 2, prepared slide; 3, hand-operated shutter plate; 4, shutter opening; 5, disk; 6, drain tray.

The method of sampling the water droplets is shown in Fig. 3. The open end of the receiver is closed with the shutter and a prepared 3 in. microscope slide is inserted. The slide is prepared by depositing two layers of magnesium oxide smoke, each layer resulting from the burning of 8 in. of 1/10 in. magnesium ribbon. The assembly is placed as close to the disk as convenience of operation permits and so orientated that droplets strike and enter the oxide normally. The shutter is translated by hand at such a speed as will give an acceptable density of craters. The variation of d with speed, disk and liquid feed rate is shown in Fig. 4.

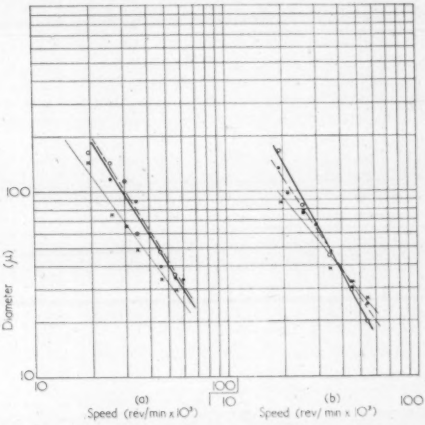

Fig. 4. Variation of Sauter mean diameter with speed

(*a*) 3 cm disk, (*b*) 5 cm disk.
Feed — — • — —, 0·771 cm³/s.
——○——, 0·421 cm³/s.
——×——, 0·121 cm³/s.

It was not found possible when employing the brake to adjust the tension so as to give a desired speed reduction equal to that of a given atomising load owing to the speed drift already noted and the difficulty of exact adjustment of the brake. The technique employed, therefore, was as follows. The brake band was tensioned to a definite value and a time count was taken with the brake in operation. The brake band loop was then held free from the shank and a control count taken after allowing about 2 s for the speed to rise to the new stable value. Alternative loaded and unloaded positions were counted for about 10 pairs. The tension was then changed and the procedure repeated until three or more groups of corresponding readings had been obtained and the required range of tensions covered. A plot was then made of resultant net tension against time increment and the tension and hence the energy expended was found by interpolation for the values of time interval obtained in the earlier experiments. The atomising efficiency is

$$6\sigma Q/2\pi rd(W - w)Ng \qquad (6)$$

Curves for the several conditions are shown in Fig. 5.

The most significant fact shown by these curves is that throughout the whole range of the variables the efficiency is very low and it is instructive to compare with Fig. 5 the efficiency of a small high speed air-driven disk atomiser.

For obvious reasons a band brake cannot be employed in such a case but the efficiency can be assessed with sufficient accuracy for comparative purposes in the following way.

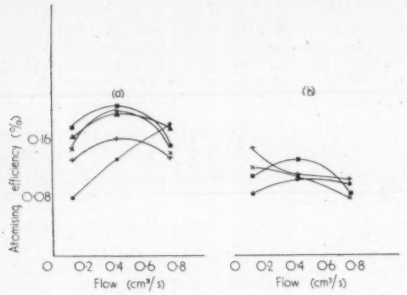

Fig. 5. Efficiency of atomisation (*a*) 3 cm disk, (*b*) 5 cm disk

● 20 000 rev/min. + 50 000 rev/min.
× 30 000 rev/min. ▲ 60 000 rev/min.
■ 40 000 rev/min.

The work done by unit mass of air expanding in the stator of an air-driven atomiser is

$$\frac{\eta\gamma p_1}{(\gamma-1)\rho_1}\left[1-\left(\frac{p_2}{p_1}\right)^{\frac{\gamma-1}{\gamma}}\right] \tag{7}$$

If n is the number of globules produced, the efficiency of utilization of this work is

$$\frac{n\pi d^2\sigma(\gamma-1)\rho_1}{\eta\gamma p_1 g\left[1-\left(\frac{p_2}{p_1}\right)^{\frac{\gamma-1}{\gamma}}\right]} \tag{8}$$

To obtain a representative figure for this quantity some results due to May[2, 3] have been employed. It may be shown from his Fig. 4 that the air consumption is related to supply pressure by the approximate expression

$$\text{Volume } (ft^3/\text{min}) = 0{\cdot}265\, p_1^{0{\cdot}72} \text{ (pressure in lb/in.}^2 \text{ gauge)} \tag{9}$$

From the same figure it may be shown that the supply pressure is closely related to the globule size by

$$\text{Globule size } (\mu) = 124{\cdot}2 p_1^{-0{\cdot}71} \tag{10}$$

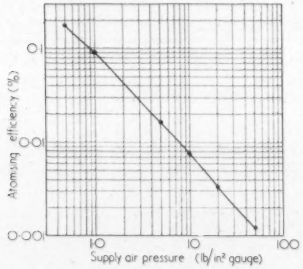

[Reproduced from *The Atomisation of Liquid Fuels*.]

Fig. 6. Efficiency of air driven atomiser

For a flow of 1 cm³/min of water, the efficiency defined by equation (8) can be calculated for the range of supply pressures used and gives the results shown in Fig. 6. It is assumed that the air expands isentropically, that the whole pressure range is effective and that all globules are "main droplets."

It will be seen that the efficiencies at low pressure are of the same magnitude as those in the present experiments, but that the efficiency declines seriously with rising supply air pressure. The reasons are as follows: (1) Expression (7) does not include the efficiency with which the kinetic energy of the air issuing from the nozzles is converted into rotational energy in the rotor; (2) air is consumed in providing the pressure rise necessary to keep the rotor airborne; (3) for atmospheric exhaust pressure a supply air pressure above the critical value $14{\cdot}7/0{\cdot}53 = 27{\cdot}7$ lb/in.^{2} abs., or 13 lb/in.^{2} gauge requires a divergence in the nozzle holes to accommodate the supersonic air velocity and an inlet pressure above this value cannot usefully be employed; (4) The expansion of the air involves considerable internal reheating of the air itself thus raising the expansion index above γ and depressing η.

It is also instructive to compare the disk atomiser with a representative performance of a typical atomiser of another type. Fig. 7 shows the droplet size distribution[4] from a

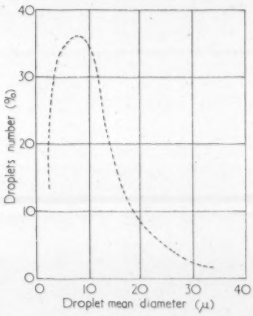

Fig. 7. Spray characteristics of injection type atomiser

plain pressure atomiser having four holes 0·016 in. diameter and operating with an effective pressure of 3970 lb/in.^{2} The test liquid was gas oil, $\sigma = 29$ dyn/cm. The specific available energy in this case is simply p/ρ and an analysis of the spray shows the atomising efficiency to be 0·04%; a very low value and commensurate with those of spinning disks.

The energy given to a test liquid by any atomising device may be expended (*a*) usefully, in creating new surface; (*b*) in providing kinetic energy of the flung globules; and (*c*) in deformation of globules, films and ligaments resulting in internal heating. It is not fully known at what stage the globules are formed as a final stable dispersion and whether, for example, (*a*) derives from (*b*). For centrifugal atomisers, Hinze and Milborn[5] distinguish three modes of fracture: (1) dropwise, by the detachment from the rotating edge of discrete droplets; (2) by the break-up of involute shaped ligaments extending from the edge; and (3) by the break-up of a rotating water sheet embracing the disk. They conducted experiments with a hollow conical atomiser and concentrated on the transition from mode (2) to mode (3), but show also

the boundary between mode (1) and mode (2). This transition occurs when

$$\left(wD\sqrt{\frac{\rho D}{\sigma}}\right)^{0\cdot25}\left\{\frac{Q}{D}\sqrt{\frac{\rho}{\sigma D}}\left[\frac{\mu}{\sqrt{(\rho\sigma D)}}\right]^{0\cdot167}\right\} > 4\cdot55\times10^{-3} \qquad (11)$$

In the present experiments, the mode of fracture is dropwise, mode (1), only in the case where the 5 cm disk is employed with the smallest rate of feed, i.e. 0·121 cm³/s. If mode (1) is assumed, the division of energy is as suggested in (*a*), (*b*) and (*c*) above, and an energy balance may be exhibited as shown in Fig. 8.

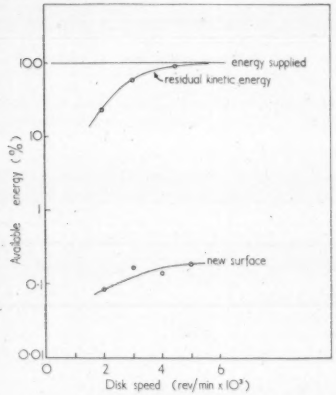

Fig. 8. Energy distribution for 5 cm disk (feed 0·121 cm³/s)

CONCLUSIONS

The atomising efficiency in all the experiments discussed is very low, showing an extreme range of efficiency from 0·08–0·20%. The 3 cm disk is clearly superior to the 5 cm disk and there is some evidence that in both cases the efficiency tends to be greatest for a mean flow value of 0·421 cm³/s. The values of efficiency are believed to be least accurate for a flow of 0·121 cm³/s, owing to the difficulty of measuring accurately small differences in time between the load and no load conditions for 250 pulses at the higher speeds. In the worst case this difference averaged only 300 μs.

ACKNOWLEDGEMENTS

The author is indebted to Professor W. J. Kearton, Harrison Professor of Mechanical Engineering at Liverpool University for permission to use the facilities of the mechanical engineering department.

He is also indebted to Mr. K. R. May, Ministry of Supply, Microbiological Research Department, Porton, for helpful information by private letter, and to Mr. H. D. Makinson for assistance with experimental work and the preparation of drawings.

REFERENCES

(1) RYLEY, D. J. *J. Sci. Instrum.*, **35**, p. 237 (1958).

(2) MAY, K. R. *J. Appl. Phys.*, **20**, p. 932 (1949).

(3) MAY, K. R. Private communication to author.

(4) GIFFEN, E., and MURASZEW, Q. *The Atomisation of Liquid Fuels*, p. 84 (London: Chapman and Hall, Ltd., 1953).

(5) HINZE, J. O., and MILBORN, H. *J. Appl. Mech.*, **17**, p. 145 (1950).

Distribution of relaxation times in a symmetrically stressed renneted milk gel

By G. W. SCOTT BLAIR, M.A., D.Sc., F.R.I.C., F.Inst.P., and J. BURNETT, National Institute for Research in Dairying, University of Reading

[*Paper first received* 28 *July, and in final form* 4 *November*, 1958]

Applying the graphical method of the "Central Limit Theorem," it is found that repeated relaxation experiments on suitably prepared renneted milk gels indicate a log-normal distribution of relaxation times, under optimal temperature conditions. This depends on minimizing strain-stiffening by alternating the direction of the stresses and also on the use of a particular convention for fixing the time zero. The disparity between the immediate elastic displacement of these gels under load and the immediate part of their recovery, previously ascribed to a type of thixotropy, is now explained in terms of static fatigue.

In an earlier paper[1] the authors have discussed the form of the stress-time curve when renneted milk gel is allowed to relax at a constant strain. A curve was given (Fig. 2) showing that, following a number of stresses in the same direction, good straight lines are obtained when $\log(P/P_0)$ is plotted against $\log t$, P being the pressure t s after the beginning of loading and P_0 the maximum pressure when the constant strain is just reached. The two curves shown represented, in fact, the eighth and ninth strainings, the loading being always in the same direction. Repeated loading in one direction stiffens the gel, whereas change of direction softens it. The log-log curves, after the first few runs, coincide, independently of the stiffening and softening.

It was pointed out that the use of the log-log plot is convenient when simple distributions of relaxation times are not apparent. Since publishing this earlier paper, however, it has been thought worth while to look further into this matter.

Feltham[2, 3] has shown that a normal distribution of entropies of activation leads to a log-normal spectrum of relaxation times, as originally proposed by Wiechert.[4] Feltham has further shown that, under certain conditions, "the (power-law) relation describing the stress relaxation can be derived on the assumption of the superposition of a spectrum of Maxwellian relaxation elements, the spectrum being approximately Gaussian on a logarithmic base." A comparatively good straight line was obtained, using data

for polymethylmethacrylate from Jenckel and Klein[5] when the integral of the log-normal distribution function was plotted against a power-law distribution of Maxwellian relaxation times [Fig. 5 in Ref. (3)]. This linearity is, of course, only approximate and is in any case limited to a certain range of relaxation times, though in the figure shown by Feltham this stretches from 0·1 to 100 s.

In general, fitting a distribution function to experimental data is a laborious business, but Grogg and Melms[6] have recently applied to relaxation data from flour doughs, a graphical method ("The Central Limit Theorem") which they ascribe to K. T. Whitby (reference not given).

The main feature of this is that, if the data plotting $100P/P_0$ against time on probability-log paper are so closely linear that a straight line can safely be drawn through the points by inspection, then it is reasonable to assume an approximately log-normal distribution of relaxation times. This really follows from Wiechert's original work, as interpreted by Feltham,[3] who derives the following equation

$$\frac{\sigma_0}{\sigma} = \frac{1}{2}\left[1 + \operatorname{erf}\left(b \ln \frac{t'_{rel}}{t}\right)\right]$$

where σ is stress at time t, σ_0 is initial stress, t'_{rel} is relaxation time of greatest frequency and, if

$$t \geqslant t'_{rel},\ \operatorname{erf}\left[b \ln (t'_{rel}/t)\right] = -\operatorname{erf}\left[b \ln (t/t'_{rel})\right]$$

which means that we can approximately equate the half-relaxation period, which we have called τ, to the geometric mean relaxation time as Grogg and Melms define this. Likewise, since in a normal distribution, 34% of the relaxation times will lie between this geometric mean and a time removed from it by one geometric standard deviation (g.s.d.), the g.s.d. can be taken by interpolation or, if necessary, extrapolation as the ratio of the time corresponding to a value of 16% for $100P/P_0$, to the value of τ.

It seemed worth while, therefore, to see whether, in so complex a system as milk gel, the data plotting $100\ P/P_0$ on probability–log paper* are sufficiently linear to justify a graphical determination of these statistical parameters.

Replotting the relaxation data from the previous paper, in this way, gives the not very encouraging curve shown in Fig. 1.

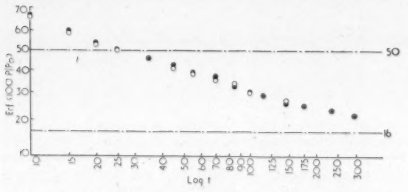

Fig. 1. Log-normal distribution for hardened gels (duplicates)

There is a decided curvature at the beginning of the experiment. However, in this experiment, conditions were much complicated by strain-stiffening; and it seemed worth while to examine data from another experiment in which an exactly similar one-hour old gel was strained eight times in alternate directions, so that there was very little stiffening or softening. The data from the eight relaxations were so similar that it seemed best to average the eight values of P for each reading-time and to plot a single curve. This is shown in Fig. 2.

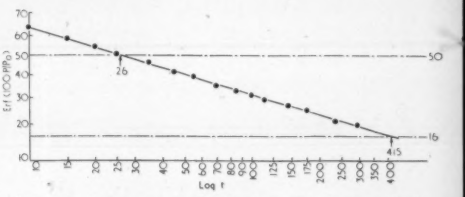

Fig. 2. Log-normal distribution for symmetrically stressed gel

Here it is apparent that the linearity is so good that a log-normal distribution may readily be assumed. The value of τ is found to be 26 s and the g.s.d. is 15·9.

In Fig. 3, the same data are given, plotting log (P/P_0) against log t, using the same time zero.

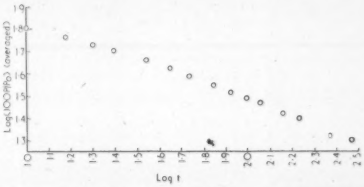

Fig. 3. Power distribution for symmetrically stressed gel

Taking the zero from the start of relaxation and not, as previously, from the start of loading, it is seen that the power-law plot shows some curvature at the beginning of the experiment. The probability plot is much more linear. This is different from the case where there was considerable strain stiffening. A comparison between Figs. 2 and 3 shows that, when the probability-log time plot is linear, the power plot is only approximately so. (This is apparent even when the same zero is taken.)

These experiments were done at a temperature of 32° C. Others were done at other temperatures ranging from about 20 to 40° C. The log-normal distribution curves were linear only over the temperature range of about 30 to 35° C, i.e. the optimum condition for the action of the enzyme (rennin). The more the temperature deviates from this range, the greater would seem to be the divergence from the log-normal distribution. The reason for this is not known.

It was shown in an earlier paper[7] that, in elastic recovery, the behaviour of these gels approximates to a simple model comprising two dashpots and two springs. Now it appears that, in relaxation, even in the absence of stiffening, an infinite number of these units is required. This implies no more than that the use of the Burgers model to account for elastic recovery is only an approximation, as, indeed, is the use of all such models. Under more complex conditions, more elements must be introduced.

* Grogg and Melms, like most other workers, take the time from the start of the reduction in stress, i.e. when the constant strain has been reached. As explained in the earlier paper, we have a preference for taking as time-zero the start of the loading but, for the present purpose, we have conformed to Grogg and Melms' usage.

Indeed, even in simple elastic recovery, it had already been noticed that some addition to the Burgers model would be needed. Thus, in our earlier paper (Scott Blair and Burnett[1]), we described how, when a load is put on to a gel and later removed, the immediate elastic displacement is very much larger than the immediate elastic recovery; and this phenomenon, unknown to us at the time for any other material, was tentatively ascribed to a thixotropy of the Maxwell dashpot in the Burgers model. Such a thixotropy would lead to a curvature in the Maxwell relaxation plot and would account for the need to introduce logarithmic time if linearity is to be restored, when plotting against the logarithm of the dissipating stress. (The linearity of this latter plot does not, of course, depend on the hypothesis of thixotropy.)

We are indebted to Prof. M. Reiner for a very interesting suggestion, made in a personal communication. Reiner suggests that the "immediate" elastic component is not really instantaneous (acoustic) but lightly damped; and that, during the creep, stress is gradually transferred from the damping dashpots to the springs in such a way that the strength of some of them is exceeded, producing local ruptures. (We have, in fact, no experimental evidence that any of the elastic reaction of these materials is truly acoustic.) Such "static fatigue" has been found, under certain conditions, in concrete; and is discussed in a paper by Reiner[8] given at the Third International Congress on Rheology (1958).

ACKNOWLEDGEMENT

We are indebted to Mr. A. Graham, of the National Gas Turbine Establishment, for helpful discussions.

REFERENCES

(1) Scott Blair, G. W., and Burnett, J. *Brit. J. Appl. Phys.*, **10**, p. 15 (1959).
(2) Feltham, P. *Bull. Brit. Soc. Rheol.*, No. 39, p. 4 (1953).
(3) Feltham, P. *Brit. J. Appl. Phys.*, **6**, p. 26 (1955).
(4) Wiechert, E. *Ann. Phys* (*Leipzig*), **50**, pp. 335, 546 (1893).
(5) Jenckel, E., and Klein, E. *Z. Naturforsch.*, 7a, p. 619 (1952).
(6) Grogg, B., and Melms, D. *Cereal Chem.*, **35**, p. 189 (1958).
(7) Scott Blair, G. W., and Burnett, J. *Lab. Pract.*, **6**, p. 570 (1957).
(8) Reiner, M. *Rheol. Acta.* (In process of publication.)

Volume of drops of aqueous solutions transferred to a slide by a "micro-rod"

By A. E. Hawkins, Ph.D., A.Inst.P., Department of Physiology, Royal Veterinary College, London, N.W.1

[*Paper first received* 28 *August, and in final form* 16 *October*, 1958]

It is shown that it is possible to estimate the volume of aqueous solution transferred by a "micro-rod" from a liquid surface to a clean glass surface. It is also shown that if several aqueous solutions are transferred it is possible to estimate the relative proportions of the solutions comprising the mixture on the glass surface.

INTRODUCTION

Clarke and Williams[1] have described a new technique for the identification of alkaloidal substances which has been found to have wide application.[2–10] "Micro-drops" of liquid are obtained with "micro-rods" which are made in the following manner. A piece of soft glass rod, 5 mm in diameter and 12 cm long, is heated in the middle and pulled out until its length is about 20 cm. It is then broken at its thinnest point, which should have a diameter of the order of 1 mm. The narrow ends are ground flat and thoroughly washed to remove glass splinters. The surface of a solution of the material to be tested is touched with a micro-rod and the adhering drop of liquid is transferred to a clean glass surface. A similar drop of reagent is now added by means of another micro-rod, and the liquid on the glass is stirred. For micro-crystalline tests a single reagent is normally all that is required, but for colour tests it is often necessary to use several successive drops of different reagents. In the latter case it is evident that it is of some importance to know the volume of the liquid transferred by the micro-rod, and the relative proportions of the various liquids making up the mixture on the glass.

An approximate theory has been worked out to enable the order of magnitude of the values to be calculated, and direct measurements have been made to check the theory. An exact analysis would be very difficult, if not impossible, and in any case would be unavailing because of the variables introduced by the technique itself. For example: (i) the rods are not exactly circular in cross-section; (ii) they are selected for size by eye; (iii) they are not precision ground; and (iv) they are liable to be moved laterally during the transfer and mixing of the liquids.

For experimental purposes distilled water was used as the liquid and clean microscope slides were used to provide the glass surfaces. It must be noted that the results obtained are only valid for aqueous solutions with a surface tension near that of water. Almost all the liquids used in micro-tests are 5% aqueous solutions of inorganic salts, and such solutions have a surface tension only 1 or 2% different from that of water.[11]

THE INITIAL DROP PICKED UP BY A ROD

When a micro-rod touching a liquid surface is lifted, the adhering liquid first takes up the shape of a surface of revolution. Since the pressure on opposite sides of the surface may be supposed to be the same, the only forces acting on any portion are the surface tensions round the boundary. It can be shown that, under these conditions, the surface is a catenoid.[12] Considering a vertical cross-section, as in Fig. 1(*a*), it seems that, with further lifting of the rod, the curves approach one another until the points *A* and *B*, where the tangents are vertical, coincide. Then the liquid

breaks away and the upper portion is left suspended from the rod as a drop.

The equation of the catenary is $y = a \cosh(x/a)$ if the x-axis is a depth a below the lowest point of the curve and thus may be expanded as $y = a\left(1 + \frac{x^2}{2a^2} + \frac{x^4}{4!a^4} + \cdots\right)$

Therefore, if the fourth and higher terms of x/a are neglected, $y = a + (x^2/2a)$, which, when the origin is removed to the lowest point of the curve, becomes $y = x^2/2a$, which is the equation of a parabola.

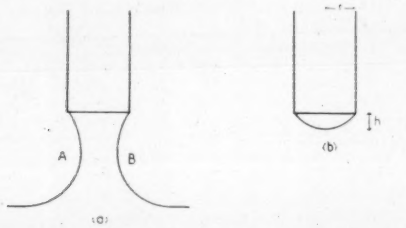

Fig. 1. (*a*) Vertical cross-section of liquid lifted by a rod (*b*) Vertical cross-section of liquid left on a rod after break

If it is assumed that this curve is, in fact, a parabola, it is possible to calculate the volume of the liquid above the breaking point. This volume is given by $\pi pr^2/5$, where p is the distance from the base of the rod to the breaking point and r is the radius of the rod. It has not been found possible to determine an equation giving the equivalent volume for the catenoid.

After the break occurs, the liquid suspended on the base of the rod forms what appears to be a spherical segment as in Fig. 1(*b*). The volume of the spherical segment is given by $(\pi h/6)(3r^2 + h^2)$, where r is the radius of the rod and h the depth of the segment.

In order to test whether $\pi pr^2/5$ is valid, the following experiment was performed and values for the volume of the drop were calculated according to this formula and also using $(\pi h/6)(3r^2 + h^2)$.

For experimental purposes the rod was fixed and distilled water was placed in a watch glass on a platform, which was so arranged that it could be moved vertically very slowly in either direction. The break-away was observed through a low-power travelling microscope. The break occurred too rapidly for p to be measured, and it was taken as half the distance between the ground base of the rod and the free surface of the water at the moment when the break occurred. The depth of the pendant drop h was determined. Several rods with a considerable variation of known radius r were used and each rod was used several times and average values for h and p obtained. As the distances measured were, in general, of the order of 0·1 cm, both the theoretical and experimental volumes were subject to an unavoidable error. The volumes obtained are given in Table 1, and it appears from these figures that $\pi pr^2/5$ is a justifiable formula.

As a confirmatory experiment the average weight of the drop of water picked up by a rod was also determined. This was done by suspending a small piece of filter paper from a torsion balance and touching the drop-laden rod to the paper. The torsion balance available covered the range 0–10 mg + 0·01 mg, and it was therefore necessary to use twenty drops to obtain a reasonable accuracy. The rate of evaporation of the water from the filter paper was determined, and it was found to be low enough not to affect the second decimal place for rods with a radius of 0·05 cm or above, but with thin rods it was impossible to obtain more than the order of magnitude of the weight of the drops. The results for the average drop weights are given in Table 1, the values for successive determinations with each rod being very consistent.

Table 1. *The volume and weight of a drop suspended from a rod after touching to distilled water*

Radius of rod (cm)	Volume of drop $\pi pr^2/5$ (μl.)	Volume of drop $(\pi h/6)(3r^2+h^2)$ (μl.)	Weight of drop Unwaxed rod (mg)	Weight of drop Waxed rod (mg)	K	Q
0·077	0·29	0·29	0·36	0·30	0·053	0·64
0·076	0·29	0·31	0·33	0·28	0·052	0·71
0·069	0·23	0·24	0·26	0·24	0·048	0·73
0·068	0·22	0·23	0·25	0·28	0·056	0·73
0·067	0·20	0·24	0·24	0·23	0·048	0·80
0·064	0·18	0·21	0·25	0·25	0·053	0·80
0·056	0·12	0·12	0·18	0·15	0·037	0·69
0·051	0·10	0·12	0·12	0·12	0·033	0·91
0·051	0·12	0·10	0·14	0·13	0·034	0·76
0·050	0·10	0·10	0·12	0·10	0·027	0·80
0·049	0·10	0·08	0·12	0·11	0·030	0·68
0·048	0·10	0·10	0·12	0·11	0·031	0·91
0·029	0·02(0)	0·01(9)	0·0(2)	—	0·01	0·78
0·027	0·01(9)	0·01(8)	0·0(3)	—	0·01	0·92
0·026	0·01(6)	0·01(4)	0·0(1)	—	0·01	0·80
0·025	0·01(5)	0·01(5)	0·0(2)	—	0·01	0·96

Owing to the nature of filter paper, these values inevitably include much of the water on the side of the rod which has not been allowed for in the theory above, and which takes little or no part in the micro-tests. The experiment was repeated after the sides of the rods had been coated with a beeswax-resin mixture to prevent water rising up the rods. The results are also given in Table 1. It will be noted that the average weights have decreased, despite the fact that it was impracticable to wax the periphery of a rod to the very tip.

Although the agreement between the calculated values and those obtained in this second experiment was again good, since the critical physical parameter is surface tension it was desired to include this in the theory. A calculation of the size of the drop using surface tension proved impracticable, but it is possible to show by the theory of dimensions that the weight of a drop of water formed at the end of, and detached slowly from, a vertical thick-walled capillary tube is given by $mg = KrT$ where m is the mass of the drop, T the surface tension of water, r the external radius of the tube and K a constant.[13] As there is a slight similarity between the two arrangements, K was calculated assuming that the mass of the drop picked up by a micro-rod obeyed this formula, but, as may be seen from the values given in Table 1, K was not found to be constant.

Since a formula for the volume of the drop with the radius of the base of the rod as the only independent variable is more convenient than $\pi pr^2/5$, the volume was expressed as Qr^3 and the value of Q determined from the experimental data. As may be seen in Table 1, the value of Q can be taken as constant. The average value is $\pi/3{\cdot}97$ which has been approximated to $\pi/4$ and the volume of the drop picked up by a rod of radius r is taken as $\pi r^3/4$ in the following sections. This result means that the distance between the

ground surface of the rod and the free surface of the water, when severance of the catenoid occurs, bears a constant relation to the radius of the ground surface. The experimental results indicate that the distance is given by $2{\cdot}5\,r$.

THE TRANSFER OF THE DROP TO THE SLIDE

When the rod is applied to the glass the liquid takes the form shown in Fig. 2(*a*). If it is assumed that the vertical cross-section of the meniscus is an arc of a circle, then its radius is $(R - r)$, where R is the radius of the wetted portion

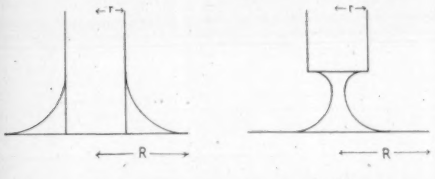

Fig. 2. (*a*) Vertical cross-section of liquid when a rod is touched on to a glass surface
(*b*) Vertical cross-section of liquid when a rod is lifted from a glass surface

of the glass and r is the radius of the base of the rod. The volume of the liquid involved is given by:

$$\pi\left[\left(\frac{10-3\pi}{6}\right)R^3+\frac{r^3}{3}+(\pi-3)R^2r+\left(\frac{2-\pi}{2}\right)Rr^2\right]$$

But this volume must be equal to that of the liquid suspended from the rod initially. This will be taken as $\pi r^3/4$. Thus

$$\left(\frac{10-3\pi}{6}\right)R^3+\frac{r^3}{12}+(\pi-3)R^2r+\left(\frac{2-\pi}{2}\right)Rr^2=0 \qquad (1)$$

In practice r/R is required, so, dividing through by R^3, the following equation is obtained:

$$0{\cdot}096+0{\cdot}083(r^3/R^3)-0{\cdot}571(r^2/R^2)+0{\cdot}142(r/R)=0 \qquad (2)$$

Solving this cubic equation graphically gives $r/R = 0{\cdot}59$.

By using a 1% aqueous solution of methylene blue the diameter of the wetted area can be measured after the liquid has evaporated to dryness. The areas are roughly circular in shape, although very irregular, and the diameters were measured in two directions at right angles. Each of six rods of the radius used in micro-tests was used to produce five drops on a glass slide, in the same way as in a micro-test, with the results given in Table 2. The average value for r/R obtained is thus $0{\cdot}62$, which is in reasonable agreement with the calculated value of $0{\cdot}59$.

Table 2. *The ratio of the diameter of a rod to the diameter of the wetted area*

Radius of rod (cm)	*Ratios*					*Average ratio*
0·056	0·73	0·55	0·56	0·57	0·58	0·60
0·051	0·67	0·62	0·69	0·56	0·63	0·63
0·051	0·61	0·66	0·64	0·63	0·68	0·64
0·050	0·61	0·63	0·76	0·63	0·59	0·64
0·049	0·60	0·66	0·61	0·55	0·63	0·61
0·048	0·62	0·58	0·61	0·59	0·54	0·59

THE VOLUME OF LIQUID LEFT ON THE SLIDE

When the rod is lifted off the slide the liquid runs in on both the slide and the base of the rod as in Fig. 2(*b*). To calculate the volume left on the slide at break it is assumed that the ratio of the radius of revolution of the catenoid at the rod (*a*) to the radius of revolution of the catenoid at the slide (*b*) at break is the same as r/R just determined. Assuming again that break occurs at the mid-point and that the curves are parabolas, the volume left on the rod is $\pi qa^2/5$ and the volume left on the slide is $\pi qb^2/5$, where $2q$ is the distance between rod and slide at break. Thus, as

$$\frac{a}{b}=\frac{r}{R},\quad V_{slide}=\frac{V}{1+(r/R)^2}\quad\text{and}\quad V_{rod}=\frac{V(r/R)^2}{1+(r/R)^2}$$

where V is the volume of the initial drop hanging on the rod. That is, $V_{slide} = V/1{\cdot}35$ and $V_{rod} = 0{\cdot}35V/1{\cdot}35$ since $r/R = 0{\cdot}59$. As $V = 0{\cdot}25\pi r^3$, $V_{slide} = 0{\cdot}58r^3$ and $V_{rod} = 0{\cdot}204r^3$.

After severance the liquid hangs as a small cap (again assumed to be a spherical segment) at some point on the foot of the rod, and it is possible to determine the diameter and depth before evaporation occurs if two operators each using a vernier microscope carry out the two measurements simultaneously. Experimental and theoretical values for the volume of the drop left on the rod after touching to the slide are given in Table 3. Reasonable agreement having been obtained it would appear satisfactory to assume that the volume of liquid remaining on the slide is given by $0{\cdot}58r^3$.

Table 3. *The volume of a drop on a rod after touching to a slide*

Radius of rod (cm)	*Theoretical volume* $0{\cdot}204r^3$ (μl.)	*Spherical segment* (μl.)
0·056	0·03	0·04
0·051	0·03	0·03
0·051	0·03	0·03
0·050	0·03	0·03
0·049	0·03	0·03
0·048	0·02	0·04

THE EFFECT OF ADDING A SECOND DROP

In practice a new rod is used to add a drop of a second liquid to the original drop. However, when the radii of over one hundred rods were measured it was found that 90% were within the range $0{\cdot}05 - 0{\cdot}065$ cm, and for this work the rods are assumed to have the same radius r. Thus to $0{\cdot}58r^3$ of liquid A on the slide there is added $\pi r^3/4$ of liquid B.

The total volume of liquid is, therefore, $1{\cdot}37r^3$ which is spread out as it is in Fig. 2(*a*) and thus equation (2) becomes, for this case:

$$0{\cdot}096-0{\cdot}103(r^3/R^3)-0{\cdot}571(r^2/R^2)+0{\cdot}142(r/R)=0 \qquad (3)$$

Solving graphically gives $r/R = 0{\cdot}53$. This ratio was determined experimentally as before, except that the first drop of methylene blue was applied, the rod dried and then a second drop applied. The average value for r/R was found to be $0{\cdot}51$.

THE VOLUME OF LIQUID REMAINING ON THE SLIDE AFTER ADDING THE SECOND DROP AND REMOVING THE ROD

As the total volume of liquid is $1{\cdot}37r^3$ and r/R is $0{\cdot}53$, the volume on the slide is calculated to be $1{\cdot}07r^3$ and the volume left hanging from the rod is calculated to be $0{\cdot}30r^3$.

In order to check these figures experimentally the rod was fixed in position and the first drop of water was applied to the slide by moving the platform up to the rod. After drying the rod and recharging with water the second drop was applied to the first and finally the dimensions of the drop remaining on the rod were determined. The results are given in Table 4.

Table 4. *The volume of a drop remaining on a rod after applying a second drop*

Radius of rod (cm)	Theoretical volume $0{\cdot}30r^3$ (μl.)	Spherical segment (μl.)
0·056	0·05	0·06
0·051	0·04	0·05
0·051	0·04	0·05
0·050	0·04	0·05
0·049	0·04	0·04
0·048	0·03	0·06

The experimental values are in all cases higher than or equal to the theoretical, but of the same order of magnitude, hence it appears that the figure of $1{\cdot}07r^3$ for the volume of the mixture of the two liquids A and B on the slide is approximately correct.

As there was a volume $0{\cdot}58r^3$ of A on the slide and a volume $0{\cdot}79r^3$ of B on the rod it follows that, if complete mixing has occurred before removing the rod, the volume $1{\cdot}07r^3$ after the rod is removed is made up of a volume ratio of 1 of A to 1·4 of B.

THE EFFECT OF ADDING MORE DROPS

The theory given above can be applied for the addition of further drops. If a drop of a liquid C be added, r/R becomes 0·48 and there should be left a total volume of liquid on the slide of $1{\cdot}5r^3$, made up of 1 part of A to 1·4 of B and 1·7 of C. If a drop of a liquid D is also added the figures become: $r/R = 0{\cdot}46$, total volume on slide $1{\cdot}9r^3$ made up of 1 part A to 1·4 of B, 1·8 of C and 2·2 of D.

It is evident from these figures that it may be necessary either (i) to use different concentrations of reagents, or (ii) to use a particular order, when several successive reagents are being used. For example, in the micro-scale technique for the well-known diazo test,[3] micro-drops of the test solution, dilute hydrochloric acid, sodium nitrite solution and alkaline β-naphthol solution are added successively in that order. If the hydrochloric acid and the β-naphthol are of the same normality, the final test drop will be alkaline and coupling to form the dye will take place.

ACKNOWLEDGEMENTS

The author is indebted to Prof. E. C. Amoroso for his encouragement in this work and to Dr. E. G. C. Clarke for bringing the problem to his notice. The author also wishes to thank Miss G. Tomlinson for her assistance with the measurements.

REFERENCES

(1) Clarke, E. G. C., and Williams, M. *J. Pharm. and Pharmacol.*, **7**, p. 255 (1955).
(2) Clarke, E. G. C., and Williams, M. *Bull. Narcotics*, **7**, p. 33 (1955).
(3) Clarke, E. G. C. *J. Pharm. and Pharmacol.*, **8**, p. 202 (1956).
(4) Clarke, E. G. C. *J. Pharm. and Pharmacol.*, **9**, p. 187 (1957).
(5) Clarke, E. G. C. *J. Physiol.*, **135**, p. 28P (1957).
(6) Williams, M. *J. Physiol.*, **135**, p. 35P (1957).
(7) Clarke, E. G. C. *J. Pharm. and Pharmacol.*, **9**, p. 752 (1957).
(8) Clarke, E. G. C. *J. Pharm. and Pharmacol.*, **10**, p. 194 (1958).
(9) Clarke, E. G. C. *Nature* [*London*], **181**, p. 1152 (1958).
(10) Clarke, E. G. C. *J. Pharm. and Pharmacol.*, **10**, p. 642 (1958).
(11) Hodgman, C. D. (Ed.). *Handbook of Chemistry and Physics*, 36th Ed., p. 1718 (Cleveland: Chemical Rubber Publishing Co., 1954).
(12) Ramsey, A. S. *Hydrostatics*, p. 164 (Cambridge: University Press, 1936).
(13) Drysdale, C. V., and others. *The Mechanical Properties of Fluids*, p. 26 (London: Blackie and Son, Ltd., 1923).

Correspondence

The problem of exo-electron emission phenomena

I should like to add some comments and further information to the recent survey on exo-electron emission phenomena communicated to your *Journal* by Dr. L. Grunberg.[1]

In 1953 I made some measurements on the induced external photoelectric effect of polycrystalline layers of alkali halides by means of a Geiger–Müller counter.[2] The results showed that the spectral distribution of the induced photoelectric emission (radio-photostimulation–coelectronemission) showed a maximum in the vicinity of 4800 Å for sodium chloride and 5700 Å for potassium chloride layers. These results suggested that the induced emission was connected with the existence of *F*-centres in the crystals forming the layer and they were discussed in conjunction with the work of Gudris and Kuligowa,[3] Fleischmann,[4] Apker and Taft[5] and Kramer.[6] It was clear that if the phenomenon of induced emission was due to *F*-centres, it should also be possible to observe an increasing emission with time due to the increasing concentration of *F'*-centres as the *F*-centres decayed. Such an observation was reported by the author in 1955.[7]

The influence of the electric field within the counter has been mentioned by the author, and it has also been observed that by applying a retarding potential to an internal grid it was possible to stabilize the operation of a counter using an aluminium cathode.[8] The opinion was expressed that exo-electrons were the cause of the instability of counters when they were not operated in complete darkness.[8] Further observations on the role played by the gaseous atmosphere on the emission phenomena have also been published.[9–11]

My own measurements and those of other workers[12] suggest that two mechanisms for the emission of exo-electrons are possible: (*a*) chemical reactions accompanied by electron or negative ion emission and (*b*) emission of electrons from filled electron traps generated in the surface layers. It is

conceivable that both mechanisms could operate consecutively, electrons initially being emitted by process (*a*), and then by (*b*) as the semi-conducting layer builds up on the surface (e.g. an oxide layer on a metal surface).

Recent work suggests that one must take care to avoid spurious counts arising from the development of surface charges or from vapours diffusing into the counter.[13, 14] Such effects although not related to the emission of exo-electrons are nevertheless of some value for the examination of certain other properties of solid surfaces.

Grunberg and Wright have studied the exo-electron emission phenomena from abraded aluminium and zinc surfaces[15] and report that the emission is selective with wavelength in the visible region. Grunberg maintains that this suggests that mechanism (*b*) is the important one in causing emission. However, other workers[16, 17] have not observed this selectivity with abraded surfaces (plasto-photostimulated co-electron emission). Whilst my own studies of radio-photo stimulation co-emission of electrons with an oxidized aluminium counter[11, 18] gave no possibility of observing any selective character of the emission. I observed only a gradual increase in emission with time and with accelerating voltage on the grid, as had already been reported by other workers. It has been suggested that this effect could give information on the oxidation mechanism of an aluminium surface.[19]

In recent studies made by myself and my co-workers a Geiger–Müller counter fitted with a grid has been used.[20, 21] Using light filters and a different light source from that used by Grunberg and Wright[15] no evidence of selective emission at 4700 Å or over the range 5000–7500 Å was observed. It would be desirable to investigate this aspect further, but preferably avoiding the use of carborundum as an abrasive, since it has been established that this abrasive if it becomes embedded into the surface layers of soft metals can by itself give rise to electron emission.[22]

Zaklad Fizyki Doswiadczalnej, Uniwersytet Wroclawski, Wroclaw, Poland.

B. SUJAK

[22 *May*, 1958]

REFERENCES

(1) GRUNBERG, L. *Brit. J. Appl. Phys.*, **9**, p. 85 (1958).
(2) SUJAK, B. *Acta phys. Polon.*, **12**, p. 241 (1953).
(3) LUKIRSKY, P., GUDRYS, N., and KULIKOWA, L. *Z. Phys.*, **37**, p. 308 (1926).
(4) APKER, L., and TAFT, E. *Phys. Rev.*, **79**, p. 964 (1950); **81**, p. 698 (1951).
(5) FLEISCHMANN, R. *Z. Phys.*, **84**, p. 727 (1933).
(6) KRAMER, J. *Z. Phys.*, **129**, p. 34 (1951).
(7) SUJAK, B. *Acta phys. Polon.*, **14**, p. 263 (1955).
(8) SUJAK, B. *Acta phys. Polon.*, **14**, p. 489 (1955).
(9) SUJAK, B. *Zeszyty Naukowe Uniwersytetu Wroclawskiego*, **1***B*, p. 151 (1956).
(10) SUJAK, B. *J. Phys. Soc., Japan*, **11**, p.719 (1956).
(11) SUJAK, B. *Acta phys. Austriaca*, **10**, p. 460 (1957).
(12) SUJAK, B. Paper read on 15.11.1957 in Technische Universität—Berlin Charlottenburg (see *Phys. Verh.*, **8**, p. 254 [1957] paper will be published in *Phys. Blätter*).
(13) SUJAK, B. *Z. ang. Phys.*, **9**, p. 404 (1957); *Czechosl. J. Phys.*, **1**, p. 627 (1957).
(14) SUJAK, B. *Czechosl. J. Phys.*, **8**, p. 616 (1958); *Z. ang. Phys.*, **10**, p. 531 (1958).
(15) GRUNBERG, L., and WRIGHT, K. H. R. *Nature* [*London*], **174**, p. 657 (1954); *Proc. Roy. Soc. A*, **232**, p. 403 (1955).
(16) EDLINGER, W., and MÜLLER, H. *Anz. d. math.-nat. Kl. Oester. Akad. d. Wiss.*, **163**, p. 89 (1954).
(17) MÜLLER, H., and WEINBERGER, F. *Acta phys. Austriaca*, **10**, p. 409 (1957).
(18) SUJAK, B. *Acta phys. Polon.*, **16**, p. 49 (1957).
(19) HRBEK, A., and VLASAKOVA, L. *Czechosl. J. Phys.*, **7**, p. 626 (1957).
(20) SUJAK, B., and MADER, J. *Z. Naturforsch.*, **13***a*, p. 55 (1958).
(21) BOJKO, I., PIROG, M., and SUJAK, B. *Z. Naturforsch.*, **13a**, p. 799 (1958).
(22) LINTNER, K., and SCHMID, E. *Radex-Rundschau*, **1**, p. 23 (1956).

The article *A survey of exo-electron emission phenomena* was intended as a guide for the uninitiated to the subject and within the space allocated it was impossible to do justice to all the workers in the field. It is fortunate that the present letter remedies this with respect to Mr. Sujak's work.

In the latter part of his communication Mr. Sujak raises the controversy of chemo-emission *versus* emission from electron traps. As the survey has clearly shown the atmosphere present and surface films affect the emission greatly. Experimental results obtained with Geiger counters, in which specimens are exposed to the counting gas should be accepted with considerable caution. This applies to a large number of data, including those by Sujak and our own. Much of the work requires confirmation with instruments which allow a better control of the ambient atmosphere, such as electron-multipliers.

Similar caution is necessary with respect to "photo-stimulation" in which light-filters are used to restrict the range of wavelengths. Parasitic transmission in the near ultra-violet may affect the results and we have also found that intense light-sources may change the relative transmissivity of different filters through bleaching. The use of monochromators suffers from the disadvantage of a low signal/noise ratio, owing to the low output of photons.

We are, at present, investigating the effect of these factors in relation to previously obtained data. The results of these investigations will be published in due course.

Mechanical Engineering Research Laboratory, Thorntonhall, Glasgow.

L. GRUNBERG

[11 *August*, 1958]

Notes and comments

Elections to The Institute of Physics

The following elections have been made by the Board of The Institute of Physics:

Fellows: A. S. Douglas, J. Franks, K. D. Froome, D. E. R. Godfrey, E. O. Hall, G. W. Hamstead, H. K. Henisch, S. C. Jain, W. O. Lock, S. G. G. Macdonald, G. W. A. Morris, B. G. Owen, K. I. Roulston, A. H. Ward, P. E. Watson, R. W. H. Wright.

Associates: K. H. J. Adams, K. V. Aubrey, G. S. Barlow, F. Baynes, A. C. Benson, C. E. Brindley, R. Brymner, A. C. Chapman, J. C. Cooper, C. W. Dally, B. L. Davies, V. Deshpande, R. O. W. Fletcher, I. V. Hansford, T. Hatherton, P. J. Heywood, G. Jackson, D. A. James, J. G. Jones, M. J. Jones, E. A. Kellett, W. E. Laker, B. D. Lambourn, I. G. Main, W. J. G. Massey, D. May, E. J. W. Morrison, T. R. Morgan, P. Muff, J. J. Parker, B. L. Rees, A. D. Reid, R. Riley, D. M. Roycroft, J. W. Saunders, J. Seymour, A. Shilton, A. Skertchly, E. J. Smith, W. A. Smith, Sister St. Joan of Ark, G. W. Taylor, B. J. Thompson, J. A. Wesson, D. F. White, R. C. Wratten, J. Zarzycki.

Forty-three Graduates, seventy-four Students and four Subscribers were also elected.

Australian conference on solid state physics

The Australian Branch of the Institute of Physics announces that it is arranging a conference on Solid state physics to be held from 17–24 August, 1959 in Melbourne. There will be a number of overseas visitors attending the conference.

Details may be obtained from the convenor of the organizing committee, Dr. W. Boas, C.S.I.R.O., Tribophysics Laboratory, University of Melbourne, Carlton, N.3, Victoria, Australia.

Symposium on interferometry

A symposium on interferometry is to be held at the National Physical Laboratory from 9–11 June, 1959. The symposium is designed for specialists and will not deal primarily with technical applications. There will be four half-day sessions devoted to the presentation of papers and to discussion, and a fifth session for the viewing of demonstrations.

About 20 main papers have been invited and will be printed and circulated in advance. Additional short contributions will be welcomed in the form of contributions to the discussion on the main papers, or in the form of demonstrations.

Attendance is by invitation, and applications should be made to Mr. L. H. McDermott at the National Physical Laboratory, Teddington, Middlesex.

Lapis

A new monthly journal entitled *Lapis* was first published in October, 1958. The first issue list patents (Government and industrial) available for manufacture under licence; inventors seeking manufacturers; inventions for which provisional patents are being taken out and manufacturers sought; agents seeking agencies, and companies seeking agents.

The journal is published by Kenneth Mason Publications, 1 Old Burlington Street, London, W.1. Subscription price is £10 10*s.* p.a.

Errata

The following errors occurred in the January issue of this *Journal*:

In the paper by E. H. Andrews which appeared on p. 39, the figure 2 should appear in the numerator instead of the denominator in the headings of columns 5 and 6 of Table 2.

In the paper by G. F. Eveson, E. W. Hall and S. G. Ward which appeared on p. 43. Equation (1), Table 2 should read:

$$v_\infty/v = 1{\cdot}001 - 0{\cdot}272d/D$$

Equation (9) should read:

$$\frac{v_\infty}{v} = \frac{2}{3}\sinh\alpha \sum_{n=1}^{\infty} \frac{n(n+1)}{(2n-1)(2n+3)}\gamma \qquad (9)$$

Journal of Scientific Instruments

Contents of the February issue

ORIGINAL CONTRIBUTIONS

Papers

Nuclear spin pulse apparatus. By K. Luszczynski and J. G. Powles.
Wide range recording anemometer. By A. N. Rapsey.
Two emission stabilizers for electron-bombardment furnaces. By D. Allenden.
Three-beam interferometer. By P. Hariharan and D. Sen.
Photoelectric setting methods for a three-beam interferometer. By P. Hariharan, D. Sen and M. S. Bhalla.
Mechanical structure-factor computer. By W. Schaffer.
Liquid manometer with electromagnetic balance indicator. By J. F. Kemp.
Two-layer anti-reflexion coating for low refractive index glass. By L. Holland and T. Putner.
Continuous reading balance for oxidation studies. By E. Dempsey.
Thermostat suitable for controlling air temperature, particularly in biological research. By J. W. L. Beament and K. E. Machin.
Electron bombardment apparatus for vacuum evaporation. By J. C. Kelly.
Recording optical lever. By R. V. Jones and J. C. S. Richards.
Evaporation of metals by electron bombardment. By O. S. Heavens.

Laboratory and workshop notes

Multi-channel time recorder for time and motion studies. By W. G. Whittlestone.
Controlled-atmosphere electric furnace. By A. C. Frostick and J. H. Weymouth.
Bellows-operated water switch. By J. Preston.
Zone refiner for laboratory use. By T. Fohl and R. W. Christy.
Coolable vacuum-tight window seals for optical use. By V. Roberts.

Correspondence

Simple attachment to the Sucksmith ring balance for use at low temperatures. From J. Crangle and M. J. C. Martin.

NOTES AND NEWS

New instruments — Notes and comments

THIS JOURNAL is produced monthly by The Institute of Physics, in London. It deals with all branches of applied physics (including theory and technique). All rights reserved. Responsibility for the statements contained herein attaches only to the writers.

EDITORIAL MATTER. Communications concerning editorial matter should be addressed to the Editor, The Institute of Physics, 47 Belgrave Square, London, S.W.1. (*Telephone:* Belgravia 6111.) Prospective authors are invited to prepare their scripts in accordance with the *Notes on the preparation of contributions*. (Price 2*s.* 6*d.* including postage.)

REPRODUCTION. The Institute of Physics is a signatory to The Royal Society's Fair Copying Declaration. Details may be obtained upon application from The Royal Society, London, W.1.

ADVERTISEMENTS. Communications concerning advertisements should be addressed to the agents, Messrs. Walter Judd Ltd., 47 Gresham Street, London, E.C.2. (*Telephone:* Monarch 7644.)

CLAIMS FOR MISSING JOURNALS. Claims from regular subscribers to this *Journal* for missing numbers will only be considered if received within 60 days of the date of mailing plus normal outward time of transit and time for lodging the claim. Losses attributable to failure to notify a change of address or to similar omissions will not be considered.

SUBSCRIPTION RATES. A new volume commences each January. The charge is £6 per volume ($17 U.S.A.), including index (post paid), payable in advance. Single parts, so far as available, may be purchased at 12*s.* 6*d.* each ($1.75 U.S.A.), post paid, cash with order. Orders should be sent to The Institute of Physics, 47 Belgrave Square, London, S.W.1, or to any bookseller.

Summarized proceedings of a colloquium on X-ray fluorescence analysis—London, February and April 1958

X-ray fluorescence as an analytical technique was the subject of a joint meeting of the Applied Spectroscopy and X-ray Analysis Groups of The Institute of Physics held in London on 21 February, 1958 (and repeated on 1 April). A summarized account of the papers read by the principal speakers and of the ensuing discussions at the two meetings is given below.

The colloquium was opened by Mr. H. M. DAVIS and Mr. H. I. SHALGOSKY [U.K. Atomic Energy Authority (Research group) London], with a paper on "The basic principles of X-ray fluorescence spectroscopy." The X-rays produced when an element is bombarded in a vacuum by a monochromatic stream of electrons of sufficient energy consist of a continuum and a superimposed line spectrum which is characteristic of the target material (Fig. 1). The line spectra

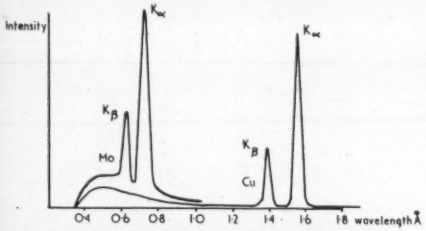

Fig. 1. Relationships of X-ray lines to continuum in K series spectra of molybdenum and copper

of the elements were studied by Moseley who was able to show that the wavelengths of corresponding lines varied in a systematic manner with atomic number (Z). The law he deduced is expressed by the following equation:

$$1/\lambda = c(Z - \sigma)^2 \qquad (1)$$

where c and σ are constants appropriate to the line under consideration and Z and λ have their usual significance. For the $K\alpha$ lines the equation becomes

$$1/\lambda_{K\alpha} = 8{\cdot}2303 \times 10^4 (Z - 1)^2 \qquad (2)$$

The intensity I of a particular line emitted by the target material was found empirically to depend on the target current i and on the potential employed to accelerate the electron beam in the following manner:

$$I = K.\, i\,(V - V_c)^n \qquad (3)$$

where K and n are constants, V is the accelerating potential and V_c is a critical potential depending upon the line and the target element. Above a certain value of V it was found that all the lines in the spectrum of an element were excited and that further increase merely increased their intensities relative to the continuum.

The continuum has a well-defined minimum wavelength corresponding to

$$\lambda_{min} = hc/eV = 12430/V(\text{Å}) \qquad (4)$$

with the usual notation (Fig. 2). This wavelength corresponds with complete conversion of the energy of an electron in an encounter with the nucleus of one of the atoms of the target. The probability of this process is very low, however, and in general the electron will give up its energy in a series of encounters in the form of heat or quanta of lower energy than that corresponding to λ_{min}. Hence the spectrum is continuous from λ_{min} to very long wavelengths.

The efficiency of conversion of electrical energy into X-radiation has been determined empirically as,

$$\epsilon = 1{\cdot}1 \times 10^{-9} ZV \qquad (5)$$

and for a tungsten target bombarded with 50 keV electrons is 0·4 %.

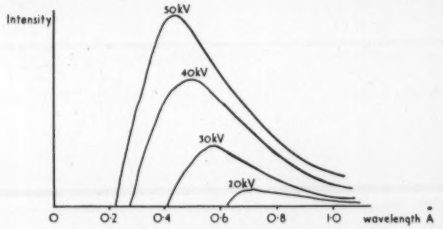

Fig. 2. X-ray continuum

The use of the line spectra produced by direct electronic bombardment for analytical purpose is attractive, but there are many practical difficulties in the general application of the technique. These are briefly as follows:

(*a*) the X-ray tube in which the specimen is to form the anticathode must be opened, cleaned, reassembled and outgassed before each analysis
(*b*) the specimen must possess high electrical conductivity
(*c*) the specimen must be capable of dissipating large amounts of thermal energy, since only a small fraction of 1 % of the energy of the bombarding electrons is converted into X-radiation and the remainder appears as heat
(*d*) the material under examination must be non-volatile and capable of being rapidly and completely outgassed.

These requirements restrict the method to a few metallic elements or their alloys, and greatly diminish its potential usefulness.

Fluorescent spectra. It is possible to excite the line spectrum of any specimen by bombarding it with X-ray photons of sufficient energy. Photoelectric absorption of the incident radiation then occurs accompanied by fluorescent emission of the characteristic spectrum of the material under examination. This method of excitation has immense advantages over that already discussed, in that the physical characteristics

of the specimen are for the most part no longer of importance, and the X-ray tube supplying the primary radiation may be designed for maximum efficiency and permanently sealed off. The excitation process, moreover, does not give rise to an X-ray continuum, and much greater accuracy is therefore possible in the measurement of small line intensities. The only disadvantage is that the overall efficiency of the excitation process referred to the power dissipated by the X-ray tube is only a few per cent of that attainable by direct bombardment.

The universal applicability, rapidity and convenience of the fluorescence method have, however, made it the basis of nearly all modern X-ray spectroscopy.

Production of fluorescent spectra. The absorption of X-radiation by matter is governed by the equation

$$I = I_0 \exp(-\mu x) \qquad (6)$$

where I_0 and I are the incident and transmitted intensities respectively, μ is the absorption coefficient of the material at a particular wavelength and x is the thickness of the specimen. If μ is plotted as a function of the wavelength of the incident radiation, an absorption curve similar to that shown in Fig. 3 is obtained which exhibits sharp increases as the wavelength decreases.

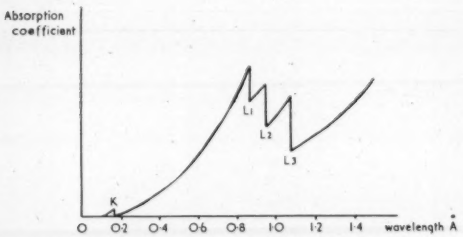

Fig. 3. *K* and *L* absorption edges of platinum

These increases occur at wavelengths at which the incident quanta have just sufficient energy to eject an electron completely from one of the subshells of the receiving atom. The most energetic quanta are required to eject electrons from the *K* shell, since these are the most strongly bound. A simplified energy level diagram is given in Fig. 4.

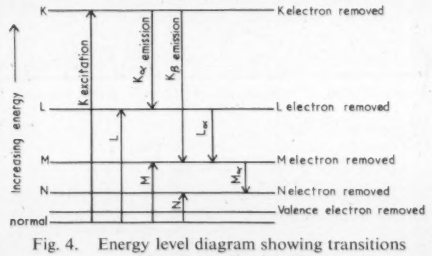

Fig. 4. Energy level diagram showing transitions giving rise to line spectra

From this it can be seen that removal of a *K* shell electron makes possible transfer of an electron to the shell from any of the lower levels in the atom. Each such transition is accompanied by emission of a quantum of energy equivalent to the difference in binding energies of the shells involved. The radiation so produced forms the *K* series of lines.

The *L* spectrum will appear when the incident quanta have the required energy to eject an electron from the *L* shell, but will also be produced if the shell loses an electron to the *K* shell. Similar processes will occur in all other shells, and thus radiation sufficiently energetic to remove the *K* electrons will excite the entire spectrum of the element.

The wavelengths of the *M*, *N*, etc., series of lines are, in general, so great that they are readily absorbed in air and hence they are of little analytical interest. Attention is thus concentrated upon the *K* and *L* series. The number of lines in these series which are of importance to the analyst does not exceed seventeen for elements of atomic number 30 and above, and is progressively less for the lighter elements. This is because some transitions are "forbidden" or of low probability, while others involve changes in potential so nearly equal that the lines produced form close doublets and are not normally resolved. The lines of most importance are the $K_{\alpha_1} + K_{\alpha_2}$, $K_{\beta_3} + K_{\beta_1}$, L_{α_1}, L_{β_1}, L_{α_2} and L_{β_2}. The intensity of the K_α doublet is usually four or five times that of the K_β doublet, and the intensities of $L_{\alpha_1} : L_{\beta_1} : L_{\beta_2} : L_{\alpha_2}$ lines are as 100 : 50 : 20 : 12 for tungsten. The wavelengths of the *L* lines of elements 20 to 48 are strongly absorbed by reason of their long wavelength and are of no great analytical importance. The *K* lines of elements below 20 in atomic number become increasingly difficult to detect by reason of their long wavelength, even when the spectrograph is evacuated to minimize air absorption.

Primary source of X-rays. From the foregoing it is possible to summarize the general requirements for the primary source of radiation. It must:

(*a*) contain all wavelengths required for excitation of the characteristic spectra of the heaviest elements,
(*b*) illuminate the specimen as intensely as possible,
(*c*) be free from strong characteristic lines arising from the anticathode or any impurities present in the tube.

Requirements (*a*) and (*b*) dictate the use of high accelerating potentials in order that λ_{min} of the continuum shall be low and the integrated area under the graph of intensity *versus* wavelength large. Requirement (*c*) implies that the *K* lines of the anticathode should certainly not be generated and that the *L* lines should be weak. It thus imposes an upper limit (depending upon the atomic number of the anticathode material) on the accelerating potential which can be employed. Purity of the target material and careful choice of the materials used in the construction of the tube are, of course, essential.

The usual compromise is to employ a tube with a tungsten target at an operating potential of 50–60 kV. The critical excitation potential for the *K* lines of tungsten is 69·5 kV. These are therefore not excited and the *L* lines are fairly weak. At 50 kV, λ_{min} for the continuum is 0·25 Å and the radiation will excite the *K* spectra of elements of atomic numbers 63 and below, and the *L* spectra of all elements will be excited.

The window of the tube must not absorb any appreciable fraction of the radiation and must not fluoresce within the wavelength range of the spectrograph for which the tube is intended. For these reasons a light element, usually beryllium, is employed.

Analysis of spectrum. In the majority of spectrographs crystals of suitable materials are employed either as reflexion or transmission diffraction gratings. Both plane crystal and focusing spectrographs are used and have special merits and demerits. The more important types are discussed below.

The choice of crystals depends on a number of factors, but

general requirements are that it must be possible to obtain large pure crystals and that the interplanar spacing in the orientation employed shall give adequate wavelength separation.

The most widely used crystals for reflexion spectrographs are:

lithium fluoride	$d_{(200)} = 2{\cdot}02$ Å
quartz	$d_{(01\bar{1}0)} = 3{\cdot}34$ Å

Mica is the only really practicable diffracting agent for transmission spectrographs.

The plane reflexion spectrograph. The arrangement of a typical spectrograph is shown in Fig. 5. In order to make maximum use of the radiation generated by the source it is necessary to illumine a large area of the specimen and to place

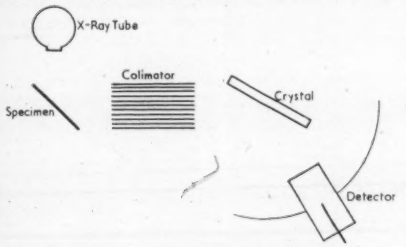

Fig. 5. Plane crystal spectrograph

the specimen as close to the source (i.e. the anticathode spot) as practicable. The latter is one of the most important design features of an X-ray spectrograph since the inverse square law applies.

A collimator is placed between the specimen and the analysing crystal in order to define the direction of the fluorescent radiation and prevent scattered primary radiation from reaching the detector. The device usually employed is an open-ended box containing a set of parallel blades, known as the Soller slit collimator. The length and separation of the blades determine the angular resolution obtainable from the apparatus. Here it is necessary to effect a compromise between the loss of energy in the collimator and acceptable resolution. In a typical instrument the collimator blades are 4in. long, spaced 0·010 in. apart, and the resulting angular resolution is 0·4° at half maximum intensity. This degree of resolution is satisfactory for most purposes as it enables the K_β line of any element to be separated from the K_α line of the element of next higher atomic number.

The angle at which the diffracted ray has maximum intensity is determined by the Bragg relation:

$$n\lambda = 2d \sin \theta \qquad (7)$$

where d is the interplanar spacing of the crystal and λ the wavelength of the incident radiation (see Fig. 6). The analogy with the optical diffraction grating will be obvious.

The analysing crystal is mounted on a goniometer which is coupled through precision gearing to an arm carrying the detector. The gearing is arranged so that the angular movement of the detector arm is double that of the crystal, and it is thus always correctly alined to receive the reflected radiation. The goniometer may be motor driven at various rates to scan the spectrum automatically when required.

The maximum wavelength that can be diffracted by a crystal is determined by the Bragg equation and is equal to $2d$. The reflected intensity falls off rapidly, however, at angles greater than 60°, and it is therefore undesirable to use a crystal to analyse wavelengths greater than its interplanar spacing. The effective wavelength range of the spectrograph is 0·4–3·0 Å, the lower limit being set by the primary source and the upper by absorption within the spectrograph and detector window.

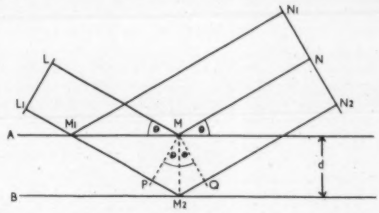

Fig. 6. Illustration of Bragg's law of reflexion from atomic planes in a crystal

Focusing reflexion spectrograph. A focusing crystal spectrograph is shown diagrammatically in Fig. 7. The analysing crystal is bent with radius of curvature $2R$ and receives radiation from a point of the circumference of a circle of radius R. Radiation from the source S then converges at the point F which is situated on the same circle (the Rowland circle of optical spectroscopy). The focus so obtained is imperfect but may be greatly improved by grinding the crystal surface to a radius of curvature R. When this is done each ray from the source makes the same angle θ with the particular lattice plane that it meets and the reflected rays converge to a true focus at F. By this means, the whole surface of the crystal is made effective in concentrating radiation on the detector at F.

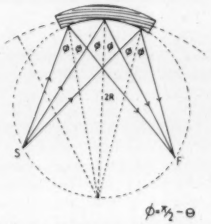

Fig. 7. Reflexion from curved crystal, corrected for astigmatism

If the distance of the source slit from the centre of the crystal face is l then:

$$l = 2R \sin \theta \qquad (8)$$

Substitution for $\sin \theta$ in the Bragg equation then gives the following modified relation:

$$l = nR\lambda/d \qquad (9)$$

which is the required condition for reinforcement at F. In order to maintain l within reasonable limits it is necessary to employ several different curvatures of crystals for the 0·5–3 Å range.

If a slit is used at the source no slit is necessary at the detector, since the radiation is monochromatic on leaving the

crystal. The resolution and efficiency obtainable with a given slit depend, however, on the accuracy of the geometry of the bent and ground crystal.

Transmission spectrograph. A curved crystal transmission spectrograph has been produced by the General Electric Company of America. In this type of instrument a very thin section of mica is employed as the grating and this is placed between the specimen and the detector. As fluorescent X-rays are relatively soft, the thickness of the analysing crystal must not exceed a few thousandths of an inch to ensure that absorption is reasonably small. The maximum intensity of diffraction is obtained when the incident beam is attenuated by a factor $1/e$. Thus over the range 0·5 to 3·0 Å it is desirable to have available crystals of several thicknesses. The reflecting planes of the crystal are nearly normal to the surface and, as the spectrum is scanned, the curvature is continuously adjusted so that the diffracted rays are brought to a focus at a point on a circle of fixed radius. The detector rotates around this circle. The interplanar spacing ($33\bar{1}$) of the mica crystal is only 1·5 Å and dispersion is sufficiently high for resolution of the K_{α_1}, K_{α_2} doublet to be possible with fine slits.

The chief advantage of the focusing spectrograph over the plane grating type lies in the high spectral intensities which may be achieved using small specimens (about 1 mg) placed close to the source slit. The size of the slits controls resolution obtainable and this can be improved only at the expense of sensitivity. In practice, angular resolution similar to that of the plane crystal instrument (about 0·3–0·4 Å) is employed.

Fundamentally, however, spectral intensity depends upon the surface brightness of the specimen and its superficial area. In the plane crystal spectrograph the cross-sectional area of the collimator may be large without impairment of resolution. Thus the amount of radiation reaching the detector may be as great as in the focusing type of instrument when sample size is not a limitation.

Detectors. In the modern spectrograph electrical methods of detection are universally employed. The most commonly used detector is the Geiger counter which has much to commend it because of the simplicity of the associated electronic equipment. Such counters are usually filled with a mixture of argon and bromine at a pressure near atmospheric. The efficiency of detection falls off rapidly with diminishing wavelength and is reduced to about 10% at 0·5 Å. Counters having improved efficiencies at short wavelengths are now being developed.

The chief limitation of Geiger counters lies in the large dead time, the period after a count has taken place during which the counter is inoperative. The dead time τ is commonly in the range 200–300 μs; thus if the observed rate of counting is N, the true rate N' is given by:

$$N' = N/(1 - N\tau) \qquad (10)$$

The accurate determination of dead time presents considerable difficulty and it is unwise to apply corrections greater than 10%. Thus the practical limit for counting rate lies at about 2000 counts per second.

An alternative form of detector, which is of importance since in itself it is capable of furnishing a degree of spectral resolution, is the proportional counter. The output pulses obtained from this detector are dependent in amplitude on the energy of the incident photons. Thus it is possible in the associated electronic equipment to discriminate against pulses arising from sources other than radiation of the energy it is desired to record. The method has the additional advantage that corrections due to dead time are negligible.

Scintillation counters of the thallium-activated sodium iodide type may be used in conjunction with suitable photomultipliers. This system is much superior to the gas-filled counter at short wavelengths, but is inferior for soft radiations as the pulse amplitude is little greater than the unavoidable background produced by the photomultiplier. Resolving time is again very short (about 0·25 μs) and high counting rates may safely be employed.

The quantum efficiency of the photocathodes employed in the multiplier photocells is, however, low (less than 10%), and because of this the statistical spread in the amplitude of the output pulses from the photomultiplier is very large. Amplitude discrimination is therefore of limited value in improving spectral resolution in the case of the scintillation counter.

Power supplies. The power required by the primary X-ray tube is in the region of 1 kW (20 mA at 50 kV). Two principal methods of compensating for the effects of mains fluctuations exist:

(*a*) electronic stabilization of the tube current and voltage usually to about 0·1%,

(*b*) monitoring the primary X-ray output by means of an independent Geiger tube, and applying the resulting signal to correct results obtained from the spectrum counter. For example, it may be arranged that when the monitor channel has registered a predetermined number of counts the spectrum count is automatically terminated. By this means, complete compensation for all changes in the intensity of the primary radiation can theoretically be secured. The value of the method, of course, depends upon consistent behaviour of the two Geiger counters.

Electronic equipment. This normally consists of a scaler which can be arranged to count either on a fixed count or fixed time basis, together with a ratemeter recorder. A stabilized source of E.H.T. for the detector is also provided. If proportional or scintillation counting is employed a stable amplifier and pulse amplitude discriminator will be required in addition.

Use of the spectrograph. The specimen will often require no preparation before analysis. Powders may require grinding to uniform size, however, to ensure homogeneity and solid specimens are preferably lapped to produce a flat surface for irradiation.

From consideration of mass absorption coefficients it is found that a sample depth of 0·020 in. is effectively infinite for most materials. A thickness giving optimum line-to-background ratio can be determined, but the improvement to be secured is worthwhile only in special cases.

It has been seen that comparatively simple line spectra are produced by X-rays and it is usually found that, even in the analysis of complex mixtures, one or more lines characteristic of each element present are free from interference. A preliminary qualitative examination using the ratemeter recorder is, in general, essential. Such an examination can be carried out for all elements of atomic number greater than 20 in approximately thirty minutes. Quantitative interpretation of the ratemeter record is unlikely, however, to be straightforward, except where components are few. In the latter case, comparison of the ratemeter record with standard traces, obtained from samples of known and similar composition, will enable reasonably accurate estimates of composition to be made.

In general, however, the intensity of the characteristic radiation emitted by an element will be greatly dependene upon the composition of the specimen. It is clear that there

will be general absorption of the fluorescent radiation by the matrix. Thus the determination of a light element emitting long wavelength radiation in a heavy matrix of high absorption coefficient may be difficult, if not impossible. Determination of a heavy element in a light matrix, however, presents no difficulty down to very low concentrations. There are also effects due to selective absorption and enhancement to be taken into account. It was seen above that sharp increases in the absorption coefficient of an element occur at the wavelengths at which the various line series of its spectrum are excited. When elements of nearly equal atomic number are present in the same specimen the fluorescent radiation of the element of higher atomic number will be absorbed, while that of the lighter element will be enhanced. For example, if zinc and nickel are present together, the zinc K_α line (1·436 Å) will be strongly absorbed by the nickel (K_{abs} = 1·49 Å). The K spectrum of the nickel will be correspondingly enhanced. Similar inter-actions will occur between the L absorption edges of heavy elements and the K radiation of lighter elements, giving rise to selective absorption of the K radiation and enhancement of the L radiation.

Because of these effects, the analysis of mixtures must, in general, be carried out by making known additions of the wanted elements to the specimen or, alternatively, by addition of a suitable internal standard or standards.

The method of known addition is to be preferred where only a few samples of similar composition are to be analysed. Two such additions are normally adequate, and it has been found that grinding in an automatic mortar for 10–15 min is sufficient to ensure homogeneity in the case of powders. If the amounts to be added are small, dilution in several stages with 10 min grinding at each stage has been found desirable. Counts are carried out on the lines of interest and the adjacent background; the difference between line and background are then plotted against concentration for each element. The original concentrations are then determined in the normal way by extrapolation. The sample must, if necessary, be converted to powder or dissolved so that the additions can be made.

When many samples have to be examined for one or more elements and their compositions may vary widely, addition of a suitable internal standard is the most satisfactory method. The ratios of the element and internal standard line intensities are then determined, and concentrations of the element calculated from a knowledge of the ratios obtained with known or prepared specimens. The element used as standard must, of course, be absent from the range of samples to be examined, and should preferably be of adjacent atomic number to the element of interest so that it will undergo similar enhancement and absorption. This method is capable of giving very rapid results once the standardizations have been performed, and analysis for a single element would normally not require more than 30–40 min. Where samples are to be analysed in the solid state without conversion to powder or solution, a sufficient number of analysed standards must be available to enable calibration curves to be prepared.

The weight of sample required for analysis varies with the type of spectrograph. With the plane grating spectrograph sample weights of 1–2 g are usually adequate, though considerably smaller specimens (about 50 mg) may be analysed by briquetting with suitable diluents of low absorption, masking the sample holder, etc. Samples of about 1 mg in weight can be dealt with by focusing spectrographs and point-by-point analyses of surfaces may be carried out with such instruments.

Statistical accuracy. In accurate quantitative analysis it is necessary to count both line and background intensities at fixed goniometer settings. The usual practice is to record the time required to register a fixed number of counts.

It is easily shown that the standard deviation of the difference between line and background intensities is given by:

$$\sigma = (R/N)^{\frac{1}{2}} (R + 1)^{\frac{1}{2}}/(R - 1) \qquad (11)$$

where $R = T_B/T_L$;

T_L = time for N counts at the line position; and
T_B = time for N counts at the background position

Calculated values for the coefficient of variation at various line/background ratios for N = 25 600 are as follows:

Line–Background / Background	0·01	0·1	1·0	10	100
Coefficient of Variation (%)	89	10	1·5	0·7	0·63

The time required to record 25 600 counts is usually a few minutes and, in general it is practicable to record counts up to 10^6 where high accuracy is required.

Applications of the spectrograph. The literature of the subject is comparatively small and has appeared for the most part within the last five years. As might be expected from the fact that, until very recently, X-ray spectrographs were produced only in the U.S.A., nearly all the articles that have been published are of American origin. Papers dealing with the determination of an element or elements in a particular type of sample are relatively few, and it seems this can only be ascribed to the wide acceptance of the X-ray spectrograph as an analytical tool of general application.

In the experience of Mr. Davis and Mr. Shalgosky, a few calculations nearly always suffice to show whether or not a particular determination is likely to be successful and, if so, what limit of detection will be practicable. For example, if the limit of detection of an element in a particular matrix is known, the corresponding figure for the same element in a sample of different composition may be derived from calculations of the mass absorption coefficients of the matrices. If samples of the new material are available in a suitable form, however, a complete qualitative survey of the spectrum can be carried out on the instrument in about half an hour (much less if only a portion of the spectrum is of interest) and from this record semi-quantitative assessments may be made.

As a broad generalization, it may be said that the sensitivity of the instrument is a maximum when dealing with elements of medium atomic number, the K spectra of which are strongly excited and detected with high efficiency.

Sensitivity will be reduced for the heavier elements ($Z > 63$) because only the comparatively weak L spectra can be excited. The determination of the lighter elements ($Z < 26$) becomes progressively more difficult because their fluorescence is strongly absorbed in air and in the windows of the instrument and detector. Air absorption may be greatly reduced by evacuation of the spectograph chamber, but the residual absorptions are sufficient to prevent analysis for elements of atomic numbers below 19.

Most elements in the periodic system may be determined down to 0·1% unless the circumstances are very unfavourable (e.g. light element in a strongly absorbing matrix). Considerably lower limits of detection may be achieved when conditions of excitation and absorption are favourable, and in the best circumstances impurities on the parts per million scale have been detected with certainty.

Mr. Davis and Mr. Shalgosky then gave a brief account of some experiences with the Philips X-ray spectrograph, shown in Fig. 8. In this instrument the beam from the X-ray tube, which is powered by a fully stabilized 50 kV 20 mA supply, is directed upwards onto the sample contained in a holder having in its base a Terylene window 0·00025 in. thick. Collimation is effected by a Soller slit 4 in. long with blades 0·010 in. apart and the angular resolution attained is 0·4° (2θ) at half maximum intensity. The goniometer may be

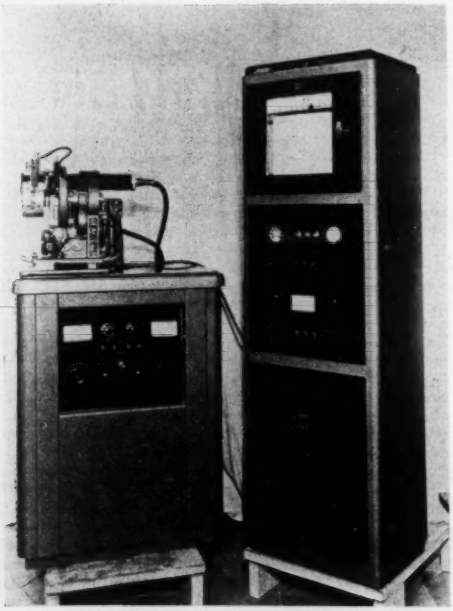

Reproduced by courtesy of Philips Electrical Ltd.

Fig. 8. The Philips X-ray spectrograph

set to 0·01° (2θ), thus ensuring high reproducibility in the measurement of peak intensities, and has five speeds of automatic traverse. Quartz, sodium chloride, lithium fluoride and topaz crystals are available and almost the whole of the path of the fluorescent beam can be evacuated. Geiger, proportional or scintillation counting may be employed, the last two with pulse amplitude analysis if desired. The output of the detector is fed to a ratemeter recorder *via* a scaling circuit which provides facilities for fixed time and fixed count measurements.

The intensity and spectral distribution of the radiation from the Philips X-ray tube has been found to remain constant over long periods of time involving 1 000 hours operation. This characteristic is of great value, since calibrations need checking only at infrequent intervals.

The application of X-ray spectrography to the determination of the major and minor constituents of alloys and ores is now well established, and experiments with the Philips apparatus amply confirm the claims made by other workers. The applications described below, however, show how determinations in the parts per million range may be carried out in favourable cases.

The determination of lead in Santowax. Santowax, a mixture of terphenyls, is an extremely inert material which might prove useful as a combined moderator and coolant in a nuclear reactor. The lead content was of interest and an optical spectrographic determination on the ash gave such a low result that a confirmatory method was required. The nature of the material rendered wet chemical methods inapplicable.

A ratemeter record of the Santowax spectrum showed no evidence of the presence of lead. A specimen containing a known amount of lead was prepared by melting the Santowax with lead stearate and then casting in a mould to a disk 1 in. diameter and 0·5 in. thick. Dilutions were made with successive additions of Santowax until a specimen containing 0·8 p.p.m. added lead was obtained. The ratemeter record still showed a peak due to the presence of lead, and it was concluded that the original must have contained less than 1 p.p.m.

The determination of strontium in milk powder ash. Since milk powder is virtually constant in composition, the X-ray determination of strontium may be carried out by direct measurement of the intensity of the $K\alpha$ line. The conditions employed were:

tungsten target X-ray tube, 48 kV and 20 mA; lithium fluoride crystal; vacuum path; argon-filled Geiger counter; strontium K_α line 25·15° (2θ), background 24·50° (2θ), time to collect 51 200 counts measured.

The ratio between the background count rates at 24·5° and 25·15° was determined with strontium-free calcium phosphate, and subsequent background measurements at 24·5° were corrected by the appropriate factor. A linear calibration graph was obtained when successive additions of 50 mg potassium chloride containing 0·1% strontium as chloride were made to 1 g of one of the samples, the strontium line intensity (corrected for Geiger dead-time and background) being plotted against the strontium content of the sample (corrected for dilution). The results obtained from six samples which had been analysed by two other methods are shown in the table. The "theoretical" coefficient of variation of the X-ray method with a counting time of 30 min is about 10%.

Strontium in six samples of milk powder ash

Method	*Strontium content (p.p.m.)*					
Flame photometry	33	50	64	49	40	31
Radioactivation	32	—	62·5	51·5	38	33
X-ray	34	53	65	54	43	33

The determination of chromium, manganese, iron, cobalt, nickel, copper and zinc in beryllium metal. The sensitivity of the spectrograph for iron and nickel in beryllium was determined using mixtures of the elements in powder form and, from the known relative sensitivity of the instrument for other elements, the sensitivities for chromium, manganese, cobalt, copper and zinc were calculated. The fluorescent spectra of the samples (which, if in powder form were first briquetted) were recorded over the range 40 to 70° (2θ) at 2° per minute using a lithium fluoride crystal, a tungsten target X-ray tube operating at 48 kV and a vacuum path for the fluorescent radiation. The intensity of the lines due to the above seven elements and that due to tungsten (from the primary radiation)

were measured on the ratemeter record. It was found possible to use the tungsten line as an internal standard to correct for variations in the thickness and density of the sample, the tube current and, within limits, the area and absorption coefficient of the specimen. The time for the determination of the seven elements was about 30 min and the health hazard to the operator due to the handling of the beryllium was negligible. The coefficient of variation of replicate determinations was 3% and the limits of detection for the elements determined, taken as the concentrations which would give a peak of two divisions on the recording (full-scale deflexion = 100 divisions), are shown below.

Element	Cr	Mn	Fe	Co	Ni	Cu	Zn
Limit of detection (p.p.m.)	30	17	10	6	5	30	7

Mr. K. M. BILLS (Mond Nickel Co., Birmingham) gave an account of metallurgical analysis with the X-ray spectrometer made by the General Electric Company of America. A General Electric unit was installed during 1954 in the Physics section of the Mond Nickel Company's Research Laboratory at Bayonne (New Jersey). This instrument was initially used for special research analyses such as the determination of the thickness of nickel plate and the analysis of archaeological specimens. It was first employed in production analysis for the determination of tungsten and molybdenum in high temperature alloys, and the striking success of the technique resulted in the purchase of a second instrument specifically for analysis. This instrument now handles about one half of the total analytical demand of the Bayonne plant. It was found that not only is the technique far more rapid than wet chemical methods, but the results are appreciably more accurate than ordinary routine determinations; indeed, the provision of adequate calibration standards is one of the major problems encountered so far.

Similar equipment has been recently installed in the Physics Section of the Company's Birmingham Reasearch Laboratory. The Analysis Section, faced with a rising demand for increasingly difficult determinations, has had the use of the equipment for a general investigation into X-ray fluorescence, the main purpose being to discover the extent to which this technique can take over the Research Department's analytical load. This preliminary work is not yet complete but the general conclusions are already clear. X-ray fluorescence is the most reproducible and precise physical method of analysis so far encountered. It is estimated that at least 50% of the present analytical demand could be handled by this technique. The greater part of this work would consist of major element determinations in the range of 5–75% content and so would replace chemical procedures. Moreover, the sensitivity of the method has been found to be surprisingly good. For example, titanium, one of the less sensitive elements, has been determined at a level of 0·1% in 80/20 nickel-chromium base alloys, and it is clear that this method could handle with advantage some of the work normally considered the special province of the optical spectrograph.

The principal features of the General Electric spectrometer may be noted in Fig. 9. The X-ray tube holder and the sample compartment may be seen on the right, the crystal holder in the centre and the detector head, incorporating a preamplifier stage, on the left.

The sample, preferably in the massive form with one face turned or ground to a standard finish, is introduced into the sample carrier, which presents an area of about $\frac{3}{4} \times \frac{1}{2}$ in. for excitation by the primary beam. The secondary X-rays, which are emitted from the sample at all angles, are roughly collimated before being dispersed by a lithium fluoride crystal. Upon leaving the crystal the X-rays are collimated by a fine Soller slit and are measured by the detector, which is a gas-flow proportional counter. It is considered that, at the present time, the gas-flow counter is the simplest and most reliable device for measuring the widest possible range of wavelengths. A helium path can be provided for the fluorescent beam to deal with elements of low atomic number, although this is hardly economic practice in this country. The pulses produced by the detector are either counted by means of a scaler unit or, for qualitative work, the count rate may be displayed on a pen recorder.

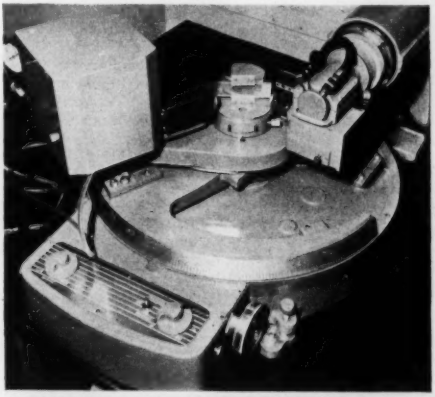

Reproduced by courtesy of the General Electric Company of America

Fig. 9. The General Electric type XRD-5 X-ray spectrometer

Two methods of evaluation may be employed for quantitative analysis. Either the time to accumulate a predetermined number of counts or (preferably) the total counts accumulated in a fixed period of time may be measured and plotted against the chemically analysed contents of the appropriate standards to produce the calibration curve.

The accuracy of analysis with this instrument is ultimately dependent on the stability of the primary beam. Since only one detector is used the various spectrum lines emitted by the alloy are measured sequentially. An inferior form of internal standard technique can be employed, but with massive samples which properly fill the "optics" there is no positive evidence that this particular method effects any worthwhile improvement. With adequate samples and standards a coefficient of variation of about 0·5% of the content has been obtained, and the average time required for a single determination is of the order of 60 s.

Experience of this technique had been most encouraging but a number of problems remain to be solved. First and most important of these is to extend the range of the method to elements of low atomic number—at least to aluminium. Secondly, if the sensitivity could be improved by a factor ten to one hundred, the method could well become the ideal analytical technique. Finally, in spite of the high accuracy already achieved, experience is still required to deal with

contents above 50% and, in particular, some method is required to overcome fluctuations in the intensity of the primary beam which may occur in spite of the rigid control of voltage and current supply.

Dr. E. T. HALL (Research Laboratory for Archaeology, Oxford), has been interested in the use of X-ray fluorescence for the analysis of ancient coinage and other archaeological specimens for nearly ten years, the important factor in this field being the non-destructive features of the technique. His original instrument was a hand-operated flat crystal apparatus and it proved that, even working at 3 mA unrectified current and 30 kV peak voltage, ample resolution and intensity was obtainable for many problems in archaeology. The main disadvantage of this instrument was that each peak had to be scanned individually and the number of counts accumulated in a given time recorded manually, a tedious and lengthy business.

When the Archaeological Research Laboratory was started in Oxford three years ago it was realized that if any useful results were to be obtained from X-ray spectrometry, a very large number of specimens would have to be analysed since statistical methods would be necessary. A completely automatic instrument was therefore built, having the following facilities:

(*a*) the crystal and detector are set sequentially by a control mechanism in up to twenty-four positions, with an accuracy better than one minute of arc;
(*b*) the number of counts accumulated in a given period of time, variable between 10 s and 3 h, is printed out;
(*c*) alternatively the spectrometer can be scanned at variable speeds by a synchronous motor and the pulses from the counter fed to a ratemeter, the ouptut of which is displayed on a standard potentiometric recorder. In this way the whole spectrum, or pre-selected portions of it, can be traced to permit detailed qualitative examination.

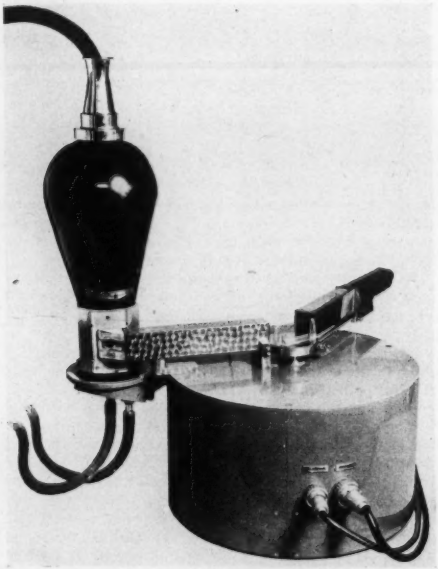

Fig. 10. Single-channel X-ray spectrometer as used in the Archaeological Research Laboratory, Oxford

In use this machine can in most instances analyse coins or pottery at a speed of half a minute per element. The spectrometer with its control gear is shown in Figs. 10 and 11. An improved form of the apparatus has been put on the commercial market as the Solartron automatic fluorescent spectrometer, a block diagram of which is given in Fig. 12.

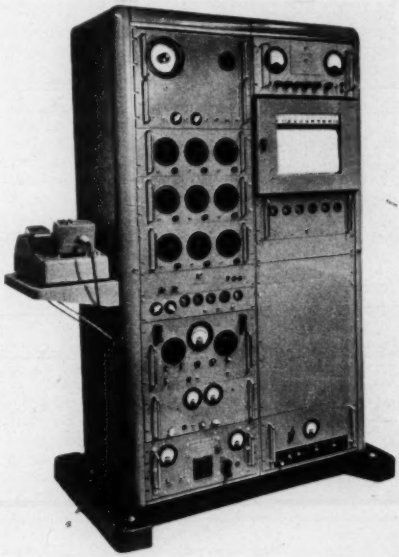

Fig. 11. Control gear for single-channel instrument shown in Fig. 10

In most X-ray instruments it is considered essential to provide a high degree of current and voltage stabilization. This compensates for the more obvious sources of variation of the beam intensity. There are, however, two possible sources of variation in addition. These are sputtering of the tube window and pitting of the target, and both have a similar effect, namely a gradual drift of the peak of the continuum towards the high energy direction. A monitoring technique involving the use of a second "standard" channel is therefore considered essential, and there are three possible methods of application:

(*a*) by observing the undispersed fluorescent beam from the standard, including any scattered radiation;
(*b*) by collimating the fluorescent beam from the standard and selecting one particular line for comparison;
(*c*) by use of the "double-beam" technique, in which two complete optical systems are ganged together in such a way that the two channels are simultaneously counting on the same element in the standard and sample respectively.

The last method is the only one which provides complete compensation for all possible variations in tube output, including spectral drift, and is incorporated in the Solartron instrument.

Four methods of presentation of results are provided:

(i) sequential counting of peak intensities on a single channel for a fixed time, results being printed out;
(ii) sequential recording, as above, using a potentiometric recorder;
(iii) using two channels, recording the time taken to reach a fixed number of "standard" counts in each position;
(iv) using two channels and two ratemeters, presenting results on a ratio-recorder

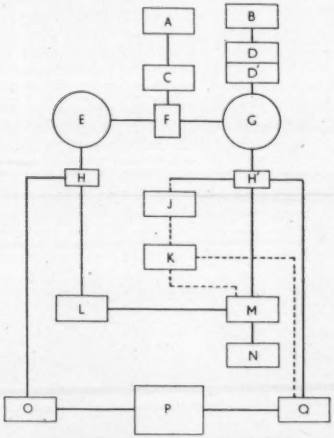

Reproduced by courtesy of Solartron Ltd.

Fig. 12. Block diagram of Solartron automatic spectrometer

A, generator control (stabilizer); *B*, servo-amplifier; *C*, X-ray generator; *D*, *D'*, multi-channel transmitter–control unit; *E*, "monitor" spectrometer; *F*, X-ray tube; *G*, "analysis" spectrometer; *H*, *H'*, probes; *J*, linear pulse amplifier; *K*, pulse height discriminator; *L*, "monitor" scaler or timer; *M*, "analysis" scaler; *N*, printer; *O*, "monitor" ratemeter; *P*, ratio or time-based recorder; *Q*, "analysis" ratemeter.

Other details of design in the Solartron apparatus are tabulated below:

Detectors. At present Mullard Geiger counters types MX118 and MX122 are used. These tubes, in common with other types, are somewhat temperature dependent, but since their temperature coefficients are extremely similar, a monitoring technique will afford complete compensation. Research is being carried out on the use of gas-flow proportional and scintillation counters.

Wavelength limitations. The spectrometer is built on a $\frac{1}{4}$ in. thick steel table top in order to support a vacuum chamber. This will enable the atomic number range to be extended from scandium, the present limit, to aluminium. Active research is progressing to achieve this and the present apparatus is being produced so that the additional components can be added in due course.

Operating conditions. A Machlett type OEG 60 X-ray tube operating at 30 mA and 60 kV is used. Lithium fluoride crystals are fitted on both channels and the Soller slit collimators consist of 8 in. long wave-guide tubes packed with nickel tubing (measuring $0{\cdot}4 \times 0{\cdot}030$ in.).

In the Solartron instrument a specially-designed "cosec" potentiometer geared to the crystal spindle provides a bias voltage appropriate to the wavelength, for use in pulse-height discrimination with scintillation or proportional counters.

Dr. Hall concluded with an interesting account of some applications of X-ray fluorescence to the examination of archaeological specimens.

For many years Applied Research Laboratories (U.S.A.) have been prominent in developments in direct-reading spectroscopy, and since 1951 have been applying the experience gained in this field to X-ray fluorescence. Mr. W. RAMSDEN [Applied Research Laboratories (Gt. Britain) Ltd., Harpenden] gave an account of the A.R.L. programme.

Early experience led to the adoption of a curved crystal optical system, with its attendant advantages of good resolution and high speed. It should be realized that adequate resolution is just as important in X-ray spectroscopy as in optical emission spectroscopy, while provision of good signal strength allows more flexibility in the choice of detector. The components of the system are: X-ray source, sample, primary slit, curved crystal, detector slit and detector. This system can, therefore, examine only one constituent of a sample. To record additional elements, it is necessary to scan the spectrum by moving both detector and crystal or to provide extra monochromators. The former approach resulted in the development of the X-ray Scanning Quantometer and the latter of the X-ray Industrial Quantometer, now superseded by the multi-channel Production X-ray Quantometer.

A rugged industrial version of the basic monochromator has also been developed, known as the Quantrol, which permits single constituents to be monitored in solid or liquid, continuous or discontinuous moving systems.

The recording system used with all X-ray Quantometers is identical with that used for several years in optical emission direct-reading spectrographs. The signal from the detector is fed into capacitors of high insulation resistance during the irradiation of the sample; the voltage on the "integrator" is then displayed on a strip-chart recorder. In multichannel instruments a sequential relay system displays the voltages built up on a group of integrators at intervals of 2·5 s. The precision of the recording system is of the order 0·1% of the quantity being measured. The X-ray power supply used is identical in all instruments, comprising a Machlett type OEG-60 end window X-ray tube, powered from a full-wave rectified and filtered supply.

The first instrument developed, the X-ray Scanning Quantometer, used two separate crystals of lithium fluoride, one bent to an 8 in. radius and ground to a 4 in. radius, covering wavelengths from 1·0 to 3·88 Å, the other bent to 22 in. radius and ground to 11 in. radius, covering the range 0·35 to 1·0 Å. With an air path, using *K* and *L* spectra, the wavelength range 2·74 (titanium) to 0·9 Å could be covered. With a helium atmosphere, the upper wavelength limit could be extended to potassium. Fig. 13 shows the internal scanning mechanism of this instrument.

The multichannel Production X-ray Quantometer provides the most comprehensive facitilies for X-ray fluorescence analysis available at the present time. The basic form of the instrument comprises six pairs of monochromatic spectrometers arranged radially round the sample and X-ray tube,

which with an internal standard channel allows thirteen channels to be recorded simultaneously. An extension allows ten more monochromators to be added, so that up to twenty-three channels can be recorded simultaneously. Each monochromator is supplied with the appropriate curved crystal and

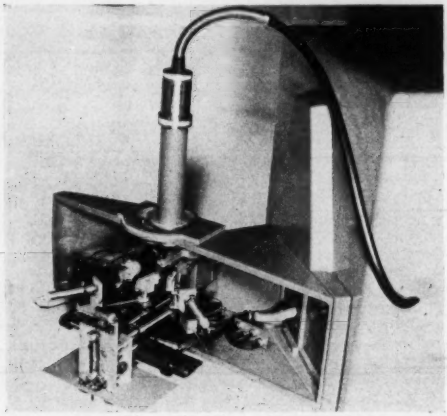

Reproduced by courtesy of the Applied Research Laboratories

Fig. 13. Internal scanning mechanism of A.R.L. X-ray Scanning Quantometer

detector for the wavelength in question. A helium "boot" is available so that several monochromators may be used for elements below atomic number 20. The materials Li F, quartz, NaCl, ADP, EDT are available as crystal material, and total integrating devices such as Geiger counters, flow Geigers, or Multitrons are supplied as detectors. The spectral range covered by the instrument is 0·35 to 10·2 Å. Although the Production X-ray Quantometer is, as its name implies, intended primarily for production control work, a

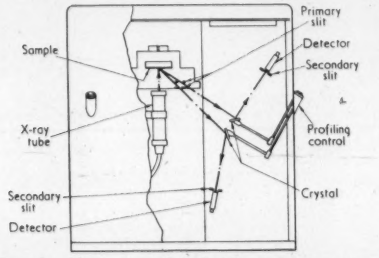

Reproduced by courtesy of Applied Research Laboratories

Fig. 14. Typical dual monochromator plate in Production X-ray Quantometer

pair of monochromators can be replaced by a scanning spectrometer using a lithium fluoride crystal. A sectional view of the instrument, showing a pair of monochromators in position, is shown in Fig. 14.

Improvements in curved crystal techniques and in detectors, and provision of multichannel recording have resulted in considerable gains in resolution, speed and sensitivity, and the way is now open for X-ray fluorescence to be investigated as a comprehensive analytical scheme, complete in itself. Its principal limitation at present is the mutual interference of elements due to absorption, but in this respect it has the advantage over optical spectroscopy that the effect follows well-defined laws and corrections may be easily applied.

Mr. J. R. STANSFIELD (Hilger and Watts, Ltd., London) described recent developments by his company in X-ray fluorescence. Two instruments are being developed, one of which is now in production.

Fig. 15 shows the simpler unit. At the back and to the right can be seen the Machlett type OEG-60 tungsten-target X-ray tube which excites the fluorescent radiation. The tube is fed from an ENRAF Diffractis G generator,* the input voltage to which is stabilized. A three-phase rectifying circuit is used which is capable of giving the required output substantially free from ripple. The housing around the end of the X-ray tube takes samples up to $2 \times 2\frac{1}{2} \times 2\frac{3}{8}$ in. with ease, and larger samples if necessary; it will also take a standard sample for comparative measurements. There is a tungsten-alloy shutter in front of the X-ray tube, and this is inter-locked with the hinged cover over the samples so that it is impossible to stand inadvertently in the direct beam from the tube. The fluorescent radiation passes through the Soller slits to the crystal and after reflexion is received by the Geiger counter. The hand control (in front of the picture) allows the crystal

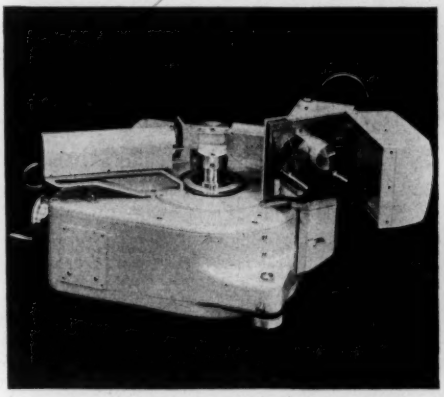

Reproduced by courtesy of Hilger and Watts Ltd.

Fig. 15. Hilger X-ray spectrometer

and the counter to be turned in the correct relationship to the required angle. A pen recorder is provided and, in the body of the instrument, a multi-speed motor for scanning spectral lines in qualitative or exploratory work; for routine analysis each line is measured in turn statically, when readings are made on a scaler in a separate console. This console contains the supply circuits for the main instrument, the voltage stabilizers, the recorder and two scalers—one to count the pulses from the measuring Geiger tube, and one, fed from the

* HOEKSTRA, G. D. A. *Hilger J.*, **3**, p. 19 (1956).

monitor, to control the measuring time. The instrument is built on the same foundations as the Hilger type Y-115 X-ray diffractometer, which can thus be easily converted to a fluorescence analyser.

The resolution of the instrument, using a lithium fluoride crystal and 0·005 in. separation Soller slits 4 in. long, is adequate for most analytical work, and, for example, lines having wavelengths of 2·08 and 2·10 Å respectively are clearly separated. For light elements down to titanium satisfactory analyses can be made, and in stainless steel concentrations down to at least 0·05% can be detected. Other work on stainless steels has established that good working curves can be obtained for titanium over the range 0–1% and nickel, chromium, niobium and molybdenum have been determined with an accuracy well within 1%. Nimonics, difficult to analyse for their major constituents by ultra-violet spectroscopy, are also within the field of this instrument, and possible interferences between different elements in this and other heat-resisting alloys is a matter at present under investigation.

The general principle of the automatic instrument is illustrated in block form in Fig. 16. The spectrometer has scintillation counters as detectors and an automatic scanning

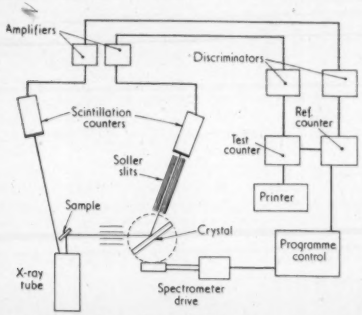

Reproduced by courtesy of Hilger and Watts Ltd.

Fig. 16. Block diagram of Hilger automatic X-ray spectrometer

system. The sample is irradiated from underneath, and the fluorescent radiation, after reflexion by the crystal, is passed through a Soller-slit system and detected by a slice of thallium-activated sodium iodide (by Hilger and Watts Ltd.) and a photomultiplier (by E.M.I. Ltd.). A similar detector is used to monitor the primary beam.

A separate console is used to set the analytical programme and record the results. Elements in the sample are determined in sequence, and a plug-board allows for the very easy selection of any chosen set of elements—up to nine in the experimental model. In operation, the detector and the crystal move to the correct position for the first element, the scintillations produced by the two X-ray beams are counted, and, when the monitor has received a pre-set number, the count in the measuring channel is printed out. The instrument then automatically moves to the next position and the operation is repeated. This sequence is repeated until all the elements have been determined, when the spectrometer returns to its stand-by position ready to analyse the next sample. A production prototype of this instrument is now under way.

DISCUSSION

The general discussion was opened by Mr. B. D. BURNS (A.R.D.E., Fort Halstead), who drew attention to the surprising interest in the subject which had been revealed by the meeting and congratulated the organizers. He pointed out that the various contributors had implied, by their concentration on the discussion of instrument errors, that this is the primary source of error. He suggested that, in general, far greater sources of error, particularly in the analysis of complex alloys such as modern stainless steels, arise from errors in the calibration curves obtained with standard comparison compositions. If the unknown alloy is of very similar composition to that of the standards, such calibration errors may well be small, but in general, the variations with alloy composition of absorption coefficient for any particular radiation combined with the incidence of mutual fluorescence excitation between the elements in the alloy can give rise to serious calibration discrepancies, even with changes in composition of the order of 1%. This is particularly true for alloys containing elements of high atomic number, e.g. molybdenum, niobium and tungsten, and the difficulty is generally more serious the lower the atomic number of the element being determined.

In an analysis of molybdenum and niobium bearing stainless steels this difficulty was encountered particularly when determining chromium. The intensity of chromium radiation was significantly affected by small variations in molybdenum and niobium contents and also by differences in the amount of fluorescence excitation by iron and nickel radiations. The scatter of points in the calibration curve for chromium could be significantly reduced by the application of absorption corrections, but a more effective and simpler correction was obtained by plotting "counts per 1% chromium" against the quantity $\Sigma_{Cr}\mu_A . N_A$ for all elements present in the alloy, where $_{Cr}\mu_A$ is the absorption coefficient of element A for chromium radiation and N_A is the atomic content of A. This procedure effectively corrected for variations in the absorption coefficients, including the reduction of intensity of excited radiation due to any mutual fluorescence excitation. It did not, however, correct for the enhancement of intensity of any characteristic radiation augmented by mutual fluorescence.

Calibration curves of this type display a smaller standard deviation and permit a considerable reduction in the number of standards necessary to give reliable calibrations. They also enable a wider range of alloy compositions to be covered by one set of callibration curves.

Considering the question of future development of the technique, the outstanding requirement is to extend the method to the elements of lower atomic number. For such elements it is essential to use vacuum operation (or hydrogen or helium atmospheres) and to utilize highly efficient analysing crystals. For elements down to potassium, lithium fluoride has excellent stability and reflexion efficiency and can be readily bent or shaped. The efficiency of a cleaved lithium fluoride surface can be increased by up to about seven times by treatment involving abrasive and surface distortion by ultrasonic waves. For elements down to aluminium, crystals of E.D.D.T. (ethylene di-amine di-tartrate) have proved effective while American workers have used A.D.P. (ammonium dihydrogen phosphate) down to magnesium. There remains, however, a need for crystals of greater efficiency in reflecting these long wavelengths. It is also desirable that such crystals should be stable in the atmosphere even under prolonged irradiation, and that they can be formed or shaped as desired.

A number of film-recording spectrographs have been

developed at A.R.D.E., Fort Halstead, and have proved invaluable in a wide range of research rather than routine applications. The wide angle spectrographs with fixed curved focusing crystals of lithium fluoride record simultaneously a wide range of wavelengths without oscillation of the camera or crystal; the transmission type covers the range 1·5 Å downwards, i.e. elements heavier than copper, while the reflexion type can record wavelengths from 1·5 to approximately 4 Å i.e. elements from copper to potassium.

The wide apertures used in these cameras necessarily involve some loss in resolution and sensitivity due to the higher background intensity, and for more precise work it is advantageous to collimate the excited radiation incident on the crystal and to maintain the recording range by oscillating the camera and its fixed crystal. A vacuum spectrograph in which elemental analysis down to oxygen has been achieved has also been developed.

Mr. M. G. Harwood (Mullard Radio Valve Co., Mitcham) considered that the possibility of electron excitation should not be overlooked. This technique scores with very small specimens, and with elements of low atomic number where the fluorescent yield might be very different from that obtained by conventional X-ray excitation. He also drew attention to the possible use of plane diffraction gratings as dispersive media for the longer wavelengths. He thought that the intensity problem might be solved by the development of more selective non-dispersive systems.

Mr. E. F. Priestley (A.R.D.E., Fort Halstead), referring to Mr. Harwood's suggestion of the use of gratings, pointed out that in the fluorescence analysis of the lighter elements the X-ray output is necessarily much lower than in the electron-excited spectra obtained with Mr. Harwood's spectrograph, and the low efficiency of the grating compared with a high efficiency crystal becomes important. In the region of aluminium K it has been found that a 1 min exposure using an E.D.D.T. crystal gives a line of good density (about 0·3). With the same specimen and excitation conditions a Siegbahn diffraction grating required at least ten times as long an exposure to give a comparable density, and although there is some reason to believe that conditions are more favourable to the diffraction grating at longer wavelengths, there is still a need for efficient crystals with spacings larger than E.D.D.T. for use with elements lighter than aluminium.

The precision of X-ray analysis was discussed by Mr. K. J. Marsh (British Petroleum Co., Sunbury on Thames) who considered that the use of the term $\sqrt{N}$ for describing the accuracy of an analysis is entirely misleading and gives a false impression of the precision which can be attained in practice. Its chief function is to serve as a guide to the best counting procedure to be adopted in an analysis. The long term-repeatability of a technique is the only measure of precision which is significant.

A series of repeat readings on the lead L_{α_1} peak from a solid metal sample taken over a month has shown that there are significant contributions to the total error due to day-to-day variations in the generator output and to setting on the peak. In the analysis of platinum catalysts Mr. Marsh endeavoured to minimize these by taking the mean of six settings on the peak and background and correcting the day-to-day variations with a solid standard. Using this technique he made a comparison of the X-ray and chemical analyses of fifty-one samples. These contained about 0·5% platinum on an alumina base and the standard deviation of the regression equation relating the two sets of values was 0·003%. This, of course, includes the errors of both methods. The X-ray measurements were made in the course of three months, so that this figure gives a good indication of the long-term precision which can be obtained.

The use of some very interesting micro-techniques in X-ray analysis as developed in Dr. Cosslett's group at Cambridge University was described by Dr. K. Nixon. In these techniques accurately focused electron beams of very small cross-section (1 μ diameter) are used for direct and fluorescent excitation. The beam can be scanned across a surface and the resulting signal may be displayed on a cathode-ray tube using a television type raster. Thus a point-to-point analysis can be made for a particular element with a resolution of 200 Å. Using a static beam a selected volume of 1 μ^3 may be analysed, with a detection sensitivity of 10^{-14} g. Although the equipment is costly it has great potential value in the examination of surfaces and inclusions.

U.K.A.E.A. (Research Group),
C.37 Royal Arsenal,
Woolwich, S.E.18.

F. W. J. Garton
H. M. Davis

Summarized proceedings of a conference on X-ray analysis—Manchester, April 1958

The annual Spring Conference of the X-ray Analysis Group of The Institute of Physics was held at the Manchester College of Science and Technology on 18 and 19 April, 1958. The papers and discussions ranged over a wide field including structural studies, apparatus and techniques of analysis.

The programme for the Conference was drawn up after members of the Group had been invited to offer contributions in any field of X-ray analysis and crystallography. As a result the papers selected for the three sessions covered a wider range of topics than is usual at these conferences. Another special feature was that most of one session was devoted to papers by research students. A brief report of the students' papers has appeared in *Nature*.[1]

Prof. E. G. Cox (University of Leeds) opened the Conference and took the Chair for the first session which began with three papers involving optical diffraction methods.

The first was presented by Mr. B. J. Thompson (Manchester College of Science and Technology) who described applications of an optical diffractometer which had been modified[2, 3] so that the diffraction pattern of a mask could be re-combined to form an image of the original mask. The effect of series termination errors in Fourier synthesis was demonstrated in a series of slides showing the [010] projection of bishydroxydurylmethane[4] with the diffraction pattern of the mask limited by various circular apertures. Fig. 1 reproduces the slide for which the diffraction pattern was restricted to reflexions with $\sin\theta \leqslant 0{\cdot}22$ (CuKα radiation). Fig. 1(*a*) shows one of the twenty-eight molecules constituting the diffracting mask, Fig. 1(*b*) the diffraction pattern passed by the limiting aperture and Fig. 1(*c*) the re-combined image. The results may be compared with a calculated Fourier

projection [Fig. 1(*e*)], based on information derived from real atoms, using the reflexions indicated in the weighted reciprocal lattice [Fig. 1(*d*)].

Mr. Thompson also put forward some tentative ideas for using the diffractometer to modify the transforms of approximate structures by the weighted reciprocal lattice; the re-combined image appears to be nearer the true structure than the approximate structure.

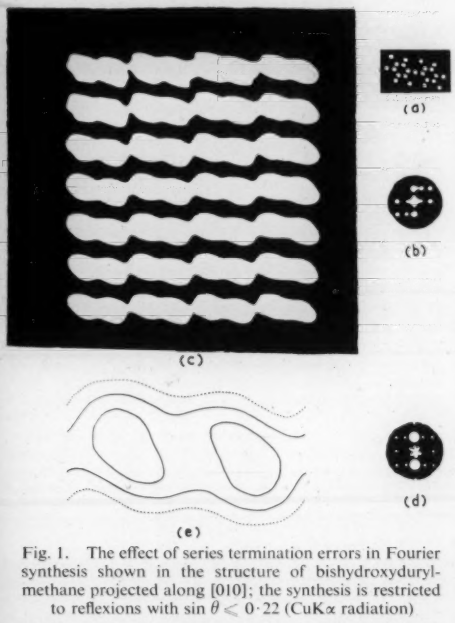

Fig. 1. The effect of series termination errors in Fourier synthesis shown in the structure of bishydroxyduryl-methane projected along [010]; the synthesis is restricted to reflexions with $\sin\theta \leqslant 0{\cdot}22$ (CuKα radiation)

(*a*) One of the twenty-eight molecules constituting the diffracting mask; (*b*) the diffraction pattern passed by the limiting aperture; (*c*) the re-combined image obtained from the diffraction pattern in (*b*); (*d*) the weighted reciprocal lattice; (*e*) calculated Fourier projection using data represented in (*d*) and phase angles calculated from atomic scattering factors of real atoms.

In the discussion Dr. J. W. JEFFREY (Birkbeck College, London) suggested that superstructures might be investigated by re-combining those reflexions which arise only from the superstructure.

In the second paper Dr. B. T. M. WILLIS (Atomic Energy Research Establishment, Harwell) described the use of the optical diffractometer to determine the diffraction from gratings representing structures with stacking faults. The diffractometer had been modified to allow photoelectric measurements of the intensity of the diffraction pattern. Light was admitted to a photomultiplier through an adjustable slit in the plane of the diffraction pattern and the slit was moved by a micrometer so as to scan the pattern. Gratings were prepared which represented the stacking of 1000 atomic layers of different types of faulted structures, and the corresponding intensity distributions in the diffraction patterns were determined by the diffractometer.

Gratings representing the face-centred-cubic structure with deformation faulted (111) planes gave broadened and displaced reflexions in accordance with Paterson's theory.[5] Two-dimensionally faulted gratings (for which no theory is available) gave reflexions with components of displacement Δ along the two stacking directions in accordance with Paterson's equation for faults on one set of planes only—

$$\Delta = \tfrac{1}{6} - (1/2\pi)\arctan\left[\sqrt{3}(1-2\alpha)\right]$$

—provided that the stacking fault parameter α (assumed equal for both sets of planes) was less than about 0·15.

Prof. K. DORNBERGER-SCHIFF (German Academy of Science, Berlin) wondered whether the problem of faulted structures could be attacked by calculating a Patterson distribution, which is the Fourier transform of the intensity distribution, rather than by trial and error methods. Prof. COX referred to the practical difficulties of this approach and Dr. I. G. EDMUNDS (Manchester College of Science and Technology) mentioned particularly the difficulty of obtaining accurate experimental data.[6]

Dr. A. ELLIOTT (Courtaulds Ltd., Maidenhead) then presented a paper by himself and Dr. B. R. MALCOLM (University of Edinburgh) on "The sense of the α-helix in poly-L-alanine." The α-helix structure for the folded form of the synthetic polypeptides,[7–11] when based on atomic dimensions found in simple molecules, is determined within narrow limits except for the helix sense. Examination of models of α-poly-L-alanine (—CH . CH_3 . CO . NH—) shows that like-handed helices can pack in a hexagonal arrangement in which the direction of the polypeptide sequence is quite random; opposite-handed helices do not pack well in a hexagonal arrangement. In testing proposed structures with the aid of their reflecting diffraction spectrometer,[12] Dr. Elliott and Dr. Malcolm had therefore examined only those with a random sequence direction of like-handed helices. The diffracting masks represented three fibre axis repeats of 27 Å each.

For a structure with the random arrangement of a polypeptide sequence direction, but with regular inter-chain distances and hexagonal packing, the diffraction pattern consists of both sharp reflexions and layer-line streaks. Cochran[13] has shown that the transform for the sharp reflexions is obtained by adding the transforms of the individual "up" and "down" chains, when these are superposed on a common chain axis with the appropriate displacement parallel to the chain axis; the transform for the layer-line streaks is obtained by subtracting these same individual transforms.

With any reasonable values for the atomic co-ordinates it was found that the observed distribution of intensity of the sharp reflexions fits the transform fairly well for the right-handed helix, but is grossly wrong for the left-handed form. The difference of the transforms of "up" and "down" chains was measured by making a mask in which the axes of the "up" and "down" chains are separated by a suitable distance d. Along row lines where ξ has the values $1/2d$, $3/2d$, $5/2d$, etc., the contributions from the individual chains differ in phase by π, and along these lines the differences of the transforms of the chains are obtained. The predicted layer-line streaks give semi-quantitative agreement with the observed layer-line streaks in the X-ray fibre photographs.

In making "A contribution to the understanding of glass formation" Dr. L. CARTZ (Cavendish Laboratory, Cambridge) considered the question of why some materials form glasses whilst others form only crystals. The work of Warren[14] showed that the silicon atom is surrounded by

four oxygen atoms and that the next silicon atom is about 3 Å away. This work did not show how the silicate tetrahedra were linked together. Two crystalline forms of silica, tridymite and cristobalite, are stable in the range 1000–1700° C. The two are different in the angles between the terminal groups of three oxygen atoms about the silicon–oxygen–silicon axis. Extensive stacking faults, depending on the thermal history are very common.

If the energy associated with these different linkages is similar and the "unit" is of low symmetry, a model can be made of random cristobalite and tridymite linkages. The diffraction pattern is calculated assuming that the scattering is determined by the radial distribution function about each atom and thus, for large distances, the summation can be replaced by integration. The comparison with the observed data shows that this model is certainly a reasonable one, but it is not necessarily unique.

Evidently the crystal forms associated with the formation of a glass must have a low energy of transition. If the slopes of the free energy-temperature curves are similar, the transition will be sluggish and stacking faults will occur. In extreme cases glasses will be found.

During the discussion Dr. Cartz agreed with the Chairman, Prof. Cox, that up-to-date structural information on tridymite and cristobalite would be a great help in this kind of work. Dr. G. D. REICK (Philips, Eindhoven) pointed out that the devitrification properties of silica glass depend on its history and suggested that differences might be observable in the diffraction patterns. Dr. Cartz confirmed that such differences were observed in samples with different thermal histories and considered that this might be due to the different probabilities of the two types of linkage. Mr. ROOKSBY (G.E.C. Ltd., Wembley) considered that the restriction of the linkage to either tridymite-like or cristobalite-like was improbable and preferred the statistical variation in orientation and bond angle between the tetrahedral groups proposed by Warren. Dr. Cartz said that it was hoped to obtain a very good fit with the experimental data and then to find what extreme variations in the model were possible.

"The structural and optical properties of ferroelectric lead metaniobate" were described by Mr. M. H. FRANCOMBE (G.E.C. Ltd., Wembley). Most of the known oxide ferroelectrics belong to the large class of pseudo-cubic perovskite-type structures. On cooling through the Curie point the structures distort from cubic, usually to tetragonal symmetry, because of ferroelectric strain effects. Further transitions occur at lower temperatures as the polar moment re-orients itself in the cell. Lead metaniobate ($PbNb_2O_6$) reported by Goodman[15] appeared to be unrelated to the perovskite-type niobates. The Curie point is very high (570° C) and there are no transitions at lower temperatures. X-ray single-crystal studies[16] have shown the structure to be orthorhombic. An alternative monoclinic unit cell with a common *c*-axis might also be chosen. The electrical permittivities measured along the plate edges, which are parallel to the *a*- and *b*-axes of the orthorhombic cell, show sharp maxima at the Curie point. In the perpendicular direction there is no permittivity anomaly. The crystal plates can be seen to be complex twins in convergent polarized light.

These observations indicate that the crystals break down into a network of 90° domains. The domain boundaries do not alter in electric fields or under mechanical pressure. Above the Curie point the domain pattern disappears and the X-ray pattern shows the structure to be truly tetragonal. The change from orthorhombic to tetragonal form is accompanied by a large discontinuous change in the unit cell dimensions.

The structure of lead metaniobate at 700° C was identified, by comparing powder photographs with those of some alkali tungsten oxide structures,[17] as similar to that of potassium tungsten bronze K_xWO_3. This structure was described by Magneli.[18] The Pb^{2+} ions occupy four pentagon and one tetragon sites, the tetragon sites forming perovskite-type units in the unit cell. As Pb^{2+} ions are removed from the material, considered as $PbO \,.\, x(Nb_2O_5)$, the lattice parameter changes abruptly and all ferroelectric properties disappear. This is presumably due to the removal of the Pb^{2+} ions from the tetragon, perovskite-type sites.

The existence of perovskite-type units suggests analogy with barium titanate ($BaTiO_3$) and potassium niobate (KN_bO_3) with polarization vectors along the face diagonals. The resultant polar moment is along the [101] axis of the monoclinic structure, or along the *b*-axis of the orthorhombic structure. It is possible that the polar axis can lie along one of the edges of the perovskite unit distorting it tetragonally. Some experimental observations indicate tetragonal distortion by a ferroelectric strain along the short *c*-axis of the bronze cell. Above the Curie point the perovskite units become cubic. The tetragonal and monoclinic phases have never been found at the same composition and thus, unlike the pseudo-cubic ferroelectrics, each structure shows only one Curie point transition.

It seems that in the bronze-type ferroelectrics the polar moments originate in perovskite-type units which are linked together in a more complex way than in the pseudo-cubic structures.

Dr. R. F. YOUELL (University of Leeds) described "Some recent X-ray investigations on iron silicate minerals" by himself and Mr. R. STEADMAN. The kaolin and chlorite groups of hydrous-layer silicate structures include a large number of iron-bearing minerals in which the amount of iron present can vary widely. The introduction of iron into a silicate containing aluminium and magnesium ions profoundly modifies the diffraction pattern because of the higher diffracting power. The thermal decomposition is influenced by the presence of iron.

Brindley[19] showed that chamosite was a kaolin mineral with a variable diffraction pattern which he interpreted as mixtures of orthohexagonal and monoclinic structures. It is now clear that an intermediate structure with random disorder in the *a*-direction is also present. The structure with no translation between layers is orthohexagonal and the structure with translation between all layers is monoclinic. If the translations are random the situation is analogous to that of metallic cobalt described by Edwards and Lipson[20] and Wilson.[21] Attempts to classify chamosites chemically have not been successful, but it seems that an isomorphous series exists between the iron-rich chamosites and aluminous kaolin.

The mineral cronstedtite was described by Hendricks[22] as a kaolin structure having an orthohexagonal unit cell of three layers. Recent work suggests the existence of one-, two-, three- and six-layer structures. In this structure the silicon is replaced by the tetrahedral ferric iron. At 220° C the ferric iron is oxidized with contraction of the lattice. At 720° C the structure changes completely to a cubic spinel with the cube diagonal parallel to the *c*-axis of the cronstedtite. The spinel seems to have the regular arrangement of magnetite but is more stable to heat treatment. Conversion to haematite occurs between 750 and 900° C, and at higher temperatures free silica can be detected.

Greenalite is orthohexagonal like chamosite and not like chrysotile as proposed by Gruner.[23] The virtual absence of

aluminium would be expected to reduce the a_0 and b_0 and increase the c_0 parameters compared with chamosite. The higher proportion of ferric iron would be expected to increase all the cell dimensions. In fact, the cell dimensions are all greater in greenalite. Greenalite oxidizes to a ferric form at 250–300° C with deterioration of the structure. Detailed thermal decomposition studies have not been possible because of the interference from impurities.

Dr. E. J. W. WHITTAKER (Ferodo Ltd., Chapel-en-le-Frith) said the fact that greenalite does not belong to the chrysotile-antigorite group accords with the lack of iron substitution in the latter. There did not seem to be any explanation of this difference in behaviour of the ferric and magnesium ions which are similar in size. In reply to a question by Dr. J. ZUSSMAN (University of Manchester) Dr. Youell said that whereas some chamosites have composition intermediate between di- and tri-octahedral, the chlorites have not yet been sufficiently thoroughly investigated to be able to say whether there were any chlorites with about five octahedral atoms per formula instead of the six in the ideal structure.

The second session, under the Chairmanship of Dr. C. W. BUNN (Imperial Chemical Industries Ltd., Welwyn Garden City), was large devoted to the papers by students.

"The crystal structures of chromous and chromic chloride" were described by Mr. R. MAITLAND (King's College, Newcastle upon Tyne). The trifluorides have been recently classified by Hepworth, Jack, Peacock and Westland[24] into three main groups distributed in specific regions of the periodic table. In the first long period they are all isostructural with VF_3; this class includes CrF_3. The chromium atom is on the three-fold axis in the space group $R3c$ and there is only one variable parameter for the fluorine. The bi-molecular structure can be considered as a distortion of the unimolecular cubic structure of the ReO_3 type of trifluoride structure, in which there is close packing of the fluorine atoms with one quarter of the sites vacant. The six fluorine atoms in the CrF_3 unit cell form a regular octagon round the chromium atom at a distance of 1·90 Å.

CrF_2, space group $P2_1/n$, is a monoclinic distortion of the rutile structure. The chromium-fluorine bond lengths in the octagon are 2·43, 2·01, 1·98 Å. The magnetic moment agrees with the value for the four unpaired electrons in the 3*d* orbitals of the divalent chromous ion. Considerations of the orbitals lead to the conclusion that two of the fluorine atoms are held either by ionic bonds or by linear hybrid 4*d*4*p* bonds. In either case these two bonds would be longer than the other four bonds in the CrF_6 octahedron.

The electron occupation of the $d\gamma$ orbital is unsymmetrical for chromium in contrast to the symmetrical configuration in divalent manganese, iron, cobalt and nickel. The difluorides of these metals all have the rutile structure in which the octahedron of fluorine atoms is regular. Cupric fluoride, which is isostructural with chromous fluoride,[25] also has a corresponding unsymmetrical occupation of the $d\gamma$ orbital.

The octahedral co-ordination is not a consequence of the favourable ionic radius, but is due to the covalent d^2sp^3 bond hybridization. This is almost certainly true in the trifluoride where the fluorine–fluorine distance is less than 2·70 Å, the ionic diameter of the fluorine ion. In the difluoride no fluorine–fluorine distance is less than 2·70 Å but this does not exclude covalent bonding.

Mr. ROOKSBY, contributing to the discussion, said that field theory had been invoked to explain structure deformation in other compounds containing transition elements. In these the deformation disappears at some elevated temperature, as in nickel chromium oxide above 35° C. The close relationship to the rutile-type structure suggests that the deformation in the difluoride of chromium might be removed at some higher temperature.

Details of "Some methods and applications of micro-analysis with fine focus X-ray tubes" were given by Mr. J. V. P. LONG (Cavendish Laboratory, Cambridge). Two techniques were described. The first method used a 1 μ focus tube in which the thin foil target formed part of the vacuum wall. The specimen, in the form of a thin section, was placed a fraction of a millimetre from the source and a photographic plate was placed some centimetres from the source. The resolution of the magnified image is of the same order as the source size. A 1 or 2 mm aperture in the plane of the photographic plate will transmit X-rays which have traversed an area of only a few microns across in the specimen. A crystal spectrometer was used to select, from the transmitted beam, particular wavelengths on the high and low energy sides of the absorption edge of the element in question. The monochromator was arranged to alternate between two fixed angular positions, corresponding to the selected wavelengths, during the measurement and the ratio of the transmission measured after correction for background count rate and for the measured ratio without the specimen.

The method has been used for estimating calcium in rock specimens and in biological materials. Wavelengths of 3·00 and 3·14 Å were selected from the continuous radiation of an aluminium target. It was found possible to show the presence of a high lime gel in the presence of natural gel and low lime gel in a cavity about 1·5 mm long in a larnite spinel rock.

The second technique makes use of the very high specific loading of the point focus X-ray tube to form a small intense beam which can be used to excite characteristic radiation in the specimen. The specimen was mounted very close to the source and the fluorescence radiation was collected in a proportional counter or a crystal spectrometer. Correction must be made for the absorption by the specimen of both the incident radiation and the fluorescence radiation. The minimum detectable mass of calcium for a 50 μ aperture and a counting period of ten minutes is 7×10^{-11} g.

The absorption method is not well suited to quantitative analysis since the sensitivity is limited by the height of the absorption jump which can be detected. It can provide accurate information about the distribution of mass of an element in a thin specimen without interference from the matrix material. The spatial resolution of the fluorescence method is unlikely to be so good but the sensitivity is higher. Quantitative applications will require a knowledge of the absorption coefficients of the specimen, but it may be possible to measure these in the way already described at the same time as the fluorescence measurements are made.

Mr. S. HOSOYA (University College, Cardiff) described "The structure of α- and β-thioanthrene dioxide." The α-isomer has the higher melting point and the smaller dipole moment. Taylor[26] forecast that the α-form would be *anti-cis* and the β-form *trans*. Both structures have been determined. The orientation of the molecules was indicated by the optical anisotropy and the sulphur–sulphur vector was obvious in the Patterson projections.

In the α-isomer the molecules of the *anti-cis* form are on the diad axes in the space group $Fdd2$. The present R value for the projection on (001) for this structure is 0·12. The β-isomer contains molecules of the *trans*-form in the space group $P2_1/n$. The present R value for the projection on (001) is 0·16 and for the projection on (100) R is 0·22.

The *anti-cis* form and the *syn-cis* form are conformational

isomers and not distinct chemical entities; one can be changed into the other by turning the molecule inside out. The *trans*-form remains *trans* when turned inside out. Only two isomers are known and it may be that the oxygen–oxygen interaction prohibits the *syn-cis* form, at least in the crystalline state.

In diphenyl sulphone two oxygen atoms are attached to each sulphur. In spite of the small separation of the oxygen atoms the molecule is still folded and not plane as might have been expected.

Three-dimensional refinement is in progress from which it is expected that accurate calcium–sulphur bond lengths will be available for comparison with the results of Lynton and Cox.[27]

Mr. R. Hine (University College, Cardiff) gave a paper on the crystal structure of (+) S-methyl-L-cysteine-S-oxide. The space group is $P2_12_12_1$ and there are four molecules in a unit cell with dimensions $a = 5.82$ Å, $b = 7.4$ Å, $c = 16.4$ Å.

The structure was solved by a sign-relation method[28] which gave the signs of fifty-two out of 115 reflexions. Both the [100] and [010] projections have been refined to give agreement residuals of about 14%. There is considerable interest in the absolute configuration at the asymmetric sulphur atom and this was determined by a direct comparison with that of the laevorotatory α-carbon for which the absolute configuration is known.[29] The crystal structure is characterized by a network of short distances between the nitrogen atom of the amino group and surrounding oxygen atoms. It is suggested that these short distances represent electrostatic bonding between the $-NH_3$ group and the negatively charged oxygens. The nitrogen takes part in five of these linkages, which are all about 2·7–2·8 Å. As a result the molecules are pulled into sheets with the nitrogen and oxygens inwards and with the short nitrogen–oxygen distances spiralled around the screw axes. A sulphur–oxygen distance of 1·48 Å suggests that no abnormal lengthening has occurred in this bond, but this will be clearer when a three-dimensional refinement of the structure has been carried out. The structure of the (−)S diastereoisomer is being investigated to provide further information about the sulphur–oxygen bond.

In the discussion Dr. J. C. Speakman (University of Glasgow) said that there is *prima facie* evidence for the view that in certain crystals more hydrogen bonds are formed by a given atom than there are hydrogen atoms available. It would be of great interest to attempt to locate these hydrogen atoms in such cases as +S-methyl-L-cysteine-S-oxide. Mr. Hine replied that the proposed three-dimensional analysis might throw light on this problem.

Dr. C. W. Bunn inquired about the van der Waals' radius of sulphur and suggested that more consideration should be given to the inclusion of van der Waals' distances in presenting the results of structure determinations. Dr. Beryl M. Oughton (Chemical Crystallography Laboratory, Oxford) said that in hexagonal L-cysteine the sulphur atoms make several close contacts suggesting a van der Waals' radius for sulphur of about 1·65 Å, which is 0·2 Å less than Pauling's value.

Mr. H. C. Watson (Manchester College of Science and Technology), giving the last of the students' papers, described a re-determination of the structure of β-naphthol.[30–33] The newly assigned space group is Ia; two sets of non-equivalent molecules occupy general positions in a unit cell of dimensions $a = 8{\cdot}18$ Å, $b = 5{\cdot}95$ Å, $c = 36{\cdot}3$ Å, $\beta = 119° 52'$. The [100] and [010] projections, which are both non-centrosymmetric, were deduced independently by comparing the optical transforms of "naphthalene molecules" (i.e. β-naphthol molecules with the oxygen atoms omitted) with the weighted-reciprocal-lattice sections.[34] Mr. Watson explained how both the orientations and the approximate intermolecular separations of the non-equivalent molecules were determined by this technique. Fourier methods revealed the positions of the oxygen atoms; subsequent refinement of the [100] and [010] projections reduced the agreement residuals to 11 and 13% respectively.

The molecules can be arranged in two ways, *A* and *B*, so as to give the observed [100] and [010] projections but different [001] projections. Structure *A* was rejected because in it one of the intermolecular oxygen–oxygen distances is 1·8 Å, whereas the corresponding distance in *B* has the usual value of 2·7 Å. Examination of the intensities of a number of general reflexions *hkl* confirmed that *B* is the correct structure.

Prof. Cox remarked that structures such as this, in which there is more than one molecule in the asymmetric unit, are particularly useful for the study of intermolecular distances and forces. They enable us to see how much intermolecular distances between atoms can vary with environment and therefore give us some idea of the precision which we can assign to the "van der Waals' radius" of an atom.

Dr. Bodil Jerslev (Royal Danish School of Pharmacy, Copenhagen) read a paper on the crystal structure of oximes. The crystal structure of *syn-p*-chlorobenzaldoxime was established some years ago from two well-resolved electron-density projections.[35] The molecules are held together in pairs by two hydrogen bridges between nitrogen and oxygen in adjacent molecules. Although no trace of the hydrogen could be seen at this stage it was argued[36] that from the molecular geometry one would expect the hydrogen to be attached to nitrogen rather than to oxygen so that the formula of the oxime in the crystalline state should be written I instead of the classical II.

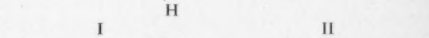

I II

To decide between these two possibilities Dr. Jerslev has refined the structure determination by means of a three-dimensional Fourier synthesis involving 1600 independent reflexions and difference syntheses of the two projections.[37] The resulting electron density maps give strong indications that the hydrogen atom of the oxime group is covalently bound to oxygen and, therefore, that the classical oxime formula is correct. The hydrogen bonds O–H . . . N appear to be non-linear with a deviation of the oxygen–hydrogen bond of about 20° from the line O . . . N.

Dr. Jerslev then surveyed the crystal structures of different oximes published by herself and by other authors. A common structural feature is association of the molecules by hydrogen bonds . . . N–O . . . N–O between the oxime groups in neighbouring molecules.[37] Relations between the degree of association and the molecular geometry were also discussed.

Prof. Cox observed that at first sight it would appear that the oximes, $R_1R_2C = N{-}OH$, would be very suitable substances in which to determine an accurate standard value for the C = N double bond. Unfortunately, this is not the case, because the hydrogen bonding reacts on the C = N bond and alters its length by an amount which is difficult to estimate with accuracy. An accurate experimental value for the 100% C = N double bond is still not available.

Dr. G. J. BULLEN (University College, London) said that the carbon–carbon bond length in glyoxime is 1·44 Å across a centre of symmetry. He asked whether the shortening of this bond is due to conjugation and also whether the carbon–nitrogen bond is longer than in other compounds. Dr. Jerslev replied that the shortening *is* due to conjugation but that the carbon–nitrogen bond length is not abnormal.

Dr. S. C. WALLWORK (University of Nottingham) concluded the second session with a review of the crystallographic evidence for polarization bonding. The term "polarization bonding" was introduced[38] to explain the short intermolecular distance reported in the structure of *p*-nitroaniline[39] and has been applied to molecular compounds of the charge-transfer type.[40–43]

Donohue and Trueblood[44] have questioned the crystallographic evidence for polarization bonding. They have re-determined the structure of *p*-nitroaniline and find that there are no unusual intermolecular distances. They also criticize the structure for the chloranil-hexamethylbenzene complex published by Harding and Wallwork[43] because of the distorted shapes of the molecules and because the quoted standard deviations σ in the atomic co-ordinates are greater for chlorine than for carbon atoms. Dr. Wallwork agreed that these criticisms are quite justified: the σ-values, which were previously erroneous, have now been re-calculated from the original data and are so large that none of the molecular distortions previously reported is significant.

Dr. Wallwork proceeded to review X-ray and other data on ten molecular complexes of the "charge-transfer" type which have been examined at Nottingham University. Although no very short intermolecular distances have been found there is evidence of slight reductions in van der Waals' distances, which vary from one complex to another in an understandable way. A common structural feature of these complexes is the plane-to-plane stacking of donor and acceptor molecules; this permits the calculation of the mean perpendicular distance between the molecular planes solely from the cell dimensions and a knowledge of the orientation of the molecules, i.e. without accurate atomic co-ordinates. These separations are all below the normal van der Waals' separation, if the latter is taken as 3·5 Å for contact between two aromatic rings, and decrease with increasing stability of the complexes, as far as can be judged. Low-temperature refinements of these structures are contemplated with a view to obtaining accurate intermolecular distances.

In the discussion Dr. J. H. ROBERTSON (University of Leeds) pointed out that one of the most simple, yet convincing, demonstrations of the existence of "polarization bonding" is obtained by observing the anisotropy of the colour of these crystals. In layer structures where flat molecules are arranged parallel to one another it is usual to find the refractive indices greatest in the plane of the layers: it is also usual to find the optical absorption greatest in this plane, that is, the density of colour is maximum when the electric vector of the incident light lies in the plane of the molecule. In these crystals, however, while the maximum refractive indices lie in the molecular plane as usual, absorption of visible light is greatest when the electric vector is perpendicular to the plane. Evidently *something* is going on between the molecules, normal to the aromatic rings. These remarks were taken by Dr. Wallwork as an opportunity for showing a slide, in colour, illustrating just the effect to which Dr. Robertson had referred.

Dr. A. HARGREAVES (Manchester College of Science and Technology) presented a paper by Dr. F. FOSTER and himself which gave an account of statistical tests for determining whether a crystal consisting of atoms of widely differing weights is centrosymmetrical or non-centrosymmetrical. When atoms of differing weights are considered, the probability distribution of X-ray intensities depends not only on the presence or absence of centres of symmetry but also on the presence of other symmetry elements and on the relative weights of the atoms.[45] The problem of determining the theoretical distribution for each symmetry type and for various relative weights of atoms is rather formidable. A more practicable approach is to calculate the various theoretical moments of Z (the ratio of the intensity of a reflexion to the local average intensity) which can then be compared with practical moments of Z.

Expressions for moments of Z have been deduced, from a moment-generating function developed by Dr. Foster, for the seven different types of structure factor formulae which are included amongst the triclinic, monoclinic and orthorhombic space groups and the associated plane groups; special positions and hypersymmetry can be taken into consideration.

A particularly important practical case is that in which there is one heavy atom and several light atoms of approximately equal weight. Dr. Hargreaves presented a slide showing a family of curves which provides sufficient data to enable the second moment of Z to be calculated in a few seconds for any heavy atom, any number of light atoms and for any distribution type. Similar families of curves provide data for higher moments.

In the discussion Prof. H. LIPSON (Manchester College of Science and Technology) made a plea for the correct use of the terms "centric" and "acentric" which should be reserved for intensity distributions and should not be confused with the terms "centrosymmetrical" and "non-centrosymmetrical" which refer to structures.

Dr. D. C. PHILLIPS (The Royal Institution, London) read a paper by Dr. U. W. ARNDT and himself describing a new type of single-crystal X-ray diffractometer. In this instrument the survey of diffraction spectra from a crystal is carried out by instrumental adjustments which provide linear translations along reciprocal lattice axes. This eliminates the necessity for computing settings of the instrument, such as are usually required to determine the crystal and counter orientations for each individual measurement with a diffractometer, and makes possible completely automatic data collection: in general, only one adjustment of constant magnitude is required between consecutive measurements.

The design of the instrument is based directly on the reciprocal lattice representation of the genesis of X-ray reflexions. Fig. 2 shows how the principles involved can be applied in a two-dimensional arrangement: XCO is the direction of the incident X-ray beam and C the position of the crystal specimen; AOB represents a slide, pivoted at O and carrying a second slide PQ at right angles to itself which can be moved along OA by means of a micrometer screw. The distance PQ can be varied in the same way. The point P is constrained to remain always in the circumference of the circle XPO by means of a link of fixed length CP, pivoted at C and P, and any rotation of the slide system PQO necessary to satisfy this condition is transmitted to the crystal at C by means of the parallel linkages CD–OB and DB–CO. The slide system PQO thus represents a reciprocal lattice net and the circle XPO represents the circle of reflexion.

According to the standard construction, CP represents the direction of the reflexion corresponding to the reciprocal lattice point P. The X-ray counter is therefore mounted on the arm CP. Then if PQ is kept constant in length, movement of Q along OA will result in the scanning of all the reflexions

corresponding to reciprocal lattice points in the line *RP* which is parallel to *OA* and distant *PQ* from it. Such a device can be used in scanning all the reflexions corresponding to points in a central reciprocal lattice sheet.

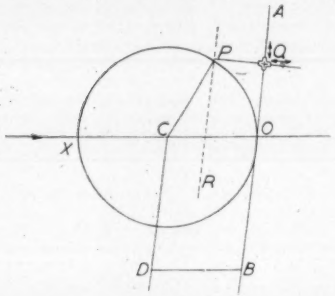

Fig. 2. Principles underlying the survey of spectra with the single-crystal X-ray diffractometer explained in terms of the reciprocal lattice representation of the genesis of X-ray reflexions

The foregoing principles have been extended to three dimensions by introducing a third slide, perpendicular to the other two, in the reciprocal lattice analogue. By means of this additional slide each non-central reciprocal lattice sheet can be brought into a position in which it can be scanned systematically by operation of the other two slides.

Details of the construction and use of the diffractometer were discussed by Dr. Phillips. The development of the instrument has been sponsored by the National Research Development Corporation.

The next paper, by Dr. E. R. Pike, Prof. A. J. C. Wilson and Dr. J. W. Hughes (University College, Cardiff) was concerned with the problems which arise when the maximum accuracy is desired in the measurement of lattice parameters with the counter diffractometer. Dr. Pike, presenting the paper, discussed the factors which cause a departure from the ideal case in which the lattice parameter is given by the Bragg equation, with a small correction for the slight departure from unity of the refractive index of the material.[46]

Lack of true monochromaticity of the incident X-ray beam gives rise to a range of diffraction angles; the angular distribution $f(\theta)$ will differ slightly from the spectral distribution because of the non-linear nature of the transformation. A small "dispersion correction" is required for this effect if the centres of gravity of the distributions are used.[47]

Geometrical effects, due to finite extension of the source, specimen and receiving slit, cause a single wavelength element to be "smeared out" over a range of angles by the so-called aberration function $g(\theta)$.

The observed profile is the fold or convolution of the functions $f(\theta)$ and $g(\theta)$, and its form depends in a critical and complicated way on the form of $g(\theta)$. To determine lattice parameters from the ideal peak positions, the observed profile and the aberration function would have to be "unfolded." This is impracticable in most cases as the profiles of the functions are not known accurately enough and, in any case, the mathematics of the process are very lengthy.

An alternative process involves the use of the centres of gravity of the profiles rather than their peaks. The centre of gravity of the observed profile is calculated and the shift G due to the aberration function is subtracted. This gives θ for the centre of gravity of the ideal profile. The lattice parameter may now be calculated from the Bragg equation, using the wavelength of the centre of gravity of the spectral profile, provided that the small correction for dispersion has been applied. The shifts G caused by all the major aberrations have been worked out[48, 49] and are much easier to calculate than the actual profiles of the aberration functions; they have all been reasonably confirmed experimentally.

Since the tails of a profile die away slowly, and since also the lines are superimposed upon a continuous background, there is no definite beginning or end to each line. It is therefore necessary to "truncate" the profiles somewhere in the tails and use a finite portion only. Discussing the resulting errors, Dr. Pike said that they can be reduced to the order of one or two parts in 10^6 in d provided a satisfactory procedure, which he described, is adopted.

An investigation of the statistical limitations in counting X-ray quanta has shown that surprisingly few counts are required at each point to give an accurate centre of gravity. The actual number depends on the peak-to-background ratio, range of integration and monitor count, if used. Because of the higher peak-to-background ratio obtainable, proportional or scintillation counters have a very marked advantage over the Geiger counter for this type of work.

A paper on "A high-temperature X-ray camera" by Mr. B. A. Hatt, Mr. P. J. C. Kent and Dr. G. I. Williams was presented by Mr. Hatt (Fulmer Research Institute Ltd., Stoke Poges).

The camera was designed for studying the reactive metals titanium, zirconium and uranium. Existing types of high-temperature cameras were considered unsuitable because of specimen contamination introduced by the relatively poor vacua attainable and the difficulties of outgassing the camera interior, particularly the furnace assembly.

Essential features of the new design are the construction of the camera in glass and the use of a radiant heater situated outside the camera. These eliminate contamination due to a conventional furnace assembly and facilitate outgassing of interior walls. Specimen temperatures up to 1000° C are attained and a vacuum better than 1×10^{-6} mm of mercury can be maintained in operation.

On studying the β–α transformation in zirconium–titanium alloys, it was found that the β-high temperature phase was not retained on quenching to room temperature, complete transformation to α taking place. Earlier work showing that the β-phase could be partially retained on quenching was repeated only by operating the camera at an inferior vacuum of 10^{-3} mm of mercury, thus contaminating the specimen.

These results show the importance of the role played by contamination, thus emphasizing the need for suitable precautions in X-ray studies at high temperature, and also in those studies where interpretation of results obtained with other techniques is based on X-ray identification.

Mr. K. J. Marsh (British Petroleum Company Ltd., Sunbury-on-Thames) described the "Application of X-ray spectrographic analysis in the petroleum industry." Any method of analysis must be repeatable over long periods. Measurements made several times a day on the intensity of a lead peak, using a metal specimen, over a period of a month showed a significant error in setting on the peak as well as from the day-to-day variation of the generator output. The practice now adopted is to take the mean of several peak

settings and correct for generator variations by reference to the solid standard.

Analysis of lead tetraethyl in gasolines in the concentration range 0·01 to 0·10% is straightforward. The X-ray method requires no special sample preparation and, provided the sample is thicker than the critical value, the fluorescence radiation intensity is independent of the size of the sample. The $PbL\alpha_1$ peak was selected for measurement and the background in the neighbourhood subtracted. Calibration was carried out using a set of standard solutions of tetraethyl lead in toluene and in iso-octane, which are at the extreme ends of the density range normally encountered. The value obtained directly from the corrected peak height was corrected for sample density by interpolation between the toluene and iso-octane standards. The analysis takes twenty-five minutes including calculation, compared with eight hours for a chemical analysis. The standard deviation at all concentrations in the normal range is about 1%, which is within the limits laid down for the chemical method.

Analysis of platinum in alumina-based catalysts requires high accuracy. The $PtL\beta_1$ line was well resolved and was used for measurement. The variability due to water absorption by the alumina was overcome by heat treatment. There is a considerable saving of time compared with the chemical method and there is no loss of accuracy.

In discussing this paper Dr. P. T. DAVIS ("Shell" Research Ltd., Thornton) expressed surprise that the intensity/concentration calibration curves for lead in gasoline depended only on the density of the matrix. It would be expected to depend on the carbon : hydrogen ratio as well. Mr. Marsh replied that there was some connexion between the carbon : hydrogen ratio and density itself, but the details of the variation had not been investigated.

The final paper of the Conference by Mr. L. BROWN, Mr. A. W. PORTER and Mr. J. G. STENNER (Courtaulds Ltd., Coventry) on "An X-ray study of filament spinning" was read by Mr. Brown. A sealed-off X-ray tube, flexibly mounted on a mobile chassis, was used to take photographs of running cellulose yarn at various stages of the viscose spinning process, from the spinning bath to the collecting bobbin. This has provided structural information about the nature of the yarn during coagulation and regeneration, which is unobtainable by examination of the static samples because of the speed of the chemical reaction. The results show that the freshly spun yarn has a molecular sheet structure with low orientation. The peak observed at 4·4 Å corresponds to the intermolecular spacing within a single sheet. This agrees with the findings of Hess, Keissig and Koblitz.[50] During regeneration the sheets come closer together, probably with some hydrogen bonding as the sheets pack into a swollen cellulose II structure. The pattern shows a high degree of orientation because of the stretching applied during spinning. After drying the yarn becomes largely crystalline cellulose II with a sharp reflexion at 7·2 Å instead of the diffuse reflexion observed with the wet yarn. Yarn dried at above 100° C shows a further equatorial reflexion at 5·6 Å indicating the presence of cellulose IV. Kost[51] has suggested that the formation of cellulose IV is due to stretching in hot acid. The present investigation shows that it is due to hot drying. Cold dried, hot streched yarn, does not contain any cellulose IV.

The equipment used is versatile and is now being used to study other spinning and stretching processes as well as to clear up some further points in the present investigation.

Replying to a question by Dr. STADLER (King's College, Newcastle-upon-Tyne), Mr. Brown said that attempts to study the fibres using polarized light had been very disappointing and the X-ray method appeared to be a much more profitable line of attack.

A. HARGREAVES
E. STANLEY

REFERENCES

(1) GORDON, R. L. *Nature* [*London*], **181**, p. 1645 (1958).
(2) HANSON, A. W., and TAYLOR, C. A. *Proceedings of Symposium on Astronomical Optics and Related Subjects, University of Manchester*, 1955. Ed.: Z. Kopal (Amsterdam: North Holland Publishing Co., 1956).
(3) MENARRY, A. Ph.D. Thesis (University of Manchester, 1957).
(4) CHAUDHURI, B., and HARGREAVES, A. *Acta Cryst.*, **9**, p. 793 (1956).
(5) PATERSON, M. S. *J. Appl. Phys.*, **23**, p. 805 (1952).
(6) STEEPLE, H., and EDMUNDS, I. G. *Acta Cryst.*, **9**, p. 934 (1956).
(7) PAULING, L., and COREY, R. B. *Proc. Nat. Acad. Sci. U.S.A.*, **37**, p. 241 (1951).
(8) PERUTZ, M. F. *Nature* [*London*], **167**, p. 1053 (1951).
(9) BROWN, L., and TROTTER, I. F. *Trans Faraday Soc.*, **52**, p. 537 (1956).
(10) ELLIOTT, A., and MALCOLM, B. R. *Nature* [*London*], **178**, p. 912 (1956).
(11) PAULING, L., COREY, R. B., YAKEL, H. L., and MARSH, R. E. *Acta Cryst.*, **8**, p. 853 (1955).
(12) ELLIOTT, A., and ROBERTSON, P. *Acta Cryst.*, **8**, p. 736 (1955).
(13) COCHRAN, W. Private communication.
(14) WARREN, B. E. *J. Amer. Ceramic Soc.*, **19**, p. 202 (1936).
(15) GOODMAN, G. *J. Amer. Ceramic Soc.*, **30**, p. 368 (1953).
(16) FRANCOMBE, M. H. *Acta Cryst.*, **9**, p. 683 (1956).
(17) FRANCOMBE, M. H., and LEWIS, B. *Acta Cryst.*, **11**, p. 696 (1958).
(18) MAGNELI, A. *Arbir. fur Kemi.*, **1**, p. 213 (1949).
(19) BRINDLEY, W. G. *Min. Mag.*, **29**, p. 502 (1951).
(20) EDWARDS, O. S., and LIPSON, H. *Proc. Roy. Soc. A*, **180**, p. 268 (1942).
(21) WILSON, A. J. C. *Proc. Roy. Soc. A*, **180**, p. 277 (1942).
(22) HENDRICKS, ST. B. *Amer. Mineralogist*, **24**, p. 529 (1939).
(23) GRUNER, J. W. *Amer. Mineralogist*, **21**, p. 449 (1936).
(24) HEPWORTH, M. A., JACK, K. H., PEACOCK, R. D., and WESTLAND, G. J. *Acta Cryst.*, **10**, p. 63 (1957).
(25) BILLY, C., and HAENDLER, H. M. *J. Amer. Chem. Soc.*, **79**, p. 1049 (1957).
(26) TAYLOR, T. W. J. *J. Chem. Soc.*, p. 625 (1935).
(27) LYNTON, H., and COX, E. G. *J. Chem. Soc.*, p. 4886 (1956).
(28) GRANT, D. F., HOWELLS, R. G., and ROGERS, D. *Acta Cryst.*, **10**, p. 489 (1957).
(29) PEERDEMAN, A. F., VAN BOMMEL, A. J., and BIJVOET, J. M. *Proc. K. Ned. Akad. Wetensch. B.*, **54**, p. 16 (1951).
(30) HARGREAVES, A., and WATSON, H. C. *Acta Cryst.*, **10**, p. 368 (1957).
(31) WATSON, H. C., and HARGREAVES, A. *Acta Cryst.*, **11**, p. 556 (1958).
(32) KITAIGORODSKII, A. I. *Dokl. Akad. Nauk. SSSR*, **50**, p. 319 (1945).
(33) KITAIGORODSKII, A. I. *Izv. Akad. Nauk, SSSR, Khim. Nauk.*, **6**, p. 561 (1947).
(34) HANSON, A. W., LIPSON, H., and TAYLOR, C. A. *Proc. Roy. Soc. A*, **218**, p. 371 (1953).
(35) JERSLEV, B. *Nature* [*London*], **166**, p. 741 (1950).

(36) PITT, G. J. *Ann. Rep. Chem. Soc.*, **47**, p. 457 (1950).
(37) JERSLEV, B. *Nature [London]*, **180**, p. 1410 (1957).
(38) MCKEOWN, P. J. A., UBBELOHDE, A. R., and WOODWARD, I. *Acta Cryst.*, **4**, p. 391 (1951).
(39) ABRAHAMS, S. C., and ROBERTSON, J. M. *Acta Cryst.*, **1**, p. 252 (1948).
(40) MULLIKEN, R. S. *J. Amer. Chem. Soc.*, **74**, p. 811 (1952).
(41) MULLIKEN, R. S. *J. Phys. Chem.*, **56**, p. 801 (1952).
(42) HARDING, T. T., and WALLWORK, S. C. *Acta Cryst.*, **6**, p. 791 (1953).
(43) HARDING, T. T., and WALLWORK, S. C. *Acta Cryst.*, **8**, p. 787 (1955).
(44) DONOHUE, J., and TRUEBLOOD, K. N. *Acta Cryst.*, **9**, p. 960 (1956).
(45) HARGREAVES, A. *Acta Cryst.*, **8**, p. 12 (1955).
(46) WILSON, A. J. C. *Proc. Cambridge Phil. Soc.*, **36**, p. 485 (1940).
(47) PIKE, E. R. Submitted to *J. Appl. Phys.*
(48) WILSON, A. J. C. *J. Sci. Instrum.*, **27**, p. 321 (1950).
(49) PIKE, E. R. *J. Sci. Instrum.*, **34**, p. 355 (1957).
(50) HESS, K., KEISSIG, H., and KOBLITZ, W. *Z. Elektrochem. Ang. Physik. Chemie*, **55**, p. 697 (1951).
(51) KOST, W. *Forschungsberichte des Wirtschafts und Verkehrministeriums, Nordhein-Westfalen* No. 93 (1954).

ORIGINAL CONTRIBUTIONS

Evaluation of approximate methods of applying binary scale factors in pulse-counting systems of measurement

By W. T. BANE, B.Sc., A.M.I.E.E., and M. P. ATKINSON, B.Eng., Control Mechanisms and Electronics Division, National Physical Laboratory, Teddington, Middlesex

[*Paper first received* 1 *September, and in final form* 2 *October*, 1958]

An approximate system of applying binary scaling factors in pulse-counting systems of measurement is described and the errors involved are evaluated. This system forms the basis of a series of developed systems whose errors are also discussed. The effects producing the errors are not arithmetic, and complete proofs are lacking for some of the expressions, which, however, have been checked over the first part of their range.

1. INTRODUCTION

Pulse-counting techniques have been used in various applications for measuring the position of a moving mechanical member. In such systems "marks" placed on the member are counted as they pass beneath a sensing head so that the number held by the counter is a digital indication of the position of the member relative to that at which the counter was set to zero. It is, of course, necessary to sense the direction of passage of the marks and the counter must be capable of increasing or decreasing its count appropriately.

The "marks" can be a change in any physical quantity to which a sensing head will respond. The variation in light intensity from a pattern of interference fringes has been used with a photoelectric head[1] as well as simple shadows.[2] Use has also been made of the change in electrical coupling between a configuration of conductors carried by the member and a second configuration on the sensing head.[3] In the description that follows, we are not concerned with the physical realization of the "mark" which is taken to be a discrete point on the member.

In these systems it is sometimes necessary to introduce an easily variable scaling factor into the digital measurement. It can, of course, be effected by directly multiplying the count but this may entail a relatively large increase in the complexity of the equipment associated with counting. On the other hand a variable mechanical magnification can be introduced into the system but this will rarely give a neat solution and often an impracticable one.

The basis of a simple, but approximate, method of scaling is described in the next section.[4] This method, together with many of the variants that will be described, was first suggested by Mr. R. H. Tizard, formerly of the National Physical Laboratory.

2. METHOD OF SCALING

In a counting system, the "marks" on the moving member are usually fixed at equal intervals along the moving member, the distance between adjacent marks determining the accuracy to which the distance moved can be measured by the system, since movement within one interval causes no change in the number counted. Scaling the distance implies that each interval must be equivalent to some number other than one (i.e. the scaling factor). The scaling factor is usually defined as lying between 0 and 1. If the scaling factor S is quoted to R binary digits and S_{-r} is the coefficient of 2^{-r} in S, then after moving a distance D, the number we require in the counter is $D \,.\, S$. That is

$$\frac{DS_{-1}}{2} + \frac{DS_{-2}}{2^2} + \frac{DS_{-3}}{2^3} \cdots + \frac{DS_{-r}}{2^r} \cdots + \frac{DS_{-R}}{2^R}$$

Now consider the disposition of marks in Fig. 1, in which

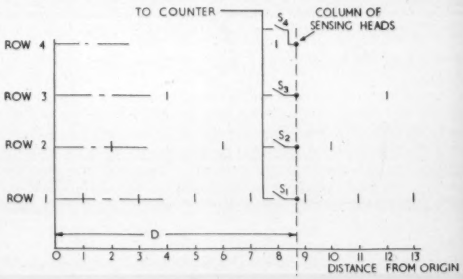

Fig. 1. Disposition of marks for binary scaling

there is a sensing head associated with each row. Marks on row 1 appear at positions 1, 3, 5, 7, etc., along the D axis. In row 2 the marks have double the spacing of those on row 1 at positions 2, 6, 10, etc. The spacing in row 3 is double that in row 2 and so on.

The marks counted on row 1 in moving a distance D from the origin will approximate to $\frac{D}{2}$ with an error which varies from $+\frac{1}{2}$ to $-\frac{1}{2}$ as D increases between adjacent marks. The marks counted on row 2 will approximate to $\frac{D}{4}$ again with an error between $+\frac{1}{4}$ and $-\frac{1}{4}$. On row r, the number of marks counted will approximate to $\frac{D}{2^r}$ with the same range of possible error. Each row can therefore represent one digit of the scaling factor; row r, for instance, is equivalent to the term $\frac{S_{-r}}{2^r}$ in the scaling factor. By adding together the counts from those rows whose equivalent "S" coefficient is 1, we can get a total count which approximates to the desired count of $D \,.\, S$.

3. ERRORS IN THE BINARY SYSTEM

With a scaling factor quoted to R binary places, the system requires R rows containing 1, 2, 4 . . . 2^{R-1} marks respectively, a total of $(2^R - 1)$ marks in the range $0(A)$ to $2^R(B)$ as illustrated in Fig. 2(*a*). No mark is present at positions 0, 2^R, 2^{R+1}, 2^{R+2}, etc., along the D axis. If we start at A with the counter at zero and move to B, the total count registered with a scaling factor S will be

$$S_{-1} \times 2^{R-1} + S_{-2} \times 2^{R-2} \ldots + S_{-(R-1)} \times 2 + S_{-R} \times 1$$

The total count we require is $2^R \times S$ which is also

$$2^{R-1} \times S_{-1} + 2^{R-2} \times S_{-2} + \ldots + S_{-R} \times 1$$

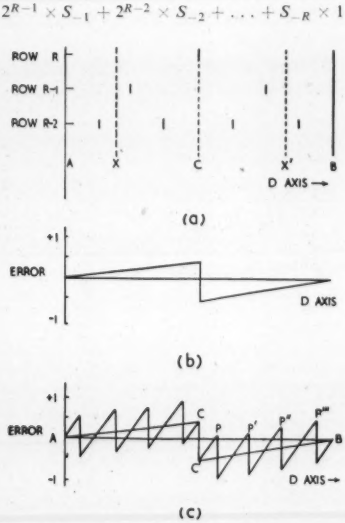

Fig. 2. Error pattern in the basic system

Thus the error between the actual and desired counts will be zero at A and B and the pattern of errors between A and B is repeated for each subsequent range of 2^R along the D axis. To obtain the value of the maximum error, therefore, only the range AB need be considered.

Row "R" contains only one mark in this range, at a position C, halfway between A and B. The pattern of marks from A to C is a mirror image about C of the pattern from B to C. Consider the errors at X and X' where $AX = BX'$. If the error in the count in moving from A to X is E, then the error is the count in moving from B to X' must also be E. The error, in the count, in moving from A to X' must therefore be $-E$. The errors at X and X' are therefore equal in magnitude but of opposite sign. Thus for any positive error in the system there is an equal negative error, and the sum of the distances from A at which these errors occur is 2^R.

Now if row R is not included then the system becomes one in which the scaling factor is quoted to $(R - 1)$ places, with zero error at C and the errors in the range A to C are repeated in the range C to B. With the inclusion of row R, therefore, the error changes from $+\frac{1}{2}$ to $-\frac{1}{2}$ at C (because of the "mirror" effect at C), causing some proportion of $\frac{1}{2}$ to be added to errors in the range AC and some proportion of $(-\frac{1}{2})$ to be added to those in the range BC. This effect is shown in Fig. 2(*b*). Thus the maximum positive error will always occur in the range AC and the maximum negative error in the range CB, and if the coefficient of 2^{-R} in the scaling factor is 1, then for a maximum negative error the coefficient of 2^{R-1} in the distance AD must also be 1.

Now assume that the $(R - 1)^{th}$ and $(R - 2)^{th}$ rows are not included in our scaling factor, but the $(R - 3)^{th}$ row is. This row contains 8 marks at intervals of $2^{(R-3)}$. Fig. 2(*c*) shows the effect of this row on the errors. At point P, the error changes from $+\frac{1}{4}$ to $-\frac{1}{4}$ about the error line $C'B$. Then again at P', P'', etc. The new error lines will all have the same slope and since the pattern of marks in the range PP' is the same as that in the range $P'P''$, the maximum negative error will occur in this range PP', that is, in the range $(2^{R-1} + 2^{R-4}) < D < (2^{R-1} + 2^{R-3})$.

The coefficients of 2^{R-2} and 2^{R-3} in D will be 0 and that of 2^{R-4} will be 1. Extending this argument, it is clear that for any scaling factor S, the maximum negative error will occur at distance D from A such that the coefficient D_r of 2^{r-1} in D equals the coefficient S_r of 2^{-r} in S. Similarly the maximum positive error occurs at position D' where $D' = 2^r - D$. Thus D_r and S_r will be dissimilar.

In Appendix 1, an expression for the maximum possible error obtainable with a scaling factor quoted to R places is derived. For all but the lowest few values of R, this may be approximated by

$$(E)\max \simeq \frac{3R + 7}{18} \qquad (1)$$

When using pulse counting methods the zero can be set at any desired position along the axis of movement merely by setting the counter to zero with the moving member at this position. This may, however, introduce an additional error. In fact, if the zero is set at a position where the error has a maximum negative value, then the error in the count at the position where maximum positive error occurs will be twice the value given by equation (1).

4. DEVELOPMENTS OF THE BASIC SYSTEM

There are two possible methods of obtaining scaling factors less than $\frac{1}{2}$ (factors where $S_{-1} = 0$), from the basic

array. The count from row 1 can be omitted (since $S_{-1} = 0$), making the system equivalent to one with $(R - 1)$ rows with double the basic interval, or the scaling factor can be doubled in order to use the first $(R - 1)$ rows of the pattern and the resulting answer in the counter divided by two by shifting the position of the binary point in the counter. Row R in the pattern is now redundant. In both cases, only $(R - 1)$ rows are required, but in the second system each pulse increases the count by $\frac{1}{2}$ instead of by 1, and the resulting error is therefore halved. Fig. 3(*a*) illustrates this system. Row 1 of the pattern is now equivalent to s_{-2} in the scaling factor and pulses from the pattern are fed into a scale-of-two stage before passing into the counter.

As described, this improved accuracy can only be obtained for scaling factors smaller than $\frac{1}{2}$, since there is no provision for the s_{-1} term of the scaling factor. In the original system, this term was obtained from row 1 of the pattern by feeding the pulses direct to the counter instead of *via* the scale-of-two stage.

This suggests a method by which scaling factors greater than $\frac{1}{2}$ could be obtained with an improved accuracy. The method is illustrated in Fig. 3(*b*). This is similar to the

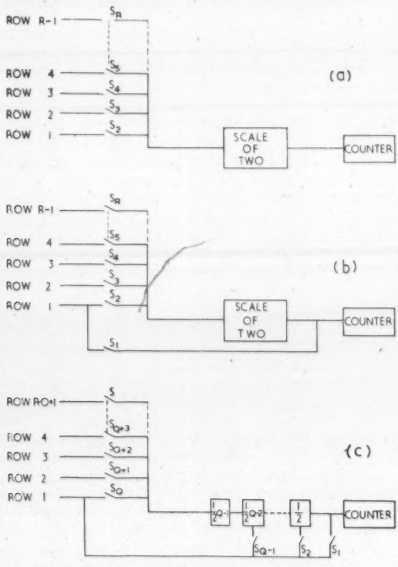

Fig. 3. Modified counter systems

system of Fig. 3(*a*) but the pulses from row 1 are now fed directly to the counter *via* switch S_1 as well as to the scale-of-two stage *via* switch S_2.

The resulting count now approximates to

$$D\left[\frac{S_{-1}}{2} + \frac{1}{2}\left(\frac{S_{-2}}{2} + \frac{S_{-3}}{2^2} + \ldots\right)\right]$$

which is the required value. Now, however, the first two digits of the scaling factor are derived from row 1 of the pattern. The maximum error produced by assuming that the count from row 1 is equal to $D/2$ is $\frac{1}{4}$. The maximum error from the remaining terms is now $\frac{1}{2}$ the value given by equation (1) of section 3 for $(R - 1)$ terms. The maximum error of the system is the sum of these two, which is

$$\frac{1}{2} + \frac{3(R-1)+7}{2 \times 18} = \frac{3R + 13}{36} \qquad (2)$$

which is smaller than the original value for all values of R.

The system is capable of further extension. If the first Q digits of the scaling factor are obtained from row 1 by switching the pulses produced from this row into chosen stages of a counter whose binary point has been shifted to compensate for the increased number of pulses it receives, a system as illustrated in Fig. 3(*c*) results. Only rows 1 to $(R - Q + 1)$ of the pattern are now required and the pulses from the pattern are fed *via* switches $S_Q \ldots S_R$, to the $\frac{1}{2^{(Q-1)}}$ stage of the counter. The pulses from row 1 are also fed, *via* switches $S_{(Q-1)} \ldots S_1$ to each stage of the counter from $\frac{1}{2}Q - 2$ to 1.

The error produced by this system is the sum of the errors due to the pattern of $(R - Q + 1)$ rows and the error due to the remaining $(Q - 1)$ digits of the scaling factor derived from row 1.

The total count from the pattern is divided by $\frac{1}{2^{(Q-1)}}$ before reaching the integer stages of the counter. The error from this source is therefore

$$\pm \frac{1}{2^{(Q-1)}} \frac{3(R-Q+1)+7}{18} \text{ from equation (1)}$$

Each pulse from row 1 causes a number

$$S_1 + \frac{S_2}{2} + \ldots + \frac{S_{Q-1}}{2^{Q-2}}$$

to be added to the counter. These pulses occur at positions 1, 3, 5, etc., along the D axis, and the count produced will therefore approximate to

$$\frac{D}{2}\left[S_{-1} + \frac{S_{-2}}{2} + \ldots + \frac{S_{(Q-1)}}{2^{Q-2}}\right]$$

with an error of up to $\frac{1}{2}$ the value of a count. The error will therefore be a maximum when $S_1 = S_2 = S_3 \ldots = S_{Q-1} = 1$, and will then be equal to

$$\pm \frac{1}{2}\left(1 + \frac{1}{2} + \frac{1}{4} \ldots + \frac{1}{2^{Q-2}}\right) = \pm \left(1 - \frac{1}{2^{Q-1}}\right) \qquad (3)$$

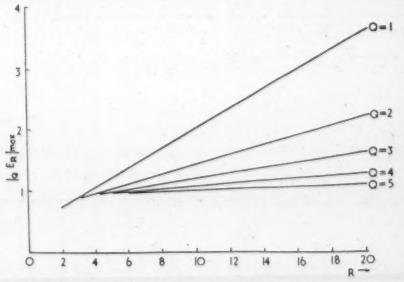

Fig. 4. Maximum error of modified scaling system

The maximum possible error of the system is therefore the sum of these two values, i.e.

$$ {}_{Q}E_{R\,max} = \pm\left\{\frac{1}{2^{Q}-1}\left[\frac{3(R-Q)+10}{18}\right] + \left(1-\frac{1}{2^{Q}-1}\right)\right\} $$

$$ = \pm\left\{1 + \frac{1}{2^{Q}-1}\left[\frac{3(R-Q)-8}{18}\right]\right\} \qquad (4) $$

If the effect of zeroing is taken into account, the maximum possible error is twice the value given by equation (4).

If all the digits of the scaling factor are obtained from row 1, then $Q = R$ and equation (4) falls down. The actual error is given by equation (3) with $Q = R + 1$.

Fig. 4 shows the values of $({}_{Q}E_{R})_{max}$ derived from equation (4) plotted as a function of R for different values of Q. The curve for $Q = 1$ corresponds to that for equation (1).

5. MAXIMUM ERROR REFERRED TO THE MOVING MEMBER

For some applications it is necessary to know the maximum error that can occur for a given R in terms of movement of the mechanical member carrying the marks. For example, if the position of the member is to be controlled in accordance with a number set into the equipment, it will be important to know the worst error in terms of the displacement of the member from its required position.

The maximum error referred to the member will not occur at the same value of R as that for the maximum error in the scaled result (except in a few, almost trivial, cases).

In Appendix 2 an expression has been derived for the maximum error (including zeroing), $|F|_{max}$, referred to the source. The expression refers to the basic system of section 3 and for all but the lowest values of R may be conveniently approximated by

$$ |F|_{max} = \frac{2}{3}\left[\frac{3(R-x)+25}{3+4(\frac{1}{2})^{x}}\right] - 2 \qquad (5) $$

Where x takes on the following values for different values of R

R	x
2	1
3	2
4–8	3
9–21	4
22–46	5

A complete justification for this result has not been found; the expression has been derived by the use of one assumption about the form of the scaling factor for the maximum error. There is a certain amount of evidence for making this assumption and it has been found to be true for values of R up to 10.

6. PRODUCTION OF THE BASIC PATTERN BY A COUNTER

A bi-directional counter operating from a series of pulses on a single channel may be made to develop the basic pattern as follows. The pulses corresponding to row 1 in Fig. 1 are derived from the first stage (the least significant) by causing it to generate an "add" pulse each time the stage changes from 0 to 1 when the counter is adding and vice versa when it is subtracting. Similarly, pulses corresponding to row 2 can be derived from the second stage, and so on.

Table 1 illustrates this for a four-stage counter; the pulse outputs may be compared with the pattern of Fig. 1.

Table 1. *Pulse pattern in a binary counter*

Number of pulses fed to counter	*State of counter stages*				*Pulses emitted when adding or subtracting*			
	1	2	3	4	R1	R2	R3	R4
0	0	0	0	0				
					1			
1	1	0	0	0				
						1		
2	0	1	0	0				
					1			
3	1	1	0	0				
4	0	0	1	0				
					1			
5	1	0	1	0				
						1		
6	0	1	1	0				
					1			
7	1	1	1	0				
								1
8	0	0	0	1				
					1			
9	1	0	0	1				
						1		
10	1	1	0	1				

Such a method of generating the pulse trains can be used in conjunction with the methods of scaling that have been described. It has the advantage that providing the auxiliary counter is zeroed at the same time as the main one, the additional effect of zeroing is greatly reduced, since "zero" is always set effectively between "0" and "1" on the pattern of Fig. 1. The maximum error due to this is therefore equal to the scaling factor.

If the pulses to this auxiliary counter are obtained from a single row of equally spaced marks it is possible to modify the system of scaling described in section 4 of the paper. The scaling factor for the first Q digits can now be obtained from this single row (rather than from stage "1" of the counter).

With this system, the error due to this part of the scaling factor can vary between 0 and $\left(1-\frac{1}{2^{Q}}\right)$ which is not symmetrical. The maximum positive error will be

$$ \left(1-\frac{1}{2^{Q}}\right) + \frac{1}{2^{Q}}\left[\frac{3(R-Q)+7}{18}\right] = $$

$$ = 1 + \frac{1}{2^{Q}}\left[\frac{3(R-Q)-11}{18}\right] \qquad (6) $$

7. USE OF A SINGLE FED-BACK COUNTER

Having devised a method of generating the basic pattern of pulses from one counter and counting the resulting pulses on a second, the next obvious step is to try to devise a scheme in which both functions are performed by the same counter. Such a scheme will have the obvious first advantage that the complexity of the electronics will be approximately halved.

One possible arrangement is shown in Fig. 5, where the unscaled pulses are fed to a counter that, as before, produces the basic pattern. The resulting pulses are fed back *via* the scale-factor switches S_1' to S_4' and a delay to the input of the counter. Another arrangement, in which the fed-back pulses are used to block an equivalent number of primary input pulses, is also possible. However, such an arrangement

appears to have no obvious advantages over that of Fig. 5 and it will not be discussed.

The system of Fig. 5 is one in which a proportion $S'T$ of the actual number T in the counter is fed back into the counter. The total count must equal $X + J$.

Therefore $$X + J = T$$
$$J = S'T$$
hence $$X + S'T = T \qquad (7)$$

In this case the actual scaling factor S between X and T (such that $S \,.\, X = T$) will be

$$S = \frac{1}{1 - S'}$$

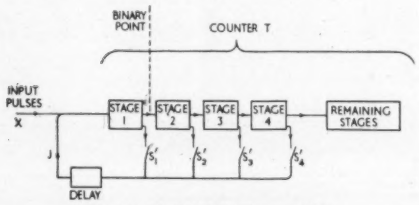

Fig. 5. Feed-back scaling system

This will always be greater than unity, but can be limited to values less than unity by inserting the binary point after "stage 1" of the counter (as shown in Fig. 5) and limiting S' to the range 0 to $\frac{1}{2}$.

Now if S' is set up on the switches S'_1 to S'_R the number of pulses along the line J will approximate to the required number $S'T$. There will be an error present. The pulses to switch S'_1 will occur at values of T of 1, 3, 5, etc. Those to S'_2 will occur at 2, 6, 10, etc. Thus S'_1 corresponds to row 1 of Fig. 1, S'_2 to row 2 and so on. The error in $S' \,.\, T$ can therefore be derived in the same manner as the error in $S \times D$ of section 4.

From equation (7), any error in $S'T$ will result in an equal and opposite error in X, that is, the distance moved by the member. This error can be calculated from equation (1) in section 3, with the following limitations:

(1) The count T (which corresponds to "D" in the system of Fig. 1) does not increase continuously between counts. The error in $S'T$ is therefore constant between counts, and is that of the system of Fig. 1 at points immediately following each pulse. The maximum positive error is therefore greater than the maximum negative error by the value of the scaling factor. The array for evaluating the errors is that of Fig. 7, without the row "D_X."

(2) If the scaling factor S' is limited to values less than unity, $S'_{-1} = 0$. The error is therefore that due to a scaling factor of $(R - 1)$ digits.

The error in the distance moved for a given scaling factor and given count T will be the error in X plus or minus one, (since D can have any value within one count interval without affecting X), including the effect of zeroing.

Thus the maximum error is negative and has a value

$$|\bar{F}|_{max} \simeq 1 + \frac{3(R-1)+7}{18} = \frac{3R+22}{18} \qquad (8)$$

The error in the count T for a given X can be found by a method similar to that used to evaluate the error in position for the original system of Fig. 1 (see section 5 and Appendix 2).

Since, from equation (7)

$$T = \frac{X}{1 - S'}$$

the error in T will be the error in X, evaluated from equation (8) divided by $(1 - S')$.

By applying the method used in Appendix 2 to evaluate this error it has been found that

$$|\bar{E}|_{max} \simeq \frac{1}{6} \cdot \frac{3(R-x)+52}{3 + 4(\frac{1}{4})^x} - 1 \qquad (9)$$

where x takes on the following values for different R:

R	x
2	1
3	2
4	3
5–9	4
10–37	5

As with equation (5), no complete proof has been found for equation (9). A similar assumption has been made to obtain both equations (5) and (9), and the assumption checked for values of R up to 10.

The electronics associated with this system is similar to that of the developed system of section 4 with $Q = 1$, and the accuracy of the two systems is comparable. This latter system has the advantage that only one row of marks and one sensing head are required, making the mechanical design considerably more simple.

8. Relationship with Multiplication of Binary Numbers

The basic system of section 3 can be shown to correspond to the multiplication of one binary number by another when each sub-product is rounded off to the point before being totalled. The multiplicand may extend indefinitely above and below the point; the multiplier is restricted to a given number of places below the point and none above. An example is shown below.

```
101110·110111
      ·1101
-------------
 10111·
  1100·
   000·
    11·
-------------
100110·
```

Similarly, the developed systems of section 4 correspond to multiplication where each sub-product is rounded off to a number of places below the point corresponding to the value of Q. The example is repeated for $Q = 1$.

```
101110·110111
      ·1101
-------------
 10111·1
  1011·1
   000·0
    11·0
-------------
100110·0
```

9. SIMILAR SYSTEMS IN CODED DECIMAL NOTATION

It is possible to devise systems of approximate scaling where the scaling factor is set in codes other than plain binary and for certain applications these may have practical advantages. In particular, some form of coded decimal notation would be useful. A pattern of marks in the 4, 2, 2, 1 code is shown in Fig. 6. Here, the count from the first row is approximately $\frac{4D}{10}$, from the second and third $\frac{2D}{10}$, from the fourth $\frac{D}{10}$, from the fifth $\frac{4D}{100}$, etc. Using such a pattern, the scaling factor may be set up in coded decimal notation.

To evaluate the errors in such a system is of far greater difficulty than evaluation in the binary system. No serious attempt has so far been made and the existence of such systems is merely noted.

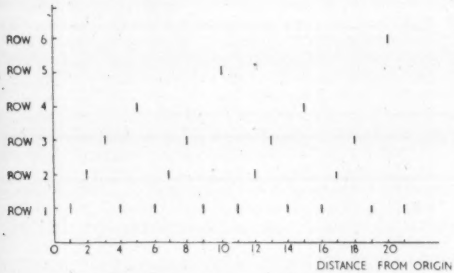

Fig. 6. Disposition of marks for decimal scaling

10. ACKNOWLEDGEMENTS

The authors wish to acknowledge their indebtedness to Mr. R. H. Tizard, who suggested the basic system of scaling together with many of its variants. They would also like to acknowledge the help of Mr. J. D. Gilbert in the tiresome work of checking the validity of some of the expressions.

This work has been carried out as part of the research programme of the National Physical Laboratory and is published by permission of the Director of the Laboratory.

11. REFERENCES

(1) GUILD, J. *The Interference Systems of Crossed Diffraction Gratings. Theory of Moiré Fringes* (London: Oxford University Press, 1956).

(2) BANE, W. T., and BARBER, D. L. A. *J. Sci. Instrum.*, **33**, p. 483 (1956).

(3) WINTER, A. J. *Electronics*, **26**, p. 214 (1953).

(4) TIZARD, R. H., BANE, W. T., and ATKINSON, M. P. Brit. Pat. Appl. No. 13,438/56.

APPENDIX 1

Referring to Fig. 1, let D be represented by the binary series

$$D = d_N(2)^N + \ldots + d_{-M}(2)^{-M}$$

The number of pulses generated by track 1 will be

$$C_1 = \tfrac{1}{2}[d_N(2)^N + \ldots + d_1(2)^1] + d_0.$$

Let $I_1 = \dfrac{D}{2} - C_1$

Then $I_1 = -\tfrac{1}{2}d_0 + \tfrac{1}{2}[d_{-1}(2)^{-1} + \ldots + d_{-M}(2)^{-M}]$

Let $I_2 = \dfrac{D}{4} - C_2$

Then $I_2 = -\tfrac{1}{2}d_1 + (\tfrac{1}{4})[d_0(2)^0 + d_{-1}(2)^{-1} + \ldots + d_{-M}(2)^{-M}]$

and so on for I_3, etc.

Let the scaling factor S be represented by the binary series

$$S = s_{-1}(2)^{-1} + \ldots + s_{-R}(2)^{-R}$$

Then the error in scaling according to the method described in section 2 of the paper is given by

$$E = s_{-1}I_1 + s_{-2}I_2 + \ldots$$

This sum is represented by the array of Fig. 7.

From this array it is seen that, irrespective of S, E will be a maximum when

$$d_{-1} = 1 \text{ and similarly for } d_{-2}, \text{ etc.}$$

Therefore, for a maximum, rows d_{-1} to $d_{-\infty}$ can be replaced by a single row whose d coefficient d_x is unity and whose elements are $\frac{1}{2}$, $\frac{1}{4}$, $\frac{1}{8}$, etc.

In a similar manner, for a minimum, this d coefficient is zero.

In section 3 of the paper, the following facts were deduced:

(1) Maximum positive error = maximum negative error.

(2) Maximum positive error for a given scaling factor occurs when $d_r \neq S_{-(r+1)}$ and $d_x = 1$ and maximum negative error occurs when $d_r = S_{-(r+1)}$ and $d_x = 0$.

These facts can be verified by examining the array of Fig. 7. (2) can be seen by considering the sum of row d_r and column $S_{-(r+1)}$ under the four possible combinations of these two digits. (1) follows from (2) since the sum of any column is zero, and with a given scaling factor the sum of maximum and minimum errors is the sum of all the numbers in columns whose "S" digit is "1." Thus the sum of maximum positive and negative errors is zero.

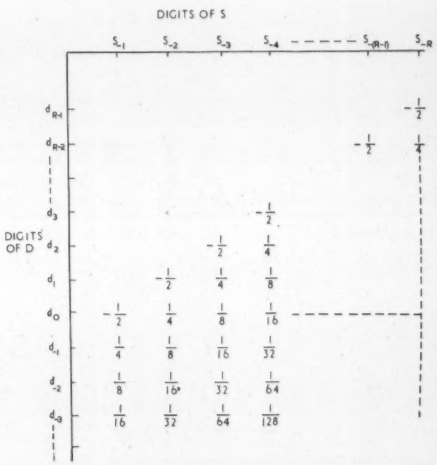

Fig. 7. Array for evaluating scaling errors in the basic system

Further, it can be seen that for a maximum error $S_{-1} = 1$ and S_{-R} must also be 1.

To determine the form of scaling factors which will produce the possibility of the largest errors it has been found necessary to show that the maximum error E_1 obtainable with scaling factor S_1 is equal to E_2, that obtainable for a scaling factor S_2 whose central $(R-2)$ digits are the complement of those of "S."

Now if E_1 occurs at a value of $D = D_1$ then E_2 will occur at a value D_2 where the central $(R-2)$ digits of D_2 are the complement of those of D_1. An error $-E_2$ for scaling factor S_2 will occur at a position D_3 whose central $(R-2)$ digits are the same as those of D_1 but whose extreme digits are the complement of those of D_1, and with $d_x = 0$ instead of 1.

Consider the sum of E_1 and $-E_2$. The contribution of row $d_{(R-1)} = -\frac{1}{2}$. That of row $d_{R-2} = -\frac{1}{4} + \frac{1}{4} + \frac{1}{4}$ (since $S_R = 1$ for both E_1 and $-E_2$) = 0. Similarly the contribution of all other rows except d_0 and d_x is equal to zero. For E_1, $d_0 = 0$ and $d_x = 1$, and for $(-E_2)d_0 = 1$ and $d_x = 0$. The combined contribution of these two rows is therefore

$$-\frac{1}{2} + \frac{1}{2} + \frac{1}{4} + \quad + \ldots + \frac{1}{2^R} + \frac{1}{2^R} = +\frac{1}{2}$$

Therefore

$$E_1 + (-E_2) = -\frac{1}{2} + 0 + 0 \ldots + \frac{1}{2} = 0$$

Therefore

$$E_1 = E_2$$

For a maximum positive error $d_0 = 0$ and $d_x = 1$, and $d_r \neq S_{(r+1)}$. If we incorporate these conditions in the array of Fig. 7, and move row d_x into the place of row d_0, we arrive at the array of Fig. 8(*a*). In this array, the $+\frac{1}{2}$ term due to d_x and S_{-1} has been omitted as it will always be present in considering maximum positive errors.

Now we have just shown that the sum of this array remains unaltered if we complement the central $(R-2)$ digits of both S and D. Therefore S_{-2} can be 0 or 1 and the maximum error will be the same. Make $S_{-2} = 0$ and incorporate this in the array. The resulting array is shown in Fig. 8(*b*), after removing all elements which are independent of digits S_{-3} to S_{-7}. That part of the array not enclosed by line OP is similar in form to that of Fig. 8(*a*), and its sum can therefore be made the same whether S_{-3} is 0 or 1. But the extra part of the array (within QP) will always be greater for $S_{-3} = 1$ than for $S_{-3} = 0$. Therefore S_{-3} is unity.

If we now incorporate this condition in the array of Fig. 8(*b*), remove all elements independent of S_{-4} to S_{-7}, omit row d_2 (since for $S_{-3} = 1$, $d_2 = 0$), the array of Fig. 8(*c*) can be deduced. Once more, that part of the array not enclosed by QR is similar to the array of Fig. 8(*a*) and its sum can be made the same whether S_{-4} is 0 or 1. Now, however, the elements enclosed by QR are negative and S_{-4} must be zero for a maximum positive sum of the array.

This process can be continued and it can be shown that the maximum sum of the array occurs when the central $(R-2)$ digits of "S" are alternately 0 and 1, starting with either 0 or 1, and with the first and last digits of "S" equal to unity.

Thus for an eight-digit number the values of S which will give a maximum possible error are 10101011 and 11010101. This form is true for "S" quoted to any number of places.

It can be seen from the array of Fig. 7 that the error E is:

$$E = d_x\left(\frac{1}{2}S_{-1} + \frac{1}{2^2}S_{-2} + \ldots\right) + \\ + d_0\left(-\frac{1}{2}S_{-1} + \frac{1}{2^2}S_{-2} + \frac{1}{2^3}S_{-3}\ldots\right) + \\ + \ldots + d_{R-1}\left(-\frac{1}{2}S_{-R}\right)$$

If the conditions $d_x = 1$, $S_{-1} = 1$, $S_{-R} = 1$ and $S_{-R} = d_{R-1}$ are inserted in this and $\bar{S}_{-R}$ represents the complement of S_{-R} (therefore $d_{R-1} = \bar{S}_{-R}$), then

$$E = \frac{1}{2} + \frac{1}{2^2}\cdot S_{-2} + \frac{1}{2^3}S_{-3} \ldots + \frac{1}{2^R} + \\ + \frac{1}{2^2}(\bar{S}_{-2}S_{-3} + \bar{S}_{-3}S_{-4} + \ldots + \bar{S}_{-(R-1)}\cdot 1 + \\ + \frac{1}{2^3}(\bar{S}_{-2}S_{-4} + \bar{S}_{-3}S_{-5} \ldots + \bar{S}_{-(R-2)}\cdot 1) + \ldots$$

The digits S_{-2} to $S_{-(R-1)}$ must be alternately 0 and 1 for

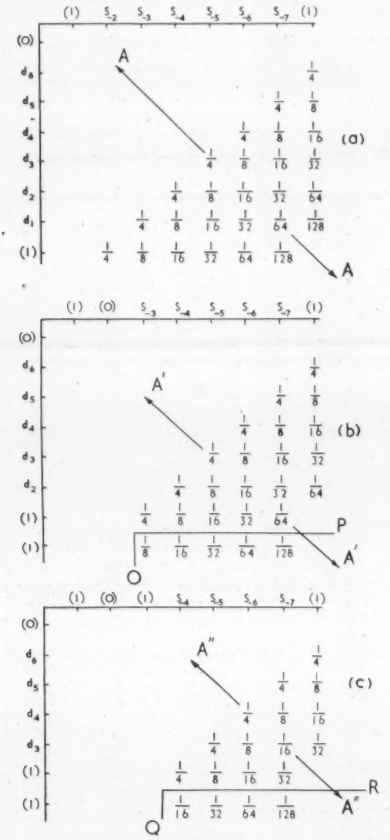

Fig. 8. Successive arrays used in evaluating scaling error

a maximum, with S_{-2} taking either value. If R is even and $S_{-2} = 1$ then $S_{-(R-1)} = 0$ and

$$(E)_{max} = \frac{1}{2} + \frac{1}{2^2} + \frac{1}{2^4} + \ldots + \frac{1}{2^{R-2}} + \frac{1}{2^R} + \\ + \frac{1}{2^2}\left(\frac{R}{2} - 1\right) + \frac{1}{2^3}(0) + \frac{1}{2^4}\left(\frac{R}{2} - 2\right) + \\ + \frac{1}{2^5}(0) + \ldots + \frac{1}{2^{R-2}} \times \left(\frac{R}{2} - \frac{R-2}{2}\right) \\ = \frac{1}{18}\left(3R + 7 + \frac{1}{2^{R-1}}\right)$$

If R is odd, and $S_{-2} = 0$, then $S_{-(R-1)} = 0$ and

$$(E)_{max} = \frac{1}{2} + \frac{1}{2^3} + \frac{1}{2^5} \ldots + \frac{1}{2^R} + \\ + \frac{1}{2^2}\left(\frac{R-1}{2}\right) + \frac{1}{2^4}\left(\frac{R-3}{2}\right) + \frac{1}{2^6}\left(\frac{R-5}{2}\right) \ldots \\ = \frac{1}{18}\left(3R + 7 - \frac{1}{2^{R-1}}\right)$$

The sum for any R is therefore

$$(E)_{max} = \frac{1}{18}\left[3R + 7 + \frac{1}{2}\left(-\frac{1}{2}\right)^R\right] \simeq \frac{1}{18}(3R + 7) \text{ for large } R$$

APPENDIX 2

The error referred to the source is the number of basic intervals by which D is in error for a particular value in the counter. This error is therefore the error in the count, divided by the scaling factor "S."

The distribution of errors in D along the D axis for a given scaling factor is therefore similar in form to the distribution of errors in the counter, the magnitudes of the errors being scaled up by the factor $1/S$. The positions at which maximum errors occur for a given S is therefore the same in both cases.

The value of S which produces a maximum possible error in D is not, however, the same as that which produces the maximum count error. For with a scaling factor $S_{-1} = S_{-2} = \ldots = S_{-(R-1)} = 0$ and $S_{-R} = 1$, the distance D can be in error by 2^{R-1} basic intervals, the distance the sensing head can move without changing the count.

If values of S between $\frac{1}{2}$ and 1 are considered, and S is quoted to R places, then $S_{-1} = 1$ and $S_{-R} = 1$, some indication of the form of S for maximum error in D can be obtained. The relationship between corresponding digits in S and D found in section 3 of the paper still holds, i.e.

For maximum positive error $d_n \neq S_{-(n+1)}$, $d_x = 1$

For maximum negative error $d_n = S_{-(n+1)}$, $d_x = 0$.

The value of S which will give a maximum value of

$$\frac{\textit{Sum of array of Fig. 7}}{\textit{Scaling factor}(s)} \qquad (a)$$

is required.

The sum of row d_x is always equal to the scaling factor and therefore, when divided by S, equals 1. This row can therefore be ignored, in searching for the value of S to give a maximum value to (a).

If we insert in Fig. 7 the condition S_{-1}, $S_{-R} = 1$ and $d_n \neq S_{-(n+1)}$ and leave out rows d_{-1}, d_{-2} . . . then only the array from row d_2 upwards is left, and $S_{-2} = 0$ will give a greater sum. Inserting this condition into the array, an array results similar in form to that of Fig. 8(a). The sum of the array is therefore the same whether S_{-3} is 0 or 1, and the factor (a) will therefore always be greater when $S_{-3} = 0$.

By extending the last argument, it can be shown that if any digit from s_{-4} to $s_{-(R-2)}$ inclusive is unity, it must be followed by a digit that is zero.

It has not been found possible to derive any further conditions for the required value of S. However, it seemed likely that the number would be of the form

$$\begin{aligned} s_{-1} &= 1 \\ s_{-2} &= 0 \\ s_{-3} &= 0 \\ s_{-4} &= 0 \\ &\vdots \\ s_{-(x+1)} &= 0 \\ s_{-(x+2)} &= 1 \\ s_{-(x+3)} &= 0 \end{aligned}$$

The latter group repeated until

$$s_{-R} = 1$$

The necessary conditions that have been derived allow this supposition to be checked by trial and error with a considerable reduction in the labour involved. For example, only 52 trials are necessary to check the assumption for R up to ten digits. Table 2 shows S for these values of R and it is seen that the assumption is correct for this range.

Table 2. *Scaling factors which produce a maximum displacement error*

R	S for maximum error referred to source	Corresponding value of x
1	1	
2	11	1
3	101	2
4	1001	3
5	10011	3
6	100101	3
7	1001011	3
8	10010101	3
9	100010101	4
10	1000101011	4

It has been assumed that this form for S applies for all R and a general expression has been derived for the corresponding error referred to the source with the effect of unrestricted zeroing included

$$|\bar{F}|_{max} = \frac{2}{3}\,\frac{3(R-x) + 25 + 2(-\frac{1}{2})^{R-x}}{3 + 4(\frac{1}{2})^x 1 - (-\frac{1}{2})^{R-x+1}} - 2 \qquad (10)$$

Using this equation, values of x can easily be found by trial and error for each value of R. They are given in Table 3.

Table 3. *Value of R and X*

R	x
2	1
3	2
4–8	3
9–21	4
22–46	5

Equation (10) may be conveniently approximated by dropping the last terms in both numerator and denominator. The worst error occurs for $R = 2$ and it amounts to 13%. For $R = 3$ it drops to 1% and afterwards is less than 0·25%.

Some experimental results on the impact sensitivity of mercury fulminate

By M. P. MURGAI, Ph.D.,* and A. K. RAY, Ph.D., Defence Science Laboratory, N.P.L. Buildings, New Delhi, India

[*Paper first received* 3 *February, and in final form* 29 *September*, 1958]

An account is given of some experimental results, namely, 50% explosion efficiency heights, times of impact and pressures on the impact sensitivity of mercury fulminate. These pressure estimations, together with similar measurements by other workers, have been compared to the theoretical calculations by one of the authors in an earlier publication.[6] There is a general agreement between the experimental and theoretical pressures.

In the investigations on the impact sensitivity of explosives described in the literature[1-4] one particular aspect of the problem—namely, a systematic estimation (experimental or theoretical) of pressures characterizing a specific level of efficiency of explosion—has been, comparatively speaking, less explored. Taylor and Weale[1] estimated the pressure required to detonate mercury fulminate by comparing it with that required to produce a dent in a lead slab. Bowden and others,[2, 5] in their experiments on the mechanism of initiation of explosives, have only made an approximate assessment of the upper limit of pressures reached in these investigations from considerations relating to the hardness and flow of metals. Recently Hollies, Legge and Morrison[3] have determined pressures that would cause 50% explosion efficiency in the initiator explosives by measuring the time of impact, 50% explosion efficiency height and the coefficient of restitution. However, they did not carry out these measurements for a wide range of heights and weights. The main objective of the present investigation was to carry out such measurements for a range of impacting weights and to compare these values with those based on the theory given by one of the authors in an earlier publication.[6] The experimental pressures have been determined from the measurements of the times of impact and rebound heights, etc.

The next section describes the experimental set-up—the impact sensitivity apparatus and the arrangement for measuring the times of impact. The experimental and theoretical results on the pressure estimation, as well as the percentage efficiency *versus* height curves for various masses, are then given, followed by a discussion of the results.

EXPERIMENTAL

A sketch of the apparatus used for studying the impact sensitivity of initiator explosives is shown in Fig. 1(*a*). On a solid circular base made of cast iron (weight about 130 lb) a vertical rod graduated in centimetres was erected. At the central part of the base there was a cylindrical cavity in which the anvil and the other striking devices fitted properly. The striking pin, made of high-speed steel, had a flat circular area of 0·178 cm^2 and fitted into a sleeve resting over the mild steel tempered anvil, the details being shown in Fig. 1(*b*). The height of the spherical balls could be adjusted by sliding the electromagnet along the vertical rod. The pole-piece of the electromagnet was made concave so that the striking balls would fit exactly in the same position every time. The central portion of the striking pin head and the pole of the concave electromagnet were always kept in the same vertical line. This was achieved by means of a plumb line, at one end of which was attached a cylindrical rod fitted with a spindle. While adjusting, the spindle was allowed to fit in a small hole in the pole of the concave electromagnet.

The fulminate of mercury was prepared in the laboratory. In carrying out the experiments attempts were made to have

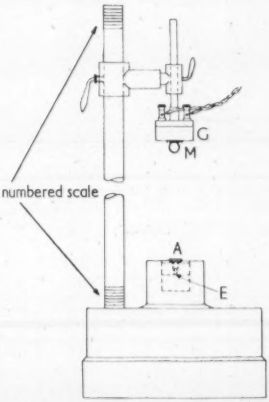

Fig. 1(*a*). Sketch of the impact sensitivity apparatus
E, explosive; *A*, striking pin; *G*, pole-piece; *M*, ball.

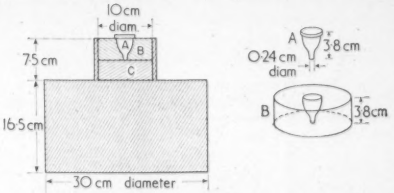

Fig. 1(*b*). Details of striking pin and anvil
A, striking pin; *B*, sleeve; *C*, anvil.

uniform crystal sizes throughout. Experiments were conducted with different balls at different heights. The heights were all taken in geometric progression to facilitate the probit analysis for obtaining 50% explosion efficiency heights. Precautions were taken to see that measured quantity of charges (0·1 to 0·2 g), spreading over a measured area (diameter 0·5 to 0·65 cm), were taken every time. In each weight and height at least fifty samples were tried and the

* Now a Research Fellow at University of Harvard, Massachusetts, U.S.A.

number of explosions at the first trial (with a sample of fulminate) were taken into account for calculating the explosion efficiency. In all the experiments the charge below the striking pin was kept under a static load and steel balls of various sizes were dropped on the striking pin by release from the electromagnetic. Whenever the ends of the striking pins were pitted by explosion, they were reshaped on a lathe and finally polished by using fine grain emery paper. This was necessary after ten to fifteen detonations. The initiator was placed in the dessicator between tests. In collecting data, the partial explosions were not taken into account.

The time of impact was measured by using an electronic counter, with a 10^6 c/s crystal oscillator, fitted in the circuit shown in Fig. 2. The pulses obtained from the oscillations

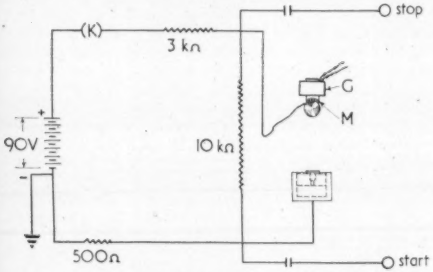

Fig. 2. The electrical circuit used with the electronic counter for measuring time of impact

are fed to a binary counting system, employing multivibrators, through a thyratron. A voltage pulse makes the thyratron conducting and a current passes. The latter is closed by a second pulse of the same magnitude. The time interval between the two pulses is displayed on the decaded units of the counter. Two such successive pulses were achieved in the above arrangement by connecting the ball through a wire (enamelled copper 30–35 s.w.g.) as shown in Fig. 2. At the instant the ball comes in contact with the striking pin a positive pulse is developed at A, which starts the counter, while a second voltage pulse developed at B, when the ball rebounds, stops the counter. Measurements of the times of contact with salts like mercury iodide, sodium chloride, etc., showed that they were sensibly the same. The authors assumed, therefore, that the times under actual conditions of explosion, would not be very much different from those with the non-explosive salts on the anvil and have taken the latter times for the corresponding masses and heights in the following analysis.

EXPERIMENTAL AND THEORETICAL RESULTS

If t be the experimentally measured time, h the height of fall of the ball, m its mass, e the coefficient of restitution (estimated value of e in the present observations is 0·3) and A the area of cross-section of the striking pin, the average pressure p is given by

$$p = [m2gh(1 + e)]/tA$$

Results of about one thousand explosions are given in the table. The figures in brackets in column one indicate the number of explosions in each case. The 50% explosion efficiency heights have been determined from both the graphical plot of efficiency *versus* height for each mass, given in Fig. 3, as well as by the method of probit analysis (based on the procedure given in Ref. 7). The last column gives the

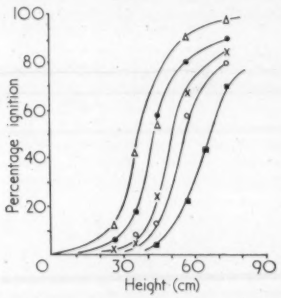

Fig. 3

△ m = 101·9 g. ○ m = 28 g.
● m = 60·8 g. ■ m = 19 g.
× m = 44·45 g.

theoretical pressures based on a treatment given by one of the authors earlier.[6] The two values of the pressures correspond to the two values of the elastic constants. The impact assembly consists of parts made of mild steel and a thin layer of the explosive, having elastic constants presumably less than that for the former. The latter gets deformed (plastically) more than the other members. In a

Experimental and theoretical results

Weight of steel ball W(g)	*Radii of balls* R(cm)	50% *explosion efficiency heights* h(cm) *Obtained graphically*	*Obtained by probit analysis*[6]	*Times of contact* (μs)	*Experimental pressures**	*Theoretical pressures*[6] (1)	(2)
					10^9 dyn/cm^2		
101·90 (250)	1·46	36	40	87	2·4	5·89	2·16
60·80 (230)	1·23	43	44	82	1·7	5·68	2·08
44·45 (250)	1·11	51	52	72	1·4	5·71	2·09
28·00 (250)	0·95	57	55	69	1·2	5·04	1·84
19·00 (130)	0·76	66	67	64	0·92	4·70	1·72

* Experimental values reported by other workers[1,3] are 1·56 – 1·95 × 10^9 and 1·06 × 10^9 dyn/cm^2 respectively.

composite assembly, the maximum stress generated during impact would very likely be determined by the least elastic of the members, and the situation would not be expected to change radically in this assembly where the least elastic member is placed. When applied to the above it would mean that the maximum stresses produced should not be very much different with respect to the position of the explosive; that is, whether it is under the striking pin or above it. For the purposes of calculating pressures, therefore, it is assumed to be above the striking pin. Having made this assumption, its plastic deformation and the change in the elastic constants on the rate of loading may be taken into account in a general way by considering two types of impact —one steel-to-steel and the other from steel to a solid having an elastic constant one-tenth that of steel. That is the basis of the two sets of calculations given in the table and shown as (1) and (2) in the last column.

DISCUSSION

In view of the difficulties of the problem enumerated above, the agreement of the theoretical pressures may be considered reasonable. (It is interesting to note that the expression for the peak pressure in a plane stress wave in a cylindrical rod namely, $p = \rho cv$, ρ being the density of the medium, c the velocity of sound and v the particle velocity, when applied to the above assembly gives pressures of the correct order of magnitude if v is assumed to be equal to the velocity of the fall of the ball, namely $2gh$, h being the height of fall. The pressures calculated for minimum and maximum values of h range from $1{\cdot}05 \times 10^9$ to $1{\cdot}37 \times 10^9$ dyn/cm^2.) The systematic decrease in experimental pressure is due to the fact that, for such an assembly, lesser weights require lesser energies (which would generate lesser impulsive stresses on the explosive sample) to cause explosions. These energies (and hence the pressures) are to a very great extent determined, in addition to the general rigidity of the apparatus, by the other dynamical details like hardness of the members of the striking assembly, the method of making the explosive pellet, crystal size distribution, shape and the work hardening of the striking pin and the anvil while running the experiment. It is indeed difficult to take account of all these factors in a straightforward scheme of mathematical analysis of the problem. While these features, therefore, complicate the agreement of the experimental and theoretical values, they would also explain some of the inconsistencies between the present results and that of some of the other workers mentioned below.

The product of mass and height for 50% efficiency change by a factor of about three, throughout the range of weights employed by the authors. This (as also do some results relating to the heights for some individual masses) seems to be in contradiction to the results of Taylor and Weale[4] for mercury fulminate, who observed that this product remains sensibly constant. A detailed examination of this point, however, shows that the inconsistency is only an apparent one.* As mentioned by these authors,[4] it was not true for all their impact machines, especially those which showed lack of rigidity due to various causes like looseness of the explosive pellet, permanently deformed striking pins, etc. In fact these authors mention in their paper that in one of their set-ups, when the hardened steel rollers were replaced by mild steel pistons (the present authors used high-speed steel striking pins) "not only much greater energies were required to cause ignitions but smaller weights appeared to produce ignitions, with lesser kinetic energies than did the larger weights." This is similar to the present authors' observations. Taylor and Weale also mention that this departure from the constant mxh criterion had been observed even earlier. Workers[2, 3, 8] in this field of investigation, after Taylor and Weale, have also not confirmed the universality of this relation. For example, the calculations from the results of Powell, Skelly and Ubbelohde[8] and Hollies, Legge and Morrison,[3] show that this product changes by a factor of about 2 and 1·5 respectively for mercury fulminate, and more for other initiator explosives. The range of impacting weights used by these workers, however, is much smaller than used by the present authors.

It appears that these rather divergent results for different impact machines are due to the various differences in their dynamical details already referred to. These apparently go a long way to determine their overall performance. This seems to be the explanation of the apparent contradictions in the present results mentioned above. While this would also partly explain the discrepancy between the experimental and theoretical mass *versus* height curve discussed by one of the authors[6] in an earlier publication, it may be mentioned here that the basis of this theoretical analysis, namely the assumption of constant pressure characterizing 50% explosion efficiency, would not strictly hold for all assemblies and would be true only for some typically rigid ones.

These studies relating to the measurement of maximum pressures, and pressure time relations are of interest in considering theoretically the hypothesis of hot spot formation prior to the initiation of explosion, as done by one of us in an earlier publication.[6]

ACKNOWLEDGEMENTS

The authors are grateful to Prof. D. S. Kothari, Scientific Adviser to the Minister of Defence, Government of India, for his interest during the course of this investigation. Thanks are due to Dr. Thiruvenkatachar, Mr. A. N. Murty, Mr. M. G. Rao and Mr. D. Ray for useful discussions.

REFERENCES

(1) Taylor, W., and Weale, A. *Trans Faraday Soc.*, **34**, p. 995 (1938).
(2) Bowden, F. P., and Gurton, O. A. *Proc. Roy. Soc. A*, **198**, 350 (1949).
(3) Hollies, N. R. S., Legge, N. R., and Morrison, J. L.: *Canad. J. Chem.*, **31**, p. 746 (1953).
(4) Taylor, W., and Weale, A. *Proc. Roy Soc. A*, **138**, p. 92 (1932).
(5) Bowden, F. P., and Yoffe, A. D. *The initiation and growth of explosion* (London: Cambridge University Press, 1952).
(6) Murgai, M. P. *J. Chem. Phys.*, **25**, p. 762 (1956).
(7) Fisher, R. A., and Yates, E. *Statistical Tables for Biological, Agricultural and Medical Research*, p. 8 (London: Oliver and Boyd Ltd., 1948).
(8) Powell, W. J., Skelly, H., and Ubbelohde, A. R. *Phil. Trans A*, **241**, p. 287 (1948).

* The authors are grateful to the referees, who examined this point in greater detail by fitting the following relation similar to Taylor and Weale to the data in the table

$$W(h - 33{\cdot}9) = 619$$

The presence of a factor as much as 33·9 indicates that the apparatus was not rigid and for that reason the value of the pressures would be less than that given in the Table. The above relation fits quite well throughout except, unaccountably, for the ball of radius 1·11 cm.

Alternative method of correlating forced convection heat transfer data

By P. H. PRICE, B.Sc., Ph.D., Assoc.I.Mech.E., Department of Mechanical Engineering, University of Manchester

[*Paper first received* 27 *August, and in final form* 3 *October*, 1958]

The use of a heat transfer coefficient as a general parameter of forced convection heat transfer is shown to be unsatisfactory, and an alternative correlation making explicit allowance for pipe wall temperature variations is derived. In the derivation it is assumed that radial heat transfer in the fluid may be represented as due to an effective conductivity, and that longitudinal heat transfer is by fluid transport only. The effective conductivity and the fluid forward velocity may be arbitrary functions of radial distance.

The correlation shows that the difference between wall and mean fluid temperature at any distance along the tube is composed of an entry condition term which diminishes with distance along the pipe, plus a series of terms due to temperature variations along the pipe wall. The values of the coefficients of these terms have been calculated for two ideal cases, and experimental values are being sought. Some implications of the correlation are discussed.

NOTATION

A, constant.
B, constant.
C, constant.
D, pipe diameter.
K, effective fluid thermal conductivity including turbulence.
L, pipe length.
R, function satisfying equation (3).
V, fluid mean velocity.
Z, function of z.

a, pipe radius.
c, specific heat.
f, functional symbol.
g, functional symbol.
h, heat transfer coefficient.
k, true fluid thermal conductivity.
r, distance from axis of pipe.
s, z/L.
v, fluid local velocity.
z, distance parallel to axis of pipe.

β, constant.
γ, constant.
δ, thickness of laminar sub-layer.
θ, local temperature.
θ_m, mean temperature.
λ, distance parallel to axis of pipe.
ν, fluid kinematic viscosity.
ρ, density.
ϕ, wall temperature.

INTRODUCTION

Exact analytical solutions of forced convection heat transfer problems are possible only in extremely simple cases; consequently a large number of experimental investigations have been made, and their results expressed in terms of dimensionless groups. Comparison of the results obtained in different investigations shows discrepancies which may amount to a factor of two. Such discrepancies necessitate the use of plant design data obtained under conditions as close as possible to those under which the projected plant will operate; hence the large number of investigations which have been reported. If closer correlation were possible, greater confidence in the data would be justified, and plant design using these data would require less preliminary experiment.

An expression used almost universally in reporting forced convection data is the "heat transfer coefficient." This is the rate of heat transfer between fluid and pipe wall per unit area of wall, divided by the difference between some mean fluid temperature and a mean wall temperature. The mean fluid temperature is usually taken as the "mixing cup" temperature since this is of importance in practice, and is also the most conveniently measured mean temperature. To avoid difficulties arising in taking mean fluid and wall temperatures along the length of the pipe, attention may be restricted to a short length of pipe in which wall and mean fluid temperatures may be considered constant, and a local heat transfer coefficient derived. In plant design an overall heat transfer coefficient is a great help if available, but existing overall coefficients may not be relevant to new plant.

The concept of a heat transfer coefficient may have been carried over into forced convection studies from Newton's experimentally derived cooling law in natural convection. Alternatively, it may have arisen by considering a fluid in highly turbulent pipe flow to consist of a thin sub-layer of fluid near the wall in laminar flow surrounding a core in which turbulence maintains a constant temperature over any cross-section. The temperature of the core is very nearly the mixing cup temperature because the amount of fluid flowing in the laminar sub-layer is small. The thin laminar sub-layer is then the only obstacle to heat transfer between fluid and wall; neglecting its heat capacity, a heat transfer coefficient may be regarded as operating across it. In this case, the local heat transfer coefficient is constant along the pipe, and is equal to the overall coefficient if arithmetic mean values of wall and mixing cup fluid temperature along the pipe are used. This coefficient may be written as $h = k/\delta$, where k is the thermal conductivity of the laminar sub-layer and δ is its thickness.

The factors affecting δ would appear to be fluid velocity V (mean velocity and maximum velocity are almost identical if the laminar layer is thin), and kinematic viscosity ν. The diameter of the tube should not be important, since it is assumed large compared with δ. Hence δ is proportional to ν/V, a reasonable result indicating that the thickness of the laminar sub-layer varies directly as viscosity and inversely as velocity. Thus the heat transfer coefficient should be proportional to kV/ν, which means that Nusselt number hD/k is proportional to Reynolds number VD/ν. This result is not found to hold in practice.

Experimental attempts to resolve this situation have involved the study of additional variables, particularly fluid specific heat, and simplification by considering only local heat transfer coefficients. Theoretical considerations have assumed the existence of a buffer layer between the laminar layer and the turbulent core, or have pursued analogies between transfer of mass, momentum, and heat. None of

these procedures have produced a satisfactory correlation over a wide field. In this paper it is hoped to provide a possible basis for such a correlation.

It is not proposed that this correlation should generally replace the heat transfer coefficient as a design parameter, but that it should enable accurate allowance to be made for effect of pipe or heater temperature distribution when a heat transfer coefficient is chosen for a particular design purpose. Such an effect could arise, for example, in the application of results from a fuel can heat transfer rig having constant or linear heater temperature, to a highly rated nuclear reactor in which the fuel temperature follows a cosine function.

THEORY OF ALTERNATIVE CORRELATION

The following assumptions will be made:

(1) The fluid velocity profile does not vary along the length of the pipe.

(2) The conduction of heat in the fluid parallel to the axis of the pipe may be ignored in comparison with the transport of heat in this direction.

(3) The effective radial thermal conductivity K, consisting of the superimposed effects of true conductivity and turbulent diffusion, will be assumed to depend on radial distance r.

(4) The effective conductivity K, specific heat c, and density ρ, will be assumed independent of temperature θ. This assumption is valid for K, which is largely governed by turbulence; it is not particularly good for c and ρ.

If z is measured parallel to the axis of the pipe, a heat balance on the element of fluid between r and $r + dr$, z and $z + dz$, gives the equation:

$$c\rho vr\frac{\partial\theta}{\partial z} = \frac{\partial}{\partial r}\left(Kr\frac{\partial\theta}{\partial r}\right) \tag{1}$$

In order to solve this equation it is necessary to know:

(1) K and v in terms of r.

(2) The fluid temperature distribution in terms of r at the initial value of z.

(3) The pipe wall temperature distribution in terms of z. This must also be the temperature of the fluid at the wall.

For simple cases, solutions of equation (1) have been found by Graetz,[1] Nusselt,[2] Lévêque[3] and Latzko.[4]

Equation (1) is very similar to equation (2) governing the unsteady flow of heat in a long cylinder in which the thermal properties may depend on distance r from the axis of the cylinder

$$c\rho r\frac{\partial\theta}{\partial t} = \frac{\partial}{\partial r}\left(kr\frac{\partial\theta}{\partial r}\right) \tag{2}$$

In this equation t denotes time and k denotes thermal conductivity.

Equation (2) has been the subject of much study, but even if c, k and ρ are assumed constant, it has not proved possible to relate the rate of heat transfer to or from the cylinder to a difference between cylinder surface temperature and cylinder mean temperature. This would be exactly analogous to determining a local heat transfer coefficient for forced convection. It follows that the concept of a forced convection heat transfer coefficient has no satisfactory theoretical basis.

It becomes apparent that the temperature distribution in the heated or cooled fluid is governed by the initial temperature distribution in the fluid and by the temperature or heat transfer condition existing at the fluid boundary. If K, c and ρ are independent of temperature, then the effects of initial temperature and boundary condition are independent, and may be evaluated separately. Even if K, c and ρ are not independent of temperature, the effect of the initial temperature distribution dies away. The effect of boundary condition is therefore the major consideration.

Boundary conditions of major importance in forced convection are:—

(i) Prescribed wall temperature.

(ii) The concentric parallel or counter-flow heat exchanger.

The case of prescribed heat flux into the fluid should be mentioned. Although the fluid mean temperature is defined immediately in this case, it may be of interest (as in the case of the nuclear reactor) to find the maximum wall temperature occurring. This may be done by inverting equation (5).

In this section attention will be concentrated on the prescribed surface temperature case, but some mention of heat exchanger conditions will be made in paragraph (viii) of the discussion.

In the case of a conducting cylinder, an expression for the temperature distribution in terms of an arbitrary wall temperature history may be derived by Duhamel's method. Such an expression has some use on conduction problems and will lend itself to the purpose of this section. It is first necessary to find a solution of equation (1) for the case of fluid at zero temperature entering a pipe of constant wall temperature ϕ_0. It is shown in Appendix 2 that this solution is

$$\theta = \phi_0 - \phi_0\sum_{n=1}^{\infty} A_n R(r, \gamma_n)\exp(-\gamma_n z)$$

where R satisfies the equation

$$\frac{d}{dr}\left(Kr\frac{dR}{dr}\right) + \gamma c\rho vrR = 0 \tag{3}$$

γ_n satisfies the equation $R(a, \gamma_n) = 0$ where a is the radius of the pipe, and

$$A_n = \int_0^a vrR(r, \gamma_n)dr \Big/ \int_0^a vrR^2(r, \gamma_n)dr$$

By Duhamel's method, the fluid temperature distribution θ due to wall temperature variation $\phi(\lambda)$ in $0 \leqslant \lambda \leqslant z$ is

$$\theta = \sum_{n=1}^{\infty}\gamma_n A_n R(r, \gamma_n)\exp(-\gamma_n z)\int_0^z \phi(\lambda)\exp(\gamma_n\lambda)d\lambda$$

If V is the mean fluid velocity, the mixing cup mean temperature θ_m is given by

$$\begin{aligned}\theta_m &= \frac{2}{a^2V}\int_0^a rv\theta dr \\ &= \frac{2}{a^2V}\sum_{n=1}^{\infty}\gamma_n A_n\exp(-\gamma_n z)\int_0^a rvR(r,\gamma_n)dr\int_0^z\phi(\lambda)\exp(\gamma_n\lambda)d\lambda \\ &= \sum_{n=1}^{\infty} B_n\gamma_n\exp(-\gamma_n z)\int_0^z\phi(\lambda)\exp(\gamma_n\lambda)d\lambda \end{aligned} \tag{4}$$

But

$$\begin{aligned}\int_0^z\phi(\lambda)\exp(\gamma_n\lambda)d\lambda &= \left[\frac{\phi(\lambda)\exp(\gamma\lambda)}{\gamma}\right]_0^z - \frac{1}{\gamma}\int_0^z\frac{d\phi}{d\lambda}\exp(\gamma\lambda)d\lambda \\ &= \exp(\gamma z)\left[\frac{1}{\gamma}\phi(z) - \frac{1}{\gamma^2}\frac{d\phi(z)}{dz} + \frac{1}{\gamma^3}\frac{d^2\phi(z)}{dz^2} - \cdots\right] \\ &\quad - \left[\frac{1}{\gamma}\phi(0) - \frac{1}{\gamma^2}\frac{d\phi(0)}{dz} + \frac{1}{\gamma^3}\frac{d^2\phi(0)}{dz^2} - \cdots\right]\end{aligned}$$

Therefore

$$\theta_m = \sum_{n=1}^{\infty} B_n\left[\phi(z) - \frac{1}{\gamma_n}\frac{d\phi(z)}{dz} + \frac{1}{\gamma_n^2}\frac{d^2\phi(z)}{dz^2} - \ldots\right]$$
$$- \sum_{n=1}^{\infty} B_n \exp(-\gamma_n z)\left[\phi(0) - \frac{1}{\gamma_n}\frac{d\phi(0)}{dz} + \frac{1}{\gamma_n^2}\frac{d^2\phi(0)}{dz^2} - \ldots\right]$$

If the fluid initial temperature is θ_0, instead of zero, a term for the decay of initial temperature must be added to this expression to give

$$\theta_m = \sum_{n=1}^{\infty} B_n\left[\phi(z) - \frac{1}{\gamma_n}\frac{d\phi(z)}{dz} + \frac{1}{\gamma_n^2}\frac{d^2\phi(z)}{dz^2} - \ldots\right]$$
$$- \sum_{n=1}^{\infty} B_n \exp(-\gamma_n z)\left[\phi(0) - \frac{1}{\gamma_n}\frac{d\phi(0)}{dz} + \frac{1}{\gamma_n^2}\frac{d^2\phi(0)}{dz^2} - \ldots\right]$$
$$+ \theta_0 \sum_{n=1}^{\infty} B_n \exp(-\gamma_n z)$$

It may be shown analytically, or by physical considerations, that

$$\sum_{n=1}^{\infty} B_n = 1$$

In a very long tube in which entry conditions may be ignored

$$\theta_m = \phi - C_1\frac{d\phi}{dz} + C_2\frac{d^2\phi}{dz^2} - \ldots \qquad (5)$$

where ϕ is the pipe temperature at the point where the mean fluid temperature is θ_m. In a tube of moderate length, the entry condition effect approximates to

$$(\theta_0 - \phi_0)B_1 \exp(-\gamma, z)$$

The coefficients C_1, C_2, . . . , etc., depend only on the fluid properties and type of flow existing. Values of C_1, C_2 and C_3 calculated for laminar flow, and for slug flow, are given in Appendix 1. In slug flow the fluid velocity is assumed to be constant over the cross-section; this is a crude approximation to turbulent flow.

It is suggested that in fundamental heat transfer investigations these coefficients might be found in terms of the variables mentioned in paragraph (i) of the discussion. For design purposes, a known local heat transfer coefficient for appropriate flow but different temperature conditions may be modified as suggested in paragraph (ii) of the discussion. An overall heat transfer coefficient leads directly to a value of the fluid exit temperature; such information may be modified from one wall temperature condition to another for the same fluid flow conditions as described in paragraph (iii) of the discussion.

DISCUSSION

(i) In the laminar flow coefficients k represents the true thermal conductivity, and in the slug flow coefficients K represents an effective conductivity. In turbulent flow, a more detailed examination of the preceding analysis suggests that the dimensional terms in C_n should be

$$(VD^2c\rho)^n/kK^{n-1} \qquad (6)$$

where k is evaluated at the temperature of the laminar sublayer, and c is at the mean temperature of the fluid.

Physical and dimensional considerations indicate that $K = c\rho VD/f(Re)$. Inserting this into expression (6) gives

$$VDc\rho D^n f^{n-1}(Re)/k$$

Expression (5) then becomes

$$\theta_m = \phi - \beta_1\frac{VDc\rho}{k}\frac{D}{L}\frac{d\phi}{ds} + \beta_2\frac{VDc\rho f(Re)}{k}\left(\frac{D}{L}\right)^2\frac{d^2\phi}{ds^2} \cdots$$

where β_1, β_2, . . . , etc., are dimensionless constants

$s = z/L$ and is dimensionless

L = length of pipe considered.

Rearranging

$$\frac{k(\theta_m - \phi)f(Re)}{VDc\rho} = -\beta_1 f(Re)\frac{D}{L}\frac{d\phi}{ds} + \beta_2 f^2(Re)\left(\frac{D}{L}\right)^2\frac{d^2\phi}{ds^2} \cdots$$

So for a particular form of wall temperature distribution, of which ϕ_w is a parameter, the appropriate dimensionless heat transfer correlation is seen to be

$$\frac{k(\theta_m - \phi)f(Re)}{\phi_w VDc\rho} = g\left[\frac{D}{L}f(Re)\right]$$

The form of f depends only on the geometry of the pipe or duct in which the flow takes place. The function g is dependent upon this, and also on the nature of the temperature distribution along the pipe.

(ii) The conservative reader who is familiar with a heat transfer coefficient defined in the notation of this paper as

$$h = \frac{c\rho VD}{4(\phi - \theta_m)}\frac{d\theta_m}{dz}$$

may be interested to substitute into this expression for θ_m from equation (5).

If $d^2\phi/dz^2$ is ignored, this gives

$$h = c\rho VD/4C_1$$

showing that C_1 is related to existing concepts of a heat transfer coefficient.

If it is assumed that K is very large, as in extremely turbulent flow, it follows from expression (6) that C_2 and higher coefficients may be ignored, and

$$h = \frac{c\rho VD}{4C_1} = \frac{c\rho VD}{4}\frac{d^2\phi}{dz^2}\Big/\frac{d\phi}{dz}$$

showing that wall temperature variations must be considered even in local heat transfer coefficients for highly turbulent flow.

(iii) Neglecting second and higher order derivatives in equation (5) gives

$$\theta_m = \phi(z - C_1)$$

which states that the mean fluid temperature at any point is equal to the wall temperature at a distance C_1 earlier. This is an approximation only.

(iv) In the case of flow parallel to the fins of a finned surface the correlation (5) still applies, but with different values of C_1, C_2, etc.

(v) In the case of flow parallel to two surfaces at different temperatures, the mean fluid temperature is expressed as the sum of two series each similar to (5), but with different values of C_1, C_2, etc., in each series.

(vi) In the case of flow along a pipe of constant wall temperature, taking the wall temperature as zero, Appendix 2 shows that the fluid temperature is

$$\theta = \theta_0 \sum_{n=1}^{\infty} A_n R(r, \gamma_n) \exp(-\gamma_n z)$$

and

$$\theta_m = \theta_0 \sum_{n=1}^{\infty} B_n \exp(-\gamma_n z)$$

After the higher harmonics have damped out, this becomes

$$\theta_m = \theta_0 B_1 \exp(-\gamma, z)$$

(vii) This analysis does not apply to flow parallel to surfaces carrying high transverse fins. In the case of transverse fins or "turbulence promoters" expression (4) is of interest. It shows that a series of temperature "harmonic modes" exist in the fluid, each damping out with its own time constant γ_n. Thus the higher harmonics damp out faster than the first harmonic, and after a certain distance along the pipe heat remains only in the first harmonic mode from which it is transferred relatively slowly. A similar effect occurs in the solution of conduction problems using Fourier series. If the fluid is then caused in some way to mix, the resulting temperature is approximately constant across the pipe, and some heat from the first harmonic mode is moved into higher modes from which it is transferred more easily.

(viii) The concentric heat exchanger may have fluids in parallel or counter flow. Let subscripts 1 and 2 refer to inner and outer fluid respectively; symbols without suffixes refer to both tubes. Take z increasing in the direction in which

$$\frac{1}{a_1^2 c_1 \rho_1 V_1} + \frac{1}{(a_2^2 - a_1^2) c_2 \rho_2 V_2} > 0$$

This makes the difference in mean temperatures of the fluids diminish as z increases. If this expression is zero, the difference in mean temperatures remains constant whatever heat transfer assumptions are made.

Let $\bar{\theta}$ be the equilibrium value to which the temperatures of the two fluids converge. Then it may be shown that the temperature distributions in each fluid are of the form

$$\theta = \bar{\theta} + \sum_{n=1}^{\infty} A_n R(r, \gamma_n) \exp(-\gamma_n z)$$

The values of A_n are chosen to suit the entry conditions of the respective fluids. In the parallel flow exchanger the higher harmonics damp out in both fluids. In the counter flow exchanger the harmonics damp out in the fluid flowing in the direction of z increasing; the harmonics build up in the other fluid as it flows in the direction of z decreasing. Therefore in moderately long exchangers of either type a correlation is

$$\theta = \bar{\theta} + B_1 \exp(-\gamma_1 z)$$

in the fluid flowing in the direction of z increasing. $\bar{\theta}$, B_1 and γ_1 depend upon flow conditions, thermal properties and entry temperatures of each fluid.

(ix) Much more theory may be constructed on the basis described in this paper. Before proceeding with this, it was considered desirable to examine the validity of the results so far obtained. Since published results do not include sufficient information on wall temperature distribution to permit their analysis in the terms of this paper, an apparatus for this purpose has been constructed in this Department, and an experimental programme is proceeding.

REFERENCES

(1) GRAETZ, L. *Ann. Phys.* [*Leipzig*], **25**, p. 337 (1885).
(2) NUSSELT, W. *Z. d. Ver deutsch. Ing.*, **54**, p. 1154 (1910).
(3) LÉVÊQUE, J. *Ann. d. mines* (12), **13**, pp. 201, 305, 381 (1928).
(4) LATZKO, H. *Z. f. angew. Math. u. Mech.*, **1**, p. 268 (1921).

APPENDIX 1

Values of C_1, C_2 and C_3 for laminar flow and slug flow

	Laminar flow	*Slug flow*
C_1	$\frac{11}{192}\left(\frac{VD^2c\rho}{k}\right)$	$\frac{1}{32}\left(\frac{VD^2c\rho}{K}\right)$
C_2	$\frac{59}{15360}\left(\frac{VD^2c\rho}{k}\right)^2$	$\frac{1}{768}\left(\frac{VD^2c\rho}{K}\right)^2$
C_3	$\frac{129737}{495452160}\left(\frac{VD^2c\rho}{k}\right)^3$	$\frac{11}{196608}\left(\frac{VD^2c\rho}{K}\right)^3$

APPENDIX 2

Solution of equation (1) *for constant wall temperature and zero initial fluid temperature*

This is found from the case of fluid at temperature θ_0 entering a pipe of zero wall temperature.

Suppose that a solution of equation (1) exists in the form $\theta = R(r)$. $Z(z)$ where R is a function of r only, and Z is a function of z only. Then

$$c\rho v r R \frac{dZ}{dz} = Z \frac{d}{dr}\left(Kr \frac{dR}{dr}\right)$$

$$\frac{1}{Z}\frac{dZ}{dz} = \frac{1}{c\rho v r R}\frac{d}{dr}\left(Kr \frac{dR}{dr}\right)$$

But the left-hand side of this equation is a function of z only, and the right-hand side is a function of r only, therefore each side of the equation must be a constant

$$\frac{1}{Z}\frac{dZ}{dz} = \frac{1}{c\rho v r R}\frac{d}{dr}\left(Kr \frac{dR}{dr}\right) = -\gamma$$

The minus sign is chosen in order that the temperature should diminish as z increases. It follows that

$$Z = \exp(-\gamma z)$$

and

$$\frac{d}{dr}\left(Kr \frac{dR}{dr}\right) + \gamma c\rho v r R = 0 \qquad (3)$$

Physical considerations indicate that by choosing suitable values of γ, denoted by γ_1, γ_2, etc., a set of solutions of equation (3) exists, each solution vanishing at $r = a$, the radius of the pipe. Let them be denoted by $R(r, \gamma_n)$. It is easy to show that

$$\int_0^a v r R(r, \gamma_p) R(r, \gamma_q) dr = 0 \quad \text{if} \quad p \neq q$$

Then if it is assumed that unity can be expressed as an infinite sequence of these functions, the initial temperature distribution θ_0 may be written

$$\theta_0 = \theta_0 \sum_{n=1}^{\infty} A_n R(r, \gamma_n)$$

where

$$A_n = \int_0^a v r R(r, \gamma_n) dr \Big/ \int_0^a v r R^2(r, \gamma_n) dr$$

therefore

$$\theta = \theta_0 \sum_{n=1}^{\infty} A_n R(r, \gamma_n) \exp(-\gamma_n z)$$

Hence the solution for the case of fluid at zero temperature entering a pipe of constant temperature T_0 is

$$\theta = \theta_0 - \theta_0 \sum_{n=1}^{\infty} A_n R(r, \gamma_n) \exp(-\gamma_n z)$$

Method for size-distribution determinations of non-volatile droplets by electron microscopy

By W. J. Harris, Chemical Defence Experimental Establishment, Porton Down, Wilts.

[*Paper received* 21 *July*, 1958]

The droplets are sampled on a thin wet film of gelatin solution and washed away when the gelatin has set. Replicas are taken of the impressions left by the spread-out droplets. The replica diameters are converted to droplet diameters by the application of a spread factor which although determined for larger droplets by light microscopy may be reliably applied to droplets in the electron microscope size range.

When liquid droplets are sampled on to a clean solid surface which they wet, they generally spread to an equilibrium position in which they assume the nature of plano-convex lenses. May* has related the diameter of such a lens to the diameter of the droplet producing it by the application of a spread factor obtained in terms of the focal length of the lens and the refractive index and angle of contact of the liquid, and has developed a technique for light microscope size-distribution determinations of non-volatile droplets down to about 1 μ diameter. For obvious reasons this method of making measurements on the droplets themselves cannot be used for electron microscopy even with seemingly non-volatile droplets.

The method to be described is applicable to droplets of non-volatile liquids which do not mix with water. Electron microscope measurements are made on replicas of the spread-out droplets and a spread factor determined by light microscopy is applied to convert these measurements to actual droplet sizes. Although the spread factor determination is made on larger droplets it may be reliably applied to droplets in the electron microscope range.

METHOD

The droplets are sampled, either by sedimentation or electrostatic precipitation, on a thin wet film of a 2% gelatin-water solution on a glass slide and spread out to form biconvex lenses on the surface. When the film has dried out, the liquid from the droplets is removed by washing with some suitable solvent which does not attack the gelatin (e.g. benzene) leaving behind replica impressions of the lenses (Fig. 1). The gelatin replica is flooded with firstly a 2% collodion-amyl acetate solution and then, when dry, a 10–20% solution. The dried out collodion film is mechanically stripped with transparent sticky tape which is separated from the portion of replica to be examined by cigarette paper. It is advisable to select an area for examination near the centre of the dried gelatin film as sometimes distortion of the droplet replicas occurs near the edges during drying. Similarly, a reasonably thick collodion film minimizes the risk of producing distortion during mechanical stripping. The collodion negative replica is metal shadowed and carbon is evaporated on to it. The composite collodion-carbon film is cut into $\frac{1}{8}$ in. squares which are allowed to float collodion surface downwards on the surface of a dish of distilled water. The floating portions of film are caught on electron microscope specimen screens resting on small pieces of filter paper and these, when dry, are placed on a filter paper wick soaked in butyl acetate. In 30–60 s the collodion of the composite film is completely dissolved away leaving positive carbon replicas mounted on the specimen screens. When the butyl acetate has evaporated from the small pieces of filter paper, the specimen screens may be lifted off, examined in the electron microscope and the diameters of the droplet replicas measured. It has been found that mounting the specimen screens on the small portions of filter paper and using butyl acetate considerably reduces the likelihood of the carbon replicas being damaged during handling or drying out.

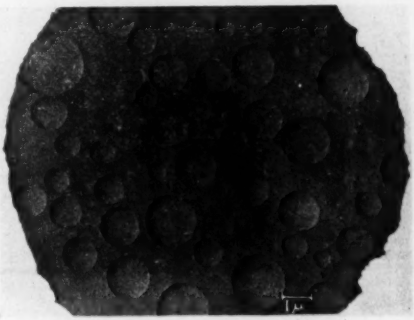

Fig. 1. Carbon replica of lens impressions

DETERMINATION OF THE TRUE DIAMETER OF THE DROPLET

If a spread-out droplet on the dried gelatin is viewed with a light microscope using a plane mirror without condenser, it will be observed that an image of a distant object (e.g. bars of a window) will be formed above the droplet. When the droplet is washed away another image will be formed, this time beneath the droplet replica.

Referring to Fig. 2, the explanation of these observations is as follows. The droplet has spread to form a biconvex

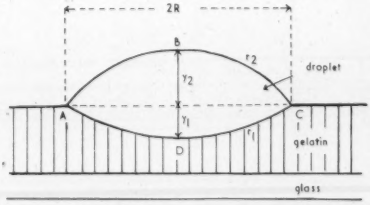

Fig. 2. Cross-section of droplet-gelatin lens

* May, K. R. *J. Sci. Instrum.*, **22**, p. 187 (1945).

lens $ABCD$, the lower portion of which ADC gives rise to the formation of a plano-concave gelatin lens ADC. The image formed above the droplet is a real image resulting from the combination of the two lenses and the image formed beneath the droplet after washing is a virtual image formed by the plano-concave lens. If a microscope with a micrometer on the fine focusing adjustment is used, the measured distance between the gelatin surface AC and the upper focal point will be the focal length of the combination. Let this be F. The distance from AC to the lower focal point will be the focal length of the plano-concave lens ADC. Let this be f_1.

The focal length f_2 of the biconvex droplet lens $ABCD$ may be found by substitution in the formula for the focal length of a combination and will be given by

$$f_2 = -f_1F/(f_1 + F)$$

If r_1 is the radius of curvature of ADC and μ_1 the refractive index of gelatin

$$r_1 = f_1(\mu_1 - 1)$$

The radius of curvature (r_2) of surface ABC is given by

$$r_2 = \frac{f_2r_1(\mu_2 - 1)}{r_1 - f_2(\mu_2 - 1)}$$

where μ_2 is the refractive index of the liquid.

10 μ and 30 μ diameter, a size range in which light microscope measurements are most easily and accurately made. Five or so determinations appear to be entirely adequate and multiplying the measured droplet replica diameters by the average value will give the original droplet diameter.

RESULTS

The following table gives a typical set of spread factor determinations for dioctyl phthalate.

Work has also been done with "Fog" oil (refractive index 1·518) and a lubricating oil (refractive index 1·491) giving mean spread factors of 0·51 and 0·45 respectively.

Since the mean spread factor is determined on 10–30 μ diameter droplet lenses it was desirable to ascertain if it could be applied reliably to droplets in the electron microscope range. Unsuccessful attempts were made to produce a homogeneous cloud of very small droplets so that light scattering measurements of droplet size could be made for correlation with sizes determined by the application of the spread factor to the droplet replica diameters. Instead, heterogeneous aerosols were generated and the average rate of fall of the largest droplets was timed in a Schaefer type sedimentation cell. The droplet diameter was determined

Typical set of spread factor determinations

$2R$ (μ)	F (μ)	f_1 (μ)	f_2 (μ)	r_1 (μ)	r_2 (μ)	y_1 (μ)	y_2 (μ)	D (μ)	$D/2R$
11·6	90	31	23	16·43	34·74	0·49	0·95	5·25	0·45
12·4	100	39	28	20·67	40	0·49	0·9	5·43	0·44
17·6	132	58	40·3	30·74	53·64	0·55	1·29	7·5	0·43
20·8	188	64	47·7	33·92	80·15	0·68	1·64	9·1	0·43
22	158	83	54·4	43·99	65·92	0·94	1·39	9·46	0·43

Refractive index of gelatin (μ_1) = 1·53
Refractive index of dioctyl phthalate (μ_2) = 1·485
Mean spread factor = 0·436

Let y_1, y_2 be the heights of the segments ADC, ABC of spheres of radii r_1 and r_2 respectively, then

$$y_1 = r_1 - \sqrt{(r_1^2 - R^2)}$$

where R is the radius of the droplet replica

and

$$y_2 = r_2 - \sqrt{(r_2^2 - R^2)}$$

The total volume of the two segments is

$$\pi/6\left[y_1^3 + 3R^2(y_1 + y_2) + y_2^3\right]$$

and equals the volume $\pi D^3/6$ of the original droplet of diameter D. Hence

$$D = \left[y_1^3 + 3R^2(y_1 + y_2) + y_2^3\right]^{\frac{1}{3}}$$

In practice y_1^3, y_2^3 are small enough to be neglected so that

$$D = \left[3R^2(y_1 + y_2)\right]^{\frac{1}{3}}$$

It has been assumed that the surfaces of the lenses are spherical and from the sharpness of the images produced it is evident that this must be so, for where there is any tendency for the surface to be otherwise the images are blurred or multiple.

SPREAD FACTOR

The ratio $D/2R$ is the spread factor and should be determined for a number of the spread-out droplets between by the application of the Stokes–Cunningham law and compared with the average largest drop diameter of the same aerosol determined by the replica technique. This process was carried out on three separate dioctyl phthalate aerosols having different maximum droplet sizes. The close agreement between the two methods of diameter determination shown in the following table indicates that the spread factor determined on large droplets may be reliably applied to droplets in the electron microscope range.

Stokes–Cunningham diameter (μ)	*Replica technique diameter* (μ)
1·35	1·33
0·7	0·66
0·25	0·3

Owing to the difficulty of producing extremely small droplets of non-volatile liquids it is not possible to indicate a resolving limit for the technique. The smallest droplets so far found in experimental aerosols and sized by the replica technique, have been of 0·04 μ diameter.

ACKNOWLEDGEMENT

The paper is reproduced with the permission of the Controller of Her Majesty's Stationery Office and Crown copyright is reserved.

New method for increasing the X-ray reflection power of lithium fluoride crystals

By E. F. Priestley, Ministry of Supply, Armament Research and Development Establishment, Fort Halstead, Kent

[*Paper received* 20 *October*, 1958]

Bending and quenching methods for increasing the dislocation density and hence the X-ray reflection power of lithium fluoride have been found ineffective when applied to certain crystals of British origin. An ultrasonic treatment is described which, with abrasion of the surface, gave a gain in reflection intensity of up to 3½ times at 2·0 Å and 7 times at 0·6 Å.

Birks and Seal[1] have described methods of increasing the dislocation density within lithium fluoride crystals and hence their X-ray reflexion intensity by up to ten times without excessive line broadening. Such a gain is of great value in a flat crystal monochromator or spectrograph, especially when used for dispersing weak radiation in X-ray fluorescence analysis.

These results applied to crystals of American origin and an investigation was carried out to test the value of the methods described when using crystals grown in this country by Messrs. Taylor, Taylor and Hobson (Leicester).

The quenching and bending methods used by Birks and Seal were found to be of little value when applied to the crystals available for test, since they either fractured or gave gains of little more than 50%. Abrasion, however, gave a gain of up to three times for manganese Kα radiation and two times for molybdenum Kα.

Since abrading the surface gave this moderate but useful gain, it was reasonable to expect that the production of dislocations in greater depth than is possible by abrasion would give greater gain, especially with the shorter wavelengths.

It was thought that ultrasonic vibration might produce the desired effect and tests were carried out using the only equipment available—a Mullard ultrasonic soldering iron.

The heating circuit was cut out by the removal of its fuse, and the smooth tip of the iron stroked gently across the oiled surface of a freshly cleaved crystal for 2 to 3 min.[2] Examination in the X-ray spectrometer showed that the intensity of the X-ray spectrum at 2·0 and 0·6 Å was about 3 and 4 times respectively greater than that found for the virgin surface. Thus the overall gain was similar to that obtained by abrasion, but was greatest at the short instead of the long wavelength end.

Abrading the cleaved surface of another crystal before applying the ultrasonic treatment gave gains of about 3½ and 7 times at 2·0 and 0·6 Å respectively.

Fig. 1 shows a series of records made with crystals subjected to various treatments together with one (ground and lightly polished) supplied with the Norelco spectrometer used for these experiments. The response of this crystal (included for comparison) is seen to be very similar to our own crystals after abrasion. All crystals were 75 × 25 mm in area and about 5 mm thick. "Dead time" correction would increase the effective height of the higher peaks and this has been allowed for in the figures quoted.

For an untreated crystal the line breadth at half-peak height was found to be about 0·4° in 2θ, representing the combined effect of the crystal rocking angle and the effective angular aperture of the collimating system, estimated to be about 0·3°. The fully treated crystal [Fig. 1(*e*)] showed an increase at the long-wavelength end of about 0·2°, and negligible broadening at the shorter wavelengths. The ultrasonic vibration had not therefore significantly altered the X-ray resolving power of the crystal.

In order to follow the changes taking place in the dislocation density as revealed by etch pits, the laminae were cleaved perpendicular to the treated surface, etched in dilute hydrochloric and acetic acid with ferric chloride and examined at magnifications of about 450×. Fig. 2(*a*) shows a typical area of the cleavage face of an untreated crystal which had clusters of dislocations randomly distributed throughout the block. It is this observation which leads us to suggest that

Fig. 1. Spectrograph records of the same specimen with crystals subjected to various treatments

(*a*) As cleaved; (*b*) Norelco crystal; (*c*) abraded; (*d*) vibrated; (*e*) abraded and vibrated.

our initial material may well be less perfect structurally than that used by Birks and Seal, and this may explain the difference in its behaviour under treatment. The abraded crystal (*b*) shows a high concentration of etch pits near the surface very similar to those shown by Birks and Seal, but those treated by ultrasonic vibration, as in (*c*), show a greater tendency for the pits to lie in a lattice-like array, with well marked lines running in (110) directions. In (*d*) the deeper penetration of the double treatment may be seen with the same cross pattern of lines typical of the ultrasonic method.

No damage to the crystals occurred during any of the tests. Repeated cycles of abrasion and ultrasonic treatment gave

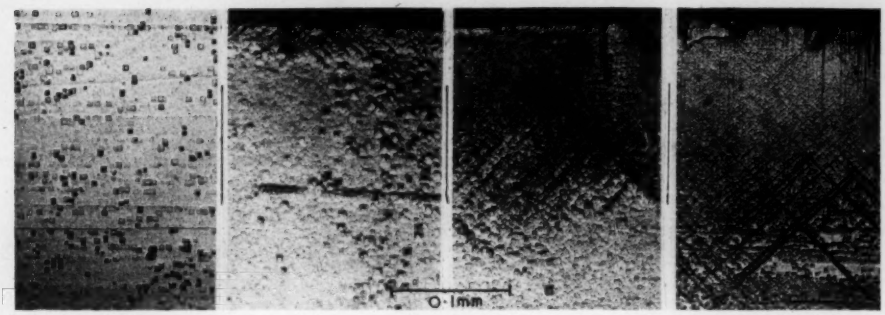

(*a*) (*b*) (*c*) (*d*)

Fig. 2. Micrographs showing concentration of etch-pits after various treatments
(*a*) Untreated; (*b*) abraded; (*c*) vibrated; (*d*) abraded and vibrated.

only a slight gain. Since it appears, however, that the effect of the ultrasonic treatment does not penetrate more than about 0·3 mm into the crystal it is conceivable that vibrations of higher frequency or amplitude might give improved response at the very short wavelengths.

Acknowledgement is due to Mr. B. D. Burns for encouragement in this work. The figures illustrating this report are reproduced by permission of the Controller of H.M. Stationery Office, and Crown Copyright is reserved.

REFERENCES

(1) Birks, L. A., and Seal, H. T. *J. Appl. Phys.*, **28**, p. 541 (1957).
(2) U.K. Pat. Appl. No. 5536/58.

Ferromagnetic after-effect in mumetal

By L. Castelliz, Ph.D., and W. W. H. Clarke, Ph.D., A.Inst.P., A.M.I.E.E., Components Division, E.M.I.-Cossor Electronics Ltd., Halifax, Nova Scotia

[*Paper first received* 18 *September, and in final form* 4 *November*, 1958]

Study of the magnetic performance of Ludlam mumetal sheets incorporated in extremely precise deflexion yokes has revealed a magnetic after-effect having a magnitude and decay time which appear to place it in a different category from reported phenomena of this general nature. This paper describes the phenomenon, which has been measured, and includes a description of the mechanism which is believed to be responsible for it. The effect is partially submerged by the well-known eddy current delay, measurements of which have also been made. The dependence of both after-effects on various parameters such as annealing treatment, thickness and spacing of the mumetal sheets and temperature, has been revealed qualitatively by the experiments, and it is the difference in their behaviour under these parametric variations which has enabled them to be properly distinguished.

1. INTRODUCTION

Fundamentally, magnetic delay effects are of two types: those originating from the flow of time-decaying currents which produce magnetic fields in a sense opposing the change of magnitization (eddy currents) and those associated with the re-orientation of the electron spin moments whose parallel coupling is responsible for ferromagnetism. The former category is well understood though the exact evaluation of particular cases is sometimes difficult, and in the latter category both the "natural" delay which is a time of the order of the reciprocal Larmor frequency[1] and the "long" delay first observed by Ewing,[2] and later attributed[3, 4] to the presence of carbon or nitrogen atoms in the α-iron lattice, are well known. Associated phenomena to the latter category concern the slow response of nuclear magnetic moments in some materials, on which subject a number of papers[5, 6] have appeared. The present phenomenon is believed to be of similar nature to the nuclear magnetic moment time lag, caused by a weak coupling between the spin system and the vibrational system of the crystal lattice.[7]

The experiments which revealed this time lag were performed with thin mumetal laminations in which eddy currents also caused small back magneto-motive forces, decaying with time. However, these two different after-effects were readily isolated once a sensitive experimental procedure was devised. Measurements at different temperatures, and using different thicknesses of mumetal, confirmed the different interpretations of the two parts of the after-effect curve.

2. EXPERIMENTAL ARRANGEMENTS

For the purposes of this paper a deflexion yoke may be treated simply as a pair of orthogonal coils arranged around the neck of a cathode-ray tube with a cylindrical sleeve, made up of thin annular mumetal washers and fibre spacing washers over them. Fig. 1 is a photograph of a typical yoke assembly.

The angular deflexion of the electron beam is proportional to the field in the air gap of the deflexion coils. Since this is driven by the magnetic flux with which the magnetic material responds to a magnetizing field, the air gap field and hence the deflexion of the electron can reveal anomalous

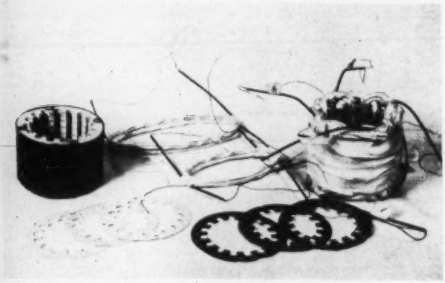

Fig. 1. Simple deflexion yoke

time response of the magnetic material. To do this a step function of current is applied, and it is convenient to examine the response to a step of current from a high value to zero, because circuits to maintain zero injected current after the step can readily be made. The step function, of course, applies to the yoke as an LCR circuit, where R is (almost entirely) a parallel external damping resistor. In the absence of a core material time effect, the response of this circuit is well known, and the values of LC and R used in these experiments were such that near-critical damping was used, and that 99·9% response to the change was completed in some 10 μs.

The form of the approach for critical damping is $1 - e^{-t/\tau_0}(1 + t/\tau_0)$, where $\tau_0 = \sqrt{LC}$. Hence the measurements described were all made at times when the response to the Heaviside function was substantially complete.

A linear current sweep locked to the high current pulses was applied to the other axis, permitting the slow approach to be seen. Fig. 2 shows the approximate form of the waveforms on the cathode-ray-tube face. The equipment used for the experiment is illustrated in the block schematic of equipment and circuit schematic of pulse drive unit in Fig. 3.

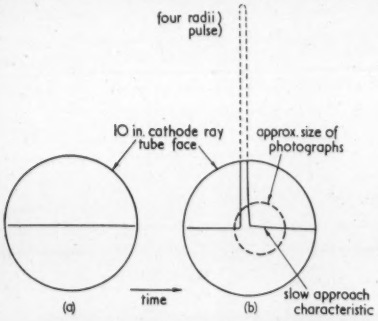

Fig. 2. Cathode-ray-tube wave forms
(*a*) Reference scan; (*b*) scan and pulse wave form.

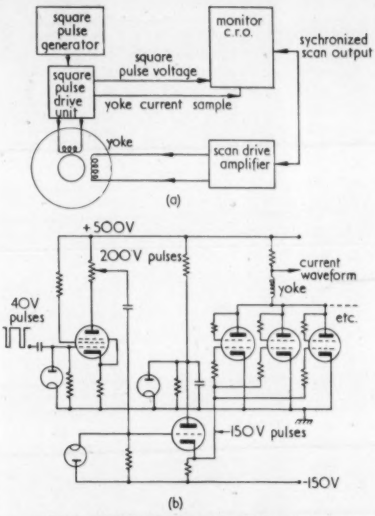

Fig. 3. (*a*) Block diagram of the equipment.
(*b*) Circuit diagram of the pulse drive unit

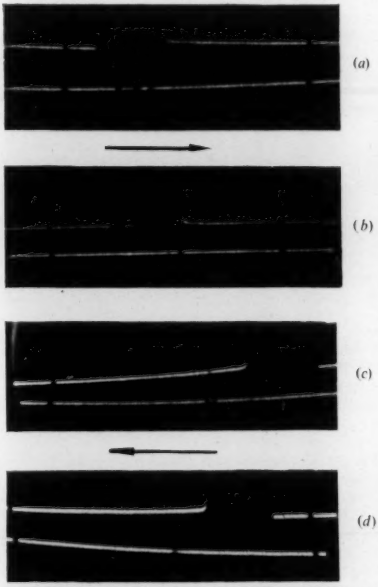

Fig. 4. Some representative slow approach photographs (arrow shows direction of time)
(*a*) Yoke No. 23; (*b*) yoke No. 30; (*c*) yoke No. 23 at +25° C; (*d*) yoke No. 23 at −10° C.

Settling-time to 99·9% of amplitude for varying parameters

Yoke No.	*No. of lam.*	*Thickness* (in.)	*Annealing temperature* (°C)	*Annealing time* (h)	*Cooling speed*	*Protecting atmosphere*	*Settling-time to 99·9% B_0* (μs)
1	50	0·008	1100	3	50° C/h	H_2	63
29	50	0·008	900	4	air quenched from 750° C	H_2 purified	49
5	10	0·008	1100	3	50° C/h	H_2	75
27	10	0·008	900	4	air quenched from 750° C	H_2	75
28	5	0·008	900	4	air quenched from 750° C	H_2	136
2	50	0·004	1100	3	50° C/h	H_2	51
22	50	0·004	900	4	air quenched from 750° C	H_2	51
25	50	0·004	900	4	air quenched from 750° C	H_2	66
21	39	0·004	900	4	air quenched from 750° C	H_2	101
30	50	0·004	1080	8	50° C/h	H_2 purified	30
31	50	0·004	1080	8	air quenched from 650° C	H_2 purified	44
24	50	0·002	900	4	air quenched from 750° C	H_2	115
23	10	0·001	900	4	air quenched from 750° C	H_2	243

To ensure accuracy, the picture obtained was photographed, and then the camera was displaced very slightly normal to the linear sweep trace and another exposure taken, on the same photograph, of the trace without the heavy current pulse. This provided a zero amplitude reference base line to measure amplitude as a function of time without any inaccuracy due to camera or to curvature of the trace. From these photographs (Fig. 4) measurements were taken by projecting them on to a large screen and tracing the outlines.

The pictures are almost full size, as shown in Fig. 4, and this is a portion of the picture on a 10 in. diameter screen. Hence a deflexion of 4 radii corresponds to 20 in., and a residual 0·1% of amplitude is some 0·020 in. on the scale of the photographs. There is therefore reason to believe that the experimental accuracy obtained with enlarged traces is of the order 0·01% of the Heaviside function.

3. EXPERIMENTAL RESULTS

The settling time to 99·9% of amplitude, commonly used as a measure for the response qualities of magnetic deflexion yokes, has been measured for a series of yokes using cores with variation of the following parameters: method of annealing the laminations after punching, thickness and number of laminations. Settling times, covering a range of from 30 to 243 μs, were measured. Part of the results is listed in the table. A few complete $B(t)$ curves are shown in Figs. 5, 6 and 7.

3.1 *Effect of heat treatment on settling-time.* Whereas annealing temperature within the investigated limits, i.e. between 900 and 1100° C, does not affect approach-time substantially, an essential improvement has been observed when the annealing-time was raised from 4 to 8 hours and simultaneously the protecting atmosphere was purified by passing the electrolytic H_2 over a common laboratory tower

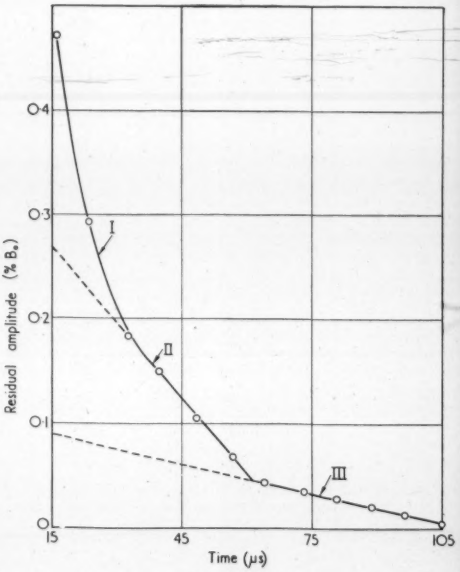

Fig. 5. The three sections of the response curve

I, circuit response; II, eddy current delay; III, ferromagnetic after-effect.

system. The yokes whose laminations were submitted to this procedure exhibited settling-times, as defined above, shorter than 45 μs. The minimum time of 30 μs was obtained when the longer annealing-time in purified H_2 was combined with a slow cooling rate, i.e. 50° C/h to room temperature. Quenching at 650° C, the usual permalloy treatment, desirable for other aspects of deflexion yoke performance, results in a slightly elevated settling-time.

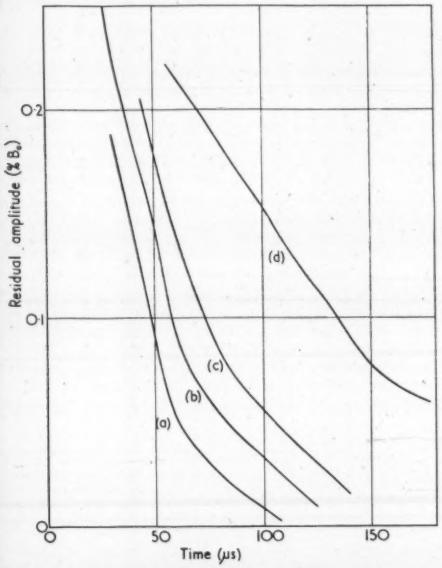

Fig. 6. Settling time for 0·008 in. yokes with different numbers of laminations

(*a*) Yoke No. 29; (*b*) yoke No. 1, 50 laminations; (*c*) yoke No. 27, 10 laminations; (*d*) yoke No. 28, 5 laminations.

3.2 *Influence of lamination thickness and number of laminations.* Lamination thicknesses of 0·004 and 0·008 in. were compared, the latter giving a slight (10 to 20%) increase of settling-time. Laminations etched from 0·004 to 0·002 in. exhibited remarkably long times, varying from 115 to 243 μs depending on the other parameters. A clear connexion exists between the observed settling-times and the number of laminations as may be seen from Fig. 6 and by comparing the values for yokes Nos. 1, 27 and 28 in the table.

3.3 *Influence of temperature.* The two curves of Fig. 7 are typical of the results obtained by measurements at different temperatures. Cooling was done with dry ice and although temperature equalization was not reached, a clear increase of the magnetic time lag with lower temperature may be noticed.

4. DISCUSSION OF THE EXPERIMENTAL RESULTS

The results described in section 3.1 distinctively show the influence of non-magnetic impurities on the magnetic-time lag. The shortest delay-times are achieved with the method which provides the most efficient refining of the mumetal. For a relatively pure material internal strains introduced by the cooling process, if not allowed to relax by plastic flow, may prevail over the influence of impurities on settling-time as a comparison between the slowly cooled yoke 30 and the air quenched yoke 31 indicates.

Comparisons between $B(t)$ curves of 0·008 in. and 0·004 in. laminations have shown that only that part of the curve marked as part II in Fig. 5 changes its slope in the sense which is expected for eddy current delay. Part III of the curve is not affected substantially. Unfortunately, these measurements were not extended to thinner laminations reduced by cold rolling. Thickness reduction by etching roughens alloy surfaces microscopically and produces surface stresses which are primarily responsible for the long magnetic delay-times measured on the 0·002 in. and 0·001 in. laminations. However, the results obtained on 0·008 in. and

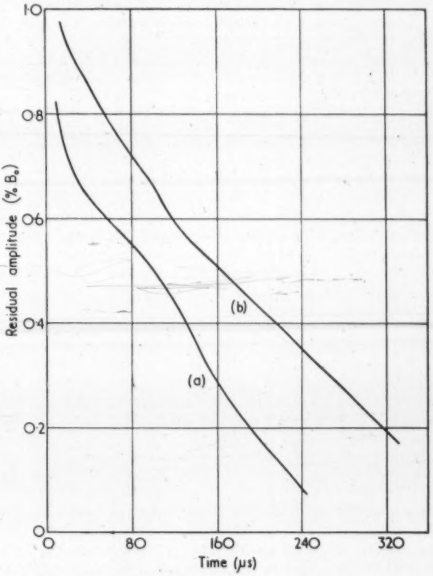

Fig. 7. Influence of temperature on settling-time for yoke No. 23

(*a*) About +25° C; (*b*) about −10° C.

0·004 in. laminations seem to justify the assignment of eddy current delay and ferromagnetic after-effects to parts II and III respectively in Fig. 5. The conclusion is also confirmed by the fact that the influence of temperature mainly involves part III of the curves in Fig. 7. The influence of this temperature change on eddy current delay is estimated at only a few per cent. Part I, the natural current response is not shown in that figure.

As Fig. 6 shows, the influence of the lamination number expresses itself in both parts of the slow approach curves. Since with respect to their final application the total length of the lamination stack had to be the same for all yokes, the

spacing between mumetal laminations, provided by fibre washers, increases with decreasing number. There is little doubt that the longer approach-times of the 10 and 5 lamination yokes are associated with their greater spacing rather than with their mere number. With greater spacings, the air path of the flux and with it the normal flux component increase. That will cause greater eddy current losses but also provide a larger number of re-orientation processes of the Larmor vector the influence of which is discussed in the following section.

5. CONCLUSIONS

Summarizing the results the following characteristics are noted:

(*a*) Under the experimental conditions magnetic-time lags of the order 10^{-5} to 10^{-4} s have been observed on thin mumetal sheets.
(*b*) Differences in response-times, spreading over nearly one decade, are related to differences in the state of purification and stress relief of the sheets.
(*c*) The observed delay-times and the oscillation-times of the field exciting current are of the same order of magnitude.
(*d*) The lag is temperature-dependent.

An attempt to reconcile this type of ferromagnetic after-effect with the reported and more or less sufficiently explained types, did not lead to a satisfactory result as will be indicated below.

Ewing's type, attributed to a re-orientation process of the small metalloid atoms in the interstitial holes of the bcc α-Fe lattice, i.e. to a transition from the random distribution in the stress-free state to a preferred position in the magneto-strictively distorted cell is unlikely to occur in the close packed fcc lattice of mumetal. Furthermore, the observed short relaxation times are not compatible with position changes of material particles.

The Jordan lag, comprising a rather complex group of after-effect phenomena, has not yet found a theory which could be claimed as completely satisfactory. It is clearly connected with either elastic or plastic deformation. The attempt of Preisach,[8] therefore, to relate the results of his experiment on a 40% Ni–Fe alloy to a time lag of irreversible wall displacements might be a good approach to an understanding of at least a part of these phenomena. However, the present results are distinct from the reported observations of Jordan lag in the first place by their marked temperature dependence, and in the second place by their shorter duration. Within the concept of wall displacement a temperature dependent impediment could only be understood in terms of diffusion and plastic flow processes which would again generate relaxation times much higher than observed. Indeed, attempts have been made[9] to explain the long-time Ewing's lag by diffusion retarded wall displacements.

It is still possible that a more refined domain theory could provide a satisfactory explanation of the experimental results, but the authors hold the opinion that the alternative explanation is more justified.

It is known that the second-order magnitude phenomenon of interaction between spin and lattice systems in ferromagnetics is strongly dependent on temperature without material diffusion or mechanical stress relief processes being involved. The spins precess about the Larmor cone axes which at any moment of time and in any Weiss domain are determined by the condition that the sum of magnetic torque energy, anistropy energy and energy of internal strains is a minimum. When the spin moments re-orient in response to a change in the external field, the semiapex angle of the precession cone at first goes through intermediate values until temperature equalization is reached by coupling with the vibrational lattice system. According to A. Akhieser,[7] at low temperatures the relaxation-time for an exponential approach to temperature equalization is given by

$$\tau = \pi \frac{Ma^2}{\hbar} \left(\frac{\Theta_c}{\Theta}\right)^3 \frac{\Theta_c}{T} \exp\left(\frac{1}{4}\frac{\Theta^2}{T\Theta_c}\right)$$

where M = atomic mass, a = lattice constant, Θ_c = Curie temperature, and Θ = Debye temperature.

For transition metals with incomplete 3d-shells, τ lies in a narrow range of a few microseconds at 10° K. The range of validity of the formula is restricted to ideal crystals without lattice imperfections. On the other hand, spin relaxation times of nuclear moments covering a range of six decades from 10^{-4} to 10^{+2} s have been measured on real crystals. It seems conceivable to assume that in real transition metal lattices electron spin relaxation-times will cover at least a range of some 3 decades.

In the practical case, there is not one coupling factor to be treated between spin and lattice systems, but rather a spectrum giving rise to a range of relaxation-times, of which only the longest have been observed. Since in the range of observation the after-effect appears to be linear with time, it may be inferred that the distribution of relaxation-times contributing to this is similar to the energy distribution of β-ray spectra. For these reasons it is felt to be preferable to define the after effect magnitude by extrapolation of the straight line to the B_0 ordinate, and its duration by a total time analagous to the "range" of β-particles.

This concept of the after effect may permit an explanation of the anomaly that the present experimental results tend to relate longer relaxation-times to lattice imperfections, whereas it is generally accepted that the gross effect of lattice imperfections is to increase the spin/lattice coupling. Imperfections in general alter the quadrupole moment of the lattice and this will mostly result in higher values, but according to the characteristics of a probability distribution, in a sufficient number of cases to be significant, a very low quadrupole moment may be caused to occur. If the quadrupole moment of the ideal lattice has a value defined by a very narrow "normal" distribution, then a major widening of this distribution due to imperfections could result in a greatly increased probability of low coupling.

It is anticipated that further work in this field will supply additional useful information. In particular it is believed that experiments covering a wider range of similarly produced lamination thicknesses should prove fruitful. It should also be feasible to do quantitative studies of the effect of temperature.

It is to be expected that other ferromagnetic materials will also exhibit an after-effect of the type discussed if studied under similar conditions. In experiments on manganese–zinc ferrite cored yokes the effect was not observed.

From the point of view of experimental technique it is believed that the use of the deflexion yoke as a medium for investigating second-order magnetic phenomena is to some extent novel. The high measurement accuracy of the reported results indicates its usefulness in this respect.

6. ACKNOWLEDGEMENTS

The authors are indebted to Cossor (Canada) Ltd. for permission to publish this paper which describes some results

obtained in carrying out a general research programme on deflexion yokes.

7. REFERENCES

(1) BOZORTH, R. M. *Ferromagnetism*, p. 808 (New York: Van Nostrand Co. Inc., 1956).
(2) EWING, G. A. *Proc. Roy. Soc.*, **46**, p. 269 (1889).
(3) RICHTER, G. *Probleme d. Technischen Magnetisierungskurve*, p. 93 (Berlin: Springer Verlag, 1938).
(4) SNOEK, J. L. *Physica*, **6**, pp. 161, 797 (1939).
(5) BLOEMBERGEN, N. *Phys. Rev.*, **73**, p. 674 (1948).
(6) HABER, E. C. *Phys. Rev.*, **80**, p. 580 (1950).
(7) AKHIESER, A. *J. Phys., USSR*, **10**, p. 217 (1946).
(8) PREISACH, F. *Z. Phys.*, **93**, p. 245 (1935).
(9) SNOEK, J. W. *Physica*, **5**, p. 663 (1938).

Production of X-rays during a low-pressure gas discharge

By R. F. THUMWOOD, B.Sc.(Eng.), Ph.D., Queen Mary College, London, E.1

[*Paper received* 10 *September*, 1958]

The impulse breakdown of several gases at pressures of a few microns of mercury has been investigated. During the first stage of the discharge, a microsecond burst of X-rays is emitted from a spot of about 8 mm diameter on the anode electrode. If the initial voltage applied to the tube is 600 kV, a single X-ray pulse will produce a legible radiograph through about 5 cm of steel.

The mechanism of the discharge has been studied and high-speed photographs of the visible discharge show a luminous column moving from cathode to anode. Steenbeck's theory[3] has been extended to show qualitatively the probable sequence of events during the discharge.

It has been known for many years that a low-pressure gas breakdown process may be used for the production of short but intense bursts of X-rays.[1, 2, 3] Work carried out in both Germany and the U.S.A. just before the war led to successful designs of flash X-ray tubes capable of producing useful outputs in times of the order of a microsecond.[4, 5] These tubes have been developed and used almost exclusively for ballistics research, although there are a few other applications where short-exposure radiography has been used.

It is believed that at present all commercially available tubes are of the so-called "high vacuum" type, in which the residual gas pressure is as low as the manufacturer can make it (less than 10^{-6} mm of mercury). In the operation of these tubes a small arc is started at the cathode which injects into the inter-electrode space sufficient vapour for the breakdown process to take place. A detailed study of the mechanism of these tubes has already been made.[6]

The older type of tube, in which a permanent gas is employed, has been comparatively neglected, except as a possible means of irradiating food and as an object of study for its own sake. It is possible, however, if higher-voltage X-rays are required, that the gas-filled tube will again have its uses. The present article is concerned with the construction and performance of a gas-filled tube which operated at voltages up to 600 kV and currents of several kiloamperes peak value.

DESCRIPTION OF APPARATUS

The form of the discharge tube and the connexions to the high-voltage supply are shown in Fig. 1. The tube itself was made of thirty-three sections of borosilicate glass, each 30 cm diameter and 2·5 cm long. Adjacent sections of glass were separated by aluminium disks of 40 cm diameter, the whole assembly being joined and made vacuum-tight by an epoxy resin glue. Each aluminium disk was perforated by a central hole which was 5 cm diameter at the topmost or cathode end, and increased linearly up to 20 cm diameter at the anode end. This elaborate form of construction greatly reduced difficulties due to surface breakdown along the walls of the discharge tube.

The cathode electrode was a disk of mild steel, slightly hollow on its front surface, and pierced by a hole about 0·5 cm in diameter; within this hole was mounted a trigger

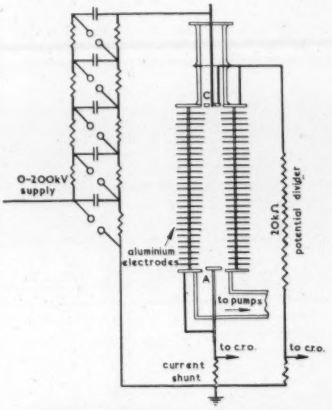

Fig. 1. Diagram of discharge tube showing electrical connexions and monitoring points
A, anode; *C*, cathode.

electrode, also of mild steel. In operation a high-voltage pulse applied between the trigger rod and the cathode served to initiate the main discharge. A plane disk of tungsten formed the anode electrode.

For use with common gases the diffusion pump was baffled to restrict its speed and a dynamic pressure balance obtained

by means of a controllable leak valve, but for xenon and krypton the pumps were isolated and a static pressure set up. Owing to the release of gas from the electrodes and walls of the tube it was necessary to re-evacuate the tube after two or three discharges.

The high-voltage supply was a five-stage Marx generator using the Goodlet connexions. The effective discharge capacity was 0·005 μF, and the total loop inductance, including the discharge tube, was about 10 μH. The potentiometer served the double purpose of providing a voltage monitoring point and also of making the tube self-triggering.

The discharge process was studied by means of an oscilloscope having two tubes driven by a single time-base circuit, so that any pair of the three quantities—current, voltage and X-ray output—could be recorded simultaneously. For this purpose the X-rays were detected by a scintillation phosphor of tetraphenyl butadiene in polystyrene coupled to a photomultiplier. The output of this multiplier passed through an amplifier of 16 Mc/s bandwidth and times 10 gain directly to the cathode-ray oscilloscope tube plates.

EXPERIMENTAL RESULTS

Total X-ray output. With all the gases tested it was found that a fairly well-defined optimum gas pressure in the region 10^{-3} to 10^{-2} mm of mercury existed for the production of X-rays. At lower pressures the discharge tube suffered from external breakdown troubles, and at higher pressures the whole process took place so rapidly that most of the supply voltage was lost across the circuit inductance. For this reason it was not possible to make experiments over a wide range of pressure except at rather low voltages. The triggering system was not strictly necessary as breakdown would always take place eventually, but it was convenient to ensure initiation of the discharge at the beginning of the voltage wave from the impulse generator.

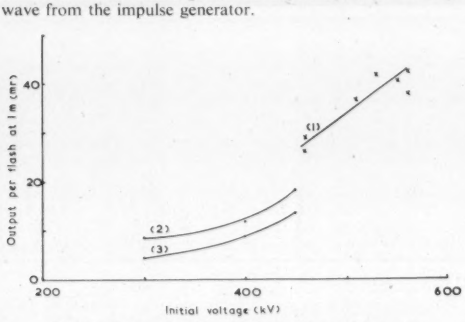

Fig. 2. Measured X-ray output of gas-filled tube

Curve (1), argon, $p = 3 \times 10^{-3}$ mm of mercury; curve (2), air, $p = 4 \times 10^{-3}$ mm of mercury; curve (3), air, $p = 4 \times 10^{-3}$ mm of mercury, 0·58 mm copper filter.

Measurements of X-ray output were made with a small ionization chamber, type BD. 11 (by Baldwin Instrument Co.), and a Farmer electrometer. Results for air at a pressure of 4×10^{-3} mm of mercury are shown in Fig. 2. It is possible to estimate, on the basis of published data for d.c.-supplied X-ray tubes, the maximum output in röntgens at one metre for a capacitor-supplied tube.[7] From this point of view the gas discharge tube is about 25% efficient. Reliability varied with the nature of the gas filling, being worst with hydrogen, which tended to cause discharges external to the tube, and best with argon, krypton and xenon, when almost 100% reliability up to 500 kV was found. The optimum pressures for various gases are shown in the table.

Pressure for maximum X-ray output

Gas	p(mm Hg) ($\times 10^{-3}$)
Air	3
Oxygen	3
Hydrogen	7
Argon	4·5
Krypton	1·5
Xenon	1·2

In order to assess the potential usefulness of the system for short exposure radiography, a standard penetration test was used. This consisted of a steel step wedge in conjunction with Ilford Industrial "A" X-ray film and Ilford "Standard" salt screens. A single exposure at a distance of one metre was made and the film developed in Ilford I.D. 11 developer for five minutes at 20° C with continuous agitation. A densitometer was then used to find the thickness of steel corresponding to a density of one above fog level. On this basis it was found that approximately 2 cm of steel were penetrated when the initial charging voltage was 500 kV. This is, of course, not the usable limit of the tube, as readable density is produced through as much as 5 cm of steel. Pin-hole pictures of the anode show a well-defined focal spot of about 8 mm diameter but some radiation is emitted from the whole surface of the anode.

Oscillograms. Typical oscillograms recorded under optimum conditions of X-ray output are shown in Fig. 3. These oscillograms are for air filling, but no significant differences are found with other gases.

Use of image tube as high-speed shutter. The visible signs of the discharge were a luminous column down the centre of the tube, of a colour characteristic of the gas in use, together with a bright spray of incandescent tungsten particles shooting upwards from the centre of the anode. (This vaporization of the anode surface is very marked at higher voltages and the anode has to be replaced at intervals.) To obtain information about the formation of the glowing discharge column, high-speed photographs were taken by using an image tube as a fast shutter. Synchronization of the shutter was achieved by standard pulse delay circuits operated by the voltage wave coming from the potentiometer. By varying the delay timing it was possible to obtain a sequence of pictures corresponding to the various stages of the discharge. Since the total duration of the X-ray producing part of the discharge was only 1 μs it was necessary to use a shutter speed of 0·1 μs to obtain useful results. The relatively low intensity of the visible glow and the necessarily short exposure time made it difficult to secure adequate photographic records, especially during the initial stages of the discharge. The best results were obtained using an argon filling for the tube, presumably because of the colour match between the emitted light and the response of the image tube cathode.

One set of pictures is shown in Fig. 4, where exposures are spaced approximately equally within the first microsecond of the discharge and the last exposure corresponds to the voltage and current zero. Similar results were obtained for all the gases tested but, as explained above, are not suitable for reproduction.

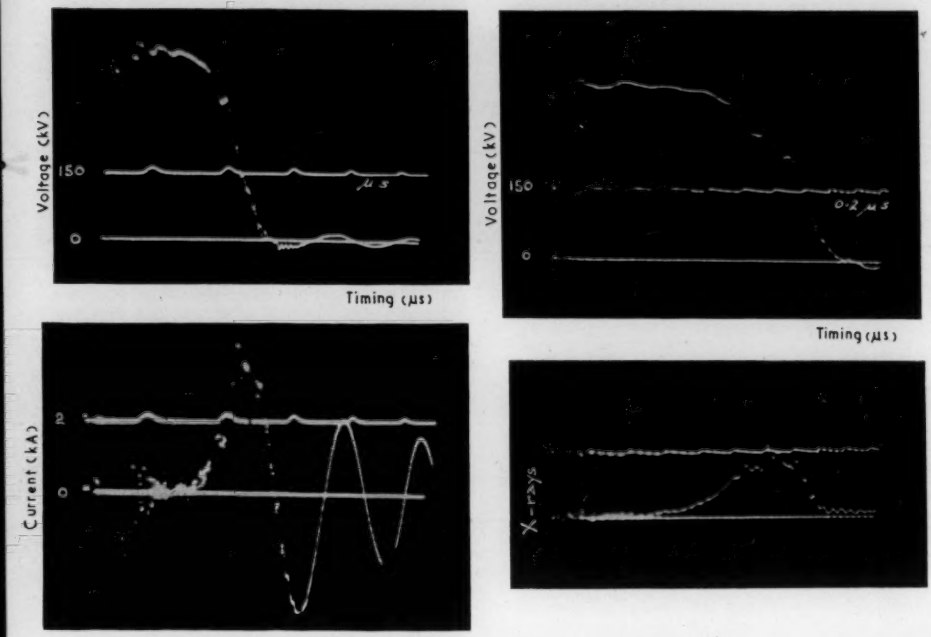

Fig. 3. Typical oscillograms showing relation between voltage and current and voltage and X-ray output

The photographs show a region of luminosity starting at the cathode and extending towards the anode during the discharge. The end of the luminous region appears always to be pointed or constricted. In a few records there appeared two constrictions separated by some 20 cm. At the anode end of the tube there were usually some bright flashes which coincided with external breakdown of some of the lower sections of the tube. This indicates that the potential distribution becomes non-uniform early in the discharge process, and it was the occurrence of these breakdowns which set a limit to the usable tube voltage.

By examining many sets of records it is clear that one bright spot always appears in the centre of the anode early in the discharge. This is assumed to be incandescence of the anode surface due to electron bombardment, and shows that a high degree of focusing exists, at least in the early stages of the discharge. No trace of the evaporation of luminous particles of tungsten was found on the photographic records, although this was one of the most marked features of the discharge as observed with the naked eye. This is, perhaps, not surprising, as such a process would be comparatively very slow and of much lower intrinsic brightness. A general glow of diminishing brightness was observable for about 10 μs after the initial phase of the discharge.

THEORY OF LOW-PRESSURE DISCHARGE

It is clear from the experimental evidence that electron currents of several thousand amperes flow while the potential across the tube is about 250 kV. This is only possible if the greater part of the space charge due to electrons is neutralized by positive ions which have been formed in the discharge space by electron collisions. A simple calculation indicates that about one electron in ten will be involved in such an ionizing collision, provided that the potential distribution is fairly linear (as it should be at the beginning of the discharge). The first requirement for an increase in current above that specified by the Child–Langmuir equation is that positive ions shall be formed in sufficient numbers to form an extractive field in the cathode region, but this in itself is not enough to produce the high currents actually recorded. Neutralization of the electron space charge at the cathode would result only in the formation of a virtual cathode further along the beam. An extension of this argument implies that ultimately the electrons close to the anode will have to be neutralized.

This process would be more plausible if it could be demonstrated that space-charge neutralization did, in fact, take place most rapidly in the region near the cathode, and it is suggested that the following extension of a treatment, due originally to Steenbeck[3] and later elaborated by Funfer,[8] will bear this interpretation.

Considering first the region near the anode, making the assumption that a positive ion will remain in the position in which it was formed throughout the rest of the process, let

σ_+ = linear density of positive charge (C/m).
σ_- = linear density of negative charge.
$i_{(t)}$ = electron current.

p = gas pressure (mm of mercury).
$S_{(V)}$ = ionization coefficient (ion pairs per metre per mm of mercury per electron).

Then at a time t the linear charge density due to positive ions in the anode region will be the result of all previous ionizing collisions

$$\sigma_+ = \int_0^t i_{(t)} p S_{(V)} dt \text{ (C/m)} \quad (1)$$

If the effects of inductance are ignored and only a capacitance discharge considered

$$i = -C(dV/dt) \quad (2)$$

At energies greater than a few hundred volts the ionization coefficient may be represented fairly accurately by $S = k/V$ where $k = 6 \times 10^6$ for air, in the present system of units. The use of this approximation was first suggested by

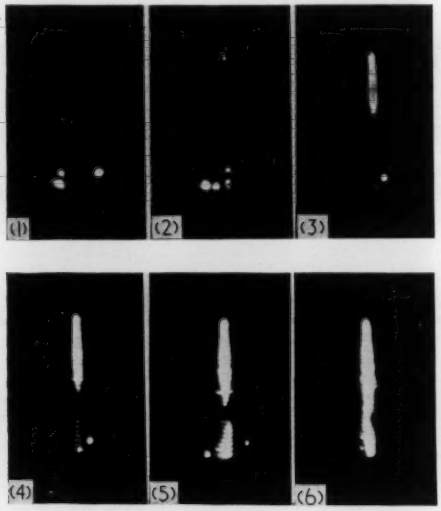

Fig. 4. Successive stages of discharge in argon
$p = 3 \times 10^{-3}$ mm of mercury; exposure approximately 10^{-7} s.

Bennett[9] and has been more recently examined by Spangenberg.[10] So that

$$\sigma_+ = -pCk \int_{V_0}^{V} \frac{dV}{V} = pCk \log \frac{V_0}{V} \quad (3)$$

where V_0 is the initial charged voltage of the capacitor.

The linear charge density due to electrons is given by

$$\sigma_- = \frac{i}{\sqrt{(2eV/m)}} = \frac{-CdV/dt}{\sqrt{(2eV/m)}} \text{ (C/m)} \quad (4)$$

Now even if there are no positive ions there will still be an electron current of a value determined by the Child–Langmuir law. This current is small (of the order of 5 A) but without it the discharge process could never start. The charge density at the anode produced by this current is

$$\sigma_0 = i_0/\sqrt{(2eV_0/m)} \quad (5)$$

and will be assumed to remain constant throughout the process. The total electron current is then controlled by the requirement that

$$\sigma_- = \sigma_0 + \sigma_+ \quad (6)$$

Substituting from equations (3) and (4)

$$-C(dV/dt) = \sqrt{(2eV/m)}[pCk \log (V_0/V) + \sigma_0] \quad (7)$$

Writing $\sigma_0/pCk = \log \beta$ this equation may be rearranged as:

$$dt = -\sqrt{(m/2e)} \frac{dV}{pkV^{\frac{1}{2}} \log (\beta V_0/V)} \quad (8)$$

Substituting $\exp(2x) = \beta V_0/V$ and with the boundary condition $t = 0$, $V = V_0$

$$t = \sqrt{(m/2e)} \frac{(\beta V_0)^{\frac{1}{2}}}{pk} \int_{\frac{1}{2}\log\beta}^{\frac{1}{2}\log(\beta V_0/V)} \exp(-x)/x \, dx \quad (9)$$

The exponential integral $E_1(x) = \int_x^\infty \exp(-x)/x \, dx$ is tabulated, so that

$$t = \sqrt{(m/2e)} \frac{(\beta V_0)^{\frac{1}{2}}}{pk} \left[E_1(\tfrac{1}{2}\log\beta) - E_1\left(\tfrac{1}{2}\log\frac{\beta V_0}{V}\right) \right] \quad (10)$$

The current wave-shape may be then found from

$$i = -C\frac{dV}{dt} = \sqrt{(2e/m)} pkCV^{\frac{1}{2}} \log \frac{\beta V_0}{V} \quad (11)$$

These equations have been plotted (Fig. 5) for the following conditions: $V_0 = 200$ kV, $C = 0{\cdot}005$ μF and

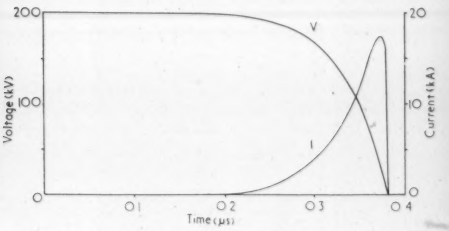

Fig. 5. Calculated current and voltage waveforms using modified Steenbeck theory
$C = 0{\cdot}005$ μF; $p = 3 \times 10^{-3}$ mm of mercury.

$p = 3 \times 10^{-3}$ mm of mercury. The agreement with the experimentally obtained curves is poor in respect to duration of discharge and this may be due to several causes. Probably the most significant is the omission of the circuit inductance from the calculation. Another gross assumption is the immobility of the positive ions, and this tends to produce an underestimate of the time of the discharge.

The form of the equation is interesting, in showing that the duration of discharge, measured from the time of voltage application, depends on the initial space-charge limited current, and hence on the tube dimensions. Also the lower the applied voltage V_0 the shorter will be the discharge time. This indicates that it is the anode region which controls the discharge, since if some other point in the tube is considered

where the voltage is always less than V_0, the discharge time would be less.

This theory is known to fail for the combination of short anode-cathode distance and low pressure (less than 10^{-4} mm of mercury), and Funfer has postulated a release of gas from the anode surface in order to overcome this difficulty. A more likely explanation is a release of gas from the triggering spark at the cathode, and this has been considered in some detail by Flynn.[6]

DESCRIPTION OF THE DISCHARGE PROCESS

On the basis of the above analysis it is possible to describe qualitatively the sequence of events in a low-pressure discharge of the type considered.

The initial potential distribution will be of the type shown in Fig. 6, curve (*a*). Since neutrality is achieved most rapidly

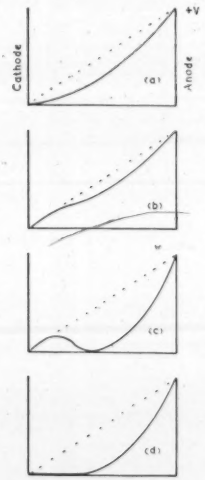

Fig. 6. Probable stages in the development of non-linear potential distribution

(*a*) Initial potential distribution; (*b*) space charge neutralized near cathode; (*c*) formation of virtual cathode; (*d*) filling of trap by slow electrons.

near the cathode, the potential distribution tends to move to (*b*). But this situation is analagous to that of a tetrode, and a virtual cathode will form as in (*c*) [see, for instance, Ref. (10), p. 260]. Again, it is not possible to neglect the electron trap formed by the hump in the potential distribution, and low-speed electrons will tend to accumulate to give a distribution as in (*d*).

The net result is that a region of ionization should gradually extend from the cathode towards the anode. The strongest experimental evidence for this is the incidence of external breakdown at the anode end of the tube, confirming that the potential has been redistributed as predicted. The high-speed photographs also tend to confirm the theory, but so far it has not been possible to show that the curve of excitation cross-section follows the same general trend as the ionization cross-section. Hence it is not necessarily true that the luminous regions show where space-charge neutrality is achieved.

CONCLUSIONS

The use of a low-pressure gas discharge for the production of intense pulses of X-rays had been re-investigated. It has been established that any of several gases may be used, although the optimum pressure for maximum output varies from gas to gas. Because of the better focusing properties of the heavier gases, it is possible to work with them at higher voltages without external breakdown of the discharge tube.

As a flash X-ray source the gas-filled tube has the merits of a small focal spot, high efficiency, reliability and long life, and the possibility of high voltage operation. Against this must be set the disadvantages of its complicated construction and the necessity for continuous pumping and accurate control of gas pressure.

The discharge mechanism requires the progressive neutralization of electron space charge by the formation of positive ions. This occurs more readily at the cathode end of the tube, and the potential distribution is changed so that the stress increases at the anode end. This non-linear distribution of potential causes external breakdown troubles which eventually set an upper limit to the working voltage.

REFERENCES

(1) BRASCH, A., and LANGE, F. *Naturwissenschaften*, **18**, pp. 16, 765 (1930); *Z. Phys.*, **70**, p. 10 (1931).

(2) KINGDON, K. H., and TANIS, H. E. *Phys. Rev.*, **53**, p. 128 (1938).

(3) STEENBECK, M. *Wiss. Veroff Siemens Werken*, **17**, p. 363 (1938).

(4) SLACK, C. M., and EHRKE, L. F. *J. Appl. Phys.*, **12**, p. 165 (1941).

(5) SCHAAFS, W. *Z. Angew. Phys.*, **1**, p. 462 (1949).

(6) FLYNN, P. T. G. *Proc. Phys. Soc.* [*London*], **13**, p. 748 (1956).

(7) THUMWOOD, R. F. *Proceedings 3rd International Congress High Speed Photography*, p. 238 (London: Butterworths Scientific Publications, 1956).

(8) FUNFER, E. *Z. Angew. Phys.*, **5**, p. 426 (1953).

(9) BENNETT, W. H. *Phys. Rev.*, **45**, p. 890 (1934).

(10) SPANGENBERG, K. *Vacuum Tubes* (New York: McGraw-Hill Book Co. Inc., 1948).

Notes and comments

Register of British manufacturers

The 1959 edition of the F.B.I. register of British manufacturers provides a comprehensive guide to a substantial cross-section of British industry, listing the products and services of over 7500 firms who are members of the Federation of British Industries, under more than 5400 alphabetical headings. The headings used are: products and services, addresses, trade associations, brands and trade names, trade marks. In addition there are language glossaries in French, German and Spanish.

The register is published by Kelly's Directories Ltd., and Iliffe and Sons Ltd., Dorset House, Stamford Street, London, S.E.1. The price is 42*s*.

Health Physics

The latest addition to the several new periodicals, associated with applied physics, which have recently appeared is entitled *Health Physics* and is the official journal of the Health Physics Society, founded at the University of Michigan in 1956. The Society met during 1957 in Pittsburgh and a selection of the papers then presented are to be published in the first few issues of the new periodical. Health physics is defined as "a study and practice dealing with any and all factors relating to damage from ionizing radiation and the prevention of such damage". In addition to specialist papers, survey sheets and notes and new items are promised.

The subscription rate is £6 ($17) p.a. and the publisher is Pergamon Press Ltd. Members of the Health Physics Society subscribe at special rates.

Control

The first issue of a new monthly periodical entitled *Control* has recently appeared. Its aim is stated to be the covering of "every aspect of control engineering for the engineer, scientist and user of control equipment," including systems, instrumentation, data processing, engineering and applications. The Editor is Mr. C. T. Rivington and he has a distinguished panel of editorial consultants. This issue, published in July, contains the following articles: "Electronic systems for industrial measurement and control" by M. V. Needham; "Dynamics of mechano-pneumatic systems" by J. E. Samson; "What is control engineering?" by C. M. Burrell and J. K. Lubbock; "Computer control of machine tools" by D. T. N. Williamson; "An elementary survey of digital codes" by G. C. Tootill. A buyers' guide and the usual regular features of this type of commercial periodical are also included.

Control is companion to the publisher's *Nuclear Power* and is produced in the same attractive modern format. Once more it is our pleasure to wish success to another contemporary resulting largely from the application of physics in industry.

The magazine is produced by Rowse Muir Publications Ltd., 3 Percy Street, London, W.1. The price is £2 2*s*. 6*d*. p.a. plus 10*s*. postage in the U.K., £3 3*s*. overseas, and $8 in the U.S.A. and Canada.

Journal of Scientific Instruments

Contents of the March issue

SPECIAL ARTICLE

Theory and design of getter-ion pumps. By L. Holland.

ORIGINAL CONTRIBUTIONS

Papers

High-temperature X-ray diffractometer. By J. Spreadborough and J. W. Christian.

Acoustic gas analyser. By L. Molyneux.

Electrolytic hygrometers for measurements in gases down to a few parts per million. By J. K. Crawshaw and F. G. Davidson.

Photographic method for pulse amplitude analysis. By P. J. Kennedy and P. J. Dean.

Electrometer for measuring the variation with concentration of the low frequency dielectric constant of aqueous ionic solutions. By V. I. Little.

Large scale laboratory freeze-drying apparatus. By P. M. Grant and R. B. Ward.

Cryostat for measuring the electrical properties of high resistance semiconductors at low temperatures. By W. H. Mitchell and E. H. Putley.

Method of determining the dynamic constant of liquid-containing membrane manometer systems. By R. J. Linden.

Laboratory and workshop notes

O-ring vacuum valve for use with a visible flow industrial glass apparatus. By G. S. Martin and A. Lench.

Vacuum valve indicator light. By D. H. Cooper.

Liquid-air level controller for cold traps. By K. H. Purser and J. R. Richards.

Simple monitor of equipment on a three-phase supply. By T. S. Holdon.

Inexpensive electronic relay for use with toluene regulators. By M. I. Pope.

Wave-guides for use in low temperature cryostats. By A. Caister, S. J. Fray and W. C. Hopper.

Orientation control for germanium wafers. By B. J. Coughlin, G. L. Davis and R. L. Kingsnorth.

Improved machine for lapping very thin slices of semiconductor material. By D. Baker.

Simple light source of about 10 mμs duration. By G. Porter and E. R. Wooding.

Photomultiplier window for a liquid scintillator. By R. M. Tennent.

NOTES AND NEWS

New instruments, materials and tools — New books

THIS JOURNAL is produced monthly by The Institute of Physics, in London. It deals with all branches of applied physics (including theory and technique). All rights reserved. Responsibility for the statements contained herein attaches only to the writers.

EDITORIAL MATTER. Communications concerning editorial matter should be addressed to the Editor, The Institute of Physics, 47 Belgrave Square, London, S.W.1. (*Telephone*: Belgravia 6111.) Prospective authors are invited to prepare their scripts in accordance with the *Notes on the preparation of contributions*. (Price 2*s*. 6*d*. including postage.)

REPRODUCTION. The Institute of Physics is a signatory to The Royal Society's Fair Copying Declaration. Details may be obtained upon application from The Royal Society, London, W.1.

ADVERTISEMENTS. Communications concerning advertisements should be addressed to the agents, Messrs. Walter Judd Ltd., 47 Gresham Street, London, E.C.2. (*Telephone*: Monarch 7644.)

CLAIMS FOR MISSING JOURNALS. Claims from regular subscribers to this *Journal* for missing numbers will only be considered if received within 60 days of the date of mailing plus normal outward time of transit and time for lodging the claim. Losses attributable to failure to notify a change of address or to similar omissions will not be considered.

SUBSCRIPTION RATES. A new volume commences each January. The charge is £6 per volume ($17 U.S.A.), including index (post paid), payable in advance. Single parts, so far as available, may be purchased at 12*s*. 6*d*. each ($1.75 U.S.A.), post paid, cash with order. Orders should be sent to The Institute of Physics, 47 Belgrave Square, London, S.W.1, or to any bookseller.

Summarized proceedings of a Conference on solid state memory and switching devices—London, September 1958

Some of the newer devices which may form the basis of present or future computers were discussed at a Conference of the Electronics Group of The Institute of Physics held in London on 26 and 27 September, 1958. The papers and discussion are summarized in the present report.

INTRODUCTION

The Conference, which was attended by over 150 representatives of Government and industrial research laboratories and of Universities, opened with a discussion of users' requirements. Mr. T. H. FLOWERS (Post Office Engineering Research Station, Dollis Hill) surveyed the special requirements of computers and telephone exchanges. Any such machine must have a permanent memory which can survive power failures and similar hazards and does not deteriorate with continued reading. Computers use punched card or tape and magnetic tape for the storage of the primary data and programme instructions. The time of access to any part of the record is not usually of prime importance. Electronic telephone exchanges require a memory capable of holding up to 10^6 binary digits, with an access time of a few milliseconds. Punched cards, even when scanned photoelectrically, are too slow for this purpose. Magnetic drums have been proposed: their cost is low and their storage capacity adequate, but the access time (approximately 20 ms) is long enough to be a handicap. Ferrite matrices with non-destructive read-out would be satisfactory if they were not so costly. A flying-spot cathode-ray tube scanner[1] has been proposed. This memory is, however, expensive to make and inconvenient if the record has to be changed frequently.

In addition to the permanent memory for the primary data and programme, a computer requires a means of remembering numbers arising at an intermediate stage of the calculation until they can be used in later processes. The requirements of a temporary memory are fast access and the ability to change the information quickly. Barrier-grid cathode-ray tubes now have a storage capacity of 128×128 bits together with an extended time between regeneration cycles. Ferrite core matrices are favoured in computers, and matrices of 128×128 cores are now being operated. The size is limited by the signal-to-noise ratio in reading, and this in turn depends on the squareness of the $B - H$ hysteresis loop. Reading is destructive and therefore to preserve the information it must be re-written after reading. The combined read-and-write cycle takes up to 15 μs.

Ferroelectric matrix memories may be cheaper than ferrite ones, since wiring is done by depositing metallic lines on each side of a crystal plate; but so far no entirely suitable crystals are available and the indications are that the operating rate would be slower than for ferrites.

Mercury and magnetostriction delay lines can be made into iterative pulse stores of 10^2 to 10^3 pulse positions at a spacing of 0·2 to 2 μs; the access time is the time of circulation of a pulse train and is usually between 0·1 and 1 ms.

Future memory requirements of computers and telephone exchanges are likely to be very different. Computers are likely to need the present temporary memories increasing by an order of magnitude in both size and speed. Thin magnetic films and superconductive devices are being examined for this purpose. Increased size and speed of memories is unimportant in telephone exchanges, but low cost and high security against loss of information by faults have not yet been adequately realized. What is wanted is the permanence and cost per digit of the magnetic drum combined with the random access of core matrices and the speed of delay lines.

Dr. J. E. FLOOD (Siemens Edison Swan Ltd., London) pointed out that storage of digits along a line, as in a magnetic tape, an ultrasonic delay-line circulating store, or the Twistor,[2] is more economical than a matrix where each unit can represent only one digit. A memory in which digits are stored as elements of area of a surface, as in the cathode-ray tube or magnetic drum store, is yet more economical. If it could be realized, a volume store would be best of all.

Dr. A. C. MOORE (Royal Radar Establishment, Malvern) stated that the barrier-grid cathode-ray storage tube could be operated so as to store one of twenty different intensity levels at each of 2×10^4 positions—an obvious improvement on a device which stores only a binary digit at each point. Opinion at the Conference was divided as to whether a multi-state system would be as reliable as a two-state one.

FERRITE MEMORY DEVICES

Memory devices based on ferromagnetic materials having a substantially square hysteresis loop were surveyed by Mr. J. H. RICHARDS (Mullard Research Laboratories, Salfords). A toroid of such material may have its remanent magnetic flux in either direction, and is therefore capable of storing a binary digit. Such cores can be combined into matrices as

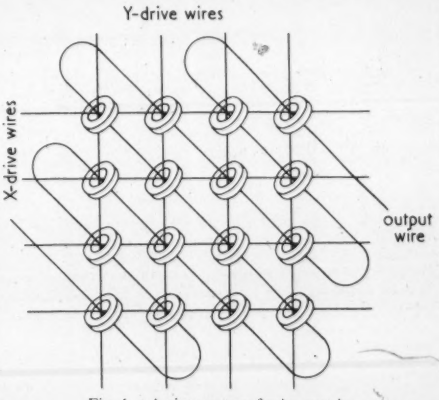

Fig. 1. A sixteen-core ferrite matrix

shown in Fig. 1. If H_m is the field required to saturate the core, current pulses, producing a magnetic field of amplitude $\frac{1}{2}H_m$, applied simultaneously along row X and column Y, will switch only the core so defined. Other cores will receive only half-amplitude pulses and will not be switched. Information may be written into the matrix as binary digits 0 or 1 by successively applying coincident pulses to pairs of co-ordinate wires. To read the information, coincident pulses are applied in a direction tending to switch to the state representing 0. The resulting flux change is small if a 0 has been stored but large if a 1 has been stored.

Since only one core is read at once, the output may take the form of a diagonal wire threading all cores. However, in a $N \times N$ matrix, $2(N-1)$ cores will be disturbed on reading, and the output from these may well exceed that from the core being read. Fig. 2 shows that the output pulse

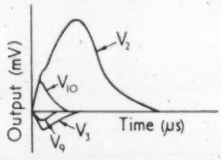

Fig. 2. Voltage outputs of cores in ferrite matrix
V_2: output of switched core; V_3, V_9, V_{10}: outputs of disturbed cores under various conditions.

from the disturbed cores is shorter than that from the switched one. Discrimination against the total disturbed signal can be improved by threading the output winding in opposite directions through alternate cores and by examining the output about 1 μs after the switching pulses are applied or, alternatively, applying two reading pulses first in the 1 and then in the 0 direction and integrating the output over the total reading period.

The earlier materials used for cores were magnesium manganese ferrites. Copper manganese ferrites have recently been found to have similar hysteresis loops. Fig. 3(*a*) shows a family of pulse response curves taken with varying driving pulse amplitudes. As this amplitude increases, the output pulse increases in amplitude and decreases in duration. Fig. 3(*b*) shows the reciprocal of the switching time τ as a function of the pulse amplitude. The linear portion of the curve is given by

$$(H_m - H_c)\tau = s \qquad (1)$$

where H_m is the maximum field during the pulse, H_c is approximately equal to the coercive field and s is a constant. Galt has derived the theoretical relation

$$s = \beta d / M_s \qquad (2)$$

where M_s is the saturation magnetization, β the viscous damping of domain wall motion and d the distance between domain walls. When a matrix is switched by two coincident currents in the manner described above, the necessity of operating over the squarest hysteresis loop limits the maximum field H_m to about $1{\cdot}4\,H_c$. It is therefore clear that to obtain the smallest switching time a material of a low value of s must be used.

The switching current required can be reduced by using smaller cores. Core apertures of 0·08 in. have been used, but recently 0·05 in. cores have been employed and Looney has used ferrite beads fired directly on to 0·002 in. diameter wires.

The memories described above have an access time of the order of 1–1·5 μs with materials of coercive field approximately equal to one oersted. The complete operation of

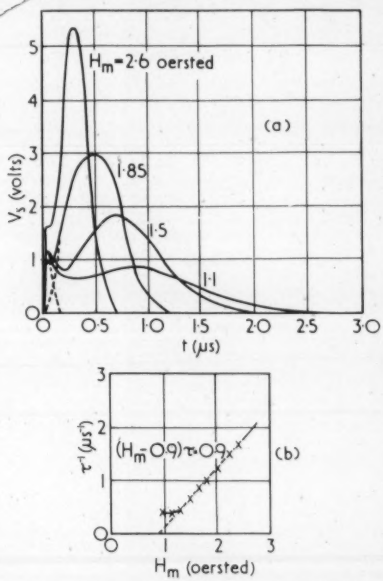

Fig. 3. (*a*) Pulse response curves obtained from a manganese–magnesium ferrite
(*b*) Reciprocal of switching time t as a function of pulse amplitude H_m

reading and re-writing the information takes 5–10 μs. Much smaller switching times are possible with ferrites if they do not have to be used under coincident current conditions. Fig. 4 shows the principle of a high-speed memory using two cores per digit. The read, write and digit pulses are approximately 100 mμs long. The digit pulse is of opposite sign for 1 and 0. It will be seen that when writing 1, the digit and write pulses add in core B, which therefore switches further than core A, though still not completely. Core A switches furthest when writing 0. On reading, both cores are returned to point P of the hysteresis curve so that B or A gives the greater output according as a 1 or a 0 has been stored. The polarity of the output pulse therefore depends on whether a 1 or a 0 has been stored. This system has the advantage that the pulse amplitudes are not critical and heating is small because the cores are not fully switched.

Mr. R. G. George (Standard Telecommunication Laboratories, Enfield, Middlesex) pointed out that a ferrite plate drilled with holes has the advantage that the wiring can be printed, though it does require two holes per digit and a switch to select the digit. The operating current can be between 40 and 80 mA and temperature compensation is good. A memory holding 5×10^4 digits is possible with an

access time of 50 μs. Very high speeds can be obtained only at the expense of high currents. A future development is the possibility of devices based on the switching of the pattern of magnetic flux round a series of holes in a ferrite plate.

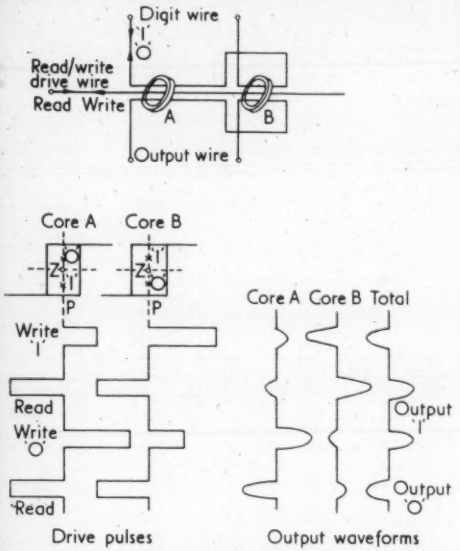

Fig. 4. Principle of high-speed memory using two cores per bit

Dr. R. E. HAYES (Plessey Co. Ltd., Towcester) stated that s of equation (1) is similar for ferrites and metals. Hence the switching time can be diminished only by over-driving the core. One way of doing this with the simple matrix of Fig. 1 is to add a series of diagonal Z wires. A pulse producing a field $\frac{1}{2}H_m$ is sent along the Z wire which passes through the core being read or written. The particular diagonal wire required is selected by a switch matrix operated by the control which selects the X and Y wires. To get the full benefit from an overdriven core, the rise time of the current drive must be small compared with the switching time. Thus larger currents with smaller rise times are necessary, resulting in increased power consumption and cost.

FERROELECTRIC MEMORY DEVICES

Ferroelectric devices were surveyed by Mr. D. CAMPBELL (Plessey Co. Ltd., Towcester). A ferroelectric for use in a memory device must have a low coercive field E_c, a high spontaneous polarization P_s (so as to give a large output on switching) and should preferably have a large temperature range for operation. Barium titanate with $E_c = 1$ kV/cm; $P_s = 26\ \mu$C/cm^2 (higher by an order of magnitude than other materials); and a temperature range 0–80° C, fulfils these conditions. Unfortunately, although crystals grown hydrothermally using potassium fluoride as a flux have a suitable thickness (approximately 0·1 mm), they have to be selected and re-oriented for use. It appears impossible to reduce the cost of a matrix memory below about one shilling per digit, particularly as the size is at present limited to about 20 × 20 elements. At 5 kV/cm the response time is approximately 1 μs. As with ferrites, the reciprocal of the response time is proportional to the field above a threshold limit. Repetition rates greater than 100 kc/s cause heating of the crystal. Switching is additive if the individual pulses are separated by less than the response time. The coercive field is not a constant but depends on frequency. The general effect is that, no matter what voltage is applied, the crystals switch if left long enough. Frequent regeneration of information is therefore needed. Some crystals show a decay of P_s with continuous switching; this appears to be due to crystal imperfections, but is not fully understood. A ferroelectric memory would occupy less space than a matrix of the smallest ferrite toroids and the power consumption would be similar.

Dr. T. B. TOMLINSON (Computer Developments Ltd., Kenton, Middlesex) remarked that the variable coercive field prevented the use of a ferroelectric in the electrostatic analogue of Fig. 1, owing to the possibility of switching occurring with half-amplitude pulses. A possible solution is to connect the capacity formed by the ferroelectric to the potential supply through a non-ohmic resistance R having a characteristic of the type $i \propto V^n$ where $n > 1$. The switching pulse voltage V_0 is several times greater than the value required to switch the ferroelectric if directly connected. The pulse width T must be sufficient to ensure complete switching for a full pulse. Resistance R must have such a value that when a pulse $\frac{1}{2}V_0$ is applied, the rate of rise of voltage across the ferroelectric is slow enough for the final voltage after a time T to be less than the switching voltage by a factor of five or more. When the full voltage pulse V_0 is applied, the initial charging current is greater by a factor 2^n than that for the half pulse. The rise of potential is correspondingly more rapid and the switching field is developed within the period T. By this means, the effective value of half pulses could be reduced by a fifth or less; an extremely large number of such pulses would be required to produce switching. The resistance element could take the form of a semiconducting layer deposited between the crystal and the electrodes.

Dr. J. C. BURFOOT (Queen Mary College, London) considered that neither heating of the crystal at switching frequencies above 100 kc/s nor decay of the information were serious limitations. The former can be dealt with by air-blast cooling and the latter by re-writing the information about once per second. A more serious limitation is the small size of the crystals and the fact that the crystal plates usually taper in thickness. The decay of polarization with use is probably due to deficient electrodes. Cases are known where the polarization *increases* several-fold during use.

Mr. C. F. OXBROW (Signals Research and Development Establishment, Christchurch, Hants) observed that the frequency dependence of the coercive field is particularly serious when the ferroelectric is used in a matrix circuit which is the electrostatic analogue of Fig. 1. The shift register circuit[3] avoids this difficulty. Alternatives to barium titanate which have been studied are guanidine aluminium sulphate hexahydrate (GASH) and triglycine sulphate (GS). GASH is not likely to be satisfactory because of its low operating speed and because large crystals tend to grow with a permanent polarization which cannot easily be removed; GS is a promising material in spite of its low Curie temperature of 47° C. The coercive field is less than that of barium titanate, and this compensates for the thicker crystal slices

which the friable nature of the crystal makes necessary. Switching times of 10 μs have been obtained. It has been confirmed[4] that in GS there are two different mechanisms of domain reversal as suspected, but not proved, for barium titanate. At low fields there is a logarithmic relation between the reciprocal of the electric field and the switching speed; at high fields the relation is linear. These relations are ascribed to nucleation of domains and domain wall motion respectively.

MAGNETIC THIN FILMS

The fundamental properties of thin magnetic films were discussed by Mr. M. WILLIAMS (General Electric Co. Ltd., Wembley). The magnetization of a thin film of high permeability material will always lie very nearly in the plane of the film. This is because a large demagnetizing field would be produced by a component of magnetization perpendicular to the plane of the film. Such films commonly consist of single magnetic domains[5, 6] This is because[7] the demagnetizing field is very small when the magnetization lies in the plane of the film; consequently the small reduction of magnetostatic energy when new domains are formed may be insufficient to supply the domain wall energy.

Films may be produced by vacuum evaporation of a high permeability alloy on to a heated glass substrate. If deposition occurs in a magnetic field parallel to the substrate, the film will have uniaxial anisotropy, the easy axis of magnetization being parallel to the field. The hysteresis loop of such a film depends on the direction in which the measuring field is applied. Measuring fields in the easy direction produce a rectangular hysteresis loop: this changes to a sloping line for fields in the perpendicular direction.[8, 9] A measuring field applied along the easy direction of magnetization in the presence of a steady perpendicular field gives an S-shaped hysteresis loop with reduced coercive force and switching time.[6, 10] This behaviour agrees with that expected for a single domain with uniaxial anisotropy. The simple theory requires that the coercive field in the case of the rectangular hysteresis loop should be proportional to the anisotropy constant and equal to the field needed to produce saturation in the case of the sloping line loop. In practice, the coercive force is rather smaller. This may be due to a reversal of magnetization by the process of domain wall movement. The sloping line is usually curved, which suggests that when the magnetization is inclined at a large angle to the easy direction the torque tending to aline it in this direction is greater than that given by the simple theory.

The anisotropy constant can be reduced if the film is deposited in a rotating magnetic field, but some magnetic orientation usually persists unless the field is very well balanced.

A film subjected to a radio-frequency magnetic field and a perpendicular steady field (both in the plane of the film) exhibits resonance. This can be interpreted[10] in terms of a Landau–Lifschitz equation giving the rotation of the magnetization vector **M** in terms of the torque **T** acting on it:

$$d\mathbf{M}/dt = \gamma\mathbf{T} - (\lambda/\mathbf{M}^2)\mathbf{M} \times \mathbf{T} \qquad (3)$$

The first term corresponds to a rapid precession of **M** about the direction of an applied field: the second represents a slow approach of **M** towards the field direction at a rate determined by the damping constant λ. Any opposition to the precession causes a new precession towards alinement with the field. In thin films, such opposition is provided by the strong demagnetizing field which appears when the magnetization moves out of the plane of the film. A steady magnetic field in the plane of the film will cause the magnetization vector to precess out of the film. This will produce a strong demagnetizing field, the magnitude of which increases with the strength of the applied field. The magnetization vector will then precess about this demagnetizing field, and resonance can therefore occur in a r.f. field of appropriate frequency. The theory leads to a correlation between the resonance behaviour on the one hand and the coercive field and switching time on the other.

The size of a thin film element which can be switched by a uniform field is fixed approximately by the available current, the coercivity and the tolerable ratio of demagnetizing field to coercivity. The output e.m.f. depends on film size and switching rate. If the internal and external fields are reduced, the switching speed falls in proportion. Thus, although coercivity reductions make possible the use of larger films, the available e.m.f. will not necessarily increase. On the other hand, the gain-bandwidth product in the pick-up amplifier is inversely proportional to the flux and therefore to the coercivity.

Non-destructive read-out can be obtained from thin films by applying a limited cross-field pulse and measuring the magnetization change along the easy axis. The sign of this change depends on the initial orientation of the magnetization along this axis.

A new switching system being developed at the General Electric Co. Ltd. uses a cross-field pulse as one of the selection pulses. This lowers the switching threshold and

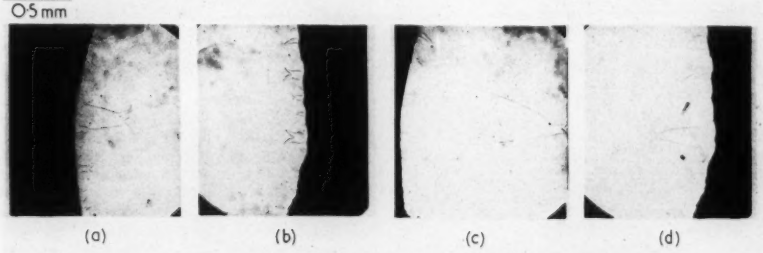

Fig. 5. Reversed domains at edges of thin ferromagnetic film
(a, b) $H = -0{\cdot}2$ oersted. (c, d) $H = -0{\cdot}3$ oersted.

enables a field along the easy axis to perform the switching. The cross field can be fairly strong, since a rectangular hysteresis loop is not needed.

The chief problem in matrix construction is the design and fabrication of conductors. Considerable magnetic and electrostatic interaction occurs between adjacent conductors. Vacuum-deposited metals or dielectrics can break up previously deposited films. Lacquer insulation will not stand the temperature needed for the preparation of magnetic films. The only reported matrix has been built of printed circuit boards.

Though film performance surpasses that of ferrite toroids, many problems must be solved before satisfactory matrices can be constructed. Such matrices would make feasible access time of approximately 100 mμs.

Mr. C. E. FULLER (Mullard Research Laboratories, Salfords) pointed out that below the critical field values for rotation, magnetization must take place by domain wall movement. This process has been studied by slowly reversing a field in the easy direction and examining the domain structure by the magnetic colloid technique. Fig. 5 shows that at low fields the demagnetizing effect is sufficient to produce at the edges of the film reversed domains extending perpendicular to the easy direction. Increase of field causes the reverse domains to grow. Fig. 6 shows that at a reverse field of 0·6 oersted the reverse domains from either side link up across the middle of the film. Further increase of field causes the walls to move out to the upper and lower edges of the film. Magnetization by domain wall movement of this nature would result in a fairly square hysteresis loop, the coercive field being that required to cause the nucleated domains to link up across the film.

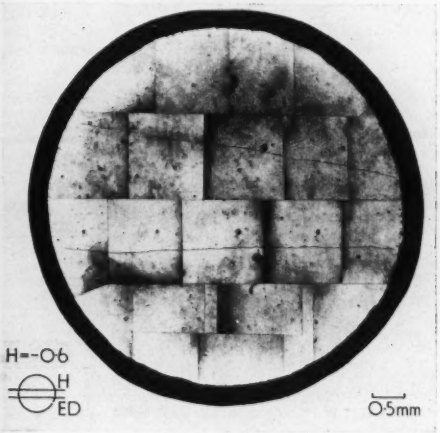

Fig. 6. Composite micrograph showing a reversed domain extending across a film at high reversing fields

Domain wall movement under inhomogeneous fields was discussed by Dr. A. C. MOORE and Mr. A. S. YOUNG (Royal Radar Establishment, Malvern). A reverse field was applied along the easy axis of a single domain film. The field had a gradient parallel to the easy axis, and its peak intensity was greater than the coercive field. A single domain, formed in the high field region, progressed through the film under the action of a decreasing drive field to a point where the field was insufficient to overcome the resistance to domain wall movement. The resulting zig-zag boundary is shown in Fig. 7. The field gradient was obtained by laying a current-carrying wire across the film, thus obtaining a symmetrical

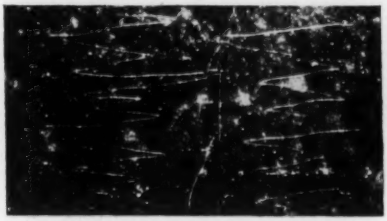

Fig. 7. Domain boundaries due to inhomogeneous reverse field

picture with two domain boundaries. The domain walls make a small angle with the magnetization direction as this minimizes the energy of the boundary. The inner points of the wall occur where the reverse field is equal to the coercive field; the outer points lie where the field has about half this value. The angle between the domain walls and the magnetization direction is determined by the material itself. If the field gradient is changed, this angle remains unaltered and the points of the domain wall remain in the same field range; only the pitch of the zig-zag is changed. The domain pattern shows no obvious change when the field is removed. In a typical 80/20 nickel–iron film 1500 Å thick, the inner points of the domain wall occurred at 3·2–4·0 oersted and the outer ones at 1·2–2·0 oersted. The hysteresis loop was rectangular, with a coercive field of 3·3–3·7 oersted. The field strength at points where the domain walls are held up (the inner points of Fig. 7) show a scatter indicating a variability of coercive field throughout the specimen. There is evidence that this is due to mechanical stresses in the films and to lattice imperfections rather than variations in chemical composition.

Mr. E. M. BRADLEY (British Tabulating Machine Co. Ltd., Stevenage) described hysteresis loop measurements in which the change of flux was measured in the plane of the film but perpendicular to the applied field. If magnetization reversal occurs by domain wall movement, no flux change should be observed in this direction: if by a coherent rotational process, then a flux change will be observed which can be compared with theoretical calculations. Experimental curves differed from theoretical curves based on the coherent rotation model in (*a*) the lack of predicted discontinuities, and (*b*) the low ratio of coercive field in the easy direction to the field required to saturate in the perpendicular direction. With thicker films, the proportion of flux rotating is smaller, showing that wall motion and rotation occur simultaneously.

SUPERCONDUCTING MEMORY DEVICES

The present status of superconducting memory devices was surveyed by Dr. E. H. RHODERICK (Services Electronics Research Laboratory, Baldock). The first serious attempt at applying superconductivity phenomena to computer circuitry was the cryotron.[11] This uses the destruction of super-

conductivity in a tantalum wire (known as the gate) by the magnetic field of a coaxial superconducting solenoid. In this way it is possible to achieve *current gain*, i.e. to use one current to control a larger current. Two cryotrons can be connected to form a bistable flip-flop. The maximum rate of such a flip-flop is about 10 kc/s, the limit being set primarily by heating effects. In the absence of heating effects a fundamental limit to the speed is the time taken for the superconducting-normal transition to reach completion. This time is determined by eddy-current effects, and can be reduced by using thin evaporated films. The gate of a thin film cryotron may consist of a narrow strip of tin film and the control solenoid can be replaced by a strip of lead film perpendicular to the gate and separated from it by a thin layer of insulation. Current gain is achieved if the width of the control strip is less than that of the gate. Most current cryotron research is devoted to developing techniques of making thin films, since without a sure understanding of the factors which influence the structure of a film (nature and temperature of substrate, rate of deposition, residual gas, etc.), consistent results cannot be achieved. Switching times of approximately 1 μs have been claimed for flat film cryotrons.

Since a superconducting ring can carry a persistent current circulating in either direction, it can provide the basis of a bistable memory device. The most advanced application of such persistent currents is the Crowe[12] cell. This employs a thin lead film containing two holes separated by a narrow bridge, which in practice consists of a circular aperture divided in two by a narrow cross-bar, rather like the London Transport sign. Drive and sense wires are placed on opposite sides of the cross-bar and parallel to it. A current pulse sent through the drive wire can, under suitable conditions, induce a persistent current in the lead film. This persistent current flows in a figure of eight pattern, circumscribing the two holes in opposite directions. The direction of the current through the cross-bar determines whether a 0 or 1 is stored. An advantage of this type of cell is that the magnetic field is confined to a much smaller region than in the case of a simple ring. As in the case of the cryotron, the speed of operation is determined by heating effects. Measurements by R. F. Broom at the Services Electronics Research Laboratory showed that the thermal relaxation time, which limits the speed of switching from the 0 to 1 state, can be as short as 40 mμs. This refers to a cell in which the cross-bar was of lead, 500 Å thick, deposited on a mica substrate. The thermal relaxation time of an identical cell on a glass substrate was appreciably longer.

The Crowe cell is already very promising as regards switching time. The aperture may be as small as 1 mm diameter. This permits a packing density of 10^4 per ft^2 or 10^6–10^7 bits per ft^3. The cell quoted dissipated 10^{-10} J when switched, so that 10^{10} elements could be switched per second for a dissipation of 1 W, which would evaporate about 2 l. of liquid helium per hour. However, the problem of the reproducibility of thin films is not an easy one, and little is known about their stability. The importance of electron microscope studies of the structure of evaporated films cannot be over-emphasized.

Dr. E. MENDOZA (University of Manchester) stated that the factor which would decide whether superconducting devices could be employed in practical computers was their power dissipation, which determined the quantity of liquid helium. Although simple techniques exist for handling liquid helium supplied by the National Physical Laboratory, it may eventually be simpler and more economical for a helium liquefier to be incorporated in the memory unit. It should be possible to design a liquefier functioning like a domestic refrigerator and keeping a volume of about 1 ft^3 cold indefinitely. Quite a small unit could handle a power of 10 W. Rough estimates indicate that this should suffice for a large, fast memory. A wire-wound cryotron dissipates 0·1 erg/flip. It is not impossible to imagine printed cryotrons with a power dissipation of 10^{-7} erg/flip. Ordinary-sized liquefiers could therefore cope with repetition rates of 10^8/s, allowing for 10^4 units flipping simultaneously. Gain of heat by conduction along leads is unimportant because such leads are few in number and methods of reducing the conduction are well known. It therefore appears that from the point of view of low-temperature technology there is no insuperable problem in the practical application of superconducting devices.

Dr. R. E. HAYES (Plessey Co. Ltd., Towcester) stated that the commercially available Collins Liquefier manufactured by A. D. Little and costing about £30 000 ($11 000) could supply about 4 l. of liquid helium per hour, which would suffice for a power dissipation of 3 W. The liquid nitrogen required could be obtained from a Philips liquefier costing about £2300. The capital cost of the low-temperature plant for a computer is therefore not excessive. For comparison, the present cost of a high-speed valve computer is at least £100 000.

The University,
Reading.

T. B. RYMER

REFERENCES

(1) HOOVER, C. W., STAEHLER, R. E., and KETCHLEDGE, R. W. *Bell System Tech. J.*, **37**, p. 1161 (1958).

(2) BOBECK, A. H. *Bell System Tech. J.*, **36**, p. 1319 (1957).

(3) ANDERSON, J. R. *I.R.E. Trans on Electronic Computers*, p. 184 (1956).

(4) FATUZZO, E. *Helv. Phys. Acta*, **31**, p. 309 (1958).

(5) FOWLER, A., FRYER, E. M., and STEVENS, J. R. *Phys. Rev.*, **104**, p. 645 (1956).

(6) OLSON, C. V., and POHM, A. V. *J. Appl. Phys.*, **29**, p. 274 (1958).

(7) KITTEL, C. *Phys. Rev.*, **70**, p. 965 (1946).

(8) BECKER, R. *Z. Phys.*, **62**, p. 253 (1930).

(9) STONER, E. C., and WOHLFARTH, E. P. *Phil. Trans Roy. Soc. A*, **240**, p. 599 (1948).

(10) SMITH, D. O. *J. Appl. Phys.*, **29**, p. 264 (1958).

(11) BUCK, D. A. *Proc. Inst. Radio Engrs.*, **44**, p. 482 (1956).

(12) CROWE, J. W. *I.B.M. J. Res. Developm.*, **1**, p. 295 (1957).

Investigation of the ignition of a gas by an electric spark

By D. R. Lintin, B.Sc., and E. R. Wooding, Ph.D., D.I.C., A.Inst.P.,* Safety in Mines Research Establishment, Sheffield

[*Paper first received* 10 *January, and in final form* 20 *October*, 1958]

By using flashes of microsecond duration it has been possible to obtain a series of shadowgrams showing the development of steadily propagating flames.

About 100μs must elapse before any difference can be detected between the flame kernels which will propagate and those which subsequently degenerate. The critical radius, at which this difference becomes apparent, has been measured in various mixtures of methane and air. The time to reach this critical stage has been determined. The flame speed has been calculated and after assuming a value for the final flame temperature, the burning velocity has been estimated.

From the results obtained it has been possible to outline the mode of growth of the flame and to state which conditions favour ignition.

1. Introduction

In the ignition of a gas by an electric spark there are many features still to be investigated. Arnold and Sherburne[1] have studied the growth of a flame in a flowing gas and Olsen and others[2] examined incipient flames after the passage of a relatively energetic spark. In the present work, various stages are studied in the development of a flame from a spark having just sufficient energy to cause ignition. Shadowgrams of the flame are obtained with a microsecond pulse of collimated light, a method having high temporal resolution and causing no interference with the combustion processes.

An investigation of a critical stage in the growth of a flame is described and other features of the flame are examined. The existence of a critical stage has been postulated in the ignition theories of Jost,[3] Lewis and von Elbe[4] and Burgoyne and Weinberg.[5] At this stage it is possible to decide if a flame kernel will propagate or degenerate.

2. Method of Investigating Incipient Flames

The progress of the flame front was followed by means of shadowgrams taken at predetermined intervals after the igniting spark had passed. The apparatus (Fig. 1) consisted of a flash-tube F, and condensing lens L_1, which illuminated a pinhole P, followed by a lens L_2 which caused a parallel beam of light to pass through the flame and fall on a photographic emulsion in filmholder K. When the ignition gap broke down, an electronic delay unit D was initiated and after a predetermined time, the flash-tube fired. The ignition chamber I and its ancillary circuits are described in the next section.

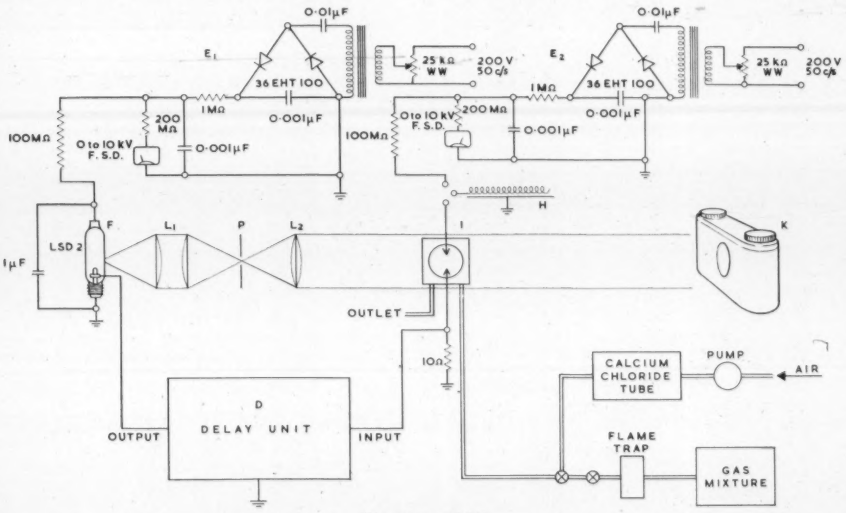

[Crown copyright]

Fig. 1. Apparatus for high-speed shadow recording

* Now at Sheffield University.

A 1 μF capacitor released about 25 J of energy through the flash tube (Mullard LSD 2), the light falling to half its peak intensity in about 5 μs. The tube was triggered by a high potential pulse produced when the thyratron V_4 in the delay unit (Fig. 2) fired. The delay between the igniting spark and the flash was the time taken to fire valve V_3 and charge capacitor C up to the striking potential of valve V_4, plus the time of initiation of the flash tube. The reproducibility of triggering was improved by illuminating the flash tube with a 5 W tungsten lamp.

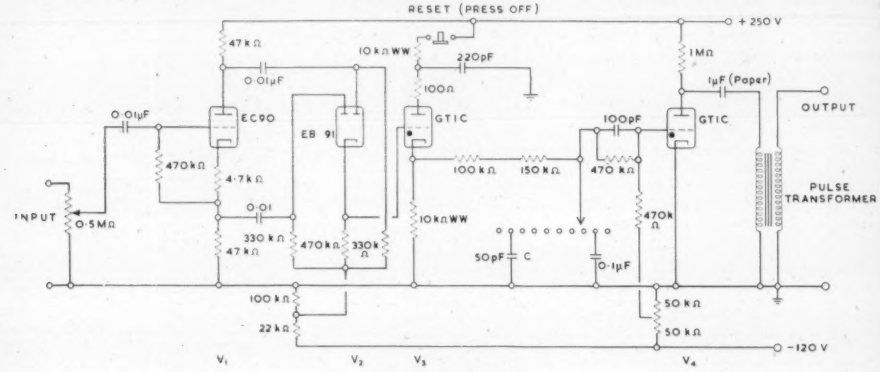

[Crown copyright]

Fig. 2. Delay unit

3. THE IGNITION SYSTEM

The igniting spark occurred when a fixed gap broke down under a high potential and discharged a delay cable H. The spark gap was enclosed in a chamber which could be filled with inflammable gas at atmospheric pressure.

The ignition chamber (Fig. 3) was constructed from a block of perspex 12 × 5 × 5 cm, with brass electrodes mounted in polytetrafluoroethylene bushes. Light was transmitted through plate glass windows and the volume of gas enclosed was 14 cc.

The arrangement of the electrodes shown in Fig. 4, was chosen because it had less influence on the flame growth than any other arrangement examined. (See Addendum.) Gold wires of 0·0025 cm diameter were soldered to the brass cones so that the energy abstracted from the flame was a minimum. Gold was used since it was expected to have little influence on the oxidation of methane. Although its melting point is 1100°C, wires of less than 0·2 cm length did not melt in the incipient flames.

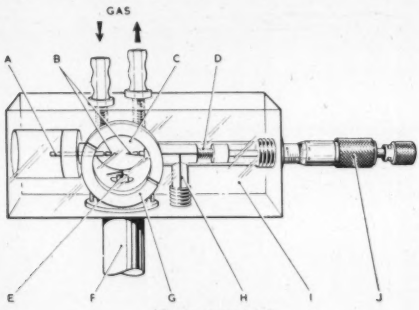

[Crown copyright]

Fig. 3. Ignition chamber

A, high potential electrode connexion; *B*, detachable electrode tips; *C*, combustion space; *D*, return spring; *E*, lead through for trigger electrode; *F*, supporting pillar; *G*, window retaining ring; *H*, low potential electrode connexion; *I*, perspex body; *J*, adjusting micrometer.

The electrical energy was obtained from a length of Hackethal delay cable, type HH2000, previously charged to several kilovolts. Since the cable was not correctly terminated by the discharge circuit an oscillatory spark occurred lasting about 0·5 μs. The cable was suspended by polythene filaments so that it could be swung to one side, charged to a chosen potential by the generator E_2 and then swung back to discharge through the ignition chamber. A small spark passed between the cable and terminal of the ignition chamber, connecting them electrically only while the igniting spark was passing. Consequently the flame could grow undisturbed by electric fields.

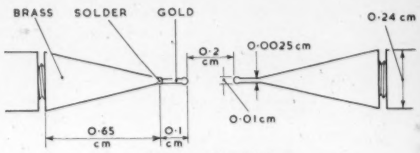

[Crown copyright]

Fig. 4. Electrode orientation and dimensions

It was estimated that the igniting spark released about a millijoule of electrical energy during an interval of about 0·5 μs. The energy depended on the potential to which the delay cable was charged, and was varied for each gas mixture.

The length of the spark channel was 0·2 cm and its apparent

radius as measured on a direct photograph was 0·003 cm. Hence the energy density was of the order of 10^2 J cm^{-3} and the temperature calculated from specific heats was of the order of 10^4 °K.

The gas mixtures were stored in iron gasholders after the gases had been measured, brought to a known humidity and mixed.

The gas composition is expressed as the equivalence ratio ϕ, where

$$\phi = \frac{\text{percentage by volume of methane in mixture}}{\text{percentage by volume of methane in stoichiometric mixture}} \quad (1)$$

The gas was passed through a saturated solution of calcium chloride ($CaCl_2.6H_2O$) which reduced the relative humidity to 31% and after each ignition the apparatus was flushed out with dry air (r.h. $< 10\%$).

4. BEHAVIOUR OF THE APPARATUS

The optical resolution of the system depended on the quality of the collimating lens and on the size of the pinhole. When an f/15 lens of 42 cm focal length was used in conjunction with a pinhole of 0·028 cm diameter, the minimum distance that could be resolved in the image plane was 0·031 cm corresponding to 0·005 cm in the region of the flame. After the flame speed had been measured it was found that the maximum displacement during the flash was of the order of 0·01 cm but this could only limit the resolution during the first observation.

The accuracy of collimation was determined by measuring the separation of the images of two wires which were a known distance apart.

Weinberg[6] has shown how a ray of light is deflected by a flat flame. From his work it can be seen that a spherical flame illuminated by parallel light should form a circular bright ring on a uniformly illuminated background. Just inside the ring is a region of low illumination increasing toward the centre of the image. As a result of diffraction there is a narrow zone of low illumination just outside the bright ring. This is the type of image which has been recorded in Fig. 5. This deflexion causes the shadow to be larger than the flame diameter. The enlargement was determined by measuring the displacement of the lines of a grid placed between the collimating lens and the flame. From records such as Fig. 11 it was calculated that flames of diameter 0·1 to 1·2 cm were enlarged by a factor of 1·18 if the diameter of the centre of the bright zone in Fig. 5 were measured.

The minimum delay obtainable was 23 μs and the reproducibility of the system such that the standard error varied from 2 μs with a delay of 25 μs to 30 μs with a delay of 1 ms.

Although the rated peak current of the GT 1C thyratron was exceeded by a factor of 50 or more, the delay unit operated for several months before it became necessary to replace valve V_4.

5. GENERAL CHARACTERISTICS OF AN INCIPIENT FLAME

The shadowgrams of incipient flames (Fig. 5) show (*a*) a propagating kernel and (*b*) a kernel which degenerates, the equivalence ratio of the gas being 0·9 in each case. Each shadowgram is of a different flame since the photographic system could be used to obtain single records only. The polarity of the right-hand electrode was positive.

The first observation of the flame was made 23 μs after the igniting spark had passed. No shock wave was detected. The flame envelope was approximately cylindrical with slight corrugations but there was no evidence of any part of the spark being more effective than another in causing ignition. Between 50 and 100 μs, the corrugations disappeared and the

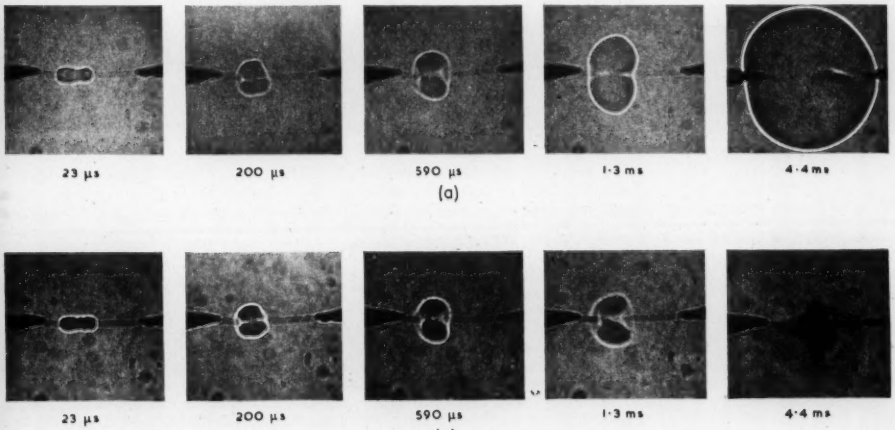

[Crown copyright]

Fig. 5. Shadow of incipient flame in a methane/air mixture, $\phi = 0·9$

(*a*) Ignitions: the radius of the flame kernel grows steadily; (*b*) Non-ignitions: after an initial growth the flame kernel dies away.

flame became nearly spherical. During the next 200 μs there were the first detectable differences between propagating and degenerating flames. A propagating flame continued to grow but at a diminished speed, and a flame which later degenerated grew slower still. After 500 μs the flame usually became oblate. It had indentations where it was penetrated by the electrodes, although the thermal capacity of the gold wire was only 10^{-5} J cm^{-1}. After 1 ms the rate of growth of the propagating flame fell to its lowest value but rose after about 3 ms, reaching the value expected for a steady flame after 5 ms. The degenerating flame became turbulent and diffuse after 1 ms, lost its structure after 2 or 3 ms and disappeared completely after 5 ms.

It was calculated that the buoyancy of the hot gas caused the flame kernel to rise a distance of about $5 \cdot 10^{-4}$ cm, during the first millisecond. This distance was too small to be detectable in the shadowgrams.

6. IMPORTANT STAGES IN THE GROWTH OF A FLAME

The radii of the propagating and degenerating flames are plotted in Fig. 6 for $\phi = 0 \cdot 9$ and similar results were obtained for other gas mixtures. Each point is the average of five

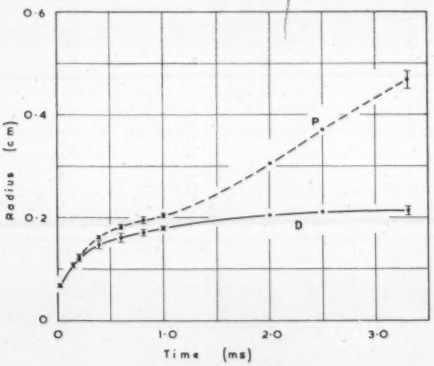

[Crown copyright]

Fig. 6. Growth of flame kernels, $\phi = 0 \cdot 9$
P, propagating flame; *D*, degenerating flame

determinations and the standard deviation is shown. From these curves, it has been possible to determine the radius at the critical stage, the radius associated with a minimum in the flame speed and the final radius when the degenerating flame disappeared.

In this work, the critical stage is defined as that stage at which a difference is first detectable between the rates of growth of propagating and degenerating flame kernels. Experimentally, the critical stage was taken to be that at which the radii of propagating and degenerating flames just differed by more than the standard deviation of a measurement.

Ideally, the critical radius should be determined when the energy of the igniting spark is varied in the region of the minimum igniting energy. Since it was not possible to control the energy with adequate precision, the potential was adjusted until 50 $\pm$ 20% of the sparks caused ignition. An increase or decrease in spark energy of about 5% caused 100% or zero ignitions respectively. The radii of the propagating flames were then increased by about 10% and those of the degenerating flames decreased by a similar amount. The experimental values of the critical radius are plotted in Fig. 7 against gas composition and the times taken for an incipient flame to grow to the critical radius are plotted in Fig. 8.

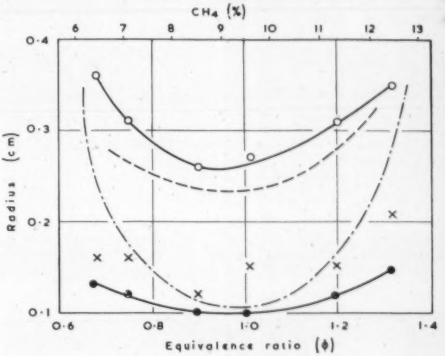

[Crown copyright]

Fig. 7. Radii which are important in the growth of flames in various methane/air mixtures

—●— critical radius
— — — Arnold and Sherburne[1]
× × minimum velocity
—·— Blanc and others[7]
—○— extinction.

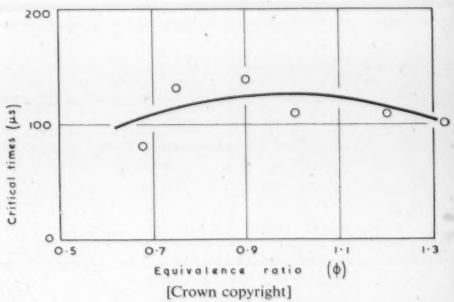

[Crown copyright]

Fig. 8. Time for kernels to reach critical stage

A critical radius has also been determined by Arnold and Sherburne[1] after an arbitrary time of 200 μs. The values which they obtained were greater than those reported in this paper owing to a different definition of the critical stage.

It was found that the radius of the degenerating flame tended to a constant value which we have called the extinction radius. Experimental values were obtained by extrapolation of the radius/time curve to 5 ms because the flame kernel although still expanding slightly became too diffuse to measure after 2 to 5 ms. The extinction radii plotted in Fig. 7 are larger than any of the other characteristic radii.

The quenching radii determined by Blanc and others[7] are also plotted in Fig. 7 for comparison. They determined these radii by igniting gas mixtures between two parallel glass plates and decreasing their separation until the spark energy required to cause a flame to propagate was greater than the minimum igniting energy. Energy is removed from the flame front by conduction at a rate dependent upon the distance from the solid wall. Consequently the flame front becomes curved and the divergence of energy through it increases. It is apparent in Fig. 7 that the quenching radii are larger than the critical radii.

7. FLAME SPEED AND BURNING VELOCITY

The flame speed was calculated from the variation of radius with time. It was subsonic (of the order of 10^4 cm s^{-1}) when the first measurement was made and fell in an exponential manner to attain a minimum of the order of 10^2 cm s^{-1} after one or two milliseconds. Subsequently the speed increased and attained a constant value after about 5 ms.

A flame increases in radius at a rate v as a result of the flame front propagating through the unburned gas at a velocity S and the gas expanding as it is heated from its initial temperature T_0 to a final temperature T_F. The flame speed v is related to the burning velocity S by the relation

$$v = S\,T_F/T_0 \qquad (2)$$

If any reaction occurs subsequently in the burned gas, this relationship is invalid.

A value of the burning velocity was estimated from the flame speed v using equation (2) and values of T_F published by Smith and others.[8] The published values of T_F are those of a steadily propagating flame and are possibly a fifth of the value attained in the incipient flame at an early stage. Consequently the estimate of burning velocity is an upper limit.

The variation of the estimated burning velocity with time is shown in Fig. 9 for a gas mixture of equivalence ratio 0·9.

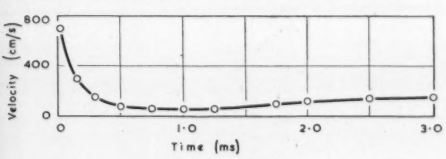

[Crown copyright]

Fig. 9. Upper limiting value of burning velocity obtained by assuming a value of final flame temperature, $\phi = 0{\cdot}9$

It is initially about 25 times greater than the steady value S_u determined by Coward and Hartwell[9] and since T_F is in error the true value of the burning velocity at this time must be about five times the steady value. The minimum value S_m is about half S_u but the velocity attained after 5 ms is in reasonable agreement with the values of Coward and Hartwell.

The minimum velocity S_m, the final value S_u, the velocity S_c at the critical stage and values determined by Coward and Hartwell are plotted in Fig. 10 against the equivalence ratio of the gas mixture.

The radii of flames having the minimum flame speed are plotted in Fig. 7.

8. TEMPERATURE OF THE FLAME KERNEL

Accurate calculations of burning velocity could be made if the flame temperature were known, so an attempt was made to deduce the temperature within the flame kernel, assuming that a ray passing through a spherical flame encountered a constant refractive index within the burnt gas. Then the temperature could be calculated by measuring the deflexion

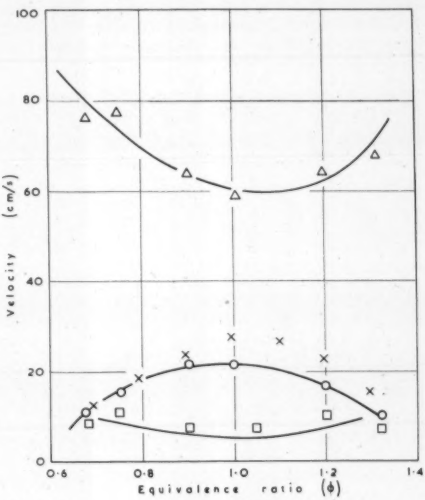

[Crown copyright]

Fig. 10. Burning velocities

△ critical velocity S_c; × Coward and Hartwell's[9] values;
○ steady velocity S_u; □ minimum velocity S_m.

of a ray of light on passing through the flame. The optical system described above was used with a grid placed immediately behind the collimating lens so that the shadow was dissected as in Fig. 11 (compare, Ellis and Morgan[10]).

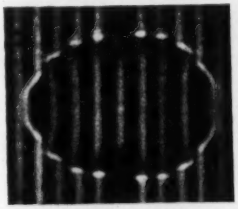

[Crown copyright]

Fig. 11. Dissected shadowgram

The angular deflexion α of a ray on passing through the flame can be calculated from the displacement which the image of the grid lines suffers. If refractive indices of the burnt and unburnt gas are n and n_0, a ray which encounters the flame kernel at an angle θ to the radius is deflected through an angle

$$\alpha = 2\,\frac{(n_0 - n)}{n}\tan\theta$$

If n were constant throughout the flame kernel a plot of α against $\tan\theta$ should be a straight line. If n varies with radius, α must be calculated by means of a relationship derived by Schardin.[11] From the graph of α plotted against $\tan\theta$ in Fig. 12, it appears that the temperature is fairly constant near the centre of the flame kernel and then varies with increasing radius. This is consistent with the spark causing an initial rapid heating of the gas and heat being conducted away subsequently.

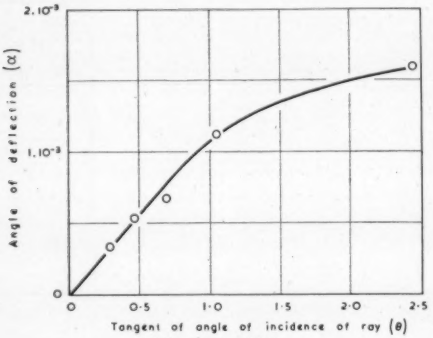

[Crown copyright]

Fig. 12. Deflexion of ray on passing through flame kernel

9. DISCUSSION

The equations of continuity of a laminar flame have been stated by Courant and Friedrichs[12] and simplifying assumptions were made by Evans[13] and Hirschfelder and Curtis.[14] For a flame with spherical symmetry the energy equation is

$$\frac{\partial}{\partial t}[\rho e] + \operatorname{div}[MI - F] = 0 \qquad (3)$$

where ρ is the gas density, M is the mass velocity of flame per unit cross-sectional area, e is the specific internal energy of the gas mixture per unit mass of gas, I is the enthalpy per unit mass, and F is the net energy flowing through the flame front per unit area in unit time.

$$I = i + \varepsilon + H$$

where i is the specific enthalpy of the gas, less the contribution of the spark energy, ε is the enthalpy resulting from the energy release in the spark, and is a function of r and t, while H is the heat of combustion of the mixture per unit mass.

The simplifying assumptions are that the viscosity of the gases has a negligible effect on the equations of continuity and that the flame velocity is small enough for pressure differences to be negligible.

The behaviour of the incipient flame is governed by the function $[\rho e]$. When $[\rho e]$ is constant

$$\operatorname{div}[MI - F] = 0 \qquad (4)$$

The radius of the flame tends to infinity as $[\rho e]$ tends to a constant value so that this is a condition for steady combustion. Assuming that only the radial components of relation (4) are varying

$$\frac{1}{r^2}\frac{\partial}{\partial r}[r^2(MI - F)] = 0 \qquad (5)$$

and

$$[r^2(MI - F)] = g(\phi)$$

where $g(\phi)$ is a function which is related to the gas composition and is independent of time.

At the critical stage, a minimum value of $[\rho e]$ is expected so that equations (4) and (5) are valid. Also the second derivative of $[\rho e]$ must be positive and

$$\frac{\partial^2}{\partial r^2}(r^2 MI) > \frac{\partial^2}{\partial r^2}(r^2 F) \qquad (6)$$

i.e. the critical radius is defined by the enthalpy flow through the flame front.

Since the initial contribution to $[\rho e]$ from the spark is about an order greater than the contribution from the combustion reaction, $[\rho e]$ falls rapidly until a minimum is reached.

The time taken to reach the critical stage after the passage of a spark could be the time taken for the combustion reaction to release energy. Norrish and others[15] observed that certain radicals appeared after 10^{-4} s when a combustion reaction was initiated by an intense flash and a range of hydrocarbon-oxygen mixtures was studied. If the enthalpy due to the spark is too low or the geometry of the system causes the flux to be too great then the flame kernel degenerates. Since the critical stage occurs when r is small, M and I must be large and positive.

The flame could be extinguished if $[\rho e]$ were reduced by increasing the flux of energy through the flame front. This can be achieved by increasing the curvature by turbulence or by passing the flame through a gap of appropriate dimensions (the quenching distance).

The existence of a minimum in the flame speed indicates the existence of a further important stage in the development of the flame. This stage has been found to occur when the radius of the flame is approximately equal to the quenching radius.

Olsen and others[2] found that the product of burning velocity and final flame temperature fell to a minimum after about 1 ms in propane but that there was no such minimum with hydrogen. They suggested that the combustion reaction in propane was not complete until after 1 ms and the present results indicate that the reaction in methane occurs in two stages.

If this is the case then there should be a minimum in the energy density during the interval, accompanied by a minimum in the flame speed. During this interval the flame should be most susceptible to the removal of energy so that the quenching radius could be equal to the radius at which the minimum speed occurs.

10. CONCLUSIONS

The development of a steady flame from an electric spark passed through a stationary gas has been recorded by allowing short duration flashes to form a shadow of the flame front on a photographic film. Several important stages in the development have been studied quantitatively.

The critical stage has been investigated and the critical radius which has been postulated in a number of ignition theories has been measured. It is thought that this stage coincides with the first release of energy from the gas by the combustion process. The critical radius and the time taken to attain it are dependent on the gas composition.

Those flame kernels which fail to propagate tend to a constant radius which is dependent on the spark energy and to some extent on the gas composition. Such a relationship would exist if the growth were the result of thermal conduction only and no exothermic chemical reaction occurred. Since there were uncontrollable variations in the spark, it was

not possible to discover the reason for some flame kernels failing to propagate.

The speed of the flame was subsonic 23 μs after the passage of an igniting spark. It then fell almost exponentially to a value less than that associated with a steady flame but rose to the expected value after 5 ms. The minimum speed is thought to be associated with a delayed release of energy by the combustion reaction.

The burning velocity was estimated from the flame speed and published values of the final flame temperature. This estimate is an upper limiting value since the temperature immediately after the igniting spark passed was about five times the final flame temperature. An attempt to determine the temperature within the flame kernel was unsuccessful.

time that the energy density is as large as possible at the critical stage.

(*d*) The electrodes should be as small as possible and no solid surfaces should be present to remove energy until the flame is greater than the quenching radius.

It has been possible to indicate the way in which spark energy may be related to the characteristics of an inflammable gas mixture [equation (5)]. Further experiments are required to relate temperature to time and position in the flame. The use of flash photolysis and kinetic spectroscopy (Porter[16]) would be a means of obtaining very useful information on the gas reaction which appears to occur in two stages. This would also provide a means of determining the minimum density of energy necessary for ignition.

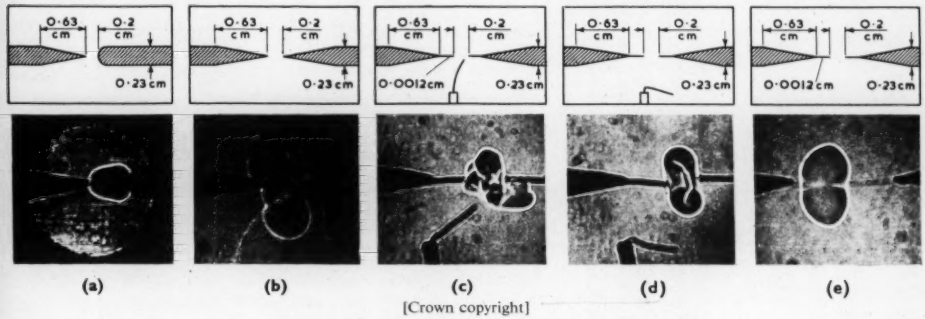

[Crown copyright]

Fig. 13. Influence of arrangement of electrodes and igniting circuit

Conditions under which records were obtained:

(*a*) Electrodes—brass point to hemisphere. Electric field applied for duration of spark. Breakdown occurs when delay line is brought into contact with outer end of one electrode.
(*b*) Electrodes—brass point to point. Electric field applied permanently by capacitor. Breakdown occurs by chance.
(*c*) Electrodes—brass with gold wire tips. Electric field applied permanently by capacitor. Breakdown occurs when pulse is applied to third electrode.
(*d*) Electrodes—brass with gold wire tips. Electric field applied permanently by capacitor. Breakdown occurs by chance. Third electrode inoperative.
(*e*) Electrodes—brass with gold wire tips. Electric field applied for duration of spark only. Breakdown occurs when charged delay line is brought into contact with outer end of one electrode.

The steady burning velocity can be determined accurately if the flame speed is measured about 10 ms after the passage of the igniting spark. Then the flame is propagating steadily and the flame temperature is the steady value.

The radius of the flame when the speed is a minimum is approximately equal to the quenching radius. It is inferred that the energy density in the flame front must be a minimum at this time so that removal of further energy causes extinction. A minimum energy would be concomitant with a delayed release of energy or the combustion reaction proceeding in two stages.

The ideal conditions for ignition by a spark appear to be:

(*a*) The electrode separation should be twice the critical radius. If less than this, energy is removed from the gas before the chemical reaction has commenced, if greater, the density of energy from the spark is diminished. These effects are also apparent in the relation between minimum igniting energy and electrode separation published by Blanc and others.[7]

(*b*) The gas should not be turbulent; then no convolutions of the flame front can occur to increase the flux of energy into the unburned gas.

(*c*) The energy of the spark should be released in such a

ADDENDUM

Influence of electrode on flame kernel. Fig. 13 has been added to illustrate the importance of the electrode shape and orientation on the growth of the flame kernel. For the measurements of flame radii, the electrodes (Fig. 13(*e*)) were selected which appeared to cause least disturbance. It was also found to be essential that the electric field should be removed as soon as the igniting spark had passed. The polarity of the right hand electrode is positive in each case.

ACKNOWLEDGEMENT

This paper is published by permission of the Ministry of Power. The authors wish to express their gratitude to Dr. J. H. Burgoyne and Dr. F. J. Weinberg for stimulating discussion of the work. They are also indebted to those members of S.M.R.E. staff who assisted with construction of apparatus and the production of this report.

REFERENCES

(1) Arnold, J. S., and Sherburne, R. K. *4th Symposium (International) on Combustion* 1952, p. 139 (Baltimore: Williams and Wilkins Co., 1953).

(2) Olsen, H. L., Gayhart, E. L., and Edmonson, R. B. *4th Symposium (International) on Combustion* 1952, p. 144 (Baltimore: Williams and Wilkins Co., 1953).
(3) Jost, W. *Explosion and Combustion Processes in Gases* (London: McGraw Hill Publishing Co. Ltd., 1946).
(4) Lewis, B., and von Elbe, G. *Combustion, Flames and Explosions of Gases* (New York: Academic Press Inc., 1951).
(5) Burgoyne, J. H., and Weinberg, F. J. *Fuel*, **35**, p. 436 (1954).
(6) Weinberg, F. J. *Proc. Roy. Soc. A* **235**, p. 510 (1956).
(7) Blanc, M. V., Guest, P. G., von Elbe, G., and Lewis, B. *J. Chem. Phys.*, **15**, p. 798 (1947).
(8) Smith, R. W., Edwards, H. E., and Brinkley, S. R. *Report of Investigations* 4938 (Pittsburgh: U.S. Bureau of Mines, 1953).
(9) Coward, H. F., and Hartwell, F. J. *J. Chem. Soc.*, pp. 1996 and 2676 (1932).
(10) Ellis, O. C. de C., and Morgan, E. *Trans Faraday Soc.*, **30**, 287 (1934).
(11) Schardin, H. Forschungscheft 367. Supplement to *Forschung auf dem Gebeite des Ingenierwesens*, **5** (1934).
(12) Courant, R., and Friedrichs, K. O. *Supersonic Flow and Shock Waves* (London: Interscience Publishers Ltd., 1948).
(13) Evans, M. W. *Chem. Rev.*, **51**, p. 363 (1952).
(14) Hirschfelder, J. O., and Curtiss, C. F. *J. Chem. Phys.*, **17**, p. 1076 (1949).
(15) Norrish, R. G. W., Porter, G., and Thrush, B. A. *Proc. Roy. Soc. A.*, **216**, p. 165 (1953); **227**, p. 422 (1955).
(16) Porter, G. *4th Symposium (International) on Combustion* 1952, p. 248 (Baltimore: Williams and Wilkins Co., 1953).

Unifying design principle for the resistance network analogue

By F. C. Gair, M.Sc., Associated Electrical Industries Ltd., Aldermaston, Berks.

[*Paper first received* 24 *July, and in final form* 10 *September*, 1958]

The object of the present paper is to simplify the design of resistance network analogues. This is achieved, without any loss of accuracy, by the use of what can be called the "cell principle," which is an extension and generalization of the method of MacNeal.[2] Poisson's equation is integrated over the volume of a representative small cell. In this form it is much easier to appreciate the analogy with the resistance network, and hence to arrive immediately at the relevant design parameters. The method applies not only to the usual type of network with equal meshes, but also to networks with unequal meshes, or subdivided meshes, and further to the representation of the Dirichlet, Neumann or Fourier boundary conditions on rectangular or arbitrarily curved boundaries.

More complicated equations than Poisson's can also be represented by a resistance network. By considering these equations as generalizations of Poisson's equation in an appropriate Riemann space, the corresponding design parameters are achieved. This formulation can equally well be used as the basis for any numerical solution of the equations.

The whole field of resistance network analogue design has been outlined in a review article by Liebmann.[1] However, it appears that he was unaware of a paper by MacNeal,[2] which presents a very useful and revealing interpretation of the finite difference network approximation to Poisson's equation in two dimensions. The application of MacNeal's method will be called the "cell principle." Although Liebmann[3] arrived at some aspects of the cell principle in three dimensions, he did not apply it to the design of curved boundaries or subdivided networks. These points are, therefore, given special attention here.

MacNeal's presentation is given in terms of an irregular cell structure to illustrate the generality of his concept. However, for reasons of utility, the presentation here will be given, in the first instance, in terms of a regular cell structure. This emphasis is in keeping with the practical advantages of having network points, in so far as possible, in a rectangular array, with the modifications near a curved boundary kept to a minimum.

The method will be illustrated here for Poisson's equation in both two and three dimensions, and then later for a more general class of equations. Thus, in this general form, the cell principle is seen to apply to every aspect of resistance network design.

POISSON'S EQUATION

Consider the solution of Poisson's equation

$$\nabla^2 f = g \qquad (1)$$

in the domain D, together with appropriate boundary conditions on B, the boundary of D (Fig. 1). Equation (1) is a differential equation which must be satisfied in domain

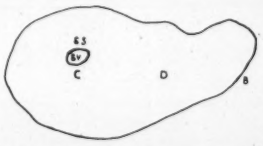

Fig. 1. Domain D showing representative cell C

D, which contains an infinite number of points. However, in a numerical, or resistance network analogue solution, we must be satisfied to represent D by a finite number of point P. Hence it is necessary to consider the solution of

$$Hf = g \qquad (2)$$

at a finite number of points P in D, where H is a finite difference operator such that Hf is an approximation of $\nabla^2 f$.

In the numerical solution of equation (2), H can be interpreted as a square matrix with known coefficients, f as an unknown column matrix, and g a known column matrix. The only necessary condition for a solution is that H should be non-singular. This degree of flexibility in the form of H means that a method for a numerical solution can be devised (in theory) for cases where curved boundaries, or other complications, are involved—see, for example, Viswanathan.[4]

However, it is only possible to represent equation (2) on a resistance network when H has certain properties. For example, H must be symmetric, i.e.

$$h_{ij} = h_{ji}$$

Further

$$\sum_i h_{ij} \leqslant 0$$

and

$$h_{ij} \geqslant 0 \qquad i \neq j$$

These conditions are necessary because they are always fulfilled in the corresponding matrix representation of a resistance network. They arise from the physics of the model—namely that network nodes are connected together in pairs by resistors which are "positive" and "symmetrical." Fortunately it is possible to convert H into a suitable form by multiplying it by a diagonal matrix, each diagonal element of which is proportional to the volume of the "cell" associated with each point P in D.

TRANSFORMATION OF POISSON'S EQUATION

In order to appreciate the relative simplicity of this procedure we will revert from the above algebraic concepts to more intuitive geometrical ones. Rather than modifying equation (2) to the required form, we will transform equation (1) before introducing the finite difference approximation. In this way we will be led directly to the appropriate form. Moreover the method will seem "natural" and "obvious" from a geometrical viewpoint.

Divide the domain D into a finite number of small cells C. Let a representative cell C have volume δv and be bounded by surface δS (Fig. 1). Now integrate equation (1) throughout the volume of C, and transform the left-hand side by Gauss's theorem, to get

$$\iint_{\delta S} \frac{\partial f}{\partial n} dS = \iiint_{\delta v} g\, dv \tag{3}$$

where $\partial f/\partial n$ is the derivative of f in the direction $\boldsymbol{n}$, the outward normal to δS.

TWO-DIMENSIONAL CASE

In the above we have considered a three-dimensional domain, with cells of volume δv, bounded by surfaces δS. However, the method applies equally well when the domain is two-dimensional, and equation (3) is replaced by

$$\int_{\delta s} \frac{\partial f}{\partial n} ds = \iint_{\delta S} g\, dS \tag{4}$$

where the representative cell has area δS, and is bounded by the closed curve δs, where $\boldsymbol{n}$ is the outward normal to δs. We will illustrate the method first with the two-dimensional case given by equation (4). The generalization to equation (3) will then follow easily.

Rectangular mesh system. The finite difference approximation of equation (4) which will be the direct analogue of the resistance network is therefore considered next. The cell C will be represented on the analogue only by its representative "mesh point" P, the position of which within the cell will be precisely specified. In the interior of the region D we will choose these mesh points P at the points of intersection of a rectangular array (the dotted lines in Fig. 2). Then a suitable choice for the associated cells is such that the cell boundaries coincide with another rectangular array (the continuous lines in Fig. 2), each line of which bisects

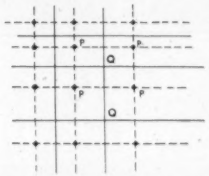

Fig. 2. Rectangular mesh-cell system

the intervals PP between neighbouring mesh points. Denote a typical point of intersection of the second array by Q (Fig. 2).

It is now worth noting a "certain reciprocity" between P and Q. Each interval PP is bisected at right angles by a line QQ, whereas each Q is at the centre of a rectangle $PPPP$. We will say that this reciprocity is "complete" when the converse properties hold as well. The reciprocity of P and Q will be complete only when one of the two systems (and therefore the other) forms a lattice, i.e. a periodic system in space as defined in crystal analysis. Thus if P indicate lattice points, Q are the reciprocal lattice points. However, even for the general case of Fig. 2 when neither system forms a lattice, the reciprocity is sufficient to make possible the choice of either P or Q for the mesh points. In the following, however, we will retain our original choice P.

Now let us direct our attention to a typical cell C_0, of area δS_0, with representative point P_0 (Fig. 3). Cell C_0 is a

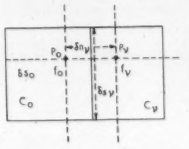

Fig. 3. Two neighbouring cells C_0, C_ν

rectangle with perimeter δs_0 and four sides δs_ν, $\nu = 1, \ldots 4$. The neighbouring cell with common boundary δs_ν is denoted by C_ν, with representative point P_ν.

Equation (4) can now be rewritten as

$$\sum_\nu \int_{\delta s_\nu} \frac{\partial f}{\partial n} ds = \iint_{\delta S_0} g\, dS \tag{5}$$

and no approximations of any kind have yet been made.

The following approximations are now made:

$$\int_{\delta s_\nu} \frac{\partial f}{\partial n} ds = \frac{\delta f_\nu}{\delta n_\nu} \delta s_\nu \tag{6}$$

$$\iint_{\delta S_0} g\, dS = g_0 \delta S_0 \tag{7}$$

where f_ν, f_0, g_ν, g_0 are the values of f, g at P_ν and P_0, $\delta f_\nu = f_\nu - f_0$ and δn_ν is the (positive) distance between P_ν and P_0. An intuitive knowledge of the degree of approximation involved in equations (6) and (7) can be gained from geometrical considerations. Equation (7) is, in general, most accurate when P_0 is at the centre of C_0, whereas equation (6) is best when δn_ν and δs_ν bisect each other at right angles. These "optimum" conditions can be achieved when the mesh points P form a lattice. Unfortunately such optimum conditions are, in general, impossible near an oblique or curved boundary.

Using equations (6) and (7), equation (5) can be converted to the finite difference form

$$\sum_\nu \frac{\delta f_\nu}{\delta n_\nu}\delta s_\nu = g_0 \delta S_0 \tag{8}$$

This is a direct analogue of a resistance network with conductances G_ν and nodal voltages V_0, from which currents i_0 are fed out (Fig. 4) such that

$$\left.\begin{aligned} G_\nu &\propto \delta s_\nu/\delta n_\nu \\ V_0 &\propto f_0 \\ i_0 &\propto g_0 \delta S_0 \end{aligned}\right\} \tag{9}$$

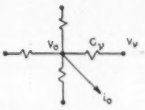

Fig. 4. A network point and its four neighbouring points

The following should be noted: $\delta s_\nu/\delta n_\nu$ is always positive and symmetrical with respect to P_0 and P_ν. These are exactly the required properties for proportionality to G_ν, the conductance between P_0 and P_ν; δS_0 and $\delta s_\nu/\delta n_\nu$ are geometrical properties of the mesh and cell structures. Hence once a diagram of these is drawn, the design of the resistance network follows directly.

Equation (8) can be rewritten in operator form as

$$Kf = g\delta S \tag{10}$$

Comparing this with equation (2) it can be seen that H has been converted into the desired form K on multiplication by δS. From the algebraic viewpoint considered earlier, δS is the appropriate diagonal matrix referred to then.

Physical interpretation. The following physical interpretation of equation (4), and similarly equations (5) and (3), is often useful. $\int_{\delta s} \frac{\partial f}{\partial n} ds$ is the "flow" or "flux" into C through its boundary δs, which must equal $\iint_{\delta s} g\,dS$, the "amount lost" in C. Just what the "flow" and "amount lost" represent depends on the precise physical interpretation (or designation) given to f, the "potential function" which governs the "flow." A similar interpretation applies to equations (8) or (10).

Straight boundary along mesh points. Consider now the network representation at a straight boundary (Fig. 5). Here one side of the rectangular cell C_0 coincides with the boundary B of the domain D. On this side of the cell, of length δs_B say, the approximation (6) is replaced by

$$\int_{\delta s_B} \frac{\partial f}{\partial n} ds = \left(\frac{\partial f}{\partial n}\right)_0 \delta s_B \tag{11}$$

It is usually necessary to choose P_0 on B for a boundary cell (as in Fig. 5), and not at a point inside C_0.

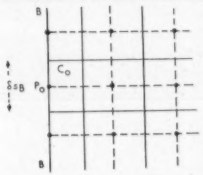

Fig. 5. Cell structure at a straight boundary along the mesh points

Corresponding to equation (8) we now have

$$\sum_\nu \frac{\delta f_\nu}{\delta n_\nu}\delta s_\nu = g_0\delta S_0 - \left(\frac{\partial f}{\partial n}\right)\delta s_B \tag{12}$$

where ν is summed over the sides of C_0 neighbouring other cells only; such sides can be called "interior intervals." The current must now satisfy

$$i_0 \propto g_0\delta S_0 - (\partial f/\partial n)_0 \delta s_B \tag{13}$$

Curved or oblique boundary. A network representation for an example of this general case is shown in Fig. 6. It is necessary to distort the rectangular pattern, both of the meshes and of the cells, in order to accommodate the curved boundary. Here a typical boundary cell will itself be bounded by a number of "interior intervals" δs_ν (taken straight for convenience) and a single "boundary interval" δs_B which is part of B.

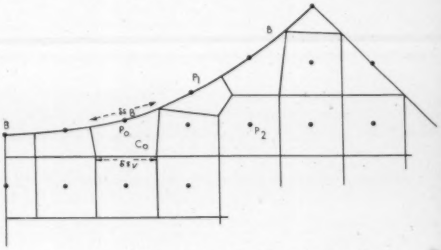

Fig. 6. Cell structure at a curved boundary

In a similar way to the previous case, we make the approximations

$$\int_{\delta s_\nu} \frac{\partial f}{\partial n} ds = \frac{\delta f_\nu}{\delta n_\nu}\delta s_\nu$$

along "internal intervals"

and

$$\int_{\delta s_B} \frac{\partial f}{\partial n} ds = \left(\frac{\partial f}{\partial n}\right)_0 \delta s_B$$

for "boundary intervals" δs_B. Equations (8) and (12) again result, but with the wider interpretation to the cells as they occur in Fig. 6.

It will be noticed that some resistors are needed in a "diagonal" direction, e.g. between P_1 and P_2. The method is therefore similar in this respect to that of Huard de la Marre.[5] However, the present author's method is intuitive, geometrical and direct, whereas his is algebraic and more involved.

A certain amount of practice and judgement is necessary in order to choose a suitable cell and mesh structure to "match" a given curved boundary. Again the degree of approximation can be appreciated geometrically. Insofar as possible we attempt to make the interior boundaries of the cells δs_ν and the mesh intervals δn_ν bisect each other at right angles, and to place the representative points at the "centres" of their corresponding cells.

THE BOUNDARY CONDITIONS

Dirichlet's condition. Here f is specified on B, and corresponding values of V must be imposed on the boundary of the network.

Neumann's condition. $\partial f/\partial n$ is specified on B. Corresponding currents must be fed from boundary points according to equation (13).

Fourier's condition. $[(\partial f/\partial n) + \alpha f]$ is specified on B, where α is positive. In order to represent this on the network, consider the following. Write the condition

$$(\partial f/\partial n)_0 + \alpha f_0 = \beta$$

where β is known on B, and f_0 is a typical function value at a representative boundary point on the network. This can be rewritten as

$$(\partial f/\partial n)_0 = \alpha \delta \bar{f}$$

where $$\delta \bar{f} = f - f_0$$

and $$\bar{f} = \beta/\alpha$$

Then equation (12) can be written

$$\sum_\nu \frac{\delta f_\nu}{\delta n_\nu} \delta s_\nu + \alpha \delta \bar{f} \delta s_B = g_0 \delta S_0 \qquad (14)$$

The new term $\alpha \delta \bar{f} \delta s_B$ is represented on the network simply by a conductance $\bar{G} \propto \alpha \delta s_B$ (Fig. 7) between network points

Fig. 7. Method of setting Fourier's boundary condition at a network boundary point

at potentials $\bar{V}$, $V_0 \propto \bar{f}$, f_0. Thus corresponding to each boundary point f_0, we must construct an additional point $\bar{f}$. The potentials $\bar{V}$ must be imposed at these points.

SUBDIVISION OF THE MESH

In a numerical solution of Poisson's equation it is an advantage to be able to choose a fine mesh in regions where f is expected to fluctuate rapidly, and to use a coarser mesh elsewhere. This practice is well established in the relaxation method of solution. The use of "subdivided meshes" also makes this possible on a resistance network. A number of somewhat different designs are possible, e.g. Liebmann,[3] Palmer and Redshaw.[6] These authors give analytical derivations of their design formulas.

A much faster way of achieving these results is to use the cell principle.

It is illustrated in Fig. 8 how cells can be chosen in a region where there is a change-over from fine to coarse mesh. Fig. 8 actually corresponds to the design of Palmer and

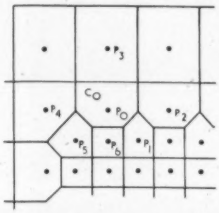

Fig. 8. Cell structure illustrating subdivision of the mesh

Redshaw. The appropriate design values come immediately from the interpretation of equation (8) for the cells as they occur in Fig. 8. There are, for example, six resistors terminating on P_0 corresponding to the six "interior boundary intervals" δs_ν of the cell C_0. The conductance between P_0 and P_1 is then given by

$$G_1 \propto (\delta s_1/\delta n_1) = \tfrac{1}{2}$$

whereas
$$G_2 \propto (\delta s_2/\delta n_2) = \tfrac{1}{2}$$
$$G_3 \propto (\delta s_3/\delta n_3) = 1 \quad \text{etc.}$$

and
$$G_6 \propto (\delta s_6/\delta n_6) = 1$$

and similarly for resistors in any other part of the region.

The cell principle will also yield Liebmann's formulas by choosing a slightly different cell structure. In fact, corresponding to any possible cell structure, we can immediately deduce the corresponding network design. A combination of convenience and geometrical intuition will lead us quickly to the most suitable and accurate representation.

CURVILINEAR OR OBLIQUE MESH SYSTEMS

So far we have confined our attention to the simplest mesh system, where the basic mesh points are in a rectangular array. This is usually the most satisfactory system. However, other more complicated systems can sometimes be employed with advantage. The corresponding resistance networks for these can still be designed from equations (8), (9), etc., provided δs_ν and δS_0 are taken from the appropriate geometry.

For example, the typical cell for polar co-ordinates r, θ is shown in Fig. 9

where
$$\left.\begin{aligned} \delta s_1 &= r(\delta s_1)\delta\theta \\ \delta s_2 &= \delta r \\ \delta S_0 &= r_0 \delta r \delta\theta \\ \delta n_1 &= \delta r_1 \\ \delta n_2 &= r\delta\theta_2 \end{aligned}\right\} \qquad (15)$$

and the design follows immediately from equation (9).

It is also possible to design a resistance network corresponding to mesh points on oblique axes. A typical structure is shown in Fig. 10. Each cell is a hexagon with opposite

sides equal and parallel. Again, as for the rectangular mesh system of Fig. 2, there is a certain reciprocity between the mesh and cell structures making it possible to choose either system as the mesh system and the other as the cell system.

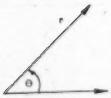

Fig. 9. Typical cell of a plane polar mesh-cell system

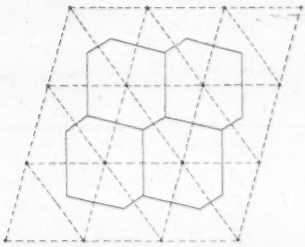

Fig. 10. Oblique mesh-cell system

THREE-DIMENSIONAL CASE

For simplicity of exposition, we have illustrated the various applications of the cell principle so far for the two-dimensional case of equation (4), with its two-dimensional network analogue. The generalization to three dimensions follows merely by changing all appropriate line and surface elements into surface and volume elements respectively.

Thus equation (3) is a generalization of equation (4), and further, for example,

$$\sum_{\nu} \frac{\delta f_\nu}{\delta n_\nu} \delta S_\nu = g_0 \delta v_0 \tag{16}$$

$$G_\nu \propto \delta S_\nu / \delta n_\nu \quad V_0 \propto f_0 \quad i_0 \propto g_0 \delta v_0 \tag{17}$$

$$\sum_{\nu} \frac{\delta f_\nu}{\delta n_\nu} \delta S_\nu = g_0 \delta v_0 - \left(\frac{\partial f}{\partial n}\right)_0 \delta S_B \tag{18}$$

$$\sum_{\nu} \frac{\delta f_\nu}{\delta n_\nu} \delta S_\nu + \alpha \delta f \delta S_B = g_0 \delta v_0 \tag{19}$$

replace equations (8), (9), (12) and (14); ν is now summed over all the sides δS_ν of the volume element δv. Thus we usually have $\nu = 1 \ldots 6$, and the resulting network is three-dimensional.

The various applications to curved boundaries, boundary conditions, subdivided meshes, and curvilinear or oblique mesh systems are generalized to three dimensions in a like manner. It must be admitted, however, that a three-dimensional geometry is more difficult to draw and visualize than a two-dimensional one. We therefore seek an analytic formulation which will be complementary to the geometrical approach. This will have the added advantage of helping us to recognize Poisson's equation when given analytically in an unfamiliar co-ordinate system.

Poisson's equation in curvilinear co-ordinates. We will use the results of tensor calculus to express Poisson's equation in the desired form.

Let z^i be orthogonal Cartesian co-ordinates, x^i be general curvilinear co-ordinates, a_{ij}, a^{ij} be the co-, contra-variant metric tensor, and $a = det\ a_{ij}$.

Note that a_{ij} and a^{ij} are reciprocal matrices and

$$a_{ij} = (\partial z^m/\partial x^i)(\partial z^m/\partial x^j) \tag{20}$$

Now Poisson's equation (1) can be written[7]

$$(\partial/\partial x^i)[\sqrt{a}\, a^{ij}(\partial f/\partial x^j)] = g\sqrt{a} \tag{21}$$

In orthogonal co-ordinates this reduces to

$$\frac{\partial}{\partial x^1}\left(\frac{h_2 h_3}{h_1}\frac{\partial f}{\partial x^1}\right) + + = g\, h_1 h_2 h_3 \tag{22}$$

where

$$a_{ij} = \begin{bmatrix} h_1^2 & . & . \\ . & h_2^2 & . \\ . & . & h_3^2 \end{bmatrix} \tag{23}$$

and $h_1 dx^1$, $h_2 dx^2$, $h_3 dx^3$ are elements of length along the co-ordinate directions.

Now for case (22), we already know the resistance network design from equations (16) and (17). In particular, if we choose the curvilinear co-ordinate system as our mesh system, then corresponding to co-ordinate direction x^1 we have

$$\delta S_1 = h_2 \delta x^2 h_3 \delta x^3$$

$$\delta n_1 = h_1 \delta x^1$$

$$G_1 \propto \left(\frac{h_2 h_3}{h_1}\right)\frac{\delta x^2 \delta x^3}{\delta x^1} \tag{24}$$

and similarly for x^2, x^3.

Corresponding to the volume, we have

$$\delta v = h_1 h_2 h_3 \delta x^1 \delta x^2 \delta x^3$$

$$i_0 \propto g_0 h_1 h_2 h_3 \delta x^1 \delta x^2 \delta x^3 \tag{25}$$

As an illustration, consider a resistance network for Poisson's equation in spherical polar co-ordinates r, θ and ϕ.

$$x^1 = r \qquad x^2 = \theta \qquad x^3 = \phi$$
$$h_1 = 1 \qquad h_2 = r \qquad h_3 = r \sin\theta$$

Equation (22) then becomes

$$\frac{\partial}{\partial r}\left(r^2 \sin\theta \frac{\partial f}{\partial r}\right) + \frac{\partial}{\partial \theta}\left(\sin\theta \frac{\partial f}{\partial \theta}\right) + \frac{1}{\sin\theta}\frac{\partial^2 f}{\partial \phi^2} = r^2 \sin\theta\, g$$

and

$$G_r \propto r^2 \sin\theta\, (\delta\theta\delta\phi/\delta r)$$
$$G_\theta \propto \sin\theta\, (\delta\phi\delta r/\delta\theta)$$
$$G_\phi \propto (1/\sin\theta)(\delta r\delta\theta/\delta\phi)$$
$$i_0 \propto r^2 \sin\theta\, g\delta r\delta\theta\delta\phi$$

GENERALIZATION OF POISSON'S EQUATION

Equations (24) and (25) are the design formulae for equation (22). They were derived on the assumption that h_1, h_2, h_3 had a special geometrical significance with respect

to curvilinear co-ordinates x^i in a Euclidean space. However, such a geometrical interpretation is not necessary. In fact equations (24) and (25) will be the appropriate design formulae for any equation of the form (22) where h_1, h_2, h_3 are known positive functions of the co-ordinates x^i. Thus we can make the following more general formulation. Any equation of the form

$$\frac{\partial}{\partial x^1}\left(\mu_1\frac{\partial f}{\partial x^1}\right) + + = g^{*\,\prime\prime} \tag{26}$$

where μ_i, g^* are functions of x^i and μ_i are always positive, can be represented on a resistance network with design formulae

$$\left.\begin{aligned} G_1 &\propto \mu_1\,(\delta x^2\delta x^3/\delta x^1) \quad \text{etc.} \\ V_0 &\propto f_0 \\ i_0 &\propto g_0^*\delta x^1\delta x^2\delta x^3 \end{aligned}\right\} \tag{27}$$

The above formulation is a three-dimensional one. If the problem depends on only two co-ordinates x^1, x^2 then equations (26) and (27) become

$$\frac{\partial}{\partial x^1}\left(\mu^1\frac{\partial f}{\partial x^1}\right) + = g^* \tag{28}$$

$$\left.\begin{aligned} G_1 &\propto \mu_1\,(\delta x^2/\delta x^1) \quad \text{etc.} \\ V_0 &\propto f_0 \\ i_0 &\propto g_0^*\delta x^1\delta x^2 \end{aligned}\right\} \tag{29}$$

and similarly for problems depending on only one co-ordinate x^1. Equation (28) is of considerable practical importance.

To show how simply these formulae can be applied, a number of examples are now given.

Cylindrical polar co-ordinates

$$\frac{\partial}{\partial r}\left(r\frac{\partial f}{\partial r}\right) + \frac{\partial}{\partial\theta}\left(\frac{1}{r}\frac{\partial f}{\partial\theta}\right) + r\frac{\partial^2 f}{\partial z^2} = rg \tag{30}$$

$$G_r \propto r(\delta\theta\delta z/\delta r)$$

$$G_\theta \propto 1/r(\delta z\delta r/\delta\theta)$$

$$G_z \propto r(\delta r\delta\theta/\delta z)$$

$$i_0 \propto rg\delta r\delta\theta\delta z$$

Axial symmetry. [See also Liebmann[3]]

$$\frac{\partial}{\partial r}\left(r\frac{\partial f}{\partial r}\right) + r\frac{\partial^2 f}{\partial z^2} = rg \tag{31}$$

$$G_r \propto r(\delta z/\delta r)$$

$$G_z \propto r(\delta r/\delta z)$$

$$i_0 \propto rg\delta r\delta z$$

Generalization of axial symmetry. [See also Liebmann[8]]

$$\frac{\partial}{\partial r}\left(r^K\frac{\partial f}{\partial r}\right) + r^K\frac{\partial^2 f}{\partial z^2} = r^K g \tag{32}$$

$$G_r \propto r^K(\delta z/\delta r)$$

$$G_z \propto r^K(\delta r/\delta z)$$

$$i_0 \propto r^K g\delta r\delta z$$

Helical symmetry. [See also Liebmann[9]]

$$\frac{\partial}{\partial r}\left(r\frac{\partial f}{\partial r}\right) + r\left(1 + \frac{\lambda^2}{r^2}\right)\frac{\partial^2 f}{\partial\zeta^2} = rg \tag{33}$$

$$G_r \propto r(\delta\zeta/\delta r)$$

$$G_\zeta \propto r[1 + (\lambda^2/r^2)](\delta r/\delta\zeta)$$

$$i_0 \propto rg\delta r\delta\zeta$$

Spherical symmetry [See also Liebmann[10]]

$$\frac{\partial}{\partial r}\left(r^2\frac{\partial f}{\partial r}\right) = r^2 g \tag{34}$$

$$G_r \propto r^2(1/\delta r)$$

$$i_0 \propto r^2 g\delta r$$

Geometrical interpretation in Riemann space. By comparing equations (22) and (26) we see that these are formally the same provided

$$\mu_1 = h_2h_3/h_1 \quad \text{etc.}$$

i.e.

$$h_1^2 = \mu_2\mu_3 \quad \text{etc.} \tag{35}$$

Thus we can always interpret equation (26) as representing Poisson's equation in a three-dimensional Riemann space with metric

$$a_{ii} = \begin{bmatrix} \mu_2\mu_3 & . & . \\ . & \mu_3\mu_1 & . \\ . & . & \mu_1\mu_2 \end{bmatrix} \tag{36}$$

However, the corresponding interpretation is not possible for the two-dimensional case (28), unless $\mu_1\mu_2 = 1$. Thus for plane polar co-ordinates r, θ

$$\frac{\partial}{\partial r}\left(r\frac{\partial f}{\partial r}\right) + \frac{1}{r}\frac{\partial^2 f}{\partial\theta^2} = g^* \quad \text{[see also equations (15) and (30)]}$$

$$\mu_1\mu_2 = 1$$

and the two-dimensional Riemann interpretation is possible; whereas for the axial plane with co-ordinates r and z, given by equation (31)

$$\mu_1\mu_2 \neq 1$$

and this interpretation is not possible. However, equation (28) can always be regarded as a degenerate three-dimensional problem.

In contrast to this, no such limitation arises for the one-dimensional case, e.g. equation (34).

Further points to note concerning the formulation (26), (27). The formulation (26), (27) is directly applicable to an anisotropic medium involving different values of μ_1, μ_2, μ_3.

It is possible to represent equation (26) on a resistance network when g^* is a function of f or $\partial f/\partial t$ [see also Liebmann[1]]. In particular if g_0^* contains a term of the form $\mu_0 f_0$, where μ_0 is positive, then this term can be represented by attaching a resistor of conductance

$$G_0 \propto \mu_0\delta x^1\delta x^2\delta x^3 \tag{37}$$

between f_0 and $f = 0$ [see also Liebmann[8]].

Any equation of the form

$$\lambda_1\frac{\partial}{\partial x^1}\left(\mu_1^*\frac{\partial f}{\partial x^1}\right) + + = g^{**} \tag{38}$$

where each λ is separable, of the form

$$\lambda_1 = \lambda_{11}(x^1)\lambda_{10}(x^2, x^3) \quad \text{etc.}$$

can be put in the form of equation (26), merely by putting

$$g^* = g^{**}/(\lambda_{11}\lambda_{22}\lambda_{33})$$
$$\mu_1 = \lambda_{10}\mu_1^*/(\lambda_{22}\lambda_{33}) \quad \text{etc.}$$

Thus equation (38) can be represented on a resistance network.

APPLICABILITY AND ACCURACY

Although the above methods of constructing the finite difference equations for a numerical solution have been moulded to fit the requirements of the resistance network analogue, they can be generally used as a basis for a numerical solution by any other method.

Essentially the errors in a resistance network analogue solution are of two kinds—experimental and truncation. The experimental errors are fairly obvious in any given set-up. The truncation errors, due to the finite difference approximations made in the design, are more difficult to estimate. A completely satisfactory method to eliminate truncation error would be to modify the difference correction method of Fox[11] in an appropriate manner. However, for curved boundaries or complicated boundary conditions this modification still appears to present some difficulties [see also Fox[12]].

CONCLUSION

The cell principle has been demonstrated as a general method for the design of resistance network analogues. Its geometrical and physical nature leads to a simple and direct understanding of the subject. Its usefulness lies in the speed with which it can be applied to every aspect of the design. The method can therefore be of great use to the designer of resistance network analogues.

ACKNOWLEDGEMENTS

The author would like to thank Dr. R. Bullough for helpful suggestions, and Dr. T. E. Allibone, Director of the Research Laboratory, Associated Electrical Industries, for permission to publish this paper.

REFERENCES

(1) LIEBMANN, G. *Actes des Journees Internationales de Calcul Analogique, Bruxelles*, p. 346 (1956).
(2) MACNEAL, R. H. *Quart. Appl. Math.*, **11**, p. 295 (1953).
(3) LIEBMANN, G. *Brit. J. Appl. Phys.*, **5**, p. 362 (1954).
(4) VISWANATHAN, R. V. *Math. Tables Aids Comput.*, **11**, p. 67 (1957).
(5) HUARD DE LA MARRE, P. *Actes des Journees Internationales de Calcul Analogique, Bruxelles*, p. 385 (Brussels: Association International de Calcul Analogique, 1956).
(6) PALMER, P. J., and REDSHAW, S. C. *J. Sci. Instrum.*, **34**, p. 407 (1957).
(7) SYNGE, J. L., and SCHILD, A. *Tensor Calculus*, p. 58 (Toronto: University of Toronto Press, 1952).
(8) LIEBMANN, G. *Phil. Mag.*, **61**, p. 1143 (1950); see also Corrigendum, *Phil. Mag.*, **2**, p. 576 (1957).
(9) LIEBMANN, G. Private communication (1953).
(10) LIEBMANN, G. *Brit. J. Appl. Phys.*, **5**, p. 412 (1954).
(11) FOX, L. *The numerical solution of two-point boundary problems in ordinary differential equations* (Oxford: University Press, 1957).
(12) FOX, L. *Phil. Trans*, **242**, p. 345 (1950).

Effect of deformation of the surface texture on rolling resistance

By J. HALLING, B.Sc., Mechanical Engineering Department, University of Liverpool

[*Paper first received* 11 *July, and in final form* 20 *August*, 1958]

The paper describes the results of a series of experiments showing the variation of the coefficient of rolling resistance λ, with increasing load for hard steel rollers on a variety of steel surfaces. It was found that the initial value of λ, and the rate of change of λ with increasing load, were both reduced by a series of loading cycles in which the maximum load in any given cycle exceeded the maximum load of the preceeding cycle. These changes were also found to be greater for the rougher surfaces.

The effect of yield stress was also studied and increasing yield stress produced slightly larger values of λ. In all the tests a change of behaviour occurred at a load which was markedly dependent on the bulk yield stress of the material and marginally dependent on the surface roughness.

The experimental results are interpreted in terms of the resistance to rolling being dependent on two factors; (*a*) the hysteresis loss concept, and (*b*) the requirement for the smooth roller to surmount the irregularities on the surface.

In a previous paper[1] the author has investigated the dependence of the resistance to pure rolling on the surface texture of ground steel surfaces. The results were expressed as a static coefficient of rolling resistance λ which was found to decrease with increasing load and for any given load had a larger value for the rougher surfaces. The coefficient λ is defined in equation (1) where P is the applied load, M the resisting torque, R the radius of the roller and Q the resisting force.

$$\lambda = M/P = QR/P \qquad (1)$$

The results for this investigation, where the maximum load P was restricted to 80 lb, satisfied the experimental law;

$$\lambda = \frac{K}{n}\left(1 - \frac{\log_{10} P}{K}\right) \qquad (2)$$

where K and n are constants depending on the surface texture.

It was also observed that the presence of a lubricant film did not affect the experimental results. From these results it was concluded that the rolling resistance was dependent on the surface texture with a secondary contribution due to the hysteresis effects.[2, 3]

EXPERIMENTAL STUDY OF THE EFFECT OF SURFACE DEFORMATION

The apparatus used in the previous investigation[4] was employed. Two pairs of identical rollers were accurately located with their axes parallel and equally disposed on either side of the loading axis as shown in Fig. 1. The rollers were supported by four similar test surfaces. A thrust load was applied to the system which was then inclined until the first movement of the central block was initiated, the upper and lower blocks being rigidly located. From the values of the applied load and the inclination the value of λ was determined.

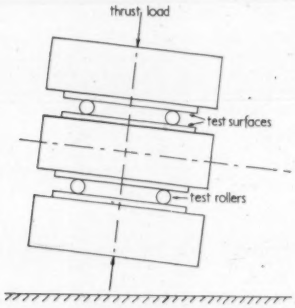

Fig. 1. Principle of the apparatus

The rollers were $\frac{1}{2}$ in. diameter, $1\frac{1}{4}$ in. length, made from a ball bearing steel having a yield stress in excess of 100 t/in.^{2} and a Vickers diamond pyramid hardness number of 835. Their surface finish was better than 3 μ in. c.l.a. (centre line average) as measured by a Talysurf (by Taylor, Taylor and Hobson Ltd.). Test surfaces were produced by surface grinding with a width equal to the axial length of the rollers so that end effects were minimized. The material of these specimens had a yield stress of 24 t/in.^{2} as determined by a standard tensile test, an ultimate tensile strength of 42 t/in.^{2} and a Vickers diamond pyramid hardness number of 193. The average c.l.a. values for each of the three groups of surfaces considered were 15, 27 and 59 μ in. as measured across the direction of machining.

After cleansing in ethylene trichloride vapour and washing in acetone to remove grease and dust particles, the test surfaces were assembled in the apparatus. The central block was oscillated over its full traverse ten times, whence it was

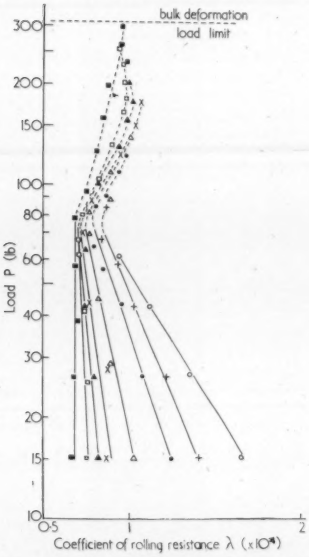

Fig. 2. Variation of the coefficient of rolling resistance with load in the successive load cycles

Initial c.l.a. value, 15 μ in.

○ = 1st load cycle
+ = 2nd load cycle
● = 3rd load cycle
△ = 4th load cycle
× = 5th load cycle
▲ = 6th load cycle
□ = 7th load cycle
■ = 8th load cycle

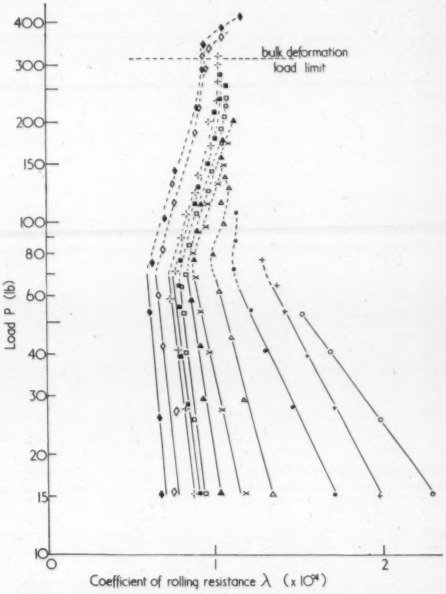

Fig. 3. Variation of the coefficient of rolling resistance with load in the successive load cycles

Initial c.l.a. value, 27 μ in.

○ = 1st load cycle
+ = 2nd load cycle
● = 3rd load cycle
△ = 4th load cycle
× = 5th load cycle
▲ = 6th load cycle
□ = 7th load cycle
■ = 8th load cycle
+ = 9th load cycle
◇ = 10th load cycle
♦ = 11th load cycle

found that repeatable values of λ could be obtained from an average of five determinations. This procedure was repeated for a number of values of increasing load. The load was then reduced to its residual value of 15·7 lb per roller arising from the dead weight of those parts of the apparatus which were supported by the rollers. The same procedure was then adopted for a further series of increasing loads up to a value in excess of the maximum load attained in the first loading cycle. The load was again reduced to its residual value and further loading cycles were obtained where the maximum load in any given loading cycle was in excess of the maximum load previously attained.

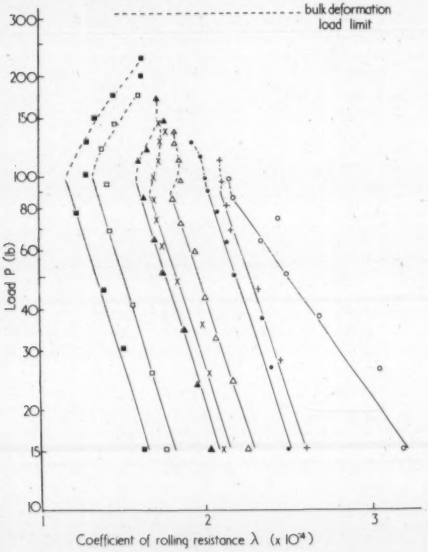

Fig. 4. Variation of the coefficient of rolling resistance with load in the successive load cycles

Initial c.l.a. value, 59 μ in.

○ = 1st load cycle
+ = 2nd load cycle
● = 3rd load cycle
△ = 4th load cycle
× = 5th load cycle
▲ = 6th load cycle
□ = 7th load cycle
■ = 8th load cycle

The results for the three groups of surfaces are plotted on a semi-log basis in Figs. 2, 3 and 4. These figures also indicate the load at which bulk deformation of the material would be expected to occur and are justified by experiments described later in the paper.

EXPERIMENTAL STUDY OF THE EFFECT OF YIELD STRESS

Groups of surfaces were produced from a variety of steels having the properties shown in the table. The surface texture of all the specimens in these groups was produced by surface grinding having values in the range 7–12 μ in. c.l.a.

Using the same rollers as before the variation of the coefficient of rolling resistance with increasing load was determined. The results are shown in Fig. 5.

Mechanical properties of the steel test pieces

Group	Vickers diamond pyramid hardness No.	Elongation (%)	Yield stress (t/in²).	Ultimate tensile stress (t/in.²)
A	193	32	24	42
B	274	21	47	58
C	598	8	91	115

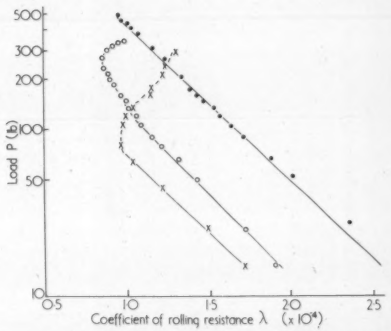

Fig. 5. Variation of the coefficient of rolling resistance with load for surfaces having different yield strengths

× = Group *A*, 24 t/in.² yield strength
○ = Group *B*, 47 t/in.² yield strength
● = Group *C*, 91 t/in.² yield strength

DISCUSSION OF THE RESULTS

Examination of the slopes of the linear part of the curves in Figs. 2, 3 and 4 indicate a relatively large change after the first loading cycle with subsequent changes such that the greatest overall change occurs for the smoothest surfaces. For all the surfaces the departure from linearity occurs at about the same load value, being slightly higher for the rougher surfaces.

In Fig. 6 the value of λ at the commencement of each

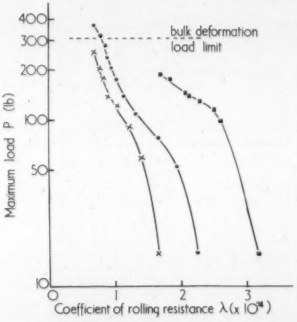

Fig. 6. Variation of the values of λ at the minimum load in Figs. 2, 3 and 4, with the maximum load previously sustained by the surface

× = 15 μ in. c.l.a.
● = 27 μ in. c.l.a.
■ = 59 μ in. c.l.a.

loading cycle is shown with respect to the maximum load attained in the preceding load cycle. The inflexion of these curves occur at a load equivalent to that at which non-linearity is first observed in Figs. 2, 3 and 4. Furthermore, the rate of change of λ with increasing values of the previous maximum load is greater for the rougher surfaces, particularly after the load has exceeded the value corresponding to the departure from linearity. In Fig. 5 it is observed that the non-linear relationship occurs at a higher load for the surfaces having the higher yield stress. Indeed, for the surfaces having a yield stress of 91 t/in.^{2} linear behaviour was observed throughout the complete load range of the apparatus. Increase of yield stress also shows a slight increase in corresponding values of λ, although it must be recalled that the surface textures for these surfaces were not identical.

DEFORMATION OF THE SURFACE TEXTURE

The degree of plastic deformation of the surface irregularities will tend to decrease with increasing load since:

(i) any plastic deformation of a single asperity will increase its load carrying area;
(ii) the plastic deformation will work-harden the tips of the irregularities, thus enhancing their load carrying capacity;
(iii) as deformation proceeds those irregularities initially below the contact area will become load carrying contacts.

These conditions, and particularly (ii) above, are of considerable interest, since the load may be such that although the irregularities are able to support it the underlying bulk material begins to be plastically deformed. Since these tests were designed to study the effect of the deformation of the surface texture, it was necessary to limit the load to a smaller value than that required to initiate such bulk deformation.

To ascertain this loading limit the width of the indentation produced by a variety of cylinders at a number of loads was determined. These results are shown in Fig. 7, and indicate

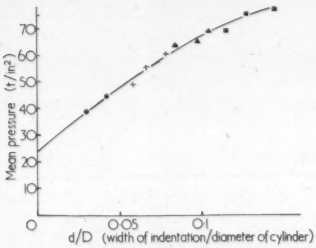

Fig. 7. The relationship between the mean pressure and the width of indentation produced by a number of cylinders

Bulk yield stress of the material, 24 t/in.^{2}
● = 1·25 in. diameter cylinder
+ = 0·75 in. diameter cylinder
▲ = 0·50 in. diameter cylinder
■ = 0·25 in. diameter cylinder

that bulk deformation will be initiated when the applied load produces a mean stress of value roughly equal to the bulk yield stress of the material. In a test where this limiting load was exceeded, the value of λ shows a marked increase as this load value is attained (see Fig. 3). It is also of interest to note that where this limiting load was exceeded the irregularities are still markedly present on the surface although they are less pronounced for the smoother surface (Figs. 8 and 9).

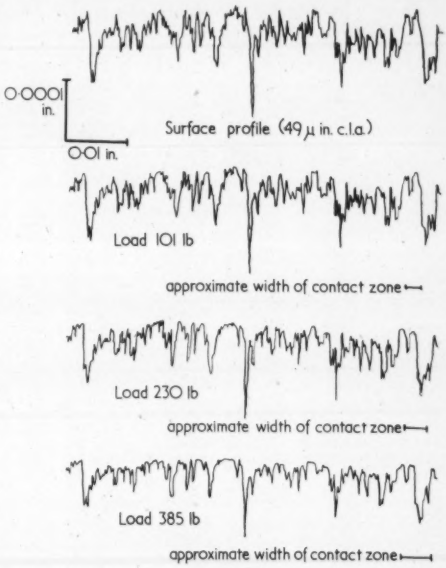

Fig. 8. Surface profiles before and after rolling for a rough surface

HYSTERESIS EFFECTS

In a previous paper[1] it was demonstrated that a reduction of λ with increasing load was not compatible with the elastic hysteresis concept of rolling resistance for a smooth roller on a smooth plane. For rough surfaces the elastic work

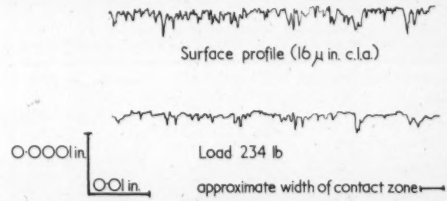

Fig. 9. Surface profiles before and after rolling for the smoothest surfaces

done is given by the product of the applied loading and the elastic deflexions, which are themselves some function of the applied load. Thus from the standpoint of the elastic hysteresis concept, the value of λ must necessarily increase with increasing load or in the limit be independent of load,

e.g. if the surface irregularities are assumed to have spherical tips it can be shown that

$$\lambda = A\phi P^{\frac{1}{2}} \tag{3}$$

where A is a constant for a given system and ϕ is the elastic hysteresis loss function.

Although the experimental results are contrary to the requirements of the hysteresis loss concept, it is interesting to note that this discrepancy becomes reduced with succeeding load cycles. Indeed, in the final loading cycle for the smoothest surface it is noted that the value of λ is virtually independent of the load. Examination of the surface profile for this load condition (Fig. 9) indicates the considerable degree to which the surface irregularities have been eliminated by plastic deformation.

CONCLUSIONS

From the results it is concluded that the rolling resistance is determined by the following two factors:

(i) the losses arising from the hysteresis effects due to the forward compression and rearward expansion of the materials which occurs as rolling proceeds,
(ii) the requirement for the roller to surmount any irregularities on the surfaces.

Condition (i) would appear to require an increase of λ with increasing load, a situation which is approached when the surface finish is improved by plastic deformation of the irregularities.

Condition (ii) is illustrated by the following interpretation of the results:

(*a*) the greater changes in λ with increasing load in the first loading cycle, where some plastic deformation of the irregularities occurs as the load is increased;
(*b*) the reduction in the values of λ with successive loading cycles, also due to the successive reduction in the size of the irregularities. The greatest change occurs for the rougher surfaces, which is in agreement with this hypothesis;
(*c*) in a given loading cycle, when the load is less than the previous maximum load, it is assumed that the surface irregularities are deforming elastically. Thus the reduction of λ with increasing load is accountable to the elastic deformation of the irregularities reducing the resistance to motion. It must be appreciated that the relatively large radius of the roller limits its penetration into the texture, so that even small deformations of the irregularities will be significant. For the rougher surfaces, where the irregularities are still pronounced after successive loading, this elastic effect is still noticeable in the results for the final loading. With the smoothest surface, however, the value of λ is virtually independent of load in the final loading and the irregularities have been considerably eliminated.

The divergence from linearity of the $\lambda \simeq \log_{10} P$ curves occurs at a load which is dependent on the bulk yield strength of the material. This load is marginally greater in successive loadings and also for the rougher surfaces. It is, therefore, assumed that this divergence probably occurs when the tips of the isolated irregularities have been deformed and there is a relatively sudden increase in the number of load-carrying contacts available.

ACKNOWLEDGEMENTS

The author would like to thank Prof. W. J. Kearton and the University of Liverpool for providing the facilities for this investigation and gratefully acknowledges the generosity of British Timken Ltd. for supplying the various test specimens.

REFERENCES

(1) Halling, J. *Brit. J. Appl. Phys.*, **9**, p. 421 (1958).
(2) Tabor, D. *Phil. Mag.*, **43**, p. 1055 (1952).
(3) Tabor, D. *Proc. Roy. Soc. A*, **229**, p. 198 (1955).
(4) Halling, J. *J. Sci. Instrum.*, **32**, p. 8 (1955).

Use of an electronic analogue computer with resistance network analogues

By J. Ph. Korthals Altes, Department of Physics, Delft University of Technology, The Netherlands

[*Paper first received* 6 *May, and in final form* 1 *August*, 1958]

This paper describes a method of solving partial differential equations of the elliptical type, with the aid of an electronic analogue computer in conjunction with a resistance network. Although this method is iterative the adjustments are made automatically by means of electronic memory elements and a switching mechanism. Some results are given.

In case the iteration process proves to be divergent an additional voltage source connected with a well-chosen node may offer a solution.

INTRODUCTION

In the equation

$$\nabla^2\phi = f(\phi)$$

the left-hand side is expanded in finite differences. An analogue for this is a network of electrical resistors. Into the nodes a series of currents I have to be fed, which are proportional to the right-hand side $f(\phi)$. Since ϕ, and therefore $f(\phi)$, is unknown at first, these currents cannot immediately be adjusted to their right values. It is possible however to adjust the currents roughly, followed by successive readjustments.(1) This implies an iterative process which requires much time. An automatic system using a servo mechanism and potentiometers to readjust in turn the currents is made by Sunvic Controls Ltd. Karplus has developed a method making the iteration process superfluous.(2) In his system each node is connected with the input of an analogue computer which creates a voltage proportional to $\phi - f(\phi)$. The currents I are injected through resistors. The entire apparatus adjusts itself to the solution instantaneously. The number of analogue computers needed in Karplus' system is equal to the number of nodes of the network. This number can be reduced to one by using an automatic iterative process, which reintroduces an adjustment time. But the time thus

required is only a slight fraction of what is needed to measure the voltages at the nodes.

Fig. 1 shows the block diagram of a one-dimensional network with nine nodes. The network consists of the resistors R. The currents are injected through resistors r. M_1 to M_9 are memory elements which maintain the voltages

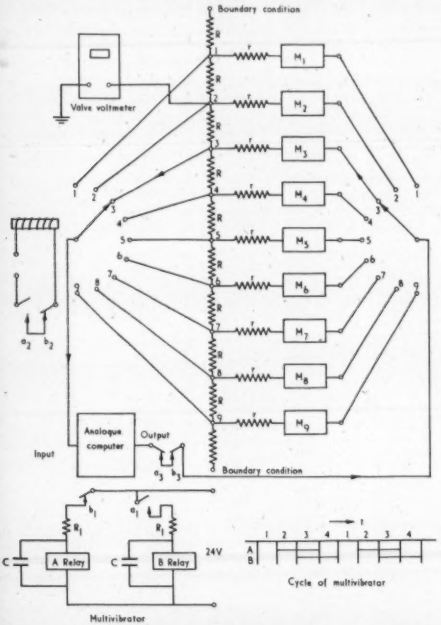

Fig. 1. Diagram of a one-dimensional network and the switching-mechanism
M = memory element

received in turn from the analogue computer. A stepping switch with two decks (one on the left-hand side, one on the right-hand side of the figure) provides the simultaneous connexions: "node n—input computer" and "output computer—memory element n." After adjusting the memory elements in turn, the cycle repeats until the iteration process converges to a limit. Now only one analogue computer is necessary for the entire apparatus while each node requires a memory element. The network is supplied with direct current and the analogue computer is equipped with d.c. amplifiers.

Independently of the author, Hutcheon[3] has developed a similar system which differs in detail from the system presently discussed. The memory elements (the properties of which are discussed later) used in the present system maintain the voltage during a considerably longer time. This makes it possible to use a larger number of nodes without the switching mechanisms having to function very rapidly. The scanning mechanism used here is also simpler. Hutcheon applies a feedback system in conjunction with the memory elements. This implies that the electronic memory elements described here should be more accurate.

THE SWITCHING MECHANISM

Relays A and B form a multivibrator, which determines the frequency of the iteration process. The cycle consists of four parts as indicated at the bottom right. The situation of the switches a_1, a_2, a_3, b_1, b_2 and b_3 in Fig. 1 belongs to part 1 of the cycle. The stepping-switch becomes activated only when both a_2 and b_2 are closed (part 2 of the cycle of the multivibrator). To prevent undesired transient voltages, the output of the computer is applied to the input of a memory element, only when a_3 and b_3 are closed (part 1 of the cycle). In this situation the stepping-switch is at rest, since during parts 3 and 4 the stepping switch is not activated. The frequency of the multivibrator determined by C and R_1 may be increased to ± 20 c/s. Then with the 9 nodes two iterations can be completed in one second. The number of iterations required depends on the rate of convergence of the iteration process. For some equations this number is only 3 or 4; other equations may require 20 or more iterations.

THE ELECTRONIC MEMORY ELEMENTS

The memory elements have the property to maintain the output voltage for some time after the connexion between the computer and the input has been interrupted, even if a load is present. Fig. 2 shows the circuit diagram, which can be interpreted as two cathode followers in series. The second valve fixes the anode voltage of the first one, which does not exceed 45 V in the whole range. The anode current is limited to a maximum of 70 μA by the high cathode resistor R_1. As the grid current is reduced to 10^{-10} A, the "loss of memory" with a capacitor of 47 nF is not more than 0·2 V/min. The second cathode follower can supply the required feed-in

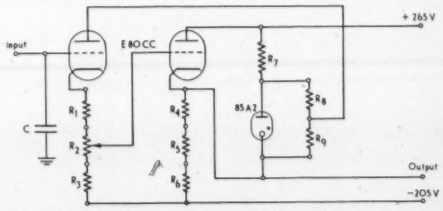

Fig. 2. Diagram of the electronic memory element

$R_1 = 150$ kΩ
$R_2 = 50$ kΩ
$R_3 = 3{\cdot}9$ MΩ
$R_4 = 10$ kΩ
$R_5 = 10$ kΩ
$R_6 = 8{\cdot}2$ kΩ
$R_7 = 100$ kΩ
$R_8 = 200$ kΩ
$R_9 = 200$ kΩ
$C = 47$ nF

current. The value of the output voltages and the node voltage lies between -60 and $+60$ V. In this range the memory elements operate satisfactorily. The gain of the combination is 0·91. After a warming-up period of about one hour the drift is negligible.

RESULTS

With the one-dimensional network of Fig. 1 a number of equations have been solved.

Hutcheon and Spalding[4] recently discussed the solution of an equation similar to the first equation to be described here under example (*a*). Example (*b*) pays attention to the solution of an eigenvalue problem. Finally the possibility of solving equations with diverging iteration processes is treated where the method described can not be used without some alterations.

Example (*a*).—Liebmann as well as Karplus solved the equation

$$\frac{d^2\phi}{dx^2} = \frac{4}{9}\frac{1}{\sqrt{\phi}}$$

Fig. 3 shows the block diagram of the electronic computer for producing a voltage

$$V = \phi - \frac{4}{9}\frac{1}{\sqrt{\phi}}$$

at the input of the memory elements.

M is a memory element, which maintains the voltage of a node while the stepping switch moves from this node to the

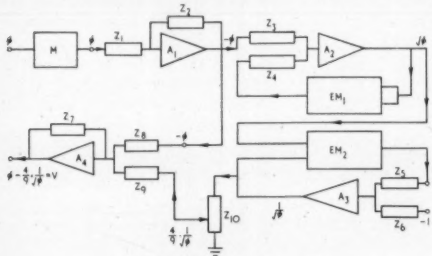

Fig. 3. Wiring of the analogue computer

next, thus preventing disturbing signals (for instance $\phi = 0$, so $1/\sqrt{\phi} \to \infty$). Amplifier A_1 changes the sign of ϕ. Amplifier A_2 with an electronic multiplier EM_1 in the feed-back path creates $\sqrt{\phi}$. The multiplier is based on the "pulse-height pulse-width" modulation system. The second multiplier EM_2 in the feed-back path of the third amplier forms $1/\sqrt{\phi}$. Finally amplier A_4 adds the voltages $-\phi$ and $1/\sqrt{\phi}$ and changes the sign.

Table 1 shows that the results of the method described are practically identical to those of Karplus.

Table 1. *Results of the equation*

$$\frac{d^2\phi}{dx^2} = \frac{4}{9}\frac{1}{\sqrt{\phi}}$$

x (*arbitrary units*)	ϕ (*exact value*)	ϕ (*by Karplus*)	ϕ (*by the author*)
0	0	0	0
1	1·00	1·03	1·07
2	2·52	2·52	2·51
3	4·33	4·25	4·26
4	6·35	6·26	6·23
5	8·55	8·46	8·46
6	10·9		10·8
7	13·4		13·3
8	16·0		16·0
9	18·7		18·7
10	21·5		21·7

The deviations of the first values are caused mainly by the mathematical distinction between a finite difference and a differential equation. This high accuracy is mainly caused by the fact that the voltage $\frac{4}{9}\frac{1}{\sqrt{\phi}}$ is small compared to ϕ. Therefore an error of a few per cent in the value of $\frac{4}{9}\frac{4}{\sqrt{\phi}}$ scarcely affects the final result.

Example (*b*). The equation

$$\frac{d^2\phi}{d\rho^2} + \frac{1}{\rho}\frac{d\phi}{d\rho} = -\beta^2(1 - 4\rho^2)\phi$$

(in which β is an eigenvalue) refers to the temperature distribution in a cross-section of a cylindrical tube through which a laminar flow passes (the problem which was investigated by Graetz[5]).

Three specific boundary conditions are given:

(1) $\phi = 1$ for $\rho = 0$.
(2) $\phi = 0$ for $\rho = 0{\cdot}5$.
(3) $d\phi/d\rho = 0$ for $\rho = 0$.

This is only possible for discrete values of β.

Fig. 4 shows the situation in node n. The magnitudes of the resistors cannot be equal, but must be calculated according to the following formulas:

$$R_n = R_0/(n - \tfrac{1}{2}) \quad \text{and} \quad r_n = CR_0/h\rho(1 - 4\rho^2)$$

We find that

$$V_n = (1 + C\beta^2)\phi_n = K\phi_n$$

in which h is the interval in ρ and C a constant. The gain K has to be adjusted experimentally to fit the third boundary

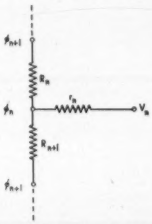

Fig. 4. Situation in node n

condition, that is approximated by $\phi_1 = \phi_0$. In this way an eigenvalue and the eigenfunction can be found. Since only one amplifier is used to adjust K for all nodes this operation is quite simple.

The first eigenvalue β_0 obtained in this way was 5·50 instead of 5·41, the theoretical value. Table 2 shows the first eigenfunction.

Table 2. *Results of the equation*

$$\frac{d^2\phi}{d\rho^2} + \frac{1}{\rho}\frac{d\phi}{d\rho} = -\beta^2(1 - 4\rho^2)\phi$$

ρ	ϕ (*exact value*)	ϕ (*by analogue*)
0	1·00	1·00
0·05	0·98	1·00
0·10	0·93	0·96
0·15	0·85	0·88
0·20	0·74	0·77
0·25	0·62	0·65
0·30	0·48	0·51
0·35	0·35	0·37
0·40	0·22	0·24
0·45	0·11	0·11
0·50	0·00	0·00

The positive deviations of the measured values are mainly caused by the approximation for the third boundary condition.

Only β_0 can be found because the iterative process is divergent for higher values of β.

THE ITERATION PROCESS

The iteration process described is not always convergent (neither is Karplus' system).

The equation $d^2\phi/dx^2 = K\phi$ serves as an example.

For $K < 0$ the solution is $\phi = C \sin(\sqrt{(-K)}\, x + \psi)$. In general the constants C and ψ are determined if ϕ is given for two values of x. If, however, for $x = 0$ and $x = b$; $\phi = 0$, the constants ψ and C are zero, unless $\sqrt{-K} = m(\pi/b)$ (where $m = 1, 2, 3, \ldots$).

In this case C (and therefore the equation) is indefinite. These values of K are the so-called homogeneous eigenvalues of the equation, which are not only defined by the equation, but also by the values of x for which ϕ is given.

When solving the equation with the present network one finds that as long as the value of $|K|$ does not exceed the first homogeneous eigenvalue, the iteration process is convergent ($m < 1$). Otherwise the iteration process is divergent.*

Example. Let K be $-0{\cdot}36$ and

$$\phi = 1 \quad \text{for} \quad x = 0$$
$$\phi = 0 \quad \text{for} \quad x = 10$$

(e.g. for $x = 5$, $\phi = -0{\cdot}51$).

The homogeneous eigenvalues are

$$\sqrt{-K} = m(\pi/10)$$

with solutions

$$K_1 = -0{\cdot}0986\ldots, \quad K_2 = -0{\cdot}394, \text{ etc.}$$

The value $K = -0{\cdot}36$ lies in between K_1 and K_2, and the process is divergent. Now one tries to divide the interval into two parts both giving a convergent solution. Here equal parts are tried and two systems are obtained with the boundary conditions:

$$\left.\begin{aligned} \phi &= 1 \quad \text{for} \quad x = 0 \\ \phi &= -0{\cdot}51 \quad \text{for} \quad x = 5 \end{aligned}\right\} 1$$

$$\left.\begin{aligned} \phi &= -0{\cdot}51 \quad \text{for} \quad x = 5 \\ \phi &= 0 \quad \text{for} \quad x = 10 \end{aligned}\right\} 2$$

The iteration process for both parts is convergent since $|K|$ now is smaller than the homogeneous eigenvalue of every part ($\sqrt{-K} = m(\pi/5)$ or $K_1 = -0{\cdot}394$). If one connects the fifth node with an additional voltage source of $-0{\cdot}51$ V with small internal resistance, both systems adjust themselves. When the final position has been reached no current flows from the additional voltage source into the node, if this source has the right value.

To find the solution experimentally one should take the following steps:

(1) Connect the nodes consecutively with an additional voltage source until a node has been found for which both parts converge.

(2) Then adjust the voltage gradually until no current flows from the voltage source. This situation is easily detected by an ammeter. In this example node 5 appears to be the only node for which the first condition is fulfilled. For smaller values of K, for instance $K = -0{\cdot}1$ or $K = -0{\cdot}2$, there is a choice.

* The node voltages increase more and more rapidly, and even if the solution should be present every disturbance causes the solution to disappear.

Table 3 shows the experimental results of the case treated.

Table 3. *Results of the equation*

$$\frac{d^2\phi}{dx^2} = -0{\cdot}36\,\phi$$

x	ϕ (exact value)	ϕ (by analogue)
0	+1	+1
1	+2·80	+2·76
2	+3·61	+3·54
3	+3·16	+3·08
4	+1·61	+1·57
5	−0·51	−0·54
6	−2·43	−2·43
7	−3·53	−3·51
8	−3·38	−3·31
9	−2·05	−2·04
10	0	0

Here again the deviations are caused mainly by the mathematical distinction between a finite difference and a differential equation. For values of $|K|$ satisfying $|K_2| < |K| < |K_3|$ two additional voltage sources are required, etc. The adjustment of these voltages induces a new iterative process which is superposed on the described one.

The method described here can also be applied to linear equations of the type

$$\frac{d^2\phi}{dx^2} + \frac{m}{x}\frac{d\phi}{dx} = K \,.\, f(x) \,.\, \phi$$

Generally it is not possible to indicate when the iteration

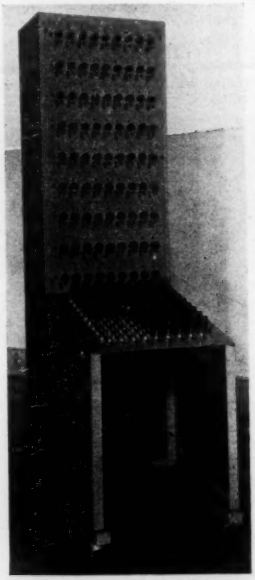

Fig. 5. Two-dimensional network, memory elements and switching-mechanism

process for non-linear differential equations becomes divergent. The method described can still be used, although the positioning of an additional voltage source(s) is less simple, since the stability of the iteration process now also depends upon the magnitude of the voltage. Recently an apparatus has been completed with a two-dimensional resistance network and 81 memory elements (Fig. 5).

ACKNOWLEDGEMENT

This investigation has been performed at the Instrumentation Department of Prof. dr. ir. C. J. D. M. Verhagen as part of the work prescribed for the degree of Physical Engineering at the Delft University of Technology. Much appreciated advice was given to the author by Dr. C. G. 't Hooft, whose idea it was to use electronic memory elements as well as working out the development of these. For the translation into English the author wishes to thank Mr. Ph. J. Kohnstamm and Mr. F. N. Leddy.

REFERENCES

(1) LIEBMANN, G. *Proceedings International Analogy Computation Meeting, Brussels*, 1956, p. 346 (Brussels: Presse Académie Européaine, 1956).

(2) KARPLUS, P. D. *Brit. J. Appl. Phys.*, **6**, p. 356 (1955).

(3) HUTCHEON, I. C. *Brit. J. Appl. Phys.*, **8**, p. 370 (1957).

(4) HUTCHEON, I. C., and SPALDING, D. B. *Brit. J. Appl. Phys.*, **9**, p. 185 (1958).

(5) SCHENK, J., and DUMORÉ, J. M. *Appl. Sci. Res., A.* **4**, p. 39 (1954).

Analysis of a polydisperse aqueous spray from a high-speed spinning disk atomizer

By D. J. RYLEY, M.Sc.(Eng.), A.M.I.Mech.E., Department of Mechanical Engineering, University of Liverpool

[*Paper first received* 25 *August, and in final form* 26 *November*, 1958]

The analysis covers experiments made using flat rotating disks of 2, 3 and 5 cm diameter having controlled matt working surfaces. Rotational speeds varied from 19 000–70 000 rev/min and water feed rates were 0·121, 0·421 and 0·771 g/s. The independent variation of Sauter mean diameter (S.m.d.) and of maximum droplet diameter with disk size, liquid flow rate and rotational speed were found and the general correlation is expressed using dimensionless groups. The extent of the dispersion is numerically expressed as a Rosin–Rammler distribution constant.

Good correlation was found between both (*a*) S.m.d. and (*b*) maximum droplet diameter, and the appropriate products of dimensionless groups. The distribution constant is expressed empirically in terms of speed and flow rate, but the correlation is less satisfactory than in the case of (*a*) and (*b*). No information is given on the mode of fracture, but limitations of the analytical method are explored.

LIST OF SYMBOLS

$D = 2r$, disk diameter (cm)
$n = \omega/2\pi$, disk speed (rev/min or rev/s)
$L = 2\pi r$, length of wetted periphery (cm)
d_m, linear diameter of droplet of maximum size (cm or μ)
d_1, absolute size constant in Rosin–Rammler equation (cm or μ)
R, cumulative volume of droplets (see text)
q, distribution constant in Rosin–Rammler equation
Q, rate of liquid feed (g/s)
T, flow rate, i.e. specific rate of liquid feed from edge of disk (g cm^{-1} s^{-1})
μ, viscosity of liquid (g cm^{-1} s^{-1})
ρ, liquid density (g/cm^3)
σ, surface tension (dyn/cm)
K, dimensionless constant

The Sauter mean diameter is defined as $d_{vs} = \Sigma Nd^3/\Sigma Nd^2$ where N is the frequency of occurrence of a globule of linear diameter d. It is the diameter of a droplet in an imaginary homogeneous spray having the same volume and total surface area as the actual heterogeneous spray.

INTRODUCTION

The spinning disk atomizer has become a standard research device for the production of liquid sprays having a high uniformity of globule size. A summary of the state of knowledge on this subject as it existed in 1952 is given by Friedman, Gluckert and Marshall[1] in the introduction to their own paper on centrifugal disk atomization, and a very full list of references is presented. The principal work since that time is due to Boshoff[2] who investigated the effect on drop size of much larger disks, and Pattison and Aldridge[3] who employed large disks with radial grooves.

Walton and Prewett[4] investigated a number of liquids and employed various speeds and disk sizes. They observed that the spray formed comprised large uniform ("main") droplets, together with a number of smaller ("satellite") droplets, and they gave the relation between the size of the main droplets and the operating parameters thus

$$d = 3 \cdot 8(\sigma/D\rho)^{1/2}/\omega \qquad (1a)$$

The constant was obtained by a separate experiment, and equation (1*a*) is seen to contain no reference to the viscosity or feed rate of the test liquid. The rotating element in these experiments provided in all cases a horizontal circular surface with either a 45° bevelled edge or a 90° edge of unspecified depth.

Friedman and others[1] made a very full investigation of drop size, power consumption and size dispersion with varying speeds, liquids and feed rates using some thirteen different disks. Only three of these disks appear to have any degree of geometric similarity, and in each case these have radial vanes which ensure that no slipping occurs between the disk and the liquid at the time of release.

EXPERIMENTAL

The experiments to be described employed three geometrically similar flat-topped disks of respective diameters 2,

3 and 5 cm. These disks were driven electrically at speeds ranging from 20 000 to 70 000 rev/min approximately, using equipment described at length in an earlier paper by the present writer.[5] As the present experiments were in the nature of calibration experiments for future work on wet saturated steam, no attempt was made to secure uniformity in the spray by separating the satellite drops.

The spray was sampled using 3 in. standard plain microscope slides smoked with magnesium oxide smoke.[6] Two layers of oxide were deposited, each layer resulting from the burning of 8 in. of 0·1 in. magnesium ribbon. The method of sampling has been described elsewhere by the writer.[7] Briefly, it consisted of bringing a protected, smoked slide into close proximity to the disk and employing a hand shutter to gain the correct time of exposure. The distance of flight from disk to slide was adjusted so that the smallest globules reached the slide. To ensure that this distance was less than the least trajectory some preliminary experiments were conducted using water coloured with dye. White blotting paper strips were laid radially and horizontally just below the disk and coloured stains revealed the positions of globule descent. Some skill was necessary to judge the exposure time and orientation of the slide to ensure an acceptable density of craters and a reasonably normal entry of droplets of all sizes into the oxide. In many earlier attempts a number of exposed slides were rejected on account of "smudges" and "tails" before a satisfactory sample was obtained.

A count was then made, using a low-power microscope with an eyepiece scale, of some 500 craters selected from the central area of the slide. In a few cases where the size range was very small the count was limited to 250–300 craters. The scale was arranged to appear horizontal in the field of view, and the slide was translated vertically from edge to edge. Craters were measured as they traversed the scale, and after each complete transit of the slide it was moved horizontally to displace the field of view a distance equal to the diameter of the field of view.

RESULTS

In order to investigate the effect of the working surface, the 5 cm disk was roughened in the first instance in a haphazard manner by rubbing with fairly fine emery cloth. Surface indentations and scratches were thus randomly disposed. By measuring a surface record made by a Taylor–Hobson Talysurf machine it was found that an average scratch was $4{\cdot}5 \times 10^{-5}$ in. deep. Fig. 1 shows a plot of the Sauter mean diameter (S.m.d.) for this case, which may be regarded as one of uncontrolled roughening, and the experimental points reveal considerable scatter. To obtain a reproducible surface for all tests, the practice was adopted of placing the disk working-face downward on a sheet of glass and grinding the top and later the edge with a paste of water and carborundum powder. Powder No. 180 was used in the first instance, but No. 60 was subsequently adopted. The improvement due to control of roughening is clearly seen in Fig. 1. It became general practice to grind all disks thus before a test and to start the liquid flow before the disk commenced to spin. It was thus possible to prevent the working surface from becoming dry at any time before sampling the spray.

Tests were conducted on disks of diameters D of 2, 3 and 5 cm respectively. The water feed rate was determined by weighing the efflux for a fixed head over a suitable period of time, and the values of feed rate Q were 0·121, 0·421 and 0·771 g/s respectively. The nominal standard speeds n were 19 500, 25 200, 30 000, 34 800, 45 000 and 54 500 rev/min, respectively, which were measured photoelectrically in the manner described in Ref. (5). A few tests were included at higher speeds with the smaller disks, but balancing difficulties imposed a speed limit for the 5 cm disk. Table 1 lists experimental data for the whole range of main experiments.

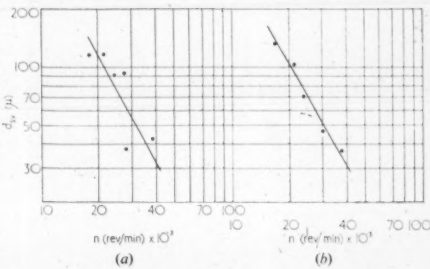

Fig. 1. Effect of roughening 5 cm disk. Flow rate 0·0491 g cm^{-1} s^{-1}

(*a*) uncontrolled roughening; (*b*) controlled roughening.

ANALYSIS

The functional relationships between the variables were considered too complicated for direct analysis, and the method of employing dimensionless groups was therefore adopted. The following quantities were thought to be of importance:

(i) flow rate, i.e. feed rate/unit periphery of disk T;
(ii) disk speed n;
(iii) viscosity of test liquid μ;
(iv) surface tension of test liquid σ;
(v) density of test liquid ρ;
(vi) disk radius $r = D/2$;
(vii) Sauter mean diameter of droplet d_{sv}.

For the general case of the analysis, the viscosity and density of the reception medium ought to be included, but as the latter is necessarily air in every case, these quantities are omitted. The variables may be related by dimensional analysis in the following general way:

$$\frac{d_{sv}}{r} = f\left(\frac{T}{\mu}, \frac{T}{\rho n r^2}, \frac{T^2}{\sigma \rho r}\right) \tag{1}$$

Experimental work is found to justify a relationship of the form

$$\frac{d_{sv}}{r} = K\left(\frac{T}{\mu}\right)^a \left(\frac{T}{\rho n r^2}\right)^b \left(\frac{T^2}{\sigma \rho r}\right)^c \tag{2}$$

These groups are similar to those employed by Friedman and others, except that they added in the first instance a further group (L/r), where L is the length of the wetted periphery, to accommodate the differing construction of their several disks. This group was later omitted. With the present flat (i.e. unvaned) disks, the group assumes a constant value and may be eliminated. Groups having the indices a and b [equation (2)] can be rearranged to reveal a ratio of inertial to viscous forces, and are thus Reynolds criteria, while the group having the index c can be shown to be a ratio of inertial to surface tensile energies, and is thus a Weber criterion.

Table 1. *Experimental results*

Test No.	Disk diameter D (cm)	Speed n (rev/min $\times 10^{-3}$)	Specific feed ($g\,cm^{-1}\,s^{-1}$)	d_{av} (μ)	d_m (μ)	q
1	5	19·25	0·0491	133·2	237	3·61
2	5	25·2	0·0491	76·2	154	3·34
3	5	29·6	0·0491	62·1	113	4·81
4	5	34·8	0·0491	46·3	89	4·69
5	5	45·5	0·0491	30·0	72	3·00
6	5	54·5	0·0491	24·2	41	4·22
7	5	19·3	0·0268	161·4	296	2·87
8	5	25·2	0·0268	83·3	160	2·84
9	5	34·9	0·0268	43·7	83	4·15
10	5	45·5	0·0268	29·2	59	3·60
11	5	54·5	0·0268	19·7	35	3·83
12	5	19·5	0·0077	86·2	237	6·56
13	5	25·3	0·0077	77·2	149	5·30
14	5	30·0	0·0077	52·8	131	6·80
15	5	34·5	0·0077	37·6	65	6·80
16	5	45·5	0·0077	32·1	59	9·40
17	5	54·5	0·0077	26·1	30	8·40
18	2	25·2	0·123	163·0	266	3·40
19	2	30·0	0·123	98·1	201	3·99
20	2	34·8	0·123	86·4	177	4·57
21	2	45·5	0·123	70·8	149	3·79
22	2	54·5	0·123	63·0	131	4·37
23	2	70·0	0·123	37·7	65	5·48
24	2	19·4	0·0193	113·4	189	4·63
25	2	25·2	0·0193	91·3	154	6·35
26	2	34·8	0·0193	58·7	95	7·57
27	2	45·5	0·0193	39·1	59	8·40
28	2	54·5	0·0193	32·4	53	8·75
29	2	70·0	0·0193	33·8	53	8·74
30	2	19·5	0·067	121·2	325	2·85
31	2	25·2	0·067	99·4	177	3·58
32	2	30·0	0·067	113·1	237	3·65
33	2	34·0	0·067	67·4	142	4·20
34	2	45·5	0·067	59·8	160	4·02
35	2	54·5	0·067	43·9	77	5·05
36	2	70·0	0·067	34·1	72	5·47
37	3	19·5	0·0447	197·5	305	3·26
38	3	25·2	0·0447	113·0	266	4·32
39	3	30·1	0·0447	116·0	207	4·48
40	3	34·9	0·0447	59·4	119	3·55
41	3	44·5	0·0447	47·5	113	4·33
42	3	54·5	0·0447	35·8	77	6·10
43	3	25·4	0·0822	115·4	249	3·52
44	3	30·0	0·0822	126·6	237	3·51
45	3	34·8	0·0822	88·2	177	3·86
46	3	45·5	0·0822	39·6	72	8·40
47	3	54·5	0·0822	34·9	59	6·15
48	3	60·0	0·0822	33·9	65	4·15
49	3	19·5	0·0129	142·4	255	5·00
50	3	25·2	0·0129	74·8	149	7·58
51	3	30·1	0·0129	62·7	119	6·35
52	3	34·8	0·0129	48·7	83	6·80
53	3	45·5	0·0129	33·6	65	9·40
54	3	54·5	0·0129	29·5	41	6·60

Figs. 2, 3 and 4 show respectively the independent variations of d_{sv} with r, T and n. Fig. 2 shows that, in general, log d_{sv} varies inversely with log D, but that the variation only approximates to linearity at the higher values of speed n. At the lower speeds there is evidence of a maximum value

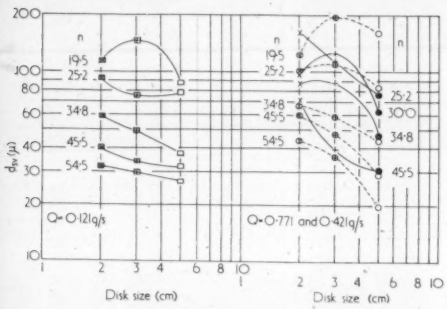

Fig. 2. Effect of disk size on droplet size; n is given in rev/min × 10^{-3}

● = 5 cm disk
+ = 3 cm disk } at 0·771 g/s feed rate.
× = 2 cm disk

○ = 5 cm disk
⊕ = 3 cm disk } at 0·421 g/s feed rate.
⊗ = 2 cm disk

□ = 5 cm disk
⊞ = 3 cm disk } at 0·121 g/s feed rate.
⊠ = 2 cm disk

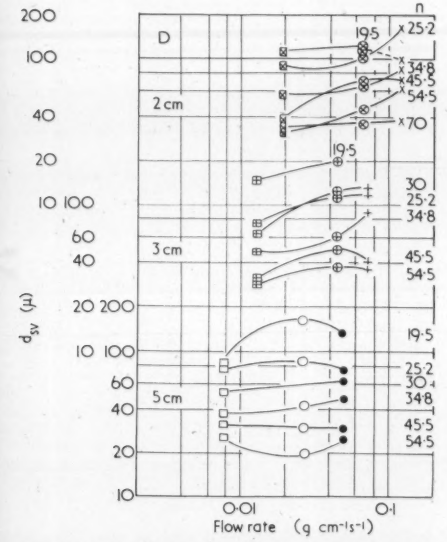

Fig. 3. Effect of flow rate on droplet size; n is given in rev/min × 10^{-3}. (Key as Fig. 2)

of d_{sv} near the value $D = 3$ cm. The average slope was $-0{\cdot}47$ compared with the value $-0{\cdot}2$ given by Friedman and others for disks of differing types. These authors concede, however, that their value was based on inadequate data, and that the value $-0{\cdot}2$ was chosen because it agreed with the dimensional analysis. Fig. 3 shows that the general tendency of d_{sv} is to rise slowly as the flow rate T is increased. Again there is evidence of the operation of an unknown factor, and the assumption of an average slope of 0·19 is a simplification to permit the analysis to proceed. The corresponding value given by Friedman and others is 0·2. This is based on two different disks of somewhat similar construction to those present, and on fewer experimental points than in the present case.

Fig. 4 shows that d_{sv} varies inversely with the speed n in a straightforward manner. The average slope is here 1·41

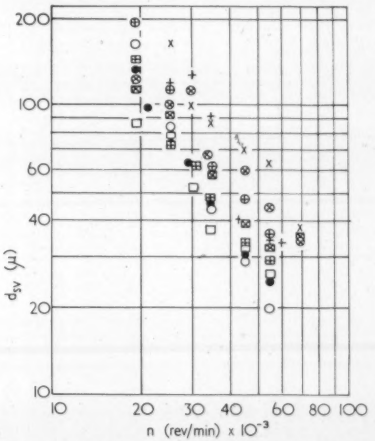

Fig. 4. Effect of speed on droplet size. (Key as Fig. 2)

and is to be compared with the value 0·6 found by Friedman and others.

The experimental determination of these powers determines uniquely the values to be assigned to the indices a, b and c in equation (2), and also implies the values of the powers to be associated with σ, ρ and μ respectively. The constant K is also determined, and equation (2) becomes

$$\frac{d_{sv}}{r} = 3{\cdot}81 \times 10^{-5}\left(\frac{T}{\mu}\right)^{1{\cdot}48}\left(\frac{T}{\rho n r^2}\right)^{1{\cdot}41}\left(\frac{\sigma\rho L}{T^2}\right)^{1{\cdot}35} \qquad (3)$$

L having been employed in the last group instead of r to facilitate comparison with equation (4). Equation (3) may be compared with the form given by Walton and Prewett in equation (1a) and the final equation of Friedman and others thus:

$$\frac{d_{sv}}{r} = 0{\cdot}4\left(\frac{\mu}{T}\right)^{0{\cdot}2}\left(\frac{T}{\rho n r^2}\right)^{0{\cdot}6}\left(\frac{\sigma\rho L}{T^2}\right)^{0{\cdot}1} \qquad (4)$$

For comparison of equations (3) and (1a), the present results may be written

$$d_{sv} = \text{constant} \times \frac{\sigma^{1{\cdot}35}T^{0{\cdot}19}}{\rho^{0{\cdot}06}\omega^{1{\cdot}41}r^{0{\cdot}47}\mu^{1{\cdot}48}} \qquad (5)$$

Table 2 gives a comparison of the powers for different physical quantities obtained by different investigators. The general correlation between d_{sv} and the other variables is shown in Fig. 5.

Table 2. *Comparison of powers of physical quantities*

Variation of d_{sv} with:	*Ryley*	*Walton and Prewett*	*Friedman and others*
Disk radius r	−0·47	−0·5	−0·2
Speed ω or n	−1·41	−1·0	−0·6
Surface tension σ	1·35	0·5	0·1
Liquid density ρ	−0·06	−0·5	−0·5
Viscosity μ	−1·48	0	0·2
Specific feed T	0·19	0	0·2

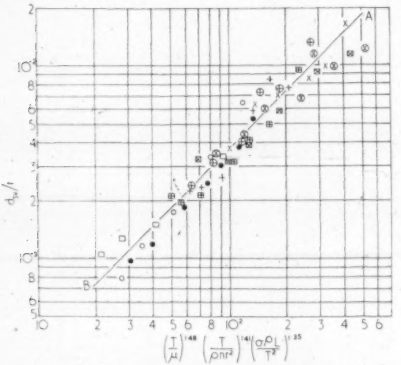

Fig. 5. General correlation of droplet size. Line AB is

$$\frac{d_{sv}}{r} = 3{\cdot}81 \times 10^{-5}\left(\frac{T}{\mu}\right)^{1\cdot48}\left(\frac{T}{\rho n r^2}\right)^{1\cdot41}\left(\frac{\sigma\rho L}{T^2}\right)^{1\cdot35}$$

(Key as Fig. 2)

Maximum size of droplet. Each slide was carefully inspected for the crater of maximum size. It was generally assumed that this crater was formed by a single large droplet discretely produced and that no coalescence had occurred in flight. In cases, however, in which a single large crater was found to be several sizes in excess of the next largest it was rejected on the presumption of a coalescence. This arbitrary procedure occurred on four occasions. Fig. 6 shows the general correlation between d_m and the dimensionless groups defined by

$$\frac{d_m}{r} = 7{\cdot}41 \times 10^{-5}\left(\frac{T}{\mu}\right)^{1\cdot48}\left(\frac{T}{\rho n r^2}\right)^{1\cdot41}\left(\frac{\sigma\rho L}{T^2}\right)^{1\cdot35} \quad (6)$$

and it will be seen that most experimental values conform reasonably to this equation. It is noticeable that the conformity becomes poorer as d_m/r increases. Friedman and others quote a corresponding relation

$$\frac{d_m}{r} = 1{\cdot}2\left(\frac{T}{\rho n r^2}\right)^{0\cdot6}\left(\frac{\mu}{T}\right)^{0\cdot2}\left(\frac{\sigma\rho L}{T^2}\right)^{0\cdot1} \quad (7)$$

The ratio of d_m/d_{sv} for the whole series of tests was found to be about 2, suggesting that the maximum droplet size to be expected in any aqueous spray from this type of atomizer is approximately twice the Sauter mean value. Friedman and others quote a value of 3.

Size dispersion in spray. From the several available methods of expressing quantitatively the extent of the size dispersion in a spray, that chosen was due to Rosin and Rammler,[8] whose equation may be written

$$R = \exp\left[-(d/d_1)^q\right] \quad (8)$$

where R is the cumulative volume (or weight) of droplets of size greater than d expressed as a ratio of the total volume (weight) of the sample, d_1 is the absolute size constant, and q is the distribution constant.

The absolute size constant may be regarded as a size representative of the spray, but is not here of consequence. The distribution constant is significant here as a measure of the dispersion, and a rising value of q denotes increasing uniformity in the spray.

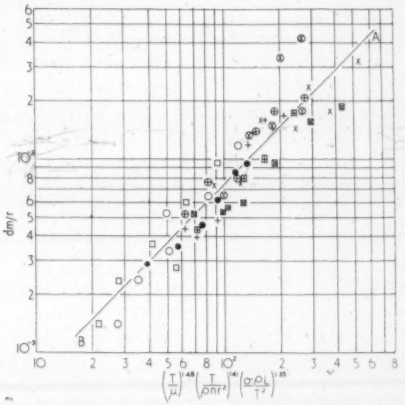

Fig. 6. General correlation of maximum droplet size. Line AB is $\frac{d_m}{r} = 7{\cdot}41 \times 10^{-5}\left(\frac{T}{\mu}\right)^{1\cdot48}\left(\frac{T}{\rho n r^2}\right)^{1\cdot41}\left(\frac{\sigma\rho L}{T^2}\right)^{1\cdot35}$

(Key as Fig. 2)

For each test calculations were made of R and d and these quantities were plotted on Rosin–Rammler graph paper. The best straight line was drawn through the experimental points and the required value of q was found from the reciprocal of the slope. The collected results are shown in Fig. 7. Although there is considerable scatter it is clear that q rises with the speed n and falls with increasing feed rate Q, and an attempt was made to obtain an empirical expression relating the several quantities. Thus independent plots of $q - n$ and $q - T$ established that q tends to vary directly with n to the power 0·53 and inversely with T to the power 0·29. The best empirical relationship was therefore found to be

$$q = 7{\cdot}9 \times 10^{-3} n^{0\cdot53} T^{-0\cdot29} \quad (9)$$

(where n is in rev/min) which is shown in Fig. 8. The correlation between the experimental points, and the function defined by equation (9) is much weaker than in the case of equations (3) and (6).

CONSIDERATION OF RESULTS

Inspection of Table 2 shows that whereas, with the exception of μ, the sign of the variation of d_{sv} with the several

physical quantities involved is agreed, there is considerable divergence of view concerning the magnitude of the powers, particularly in respect of σ, ρ and μ. There is clearly a need for additional experimental work of the present type on plane disks using non-aqueous liquids, an enquiry outside the purpose of the present investigation.

Although the relationships given by equations (3) and (6) show good correlation with the experimental points from which they were derived, it is unreasonable to suppose that the dimensionless groups chosen, or indeed any combination of such groups, will give a very close mathematical description of the interplay of the several variables affecting the spray. A consideration of the placing of experimental points in Figs. 2 and 3 shows that additional unrecognized influences are involved, and curves such as Figs. 4 and 7 of Ref. (1) as well as those just cited betray the inadequacy of expressing the functional relation between two variables in a spray by a simple power law. It is likely that the mode of formation of the droplets at the disk periphery influences the results, and in default of knowledge on this matter the postulation of certain dimensionless groups has been made with ease of experimental manipulation in mind. It is well known, for example, that n is the most significant variable influencing d_{vr}. Nevertheless, any choice of groups necessarily omits reference to such considerations as, say, the effect of the air boundary layer surrounding the disk or the electrostatic charges which accompany the vigorous production of new surface.

Although the groups (T/μ) and $(T/\rho m r^2)$ have the structure of Reynolds criteria, it is not apparent in what manner they may be related to, say, flow over the disk surface or the flight of a droplet; two contexts in which such criteria would seem relevant. Similarly, although $(T^2/\rho\sigma D)$ has the structure of a Weber number, its connexion with a deformed droplet in flight is obscure.

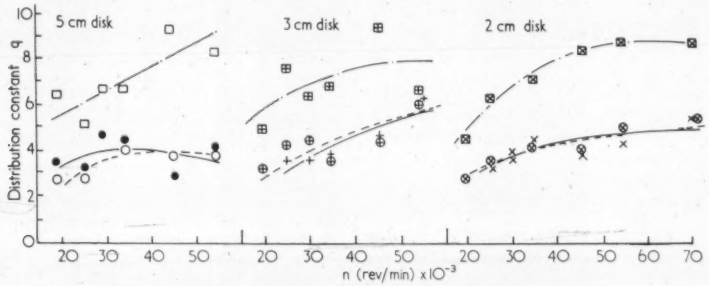

Fig. 7. Effect of speed, feed and disk size on distribution constant
—·— = 0·121 cm³/s – – – – = 0·421 cm³/s ——— = 0·771 cm³/s
(Key as Fig. 2)

The magnesium oxide-coated slide is known to have limitations as a reception medium for droplets. The upper limit of crater size for which satisfactory results can be obtained is given by May as 200 μ. In the present experiments the largest droplets were about 325 μ. Such droplets are structurally weaker than the smaller ones and probably deform on striking the oxide surface, causing a larger crater than if they were more rigid. A progressive crater error is thus to be expected as the droplet size increases. This is one contributory factor to the worsening agreement between equation (6) and the experimental results as d_m/r increases. The crater corrections obtained by May have been applied in these results. These corrections were unfortunately overlooked by Friedman and others, whose results must be regarded as in error to this extent and whose correlation of different drop sizing methods (their Fig. 3) might thereby be improved. Also, it is not clear from the text whether these workers employed magnesium oxide slides for their largest droplets which range in size up to about 550 μ.

While every care was taken to obtain a true sample of droplets, it is not possible to obtain a slide for which all the craters can be measured. In most cases a few craters will be misshapen, will overlap and some shallow depressions will result from droplets which have bounced from the surface. It cannot be assumed that defective craters will be random in their incidence as regards size. An average slide admitted sizing of about 80% of all the craters, and in about twenty tests the value was 90%. Errors in sizing, from whatever cause they arise, are more significant in the final value of d_{vr} for large than for small droplets.

Concerning size dispersion, two factors are clearly involved; the extreme range of droplet sizes and the distribution of frequencies within that range. Fig. 9 shows the results of two actual tests in which the total count is the same and which have the same value of q. It is clear, however, that

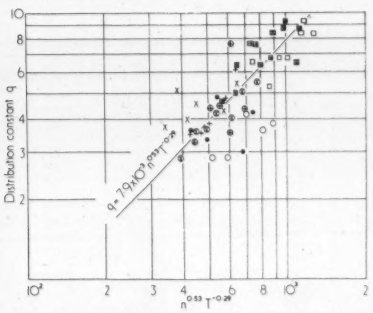

Fig. 8. General correlation of distribution constant; n is given in rev/min. (Key as Fig. 2)

while the peaked portions of the curves are broadly similar in shape, one curve shows a much greater extreme size variation than the other, although the number of extreme-sized droplets is admittedly small. This illustrates the limitations of a single parameter such as q to describe a dispersion. The difference in the distribution of the frequencies for a given value of q may be more marked in the case of sprays taken at low speeds in which no unique outstanding modal size is observed. This limitation in the scope of q must be regarded as another factor contributing towards the scatter on Fig. 8.

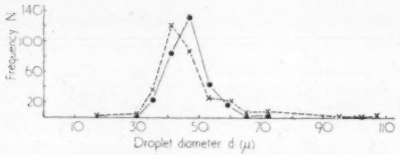

Fig. 9. Comparative frequency distribution curves

The values of q here obtained may be compared with those found by Hinze and Milborn[9] using a spinning cup and unspecified test liquids. For atomization by ligament formation they quote values of q in the range 4·3–9·4, and for atomization by film formation values in the range 7·3–8·6. The atomization categories of the present experiments are not known with certainty. Hinze and Milborn quote the change over from ligaments to film as occurring when

$$\frac{Q}{D}\sqrt{\left(\frac{\rho}{\sigma D}\right)}\left[\omega D\sqrt{\left(\frac{\rho D}{\sigma}\right)}\right]^{0\cdot60}\left[\frac{\mu}{\sqrt{(\rho\sigma D)}}\right]^{0\cdot167}=133 \quad (11)$$

They also suggest a transition between dropwise and ligament formation which may be shown to occur when

$$\left[\omega D\sqrt{\left(\frac{\rho D}{\sigma}\right)}\right]^{0\cdot25}\left\{\frac{Q}{D}\sqrt{\left(\frac{\rho}{\sigma D}\right)}\left[\frac{\mu}{\sqrt{(\rho\sigma D)}}\right]^{0\cdot167}\right\}>4\cdot55\times10^{-3} \quad (12)$$

If, as is reasonable, these criteria be accepted as valid for the present tests, the majority occur in the ligament range. It is noteworthy that both the Hinze and Milborn investigation and that here reported show a limiting value of dispersion uniformity at $q = 9\cdot4$.

ACKNOWLEDGEMENTS

The writer is indebted to Prof. W. J. Kearton, late Harrison Professor of Mechanical Engineering at Liverpool University, for permission to use the facilities of the department.

He is also indebted to Mr. H. D. Makinson for help with the tedious work of analysing slides.

REFERENCES

(1) Friedman, S. J., Gluckert, F. A., and Marshall, W. R. *Chem. Eng. Prog.*, **48**, p. 181 (1952).
(2) Boshoff, W. H. *Proc. Instn Mech. Engrs A*, **166**, p. 443 (1952).
(3) Pattison, J. R., and Aldridge, J. D. *Engineer*, **203**, p. 514 (1957).
(4) Walton, W. H., and Prewett, W. C. *Proc. Phys. Soc. (London) B*, **62**, p. 341 (1949).
(5) Ryley, D. J. *J. Sci. Instrum.*, **35**, p. 237 (1958).
(6) May, K. R. *J. Sci. Instrum.*, **22**, p. 187 (1945).
(7) Ryley, D. J. *Brit. J. Appl. Phys.*, **10**, p. 93 (1959).
(8) Rosin, P. O., and Rammler, E. *J. Inst. Fuel*, **7**, p. 29 (1933–4).
(9) Hinze, J. O., and Milborn, H. *J. Appl. Mech.*, **17**, p. 145 (1950).

Excitation and ionization rates of mercury in discharge plasmas

By M. A. Cayless, B.Sc., A.R.C.S., A.Inst.P., The British Thomson-Houston Co. Ltd., Rugby

[*Paper received* 17 *September*, 1958]

Excitation and ionization rates of mercury by inelastic electron collisions in gas discharge plasmas with Maxwellian electron energy distributions have been calculated from the collision cross-section data for electron temperatures between 5000 and 54 000° K. Published cross-section data have been used where available, and estimates have been made in several cases of interest for which no data are known.

In the theory of low-pressure discharges it is necessary to know the rates of formation of excited states and ions in the discharge plasma by inelastic electron collisions. These may be calculated when the electron energy distribution and the cross-section curves of the transitions are known. The latter are usually available numerically as the result of quantum-mechanical calculations or experimental determinations [see, for example, Ref. (1)], and the excitation and ionization rates are obtained by numerical integration over the electron energy distribution. This is readily performed with an automatic digital computer.

These calculations have been carried out for various transitions in the case of mercury with a Maxwellian electron energy distribution. This is a satisfactory representation of many steady state discharges in the medium pressure range, 0·1 to 100 mm of mercury.[2]

At lower pressures, or where striations or oscillations are present, the distribution may differ from the Maxwellian [see, for example, Ref. (3)] and these calculations are inapplicable. At higher pressures the plasma may approximate to thermal equilibrium and a different approach may be used.[4]

THEORY

Let Q_{xy} be the cross-section for the transition from state x to state y. Then the transition rate in the plasma per unit x concentration per electron per second is given by

$$Z_{xy}=\int_0^\infty f(E)v(E)Q_{xy}(E)dE \quad (1)$$

where E is the electron energy, $v(E)$ is the electron velocity, and $f(E)dE$ the fraction of electrons with energies between E and $E + dE$.

For a Maxwellian distribution

$$f(E)dE=2(E/\pi)^{1/2}(kT_e)^{-3/2}\exp(-E/kT_e)dE \quad (2)$$

where T_e is the electron temperature, m_e the electron mass, and k is Boltzmann's constant. Expressing E in electron volts, therefore,

$$Z_{xy} = 2\left(\frac{e}{k}\right)^2\left(\frac{2k}{\pi m_e}\right)^{1/2} T_e^{-3/2}\int_0^\infty Q_{xy} V \exp\left(-\frac{eV}{kT_e}\right) dV \quad (3)$$

where e is the electronic charge and V the voltage of the electrons.

Equation (3) has been evaluated for mercury transitions with electron temperatures between 5000 and 54 000° K using a Pegasus digital computer. The quadrature was performed using Simpson's rule and a sufficient number of suitably spaced ordinates to ensure that the results are well within the accuracy of the data. A correction term was added to include the part of the integral beyond the highest ordinate by assessing the cross-section to be constant from then on. This correction was always very small, and quite negligible at low values of T_e.

The following numerical values were used:

$$e/k = 11\,600^\circ\ \mathrm{K\ V^{-1}}$$
$$k = 1{\cdot}380 \times 10^{-16}\ \mathrm{erg\ ^\circ K^{-1}}$$
$$m_e = 9{\cdot}11 \times 10^{-28}\ \mathrm{g}$$

DATA

The table shows the levels considered and the energy values used. These were obtained from the spectral wavelengths and rounded to three figures, well within the accuracy of the cross-section data, to provide a self-consistent scheme. For this purpose the 6^3D levels are considered as one, at the 6^3D_2 level.

Energy values used in the calculations

Level	Energy above ground state (eV)
6^3P_0	4·67
6^3P_1	4·89
6^3P_2	5·46
6^1P_1	6·70
7^3S_1	7·73
6^3D	8·85
Hg^+	10·43

The cross-sections used for ionization from the ground state are taken from Nottingham's data[5] and shown in Fig. 1. His values for Hg^+ were obtained from his measurements of the total cross-section, including multiply charged ions, by using the relative proportions determined by Bleakney.[6]

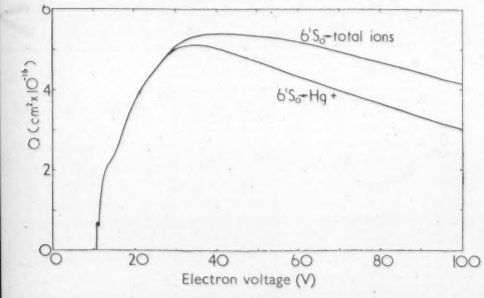

Fig. 1. Ionization cross-sections for the ground state, after Nottingham

For the excitation of the 6^3P states from 6^1S_0, the curves used by Kenty[7] have been used. The linear extrapolations shown in Fig. 2 are sufficiently accurate to provide corrections at high electron temperatures, and were made with the aid of Penney's calculations[8] and the data of Arnot and Baines,[9] Nottingham[5] and Massey and Burhop.[10]

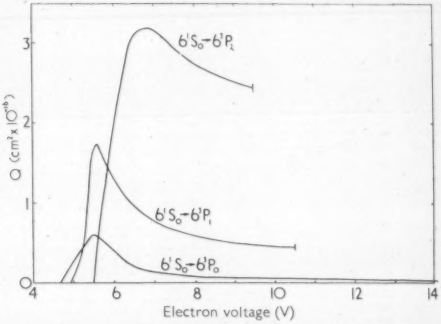

Fig. 2. Excitation cross-sections for the 6^3P levels, after Kenty

For transitions between the 6^3P_2 and 6^3P_1 levels, and transitions involving 7^3S_1, the curves used by Kenty,[7] taken from Yavorski's calculation[11] have been used. These are shown in Figs. 3 and 4, the latter transposed to zero origin. Transitions to the 6^3D states, considered as one, were found to be satisfactorily accounted for by Kenty,[7] who evaluated the rates for a particular discharge by assuming cross-section curves as for 7^3S_1, but 10% larger and transposed to the

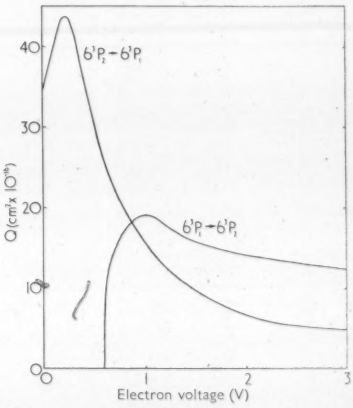

Fig. 3. Cross-sections for transitions of the first and second kind between 6^3P_1 and 6^3P_2, after Yavorski

appropriate excitation potentials. The same procedure has been followed in the present calculations. No data are known for transitions involving 6^3P_0, but a qualitative discussion is given by Kenty.[7]

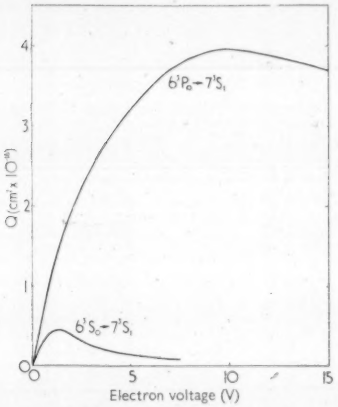

Fig. 4. Cross-sections for excitation of 7^3S_1 from the ground state and 6^3P_0, after Yavorski. (Origin transposed)

For excitation of 6^1P_1 from 6^1S_0, Penney's calculated cross-section was used,[8] normalized so that his curve for 6^3P_2 fits that of Fig. 2. This is shown in Fig. 5.

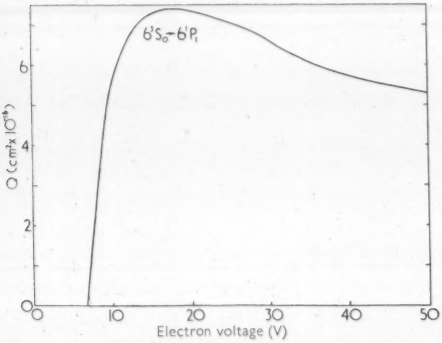

Fig. 5. Excitation cross-section for 6^1P_1, after Penney

RESULTS AND DISCUSSION

The excitation and ionization rates obtained for electron temperatures between 5000 and 54000° K are shown in Figs. 6 to 12.

Fig. 12 shows the rate of formation of singly ionized mercury. Multiple ionization is less than 0·5% of this over the whole range and the total ionization curve is indistinguishable on this scale. Exact integration using the approximate cross-section formula $Q = \alpha(V - V_i)$ is often used [for example, in Ref. (12)], and the circles in Fig. 12 show the ionization rate obtained in this way using the values $\alpha = 1{\cdot}025 \times 10^{-16}$ cm^2 V^{-1} and $V_i = 10{\cdot}43$ V. Agreement is good at low electron temperatures only.

Fig. 13 shows the ionization rate from the 6^3P levels, assuming that the cross-section is the same as that from the

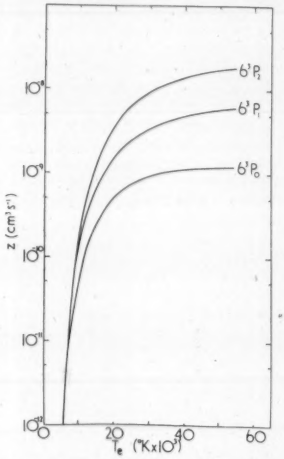

Fig. 6. Rate of excitation of the 6^3P levels

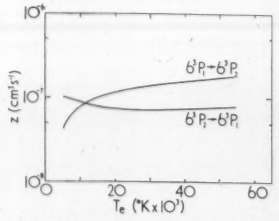

Fig. 7. Rate of transitions between 6^3P_1 and 6^3P_2 by electron collisions of the first and second kind

ground state. Although there is no sound justification for this assumption, the rates obtained are of interest since a similar assumption, but using a linear approximation to the cross-section curve, has been used by Waymouth and Bitter[12] in their treatment of the fluorescent lamp discharge. There is evidence that the real rates may be as much as ten times larger. At low electron temperatures (less than 20000° K) ionization from the ground state is small and step-wire ionization *via* 6^3P is predominant.[7, 13] At higher electron temperatures direct ionization becomes more important, as may be seen from Fig. 12.

Because of the high transition rates between 6^3P_2 and 6^3P_1, there will be a high degree of excitation of the latter, the resonance level, *via* the former, which is metastable. This has been demonstrated experimentally by Kenty,[7] who also discusses the matter further.[13]

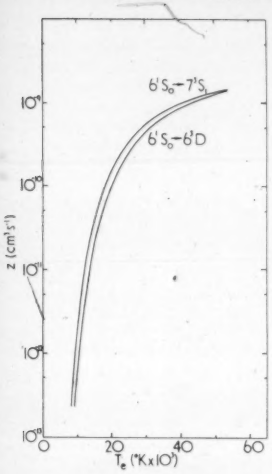

Fig. 8. Rates of excitation of 7^3S_1 and 6^3D from the ground state using Yavorski's cross-section for 7^3S_1, increased by 10% for 6^3D, after Kenty

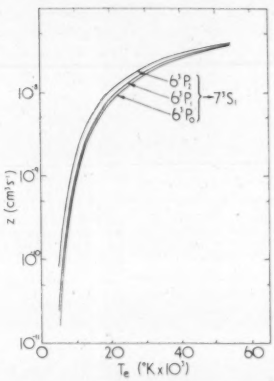

Fig. 9. Rates of excitation of 7^3S_1 from the 6^3P states assuming Yavorski's cross-section for 6^3P_0 to apply in each case

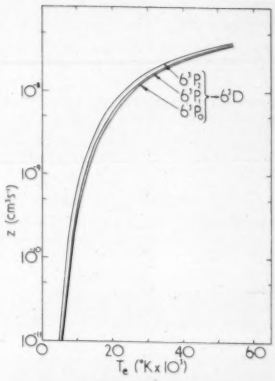

Fig. 10. Rates of excitation of 6^3D from the 6^3P states assuming Yavorski's cross-section for 6^3P_0–7^3S_1, increased by 10%, to apply in each case

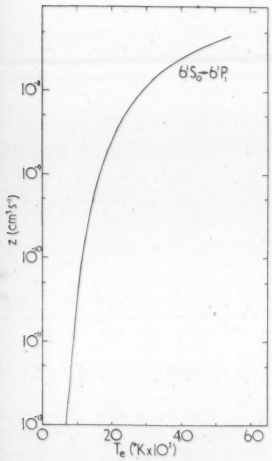

Fig. 11. Rate of excitation of 6^1P_1 from the ground state using Penney's cross-section

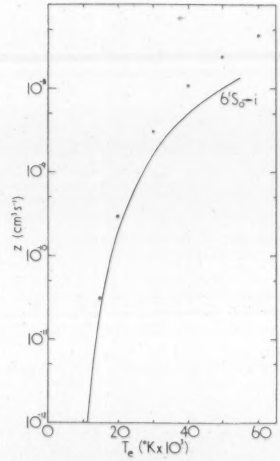

Fig. 12. Rate of ionization from the ground state using Nottingham's cross-section. Multiple ionization negligible on this scale. The circles show the result of using the approximate cross-section
$Q = 1{\cdot}025 \times 10^{-16}(V-10{\cdot}43)\ \mathrm{cm}^2$

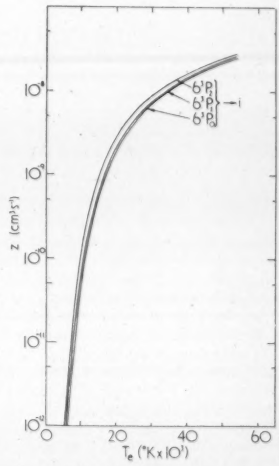

Fig. 13. Rates of ionization from the 6^3P states obtained by assuming Nottingham's cross-section to apply to these cases. The real rates may exceed these by as much as a factor of ten

Because of the high relative cross-sections for excitation of 6^1P_1, the 1849 resonance line becomes increasingly important as the electron temperature is increased. The fact that the negative glow of a mercury rare gas discharge is known to emit a higher proportion of 1849 radiation than the positive column is probably explained in this way.

ACKNOWLEDGEMENTS

The author wishes to thank his colleagues at the Research Laboratory of the British Thomson-Houston Co. Ltd., with whom he has had many valuable discussions.

REFERENCES

(1) BRODE, R. B. *Rev. Mod. Phys.*, **5**, p. 257 (1933).
(2) EASLEY, M. A. *J. Appl. Phys.*, **22**, p. 590 (1951).
(3) LOEB, R. B. *Basic Processes of Gaseous Electronics*, Chapter 4 (California: University of California Press, 1955).
(4) ELENBAAS, W. *The High Pressure Mercury Vapour Discharge* (Amsterdam: North Holland Publishing Co., 1951).
(5) NOTTINGHAM, W. B. *Phys. Rev.*, **55**, p. 203 (1939).
(6) BLEAKNEY, W. *Phys. Rev.*, **35**, p. 139 (1930).
(7) KENTY, C. *J. Appl. Phys.*, **21**, p. 1309 (1950).
(8) PENNEY, W. G. *Phys. Rev.*, **39**, p. 467 (1932).
(9) ARNOT, F. L., and BAINES, G. O. *Proc. Roy. Soc. A*, **151**, p. 256 (1935).
(10) MASSEY, H. S. W., and BURHOP, E. H. S. *Electronic and Ionic Impact Phenomena* (Oxford: The University Press, 1952).
(11) YAVORSKI, B. *Bull. Acad. Sci. U.S.S.R.*, **9**, p. 233 (1945); *J. Phys. U.S.S.R.*, **10**, p. 476 (1946).
(12) WAYMOUTH, J. F., and BITTER, F. *J. Appl. Phys.*, **27**, p. 122 (1956).
(13) KENTY, C. *Phys. Rev.*, **80**, pp. 95, 96 (1950).

Analysis of the lighter elements by total reflexion of their characteristic X-ray wavelengths

By A. FRANKS, Ph.D., A.Inst.P., and R. F. BRAYBROOK, B.A., National Physical Laboratory, Teddington, Middlesex

[*Paper received* 15 *January*, 1959]

The analysis of characteristic X-ray wavelengths in the region of 10 Å has been achieved by a technique employing total external reflexion.

Two convenient techniques are available for direct quantitative analysis using characteristic X-rays. The first is the well-established fluorescent technique in which a beam of X-rays incident on a sample excites the characteristic radiation, which is then analysed with a crystal spectrometer. The second method differs from the first only in the mode of excitation; the characteristic radiation is produced by direct electron bombardment. In most commercially available equipment, analysis is limited to elements having atomic numbers exceeding 20.

The difficulties in dealing with the lighter elements mainly concern the analysing and detection techniques. A further handicap is the absorption of the radiation in air so that a hydrogen or helium atmosphere, or preferably a vacuum enclosure, is essential.

Although the detecting device can be a photographic plate, a counter is more convenient; conventional Geiger or proportional counters cannot, however, be used owing to the heavy absorption in their windows. The authors have found an open (i.e. windowless) photomultiplier, with copper-beryllium electrodes similar to that described by Allan,[1] to be satisfactory.

The analyser cannot be one of the crystals in common use in spectrometers because the lattice spacings are too small to permit Bragg diffraction to occur. Efforts are being made in various laboratories to obtain a really satisfactory crystal with a sufficiently large spacing.

The aim of this work is to investigate the use of total external reflexion of X-rays as a means of analysis of wavelength. The refractive index of all materials for X-rays is slightly less than unity. Hence X-rays which are incident at a sufficiently small glancing angle will be totally reflected.[2] The critical angle of reflexion is proportional to wavelength and thus it would appear that an analysis could be obtained by measurement of the critical angle. In practice the authors have found that the critical angle is not sharp and must be evaluated from a graph of intensity I *versus* glancing angle θ.

The experimental technique is simple and is illustrated in Fig. 1. A collimated X-ray beam from the sample is incident on the reflector, which can be rotated as indicated by means of a micrometer screw. The detector may remain stationary

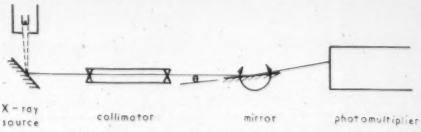

Fig. 1. The total reflexion analyser

since the angles of reflexion are sufficiently small and the collecting electrode is relatively large. Fig. 2 shows the results obtained from aluminium and magnesium samples ($\lambda = 8{\cdot}32$ and $9{\cdot}87$ Å respectively). The reflected intensities I are given relative to the incident intensity I_0 and the zero of the glancing angle θ is only approximately correct.

The accuracy of individual measurements was about 5%; the errors were due to statistical counting errors and to the mechanical difficulties of accurately adjusting the reflector.

The advantages of total reflexion are:

(i) simplicity of apparatus;
(ii) the intensity of the reflected beam is high, since the reflexion is very nearly total.

The disadvantages are:

(i) the sharpness of the critical angle decreases with increasing wavelength. Sharpness should be enhanced by use of a reflector of low absorption coefficient,[2] but no worth-while improvement was obtained by substituting a beryllium reflector for the glass one. It has not been found possible to separate the C_K and O_K radiations ($\lambda = 44{\cdot}5$ and $23{\cdot}6$ Å respectively);

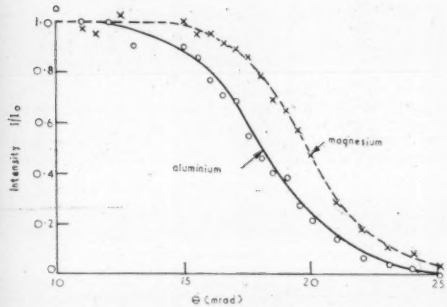

Fig. 2. Graphs of relative intensity *versus* glancing angle for Al_K and Mg_K radiations

(ii) an additional factor which decreases the resolution is the effect of white radiation of wavelength longer than the characteristic. This radiation will be reflected at angles greater than the characteristic critical angle so that the intensity curve will drop less sharply. The effect can be reduced by the insertion of thin filters, and in order to produce the curves in Fig. 2, a 0·0003 in. aluminium filter was used;

(iii) the (I, θ) curve for mixed radiation from neighbouring light elements will be intermediate between the curves obtained from pure samples of each. A satisfactory analysis would require the preparation of suitable standard specimens. It would appear that the accuracy of the analysis is not comparable to that in the range covered by crystal spectrometers.

CONCLUSIONS

The method is satisfactory as it stands in the region of aluminium, magnesium and sodium, especially for the determination of these pure elements or in combination with a heavier element. The analysis of mixtures of light elements presents many difficulties even with the help of standard samples. For the analysis of even lighter elements the method may prove of some use if it is combined with a technique employing partial filtration by using thin absorbing screens.[3]

ACKNOWLEDGEMENTS

The work described above has been carried out as part of the research programme of the National Physical Laboratory and this paper is published by permission of the Director of the Laboratory.

REFERENCES

(1) ALLAN, J. S. *Rev. Sci. Instrum.*, **18**, p. 739 (1947).
(2) COMPTON, A. H., and ALLISON, S. K. *X-rays in Theory and Experiment* (London: Macmillan and Co. Ltd., 1935).
(3) TOMBOULIAN, D. H., and BEDO, D. E. *Rev. Sci. Instrum.*, **26**, p. 747 (1955).

Correspondence

On the use of coarse gratings in ultrasonics

It is well known that the Debye Sears' diffraction effect produced by high-frequency sound waves traversing a liquid gives a simple and accurate method of finding the wavelength of those sound waves in the liquid. A photograph of the diffraction spectra taken by a long focus camera of known focal length F yields the linear separation D between the different orders, and the wavelength of the sound waves λ^* can then be calculated using the relation $\lambda^* = F\lambda/D$ where λ is the wavelength of the monochromatic light used. Since $\delta\lambda^*/\lambda^* = -\delta D/D$ it follows that the percentage error in the determination of λ^* is same as that in the measurement of D.

The writer* has used an alternative technique of measuring the wavelength of the sound waves which makes use of a suitable coarse transmission grating—periodicity $\Delta > \lambda^*$—and a spectrometer. The beam of light from the collimator passes normally through the optical and acoustic gratings in succession, the former being mounted on the prism table, while the optical cell containing the latter is mounted on an independent platform in front of the telescope. The diffraction orders generated by both gratings are then viewed through the telescope, and the table is turned through an angle i till the apparent spacing of the diffraction orders of the optical grating becomes equal to that of the other, when exact coincidence between the two sets takes place. The wavelength of the sound waves is then given by $\lambda^* = \Delta \cos i$ and, if a proper value for Δ is chosen, the angle i is large and the wavelength is found very accurately.

The photographic method, however, has the advantage that once the photograph is taken measurements on the plate can be made leisurely. In this case also a transmission coarse grating may be used with advantage. After the photograph of the diffraction spectra generated by the acoustic grating is taken and the sound field in the optical cell is turned off, a coarse grating may be mounted normal to the beam of light in front of the optical cell, and a photograph of the diffraction spectra produced by that grating be taken on the same plate just below the photograph of the other spectra, allowing the same exposure time. After developing the plate, measurements can be made of the distances D and d, that is between the diffraction spectra generated by the acoustic and optical gratings respectively. It is obvious then that $d/D = \lambda^*/\Delta$, and in calculating λ^* neither the focal length of the camera lens nor the wavelength of the monochromatic light is needed, If d and D are arranged to be of the same order of magnitude by setting the grating at a known angle of incidence i, though the same error which is likely to be of the same sign occurs in the measurement of each, the ratio d/D obtained as the result

of a number of measurements is free from the effects of that error. Therefore $\lambda^* = (d/D)\Delta \cos i$ is obtained to the same degree of accuracy as Δ, the exact value of which can be obtained from the manufacturer of the grating. Though collimation is important, imperfections of the optical cell and of the camera lens produce similar distortion in both spectra, and so the ratio d/D remains unaffected.

If the coarse grating consists of strictly opaque and transparent elements of width b and c respectively, $(b + c) = \Delta$, another useful purpose is served by this method. A comparison of the intensities of the diffraction spectra produced by the acoustic grating with that produced by the optical grating becomes possible and a microdensitometer record of the former can be standardized with respect to the latter, particularly since the photographs are taken giving the same exposure time. This is possible because the record of the optical grating spectra for normal incidence represents known intensities. If the grating has N grating elements and if the amplitude of the vibrations transmitted normally through a transparent element is a, the intensity of the mth order is given by the expression

$$I_m = \frac{N^2a^2 \sin^2\{m\pi[b/(b+c)]\}}{\{m\pi[b/(b+c)]\}^2}$$

and the intensity of the zero order is given by N^2a^2. The writer has used a grating of strictly opaque and transparent elements, $\Delta = 0{\cdot}0069$ cm, and actual measurement of the intensities of the different orders using a photomultiplier has shown that the formula given above can be relied upon to give the relative intensities accurately.

Raman and Nath's† theory of Debye Sears' effect has yielded a method of comparing the intensities of ultrasonic fields or the intensities of portions of the same ultrasonic field in an absorbing medium. The method involves the estimation of the relative intensities of the diffraction spectra produced by each. The writer has successfully used his coarse grating of strictly opaque and transparent elements in such investigations.

University College,
Trivandrum,
Kerala State,
India.

G. M. SREEKANTATH
[28 July, 1958]

* SREEKANTATH, G. M. *Curr. Sci.*, **25**, p. 355 (1956).
† RAMAN, C. V., and NAGENDRA NATH, N. S. *Proc. Indian Acad. Sci.*, *A* **2**, pp. 406, 413 (1935).

Comments on the A.S.T.M. Powder Data File—4

The writers have now prepared a fourth booklet, bearing the above title, which contains further additions to the lists previously published and described in The Institute's journals.* Copies of the present booklet have been distributed in the same way as were the others. Those who have not received copies of the booklet in this way may obtain them (free of charge) on request from The Institute or from us.

It is hoped that similar lists of comments will be published at approximately annual intervals. Users of the Data File are urged to send to the writers any material that they feel should be included in future issues.

Viriamu Jones Laboratory,
University college, Cardiff,
Great Britain.

J. W. HUGHES
ISABEL E. LEWIS
A. J. C. WILSON
[8 January, 1959]

* HUGHES, J. W., LEWIS, ISABEL E., and WILSON, A. J. C. *Brit. J. Appl. Phys.*, **9**, p. 123 (1958); *J. Sci. Instrum.*, **35**, p. 120 (1958).

Journal of Scientific Instruments

Contents of the April issue

ORIGINAL CONTRIBUTIONS

Papers

Use of radial gratings in a small inclinometer. By A. Lewis and I. R. Young.
Resistance strain gauges of low temperature sensitivity. By G. R. Higson.
Automatic scanner for electrophoresis and chromatography paper strips. By G. Smiljanic and T. Rabuzin.
Recording projection micrometer. By N. A. Hunt, P. C. Russell, E. A. Stewardston and J. E. Wilson.
Tensile testing machine for microscopic specimens. By D. M. Marsh.
Linear voltage temperature furnace for thermal analysis. By A. J. Martin and K. L. Edwards.
Liénard phase plane integraph. By R. Butler.
Analogue computer for the solution of product integrals. By F. D. Penny and J. W. McHugo.
Apparatus for the measurement of specific heat of metals. By W. H. Martin and J. Rixon.
The design of mercury thermometers for calorimetry. By J. A. Hall and Vera M. Leaver.
Method of double-beam spectrophotometry in the vacuum ultra-violet. By J. F. James.
Method of reducing the effects of vibration in a magnetic ring balance. By C. A. Clark and J. E. Whittle.
Contour mapping microdensitometer. By P. Hariharan and M. S. Bhalla.

Laboratory and workshop notes

Photoconductive detector of radiation of wavelength greater than 50 T. By S. J. Fray and J. F. C. Oliver.
Simple evaporator for radioactive metals. By L. W. Barr and D. A. Blackburn.
Method for operating a galvanometer amplifier from a low resistance input circuit. By G. G. E. Low.
Growth of uniform circular cylindrical crystals of predetermined orientation. By E. V. Vernon.

Correspondence

Recording optical lever. From R. V. Jones and J. C. S. Richards.
Comments on the A.S.T.M. Powder Data File—4. From J. W. Hughes, Isabel E. Lewis and A. J. C. Wilson.

NOTES AND NEWS

New instruments, materials and tools

THIS JOURNAL is produced monthly by The Institute of Physics, in London. It deals with all branches of applied physics (including theory and technique). All rights reserved. Responsibility for the statements contained herein attaches only to the writers.
EDITORIAL MATTER. Communications concerning editorial matter should be addressed to the Editor, The Institute of Physics, 47 Belgrave Square, London, S.W.1. (*Telephone:* Belgravia 6111.) Prospective authors are invited to prepare their scripts in accordance with the *Notes on the preparation of contributions*. (Price 2*s*. 6*d*. including postage.)
REPRODUCTION. The Institute of Physics is a signatory to The Royal Society's Fair Copying Declaration. Details may be obtained upon application from The Royal Society, London, W.1.
ADVERTISEMENTS. Communications concerning advertisements should be addressed to the agents, Messrs. George Jackson (Fleet St.) Ltd., Cliffords Inn, Fleet Street, London, E.C.4. (*Telephone:* Holborn 3611–2.)
CLAIMS FOR MISSING JOURNALS. Claims from regular subscribers to this *Journal* for missing numbers will only be considered if received within 60 days of the date of mailing plus normal outward time of transit and time for lodging the claim. Losses attributable to failure to notify a change of address or to similar omissions will not be considered.
SUBSCRIPTION RATES. A new volume commences each January. The charge is £6 per volume ($17 U.S.A.), including index (post paid), payable in advance. Single parts, so far as available, may be purchased at 12*s*. 6*d*. each ($1.75 U.S.A.), post paid, cash with order. Orders should be sent to The Institute of Physics, 47 Belgrave Square, London, S.W.1, or to any bookseller.

Superconducting computer elements*

By E. H. RHODERICK, M.A., Ph.D., Services Electronics Research Laboratory, Baldock, Herts.

A survey is made of the present status of superconducting circuit components, including both active elements of the "cryotron" type and passive elements such as persistent current memory cells. The factors which affect the speed of operation of these devices are discussed, and the future shown to be closely linked with developments in the technology of thin metallic films.

1. INTRODUCTION

Much consideration has recently been given to the possibility of applying the phenomenon of superconductivity to the design of circuit elements for computers. The present cost of commercially available helium liquefiers is much less than that of a large computer, and the philosophy underlying the current interest in superconducting circuits is that it may well be expedient to tolerate the added cost and complication of a low-temperature cryostat if, in return, significant improvements in the cheapness, reliability and speed of operation of the circuit elements themselves may be realized. From this point of view, the progress which has already been made with superconducting circuit components is sufficient to show that they hold considerable promise for computer applications. Another important feature of superconducting elements is that, because of their zero resistance, they dissipate no power in the quiescent state. This, although of secondary interest to the computer engineer, is an essential prerequisite for circuits which have to operate at liquid helium temperatures, since the consumption of liquid helium would otherwise be prohibitive.

2. SUMMARY OF SOME FUNDAMENTAL PROPERTIES OF SUPERCONDUCTORS

A comprehensive account of the subject of superconductivity is given in several standard texts, such as that by Shoenberg,[1] but the application of superconductivity to the design of circuit elements can be understood if the following fundamental properties of superconductors are appreciated.

(*a*) *Disappearance of resistance below a critical temperature* (T_c). The transition is very sharp in perfect superconductors, taking place within about 10^{-3}° K, but is less sharp in impure or strained superconductors. As far as can be determined, the residual resistance is truly zero.

(*b*) *Perfect diamagnetism* (*Meissner effect*). In the superconducting state the magnetic induction $\boldsymbol{B}$ always vanishes. The fact that $\boldsymbol{B}$ is zero involves the existence of superficial currents which produce an internal field exactly cancelling the applied field; since these currents are not truly superficial but occupy a very thin surface layer, $\boldsymbol{B}$ falls to zero within a very small distance known as the penetration depth, λ. For most superconductors, λ is of the order of 10^{-5} cm.

(*c*) *Destruction of superconductivity by a magnetic field.* For all superconductors, the application of a magnetic field above a critical value H_c destroys superconductivity. For a perfect superconductor, the transition is very sharp provided demagnetizing effects are negligible. The value of H_c varies with temperature, being approximately represented by the parabolic law $H_c = H_0[1 - (T/T_c)^2]$. Values of T_c and H_0 for some of the more useful superconducting metals are given in the table.

Critical temperatures and critical magnetic fields at 0° K for some superconducting metals

	Niobium	*Tin*	*Tantalum*	*Lead*
T_c (° K)	8·0	3·7	4·4	7·2
H_0 (G)	2600	304	975	805

(*d*) *Destruction of superconductivity by a current.* There is a maximum current which superconductors can carry without losing their superconductivity. For specimens with dimensions large compared with λ, the critical current I_c is given by Silsbee's criterion, i.e. I_c is that current which produces a magnetic field H_c at the surface. For a circular wire of radius r, I_c is given by $H_c = 2I_c/r$ in electromagnetic units. For large specimens the resistance R rises discontinuously from zero to approximately $0{\cdot}5\,R_n$ at $I = I_c$, then approaches R_n asymptotically, R_n being the normal resistance. I_c varies with temperature in a manner similar to H_c.

3. THE CRYOTRON

The first suggestion that superconductivity might have some application to computer circuits came from Buck,[2] who suggested the use of property (*c*) to make a switching device called the cryotron. This consists of a superconducting tantalum wire, called a gate, which is surrounded by a solenoid of niobium, called the control winding, so that a sufficiently large current through the latter can restore the resistance of the former. Tantalum is chosen for its low value of H_c at 4·2° K, and niobium for its high value. The cryotron is very similar in operation to a relay, with the important difference that its resistance in the "open" state is not infinite. Since the resistance of the gate can be used to control a current, the device is a current amplifier. In order to have current gain, i.e. to enable a current I in the control winding to produce a variation greater than I in the current in the gate, it is necessary that the current I' in the control winding which produces a magnetic field H_c along the axis of the solenoid shall be less than the critical current I_c which, when flowing in the gate circuit, causes the self-destruction of superconductivity in the gate in accordance with property (*d*). The condition for this to be so is $4\pi n > 2/r$, where n is the number of turns per unit length of the control winding and r is the radius of the gate. The ratio $(4\pi n)/(2/r) = 2\pi nr$ is called the "current gain," and the condition that the gain shall exceed unity is necessary for the output of one cryotron to be used to control another.

Cryotrons can be used for the construction of many types of logical circuit, such as binary adders, shift registers, "and" and "or" gates, and matrix switches.[2, 3] The most extensive

* Based on a lecture given at the Electronics Group Conference on Solid State Switching Devices, held at University College, London, on 27 September, 1958.

application of cryotron circuits on record seems to be the catalogue memory described by Slade and McMahon.[4] Cryotrons can also be connected so as to form a bistable flip-flop circuit, as shown in Fig. 1. The operation of the

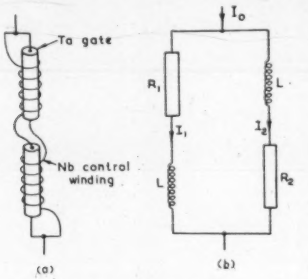

Fig. 1. Cryotron flip-flop circuit
(*a*) Physical arrangement; (*b*) electrical circuit.

flip-flop circuit depends on the fact that if a circuit contains two parallel branches, one of which is completely superconducting while the other is partially in the normal state, then the current will flow entirely in the superconducting branch since the resistance ratio is infinite. Clearly, if $I_0 > I'$, there are two stable states: (*a*) $I_1 = I_0$, $I_2 = 0$, $R_1 = 0$, $R_2 \neq 0$, and (*b*) $I_1 = 0$, $I_2 = I_0$, $R_1 \neq 0$, $R_2 = 0$. To trigger the circuit from one state to the other two additional cryotrons are needed, and a further cryotron is necessary to interrogate the device, making a total of five as shown in Fig. 2.

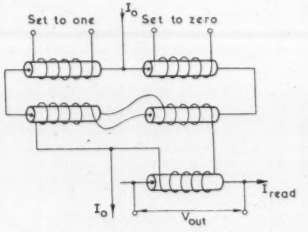

Fig. 2. Cryotron flip-flop circuit with state selection and read-out cryotrons

The method of switching this circuit is by inserting resistance in the superconducting leg by means of the triggering cryotron, and then waiting for the current through this leg to decrease until it is insufficient to hold the opposite gate normal. During this interval the circuit acts as a passive network, the time constant of which depends on the total inductance and resistance in the circuit; there is no regeneration as in a valve flip-flop circuit. An analysis by Morin[5] of the mode of operation of a cryotron flip-flop circuit shows that the total switching time is about $11 \times L/R$, where L and R are the inductance and resistance respectively of a single cryotron, assuming them all identical. Of this, about $4 \times L/R$ is the time taken for triggering from one state to the other, while a further $7 \times L/R$ is needed for transients to die away. A similar conclusion has been reached by Aharoni, Frei and Shtrikman.[6] The L/R ratio can be made smaller by decreasing the radius of the gate; if n is increased so as to keep the gain constant, $L/R \propto r^{-2}$. In a particular cryotron flip-flop circuit studied by Morin, the gate was of 0·009 in. diameter tantalum wire and the control winding had 220 turns per inch. For this construction $L/R = 12{\cdot}5\ \mu s$, so that $11\ L/R \simeq 140\ \mu s$. One would therefore expect to be able to trigger and reset the flip-flop in 280 μs, or about 4000 times per second. In practice, however, the maximum frequency of operation was 1000 c/s. The reason for this was the production of heat during switching. During both the switching interval and the decay of the transients, current flows through a gate which is in the normal state. The resulting Joule heat raises the temperature of the gate and reduces the value of H_c; in some cases the gate may even rise above T_c. The physical construction of the cryotron is such that the thermal time constant of the gate is quite long, of the order of 100–1000 μs, since the control winding and its insulation act as a thermal insulating jacket. In the particular design mentioned, the maximum speed was limited by this heating effect. The relative importance of the heating effect can be reduced by increasing the number of turns on the control winding, so that I' is reduced, but this puts up the value of L. The fastest operation of a cryotron on record is that reported by the General Electric Co. of America,[7] who claim a switching time of 10 μs. The flip-flop circuit could be set and cleared at a rate of 20 kc/s, which implies a recovery time of 15 μs. This was achieved by using a very small diameter gate consisting of a layer of superconductor deposited on an insulating cylinder; in this way one can increase the normal resistance and so reduce L/R without changing the gain. It is doubtful whether the solenoid type of cryotron is capable of much faster operation than this, and partly because of this and partly because of its structural complexity, development work on it seems to have been completely discontinued.

4. THE THIN FILM CRYOTRON

Apart from the heating effects mentioned above and the difficulty of achieving a design with L/R less than some microseconds, there is a more fundamental difficulty in the way of achieving fast operation with a solenoid type of construction. Due to the Meissner effect, magnetic flux is completely excluded from the gate wire when it is in the superconducting state. When the superconductivity is destroyed by a magnetic field greater than H_c, flux penetrates into the wire. The normal region starts as a thin sheath which grows inwards, enclosing a diminishing superconducting core. As the flux moves inwards, eddy currents are induced in the normal region and circulate circumferentially. These eddy currents produce Joule heating and also retard the growth of the normal phase. The time, τ, taken for the entire wire to become normal depends on the amount by which H exceeds H_c. According to Pippard[8] τ is proportional to $\sigma r^2 H/(H - H_c)$, where σ is the conductivity and r the radius of the wire, so that the delay decreases with decreasing r. For 0·009 in. tantalum, even values of $(H - H_c)/H$ as high as 0·25 cause delays of approximately 10 μs. A similar phenomenon occurs during the normal-to-superconducting transition, though here the situation is more complicated since there cannot be a continuous sheath of the superconducting phase surrounding a core of normal material, otherwise the flux in the normal region would be unable to escape. It is clear that, even with the smallest wire which is practicable, eddy current delays are going to limit the speed of the transition to the order of a microsecond. To achieve

faster switching times it is necessary to reduce at least one of the dimensions quite drastically, and this can most easily be done by using a thin film. Films of lead and tin can easily be prepared by evaporation with thicknesses of 10^{-5} cm or less; such films are comparable with the penetration depth and the superconducting-to-normal transition in them is inherently very fast since, apart from the dimensional factor discussed above the mechanism of flux penetration is altogether simpler than in the case of a wire of dimensions greater than λ. According to Pippard there can be no superconducting-normal boundary parallel to the face of a thin film of dimensions of the order of λ. The transition involves the growth of islands of the normal phase which occupy the whole thickness of the film.

The first step in making a thin film cryotron is obviously to use a narrow strip of thin film as the gate; the next logical step is to use a second strip of film as the control circuit. This is possible in principle if one adopts the geometry shown in Fig. 3. Here the control strip is at right angles to the gate.

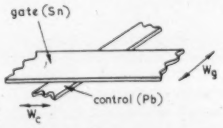

Fig. 3. Crossed film cryotron

The field which makes a portion of the gate go normal is a field transverse to the control strip, and the amount of the gate that goes normal is limited to a length of the order of the width of the control strip. If one assumes that the current distribution in the strips is uniform and that Silsbee's criterion holds, the current gain should be greater than unity provided the width of the control strip is less than that of the gate, since the field at the surface of the gate due to a current I in the control strip is $2\pi I/w_c$, while the field due to the same current in the gate is $2\pi I/w_g$. In practice neither of these assumptions is valid, and the width of the control strip must be very much less than that of the gate if a gain greater than unity is to be achieved. The amount of resistance introduced into the gate is small, of the order of $0{\cdot}1\,\Omega$, since only a small fraction of it is driven normal. On the other hand, the inductance of such a device should be very small, of the order of 10^{-8} H or less, so that L/R ratios of $0{\cdot}1\,\mu$s or less should be achievable.

Several laboratories in the United States are working on devices of this type. So far they all use tin for the gate and lead for the control, since these metals are easy to evaporate; the choice of tin for the gate and lead for the control is made because tin has a much lower critical field than lead (100 and 700 G respectively at 3° K). Flip-flop circuits made with thin film cryotrons have been constructed and shown to have two stable states, but no measurements of switching times have yet been reported. Most of the effort so far has been concentrated on the art of preparing evaporated films, involving intensive studies of the way in which various factors, such as the nature and temperature of the substrate, the rate of deposition, etc., influence the structure of the film. This seems to be a sensible approach, since until such problems are well understood it is impossible to say to what extent any observed superconducting properties of a film are representative of the behaviour of films in general rather than of the method of preparation.

The use of tin, for which $T_c = 3{\cdot}7°$ K, involves operating the helium cryostat under reduced pressure, since the boiling point of helium at atmospheric pressure is 4·2° K. This is a slight complication, though not a great one, and it would certainly be desirable to have available a film with a low value of H_c at 4·2° K. Tantalum immediately suggests itself for this purpose. Unfortunately tantalum is an exceedingly recalcitrant metal from the point of view of making evaporated films because of its high melting point (2850° C) and because of its excellent properties as a "getter." Tantalum films have been made in this laboratory,[9] using a vacuum of approximately 10^{-6} mm. The films exhibited superconductivity, but with a critical temperature of 1·6° K compared with 4·4° K for bulk tantalum. It is probable that the vacuum, although perfectly adequate in the case of tin and lead, is not good enough to avoid serious contamination of the tantalum during evaporation. The appropriate vacuum conditions for the evaporation of different metals are poorly understood, and it is clear that there is much yet to be done in the field of evaporated film technology.

5. PERSISTENT CURRENT MEMORY DEVICES

Attention has recently been attracted to the possibility of using a persistent current in a superconducting ring as a memory device. Such currents can be maintained indefinitely (for periods of years, at least) and, since the current can circulate either way, one has the essentials of a two-state memory. The idea of using persistent currents for this purpose seems to have been suggested simultaneously by Buckingham,[10] Crowe[11] and Crittenden.[12] The simplest device is that proposed by Buckingham, who called it the "Persistatron." This consists of a lead ring which has two wires connected asymmetrically to the periphery (Fig. 4). If a current I is passed through the system when the ring is superconducting, it divides between the two segments inversely in the ratio of their inductances, i.e. $I_1 = IL_2/(L_1 + L_2)$ and $I_2 = IL_1/(L_1 + L_2)$. If I is increased

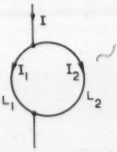

Fig. 4. The "Persistatron"

until I_1 reaches I_c, I_1 cannot increase further without making the left-hand segment go normal, and as soon as this happens any further increase in I can only increase I_2. One now has $I_1 = I_c$ and $I_2 = I - I_c$. This situation is a superposition of currents $IL_2/(L_1 + L_2)$ in L_1 and $IL_1/(L_1 + L_2)$ in L_2, together with a current $[IL_2/(L_1 + L_2) - I_c]$ circulating clockwise through the entire ring. If I is now reduced to zero, no branch of the ring is made to go normal, and, of the reduction I in the net current through the ring, an amount $IL_2/(L_1 + L_2)$ is withdrawn from the left segment and an amount $IL_1/(L_1 + L_2)$ from the right segment. The circulating current therefore remains after I reaches zero, and will persist until it is reversed by increasing I sufficiently in the opposite direction.

Although the basic principle of the Persistatron has been shown to work, it has not been exploited to any degree, so that it is not known how fast it can be made to switch. It is fairly clear, however, that in order to get away from eddy current problems the dimensions must be made very small, as in the case of the cryotron, e.g. by making the ring an annulus of thin film. It is also advantageous to drive the ring by induction rather than by a direct connexion, since

this will enable a two- or three-dimensional array of such elements to be constructed in the usual manner. These considerations, together with an examination of the problems of fabricating such a device, lead quite logically to the type of memory cell developed by Crowe[11] at the I.B.M. laboratories. In this, the ring becomes a hole in a thin lead film, with a narrow cross-bar running across a diameter. The persistent currents follow a figure-eight shaped path, passing along the cross-bar and then dividing and returning around the two halves of the periphery of the hole as shown in Fig. 5. This construction has the great advantage that

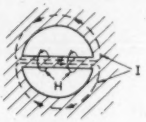

Fig. 5. Crowe cell, showing lines of current flow and magnetic field lines

the magnetic field of the persistent current is highly localized. The magnetic field lines are closed loops surrounding the cross-bar. To energize the cell, inductive coupling is provided by a drive wire mounted parallel with the cross-bar and separated from it by a thin layer of insulation; if the cross-bar is normal, lines of force set up by a current in the drive wire will link the cross-bar and provide almost perfect coupling. The signal output is obtained from a similar wire (the sense wire) situated on the opposite side of the film from the drive wire. In the Crowe cell the lead film and cross-bar are about 1000 Å thick, and both the drive and sense wires are strips of evaporated lead film.

At the present moment, the Crowe cell is in a more advanced state of development than any other superconductive device, so that a fuller account of it seems justified. To understand the operation of the device, consider the simplified circuit shown in Fig. 6, which is electrically equivalent. The

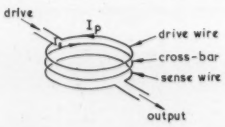

Fig. 6. Crowe cell: equivalent circuit

secondary winding (i.e. the film and cross-bar) is superconducting. The primary (drive wire) and sense loop are not necessarily superconducting, though it is desirable that the drive circuit should be superconducting to eliminate power dissipation. Suppose that the secondary inductance and resistance are L and R, and that the mutual inductance between primary and secondary is M. Then the secondary current satisfies the equation

$$L(dI_s/dt) + RI_s = M(dI_p/dt)$$

(for convenience, I_p and I_s are defined to have opposite directions). Owing to the tight coupling between primary and secondary, $M \simeq L$. For the case when the secondary is superconducting ($R = 0$) and $L = M$, integration gives $I_p - I_s =$ constant. Now suppose that $I_s = I_p = 0$ initially, and apply to the primary a linearly rising current so that $dI_p/dt = p$. Then the constant is zero and $I_s = I_p$; I_s therefore follows I_p until it reaches the critical current I_c at which the cross-bar begins to go normal. (The cross-bar goes normal before the rest of the film because the current density in it is much higher.) Because the superconducting-to-normal transition is not instantaneous, I_s overshoots I_c slightly before the secondary becomes completely normal. When the secondary resistance becomes R_n, the resistance of the cross-bar in its normal state, I_s begins to decrease exponentially to the value Mp/R_n (Fig. 7). One would

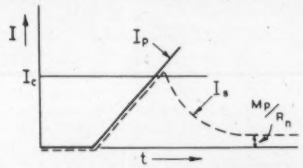

Fig. 7. Variation of primary and secondary currents in Crowe cell

expect that, as soon as I_s decreases below I_c, the cross-bar would become superconducting again, and that I_s would then begin to increase in accordance with the rule $I_p - I_s =$ constant; in this way I_s would oscillate around the level I_c. However, this is not what happens. Because of the overshoot, the secondary resistance is different from zero for a short interval of time, and during this interval Joule heating raises the temperature of the cross-bar slightly. This reduces the critical current so that I_s has to decay further before the cross-bar can go normal. [The critical current I_c varies with temperature in much the same way as H_c (see Section 2*d*).] This increases the time during which R is different from zero and causes additional heating. The relevant thermal constants of the I.B.M. design are such that this process diverges, and the cross-bar remains in the normal state long enough for the exponential decay to proceed almost to completion. This picture enables us to understand the behaviour of the cell when a trapezoidal current pulse is applied to the drive wire, as in Fig. 8. When I_p rises above I_c, I_s decays exponentially as already described, except that, since I_p is constant at the top of the pulse, I_s decays towards zero rather than to Mp/R_n. For simplicity, assume that I_s falls completely to zero, although experiments indicate that the exponential decay is arrested by the return of super-

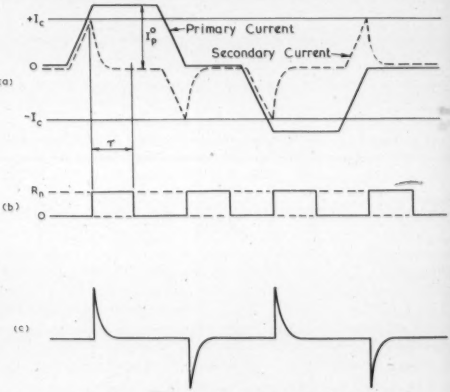

Fig. 8. Crowe cell: non-storing mode
(*a*) Primary and secondary currents; (*b*) secondary resistance; (*c*) output signal.

conductivity to the cross-bar when I_s falls to approximately $I_c/10$. Throughout this exponential decay the cross-bar is normal and heat is being produced. When the cross-bar temperature has ceased rising, it decays towards 4·2° K in a roughly exponential manner, and the interval that elapses before it reaches 4·2° K will be called the thermal recovery time, τ. Provided the width of the drive pulse exceeds τ, the falling edge induces a current in the secondary which is given by $I_p - I_s = I_p^0$, and as soon as I_s reaches $-I_c$, the above behaviour is repeated. After the cross-bar has cooled for the second time, it is in the same state as initially: there is no persistent current and no stored information. To determine the signal induced in the sense wire, note that for perfect coupling this is equal to $M(dI_p/dt) - L(dI_s/dt) = RI_s$, i.e. the output voltage is equal to the ohmic drop across the cross-bar. The output signal is therefore found by multiplying I_s by the secondary resistance, which is either 0 or R_n. If a second identical drive pulse is applied at a time greater than τ after the first, the cycle is repeated. The response to the second pulse is independent of the sign of the latter apart from the fact that it determines the polarity of the output signal, as shown in Fig. 8.

There is an alternative mode of operation in which the cell stores information, as shown in Fig. 9. Suppose that by some means the cell is left with a persistent current, which is necessarily less than I_c. If a drive pulse of amplitude less than I_c and of the appropriate polarity is applied, then I_s

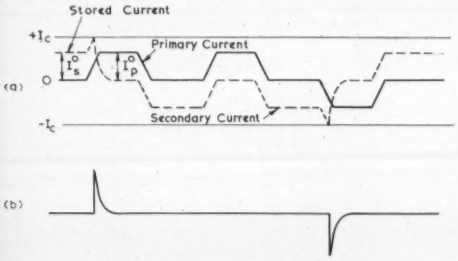

Fig. 9. Crowe cell: storing mode
(*a*) Primary and secondary currents; (*b*) output signal.

increases. If $I_p^0 + I_s^0 > I_c$, then I_s will reach I_c and one gets the usual decay of I_s towards zero followed by a thermal recovery time τ. If the length of the drive pulse exceeds τ, then its falling edge induces a current I_p^0 in the secondary, which is insufficient to make the cross-bar go normal. The cell is left with a persistent current $-I_p^0$ and stores this indefinitely. A second pulse of the same polarity as the first simply reduces I_s to zero then returns it to $-I_p^0$; it therefore does not change the state the cell is in. A drive pulse of opposite polarity makes I_s fall below $-I_c$, decay to zero and subsequently rise to $+I_p^0$. The cell is therefore cleared.

Both these modes can be observed. The procedure prescribed by Crowe for setting up the storing mode consists in applying a priming pulse which exceeds I_c, but then decays rapidly to a value less than I_c in a time shorter than the thermal recovery time; in this way the trailing edge of the pulse is insufficient to drive the cross-bar normal, and a persistent current is set up. This feature of the device is something of a disadvantage since a special priming pulse is needed, and also because it is necessary to resort to single-shot operation to be sure how the cell is functioning.

One advantage claimed for the I.B.M. device is that, provided the cross-bar is not driven normal, there is no coupling between drive and sense wires, consequently no "delta" noise. This is true in principle provided that the drive wire, cross-bar and sense wire are accurately alined. Any departure from true alinement causes coupling between drive and sense wires. It seems probable, however, that if the drive and sense wires consist of strips of evaporated film, sufficiently accurate registration of the masks can be achieved to ensure that direct coupling of drive and sense wires is negligible compared with the cross-talk between the connecting leads.

As far as operating characteristics of the Crowe cell are concerned, some data obtained with replicas of the device made by Broom[13] in this laboratory may be quoted. The cells were made of evaporated lead films with cross-bars in the range 400–1000 Å thick and 0·1 mm wide. The holes were deliberately made fairly large (5 mm diameter) for ease of construction and to give a fairly big output pulse. Both glass and mica were used as substrates, with a considerable difference between the thermal recovery times in the two cases. The recovery time, determined from the minimum length of drive pulse which was capable of switching the cell, was found to be about ten times shorter with a mica substrate than with a glass one. Glass is known to be an extremely poor conductor of heat at liquid helium temperatures, and though there seems to be no corresponding information available for mica, it seems probable that mica, being crystalline, will have a much higher thermal conductivity. This result suggests that the principal path by which heat leaves the cross-bar is by conduction through the substrate rather than by direct transfer to the helium bath. The fastest cell yet made by Broom, having a lead cross-bar 500 Å thick × 0·1 mm wide deposited on 0·07 mm thick mica, gave a symmetrical output pulse with rise and fall times of 15 mμs when operated in the storing mode. This is slightly more than the stated rise time of the oscillograph amplifier (12 mμs), so that the real rise and fall times of the output pulse are probably not more than 10 mμs. The rise time is determined by the speed of the superconducting-normal transition, the fall time by the L/R ratio of the cell, so that an upper limit of 10 mμs can be placed on both of these. The cell could be switched with pulses of 30 mμs duration, so that the thermal recovery time was no longer than 30 mμs. (The thermal recovery time must, of course, exceed the decay time of the output pulse, since the cross-bar must be normal throughout the latter interval.) At the present time, more accurate measurements of the various time constants are limited by the difficulty of obtaining sufficiently fast circuitry. With the cell dimensions quoted here, the critical current is about 300 mA and the output pulses are about 50 mV in amplitude.

6. PROGNOSIS

It is clear that the future of superconductive switching and memory devices is linked very closely with thin films, from the point of view of both speed and ease of mass production. As far as switching devices of the cryotron type are concerned, the use of evaporated films is in a very preliminary stage and no prediction of their potentialities in this field can possibly be made at the moment. The American approach of undertaking a thorough study of the mechanism by which evaporated films are formed and of their physical properties, before attempting any serious device work, seems essentially sound. Without this there can be no real understanding of the mode of operation of any device, nor can the problem of reproducibility be tackled. The importance

of examining the structure of films with an electron microscope cannot be too heavily emphasized.

The situation with regard to persistent current memories is somewhat clearer. The figures quoted show that, from the point of view of speed, the Crowe cell is already very promising. It is reasonable to suppose that the thermal recovery time can be reduced to the 10 mμs region by careful design of the cell, though at the moment the mechanism of heat dissipation is not understood sufficiently well to be able to predict the optimum design. As far as size is concerned, the hole diameter can certainly be reduced to 1 mm, so that one should be able to pack between fifty and a hundred cells into a square inch. Whether this means one can pack 10^4 cells into a square foot is another matter, since the problem of evaporating films of this area is by no means trivial. The thickness of the substrate plus film, sense and drive wires is about 0·1 mm, and if one adopts the device of using a superconducting screen between layers it should be possible to achieve at least twenty layers per inch, thus obtaining between 10^6 and 10^7 bits per cubic foot.

The remarks made above about the importance of a thorough study of the technique of preparing films apply with equal force to persistent current devices. Apart from the fact that the physical structure of the film may affect the heat relaxation time, the question of reproducibility is of great importance. Experience in this laboratory suggests that with a simple evaporating plant it is hard to control film thickness to better than 20%, the spread in I_c being greater than this. Another problem about which very little is known is that of the stability of thin films.

The more general question of the extent to which the merits of superconductive circuitry compensate for the problems of working at liquid helium temperature, and just what these problems are, is difficult to answer until the exact form a superconducting memory or switching unit may take is somewhat clearer. The Crowe cells dissipate about 10^{-10} joules when switched, so that 10^{10} cells can be switched per second for a dissipation of 1 W, which would evaporate about 2 litres of helium per hour. The latter figure is well within the range of a modern helium liquefier. The heat lost by conduction along a 0·001 in. diameter copper wire 1 m long, having one end at 4° K and the other at 300° K, is about 10^{-4} W, so a large number of leads into the cryostat could be tolerated as far as helium consumption is concerned. However, time of flight difficulties and the problem of eliminating cross-talk between a closely packed bunch of wires make it desirable to avoid having a vast number of leads running down into the cryostat. The future of superconducting memory devices may well depend on whether the concomitant switching circuits can also be operated at liquid helium temperature.

REFERENCES

(1) SHOENBERG, D. *Superconductivity*, 2nd Ed. (Cambridge: University Press, 1952).

(2) BUCK, D. A. *Proc. Inst. Radio Engrs*, **44**, p. 482 (1956).

(3) RICHARDS, R. K. *Digital Computer Components and Circuits*, p. 432 *et seq.* (New York: D. Van Nostrand Co. Inc., 1957).

(4) SLADE, A. E., and MCMAHON, H. O. *Proceedings of the Eastern Joint Computer Conference*, p. 115 (New York: American Institute of Electrical Engineers, 1957).

(5) MORIN, J. O. *The Cryotron as a Storage Element*. Massachusetts Institute of Technology Servomechanisms Laboratory Report No. 7138-R-15 (1956).

(6) AHARONI, A., FREI, E. H., and SHTRIKMAN, S. *Proc. Inst. Radio Engrs*, **46**, p. 780 (1958).

(7) *Gen. Elect. Rev.*, **61**, p. 41 (1958); also V. L. NEWHOUSE. Private communication.

(8) PIPPARD, A. B. *Phil. Mag.*, **41**, p. 243 (1952).

(9) OLIVER, D. J. Unpublished work at Services Electronics Research Laboratory.

(10) BUCKINGHAM, M. J. *Proceedings of Madison Conference on Low Temperature Physics* (Madison: University of Wisconsin Press, 1958).

(11) CROWE, J. W. *Proceedings of Madison Conference on Low Temperature Physics* (Madison: University of Wisconsin Press, 1958); see also *I.B.M. Journal*, **1**, p. 295 (1957).

(12) CRITTENDEN, E. C. *Proceedings of Madison Conference on Low Temperature Physics* (Madison: University of Wisconsin Press, 1958).

(13) BROOM, R. F. Unpublished work at Services Electronics Research Laboratory.

ORIGINAL CONTRIBUTIONS

High-resolution shadow-casting technique for the electron microscope using the simultaneous evaporation of platinum and carbon

By D. E. BRADLEY, Associated Electrical Industries Ltd., Aldermaston, Berks.

[*Paper first received* 31 *October*, 1958, *and in final form* 7 *January*, 1959]

Conventional shadowcasting techniques using heavy metals as shadowing materials suffer from a limited resolution imposed by the granulation of the metal. The paper describes a method for the simultaneous evaporation of platinum and carbon. This produces a deposit which does not granulate but at the same time has the high electron scattering power required for shadowing purposes. The properties of the deposit relating to its suitability as a shadowing material are fully discussed. The method is illustrated by means of various applications, one of which, the cleavage face of a sucrose crystal, exhibits monomolecular steps 11 Å high.

With the development of carbon and silicon monoxide replicas and the ultra-microtome, fuller use can be made of the high resolving power of modern electron microscopes. However, it is almost always necessary to shadow replicas and other specimens,(1) either to increase their contrast or to measure the heights of projections. This paper describes a new self-shadowing replica method capable of resolving steps 10 Å in height.

Existing shadowing techniques, using heavy metals, carbon or silicon monoxide provide only limited resolution. Heavy metals aggregate into small crystallites; carbon and silicon monoxide produce insufficient contrast to permit the attainment of high resolution. Thus there exists a need for a replica r shadowing material with high electron scattering power, the same time providing an amorphous deposit when evaporated. In addition the deposit must not granulate when subjected to electron bombardment. One possible approach to this problem is the simultaneous evaporation of carbon and a heavy metal.

The first development in this direction was by Knoch and König[2] who obtained what was effectively a platinum/carbon deposit by combining the evaporation of platinum with the deposition of carbon by the gas-discharge method.[3] The disadvantages of employing ion bombardment in the preparation of replicas are obvious, and it is clear that a straightforward simultaneous evaporation would be preferable. This has been achieved by other authors,[4, 5] but their attempts have suffered from a lack of control of the relative amounts of carbon and metal evaporated.

The present author has achieved the simultaneous evaporation of platinum and carbon by passing a heavy current through the points of two rods consisting of platinum and carbon intimately mixed together.[6] The points are lightly sprung together in a vacuum in a manner similar to that used in the evaporation of pure carbon.[7] Intense local heating at the points evaporates both platinum and carbon, producing a coherent amorphous deposit. The object in developing this method was to enable the composition of the deposit to be easily controlled and to provide a simple and reproducible method of evaporation. Preliminary observations on the technique have already been published elsewhere.[6] This paper describes in detail the method used for the preparation of the platinum/carbon rods, the nature of the deposit and the results obtained.

PREPARATION OF THE PLATINUM/CARBON RODS

It has been found necessary to evaporate the platinum and carbon through an aperture to prevent gas-scattered carbon from reaching the target. This scattered material often causes a very coarse background structure on the specimen (Fig. 5). However, the use of an aperture decreases the carbon content of the deposit, making it easily recrystallizable. This decrease must, therefore, be offset by increasing the carbon content of the rods. The composition of the rods, given in the description of their preparation, is such that the deposit obtained by evaporation contains the maximum permissible amount of platinum when an aperture is not used. If this quantity is exceeded, a crystalline deposit will be obtained. When apertures of 2·0 mm diameter or less are used, the amount of carbon required is two to three times that given.

It was found that metal powders and carbon did not bond together under the influence of high hydrostatic pressure alone. In the method described here, the powders are mixed with organic material, compressed, and then extruded into rods. Interlacing graphite particles or crystals, which harden the rods, are produced by the breakdown of the organic material or heating. The details are given below.[8]

(i) Finely divided platinum powder (200 mesh) and carbon powder [made by filing carbon rods type LINK WLO or WLI (by the Morgan Crucible Co.)] are well mixed in a pestle and mortar. (Weights 2·0 g platinum, 0·3 g carbon.)

(ii) A 10% aqueous solution of acacia (gum arabic) is now added, 0·45 ml. per gramme of mixture. The powders and solution are mixed to a paste, assisted if necessary by additional water. The paste is now dried with a stream of hot air and the mixture ground up.

(iii) A similar quantity of a 15% solution of pitch (or Apiezon W wax, by Metropolitan-Vickers Electrical Co. Ltd.) in chloroform is added together with one drop of linseed oil to each gramme of original platinum/carbon mixture. The pitch helps to hold the rods together before baking, and the linseed oil facilitates the extrusion described below. A few millilitres of ether added at this stage assists in mixing the components thoroughly. This paste is dried as much as possible with hot air. If the final rods are soft and crumble easily, the quantity of pitch solution used can be increased to double the amount given.

(iv) The mixture, now in the form of lumps of material resembling plasticine in texture, is broken down as much as possible. It is then placed in a test tube and warmed gently over a bunsen, at the same time being shaken, until all excess moisture and solvents are driven off. As soon as smoke appears the test tube is removed from the heat. The powder is now returned to the pestle and mortar and reground.

(v) The powder is next fed into a simple press, which consists of a short length of $\frac{1}{4}$ in. hardened silver-steel rod with a $\frac{3}{32}$ in. hole drilled down the whole length. About $\frac{1}{4}$ in. of $\frac{3}{32}$ in. silver-steel rod is inserted in one end to act as a bung, and the powder fed into the other end. When the tube is full of powder a drop of 10% linseed oil in benzene is introduced. A longer piece of silver-steel rod is now inserted into the tube, and the whole placed in a vice so that the mixture can be compressed. When the vice has been tightened as much as possible without bending the silver-steel rod, it is loosened and the assembly moved so that the bung can be pushed out and the mixture extruded. The resulting rod is somewhat soft and must be handled with care.

(vi) The next stage consists of baking the rod. The soft freshly extruded rod is allowed to dry in air for about an hour to remove as much benzene as possible. It is then inserted in a length of glass tubing through which nitrogen or any inert gas can be passed. To prevent combustion of the organic compounds during baking it is heated in a stream of the gas, gently at first, over a 450 W electric bunsen until all the linseed oil has been driven off (about twenty minutes), This baking is essentially for distilling off unwanted liquids.

(vii) The final "curing" process is carried out after cooling the baked rod and removing it from the glass tube. It consists of heating the rod to 500° C in a molybdenum foil boat at a pressure of about 10^{-2} mm of mercury for twenty minutes. Degassing the rods at 1200° C (by radio-frequency heating or electron bombardment) at a pressure of 10^{-5} mm of mercury enables a more controllable evaporation to be obtained.

When the rod is cool, it is removed from the vacuum and sharpened in a drill using grade 0 emery paper.

Platinum/carbon rods made in this way have been found to be hard, and to evaporate easily. Two grammes of platinum metal yield about 7 cm of rods in units of up to 1 cm in length; these are sufficient for between twenty and thirty evaporations.

THE EVAPORATION

This is carried out by the method used for evaporating carbon.[7] The pointed rods are mounted in small chucks and sprung lightly together in an evaporating plant (an oil diffusion pump was used here). A good vacuum (10^{-4} to 10^{-5} mm of mercury) is required. A heavy alternating current of about 50 A passed through the points causes

the rods to evaporate. The most satisfactory electrical supply is obtained from a transformer rated at 22 V, 20 A. The rods are connected across the secondary, and a variable transformer, which is pre-set, is connected across the primary coil.

With the source-target distance of about 4 cm used here, a deposit of suitable thickness is obtained in less than one second. The aperture, which has already been mentioned, is fitted into a large screen. It should be between 1 and 2 mm in diameter, and placed 1–1·5 cm from the source. When such an aperture is used, the deposit covers only a small area. The deposit is thinner at the edge of the area covered, so that specimens of varying thickness can be mounted.

The most satisfactory method for preparing platinum/carbon shadowed specimens for the electron microscope is as pre-shadowed replicas. For example, in the case of the surface of cleaved rock salt, a layer of platinum/carbon is deposited at the desired angle, and then a further thin layer of carbon is deposited normally. The combined film is floated on to water and mounted on specimen support grids. It is not always necessary to use the carbon backing since the platinum/carbon film is self-supporting when mounted on grids of a suitable design (type A.E.I. by Smethurst Highlight Ltd.). Platinum/carbon deposits can, of course, be used for shadowing in the conventional manner.

THE DEPOSIT

The composition of deposits obtained by the method given is not known, but consideration of vapour pressure figures indicate that the platinum content is greater than that of the rods (the vapour pressure of platinum is seventy times that of carbon at about 3500° C). The electron micrographs obtained also suggest that the mean atomic number is high, since the contrast is good with little noticeable "pile-up" effect.

Platinum/carbon films are effectively non-crystalline since they give a halo diffraction pattern, shown in Fig. 1(*a*). This is the kind of pattern to be expected from an amorphous deposit, but if it is considered as a specimen consisting of extremely small crystallites, then the particle size estimated from the ring breadth is about 8 Å, only twice the size of the unit cell of platinum. Fig. 1(*b*) shows the ring pattern obtained from a crystalline platinum deposit, and it can be seen that the two haloes of Fig. 1(*a*) correspond to the main reflexions of the platinum pattern.

Platinum/carbon deposits granulate under the influence of heavy electron bombardment if the metal content is too high. With a sufficiently high carbon content, however, it is not possible to cause granulation, and obviously the most suitable composition for the rods is that which gives a deposit containing the highest proportion of platinum that will not granulate under normal electron microscope operating conditions. The composition of the deposit may be conveniently varied as follows. A set of rods containing 10, 30 and 50% carbon (90, 70 and 50% platinum) are prepared. These may now be used in different combinations to give a source containing intermediate quantities. The composition of the deposit can thus be varied at will to accommodate various aperture systems and different electron beam intensities.

A simple and very sensitive method for the detection of crystallites in evaporated deposits consists of examining the films under dark field conditions. A diffraction pattern is obtained on the screen, and the objective aperture is positioned so that a small part of the brightest ring or halo can be seen through it. A dark field image is now obtained, and any crystallites contributing to the selected arc appear as bright specks; for example, Fig. 2(*b*) shows a crystalline platinum deposit. If there are no specks, then the specimen is amorphous, as in Fig. 2(*a*) which shows a platinum/carbon film.

SIMULTANEOUS EVAPORATION OF PLATINUM/IRIDIUM/CARBON RODS

The simultaneous evaporation of carbon and a number of other heavy metals has been attempted. These include tungsten, iridium, tantalum, rhenium and gold. All save iridium could not be evaporated satisfactorily for various reasons. A stable deposit was obtained using iridium, but the evaporation was difficult and required a higher temperature and more current than was the case with platinum. However, it is possible to evaporate rods containing 40% platinum, 30% iridium and 30% carbon without difficulty. The deposit obtained with a 2 mm evaporating aperture gave a characteristic halo pattern and could not be granulated in the electron microscope. It seems likely that it contained a reasonably high percentage of iridium, which would assist in inhibiting granulation because of its high melting point. Thus the advantage of incorporating iridium is that a stable deposit with a higher electron scattering power can be obtained. Further study of this technique is to be carried out.

BACKGROUND STRUCTURE

Diffraction and dark field evidence proves conclusively that any background structure found on platinum/carbon films is due to an unevenness in the deposit, contrast being produced by a self-shadowing effect. This is distinct from the case of evaporated metal films, where the background is produced by discrete crystallites and much of the contrast arises from diffraction effects.

A very fine structure, smaller than that occurring on evaporated metal films, appears when platinum/carbon films are deposited on atomically smooth surfaces such as mica, in spite of the use of an aperture. It must be emphasized that fine detail of this nature is particularly sensitive to the focus of the instrument; it may thus vary in appearance from one micrograph to another. Even when allowing for this factor the background structure seems to vary considerably and inconsistently on the surfaces examined so far. Its origin is not known, but many possibilities, such as damage by heat radiation to the specimen, have been eliminated by varying conditions of evaporation, for example the aperture size. In some cases, as in Fig. 7, the structure is completely absent. It seems probable that the migration of atoms of shadowing material may have some bearing on its formation, producing an uneven film in the earliest stages of deposition. The roughness of the deposit will be accentuated by pile-up effects in the later stages, and will, of course, be made visible by shadowing. This idea is to some extent supported by the fact that lower angles of shadowing produce coarser background effects as can be seen from Fig. 6. It is likely that this effect, which could be described as "statistical," will not occur on surfaces with a structure of the same order of size as the irregularities present in the first few atomic layers of the platinum/carbon film. Any structure of suitable dimensions and distribution is likely to reduce migration or other characteristics, which may contribute to statistical irregularities in the shadowing layer.

If the fine background is due to a "statistical" effect, it will not be a very serious impediment since it will only occur

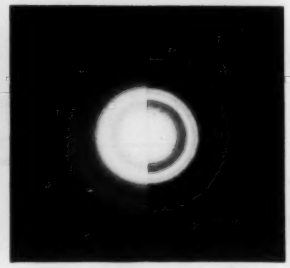

(*a*) (*b*)

Fig. 1. Electron diffraction patterns of (*a*) platinum/carbon film, (*b*) platinum metal on carbon film

Fig. 3. Penumbra of a shadow on the surface of a cleaved sucrose crystal. Platinum/carbon replica, angle 2 : 1 (× 190 000)

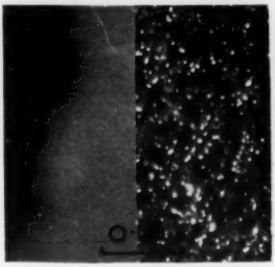

(*a*) (*b*)

Fig. 2. Dark field electron micrographs (× 75 000) of (*a*) platinum/carbon film, (*b*) platinum metal on carbon film

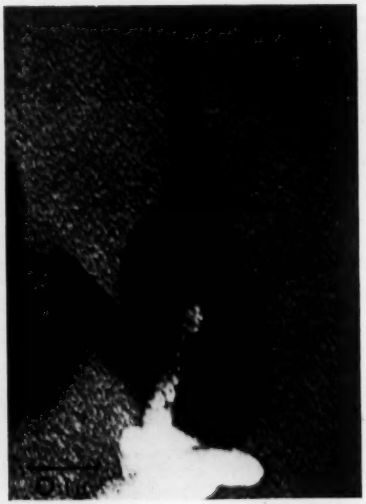

Fig. 4. Platinum/carbon shadowed molybdenum oxide smoke illustrating shadow sharpness. Angle 2·5 : 1 (× 110 000)

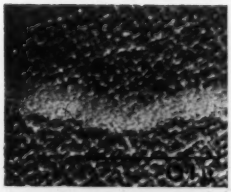

Fig. 5. Platinum/carbon shadowed edge of a 50 Å thick carbon film. Angle 3 : 1 (× 250 000). (Print not reversed; shadowing direction top to bottom)

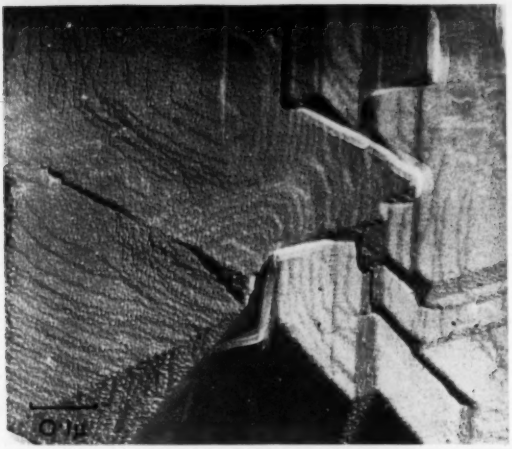

Fig. 6. Platinum/carbon replica of sodium faujasite crystal surface. Angle 2 : 1 (×125 000)

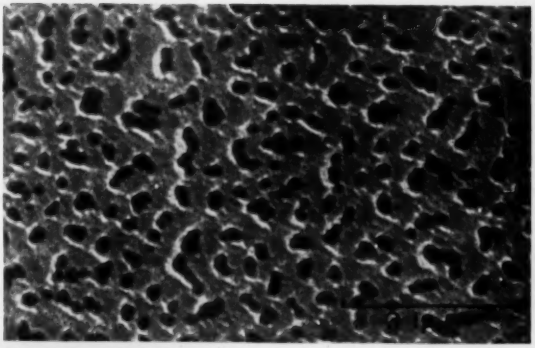

Fig. 7. Platinum/carbon shadowed gold particles evaporated on to cleaved rock salt. Angle 2 : 1 (×330 000). (Print not reversed)

Fig. 8. Monomolecular steps on a cleaved sucrose crystal. (Platinum/carbon replica.) Angle 2 : 1 (×250 000)

on nearly atomically smooth surfaces. If it is due to some other cause, it will be a more serious problem since it will mask the finest surface detail. As yet no suitable test specimen has been found to establish this point.

An important effect to be noted in the deposition of platinum/carbon films is the masking of fine detail if too thick a shadowing film is used. This is shown in Fig. 3. The specimen consists of a large particle on the surface of a cleaved sucrose crystal which has cast a shadow with a distinct penumbra at the edges. The sucrose crystal is covered with very fine steps, which are only visible in the thinly shadowed area of the penumbra. It can be seen that they disappear where the shadowing film attains its full thickness. As has already been mentioned, the evaporation produces a deposit, the thickness of which varies, so that there is no difficulty in selecting a specimen of correct thickness. Too thick a film can be easily recognized by excessive shadow contrast. Where very thin films are used, it may be necessary to increase the contrast photographically.

Some increase in contrast can be obtained in the electron microscope by phase contrast effects produced by underfocusing the image slightly. However, as has been stated this must be carefully limited. The micrographs here were underfocused by no more than 2 μ.

RESULTS

It has been found that platinum/carbon shadowing gives extremely sharp shadows, even at the abnormally short working distances used. A shadowed particle of molybdenum oxide smoke is shown in Fig. 4 to illustrate this point. It appears that the presence of an aperture does not in any way increase the shadow sharpness, but, as has been mentioned, cuts out scattered carbon. The specimen is therefore composed of atoms which have arrived directly and in a straight line from the source. As a result, holes such as that shown in Fig. 4 are visible in the densest part of large shadows when the platinum/carbon film is not backed with carbon. The presence of these holes indicates that surface migration is limited and supports the hypothesis that scattered carbon produces the coarse background structure found in the absence of an aperture.

The sharp shadows obtainable enable the edges of thin films to be shadowed and the film thickness to be measured directly in the electron microscope. Fig. 5 shows the edge of a 50 Å thick carbon film shadowed at $\tan^{-1}\frac{1}{3}$. Fig. 5 was obtained by coating a glass slide with carbon, then stripping off some of the carbon by backing it with Formvar, which was removed with adhesive tape. The film edge was shadowed without using an aperture because of lining-up difficulties, and a further backing layer of carbon applied. The composite specimen was then floated on to water and mounted on a grid. The film edge was easily located in the electron microscope. Though the difficulties of mounting the film edge across a grid increase as the initial deposit becomes thinner and less easily visible, it seems likely that the technique could be used to measure evaporated deposits as thin as 10 Å with a reasonable degree of accuracy.

One of the most readily obtainable types of structure which are useful in testing electron microscope replicas are step structures. They can be easily obtained as cleavage steps in many crystalline substances. Fig. 6 shows steps on the surface of a crystal of sodium faujasite. These steps are very small (less than 10 Å high) as estimated from the shadow length, taking into account the variation of the angles of the different faces with respect to the shadowing direction. The layer structure of the crystals is clearly shown and some form of spiral is also visible. The electron micrograph also shows the effect of different shadowing angles on the background structure.

Evaporated gold particles deposited on freshly cleaved rock salt provide a useful test specimen for the shadowing method. Fig. 7 shows an electron micrograph (print not reversed) of the particles obtained by depositing the equivalent of about 20 Å of gold on the rock salt surface. They were shadowed at $\tan^{-1}\frac{1}{2}$ with platinum/carbon. It can be seen that the shadows are very sharp and that the thickness of the gold particles varies from less than 10 to 20 Å.

A source of very fine steps is the cleavage face of a sucrose crystal. Cleavage steps of greatly varying height are found, and some of them, as in Fig. 8, split up into a number of smaller steps. It is possible to estimate the height of the larger step from the shadow length, the result being about 200 Å. This step splits up into eighteen units, the average height of which must therefore be about 11 Å. X-ray data gives the unit cell dimension normal to the cleavage plane as about the same value, so that the steps shown must be monomolecular.

CONCLUSIONS

It is clear that a platinum/carbon deposit provides a shadowing material capable of revealing very fine detail. It is difficult to place a definite limit on the resolving power of such a technique as shadow-casting, since this depends to a great extent on the nature of the specimen. However, it can be stated that steps less than 10 Å in height can be revealed by platinum/carbon shadowing. The ultimate capabilities of the method can only be assessed after it has been applied to a wide variety of specimens which have also been studied by conventional techniques.

The very fine background which still appears in many cases may well be a statistical effect common to other types of evaporation. Its presence can only be detected with a non-granular deposit of high scattering power, because of the small dimensions involved; it is thus unlikely to be observed using metal deposits.

It is interesting to note that platinum and iridium appear to be the only metals which fully satisfy all the somewhat critical conditions required for simultaneous evaporation with carbon.

ACKNOWLEDGEMENTS

The author would like to thank Mr. G. Rickards for his help with the electron microscope, Mr. G. A. Bassett (Tube Investments Ltd., Cambridge) for suggesting the examination of evaporated gold deposits on cleaved rock salt, Mr. D. P. R. Petrie, Dr. J. S. Halliday and Mr. R. Phillips for their interest and advice, and Dr. T. E. Allibone, Director of the Research Laboratory, Associated Electrical Industries Ltd., for permission to publish this paper.

REFERENCES

(1) WILLIAMS, R. C., and WYCOFF, R. W. G. *J. Appl. Phys.*, **17**, p. 23 (1946).
(2) KNOCH, M., and KÖNIG, H. *Z. Wiss. Mikr.*, **63**, p. 121 (1956).
(3) KÖNIG, H., and HELWIG, G. *Z. Phys.*, **129**, p. 491 (1951).
(4) SKATULLA, W. Private communication.
(5) JAYME, G., and HUNGER, G. *Mikroskopie*, **13**, p. 24 (1958).
(6) BRADLEY, D. E. *Nature* (*London*), **181**, p. 875 (1958).
(7) BRADLEY, D. E. *Brit. J. Appl. Phys.*, **5**, p. 65 (1954).
(8) BRADLEY, D. E. Patent application No. 26815/58.

Flow of heat in a composite solid

By T. P. Newcomb, M.Sc., A.Inst.P., Ferodo Ltd., Chapel-en-le-Frith, Stockport, Cheshire

[*Paper received* 15 *September*, 1958]

A solution is given to the problem of heat conduction in a composite solid consisting of two infinite slabs between parallel boundaries, when the interface is subjected to a thermal flux which decreases linearly with time, whilst at the two outer parallel boundaries there is no flow of heat. No assumptions are made concerning the way the heat is shared between the two bodies. This solution is applied to the problem of braking with uniform deceleration and possesses the advantage over previous solutions in that it can be used even when the brake applications are of long duration (over ten seconds). Typical curves showing the transient temperatures developed during braking are given.

During the process of braking two surfaces are in contact, one of which is rotating with respect to the other. If the deceleration of the body, the motion of which is to be controlled, is uniform, then the rate of heat generation H at the friction surfaces decreases linearly with time t, with $H = Q(1 - at)$ where a and Q are constants. At the working surface the heat developed is dissipated into each contacting body, and the determination of the transient temperatures reached at the interface or inside the contacting solids during a brake application reduces to considering the flow of heat in a composite solid. In the case of braking in an automobile, the curvature and dimensions of brakes and drums are sufficiently great that the errors, introduced by considering the concentric cylindrical portion of drum and lining to be developed into a flat rectangular plate (without edge effects) and the flow of heat to be uni-dimensional, are small enough to be neglected. In previous papers[1–4] solutions have been presented to the problem of the linear flow of heat in an infinite slab, when the heat shared between drum and lining was considered to be the same as that when both contacting bodies were of infinite thickness. This assumption is not in serious error if the thermal constants of the brake lining material are sufficiently low (say with a thermal diffusivity of 10^{-3} cm^2/s) and if the brake application is of short duration (up to 10 s). However, some brake lining materials are of higher thermal conductivity and diffusivity, and surface temperature calculations applied to each slab, based on the above method of heat sharing, violate the condition that at the common interface the temperatures must be identical throughout a long brake application. In this paper an exact solution is given to the problem of the flow of heat in a composite body, consisting of two infinite slabs between parallel boundaries, in which the interface is subjected to a thermal flux which decreases linearly with time, whilst at the other boundaries there is no flow of heat. The method of analysis used to solve the problem is based on the Laplace transformation which readily enables the temperature distribution in brakes to be determined.

THE EQUATIONS AND THEIR FORMAL SOLUTION

Consider the linear flow of heat in a composite solid consisting of two parallel faced infinite slabs, where $-l < x < 0$ represents one medium with physical properties K_1, ρ_1, c_1, k_1, v_1 and $0 < x < d$ is the other medium with physical properties K_2, ρ_2, c_2, k_2, v_2. The quantities K, ρ, c, k, v, with suffixes for whichever body is considered, refer respectively to the thermal conductivity, density, specific heat, thermal diffusivity and the temperature rise at any point x in the medium concerned. At the surface of contact $x = 0$ there exists a total thermal flux $Q(1 - at)$, whilst at the other boundaries there is no flow of heat perpendicular to the planes. Initially the two bodies are at zero temperature.

The partial differential equations to be solved are

$$\frac{\partial^2 v_1}{\partial x^2} - \frac{1}{k_1}\frac{\partial v_1}{\partial t} = 0, \quad -l < x < 0, \quad t > 0 \tag{1}$$

$$\frac{\partial^2 v_2}{\partial x^2} - \frac{1}{k_2}\frac{\partial v_2}{\partial t} = 0, \quad d > x > 0, \quad t > 0 \tag{2}$$

subject to the boundary conditions.

$$\partial v_1/\partial x = 0 \quad \text{at} \quad x = -l; \quad \partial v_2/\partial x = 0 \quad \text{at} \quad x = d \tag{3}$$

$$v_1 = v_2 \quad \text{at} \quad x = 0 \quad t > 0 \tag{4}$$

$$K_2(\partial v_2/\partial x) = -Q_2(1 - at) \quad \text{at} \quad x = 0 \tag{5}$$

$$K_1(\partial v_1/\partial x) = Q_1(1 - at) \quad \text{at} \quad x = 0 \tag{6}$$

where $$Q = Q_1 + Q_2$$

Introducing the Laplace transform defined as

$$\bar{v} = \int_0^\infty \exp(-pt)v(x, t)dt \tag{7}$$

the subsidiary equations become

$$(d^2\bar{v}_1/dx^2) - q_1^2\bar{v}_1 = 0. \quad -l < x < 0 \tag{8}$$

$$(d^2\bar{v}_2/dx^2) - q_2^2\bar{v}_2 = 0. \quad d > x > 0 \tag{9}$$

where $$q_1^2 = p/k_1 \quad \text{and} \quad q_2^2 = p/k_2 \tag{10}$$

These have to be solved with

$$d\bar{v}_1/dx = 0 \quad \text{at} \quad x = -l \tag{11}$$

$$d\bar{v}_2/dx = 0 \quad \text{at} \quad x = d \tag{12}$$

and $\bar{v}_1 = \bar{v}_2$, $K_1\dfrac{d\bar{v}_1}{dx} = Q_1\left(\dfrac{1}{p} - \dfrac{a}{p^2}\right)$,

$$K_2\frac{d\bar{v}_2}{dx} = -Q_2\left(\frac{1}{p} - \frac{a}{p^2}\right), \quad \text{at} \quad x = 0 \tag{13}$$

where $$Q = Q_1 + Q_2$$

A solution of equation (8) which satisfies condition (11) is

$$\bar{v}_1 = [A\cosh q_1(l + x)]/\cosh q_1 l \tag{14}$$

and a solution of equation (9) which satisfies equation (12) is

$$\bar{v}_2 = [E\cosh q_2(d - x)]/\cosh q_2 d \tag{15}$$

The unknowns A and E are found from equation (13), and equations (14) and (15) then reduce to

$$\bar{v}_1 = \frac{k_1^{\frac{1}{2}}Q}{K_1}\left(\frac{1}{p^{3/2}} - \frac{a}{p^{5/2}}\right)\left[\frac{\cosh q_2 d\cosh q_1(l + x)}{\sinh q_1 l\cosh q_2 d + \sigma\sinh q_2 d\cosh q_1 l}\right] \tag{16}$$

$$\bar{v}_2 = \frac{k_1^{\frac{1}{2}}Q}{K_1}\left(\frac{1}{p^{3/2}} - \frac{a}{p^{5/2}}\right)\left[\frac{\cosh q_1 l \cosh q_2(d-x)}{\sinh q_1 l \cosh q_2 d + \sigma \sinh q_2 d \cosh q_1 l}\right] \quad (17)$$

where $$\sigma = \frac{K_2}{K_1}\left(\frac{k_1}{k_2}\right)^{\frac{1}{2}}$$

Applying the inversion theorem for the Laplace transformation[5] in the usual way to equations (16) and (17), one obtains

$$v_1 = \frac{Qk_1^{\frac{1}{2}}}{K_1(u+\sigma w)}\left(t\left(1-\frac{at}{2}\right) + \frac{1}{2}(1-at)(w^2+z^2) - \frac{a}{24}(w^4+6w^2z^2+z^4) - \frac{1}{120(u+\sigma w)}\right.$$
$$\left\{20[u^3+3uw(w+\sigma u)+\sigma w^3]\left[1-a\left(t+\frac{w^2+z^2}{2}\right)\right]\right.$$
$$\left.\left. - a[u^5+10u^2w^2(u+\sigma w)+5wu(w^3+\sigma u^3)+\sigma w^5]\right\}\right.$$
$$\left. - \frac{a}{36(u+\sigma w)^2}[u^3+3uw(w+\sigma u)+\sigma w^3]^2\right)$$
$$- \frac{2Qk_1^{\frac{1}{2}}}{K_1}\sum_{m=1}^{\infty}\left(\frac{1}{\beta_m^2}+\frac{a}{\beta_m^4}\right)$$
$$\times\left[\frac{\cos\beta_m w\cos\beta_m z}{(u+\sigma w)\cos\beta_m u\cos\beta_m w-(w+\sigma u)\sin\beta_m u\sin\beta_m w}\right]$$
$$\times\exp(-\beta_m^2 t) \quad (18)$$

and

$$v_2 = \frac{Qk_1^{\frac{1}{2}}}{K_1(u+\sigma w)}\left(t\left(1-\frac{at}{2}\right) + \frac{1}{2}(1-at)(u^2+y^2) - \right.$$
$$\left. - \frac{a}{24}(u^4+6u^2y^2+y^4) - \frac{1}{120(u+\sigma w)}\right.$$
$$\times\left\{20[u^3+3uw(w+\sigma u)+\sigma w^3]\left[1-a\left(t+\frac{u^2+y^2}{2}\right)\right]\right.$$
$$\left.\left. - a[u^5+10u^2w^2(u+\sigma w)+5wu(w^3+\sigma u^3)+\sigma w^5]\right\}\right.$$
$$\left. - \frac{a}{36(u+\sigma w)^2}[u^3+3uw(w+\sigma u)+\sigma w^3]^2\right)$$
$$- \frac{2Qk_1^{\frac{1}{2}}}{K_1}\sum_{m=1}^{\infty}\left(\frac{1}{\beta_m^2}+\frac{a}{\beta_m^4}\right)$$
$$\times\left[\frac{\cos\beta_m u/\cos\beta_m y}{(u+\sigma w)\cos\beta_m u\cos\beta_m w-(w+\sigma u)\sin\beta_m u\sin\beta_m w}\right]$$
$$\times\exp(-\beta_m^2 t) \quad (19)$$

where

$$u = l/k_1^{\frac{1}{2}} \quad w = d/k_2^{\frac{1}{2}} \quad z = (l+x)/k_1^{\frac{1}{2}} \quad y = (d-x)/k_2^{\frac{1}{2}} \quad (20)$$

and $\pm\beta_m$, $m = 1, 2, 3 \ldots$ are the roots of the equation

$$\cos\beta w\sin\beta u + \sigma\sin\beta w\cos\beta u = 0 \quad (21)$$

and these roots are real and simple.

Thus, if Q, a and the physical properties of the contacting bodies are known, the temperature rise at the interface (where $u = z$ and $w = y$) and inside either body may be determined from equations (18) and (19). These results may be compared with previous solutions[1–4] where the heat flow is assumed to be shared at the friction surface as if both media were infinite in thickness. In Fig. 1 curves are shown of the quantity $K_1 v/Qk_1^{\frac{1}{2}}$ at the friction surface, calculated from the exact solution for a 16 s brake application for brake linings with diffusivities of $k_2 = 3{\cdot}3 \times 10^{-3}$ cm²/s (conventional material) and $k_2 = 3{\cdot}3 \times 10^{-2}$ cm²/s (sintered material), together with values of $K_1 v/Qk_1^{\frac{1}{2}}$ determined from the equation

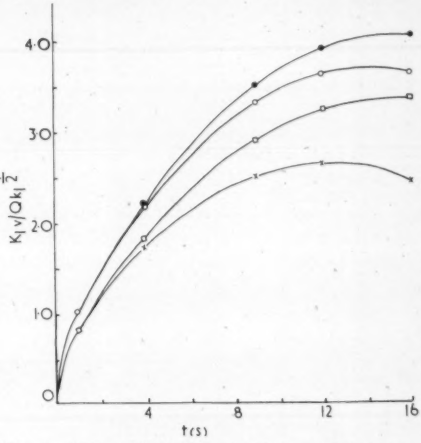

Fig. 1. Values of $K_1 v/Qk_1^{\frac{1}{2}}$ at the friction surface during 16 s brake application

○, ● = calculated from exact and previous solutions respectively for $k_2 = 3{\cdot}3 \times 10^{-3}$ cm²/s.
×, □ = $k_2 = 3{\cdot}3 \times 10^{-2}$ cm²/s.

$$\frac{K_1 v}{Qk_1^{\frac{1}{2}}} = \frac{1}{(1+\sigma)}\left[\frac{2t^{\frac{1}{2}}}{\pi^{\frac{1}{2}}}(1-\tfrac{3}{2}at) + 4t^{\frac{1}{2}}\sum_{n=1}^{\infty} i\,\mathrm{erf}\,c2n\lambda - 16at^{3/2}\sum_{n=1}^{\infty} i^3\,\mathrm{erf}\,c2n\lambda\right]$$

derived previously by the author.[4] These curves show that the exact solution may give surface braking temperatures of 10 to 30% (depending on the material used) lower than that based on previous assumptions for long brake applications.

APPLICATION OF THEORY

If a brake lining slides against a rotating drum with an initial surface speed r cm/s and produces a constant drum deceleration of f cm/s², then after t seconds of braking the instantaneous speed is $(r - ft)$ cm/s. Hence the instantaneous energy H generated at the friction surface is

$$H = \frac{Fr}{A_2 J}\left(1 - \frac{ft}{r}\right) = Q(1-at) \quad (22)$$

where A_2 = area of brake linings (cm²); F = tangential force acting at the friction surface (dyn); J = mechanical equivalent of heat, taken as $4{\cdot}18 \times 10^7$ erg/cal; $Q = Fr/A_2 J$; and $a = f/r$.

Thus for any brake application the quantities Q and a may be determined experimentally. In the brake of a typical automobile $d_1 = 0{\cdot}625$ cm, $K_1 = 0{\cdot}12$ cal cm^{-1} s^{-1} °C^{-1},

$k_1 = 0{\cdot}12$ cm^2/s and $d_2 = 0{\cdot}48$ cm, $K_2 = 1{\cdot}8 \times 10^{-3}$ cal cm^{-1} s^{-1} °C^{-1}, $k_2 = 3{\cdot}3 \times 10^{-3}$ cm^2/s. If the braking time T from an initial sliding surface speed of 1308 cm/s is 16 s the resulting value of Q is 105 cal cm^{-2} s^{-1}.

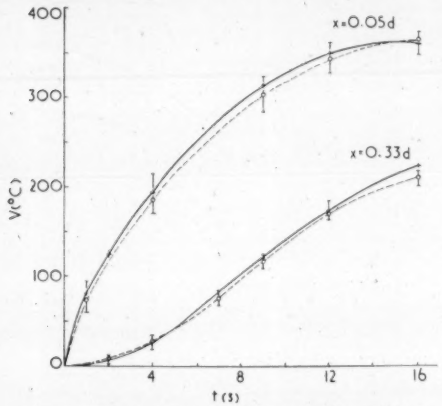

Fig. 2. Typical curves of transient temperature rise at different depths in a brake lining

× = calculated values. ○ = mean experimental values. The range of values is also shown.

Experimental verification of equation (19) has been made by measuring transient temperatures inside the linings at depths corresponding to $x = 0{\cdot}05d$ and $x = 0{\cdot}33d$ when the physical quantities involved are as stated previously. Temperature measurements during each application of the brake were made by fine gauge copper-constantan thermocouples, the outputs of which were fed into an amplifier and then to an Evershed and Vignoles recorder having a response of approximately $\frac{1}{16}$ s. The agreement between temperatures determined experimentally and theoretically from equation (19) at various times during the braking application are illustrated graphically in Fig. 2.

ACKNOWLEDGEMENTS

The author wishes to thank Dr. R. T. Spurr of the Research Division of Ferodo Ltd. for assistance and criticism, and the directors of Ferodo Ltd. for permission to publish this paper.

REFERENCES

(1) ODIER, J., and LEUTARD, P. *C.R. Acad. Sci.* (*Paris*), **244**, p. 1141 (1957).
(2) ODIER, J., and LEUTARD, P. *C.R. Acad. Sci.* (*Paris*), **244**, p. 1321 (1957).
(3) BANNISTER, F. K. *Engineering* (*London*), **183**, p. 304 (1957).
(4) NEWCOMB, T. P. *Brit. J. Appl. Phys.*, **9**, p. 370 (1958).
(5) CARSLAW, H. S., and JAEGER, J. C. *Conduction of Heat in Solids*, 1st Ed., p. 244 (Oxford: Clarendon Press, 1947).

Deposition of unipolar charged aerosol particles by mutual repulsion

By W. W. FOSTER, B.Sc., A.Inst.P., Ph.D.,* Torry Research Station, Aberdeen

[*Paper received* 10 *November*, 1958]

A simple theory of the deposition of unipolar charged aerosols by their mutual repulsion is developed. The application of this theory enables the average radius and the average charge of the particles to be determined from measurements of the mass of smoke deposited on metal surfaces and the charge given up by the particles. This new method offers a means of determining the rate of coagulation of unipolar charged aerosols. Experiments with wood smokes indicate that the simple theory of deposition is correct. The calculated average radius of the wood smoke particles examined compares favourably with that determined from measurement of the optical density and mass concentration of the smoke. The charge determined by the new method is consistent with that calculated on the basis of corona charging theory.

LIST OF SYMBOLS

a = radius of spherical aerosol particle
b = number of cylinders of length l in which charged particles are deposited
$\beta = (Fc_0/2\pi k_0\eta d)(n^2e^2/a^4)$
c, c_0 = mass concentration of aerosol at times t and $t = 0$ respectively
C = constant of integration in $V_m = \int Edr$
d = density of each aerosol particle
e = elementary charge
E = electric field strength
F = slip factor for correcting Stokes' drag
G = root mean square velocity of ions
i = current per unit length of corona electrode
I' = current due to deposition of charged particles inside cylinders
k = Boltzmann's constant
k_0 = dielectric constant of medium
l = length of individual cylinders in which charged particles are deposited
Λ = mobility of ions
M = rate of deposition of charged particles in a given length of cylinder
M_c = mass of particles deposited in charging unit in time t
n = number of elementary charges on a particle
n_d, n_f = number of elementary charges acquired by ion diffusion and field charging mechanisms respectively
N_0 = number concentration of ions
η = viscosity of medium
P = rate of deposition of particles in cylinder of length x
P_b = mass of charged particles deposited on b cylinders in time t
P_c = mass of particles entering charging unit in time t
r, r_0 = radial positions in cylinder

* Member of the staff of the Herring Industry Board.

R = radius of cylinder in which charged particles are deposited
ρ, ρ_0 = charge concentration of aerosol at times t and $t = 0$ respectively
ρ' = charge concentration in corona space due to ions and to charged particles
t = time
t_c = time for aerosol to pass from charging unit to centre of set of cylinders
t_u = time for aerosol to pass from smoke box to centre of charging unit
T = absolute temperature
v = velocity of particle relative to medium
V = velocity of medium carrying aerosol
V_m = potential difference between corona and outer electrodes of charging unit
W = rate of deposition of charged particles in a given length of cylinder
x = distance

INTRODUCTION

During investigations[1] of the mechanisms of the deposition of wood smoke on surfaces, a method was developed for increasing the rate of deposition by charging the particles with the same sign and allowing them to precipitate in their self-generated electric field. Although it is well known that unipolar charged aerosols disperse rapidly, it appears that very little theoretical work, tested experimentally, has been published. Wilson[2] derived equations for the deposition of a stationary charged cloud inside a tube, but these were not confirmed experimentally. Calculations have been given for the rate of deposition from a moving cloud on to a solid sphere under the influence of coulombic, induced and space charge forces[3] and on to plates,[4] these calculations being tested experimentally. The present study was therefore made in the absence of published work about deposition resulting purely from the mutual repulsion of charged particles in a moving cloud.

To test the theory developed it was convenient to use wood smoke, which contains homogeneous spherical tarry droplets formed during cooling of the products of the distillation and degradation of heated wood. Under the experimental conditions to be described the particles were apparently in equilibrium with the residual vapours and, after deposition, they did not evaporate appreciably before being weighed.

To simplify the analysis, it is assumed initially that wood smokes are monodisperse, the effects of polydispersity being discussed later.

THEORY OF SPACE CHARGE DEPOSITION

In an infinitely long cylindrical cloud of uniform mass concentration containing spherical particles of equal radius a, each supporting a like charge ne, the electric field strength at a point distant r_0 from the axis of the cloud is due only to charges within the cylinder of radius r_0. The force on each particle in the cloud is directed radially outwards and the cloud expands. When a particle moves from the radial position r_0 to a position r, the total charge affecting the movement of the particle is unchanged. By Gauss' theorem

$$2\pi r k_0 E = 4\pi \,.\, \pi r_0^2 \,.\, \rho_0$$

or

$$E = 2\pi r_0^2 \rho_0 / k_0 r \qquad (1)$$

where E is the field strength at r, ρ_0 is the initial space charge concentration and k_0 is the dielectric constant of the medium.

The force Ene on the particle at r is balanced by the drag due to the medium. If the radius a of the particles is of the order $0{\cdot}1\ \mu$, and the medium is air at about atmospheric pressure and room temperature, Stokes' law modified for slip may be assumed. Thus, the radial velocity of the particle is

$$dr/dt = r_0^2 Fne\rho_0 / 3k_0 a\eta r \qquad (2)$$

where F is the slip factor, $[1 + (0{\cdot}83 \times 10^{-5}/a)]$[5], and η is the viscosity of the medium.

Rearranging equation (2) and integrating

$$r = r_0\sqrt{(1 + \beta t)} \qquad (3)$$

where

$$\beta = 2ne\rho_0 F / 3k_0 a\eta$$

As the cloud expands the total charge between concentric cylinders of initial radii r_0 and $(r_0 + dr_0)$ remains constant, but the charge concentration decreases from ρ_0 to ρ. Thus using equation (3)

$$2\pi r_0 dr_0 \rho_0 = 2\pi r dr \rho = 2\pi r_0\sqrt{(1 + \beta t)} dr_0 \sqrt{(1 + \beta t)}\rho$$

Therefore

$$\rho = \rho_0/(1 + \beta t) \qquad (4)$$

Extending equation (2) to the general case and substituting

$$\frac{3ne}{4\pi a^3 d} \cdot \frac{c_0}{1 + \beta t} \text{ for } \rho,$$

$$\frac{dr}{dt} = \frac{rF}{4\pi k_0 \eta d} \cdot \frac{n^2 e^2}{a^4} \cdot \frac{c_0}{1 + \beta t} \qquad (5)$$

where d is the density of each particle and c_0 is the mass concentration of the aerosol at time $t = 0$.

Equations (1) to (5) are calculated for an infinite cylindrical cloud in a stationary medium, the concentration of the cloud being constant throughout the cylinder at any time. The equations are valid when the cloud is enclosed by a conducting cylinder of radius R when $r \leqslant R$. Assume now that the cloud is being carried along by the suspending medium inside the cylinder, and is being continually replenished at an arbitrary origin where $x = 0$ and the space charge concentration is ρ_0. As a result of the precipitation of particles on the walls of the cylinder the space charge concentration decreases downstream from the origin. This uneven distribution of charge results in the generation of axially directed components of electric field tending to accelerate the particles, thus making them move along the cylinder faster than the carrying medium. It would be difficult to calculate the radial field strength and the radial velocity of charged particles in such a system. It has therefore been assumed that if the velocity of the particles is not measurably different from that of the carrying medium, then the axially directed components of electric field may be neglected and the field can be considered to be entirely radial. The following equations are derived using this simplification.

Referring to Fig. 1, let the mass concentration at $x = 0$ and x be c_0 and c respectively and let V be the velocity of the medium along the cylinder. If the aerosol in the annular

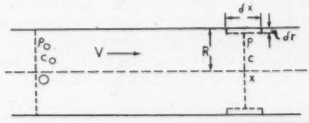

Fig. 1. Transverse section of cylindrical cloud of charged particles

volume $2\pi R\delta x\ \delta r$ is precipitated in time δt, the mass precipitated per unit area per unit time is $M = c(\delta r/\delta t)$.

In the limit $\delta r/\delta t = dr/dt$ and from equation (5)

$$M = \frac{cRF}{4\pi k_0 \eta d} \cdot \frac{n^2e^2}{a^4} \cdot \frac{c_0}{1+\beta t}$$

Now $t = x/V$ and $\beta = (c_0F/2\pi k_0\eta d) \cdot (n^2e^2/a^4)$

Therefore
$$M = \frac{\beta R c_0}{2[1+(\beta x/V)]^2} \quad (6)$$

P, the total mass precipitated per unit time between $x = 0$ and x is obtained by integrating $2\pi RMdx$

Thus
$$P = \frac{\pi R^2 c_0 \beta x}{1+(\beta x/V)} \quad (7)$$

or
$$x = \pi R^2 c_0 V(x/P) - (V/\beta) \quad (8)$$

Any particular length of the cylinder acquires a net charge on the outside only from deposited particles. If the cylinder is earthed and a mass W is precipitated per unit time on the length of cylinder, the current to earth is

$$I' = 3Wne/4\pi da^3 \quad (9)$$

APPARATUS

The general arrangement of the apparatus is shown in Fig. 2. The smoke generator consisted essentially of a vertical cylinder containing a horizontal grid supporting a bed of oak wood sawdust particles nearly midway along the cylinder.[6] Air was heated electrically in the section of the cylinder below the grid and passed through the bed of sawdust with sufficient velocity to keep the particles in a state of violent agitation. After losing weight by distillation and degradation at 314 ± 2° C, the spent sawdust was collected in a small cyclone separator. The amount of smoke being generated was maintained by supplying fresh sawdust to the bed at a controlled rate using a worm feed. Small centrifugal fans were used to direct air and smoke through the system. Rates of flow indicated by pressure drops across Venturi orifice plates were kept constant to within ±5% by controlling the fans and stopcocks. The smoke was passed through a box of capacity 50 l. in which the optical density was measured by a double-beam meter using unfiltered light from a tungsten lamp.[7, 8]

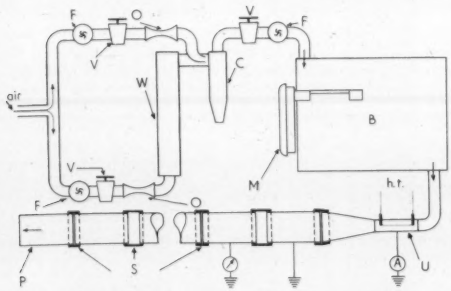

Fig. 2. Apparatus for generating wood smoke and depositing charged particles inside cylinders

A, ammeter; *B*, smoke box; *C*, cyclone; *F*, fan; *M*, smoke meter; *O*, Venturi orifice; *P*, precipitator; *S*, Sellotape; *U*, charging unit; *V*, valve; *W*, wood smoke generator.

After leaving the box, the wood smoke particles were charged—for subsequent deposition in the absence of an applied field—in a concentric cylinder corona field. To avoid errors in the measurement of corona current resulting from conduction through the deposits of smoke constituents on the insulators, the charging unit shown diagrammatically in Fig. 3 was designed. When smoke constituents were deposited on the insulators, the resulting current from the corona electrode passed directly to earth. In this way the true corona current from the wire was measured by the meter placed in the position shown. Stainless steel wires of various diameters were tested for suitability as corona electrodes. It was found that the accumulation of tar on very fine wires led to a fall-off in the corona current after smoking for only one hour. This effect was particularly marked when, in an attempt to obtain uniform field conditions in the manner suggested by Kraemer and Johnstone,[3] a 43 s.w.g. corona wire was used with an aluminium liner inserted into the charging tube in the position indicated in Fig. 3. The use of very fine wires was therefore discontinued in favour of 36 s.w.g. stainless steel wire, which was found to be satisfactory.

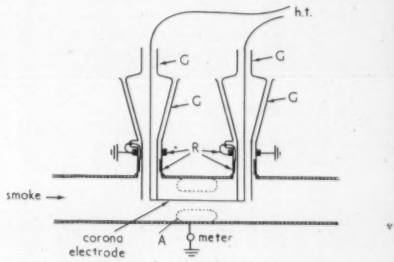

Fig. 3. Apparatus for charging smoke particles

A, aluminium liner (used in one experiment); *R*, earthed ring electrodes (to prevent tracking current from passing through meter); *G*, B14 Pyrex cones and sockets.

After being charged, the particles were dispersed inside a stainless steel tube consisting of short cylindrical sections joined by Sellotape (Fig. 2). For the purpose of testing the theory, cylinders of internal radii 0·685, 2·50 and 4·20 cm were used, the corresponding lengths being 12·4, 15·25 and 11·5 cm. The particles leaving the tube were deposited in a two-stage electrical precipitator. This precipitator consisted of an earthed tube of radius 4·2 cm about 70 cm long in which were supported axially a 36 s.w.g. charging wire about 10 cm long and an aluminium rod 1·27 cm in diameter and about 60 cm long, the wire and the rod being at a potential of about 10 kV. Where necessary, expansion or contraction pieces were placed in the train. The deposits on each portion of the whole train were weighed to an accuracy of ±0·5 mg.

To ensure uniform electric field conditions in any set of cylinders when this was necessary, cylinders of the same diameter and at least one diameter long were joined upstream and downstream of the set. Sets of cylinders were spaced about 1 cm apart, the gap being bridged by Sellotape (Fig. 2). The electrical resistance of this band of Sellotape was always greater than about $10^7\ \Omega$ even when the smoke deposit was heavy. The charge from deposited particles was passed

directly to earth or through a galvanometer of resistance 1800 Ω and current sensitivity 0·0145 μA/cm. All sections of the train from which the current was not being measured were earthed. When the current from more than one set of cylinders was being measured, it was passed either through the galvanometer or to earth by means of double-pole double-throw switches. Occasionally, stray corona points outside the charging and precipitation units caused leakage currents to earth from the cylinders, and this could be confused with that due to charged smoke. When necessary, this source of error was eliminated by shielding the cylinders with earthed aluminium foil encased in polythene sheeting.

The rate of flow of smoke through the train was too small for accurate measurement with a vane anemometer and too large for convenient measurement by aspiration. It was therefore determined indirectly in a few experiments from measurements of the total amount of smoke precipitated in the train P_t, and the mass concentration of the smoke, found by sampling at a slow, accurately known rate from a region between the smoke box and the train. Since in all other experiments the rate of flow of smoke through the train could be controlled, the mass concentration of the smoke in the box containing the optical density meter was calculated from the known volume of smoke passed through the train and the mass precipitated P_t.

EXPERIMENTAL

Deposition of charged wood smoke particles. If P_b is the mass of smoke particles deposited in time t on b cylinders each of length l, then from equation (8),

$$b = \pi R^2 c_0 V t(b/P_b) - (V/l\beta) \qquad (10)$$

Furthermore, according to equation (9), if the current to earth due to the deposition of a mass W per unit time (equal to P_b/t for b cylinders) is I'

$$I' = (3P_b/4\pi t d)\,(ne/a^3) \qquad (11)$$

Thus, by measuring the mass of smoke deposited on a number of consecutive cylinders and plotting b against b/P_b, the quantities $\pi R^2 c_0 V t$ and $V/l\beta$ can be found from the gradient of the line and the intercept of the line on either of the axes. The mass concentration, c_0, and β, can therefore be evaluated and $n^2e^2 \cdot F/a^4$ determined; ne/a^3 can also be found using equation (11). The average particle radius and charge can therefore be calculated from $n^2e^2 \cdot F/a^4$ and ne/a^3.

To determine whether the axially directed components of electric field inside tubes due to the charged particles made them move appreciably faster than their carrying medium, the transit times of both charged and uncharged smokes through a 300 cm long cylinder of radius 4·2 cm were measured. It was found that over a wide range of charging voltages the transit time was not affected by charging the particles. It was concluded that since the effect of the axial field was negligible, the simple theory developed above was valid.

It was found that in all experiments there was a linear relationship between b and b/P_b and typical plots are given in Fig. 4. The gradient of each line $\pi R^2 c_0 V t$ was usually slightly less than the total mass of smoke P_t deposited in the whole train, the overall average ratio $\pi R^2 c_0 V t/P_t$ for results presented here being 0·912.

For convenience, the experiments to be discussed are numbered serially in Table 1. The general experimental conditions described are the rate of flow, the optical density and the mass concentration c of the smoke; the magnitude and polarity of the voltage V_m applied to the corona electrode of the charging unit, and the corresponding current per unit length of corona electrode i; the ratio of the mass of smoke deposited in the charging unit M_c to the total mass of smoke which entered the charging unit P_c; the radius R of the tube in which charged smoke deposited; and the age of the smoke before and after charging, t_u and t_c respectively, the times in which smoke passed from the smoke box to the centre of

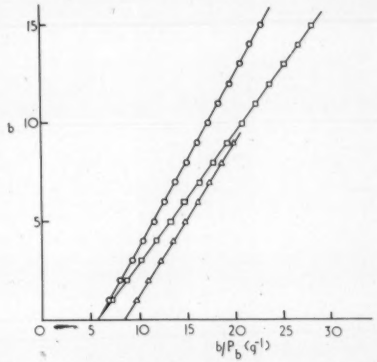

Fig. 4. Application of theory of deposition of charged particles to experimental results
○ = experiment 11 □ = experiment 12 △ = experiment 14

the charging unit and from there to the set of cylinders where measurements were being made. The ageing times t_u and t_c varied according to the radius and length of the tubes before and after charging, and on the rate of flow of the smoke. Table 1 also gives calculated values of particle radius a and number of elementary charges n. It appears from these tabulated results that the mass concentration c had decreased by about 2% when the age of the uncharged smoke was about 16 s. This was shown to be due to deposition of the uncharged smoke particles inside the cylinder before the smoke reached the charging unit. Since the change in c could be accounted for in this way, there appeared to be no marked tendency for particles to grow by condensation or to evaporate. This stability of wood smoke makes it a particularly useful material for studying the deposition of charged particles.

A number of experiments were conducted to determine the effects of various parameters on the calculated particle radius a and number of elementary charges n, and these are described below.

Definition of V, velocity of smoke along cylinder. (*Experiments* 1, 2 *and* 3.) To calculate a and n using the above theory it was necessary to know the effective velocity V for different flow conditions. Cylinders of three radii, 0·685, 2·50 and 4·20 cm, were used, the conditions being turbulent in the cylinder of radius 0·685 cm and generally laminar in the cylinder of radius 4·20 cm. In each experiment, charged smoke was passed through a set of cylinders of small radius first and then through a set of large radius. In experiment 1, expansions of the smoke were effected slowly to reduce aerodynamic instability, the included angle of the expansion pieces being just less than 10°. In experiments 2 and 3, turbulence was promoted at the inlet of the cylinder of smallest radius by an abrupt change of radius from 1·27 to 0·685 cm. To induce steady flow conditions in the large

Table 1. *Details of experiments using charged wood smoke particles, with calculated values of particle radius and number of elementary charges*

Identification number of experiment	Flow rate (l./s)	Mass concentration (mg/l.)	Optical density*	Corona conditions† Voltage, V_m (kV)	Current, i (μA/cm)	$\frac{M_c}{P_c}$	R (cm)	Age of smoke t_u (s)	Age of smoke t_c (s)	Particle radius (μ)	Number of elementary charges, n
1*a*	1·40	0·271	0·21	+6·98	3·16	0·178	2·50	0·94	0·78	0·103	19·3
1*b*							4·20		3·93	0·099	16·0
2*a*	1·15	0·254	0·20	+6·15	1·21	0·116	0·685	1·14	0·70	0·110	19·1
2*b*							4·20		2·39	0·110	17·0
3*a*	1·15	0·243	0·20	+6·23	1·21	0·131	0·685	1·14	0·70	0·102	15·2
3*b*							4·20		2·39	0·088	8·7
4*a*	0·75	0·256	0·20	+6·20	0·95	0·212	2·50	16·4	1·66	0·141	30·8
4*b*	0·75	0·245	0·20	+6·20	1·35	0·195	2·50	16·2	1·66	0·141	31·9
5*a*	0·75	0·273	0·20	+6·16	1·34	0·220	2·50	2·16	1·66	0·118	23·8
5*b*	0·75	0·263	0·20	+6·16	1·18	0·221	2·50	2·16	1·66	0·118	24·5
6*a*	0·75	0·254	0·20	+6·18	1·53	0·234	2·50	16·4	1·66	0·144	24·5
6*b*	0·75	0·263	0·20	+6·18	1·15	0·209	2·50	2·16	1·66	0·098	14·0
7	1·40	0·253	0·21	+6·15	1·53	0·124	2·50	3·38	0·78	0·116	21·1
8	1·40	0·251	0·20	+6·17	1·22	0·088	2·50	3·38	0·78	0·122	22·6
9	1·15	0·269	0·20	+6·18	1·27	0·141	0·685	1·14	0·21	0·118	23·1
10	1·40	0·286	0·21	+5·70	0·39	0·059	2·50	0·94	0·57	0·106	11·6
11	1·40	0·276	0·21	+6·20	1·38	0·109	2·50	0·94	0·57	0·093	11·6
12	1·40	0·282	0·21	+7·20	4·23	0·207	2·50	0·94	0·57	0·090	14·1
13	1·40	0·260	0·21	+8·71	12·2	0·339	2·50	0·94	0·57	0·098	23·9
14†	1·15	0·266	0·21	+3·68	1·58	0·037	2·50	1·14	0·70	0·089	8·2
15	1·23	0·269	0·19	−6·00	0·34	0·073	2·50	1·07	1·61	0·075	4·6
16	1·23	0·284	0·21	−6·00	0·38	0·091	2·50	1·10	0·65	0·102	12·3
17	1·40	0·260	0·20	−6·69	1·80	0·199	2·50	0·94	0·57	0·100	21·4
18	1·40	0·260	0·20	−7·74	9·67	0·457	2·50	0·94	0·57	0·089	27·9

* Length of light path in optical density meter = 30·5 cm.

† In all experiments except number 14, the radius of the outer electrode was 1·27 cm and the radius and length of the inner electrode were 0·0096 and 6·0 cm respectively. The corresponding conditions in experiment 14 were 0·47, 0·0044 and, approximately, 3·0 cm.

diameter tube, the included angle of the expansion piece between the tubes of radii 0·685 and 4·20 cm was about 7°. In the absence of wood smoke, the aerodynamic conditions in the tubes were examined, using a 20 s.w.g. wire probe coated with fuming titanium tetrachloride. The fumes were observed by means of glass tubes which were substituted for some of the metal tubes. It was found that in the tube of radius 4·20 cm the fumes flowed in wavy filaments indicating that the conditions were generally laminar; the fumes in the tube of radius 2·50 cm mixed in the air stream and there was less tendency for filament formation; in the tube of radius 0·685 cm the fumes mixed completely throughout the tube, there being no filamenting, and conditions were clearly turbulent. Experiments 1, 2 and 3 listed in Table 1 showed that, for each consecutive pair of cylindrical sections, the calculated values of particle radius and charge agree fairly well when V is assumed to be equal to the total flow rate divided by the cross-sectional area of the cylinder. This definition was therefore used in all subsequent calculations.

Reproducibility in duplication of experimental conditions. (*Experiments* 4 *and* 5.) In these experiments a common stream of smoke was divided into two equal streams, as indicated by equal pressure drops across identical Venturi orifice plates in each stream. The particles in each stream were then charged in identical charging units and precipitated in tubes of equal radius. The results of these experiments show that there is good agreement between pairs of concurrent determinations of a and n, and suggest that the errors are small in the measured values of the mass of smoke precipitated and the charge relinquished on deposition.

Effect of polarity and rate of charging on particle radius. (*Experiments* 1*a*, 2*a*, 3*a and* 9–18.) The polarity and magnitude of the voltage applied to the corona electrode were varied to determine whether, for wood smoke, these factors had any effect on the average particle radius calculated from the results of precipitation inside cylinders. Results obtained with smokes of about the same age before and after charging are compared, so that possible effects due to coagulation which might have arisen in separate experiments can be ignored.

The fraction of the total entrant aerosol which was precipitated in the charging unit M_c/P_c is presented in Table 1, since this fraction is dependent on the charging rate. Although this fraction varied from 0·037 to 0·339 for positive corona and from 0·073 to 0·457 for negative corona, there was apparently no tendency for the average radius of the emergent aerosol to vary with M_c/P_c. The overall average radius for positively charged particles was about 10% more than that for negatively charged particles. It would seem from these results that there was no marked tendency for wood smoke particles of any particular size to be preferentially precipitated during charging, whatever the sign of the charge.

Effect on particle radius of ageing before and after charging. It was shown above that neither the polarity nor the rate of charging appear to have any substantial effect on the average particle radius. Irrespective of the charging conditions, therefore, the values of particle radius calculated from results of experiments in which t_u varied from 0·94 to 16·4 s may be compared. It can be seen from Table 1 that, although there is considerable scatter in the results, the particle radius

appears to increase as t_u increases and that this increase is quite marked when t_u is about 16 s.

In determining the effect of t_c on the particle radius, smokes having about the same t_u value were examined, the particle radius being determined in a number of consecutive sets of cylinders. A range of charging conditions were used in these experiments, as indicated in Fig. 5. Although there seems to be no systematic relationship between the rate of charging and the change of particle radius with t_c, there appears to be an overall tendency for the particle radius to increase as the charged smoke ages.

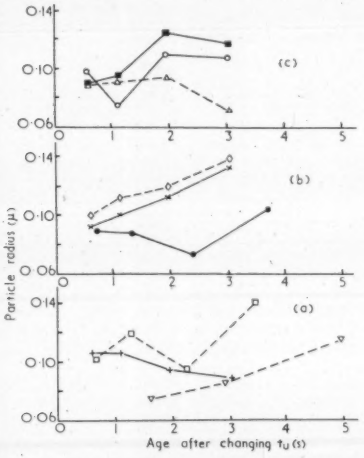

Fig. 5. Effect of ageing on average radius of charged wood smokes

– – – – = negative corona. ——— = positive corona.
(*a*) Low charging rates; (*b*) medium charging rates; (*c*) high charging rates.

Symbol	Corona conditions V_m (kV)	i (μA/cm)
○	+8·71	12·2
■	+7·2	4·23
△	−7·74	9·67
●	+6·2	1·38
×	+3·68	1·58
◇	−6·69	1·18
+	+5·7	0·39
⊡	−6·0	0·38
▽	−6·0	0·34

DISCUSSION

Applying experimental results to equation (10) it has been shown that there is a linear relationship between b and b/P_b, and that the gradient of this line ($\pi R^2 c_0 V t$) is usually about 10% less than P_t, the actual mass of particles entering the corresponding set of cylinders. These two facts offer strong support for the theory presented. The value of the average particle radius a and number of elementary charges n will now be compared with those obtained by other methods of calculation.

Particle radius from the Lambert–Beer relationship. According to the results of other experiments[8] there appears to be a linear relationship between the optical density and the mass concentration of wood smoke generated by burning sawdust. Using values of the refractive and absorption indexes of such wood smoke particles, it was shown theoretically that the Lambert–Beer law should be valid over the range of optical densities and mass concentrations encountered in practice. On this basis, a method was given for calculating the average particle radius from the optical density per unit mass concentration. For the smokes listed in Table 1 the optical density and mass concentration are well within the range in which the Lambert–Beer law is valid. Furthermore, the refractive index of wood smoke particles generated at a constant temperature, as in the present experiments, agrees very well with that for particles obtained by burning sawdust; and the absorption indexes of the two types of smoke are about equal.[1, 8] In determining the overall average radius the results of experiments 1*a*, 2*a*, 3*a* and 9–18 were used, since in these experiments t_u was about 1 s and the effects which might have arisen from differences in t_u could be ignored. The overall average optical density per unit mass concentration for these experiments was $76{\cdot}4 \times 10^4$ l/mg and the corresponding average particle radius was found to be $0{\cdot}173\ \mu$. According to Table 1 the overall average radius of these smokes is $0{\cdot}038\ \mu$. It is considered that this general agreement is fairly satisfactory, in view of the fact that different methods of averaging are implicit in the two ways of determining the particle radius.

Calculation of the charge on wood smoke particles. The following calculations were made to determine whether the charges obtained on the basis of results of the deposition of charged smokes inside cylinders were consistent with those to be expected on the basis of the theory of corona charging.

The rate of charging of a particle in the space between a corona electrode and a coaxial outer electrode decreases with increasing time, since the approaching ions are repelled by the acquired charge. The rate of charging is eventually negligible.[9] Theoretical descriptions have been given of the mechanisms of the charging of a spherical particle at infinite dilution. Two processes occur: field charging, in which ions are forced on to the particle under the influence of the applied electric field; and diffusion charging, in which ions share the thermal energy of the gas molecules and the particle is charged by the absorption of ions.

The specific resistance of wood smoke particles is about $5 \times 10^6\ \Omega$ cm.[1] The time constant of an asymmetrically charged cube of this material is of the order of a microsecond. To a first approximation, the time constant of a spherical wood smoke particle would also be of the order of a microsecond. This time is negligible in relation to the total time during which a particle is in the corona field (approximately 10^{-2} s) so that wood smoke particles may be regarded as perfect conductors during charging. For such a spherical conducting particle of radius a in an electric field of strength E containing ions of concentration $N_0 e$ and mobility Λ, the number n_f of elementary charges e acquired in time t during field charging is[10]

$$n_f = \frac{3Ea^2}{e} \cdot \frac{t}{t + (1/\pi N_0 e \Lambda)} \qquad (12)$$

The following equation[9] has been used to calculate the number n_d of elementary charges acquired during diffusion charging. Thus

$$n_d = \frac{akT}{e^2} ln\left(1 + \frac{\pi a G N_0 e^2 t}{kT}\right) \qquad (13)$$

where k is Boltzmann's constant, G is the root mean square velocity of ions and T is the absolute temperature.

Equations (12) and (13) apply when the charging processes are separate, but no solution appears to have been given in the literature for the case when both processes occur simultaneously. Kraemer and Johnstone[3] assumed that n_f and n_d are additive and obtained very good agreement with experimentally determined values of charge. The same assumption was therefore made in the present work.

To calculate n_f and n_d, N_0e and E must be known. At a point distant r from the axis of a concentric cylinder corona system[10]

$$N_0e = (i/2\pi r)\,(1/\Lambda E) \tag{14}$$

where i is the corona current per unit length of corona electrode. The value of E may be found by solving Poisson's equation

$$(dE/dr) + (E/r) - 4\pi\rho' = 0 \tag{15}$$

where the space charge concentration at any point is

ρ' = charge concentration due to ions plus charge concentration due to particles

$$= N_0e + ne(3c/4\pi a^3 d) \tag{16}$$

where ne is the charge on each particle and c is the mass concentration. The effect of ρ' is to alter the normal electric field distribution, reducing E near to the corona electrode and increasing it near to the outer electrode.

When $n = 0$[10]

$$E = \sqrt{[(2i/\Lambda) + (C^2/r^2)]} \tag{17}$$

where C is obtained by equating the applied voltage V_m with $\int E dr$. When the corona current is large, C^2/r^2 may be neglected and

$$E = \sqrt{(2i/\Lambda)} \tag{18}$$

Equation (15) has been solved[11] for the case in which space charge due to ions is supplemented by that due to large particles, field charging being predominant and complete, i.e. $n = 3Ea^2/e$. Such a space charge can considerably distort the normal distribution of E. It has been shown[12] that in typical industrial conditions, for instance, E may be three to four times greater than $\sqrt{(2i/\Lambda)}$ over most of the inter-electrode space.

As the particle radius decreases the diffusion charging mechanism eventually predominates. Since there is no simple formula for n_d, no attempt was made to solve equation (15) and to calculate the variation of E with r. It should be noted, however, that for a constant value of c, the effects of particle space charge on the distribution of E become more pronounced as a decreases, since the space charge concentration is approximately proportional to $1/a$ in field charging and to $1/a^2$ in diffusion charging, the space charge concentration per unit mass concentration thus increasing as the particle radius decreases.

The effect of various assumed electric field distributions on $n_f + n_d$ was determined for particles of radius 0·08, 0·10 and 0·15 μ, since these values appear to straddle the range of particle size for wood smokes (Table 1). The charging conditions, assumed similar to those in experiments 2–9 and 11 were: radius of earthed electrode, 1·27 cm; radius of corona electrode, 0·0096 cm; length of corona electrode, 6·0 cm; positive potential of corona electrode, 6·2 kV; corona current, 7·20 μA (1·20 μA/cm); time in charging zone, 0·03 s. It was found[1] that the ratio of the charge acquired at $r = 0{\cdot}1$ cm to that acquired at $r = 1{\cdot}27$ cm is about 3 : 1 when equation (17) is assumed, and about 1·5 : 1 when equation (18) is assumed. Furthermore, about 85% of the particles in the field assumed to vary with r [equation (17)] have a charge which is within about +25% and −5% of that found by assuming $E = \sqrt{(2i/\Lambda)}$ at a position $r = 0{\cdot}9$ cm, corresponding to the radius of the cylindrical shell which divides the inter-electrode volume into two equal parts. In calculating $n_f + n_d$ for particles charged under conditions listed in Table 1 therefore, the approximation was made that the average charge corresponds to that for a particle at $r = 0{\cdot}9$ cm in a field of strength $\sqrt{(2i/\Lambda)}$.

Values of $n_f + n_d$ were calculated for particles charged under known corona conditions (Table 1), assuming the values of particle radius determined from results of measurements of deposition inside cylinders. As can be seen from Fig. 6 the agreement between n and $n_f + n_d$ is fairly good

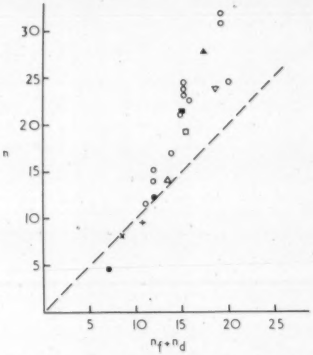

Fig. 6. Charge on wood smoke particles calculated from theories of deposition inside cylinders (n) and of corona charging ($n_f + n_d$)

	Corona conditions		
Symbol	V_m (kV)	i (μA/cm)	*Experiment*
×	+3·7	1·58	14
+	+5·7	0·39	10
○	+6·2	1·20	2*a*, 3*a*, 4–9, 11
□	+6·98	3·16	1*a*
△	+7·2	4·23	12
▽	+8·71	12·2	13
•	−6·0	0·36	15, 16
■	−6·69	1·80	17
▲	−7·74	9·67	18

except at the higher values of n. It is possible that this discrepancy arises from an underestimation of the value of the electric field strength during charging. The effect on $n_f + n_d$ of assuming a greater average field strength than $\sqrt{(2i/\Lambda)}$ was therefore investigated. It was found[1] that for experiments in which the corona wire was at a positive potential of about 6·2 kV, the agreement between n and $n_f + n_d$ is better when, in equations (12), (13) and (14), it is assumed that $E = 4\sqrt{(2i/\Lambda)}$ instead of $\sqrt{(2i/\Lambda)}$. Thus, it would seem that these results accord with other theoretical findings,[11] which indicate that the field strength throughout most of the space in a concentric cylinder corona system may be three to four times greater than $\sqrt{(2i/\Lambda)}$.

The velocity of charged particles in externally applied and self-generated electric fields. To determine whether the average radius of polydisperse aerosols might be expected to vary with time in applied and self-generated electric fields, the velocities of particles during and after charging were calculated. The velocity v of a spherical particle of radius a and charge $(n_f + n_d)e$ in a field of strength E was calculated for low, medium and high charging rates, similar to those

Table 2. *Velocity of charged particles in a concentric cylinder corona system*

Radius of outer electrode = 1·27 cm Radius of inner electrode = 0·0096 cm Length of inner electrode = 6·0 cm

Particle radius (μ)	Velocity (cm/s) Low charging rate: $V_m = 5{\cdot}7$ kV; $i = 0{\cdot}38$ μ A/cm			Medium charging rate: $V_m = 6{\cdot}2$ kV; $i = 1{\cdot}20$ μ A/cm			High charging rate: $V_m = 8{\cdot}7$ kV; $i = 12{\cdot}2$ μ A/cm	
	$E = \sqrt{(2i/\Lambda)}$	$E = 2\sqrt{(2i/\Lambda)}$	$E = 4\sqrt{(2i/\Lambda)}$	$E = \sqrt{(2i/\Lambda)}$	$E = 2\sqrt{(2i/\Lambda)}$	$E = 4\sqrt{(2i/\Lambda)}$	$E = \sqrt{(2i/\Lambda)}$	$E = 2\sqrt{(2i/\Lambda)}$
0·05	0·685	1·25	2·36	1·46	2·87	6·09	7·22	16·6
0·08	0·606	1·16	2·31	1·30	2·71	6·19	6·74	17·0
0·10	0·583	1·14	2·37	1·26	2·71	6·41	6·75	17·6
0·15	0·565	1·16	2·55	1·24	2·83	7·15	7·12	19·9
0·20	0·566	1·21	2·77	1·27	3·03	8·00	7·69	22·5

obtaining in the experiments described above, using the following equation:

$$v = \frac{Ee}{6\pi\eta} \cdot \frac{(n_f + n_d)F}{a} \qquad (19)$$

Since it appeared that the average field strength might be much greater than $\sqrt{(2i/\Lambda)}$, the velocities were determined for multiples of this value, as indicated in Table 2. The columns in Table 2 referring to low and medium charging rates show that, as the particle radius increases from 0·05 to 0·20 μ, v decreases by about 20% for the lowest assumed value of E and increases by about 20% for the highest assumed value of E. For the high charging rate the velocity varies only slightly with radius for the lowest assumed value of E but increases markedly with increasing radius when twice this value of E is assumed. Similar results, not quoted here, were found for negative corona conditions.

In the experiments described above there appears to be no dependence of the average particle radius on the charging rate. From this observation and the above theoretical considerations it would seem that for low and medium charging rates the electric field strength is probably about $2\sqrt{(2i/\Lambda)}$ and for high charging rates is nearer to $\sqrt{(2i/\Lambda)}$.

The radial velocity of any particle of radius a and charge $(n_f + n_d)e$ in a polydisperse cloud of particles of space charge concentration ρ is, from equation (2), $\frac{r\rho e}{3k_0\eta} \cdot \frac{(n_f + n_d)F}{a}$. Apart from a difference in magnitude, for any given cloud this velocity varies with particle radius in exactly the same way as that for particles in an externally applied electric field [equation (19)]. It follows that since there appears to be no marked tendency for particles of different sizes to move at different velocities in the charging unit, it is likely that there should be no tendency on this account for the average radius of charged smoke particles to change as the smoke passes along the cylinder. The observed general tendency for the average radius to increase as t_c increases might therefore be due to coagulation of the charged smoke particles. This result accords with theoretical discussions[13, 14] which show that coagulation due to Brownian movement can never be prevented by the mutual repulsion of charged particles, except when each particle has an infinite charge. The measurement of the rate of coagulation of charged aerosols is difficult, chiefly because the particles disperse rapidly on to containing walls. Although the results presented here and the subsequent argument cannot be considered to be conclusive, it would seem that this method of determining the average radius of charged aerosols might be useful when studying their coagulation, especially when applied to aerosols initially monodisperse or of known size distribution.

CONCLUSIONS

A theory of the deposition of charged aerosols by their mutual repulsion inside a cylinder is verified experimentally. The average radius and charge on the particles is then calculated; the average radius is about 70% less than that calculated from the Lambert–Beer relationship for the aerosols; the average particle charges agree fairly well with those calculated from corona charging theory, except at high values of charge. It is possible that the latter discrepancy might arise from an underestimation of the average field strength during charging.

Experimental results appear to indicate that the average radius of charged particles increases as the aerosol ages. According to other experimental results and calculations based on theory, this effect might be due to coagulation of the particles, rather than to selective deposition of particles of different sizes.

ACKNOWLEDGEMENTS

The work described was carried out at Torry Research Station of the Department of Scientific and Industrial Research by staff of the Herring Industry Board as a part of the programmes of the Board and the Department. The author is indebted to Dr. A. C. Jason for advice in the course of this work. Miss M. Cole assisted with the experimental work. Crown copyright is reserved.

REFERENCES

(1) Foster, W. W. Ph.D. Thesis (University of Aberdeen, 1957).
(2) Wilson, I. B. *J. Colloid Sci.*, **2**, p. 271 (1947).
(3) Kraemer, H. F., and Johnstone, H. F. *Industr. Engng Chem.* (Industr.), **47**, p. 2426 (1955).
(4) Splinter, W. E. Ph.D. Thesis (Michigan State University, 1955).
(5) Davies, C. N. *Proc. Phys. Soc.* (*London*), **57**, p. 259 (1945).
(6) Nicol, D. L. Brit. Pat. No. 781 591 (September 1954); *Dep. Sci. Industr. Res., London, Food Investig. Bd. Rep.*, p. 41 (1954), p. 31 (1955).
(7) Jason, A. C. *Process Control and Automation*, **3**, p. 61 (1956).
(8) Foster, W. W. *Brit. J. Appl. Phys.* To be published.
(9) White, H. J. *Trans Amer. Inst. Elect. Engrs*, **70**, p. 1186 (1951).
(10) Pauthenier, M., and Moreau-Hanot, M. *J. Phys. Radium*, **3** (7), p. 590 (1932).
(11) Pauthenier, M., and Moreau-Hanot, M. *J. Phys. Radium*, **6** (7), p. 257 (1935).
(12) Lowe, H. J., and Lucas, D. H. *Static Electrification, Brit. J. Appl. Phys.*, **4**, Suppl. 2, p. S40 (1953).
(13) Whytlaw-Gray, R., and Patterson, H. S. *Smoke: a study of aerial disperse systems* (London: Edward Arnold and Co., 1932).
(14) Gillespie, T. *Proc. Roy. Soc., A*, **216**, p. 569 (1953).

Viscous properties of thixotropic materials

By D. G. Osborne, B.Sc., Ph.D., A.Inst.P.,* and S. Thornton, B.Sc., Ph.D., F.Inst.P.,† Department of Physics, Durham Colleges in the University of Durham

[*Paper first received* 10 *November*, 1958, *and in final form* 9 *January*, 1959]

Measurements have been made on the viscous properties of thixotropic suspensions of titanium dioxide pigments in linseed stand oils. The effects of changes in concentration and temperature have been noted. The viscosity under steady flow conditions cannot be adequately defined by a single coefficient but it is convenient to display the results graphically, plotting shear stress against velocity gradient. It is shown that the shear stress required to maintain any steady velocity gradient has two components, one being independent of temperature and the other proportional to the viscosity of the medium as this changes with temperature.

The samples studied took some time to attain steady conditions of flow and the approach to this state, the "thixotropic relaxation", occurs in a very complicated way. Two qualitative conclusions could be drawn: that the magnitude and speed of thixotropic change decreased with increasing values of shear stress, and that the magnitude and speed of thixotropic change (at the same shear stress) increased with increasing concentration.

For liquids where viscosity varies with velocity gradient, practical difficulties arise in making absolute determinations of viscosity, because normal viscometers impose a range of shear stresses on the liquid. Thornton[1] gave a theory for calculating the shear stress and the corresponding velocity gradient at one location in a suitable viscometer. Working one instrument under different conditions enables a set of such values to be calculated. Thornton and Rae[2] used this method to study anomalous flow, analysing readings made with a Poiseuille tube and a concentric cylinder viscometer. The agreement between the two sets of results confirms the usefulness of the method in assessing the properties of an anomalous fluid independently of the measuring instrument. The fluids used by Thornton and Rae were instantaneously thixotropic, that is of the type where a change in the shear stress produces an immediate change in the velocity gradient (apart from a slight inertia effect).

The present paper describes an extension of this work to the more general case of normally thixotropic fluids. These change their flow properties slowly, "thickening" or "thinning" gradually when a different shear stress is applied and only reaching a sensibly steady state of flow after a period of time. Such changes in flow properties are reversible. To describe these properties fully it is necessary to give the relation between shear stress and velocity gradient when steady conditions obtain and also to express, in some way, the time dependence of flow during build-up and breakdown. In theory the procedure is simple; in practice, especially in the latter investigation, the experimental difficulties are great.

The investigation required samples with a high degree of reproducibility of viscous flow behaviour over long periods to allow for the considerable time taken to get a full set of readings. As the anomaly, or departure from normal Newtonian flow, was the factor to be investigated, this had to be pronounced, though in practice too great a variation in the viscosity made accurate viscometry impossible. At this stage the aim was to measure thixotropy and anomalous flow, and not to find the viscous properties of any fluid which might be called thixotropic; hence the samples were prepared and selected with care and only those showing the phenomena sought were studied in detail. Suspensions of chemically inert pigments in comparatively unreactive oil media proved most promising in meeting these difficult requirements, and with experience it was possible to obtain suspensions which showed negligible irreversible ageing effects during the course of the experiments. Ageing, detected as an irreversible change in the steady-state viscosity over a period of time, was found to occur in all the samples prepared. The rate of change decreased rapidly in the first few weeks after milling and specimens stored for several months before use in the viscometer gave reproducible results, ageing effects then being less than the experimental error. The suspensions were stored at 25° C and most of the experiments conducted at the same temperature. The suitability of a sample for detailed study could not be determined before it had been aged and this made the process of selection somewhat lengthy. Difficulties due to sedimentation of the pigment were overcome by working in the concentration range where sedimentation was negligible during the period of investigation.

With such materials it was possible to perform fairly accurate measurements on the viscous properties under steady flow conditions, but the extended investigation into the time dependence of the flow during build-up or breakdown of structure was not so accurate. For this purpose the anomaly, or change in flow properties between two steady conditions of flow, had to be large and the relaxation times neither too short for accurate measurements to be made nor too long for ageing effects to be troublesome. These are very stringent conditions indeed, and it was found necessary to test many samples whilst seeking one suitable for this work. None of the samples produced permitted a very accurate study of thixotropic relaxation to be made, but the results give a qualitative description of thixotropic behaviour, indicating the factors which influence the magnitude and speed of thixotropic change and which may, therefore, facilitate the choice of materials for a more quantitative study.

Apparatus and Method of Tests

The viscometer used was of the concentric cylinder type and was essentially that described by Thornton and Rae.[2] In most of the experiments it was used as a constant torque apparatus and the torque, which was measured by the angular deflexion of a suspension wire carrying the inner cylinder, was held constant by a servo-mechanism which controlled the speed of rotation of the outer cylinder, or "cup." The servo-mechanism was actuated by a beam of light reflected from a mirror attached to the base of the suspension wire; the setting of the mirror decided the torque applied. In practice it was found convenient to have several mirrors which could be pre-set so that the torque applied

* Now at University College of Ghana, Achimota, Ghana.
† Now at UNESCO Technical Assistance Mission to Liberia, Monrovia, Liberia.

could be maintained at one of several selected values and changed to another value as required. A self-recording apparatus facilitated measurement of the speed of rotation of the outer cylinder, an electronic pen recorder being used so that an immediately visible trace was obtained.

In the instrument used the observed variables are the speed of rotation of the outer cylinder W, and the corresponding values of the applied couple C. The couple acting determines the shear stress f_a at the boundary of an inner cylinder of radius a, the relation being

$$f_a = C/(2\pi a^2 L) \qquad (1)$$

where L is the effective depth of immersion in the specimen. Subsidiary experiments, using different depths of immersion, allowed an end correction to be measured. This was found to be equivalent to an increase in the depth of immersion and independent of the speed of rotation. Examination of the surface during rotation showed that any "Weissenberg effect" was too small to be detected.

Thornton[1] derived an expression for the viscosity of the fluid adjacent to the inner cylinder if the outer cup was of infinite radius, and showed how this could be modified by a series of approximations for the experimental condition of a finite sized cup. The rate of shear strain, or velocity gradient, can be calculated directly in a similar way, and this is outlined in the Appendix. If the radii of the inner and outer cylinders are a and b, the difference between the velocity gradients at each (g_a and g_b) is given by

$$g_a - g_b = 2C(dW/dC) \qquad (2)$$

As before, C is the couple acting and W the angular velocity of the cup, the inner cylinder being stationary. The value of g_b could only be determined approximately, as indicated in the Appendix, but the magnitude of g_b was usually no more than 2% of g_a in the experiments considered.

Thus values for the velocity gradient g_a and the shear stress f_a in steady flow are obtained. For convenience the suffices will now be omitted. The ratio f/g is the viscosity. Data were obtained at different temperatures and pigment concentrations.

The experiments from which the steady-flow values of f and g were calculated were also used for the investigation of flow time-dependence (i.e. thixotropic relaxation). The speed of rotation of the outer cylinder was allowed to reach a steady value for a constant applied torque; the torque was then changed to a new value. The speed of rotation of the outer cylinder necessary to maintain this new torque relaxed gradually with time and this relaxation was observed. This experiment was repeated for different initial torques C, changing each time to a new torque in the same ratio to the first, kC, where k was kept constant and C differed for each experiment. Taking the speed W after a selected time t from the start of relaxation in each experiment, graphs were plotted of speed against torque just as in the analysis for steady flow. These graphs showed values of cylinder speed W under an imposed torque kC, at a time t after changing from an initial steady flow condition under an imposed torque C. The torque acting gave the shear stress at the inner cylinder as before, and the slope of the curves of W against kC gave values for the velocity gradient g_a at the time t. Series of these curves permitted the drawing of further curves showing how the velocity gradient relaxed with time under a given shear stress after a defined pre-history. This flow time-dependence was studied for different ratios k under a range of shear stresses and for different concentrations.

EXPERIMENTAL RESULTS

From the many different thixotropic samples prepared and tested, eleven have proved satisfactory from the point of view of reproducibility of viscous behaviour. With these at least forty curves relating shear stress to velocity gradient have been obtained for steady flow conditions and all follow a common pattern. In the case of the temperature dependence studies, three separate sets of experiments were performed and all were in agreement. The effect of concentration was given a detailed investigation in only one case, using a particular pigment (rutile titanium dioxide, mean particle diameter about 0·25 μ) in a particular linseed stand oil, but these results may be taken as reliable since they involved replication from three-fold to ten-fold for the different concentrations used. Moreover, it is clear from less accurate experiments on other suspensions that their viscous properties vary with concentration in substantially the same way as the one described.

It was found that the steady cylinder speed, at a given torque, was independent of the previous flow history of the sample. Thus the material relaxed eventually to the same viscous state regardless of whether it had previously been in a "thicker" or "thinner" condition. This was found true for all the samples tested.

To facilitate concise presentation the experimental results are considered under two headings, and typical examples have been chosen from the samples tested to illustrate the observed properties.

The effect of temperature and concentration on steady flow. Typical curves showing the relation between steady-flow values of shear stress and velocity gradient are given in Figs. 1 and 2. The values are in c.g.s. units; velocity

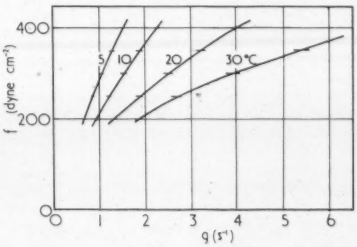

Fig. 1. Shear stress as function of velocity gradient for steady flow at different temperatures: 30% rutile titanium dioxide in linseed oil

gradient g as s^{-1}, and shear stress f as dyn cm^{-2}. Temperature is expressed in degrees Centigrade and concentration as percentage of solid by volume. Fig. 1 shows the effect of temperature changes. At any shear stress the viscosity is the ratio of shear stress to velocity gradient, and it is clear from the figure that the viscosity at any one shear stress decreases with increasing temperature, as would be expected. The sample used had a 30% concentration by volume of 0·25 μ rutile titanium dioxide pigment in a specially prepared linseed stand oil of viscosity 5·0 P at 25° C. This specimen had been stored at a constant temperature of 25° C for five months after milling to allow it to reach a stable condition, and by the time the experiments were performed the ageing effects, attributed to chemical reaction between the pigment and the medium, had become so small that irreversible viscosity

changes were within the limits of uncertainty associated with the method of measurement. Fig. 2 shows a similar set of curves for differing concentration, the viscosity increasing with increasing concentration. The pigment and oil used were similar to those for the studies on temperature dependence. Care was taken to ensure that each sample had aged to a stable condition before measurements were taken.

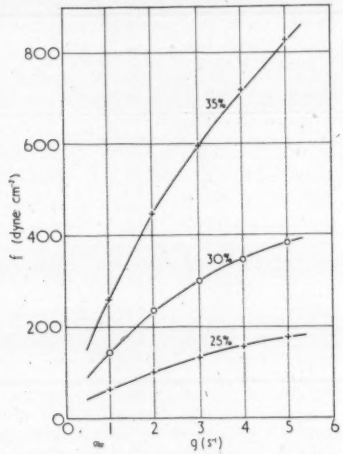

Fig. 2. Shear stress as function of velocity gradient for steady flow at different concentrations: rutile titanium oxide in linseed oil at 25° C

The accuracy of these curves was checked both by testing their reproducibility and by estimating the effect of likely errors in measuring the quantities from which stress and velocity gradient were calculated. The significant errors lay in controlling the couple by the deflexion of the suspended inner cylinder (error up to one degree of deflexion due to a dead-space, introduced to minimize "hunting," in the controlling device) and in measuring the speed of rotation of the outer cylinder (computed error up to 2·5% due to variations in the tachometer output, accuracy limits of the pen recorder and temperature fluctuations within the sample of up to 0·2° C). It was necessary to evaluate the tangents to the curves of angular velocity W plotted against torque C, and to estimate the error in these. From the estimated uncertainties in the values of W and C the probable error in the slope of a chord joining two consecutive readings was calculated, providing an upper bound for the error in the slope of the curve. These errors are undoubtedly greater than the errors actually resulting from the measured slopes of tangents to the smoothed curve, which were obtained with an optical device of relatively high accuracy, but they are given as a guide to the accuracy of those measurements. In presenting the results the magnitude of the abscissae in Fig. 1 represents the probable errors calculated in this way, together with an allowance for slight inaccuracy in determining the apparatus constants. The effects of ageing, random external vibration and slight eccentricity of the inner cylinder with respect to the outer were independently examined and found to be negligible.

The effect of thixotropic relaxation on viscous flow. To study these properties the suspensions were given the prescribed treatment whereby the speed of the outer cylinder rotation was allowed to relax to a steady value at a constant couple kC after it had initially been steady at a couple C. The values of k first chosen were 0·5 and its reciprocal 2·0, to facilitate the investigation of both build-up and breakdown between the same limits. It was later found more convenient to work with k (and k^{-1}) as 0·64 or 0·8. On imposing a k-fold increase in the torque the subsequent variation in angular velocity of the outer cylinder could be followed, indicating a progressive "thinning" of the specimen after a sudden increase of torque. The corresponding variation in the velocity gradient at the inner cylinder, which is shown in Fig. 3, is in the same sense but much smaller. This behaviour was typical of many specimens and will be discussed later.

Fig. 3 shows typical curves of velocity gradient against time (in minutes) at constant shear stress for the 30% volume

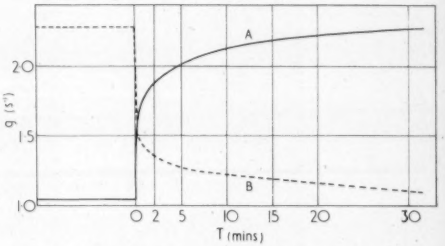

Fig. 3. Relaxation of velocity gradient under constant shear stress. (The horizontal line before the origin of the time axis represents steady flow before imposing a change of stress)

concentration of rutile titanium dioxide in a linseed stand oil (viscosity 5 P) at 25° C with k equal to 0·8 and 1·25. The curve A is for a change in shear stress from 262 to 327 dyn cm^{-2} with the material thinning in consequence; the velocity gradient increases to maintain the increased value of stress. Curve B shows the velocity gradient decreasing as the material thickens after reducing the shear stress from 327 back to 262 dyn cm^{-2}.

DISCUSSION OF RESULTS

The change in the steady-flow properties with temperature may be caused by changes in the viscosity of the medium and by changes in the magnitude of inter-particle forces. There will also be an effect due to the change in concentration (on heating, the liquid medium expands more than the pigment), but on calculation this effect is found to be very small.

The temperature variation of the medium viscosity n was measured so that the shear stress necessary to maintain a given velocity gradient in the sample could be compared with the viscosity of the medium as it changed with temperature. Fig. 4 shows the relationship, each set of points representing the shear stress required to maintain the velocity gradient indicated by the number beside them. Some difficulty was found in maintaining a uniformly low temperature throughout the sample and the values for the lowest temperature (the highest medium viscosity) are only approximate. Over the

range of temperatures from 5 to 30° C (viscosity range of medium 15 to 3·4 P) the relationship between stress and medium viscosity is approximately linear. The equation to any line in Fig. 4 may be written as

$$f = f_0 + An \qquad (3)$$

where the values of f_0 and A depend on the velocity gradient. It is convenient to express A as the product ag and Fig. 5 shows that f_0 and a both approach constant values at high velocity gradients. At these high velocity gradients, with f_0

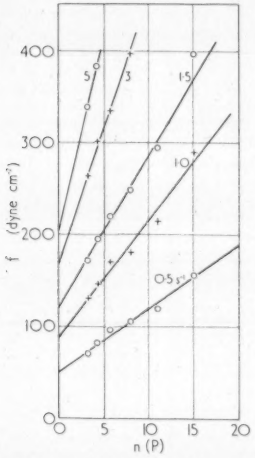

Fig. 4. Shear stress f at constant velocity gradient and different temperatures expressed as a function of medium viscosity n

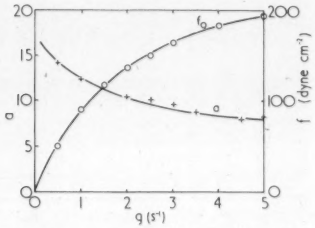

Fig. 5. Variation in parameters f_0 and a with velocity gradient

and a constant, equation (3) is identical with that suggested by Bingham and others for false-bodied materials and by Goodeve[3] for thixotropic materials under steady-flow conditions. Over the whole range of velocity gradients *ang* represents a resistance to flow proportional to the viscosity of the medium and f_0 represents a resistance to flow independent of the medium viscosity. Fig. 6 shows the separate contributions of the two terms (to the total shear stress at differing velocity gradients) for this sample at 25° C. Fig. 7 shows the results of applying a similar analysis to the results given by Rae[5] for the temperature dependence of the flow properties of an instantaneously thixotropic (false-bodied) material.

The term f_0 is independent of medium viscosity and must be attributed to the properties of the particles suspended in the medium rather than the medium itself. Its change in value with velocity gradient suggests changes in the structure of the system. The value of f_0 does not depend on temperature and Goodeve,[3] Goodeve and Whitfield[4] and Rae[5] have already suggested that the effect of inter-particle forces is sensibly independent of temperature.

The component *ang* of the shear stress is proportional to the viscosity of the medium. This is similar to the ordinary Newtonian flow which might be expected in a suspension of

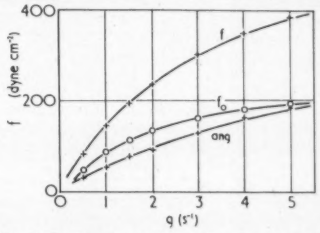

Fig. 6. Components of shear stress for normally thixotropic fluid

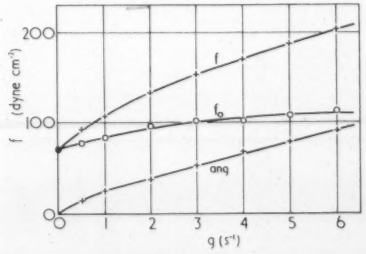

Fig. 7. Components of shear stress for instantaneously thixotropic fluid

non-interacting particles. The resistance to liquid flow will depend on the viscosity of the liquid and on the structure (e.g. amount of liquid immobilized by flocculates) of the system. The variation of a with velocity gradient, like that of f_0, could be explained by a breakdown of structure at high shear stresses. The indication is that under steady-flow conditions the shear stress, at all values of the velocity gradient, is given by the sum of two components: one required to overcome the hydrodynamic resistance to flow presented by the particles (in the state of flocculation in which they exist at that velocity gradient) and another due to inter-particle or inter-flocculate attraction.

The results for thixotropic relaxation were more qualitative in character. Several experiments showed, on calculation, rather small changes in the velocity gradient of the fluid adjacent to the inner cylinder, even when the relaxation of cylinder speed at constant torque was quite large. This demands greater changes in velocity gradient to have occurred in regions of the cup away from the inner cylinder and in these regions the shear stress, both before and during the

relaxation period, would be less than near the surface of the inner cylinder. Thus thixotropic relaxation is more pronounced at low values of shear stress, a result in accord with the steady-flow observation that only small changes of structure occur between states at high shear rates and stresses. Curves of velocity gradient against time were obtained for differing values of shear stress but with the same ratio between final and initial values k, showing that steady conditions were approached more rapidly at lower values of shear stress. The presence, after a change of shear stress, of an instantaneous change in the velocity gradient followed by a relaxation of uncertain form made it impossible to define a single relaxation time.

It is only possible to compare the thixotropic properties of different substances when it is recognized that these properties depend on the shear stress under which relaxation occurs. For systems of differing concentration it was found that the magnitude and speed of thixotropic change (at the same shear stress) increased with increasing concentration of pigment. For the familiar false-bodied (instantaneously thixotropic) materials studied by Thornton and Rae[2] the change is large and instantaneous; for the limit of zero concentration (when the medium behaves as a Newtonian fluid) the thixotropic change may be considered of zero magnitude and infinite slowness. The normally thixotropic suspensions considered in this paper are intermediate between these two extremes, and provide a general type of flow behaviour with the others as limiting cases.

CONCLUSION

The results given and discussed show that the method of measurement used enables the flow properties of thixotropic fluids to be studied. The general equation

$$f = f_0 + ang \tag{4}$$

where f_0 and a are parameters depending on g, describes the steady flow and its temperature variation. This one equation represents the steady flow properties of normally thixotropic and instantaneously thixotropic (false-bodied) materials, and it reduces to cover Newtonian fluids as a special case.

Time-dependent properties were found to be very complex and only qualitative conclusions could be drawn. These are:

(i) the magnitude and speed of thixotropic change decreased with increasing values of shear stress for all the suspensions studied;

(ii) the magnitude and speed of thixotropic change (at the same shear stress) increased with increasing concentration.

These factors must determine the selection of suitable materials for further study.

ACKNOWLEDGEMENTS

The work described was done in the Department of Physics of the Durham Colleges in the University of Durham and we wish to express our thanks to Prof. J. E. P. Wagstaff and Prof. G. D. Rochester for the facilities there placed at our disposal: also to the British Titan Products Co. Ltd. and Lewis Berger Ltd. for samples of materials, and especially to the Department of Scientific and Industrial Research for a Research studentship held by one of us (D. G. O.).

REFERENCES

(1) THORNTON, S. *Proc. Phys. Soc.* (*London*) *B*, **66**, p. 115 (1953).

(2) THORNTON, S., and RAE, D. *Proc. Phys. Soc.* (*London*) *B*, **66**, p. 120 (1953).

(3) GOODEVE, C. F. *Trans Faraday Soc.*, **35**, p. 342 (1939).

(4) GOODEVE, C. F., and WHITFIELD, G. W. *Trans. Faraday Soc.*, **34**, p. 511 (1938).

(5) RAE, D. Ph.D. Thesis (University of Durham, 1952).

APPENDIX

Measurement of velocity gradient using a concentric cylinder viscometer

The theory of measurement follows that of Thornton,[1] but it is adapted to permit immediate calculation of the velocity gradient rather than the viscosity.

Let the torque acting be C and the angular velocity of the outer cylinder be W, the inner cylinder of the viscometer being at rest. Let a and b denote the radii of the inner and outer cylinders, and f and g the shear stress and velocity gradient in a cylindrical element of fluid between the radii r and $r + \delta r$. The difference in velocity across this element is $g \,.\, \delta r$ and hence the difference in angular velocity is given by

$$\delta W = g \,.\, \delta r/r \tag{5}$$

The angular velocity across all the elements between radii a and b is that between the two viscometer cylinders

$$W = \int_0^W dW = \int_{r=a}^{r=b} (g/r) \,.\, dr \tag{6}$$

The shear stress at the boundary of the inner cylinder is given in the text; at the boundary of a cylinder of radius r it is given by

$$f = C/(2\pi r^2 L) \tag{7}$$

where L is the effective depth of immersion. Differentiating equation (7) with respect to r and substituting in equation (6), we get

$$W = \int_{f_b}^{f_a} (g/2f) \,.\, df \tag{8}$$

The relationship between f and g is unknown, but equation (8) states that the observable angular velocity W is given by the area under the curve of $(g/2f)$ against f between the limits of f_b and f_a.

If the instrument is now run at a new torque $C + \delta C$ instead of C the limits of f_b and f_a will change. The change in area under the curve due to this change in limits gives the difference in angular velocity between the two experiments [this is called δW but must not be confused with the same expression in equation (5), which refers to changes in angular velocity between different parts of the viscometer and not between experiments conducted under different torques]. Hence we have

$$\delta W = (g_a/2f_a) \,.\, \delta f_a - (g_b/2f_b) \,.\, \delta f_b \tag{9}$$

Differentiating equation (7) with respect to C for any constant value of r we have that

$$(\delta f/f)_r = \delta C/C \tag{10}$$

Taking values for r of a and b and substituting in equation (9) we find

$$\delta W = (g_a - g_b)\,(\delta C/2C)$$

which may be rearranged to

$$g_a - g_b = 2C(dW/dC)$$

which is quoted in the text of the paper [equation (2)].

Figs. 8, 9 and 10 illustrate this analysis, Fig. 10 showing how a change in torque changes the area representing the angular velocity between the cylinders.

The velocity gradient at the outer cylinder

Equation (2) gives a value for $(g_a - g_b)$. If the viscometer were of infinite radius, f_b, and hence g_b, would be zero. For an ordinary viscometer it is desirable to calculate the value of g_b so that g_a may be found.

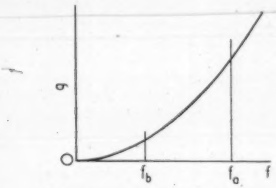

Fig. 8. Hypothetical curve of stress against velocity gradient

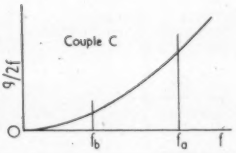

Fig. 9. Curve for function $(g/2f)$ against f

From equation (7) the shear stresses at the inner and outer cylinders are in the ratio

$$f_a/f_b = b^2/a^2 \qquad (11)$$

and if b is considerably greater than a it follows that g_b must be considerably less than g_a.

Using the equations for f_a and $(g_a - g_b)$, a graph relating experimental values for these two quantities may be plotted. In the apparatus used the value of (b^2/a^2) was ten, so that f_b was one-tenth of f_a. The value of g_b for any given value of f_a would be g_a at a stress $f_a/10$; it is therefore given to a first approximation by the value of $(g_a - g_b)$ at $f_a/10$.

The method is then one of successive approximation, but in a typical case the first correction would be less than 2% of the value of $(g_a - g_b)$. A second approximation gives a correction about 2% of the first correction, that is, only 0·04% of the total, and is not required. Considerable percentage errors in estimating g_b would have only a small effect on the accuracy of g_a. A first correction was made for all curves relating shear stress and velocity gradient.

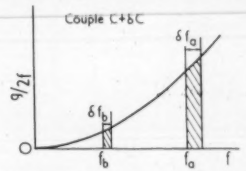

Fig. 10. Change in limits of f_a and f_b due to change in couple δC, with consequent change in area under curve

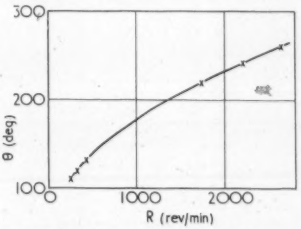

Fig. 11. Typical curve showing deflexion of inner cylinder (deg) against speed of motor driving outer cylinder (rev/min). Tangents to such curves enable velocity gradients to be calculated

Amplitude corrections for vibroscope measurements

By IAN M. STUART, M.Sc., Physics and Engineering Unit, Wool Textile Research Laboratories, Commonwealth Scientific and Industrial Research Organization, Ryde, N.S.W., Australia

[*Paper received* 19 *June*, 1958]

The dependence on amplitude of the fundamental resonant frequency for the free vibration of a string is derived for the two systems of mounting used in vibroscope measurements. It is found that in both systems a correction term of order $\frac{1}{e}\left(\frac{A}{l}\right)^2$ applies, where A is the amplitude, l the gauge length, and e a number we call the incremental strain. As this strain e is usually small (of the order 1% from most textile testing), the correction term can be important at apparently low amplitudes.

INTRODUCTION

In the vibroscope technique[1, 2] a natural mode of transverse vibration of a length of string under tension is excited, and the relationship

$$\omega = (n)\frac{\pi}{l}\sqrt{\frac{T}{\rho}} \qquad (1)$$

between the angular frequency of the vibration ω, the gauge length l, the tension T, the linear density of the string ρ and the order of the mode n, is used, usually to determine the linear density.

Equation (1) is derived by applying the condition that two points distant l apart on the string are restrained to be fixed in the plane of the vibration.

Two systems are commonly used to apply a tension to the string and restrain ends separated by a known distance. In one, which we call system 1 (see Fig. 1) the string is fixed at F and held over a peg at P by the tension in the string caused

by the weight of a mass M attached at W to the string. The angle θ must be chosen to be large enough to allow the tension to hold the string firmly onto the peg at P, and small enough to ensure that the tension in the gauge length is sufficiently determined. For small amplitudes the friction at P prevents longitudinal movement, and the string has both

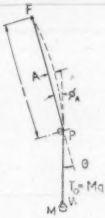

Fig. 1. String held taut over peg by weight hanging outside gauge length

θ, change of direction of string at P; A, amplitude of vibration; ϕ_A, inclination of string PF at P when amplitude is A.

ends fixed longitudinally and transversely. It is common practice to take the tension in the gauge length as that outside, that is, as $T_0 = Mg$.

In the second arrangement, which we call system 2 (see Fig. 2), the string is fixed at F and is attached at W to a mass M which hangs freely, being attached to the end of the string. Here the string is fixed both longitudinally and transversely at F, but the conditions at W are obscure, as

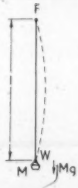

Fig. 2. String held taught by weight hanging freely

the mass can move both transversely and longitudinally. It is common practice to consider the string fixed here transversely (which we show later to be a reasonable assumption) and to take the tension in the string as the weight of the mass.

In the following sections we discuss the mechanics of these systems with regard to the part played by amplitude, both in determining the operating conditions of systems 1 and 2 and in causing the resonant frequency to change from that predicted by equation (1).

DISCUSSION OF SYSTEM 1

The relationship (1) for the frequencies of the natural modes of the transverse vibration of the string is usually derived by applying conditions of no transverse displacement y at points $x = 0$ and $x = l$, in the equation of transverse waves in the string,

$$\rho \frac{\partial^2 y}{\partial t^2} = T \frac{\partial^2 y}{\partial x^2} \tag{2}$$

It is generally conceded that equation (1) applies (apart from stiffness, damping, irregularity effects) only if the amplitude is small. This is because the approximations used in deriving the expression on the right-hand side of (2), which is the negative of the restoring force per unit length of string at position x on the string, are valid only for small angles of inclination of the string to the longitudinal axis.

Writing in an order term for the part neglected when (2) is derived, we can obtain the equation

$$\text{Restoring force per unit length at position } x \text{ on the string} = -T \frac{\partial^2 y}{\partial x^2}\left[1 + 0\left(\frac{A}{l}\right)^2\right] \tag{3}$$

However, if the ends of the string are fixed, so that to bow the string must increase in tension, the application of equation (1) with the tension given by the equilibrium tension, say T_0, is much more severely restricted than to the range of amplitudes for which we can neglect the order term in (3). If δl is the increase in length due to bowing, then neglecting terms of order $0(A/l)^2$, (to which order variations in tension along the string occur), the tension in the string is given by

$$T = T_0\left(1 + \frac{1}{e}\frac{\delta l}{l_0}\right) \tag{4}$$

where

$$e = \frac{T_0}{l_0}\frac{dl}{dT} \tag{5}$$

We assume the string is elastic, and has a variation of load with length given by $T = T(l)$ (Fig. 3). Then the value of e when the initial tension and length are T_0, l_0 is given by

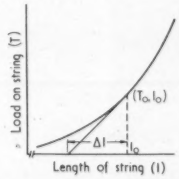

Fig. 3. Determination of incremental strain

$T = T(l)$-load-length curve of string subtangent at $T_0 = \Delta l = T_0\left(\frac{dl}{dT}\right)_{T=T_0}$. $e = \Delta l/l_0$.

the ratio of the subtangent to the $T = T(l)$ curve at the point (T_0, l_0), to the length l_0. When the string obeys Hooke's Law this curve becomes a straight line and e becomes the strain referred to the stretched length.

The incremental Young's modulus is $\frac{T_0}{A} \cdot \frac{1}{e}$, where A is the area of the section. So we call e the incremental strain.

The fundamental solution of equation (2) with boundary conditions $y = 0$ at $x = 0, l$, can be written in the form

$$y = A \sin \frac{\pi x}{l} \cos \omega t$$

where A is the amplitude of the vibration, and ω its angular frequency. If we assume that the displacement has this form, with the angular frequency ω as yet undetermined, then $\frac{\delta l}{l} = \frac{1}{4}\left(\frac{\pi A}{l}\right)^2 \cos^2 \omega t +$ higher order terms; and, neglecting the higher order terms, we see from equation (4) that

$$T = T_0\left[1 + \frac{1}{e}\frac{1}{8}\left(\frac{\pi A}{l}\right)^2 + \frac{1}{e} \cdot \frac{1}{8}\left(\frac{\pi A}{l}\right)^2 \cos 2\omega t\right] \tag{6}$$

Thus, the variation in the tension is in two forms, each of order $0\left(\frac{1}{e}\frac{A^2}{l^2}\right)$. There is an increase in the tension averaged over the cycle by an amount $T_0 \cdot \frac{1}{8e} \cdot \left(\frac{\pi A}{l}\right)^2$, and imposed

on this new average tension, an oscillatory tension of amplitude $T_0 \cdot \frac{1}{8e}\left(\frac{\pi A}{l}\right)^2$ of frequency twice that of the transverse motion, and in phase with the bowing, so that peaks in the tension occur at the positions of extreme bowing.

Consideration of the motion of the string at resonance reveals the reason for the increase in resonant frequency caused by each of these changes in the tension. From a position of zero kinetic energy at extreme bowing the string is accelerated by the restoring forces back towards the central position. This restoring force decreases as the central position is approached until it is zero in the central position, where the kinetic energy is a maximum, and the momentum of the string carries it out against the increasing restoring force on the other side. An increase in average tension raises the level of the restoring forces (which are proportional to tension [see equation (3)], and thus the string will be accelerated more rapidly back to the central position, and retarded more rapidly as the string bows out, thus raising the resonant frequency. This is a simple effect, and the change in resonant frequency can be calculated by equation (1).

$$\omega_{\Delta T} = \frac{\pi}{l}\sqrt{\left(\frac{T+\Delta T}{\rho}\right)}$$

So, for $\frac{\Delta T}{T}$ small,

$$\omega_{\Delta T} = \omega_0\left(1 + \frac{1}{2}\frac{\Delta T}{T}\right)$$

$$= \omega_0\left[1 + \frac{1}{16}\cdot\frac{1}{e}\cdot\left(\frac{\pi A}{l}\right)^2\right] \qquad (7)$$

where $$\omega_0 = \frac{\pi}{l}\sqrt{\frac{T_0}{\rho}}$$

The oscillatory tension causes the tension to be greater than its average value at the position of extreme bowing, where the restoring force is greatest and most effective in accelerating or retarding the string, and to be less than its average value when the restoring force is near zero near the central position. Thus it also must cause an increase in the resonant frequency, and it can be shown that the increase in resonant frequency per unit amplitude of tension oscillation in phase with the bowing is one-half the increase in resonant frequency per unit increase in average tension. Adding this effect to equation (7) we obtain

$$\omega = \omega_0\left[1 + \frac{3}{32}\cdot\frac{1}{e}\left(\frac{\pi A}{l}\right)^2\right] \qquad (8)$$

Application to system 1. Equation (8) applies to a string with both ends fixed longitudinally and transversely. Further, the tension to be used in computing ω_0 must be known. In system 1 the end F is fixed in the required manner but the string is held at P longitudinally by the frictional force round the peg, and transversely by the transverse component of the tension in the string. Both of these fixings may break down. Further, because of the friction round the peg, the tension in the gauge length has a degree of indeterminacy, until we make some other specification.

Transverse fixing. Referring to Fig. 1, it can be seen that the string will be held transversely at B and bouncing be prevented if the angle ϕ made by the string with the longitudinal axis at extreme bowing on the unwinding side is less than the angle θ. For y the transverse displacement given by

$$y = A \sin\frac{\pi x}{l}\cos\omega t$$

this angle $$\phi = \frac{A\pi}{l}$$

Hence, if the amplitude at which $\phi = \theta$ and bouncing commences is called A_B we have

$$A_B = \frac{l\theta}{\pi} \qquad (10)$$

So, for amplitudes less than A_B, no bouncing should occur at P.

Longitudinal fixing and tension determination. The tension T_i in the gauge length in the initial quiescent state is indeterminate to the extent that it lies in the range

$$T_0 e^{-\mu\theta} \leqslant T_i \leqslant T_0 e^{\mu\theta}$$

where $T_0 = Mg$, the weight of the mass, which is the tension outside the gauge length, and μ is the coefficient of friction between string and peg. If $\mu\theta$ is small, then $e^{\pm\mu\theta}$ can be approximated by $1 \pm \mu\theta$, and we have

$$T_0(1-\mu\theta) < T < T_0(1+\mu\theta) \qquad (11)$$

Further, by equation (6) the maximum tension in the string with fixed ends vibrating at amplitude A is:

$$T = T_0\left[1 + \frac{1}{4e}\left(\frac{\pi A}{l}\right)^2\right]$$

So, if the tension initially is $T_i = T(1+\Delta)$, where $|\Delta| < \mu\theta$, then the string can vibrate at amplitudes up to A_Δ without the tension rising above $T_0(1+\mu\theta)$, and thus causing slipping, where

$$T_0(1+\mu\theta) = T_0(1+\Delta)\left[1 + \frac{1}{4e}\left(\frac{\pi A_\Delta}{l}\right)^2\right]$$

or $$A_\Delta^2 = 4e(\mu\theta - \Delta)(l/\pi)^2 \qquad (12)$$

where we assume that the angle made by the string to its axis at the ends is small compared with θ.

If the amplitude increases above A_Δ then slipping must occur, allowing more string to be drawn in to the gauge length, and subsequently a lower tension in the central position. If the increase in amplitude over A_Δ is small enough, then on the next bowing (or half cycle) from the central position, the tension will not exceed $T_0(1+\mu\theta)$, and the string will vibrate at this new amplitude with fixed ends. The amplitude can be increased until a critical condition is reached when the central position tension is $T_0(1-\mu\theta)$, and the extreme bowing tension is $T_0(1+\mu\theta)$, corresponding to $\Delta = -\mu\theta$. The critical amplitude corresponding to this condition which is the maximum amplitude at which the string can vibrate with ends fixed longitudinally, or with no slipping, is given by

$$A_c^2 = 8e\mu\theta(l/\pi)^2 \qquad (13)$$

Once this critical condition is reached the initial tension is determinate at $T_0(1-\mu\theta)$, and calculations of ω_0 and e can be based on this tension. Thus, assuming that the condition of having enough string in the gauge length for the equilibrium tension to be $T_0(1-\mu\theta)$, the resonant frequency is given by

$$\omega = \omega_0\left[1 + \frac{3}{32}\cdot\frac{1}{e}\cdot\left(\frac{\pi A}{l}\right)^2 - \frac{1}{2}\mu\theta\right] \qquad (14)$$

where $$\omega_0 = \frac{\pi}{l}\sqrt{\frac{T}{\rho}}$$

Note.—(1) This condition can be achieved by vibrating the string at amplitudes in excess of A_c or more simply by allowing the tension outside to pull the string in the gauge length taut. The maximum difference in frequencies observable within the critical range is

$$\omega_{max} - \omega_{min} = \tfrac{1}{4}\mu\theta\omega_0 \qquad (15)$$

(2) In any future reference to system 1 mounting it will be implied that the above condition has been achieved.

DISCUSSION OF SYSTEM 2

This discussion hinges on the relative magnitudes of the frequency of the tension oscillations 2ω, and of the frequency of the natural mode of oscillation of the mass on the end of the elastic string ω_L, the latter being given by

$$\omega_L^2 = g/el \qquad (16)$$

The mass is supported by the longitudinal component of the tension in the string, which, differing from the tension in the string by $0(A/l)^2$, we take as equal to the tension in the string. As the mass executes an oscillation about a fixed mean position, the average longitudinal force on it is zero, so the average tension in the string equals the weight of the mass. There is an oscillatory tension superposed on this average tension, and this tension can be regarded as causing the longitudinal oscillation of the mass.

Now, the theory indicates that if 2ω is greater than ω_L the mass moves down as the string bows out and moves up as the string approaches its central position. Thus the tension in the string is a maximum at extreme bowing to provide a restoring force to accelerate the mass upwards, and is a minimum at the central position when the weight of the mass exceeds the string tension and the mass is accelerated downwards. Thus, the tension variation is so timed to increase the resonant frequency. The amplitude of the tension oscillation depends on the amplitude of the mass motion, and this increases as 2ω approaches ω_L. When 2ω is less than ω_L, the mass moves upwards as the string bows out; this shows the phase of the mass motion to have changed through 180° when the condition of complete coupling, or resonance at $2\omega = \omega_L$, is passed. The tension oscillation must now be such that the tension is a minimum at extreme bowing and a maximum at the central position, and thus the resonant frequency must decrease with increasing amplitude. The amplitude of the tension oscillation again increases as the condition $2\omega = \omega_L$ is approached.

The resonant frequency is given by the equation

$$\omega = \omega_L\left\{1 + \frac{1}{32}\left(\frac{\pi A}{l}\right)^2\left[\frac{1}{e}C\left(\frac{2\omega}{\omega_L}\right)\right]\right\} \qquad (17)$$

where the coupling coefficient

$$C\left(\frac{2\omega}{\omega_L}\right) = \left(\frac{2\omega}{\omega_L}\right)^2 \Big/ \left[\left(\frac{2\omega}{\omega_L}\right)^2 - 1\right] \qquad (18)$$

For $2\omega/\omega_L \gg 1$, the coefficient C approaches 1 and the amplitude correction approaches $\frac{1}{2}$ that of the fixed end system. The mass then remains almost stationary, but in an elevated mean position such that the average tension over the cycle is the mass weight. The variation in resonant frequency is that for a string with fixed ends, with the ω_0 calculated on the correct average tension, and results from the oscillation in tension only. This is the condition under which most textile testing occurs.

For $2\omega/\omega_L \ll 1$, the factor $(1/e)C(2\omega/\omega_L)$ approaches $(\omega/\omega_p)^2$, where ω_p is the angular frequency of the pendulum formed by the system. In this region the strains are vanishingly small, the string being almost unstretched. The variations in tension are those caused by the mass moving up and down sufficiently to allow the string to bow.

Between these limits there is a condition of complete coupling when $2\omega = \omega_L$ and the tension oscillation excites the natural vibrations associated with ω_L. In the vicinity of this resonance the coefficient C can be very large. It is of interest to calculate this coupling coefficient, and the actual shifts in resonant frequency for some examples of vibrating string in the literature. Stauff and Montgomery[3] vibrated fine wires mounted in system 2 to measure the change in resonant frequency caused by air damping, and provide enough information to enable the coupling coefficients to be calculated. They state that the amplitude was never allowed to exceed 0·05 cm, and making the assumption that this was the amplitude, we have constructed Table 1.

It is interesting to note that for the tungsten and gold wires the correction is negative. Further, the correction is greatest in the case of the gold wire, for which $2\omega/\omega_L$ is closest to one.

Transverse motion of mass. The mass oscillates transversely, excited into such a motion by the transverse component of the tension at W. For $\omega/\omega_p > 1$, the usual

Table 1. *Calculation of* $2\omega/\omega_L$, *coupling coefficient and shift in resonant frequency for strings vibrated by Stauff and Montgomery*[3]

Material	*Tungsten*	*Gold*	*Copper*	*Glass*
Radius a (μ)	6·77	5·24	6·65	4·62
Length l (cm)	10·13	10·53	9·45	10·11
Mass attached M (mg)	36·6	25·6	50·9	51·0
Resonant frequency f (c/s)	56	58	106	268
Density ρ (g/cm^2)	18·8	19·26	8·89	2·6
Young's modulus E (dyn/cm^2 $\times 10^{12}$)	35·5	7·85	11·1	7
Strain ($e = 10^{-3}\, M/\pi E a^2$)	0·715 $\times 10^{-5}$	3·78 $\times 10^{-5}$	3·29 $\times 10^{-5}$	11·02 $\times 10^{-5}$
$\frac{2\omega}{\omega_L} = 40\frac{M}{a^2}\sqrt{\frac{1}{\rho l E}}$	0·385	0·935	1·501	7·04
Coupling coefficient $C = \frac{(2\omega/\omega_L)^2}{(2\omega/\omega_L)^2 - 1}$	−0·174	−6·88	+1·8	+1·02
Amplitude correction* $f_A - f = \frac{\pi^2}{32} \times 10^{-4}\frac{fc}{l^2 e}$	−0·41	−3·0	+2·0	+0·76

* Amplitude assumed to be 0·05 cm.

operating condition, this motion is 180° out of phase with the motion of the string, that is, as the string bows to the left, the mass moved transversely to the right (for $\omega/\omega_p < 1$ the two motions are in phase, but this condition will no longer concern us). The amplitude of the motion depends on the ratio ω/ω_p, increasing as this ratio approaches 1, the motion of the string then exciting the natural pendulum vibration.

The mass moving 180° out of phase with the string motion results in a shifting of the node near the mass upwards, that is, in an effective shortening of the string (see Fig. 4), and it can be shown that the decrease in l,

$$\delta l = l\left(\frac{\omega_p}{\omega}\right)^2 \Big/ \left[1 - \left(\frac{\omega_p}{\omega}\right)^2\right] \qquad (19)$$

which gives an increased resonant frequency

$$\omega = \omega_0[1 + (\omega_p/\omega)^2] \qquad (20)$$

for $(\omega_p/\omega)^2 \ll 1$.

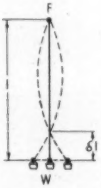

Fig. 4. Inward shift of node caused by transverse motion of mass

This result agrees with the more general one given by Rayleigh[4] who considers the shift in the nodes when each end of the string is located by a mass kept in an equilibrium position of zero transverse displacement by a restoring force proportional to the displacement.

APPLICATIONS AND DISCUSSION

Correction of vibroscope measurements. We consider the measurement of linear density by the vibroscope technique, with the string mounted in each of the systems described above. A finite amplitude causes the string to resonate at a frequency greater than that predicted by equation (1). Consequently the linear density estimated using this equation in conjunction with the observed resonant frequency will be less than the true value. For, if ρ_0 is the true linear density at the test tension T, and ρ the value estimated by use of equation (1), ω_0 the resonant angular frequency at zero amplitude and ω the observed resonant angular frequency at the test amplitude A,

$$\rho_0 = \frac{\pi^2}{l^2}\frac{T}{\omega_0^2}; \quad \rho = \frac{\pi^2}{l^2}\frac{T}{\omega^2}$$

so

$$\rho_0 = \rho\,(\omega/\omega_0)^2 = \rho(1 + k)$$

where k, which we call the correction factor, is of the order $\frac{1}{e}\left(\frac{A}{l}\right)^2$. The exact form of k depends on the mounting system. In system 1, an additional error is present if the tension substituted in these equations is that outside the gauge length. As discussed above, this is due to the friction at the peg.

To illustrate these corrections for yarns of different counts mounted at different stress levels, we consider the vibroscope testing of wool yarns of the same twist multiplier. The twist multiplier, a measure of yarn geometry, is the product of turns per unit length and the square root of the linear density. It is assumed that yarns of the same twist multiplier are characterized by the same stress-strain curve, and thus, that their incremental strains of mounting are determined solely by the stress at which they are mounted. Fig. 5(*a*) shows the stress-length curve of wool yarns of twist multiplier 200 $(\text{tex})^{1/2}$ turns/cm derived from the load length curve of a 50 tex* (approx. 18's) worsted yarn of 11 turns/in. The inset,

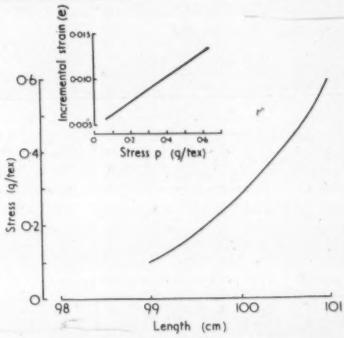

Fig. 5. Stress-length and stress-incremental strain curves for wool yarns of twist multiplier 200 $(\text{tex})^{1/2}$ turns/cm

Fig. 5(*b*), is a plot of e, the incremental strain for different values of p, the stress,† and this plot is roughly fitted in the range $0{\cdot}1 < p < 0{\cdot}6$ g/tex by

$$e = 0{\cdot}005 + 0{\cdot}0125p$$

We obtain thence the values of e, e^{-1} for the range of stress 0·1(0·1)0·6 g/tex (corresponding to loads 5(5)30 on a 50 tex wool yarn). These values are listed in Table 2.

Table 2. *Values of e, e^{-1} for different stresses on wool yarns of twist multiplier* 200 $(tex)^{1/2}$ *turn/cm*

Tension on 50 tex yarn (g)	*Stress p (g/tex)*	*Incremental strain e*	e^{-1}
5	0·1	0·0063	$1{\cdot}60 \times 10^2$
10	0·2	0·0075	1·33
15	0·3	0·0088	1·14
20	0·4	0·0100	1·00
25	0·5	0·0113	0·89
30	0·6	0·0125	0·80

Mounting by system 1. The yarn is mounted as in Fig. 1 and the equilibrium tension in the gauge length is made determinate by allowing the tension outside the peg to pull taut the yarn inside.

The linear density ρ is estimated by substituting in equation (1):

(*a*) the tension outside the gauge length T;
(*b*) the resonant angular frequency observed at amplitude A;
(*c*) the gauge length l.

* The tex is a unit of linear density used in the Textile Industry. It is the mass in milligrams of one metre of the yarn.

† If measured as load applied for tex, p is the stress (or force per unit area) divided by the bulk density of the yarn. For convenience we continue to call p the stress.

The value of the linear density corrected for the amplitude effect, and for the friction effect is then given by

$$\rho_0 = \rho(1 + k_1)$$

where $$k_1 = \frac{3}{16}\pi^2 \cdot \frac{1}{e}\left(\frac{A}{l}\right)^2 - \mu\theta$$

In Fig. 6 we plot the correction factor k_1 as a function of A/l for the range of stress values

$$p = 0{\cdot}1(0{\cdot}1)0{\cdot}6 \text{ g/tex} \quad \text{and} \quad \mu = 0{\cdot}3$$

and for two values of θ, $\theta = 5°$ and $\theta = 20°$. These sets of curves converge on corrections of $-2{\cdot}5\%$ and -10% respectively as the amplitude approaches zero.

The corrections at the amplitudes past which slipping should occur at the peg each cycle, are found by substituting (13) in (14) to obtain the result $k_1 = \frac{1}{2}\mu\theta$, $= 1{\cdot}25\%$ and 5% respectively, independent of the stress level. This is indicated in Fig. 6.

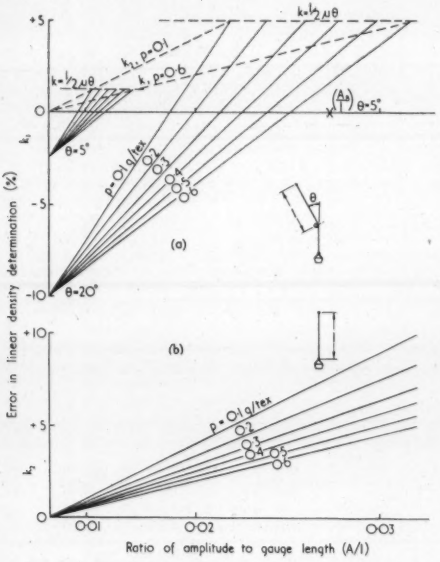

Fig. 6. Amplitude correction factor for wool yarns of twist multiplier 200 (tex)$^{1/2}$ turns/cm mounted at stresses $0{\cdot}1(0{\cdot}1)0{\cdot}6$ g/tex

(*a*) Mounting by system 1 . $k_1 = \frac{3}{16} \cdot \frac{\pi^2}{e}\left(\frac{A}{l}\right)^2 - \mu\theta$;

(*b*) Mounting by system 2 . $k_2 = \frac{1}{16} \cdot \frac{\pi^2}{e}\left(\frac{A}{l}\right)^2 . C$; $C = 1$.

For amplitudes in excess of these, the frequency of resonance is as yet unknown. As indicated by equations (15) in conjunction with (22) the maximum apparent difference in linear density observable is $\frac{3}{4}\mu\theta\rho_0$, or $3{\cdot}75\%$ and 15% of ρ_0 for $\theta = 5°$ and $20°$ respectively, which is also independent of the stress level.

For $\theta = 5°$, the amplitude at which bouncing can occur at the peg is given by

$$A/l = \theta/\pi = 0{\cdot}028$$

As can be seen from Fig. 6(*b*) this amplitude is in excess of the amplitudes at which slippage occurs for the range of stress considered.

Note. The ratio of the amplitude at which slipping should occur to the amplitude at which bouncing occurs is given by

$$\frac{A_c}{A_B} = \sqrt{\left(\frac{8e\mu}{\theta}\right)}$$

For textile yarns and fibres with $e \sim 0{\cdot}01$, $\mu \sim 0{\cdot}3$, then A_B exceeds A_c, or slipping should occur before bouncing, for the angle θ greater than several degrees.

Mounting by system 2. The yarn is mounted as in Fig. 2, and the linear density ρ is estimated as for system 1, the tension used being the weight of the mass.

The corrected linear density ρ_0 is given by

$$\rho_0 = \rho(1 + k_2)$$

where $$k_2 = \frac{1}{16} \cdot \pi^2 \cdot \frac{1}{e}\left(\frac{A}{l}\right)^2 C\left(\frac{2\omega}{\omega_L}\right)$$

$C\left(\frac{2\omega}{\omega_L}\right)$ being the coupling coefficient.

For stresses greater than $0{\cdot}1$ g/tex, and for gauge lengths less than 20 cm, the coupling coefficient lies between 1 and $1{\cdot}01$, so that under these conditions we can say that

$$k_2 = \frac{1}{16} \cdot \frac{\pi^2}{e} \cdot \left(\frac{A}{l}\right)^2$$

The correction curves for different stress levels are plotted in Fig. 6(*b*) with the coupling coefficient $C = 1$, and values of θ, μ as in system 1.

It should be noted that:

(1) The change in the correction factor, caused by a given change in the ratio of amplitude to gauge length, applicable to a yarn mounted by system 1 is three times the change in the correction factor applicable to system 2 mounting.

(2) In system 1 mounting, for amplitudes less than that which causes slipping, the friction at the peg makes the tension, and hence the resonant frequency, less than that of the same length of the same string carrying the same weight but mounted in system 2, provided the coupling coefficient is positive. When the amplitude is such that slipping is about to commence the tension behaviour in system 1 corresponds with that in system 2, provided the coupling coefficient is unity. For then, in the system 1 mounting, the tension has an average value of Mg (see definition of the critical amplitude made earlier) and this is the average tension in the system 2 mounting. As the amplitude of bowing determines the amplitude of the tension oscillation in the same way in both system 1 and system 2 when the coupling coefficient is 1, the resonant frequencies should be the same in each case [see dotted lines in Fig. 6(*a*)].

CONCLUSION

It has been shown that, in theory, a string vibrating at finite amplitude resonates at a frequency generally higher than that predicted by the classical formula. The magnitude of this shift in resonant frequency depends on a number called the incremental strain which is simply the ratio of the longitudinal stress in the string when mounted to the

incremental Young's modulus at the mounting tension. The ratio relates the increase in tension in the string due to bowing to the increase in length due to bowing, and thus to the amplitude of the vibration.

If a peg separates the gauge length of vibrating string from a region in which the tension in the string is determined, then the friction at this peg should be considered. This friction has two effects:

(*a*) For amplitudes small enough it fixes one end of the string longitudinally as well as laterally. This restraint leaves the string in the condition that to bow it must increase in tension, and this bowing causes an increase in the mean tension and an incremental oscillating tension.

(*b*) The initial tension in the gauge length can be indeterminate. If the string inside the gauge length is pulled taut by the tension outside, then the initial tension is determined, and equals that outside, less the friction force.

When the tension in the string is controlled by a weight hanging on one end, the average tension cannot exceed the mass weight, and thus bowing can cause only an incremental oscillatory tension. The magnitude of this variation depends on the coupling between the bowing motion and the natural longitudinal motion of the mass on the end of an elastic string. In textile testing, the frequency of the bowing is usually much greater than that of this longitudinal motion, and there have been no reports of difficulties caused by such coupling.

In the testing of yarns and fibres, the incremental strain is usually of the order 1%, and errors in the estimation of linear density of order 1% due to the amplitude effect would occur with amplitudes of the order 1% of the gauge length. With fine wires, where the incremental strain can be of the order 0·01% such errors would occur for amplitudes of the order of 0·1% of the gauge length.

REFERENCES

(1) MACKAY, B. H., and DOWNES, J. G. *Textile Research Journal*, **28**, p. 467 (1958).
(2) DOWNES, J. G., and LEARY, B. G. *Textile Research Journal*, **28**, p. 497 (1958).
(3) STAUFF, D. W., and MONTGOMERY, D. J. *J. Appl. Phys.*, **26**, p. 540 (1955).
(4) RAYLEIGH, J. W. S. *Theory of Sound*, **1**, p. 135 (New York: Dover Publications).
(5) CARRIER, G. F. *Quart. Appl. Math.*, **3**, p. 157 (1945).
(6) CARRIER, G. F. *Quart. Appl. Math.*, **7**, p. 97 (1949).

Investigation of Nylon "texture" by X-ray diffraction

By K. LITTLE, M.A., D.Phil.,* British Nylon Spinners Ltd., Coventry

[*Paper first received* 6 *August*, 1958, *and in final form* 16 *January*, 1959]

The manner in which minor changes in the molecular and crystalline arrangement are mirrored by corresponding changes in the X-ray diffraction pattern has been used as a method of following the effects of a number of treatments and modifications in the structure and composition of the Nylons. The crystalline diffraction pattern was taken from the branches of spherulites. Ageing after spinning from the melt, caused by the dissipation of strains (a fairly rapid process for the first two days) and uptake of water from the atmosphere (a process completed in 50 min), shows as increased distortion and crystallinity.

The effect of swelling agents is to relieve strain and convert to the more stable α form. Phenol acts as a swelling agent in concentrations greater than 2%. The effect of introducing side-chains is to decrease the probability of links between main molecular chains (e.g. hydrogen bonds) and at the same time decrease the probability of plastic flow, so that greater reversible extensibility (i.e. rubber-like elasticity) results.

The diffraction pattern of 11 Nylon, $[(CH_2)_{10}\text{–}NH.CO\text{–}]_n$, is consistent with the unit cell

$a = 9{\cdot}6 \pm 0{\cdot}5$ Å $\quad \alpha = 72 \pm 2°$
$b = 4{\cdot}2 \pm 0{\cdot}2$ Å $\quad \beta = 90$
$c = 15{\cdot}0 \pm 0{\cdot}2$ Å $\quad \gamma = 63\frac{1}{2} \pm 1°$

By the "texture" of Nylon is here meant the variation which can occur in the relations between the crystalline and non-crystalline regions of the polymer, according to its method of preparation and subsequent treatment, and which affect the properties of the polymer.

During the course of an investigation of this problem a wide variety of treatments was tried, and in this paper will be recorded observations made with some of them. The greater part of this work was completed eight years ago, but it seems that some of the observations then made are still worthy of record. Papers already published on the effects of various treatments which were used to help form an idea of the texture included work by Bergman, Fankuchen and Mark[1, 2] on the drawing of quenched monofil and the effects of phenol treatment; and by Pape, Baker and Fuller[3, 4, 5] on the effects of heat treatment, variations in the properties of certain inter-polymers and the effects of N-methylation. Hill and Walker[6] have studied the effects of hydrogen bond distribution and work has already been published by the author on the effects of irradiation on the Nylons.[7, 8]

MATERIALS USED

Nylon is the generic term for all the fibre-forming synthetic polyamides which, in common with most other high polymers, are partly crystalline and partly amorphous in character. Those which have been used in this work are as follows,

(*a*) 66 Nylon $[\text{–}(CH_2)_4\text{–}CO\cdot NH\text{–}(CH_2)_6\text{–}NH\cdot CO\text{–}]_n$
(*b*) 610 Nylon $[\text{–}(CH_2)_8\text{–}CO\cdot NH\text{–}(CH_2)_6\text{–}NH\cdot CO\text{–}]_n$

In both these polymers the molecular chains in the crystalline regions are arranged in sheets, within which the molecules are linked by hydrogen bonds. Bunn and Garner,[9] who worked out the crystal structure, found two alternative

* Now at the Nuffield Orthopaedic Centre, Oxford.

modes of packing of the sheets, the α and β forms, both of which commonly occur, together with a random mixture of the two, in a single fibre.

(*c*) 6 Nylon $[-(CH_2)_5-NH\cdot CO-(CH_2)_5-NH\cdot CO-]_n$

Here the arrangement of hydrogen bonds within the sheets is somewhat different, so that the unit cells are monoclinic, as shown by Brill[10] and Holmes, Bunn and Smith,[11] and not triclinic as with 66 and 610 Nylons.

(*d*) 11 Nylon $[-(CH_2)_{10}-NH\cdot CO-]_n$

At the time this work was done, no information was available on the crystal structure of 11 Nylon. Possible unit cells were first investigated which had packing of chains and sheets analogous to those of 66 and 610 Nylons. No simple cell, or cell in which the displacement between layers of polarized groups were of the order of 3·5 Å, could be found which fitted all the experimental data. Bunn and Garner[9] have calculated that displacements of 1·23, 3·68 and 6·14 Å are consistent with good packing of the chains. A displacement of 1·23 Å was therefore considered and a cell containing two molecular units was found for which observed and calculated spacings were in good agreement, and which would account for the intensity of the (001) reflexion (Fig. 1).

Cell parameters are:

$a = 9{\cdot}6 \pm 0{\cdot}5$ Å $\quad \alpha = 72° \pm 2°$

$b = 4{\cdot}2 \pm 0{\cdot}2$ Å $\quad \beta = 90°$

$c = 15{\cdot}0 \pm 0{\cdot}2$ Å $\quad \gamma = 63\frac{1}{2}° \pm 1°$

(*e*) Extruded and spun 66 Nylon treated with formaldehyde.

(*f*) 610 Nylon with isobutyl groups substituted for some of the hydrogen atoms in >NH groups.

(*g*) An interpolymer of 66, 610 and 6 Nylons, in the ratio 40 : 30 : 30.

(*h*) An interpolymer of 66 Nylon and 6T (terephthalic acid being substituted for part of the adipic acid during the course of polymerization).

EXPERIMENTAL

Materials were normally obtained as polymer extruded from the autoclave, or as undrawn or drawn fibres. The interpolymer was in the form of a thin sheet. Treatments received before examination are, on the whole, self-explanatory, though two points may be noted:

(*a*) in order to avoid any possible oxidation effects, the annealing process was carried out on specimens sealed in glass tubes in an atmosphere of nitrogen,

(*b*) thin films were prepared by casting a formic acid solution of the Nylon on to either a clean glass or water surface. The film produced was subsequently washed on a distilled water surface.

X-ray diffraction photographs were taken using a transmission type camera with a flat film. The specimen-to-film distance was normally 3 cm; CuKα radiation was used. Exposure times, using Ilfex film, were of the order of four hours, so that for ageing experiments a Geiger counter spectrometer was used. Ten minutes were required to scan the main reflexions. Variations in the crystalline properties of the Nylons which affect the appearance of X-ray diffraction patterns include the degree of crystallinity, crystallite sizes and shapes, distortion, orientation, partial ordering in the non-crystalline regions and the proportion of α and β forms.

To obtain electron diffraction patterns of the thin films two conditions were necessary. In the first place, the film had to be sufficiently thin for the pattern not to be lost by internal scattering of diffracted electrons. Secondly, the equipment had to be sufficiently clean for the build-up of carbon, which normally occurs in electron microscopes and electron diffraction apparatus, to be slow enough to allow a reasonable time for observation and photographing before the specimen became too thick.

RESULTS

(i) *Distribution of hydrogen-bond forming groups.* Considering first the single polymers, it was found that as the distance apart of hydrogen-bond forming groups increased, distortion also increased, and at the same time the degree of crystallinity and the size of crystallites decreased. Diffraction photographs of 11, 610 and 66 Nylons (Figs. 1, 2, 3) can be taken as typical examples, with that of 66 Nylon showing the clearest reflexions. From small angle scattering of X-rays by Nylon, Fankuchen and Mark[1] had deduced that the crystallites in their specimens were small bundles of chains rather more than 500 Å long and with 200 Å as the average width. These figures are consistent with the sizes observable directly by electron microscope examination. Although the latter show considerable variation in the size of complete crystallites (or spherulites), the sizes of the individual branches are similar (Fig. 4).

In the interpolymers, with a random mixture of the components in each molecular chain, the probability of bond-forming groups being in suitable positions for crystallite formation is greatly diminished, so that one might expect the polymers to be almost completely non-crystalline over considerable ranges of composition. In a polymer containing a high proportion of hydrogen bond-forming groups, however, the non-crystalline state must have a high internal energy, and will therefore tend to be metastable. In the present work one interpolymer 66/610/6, was examined in detail, the components being in the ratio 40-30-30. A specimen of this was obtained in an almost completely non-crystalline form. Any treatment which allowed sufficient movement of the chains relative to one another caused crystallization to occur. When a specimen was stretched the result was a fairly highly crystalline but very distorted structure; annealing and the action of swelling agents caused the formation of comparatively undistorted crystallites. These last two methods are ones which encourage free rotational movements of chain segments, rather than longitudinal movement of chains past one another, for the adjustment of positions of polar groups. The crystallites produced were smaller than those in specimens of single polymers produced under comparable conditions. An examination of the diffraction photographs of orientated specimens showed that the reflexions present were those common to β66 and 6 Nylon.

(ii) *Ageing.* After Nylon has been melt-spun there is an ageing effect which proceeds at an appreciable rate for about two days, during which time the strains set up by the rapid cooling are partially dissipated. The parameters which were used to show this (using the Geiger counter spectrometer) were the relative intensities and separation of the two main diffraction rings. The amount by which the separation of the two main diffraction rings was less than the theoretical gave an indication of the amount of distortion present, while the relative intensities of diffraction rings and the amorphous halo is related to the degree of crystallinity. During the first 50 min the changes were irregular, thereafter distortion and

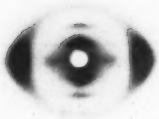

Fig. 1. X-ray diffraction pattern of extruded cold drawn 11 Nylon

Fig. 2. X-ray diffraction pattern of extruded cold drawn 610 Nylon

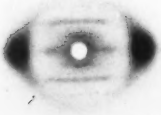

Fig. 3. X-ray diffraction pattern of extruded cold drawn 66 Nylon

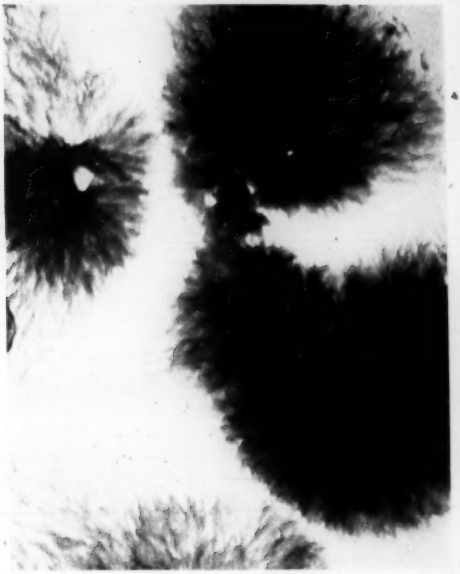

Fig. 4. Electron microscope photograph of a thin film of 66 Nylon (× 12,000)

Fig. 5. X-ray diffraction pattern of 66 Nylon before and during swelling treatment. (Sector comparison photograph)

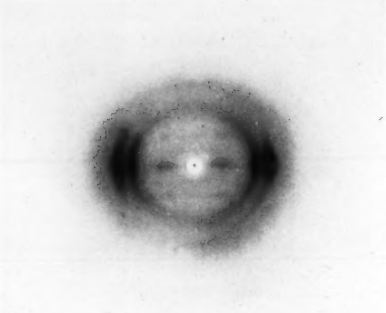

Fig. 6. X-ray diffraction pattern of 66 Nylon in contact with 4% phenol solution

Fig. 7. X-ray diffraction pattern of 66 Nylon during and after swelling treatment. (Sector comparison photograph)

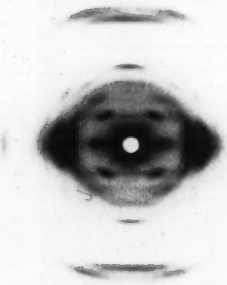

Fig. 8. X-ray diffraction pattern of orientated 66 Nylon combination of annealing and swelling treatments

Fig. 9. X-ray diffraction pattern of drawn 610 Nylon annealed

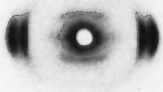

Fig. 10. X-ray diffraction pattern of drawn 610 Nylon annealed, then stretched slightly

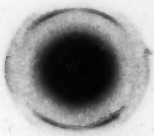

Fig. 11. Electron diffraction pattern of thin film of 66 Nylon, tilted showing orientation

degree of crystallinity both increased. Both the initial rate of cooling and the humidity of the surroundings affected the final degree of crystallinity attained. An independent observation, which also indicated that the degree of crystallinity increased, was that the heat of wetting of dry yarn decreased with increased time of storage in a desiccator after extrusion. The irregular changes during the first 50 min were related to water uptake, since the measurements of heats of wetting indicated that it took 50 min for an equilibrium amount of water to be absorbed.

(iii) *The action of swelling agents.* As a result of the increased freedom of movement of chain segments in the non-crystalline regions, both annealing and swelling agents tend to remove distortion and strain in crystallites. The effects on the degree of crystallinity are, however, quite different; in 66 Nylon annealing increases it while swelling leaves it about the same.

It was found that the more violent the swelling agent used, the greater the proportion of the crystalline regions which were converted to the α form; with a strong swelling agent the change was practically complete. To obtain further information about the mechanism of swelling, X-ray diffraction photographs of yarn in contact with 4% phenol solution were taken (Figs. 5, 6, 7). These showed an immediate decrease in spacings between molecular chains from the distorted to the calculated ordered values. The non-crystalline halo had an increased width, while a second halo appeared which corresponded with the length of the phenol molecules. The total degree of crystallinity was less than in the original material. On washing and drying the specimens, the undistorted spacings remained while the degree of crystallinity reverted to normal, the additional crystalline material assuming the α form. A point which is of some interest is that the threshold of the strength of phenol solution required to produce this marked re-organization of the crystallites is quite definite. Below about 2% phenol the solution will not re-organize hydrogen bonds within the Nylon. The precise threshold value was found by measurements of the heat of reaction of the polymer with different concentrations of phenol. These measurements also indicated that the extent of the change above this threshold increased in a linear manner with the strength of the solution.

As a result of the increased lateral ordering, it was found that for several phenol-treated specimens of 66 Nylon the 010 and 110 reflexions, with a calculated difference in spacing of 0·1 Å, were clearly resolved. Specimens with diffraction patterns showing the greatest number of crystalline reflexions were obtained by a combination of annealing and swelling processes (Fig. 8).

(iv) *Stretching and orientation.* Effects which can be produced by stretching the polyamides include increased crystallinity and distortion. Both plastic flow and reversible elasticity are possible. Related to distortion is the change in proportion of α and β forms. This is associated with the packing of sheets containing hydrogen bonds, and indicates that these sheets tend to behave as units in the rupture and formation of crystallites. In a highly ordered 610 yarn which, as a result of annealing, was mainly in the α form (Fig. 9) a tension, insufficient to cause measurable increase of the lateral distortion, changed the packing into $(\alpha + \beta)$ and β (Fig. 10).

Reversible extensibility in the polyamides is increased by the presence of small side-chains. Thus, in a sample of isobutyl-substituted 610 Nylon which was examined, the extensibility was of the order of 300%, while in normal drawn 66 Nylon it was about 8%. Thin films of these two in the electron microscope show a difference in extensibility, but not in crystalline arrangement when unstretched. Where crystallites are small, and there are no side groups and little tendency to coil, a combination of plastic flow and reversible extensibility is possible. The interpolymer 66/610/6 can be used as an illustration. A strip of the extruded material was stretched 700% of its original length, although after 300–400% stretch there was no further increase in orientation. On relaxing the length was reduced to 550% of the original. The orientation and degree of crystallinity then corresponded with an original stretch of about 150%.

For initially unorientated polyamide fibres, stretching (cold drawing) produces orientation in the direction of the fibre axis. In the thin films prepared from solution and used for electron microscope examination a different type of orientation was present. The electron diffraction pattern of a tilted thin film (Fig. 11) indicates that the (010) plane must be approximately in the plane of the film. The tilt was approximately 20° in the direction of the beam.

In the case of methoxymethylation of a polymer by reaction with formaldehyde vapour, reversible elasticity was produced which decreased when the methoxy-side chains degraded. It is the amide links in the non-crystalline regions which are affected, so that the crystallite structure remains the same. Evidence has been obtained which suggests that methoxymethylation from solution can sometimes result in direct cross-linking from one chain to another. Thus in certain specimens containing a high proportion of the α form which were methoxymethylated in a suitable manner, stretching caused an increase in the proportion of $(\alpha + \beta)$ and β packing, which was reversed on relaxing. (This methoxymethylation of amide links is presumably responsible for the fixation of proteins by formaldehyde solutions in biological procedures.)

DISCUSSION

Any picture which is formed of the arrangement of molucules in the Nylons must be in agreement with the experimental observations which have just been presented, and with those described in the papers quoted. In the electron microscope a dendritic habit is seen (Fig. 4), and from the sizes involved it is clear that the crystalline diffraction patterns are of the dendritic branches. The units within the crystals are probably better regarded as sheets than as the individual string-like molecules.

Between the crystallites the molecules are arranged in a manner which can show a greater or lesser degree of ordering. In the case of the simple polyamides there are no side chains, and cohesion between chains is caused by a certain amount of mechanical entangling, hydrogen bonds directly between chains and absorbed water hydrogen bonded to the amide groups. With the isobutyl substituted polyamides, and also with those treated with formaldehyde (before these degrade), there are small side chains. These can become intertangled, and by preventing direct hydrogen bonding between chains may well encourage a greater degree of free rotation about bonds, with consequent bending and possibly coiling, as described by Bunn[12] for rubber. From this it is clear that conditions of the polyamides which favour links between chains by hydrogen bonding will tend to make the whole polymer more rigid. When this bonding between chains is prevented, either plastic flow can occur, as in the interpolymer 66/610/6, or reversible rubber-like elasticity, when there are sufficient short side groups which by becoming entangled with one another, prevent easy slipping of molecules past one another.

ACKNOWLEDGEMENTS

The author is most grateful to Mr. A. W. Porter for help and advice on the taking and reproduction of the X-ray diffraction photographs, and to Dr. C. W. Bunn, Dr. A. Keller and Dr. R. M. Lodge for helpful discussions; also to the latter and British Nylon Spinners Ltd. for specimens and for permission to publish, and to the United Kingdom Atomic Energy Authority for the use of their electron microscope.

REFERENCES

(1) FANKUCHEN, I., and MARK, H. *J. Appl. Phys.*, **15**, p. 364 (1944).

(2) BERGMAN, M. E., FANKUCHEN, I., and MARK, H. *Textile Res. J.* **18**, p., 1 (1948).

(3) FULLER, C. S., BAKER, W. O., and PAPE, N. R. *J. Amer. Chem. Soc.*, **62**, p. 3275 (1940).

(4) BAKER, W. O., and FULLER, C. S. *J. Amer. Chem. Soc.*, **64**, p. 2399 (1942).

(5) BAKER, W. O., and FULLER, C. S. *J. Amer. Chem. Soc.*, **65**, p. 1120 (1943).

(6) HILL, R., and WALKER, E. E. *J. Polymer Sci.*, **3**, p. 609 (1948).

(7) LITTLE, K. *Nature (London)*, **173**, p. 680 (1954).

(8) LITTLE, K. *Proceedings of the 3rd International Conference on Electron Microscopy*, p. 169 (1954).

(9) BUNN, C. W., and GARNER, E. V. *Proc. Roy. Soc. A*, **189**, p. 39 (1947).

(10) BRILL, R. *Z. Phys. Chem.*, **53**, p. 61 (1943).

(11) HOLMES D. R., BUNN, C. W., and SMITH, D. J. *J. Polymer Sci.*, **17**, p. 159 (1955).

(12) BUNN, C. W. *Proc. Roy. Soc. A*, **180**, p. 40 (1942).

Inductance of an eccentric tubular conducting system

By E. E. JONES, B.Sc., Ph.D., University of Nottingham

[*Paper first received* 17 *November*, 1958, *and in final form* 7 *January*, 1959]

The inductance of an eccentric tubular conducting system is determined in a form suitable for easy application as a power series, having the distance between the axes of the two tubes as variable. The first three terms of the series are determined in closed form, and further approximations, if required, can be determined by solving in échelon certain ordinary simultaneous algebraic equations which sum up the boundary conditions of the problem. Numerical results are included in particular cases.

As indicated by the author,[1] the inductance of a conducting cable or a tubular system of conductors is a parameter of considerable practical importance. From the point of view of ease of manufacture conductors of circular cross-section are the most suitable, and for a system of non-magnetic concentric circular tubes the formula for the inductance is well known.[2] In an attempt to determine the effect of change of shape of the conductors on the inductance, the author[1] has considered the case of non-magnetic conductors of elliptic sections. In the present paper the study is extended by considering the effect on the inductance of non-collinearity of the axes of two magnetic cylindrical tubes with circular sections, this effect being important in view of the fact that in practice such a state of affairs can arise owing to faulty manufacture. The method can equally well be adapted to determine the effect of eccentricity on the capacitance of a system of circular cylindrical tubes.[3, 4, 5]

FIELD EQUATIONS AND BOUNDARY CONDITIONS

One tube has its axis through a point O and has a section formed by the annulus between concentric circles C_1, C_2 of radii r_1, r_2 respectively, with $r_2 > r_1$. The second tube has its axis through a point Q, and has a section formed by the annulus between the concentric circles C_3, C_4 of radii r_3, r_4 respectively, with $r_4 > r_3 > r_2$. A steady current I flows in one direction along the first tube and returns in the opposite direction along the second tube. It is assumed that the currents are uniformly distributed over the cross-section of the conductors, i.e. proximity effects are ignored. If the current densities are J_2 for the tube enclosed by C_1, C_2, and J_4 for the tube enclosed by C_3, C_4, then

$$I = \pi(r_2^2 - r_1^2)J_2 = -\pi(r_4^2 - r_3^2)J_4 \qquad (1)$$

Polar co-ordinates (r, θ) are used to define the cross-sectional plane, with pole at O, and initial line $\theta = 0$ along the line OQ, which is an axis of symmetry of the section.

The magnetic field intensity due to the currents present can be defined in terms of a vector potential component directed along the axial directions of the conducting tubes. This component is referred to as $A_m(r, \theta)$, $(m = 1, \ldots, 5)$, in the region bounded by C_{m-1} and C_m (C_0 is the point O, and C_5 the circle at infinity). If μ_m is the corresponding permeability for the region, then the controlling differential equation,[6] in terms of the m.k.s. system of units, is of the Poisson type

$$\nabla^2 A_m = -\mu_m J_m, \quad (m = 1, \ldots, 5)$$

with $J_1 = J_3 = J_5 = 0$.

A solution of this equation appropriate to the problem is

$$A_m = P_m + Q_m \log r + \sum_{n=1}^{\infty}(R_{mn}r^n + S_{mn}r^{-n}) \cos n\theta - \tfrac{1}{4}\mu_m J_m r^2 \qquad (2)$$

where P_m, Q_m, R_{mn}, S_{mn} are arbitrary constants. In forming this solution use has been made of the fact that the system is symmetrical about the line $\theta = 0$, i.e. $A_m(r, \theta) = A_m(r, -\theta)$. It is noticed also that $A_1(r, \theta)$ must be finite at the origin $r = 0$, i.e. $Q_1 = S_{1n} = 0$ for $n \geqslant 1$, and at large distance where the current effects cancel each other, $Q_5 = R_{5n} = 0$ for $n \geqslant 1$.

It is assumed that the constants of equation (2) can be developed in a series form as

$$P_m = \sum_{n=0}^{\infty} \delta^n P_{mn}, \quad Q_m = \sum_{n=0}^{\infty} \delta^n Q_{mn}$$

$$R_{mn} = \sum_{t=1}^{\infty} \delta^t R_{mn}^{\ t}, \quad S_{mn} = \sum_{t=1}^{\infty} \delta^t S_{mn}^{\ t} \qquad (3)$$

where $\delta = OQ$. It is noticed that when $\delta \neq 0$ only P_{mo} and Q_{mo} are non-zero, and from equation (2) the vector potential

component is of the usual form for a completely concentric system of cylindrical conductors.

From the symmetry of the system it is seen that

$$A_m(r, \theta, \delta) = A_m(r, \pi - \theta, -\delta)$$

and thus from equations (2) and (3) simultaneously this condition is satisfied if

$$\left.\begin{aligned} P_{mn} = Q_{mn} &= 0, \quad \text{when } n \text{ is odd} \\ R^t_{mn} = S^t_{mn} &= 0, \quad \text{when } n + t \text{ is odd} \end{aligned}\right\} \tag{4}$$

The functions $A_m(r, \theta)$ must satisfy certain conditions at each medium interface C_m. In order that the vector potential and the tangential component of the magnetic intensity are continuous across the circle C_m, it is required that

$$A_{m+1} = A_m \tag{5}$$

$$\mu_m \frac{\partial A_{m+1}}{\partial n} = \mu_{m+1} \frac{\partial A_m}{\partial n} \tag{6}$$

where $\partial/\partial n$ denotes differentiation along the normal to the curve C_m. In particular on C_1 and C_2 the normal derivative can be replaced by the radial derivative $\partial/\partial r$. However, for C_3 and C_4, if P is a point on C_m and OP makes an angle ϕ with the line $\theta = 0$, then

$$\frac{\partial A_m}{\partial n} = \frac{\partial A_m}{\partial r} \cos(\phi - \theta) + \frac{1}{r} \frac{\partial A_m}{\partial \theta} \sin(\phi - \theta)$$

or

$$r_m r \frac{\partial A_m}{\partial n} = r(r - \delta \cos\theta) \frac{\partial A_m}{\partial r} + \delta \frac{\partial A_m}{\partial \theta} \sin\theta \tag{7}$$

This is the form used in the second boundary equation (6) when $m = 3, 4$.

It is noted here that on C_m, $(m = 1, 2)$, the radius is $r = r_m$, whereas on C_m, $(m = 3, 4)$

$$r = r_m(\theta) = \delta \cos\theta + (r_m^2 - \delta^2 \sin^2\theta)^{1/2}$$

It is found convenient in the sequel to write $\delta = r_3\alpha$ on C_3, and $\delta = r_4\beta$ on C_4. In particular, therefore, on C_3

$$\frac{r_3(\theta)}{r_3} = 1 + \alpha \cos\theta - \tfrac{1}{2}\alpha^2 \sin^2\theta - \sum_{n=2}^{\infty} \frac{(2n-3)!\alpha^{2n} \sin^{2n}\theta}{(n-2)!n!2^{2n-2}} \tag{8}$$

for all $\alpha < 1$, i.e. $\delta < r_3$. A similar type of result holds on C_4.

THE INDUCTANCE

The inductance L per unit length of the system is defined by $IL = f_2^{-1}I_2 - f_4^{-1}I_4$, where $f_2 = \pi(r_2^2 - r_1^2)$, $f_4 = \pi(r_4^2 - r_3^2)$, namely, the areas of the regions through which the currents flow, and

$$I_2 = \int_0^{2\pi} \int_{r_1}^{r_2} A_2 r dr d\theta$$

$$I_4 = \int_0^{2\pi} \int_{r_3(\theta)}^{r_4(\theta)} A_4 r dr d\theta$$

With A_2 given by equation (2), it readily follows that

$$I_2 = \pi\{P_2(r_2^2 - r_1^2) + \tfrac{1}{2}Q_2[r_2^2(2\log r_2 - 1) - r_1^2(2\log r_1 - 1)] - \tfrac{1}{8}\mu_2 J_2(r_2^4 - r_1^4)\} \tag{9}$$

In determining I_4 use is made of the series expansion of equation (8). It will be sufficient for the purpose of this study to restrict expansions to the order of δ^4 when determining $r_3^n(\theta)$ and $r_4^n(\theta)$. These expansions are substituted into A_4 as given by equation (2), and the simple integral I_4 is readily evaluated leading to the result

$$I_4 = \pi\{P_4(r_4^2 - r_3^2) + \tfrac{1}{2}Q_4[r_4^2(2\log r_4 - 1) - r_3^2(2\log r_3 - 1)] - \tfrac{1}{8}\mu_4 J_4[(r_4^4 - r_3^4) + 2\delta^2(r_4^2 - r_3^2)] + (r_4^2 - r_3^2)\sum_{n=1}^{3}\delta^n R_{4n}\} \tag{10}$$

When the expansion formulae of equation (3) are introduced into equations (9) and (10), then $I_2 = \sum_{n=0}^{2}\delta^{2n}I_{2n}$, $I_4 = \sum_{n=0}^{2}\delta^{2n}I_{4n}$, and thus $L = \sum_{n=0}^{2}\delta^{2n}L_{2n}$, where

$$L_{2n} = (I_{2n}/If_2) - (I_{4n}/If_4) \tag{11}$$

In order to determine L_0, L_2, L_4 it is found necessary to evaluate the coefficients P_{2n}, P_{4n}, Q_{2n}, Q_{4n}, $(n = 0, 2, 4)$; R^1_{41}, R^3_{41}, R^2_{42} and R^1_{43}.

The boundary conditions on C_1 and C_2 are applied by substituting the corresponding function A_m given by equation (2) into equations (5) and (6), and equating terms in like functions $\cos n\theta$, $(n = 0, 1, \ldots)$, on each side of the equations.

The boundary conditions on C_3 and C_4 are applied by substituting equation (3) into equation (2) with the appropriate choice of the subscript m, then substituting into equations (5) and (6) using the modification of equation (7). Here again it is necessary to use expansions for $r_3^n(\theta)$, etc., derived from equation (8) to the order δ^4. The method adopted is to equate coefficients of $\alpha^n \cos m\theta$, $(n, m = 0, 1, \ldots)$, on each side of the equations derived by substituting $r = r_3(\theta)$ for the condition on C_3, and $\beta^n \cos m\theta$, $(n, m = 0, 1, \ldots)$, when $r = r_4(\theta)$ on C_4.

The resulting algebraic equations are readily solved, but in view of their number are not recorded here. In the first instance it can be shown that $Q_{20} = \frac{1}{2}\mu_2 J_2 r_2^2$, $Q_{30} = -I\mu_3/2\pi$, $Q_{40} = \frac{1}{2}\mu_4 J_4 r_4^2$, and with $P_{20} - P_{40}$ expressed in terms of these coefficients, the first approximation L_0 to the inductance as given by equations (9), (10) and (11), takes the form

$$2\pi L_0 = \mu_3 \log\frac{r_3}{r_2} + \frac{\mu_2 r_1^4}{(r_2^2 - r_1^2)^2}\log\frac{r_2}{r_1} + \frac{\mu_4 r_4^4}{(r_4^2 - r_3^2)^2}\log\frac{r_4}{r_3} + \frac{\mu_2(r_2^2 - 3r_1^2)}{4(r_2^2 - r_1^2)} - \frac{\mu_4(3r_4^2 - r_3^2)}{4(r_4^2 - r_3^2)} \tag{12}$$

This result can be compared with that stated in Ref. 2, being the inductance when $\delta = 0$, i.e. for the completely concentric conducting system.

In order to determine the second approximation to the inductance, use is made of the results $Q_{2n} = Q_{3n} = 0$ for $n \geqslant 2$, $P_{2n} = P_{3n}$ for $n \geqslant 2$, $Q_{42} = 0$. The coefficient L_2 can then be expressed in the simpler form $L_2 = -R^1_{31}/I$, and ultimately reduces to

$$2\pi L_2 = \mu_3 a_{22} b_{24}/(r_3^2 a_{24} a_{22} + r_2^2 c_{22} b_{24}) \tag{13}$$

where

$$\left.\begin{aligned} a_{mn} &= (\mu_{n+1} + \mu_n)(\mu_n + \mu_{n-1})r_n^m + (\mu_{n-1} - \mu_n)(\mu_n - \mu_{n-1})r_{n-1}{}^m \\ b_{mn} &= (\mu_{n+1} + \mu_n)(\mu_n - \mu_{n-1})r_n^m + (\mu_{n-1} - \mu_n)(\mu_n + \mu_{n-1})r_{n-1}{}^m \\ c_{mn} &= (\mu_{n+1} - \mu_n)(\mu_n + \mu_{n-1})r_n^m + (\mu_{n+1} + \mu_n)(\mu_n - \mu_{n-1})r_{n-1}{}^m \end{aligned}\right\} \tag{14}$$

In order to determine the third approximation to the

inductance, use is made of the results $Q_{44} = 0$, $R^1_{m3} = S^1_{m3} = 0$ for $m = 1, \ldots, 5$. It can be shown that

$$IL_4 = -(R^3_{31} + R^2_{32})$$

and finally

$$4\pi L_4 = \mu_3 \left(\frac{r_3^2 a_{22} a_{24} - r_2^2 c_{22} b_{24}}{r_3^2 a_{22} a_{24} + r_2^2 c_{22} b_{24}}\right)^2 \left(\frac{b_{44} a_{42}}{r_3^4 a_{42} a_{44} + r_2^4 c_{42} b_{44}}\right) \quad (15)$$

The third approximation to the inductance is then

$$L_0 + \delta^2 L_2 + \delta^4 L_4$$

Further approximations can be determined by the same method, but would be difficult to express in closed forms. However, for a given example the boundary condition equations could be solved numerically in a systematic manner.

FURTHER CONSIDERATIONS

(i) The third order approximation to the inductance of a concentric cable is derived by allowing $r_1 \to 0$ in equations (12), (13) and (15). In this case

$$2\pi L_0 = \mu_3 \log \frac{r_3}{r_2} + \frac{\mu_4 r_4^4}{(r_4^2 - r_3^2)^2} \log \frac{r_4}{r_3} - \frac{\mu_4 (3r_4^2 - r_3^2)}{4(r_4^2 - r_3^2)} + \frac{\mu_2}{4}$$

and in equations (13) and (15) a simplification is possible using

$$\frac{c_{m2}}{a_{m2}} = \frac{\mu_3 - \mu_2}{\mu_3 + \mu_2}, \quad (m = 2, 4)$$

(ii) There are conducting materials in common use, such as copper and aluminium, that have permeabilities which differ little from that of free space μ_0. In particular if

$$\mu_1 = \mu_3 = \mu_5 = \mu_0, \quad \mu_2 = \mu_4 = (1 + k)\mu_0$$

with k small so that squares and higher powers are negligible, the inductance formulae reduce to simpler forms. That of equation (12) is immediately evident, whilst equations (13) and (15) respectively become

$$L_2 = \mu_0 k (r_4^2 - r_3^2)/4\pi r_3^2 r_4^2, \quad L_4 = \mu_0 k (r_4^4 - r_3^4)/8\pi r_3^4 r_4^4$$

It is noticed that if the system is non-magnetic, or the media have the same permeability, then $L_2 = L_4 = 0$, and the eccentricity of the system has no effect on its inductance.

(iii) In order to indicate the order of magnitude of the change in inductance due to the eccentricity of the system an hypothetical example is considered.

(*a*) Table 1 indicates the change in inductance due to increase in permeability of the current-carrying medium. It is assumed that $r_1 = r$, $r_2 = 2r$, $r_3 = 3r$, $r_4 = 4r$; $\mu_1 = \mu_3 = \mu_5 = \mu_0$, $\mu_2 = \mu_4 = \gamma\mu_0$, where γ varies from 0 to 5. When $\delta = r_3 - r_2 = r$, the inner tube is in contact with the outer tube, the inductance then being L_{max}. Table 1 gives values to $L_{max} - L_0$, being the maximum variation in the inductance.

An increase of permeability increases the variation in inductance with eccentricity. However, for this example the greatest variation is less than 4%, and a close approximation is given by $L_0 + \delta^2 L_2$.

Table 1. *Variation of inductance with permeability*

γ	L_0/μ_0	r^2L_2/μ_0	r^4L_4/μ_0	$(L_{max} - L_0)/\mu_0$
1·0	0·1076	0	0	0
2·5	0·1722	0·0038	0·0004	0·0042
5·0	0·2798	0·0076	0·0008	0·0084

(*b*) In order to determine the effect of the relative sizes of the tubes on the change of inductance (Table 2) an example is considered with $\mu_1 = \mu_3 = \mu_5 = \mu_0$; $\mu_2 = \mu_4 = 5\,\mu_0$; $r_4 = 4r$, $r_3 = 3r$, $r_2 = (\nu + 1)r$, $r_1 = \nu r$. Here ν varies from 0 to 1·5 as the size of the inner tube increases, its thickness $r_2 - r_1$ remaining invariant. Since $r_3 - r_2 = (2 - \nu)r$, then L_{max} is the value of L when $\delta = (2 - \nu)r$.

Table 2. *Variation of inductance with tube size*

ν	L_0/μ_0	r^2L_2/μ_0	r^4L_4/μ_0	$(L_{max} - L_0)/\mu_0$
0	0·4614	0·0071	0·0006	0·0380
0·5	0·3608	0·0073	0·0007	0·0199
1·0	0·2798	0·0076	0·0008	0·0084
1·5	0·2204	0·0080	0·0011	0·0021

As the internal diameter of the inner tube increases from zero the change in inductance decreases, and at most is less than 9%. It follows that for tubes of the same thickness the smaller the size the greater the change in the inductance as the eccentricity becomes more pronounced.

A numerical analysis will usually be required when the distance $r_3 - r_2$ is large, as in this case the third-order approximation will not give sufficient accuracy for large eccentricity of the system. This is evident from the example studied in (*b*) when $r_2 = 0{\cdot}5r$ and $r_1 = 0$. In this case

$$L/\mu_0 = 0{\cdot}5718 + 0{\cdot}0084(\delta/r)^2 + 0{\cdot}0011(\delta/r)^4 + \ldots$$

and L_{max} is the value of L when $\delta = r_3 - r_2 = 2{\cdot}5r$. Thus $(L_{max} - L_0)/\mu_0 = 0{\cdot}0945$, a change of more than 16%, successive approximations being 0·5718, 0·6242, 0·6663. Of course this is the most unfavourable situation, and eccentricities of this magnitude are not likely in practice.

REFERENCES

(1) Jones, E. E. *Brit. J. Appl. Phys.*, **7**, p. 56 (1956).
(2) Snow, C. *Nat. Bur. Stands. Circular* 544, p. 39 (1954).
(3) Craggs, J. W., and Tranter, C. J. *Quart. J. Appl. Math.*, **3**, pp. 268, 380 (1945–46).
(4) Craggs, J. W., and Tranter, C. J. *Quart. J. Math.* (Oxford Series), **17**, p. 138 (1946).
(5) Craggs, J. W. *Quart. J. Math.* (Oxford Series), **17**, p. 131 (1946).
(6) Stratton, J. A. *Electromagnetic Theory*, p. 25 (New York: McGraw-Hill Book Co. Inc., 1941).

Image fluctuations in cascade intensifiers

By L. MANDEL, Department of Physics, Instrument Technology, Imperial College, London, S.W.7

[*Paper first received* 15 *December*, 1958, *and in final form*, 26 *January*, 1959]

The root mean square fluctuation of the number of photons emitted from the output screen of a cascade image intensifier is calculated. It is shown that the percentage fluctuation exceeds that of the primary photoelectrons by a small factor depending on the light gain per stage.

In an image intensifier incident photons forming the primary image are allowed to eject photoelectrons from a photocathode, which are accelerated to strike a luminescent screen where they produce more photons. Since both the interactions are subject to statistical fluctuations, the intensifier contributes noise to the final image and it is therefore useful to have some idea of the magnitudes involved. In cascade intensifiers each stage contributes noise, although, as is well known, the later stages have progressively less effect. Expressions for the expected fluctuations of the final image in terms of the important system parameters are derived below. As might be expected, these fluctuations become appreciable only at very low light levels.

THE SINGLE-STAGE INTENSIFIER

Consider any interaction in which a primary particle gives rise to λ secondaries, where λ is a stochastic variate. Then n incident particles making independent interactions will give rise to μ secondaries such that:

$$\left.\begin{aligned} \bar{\mu} &= \bar{n}\bar{\lambda} \\ \text{and} \quad \overline{\Delta^2\mu} &= \bar{\lambda}^2\overline{\Delta^2 n} + \bar{n}\overline{\Delta^2\lambda} \end{aligned}\right\} \tag{1}$$

A bar is used to denote the average and the Δ the deviation from the mean. These relations, which are derived in the Appendix, hold whatever the probability distributions of n and λ.

Now consider a small area of the input and output surfaces of the image intensifier and apply relations (1) to the interactions at the photocathode and at the phosphor screen in turn. In the first case the primaries n are the photons striking the cathode and the secondaries μ the photoelectrons; $\bar{\lambda}$ is the quantum sensitivity of the cathode. In the second case the primaries are the photoelectrons μ and the secondaries are the luminescence photons N. If one photoelectron produces ν photons, then, from relation (1)

$$\left.\begin{aligned} \bar{N} &= \bar{\mu}\bar{\nu} \\ \text{and} \quad \overline{\Delta^2 N} &= \bar{\nu}^2\overline{\Delta^2\mu} + \bar{\mu}\overline{\Delta^2\nu} \end{aligned}\right\} \tag{2}$$

By eliminating μ we find:

$$\left.\begin{aligned} \bar{N} &= \bar{n}\bar{\lambda}\bar{\nu} \\ \text{and} \quad \overline{\Delta^2 N} &= \bar{\nu}^2\bar{\lambda}^2\overline{\Delta^2 n} + \bar{\nu}^2\bar{n}\overline{\Delta^2\lambda} + \bar{n}\bar{\lambda}\overline{\Delta^2\nu} \end{aligned}\right\} \tag{3}$$

The fluctuations of N can therefore be evaluated once the distributions of n, λ and ν are known. Now in any time interval likely to be encountered, the incident photons will obey a Poisson distribution[1] with

$$\overline{\Delta^2 n} = \bar{n} \tag{4}$$

The distribution $p(\lambda)$ of λ is very simple if only first-order interactions, in which one photon gives rise to one photoelectron, are considered. Then:

$$\left.\begin{aligned} p(\lambda) &= \sigma \quad \text{for} \quad \lambda = 1 \\ &= 0 \quad \text{for} \quad \lambda > 1 \end{aligned}\right\} \tag{5}$$

where σ is the quantum sensitivity of the cathode and $\sigma < 1$. Hence:

$$\left.\begin{aligned} \bar{\lambda} &= \sigma \\ \overline{\Delta^2\lambda} &= \sigma(1-\sigma) \end{aligned}\right\} \tag{6}$$

Little appears to be known about the fluctuations of ν, the number of luminescence photons. It has been shown[2] that the variance of the number of ions produced by an electron brought to rest is of the order half the mean number. The distribution of the much larger number ν of luminescence photons is unlikely to differ very greatly from the Poisson form. If

$$\overline{\Delta^2\nu} = k\bar{\nu} \tag{7}$$

where k is some number of the order 1, then, from relations (3), (4), (6) and (7),

$$\left.\begin{aligned} \bar{N} &= \bar{n}\sigma\bar{\nu} \\ \text{and} \quad \overline{\Delta^2 N} &= \bar{n}\sigma\bar{\nu}(\bar{\nu}+k) \end{aligned}\right\} \tag{8}$$

Now $\bar{\nu}$ will normally be a large number. Thus, for 20 kV electrons striking a zinc sulphide/silver luminescent screen, $\bar{\nu}$ can be as great as 1300.[3] It follows that, to a good order of approximation,

$$\overline{\Delta^2 N} = \bar{n}\sigma\bar{\nu}^2 \tag{9}$$

and the percentage fluctuation

$$\sqrt{(\overline{\Delta^2 N})}/\bar{N} = 1/\sqrt{(\bar{n}\sigma)} \tag{10}$$

As might be expected, the percentage output fluctuations exceed those of the incident photons by the factor $1/\sqrt{\sigma}$. For example, when the quantum sensitivity is 10% there is a threefold increase of the percentage fluctuations. There is no significant contribution from the second interaction, but the large multiplication factor $\bar{\nu}$ causes the distribution of the emitted photons N to depart strongly from the Poisson form. This result is of importance for multi-stage tubes, in which the output of one stage is the input for the next.

THE MULTI-STAGE INTENSIFIER

It is supposed that nearly all the photons emitted from one intensifier stage fall on the photocathode of the next stage. This can be achieved, for example, by depositing the phosphor and the photocathode on opposite sides of a thin glass or mica film.

Let N_r be the number of photons emitted at the rth intensifier stage. The input to this stage will be N_{r-1} photons with N_0 photons incident at the front end of the intensifier. On applying the relations (3), (6) and (7) to the rth stage one finds:

$$\left.\begin{aligned} \bar{N}_r &= G_r\bar{N}_{r-1} \\ \text{and} \quad \overline{\Delta^2 N_r} &= G_r^2\overline{\Delta^2 N_{r-1}} - \bar{N}_{r-1}G_r^2 + \bar{N}_{r-1}G_r(\bar{\nu}_r + k) \\ &= G_r^2\overline{\Delta^2 N_{r-1}} + G_r^2\bar{N}_{r-1}(1/\sigma_r - 1) \end{aligned}\right\} \tag{11}$$

provided $\nu_r \gg k$, as before. The suffix r refers to the rth

stage and the light gain $\sigma_r\nu_r$ of the stage is denoted by G_r. These are recurrence formulae for $\bar{N}_r$ and $\overline{\Delta^2 N_r}$. By repeated application:

$$\left.\begin{aligned}\bar{N}_r &= \bar{N}_0 \prod_{i=1}^{r} G_i \\ \text{and} \\ \overline{\Delta^2 N_r} &= \bar{N}_0 \prod_{i=1}^{r} G_i^2 + \\ &+ \bar{N}_0 \prod_{i=1}^{r} G_i \sum_{s=1}^{r} (1/\sigma_{r-s+1} - 1) G_r G_{r-1} \ldots G_{r-s+1}\end{aligned}\right\} \quad (12)$$

since the variance $\overline{\Delta^2 N_0}$ of the primary photons will be $\bar{N}_0$ as before.

If the light gains of the various stages are high, relations (12) can be simplified considerably, for the last term of the summation will then be the only important one. In that case:

$$\overline{\Delta^2 N_r} \simeq \bar{N}_0 (1/\sigma_1) \prod_{i=1}^{r} G_i^2 \quad (13)$$

and the percentage fluctuations

$$\sqrt{(\overline{\Delta^2 N_r})}/\bar{N}_r \simeq 1/(\sqrt{\sigma_1 \bar{N}_0}) \quad (14)$$

as for the single stage. Although the distribution of the emitted photons departs very strongly from the Poisson form, the percentage fluctuations are those of the primary photoelectrons.

If the light gain per stage is not high, these results are slightly modified. For simplicity, assume that all stages are identical, with $\sigma_1 = \sigma_2 = \ldots = \sigma$, $G_1 = G_2 = \ldots = G$, etc. Then, from relations (12),

$$\left.\begin{aligned}\bar{N}_r &= \bar{N}_0 G^r \\ \text{and} \qquad \overline{\Delta^2 N_r} &= \bar{N}_0 G^{2r}\left[1 + \left(\frac{1}{\sigma} - 1\right)\sum_{s=1}^{r} \frac{1}{G^{s-1}}\right] \\ &\simeq \bar{N}_0 G^{2r} \frac{1}{\sigma}\left(\frac{G}{G-1}\right)\end{aligned}\right\} \quad (15)$$

for moderate gains. The percentage fluctuations are therefor increased slightly and

$$\sqrt{(\overline{\Delta^2 N_r})}/\bar{N}_r \simeq \sqrt{\left(\frac{G}{G-1}\right)}\sqrt{\left(\frac{1}{\sigma \bar{N}_0}\right)} \quad (16)$$

This situation would arise, for example, if lens systems were used to couple the intensifier stages with resulting loss of gain. With $G = 6$, there is an 11% increase in the percentage fluctuations as compared with a high gain system having the same primary photocathode. The importance of achieving a high quantum sensitivity at the first cathode is obvious from all the results.

These conclusions are, of course, analogous to well-known results in the theory of electronic amplifiers and photomultipliers. Nevertheless, it must be remembered that the cascade image tube differs from these devices in that there are *two* stochastic interactions at each intensifier stage, of which the first leads to a loss of intensity.

In practice, as would be expected, the noise is significant only for very faint primary images. At normal light levels so many photons are incident, even in a short exposure, that the fluctuations are barely observable. However, with the development of multi-stage intensifiers the point is near where a single incident photon can produce a significant photographic or visual effect. The fluctuations of the images being studied are likely, therefore, to become increasingly significant.

REFERENCES

(1) MANDEL, L. *Proc. Phys. Soc. (London)*, **71**, p. 1037 (1958).
(2) FANO, U. *Phys. Rev.*, **72**, p. 26 (1947).
(3) MANDEL, L. *J. Sci. Instrum.*, **32**, p. 405 (1955).

APPENDIX

The fluctuations of the interaction products

Let $P(n)$ be the probability distribution of the n primary particles and let $p(\lambda)$ be the probability of obtaining λ secondaries from any one primary. If $\mathscr{P}_n(\mu)$ is the conditional probability that n primaries give rise to μ secondaries, then from first principles, provided the interactions are independent:

$$\mathscr{P}_n(\mu) = \sum_{\lambda_1=0}^{\infty} \sum_{\lambda_2=0}^{\infty} \ldots \sum_{\lambda_{n-1}=0}^{\infty} p(\lambda_1)p(\lambda_2) \ldots \\ \ldots p(\lambda_{n-1})p(\mu - \lambda_1 - \lambda_2 - \ldots \lambda_{n-1}) \quad (17)$$

where it is to be understood that $p(\lambda) = 0$ for any $\lambda < 0$. The conditional mean is therefore:

$$\begin{aligned}\bar{\mu}_n &= \sum_{\mu=0}^{\infty} \mu \mathscr{P}_n(\mu) \\ &= \sum_{\lambda'=0}^{\infty} \sum_{\lambda_1=0}^{\infty} \ldots \sum_{\lambda_{n-1}=0}^{\infty} (\lambda' + \lambda_1 + \ldots \lambda_{n-1}) \\ &\qquad \times p(\lambda')p(\lambda_1) \ldots p(\lambda_{n-1}) \\ &= n\bar{\lambda} \end{aligned} \quad (18)$$

where the substitution $\mu - \lambda_1 - \lambda_2 - \ldots \lambda_{n-1} = \lambda'$ has been used.

Hence $\bar{\mu} = \sum_{n=0}^{\infty} \bar{\mu}_n P(n)$ and, from equation (18)

$$= \bar{n}\bar{\lambda} \quad (19)$$

The conditional mean square follows similarly:

$$\begin{aligned}\overline{\mu_n^2} &= \sum_{\mu=0}^{\infty} \mu^2 \mathscr{P}_n(\mu) \\ &= \sum_{\lambda'=0}^{\infty} \sum_{\lambda_1=0}^{\infty} \ldots \sum_{\lambda_{n-1}=0}^{\infty} (\lambda' + \lambda_1 + \ldots \lambda_{n-1})^2 \\ &\qquad \times p(\lambda')p(\lambda_1) \ldots p(\lambda_{n-1}) \\ &= n\overline{\lambda^2} + n(n-1)\bar{\lambda}^2 \end{aligned} \quad (20)$$

so that

$$\begin{aligned}\overline{\mu^2} &= \sum_{n=0}^{\infty} \mu_n^2 P(n) \\ &= \bar{n}\overline{\lambda^2} + (\overline{n^2} - \bar{n})\bar{\lambda}^2 \end{aligned} \quad (21)$$

Hence

$$\begin{aligned}\overline{\Delta^2 \mu} &= \overline{\mu^2} - \bar{\mu}^2 \\ &= \bar{\lambda}^2(\overline{n^2} - \bar{n}^2) + \bar{n}(\overline{\lambda^2} - \bar{\lambda}^2) \\ &= \bar{\lambda}^2 \overline{\Delta^2 n} + \bar{n}\overline{\Delta^2 \lambda} \end{aligned} \quad (22)$$

Correspondence

Electrical determination of the thermal parameters of semiconducting thermoelements

In a recently published letter, Harman* showed how the Peltier effect in a semiconductor can be used to determine the heat conductivity. However, a difficult point in heat conductivity determination is the measurement of local temperature. This problem is eliminated in the procedure described below; only the mean temperature of the semiconductor must be measured.

It can be shown that from the observation of the time dependence of the electrical potential difference across a sample, due to its own thermoelectric force, the thermal conductivity, thermal capacity and electrical conductivity may be obtained, the Seebeck coefficient being determined more accurately in another experiment.

Let us consider a sample of length $2l$ and uniform cross-section S characterized by a thermoelectric force α, a thermal conductivity K and a thermal capacity per cubic centimetre C. Two copper electrodes, so thin that their heat capacity may be neglected, are soldered to the ends of the sample. Let the current flowing through the sample be i, the Peltier heat is then equal to αiT. The current used is small enough for the Joule heat to be negligible and for the temperature difference between the ends at equilibrium to be so small (of the order of $0{\cdot}3^\circ$ C) that both α and αiT may be regarded as constant along the sample. The sample is considered to be thermally insulated.

Under these conditions the heat equation may be solved. The heat equation is

$$\frac{\partial T}{\partial t} = \frac{K}{C}\frac{\partial^2 T}{\partial x^2} \quad \text{or} \quad \frac{\partial \theta}{\partial t} = D\frac{\partial^2 \theta}{\partial x^2} \tag{1}$$

if we put $\theta(x, t) = T(x, t) - T_0$ and $D = K/C$. The boundary conditions are:

$$\theta(x, 0) = 0 \quad \text{(the sample is isothermal at time } t = 0) \tag{2}$$

$$\theta(0, t) = 0 \quad \text{(the centre of the sample is chosen as origin)} \tag{3}$$

$$\frac{\partial \theta(l, t)}{\partial x} = \frac{\alpha i T}{KS} = \frac{\alpha i T_0}{KS} = a \text{ [heat flux at the end } (x = l) \text{ due to Peltier effect, is constant]} \tag{4}$$

By a Laplace transformation the heat equation becomes $D(\partial^2\bar{\theta}/\partial x^2) = p\bar{\theta}$; its solution is

$$\bar{\theta} = P_1 \exp(q x) + P_2 \exp(-q x) \quad \text{with} \quad q^2 = p/D \tag{5}$$

Conditions (3) and (4) give

$$\bar{\theta}(x, p) = \frac{a}{pq}\,\frac{\exp[-q(l - x)] - \exp[-q(l + x)]}{1 + \exp(-2ql)} \tag{6}$$

which can be expanded into

$$\bar{\theta} = (a/pq)\sum_{n=o}^{\infty}(-1)^n\left(\exp\{-q[(2n + 1)l - x]\} - \exp\{-q[(2n + 1)l + x]\}\right) \tag{7}$$

Now $(pq)^{-1}\exp(-qy)$ is the transformation of

$$2(Dt/\pi)^{\frac{1}{2}}\exp(-y^2/4Dt) - y\,\text{erfc}\,[(4Dt)^{-\frac{1}{2}}y]$$

and thus we have finally

$$\theta = 2a(Dt/\pi)^{\frac{1}{2}}\sum_{n=o}^{\infty}(-1)^n\left[\exp(-y_-^2/4Dt) - \exp(-y_+^2/4Dt)\right] - a\sum_{n=o}^{\infty}(-1)^n\left\{y_-\,\text{erfc}\,[(4Dt)^{-\frac{1}{2}}y_-] - y_+\,\text{erfc}\,[(4Dt)^{-\frac{1}{2}}y_+]\right\} \tag{8}$$

where $y_- = (2n + 1)l - x$ and $y_+ = (2n + 1)l + x$

The temperature of the hot junction as a function of time is

$$\theta(l, t) = 2a\sum_{n=o}^{\infty}(-1)^n\Big((Dt/\pi)^{\frac{1}{2}}\{\exp[-n^2l^2/Dt] - \exp[-(n + 1)^2l^2/Dt]\} - l\{n\,\text{erfc}\,[nl/\sqrt{(Dt)}] - (n + 1)\,\text{erfc}\,[(n + 1)l/\sqrt{(Dt)}]\}\Big) \tag{9}$$

The temperature difference between the two ends of the sample is $2\theta(l, t)$ and is measured by the thermoelectric part of the electrical potential difference. It may be seen that $\theta(l, t)$ increases monotonically with time and has the limit $\theta(l, \infty) = al = \alpha iTl/KS$. For $t = \infty$ the thermoelectric part of the electrical potential difference (V_T) between the ends of the sample is given by

$$V_T(\infty) = 2\alpha\,\theta(l, \infty) = 2\alpha^2 Til/KS$$

and thus one can write, by introducing

$$l^{-1}\sqrt{(Dt)} = \tau = l^{-1}\sqrt{(tK/C)}$$

$$V_T(t)/V_T(\infty) = (4\tau/\sqrt{\pi})\left[\tfrac{1}{2} - \exp(-1/\tau^2) + \exp(-2^2/\tau^2) - \exp(-3^2/\tau^2) + \ldots\right] + 4\left[\text{erfc}\,(1/\tau) - 2\,\text{erfc}\,(2/\tau) + 3\,\text{erfc}\,(3/\tau) - \ldots\right] \tag{10}$$

The two series converge rapidly if τ is small; measurement of $V_T(t)/V_T(\infty)$ gives τ and hence K/C. The value of $\tau/2 = L^{-1}\sqrt{(tK/C)}$ ($L = 2l$ = total length of the sample) which

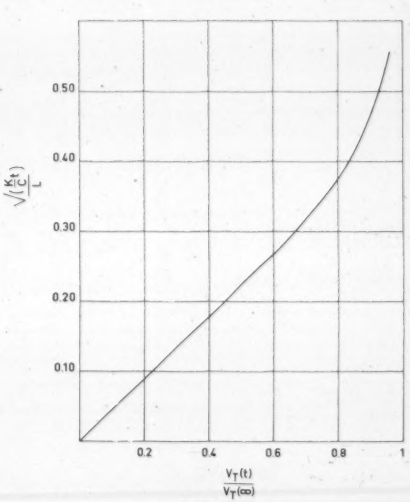

Fig. 1. The ratio $V_T(t)/V_T(\infty)$ as a function of $\tau/2$

* HARMAN, T. C. *J. Appl. Phys.*, **29**, p. 1373 (1958).

gives $V_T(t)/V_T(\infty) = 1/2$ is $\sqrt{\pi}/8 = 0{\cdot}222$, since up to this point the function is fairly linear, as may be seen from Fig. 1.

The determination of K on the same sample is very easy by use of the equation

$$\alpha i T = 2\theta\,(l, \infty)\; KSL^{-1} = V_T(\infty)\; KS\,(\alpha L)^{-1} \qquad (11)$$

and it is thus possible to measure simply and accurately the

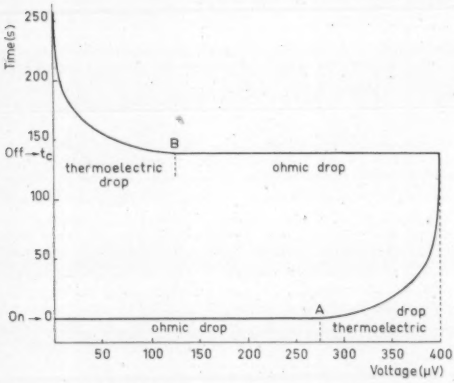

Fig. 2. The electrical potential difference between the ends of a sample as a function of time with constant current flowing through the sample

thermal capacity per cubic centimetre of the material, α being determined independently.

With a sample of bismuth telluride, 2 cm long and $0{\cdot}2$ cm^2 cross-section, the stationary state is practically obtained after 2 min. It may be shown that if after this time, the current is cut, the temperature difference and thus V_T vanishes according to

$$(\alpha aL)^{-1} V_T(t_C + t) = 1 - (\alpha aL)^{-1} V_T(t) \qquad (12)$$

where t_C is the time at which the current has been cut off. Thus the potential difference at the ends of the sample with the current on is the mirror image of the potential difference with the current off. This conclusion is very well verified by the experiments (Fig. 2).

The points A and B, corresponding to the switching on and the switching off, are difficult to locate exactly on the graph, but the fact that the beginning of the recorded curves are parabolas enables one to use a net of parabolas with common axis and vertex; the superposition of this on the curve gives a good location of points A and B.

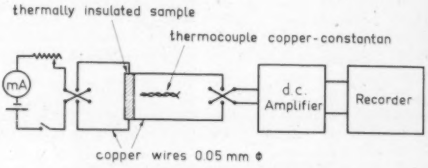

Fig. 3. Experimental arrangement

The "quality factor" $Z = \alpha^2\sigma/K$ of the sample is immediately given by the ratio of thermoelectric to ohmic drop, which is equal to $\alpha^2\sigma T/K$. The determination of σ is obviously given by the measurement of the ohmic drop Ri.

In practice, the circuit given in Fig. 3, which is calibrated with a potentiometer before each experiment, is used.

Financial support for this work was provided by the Union Carbide Corporation.

European Research Associates, S.A.,
95, Rue Gatti de Gamond,
Brussels, Belgium.

C. HÉRINCKX
A. MONFILS

[12 *December*, 1958]

Journal of Scientific Instruments

Contents of the May issue

SPECIAL ARTICLE

The Physical Society's Exhibition—London, 1959. By R. V. Jones.

ORIGINAL CONTRIBUTIONS

Papers.

Quick-acting chemical balance. By B. O. Smith and J. W. Stevens.
Geiger counter hodoscope with automatic testing. By H. S. Murdoch and H. D. Rathgeber.
Monitored Geiger counter X-ray diffractometer with automatic recording. By E. R. Pike and J. W. Hughes.
Galvanometer feedback systems. By J. A. Sirs.
Interferometer based on four diffraction gratings. By F. J. Weinberg and N. B. Wood.
High-resolution nuclear resonance apparatus. By J. B. Leane, R. E. Richards and T. P. Schaefer.
Illuminant for the colorimetry of fluorescent materials. By W. Harrison.
Automatic correction for paralysis in Geiger counting. By R. Hunt.
Controlled atmosphere levitation system. By B. Harris and A. E. Jenkins.
Infra-red absorptiometer, using interference filters, for analysis of hydrogen fluoride in gaseous mixtures. By J. A. Harrison and C. D. Reid.

Laboratory-aid workshop notes

Electrical method for detection of transition of atomization type in centrifugal atomizers. By D. J. Ryley.
Optical joint for horizontal mounting of a large scintillation crystal. By G. L. Olde and E. Brannen.
Acid machining of cylindrical crystals. By T. Broom and J. M. Summerton.

Correspondence

Obliquity corrections in transmission interference microscopes. From E. Ingelstam, L. P. Johansson and C. F. Bruce.
A method of producing eddy-current heating. From R. J. Armstrong.

NOTES AND NEWS

New instruments, materials and tools
Notes and comments

THIS JOURNAL is produced monthly by The Institute of Physics, in London. It deals with all branches of applied physics (including theory and technique). All rights reserved. Responsibility for the statements contained herein attaches only to the writers.
EDITORIAL MATTER. Communications concerning editorial matter should be addressed to the Editor, The Institute of Physics, 47 Belgrave Square, London.S.W.1. (*Telephone:* Belgravia 6111.) Prospective authors are invited to prepare their scripts in accordance with the *Notes for Authors*. (Price 3*s*. 6*d*. including postage.)
REPRODUCTION. The Institute of Physics is a signatory to The Royal Society's Fair Copying Declaration. Details may be obtained upon application from The Royal Society, London, W.1.
ADVERTISEMENTS. Communications concerning advertisements should be addressed to the agents, Messrs. George Jackson (Fleet St.) Ltd., Cliffords Inn, Fleet Street, London, E.C.4. (*Telephone:* Holborn 3611-2.)
CLAIMS FOR MISSING JOURNALS. Claims from regular subscribers to this *Journal* for missing numbers will only be considered if received within 60 days of the date of mailing plus normal outward time of transit and time for lodging the claim. Losses attributable to failure to notify a change of address or to similar omissions will not be considered.
SUBSCRIPTION RATES. A new volume commences each January. The charge is £6 per volume ($17 U.S.A.), including index (post paid), payable in advance. Single parts, so far as available, may be purchased at 12*s*. 6*d*. each ($1.75 U.S.A.), post paid, cash with order. Orders should be sent to The Institute of Physics, 47 Belgrave Square, London, S.W.1, or to any bookseller.

CONFERENCE REPORT

Summarized proceedings of a conference on nuclear fuel cycles—London, January 1959

A conference on nuclear fuel cycles, organized by The Institute of Physics in collaboration with the British Nuclear Energy Conference, was held in London on 22 and 23 January, 1959. The papers presented, and the discussion on them, are summarized in this report. A full proceedings will appear in the *Journal of the British Nuclear Energy Conference* for July.

INTRODUCTION

The conference was opened by Sir GEORGE THOMSON, President of The Institute of Physics. He welcomed the 250 delegates, and was, he said, particularly glad to see so many from European countries. Nuclear power stations had been shown to be feasible but they now had to stand their ground financially in competition with power from coal and oil. High efficiency in the use of uranium fuel could only be achieved by employing suitable fuel cycles. To determine the optimum form of cycle was a very complicated problem but, with five nuclear power stations under construction in Great Britain, it was also an urgent one. He hoped that the conference would lead to a fruitful exchange of ideas.

The conference was restricted to "once through" fuel-cycles (i.e. without reprocessing) in natural uranium, graphite, moderated systems. It consisted of three sessions, the first of which was concerned with the basic data and reactor theory involved in the design of fuel cycles. Dr. DUNWORTH, Assistant Director of A.E.R.E., Harwell, was Chairman for this session.

BASIC DATA AND REACTOR THEORY

The first paper was by Dr. H. ROSE and Mr. J. J. SYRETT (U.K.A.E.A., Harwell). Dr. Rose described the changes in isotopic composition of uranium caused by irradiation. He stressed that in a reactor using natural uranium the loss of reactivity caused by destruction of ^{235}U and growth of fission products is so closely compensated by the gain in reactivity caused by the growth of ^{239}Pu that very accurate data would be necessary to calculate the resulting balance of reactivity. [As was pointed out by Mr. MUMMERY (U.K.A.E.A., Harwell) in the discussion, the accuracy required for basic data is in the range $\pm 0{\cdot}1\%$ to $\pm 1\%$.] Such data are not available and reliable predictions of reactivity changes must therefore be based on measurement of the reactivity of irradiated fuel rods. The measurements are made by the pile oscillator method in the reactor GLEEP at Harwell and give an approximation to the "point" reactivity curve. The "point" reactivity for a given irradiation is the reactivity of a reactor in which all the fuel has that irradiation. This curve had been analysed by means of a two-group model and data adjusted, where necessary, to give a fit with the measurements. This same model and data could then be used to extrapolate from the changes as observed in the neutron spectrum in GLEEP to that in a power reactor. Mr. Mummery mentioned later that these extrapolated results had been compared and reasonable agreement obtained with measurements of the reactivity changes in the Calder Hall reactors made by Dr. F. M. Leslie, who used control rod movement during irradiation to estimate reactivity changes. Dr. Rose explained a series of slides showing the effect on the "point" reactivity curve of varying conversion factor, enrichment, neutron temperature and neutron spectrum. An important parameter derived from the "point" reactivity curve for a fuel element is the equal area point, which is the irradiation value for which the mean reactivity of a fuel element over its life is the same as its initial reactivity. Mr. Syrett said that a typical value for this is about 5000 MWD/Te. He also replied to questions on the uncertainty in this value arising from experimental errors, variations in environment, and extrapolation to different conditions during irradiation, and said that it could be as high as 20%. This is a figure worth bearing in mind when considering the appropriate degree of sophistication of the mathematical approaches. Without pile oscillator measurements the uncertainty would be greater. The equal area value is a direct measure of the efficiency of fuel, provided that fuel elements can be irradiated to this level without failure.

Mr. HUTBER (U.K.A.E.A., Harwell) raised the question of screening of the resonance in ^{240}Pu. Mr. Syrett agreed that the amount of ^{240}Pu produced at high irradiation levels was sufficient to cause considerable screening, but that there were compensating effects. Calculations, which took account of these effects, had been done at Chalk River and were in general agreement with U.K. results.

Mr. S. E. LEWIS (The Nuclear Power Plant Co. Ltd., Knutsford, Cheshire) then gave a paper on the theory of once-through fuel cycles. This is the type of cycle in which the irradiation position of a fuel element may be changed but is not returned to the reactor after chemical processing. The total irradiation may not be the same for all elements. A system in which each element may be irradiated at several positions in the same channel is called axial shuffling, and a system in which each element may be irradiated in several channels is called radial shuffling.

Mr. Lewis considered a once-through fuel cycle in which fuel is replaced continuously at a rate dependent on the rating at each point. He showed that in this case the most efficient distribution of irradiation received by a slug before removal was $\propto \frac{1}{\sqrt{\phi}}$ but that equal irradiation for all slugs was a good approximation. Relative to these an irradiation proportional to flux, as occurs in a bulk discharge system, was only 75% efficient. Using the approximation that change in "point" reactivity y depends on irradiation x according to $y = ax - bx^2$, he deduced the channel reactivity and used this to compare bulk discharge with continuous push-through fuelling from the ends or centre. The latter systems are some 40% more efficient.

Mr. Lewis gave the theoretical treatment of the question

of delayed onset of fuelling for a once-through cycle. He went on to show that an axial inversion scheme, though involving more handling, allowed a smaller range of irradiations and so was an advantage if the limit to maximum irradiation was metallurgical. As was emphasized by other speakers, the existence of a metallurgical limit is an incentive to use fuel cycles even apart from that given by the form of the variation of reactivity with irradiation. The problem of delayed onset in general aroused considerable discussion later in the symposium.

A paper by Dr. J. G. BALFOUR, Dr. D. L. BOOTH and Mr. R. S. BULLOCH (Atomic Power Projects, Whetstone, Leicester) gave the theory of perturbations of flux distribution caused by running a reactor. The first part of this paper, presented by Dr. Booth, gave a one-group theory of the axial perturbation of flux due to start-up of a reactor from the cold condition where the flux, but for variation in Wigner gaps, would be symmetrical. A series solution of the perturbed diffusion equation was used to give axial flux plots for various irradiations in steps of 285 MWD/Te channel average. The same method was used to give the perturbations resulting from axial shuffling of the type where the end slugs in a channel are replaced in the centre and *vice versa*. This is known as axial inversion. In these calculations Dr. Booth had ignored the fact that the perturbations in flux cause perturbations of temperature which have a secondary effect on flux. The effect of neighbouring channels had also been ignored. He described, in the second part of the paper, a calculation which included this "feedback" due to distortion of the temperature distribution. The basis was still that of one-group diffusion theory applied to an isotropic medium. Despite these simplifications the method involved the solution of some 500 simultaneous non-linear, differential equations by means of an electronic computer. This indicates how complex an exhaustive treatment of fuel cycles would be. Again, flux plots were given for various irradiations. Dr. Booth, replying to questions, said that the simple diffusion theory was sufficient to make comparisons between fuel cycles. Transport theory would be much more difficult to use and was probably not justified—at least at that stage.

In further discussion it was argued that the axial distribution of heat output was more biased than the flux distribution, and that there were advantages to be gained in shaping the flux distribution to increase the heat production possible from a channel for a given maximum can temperature. Dr. Booth said that simply inserting control rods from the coolant exit face (as at Calder Hall) tended to have this effect. He agreed to a suggestion that his analysis would be altered by flux rises at the ends of rods but pointed out that this effect was smaller in a hot reactor than in a cold one because of the decrease in absorption. The optimum fuel cycle depends on whether the metallurgical limit is greater or less than the reactivity limit and Mr. Hutber raised the point of whether one starts off the cycle assuming that there is no metallurgical limit since this limit cannot be accurately predicted. Mr. R. A. PEDDIE (Central Electricity Generating Board, London) pointed out that once the reactor had been built, the design of the installed charge/discharge machine limited the number of possible fuel cycle schemes.

OPTIMIZATION OF FUEL CYCLES

These practical questions anticipated the next session, on optimization of fuel cycles, for which the Chairman was Mr. L. ROTHERHAM of the Central Electricity Generating Board. The first paper was by Mr. P. R. J. FRENCH (A.E.I., Aldermaston) and Mr. C. S. LOWTHIAN (John Thompson Nuclear Energy Co. Ltd., Knutsford, Cheshire). Mr. French, who presented the paper, simplified long-term reactivity changes by considering only changes in ^{235}Pu, ^{239}Pu and ^{240}Pu. He justified this approach as being sufficiently accurate for comparison of fuel cycles which, under these conditions, was amenable to fairly simple mathematical analysis. He deduced that in this simplified case the change in the reactivity was of the form $Lx + Mx^2$ where x is the "burn up" of ^{235}U and L and M are combinations of nuclear constants. This form was used by other speakers. His diagrams illustrated quantitatively how attempts to increase k_∞ always led to a decrease in "burn up" assuming no initial excess reactivity. The calculated reactivity curves of Rose and Syrett shown in Session I had also indicated this tendency, basically due to absorption in ^{238}U being a loss of neutron economy but leading to the production of fissile ^{239}Pu. It appeared in discussion, between Mr. Lowthian and Mr. Syrett, that there was nevertheless an incentive to design for maximum k_∞, since an initial excess reactivity markedly increased the "equal area point" irradiation. The effect on capital costs of a change of lattice parameters was also important. Mr. French went on to consider whether excess reactivity would be best used to increase fuel life or to flatten the flux distribution. He also showed how to calculate the optimum allocation to flattening in a typical specific case. As mentioned by Mr. Syrett and Dr. BARDEN the two need not be mutually exclusive if fuel were left in the flattened region long enough to act as an absorber. The metallurgical limit would have to be high and was taken as infinite in Mr. French's analysis. Mr. Lowthian made the point that the reactivity has a peak value (at $\sim$1000 MWD/Te) which can be regarded as a design tolerance, since the reactivity can be employed in a number of ways. As was later mentioned by Mr. DRUMMOND (Babcock and Wilcox Ltd., London) some of this excess reactivity might be needed for absorbers to maintain stability and flexibility of operation in the presence of a positive temperature coefficient. Mr. Hutber raised the point of whether it was worth while to use enrichment to obtain this excess reactivity.

A paper by Dr. P. J. GRANT, Mr. W. OSWALD and Mr. P. D. D. RUSSELL (Atomic Energy Division, General Electric Co. Ltd., Erith, Kent) was on the same subject but treated from a more financial viewpoint. Dr. Grant said that in contrast to the preceding paper, their own started from the assumptions of shuffling and of a metallurgical limit less than the reactivity limit. He gave a warning of the dangers of planning fuel cycles in isolation. Practical considerations of load factor, interest rates and safety were likely to be important considerations. The question of safety was stressed by Dr. G. DAVIS (Commissariat a l'Energie atomique, Tel Aviv, Israel), who said that in a small country relying on a few reactors or even a single reactor, delay caused by difficulties in fuel cycling would be most unwelcome and an accident could be catastrophic. Mr. K. P. GIBBS (Central Electricity Generating Board, London) agreed that this would be so, and for that reason great care had been taken in the design of the charge/discharge machines. It did not mean, however, that it would be better not to employ fuel cycles since, to obtain an interrupted power output, it was necessary to load and unload at power and, having these facilities, it was economical to use them for fuel cycling. Dr. Grant introduced some further factors into the question of whether to design for maximum k_∞, by pointing out that a small system (with higher leakage) had smaller

capital costs. Absorbers used as flatteners improved neutron economy in the financial sense, which he regarded as the correct way to use the term. He stressed the usefulness, in optimizing designs, of a parameter that he called the cost of neutrons. He discussed the purchase price, and market values, of several fuels in some detail and came to the conclusion that enrichment was unlikely to be economic in the current design of power reactor. He pointed out that even if a high metallurgical limit allowed a high burn up, this would result in a lower market value of the irradiated element because the ^{239}Pu would be poisoned by ^{240}Pu. He showed by simple arguments that a delayed onset of fuelling was of no advantage in a once-through system, but several speakers pointed out that this was not true for systems employing shuffling or intermittent delay schemes in which, in principle, a gain of up to half a charge could be achieved. Dr. Grant's approach was to optimize the overall fuel cost but this led him to such a complicated problem that his discussion was rather qualitative. Mr. French optimized on the use of fissile material which allowed a more exact approach but was more divorced from reality. Mr. Hutber suggested that the ideal approach would be a compromise between these two. Mr. Syrett asked whether it was better to use a simplified model and optimize mathematically (as Mr. French had done) or to do full calculations for some thousands of reactor designs using a computer and choose the optimum version. Mr. Lowthian suggested that a combined approach would be ideal, in which the number of possibilities was reduced by the first method and remaining uncertainties settled by a detailed study of the second type. Two important points concerning the metallurgical limit were made. Mr. G. E. Darwin (Babcock and Wilcox Ltd., London) said that the limit was not fixed but, for a given design, depended markedly on the temperature history and on the stresses involved in handling during shuffling. The chairman, Mr. Rotherham, emphasized that the metallurgical limit could be as high as one liked if paid for in terms of absorption of neutrons in the can. Thus this limit was also a compromise between conflicting factors.

PROBLEMS IN OPERATING FUEL CYCLES IN POWER REACTORS

Professor J. Diamond (University of Manchester) then took the chair for the final session on problems likely to be encountered in operating fuel cycles in power reactors. A paper by Mr. J. C. C. Stewart and Dr. N. L. Franklin (U.K.A.E.A., Harwell) began by comparing the rapid rate of technological advance in nuclear engineering with that usually found in industries where large capital investments were involved. Capital costs would account for three-quarters of the cost per unit of electricity from nuclear power stations. By outlining a possible testing programme they showed that it would take many years to test a fuel element on load and even then the statistical accuracy of the results obtained would be poor. Also, the fuel element design would probably be constantly changing and it would be hard to decide whether a full test of a new fuel element would be economic. In a reactor operating on a fuel cycle it might be several years before a charge was completely replaced by a new type with a corresponding delay before the improved performance of the new type could be exploited. It was generally agreed that very few bursts could be allowed without seriously affecting the efficiency of the reactor, yet choosing an unduly short irradiation could lead to extra expenditure on fuel in the region of £1 000 000. Such a decision also affected the amount of chemical processing plant which would be necessary.

The varying feed to such a plant also raised problems of efficiency and safety. Mr. Hutber used this argument to plead for an integrated approach to fuel cycles in the various civil reactors. Dr. Franklin elaborated a point made in general terms by Dr. Dunworth that the problems were so complex that the practical solution could only be approached gradually as operational experience accumulated. Dr. C. P. Haigh (Central Electricity Generating Board, London) agreed and, approaching the problem from the point of view of the user of fuel, was against any move which jeopardized the status of nuclear power stations as reliable suppliers of base load requirements. He therefore argued that delayed onset, which made the discharge machines work, for a time, at the limit of their capacity, was inadvisable. (Any difficulty at that time would cause a shutdown.) For similar reasons he was in favour, at least initially, of schemes with no fuel shuffling. As an indication of the need for reliable operation of the reactor as a whole, and in particular of the discharge machines, he said that a shutdown might cost the Generating Board £8000 a day, by forcing them to use less efficient plant. Such a shutdown could be caused by a detail such as a faulty seal on the discharge machine. Dr. W. Stanners (The English Electric Co. Ltd., Leicester) suggested a compromise solution of the delayed onset problem, in which the under-irradiated first charge would be used to fuel another reactor. Dr. Franklin added that this would at the moment only be possible if no reprocessing were involved. It was also likely to be uneconomic.

CONCLUSIONS

Mr. P. W. Mummery (U.K.A.E.A., Harwell) made the closing remarks. He said that the aim of the conference, which was to show the implications of physics on the various requirements of fuel cycles and their interdependence, had been achieved. These requirements involve metallurgy, heat transfer, economics, engineering and other subjects. The conference had shown that the physics and metallurgy of the systems cannot be separated. Reactor physics predicts the criticality conditions and the distribution of heat sources in a reactor; it also deals with the dynamics of the system. It was mainly the first two factors which had been covered in the conference. The main aims of the operators would be low fuel costs and reliable operation, and these were best approached by using simple fuel cycles in the first case. With possible savings of a factor of two, the designers would have considerable financial incentives to try new and more complex systems of fuelling. The design of equipment would have to be flexible and anticipate developments so that it could gradually be brought into full use, as techniques proved their worth. Mr. Mummery looked forward to three years hence when experience with reactors of several different designs would be available. That time, he suggested, would be suitable for another conference on fuel cycles.

United Kingdom Atomic Energy Authority,
A.E.R.E., Harwell.

W. A. Cooper

Determination of the size of defects by the ultrasonic impulse echo method*

By J. KRAUTKRÄMER, Cologne

[*Paper first received* 22 *December*, 1958, *and in final form* 20 *February*, 1959]

Much to the detriment of ultrasonic testing and all attempts at standardization, it is not yet possible to compare the results from different kinds of equipment regarding the echo of a back wall or a small defect. In order to facilitate this, the relations between echo height, distance and size of circular disk defect are brought into simple and universally applicable forms. It is shown that the first back echo of a simple plate is the most convenient reference echo. With the help of a calibrated gain control as accessory to a usual flaw detector and a graphical representation of the formulae, an equivalent circular disk defect can be attributed to the actual defect.

The influence of curved contact and back wall surfaces, and the application of the method for determining ultrasonic attenuation in thick specimens, is discussed.

The detection of a small defect in a specimen by the ultrasonic impulse echo method is fairly easy. To estimate its size is a much more difficult problem. The most comprehensive information about a defect would be given by measurement of the amplitude after reflexion of the whole reflected or scattered beam, when the reflected beam is measured over as large an angle as possible. Further information could be given by the phase of the reflected wave at selected points, and also by measurement of the transverse wave pattern, which is produced when longitudinal waves are used and *vice versa*. Such a method would require a second small receiver probe, and the difficulties of coupling this probe to the specimen could probably be overcome with simple shaped pieces and immersion testing.

Because this method requires much time for measurement and calculation, and also because the instruments have not yet been developed, a method of comparing the flaw with a flat bottom hole perpendicular to the beam axis will be mentioned. Only in favourable cases can one get an indication of the real defect size by this method. Normally, it only gives an idea of the minimum size.

The method has been practised for some time and, in order to apply it generally, a large number of test blocks is necessary. They must be of the same material as the specimen and graded according to hole diameter and distance from the surface. In the case of large forgings this would mean a very costly and complicated provision. This collection of test pieces can be avoided by using one single, very simple, reference block which will provide a quick method in the far zone for all types of equipment and probes. Moreover, one can amend the method for the near zone and also for specimens with curved surfaces and consisting of materials of different absorption.

Fig. 1 shows the sound pressure amplitude along the axis of the beam from a circular crystal oscillating like a piston. In practice, the maxima and minima in the near zone are flattened out considerably because of deviation from the ideal piston form of oscillation, and because interference is restricted when short pulses are used.

The well-known law of sound pressure along the axis is

$$P = 2P_0 \sin\left[\frac{\pi}{\lambda}\left\{\sqrt{\left(\frac{D_s^2}{4} + a^2\right)} - a\right\}\right] \qquad (1)$$

where λ is the wavelength, D_s the diameter of the vibrating crystal and a the distance along the axis. The amplitude factor P_0 can be taken to be the average pressure immediately in front of the crystal when the crystal is much larger than the wavelength. For the distant field, i.e. for large distances of a compared with the diameter D_s and with the near field length of the probe, N, where $N = D_s^2/4\lambda$, equation (1) may be approximated as follows:

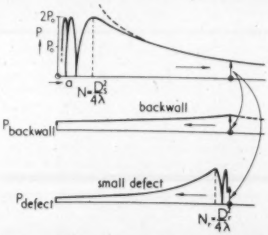

Fig. 1. Sound pressure amplitude on the axis of a piston oscillator and reflected sound pressure by the back wall and a small circular reflector at large distance

$$P \simeq P_0\, \pi\, (N/a) \qquad (2)$$

It is convenient to measure the distance in terms of the near field length, i.e. to use the "reduced defect distance" $A = aN$.

Therefore

$$P \simeq P_0\, \pi/A \qquad (3)$$

The near field of the probe is considered as an important and well-known characteristic.

A very large flat defect or a flat back wall will reflect the beam like a mirror, and the probe then acts as a microphone to its own beam at twice the back wall distance. It will measure uniform sound pressure over the whole of its surface

$$P_{back\ wall} = P_0\, \pi/2A \qquad (4)$$

If now a small, circular and completely reflecting disk is placed in the axis of the beam at so great a distance that the sound pressure $P_0\, \pi/A$ is uniform over its surface, then this

* Based on a lecture given before the Non-Destructive Testing Group of The Institute of Physics on 12 December, 1958.

may be regarded as the initial pressure of a new radiator which reradiates a similar wave back to the probe. The probe itself will therefore measure as echo:

$$P_{defect} = (P_0\,\pi/A)\,(\pi\,N_r/a) \qquad (5)$$

where $N_r = D_r^2/4\lambda$ is the near-field length of the reflector (defect), the diameter of which is D_r. If the defect size is measured in terms of the diameter of the probe one obtains the "reduced defect size" G where $G = D_r/D_s$ and equation (6) can be simplified to:

$$P_{defect} = P_0\pi^2\,(G^2/A^2) \qquad (6)$$

Equations (4) and (6) express no more than the well-known facts that: for sufficiently large distances from the probe the back wall echo decreases inversely with the distance; and the defect echo is proportional to the square of the defect diameter (i.e. proportional to its surface area) and inversely proportional to its distance. In this form they can be represented graphically for a quick solution of the problem. It must be pointed out, however, that this only applies to the far zone and as long as the wavelength is not larger than the diameter of either the probe or the defect.

To apply equation (6) in practice one has to measure the ratio P_{defect}/P_0. The unknown value of P_0 could be got from an application of equation (4) to a specimen of the same material and surface conditions, but without any defects and with a back wall normal to the beam at a distance large compared with the near zone of the probe. Also one must suppose that no absorption is involved. These are troublesome limitations, which can be avoided if P_0 is taken to be the average of the sound pressure immediately in front of the probe, but within the material under consideration. This is equivalent to saying that the back wall echo of a very thin plate is equal to P_0, the more so the thinner the choice of plate. Now very thin plates cannot be used with the single probe method because of the dead zone, i.e. the range of distance covered by the transmitter pulse and the jamming of the amplifier. But if plates of varying thickness are measured, as shown in Fig. 2, it is found that there is not much error if P_0 is measured as first back wall echo of a somewhat thicker plate, provided that it is thinner than the near-field length.

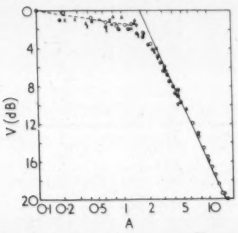

Fig. 2. Height of back echo *versus* distance for different crystal diameters, frequencies and distances in water and steel. Gain V in dB *versus* distance A in multiples of near-field depth and in logarithmic scale

○ = 8·5 mm crystal, 4·0 Mc/s in water
● = 24 mm crystal, 2·0 Mc/s in water
× = 24 mm crystal, 4·0 Mc/s in steel
□ = 17 mm crystal, 4·0 Mc/s in steel
△ = 12 mm crystal, 4·0 Mc/s in steel
▽ = 8·5 mm crystal, 4·0 Mc/s in steel
■ = 6 mm crystal, 4·0 Mc/s in steel

Fig. 2 shows in logarithmic presentation the measured curves for various probes and materials. The plate thicknesses are expressed in terms of the appropriate near-field lengths. The differences between the various probes and materials are practically negligible. Instead of the height of the echo, measured as usual in millimetres or inches on the screen of the cathode-ray tube, the amplification V is plotted in decibels, as required to bring the echo up to a certain constant height, for example 1 in. The maximum echo reached in every case on the thinnest plate just outside the dead zone was given the value 0 dB. If one takes a plate thickness between 0·3 and 1 near-field length, an average difference to the ideal extremely thin plate of roughly 1 dB may be assumed. The possible deviations are negligible when it is considered that the coupling influences in practical cases may be far larger.

Seki, Granato and Truell[1] have calculated the behaviour of the back echo with distance and confirmed experimentally that it does not drop monotonically but with some maxima and minima. The exact response is very important for accurate measurements of attenuation, but for the present purpose one may assume the average value of 1 dB mentioned above.

The straight line in Fig. 2 represents equation (4) in logarithmic scale and is the far-field back wall echo. If the appropriate straight lines representing equation (6) with the parameter G are added to the graph, one obtains Fig. 3, which is called the *AVG*-diagram, because it combines the reduced distance A in logarithmic scale, the logarithmic value of the amplification V in decibels and the reduced defect size G. In the far field the relation of the three values is given by the straight lines in the right-hand half of the graph at values of A considerably larger than 1.

For example, a probe with a near-field length of 50 mm detects a defect at a distance of 300 mm. The reduced distance A is therefore 6. The ratio of the height of the defect echo to that of a plate of, say, 20 mm thickness has been measured as 1 : 100, i.e. 40 dB. Now one can calculate from equation (6) that $G = 0{\cdot}2$ but this value can be found more easily and quickly from the *AVG*-diagram. When the probe diameter is 25 mm the equivalent circular disk diameter of the defect is seen to be $0{\cdot}2 \times 25 = 5$ mm.

It is evident that the *AVG*-diagram of the far field is valid for all types of instruments, probes and frequencies after the amplification has been calibrated on a reference block to the value 0 or, preferably, 1 dB, and when the echo from a specimen is measured under the same surface conditions as the echo from the block.

The material of the plate may be ordinary rolled steel, for measurements with all types of steel, and likewise for aluminium and its alloys. The influence of absorption is negligible in view of the small thickness involved. Thickness and even plan-parallelism is by no means critical, but the contact surface should be machined. Surface roughness is a delicate point of the method, but by using exclusively probes without direct contact, as, for example, with a thin plastic foil in between the crystal and the surface, the effect is considerably reduced. Moreover, the pressure of coupling is then of less importance.

The reference block for angle beam probes can be a wedge of appropriate angle or, for more universal application to a variety of angles, it can have cylindrically-curved surfaces as shown in Fig. 4. Table 1 gives some dimensions which are recommended for such reference blocks for some probes. It would be possible to combine the plate and cylindrical form of reference block, as in the German–

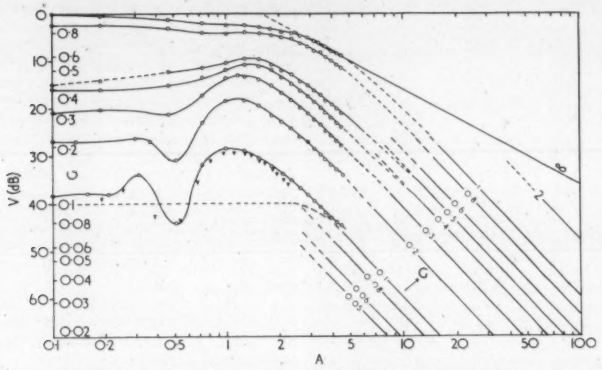

Fig. 3. *AVG*-diagram; right-hand side theoretical, left-hand side completed experimentally
○ = 2 Mc/s, 24 mm diameter ▽ = 4 Mc/s, 24 mm diameter

Dutch proposal to the International Institute of Welding (see Fig. 5).

As the end of the dead zone cannot be clearly recognized on the screen of a flaw detector, it should be communicated by the manufacturers, or they should specify for each probe

Fig. 4. Reference blocks for normal and angle probes

Table 1. *Convenient dimensions of reference blocks*

Probe	*Normal*			*Angle*	
Crystal diameter (mm)	34	24	10	10 × 10	20 × 23
Frequency (Mc/s)	1	2 4 6	4 6	4	2
d or *r (mm)*	50	20–50	20	15–30	50–100

the minimum thickness of test plate at which an error of less than 1 dB is made in setting the zero point of the gain. For exact measuring of the gain curve in the dead zone, an artificial pulse from a delay-pulse generator must be used or, with less accuracy, the bottom echo of a short water path with a continuously displacable reflector.

The value of the near-field length of the probe, which is needed for the method, may be calculated from the diameter of the crystal and the wavelength. However, it was shown experimentally that these values did not agree very well with those obtained by measurement. They should therefore be measured from equation (4) with a large reflector at distances of several times the near-field length. The manufacturers should be required to construct the probes with specified near-field lengths of convenient value and to mark the value plainly on them, as well as the crystal diameter and the frequency.

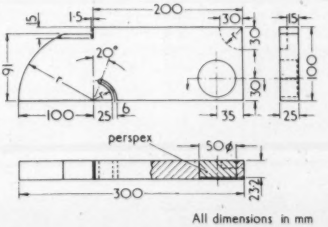

Fig. 5. Dutch–German proposal of calibration block for the International Institute of Welding, with proposed amendments

The calibrations which are provided on usual amplifier gain controls do not help in the measurement of amplification. As usual in high-frequency measurements, calibrated gain controls in decibel units are required and may easily be constructed by the manufacturers as an additional item. In future apparatus it could conveniently be built-in. It has the advantage that ratios of the echo heights of more than 1 : 1000 which may occur, can be measured exactly and with no influence of any non-linearity of the amplifier.

Table 2. *Defect diameter measured with different probes.* (*Flat bottom hole of 3·0 mm diameter at distance 125 mm in steel.*)

Frequency (Mc/s)	2			4				6		
Crystal diameter D_g (mm)	24	17	12	24	17	12	8·5	17	12	8·5
Near-field length N (experimental) (mm)	46	25	14	90	46	25	14	69	37	21
Reduced distance A of defect	2·7	5·0	8·9	1·4	2·7	5·0	8·9	1·8	3·4	5·9
Amplification V (dB)	32	36	43	24	26·5	31·5	36·5	22	27·5	32
Reduced defect size G	0·13	0·20	0·23	0·13	0·19	0·26	0·34	0·20	0·23	0·30
Defect diameter D_f (mm)	3·1	3·4	2·8	3·1	3·2	3·1	2·9	3·4	2·8	2·6

As a demonstration of the method in the distant zone, the size of a given artificial flaw (a flat bottom drill hole of 3 mm diameter) was measured using the *AVG*-graph and probes of various diameters and frequencies. Table 2 shows the results which agree with each other and with the correct figure to an accuracy which is sufficient in practice.

In the near zone a theoretical solution of the relation between A, V and G would involve very tiresome calculations. Therefore the left-hand side of Fig. 3 has been completed by measurements with circular disk reflectors in water. Even with different frequencies the results fit one another and the far field lines quite well. At small distances from the probe, simple considerations lead to the conclusion that the ratio of the echoes is proportional to the area of the reflector, i.e. to G^2 as has been shown approximately by the measurements.

This experimentally-completed diagram may be used for determination of flaw sizes at all distances. Unfortunately, the shapes of the curves in the near zone are not so generally valid as in the far zone. They depend on the form of the pulse which affects the interferences of the sound pressure in the near zone. With long pulses they are well defined by large maxima and minima, but with short pulses they are more or less flattened out. Now the length of the ultrasonic pulse depends not only on electrical data of the flaw detector, but also on the damping of the crystal. Usually the crystals are damped to a mechanical Q of values between 5 and 20 by backing with a suitable material, but the additional damping provided by the coupling to the specimen will still influence the pulse length. Therefore the near-field curves will not agree when measured with probes of different construction and with different coupling conditions. Moreover, close coupling will shift the frequency of the pulse and produce considerable pulse distortion. This is shown in Fig. 6, together with the effect of a thin plastic foil by which the difficulties of close coupling may be avoided.

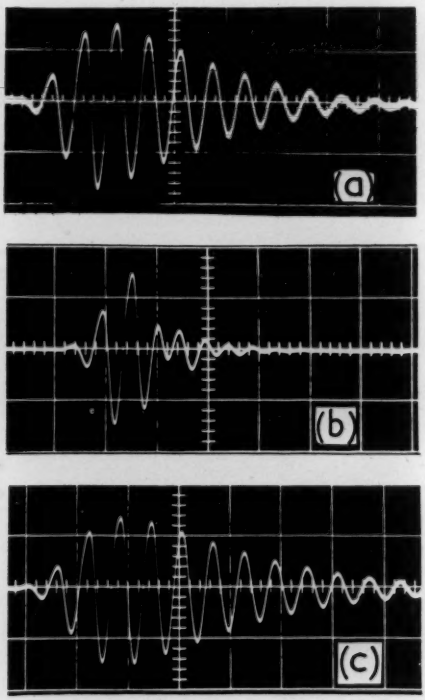

Fig. 6. Shapes of echo impulse using 4 Mc/s probe
(*a*) and (*b*) direct contact; (*c*) contact through plastic foil
(*a*) poor coupling, frequency 4·1 Mc/s
(*b*) good coupling, frequency 4·25 and 5·6 Mc/s
(*c*) shape of impulse independent of coupling, frequency 4·0 Mc/s

Strongly damped probes, for example with a value of Q of nearly 1, may be essentially better suited to this method because of the uniformity of the near field, but they have much reduced sensitivity. Further, the very short pulses have the undesirable property of being sensitive to influences which vary with frequency and from which pulse distortion will arise.

Therefore the determination of defect size within the near zone, using the usual probes, will give rise to some uncertainty. In many cases, to avoid these difficulties, the choice of a probe of shorter near zone may shift the defect to the far zone. With a special type of probe, however, it will be possible to use both zones.

In the probes which are generally in use the crystal oscillates approximately as a piston, which, in the form of a circular disk, is actually the most unfavourable oscillator from the point of view of the uniformity of the ultrasonic field. If the edges of the crystal are excited less strongly than the centre, the maxima and minima of the sound pressure on the axis will be less pronounced. The ideal solution[2] is represented by an excitation across the diameter in the form of a Gaussian probability curve (Fig. 7). The theoretical

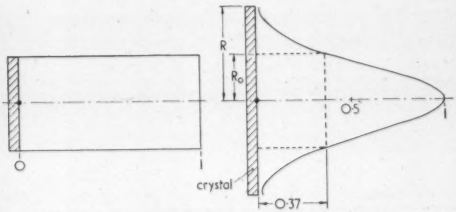

Fig. 7. Excitation of the crystal in form of a Gaussian curve $\{\exp(-\rho^2/R_0^2)\}$

curve of the near field is shown by Fig. 8, compared with that of the piston oscillator. It is completely flat and drops down in the far field, where the two types of oscillators finally behave in the same manner. The far-field angle distribution of such a Gaussian radiator is free of side lobes and zero points, as has already been mentioned by Roderick.[3]

An experimental realization by using a crystal with an electrode in the form of a star (see Fig. 9) proved to have, in fact, a rather flat response of the sound pressure on the axis and a single maximum everywhere normal to the axis. The latter behaviour of the near-field sound pressure is important for reliable flaw localizing.

Fig. 10 gives some curves of the *AVG*-graph measured with

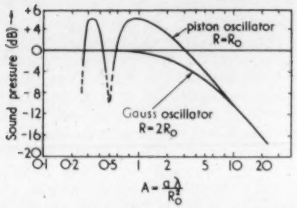

Fig. 8. Sound pressure on the axis of a Gaussian oscillator of $R = 2R_0$ and a piston oscillator with $R = R_0$, theoretical

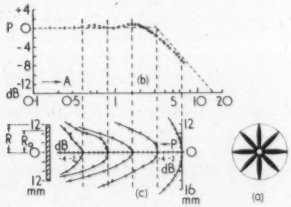

Fig. 9. Ultrasonic field of a quasi-Gaussian oscillator for 2 Mc/s, measured in water

(*a*) shape of electrode
(*b*) sound pressure on the axis
(*c*) sound pressure normal to the axis

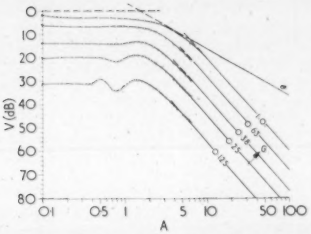

Fig. 10. Some curves of the *AVG*-diagram measured with the quasi-Gaussian probe in water. Note: reduced defect size G for Gaussian probes refers to the effective diameter $2R_0$ of the crystal

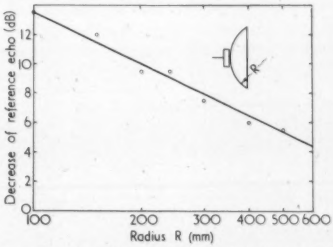

Fig. 12. Decrease of the reference echo on cylindrically-curved surface, measured with probe 24 mm diameter, 2 Mc/s on aluminium

the Gaussian probe. The remaining fluctuations could probably be avoided by better tailoring of the shape of electrode. Fig. 11 is the complete *AVG*-graph for Gaussian probes.

So far only flat contact and back surfaces and specimens without absorption have been considered. On cylindrically-curved surfaces also, a flat probe is generally used. Compared what flat surfaces there is a diminished area of contact, its sensitivity decreases and the gain V is found to be higher. Experiment shows that the near-field length remains the same. Therefore only the amplification zero has to be re-established. Instead of using reference plates with the same curvature as the specimen it is more convenient to measure once and for all the shift of amplification zero. Fig. 12 shows the correction as measured on curved aluminium blocks with a 24 mm crystal of 2 Mc/s, by contact with plastic foil. Its response will evidently depend on the material, on the probe

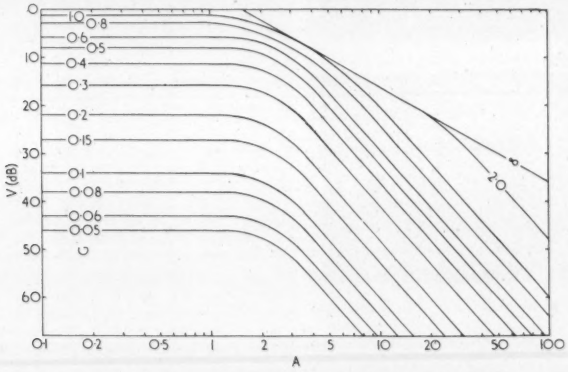

Fig. 11. Complete *AVG*-diagram for Gaussian probes

diameter and probably somewhat on the frequency. Therefor the manufacturers should furnish correction curves for steel and aluminium with their probes, to enable the use of the probes on cylindrically-curved surfaces together with the usual reference plate.

Now the influence of a curved back wall on the back echo must be considered. The echo of a flat back wall of a specimen without absorption must correspond to a point in the *AVG*-graph on the less inclined line at the top right, after a possible allowance for the curvature of the contact surface. Incidentally, the echo of a cylindrical specimen will have the same value as is obtained from a simple calculation of the spherical far-field wave. The curve of the sound pressure in the specimen is shown by Fig. 13.

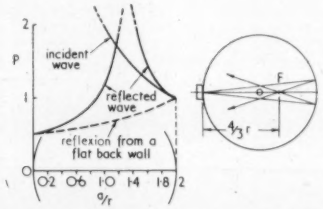

Fig. 13. Sound pressure on the axis of the crystal after reflexion at the back wall of a cylindrical specimen, calculated for distant-field conditions, to compare with echo of flat back wall

If the reflexion is from a bore hole, then the echo is smaller and the gain must be increased. It may be corrected by a factor given in Fig. 14, which is calculated as well for the far field on a purely geometrical optical basis.

The method can also be used for determining the overall attenuation in the specimen from the back wall echo. If the specimen has flat and parallel contact and back wall surfaces, and if one uses a probe with sufficiently small near-field length to permit operation in its far zone, the gain of the back echo without attenuation will be found direct from the graph, using the value A of the back wall. If the gain as measured is higher, the difference will give the attenuation over the whole path of the pulse.

For example: a specimen with a thickness of 400 mm, a probe of 100 mm near-field length (4 Mc/s, 24 mm diameter), the reduced distance being therefore $A = 4{\cdot}0$, gives from the *AVG*-graph, Fig. 3 or 11, a theoretical gain of 8 dB. If the actual gain is 28 dB, the difference of 20 dB must be ascribed to attenuation. By calculation, a mean value of the attenuation of 20 dB divided by 2×400 mm gives 25×10^{-3} dB/mm. (A rather high attenuation because there are steels, for example tool steels, with a value lower than water, i.e. 4×10^{-3} at 4 Mc/s.)

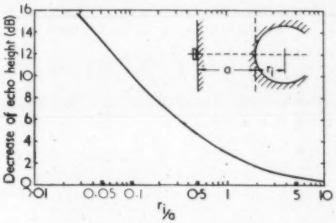

Fig. 14. Decrease of the back wall echo from cylindrical hole compared with flat back wall

In the case of cylindrically-curved contact or back surfaces one must allow first for the curvature by subtracting the corrections from Fig. 12 or a similar graph, and from Fig. 14 in the case of a bore hole.

When the attenuation in the specimen has been determined in this way at a position free from defects, the result must be applied as well to the actual estimation of defect size. If the defect lies close to the back wall the full correction must be used, otherwise there will be a smaller value in proportion to the actual depth of the defect. When the attenuation may not be assumed as uniform, as in most cases, allowance can only be made for it on the basis of empirically established curves of the distribution of the attenuation over the thickness.

REFERENCES

(1) SEKI, H., GRANATO, A., and TRUELL, R. *J. Acoust. Soc. Amer.*, **28**, pp. 230–238 (1956).

(2) HASELBERG, KL. v., and KRAUTKRÄMER, J. *Acustica*, **5**. To be published.

(3) RODERICK, R. L. *The Radiation Pattern from a Rotationally Symmetric Stress Source on a Semi-Infinite Solid, Metals Research Report* (U.S.A.: Brown University, 1950).

Energy variation with pressure and temperature in a sonic stationary wave

By A. R. INGLES, M.Sc., A.R.C.S., School of Physics and Applied Science, College of Technology, Leicester

[*Paper first received* 12 *January, and in final form* 4 *February*, 1959]

Using stationary waves in air, carbon dioxide and coal gas, the variations of the energy per wave per unit area E with pressure p at different temperatures have been plotted, and a relationship of the form $E = Kp^m$ obtained for a limited pressure range. The importance of correct impedance matching between the source and the surrounding gas is emphasized by the results.

In the course of measurements, as yet incomplete, of the velocity of sound at audio-frequencies in organic vapours and in vapour-air mixtures contained in cylindrical tubes, considerable variation was observed in the response of the receiver using different vapours at various temperatures.

It was thought, therefore, that some results of interest on the transfer of energy to stationary waves might be obtained by observing the variation in the energy per wave, using a controlled range of pressures for various temperatures and gases.

EXPERIMENTAL PROCEDURE

Two similar moving coil movements, somewhat the same as those described by Wente and Thuras[1] and as illustrated in Fig. 1, were used as source and receiver respectively, and were suspended by two thin elastic strands from a metal

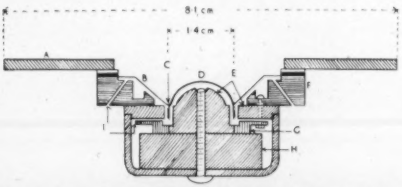

Fig. 1. Section of moving coil movement without electrical connexions

A, baffle; *B*, flexible support; *C*, coil; *D*, diaphragm; *E*, pole-pieces; *F*, ebonite; *G*, aluminium; *H*, magnet; *I*, narrow vents.

bridge placed inside a glass dessicator connected to a Speedivac pump as shown in Fig. 2.

The source faced the receiver at a distance of 7 cm, so that when the source was energized at the correct frequency a standing wave of length 14·0 cm was produced between them; they could easily be removed and replaced at the same distance apart.

The source, energized by a Dawe oscillator, was run at a constant current controlled by the oscillator volume control and measured on a Cambridge versatile galvanometer fitted with a vacuum thermojunction. After the usual period of warming up, the oscillator frequency was very stable; even so its 1000 c/s setting was occasionally checked against the 50 c/s mains using Lissajous' figures on a cathode-ray oscillograph, which was also used to measure the receiver output.

The pressure was measured directly using a vertical manometer in conjunction with a barometer and the temperature was measured on a mercury thermometer placed inside the dessicator. To minimize temperature variation the dessicator, lagged in cotton wool, was placed in a box of fibre board; the temperature was raised by an electric heater placed inside the box round the bottom of the dessicator, but not touching it; the current was controlled and measured by a Variac autotransformer and ammeter respectively; several hours were allowed for the temperature to stabilize before commencing observations.

The dessicator was filled by evacuating it, then, after checking that the mercury level in the manometer remained at a constant height for five minutes, the gas under experiment was admitted until atmospheric pressure was regained.

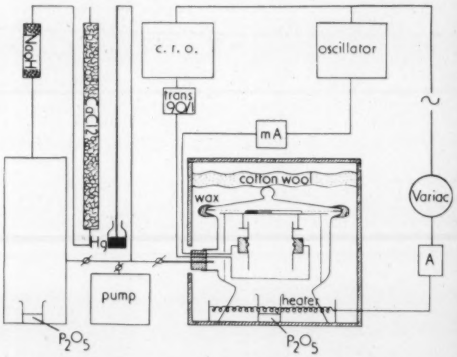

Fig. 2. Apparatus used for observing the variation in the energy per wave for various temperatures and gases

The air used was passed over sodium hydroxide, calcium chloride and stored in contact with phosphorus pentoxide prior to its entry into the dessicator in which more phosphorus pentoxide was placed; the commercial carbon dioxide used passed directly from its cylinder into the dessicator and was dried there; the coal gas was not dried at all as it caused the phosphorus pentoxide to go brown very quickly.

The data, from which the curves of wave energy against pressure were plotted, was obtained after tuning the oscillator for maximum response by measuring the maximum double amplitude on the cathode-ray oscillograph using dividers and a scale, the oscillograph being connected to the receiver, The oscillator frequency was noted, then the pressure was reduced and the procedure repeated, the oscillator being tuned each time for maximum cathode-ray oscillograph deflexion. No appreciable variation was noticed in the oscillator current at resonance. Care was taken to reduce the pressure slowly to prevent cooling in the gas; this did not occur to any appreciable extent as shown by the constancy of the frequency readings.

To increase the mechanical impedance of the source and receiver, two similar small spheres of Plasticene were made and flattened out symmetrically over the top of the hemispherical part of each diaphragm.

Apiezon grease was used to seal on the lid of the dessicator, and at temperatures above room value it was necessary also to cover up the join between lid and base with Apiezon wax.

When it was necessary to increase the pressure in the dessicator above atmospheric, a U-manometer replaced the vertical one and a load of 18 kg was applied to the lid; also the rubber bung carrying the screened leads into the dessicator was wired on. The screened leads were carried through the rubber bung in a glass tube and Picein wax applied at the glass-leads junction was found to make a leak-proof seal.

THEORY

Stationary wave energy. The energy E per wave per unit area of wave front in a stationary wave formed by the reflexion of a plane progressive wave of amplitude a, frequency $\omega/2\pi$, moving with velocity c in a gas of density ρ at pressure p, is given by Barton[2] as

$$E = \rho a^2 \omega^2 \lambda \tag{1}$$

If $\dot{y}$ and δp represent the maximum values of the particle velocity and excess pressure respectively in the progressive wave, since

$$\omega = \dot{y}/a \tag{2}$$

$$\delta p = \rho c \dot{y} \tag{3}$$

equation (1) becomes

$$E = \delta p^2 \lambda / \rho c^2 \tag{4}$$

and since

$$c^2 = \gamma p/\rho \tag{5}$$

then

$$E = \delta p^2 \lambda / \gamma p \tag{6}$$

Now the response of a pressure-operated microphone placed at the reflecting surface, as measured by the cathode-ray oscillograph deflexion D it produces, will be proportional to $2\delta p$, whence

$$E = k D^2 / \gamma p \tag{7}$$

where k is a constant, since λ is a constant.

Energy transfer and variation with pressure. The stationary wave set up at resonance in a column of gas enclosed between two reflectors, one of which contains a source, will have an ever increasing amount of energy if the power supplied by the source is constant and there is no loss of energy from the vibrating gas.

However, due to imperfect reflexion at the ends, absorption by the walls and attenuation in the gas itself, etc., energy will be lost and thus a state of equilibrium will finally be reached when the energy in the wave attains such a value that the power input is equal to the power lost. Assuming that the power lost is a function of the energy in the wave, then at equilibrium the acoustic power input will be the same function of the energy of the wave; hence the acoustic power input will be a maximum when the energy of the wave attains its maximum value.

Now the acoustic power input from the source will depend on the degree of electrical matching between the oscillator and the moving coil diaphragm, and also on the mechanical matching between the diaphragm and the gas; thus the best matching will have been obtained when the wave energy is at its maximum.

From theory given by Spandöck[3] to find the efficiency ${}_a\phi_e$ of a source, where ${}_a\phi_e$ is the ratio of the acoustic output P_a to the electric input P_e and P_m is the mechanical power, then

$$\begin{aligned} {}_a\phi_e &= {}_a\phi_m \cdot {}_m\phi_e \\ &= \frac{P_a}{P_m} \cdot \frac{P_m}{P_e} \\ &= \frac{r\dot{y}^2}{Z_m \dot{y}^2} \cdot \frac{Z_m \dot{y}^2}{(r_e + r_s) i^2} \end{aligned} \tag{8}$$

where $\dot{y}$ is the diaphragm velocity, r the radiation resistance of the gas, Z_m the mechanical impedance of the diaphragm, r_e the external (oscillator) resistance, r_s the apparent source resistance and i the current through it.

Using

$$F = iN \tag{9}$$

with

$$F = \dot{y} Z_m \tag{10}$$

to eliminate i and F between equations (8), (9) and (10), where F is the force on the diaphragm due to the current and N is the electromechanical coupling coefficient, then

$${}_a\phi_e = \frac{r}{Z_m} \cdot \frac{N^2/(r_e + r_s)}{Z_m} \tag{11}$$

For perfect matching between the vibrating diaphragm and the surrounding gas the acoustical-mechanical efficiency ${}_a\phi_m$ must be unity, thus

$$r = Z_m \tag{12}$$

The consequences of an increase in Z_m will be, firstly, r will have to be increased to re-establish the acoustical-mechanical matching, i.e. to make ${}_a\phi_m$ again unity, and secondly, the acoustical-electrical efficiency ${}_a\phi_e$ will fall owing to a decrease in the mechanical-electrical efficiency ${}_m\phi_e$, which will result in a lower output of energy from the source even though its diaphragm has been rematched to the gas.

Now the specific acoustic impedance of a gas z may be written

$$z = r + ix$$

where r and x are the specific acoustic resistance or radiation resistance and the specific acoustic reactance respectively.

Let it be assumed that in this case the value of z, given by Davis[4] for gas at the surface of a pulsating sphere in an infinite medium may be applied, then

$$z = \frac{\rho c a^2 k^2}{1 + a^2 k^2} + i \cdot \frac{\rho c a k}{1 + a^2 k^2}$$

where k is $2\pi/\lambda$, a is the radius of the spherical source, ρ is the density of the gas and c the velocity of sound; thus for a given value of λ, as in this case,

$$r = \rho c G \tag{13}$$

where G is a constant.

Also if M, R and μ are the mass, the resistance per unit velocity and the stiffness per unit displacement of the diaphragm respectively, then,

$$Z_m = (R^2 + X^2)^{1/2} \tag{14}$$

where

$$X = Mw - \mu/\omega$$

when the frequency of the forced oscillation is $\omega/2\pi$ and the reaction of the gas on the diaphragm is neglected.

Now let it be assumed that the moving coil source is

resistance controlled, then $R \gg X$; also if the resistance varies directly as the viscosity of the gas, then

$$R = H\eta$$

where H is a constant and η is the coefficient of viscosity of the gas.

For matching, from equations (12), (13) and (14),

$$\rho^2c^2G^2 = X^2 + H^2\eta^2$$

and neglecting X^2 in comparison with $H^2\eta^2$, then

$$\rho c/\eta = \text{constant} \qquad (15)$$

Also assuming, as explained previously, that at equilibrium the acoustic output of the source is a function of the energy of the wave, then let

$$P_a = f(E)$$

and since

$$P_a = P_e \cdot {}_a\phi_e$$

$$P_e \cdot {}_a\phi_e = f(E)$$

Then, assuming P_e is constant, from equations (11), (13) and (14) together with the assumptions already made in regard to R and X,

$$\rho c/\eta^2 = K_1 f(E) \quad \text{where } K_1 \text{ is a constant.}$$

Now at constant temperature, c and η are constant for a given gas and ρ is proportional to the pressure p,

whence $$p = K_2 f(E)$$

Now let $$f(E) = E^n$$

then $$p = K_2 E^n$$

or $$E = K_3 p^m \qquad (16)$$

where K_2 and K_3 are constants, the latter depending on the gas used and its temperature.

By rewriting equation (16) as

$$\log E = m \log p + \log K_3$$

and plotting $\log E$ against $\log p$, the value of K_3 and m may be found.

RESULTS AND DISCUSSION

From the results using air and carbon dioxide, shown in Figs. 3 and 4 respectively, it was considered that the maximum values of wave energy E obtained with carbon dioxide were due to impedance matching between the gas and the moving coil diaphragm; similar matching could not be attained with air using pressures up to atmospheric. Much lower values of E were expected with a gas of low density, and this was confirmed by the results using coal gas shown in Fig. 5.

The variations of wave energy E with temperature for a given gas and between different gases at a given temperature were considered to be due to changes in the impedance of the diaphragm owing to viscosity changes in the gases used.

To confirm that the maximum values of E were due to matching, the impedance of the diaphragm was raised by increasing its mass, and using carbon dioxide, as shown in Fig. 4, the pressures required for matching increased with the load. Although no matching could be expected using the loaded diaphragm with air, Fig. 3 shows the considerable decrease in E caused by the loading.

Finally, by increasing the pressure above atmospheric, matching was achieved in air as shown in Fig. 5; unfortunately, however, prior to obtaining these results, mercury from the manometer was inadvertently sucked into the dessicator and some of its spray fell on the diaphragm; although it was carefully brushed a very small amount still adhered to it, as shown by the decreased values of E given in curve L of Fig. 5 compared with those in curve A of Fig. 3, when the diaphragm was unloaded.

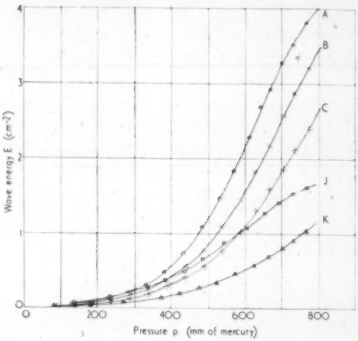

Fig. 3. Variation of wave energy with pressure for dry air at different temperatures using unloaded and loaded diaphragms

Curve A, 17·0° C, no load; curve B, 26·0° C, no load; curve C, 35·7° C, no load; curve J, 19·4° C, load 0·05 g; curve K, 20·0° C, load 0·08 g.

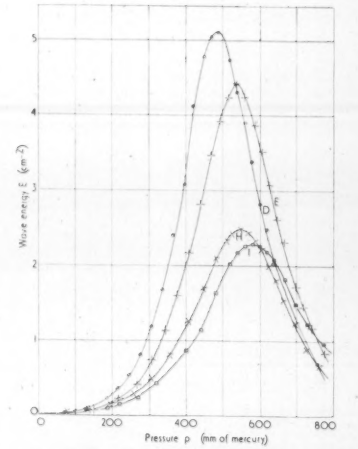

Fig. 4. Variation of wave energy with pressure for dry carbon dioxide at different temperatures using unloaded and loaded diaphragms

Curve D, 19·5° C, no load; curve E, 31·8° C, no load; curve H, 19·2° C, load 0·05 g; curve I, 18·5° C, load 0·08 g.

The value for ρc of 44·3 c.g.s. obtained from curve L of Fig. 5 for matching is therefore greater than it would have been if the slight loading had been avoided, whence the value of $24{\cdot}4 \times 10^4$ c.g.s. for $\rho c/\eta$ for air is higher than it should have been.

The commercial carbon dioxide was obtained from fermentation processes and the 3% low values for the velocity of sound, shown in Table 1, are probably due to the presence of alcohol vapour, whence the value of η used in the calculation of $\rho c/\eta$ for carbon dioxide is probably a little too high. These considerations, in some measure, may account for the differences in the three values of $\rho c/\eta$ given in Table 1.

The wave fronts generated by the source will most probably be spherical, but after several reflexions from the baffles they will become more nearly plane, as assumed in previous theory.

As the source is small not all the energy transferred to the gas will be incident on the baffle and receiver, but the bulk

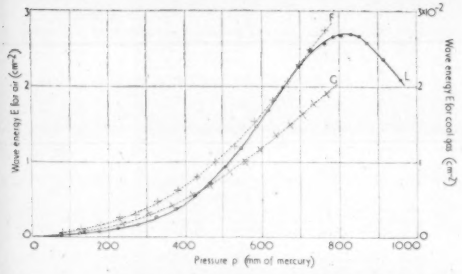

Fig. 5. Variation of wave energy with pressure for dry air when the pressure range is increased beyond atmospheric, and also for un-dry coal gas at different temperatures for pressures up to atmospheric

Curve *F*, coal gas, 19·8° C; curve *G*, coal gas, 37·5° C; curve *L*, air, 20·5° C.

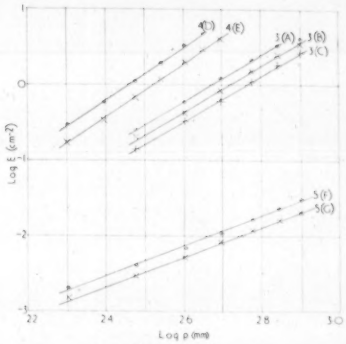

Fig. 6. Plots of log E against log p to evaluate m and K_3 in $E = K_3 p^m$ for dry air, dry carbon dioxide and un-dry coal gas

From Fig. 3: curve *A*, air, 17·0° C; curve *B*, air, 26·0° C; curve *C*, air, 35·7° C. From Fig. 4: curve *D*, carbon dioxide, 19·5° C; curve *E*, carbon dioxide, 31·8° C. From Fig. 5: curve *F*, coal gas, 19·8° C; curve *G*, coal gas, 35·7° C.

Table 1. *Summary of results*

The velocity c is given by $c = 0{\cdot}14\,n$, and ρc by $\rho c = \gamma p/c$ using values of 1·40, 1·30 and 1·37 for γ for air, carbon dioxide and coal gas respectively. The results were obtained in the alphabetical order used in the Figure reference column.

Figure reference	*Temperature* (° C)	*Frequency* $\left(\frac{n}{c/s}\right)$	*Matching pressure* $\left(\frac{p}{mm\ Hg}\right)$	*Velocity* $\left(\frac{c}{m/s}\right)$	*Velocity error* (%)	ρc (c.g.s.)	*Viscosity* (μP)	$\rho c/\eta$ (c.g.s.)	*Load* (g)
				Dry air					
3 (*A*)	17·0	2445	—	342·3	+0·2	—	—	—	0
3 (*B*)	26·0	2485	—	347·9	+0·2	—	—	—	0
3 (*C*)	35·7	2530	—	354·2	+0·3	—	—	—	0
3 (*J*)	19·4	2450	—	343·0	−0·1	—	—	—	0·05
3 (*K*)	20·0	2445	—	342·3	−0·4	—	—	—	0·08
5 (*L*)	20·5	2455	815	343·7	−0·1	44·3	181	$24{\cdot}4 \times 10^4$	small
				Dry carbon dioxide					
4 (*D*)	19·5	1940	490	271·6	−2·1	31·3	146	$21{\cdot}4 \times 10^4$	0
4 (*E*)	31·8	1990	537	278·6	−3·3	33·6	152	$22{\cdot}1 \times 10^4$	0
4 (*H*)	19·2	1930	550	270·2	−2·5	—	—	—	0·05
4 (*I*)	18·5	1920	585	268·8	−2·8	—	—	—	0·08
				Un-dry coal gas					
5 (*F*)	19·8	3520	—	492·8	—	—	—	—	0
5 (*G*)	35·7	3555	—	497·7	—	—	—	—	0

Table 2. *Values of m and K_3 in $E = K_3 p^m$*

Figure reference	*Gas*	*Temperature* (° C)	$K_3(\times 10^9)$	m	*Range* (*mm Hg*)
5 (*F*)	Coal gas	19·8	43·7	2·0	0 to beyond 800
5 (*G*)	Coal gas	35·7	30·8	2·0	0 to beyond 800
3 (*A*)	Air	17·0	9·51	3·0	0 to beyond 700
3 (*B*)	Air	26·0	6·92	3·0	0 to beyond 800
3 (*C*)	Air	35·7	5·11	3·0	0 to beyond 800
4 (*D*)	Carbon dioxide	19·5	2·46	3·5	0 to beyond 450
4 (*E*)	Carbon dioxide	31·8	1·49	3·5	0 to beyond 500

will be reflected by the baffle since the ratio area receiver/baffle is small.

An ideal pressure-operated receiver would have infinite impedance and act as a perfect reflector, thus absorbing a negligible amount of energy. In this case the impedance of the receiver is similar to that of the source Z_m, and it is interesting to consider how its response may have been affected by variation in the radiation resistance r of the gas; for example, the receiver is likely to reflect better when $Z_m \gg r$, that is at low pressure, and to absorb more energy as r approaches Z_m.

The proportionality obtained between E and p^m applies only to a limited range of pressures and does not allow of a maximum value of E, which is most likely the result of over-simplified theory; if the reaction of the gas on the source is taken into account, as outlined by Davis (Ref. 4, p. 55), then Z_m becomes a function of p as well as η; also $f(E)$ may not be of such a simple form as has been assumed.

The values of K_3 and m, taken from Fig. 6, for the three gases used are given in Table 2 and it may be noted that m varies with the gas used.

Thus to obtain stationary waves of sufficient energy per wave for successful detection in vapours and vapour-air mixtures the necessary impedance matching between the source and the medium may be achieved, or nearly achieved, by careful consideration of the design of the source, the characteristic impedance of the medium and the temperature and pressure at which it is used.

REFERENCES

(1) Wente, E. C., and Thuras, A. L. *J. Acoust. Soc. Amer.*, **3**, p. 45 (1931).
(2) Barton, E. H. *A Textbook on Sound*, p. 212 (London: Macmillan and Co. Ltd., 1926).
(3) Spandöck, F. *Technical Aspects of Sound*, Vol. 1, p. 339 (London: Elsevier Publishing Co., 1953).
(4) Davis, A. H. *Modern Acoustics*, p. 60 (London: Bell and Co. Ltd., 1934).

Effect of sound intensity on dispersion and coagulation in ultrasonic emulsification

By R. S. Krishnan, D.Sc., Ph.D.(Cantab), F.Inst.P., V. S. Venkatasubramanian, Ph.D., and E. S. Rajagopal, M.A., M.Sc., Department of Physics, Indian Institute of Science, Bangalore-12, India

[*Paper first received* 8 *December* 1958, *and in final form* 25 *February*, 1959]

The contributions of dispersion and coagulation to the process of emulsification can be determined by following the rate of emulsification, and this method is used to study the effect of sound intensity on them. After a certain threshold of intensity, below which no cavitation occurs, the dispersion increases with the sound intensity. The coagulation also increases with the sound energy, but with a residual coagulation even in the absence of the sound field. The nucleation phenomenon is also studied. All the results agree with the general theoretical considerations.

The phenomenon of ultrasonic emulsification has been studied qualitatively for a long time,[1] many of the basic processes being elucidated. The quantitative observations of Bondy and Sollner,[2] and of Claus and Schmidt[3] were not quite successful because the reproducibility achieved was only about 20%. Recently, Krishnan *et al.*[4] have paid attention to the experimental layouts and have discussed the methods of achieving consistent results to within approximately 5%.

The effect of the input energy on the process of emulsification is a very interesting problem. The earlier studies[2,5] were mostly qualitative. From general theoretical considerations, it can be said that, with the increase of sound intensity, the dispersion should increase, because of the availability of greater energy for breaking up the interface and, at the same time, the coagulation should increase because of the enhanced probability of the collisions. Because comprehensive theoretical treatments of these questions do not exist, accurate experimental studies are of considerable importance.

EXPERIMENTAL METHOD

The experiments were performed in a normal ultrasonic-emulsification arrangement in which attention was focused on producing a uniform controlled stationary sound field.[4] The rate of emulsion formation provides a convenient way of isolating and identifying the individual contributions of dispersion and coagulation to the process of emulsification.

The opposing reactions of the dispersion of the interface and the coagulation of the dispersed phase, which constitute the resultant emulsification, take place in distinct regions in ultrasonic emulsification. The dispersion occurring over the area A of the interface, gives the rate of dispersion as $\propto A$ to the first approximation, if the sound field and the interface are maintained constant. The coagulation taking place in the volume V of the emulsion, gives a coagulation factor βVc^n where n is 1 or 2 according as the dominant coagulation reaction is monomolecular or bimolecular. So the rate of emulsification is[6]:

$$\frac{\partial(Vc)}{\partial t} = A\alpha - \beta Vc^n$$

where the constants α and β depend upon the sound field, properties of the interface, etc. The concentration c of the emulsion did not exceed about 3% in these experiments and so the volume of the emulsion V can be taken as independent of time. The solution of this equation for monomolecular coagulation ($n = 1$) is:

$$c = c_\infty[1 - \exp(-at)]; \quad c_\infty = A\alpha/V\beta; \quad a = \beta \qquad (1)$$

while for the bimolecular coagulation ($n = 2$) it is:

$$c = c_\infty \tanh bt; \quad c_\infty = (A\alpha/V\beta)^{1/2}; \quad b = (A\alpha\beta/V)^{1/2} \qquad (2)$$

where t is reckoned from the start of the emulsification. Both functions are similar and represent the concentration-time curve well, an initial rapid linear increase of c being followed by a levelling off to a limiting concentration c_∞. But the experimental dependence of c_∞, a and b on A and V

are of different natures, and the experiments[6] clearly decide in favour of equation (2), the bimolecular coagulation. This result is to be expected from a general theoretical analysis of the phenomenon also.

Equation (2) is used to evaluate the individual contributions of dispersion and coagulation to the process of emulsification. The measurements were made on water-in-benzene emulsions (with magnesium-oleate as emulsifier) for experimental convenience. In all the measurements, c_∞ is estimated through the specific gravity. Where deviations from Beer's law are significant ($c > 3\%$), α is determined from the slope of the concentration-time curve at the time t_N of the start of nucleation. The general experimental procedure is as described elsewhere.

RESULTS

The observations made by varying the sound intensity are represented in Fig. 1 as a variation of c_∞ and b with $\bar{E}$ ($A = 2{\cdot}38$ cm^2; vol. of water = 2 ml.; vol. of benzene = 8 ml.). Because the exact energy used up for emulsification is difficult to estimate—no attempt ever seems to have been made in this direction—the ultrasonic energy density $\bar{E}$ itself is given, although a part of it is converted into heat. The limiting concentration c_∞ increases with $\bar{E}$ in the range studied ($I_{eq} = 0{\cdot}5$–$3{\cdot}0$ W cm^{-2}), and there is a tendency to approach a saturation level. Oyama *et al.*[7] also find this behaviour, although they have not made a detailed study. The parameter b also increases with $\bar{E}$. Because b^{-1} is a "time constant" for emulsification, this variation means that higher concentrations are reached more quickly at higher intensities. At low sound energies, the limiting concentration itself is small and it is reached only after a long time, a fact noted by Bondy and Sollner[2] also.

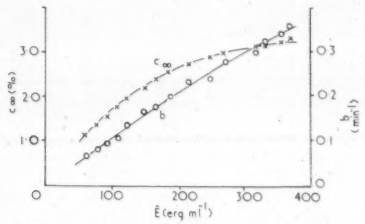

Fig. 1. Variation of c_∞ and b with $\bar{E}$

Although c_∞ and b are experimentally important quantities, the values of α and β have greater theoretical significance. They are shown in Fig. 2, where the value for $A\alpha/V$ of $0{\cdot}31\alpha$ is indicated as α^1. Within the range studied, the variations are almost linear.

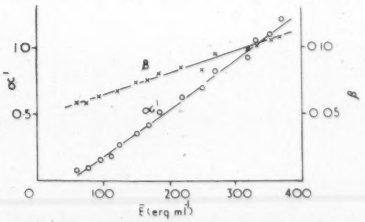

Fig. 2. Dependence of α^1 and β on $\bar{E}$

The nucleation time t_N is a characteristic of many phase transformations like crystallization, condensation, etc.[8] In ultrasonic emulsification, this nucleation time is of the order of a few minutes.[2,7,9] This phenomenon has not been carefully investigated in ultrasonic emulsification because, in the earlier measurements the fundamental requisites of uniform sound fields and clean dry emulsion chambers were not realized. The improvements made in the present experiments enabled fairly concordant results to be obtained. To find the order of the nucleation reaction, Lindstrom[10] showed that the graph of $\log t_N$ against $\log p$ should be a straight line with a slope of $-(n+1)$. Fig. 3 represents the linear variation of $\log t_N$ with $\log \bar{E}$ (t_N in minutes; $\bar{E}$ in ergs. ml.$^{-1}$), the slope of $-0{\cdot}85$ giving n to be approximately 3. But the interpretation of this order of the reaction in terms of the processes of cavitation (Noltingk and Neppiras[11]) is not straightforward, and the general explanations based on the Becker–Doring theory are not free from serious objections. The effect may also be due to simple degassing of the liquids.[13]

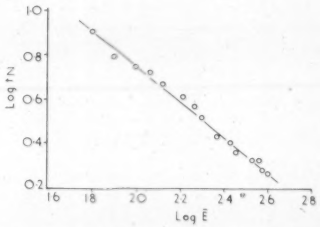

Fig. 3. Relationship between $\log t_N$ and $\log \bar{E}$

DISCUSSION

The principal contribution of the present paper is the separation of the various individual processes in emulsification, a fact which has not been effected so far. The linear variation of α with $\bar{E}$ is interesting from the viewpoint of the theory of emulsification because it shows that the energy supplied at the interface has a marked influence on the quantity of the dispersed phase produced. There seems to be a threshold value of $\bar{E}$ above which dispersion alone occurs. These factors are easily interpreted in the light of the cavitation mechanism of dispersion. A complete elucidation will require a study over a much wider range of intensities. In the region of low values of c and $\bar{E}$, the experimental errors are large, and the threshold value of $\bar{E}$ is not very exact.

The variation of β is also linear in this range, but there is a residual coagulation even as $\bar{E}$ tends to zero. Considerable perikinetic coagulation existed in the emulsion, leading to its breaking up in a few hours. The effect of the ultrasonic irradiation is only to increase the already existing coagulation, and this excess is proportional to the intensity of the sound wave. This is precisely the behaviour predicted by the principle of orthokinetic coagulation of the emulsions under ultrasonic irradiation.[12] The quantitative comparison is not easy, but the increase in coagulation is of the right order of magnitude, noting that the sound frequency and the particle sizes (about 2 μ) are different here.

ACKNOWLEDGEMENTS

The authors thank the Indian Council of Medical Research for financial assistance and for the award of a Junior Fellowship to E. S. Rajagopal. They also thank the Referee for his useful suggestions.

REFERENCES

(1) SOLLNER, K. *Colloid Chemistry*, **5**, p. 337 (New York: Reinhold, 1944).
(2) BONDY, C., and SOLLNER, K. *Trans Faraday Soc.*, **32**, p. 616 (1936).
(3) CLAUS, B., and SCHMIDT, E. *Kolloid Beih.*, **45**, p. 41 (1936).
(4) KRISHNAN, R. S., *et al. J. Colloid Sci.* To be published.
(5) BERKMAN, S., and EGLOFF, G. *Emulsions and Foams* (New York: Reinhold, 1941).
(6) RAJAGOPAL, E. S. *J. Colloid Sci.* To be published.
(7) OYAMA, L., *et al. Chem. Abs.*, **42**, p. 16 (1948).
(8) LA MER, V. K. *Ind. Eng. Chem.*, **44**, p. 1270 (1952).
(9) RICHARDS, W. T. *J. Amer. Chem. Soc.*, **51**, p. 1724 (1929).
(10) LINDSTROM, O. *J. Acoust. Soc. Amer.*, **27**, p. 654 (1955).
(11) NOLTINGK, B. E., and NEPPIRAS, E. A. *Proc. Phys. Soc.*, **64B**, p. 1032 (1951).
(12) HERMANS, J. J. *Rec. Trav. Chim. Pays. Bas.*, **58**, pp. 139, 164 (1939).
(13) KAPUSTIN, A. P. *Phys. Abst.*, **58**, No. 3520 (1955).

Temperature errors introduced by temperature-measuring probes

By I. G. DONALDSON, M.Sc., Dominion Physical Laboratory, Department of Scientific and Industrial Research, Lower Hutt, New Zealand

[*Paper first received* 23 *October*, 1958, *and in final form* 9 *February*, 1959]

Calculations are made of the thermal disturbance produced in hot ground by the presence of probes that are thermally conducting. It is found that temperatures measured with metal probes with a length/radius ratio of up to 100 : 1 may be considerably in error. Wooden probes are, however, quite satisfactory. For measurements of high accuracy thermocouple wires alone, i.e. not enclosed in any supporting probe, are quite satisfactory although copper wires should be replaced by manganin if possible. The work has a bearing on surveys being made of the heat flow from thermal regions in New Zealand.

Ground temperature measurements in and around the thermal regions of New Zealand are often made using long cylindrical probes with thermocouple junctions at the tip (and occasionally at various points along the probe), the aim being to deduce the heat flow from the mean temperature gradient. Because there is an upward flow of heat, these probes, which are often made of metal tubing, provide a low resistance path for the heat and affect the temperatures in their vicinity. Hence it is necessary to determine to what extent the presence of the conducting probe may affect temperatures of the ground.

RESULTS

The theory, given in the Appendix, is based on the fact that a finite cylinder and a prolate ellipsoid of revolution differ only near the ends, provided that the length is much greater than the radius. As most of the probes that are used have conical tips of the same or similar material, the resemblance to an ellipsoid is still greater.

Fig. 1 is the diagram of the arrangement on which the theory is based. It represents a long ellipsoid embedded in an infinite medium through which there is a steady unidirectional heat flow. By symmetry the temperature will be uniform along the plane $z = 0$ and this may be taken to represent the surface of the ground in a practical case. The analogy supposes that the portion of the probe at ground level will have the same temperature as the ground surface. Experiments made with a probe of stainless steel tubing inserted into moderately hot ground showed that the probe at ground level became slightly warmer than the ground surface. The rise in temperature was small, however, being less than a quarter of a degree. This does not constitute a direct error in the measurement of the ground temperature at the tip of the buried probe. Indeed, to the extent to which this rise reduces the temperature gradient and the heat flow along the probe, it will reduce the errors in temperature at the tip. In this sense the present theory slightly overestimates the errors due to conduction. Probes, however, are not ellipsoidal and, to the extent to which their lower parts are wider and more conducting than an ellipsoid of the same maximum diameter, the error in practice will be a little greater than the theory predicts.

If T_s is the temperature on the plane $z = 0$, then the Appendix shows that the temperature measured at any point within the probe is given by

$$T = T_s + \frac{Qz}{k_2}\left[1 - \frac{(k_1 - k_2)A}{(k_1 - k_2)A + k_2}\right] \qquad (1)$$

$$A \simeq \frac{R^2}{a^2}\left(\ln\frac{2a}{R} - 1\right) \qquad (2)$$

where k_1, k_2 are the thermal conductivities (cal cm^{-1} s^{-1} °C^{-1}) of the cylinder and the surrounding medium respectively, R is the radius of the probe (cm), a is the depth (cm) to which the probe is inserted, Q is the upward heat flow (cal cm^{-2} s^{-1}) and z is the depth measured from the ground surface.

The percentage error Δ in the temperature difference between the tip of a probe and the ground surface, arising from conduction along the probe, is

$$\frac{\Delta}{100} = \frac{(k_1 - k_2)A}{(k_1 - k_2)A + k_2} \qquad (3)$$

which, using the approximation (2) for the long cylindrical probe, gives

$$\frac{\Delta}{100 - \Delta} = \left(\frac{k_1}{k_2} - 1\right)\frac{R^2}{a_2}\left(\ln\frac{2a}{R} - 1\right) \qquad (4)$$

Thus the ratio of length to radius necessary to achieve a given accuracy may be determined for any ratio of conductivities.

In Fig. 2 a/R is plotted against k_1/k_2 for values of Δ of -5, ± 1, $\pm 0{\cdot}2$ and $\pm 0{\cdot}01$ %.

In the ground surrounding the probe the temperature is given by

$$T = T_s + \frac{Qz}{k_2}\left(1 - \left\{\left[(k_1 - k_2)\left(\frac{a^2}{e^2} - 1\right)\left(\frac{a}{2e}\ln\frac{r+e}{r-e} - \frac{a}{r}\right)\right]\Big/ [(k_1 - k_2)A + k_2]\right\}\right) \quad (5)$$

where r is one of the set of elliptic co-ordinates (r, θ, ϕ), and e is equal to $(a^2 - R^2)^{1/2}$, which is approximately equal to a for a long thin probe.

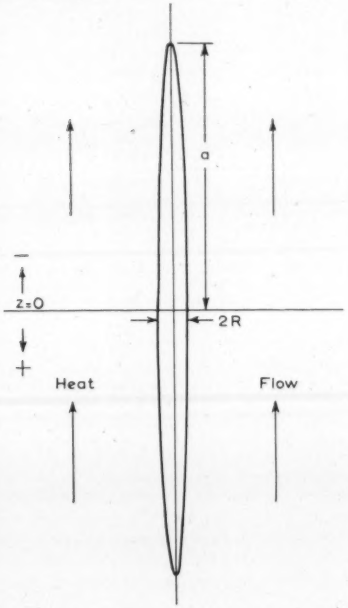

Fig. 1. The theory considers a long thin ellipsoid lying parallel to the direction of heat flow in an infinite medium. The lower half of this model is then likened to a conducting probe inserted in the ground

PRACTICAL EXAMPLES

(i) A Duralumin probe used in some New Zealand surveys is made from a tube 100 cm long, 0·8 cm in external diameter and 0·5 cm in internal diameter and contains two 27 s.w.g. thermocouple wires (copper and constantan) covered with polyvinyl chloride. The junction is soldered into the tip. This probe is inserted to depths of 5, 10, 20, 30, 50, 70 and 100 cm in grounds where the thermal conductivity lies in the range 0·5 to $3{\cdot}0 \times 10^{-3}$ cal cm^{-1} s^{-1} °C^{-1}, and through

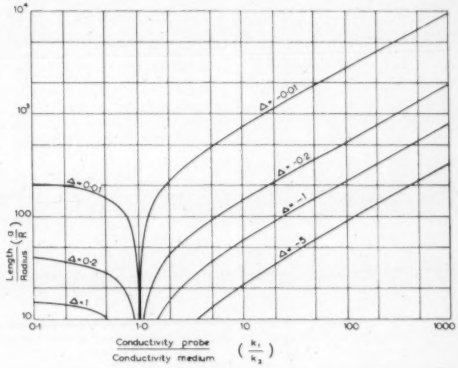

Fig. 2. The percentage change in mean temperature gradient produced by the presence of a conducting probe

which the upward heat flow may be about $1{\cdot}5 \times 10^{-3}$ cal cm^{-2} s^{-1}. This probe is also used in steaming ground[1] where the average heat flow is about 17×10^{-3} cal cm^{-2} s^{-1} and where the thermal conductivity may be 5×10^{-3} cal cm^{-1} s^{-1} °C^{-1}. There is considerable transfer of heat by water and steam movement through steaming ground and hence the "effective" conductivity of the ground may be considerably higher than that given above. Thus Benseman[2] finds that the temperature at 35 cm in steaming ground is approximately 70° C for a heat flow of 17×10^{-3} cal cm^{-2} s^{-1}; assuming that the temperature at the surface is 25° C, the effective conductivity is then approximately 13×10^{-3} cal cm^{-1} s^{-1} °C^{-1}.

The formulae given above show that the temperatures measured with this probe at various depths will differ from the original ground temperatures relative to the surface temperature, at the same depth by the percentages listed in the table.

Percentage and actual temperature errors introduced by the Duralumin probe

Conductivity of ground (cal cm^{-1} s^{-1} °C^{-1})	$0{\cdot}5 \times 10^{-3}$ *Error* (*a*)	$3{\cdot}0 \times 10^{-3}$ *Error* (*b*)	$13{\cdot}0 \times 10^{-3}$ *Error* (*c*)
Depth of insertion (cm)			
5	90% (−4·5° C)	58% (−1·5° C)	24% (−0·9° C)
10	74% (−7·4° C)	32% (−1·6° C)	9% (−0·7° C)
20	46% (−9·2° C)	13% (−1·3° C)	3% (−0·5° C)
50	15% (−7·5° C)	3% (−0·8° C)	0·6% (−0·1° C)
100	5% (−4·8° C)	0·8% (−0·4° C)	0·2% (−0·08° C)

(*a*) Temperatures given for a heat flow of $0{\cdot}5 \times 10^{-3}$ cal cm^{-2} s^{-1}.
(*b*) Temperatures given for a heat flow of $1{\cdot}5 \times 10^{-3}$ cal cm^{-2} s^{-1}.
(*c*) Temperatures given for a heat flow of $17{\cdot}0 \times 10^{-3}$ cal cm^{-2} s^{-1}.

Fig. 3 shows the manner in which the isotherms of the ground are distorted when the probe is inserted to a depth of 20 cm, (*a*) in ground, of thermal conductivity 3×10^{-3} cal $cm^{-1}\,s^{-1}\,°C^{-1}$, through which there is a heat flow of $1{\cdot}5 \times 10^{-3}$ cal $cm^{-2}\,s^{-1}$, and (*b*) in ground of thermal conductivity $0{\cdot}5 \times 10^{-3}$ cal $cm^{-1}\,s^{-1}\,°C^{-1}$ through which there is a heat flow of $0{\cdot}5 \times 10^{-3}$ cal $cm^{-2}\,s^{-1}$.

(ii) Sometimes no rigid probe is used. Suppose a compound cable consisting of five insulated copper wires and five insulated constantan wires (all 32 s.w.g.) leading to five thermojunctions is inserted into soil of conductivity 3×10^{-3} cal $cm^{-1}\,s^{-1}\,°C^{-1}$ to a depth of 35 cm. The effective conductivity of the compound cable is about 0·5 cal $cm^{-1}\,s^{-1}\,°C^{-1}$. Assuming that the upward flow of heat in the ground is $1{\cdot}5 \times 10^{-3}$ cal $cm^{-2}\,s^{-1}$, the above formulae show that the presence of the conducting wires lowers the temperature at the tip by $7{\cdot}8 \times 10^{-3}$ °C. If ten pairs of wires were used the temperature would be lowered by $14{\cdot}7 \times 10^{-3}$ °C.

If the copper wire is replaced by manganin wire, the conductivity of the combination is reduced from about 0·5 to 0·054 cal $cm^{-1}\,s^{-1}\,°C^{-1}$ and the temperature at the tip is lowered by only $0{\cdot}80 \times 10^{-3}$ °C for five couples and by $1{\cdot}52 \times 10^{-3}$ °C for ten couples.

(iii) A wooden probe 100 cm long and 2·54 cm in diameter carrying a pair of wires embedded in the wood has been used in several sectional temperature surveys of sections of the thermal regions of New Zealand. The presence of the wires should have a negligible effect. As the conductivity of the wood, approximately $0{\cdot}6 \times 10^{-3}$ cal $cm^{-1}\,s^{-1}\,°C^{-1}$, is very similar to that of dry ground, it is to be expected that a wooden probe would disturb the temperature much less than a metal one. Use of the above formulae through ground of conductivity 3×10^{-3} cal $cm^{-1}\,s^{-1}\,°C^{-1}$ shows that the temperature at the tip of the probe is raised by approximately 0·05%.

CONCLUSIONS

The above results show that for accurate measurements (to 0·01° C) of the temperature at a depth of 35 cm in the ground, a compound cable of up to ten 32 s.w.g. copper/constantan couples may be used without upsetting the ground temperatures sufficiently to affect the accuracy of the readings. For greater accuracy (to 0·001° C) it is advisable to replace the copper by manganin.

For less accurate measurements it appears that stoutly made wooden probes are quite satisfactory, but that metal probes, even fine ones, are likely to introduce large errors, especially in dry hot ground.

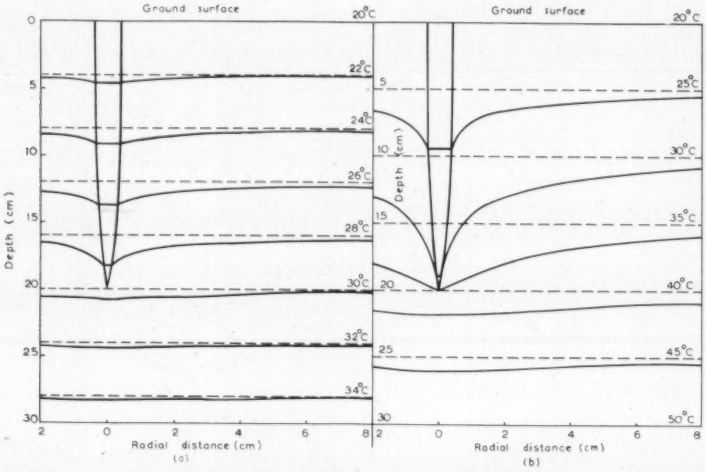

Fig. 3. Isotherms in the presence and in the absence of the conducting probe referred to in the first practical example

– – – – = undisturbed isotherms (before probe is inserted)
——— = disturbed isotherms (after insertion of probe)

REFERENCES

(1) BENSEMAN, R. F. *The natural heat output of Orakei Korako*. Internal Report R. 258 (Dominion Physical Laboratory, 1956).

(2) BENSEMAN, R. F. *Changes in the heat output from steaming ground at Orakei Korako and Wairakei*. Internal Report R. 277 (Dominion Physical Laboratory, 1957).

(3) MACROBERT, T. M. *Spherical Harmonics*, p. 198 (London: Methuen and Co. Ltd., 1947).

APPENDIX

Consider a prolate ellipsoid of revolution of length $2a$, diameter b and thermal conductivity k_1 situated in an infinite medium of conductivity k_2. Heat flows through the medium parallel to the axis of the ellipsoid at a rate Q from $z = +\infty$ to $z = -\infty$.

Laplace's equation applies both inside and outside the ellipsoid and this is given[3] in the elliptic co-ordinates (r, θ, ϕ)

$$\left.\begin{aligned} x &= (r^2 - e^2)^{1/2} \sin\theta \cos\phi \\ y &= (r^2 - e^2)^{1/2} \sin\theta \sin\phi \\ z &= r \cos\theta \end{aligned}\right\} \qquad (6)$$

as

$$\frac{\partial}{\partial r}\left[(r^2 - e^2)\frac{\partial T}{\partial r}\right] + \frac{1}{\sin\theta}\frac{\partial}{\partial\theta}\left(\sin\theta\frac{\partial T}{\partial\theta}\right) = 0 \qquad (7)$$

where the terms involving the co-ordinate ϕ are omitted because of the symmetry of the arrangement.

Inside the ellipsoid it is required that T be finite throughout, therefore

$$T = \sum_{n=0}^{\infty} A_n P_n\left(\frac{r}{e}\right) P_n(\cos\theta) \qquad (8)$$

whereas outside the ellipsoid

$$T = \sum_{n=0}^{\infty}\left[B_n P_n\left(\frac{r}{e}\right) + C_n Q_n\left(\frac{r}{e}\right)\right] P_n(\cos\theta) \qquad (9)$$

as for $\theta = 0$, $Q_n(\cos\theta)$ is not finite.

If the ellipsoid were not present then the temperature throughout the medium would be

$$T_1 = T_s + (Q/k_2)z \qquad (10)$$

$$= T_s P_0(r/e)P_0(\cos\theta) + (Qe/k_2)P_1(r/e)P_1(\cos\theta) \qquad (11)$$

This gives the temperature at $z = \pm\infty$.

Let the temperature inside the ellipsoid be $T_1 + T_{in}$ and the temperature outside be $T_1 + T_{out}$, then since T_1 gives the temperature at $z = \pm\infty$, T_{out} is zero for large values of r. Therefore

$$T_{out} = \sum_{n=0}^{\infty} C_n Q_n\left(\frac{r}{e}\right) P_n(\cos\theta) \qquad (12)$$

Now on the ellipsoid

$$T_1 + T_{in} = T_1 + T_{out} \qquad (13)$$

$$k_1(\partial/\partial N)(T_1 + T_{in}) = k_2(\partial/\partial N)(T_1 + T_{out}) \qquad (14)$$

where N denotes the outward drawn normal to the surface, but

$$\partial N/\partial r = [(a^2 - e^2\cos^2\theta)/(a^2 - e^2)]^{1/2} \text{ at } r = a \qquad (15)$$

Therefore, equation (14) becomes

$$k_1(\partial/\partial r)(T_1 + T_{in}) = k_2(\partial/\partial r)(T_1 + T_{out}) \qquad (16)$$

Substituting equations (8) and (9) in equations (13) and (14) and equating coefficients, then the temperature inside the ellipsoid is

$$T = T_s + \frac{Qz}{k_2}\left[1 - \frac{(k_1 - k_2)A}{(k_1 - k_2)A + k_2}\right] \qquad (17)$$

where

$$A = \left(\frac{a}{2e}\ln\frac{a+e}{a-e} - 1\right)\left(\frac{a^2}{e^2} - 1\right) \qquad (18)$$

and outside the ellipsoid

$$T = T_s + \frac{Qz}{k_2}\left(1 - \left\{\left[(k_1 - k_2)\left(\frac{a^2}{e^2} - 1\right)\left(\frac{a}{2e}\ln\frac{r+e}{r-e} - \frac{a}{r}\right)\right]\Big/ [(k_1 - k_2)A + k_2]\right\}\right) \qquad (19)$$

For a long narrow probe

$$a^2 - e^2 = R^2 \qquad (20)$$

$$a + e \simeq 2a \qquad (21)$$

hence

$$A \simeq \frac{R^2}{a^2}\left(\ln\frac{2a}{R} - 1\right) \qquad (22)$$

Technique for preparing thin films of α-iron

By D. G. Brandon, B.A., and J. Nutting, M.A., B.Sc., Ph.D., Department of Metallurgy, Cambridge University

[*Paper received* 16 *December*, 1958]

A technique is described for preparing foils of α-iron which are suitable for direct-transmission examination in an electron microscope. While there is no guarantee that a particular point on the foil will be thin enough for examination, results show that the technique produces foils enabling localized effects to be observed.

The direct-transmission examination of thin metal films in the electron microscope[1–4] has proved sufficiently successful to make it desirable to extend the technique to all metals and alloys. Tomlinson[5] has published details of polishing techniques for preparing foils from numerous pure metals, among them α-iron. A technique developed independently by the authors has been found to give consistent results and enables the thinned region to be taken from a pre-selected area—a factor which is of some importance when the relationship between the electron-transmission examination and the metallographic features observed using the more conventional techniques is considered.

EXPERIMENTAL PROCEDURE

The experiments were carried out on a sample of 99·97% high-purity iron (Code No. AH) supplied by the British Iron and Steel Research Association. Tensile specimens were prepared from foil of thickness 120 μ. The polishing technique is shown schematically in Fig. 1. The ends of the specimen are first blanked-off with Lacomit (by W. Canning and Co. Ltd.), a commercial blanking compound used in plating baths, and the central area is electropolished in a solution of 10 parts by volume of glacial acetic acid and 1 part of perchloric acid using a stainless-steel cathode and a current density of about 0·05 A cm^{-2} [Fig. 1(*a*)]. After polishing for fifteen minutes, the specimens are etched in 1% nital and can then be plastically deformed.

After deformation, the specimen is examined by optical microscopy. It is then blanked-off round the edges with Lacomit [Fig. 1(*b*)] and repolished in the acetic-perchloric

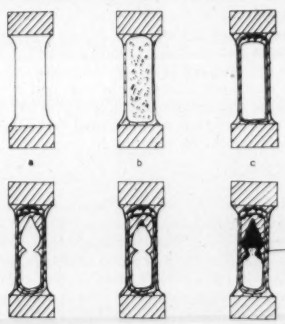

Fig. 1. Preparation sequence for thin films

acid polishing bath until perforation occurs. This always starts at the top of the specimen, at the edge of the layer of Lacomit.

When the specimen is perforated, it is removed, washed and dried, and the preferentially polished regions at the edge of the Lacomit layer are further blanked-off [Fig. 1(*c*)]. Polishing is again continued until perforation occurs a second time, when the specimen is again removed from the polishing bath, washed and dried, and a final coating of Lacomit is painted on in the shape shown in Fig. 1(*d*). The area required for examination is placed just above the waist of the unblanked-off area. In the final polishing sequence, perforation again starts at the top of the specimen and the perforated region grows slowly downwards [Fig. 1(*e*)]. When the perforated region has spread some distance down the specimen, perforation is also observed under the two overhangs forming the waist of the polishing region. Polishing is allowed to continue until the three regions in which perforation has occurred are just about to engulf the selected area *A* [Fig. 1(*f*)]. The specimen is then removed from the polishing bath and washed in methyl alcohol. The area *A* is cut away from the rest of the specimen and, after examination under an optical microscope to ascertain its geometrical relationship to the metallographic features on the original specimen, it is sectioned and mounted on copper grids for direct examination in the electron microscope.

Fig. 2. 70 μ grain size foil, 10% elongation showing dislocations

Fig. 3. Selected-area electron-diffraction pattern (same area as Fig. 2)

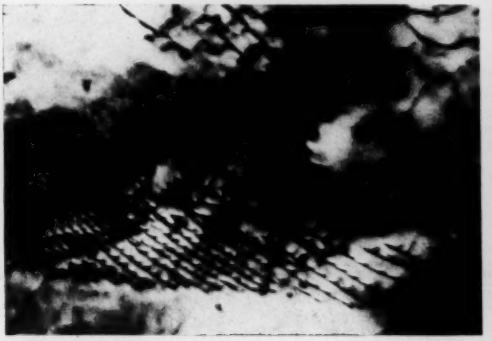

Fig. 4. 90 μ grain size foil, 7% elongation and annealed for 1 h at 550° C, showing dislocation networks forming sub-boundaries

RESULTS

Fig. 2 shows an area from a fine-grained foil given 10% deformation. The numerous networks are characteristic of deformed α-iron. A diffraction pattern from the same area is shown in Fig. 3. The diffraction spots are split into two and from their separation it is possible to calculate the misorientation across the network. The value obtained was approximately ½°. Fig. 4 shows an area from a similar specimen which has been polygonized by reheating for one hour at 550° C after 7% deformation. The dislocation arrangements are now far more regular and most of the dislocations lie in two-dimensional sub-boundary arrays.

DISCUSSION

Although there is no way of guaranteeing that a particular point on a foil will be thin enough for examination in the electron microscope, it is possible to use this technique to observe localized effects. In coarse-grained α-iron, a single-slip system observed in the optical microscope is operative over sufficiently large areas to ensure that the dislocation arrangement in the same system can be studied in thin films.

REFERENCES

(1) Hirsch, P. B., Horne, R. W., and Whelan, M. J. *Phil. Mag.*, **1**, p. 677 (1956).
(2) Whelan, M. J., Hirsch, P. B., Horne, R. W., and Bollman, W. *Proc. Roy. Soc. A*, **240**, p. 524 (1957).
(3) Nicholson, R. B., Thomas, G., and Nutting, J. *Brit. J. Appl. Phys.*, **9**, p. 25 (1957).
(4) Nicholson, R. B., and Nutting, J. *Phil. Mag.*, **3**, p. 531 (1958).
(5) Tomlinson, H. *Phil. Mag.*, **3**, p. 867 (1958).

NEW BOOKS SECTION

Contents

PAGE

Acoustics

Introduction to the theory of sound transmission, with application to the ocean . . . 259
Physical acoustics and the properties of solids . . . 259
Proceedings of the second conference on ultrasonics. 18–28 VI, 1956 . . . 259

Aerodynamics, flow and mechanics

Aerodynamik des Flugzeuges . . . 259
High speed aerodynamics and jet propulsion. Vol. III. Fundamentals of gas dynamics . . . 260
Technische hydro-und aeromechanik . . . 260
Axial flow compressors . . . 260
A handbook on torsional vibration . . . 261
Field studies of the movement of soil moisture . . . 261

Automatic control and recording instruments

Automatic process control . . . 261
Registrierinstrumente . . . 261

Chemistry and the properties of materials

Chemische Reaktionen ionisierender Strahlen (Radiation chemistry) . . . 262
Papers presented to the section on mineral chemistry. 16th International Congress of Pure and Applied Chemistry, Paris, 1957 . . . 262
Fast reactions in solids . . . 262
New chemistry . . . 262
Nomenclature of organic chemistry 1957 . . . 262
Mechanical properties of non-metallic brittle materials . . . 263
Modern materials. Advances in development and applications. Vol. 1 . . . 263
The structure and properties of porous materials . . . 263
Vacancies and other point defects in metals and alloys . . . 263

Electrical and electronic devices and properties

Propriétés et applications des transistors . . . 264
Transistor technology. Vol. 2 and Vol. 3 . . . 264
Halbleiterprobleme IV . . . 264
Principles and applications of random noise theory . . . 265
Quecksilber-niederdruckgasentladungen . . . 265
The plasma in a magnetic field. A symposium on magneto-hydrodynamics . . . 265
The principles of electrophoresis . . . 266
The theory and design of magnetic amplifiers . . . 266

PAGE

Heat thermometry and low temperature physics

Low temperature physics and chemistry. Proceedings of the fifth international conference on low temperature physics and chemistry . . . 266
Second symposium on coal preparation . . . 266
Conference on extremely high temperatures, Boston, Massachusetts, 18–19 March, 1958 . . . 266
Conduction of heat in solids . . . 267
Heat exchangers. Applications to gas turbines . . . 267
Thermische turbomaschinen . . . 267

Ionosphere

The ionosphere . . . 268
The magneto-ionic theory and its applications to the ionosphere 268

Manufacturers' publications

A story of temperature measurement . . . 268
Fifteen years of semiconducting materials and transistors . . . 268
Noble metal thermocouples . . . 268
Platinum in the glass industry . . . 268
Questions and answers on electron microscopes . . . 268
The dispersion of carbon black in rubber and its role in vulcanizate properties . . . 268
The properties and characteristics of aluminium casting alloys 268
Nickel alloys v. caustic alkalies . . . 268

Mathematics and tables

Analog simulation: solution of field problems . . . 269
Internal conversion coefficients . . . 269
Irreducible tensorial sets . . . 269
Tables of thermodynamic functions of air . . . 269

Miscellaneous and general physics

British coal mining explosives . . . 269
Fundamentals of advanced missiles . . . 270
Jahrbuch der wissenschaftlichen gesellschaft für luftfahrt E.V. (W.G.L.) . . . 270
Progress in non-destructive testing. Vol. 1 . . . 270

Nuclear and cosmic-ray physics, apparatus, techniques and data

1958 Annual international conference on high energy physics at CERN . . . 271
Bone and radiostrontium . . . 271

PAGE

Nuclear and cosmic-ray physics, apparatus, technique and data —continued

erenkov radiation and its applications 271
Effects of radiation on materials 271
Electromagnetic phenomena in cosmical physics. International astronomical union symposium No. 6 . . . 272
Extensive air showers 272
Free radicals as studied by electron spin resonance . . . 272
Glove boxes and shielded cells for handling radioactive materials 272
The nuclear handbook 273
Nuclear moments 273
Nuclear reactions. Vol. 1 273
Nuclear spectroscopy tables 274
Principles of quantum electrodynamics 274
Progress in nuclear energy. Series 1. Vol. 2. Physics and mathematics 274
Report of the United Nations Scientific Committee on the effects of atomic radiation. General Assembly. Official Records: Thirteenth Session, Supplement No. 17 (A/3838) 274
Safe handling of radioisotopes 275
Spectrum of atomic hydrogen 275
Tables of interatomic distances and configuration in molecules and ions 275
The physical theory of neutron chain reactors . . . 275

PAGE

Optics

Der lichtelektrische Effekt und seine Andwendungen . . 276
Optical properties of semi-conductors 276

Reference books

The BEAMA catalogue 276
British instruments, directory and buyers' guide . . . 277
Chemical engineering practice. Vol. 5. Fluid systems I. Vol. 6. Fluid systems II 277
The encyclopedia of chemistry (supplement) 278
Handbook of chemistry and physics 278
Handbook of physics 278
The technical writer 278

Solid state physics and crystallography

Growth and perfection of crystals 279
Preparation of single crystals 279
Solid state physical electronics 280
Solid state physics: Advances in research and applications. Vol. 7 280

Acoustics

Introduction to the theory of sound transmission, with application to the ocean. By C. B. OFFICER. (New York: McGraw-Hill Book Co. Inc.; London: McGraw-Hill Publishing Co. Ltd., 1958.) Pp. viii + 284. Price 77*s.* 6*d.*

To the average physicist it may come as a surprise that a book dealing with the theory of sound transmission should be written by a geologist. But when it is considered (1) that the sound transmission is in the sea, (2) that the propagation of sound in the sea and the earth beneath the sea is of great importance in oceanography and geophysics, and (3) that the author is also an associate in geophysics at the Woods Hole Oceanographic Institution, the authorship of the book is not so surprising after all. Professor C. B. Officer states in the preface that he is dealing primarily with the introductory theory of sound propagation in the ocean and in his acknowledgements refers to many well-known U.S. workers in this field, e.g. J. B. Hersey, M. Ewing, J. L. Worzel, and to assistance supplied by the Office of Naval Research and the Bureau of Ships, U.S. Navy. The subject is a difficult one and Professor Officer has made a praiseworthy effort in presenting the theory of sound transmission in deep and shallow seas in a stimulating and readable fashion.

The subject-matter is divided into six chapters. Chapters one and two deal with the fundamental relations of sound propagation and the general theory in terms of "normal modes" and of "rays". Chapters three and four consider respectively the transmission in shallow water (inshore seas and in deep water (the oceans). These two chapters are the heart of the book, and serve to indicate the theoretical complexities involved: the effects of depth and configuration of the bottom; the physical properties of the bottom material; the sound-velocity structure within the ocean (due to temperature and pressure gradients affecting sound velocity); the distribution of sound scatterers with the ocean; and the "shape" of the ocean surface. As the author very truly states, "a complete formulation with all possible variations of the above environmental conditions would be very difficult to obtain". The complications in shallow water transmission due to multiple reflexions between surface and bottom are dealt with on both "mode" and "ray" theories, but there is obviously much more to be done here to predict the sound distribution in a shallow sea even under the most "ideal" conditions of a flat bottom parallel to a flat water surface, isothermal water and a simple "theoretical" state of sound reflecting and absorbing sea bed.

The concluding chapters, five and six, deal respectively with reflectivity at changing boundaries and attenuation in the sea.

The book is well written, illustrated and reproduced. It can be recommended to physicists, geophysicists and geologists interested in this difficult but fascinating study of sound transmission in the sea. A. B. WOOD

Physical acoustics and the properties of solids. By P. MASON. (New York: D. Van Nostrand Co. Inc.; London: D. Van Nostrand Co. Ltd., 1958.) Pp. xii + 402. Price 67*s.* 6*d.*

Two earlier books by Dr. Mason in the Bell Laboratories Series are now well known, and the contents of this latest book are consistent with the reputation of the author and the series. It is unfortunate, however, that the title chosen for this book is so misleading. With very few exceptions the book deals solely with the generation and transmission of ultrasonic vibrations in solid materials, and is not concerned at all with physical acoustics as usually understood.

Part I explains, in the way that one would expect of Dr. Mason, the fundamentals of wave propagation in solids and includes descriptions of transducers, measuring instruments and specific applications such as delay lines, mechanical filters and ultrasonic equipment for drilling and soldering. Part II deals in considerable detail with the analytical uses of wave propagation in solids. It includes extensive discussions of thermal damping, grain and domain boundary scattering, the effects of dislocations, internal friction and similar effects.

The book will be useful to anyone engaged in the study of solid materials. It will also be an interesting introduction to the subject for more general readers, and it would make an excellent advanced textbook for the study of this branch of applied physics. A. E. DE BARR

Proceedings of the second conference on ultrasonics. 18–28 VI, 1956. (Warsaw: Polish Academy of Sciences, 1957.) Pp. 254. Price 41 zlotys.

It has been the fashion to hold congresses or symposia on ultrasonic subjects in recent years, indeed on the average they have become annual events. Some of these have dealt with industrial applications, others with more academic aspects of the subject. The report under review has a score of papers in the pure and applied fields of ultrasonics (with the latter predominating) and shows evidence of the important work in acoustics which is now being done in Poland.

Among the topics discussed there appear the formation and coagulation of aerosols, underwater echo-sounding, flaw detection in metals, methods of observing and measuring ultrasonic radiation. E. G. RICHARDSON

Aerodynamics, flow and mechanics

Aerodynamik des Flugzeuges. By H. SCHLICHTING and E. TRUCKENBRODT. (Berlin: Springer-Verlag, 1959.) Pp. xv + 455. Price DM. 52.50.

This volume and its projected companion are written by two well-known figures in German fluid mechanics to replace two German classics by Fuchs and Hopf, now outmoded by the rapid advances in aeronautical science in the last decade. They are aimed at the engineer and the engineering student who want a physical account of aerodynamics supported by experimental results and without making too many demands on mathematical technique.

The volume under review covers, in Part A, the fundamentals of fluid mechanics—the properties of air and of the atmosphere, incompressible and compressible inviscid flow and boundary layer theory. In Part B there is an introduction to the aerodynamics of aerofoils and an account of aerofoil theory for aerofoils of infinite aspect ratio. Other aspects of the aerodynamics of aerofoils will be dealt with in the companion volume.

I would take issue with the authors on one point: any attempt to understand compressible flow is, in my view, doomed to failure unless some elements of thermodynamics are discussed. It isn't appropriate to introduce the adiabatic law or the energy equation for the flow through a shock wave out of the blue for these are just as much part of fluid mechanics as are the equations of continuity or momentum. The authors are, nevertheless, to be congratulated on the amount of material they are able to convey between the single pair of covers, though as in all such works there is a danger that in

places the difficulties are too well hidden. There is no doubt, however, that it will be a useful addition to the already fairly numerous books in German in this general area.

L. HOWARTH

High speed aerodynamics and jet propulsion. Vol. III. Fundamentals of gas dynamics. Edited by H. W. EMMONS. (London: Oxford University Press, 1958.) Pp. xiii + 749. Price 140*s*.

Volume III of the Princeton series on "High speed aerodynamics and jet propulsion" is the sixth book of the series to be published. In this volume of eight sections, thirteen widely experienced scientists have endeavoured to distil the vast amount of experiment and theory accumulated in the study of gas dynamics. They have sought to emphasize fundamental aspects and approaches while, at the same time, maintaining a close touch with practical requirements and experimental results. This work should therefore be of permanent value to all who wish to deepen their understanding of this science. The sections are: *A*. The equations of gas dynamics (H. S. Tsien); *B*. One-dimensional treatment of steady gas dynamics (L. Crocco); *C*. One-dimensional treatment of nonsteady gas dynamics (A. R. Kantrowitz); *D*. The basic theory of gasdynamic discontinuities (W. D. Hayes); *E*. Shock wave interactions (H. Polachek and R. J. Seeger); *F*. Condensation phenomena in high speed flows (H. G. Stever); *G*. Gas dynamics of combustion and detonation (T. von Kármán; H. W. Emmons and R. S. Tankin; G. I. Taylor); *H*. Flow of rarefied gases (S. A. Schaaf and P. L. Chambré).

The book opens with a very general treatment (*A*), by Professor Tsien, of the equations of gas dynamics and a discussion of many different types of flow with appropriate methods of attack.

Professor Crocco's very comprehensive account of one-dimensional, steady, gas dynamics (*B*) is the longest section (285 pages) and forms a text for the design of nozzles, ducts, diffusers and other facilities. The assumptions of obliquity and uniformity, fundamental to the one-dimensional approach, are emphasized as limitations, although application can be widened by prescribing piecewise uniformity. Tangential flows, met in turbo-machinery, are left to Volume IX. There is a detailed discussion of the thermodynamics of working substances for perfect and real gases and an evaluation (with graphs) of correction factors. As the main purpose of the one-dimensional method, the flow in nozzles, diffusers and long ducts is analysed. Ideal, real, and incorrectly expanded nozzles are considered and thrust calculated. More general types of flow are considered and the method of Shapiro and Hawthorne described.

Section (*C*) on one-dimensional, non-steady, gas dynamics, by Dr. Kantrowitz, applies to flows in which the variables are functions of time and one spatial co-ordinate only. The theory of waves of finite amplitude began with Riemann and was expanded rapidly during World War II with applications to explosions and pulse jet engines (to be discussed in more detail in Vol. XII). Propagation of simple waves and the growth and decay of weak shocks are treated from a more physical standpoint than in the book of Courant and Friedrichs. Kantrowitz gives an authoritative analysis of the formation and stability of normal shock waves in steady channel flows, where the crux of the problem is the stability of smooth deceleration through the speed of sound, and where results have application to the design of supersonic diffusers.

The latter half of the book contains excellent discussion of many topics which will interest physicists and chemists. Professor Hayes (*D*) gives a penetrating discussion of gas dynamic discontinuities (shocks and combustion waves), pointing to the inadequacies of the theoretical treatments of shock structure, and Drs. Polachek and Seeger (*E*) describe the interactions between shock waves and obstacles (reflexion and refraction). Dr. Stever (*F*) treats the condensation phenomena in high speed flows, a subject of considerable importance in hypersonic wind tunnel design. Jet propulsion has caused the aerodynamicist to enter the field of physical chemistry and there is a composite section (*G*) on gas dynamics applied to combustion and detonation to which Dr. von Kármán, Professor Emmons, Dr. Tankin and Sir Geoffrey Taylor have contributed. Finally, Drs. Schaaf and Chambré (*H*) summarize the flow of rarefied gases, including free molecule and slip flow, with a review of experimental data from low density tunnels.

The volume editor must be commended on combining the efforts of so many eminent authors under one cover, but there is some overlap between sections and with other volumes of the series, while some potentially important new topics are not considered. There is no discussion of the highly energetic gas flows which are now produced in shock tubes and electrical discharges, and only passing mention of magneto-gas dynamics, of increasing interest to those studying cosmic and high temperature physics. But these can only be small criticisms in face of such a wealth of assembled knowledge.

J. D. JUKES

Technische hydro-und aeromechanik. By W. KAUFMANN. (Berlin: Springer-Verlag, 1958.) Pp. viii + 386. Price DM 37.50.

As one might expect of most second editions, this one embraces much of the first (reviewed in the *Brit. J. Appl. Phys.*, **5**, p. 457 [1954]) and adds to it some thirty-five pages of new material. This additional material increases the store of information already present without increasing substantially the depth of penetration on any one front. The additions include a more general treatment of Bernoulli's equation, a section on the viscous effects of rotation, a useful section following Wieghardt and Truckenbrodt on the energy equation for boundary layer flow, some further observations on wind resistance and the forces it generates, further contributions to aerofoil theory both in relation to the trailing-vortex system and lifting-line and lifting-surface theory, and finally there is some expansion of the section on compressible flow. This latter, at least in its treatment of boundary layer theory, removes one of the criticisms in the earlier review about the absence of any statement of the energy equation. The index is still not, in your reviewer's opinion, detailed enough and the absence of an author index is still a limitation on the book's value.

L. HOWARTH

Axial flow compressors. By J. H. HORLOCK. (London: Butterworths Scientific Publications, 1958.) Pp. xvi + 188. Price 40*s*.

This book provides a summary and a critical review of the theory and experimental data on which the design of axial-flow compressors is based. A knowledge of fluid mechanics and thermodynamics up to degree standard is assumed, and the book begins with a summary of the relevant principles of these subjects. The author then deals with both the theoretical and the experimental approaches to the problem

of two-dimensional flow through cascades of blading, and goes on to discuss "two-dimensional" methods of design based on conditions at a mean flow line. The three-dimensional flow through a compressor stage is treated in terms of the radial-equilibrium and actuator-disk theories, and this is followed by consideration of the real-fluid effects influencing compressor performance. There are chapters on stalling and surging, and compressor testing, and the book concludes with a short note on supersonic compressors.

One of the greatest merits of the book is that it brings together information from a large number of sources, and discusses from a fundamental standpoint present ideas on the various aspects of the subject. A total of 189 references are quoted. The text itself is a model of clear and precise wording.

Although not a designers' handbook in the true sense, it covers the background to axial-flow compressor design so thoroughly that it is likely to become a standard reference on the subject. H. C. WILKINSON

A handbook on torsional vibration. Compiled by E. J. NESTORIDES. (London: Cambridge University Press, 1958.) Pp. xxii + 663. Price 110*s*.

Much has been written on torsional vibrations, and this book is a collection of the useful and important material on the subject presented in a logical and convenient manner. Although the essential skeleton of the book is simple, each consideration has been developed with such thoroughness and care that the book swells to its size of over six hundred pages. The presentation is intelligent, and the important fundamental theory is fully developed. In addition, the many formulae which are recommended do not, as is often the case with handbooks, stand in solitude without explanation or reference. Each formula has adequate explanation and is either derived in the text, or the complete reference given. This feature should appeal to people who demand the confidence which comes from complete understanding. The book has been compiled with a thorough knowledge of the problems which confront the person engaged in practical design and development. Besides the basic theory, semi-empirical formulae useful at the design stage, practical points of design and experimental techniques have been fully discussed. When appropriate, every major consideration has been illustrated by completely worked out calculations. The illustration of the Holzer tabular method for the determination of the natural frequencies, for example, is a model of clarity.

The book consists of four parts, the first of which deals with the reduction of the engine to an idealized system whose natural frequencies are then found by the Holzer tabular method. There are many sample calculations for straight and branched systems, with gear and belt coupling. The second part deals with the determination of stresses in the shaft. In order to find the stresses which occur at speeds in the vicinity of the natural frequencies, the effect of damping has been very fully discussed. Much information on the damping effect of the component parts of the machine has been collected. Calculations involving damping have been illustrated using graphical means and Spaetgen's extension of the Holzer method. The third part deals very fully with the design and operation of various types of tuning disks, and the final part discusses experimental methods in connexion with torsional vibrations.

This book should prove to be an authority of immense value to design engineers, and to those with an advanced knowledge of the subject. F. A. LECKIE

Field studies of the movement of soil moisture. By W. P. M. BLACK, D. CRONEY and J. C. JACOBS. (London: Her Majesty's Stationery Office, 1958.) Pp. vi + 74. Price 6*s*.

In scope and quality the material in this Road Research Technical Paper No. 41 would be entirely suitable for publication in the *British Journal of Applied Physics*. It presents an account of 5 year measurements of the seasonal changes of water content under bare soil, grass cover, and impervious pavements, on three types of soil in southern England. The results are clearly presented and thoroughly discussed in physical and meteorological terms, and their application to the design of road and airfield pavements is reviewed in detail.

Considering the high quality of reproduction of the 52 diagrams and 9 tables the price is very low, and the paper is confidently recommended to anyone who has even a remote interest in the physics of soil water. H. L. PENMAN

Automatic control and recording instruments

Automatic process control. By D. P. ECKMAN. (New York: John Wiley and Sons Inc.; London: Chapman and Hall Ltd., 1958.) Pp. vii + 368. Price 72*s*.

Revision and expansion of the author's earlier book, *Principles of industrial process control* (1945), has produced a very readable and systematic course for students of process control. Experimental exercises and written problems are included, but except for a few historical papers, there are no references to the published literature. There is a good account of two-position control and a good chapter on regulating units includes some unusually clear words on valve sizing. In the description of the simple exponential transfer stage, however, the book inherits some of the confusion of its predecessor and the impression is still left that the presence of more than one capacitance is important in the definitions of transfer lag and time-constant.

Inevitably, the chapters relating to system design appear weakest. But this apparent weakness is largely a reflexion of the state of ignorance of the more complex processes and it might have been appropriate to give the student some idea of the nature of the material to which he may have to apply the methods he has learnt. J. MCMILLAN

Registrierinstrumente. By A. PALM. (Berlin: Springer-Verlag, 1959.) Pp. viii + 255. Price DM 27.

The author died while working on the 2nd edition of this book and the volume was completed by Dr. Roth and Dr. Schlosser. The treatment is non-mathematical, and instruments for recording measured information are systematically described.

The book deals, firstly, with various types of charts, DIN standards and shrinkage. A chapter on pens and inks follows and specially prepared charts for chemical or spark recording are then discussed. Descriptions of several forms of dotting- and multi-point recorders are followed by a chapter on chart drive mechanisms.

Part 3 deals with the problems of the measuring devices; conversion of rotary into linear deflexion; effect of damping on the accuracy of the record, and the correct choice of chart speed. Part 4 gives a more detailed description of recorders for mechanical force, movement and speed, pressure, flow and temperature. Spectral photometers and calorimeters are also discussed and, as German railways and road transport firms make frequent use of tachographs, some typical instruments are described. Most useful for the potential exporter

are the standardized measurements of recorders and indicators and the suggestions for their arrangement to give maximum information with a minimum of panel space.

Among the special instruments discussed are high-speed, fault and operation recorders and three types of maximum demand devices which present the information graphically, in printed figures or in punched code. A number of electronic self-balancing instruments are dealt with as well as spot followers and Duddell oscillographs. While much of the equipment described is of Continental design, British and American instruments have not been neglected.

A valuable feature of the book is the large number of clear illustrations and isometric diagrams, most of which are self-explanatory. The bibliography of 269 titles is fairly up to date (1957) and the index follows a list of manufacturers who helped to supply the wealth of information contained in this slender volume. P. LEWIS

Chemistry and the properties of materials

Chemische Reaktionen ionisierender Strahlen (Radiation chemistry). By H. MOHLER. (Aarau: Verlag H. R. Sauerlander and Co., 1958.) Pp. 299. Price DM 30.80.

Papers presented to the section on mineral chemistry. 16th International Congress of Pure and Applied Chemistry, Paris 1957. (London: Butterworths Scientific Publications, 1958.) Pp. 891. Price 97*s.* 6*d.*

Physicists often light-heartedly argue with their chemist friends that chemistry is a branch of physics, and the books under review do much to support this proposition. Both are published versions of conferences; one, held with commercial backing at Basel in 1956; the other, held by the I.U.P.A.C. in Paris in 1957. Apart from this, the two volumes have little in common.

The first, of which about two-thirds is in German and the rest in English, contains useful introductory chapters on the action of radiation on matter (by H. Mohler), on dosimetry, and on the fundamentals of radiation chemical reactions (both by W. Minder). There is also an authoritative chapter by Charlesby on the "Effects of atomic radiations on polymers". A patchy chapter on radiation sources is included, in which the section on linear accelerators is devoted almost entirely to the products of one firm and in which the section on reactors conspicuously lacks authenticity. Finally, there is a chapter on "Radiation-induced reactions of potential industrial importance", which is a combination of catalogue, research programme, and proposals for equipment yet to be developed, which, in the reviewer's opinion, is out of place. The production of the book is good and there is an adequate index in both English and German.

The second book under review represents the contributions of many authors. There are about 150 papers, of which about half are in English, nearly one-third in French, and just under one-sixth in German, together with two isolated papers in Italian. There are sections on "solid compounds of transition metals"; "compounds of boron with hydrogen and non-metallic elements"; "elements of the actinium series"; "chemical properties of bodies at high temperatures"; and a miscellaneous section. The volume is characterized by a high standard; a few papers that the reviewer noted were, in alphabetical order, Bagnall on polonium; Gorter on ferro- and anti-ferromagnetic compounds; Maddock on protactinium and its neighbours; Nowotny on mineral compounds of germanium; Seaborg on the actinide elements; and Sidhu on neutron diffraction.

There is, as already mentioned, a considerable physical content in the papers reproduced. The importance of structure analysis by diffraction methods is evident at even a casual glance, and among physical topics considered are: electrical properties; ferro-, ferri- and anti-ferromagnetic properties; electronic energy levels; Raman effect; spectrophotometry; infra-red spectroscopy; mass spectroscopy; solar furnaces; transistors; paramagnetic resonance spectra, etc. etc.

The book is printed in France and is without index or list of contents, apart from a "table of contents" arranged alphabetically by authors. It is thus difficult to find what is in the book, and particularly to discover where the various sections begin and end, without a good deal of trouble. This is both irritating to the reader and unjust to the contributors. J. THEWLIS

Fast reactions in solids. By F. P. BOWDEN and A. D. YOFFE. (London: Butterworths Scientific Publications, 1958.) Pp. ix + 164. Price 40*s.*

A more accurate, but perhaps rather unwieldy, title for this book would be: "Research notes on the decomposition, burning and detonation of condensed explosives." It deals chiefly with experiments on these topics carried out by the authors and their colleagues in the Physics and Chemistry of Solids Laboratory, Cambridge, and is concerned with posing problems and being up to date, rather than with being a definitive study. The tone may be indicated, for example, by the use of the present tense in the Conclusion of Chapter 4: "A detailed examination of the . . . properties of the azides is being made." It is, therefore, essentially a book for research workers in the explosives field. They have in the past been indebted to these authors for many valuable contributions and they will find the present book helpful and stimulating. T. L. COTTRELL

New chemistry. Edited by D. FLANAGAN. (New York: Scientific American, Inc.; London: G. Bell and Sons Ltd., 1958.) Pp. xi + 206. Price 13*s.* 6*d.*

Based on recent articles in *Scientific American*, the 16 sections in this book give a popular account of recent work on the borderline between physics and chemistry. Since all but one of 17 authors are active workers in their subjects, the articles are accurate, if perhaps unnecessarily elementary. Subjects covered are the chemistry of fast and high-temperature reactions; free radicals, including those due to high-energy radiation; and new methods such as the use of ultra-small quantities, infra-red spectroscopy, chelation and ion-exchange. The second half of the book deals with some new materials resulting from new methods: the rare earths; radio-isotopes; trans-uranic elements; plastics and detergents. The book is in no sense a textbook, and would be light reading for the professional chemist or physicist, since it assumes substantially no previous knowledge. It could be recommended as a very simple introduction to recent advances for those whose work lies in other fields. C. G. GARTON

Nomenclature of organic chemistry 1957. (London: Butterworths Scientific Publications, 1958.) Pp. 92. Price 15*s.*

This book contains three reports from the International Union of Pure and Applied Chemistry. (1) Definitive rules for hydrocarbons and for fundamental heterocyclic systems; (2) Definitive rules for steroids and (3) Tentative rules for Vitamin B compounds.

Though primarily intended for the guidance of organic

chemists, these reports will be of value to many physicists, in their reading of organic chemical literature and also, should they wish to refer to complex organic compounds in their own writings. The book is beautifully and accurately printed.

Perhaps it would be too much to expect that the index should contain all the compounds listed in the book; but a more complete index would have been helpful to those who are not organic chemists. Such terms as "alkadiyne," "isoprene," "toluene," "*peri*-fused" are sought in vain in the index but discussed in the book.

The organic chemists are to be congratulated on having reached so wide an international agreement on nomenclature in so complex a field. G. W. SCOTT BLAIR

Mechanical properties of non-metallic brittle materials. Edited by W. H. WALTON. (New York: Interscience Publishers Inc.; London: Butterworths Scientific Publications, 1958.) Pp. xi + 492. Price 90*s*.

This volume is a record of the proceedings of a conference, held in London in 1958, which was organized by the Mining Research Establishment of the National Coal Board in consultation with the Building Research Station. As would be expected from its origin, the materials discussed are those of interest to the mining and building industries; resins and organic glasses are not included. Of the twenty-seven papers, ten are concerned primarily with coal, six with concrete, five with rocks, four with glass and ceramic materials, one with plaster and one with graphite.

Specialized interests are well covered, but the papers include a fair proportion which attempt to provide a basic interpretation of the phenomena of brittle fracture and associated properties which will be of interest to physicists in other fields. Particular mention may be made of the paper by Evans and Pomeroy, which develops a statistical theory of fracture to account for the observed relations between size of specimen and breaking strength, the paper by Schiller on the effect of porosity on strength, the review by Miss Walton on the strength of glass, the study of the mechanism of rock fracture by Seldenrath and Gramberg, which discusses the remarkable phenomenon of longitudinal splitting under compressive loading, and Davidson and Losty's paper on carbon and graphite. The papers on the action of cutting tools are also of considerable general interest both from the theoretical and practical viewpoints.

By contrast with the success which appears to have been achieved in the explanation of the fracture of such a complex material as coal, the apparent lack of progress on the subject of concrete—judged by the papers in this volume—is disappointing. This subject appears to have got stuck at the "spring-and-dashpot" level. Whether this is due to its inherent difficulty or to an inadequate scientific effort on the part of the building industry is a matter for speculation.

While most of the papers are very readable, some could have been improved by a few words of explanation of technical terms. How many physicists know the meaning of a "balanced [explosive] charge" (p. 358) or are familiar with "frogs" in bricks (p. 51)?

With these reservations the book can be recommended.
L. R. G. TRELOAR

Modern materials. Advances in development and applications. Vol. 1. Edited by H. H. HAUSNER. (New York: Academic Press Inc.; London: Academic Books Ltd., 1958.) Pp. xi + 402. Price 89*s*. 6*d*.

The prolific evolution of new materials or of conventional materials with improved properties makes it increasingly difficult for the physicist and engineer to keep abreast of the new and improved products provided by the chemist and the metallurgist. A planned series of volumes on "Modern materials" attempts to provide some answer to this problem.

The book under review, the first volume in the series, presents a collection of 8 monographs compiled by specialist authors. The materials dealt with are wood, synthetic rubbers, fibre materials, high voltage insulation papers, glasses for nuclear applications, modern ceramics, germanium and silicon, and zirconium. The production, properties and application of these materials are described, with special emphasis on recent developments.

With such a miscellany of materials of widely differing technical importance some unevenness of treatment is probably inevitable. Thus, in the section on fibre materials, potentially a vast subject, the author has, perhaps wisely, dealt briefly with the well publicized organic fibres and has concentrated on providing information on inorganic fibres. On the other hand, the section on germanium and silicon is unnecessarily discursive in places and certainly the discussion on determination of trace impurities in germanium and silicon seems superfluous in a book of this type.

Apart from such anomalies, the book provides a useful digest of information on the various materials and is well provided with references to more detailed treatments of the subject-matter. H. J. CLULEY

The structure and properties of porous materials. Edited by D. H. EVERETT and F. S. STONE. (New York: Academic Press Inc.; London: Butterworths Scientific Publications, 1958.) Pp. xiv + 389. Price 60*s*.

This book is a record of the proceedings of the tenth symposium of the Colston Research Society held in the University of Bristol in March 1958. It includes the eighteen set papers and the complete discussion. There is an introductory lecture by Sir Eric Rideal, and other contributions include fundamental theoretical papers on porosity by Professors J. H. de Boer and D. H. Everett, valuable general discussions of sorption on various types of absorbent by Professors R. H. Barrer, A. V. Kiselev and others, and treatments of systems of practical interest, such as paper and building materials.

The value of such a volume is that the contributors have had the opportunity to expound their ideas free from some of the more stringent limitations of space and originality usually enforced in the journal literature, and so have been able to produce papers of wide scope and interest. The drawback is that along with such papers there are others which, though valuable in themselves, might equally well have appeared in the usual literature. The inclusion of all the papers and all the discussion means that the book is so large and relatively expensive that most workers will content themselves by reading it in libraries, where it should certainly find a place, whereas a smaller volume of *selected* papers might have commanded a wider sale. This would presumably have been against the policy of the Society, and perhaps made the task of the editors unduly hard. The editors and publishers are to be congratulated on the clarity of the presentation. T. L. COTTRELL

Vacancies and other point defects in metals and alloys. (London: The Institute of Metals, 1958.) Pp. 238. Price 40*s*.

The latest volume in the "Monograph and Report series", published by the Institute of Metals, conforms to the high standard of earlier issues. This monograph contains six papers and discussion on them presented at a symposium held

in December 1957. The papers deal with the role of vacancies and other point defects on the mechanical properties of metals and alloys at low temperatures (Cottrell) and at high temperatures (McLean). Their influence on diffusion in metals (Lomer), surface properties (Williams and Hayfield) and other physical properties (Broom and Ham) are also outlined, together with an account of their effects on the mechanical properties of ionic crystals (Pratt). The discussion on the papers shows both the interest aroused in the topics and the wide variety of problems to which these well-established concepts are now being applied with considerable success.

J. NUTTING

Electrical and electronic devices and properties

Propriétés et applications des transistors. By J. P. VASSEUR. (Paris: Society Francaise de Documentation Electronique, 1958.) Pp. viii + 479. Price 5540 fr.

This book, written in French, is primarily for the circuits engineer. It does, however, seek to give him a basic understanding of semi-conductor theory and the thermal and electronic processes involved in transistor action. Although each subject is taken to a considerably advanced level, each part of the book is introduced in elementary terms.

Like its several English counterparts, the book begins with a description of the diamond lattice and works its way through to the equivalent circuit of a simple transistor by way of energy bands, donors and acceptors, Czochralski pulling, alloying and diffusion, field and diffusion currents and *p–n* junctions. The introduction ends with a description of the principles of operation of the drift, field effect, *p.n.p.n.* and other types of transistor. The Mesa construction, however, does not receive a mention.

A useful section on the theory of linear four-pole networks including Thévenin's theorem and six tables of the relations between the various parameters and their matrices is followed by three long sections on transistor characteristics, linear amplification and the biasing circuits. The book ends with sections on the power handling capacity of transistors and transistor noise which are very useful and make up for the surprising lack of emphasis on high frequency operation.

Copious diagrams, tables and bibliographies enhance the value of this very capable book although the English-speaking reader will find little that is not already easily accessible in his own language.

J. HOUGHTON

Transistor technology. Edited by F. J. BIONDI. (New York: D. Van Nostrand Co. Inc.; London: D. Van Nostrand Co. Ltd., 1958.) **Vol. 2.** Pp. xiii + 701. Price 131*s.* 6*d.* **Vol. 3.** Pp. xiii + 416. Price 94*s.*

The basic principles of transistors and the properties of germanium were the main topics of Volume 1. In Volume 2 the first section deals primarily with the properties and technology of silicon and later sections discuss the general principles of transistor design. The book is a compilation of articles by a number of authors, most of whom are on the staff of the Bell Laboratories. All the material in Volume 2 has been published previously, either in journals or in special articles.

The sections on design start with *p–n* junction diodes, and include *p–i–n* junctions, the mechanism and consequences of avalanche breakdown, and the properties and possible developments at very high frequency. The triode chapter starts with switching performance, and continues with small signal a.c. transmission characteristics and other more general design aspects, including high-frequency requirements. Details of base-layer design are the subject of the final articles in this chapter. There is a separate chapter dealing with special switching devices, that is to say avalanche transistors and *p–n–p–n* switches. There is a short section on tetrodes followed by a chapter on devices sensitive to radiation, both radio-active and optical. The final sections deal with the field-effect transistor, transistor noise behaviour and the effects of surfaces on transistor design.

The collection of these papers and articles into one volume will be of great convenience to the transistor technologist and to all who are concerned with the applications of solid state physics to *p–n* junction devices.

The first part of Volume 3 of *Transistor technology* deals with the fundamental aspects of preparing *p–n* junction structures. Details are given of the basic aspects of junction formation by diffusion, by control of growth rate and by forming and solidifying a molten zone. The technique of zone-melting using a stationary temperature gradient is also discussed.

The second section of the book deals, in particular, with chemical processing in general and etching techniques, followed by the provision of ohmic contacts. Details are then given of the techniques for making alloyed junction transistors in germanium, alloyed junction diodes in silicon, diffused rectifiers and avalanche diodes in silicon and diffused-base transistors in both germanium and silicon.

The third section treats the various methods for determining bulk lifetime and surface recombination velocity, and proceeds to discuss the testing of *p–n* junction devices and the measurement of transistor characteristics.

The final section deals with transistor reliability and its assessment.

Unlike Volume 2, Volume 3 contains a considerable amount of new material specially written for this series. Of twelve chapters, seven are wholly new and two are partly so. Like Volumes 1 and 2, Volume 3 is well edited and produced, and will be welcomed by everyone engaged in the manufacture of transistors and related devices.

D. A. WRIGHT

Halbleiterprobleme IV. By W. SCHOTTKY. (Braunschweig: Friedr. Vieweg and Sohn, 1958.) Pp. vii + 381. Price DM 46.80.

Since 1953, review papers read at yearly meetings of the semi-conductors section of the association of German physical societies have been published under the title of "Semiconductor problems". The present volume covers the fourth meeting held in Heidelberg in September 1957. (There was an interruption to the yearly meetings in 1956 due to the international conference at Garmisch-Partenkirchen.) The selection of topics in this series is based on a systematic classification, projected in the first volume, to cover the whole field of semi-conductors. The progress so far achieved, by the four volumes of the series, is examined in this book.

The articles were revised and extended by the authors in conjunction with the distinguished editor of the series, Professor Walter Schottky, who has also added a large number of very useful comments throughout the book and made important contributions to the conference discussions which are collected at the end of each paper; he has set a high standard for future editors, this being the last volume he will edit. Of the seven articles in this volume three are on aspects of pure physics, two on technical applications and two on rather restricted topics. Haken describes the modern theory of exctions and considers experiments in which they are involved. Haasen and Seeger discuss dislocations in

diamond type lattices and their effect on the electrical properties of semi-conductors with special reference to a large number of experiments on germanium. Schön presents an exhaustive calculation for a simple model of a photoconducting phosphor involving two types of lattice defects on which electrons or holes can be trapped and then recombine with carriers of the opposite sign. Various experiments on light emission and photoconductivity are discussed in terms of the model and necessary extensions are considered. Dosse gives a mainly technical account of the various types of junction transistors and their application in a large number of devices. Lautz discusses the conditions under which semi-metals and semi-conductors produce efficient thermoelectric generation or refrigeration. Koswig and Stasiw describe the observed absorption spectra due to interstitial divalent impurities in alkali and silver halides. (Here Schottky's interpretation of the results, which is presented in the discussion, is far more reasonable than the authors' own.) Schottky revises and extends his previously suggested method of denoting defect centres.

The whole series can be thoroughly recommended to scientific and technical libraires. R. STRATTON

Principles and applications of random noise theory. By J. S. BENDAT. (New York: John Wiley and Sons Inc.; London: Chapman and Hall Ltd., 1958.) Pp. xxi + 431. Price 88*s*.

With the increasing interest in methods of predicting the behaviour of control systems in the presence of disturbances, presentations of the theory of random noise from this view point are welcome. The author of this volume has been able to turn the results of his practical and theoretical experience in the handling of noise problems to good account by preparing a well-organized book.

Introducing the subject-matter carefully by discussions on random processes and the properties of random processes in systems, the practical aspect of the subject is strongly maintained by a section concerned with the difficulties in the measurement of power spectra. Sympathetic understanding of the engineer's or applied physicist's conceptual aptitudes has guided the author to reserve his chapter on probability theory to the point following this introduction so that the reader is made to feel a continuity between this theory and his familiarity with spectra. One might perhaps, therefore, have considered the author's dismissal of the subject of optimum linear prediction and filtering in constant parameter systems on the basis of least mean square error in one chapter as being a little perfunctory. But at least the rules for the operation of the technique are well traversed and the extension from the limitation of the Wiener assumptions to the rather more realistic Floyd method is demonstrated. However, in the chapter which follows, providing examples of the usefulness and the possibilities of representation of random phenomena in nature by exponential-cosine correlation functions, the author is once more, very much *en famille*.

The theory and practice of analogue simulation for the investigation of noise conditions in constant parameter and time varying parameter systems and examples which are helpful in later sections of the book are provided when more difficult solutions of optimum time varying parameter systems are worked through.

Following up this chapter, the subject of errors in auto-correlation measurements is comprehensively treated, from the basic statistical theory to the consideration of the measurement of normal random noise to assessments of auto-correlation functions in the presence of extraneous noise. A section on the probabilities of no correlation and false correlations is worthy of mention. In many practical cases where the correlation is performed after envelope detection, the effect of the detector or non-linear device on the correlation function to be determined is required. This matter is fully investigated in video correlations with linear and square law envelope detectors. A method by which the solution of the integral equation involved in the optimization problem, in terms of time varying parameters is explained in detail. It is shown that simplifications to the system may be obtained in circumstances where the system is to be used for using long or very short times and that in the synthesis, this assumption may be used to obtain a simplified weighting function without having to realize the optimum weighting function valid for all circumstances.

In the final chapter, the problem of zero-crossing has been expanded to a point where an easy understanding of S. O. Rice's original analysis may be reached.

An extensive bibliography of nearly 150 references completes a very useful book for the applied scientist or engineer wishing to become familiar with the theory and methods available to solve fundamental noise problems in control systems. P. R. JOANES

Quecksilber-niederdruckgasentladungen. By M. J. SCHONHUBER. (Munchen: Hochschulbuchhandlung Lachner, 1958.) Pp. 111. Price DM. 18.

This little book, which is the text of a thesis from the Technische Hochschule, Munich, covers in considerable detail the author's work on the cause and behaviour of space charge double layers and the resulting striations in a low pressure mercury vapour discharge.

Most of the measurements were made by probes, and the introduction into the probe characteristics of additional discontinuities by the presence of fast electrons accelerated through space charge double layers is clearly demonstrated, and is treated at some length theoretically. The effect on the double layers and striations of increasing or decreasing the local plasma density by a separate discharge, or by the introduction of a molecular gas, is demonstrated by photographs of the discharge as well as by the electrical measurements.

The book is naturally very specialized, but should be of interest to those using probes in low pressure discharges.
M. P. REECE

The plasma in a magnetic field. A symposium on magneto-hydrodynamics. Edited by R. K. M. LANDSHOFF. (Stanford: University Press; London: Oxford University Press, 1958.) Pp. v + 130. Price 36*s*.

This book comprises ten papers read at the second symposium of magnetohydrodynamics sponsored by Lockheed Missile Systems Division and held in California in December 1957. The first two papers deal with the equations of motion of charged particles in electromagnetic fields and the derivation of the magneto-hydrodynamics equations. These follow two papers on the pinch effect, one on the confinement of a plasma by radio-frequency fields, three experimental papers and one theoretical paper on intense shock waves in magnetic fields, and one astrophysical paper on the stability of the gas stream from the sun. The papers are by well-known experts in this field and are of considerable interest to the specialist. No attempt has been made to review any of the subjects dealt with, nor are the papers comprehensive, and hence this is not a suitable book for the person entering this field or for the general reader. A. A. WARE

The principles of electrophoresis. By R. AUDUBERT and S. DE MENDE. (London: Hutchinson Scientific and Technical, 1959.) Pp. viii + 142. Price 25*s*.

This is indeed a welcome book. Electrophoresis, i.e. the movement of particles in relation to a liquid by the application of an electric field, is finding increasing use in many laboratories. The introduction of supporting media (gels, powders, paper, etc.) eliminates the drawback of gravitational convection, and the method can be made fully quantitative. Both theory and practice are well balanced.

The authors discuss electro-osmosis as well, but not streaming potentials or sedimentation potentials. This is a pity, because an aesthetic point of great value is missed, namely that of the four possible types of electrokinetic effects mentioned above; in the first two, an applied potential produces tangential motion, whereas in the last two tangential motion produces a potential. F. I. G. RAWLINS

The theory and design of magnetic amplifiers. By E. H. FROST-SMITH. (London: Chapman and Hall Ltd., 1958.) Pp. xix + 487. Price 75*s*.

This is probably the most complete work on this subject yet available and it is a scholarly and at the same time practical account. All aspects of the subject are dealt with, from basic principles to details of design, and the book will be of great value to engineers designing or using magnetic amplifiers.

It seems unfortunate, however, that so little should be said about the place of magnetic amplifiers in the range of amplifying devices. Apart from applications for which magnetic amplifiers are peculiarly suitable, such as the measurement of large direct currents, most of the applications for which magnetic amplifiers are suitable seem ill-defined. The author can probably decide quickly enough whether a magnetic amplifier would be suitable for any particular purpose but, beyond a brief review of actual applications and a list of reasons why electronic amplifiers are "sometimes" unsuitable for use as instrument amplifiers, he is not very helpful to the non-expert who may be wondering whether or not a magnetic amplifier would be suitable for his purpose. The properties of electronic amplifiers are much more widely known than those of magnetic amplifiers and a comparison of the properties of the various devices would have rounded off the book nicely.

But, strictly within the scope of its title, the book can hardly be faulted and will undoubtedly become a classical work on the subject. A clear account of the basic operation of transductors is followed by a detailed analysis of transient and steady state operation, including self-excited and auto-excited transductors. The frequency response of transductors is dealt with fully and high-speed transductors and magnetic amplifiers are described. Low-level amplification and magnetic modulation are also discussed.

The book, the first of a series on automation and control engineering, is attractively produced and the diagrams are very well drawn. A. E. DE BARR

Heat thermometry and low temperature physics

Low temperature physics and chemistry. Proceedings of the fifth international conference on low temperature physics and chemistry. Edited by J. R. DILLINGER. (Madison: The University of Wisconsin Press, 1958.) Pp. xxv + 676. Price $6.00.

The 225 papers presented at the Conference, held in Wisconsin in August 1957, are reproduced in this book, and grouped into twenty-six chapters according to subject. Author and subject indexes are provided.

The opening chapters deal with the physical and structural properties of ^{4}He and ^{3}He. A chapter is devoted to temperature scale and measurement at liquid He temperatures, and is followed by papers on instrumentation. The construction of Dewar systems, refrigerators and liquifiers is discussed, as well as the production and use of some low temperature devices such as superconducting memory systems. A chapter on the theory of superconductivity precedes a discussion of the properties of superconductors, the intermediate state and superconductivity in thin films.

A number of papers were presented on the thermal and electrical conductivity of elements, compounds and alloys, the measurement of specific heats, galvanomagnetic and thermoelectric effects. Mechanical properties investigated include friction, elasticity and hardness at low temperature and papers on magnetic phenomena and resonance are well represented. In the final chapter nuclear orientation experiments are discussed.

The proceedings of a conference on a rapidly expanding field such as the study of low temperature phenomena, must be published with as little delay as possible for research workers to derive the greatest benefit from the new information. This well-bound book has appeared within about a year of the Conference, the papers have been reproduced by a photo-litho process. The numerous diagrams, though not of the highest quality, are sufficiently clear. The large amount of information contained in this book, has been made readily accessible by careful grouping of the papers and by the provision of an adequate subject index. J. FRANKS

Second symposium on coal preparation. (Leeds: University of Leeds, 1959.) Pp. xiii + 513. Price 20*s*.

This second symposium, some five years after the first, included several overseas contributors amongst the authors of the eighteen papers. The papers varied from practical accounts of progress in practice in Germany, America, South Africa, Australia and this country to fundamental studies of the role of trace reagents in coal preparation, the factors governing moisture retention in fine coal, the attachment of bubbles to particles in coal flotation and studies of contact angles on coal surfaces. The physical discussions include material on fluid flow in packings and capillary phenomena.

Apart from the immediate interest of this symposium to all those concerned with either research or practice in coal preparation, the proceedings provide an interesting indication of the need of industry for classical physicists. Even the more practical papers contain certain discussions of the physics of the process under consideration. It is clear that there remains yet much to be done on the physics and chemistry of coal preparation. The organizers of the symposium are to be congratulated on bringing together in a single volume this useful picture of the present position and future prospects.
R. L. BROWN

Conference on extremely high temperatures, Boston, Massachusetts, 18–19 March, 1958. Edited by H. FISCHER and L. C. MANSUR. (New York: John Wiley and Sons Inc.; London: Chapman and Hall Ltd., 1958.) Pp. xi + 258. Price 78*s*.

This conference was held under the sponsorship of the Air Force Cambridge Research Centre, Electronics Research Directorate, which is one of the four centres concerned with electronics research and development for the United States Air Force.

The papers presented are divided into sections headed production, measurement, plasma analysis and applications. Some are theoretical, some describe work in progress or projected experiments, while others are more concerned with engineering aspects. The style and quality of the papers are very varied and the impression given is of a collection of unco-ordinated interim reports, sometimes not readily classified under the four section headings. The broad title and the headings, in fact, give little indication of the subjects covered.

Contrary to what might, at first sight, have been expected from the title of the Conference, few papers touch on the production of temperatures in the thermonuclear region or on temperature measurement under pinch conditions. Thus the section on production includes such diverse subjects as the determination of the temperature in spark channels in gases at pressures up to 35 atmospheres, exploded wires, inductive energy storage for millisecond pulses as well as experiments on the production of high temperature gas by magnetic acceleration. Similarly, the measurement section includes papers on the determination of equilibrium temperatures on plasma-jets at atmospheric pressure, computations of the radiative effects in shock wave propagation in air as well as theoretical papers on the microwave properties of plasmas and on line broadening.

In the last two sections, papers follow on means of plasma acceleration and on plasma guns and motors. Also included are descriptions of both fluid and high pressure gas stabilized vortex arc plasma generators up to four megawatts capacity. Such generators are being applied, for example, to the testing of components of rocket engines, as well as to the simulation of the intense heat fluxes encountered during the re-entry phase of hypersonic vehicles. J. W. RYDE

Conduction of heat in solids. 2nd ed. By H. S. CARSLAW and J. C. JAEGER. (London: Clarendon Press, Oxford University Press, 1959.) Pp.viii + 510. Price 84*s*.

Fifty-three years have elapsed since Carslaw produced his great work *Introduction to the theory of Fourier's series and integrals and the mathematical theory of the conduction of heat*. Later it was revised and rewritten in two volumes the second of which was entitled *Introduction to the mathematical theory of the conduction of heat in solids*. The book under review is the second edition of this work.

Owing to the death of Professor Carslaw in 1954 the preparation of the new edition devolved on Professor Jaeger who, whilst retaining the form and spirit of the earlier work, has modernized the book with great success. Two short survey chapters have been added. The first of these gives an introduction to the integral transform notation and its relationship to the classical Fourier methods. The second gives an account of the numerical methods which have assumed great importance in the last decade. The number of references to the literature has increased to over 700 which enhances the value of the book.

Although essentially a work for the mathematical physicist, the needs of the engineer have been kept in view for explicit solutions of many problems of practical interest are included together with much numerical information in the form of tables. Noteworthy topics discussed are those on heat generation; surface heating; melting and freezing; geophysical applications; anisotropic media; moving media, and substances with variable thermal properties.

The author adopts the calorie as the unit of heat. By international agreement the unit of heat is now the joule and the calorie is taking a second place although much used in expressing thermal conductivity data.

Professor Jaeger deserves the thanks of all concerned with heat conduction problems. EZER GRIFFITHS

Heat exchangers. Applications to gas turbines. By W. HRYNISZAK. (New York: Academic Press Inc.; London: Butterworths Scientific Publications, 1958.) Pp. xii + 343. Price 63*s*.

The heat exchanger, especially since it has become essential to the efficient gas turbine cycle, has been the subject of extensive study with the object of making possible the design of a highly efficient piece of apparatus of the minimum possible size. The often conflicting requirements of efficiency (or effectiveness), ease of manufacture, and minimum maintenance have to be reconciled. Dr. Hryniszak has performed a valuable service in collating much of the work on this subject, particularly in relation to the gas turbine. In fact, one of the virtues of this book is that, rather than considering the heat exchanger in isolation, it brings it into perspective as one component of a heat engine as a whole. To quote Dr. Bowden's preface, the book "is not concerned with the process of heat transfer itself but with the apparatus performing this transfer and the best way of designing and fitting it into a gas/turbine".

This study of the inter-relation of the performance of the heat exchanger and the thermodynamics of the system of which it forms part should be of value as a pattern in all applications of heat exchangers including steam generation and nuclear power.

While, as is inevitable with any subject so actively under study as this, the book is not exhaustive, it provides a thorough grounding in the work on this subject with references up to and including work published in 1954. The book deals with all topics relevant to design and includes a brief mention of corrosion and erosion troubles, the stresses set up by pressure or thermal expansion, and costing.

The reviewer was very pleased to read in the introduction a firm warning against over-elaboration of the calculations used in view of the uncertainties, especially of the experimentally determined heat transfer coefficients, inherent in designing a new heat exchanger. One may argue, however, that there is a tendency to complicate the arguments in the text too early in the treatment, and this book is not likely to appeal to those in general industry interested in designing a simple heat exchanger. This book will be most valuable to those in the more specialist fields where the heat exchanger is a vital cog in an integrated machine. G. G. THURLOW

Thermische turbomaschinen. By W. TRAUPEL. (Berlin: Springer-Verlag, 1958.) Pp. xii + 407. Price DM. 58.50.

This is the first of two volumes of an exhaustive and up-to-date presentation of a unified theory of turbomachines by Stodola's successor in Zurich. As Stodola's monumental handbook has not been reprinted since 1927 this present work fills an awkward gap, and by its high quality ought to become for the present generation of designers what Stodola's book was for the last.

The work is conceived as a rigorous treatment of the theory by a man deeply immersed in its application in the design office, and therefore not only the grand strategy of design is shown but also the designer's tactics. I am assured by my designing colleagues that it would be possible to design a turbine in detail on the information given. Some omissions there are, to be sure, and some arguments seem to be rather roundabout to a physicist, but to a designer they map out practical short cuts. The mathematical presentation in the

MKSA system of units to me is rather startling: $e^2/2$ does not at all look like the kinetic energy of a substance, even if it has been stated that the equations refer to unit mass.

The author presents his material free from ambiguity in short, well-constructed sentences, the meaning of which is easily absorbed. Great care has been taken in the presentation of the many diagrams and the phrasing of captions. The paper seems just a little less glossy than usual with Springer's books and some of the photographs consequently are somewhat indistinct and flat, but the printing is otherwise of the highest practical standard. O. KANTOROWICZ

Ionosphere

The ionosphere. By K. RAWER. (New York: Frederick Ungar Publishing Co.; London: Crosby Lockwood and Son Ltd., 1958.) Pp. 202. Price 42*s*.

This is a translation of a book originally published in German in 1951. The text has been little modified; the bibliography now contains a few references to publications with dates up to 1955. The German of the original version is in the direct style which is such a help to readers with no great knowledge of the language. The English of the translation is very poor.

The content forms an excellent introduction to the ionosphere physics of the pre-satellite era. It covers the various methods of observation—sounding by radio-waves, spectroscopy of airglow and aurorae, direct ascents, geomagnetic observations—and the results obtained, including the regular and irregular variations of the ionosphere. It concludes with a discussion of methods of prediction of ionospheric radio propagation. The treatment is rather uneven; the sections on wave propagation are full and excellent, the discussion of most of the other methods is too brief to be very helpful except as a guide to further reading. But within its limitations of size and date, "which are well known to the author", the book can be recommended as an introduction to a subject of great interest and increasing importance.

G. D. ROBINSON

The magneto-ionic theory and its applications to the ionosphere. By J. A. RATCLIFFE. (London: Cambridge University Press, 1959.) Pp. x + 206. Price 40*s*.

The equation for the refractive index of an ionized medium, which can be derived in a few lines when magnetic fields and collisions are neglected, is almost the only simple thing about ionospheric theory. The derivation of equations which might apply to the practical case of the transmission of a radio wave in the ionosphere leads to somewhat lengthy and cumbersome equations. The rather intractable nature of the subject has probably hindered the attempts to give a collective account in book form, and the present author must be congratulated on several counts, not the least of which is that he has made a unique contribution to scientific literature where it is badly needed. The monograph displays the qualities of clear insight and orderliness which are typical of the author, and it is unlikely that the magneto-ionic equations will ever be more closely related to physical phenomena than they are in this work. The basic equations are first derived both by using the macroscopic and microscopic approach. In the second part of the book an interpretation of the equations is given, and in Parts 3 and 4 the application to the terrestrial ionosphere together with some miscellaneous contributions—such as the validity of the Lorentz Term—are considered. Those who are concerned with the teaching of ionospheric physics will be profoundly grateful to Mr. Ratcliffe for writing this book, and for those whose work deals with radio waves in ionized media in any form the monograph will become an essential possession. A. C. B. LOVELL

Manufacturers' publications

A story of temperature measurement. (London: Negretti and Zambra Ltd., 1958.) Pp. 20. Gratis.

This booklet describes the evolution of the liquid-in-glass thermometer. It is fully illustrated and a bibliography is given for those who wish to read more on the subject.

Fifteen years of semiconducting materials and transistors. 2nd ed. Compiled by N. L. Meyrick. (Newmarket Transistor Co. Ltd., 1958.) Pp. 75. Gratis.

This second edition of a useful bibliography contains 2511 references to publications on the subject issued during the past 15 years.

Noble metal thermocouples. 2nd ed. (London: Johnson, Matthey and Co. Ltd., 1958.) Pp. 41. Gratis.

The second edition of this book gives a comprehensive survey of the development of noble metal thermocouples, their applications and methods of calibration. Two new sections have been added dealing with temperature measurement in glass manufacture and in the foundry.

Platinum in the glass industry. By H. MOORE. (London: The Mond Nickel Co. Ltd., 1958.) Pp. 45. Gratis.

Platinum has contributed to many improvements in glass and glass manufacture and has also enabled enormous increases to be made in the production of glass fibre. These and other aspects, including commercial glass manufacture and the control of raw materials are all covered in this booklet.

Questions and answers on electron microscopes. (New York: Philips Electronics Inc.) Pp. 12. Gratis.

Compiled from actual queries, this booklet discusses magnification, resolution, specimen preparation and fields of application and other technical matters concerning electron microscopes.

The dispersion of carbon black in rubber and its role in vulcanizate properties. By C. W. SWEITZER, W. M. HESS and J. E. CALLAN. (New York: Columbian Carbon Co., 1958.) Pp. 37. Gratis.

This 40-page booklet discusses studies made with the electron miscroscope and contact microradiograph. It has many illustrations including more than fifty micrographs together with eight graphs and seven tables.

The properties and characteristics of aluminium casting alloys. (London: The Association of Light Alloy Refiners and Smelters 1958.) Pp. 106. Price 4*s*. 6*d*.

This publication contains data for all the aluminium casting alloys to B.S. 1490: 1955. In addition to specification requirements it gives typical properties and information on the physical, foundry and other characteristics of the alloys as well as a section on heat-treatment and a guide to the selection of alloys.

Wiggin nickel alloys v. caustic alkalies. (Birmingham: Henry Wiggin and Co. Ltd., 1958.) Pp. 51. Gratis.

This 51-page booklet describes the properties of the high-nickel alloys used in the construction of plant handling caustic soda and illustrates some typical applications.

Mathematics and tables

Analog simulation: solution of field problems. By W. J. KARPLUS. (New York: McGraw-Hill Book Co. Inc.; London: McGraw-Hill Publishing Co. Ltd., 1958.) Pp. xv + 434. Price 77*s*. 6*d*.

Analogue computing devices fall into one or other of two categories. The first consists of differential analysers, in which the operations of addition, subtraction, multiplication and integration are performed mechanically by the use of gears, differentials and ball-and-disk integrators; or electronically by amplifiers and resistance-capacity networks. This type of computer is suitable where the problem can be expressed as an ordinary differential equation. The second type of device is one in which a one-to-one correspondence exists between every element of the problem and an element of the analogue. The electrolytic trough is a familiar example of such computers. It is this type of device which forms the main theme of the present volume.

The first four chapters, dealing with the mathematical background, give a concise statement of the basic differential equations of physics, useful transformations and finite difference methods. The tabulated summaries in this part will be found useful for reference. In the next four chapters, a comprehensive treatment is given of the practical realization of the various types of electrical analogue: conductive solid, electrolytic trough, resistance network and resistance-reactance network. A chapter then follows on electronic differential analysers. At first sight, this appears to be outside the scope of a book which is primarily concerned with direct analogue devices; but its inclusion is justified because the basic units are a simple extension of resistance-reactance networks. The discussion of experimental techniques concludes with a chapter on non-electrical analogues. The last four chapters present examples of the application of analogue methods to problems drawn from many branches of physics. The book can be recommended to any physicist who needs to make use of analogue computers. T. B. RYMER

Internal conversion coefficients. By M. E. ROSE. (Amsterdam: North-Holland Publishing Co., 1958.) Pp. xxi + 173. Price 40*s*.

This set of tables is nicely produced and should be easy to use. The introduction gives a clear account of the methods of calculation and the physical assumptions employed in constructing the tables. Apart from any error in the assumptions made about the nuclear charge structure, the errors of calculation are estimated to be no more than 3%.

Another set of tables of the same coefficients is available, constructed by L. A. Sliv and I. M. Band, and published by the Academy of Sciences of the U.S.S.R., reissued by permission as Report 58ICCL1 of the University of Illinois. One value in the first line of this latter table differs by a factor of over 2 from the corresponding value in Rose's Table. Sliv and Band estimate their computing error as ±2%. The only significant difference in the physical assumptions is that Sliv and Band use, in their description of the nucleus, a surface current distribution which Rose regards as negligible. However, the discrepancies vary through the tables in such a way as to suggest that this may not be their sole source. The experimenter is now in the position of having to look up both sets, and can act confidently only when they agree (as, at intermediate energies, they almost always do). It is, however, urgently necessary to locate the difference and see whether the internal conversion coefficients are exhibiting this remarkable sensitivity to the physical details of nuclear surface structure or merely to the details of computing technique. G. WYLLIE

Irreducible tensorial sets. By U. FANO and G. RACAH. (London: Academic Books Ltd.; New York: Academic Press Inc., 1959.) Pp. vii + 171. Price 54*s*. 6*d*.

The theory of the coupling of quantized angular momenta owes much to one of the authors of this book, but it must regretfully be stated that this attempt at explaining it to the uninitiated falls far short of two previous ones by humbler practitioners of the craft. The subject, which is of very great importance, can be tedious at times, but it is not really difficult—the present book makes it both. The generalization to "tensorial sets" does not seem to add anything significant and definitions, such as that for the six-j symbol, which differ slightly from the accepted ones can only lead to confusion. As a mathematician I enjoyed the reference to Desargues' theorem, but as a physicist I have to admit that the book could have managed without it. L. R. B. ELTON

Tables of thermodynamic functions of air. By A. S. PREDVODITELEV and others. (London: Cleaver-Hume Press Ltd., 1958.) Pp. 301. Price 63*s*.

This volume is the first of a series based on theoretical and numerical work carried out in various Russian research organizations. Values of the functions considered are given to four significant figures at increments of 100°K over the temperature range 6–12000°K and, for each temperature, 97 values of pressure are used over the range 0·001–1000 atmospheres. The 22 quantities listed for each temperature and pressure are: specific internal energy, enthalpy and entropy; specific heat at constant volume and constant pressure, and ratio of specific heats (c_p/c_v); velocity of sound, density, molecular weight; and the thirteen molar fractions of the constituents of air (x_N, x_O, x_A, x_{N2}, x_{O2}, x_{NO}, x_{N+}, x_{O+}, x_{A+}, x_{N2+}, x_{O2+}, x_{NO+}, and x_e). Formulae are given for interpolating between tabular values, mention being made of the number of terms to be retained for each of the tabulated functions. It is pointed out by the translator that errors exist in the entropy values, the corrections to be made being indicated for the whole range of temperature and pressure involved. R. G. SIDDALL

Miscellaneous and general physics

British coal mining explosives. By J. TAYLOR and P. F. GAY. (London: George Newnes Ltd., 1958.) Pp. vi + 175. Price 27*s*. 6*d*.

There has, in the past, been a serious lack of books of professional standard on industrial blasting explosives. Dr. Taylor is, therefore, to be thanked for following his monograph* on the physics of such explosives with a more popular work on the special explosives which have been developed for use in dusty and fiery coal mines. In addition to permitted explosives and detonators, the book deals with gas venting devices like Cardox and Hydrox, with opencast workings, with water infusion blasting, and the law on the storage and use of explosives.

For mining engineers this book is a necessity. It is also recommended to everyone interested in the application of explosives to useful ends. G. MORRIS

* *Detonation in condensed explosives* (Oxford University Press, 1952.)

Fundamentals of advanced missiles. By R. B. Dow. (New York: John Wiley and Sons Inc.; London: Chapman and Hall Ltd., 1958.) Pp. xvi + 567. Price 94*s*.

The author explains that he has replaced his initial choice of the adjective "guided" in the title by "advanced" because, with the recent progress in long-range ballistic missiles and the interest in earth satellites, he felt that the former would imply an unintended restriction on the applicability of the basic principles.

This is indeed intended as a book on basic principles but there are so many of them involved in advanced missile design that the reader cannot expect any great depth of penetration on any one subject. The subjects covered include: kinematics of flight; the applications of fluid mechanics to aerodynamics and propulsion; dynamics; applications of probability and statistics; properties of microwaves; application of infra-red radiation; radar; guidance and guided-missile systems. Each subject is developed *ab initio* and the author expresses the hope that his treatment will enable the reader to grasp the fundamentals without too many excursions into the literature. It is very easy for any specialist to be critical of the treatment of his speciality and the book must certainly be subject to such criticism subject by subject. My own view is that more reliance ought to have been placed on references to standard texts and that this would largely have nullified the criticisms that spring to my mind in, for instance, mechanics and fluid mechanics. Certainly such references would be of great help to a specialist who wishes to stray outside his own speciality.

However, when all that is said, the fact remains that the book in its 567 pages does provide a useful account of the basic facts of life for the many components which go to create an advanced missile and, however much one may feel disposed to criticize individual points, one shouldn't underestimate the advantages of having them assembled altogether by someone who can survey the whole with such first-hand knowledge as Dr. Dow's.

L. Howarth

Jahrbuch der wissenschaftlichen gesellschaft für luftfahrt E.V. (W.G.L). By H. Blenk. (Braunschweig: Friedr. Vieweg & Sohn, 1958.) Pp. 512. Price DM. 58.

This Yearbook brings together in a handsome volume the papers read before a joint meeting of the German Aeronautical Research Establishment (D.V.L.) and the Society for Aeronautical Science (W.G.L.) held at Essen in April 1957. To quote from the preface: "A glance at the titles of the papers shows the multitude of problems dealt with in aeronautical research, suggesting the influence on specialized fields of more or less related subjects; for the sake of this influence alone, any state depending on the quality of its industrial products must never discard aeronautical research, even if it has only a limited aeronautical industry." This may be special pleading, but it seems true even for the nations with a highly developed industry. However, the side effects of this research are not self evident from reading the list of contributions which on the whole keep strictly to aeronautical questions. Of the 54 contributions, all but three are in German. There are however excellent summaries in English and French, and these will help readers not familiar with the new jargon. Also attached to each paper are concise extracts from the discussion. I suspect that the Editor has done much meritorious work with a view to obtaining a text which is simple and clear in the construction of sentences and the choice of expressions and which therefore is easy to read. The illustrations, both line drawings and photographs, with a few exceptions, are informative and easy to absorb, and mathematical expressions are clearly produced without stinting space. The publishers have indeed served the authors well.

O. Kantorowicz

Progress in non-destructive testing. Vol. 1. Edited by E. G. Stanford and J. H. Fearon. (London: Heywood and Co. Ltd., 1958.) Pp. vii + 267. Price 60*s*.

The introduction of this particular series of review books is both timely and well-timed, as there is at present a significant wave of interest in non-destructive testing both nationally and internationally. Interest and action are, in fact, urgently required at this stage as the integrity of industrial products becomes of increasing prominence and as methods of automation are progressively introduced. Unfortunately, inspection has for too long been regarded in some quarters as a necessary evil and, consequently, its natural development has partly been stifled by the attitude of unenlightened managements; basic research, therefore, has been inhibited by the feeling that the topic was rather too "earthy" for academic attention.

At the outset, the editors strike right through the barriers of this restrictive convention and refreshingly state that non-destructive testing, in their view, is concerned with "every type of non-destructive measurement carried out on solids, liquids and gases with the object of examining some aspects of their physical, chemical or even biological condition".

With these defined terms of reference the chapters on neutron radiography, nuclear magnetic resonance and even the medical aspects of non-destructive testing need no apologetic introduction. They do, in fact, rather serve to emphasize the breadth and depth of the edifice that has now to be constructed in order to put non-destructive testing on its rightful pedestal in the pattern of industrial development.

The chapters on fluoroscopy, stress wave propagation, electromagnetic methods of testing, damping capacity, and thermal conductivity all critically define the present state of knowledge in the respective fields and the technical limitations to further development. Permeating these chapters one senses the emphasis that even in the so-called "accepted techniques" there is certainly no cause for any attitude of complacency, and that neither is there any lack of avenues for further development and for further basic research.

Although an international series, only one of the authors in the present book is based out of Britain. For the first volume this is perhaps inadvertently appropriate since much of the stimulus for this enlightened approach to the subject has stemmed from within this country; and, in fact, in no small measure from within the Editors' own laboratories. The fact that some of the material has had prior publication in other journals in no way detracts from the value of this collective presentation.

The book should appeal equally to those who direct and guide industrial inspection; to the individual research worker in many fields of physics and metallurgy; and in part to the medical specialist. It should also be examined in detail by those who direct university and technical college research programs, for they will find in it a rich harvest of ideas for further academic studies.

The Editors are to be congratulated on the high standard they have set and, if maintained, the series will undoubtedly be a most significant and worthwhile contribution.

R. S. Sharpe

Nuclear and cosmic-ray physics, apparatus, techniques and data

1958 Annual international conference on high energy physics at CERN. Edited by B. FERRETTI. (Geneva: CERN, 1958.) Pp. x + 358. Price 45 *fr.*

As well as differing from its predecessors in being held outside the U.S.A., last year's Rochester Conference used for the first time the *rapporteur* system in order to avoid the presentation of an overwhelming number of separate contributions. Simply to string together a summary of each submitted paper can be worse than allowing each contributor a ten minute session. However, if the *rapporteur* does his job well, as Goldhaber and Glaser do in the sections on weak interactions, it is possible to give a brief and clear account of his assessment of recent work, while retaining sufficient of the original results for the reader to form his own opinion and to use them for reference in the light of further work.

The *rapporteur* method is not followed very consistently for theoretical subjects and it is comforting to find Feyman stating that this is because so few theoretical physicists understand each other's work. It is not surprising, therefore, that the non-expert finds it difficult to perceive any general pattern of progress among the many theoretical contributions.

The volume provides the experimental physicist with an invaluable summary of recent work, especially on the production and interactions of strange particles. There are, however, no results of obviously outstanding importance. In particular, the several experiments on the existence of mass $500m_e$ particles have all given negative or indecisive answers so far.

One must applaud the decision to sacrifice uniformity of editing to speed of publication. The Organizing Committee deserve the highest praise for producing a report of this quality within three months of the conference.

N. C. BARFORD

Bone and radiostrontium. By A. ENGSTRÖM, R. BJÖRNERSTEDT, C. J. CLEMEDSON and A. NELSON. (New York: John Wiley and Sons Inc.; London: Chapman and Hall Ltd., 1958.) Pp. 139. Price 70*s*.

About one quarter of this book is devoted to methods of calculating radiation dosage, but these do not appear to possess much advantage over established methods. It is unfortunate that the roentgen and the "rem" have been used, rather than the "rad," which is a particularly suitable unit for this type of calculation. The most informative chapters are those on the determination of the distribution of mineral salts and of ingested ^{90}Sr in young and adult bone. The authors have concluded that accepted estimates of "permissible" body-burden of radiostrontium are too high.

TIKVAH ALPER

Čerenkov radiation and its applications. By J. V. JELLEY. (London: Pergamon Press Ltd., 1958.) Pp. x + 304. Price 65*s*.

The passage through a medium of a charged particle, the velocity of which is greater than the velocity of light in the medium, gives rise to the emission of visible light, the so-called "Čerenkov radiation". This fundamental phenomenon remained essentially one of academic interest until it was shown that single particles could be detected by the emission of the light and, later, that particles of the same momentum but different mass could be identified by the response of a Čerenkov counter to a beam of particles. In this way, Čerenkov radiation has now firmly established itself in the realms of high energy particle physics.

This monograph, the appearance of which will be especially welcomed by experimental physicists, is a comprehensive and lucid account of all aspects of this field. On the theoretical side, accounts are given of the extensive work carried out, mostly in Russia, and on the experimental side, clear and amply illustrated descriptions are given of the practical applications originating chiefly in the U.S.A. and Great Britain. For those interested in details of making a counter, much useful information appears on the optical properties of materials and designs of optical systems, and a chapter is devoted to the characteristics of various photomultipliers.

A full account is given of the work on the emission of Čerenkov radiation by the particles of extensive air showers of cosmic radiation, and topics of a speculative nature have been deliberately included in a final chapter to stimulate further interest.

The author sets out "to present as complete an account of the whole field as is possible in a volume of its size" and I believe he has succeeded. If the reader thinks the price of the book is a little high, let me say the quality, as well as the quantity, is there.

W. GALBRAITH

Effects of radiation on materials. Edited by J. J. HARWOOD, H. H. HAUSNER, J. G. MORSE and W. G. RAUCH. (New York: Reinhold Publishing Corporation; London: Chapman and Hall Ltd., 1958.) Pp. v + 355. Price 84*s*.

The effect of radiation upon materials is a subject of increasing interest to many scientists and of vital importance to those engaged in the peaceful uses of atomic energy. Until the 1955 Geneva conference, much of the information was classified as "Secret" or "Confidential", and there are no textbooks on the subject. The book under review is, indeed, itself not a textbook, but is a report of a colloquium on "The effects of radiation on materials", sponsored jointly by the U.S. Office of Naval Research and the Martin Company and held at the Johns Hopkins University in March 1957. The purpose of this colloquium was "to present a series of unclassified reviews that were educational in nature and gave broad coverage to this field". That this purpose is admirably achieved may (rightly) be surmised when one notes the outstanding authors who are represented:

G. J. Dienes writes on "Defects in solids and current concepts of radiation effects", J. C. Wilson on "Experimental approaches to radiation studies—radiation sources and dosimetry", E. S. Billingson on "Radiation effects on physical and metallurgical properties of metals and alloys", M. Simnad on "Influence of radiation upon corrosion behavior and surface properties of metals and alloys", R. Smoluchowski on "Effects of radiation on electronic and optical properties of inorganic dielectric materials", H. Y. Fan and K. Lark-Horovitz on "Effects of radiation on semiconductors", C. E. Weber on "Cores, liquid coolants and control rods", G. R. Hennig on "Moderators, shielding and auxiliary equipment", M. Burton on "Experimental techniques and current concepts—organic substances", A. Charlesby on "Effects of radiation on behavior and properties of polymers", and A. J. Restaino on "Radiation-induced graft copolymerization". Finally, there is a useful index and an extensive and exhaustive bibliography by H. Friedemann.

Although written for the most part by American authors, the outlook is not parochial, and credit is given to workers on this side of the Atlantic. There is some repetition, but this

is perhaps inevitable in such a work. Few misprints or errors were noted, but the statement on page 192 that boron 10 is fissionable surely needs rephrasing. Anyone who is interested in the effects of radiation on materials will do well to buy or borrow this book. J. THEWLIS

Electromagnetic phenomena in cosmical physics. International astronomical union symposium No. 6. Edited by B. LEHNERT. (London: Cambridge University Press, 1958.) Pp. xii + 545. Price 50*s*.

It is nine years since Professor Alfvén's book on *Cosmical electrodynamics* marked the beginning of a new epoch in the co-operation of physicist with astronomer, and the present volume offers 56 papers at research level in several of the topics evolved from that beginning. It seems a pity that this volume, issued in 1958, is the earliest full report of the Stockholm conference of 1956.

The branch of science which has thus become so important is the application of classical electrodynamics to the mass motion of ionized gases—the earlier treatment of which by hydrodynamics has proved inadequate. The topics especially considered in the book are experiment and theory on the stability of ionic flow when the gas carries its own magnetic fields; the application of solar eruptions to the puzzling magnetic fields characterizing certain stars; and most of all to the guiding of solar and extra-solar particles whose arrival with high energy affects profoundly our outer atmosphere. Public attention, even at the popular level, has recently been drawn to the intense radiation belts revealed outside the earth by artificial satellite and rockets.

Some cosmic radiation is known to come from certain types of solar eruption, and papers 12–17 in the book concern the mechanism of flares and other transients on the sun; but cosmic radiation also comes from more distant sources, and the latter species is modulated by the slower streams already emitted from the sun itself. Complex events studied on fortunate but rare occasions by Forbush and others, show both excess and suppression of different components and offer the chance of elucidating both solar and more distant origins of cosmic radiation, as each species is diverted into allowed and away from forbidden paths by the magnetic fields. Papers 26–46 deal with these problems, but the ultimate source of primary acceleration, galactic or other, is not discussed—the book already has more than 500 pages, and many of the treatments raise as many questions as they solve. The whole subject is in its most exciting stage.

MARTIN JOHNSON

Extensive air showers. By W. GALBRAITH. (London: Butterworths Scientific Publications, 1958.) Pp. xvi + 211. Price 40*s*.

The subject of cosmic-rays covers a very wide diversity of scientific effort from astrophysics to strange particles and the study of the properties of the ultra high energy particles, which produce the large cosmic ray air showers in the atmosphere, provides a direct link between the fields of astrophysics and high energy nuclear physics. The presence in the primary cosmic radiation of particles with energy up to 10^{18} eV is of enormous importance in understanding the astrophysical processes whereby the cosmic rays are produced, and also in the elucidation of the structure of the galactic magnetic field. At the same time, these particles give us the possibility of investigating the nature of particle interactions at an energy more than a million times greater than that produced by any man-made accelerator at present contemplated.

The greater part of this book is concerned with the structure and development of cosmic-ray showers in the atmosphere and with the relation between shower structure and the nuclear and electromagnetic interaction processes involved. A detailed account of the experimental work is given together with a very useful summary of the theoretical background. There is a chapter on the intensity variations of the very high energy particles which includes a brief discussion of theories of the origin of the cosmic rays and finally a chapter on the Čerenkov light produced by showers.

The book, although rather too specialized for the general reader, will be of great value to those working in the cosmic-ray field. This specialization is perhaps reflected in the title which does not differentiate between cosmic-ray showers and the more widely known meteorological phenomena of the same name. H. ELLIOT

Free radicals as studied by electron spin resonance. By D. J. E. INGRAM. (London: Butterworths Scientific Publications, 1958.) Pp. ix + 274. Price 50*s*.

In this timely book the author, who is eminently qualified, gives a stimulating and well-written account of the rapidly expanding field of the application of electron spin resonance (ESR) to the study of free radicals. In the first part of the book a review is given of various methods of studying free radicals, which is followed by an account of the now well established basic ideas of the experimental technique (including its possibilities and limitations) and the theory of ESR in free radicals. The remainder of the book contains a fascinating account of results obtained up to the date of completion of the manuscript.

In the preface the author mentions the difficulty of deciding the level of the book. This must have been a very real difficulty and the author has not always avoided some unevenness in treatment. For instance, the chapter on hyperfine structure would become more even, if a detailed treatment of the use of spin hamiltonians were given. More cross-references would have been useful, e.g. on p. 40 the existence of an optimum power in the detection arm of a micro-wave bridge is mentioned without reference to §3.2.1 where this is discussed in detail. These are, however, only minor points, which hardly affect the value of the book. D. BIJL

Glove boxes and shielded cells for handling radioactive materials. Edited by G. N. WALTON. (London: Butterworths Scientific Publications, 1958.) Pp. xii + 515. Price 95*s*.

The techniques and design of glove boxes and shielded cells are an important branch of nuclear technology. Glove boxes have broken the bounds of this field and are rapidly establishing their value in a number of other industrial and laboratory processes. This book is a record of the proceedings of a symposium on glove box design and operation held at the Atomic Energy Research Establishment, Harwell, 19–21 February, 1957. It includes the sixty-one papers presented at the meeting together with all the significant contributions to the discussions. The connecting theme was the possibility of standardization in design. It is clear, however, that the applications are now so diverse that standardization is only possible to a very limited extent; shielded cells are necessarily more specialized than glove boxes.

The book is extremely well produced and the illustrations are excellent. Indeed, one may ask if it would not have been more appropriate to have chosen a much cheaper mode of

presentation. The contents of the book are of unquestioned value but their nature is such that their value will decrease much more quickly than, for instance, a specialized textbook. The book is perhaps of the greatest interest to those who manufacture this kind of equipment since it presents them with a clear picture of the problems of those who design or employ the equipment.

A. G. MADDOCK

The nuclear handbook. Edited by O. R. FRISCH. (London: George Newnes Ltd., 1958.) Pp. xv + 640. Price 50*s*.

I have some hesitation in attempting a review of this publication since its aims are admirable but its achievements less so. The publishers have contributed notably in the past by their other publications on nuclear energy subjects, the consulting editor is distinguished and the individual authors are mostly well known and highly competent. Furthermore, the idea of a nuclear handbook is obviously good if it acts as a first reference and a reliable source of numerical data. In spite of these natural advantages, if they can be so described, the *Nuclear Handbook* falls far short of the high standard for which one might have hoped.

The main criticism which could be made is that the quality of the various contributions is very uneven and the volume is badly indexed. For instance, I first found the term "curie" on p. 2–3 of the section on "Radiation effects" in an expression "where Q is the source in curies" which is not very clear. Since curie was not defined I turned to the index and was referred to p. 4–10 where a definition is given in terms of a rate of decay of $3{\cdot}7 \times 10^{10}$ disintegrations/second and reference made to p. 4–26 where it is mentioned that $3{\cdot}7 \times 10^{10}$ disintegrations/second is the rate corresponding to 1 g of radium. This is a small point but indicates something of the way the book is constructed.

I find it difficult to believe that about thirty pages in Section 16 should be devoted to "Solenoids, magnets and magnetic materials" while Section 12 on "Reactors" includes in all only eighteen pages of which "Reactor theory" takes only two pages and "Reactor kinetics" rather less. The "Electronics" section is lengthened by the inclusion of some rather simple circuits and tables of valve characteristics while the section on "Vacuum" is short to the point of austerity. There is no reference at all to cosmic radiation.

These are only selected as examples of points where criticism could be made. Perhaps one should equally report that there are also some excellent sections in the volume. It would appear that it will be of limited use to some people but it is not likely to be of wide benefit to a large body of readers. Nevertheless, it would be useful if a good handbook were to be available and perhaps the publishers will find that they can use the present volume as a starting point for later editions which would meet a genuine need.

L. ROTHERHAM

Nuclear moments. By H. KOPFERMANN. English version prepared by E. E. SCHNEIDER. (New York: Academic Press Inc.; London: Academic Books Ltd., 1958.) Pp. xiii + 505. Price 93*s*.

This book gives a comprehensive account of the methods by which the spins and the moments of stable and long-lived nuclei have been determined. Although based on Prof. Kopfermann's earlier work of the same name it is an essentially new book.

The first of the four chapters is concerned with measurements on free atoms which cover the atomic beam methods and optical hyperfine structure investigations. The second chapter deals with measurements on free molecules by the molecular beam method, and by infra-red and microwave spectroscopy of gases. The third chapter takes up methods which can derive nuclear information from matter in liquid and solid form, namely nuclear magnetic resonance, pure quadrupole resonance and electron paramagnetic resonance. The fourth chapter is devoted to the interpretation of the experimental results in terms of current nuclear theory. The book closes with tables of nuclear data and references.

The book thus provides a useful compendium of all the important sources of experimental data with an adequate introduction to each. It will be found of value to lecturer and research worker alike and for reference purposes by the Honours student also.

We must be grateful to Dr. Schneider for rendering this valuable book into English. The translation is clear and uses the British convention of expressing vector quantities. Though some may share the translator's misgivings concerning the hybrid system of electric and magnetic units adopted, nobody is likely to be confused by them. The translator has considerably extended the references, tables and indexes, and has included new material published since the date of the German edition.

E. R. ANDREW

Nuclear reactions. Vol. 1. Edited by P. M. ENDT and M. DEMEUR. (Amsterdam: North-Holland Publishing Co., 1959.) Pp. xii + 502. Price 86*s*.

For many years no advanced nuclear physics book of use to the research worker existed and he leaned heavily on the 1937 articles by Bethe *et al.* and on data compilations. In the last two years, however, such books have been appearing in considerable numbers. This implies that low energy nuclear physics has reached a stage in its development where it is more work-a-day and less exciting. No longer is it true that almost any experiment one does is new and significant. At the same time many of the fundamental problems remain unsolved and the challenge is greater because the experiments are harder. They are certainly more expensive.

The book under review is the first of two volumes—the second is to include topics of low energy physics not easily connected with the idea of nuclear reactions—and stripping, other direct processes, and photo-nuclear reactions are therefore not included. The chapters are each written by a different author. This has the usual defect of non-uniformity of style or nomenclature and some duplication. When the duplication is in completely different nomenclature this seems intolerable. However, it is, in fact, an accurate reproduction of the situation in nuclear physics at the present time and so is more valuable than might at first sight appear.

The shell model, unified model and statistical model are well introduced by Elliott, Kerman and Le Couteur, and resonance reaction theory by Vogt. The experimental chapters by Fremlin, Gove, Hughes, Zimmerman and Gugelot fill in the background admirably while the article by Goldfarb on angular correlation and polarization is a good introduction to this experimental tool. In all cases the connexion between models and experiment is kept clearly in view. The introductory chapter by Eden outlines present attempts to describe nuclear structure on the basis of nucleon-nucleon interactions. Doubtless some aspects of this book will go out of date in a few years but meanwhile it is a most useful reference book for the nuclear physics researcher.

E. B. PAUL

Nuclear spectroscopy tables. By A. H. WAPSTRA, G. J. NIJGH and R. VAN LIESHOUT. (Amsterdam: North-Holland Publishing Co., 1959.) Pp. vii + 135. Price 60*s*.

This publication serves a useful purpose in collecting together a wide set of data on nuclear spectroscopy in easily available form. Where the data is based on published tabulations, references are given so that where they exist, more extensive tabulations may be consulted. It would seem, however, unnecessary to include some information so readily available elsewhere. As examples of where space and money might have been saved, tables of four-figure logarithms and a list of the names of the elements have been given. Relatively trivial calculations such as those of magnetic rigidity *versus* energy for various particles could also have been omitted with advantage. Pruning of this sort would reduce the size and cost of the volume without any loss of utility.

The use of a concise introduction to each section wherein the quantities occurring in the tables or figures are defined is a successful one, but these introductions could often have been expanded. For example, it would be convenient if in the paragraph on the longitudinal polarization of β-rays on p. 95, it had been explicitly stated that the assumptions stated on p. 44 applied.

The ordinate in Fig. 4.12 is so patently mis-scaled that it is not liable to cause error.

This is clearly a book to be obtained by every library serving nuclear physicists. It will be particularly useful to workers in the field of β-decay, but contains much useful information for workers in other fields of low energy nuclear physics.

E. H. BELLAMY

Principles of quantum electrodynamics. By W. E. THIRRING. Translated by J. BERNSTEIN. (New York: Academic Press Inc.; London: Academic Books Ltd., 1958.) Pp. xv + 234. Price 64*s*.

If one attempts to treat the interaction of particles and fields by ordinary quantum mechanical methods, it soon becomes clear that various quite ordinary physical questions get very queer answers. The recent development of quantum electrodynamics has given, among others, two of the most precise results of theoretical physics, the values of the Lamb shift and the anomalous magnetic moment of the electron. This is the region of existing field theory in which one feels most confidence, and the present translation and revision of a well-known German text will be most welcome to all who require some understanding of the field without needing at once to set to work in it. Those who intend to research in field theory will find the book a helpful preliminary to Jauch and Rohrlich's *Theory of photons and electrons*. The experimentalist who is not already well up in quantum theory and classical relativity will be wiser to start with Fermi's *Fundamental particles*.

Thirring's book is very clearly written and will be useful not only to workers in fundamental particle theory but also to those of us in solid state physics who now have to use the ideas of phonon and plasmon fields. Given its standard, more references to the original literature would have been welcome. The price is high for the size of the book. So is its value.

G. WYLLIE

Progress in nuclear energy. Series 1. Vol. 2. Physics and mathematics. Edited by D. J. HUGHES, J. E. SANDERS and J. HOROWITZ. (London: Pergamon Press Ltd., 1958.) Pp. vii + 375. Price 90*s*.

This is not a textbook. The aim has been that experts should indicate the literature, and briefly review experimental and theoretical progress along a number of paths in the field specified. The topics are well chosen for current interest, and the aim has been fulfilled admirably. There is still rapid progress in this branch of physics, and one of the merits of the book has been its reasonable speed of publication. The reader must, however, be critically aware that views expressed by its authors are neither complete nor irrevocable.

Much of the first volume reviewed the cross-sections for slow neutrons with the heavy isotopes: in the second chapter of Volume 2 Harvey and Schwarz continue this work. It has little of fundamental interest, but is exceedingly useful in thermal reactor calculations, the more so as resonance integral data are included.

The first chapter by Allen and Henkel is of interest for fast reactor physics. It deals with cross-section data for fast neutrons on the fissile nuclei and many of these data are of recent origin. Rather good agreement with simple theories is claimed, so that a convenient summary of relevant formulae is now to be desired.

The fourth chapter by R. Richmond shows that the calibration of standard neutron sources has progressed remarkably in recent years. This has come about, essentially, because many laboratories have collaborated. A valuable lesson!

Pulsed neutron methods in neutron transport measurements have attained high precision and the review by their foremost protagonists, von Dardel and Sjöstrand, reveals a need for a convincing theoretical treatment.

Development of advanced reactors with enriched fuels and complex fuel elements calls for substantial improvements in neutron transport calculations. Electronic computing machinery provides the opportunity, and is intrinsic to theoretical developments reviewed in four chapters.

To make full use of detailed cross-section data, an adequate account of the neutron spectrum is needed, and much theoretical work is current. Chapter 3 gives a valuable, but uncritical introduction to the theory. On the experimental side this review is disappointing, for no attempt has been made to contrast conflicting results.

The epithermal neutron spectrum is usually embodied by means of the resonance integral. Profuse semi-empirical treatments are discussed by Sampson and Chernick and it seems clear that a sound appreciation of the important factors would derive more readily from theoretical analysis of simple synthetic models.

Hassitt in chapter 7 gives an explicit introduction to some methods of solving neutron diffusion problems by use of high speed computers. Such machinery has long been used in the U.S.A. but it is only now coming into extensive use in Europe.

Finally Goertzel and Kalos introduce us to Monte Carlo methods, and review their applications in transport problems.

J. S. STORY

Report of the United Nations Scientific Committee on the effects of atomic radiation. General Assembly. Official Records: Thirteenth Session, Supplement No. 17 (A/3838). (New York: United Nations, 1958.) Pp. iii + 228. Price 18*s*.

The United Nations Scientific Committee on the effects of atomic radiation was set up in 1956. Its Report is a monument to international collaboration. It deals with two main problems: the magnitude of the radiation dose which individuals and populations throughout the world are receiving from a variety of sources—environmental, fall-out, clinical and occupational—and with the assessment of the biological

hazards which arise from exposure to those sources. The first, physical, problem is dealt with far more precisely than the second. New and valuable data are brought together so that a reasonable picture of levels of radiation dosage prevailing through the world can be formed. Assessment of biological damage is much more difficult. There are still wide gaps in our knowledge of the fundamental biological processes involved, and attempts at quantitative evaluation of biological effects are based on broad general assumptions which still require much experimental work to establish—or possibly to disprove—them. From this point of view, therefore, the United Nations Committee's Report adds little to the knowledge contained, for instance, in the Medical Research Council's report on *The hazards to man of nuclear and allied radiations* (1956), and the conclusions now reached differ little from those set out in that document. Considerable uncertainty concerning the magnitude of the biological hazards involved in the use of radiations, from whatever source, still prevails; and it behoves all users of radiation to take every possible step to reduce to a minimum the radiation doses received in all their applications. C. B. ALLSOPP

Safe handling of radioisotopes. (Vienna: International Atomic Energy Agency, 1958.) Pp. 99. Price 6*s*.

This book offers a collection of rules and advice for controlling the hazards associated with radioactive materials used in factories, laboratories and hospitals. Its recommendations are in general accord with the official Code of Practice adopted in Britain, though more detailed in some respects. Anyone designing an isotope laboratory or working with radioactive substances will find here a wealth of serviceable information and guidance not readily available elsewhere. Future editions of the manual would be improved by the inclusion of (*a*) a table indicating maximum permissible body burdens for commonly used radioactive materials and (*b*) notes on the design of shielding against γ-rays. J. M. A. LENIHAN

Spectrum of atomic hydrogen. By G. W. SERIES. (London: Oxford University Press, 1958.) Pp. viii + 87. Price 8*s*. 6*d*.

The most fruitful problem in atomic physics has been the precise calculation and measurement of the energies of the lines in the spectrum of atomic hydrogen. In this, the simplest of atomic problems, the strictest possible test of atomic theory is possible, and it was by attempting to reduce the difference between measured and theoretical values of these energies that quantum mechanics reached its present sophisticated state.

There are two possible ways of giving an 80-page study of the subject; to give a description of its present position or to attempt to capture the excitement of the discovery of quantum mechanics by describing its history. Dr. Series has attempted to combine these, and, in his cramped space, it is not surprising that the attempt is only partially successful. Although he gives a reasonable account of the Bohr atom, with Sommerfeld's modifications, his treatment of Schrödinger is abrupt, while Heisenberg is scarcely mentioned. However, he describes the physical basis of those paradoxes in quantum electrodynamics that bear on the Lamb shift, discusses the results of Bethe's calculation and describes the radio frequency measurements by Lamb and Retherford, and the optical measurements by Herzberg and himself. He describes the anomalies in hyperfine structure, but does not relate these to nuclear physics, and ends with a chapter on positronium, although the μ-mesic atom is not mentioned The book is entirely preoccupied with energy levels, intensities are mentioned, but not line shape, any width merely obscuring the energy. It represents a moderately successful realization of an excellent idea. W. B. THOMPSON

Tables of interatomic distances and configuration in molecules and ions. Edited by L. E. SUTTON. (London: The Chemical Society, 1958.) Pp. 385. Price 42*s*.

This compendium will be of extreme value to chemists and crystallographers, and of considerable interest to solid-state physicists. It aims to present interatomic distances and interbond angles determined by electron, X-ray and neutron diffraction; infrared, microwave and Raman spectroscopy; nuclear magnetic resonance; and one or two minor techniques up to the end of 1955. Results of accuracy less than about $\pm 0{\cdot}1$ Å are omitted, and X-ray crystallographic results are graded with two, one or no stars, in accordance with the probable accuracy of the interatomic distances quoted (up to $\pm 0{\cdot}02$ Å, $\pm 0{\cdot}05$ Å, $\pm 0{\cdot}1$ Å respectively).

The more accurate values are collected in a selected table (17 pages), followed by a main table of inorganic (97 pages) and organic (160 pages) compounds. References occupy 67 pages. "Organic" is interpreted as "containing carbon", and so includes such substances as calcite and boron carbide. The carbon compounds are arranged alphabetically by formula (C, H; other constituents alphabetical), and there is also a name index (9 pages), so that they are readily located. Inorganic compounds, however, are arranged in accordance with a scheme involving the periodic table, the electropositivity of the atoms, and the ions if the compound is ionic. There is no name index, so that a physicist is at a disadvantage in consulting this section.

The introduction (20 pages) explains the principles of the compilation and arrangement, and includes a discussion of errors in bond-length and bond-angle determination. The explanation of symmetry is probably sufficient for its purpose; the expert should heed the warning "it is meant to help the chemist rather than to inform the crystallographer". No actual misprints have been noted, but it is odd that the statement $1 \text{ Å} = 1{\cdot}002\,034 \text{ X}$ and the accompanying statement of error should have escaped notice and correction.

A. J. C. WILSON

The physical theory of neutron chain reactors. By A. M. WEINBERG and E. P. WIGNER. (Chicago: The University of Chicago Press; London: Cambridge University Press, 1958.) Pp. xii + 801. Price 112*s*. 6*d*.

The time is ripe for the publication of a standard reference work in the field of neutron chain reactor theory and Weinberg and Wigner have produced such a book. From the physicist's point of view it is the first reasonably complete and unified account of reactor theory. The authors have drawn on their personal knowledge gained at the forefront of the development of reactor theory to present in well codified form many analytical results in the field.

The book is divided into four main sections: nuclear physics of chain reactors; transport theory of neutrons; general reactor theory; heterogeneous reactor theory. The first section was written because the authors have the impression that "reactor theorists nowadays have less sophistication in nuclear physics, at least relative to the available knowledge, than did the originators of the theory", and give as their opinion that "in all really creative thinking in reactor design, a working know-

ledge of nuclear reaction theory is required". Those reactor theorists who wish to take heed of these remarks will not find a better summary of the essential nuclear physics underlying reactor theory than the one given in this volume. Every attempt is made in the book to consider the fine points in the theory. Some readers (but not those who have to teach the subject) may find the attention devoted to such details a criticism of the book, but the reviewer believes that the accurate discussions of the second order effects, and the careful attention which is paid to the differences between homogeneous and heterogeneous calculations will stand as the most important contributions made in it. The authors believe that in recent years, by ignoring such details, we have all run the risk of becoming dilettantes who deal only in automatized machine calculations of reactors without having a deep understanding of the theory. It is only in this context that one can rationalize the decision of the authors to omit any discussion of the machine methods which have revolutionized our analytical reactor design techniques.

One minor criticism of the book is that the authors have introduced the term "fermi" as the unit of cross-section in place of the more familiar name "barn". Whilst all will appreciate their attempt to honour the name of a great physicist and will agree that an old joke has now become rather stale, it is the reviewer's view that reforms of this kind can be introduced in more suitable places than textbooks.

Although the authors claim that this is not a complete exposition of all that is known in reactor theory, the book is certainly the most complete and satisfactory text available for teaching the subject. It is certain that for many years to come it will be the standard reference work on reactor theory and it can be wholeheartedly recommended to all who are working in the field. D. J. LITTLER

Optics

Der lichtelektrische Effekt und seine Andwendungen. By H. SIMON and R. SUHRMANN. (Berlin: Springer-Verlag, 1958.) Pp. xii + 747. Price DM 97.50.

With the help of such well-known workers in the field of photoelectricity as K. W. Boer, F. Eckart and W. Leo, the principal authors, H. Simon and R. Suhrmann, have produced a completely new and revised edition of their earlier book *Lichtelektrische Zellen und ihre Andwendungen*, first published in 1931. This new volume is an exhaustive and authoritative survey of the established theory and practice of photoelectricity. Since the authors' policy has been to omit work subject to current scientific dispute and discussion, the book is concerned almost entirely with photoemission and its applications. The equally important subject of photoconductivity receives slight treatment by comparison, and little reference is to be found to recent developments in this expanding field. Photovoltaic effects are dealt with in a few pages.

After a brief introductory chapter the first two important articles are concerned with the physics of photoemission and photo-conductivity. The next three chapters deal with the preparation and properties of photoemissive and photoconductive cells and photomultipliers. This completes the first half of the book. There then follows a long account of the methods and apparatus used in photoelectric measurements, and a separate chapter on the use of photocells in photometry. The book is concluded with separate sections on applications to television, image converters and numerous specialized techniques.

The principal emphasis in the book is on the manufacture of devices and their uses, and all the important subsidiary techniques and equipment needed are fully described. For example, good accounts are given of high vacuum techniques, preparation of pure starting materials and secondary electron emission. Complex equipment, e.g. monochromators, is well treated, but one feels that details of simpler and more common apparatus might well have been omitted. All the major photometric techniques are adequately described as are numerous television camera tubes. In the chapter on emission processes Suhrmann gives a well-balanced review of the emission mechanism from various surfaces. Unfortunately the only major article devoted to photoconductivity is almost entirely concerned with presenting basic ideas in solid state physics.

With the sole reservation that in a book of this length more space might have been found to discuss recent advances in photoconductivity, it is no exaggeration to describe this as a monumental volume. No better or more complete account of photoemission has ever been published. This should form an invaluable work of reference to all concerned with the subject.

The book is beautifully produced and contains a profusion of diagrams and photographs which add clarity to the text. It is remarkably free from error and each chapter is concluded with an extensive bibliography. It is regrettable that the very size and cost of this book will probably limit its circulation to the reference libraries of colleges and institutions. J. WOODS

Optical properties of semi-conductors. By T. S. MOSS. (London: Butterworths Scientific Publications, 1959.) Pp. x + 279. Price 50*s*.

This book deals firstly with the theory of reflexion, refraction and interference for conducting media, with dispersion in dielectrics and semi-conductors, and with the various processes by which light is absorbed in semi-conductors. Photoelectric effects, magneto-optical effects, and the emission of radiation from semi-conductors are then discussed.

The second part of the book, a little more than half of it, describes the detailed optical properties of the semi-conductors most thoroughly studied so far. These include the elemental semi-conductors, chalcogenides of lead, zinc, cadmium and mercury, and the group III–V compounds.

The book is thoroughly up to date and includes an extensive bibliography to which the author himself has made a considerable contribution. The treatment is intended as a review for students at Honours level, or for experimental physicists engaged in research. It will probably be found successful in meeting this objective. It is valuable in correlating a considerable range of subjects; this is done in a relatively small space so that some important topics are inevitably treated rather briefly. Students will, however, be able to pursue these where necessary from the appropriate references. D. A. WRIGHT

Reference books

The BEAMA catalogue. 4th ed. (London: Iliffe and Sons Ltd., for the British Electrical and Allied Manufacturers' Association Inc., 1958.) Pp. xvi + 840. Price £6.

The fourth edition of this catalogue serves as a useful buyers' guide to the products and services of the British electrical

industry. It contains a five-language glossary in English, German, Spanish, French and Portuguese and is divided into sections under the following headings: Electrical power plant; Electrical equipment in industry, Transport and communications; Domestic and commercial electrical appliances, lighting, accessories and installation material; Classified buyers' guide; Trade directory; Index to illustrated catalogue pages.

British instruments, directory and buyers' guide. (London: Scientific Instrument Manufacturers' Association of Great Britain, and United Science Press Ltd., 1959.) Pp. 598. Price £2 2*s*.

A valuable new addition to scientific reference books is the new *British Instruments Directory and Buyers' Guide* which combines, in one volume, the information previously available in *British Scientific Instruments* published by the Scientific Instrument Manufacturers' Association and the *Instrument Directory and Buyers' Guide* published by the United Science Press Ltd. This new publication contains all the features of the two previous volumes and, in addition, is stated to have the full support of the instrument industry. The volume serves as a complete guide and handbook to all sources of supply of British instruments for science and industry together with their components and accessories. It is claimed that it contains references to all firms in the instrument and allied industry; it is not confined to those manufacturers who are members of the Scientific Instrument Manufacturers' Association of Great Britain. In addition to the classified lists of instruments and components, the book includes a four-language glossary in English, French, German and Spanish. The headings of the various sections are as follows: The Scientific Instrument Manufacturers' Association and other associations allied to the instrument industry; List of specifications directly bearing on instrument matters issued by official bodies; List of consultants, engineers and installers of instrumentation schemes; List of firms manufacturing single or small batches of instruments to a client's order; Classified index of products; Alphabetical list of instrument and component manufacturers with overseas agents; Trade names; Manufacturers' announcements.

Chemical engineering practice. Edited by H. W. CREMER and T. DAVIES. **Vol. 5. Fluid systems I.** Pp. iv + 714. **Vol. 6. Fluid systems II.** Pp. vii + 620. (London: Butterworths Scientific Publications, 1958.) Price 95*s*. each volume.

These two volumes of the comprehensive work on *Chemical engineering practice* may be conveniently reviewed together, since both volumes are concerned with the chemical engineering of fluid systems. The subject-matter presented in both volumes forms an important field of the chemical engineer's contribution to science and technology. Consequently, the presentation of the subject-matter is of considerable interest, since much of the material has been fully treated in various specialized volumes.

Volume 5 opens logically with chapters on the transportation of liquids, the transportation of gases, and pipe systems for liquids and gases. These chapters are noteworthy for the attention given to the performance characteristics of various types of mechanical equipment together with a proper consideration of the many factors which contribute to the efficient design of any systems for transporting liquids or gases. The authors have avoided the common pitfall of detailed descriptions of particular items of equipment, and have provided a knowledgeable and instructive contribution to the overall work.

The work continues with a chapter on the design of high pressure vessels. This specialized subject is treated authoritatively, and includes a review of the fundamental considerations as well as the practical problems of design and production. The inclusion of a chapter on the production of vacuums is timely as this aspect is frequently not treated in adequate detail. The present contribution, therefore, serves a most useful purpose in discussing the various means available to the chemical engineer for producing a vacuum, together with an economic comparison of different equipment for equivalent duties. The quantitative treatment of the design problems associated with vacuum production is also adequately summarized.

Volume 5 concludes with a section on liquid-liquid systems, and the section is subdivided into chapters on liquid-liquid equilibria; liquid-liquid stagewise contact; extraction equipment; vapour-liquid equilibria; rectification in binary mixtures; multicomponent distillation, and distillation equipment. The subject-matter presented in these chapters will be familiar to those who have formally studied chemical engineering. In these chapters the authors provide a logical development of the subject and the inclusion of certain performance data maintains the subject in perspective.

Volume 6 continues the treatment of fluid systems with a section on liquid-gas systems. This section is subdivided into chapters on gas absorption; operating characteristics of packed absorption columns, and evaporation practice. The two-film theory of absorption is thoroughly developed and its application to various practical absorption systems discussed. Also of value is the second chapter of this section which collates information data on the performance of packed columns. The third chapter on evaporation practice presents the basic subject-matter for an appreciation of evaporation problems. There follows two chapters of considerable interest on fluidization and fluidized beds, and applications of fluidization. The theoretical considerations of this relatively new chemical engineering technique is fully outlined in the first of these chapters, while certain specific applications and design problems are well set out in the second chapter. These chapters thus form a valuable contribution to the whole work.

A section on multicomponent gas systems includes chapters on the liquefaction and fractionation of gases, adsorption, and refrigeration practice. Each of these specialized topics merit detailed consideration in a work of this kind and the respective chapters provide a fully adequate treatment. A further section on liquid-liquid systems includes chapters on leaching; crystallization; colloids; filtration; selection; sizing and operation of filters, and centrifuging. All of these chapters are instructive, while in particular the full bibliography to the chapter on colloids will be useful to the reader seeking more detailed knowledge on certain applications.

Volume 6 concludes with an informative chapter on sublimation and vacuum freeze drying.

It is clear that these two volumes alone contain a wealth of information both on the theoretical development and on the applications of the various techniques for dealing with the many variations of fluid systems, while each chapter contains references to detailed works. Both volumes are well presented and the subject-matter introduced in a logical sequence, so that the authoritative tone of the work as a whole is fully maintained.

H. THOMAS

The encyclopedia of chemistry (supplement). Edited by G. L. CLARK and G. G. HAWLEY. (New York: Reinhold Publishing Corporation; London: Chapman and Hall Ltd., 1958.) Pp. vi + 322. Price 80*s*.

The original volume was reviewed in the *Brit. J. Appl. Phys.*, **8**, p. 304 (1957). Retaining the same format, the supplement deals with a further selection of topics and extends and brings up to date the original work. More references appear in some of these articles, but the criticism remains—that they are scarcely complete enough to stand alone. The Preface now states that the work is a summary of chemical fundamentals "for those who are not professional chemists". It is flattering so to suggest that some of these highly condensed articles will be clear to those of us who are. In this supplement the topics give the impression of being more restricted in their fields and, as they are of about the same length, the coverage appears more satisfactory. Many of them are very good, but the section on Engineering metals and alloys, even with its 3½ pages, seems very inadequate. There are numerous good biographies, again of chemists of all nationalities. The text is curiously undecided between thixotropy and thixatropy. The article (under rheology) is correctly written about the former, but in the index, in the text (referring back to rheology) and, absurdly, as a cognate reference at the end of rheology, in the same column as the article, it is given the latter spelling. Surely, also, the Society of Chemical Industry was founded at a meeting in Widnes and not "in London in 1881". By this time, however, the great merits and the limitations of this encyclopaedia will be well known, and the supplement does add considerably to its value.

J. G. COCKBURN

Handbook of chemistry and physics. 40th ed. Edited by C. D. HODGMAN, in association with R. C. WEAST and S. M. SELBY and in collaboration with many chemists and physicists. (Cleveland: Chemical Rubber Publishing Co.; Oxford: Blackwell Scientific Publications Ltd., 1958.) Pp. xxii + 3456. Price £5.

This remarkable handbook has been appearing regularly for over fifty years and physicists owe the Editors and their collaborators a deep debt of gratitude for their painstaking herculean task in providing them with all this data and information in a single volume of a convenient size. This edition contains the following new tables: electron physics tables; physical constants of the rare earth compounds; physical constants of inorganic hydrides; thermal conductivity of oven dry wood across the grain and at various moisture content values; thermodynamic properties of the elements; thermodynamic properties of the oxides; Langevin functions; superconducting transition temperatures, magnetic; threshold fields at absolute zero, electronic; constants and Debye temperatures for superconducting elements; chelating agents; ion exchange resins.

Other sections have been revised and brought up to date by the inclusion, for example, of data about element No. 102—Nobelium.

At least one copy of this edition should be in every laboratory and library and as many individuals who can manage it should obtain a copy for their personal use.

H. R. LANG

Handbook of physics. Edited by E. U. CONDON and H. ODISHAW. (New York: McGraw-Hill Book Company Inc.; London: McGraw-Hill Publishing Co. Ltd., 1958.) Pp. xxvi + 1504. Price 194*s*.

This Handbook, published in 1958, was revised by the contributors in galley proof in an effort to make it as up to the minute as possible. This was a praiseworthy attempt to overcome the tendency of books on rapidly growing subjects to become out of date even while in the press. The editors have been defeated by the vastness of the field of physics and the single volume they have produced has over 1500 pages and weighs over 2½ kilograms, so that the description "handbook," is something of a misnomer. A handbook is not an encyclopaedia, so it is to be expected that the articles, which are by men eminent in the respective fields, are highly condensed and often presuppose a considerable knowledge of the subject. But given such a background on the part of the reader, the articles are all excellent. To single out some among many, the sections on Fundamental constants of atomic physics, Molecular optics and on Conduction in metals and Semiconductors are noteworthy.

The work as a whole is not innocent of a tendency to flatter the specialist by reminding him how much he already knows. For such it will be salutary to reflect on the versatility of the senior editor. It will astonish even those who know him as a physicist of wide learning, to see that no less than seventeen of the articles running to some 200 pages are from his own pen.

A handbook is not a dictionary and to use the index as if it were, is to be disappointed. It may be said that the index is the weakest part of the book, in that many familiar subjects, although found in the text, do not appear in the index. For example Wien's displacement law is not indexed, but Planck's law is, also the Stefan-Boltzmann law, and reference to either of these reveals a paragraph on Wein's displacement law suitably italicized. For the most part it is true that one can usually find what one needs if one knows enough to look for it in the proper place, but there is too much chance inherent in the search.

This criticism apart, the editors are to be congratulated on a monumental achievement, which many physicists will find valuable, although fewer will find the price within their means.

A. M. TAYLOR

The technical writer. By J. W. GODFREY and G. PARR. (London: Chapman and Hall Ltd., 1959.) Pp. 340. Price 45*s*.

A splendid book this.

The authors' claim that it is "an aid to the presentation and production of technical literature" is fully justified; it is an excellent textbook and reference book. One of them (Godfrey) is Editor—Technical Instruction, B.B.C., and the other (Parr), who is a Director of Chapman & Hall Ltd., and a former Editor of some well-known periodicals, takes an active part in improving the presentation of technical information. They undertook the preparation of this book "to give the writer of technical literature an insight into the technique of presentation and production as well as laying down the principles on which good writing is based". The authors state that it is suitable as a "concise introduction to the Intermediate part of the syllabus of the City and Guilds of London Institute's lectures on technical authorship".

The book is a mine of information and opens with an account of the various types of technical literature and then

deals with the technique of technical writing and style and presentation. The next chapter is about illustrations and this is followed by a 56-page illustrated account of all kinds of printing and reproducing processes. There are chapters on setting out the text, including mathematics, on editorial procedure, and on typography. The last two chapters are on the set-up of a technical publications unit and on technical authorship, dealing with the business side, copyright, indexing and so forth. The four appendices contain useful data and a glossary, and there is a critical bibliography on the presentation of technical information.

On p. 298 the authors say that "it is safer to be guarded in one's statements when reviewing another's works"; but in any case I should hate the minor criticisms that follow to detract from my wholehearted commendation of this book. Despite the reading of the script and probably the proofs by a number of experts, I found the sub-editing (which I prefer to call "copy-preparing") a little disappointing; it is best to have an expert printer's reader to do this. For example, inches, in., and " are used indiscriminately; and the hyphen is used carelessly and inconsistently; and so on.

In such a book I should expect impeccable English and while it is up to the usual standard of satisfactory writing by a competent technical writer, and is very good in places, here and there, a bad sentence has slipped through, which is a pity.

There are footnotes every few pages and in my view some of them should be in the text and most of the rest omitted, such as the Oscar Wilde anecdote appearing as a footnote on p. 67. On p. 100 it is stated that degrees Centigrade can be written ° C., or deg. C., or ° Cent. This is not so according to the latest British Standards (e.g. B.S. 350: Part I: 1959) and International agreement. The abbreviation "deg." is reserved for a temperature interval: thus 5 deg. C means an interval of 5 degrees Celsius and 5° C means that particular temperature on the Celsius (not Centigrade) scale. The information about blocks for illustration is most helpful but attention might have been called to the difference between reduction *to* one-third, and *by* one-third. The table showing the cost of blocks on p. 215 is misleading, as it refers to single blocks and there are "tricks", which the authors mention in another part of the book, for making several blocks together and so reducing cost. But enough of these sample minor criticisms.

I hope the publishers will one day render a service to the cause so dear to the authors by producing a series of cheap paper covered editions at a price which the ordinary technical writer (who is not usually affluent) can afford to buy with his own money for his own personal use, perhaps by collecting selected chapters together in booklet form. For instance, the authors of contributions to technical periodicals do not need chapters such as that on the set-up of a technical publications unit, but they do need much of this valuable book.

H. R. LANG.

Solid state physics and crystallography

Growth and perfection of crystals. Edited by R. H. DOREMUS, B. W. ROBERTS and D. TURNBULL. (New York: John Wiley and Sons Inc.; London: Chapman and Hall Ltd., 1958.) Pp. xviii + 609. Price 100*s*.

This substantial volume is a report of the proceedings of a conference held at Cooperstown, New York, on 27–29 August, 1958 on the mechanisms of growth and the perfection of crystals. The conference, sponsored by the U.S. Air Force Office of Scientific Research and the General Electric Research Laboratory, was attended by about 60 scientists actively engaged in research in this field. The report consists of a collection of papers and reviews by various authors together with recorded discussion. The photo-offset printing process used has enabled very rapid publication to be achieved, so that the reader can obtain an up-to-date picture of the main problems and lines of development in the subject.

The report is divided into six parts dealing with topics discussed in the several sessions of the conference. The first part is in an introductory lecture by Frank; emphasis is placed on the role of crystal morphology as the central connecting subject of crystal growth phenomena by which we attempt to understand, for example the kinetics of growth or the mechanical properties of crystal whiskers. The second and third parts treat the subjects of growth and strength of whiskers, and are introduced by comprehensive reviews by Nabarro and Jackson, and by Brenner. It appears that our knowledge here is still far from complete. The experimental results show that the properties of whiskers vary considerably from specimen to specimen, and it is not yet clear in terms of dislocation mechanisms why some whiskers have such high strengths. This part is concluded with a paper by Hirsch and Silcox on recent observations of dislocation loops and other defects formed by quenching in several metals.

The fourth and fifth parts deal with the growth of crystals from solvent and solute phases. Cabrera and Vermilyea, and Frank discuss recent theories of crystal growth kinetics both for pure solutions and for solutions containing impurities. This section also includes accounts by Dash and by Mitchell on the growth of crystals of silicon and silver halides with very low dislocation densities.

The report finishes with a section on the crystallization of polymers. Polymers generally give rise to spherulite structure on crystallization; Keller describes recent work showing that long chain polymers may under suitable conditions grow as single crystals.

It is clear that many points are still imperfectly understood and much experimental work remains to be done. However, the report as a whole is useful in collecting together much information obtained by diverse methods and in indicating those lines along which future research might proceed most profitably. The editors are to be congratulated on the speedy and efficient manner in which this report has been produced.

M. J. WHELAN

Preparation of single crystals. By W. D. LAWSON and S. NIELSON. (New York: Academic Press Inc.; London: Butterworths Scientific Publications, 1958.) Pp. vii + 255. Price 45*s*.

The advances in our knowledge of the solid state, which have occurred during the last decade, have depended largely upon the availability of pure and perfect crystals on which to experiment; but there are few general texts relating to this most important aspect. This book provides, therefore, a very welcome addition to the literature.

The first three chapters contain an introduction to the simpler properties of semi-conductors, a survey of methods of growing single crystals, and then apparatus, in particular vacuum technique and furnace construction, is described. Purification and analysis of material for trace impurities are examined in the next three chapters; Chapter 4 being devoted entirely to zone refining processes. The handling of very pure materials demands extreme care if contamination is to be avoided; thus, related topics such as crucible materials, etching, dry boxes, and dust-free laboratories form the subject

of Chapter 7 which, oddly, is entitled "Preparation of compounds" but contains only four pages relating to compound formation methods. The remainder of the book deals with defects in crystals, crystal growth, and the interaction of defects in crystals.

The presentation, which is non-mathematical, gives a broad coverage to the subject, and for those who wish to develop particular topics further 200 references are quoted. It is, therefore, to be regretted that the price will put this book out of the reach of many who would find it most useful.

J. G. WILKES

Solid state physical electronics. By A. VAN DER ZIEL. (London: Macmillan and Co. Ltd., 1958.) Pp. x + 604. Price 37*s.* 6*d.*

This book is claimed to be written for the fairly advanced engineering student and to cover in one volume the whole field of solid state devices in electronics. It commences with four introductory chapters headed Waves and particles, Atomic spectra, Statistics, and Structure of the solid state. As might be expected, these are rather condensed, though it must be said, very ably condensed. The subject-matter advances a good deal further than is required in later chapters and this detracts rather from the balance of the book. In places the high degree of condensation leads to steps in the argument which would not be easily surmounted at first reading, though if used as a textbook to supplement a course of lectures this criticism would not apply. The chapter on statistics is excessively mathematical though again a very good supplement to a lecture course.

Chapter 5, Semiconductors, is a very adequate introduction to this wide subject. The main criticism of this and all other chapters, which very much reduces the value of the volume, is the almost complete absence of references to other works. This is a most unfortunate omission since the large coverage of the text could make it invaluable as an entry into the whole subject if pointers were given for more detailed reading. As it is, a student must inevitably find himself in difficulties in places and would wish to seek clarification in more detailed texts.

The coverage of the rest of the chapters includes thermionic, field, secondary and photo emission, solid state diodes, transistors, photo devices, luminescence, insulators, the piezoelectric and ferroelectric effects, magnetism and magnetic materials. The last chapter includes spin resonance, superconductivity and solid state masers. The whole twenty-three chapters consist of a total of 590 pages.

Much of the exposition is so well expressed, for the engineer, that one rather regrets several chapters largely wasted in discussion on applications of devices. Perhaps this feeling results more from the impression that the space could have been so much better spent in expanding the other chapters.

Though the book is lacking in balance between the introductory theory and later descriptions of devices and their operation and is far too condensed, it is written by a natural teacher and can be well recommended to any engineer who wants to understand more of the physics of solid state electronics. (If only the author had spent time to include an adequate bibliography!)

M. E. HAINE

Solid state physics: Advances in research and applications. Vol. 7. Edited by F. SEITZ and D. TURNBULL. (New York: Academic Press Inc.; London: Academic Books Ltd., 1958.) Pp. xiv + 525. Price 100*s.*

It is an indication of the solid establishment of this series that so many references in the present volume are to articles in earlier volumes of the same series. As usual, the articles vary from considerable monographs to summaries of narrowly defined topics and I will review them in order of decreasing length.

J. Callaway's long article on "Electron energy bands in solid" is comprehensive, but not easily followed unless one is already experienced in this field. Much attention is now given to the problem of degeneracy, where electron states of substantially different character have equal energy. The alkali metals are better understood than others, but recent work on collective motions in the electron gas is unfortunately not valid at the low electron densities occurring in these metals. The recent important work on semi-conductors is well described, and a general plea made for more work on both the shape of the Fermi surface and the density of states in energy.

H. B. Huntington gives a good account of the "Elastic constants of crystals". Following Hearmon, he perhaps underestimates the possible difference between adiabatic and isothermal speeds of propagation in discussing experimental techniques. The article deals mainly with results and theory.

P. G. Klemens on "Thermal conductivity and lattice vibrational modes" is quite first-class. He emphasizes the importance of the Umklapp-processes, in which colliding entities manage to include a Bragg reflexion in the collision process, in limiting transport rates.

A. F. Wells bases his account of the "Structures of crystals" not on the Bravais lattice but on the nearest-neighbour relations. As good reviews do, it raises more questions than it solves.

J. A. Becker describes the study of clear tungsten surfaces and absorbed layers upon them by the three tools of the fast ion gauge, field emission microscope and field ion microscope. What a pity that electrostatic stresses limit the beautiful high field techniques to substances not much weaker than tungsten.

H. W. Lewis points out the suitability of treating waves which scatter every few wavelengths by correspondingly localized wave-packets. Fourier analysis being what it is, this gives us new views rather than new results at a first approximation, but these are already instructive. This approach should be pursued for more strongly non-linear phenomena.

Any solid state physicist whose department does not keep this series should protest loudly and quickly.

G. WYLLIE

Measurement of the tensile strength of brittle materials

By R. Berenbaum, Ph.D., A.R.C.S. and I. Brodie, M.Sc., A.Inst.P., Mining Research Establishment, National Coal Board, Worton Hall, Isleworth, Middlesex

[*Paper received* 9 *October*, 1958]

Three alternative methods for measuring the tensile strengths of brittle materials are investigated and compared with the conventional pull method. These are a bending test, an indentation test and a test in which disks are compressed diametrally. Experiments on plaster of Paris, coal and cement show that, apart from the bending test, the methods give results in reasonable agreement. The bending test, however, is liable to give considerably different results, and it is shown that this can be attributed to its sensitivity to surface conditions.

In measuring the tensile strengths of brittle materials it is often inconvenient to use the direct conventional method of pulling apart a suitably shaped specimen, owing to the difficulty of preparing such specimens from the materials concerned. A number of alternative methods of estimating the tensile strengths of brittle materials using specimens of simple shape are in use, but where comparisons have been made these methods have often yielded values for the tensile strength which differ considerably from that obtained from the conventional test.[1–6]

The object of the present work was to investigate these differences and to attempt to establish a simple and reliable test which could, in particular, be used for tensile strength measurements of coals, where, owing to the wide spread in results obtained, a large number of tests are required to define the distribution of strengths among similar specimens. Three methods are considered, these being a bending test, an indentation test and a test in which a disk is compressed diametrally.

THE BENDING TEST

In this test a strip or bar specimen is bent under the action of a three- or four-point loading system and the maximum tensile stress at failure estimated from the applied bending moment using the simple beam theory. Four-point loading is usually considered to be preferable since a region of constant bending moment is obtained between the two inner loading points. At the convex surface of the beam, where the maximum tension exists, the material is in a state of pure tension so that failure is caused by the action of a single principal stress only. It must be noted, however, that large undetermined stresses occur around the loading points; although these appear to be always compressive they could give rise to shear failure; however, this is rarely observed in practice.

The bending test is in common use for brittle materials but the values of tensile strengths obtained are frequently higher (often by a factor of two or more) than those obtained by the conventional test; this has been observed, for example, for concrete,[1, 2] porcelain,[3, 4] cast iron[5, 6] and also by the present authors for certain coals. The nature of the bending test suggests that quite large discrepancies could arise as a result of modification of the surface of the material under test, since it is at the surface that the maximum tensile stresses are set up. This has, in fact, been shown experimentally by measurements on glazed and unglazed porcelain,[3] which showed that a layer of glaze only one eightieth of the thickness of the specimen was sufficient to increase the bending strength by 60%. A simple theory for beams of rectangular cross-section with modified surface layers is given below in an attempt to estimate the order of magnitude of the errors to be expected from the surface effects.

Consider a beam of total height $\alpha + \beta$ which is made up of a central portion of height α, and uniform surface layers each of height $\beta/2$ strongly bonded to this central portion. These layers are supposed to have different mechanical properties from the body of the beam. Consider a short length of the beam where the radius of curvature of the neutral axis is ρ and which subtends an angle θ at the centre of curvature. Let the width of this beam be t and let E_i and E_0 be the Young's moduli respectively of the inner and outer parts of the beam.

Then the stress at the outer surface of the beam is given by

$$S_0 = [E_0(\alpha + \beta)]/2\rho \tag{1}$$

and the stress on the inner material as the interface is approached by

$$S_i = E_i\alpha/2\rho \tag{2}$$

Defining $K = \dfrac{T_0}{T_i}$

$$= \frac{\text{tensile strength of the material of the layer}}{\text{tensile strength of the central portion}} \tag{3}$$

then the position of breakage (i.e., outer face or inner face) under loading will depend on whether S_0/S_i is greater or less than K. That is if

$$\frac{E_0}{E_i}\left(\frac{\alpha+\beta}{\alpha}\right) > K \tag{4a}$$

breakage will occur at the outer face and if

$$\frac{E_0}{E_i}\left(\frac{\alpha+\beta}{\alpha}\right) < K \tag{4b}$$

then breakage will occur at the interface.

Let G_B be the bending moment applied in an actual test, when fracture of the beam occurs. On the assumption that the beam was homogeneous the tensile breaking stress would be estimated as

$$T = 6G_B/[(\alpha + \beta)^2 t] \tag{5}$$

However, in the actual case of a layered beam, it may easily be shown that the total bending moment applied to the beam is given by

$$G = (t/12\rho)\left\{E_i\,\alpha^3 + E_0\,[(\alpha+\beta)^3 - \alpha^3]\right\} \tag{6}$$

Thus substituting for ρ in equations (1) or (2) gives

$$S_0 = \frac{E_0}{E_i}\left(\frac{12G}{t}\right)\left(\frac{\alpha+\beta}{2}\right)\left\{\alpha^3 + \frac{E_0}{E_i}[(\alpha+\beta)^3]\right\}^{-1} \tag{7}$$

and

$$S_i = \left(\frac{12G}{t}\right)\left(\frac{\alpha}{2}\right)\left\{\alpha^3 + \frac{E_0}{E_i}[(\alpha+\beta)^3 - \alpha^3]\right\}^{-1} \quad (8)$$

If breakage occurs at the inner face, $G_B = G$ and $T_i = S_i$, so that from equations (5) and (8)

$$\frac{T}{T_i} = \frac{1}{\alpha(\alpha+\beta)^2}\left\{\alpha^3 + \frac{E_0}{E_i}[(\alpha+\beta)^3 - \alpha^3]\right\} \quad (9)$$

Similarly if breakage occurs at the outer face $T_0 = S_0$, then from equation (7) and by using the fact that $T_i = T_0/K$ it may be shown that

$$\frac{T_i}{T} = \frac{K\left\{\alpha^3 + (E_0/E_i)[(\alpha+\beta)^3 - \alpha^3]\right\}}{(E_0/E_i)(\alpha+\beta)^3} \quad (10)$$

Calculations have been made of the effect of modified surface layers by assuming various values for the parameters K, E_0/E_i, α and β. Some typical examples are given in Fig. 1 which show that quite large errors can be expected with even small modification to the surface.

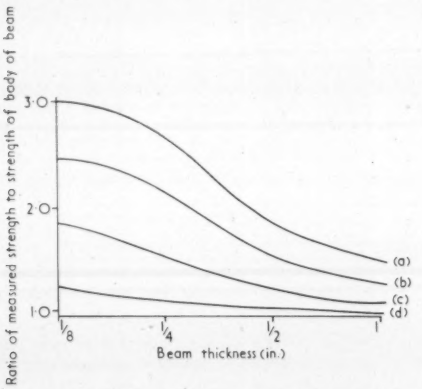

Fig. 1. The effect of skins on beam strengths

Parameters of skin assumed for curves shown

	a	*b*	*c*	*d*
Young's modulus outer/inner	2·0	1·75	1·5	1·2
Strength ratio outer/inner	3·0	2·5	2·0	1·5
Skin thickness (in.)	0·05	0·04	0·025	0·01

THE INDENTATION TEST

This test was originally devised following a study of the effect of localized forces on coal. The principle of the test (see Fig. 2) is to compress a square specimen of side a symmetrically on opposite end faces between a pair of flat ended indenters of width b. The stress distributions set up in this system were analysed by the photoelastic method for five values of b/a varying from 0·125 to 0·75 (it may be noted that case $b = 0$ has previously been investigated theoretically by Goodier[7]). The material of the indenters is assumed to be of much greater elastic modulus than the material under test, so that a constant displacement occurs. The variations of the principal stresses, P and Q, along the lines EF and GH of Fig. 2 were obtained by using the isochromatic fringe pattern to give $(P - Q)$, and Filon's method[8] of graphical integration for axes of symmetry to obtain the separate values for P and Q along these lines. Complete sets of stress trajectories for this indenter problem were obtained by the electrical analogue method recently described by Theocaris.[9]

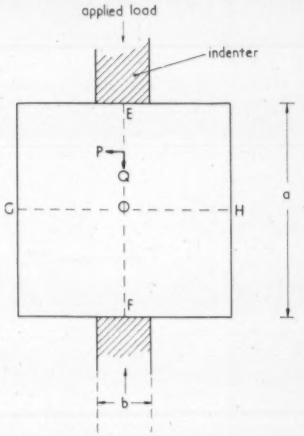

Fig. 2. Schematic diagram of indentation test

From the symmetry of the problem it will be seen that along the perpendicular bisectors EF and GH of the square specimen, the principal stresses P and Q set up by the indentation run horizontally and vertically respectively. The magnitudes of these stresses for constant indenter load are shown in Figs. 3 and 4.

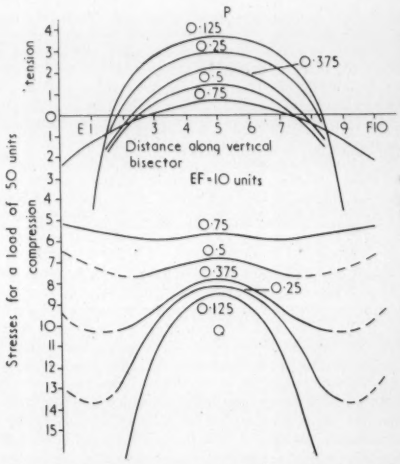

Fig. 3. Stresses along vertical bisector EF. The figures associated with each curve give the value of b/a for that curve

Detailed analyses at points in the model other than along *EF* and *GH* were not carried out, but it was found possible, by using Mesnager's theorem,[8] to deduce the approximate behaviour of the principal stresses over the rest of the model, except in the regions close to the indenter edges, from the boundary conditions and the shape of the stress trajectories. This

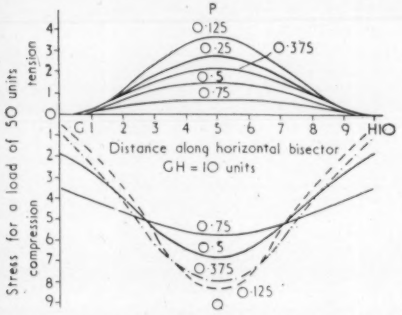

Fig. 4. Stresses along horizontal bisector *GH*. The figures associated with each curve give the value of b/a for that curve. Note: for clarity the *Q* curve for $b/a = 0{\cdot}25$ has been omitted, being close to those for $b/a = 0{\cdot}125$ and $0{\cdot}375$

showed that the maximum tensile stress along any given *P* trajectory occurs at the intersection of this trajectory with the vertical bisectors *GH*, and the maximum tensile stress in the whole specimen is found at the centre point 0. No tensile *Q* stresses occur in the specimen, except possibly in the undetermined region close to the indenter edge. It must be recognized that very large stresses occur in this region; this can be clearly seen from the isochromatic fringe pattern shown in Fig. 5, which was obtained from a model for which $b/a = 0{\cdot}5$. Fig. 6 shows the variation with b/a of the ratio of the maximum shear stress (obtained directly from the photoelastic fringe pattern) at the indenter edge to the maximum tensile stress at the centre.

A point to be resolved is whether any of the stresses around the indenter edges are tensile and, if so, whether they can become larger than the tension at the centre. A theoretical solution for a plane indenter on a semi-infinite sheet has been given by Sneddon[10] and this shows that only compressive stresses can exist in this region. A preliminary photoelastic investigation has been carried out for the present problem

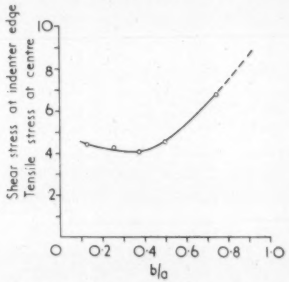

Fig. 6. Variation with b/a of ratio of shear stress at indenter edge to tensile stress at centre

and this has shown that small tensile stresses could possibly be set up since the displacement of the indenter is not infinitesimal. However, these tensile stresses appear to be insignificant compared with those set up at the centre of the indenter square. Therefore, from the point of view of breakage of brittle materials, if the material under test fails in tension a vertical crack initiated at the centre would appear. The variation of the principal stress *P* along the vertical bisector *EF* (Fig. 3) would indicate that a crack of only limited length might be expected, provided that the stresses close to the indenters are not radically altered by the presence of the crack. If, however, the specimen were to fail in shear then it would do so by a crack initiated from the indenter edge, and it is an advantage of this test that the two modes of failure can thus be easily distinguished.

The actual values of the maximum tensile and shear stresses as fractions of the applied stress were determined from the results of Figs. 4 and 6 for the various values of b/a and the results obtained are shown in Figs. 7 and 8; these results

Fig. 5. Isochromatic fringe pattern for $b/a = 0{\cdot}5$

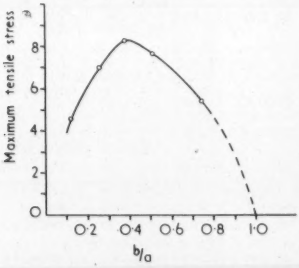

Fig. 7. Variation of maximum tensile stress with b/a for constant applied stress. Applied stress = 50 units

enable the actual breaking stresses to be determined from observations of the applied stress causing breakage. It will be noted from Fig. 6 that the ratio of the maximum shear stress in the specimen to the maximum tensile stress is never less than four, so that for the indentation test to produce tensile breakage, the shear strength of the material under test

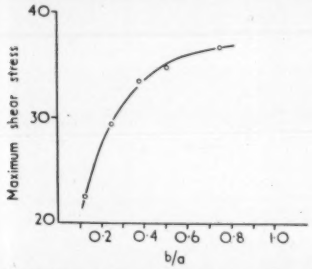

Fig. 8. Variation of maximum shear stress with b/a for constant applied stress. Applied stress = 50 units

must be at least four times greater than the tensile strength. This, in fact, appears to be the case for most of the brittle materials examined including coals, plaster of Paris and cement, for which stable central vertical cracks are produced (see Fig. 9).

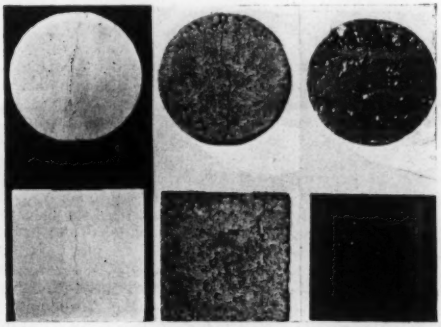

Fig. 9. Broken specimens of (*a*) plaster; (*b*) cement; (*c*) coal

A disadvantage of this test is that tensile failure is not initiated at a point where a state of pure tension exists, since at the point of maximum tensile principal stress the other principal stress is not zero but has a finite compressive value. Thus in the case of a material, the strength of which was dependent on both principal stresses, (as would be the case for a material which behaved in accordance with Griffith's theory of the propagation of cracks[11]) care would have to be taken in interpreting the results obtained.

This point can easily be checked by using the test with different sized indenters which give rise to different ratios of compressive to tensile stresses and, for the brittle materials so far examined, failure in these tests appears to be determined only by the magnitude of the tensile principal stress. Fig. 10 shows the variation of applied indenter stress for breakage as a function of the indenter width for two substances, plaster of Paris and a coal (the Top Hards of the Barnsley seam at the Rossington colliery). The full line in each case represent the result to be expected from the photoelastic analysis on the assumption that breakage is determined by the magnitude of the tensile principal stress only.

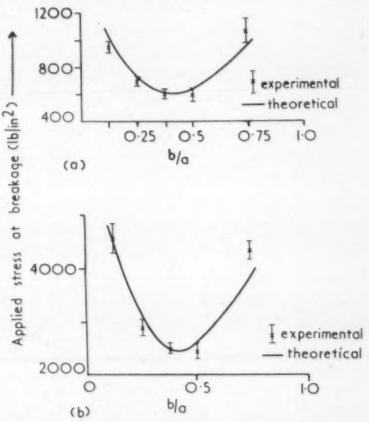

Fig. 10. Variation of breakage stress with indenter size
(*a*) Plaster of Paris (eight specimens at each indenter size); (*b*) Coal (fifteen specimens at each indenter size)

THE DIAMETRAL COMPRESSION TEST

This method is a logical extension of the indentation test and has previously been used[2, 12] for tests on concrete.

If a disk of elastically isotropic material is compressed diametrally by knife edges at opposite ends of a diameter, it can be shown theoretically that there exists across this diameter a tensile principal stress of constant magnitude which tends to pull the disk in half along this line. The magnitude of this stress P is given by[13]

$$P = 2W/\pi tD \tag{11}$$

where W is the applied load, and t and D are the thickness and diameter of the disk respectively. The other principal stress, which acts along the diameter, is always compressive but varies in magnitude from point to point along it. This stress Q is given by

$$Q = -\frac{2W}{\pi t}\left(\frac{2}{D-2y} + \frac{2}{D+2y} - \frac{1}{D}\right) \tag{12}$$

where y is the distance along the diameter measured from the centre.

If the disk is compressed between parallel planes then it can be shown, theoretically from St. Venant's principle and experimentally from photoelastic analysis, that the stresses only differ from the above theoretical solution at points the same order of distance away from the applied load as the width of the area of contact between the plane and the disk, provided this latter length is small compared with the diameter

of the disk. The theoretical value of the width of the area of contact d can be calculated from the equation[14]

$$d = 1{\cdot}6\sqrt{\left[\frac{W}{t} \times \frac{D(1-\nu^2)}{E}\right]} \qquad (13)$$

for the case where the Young's modulus for the plate is very much greater than that for the disk E; ν is the Poisson's ratio for the disk material. Calculations show that for most brittle materials d is indeed small compared with D when breakage occurs. Thus it may be concluded that the constant tensile stress across the diameter does not differ from the theoretical value, except close to the diameter ends where the stress values are undetermined. Provided that the stresses in this undetermined region do not rise to tensile values greater than that along the centre of the diameter, the stress for tensile breakage can be calculated from equation (11). While it is not easy to provide an analytical solution for the stresses close to the crushing platens, the mode of failure of plaster of Paris, coal and cement (see Fig. 9) shows that breakage is usually initiated away from the ends of the loaded diameter, and often the crack does not proceed completely to the diameter ends. This implies that the stresses close to the platens do not exceed the tensions set up along the majority of the diameter and, indeed, suggests that they are mainly compressive. There are, however, very large shearing stresses set up near to the crushing platens and in this case, in contrast to the indentation test, it is not easy to detect whether failure is initiated in tension or shear.

A further disadvantage to this test is that the compressive principal stresses which act along the loaded diameter vary from a minimum value of three times the constant tensile principal stress at the centre to large values as the crushing platens are approached. This again means that the test is only suitable for materials whose strength depends on the tensile principal stress, and disk measurements should be compared with indentation measurements to check this point.

The disk method, however, is particularly convenient for measuring tensile strengths at various orientations for substances which exhibit a strength anisotropy. This is because the tensile stresses in the disk can be set up in any chosen direction parallel to the face by a suitable choice of loaded diameter, so that specimens sliced from a single cylinder can be used to obtain a picture of the strength variation with direction. In the other tests a specimen must be cut individually for each orientation. This has made the test particularly useful for the study of coals, where the strength anistropy is often large; although some degree of elastic anisotropy has been observed for coal,[15] this is so small that it is considered that equation (11) (derived by assuming elastic isotropy) can be applied without appreciable error.

EXPERIMENTAL RESULTS

In order to compare experimentally the various methods of measuring tensile strength, specimens were prepared from 99% pure plaster of Paris. This substance was chosen because of the ease with which specimens of all shapes could be prepared and because it appears to be isotropic, homogeneous and to behave in a brittle fashion. Since the properties of plaster of Paris are sensitive to the method of preparation, comparisons must be made between specimens cast from the same plaster mix.

Measurements of tensile strength by the three methods given above were compared with results obtained from the conventional tensile test. A summary of the results obtained is given in Table 1, together with the number and dimensions of the specimens used. Since only a single mould was available to prepare the specimen for the conventional test the experiment was repeated ten times. The results in Table 1 are given as ratios of the measured strength to that of the conventional method, as this ratio should be independent of any variation in the absolute strength of the different batches.

The results for the indentation tests and the disk test are in good agreement with each other (this has also been found to be so for cement and for coal) and are in fair agreement with that obtained from the conventional test. The bending test, however, gives results which differ by a factor of about two from these. Since the bending test is particularly sensitive to the state of the surface of the specimen, it is indicated that the surface of moulded plaster of Paris is modified in some way, either by the production of a toughened surface skin or by the surface layers being put into compression during the casting and setting processes.

The effect of such modified surface layers should be much greater in thin specimens of all types, as it would be expected that the thickness of the modified layer would be approximately independent of the specimen thickness. For this reason measurements were made of the effect of size on specimen strength for the bending and disk tests.

Twenty-four disks were cast, comprising six of each of four thicknesses, all specimens being cast from the same mix of plaster. These were compressed and the tensile strengths were calculated; the results obtained are given in Table 2.

Table 2. *Variation with thickness of tensile strength of disks*

Disk thickness (in.)	0·88	0·46	0·375	0·12
Mean tensile strength (lb/in.^{2})	480	455	453	541
Standard error (lb/in.^{2})	35	28	40	30

Twenty-four beams 4 in. long and $\frac{1}{2}$ in. wide were cast, made up of six of each of four thicknesses, all specimens being cast from the same mix of plaster. These were broken with a four-point loading system as before and the results were compared with a set of disks (diameter 1 in., thickness $\frac{1}{4}$ in.) cast from the same mix. The simple beam theory is only strictly applicable to very thin beams, and a correction for calculating the maximum tensile stress at breakage for thicker

Table 1. *Comparison of methods of measuring tensile strengths*

Type of specimen	*Dimensions*	*Number produced per batch of plaster*	*Ratio of tensile strength to that from conventional test (Mean from 10 batches) (The uncertainties quoted are standard errors)*
Conventional tensile specimen	Cylindrical "dumb-bell" central diameter 0·36 in., length 1·5 in.	1	1·00
Beams for bending test	4 × ½ × ¼ in.	4–8	2·3 ± 0·3
Squares for indentation test	1 × 1 × ½ in. for $b/a = 0{\cdot}375$	6–10	0·85 ± 0·1
Disks for compression test	1 in. diameter, ½ in. thickness	6–10	0·8 ± 0·1

beams has been obtained from a photoelastic investigation of the problem, using a similar technique to Fukuhara (described in Ref. 8. p. 458) who examined beams under three-point loading. The results are given in Table 3.

A further experiment was carried out in which twelve beams of thickness 0·25 in. were cast from a single mix and, after setting, six of them were planed down to a depth of 0·05 in. on each face. All twelve were then broken under four-point loading and the results obtained were:

tensile strength of original beams = 665 ± 60 lb/in.^{2}
tensile strength of planed beams = 504 ± 45 lb/in.^{2}

The significance of these several results is discussed below.

Table 3. *Variation of strength of beams with thickness*

Beam thickness (in.)	0·125	0·25	0·5	1·0	Disks
Tensile strength (lb/in.^{2})	1060	790	655	630	440
Correction factor (distance between outer loading points = 3·5 in. *and that between inner points* = 1·5 in.)	1·00	0·95	0·92	0·90	—
Corrected Tensile strength (lb/in.^{2})	1060	750	601	566	440
Standard error (lb/in.^{2})	70	50	60	60	30

ASSESSMENT OF RESULTS

The wide disagreement between the tensile strengths obtained from bent beam measurements and those obtained from other methods can be attributed to the existence of a modified surface layer on the plaster specimens, for whereas the strength of plaster disks remains constant except for very thin specimens, for beams there is a steady variation of strength with thickness and removal of the surface of a beam does result in a decrease in strength. The fact that no significant change in disk strength was observed except at 0·125 in. thickness indicates that the "skin" depth cannot be more than about 0·05 in., and in order to obtain an estimate of the properties of this skin an attempt was made, using the results of the analysis given earlier, to calculate those parameters which would lead to the results observed above. It was found that the best agreement with experiment was obtained with a skin depth of about 0·03 in. and by assuming that both the Young's modulus and the strength of the skin are increased by factors of about two. Fig. 11 shows the observed and calculated results for the various beam thicknesses expressed as multiples of the observed disk strength, and it is seen that the observed results can be well fitted.

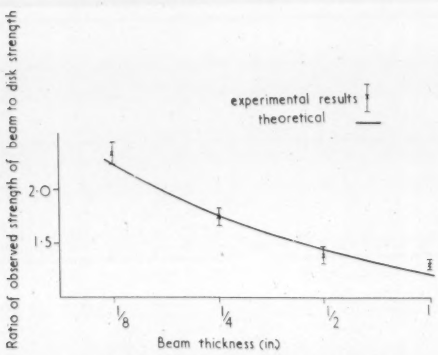

Fig. 11. Observed and calculated results for plaster beams (taking ratio of Young's moduli = 2·3; ratio of strengths 2·4; thickness of skin = 0·03 in.)

The effect of scraping the surface of the beams, however, did not produce as large an increase in strength as would be expected, presumably owing to the formation of a new skin. It must be appreciated that calculations based on skins can only be approximate, since the assumption of a sharply defined skin is unlikely to be valid; however, it appears that by using it a reasonable estimate of the properties of the surface can be obtained. This is borne out by the fact that if the above parameters are assumed for the skin, then it can be shown that the other form of tensile test are also affected to some extent. In the conventional test, using the skin parameters obtained above and assuming a constant tensile strain, it is found that the ratio of the observed strength to the actual strength of the body of the plaster is about 1·4. For the disk and indentation measurements, assuming constant lateral displacement through the thickness of the specimens, the ratio of measured strength to actual strength is found to be about 1·15. This means that the ratio of the measured disk and indentation strength to that measured conventionally should be about 0·82, which agrees remarkably well with that actually observed (Table 2).

DISCUSSION AND CONCLUSIONS

All the methods considered have the disadvantage that the material under test must be able to withstand large shear stresses; these occur close to the points of application of the load in the bending and disk tests, and at the indenter edges in the indentation test. Fortunately, for many really brittle materials, failure occurs first in tension. However, the indentation test has the advantage that it shows unmistakably whether failure has occurred in tension or shear.

The main advantage of the bending test is that a state of pure tension is set up, but this is outweighed by the sensitivity of this method to surface conditions. In many materials it appears to be difficult to prepare specimens free from surface modification, which are probably formed during the casting or machining of the specimens.[16, 17]

Both the indentation and the disk tests suffer from the disadvantage that a state of pure tension is not set up, but the effect of the other compressive principal stress can be determined by using the former test with different sizes of indenters. For the materials examined, failure in these tests appears to be determined only by the magnitude of the maximum tensile principal stress.

The main advantage of the disk test is the ease with which it can be carried out and its usefulness for materials having anisotropic tensile strength properties.

ACKNOWLEDGEMENTS

This paper forms part of the programme of research of the Mining Research Establishment and is published by permission of Dr. W. Idris Jones, Director-General of Research in the Scientific Department of the National Coal Board. The views expressed are those of the authors, and not necessarily those of the Board.

REFERENCES

(1) VOLKOV, V. G., *Trudy Moskov. Automobil-Dorozhn. Inst.*, **15**, p. 153 (1953).
(2) WRIGHT, P. J. F. *Mag. Concrete Res.*, **1**, p. 87 (1955).
(3) BETTANY, C., and WEBB, H. W. *Trans Brit. Ceram. Soc.*, **39**, p. 312 (1939).
(4) RIDDLE, F. H., and LAIRD, D. *J. Amer. Ceram. Soc.*, **5**, p. 499 (1922).
(5) MISIAG, M. *Prace Glownego Instytutu Odlewnictwa*, **4**, p. 157, (1951).
(6) LISSELL, E. O., and ITZEL, M. *Inst. Brit. Foundrymen*, Paper No. 1103 (1954).
(7) GOODIER, J. N. *Trans Amer. Soc. Mech. Engrs*, **54**, p. 173 (1932).
(8) COKER, E. G., and FILON, L. N. G. *A Treatise on photo-elasticity*, 2nd Ed. (London: Cambridge University Press, 1957).
(9) THEOCARIS, P. S. *Proc. Soc. Exper. Stress Anal.*, **14**, No. 2, p. 11 (1956).
(10) SNEDDON, I. N. *Fourier Integrals*, (New York: McGraw-Hill Book Co. Inc., 1951).
(11) GRIFFITHS, A. A. *Phil. Trans A*, **221**, p. 163 (1921).
(12) CARNEIRO, F. *Paris: Reunion des Laboratories d'Essai de Matériaux* (1947).
(13) TIMOSHENKO, S., and GOODIER, J. N. *Theory of Elasticity*, 2nd Ed. (New York: McGraw-Hill Book Co. Inc., 1951).
(14) FÖPPL, A. *Technische Mechanik*, 4th Ed., **5**, p. 350 (1933). [See also Roark, R. J. *Formulas in stress and strain.* (New York: McGraw-Hill Book Co. Inc., 1954)].
(15) MORGANS, W. M., and TERRY, N. B. *Fuel*, **37**, p. 201 (1958).
(16) GURNEY, C., p. 145, LOVE, R. J., p. 161. *Symposium on Properties of Metallic Surfaces* (London: Institute of Metals, 1952).
(17) FARMER, M. H., and GLAYSHEV, G. H. *J. Sci. Instrum.*, **30**, p. 9 (1953).

Relationship between strength and porosity for coal compacts

By D. J. MILLARD, B.Sc., Ph.D., A.Inst.P.,* National Coal Board, Central Research Establishment, Cheltenham, Gloucestershire

[*Paper received* 8 *December*, 1958]

When powdered coal is compacted by subjecting it to high pressures it is found that the quality of the compact as measured by strength tests is, for a given batch of powder, a single valued function of the porosity of the compact. The shape of this strength-porosity curve cannot be explained by treating the pores as if they only reduced the load bearing area available to withstand stresses in the compact.

The form of the observed strength-porosity curves for compacts tested at right angles to the direction of compaction has been explained in terms of the development of contacts between particles with increasing compaction, and of the changing action of pores as stress magnifiers. A strength-porosity relationship of the form $\sigma = (1 - \bar{p})\bar{p}^{-1}$ has been deduced, where $\bar{p}$ ("rationalized" porosity) is the ratio of the porosity of the compact to that of the pile of loose powder having no mechanical strength. It has been shown that this expression gives a good representation of the experimental data.

In producing fuel briquettes from powdered coal it is necessary to make a compact of sufficient strength to withstand rough handling in transit from processing plant to consumer. Whilst investigating various compacting processes it was noticed that, for a given batch of coal powder, there was a single valued relationship between the compaction achieved on briquetting and the quality of the compact as measured by various strength tests.

Now the relationship between the strength of a porous, brittle solid and its porosity is of interest in many fields. For instance, Duckworth[1] and Ryschkewitsch[2] quote an empirical strength-porosity relationship for ceramics, and Schiller[3] has devised such a relationship for gypsum plaster. Unfortunately their results do not agree with the strength-porosity relationship observed for coal compacts.

It is the object of this paper to show that the form of the strength-porosity relationship observed for coal compacts depends on the way the contacts between particles develop with increasing compaction, and on the changing action of pores as stress magnifiers. It is not sufficient merely to treat the pores as if they only reduced the load bearing area available in the material under stress.

EXPERIMENTAL WORK

A range of compacts were made by pressing samples of two coals in a 1 in. diameter mould. The samples were chosen so that the final specimens were in the form of disks about $\frac{1}{4}$ in. thick. The pressing conditions were varied to give as wide a range as possible of compactions in the final artefacts. The two coals used were Betteshanger (a low volatile "smokeless" coal) and Sherwood (a high volatile smoky coal): details of these two coals are given in the table. Before use samples of the coals were ground to pass through a 120 B.S.S. mesh sieve, and all the experiments for one coal were then carried out on a single grind of that coal. The quality of the compacts was assessed by cutting small beams from them ($1 \times \frac{1}{4} \times \frac{1}{4}$ in.) and measuring their rupture strengths in a four-point loading test. Since the compacts

* Now at the Central Electricity Generating Board, c/o Station Superintendent, Berkeley Power Station, Berkeley, Gloucester.

Details of Betteshanger and Sherwood coals

Colliery	*Betteshanger*	*Sherwood*
Seam(s)	*H*	*Dunsil, Top Hard Deep Soft*
Nominal size	−120 B.S.S. mesh	−120 B.S.S. mesh
Moisture	0·7%	7·6%
Ash	3·5%	3·1%
Volatile matter (less moisture)	17·4%	32·8%
Fixed carbon	78·4%	56·5%
Specific gravity	1·33	1·35
Screen size B.S.S. mesh		
60 × 120	1·9%	0·5%
120 × 240	29·4%	32·6%
−240	68·7%	66·9%

were known to be anisotropic with respect to the direction of the applied compacting pressure, these beams were always cut in the same way; namely, with their long axes at right angles to the direction of the applied pressure. The compaction achieved by the pressing process was expressed in terms of specimen porosities as determined by density measurements. The observed strength-porosity relationships are shown in Fig. 1.

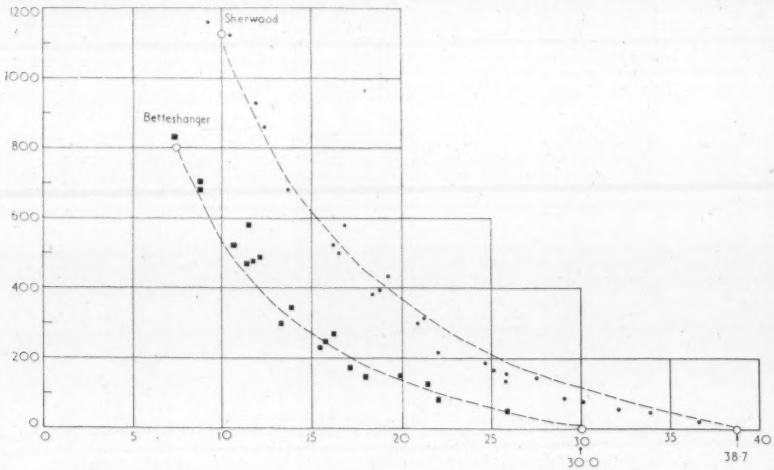

Fig. 1. Compact strength as a function of porosity for Betteshanger and Sherwood coals. The dotted curves are derived from the expression $\sigma = S_0(1 - \bar{p})\bar{p}^{-1}$

THE RELATIONSHIP BETWEEN STRENGTH AND POROSITY OF A COMPACT

When considering the relationship between the strength and the porosity of a compact, it is convenient to consider an "average" region of the compact containing one or more average pores. It is realized that in a real material there must be distributions of both pore sizes and spacings: the effect of there being such distributions need not be disturbing. Let the criterion for failure of a specimen be that there is some critical stress σ_0 that must not be exceeded. Now the actual stress at any point in a real material must depend both on the applied stress field and the perturbation of the applied field due to the pores: failure in the material will occur in a high stress region near unfavourably sited pores. Provided that the applied stress field does not vary rapidly over distances comparable with the pore size and spacing, it may be assumed, for the given pore distribution produced by compacting one size distribution of a given coal, that the weakening effect of the worst pores will be in a constant ratio to that of the average ones. Thus calculations drawn from arguments based on the "average pore" concept will be wrong by a constant, unknown, numerical factor. What follows below, however, is a dimensional argument, giving the form of the strength-porosity relationship. To obtain this relationship numerically it proves necessary to determine two constants empirically. In so doing the constant factor relating the average to the worst pores is automatically allowed for.

It is now necessary to choose a model of the pore system to be studied. Since coal compacts are permeable the model must involve interconnected pores. That chosen is a structure containing tubular pores of elliptical cross-section; the pores are interconnected and open at the ends of the tubes. They may be considered as holes running between adjacent particles in the compact. As the compacting pressure is increased the porosity of a compact is reduced. This is supposed to happen by the dimension of the pores parallel to the direction of the applied pressure being shortened (i.e. the y dimension in Fig. 2). It should be noted that the test specimens were always so orientated that they failed under tensions applied at right angles to the direction of the compacting pressure (x direction, Fig. 2).

Let us now consider a pile of particles, porosity p_{cr},

immediately prior to compacting. A plane of unit area passing through such a pile must, on the average, intercept an area of solid A' given by

$$A' = 1 - p_{cr} \tag{1}$$

The pile of powder has no mechanical strength as it can be pulled apart over a surface passing between particles, without failure of the solid material across an arbitrarily chosen plane. Let the powder be pressed and its porosity

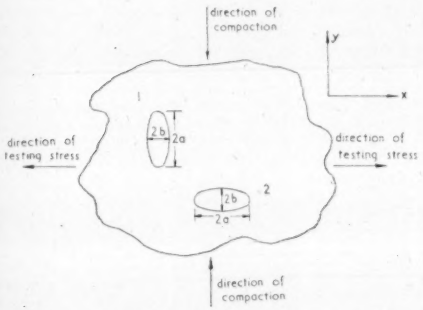

Fig. 2. Model used for the pore system. Increasing compaction is supposed to reduce the y dimensions of all pores by the same relative amount

(1) Pore giving most effective stress magnification in the tests used; (2) pore giving most effective stress magnification for tests parallel to the direction of compaction.

reduced to a lower value p. Suppose this to happen mainly by particles deforming at their points of contact rather than in the bodies of the particles. The contacts will now be joined and the structure will have some mechanical strength: it is no longer free to fall apart along a continuous surface defined by unjoined particles. The area of solid intercepted by a unit plane will now be

$$A = 1 - p \tag{2}$$

Physical intuition suggests that the increase in area ΔA will be closely correlated with the new contact area between particles that can sustain a load. Subsidiary calculations on a simple model (such as a cubic lattice of close packed spheres) have shown this to be so for specific cases. It is reasonable to suppose, therefore, that the strength of the compact will be proportional to ΔA, i.e.

$$\begin{aligned} \sigma &= S \,.\, \Delta A \\ &= S \,.\, (A - A') \\ &= S \,.\, (p_{cr} - p) \end{aligned} \tag{3}$$

where σ is the apparent applied stress to produce failure and S is a constant of proportionality involving the critical stress for failure σ_0.

To explain the observed strength-porosity relationship it is necessary to postulate that a compact is weaker than would be expected from considering the contacts between particles alone. Consider the known stress magnifications that exist at points near the edges of any holes in a stressed solid. These stress magnifications will make such points weak points in the compact. The weakest points will be at the ends of such pores as lie across the direction of the testing stresses, and these are the only points that need be considered. Once failure is started at such a weakest point the crack produced may be expected to spread across the specimen. For an isolated elliptical hole of semi-axes (a, b) the relevant stress magnification factor is $(1 + 2a/b)$ (that for simple tensile stresses parallel to the b axis). It is now assumed that this result holds for the pores under consideration. If it does the maximum applied stress, σ of equation (3), that can be withstood by the compact without σ_0 being anywhere exceeded, must be reduced by the stress magnification factor. Thus if $2a/b \gg 1$ we may write

$$\sigma = S \,.\, (p_{cr} - p)(b/2a) \tag{4}$$

It is now necessary to express $b/2a$ in terms of porosity. Consider a unit cell of linear dimension s. This is associated with, and on the average contains, one pore of length s and of cross-section of semi-axes a and b. Ignoring geometrical constants, and arguing in terms of dimensions only, the volume of the unit cell is s^3, and of the pore abs. Thus the porosity of the compact—which is the same as that of the unit cell—is of the order

$$p = ab/s^2 \tag{5}$$

Now it is supposed that as the compaction is increased all pores suffer the same relative reduction of their y dimensions (the dimension parallel to the direction of pressing). But the pores under consideration, namely those that produce the greatest stress magnification in the tensile tests, have their major (a) axis along this direction. For them the a dimension only changes, so that we may substitute for a in equation (4), using equation (5), to obtain

$$\sigma = S(p_{cr} - p)\frac{b^2}{2s^2} \cdot \frac{1}{p} \tag{6}$$

Or, defining a "rational porosity" $\bar{p}$ by

$$\bar{p} = p/p_{cr} \tag{7}$$

and collecting all other constants together,

$$\sigma = S_0(1 - \bar{p})\bar{p}^{-1} \tag{8}$$

Here S_0 is a numerical constant having the dimensions of a stress. It represents the true matrix strength of the briquette loaded by various numerical pore shape factors. The value of S_0 must be determined experimentally for any one sample of briquetted coal.

It is interesting to note that, had one considered specimens tested by stressing parallel to the direction of pressing, a different result would have been obtained from the foregoing analysis. In this case the most effective stress magnifiers would be pores with their major axes at right angles (not parallel) to the direction of pressing. Such pores would have their minor axes reduced as compacting advanced, and so would have given a reciprocal and not a direct relationship between stress magnification and porosity. Thus the final strength-porosity relationship expected would have been of the form $\sigma = S_0(1 - \bar{p})\bar{p}$.

TESTING OF THE THEORETICAL ANALYSIS

The data for testing the foregoing analysis is shown in Fig. 1, which is a graph of compact strengths plotted against porosity for Betteshanger and Sherwood coals, the compacts having been ruptured by tensile forces applied at right angles to the direction of compaction. It has not been possible to test specimens by means of stresses applied parallel to the direction of compaction.

The strengths vary from almost zero to over 1100 lb/in.^{2};

the porosities vary from 7·5 to 35%. The dotted curves are derived from the expression for briquette strength developed above. For each coal two constants had to be determined to enable the theoretical data to be fitted to the experimental results, namely p_{cr} and S_0. In each case p_{cr} was determined by extrapolating the experimental results to zero strength, and S_0 was found by fitting the calculated curves to the experimental data in the high strength regions at the points marked with large circles. It will be seen that the agreement between the predicted strength-porosity relationship and that observed experimentally is satisfactory.

The above calculations have been repeated for pore systems other than the one used here. If the compaction process were taken as varying other or more than the y dimensions of the pores, the resultant expressions (which differed in the reciprocal $\bar{p}$ term) did not provide a fit to the experimental data.

ACKNOWLEDGEMENTS

I wish to thank Dr. B. A. Lilley for the experimental results quoted in this paper.

The work described in this paper was carried out as part of the research programme of the Scientific Department of the National Coal Board. The views expressed are those of the author and not necessarily those of the Board.

REFERENCES

(1) DUCKWORTH, W. J. *J. Amer. Ceram. Soc.*, **36**, p. 68 (1953).
(2) RYSCHKEWITSCH, D. *J. Amer. Ceram. Soc.*, **36**, p. 65 (1953).
(3) SCHILLER, K. *Proceedings of the Conference on the Mechanical Properties of Non-Metallic Brittle Solids*, organized by the N.C.B. Mining Research Establishment and D.S.I.R. Building Research Establishment, London, April 1958. To be published.

Measurement of high intensity stress pulses

By J. S. BUCHANAN, B.Sc., Ph.D., A.Inst.P.,* and H. J. JAMES, B.Sc., Armament Research and Development Establishment, Fort Halstead, Kent

[*Paper first received* 1 *January, and in final form* 3 *February*, 1959]

A modified form of the Hopkinson bar technique has been applied to the study of stress pulses produced in a simple explosive-metal system. The results are used to illustrate the kind of information which can be obtained from such an experiment. This includes measurements of the pressure in the detonation wave, the changing shape of the stress pulse induced in the metal and the normal fracture stress of the metal.

1. INTRODUCTION

High explosive charges when detonated in contact with inert materials, generate high intensity stress pulses in these materials. The rise time of these pulses is extremely short: less than the time resolution of the instruments used to try and record it (i.e. 10^{-8} s) and therefore the pulses can be treated as shock waves. The amplitude of the shock at the explosive material interface is in the region of 10^{11} dyn/cm^2 and the decay behind the shock front is approximately exponential in form. As the shock wave propagates through the material it disperses rapidly; this is usually due to the expansion of the wave rather than the internal friction of the material. Studies of the propagation of these shock waves in materials have provided useful basic data on the response of materials to these very high rates of loading. The dynamic yield strength of steels[1] and the dynamic equations of state of many materials[2–7] have been measured by determining the shock wave velocity and the velocity of a free surface normal to the direction of propagation of the wave front. As yet most experimental studies have employed probe[2] or optical[3] techniques, which determine only the instantaneous peak pressure in the wave. In studies of fracture or the physics of detonation it is helpful to determine the whole profile of the wave, and it was for this reason that the following pellet method was used, despite a deep appreciation of the assumptions and errors inherent in the technique.

The first experiments to determine stress pulse shapes were the classical ones of Hopkinson[8] using his bar technique. Since then this technique has been used by several workers[9,10] and more recently Rinehart[11] has applied it to explosive-metal systems and obtained a limited amount of quantitative data on scabbing, i.e. the fracturing of a material near a free surface due to impinging compressional stress pulses. This paper describes the application of a modified form of Rinehart's adaption of the Hopkinson bar technique to a simple explosive-metal system. These experiments were exploratory, being designed to find how reproducible the system is and to see what information can be obtained from such experiments. An assumption inherent in the Hopkinson technique, and in this paper, is that the maximum of the stress pulse occurs at or very near the front of the pulse. This is a very reasonable assumption in the present experiments but is a limitation on the general application of the technique.

2. THEORY

The method used in these experiments is very similar to that used by Hopkinson.[8] Consider two plates A and B (Fig. 1) of the same material and in good contact without loading along the plane $X-Y$, such that the joint has little or no strength in tension; it will, however, transmit a compressive wave without any change in the waveform. Let a compressive wave move through A to B [Fig. 1(*a*)], it will enter B unchanged [Fig. 1(*b*)], but on reaching the free surface F will be reflected as a wave of tension [Fig. 1(*c*)]. If the wavelength λ is less than twice the thickness of B, all the wave will be in B at some time and, when the reflected wave reaches the interface $X-Y$, plate B will move away from A with all the momentum associated with the stress wave trapped in it. Plate A remains at rest. The momentum of plate B is then the total area under the stress-time curve and measurement of the velocity of B combined with a knowledge of its dimensions enable $\int \sigma\, dt$ to be determined.

* Now at A. E. Reed and Co. Ltd., Maidstone.

When λ is greater than twice the thickness of B, only part of the momentum will be trapped in B, the rest remaining in A. The amount of momentum trapped in B will be

$$M = \int_0^T \sigma \, dt \qquad (1)$$

where T is the time for the wave to travel twice the thickness of B. In the experiment B is made very thin to begin with and the thickness increased in steps. Measurement of the momentum of B in each case enables the stress-time relationship to be determined. For a pellet of unit area

$$\text{momentum} = \rho L V$$

where ρ, L and V are the density, length and velocity of the pellet respectively. Also from equation (1)

$$\text{momentum} = \bar{\sigma} T$$

where $\bar{\sigma}$ is the mean value of the stress at the surface X–Y over time T.

Now $$T = 2L/D$$

where D is the velocity of the compressive wave and also of the tension wave it produces on reflexion; D is assumed constant for all parts of the wave. (These assumptions are reasonable since D is insensitive to the actual value of the stress in the range covered in this paper[12] while the reflected tensile wave velocity is within a few per cent of the compressive wave velocity. Dispersion of the wave once it enters the pellet is unimportant, since its momentum is still trapped in the pellet.)

Therefore $$\text{momentum} = 2\bar{\sigma}L/D = \rho L V$$

and $$\bar{\sigma} = \rho V D/2 \qquad (2)$$

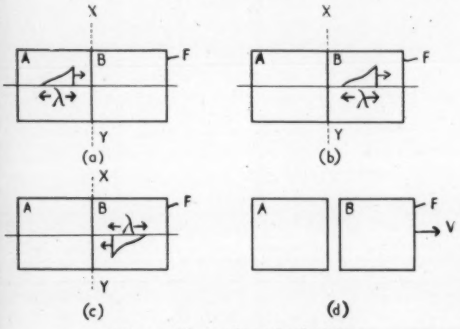

Fig. 1. Illustration of principle

A compressive pulse in plate A (a) is transmitted to plate B (b) across the plane of contact $X - Y$. This joint will transmit a compressive wave without any change in waveform but has no strength in tension. On reaching the free surface F, the pulse is reflected as a tension wave (c). When the tension wave reaches $X - Y$, the two plates separate (d), plate B moves off with velocity $= \frac{1}{M}\int \sigma \, dt$, and plate A remains at rest.

3. EXPERIMENTAL DETAILS

(i) *Object*. The experiment was designed to measure the velocity at which a small mild steel pellet was projected from the surface of a metal plate when an explosive charge was detonated in contact with the opposite surface. Various thicknesses of plate and of pellet were used.

(ii) *The explosive charge and plate*. The arrangement used is shown in Fig. 2. The explosive charge was a cylinder of tetryl (1 in. long by 1 in. diameter) and was initiated by a No. 8 Briska electric detonator. The charge was glued to the metal plate and was contained in a wooden holder to locate the detonator.

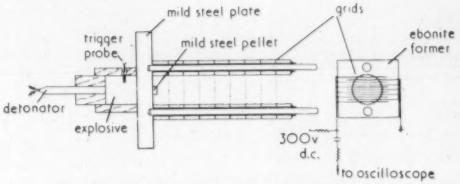

Fig. 2. Experimental arrangement

The target plates were made from mild steel (4 × 4 in. with thicknesses from $\frac{1}{4}$ to 2 in.) with the 4 × 4 in. surfaces smooth ground. The pellets ($\frac{1}{2}$ in. diameter and length $\frac{1}{32}$ to $\frac{1}{2}$ in.) were also made from mild steel and the surface in contact with the target plate was smooth ground to ensure good contact. The pellets were fastened to the plates with Tensol cement to prevent them moving prior to the firing. Some firings were carried out using Styrex rubber adhesive but there was no difference between the results obtained from similar sets using Tensol.

(iii) *Measurement of velocity*. On projection from the plate the pellet passed through eight wire grids mounted on ebonite formers. Each grid consisted of a series of coplanar wires (34 s.w.g.) about $\frac{1}{8}$ in. apart and inter-connected alternately. The grid formed part of the event circuit shown in Fig. 2 and the pellet on striking the grid shorted the two sides and thus discharged the capacitor. This gave a sharp voltage pulse which was fed into a 10 kc/s radial deflexion

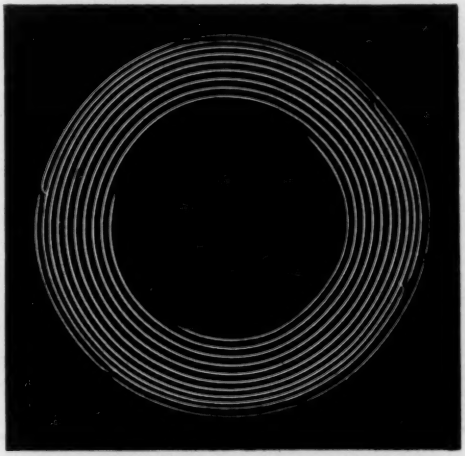

Fig. 3. Typical experimental record

spiral oscilloscope which had a trace length of 1 ms and a resolution of 1 μs. A typical record is shown in Fig. 3. A sequence of positive and negative pulses was used to enable a particular pulse to be associated with a particular grid. This was useful in analysing the records, particularly when an event failed to record. These failures were infrequent and usually associated with a fault in the electronic circuit.

It was necessary to synchronize the triggering of the oscilloscope with the passage of the pellet through the grids. Two insulated wires were twisted together and inserted into the tetryl charge. The detonation wave broke down the insulation between the wires, thus giving a signal which, after a suitable preset delay, was used to trigger the oscilloscope.

4. EXPERIMENTAL RESULTS

(i) *Results.* The results are summarized in Table 1.

Table 1. *Pellet velocities for various plate and pellet thicknesses*

Pellet length (in.)	*Plate thickness (in.)*						
	¼	½	1	1¼		1½	2
3/32		550					
	711	514	281	207	212	149	65
	770	534	280	218	211	149	65
	711	525	293	213	215	150	67
Mean	(731)	(531)	(285)	(213)		(149)	(66)
1/16	771	551	262	174	169	120	71
	758	508	262	176	173	126	62
		531	253	178	173	121	
				169			
Mean	(765)	(530)	(259)	(173)		(122)	(67)
⅛	647	467	224	158	148	83	44
	695	482	241	148	153	71	
			231	158	162	83	
Mean	(671)	(475)	(232)	(155)		(79)	(44)
¼	500	343	183	124	122	46	
	518	346	185	132	120	50	
	525	344	177	124	125	53	
				125			
Mean	(514)	(344)	(182)	(125)		(50)	
½	469	270	126	77	75		
	440	263	137	76	83		
	451	272	136	80	79		
Mean	(453)	(268)	(133)	(78)			

The velocities are given in m/s and the mean velocity of each group is given in brackets. Each column gives the velocities of the pellets of different lengths from a plate of given thickness.

The velocities of the pellets were measured from the distance–time graphs. The mean values of stress were then calculated using equation (2). A value of 7·85 g/cm^3 was taken for the density of the mild steel and a value of D of 5000 ± 100 m/s, obtained from other experiments,[12] was used. Histograms showing the shape of the stress pulse are given in Fig. 4.

(ii) *Experimental errors.* The positions of the grids were known to ±0·003 in. and the time measurements were accurate to 1 μs. Thus the variations found were not due to the method of measuring velocity as could also be seen from the quality of the distance–time plots. The physical dimensions of the pellets were accurate to ±0·001 in. and this could have caused a scatter of ±3% in the 3/32 in. thick pellet and correspondingly less in the longer pellets. The density of the pellets was measured to within ±1%. The additional scatter which appeared in some sets of results must have been due to the variability in the charge or the target plate, both of which had their dimensions fixed to ±0·001 in. The average scatter in the various sets of results is 5%. To check that the grids were not being shorted by a shock wave coming from the surface of the target plate, firings were carried out with no disks on the plates. No events were recorded until long after the disk would have arrived, if present. With the thinner target plates, which were scabbed by the charge, it was evident from the markings on the recovered pellet that the pellet had hit the grid before the scab.

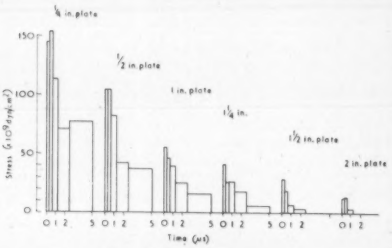

Fig. 4. Stress-time histograms

The shape of the stress pulse is shown for various thicknesses of the steel plate.

5. DISCUSSION

(i) *General.* A feature of the results in Table 1 is their reproducibility. The average scatter about the mean in the various sets of results is 5%.

Stress-time curves calculated from the experimental data are shown in Fig. 4. Following Rinehart, these are plotted in histogram form since this more truly represents the experimental results. Each histogram represents the stress at the free surface as each part of the wave reaches it. This stress distribution in time is almost the same as the spatial distribution of stress in the plate close to the free surface, the difference being due to the fact that the wave is continuously attenuating as illustrated by the series of histograms. The stress pulse attenuates rapidly as it travels through the mild steel, and the peak stress has dropped by an order while the pulse has travelled a distance less than 2 in. However, there does not appear to be much significant change in the shape of the pulse. There is an indication that there is a flat top to the stress pulse initially, but that this disappears after the pulse has travelled through 1 in. of mild steel. This would seem to contradict the results of Rinehart[11] who found that the low intensity part of the wave built up as it passed through the plate. Rinehart obtained these results using thicker (2 to 3 in.) target plates, and it is very difficult to imagine a mechanism which explains this build up of the low intensity part of the pulse.

It should be noted that the last section of the histogram for the ¼ in. target plate is probably too high owing to reverberation (i.e. multiple reflexions of the wave) occurring

in the plate before the pellet ($\frac{1}{2}$ in. in length) separated from the plate. This is the only case where this could happen.

(ii) *Detonation pressure.* The pressure generated in the detonation of tetryl has been calculated from the results. In Fig. 5 the logarithm of the peak stress in each histogram has been plotted against the thickness of the target plate and it is seen that a linear relation fits the experimental results. This relation has the form

$$\left.\begin{aligned} \log P &= -\alpha x + K \\ P &= P_0 \exp(-\alpha x) \end{aligned}\right\} \quad (3)$$

where P_0 is the initial stress at the explosive-metal interface and α is the attenuation coefficient.

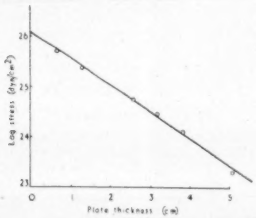

Fig. 5. Peak stress *versus* plate thickness

Stress P_0 is not the detonation pressure P_D but is related to it by the expression

$$\frac{P_0}{P_D} = \frac{\rho_2 D_2}{\rho_1 D_1} \cdot \frac{(\rho_1 D_1 + \rho_3 D_3)}{\rho_2 D_2 \quad \rho_3 D_3} \quad (4)$$

where ρ denotes density and D shock velocity. The subscripts 1, 2 and 3 refer to the undetonated explosive, the metal and the detonation products respectively. Equation (4) allows for the change in amplitude of the pressure pulse due to refraction at the explosive metal interface. It is derived by the application of the conservation laws for mass and momentum to the shock waves approaching and leaving the interface, and the boundary conditions that particle velocity and pressure must be continuous across the interface. If the usual approximation that

$$\rho_1 D_1 = \rho_3 D_3 \quad (5)$$

is made (see Pack[13] for a discussion on the validity of this approximation) equation (4) becomes

$$\frac{P_0}{P_D} = \frac{2\rho_2 D_2}{(\rho_1 D_1 + \rho_2 D_2)} = A \quad (6)$$

Putting $\rho_1 = 1{\cdot}6$ g/cm^3, $D_1 = 7500$ m/s, $\rho_2 = 7{\cdot}85$ g/cm^3 and $D_2 = 5000$ m/s

$$A = 1{\cdot}53$$

From Fig. 5, $P_0 = 2{\cdot}3 \times 10''$ dyn/cm^2 and hence

$$P_D = 1{\cdot}5 \times 10''\ \text{dyn/cm}^2$$

There are no published experimental figures for the detonation pressure in tetryl, but values have been obtained by calculation[14,15] assuming an equation of state and some knowledge of the products of detonation. Their results are summarized in Table 2.

The two figures for the pressure at a density of 1 g/cm^3 agree quite well, but there seems to be a very rapid change of pressure with density in the density range 1·5–1·6 g/cm^3. It would seem that the best value for P_D from their results for a density of 1·6 g/cm^3 is about 190×10^9 dyn/cm^2. This is to be compared with the value of 150×10^9 dyn/cm^2 obtained in these experiments. That this value is low is not unexpected since these experiments were not designed to measure detonation pressure, and the peak pressures used in Fig. 5 are mean values over the first section of the histogram. The charge diameter was small (1 in.), the charge L/D ratio was one, there was little confinement ($\frac{1}{4}$ in. wood) and there was a point source of initiation; all of these factors ensured that the wave entering the plate was not plane over the area of the pellets (0·25 in. diameter). The effect of curvature of the stress pulse as it enters the target plate and subsequently the pellet is to reduce the amount of momentum trapped in the pellet when it separates from the plate. This would then reduce the stress as calculated in paragraph (i) of Section 4 and therefore the detonation pressure calculated from these values would be low. It would be very difficult to calculate the magnitude of this reduction and this has not been attempted. However the value of 150×10^9 dyn/cm^2 sets a lower limit to the detonation pressure while the value of 190×19^9 dyn/cm obtained from Table 2 is probably close to an upper limit.

Table 2. *Detonation pressure-density relation for tetryl*

Source	*Density* (g/cm^3)	*Pressure* ($\times 10^9$ dyn/cm^2)
Cook[14]	1·0	75
	1·6	200
	1·63	210
Taylor[15]	0·5	21·3
	1·0	71
	1·5	148

(iii) *Attenuation.* The slope of the $\log P - x$ graph gives a value for the attenuation coefficient α of the pulse as it passes through mild steel. The value of α is 0·55 and thus under these experimental conditions

$$P = P_0 \exp(-0{\cdot}55\,x) \quad \text{(where } x \text{ is in cm).}$$

The attenuation coefficient as measured here includes the effect of several factors: internal friction, the fact that the wave is expanding and the effect of rarefaction waves spreading in from the boundaries of the charge. By proper design of experiment it should be possible to eliminate the effect of non-planarity of the wave and greatly reduce the effect of rarefaction waves, thus leaving internal friction free for study.

(iv) *Normal fracture stress.* When the compressive wave from the explosive charge is reflected as a tension wave from the free surface the stress may be sufficient to cause the metal to fracture. In most cases a thin crack will be formed in a plane parallel to the free surface (marked with an asterisk in Table 3) while in some cases a small piece of metal (scab) will separate completely from the plate. The stress required to produce the fracture can be found by using the histograms of Fig. 4 and Table 3. This assumes that the fracture occurs when the amplitude of the tension wave exceeds the compressive stress at the fracture plane by an amount exceeding the "fracture stress" of the material.

Table 3

Column 1 (*in.*)	*Column 2* (*in.*)	*Column 3* ($\times 10^9$ dyn/cm^2)	*Column 4* ($\times 10^9$ dyn/cm^2)	*Column 5* ($\times 10^9$ dyn/cm^2)
$\frac{1}{2}$	0·08	104	49	55
1	0·15	56	20	36
$1\frac{1}{2}$	0·14	42	11	31
$1\frac{1}{2}$	0·10	29	2	27

Column 1 gives the plate thickness and column 2 the distance of the fracture from the free surface (mean of four readings). The data for columns 1 and 2 came from firings using plates with no pellets. In column 3 the maximum value of the stress in the wave as obtained from Fig. 4 is given. The time for the wave to travel twice the distance in column 2 was calculated, and the stress corresponding to this time interval after the peak of the pulse found from Fig. 4. This stress is given in column 4. The fracture stress, column 5, is then the difference between columns 3 and 4.

A plot of the fracture stress against the compressive stress immediately before fracture occurs is given in Fig. 6. This shows an approximately linear relation between fracture stress and compressive stress, and that the fracture stress with zero compressive stress is $2{\cdot}5 \times 10^{10}$ dyn/cm^2. The ultimate tensile strength of the mild steel plates used in this experiment

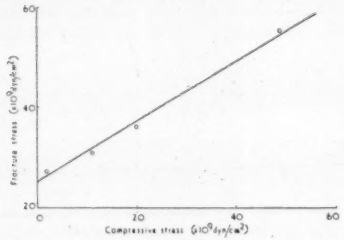

Fig. 6. Fracture stress *versus* compressive stress

was $26{\cdot}5$ t/in.$^2 = 4{\cdot}08 \times 10^9$ dyn/cm^2, i.e. the stress to produce fracture is increased by a factor of $6{\cdot}1$ in the dynamic case.

Rinehart[11] found that the fracture stresses were 16×10^9 and 9×10^9 dyn/cm^2, when the compressive stresses were $6{\cdot}2 \times 10^9$ and $3{\cdot}1 \times 10^9$ dyn/cm^2 respectively. These values were for a 1020 steel which is similar to the mild steel used in these experiments. The values he obtained for the fracture stress are much less than the values found in this experiment; the difference would seem to be more than could be explained by the slight difference in the steel plates studied. Bridgman[16] has also found that the stress required to produce cleavage fracture increases with the application of hydrostatic pressure. The physical significance of the variation of fracture stress with transient compressive stress is not understood and will not be discussed further.

(v) *Shape of stress pulse.* The shape of the stress-time pulse in the metal can be calculated from the pressure time pulse in the explosive, since it is this pulse which is refracted into the metal. The relation between the pressure distribution at the interface and the pressure distribution in the detonation wave in the explosive some distance from the interface is not known, unless the approximation made in equation (5) is used. This implies the two pressure distributions are the same. Costello[17] makes this assumption and uses a relation which was derived from the polytropic gas laws for one-dimensional gas flow.

$$p/P = \left[\left(\frac{2x}{Dt} + 1\right)^3 - 1\right]\Big/26 \qquad (7)$$

where x is the distance from the surface of the explosive where detonation occurred at time $t = 0$; D is the detonation velocity, P the detonation pressure and p the pressure behind the detonation front.

In Fig. 7 this expression has been plotted for the present experiment and the histogram of the stress pulse obtained from the $\frac{1}{4}$ in. thick target plate is also known. A value of P of 175×10^9 dyn/cm^2 was used in Fig. 7; this value was chosen to give the closest fit between the relation and the

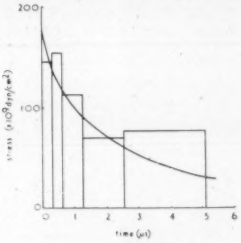

Fig. 7. Pulse shape

The theoretical relation, equation (7), has been fitted to the experimental stress histogram for the $\frac{1}{4}$ in. thick steel plate.

histogram. The agreement is as good as can be expected, considering the assumptions made in the derivation of equation (7). It does not reproduce the flattening of the top of the stress pulse apparent in the experimental results, but this is not surprising since the presence of the explosive metal interface will modify the pressure distribution in the detonation wave. The discrepancy with the last section of the histogram is not important since, as mentioned in paragraph (i) of Section 5, the histogram is probably too high owing to reverberation occurring. This is a more direct experimental check of equation (7) than that carried out by Costello and it shows that it is a useful representation of the stress pulse.

6. CONCLUSIONS

(1) The pellet technique described in this paper is a valuable and reliable method for the study of stress pulses in solids.

(2) The shape of the stress pulse changes little as the pulse passes through mild steel. This is in disagreement with Rinehart's results, where he finds that the low intensity part of the pulse builds up as it progresses through mild steel.

(3) The detonation pressure of tetryl has been estimated from the results and a value of $1{\cdot}5 \times 10^{11}$ dyn/cm^2 obtained. This value is almost certainly too low.

(4) The tensile stress required to produce a fracture in mild steel has been found as a function of the compressive stress during fracture.

(5) A comparison has been made between the experimental results and a theoretical expression for the shape of the stress pulse. This shows that the theoretical expression is in fairly good agreement with the results, though it does not show the presence of a flat top to the pulse.

ACKNOWLEDGEMENTS

The authors would like to thank Miss D. M. Sells who carried out the experimental work. Acknowledgement is made to the Controller of H.M. Stationery Office for permission to publish this paper.

REFERENCES

(1) COSTELLO, E. DE L. *Conference on the properties of materials at high rates of strain*, Institution of Mechanical Engineers (May 1957).

(2) BUCHANAN, J. S., JAMES, H. J. and TEAGUE, G. W. *Phil. Mag.*, **3**, p. 1432 (1958).
(3) WALSH, J. M., RICE, M. H., MCQUEEN, R. G. and YARGER, F. L. *Phys. Rev.*, **108**, p. 196 (1957).
(4) WALSH, J. M., and RICE, M. H. *J. Chem. Phys.*, **26**, p. 815 (1957).
(5) AL'TSHULER, L. V., KRUPNIKOV, K. K. and BRAZHNIK, M. I. *J. Expt. Theor. Phys. (U.S.S.R.)*, **34**, p. 886 (1958).
(6) GORANSON, R. W., BANCROFT, D., BURTON, B. L., BLETCHER, T., HOUSTON, E. E., GITTINGS, E. F. and LANDEON, S. A. *J. Appl. Phys.*, **26**, p. 1472 (1955).
(7) WALSH, J. M., and CHRISTIAN, R. H. *Phys. Rev.*, **97**, p. 1544 (1955).
(8) HOPKINSON, B. *Phil. Trans Roy. Soc.*, **213**, p. 437 (1914).
(9) LANDON, J. W., and QUINNEY, H. *Proc. Roy. Soc. A*, **103**, p. 622 (1923).
(10) DAVIES, R. M. *Phil. Trans Roy. Soc. A*, **240**, p. 375 (1948).
(11) RINEHART, J. S. *J. Appl. Phys.*, **22**, p. 555 (1951).
(12) BRYANT, R., and BUCHANAN, J. S. Unpublished results (1957).
(13) PACK, D. C. *Phil. Mag.*, **2**, p. 182 (1957).
(14) COOK, M. A. *J. Chem. Phys.*, **16**, p. 1081 (1948).
(15) TAYLOR, J. *Detonation in Condensed Explosives*, p. 118 (Oxford: Clarendon Press, 1952).
(16) BRIDGMAN, P. W. *Fracture and Hydrostatic Pressure*, p. 246 (American Society for Metals, 1948).
(17) COSTELLO, E. DE L. Unpublished Ministry of Supply Report (1956).

Absorption of sodium and argon by glass

By J. W. WHEELDON, B.A., B.T.H. Group Research Laboratory, The British Thomson-Houston Co. Ltd., Rugby

[*Paper received 6 February*, 1959]

Methods are described for measuring the absorption of both sodium and argon by glasses. The rate of absorption of sodium increases rapidly with temperature and is linear with time at a constant temperature. Ionization of the sodium does not change the rate of absorption. Micro-sections show that the absorbed sodium forms a layer of apparently uniform sodium concentration which advances through the glass with a sharp front. The concentration of sodium in this layer was found to be as high as 2×10^{22} atoms cm^{-3} in one case. Argon is only absorbed when ionized and the rate of absorption is more or less independent of temperature below 300° C. The argon does not diffuse through the glass and is partially evolved when heated to over 350° C.

It is well known that most glasses are attacked by sodium at temperatures above 200° C,[1] and special glasses have been developed to resist this. Nevertheless, even these are found to absorb considerable quantities of sodium in time at higher temperatures, with discoloration, stress formation and other undesirable effects. Observations with some of the more recently developed glasses were not always in accord with the earlier work and a further investigation was therefore undertaken.

An allied phenomenon is the absorption of argon by glass when ionized. This is important because a small quantity (of the order of 1%) of argon is frequently introduced into discharge tubes in order to utilize the advantageous electrical characteristics caused by the Penning effect.[2] If this argon is absorbed, the characteristics of the discharge are substantially altered.

It is found that the absorption of sodium and argon show a certain amount of parallelism, although the circumstances necessary to cause absorption in each case are quite different.

METHOD OF MEASURING THE ABSORPTION OF SODIUM

Small samples of the glass being studied were sealed in evacuated tubes of highly resistant glass, together with metallic sodium, and heated for various periods at known temperatures. The amount of sodium absorbed was determined by the increase in weight of the samples.

The tubes and samples were baked during exhaust at 450° C for 30 min and cooled to 100° C before running in the sodium. This was done by heating a short glass tube containing the distilled metal which was previously introduced into the manifold in such a position that the sodium ran into the test tube when molten. Sufficient sodium was always introduced to ensure equilibrium vapour pressure throughout the test. A hard vacuum was then obtained before sealing off. Before opening the tube at the end of the experiment the metallic sodium remaining was distilled away from the specimens. These were then removed and weighed immediately in a dry atmosphere.

SODIUM ABSORPTION MEASUREMENTS

Table 1 shows the rate of absorption of sodium by a number of glasses at various temperatures. All the glasses tested (see Table 2) absorbed sodium at sufficiently high

Table 1. *Sodium absorption against temperature*

Sodium absorption in mg 1000 h^{-1} cm^{-2}

Glass No.	*Temperature °C*		
	265	350	450
1	0·07	2·0	Rapid chemical attack
2	0·01	0·1	1·5
3	—	4·0	—

Table 2. *Glasses used in these investigations*

Glass No.	*Type of glass*
1	Sodium resistant
2	Sodium resistant
3	Kovar-sealing borosilicate glass
4	Tunsten-sealing borosilicate glass
5	Soda lime silicate glass

temperatures, and the rate of absorption increased rapidly with temperature in all cases. With some of the glasses at high temperatures the absorption becomes very rapid and clearly takes the form of chemical reaction with the sodium, forming black crystalline material.

Fig. 1 shows that the absorption rate is substantially constant with time for glass No. 1, and this was found to be the case also with the other glasses tested. The amount of scatter in the experimental points is typical of that found

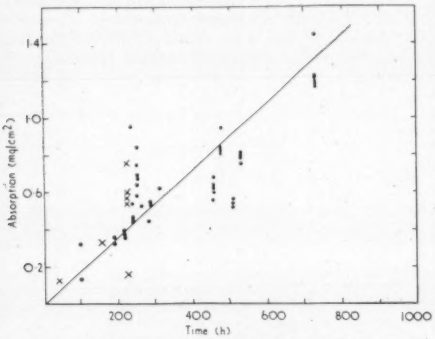

Fig. 1. Absorption of sodium by glass No. 1 at 350° C

• = absorption in presence of sodium vapour only
× = absorption in presence of a discharge

throughout this work, and is partly caused by the highly unstable nature of the loaded glass surfaces which rapidly deteriorate when exposed to the atmosphere.

With all the glasses tested, absorption of sodium was accompanied by coloration. The rate at which coloration occurs as a function of the amount of sodium absorbed varies markedly from glass to glass, but no case was found of absorption without detectable coloration. Optical transmission curves were obtained in an effort to locate the origin of this coloration, but these simply showed an increase in the ultra-violet absorption, with a movement of the cut-off towards larger wavelengths as shown in Fig. 2.

Some of the tubes were filled with inert gases (argon–neon mixtures) at 10 mm pressure and electrodes were also inserted in some and a discharge passed (at 0·53 A cm^{-2})

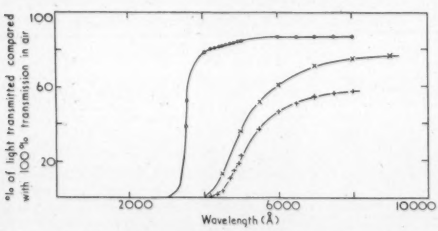

Fig. 2. Spectral transmission curves for sodium loaded polished disks of glass No. 1

○ = disk with no sodium absorbed
× = disk loaded with 0·48 mg/cm^2 sodium
+ = disk loaded with 0·96 mg/cm^2 sodium

during the absorption period. In no case was any significant difference in the absorption rate observed, compared with that for neutral sodium in vacuum. Some of these observations are shown in Fig. 1.

EVOLUTION OF SODIUM FROM LOADED GLASS

The following experiments were carried out to see whether sodium is evolved on heating glass which has previously absorbed sodium. Evacuated tubes of the glass under test, containing a small quantity of sodium, were placed in a furnace at 350° C until the glass had become discoloured by the absorption of the sodium (25 h for glass Nos. 3 and 4 and 100 h for glass No. 1). Each tube was then partially withdrawn from the furnace so that one-half was at room temperature. The free sodium quickly distilled into this half and its vapour pressure was thus reduced to that at room temperature. On continuing to heat the other half of the tube the coloration decreased, except with one glass (No. 1), but in no case did the colour disappear altogether, even after very prolonged heating (500 h). In fact, in the case of glass No. 1 the coloration increased. Thus the absorption is not completely reversible and cannot be one of simple diffusion as suggested by Fonda and Young,[1] who performed a similar experiment.

LOCATION OF ABSORBED SODIUM

To investigate further the nature of the absorption process, micro-sections were made of samples of glass No. 1 which had absorbed sodium. These show that the discoloration advances through the glass with a sharp front, as can be seen in Fig. 3. Behind the front the glass appears to have

Fig. 3. Photograph of microsection of glass No. 1

The glass is to be seen in the bottom half of the photograph. The dark band in the middle is the layer in which the sodium is absorbed. On the right-hand side the layer has flaked away, taking some of the glass with it.

absorbed sodium uniformly, but beyond it there does not appear to be any absorbed sodium. The depth of penetration increases with time of heating in sodium vapour. The process is therefore not one of simple diffusion with a fixed constant. The layer of absorbed sodium is very narrow, being of the order of 5×10^{-4} cm after 224 h at 350° C. The layer is highly stressed, and when it becomes thicker it flakes off from the glass surface as may be seen at the right of Fig. 4.

Assuming that the absorbed sodium is uniformly distributed throughout the coloured surface layer and that none has penetrated beyond the front, the concentration of sodium in this layer can be calculated. This gives the very high concentration of $2{\cdot}1 \times 10^{22}$ atoms cm^{-3}, i.e. one sodium atom every 3·7 Å for a cubic lattice. This figure may be compared with the figures 0·95 and 1·92 Å, for the mean ionic and metallic radii of sodium respectively.[3]

METHOD OF MEASURING THE ABSORPTION OF ARGON

On passing a discharge through a mixture of neon with a small admixture of argon, the latter is often observed to disappear in the course of time. Discharges in these mixtures are of technical importance because of their favourable electrical characteristics which arise from the Penning effect. Disappearance of the argon results in changes in the electrical characteristics which can be disastrous to applications (for example, the striking voltage may increase very substantially).

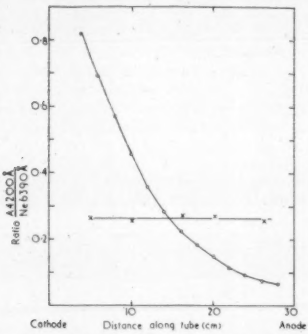

Fig. 4. Ratio of argon to neon intensities along a.c. and d.c. discharge tubes

○ = d.c. × = a.c.

One method of measuring a small concentration of one gas in another is to observe the cataphoretic migration of the minor constituent to one of the electrodes (usually the cathode) in a direct current discharge.[4] Subjective estimates of the amount of the minor constituent present can be obtained from the distance from the electrode over which its characteristic colour is visible, and are often used as measures of the amount present. Attempts to make this method objective, by using a photomultiplier as detector and interference filters to select spectral lines of each constituent (as described below), showed that, with concentrations of the order of 0·1 to 1% of argon in neon, there is no point at which the argon concentration can be sensibly said to become negligible (see Fig. 4). This method is only satisfactory at much lower concentrations.

It was decided, therefore, to use the ratio of the intensities of a group of argon lines (3850 to 4530 Å) to those of a group of neon lines (5850 to 7200 Å) at the centre of an a.c. discharge tube, under controlled conditions as a measure of the amount of argon present. Interference filters (type B20 peaking at 4200 and 6390 Å, by Geraetebau–Anstalt Balzers) have been found satisfactory for isolating these groups of lines.

The apparatus is shown diagrammatically in Fig. 5. It was designed to take 30 cm long discharge tubes of 1·2 cm internal diameter, containing 10 mm of mercury total gas pressure and run at 0·6 A. The tube is normally centred opposite the collimator as shown, but it is mounted on a slide which is useful in making the cataphoretic studies mentioned above and also for finding a suitable transparent portion of the tube in later experiments, in which metallic sodium was present.

The collimator consists of two slits, 1·2 × 0·1 cm mounted 12 cm apart, arranged so that the whole cross-section of the discharge tube is contained within the entrance pupil. This is important since radial electrophoresis occurs in the discharge and the concentration of argon is much higher in the outer region. The photomultiplier used is a type 5060 (by

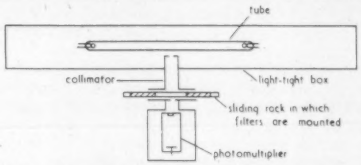

Fig. 5. Apparatus for measuring argon to neon ratio (Not to scale.)

E.M.I. Ltd.) which has a long wave cut-off at 6500 Å. The photocathode of this tube is small and does not occupy the whole of the collimator exit pupil.

In making a measurement the current is adjusted to give the same current density as if the diameter were exactly 1·2 cm and the current 0·6 A a.c. This was found necessary to obtain consistent results. After about 15 min the equilibrium temperature is reached, and it is then found that the ratio of the intensities of the two groups of lines is constant along the whole length of the tube except within 2 cm of the electrodes (Fig. 4). Freshly made discharge tubes behave erratically at first and they are therefore run for one hour to "age" them before making the first measurement.

ARGON ABSORPTION MEASUREMENTS

Argon absorption was only found to occur when a discharge was being passed, whatever glass the tube was made of. Below 300° C, the rate of argon absorption was more or less independent of temperature. No absorption was ever observed when a tube was left standing or heated at temperatures up to 250° C. On the other hand, if a tube which had already absorbed argon whilst running was then heated (without a discharge) to 350° C for a number of hours, then a substantial part of the absorbed argon was evolved into the tube. This argon was re-absorbed on continuing the discharge.

No evidence has been obtained to support the possibility

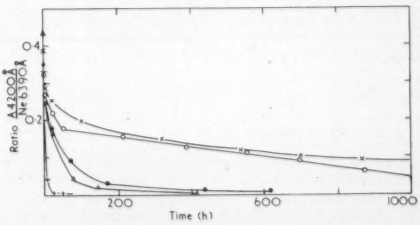

Fig. 6. Position of argon absorption in tube

× = tube wholly of glass No. 1 which only absorbs argon slowly
+ = tube wholly of glass No. 3 which absorbs argon quickly
○ = tube with ends of glass No. 3, remainder glass No. 1
• = tube of glass No. 1 containing specimen of glass No. 3
△ = tube of glass No. 1 with central section of glass No. 3

that argon diffuses right through the glass. Some tubes were surrounded by an evacuated jacket and run until no argon was present in the tube. No argon was found to have diffused into the jacket, which contained a Pirani gauge. Further, if solid specimens of a rapidly absorbing glass are introduced into a slowly absorbing tube, these absorb the argon as rapidly as if they formed an equivalent area of the tube wall (Fig. 6).

Fig. 7 shows the way in which argon is absorbed by tubes made from different glasses. A notable feature is the very rapid absorption of argon by the three glasses Nos. 3, 4 and 5 which are not sodium resistant, while in comparison the sodium resistant glasses, Nos. 1 and 2, only absorb argon slowly, the more sodium resistant, the more slowly. With the more resistant glasses the rate of absorption is quite sensitive to the surface condition. This has not been fully investigated. All the measurements quoted were made with fresh glass which was, as far as possible, untreated after manufacture.

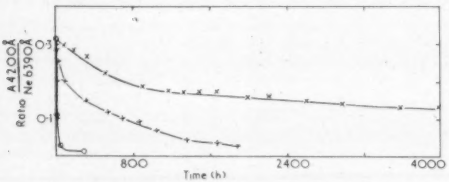

Fig. 7. Argon absorption by various glasses

+ = glass No. 1
× = glass No. 2
○ = glasses Nos. 3, 4 and 5

In Fig. 6 the curves for the sodium resistant glass No. 1, which cleans up argon slowly, and glass No. 3, which cleans up argon quickly, are reproduced from Fig. 7. In addition, a number of curves are shown which were obtained from composite tubes of these two glasses. The surface area of glass No. 3 in all these composite tubes was approximately the same, about 20% of the total tube area. These curves show that most of the absorption occurs at the glass adjacent to the main length of the discharge and not at the glass around the electrodes and leads.

CONCLUSIONS

Sodium is absorbed by all the glasses examined, at a sufficiently high temperature and is always accompanied by discoloration. The rate of absorption is constant with time and increases rapidly with temperature. Ionization of the sodium has no observable effect on the rate of absorption.

The absorption is not a straightforward diffusion process and can take the form of a thin surface layer of almost constant composition which increases in thickness with time. The concentration of sodium in this layer can be extremely high, estimated in one case at $2{\cdot}1 \times 10^{22}$ atoms cm^{-3}.

Argon is absorbed only when ionized in a discharge, and the rate of absorption is more or less independent of temperature below 300° C. At higher temperatures a partial evolution occurs. The absorbed argon is located in the surface layers of the glass and does not diffuse through in the case of a tube. In a linear discharge tube, most of the absorption occurs in the positive column region and very little near the electrodes.

In all the cases examined absorption of argon and sodium occur together, i.e. glasses absorbing sodium readily absorb argon readily, and *vice versa*.

It might be added that the rate of absorption of argon is found to be quite sensitive to the conditions of the glass surface, but this has not been fully investigated yet.

ACKNOWLEDGEMENTS

The author wishes to thank his colleagues at the Research Laboratories of the British Thomson-Houston Co. Ltd. for many helpful discussions.

REFERENCES

(1) FONDA, G. R., and YOUNG, A. H. *Gen. Elect. Rev.*, **37**, pp. 331–337 (1934).
(2) DRUYVESTEYN, M. J., and PENNING, F. M. *Rev. Mod. Phys.*, **12**, p. 87 (1940).
(3) WELLS, A. F. *Structural Inorganic Chemistry*, 2nd ed., pp. 70, 682 (Oxford: Clarendon Press, 1950).
(4) RIESZ, R., and DIEKE, G. H. *J. Appl. Phys.*, **25**, pp. 196–201 (1954).

Correspondence

Cadmium sulphide photoconductive layers

In view of the scant publicity given to the actual preparation of photoconductive layers of cadmium sulphide, the following notes on the writer's experience in this field may be of interest to readers. Since much of the work will not see further development, it is offered in its present incomplete form with qualification where necessary. The notes are not meant to be a record of completed work.

Preparation by evaporation. Layers exhibiting properties similar to those of single crystals can be prepared by evaporation of crystalline cadmium sulphide on to heated substrates.(1)

Substrates of soda glass, Pyrex glass, quartz, thin mica and rock salt have been successful. Electrodes of colloidal graphite in water (Aquadag) were painted on to these substrates and the layers evaporated over them. The electrodes were usually 1 cm wide and 1 mm apart. This layer area illuminated by 1 f.c. receives approximately 10^{-4} lm.

The starting material can be made by resubliming phosphor grade cadmium sulphide powder at 850° C in a silica tube in a vacuum. A temperature gradient of about 100° C was used in a vacuum of about 10^{-2} mm of mercury. This process removes volatile impurities and crystallizes the material. A paper dealing with layers evaporated from this material is to be presented shortly, in which it will be shown that the substrate temperature must be 500° C if the fastest speed of response(2) (about 200 μs at 1740 f.c. illumination) is to be realized. For substrate temperatures higher or lower than this, layers of longer time constant are formed. The evaporator was a quartz thimble at a temperature such that layers up to 7000 Å thick were produced in about 30 min on a substrate 10 cm distant. The pressure was better than 10^{-5} mm of mercury, though pressures as high as 10^{-3} mm were found to have no observable effect on the layer properties.

Activation can be carried out either by treatment of the initial material for evaporation, or by after-treatment. Fig. 1 shows the spectral response of three cells. Curve *A* is for a

layer evaporated on to glass at 170° C with no activation attempted. The cut-off wavelength is situated near the absorption edge for pure cadmium sulphide. Curve *B* is that of a layer, evaporated on to glass at room temperature, from a charge of cadmium sulphide which had been activated by the addition of a few parts per thousand of copper chloride

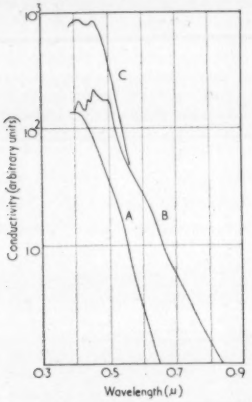

Fig. 1. Spectral response of evaporated layers

A, unactivated, 170° C substrate; *B*, initial charge copper activated, room temperature substrate; *C*, initial charge copper activated, 400° C substrate

and heated in a vacuum to 850° C before evaporation. This layer was also heated in hydrogen sulphide at 300° C to improve the dark resistance. Curve *C* is that of the copper chloride activated material evaporated on to glass at 400° C without further treatment. In both curves *B* and *C*, which become coincident, the effectiveness of the activation can be clearly seen in the long wavelength response. Layers evaporated on to room temperature substrates have low, dark resistance owing to the presence of excess cadmium donors. The dark resistance can be improved in these cases by heating them in hydrogen sulphide at 300° C. If such a treated layer is then heated in a vacuum to 300° C, the original low, dark resistance reappears. Alternate surroundings of hydrogen sulphide and vacuum have the effect of raising and lowering the dark resistance.

It has often been found that the sensitivity of the unactivated layers evaporated on to glass at 500° C can be improved many-fold by baking the layer in atmospheric air for about 15 min at 500° C. There is a slight deterioration of the fast time constant, but this is more than outweighed by the sensitivity improvement. The reason for this improvement has not been investigated. Layers thicker than a micron are tedious to make at high substrate temperatures, as only a small fraction of the material striking the substrate sticks there. At lower substrate temperatures the layers deteriorate by cracking over a period of a few days, even when thermal expansion coefficients of film and substrate are matched, so that often an advantage gained by using a low temperature activated layer is lost by layer deterioration. The reason for the deterioration is not known. Using an unfiltered tungsten light source the sensitivity of the best evaporated layers made in this way is about 10^{-4} A/lm applied. If one takes into account that only about 1/10 000 of the available visible light from a tungsten source is actually absorbed by a layer of, say, 5000 Å thickness, this sensitivity is of the order of 1 A/lm absorbed at 1 f.c.

Preparation by sputtering. Large areas of uniform thin photoconductive layers of cadmium sulphide can be made from the sputtered oxide. The oxide, in the form of a transparent conducting layer, is made by sputtering cadmium on to glass in air.[3] If such a layer is baked at 500° C in hydrogen sulphide, allowed to cool in the gas, and then baked for 15 min in air, a layer results which has similar characteristics to the high temperature substrate evaporated layers. Such layers are hard, clear and honey coloured. One such layer was 2850 Å thick and had a dark resistivity of at least $3 \times 10^8\ \Omega$ cm. At 1740 f.c. illumination the resistivity was $3 \times 10^6\ \Omega$ cm and the time constant 250 μs. This time constant was maintained for levels of illumination as low as 174 f.c., below which intensity the measuring technique was insufficient to be of any use. Resistivity was not measured at this level of illumination.

The spectral response of a sputtered layer is shown in Fig. 2, curve *A*. The cut-off wavelength is typical of pure

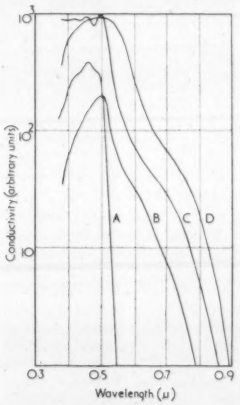

Fig. 2. Spectral response of layers made from cadmium salts

A, sputtered oxide; *B*, bromide; *C*, chloride; *D*, hydroxide

cadmium sulphide, even though the cadmium sputtering electrode was commercial grade. Some failures have been experienced with this method when attempts have been made to use layers of the order of a micron thick. It is believed that this is due to incomplete reaction with the hydrogen sulphide, though no investigation has been made of this point.

Preparation from cadmium salts. Photoconductive layers of cadmium sulphide can be prepared from ordinary laboratory reagent cadmium salts by heating them in a stream of hydrogen sulphide in a silica vessel.

Typical of such a process is that using cadmium chloride. The anhydrous salt melts at about 560° C. If such a molten layer is allowed to spread over glass, and the temperature is then lowered to 500° C, the chloride solidifies into a smooth layer. This layer is maintained at 500° C, while hydrogen sulphide is allowed to enter the system, producing a layer of cadmium sulphide. This layer is allowed to cool in the

that argon diffuses right through the glass. Some tubes were surrounded by an evacuated jacket and run until no argon was present in the tube. No argon was found to have diffused into the jacket, which contained a Pirani gauge. Further, if solid specimens of a rapidly absorbing glass are introduced into a slowly absorbing tube, these absorb the argon as rapidly as if they formed an equivalent area of the tube wall (Fig. 6).

Fig. 7 shows the way in which argon is absorbed by tubes made from different glasses. A notable feature is the very rapid absorption of argon by the three glasses Nos. 3, 4 and 5 which are not sodium resistant, while in comparison the sodium resistant glasses, Nos. 1 and 2, only absorb argon slowly, the more sodium resistant, the more slowly. With the more resistant glasses the rate of absorption is quite sensitive to the surface condition. This has not been fully investigated. All the measurements quoted were made with fresh glass which was, as far as possible, untreated after manufacture.

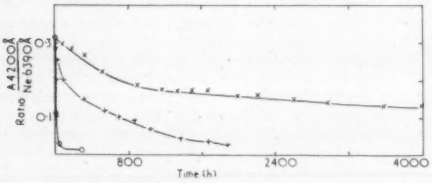

Fig. 7. Argon absorption by various glasses
+ = glass No. 1
× = glass No. 2
○ = glasses Nos. 3, 4 and 5

In Fig. 6 the curves for the sodium resistant glass No. 1, which cleans up argon slowly, and glass No. 3, which cleans up argon quickly, are reproduced from Fig. 7. In addition, a number of curves are shown which were obtained from composite tubes of these two glasses. The surface area of glass No. 3 in all these composite tubes was approximately the same, about 20% of the total tube area. These curves show that most of the absorption occurs at the glass adjacent to the main length of the discharge and not at the glass around the electrodes and leads.

CONCLUSIONS

Sodium is absorbed by all the glasses examined at a sufficiently high temperature and is always accompanied by discoloration. The rate of absorption is constant with time and increases rapidly with temperature. Ionization of the sodium has no observable effect on the rate of absorption.

The absorption is not a straightforward diffusion process and can take the form of a thin surface layer of almost constant composition which increases in thickness with time. The concentration of sodium in this layer can be extremely high, estimated in one case at $2{\cdot}1 \times 10^{22}$ atoms cm^{-3}.

Argon is absorbed only when ionized in a discharge, and the rate of absorption is more or less independent of temperature below 300° C. At higher temperatures a partial evolution occurs. The absorbed argon is located in the surface layers of the glass and does not diffuse through in the case of a tube. In a linear discharge tube, most of the absorption occurs in the positive column region and very little near the electrodes.

In all the cases examined absorption of argon and sodium occur together, i.e. glasses absorbing sodium readily absorb argon readily, and *vice versa*.

It might be added that the rate of absorption of argon is found to be quite sensitive to the conditions of the glass surface, but this has not been fully investigated yet.

ACKNOWLEDGEMENTS

The author wishes to thank his colleagues at the Research Laboratories of the British Thomson-Houston Co. Ltd. for many helpful discussions.

REFERENCES

(1) FONDA, G. R., and YOUNG, A. H. *Gen. Elect. Rev.*, **37**, pp. 331–337 (1934).
(2) DRUYVESTEYN, M. J., and PENNING, F. M. *Rev. Mod. Phys.*, **12**, p. 87 (1940).
(3) WELLS, A. F. *Structural Inorganic Chemistry*, 2nd ed., pp. 70, 682 (Oxford: Clarendon Press, 1950).
(4) RIESZ, R., and DIEKE, G. H. *J. Appl. Phys.*, **25**, pp. 196–201 (1954).

Correspondence

Cadmium sulphide photoconductive layers

In view of the scant publicity given to the actual preparation of photoconductive layers of cadmium sulphide, the following notes on the writer's experience in this field may be of interest to readers. Since much of the work will not see further development, it is offered in its present incomplete form with qualification where necessary. The notes are not meant to be a record of completed work.

Preparation by evaporation. Layers exhibiting properties similar to those of single crystals can be prepared by evaporation of crystalline cadmium sulphide on to heated substrates.(1)

Substrates of soda glass, Pyrex glass, quartz, thin mica and rock salt have been successful. Electrodes of colloidal graphite in water (Aquadag) were painted on to these substrates and the layers evaporated over them. The electrodes were usually 1 cm wide and 1 mm apart. This layer area illuminated by 1 f.c. receives approximately 10^{-4} lm.

The starting material can be made by resubliming phosphor grade cadmium sulphide powder at 850° C in a silica tube in a vacuum. A temperature gradient of about 100° C was used in a vacuum of about 10^{-2} mm of mercury. This process removes volatile impurities and crystallizes the material. A paper dealing with layers evaporated from this material is to be presented shortly, in which it will be shown that the substrate temperature must be 500° C if the fastest speed of response(2) (about 200 μs at 1740 f.c. illumination) is to be realized. For substrate temperatures higher or lower than this, layers of longer time constant are formed. The evaporator was a quartz thimble at a temperature such that layers up to 7000 Å thick were produced in about 30 min on a substrate 10 cm distant. The pressure was better than 10^{-5} mm of mercury, though pressures as high as 10^{-3} mm were found to have no observable effect on the layer properties.

Activation can be carried out either by treatment of the initial material for evaporation, or by after-treatment. Fig. 1 shows the spectral response of three cells. Curve *A* is for a

layer evaporated on to glass at 170° C with no activation attempted. The cut-off wavelength is situated near the absorption edge for pure cadmium sulphide. Curve *B* is that of a layer, evaporated on to glass at room temperature, from a charge of cadmium sulphide which had been activated by the addition of a few parts per thousand of copper chloride

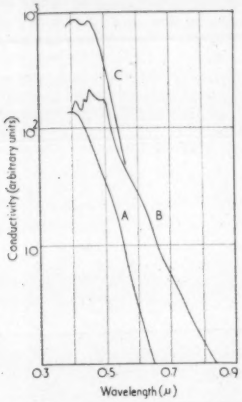

Fig. 1. Spectral response of evaporated layers

A, unactivated, 170° C substrate; *B*, initial charge copper activated, room temperature substrate; *C*, initial charge copper activated, 400° C substrate

and heated in a vacuum to 850° C before evaporation. This layer was also heated in hydrogen sulphide at 300° C to improve the dark resistance. Curve *C* is that of the copper chloride activated material evaporated on to glass at 400° C without further treatment. In both curves *B* and *C*, which become coincident, the effectiveness of the activation can be clearly seen in the long wavelength response. Layers evaporated on to room temperature substrates have low, dark resistance owing to the presence of excess cadmium donors. The dark resistance can be improved in these cases by heating them in hydrogen sulphide at 300° C. If such a treated layer is then heated in a vacuum to 300° C, the original low, dark resistance reappears. Alternate surroundings of hydrogen sulphide and vacuum have the effect of raising and lowering the dark resistance.

It has often been found that the sensitivity of the unactivated layers evaporated on to glass at 500° C can be improved many-fold by baking the layer in atmospheric air for about 15 min at 500° C. There is a slight deterioration of the fast time constant, but this is more than outweighed by the sensitivity improvement. The reason for this improvement has not been investigated. Layers thicker than a micron are tedious to make at high substrate temperatures, as only a small fraction of the material striking the substrate sticks there. At lower substrate temperatures the layers deteriorate by cracking over a period of a few days, even when thermal expansion coefficients of film and substrate are matched, so that often an advantage gained by using a low temperature activated layer is lost by layer deterioration. The reason for the deterioration is not known. Using an unfiltered tungsten light source the sensitivity of the best evaporated layers made in this way is about 10^{-4} A/lm applied. If one takes into account that only about 1/10 000 of the available visible light from a tungsten source is actually absorbed by a layer of, say, 5000 Å thickness, this sensitivity is of the order of 1 A/lm absorbed at 1 f.c.

Preparation by sputtering. Large areas of uniform thin photoconductive layers of cadmium sulphide can be made from the sputtered oxide. The oxide, in the form of a transparent conducting layer, is made by sputtering cadmium on to glass in air.[3] If such a layer is baked at 500° C in hydrogen sulphide, allowed to cool in the gas, and then baked for 15 min in air, a layer results which has similar characteristics to the high temperature substrate evaporated layers. Such layers are hard, clear and honey coloured. One such layer was 2850 Å thick and had a dark resistivity of at least 3×10^8 Ω cm. At 1740 f.c. illumination the resistivity was 3×10^6 Ω cm and the time constant 250 μs. This time constant was maintained for levels of illumination as low as 174 f.c., below which intensity the measuring technique was insufficient to be of any use. Resistivity was not measured at this level of illumination.

The spectral response of a sputtered layer is shown in Fig. 2, curve *A*. The cut-off wavelength is typical of pure

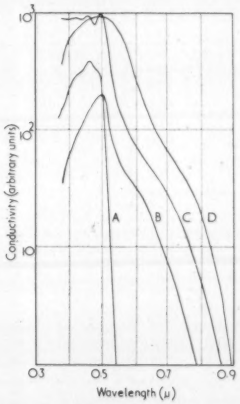

Fig. 2. Spectral response of layers made from cadmium salts

A, sputtered oxide; *B*, bromide; *C*, chloride; *D*, hydroxide

cadmium sulphide, even though the cadmium sputtering electrode was commercial grade. Some failures have been experienced with this method when attempts have been made to use layers of the order of a micron thick. It is believed that this is due to incomplete reaction with the hydrogen sulphide, though no investigation has been made of this point.

Preparation from cadmium salts. Photoconductive layers of cadmium sulphide can be prepared from ordinary laboratory reagent cadmium salts by heating them in a stream of hydrogen sulphide in a silica vessel.

Typical of such a process is that using cadmium chloride. The anhydrous salt melts at about 560° C. If such a molten layer is allowed to spread over glass, and the temperature is then lowered to 500° C, the chloride solidifies into a smooth layer. This layer is maintained at 500° C, while hydrogen sulphide is allowed to enter the system, producing a layer of cadmium sulphide. This layer is allowed to cool in the

hydrogen sulphide and is immediately photosensitive with a time constant of about 1 ms.

Alternatively, a solution of the chloride can be sprayed on to a hot sheet of glass with an atomizer. In this way a layer is built up of anhydrous chloride which is as uniform as is possible with a spraying process. This layer is then heated to 500° C, exposed to hydrogen sulphide and cooled as usual. A further alternative is to raise the temperature momentarily above the melting point of the chloride to smooth the layer. It is then reacted at 500° C as usual.

Other soluble salts, such as the hydroxide in ammonia and ammonium acetate, the sulphate, the bromide, etc., have also been tried with success. The hydroxide should have the advantage of being unactivated, but as Fig. 2 would suggest, there must have been some remaining chloride in the hydroxide.

Fig. 2 shows the spectral response of cadmium sulphide layers made from the salts; curve *A* from the sputtered oxide, and curves *B*, *C* and *D* from the bromide, chloride and hydroxide (possibly chloride activated). All these cells, except *A*, exhibit a time constant of about 1 m/s at 1740 f.c., with a sensitivity of about 10^{-2} A/lm at 1000 V/cm. This sensitivity was estimated by measuring the current passed by a cell when illuminated by a 25 W vacuum-filled household lamp of efficiency 9 lm/W, held 6 in. from the layer. The light intensity would thus have been 72 f.c. The cell tested was about 10 μ thick. With a nearly square root increase in conductivity with light intensity, the measured sensitivity would have been increased by nearly a factor of ten if measured at 1 f.c. This, considered along with the light loss due to transmission, gives a sensitivity of the order of 1 A/lm absorbed at 1 f.c.

Only a few layers have been made by the new methods of preparation reported here, and there have been some variations in performance. The methods are at present in the experimental stage, and further development will be necessary before a uniform and predictable result can be achieved.

These notes have been published by permission of the Chief Scientist, Department of Supply, Australia. The work was carried out at the Weapons Research Establishment, Salisbury, South Australia.

Research Establishment,
Australian Atomic Energy Commission,
Sutherland, New South Wales,
Australia.

R. LAWRANCE

[9 *September*, 1958]

REFERENCES

(1) BRAMLEY, A. *Phys. Rev.*, **98**, p. 246 (1955).

(2) BUBE, R. H. *J. Appl. Phys.*, **27**, p. 1237 (1956).

(3) PRESTON, J. S. *Proc. Roy. Soc. A*, **202**, p. 449 (1950).

NOTES AND NEWS

Notes and comments

Electrical instrument test service

The British Scientific Instrument Research Association has established an electrical instrument test service at their laboratories in Chislehurst, Kent. Although originally set up at the request of members of the Association, the service is now available to other firms and organizations.

Operated under the supervision of the National Physical Laboratory and using N.P.L. certified equipment, the department will test and issue certificates for instruments up to precision grade accuracy. Calibration of d.c. meters between 1 mV and 500 V and between 2 μA and 2 A can be undertaken immediately. In the near future the latter range is to be extended up to 25 A and the calibration of a.c. instruments over the ranges 1 V to 500 V and 10 mA–25 A will be undertaken. Charges for the service will be appreciably less than the cost of N.P.L. certification. It is hoped that this service will be welcomed by both manufacturers and users of instruments in this country, particularly where an independent test certificate for an instrument is required, but where the prestige value of an N.P.L. certificate is unnecessary.

Further information may be obtained from The Director of Research, The British Scientific Instrument Research Association, South Hill, Chislehurst, Kent.

Journal of Scientific Instruments

Contents of the June issue

ORIGINAL CONTRIBUTIONS

Papers

Temperature controller based on measurement of rate-of-change of temperature. By A. B. Cairnie and J. D. Pullar.
The epitasimeter: An instrument for process control by means of the continuous measurement of surface tension. By W. H. Aarts.
Apparatus for measuring the spreading coefficient of a liquid on a solid surface. J. F. Padday.
Homodyne detector for reproduction of periodic wave forms. By C. Lagercrantz.
Measurement of equivalent noise resistance of a noise thermometer amplifier By H. Pursey and E. C. Pyatt.
Double-beam infra-red grating spectrometer. By J. L. Hales.
Improved polythene-shielded net radiometer. By J. P. Funk.
Instrument for measuring liquid flows of less than a millilitre per hour. J. R. Pilbrow.
Resistance thermometer spear for field measurement. By A. C. Jason and A. Lees.
Vacuum fatigue apparatus. By N. J. Wadsworth.
Demountable vacuum seal for operation at temperatures from −188° C to 800° C. By R. Brymner and W. Steckelmacher.
Bakeable vacuum seals using aluminium-wire gaskets. By J. Holden, L. Holland and L. Laurenson.
Strobometric method of measuring the phase angles of very low currents. By S. B. Girvan and D. S. McIlhagger.
Measurement of low values of internal friction at elevated temperatures. By P. D. Southgate.

Laboratory and workshop notes

Integrator for a self-balancing potentiometer. By J. W. McHugo.
Stable radio-frequency lamp supply. By A. S. Brill and H. den Hartog, and E. R. Johnson.
Attachment to the Philips 11·46 cm diameter X-ray powder camera. By A. Barclay, F. G. Buttler and H. F. W. Taylor.
Constant-head aspirator. S. R. Howarth.
Opener for radioisotope bottles. G. R. Taylor and H. A. Malcolm.

NOTES AND NEWS

New instruments, materials and tools. New books. Notes and comments.

THIS JOURNAL is produced monthly by The Institute of Physics, in London. It deals with all branches of applied physics (including theory and technique). All rights reserved. Responsibility for the statements contained herein attaches only to the writers.

EDITORIAL MATTER. Communications concerning editorial matter should be addressed to the Editor, The Institute of Physics, 47 Belgrave Square, London, S.W.1. (*Telephone:* Belgravia 6111.) Prospective authors are invited to prepare their scripts in accordance with the *Notes for Authors*. (Price 3*s*. 6*d*. including postage.)

REPRODUCTION. The Institute of Physics is a signatory to The Royal Society's Fair Copying Declaration. Details may be obtained upon application from The Royal Society, London, W.1.

ADVERTISEMENTS. Communications concerning advertisements should be addressed to the agents, Messrs. George Jackson (Fleet St.) Ltd., Cliffords Inn, Fleet Street, London, E.C.4. (*Telephone:* Holborn 3611–2.)

CLAIMS FOR MISSING JOURNALS. Claims from regular subscribers to this *Journal* for missing numbers will only be considered if received within 60 days of the date of mailing plus normal outward time of transit and time for lodging the claim. Losses attributable to failure to notify a change of address or to similar omissions will not be considered.

SUBSCRIPTION RATES. A new volume commences each January. The charge is £6 per volume ($17 U.S.A.), including index (post paid), payable in advance. Single parts, so far as available, may be purchased at 12*s*. 6*d*. each ($1.75 U.S.A.), post paid, cash with order. Orders should be sent to The Institute of Physics, 47 Belgrave Square, London, S.W.1, or to any bookseller.

First ionization coefficients in hydrogen, neon, and argon

By D. E. Davies, B.Sc., Ph.D., A.Inst.P., and J. G. C. Milne, B.A., Ph.D.,* Department of Physics, University College of North Staffordshire, Keele, Staffs

[*Paper received* 1 *January*, 1959]

Values of the first ionization coefficient η in hydrogen have been determined in the range $40 < E/p_0 < 500$ V cm^{-1} mm^{-1} of mercury at 0° C to ±2% (where E is field strength and p_0 the gas pressure at 0° C). Evaporated metal film electrode tubes have been developed so that rigorous outgassing procedures could be adopted, and an analysis has been used whereby the values of η can be correctly calculated from the current-voltage data. Preliminary results have also been obtained for neon and argon (commercial spectroscopically pure) using the same techniques.

INTRODUCTION

Ever since Townsend[1] propounded his theory of primary ionization processes in gases by electron collision with gas molecules, a considerable amount of research has been performed in attempting to determine definite values of the first coefficient, α or η ($=\alpha/E$) for all gases; more especially the permanent gases and mixtures of them, of which air is the most important. As yet no such definitive values have been agreed upon over all the E/p_0 values of interest (where E is the strength of the electric field in which the electrons move and p_0 is the gas pressure at some standard temperature), except perhaps for the inert gases.[2, 3, 4]

Hydrogen is a gas in which several determinations have been made in the past.[5–12] Of these, values determined at $E/p_0 < 40$ V cm^{-1} mm^{-1} of mercury are in satisfactory agreement except for the results of Ayres[5] and those of Hale.[6] In Ayres' results poor vacuum techniques may well explain his serious difference from recent values. However, at $40 < E/p_0 < 500$ V cm^{-1} mm^{-1} of mercury, no such agreement has been obtained except between Rose's recent results and Ayres' old ones. Hale's results differ very considerably over all the E/p_0 range.

It therefore seemed most desirable to determine first coefficient values in this range using modern vacuum techniques and measuring instruments. Two types of experimental tube have been used: one with bulk metal electrodes in the conventional fashion, and one using evaporated metal film electrodes. The correct way of calculating the coefficients from the results has been studied and some observations made on another possible source of error. These will be dealt with in more detail in the next section.

CALCULATION OF THE FIRST IONIZATION COEFFICIENT

As is well known the current i increases with increase of electrode separation d or applied voltage V, according to the equation:

$$i/i_0 = \frac{\exp[\alpha(d-d_0)]}{1-(\omega/\alpha)\{\exp[\alpha(d-d_0)]-1\}} = \frac{\exp[\eta(V-V_0)]}{1-(\omega/\alpha)\{\exp[\eta(V-V_0)]-1\}} \quad (1)$$

at constant E/p_0, where i_0 is the photoelectric current at the cathode and d_0 and V_0 are distance and voltage corrections to compensate for the actual distance and voltage required for the electron avalanche to reach a stationary energy distribution; ω/α is a generalized secondary coefficient.

Provided d or V are small, these expressions reduce to:

$$i = i_0 \exp[\alpha(d-d_0)] = i_0 \exp[\eta(V-V_0)] \quad (2)$$

so that a graph of $\log_e i$ against d or V, should give a straight line of slope α or η respectively. This implies that the term in ω/α is $\ll 1$ and so secondary coefficient effects can be ignored. There is, however, a fundamental error in determining α or η in the above way, whether ω/α is found from sparking potential values or from the region where graphs of $\log_e i$ against d or V are curved. It is that, in practice, such $\log_e i$ against d or V curves may appear to be straight lines, but the contribution to i from the ω/α term is not negligible, but such as to give an increase in the slope. That is, ω/α has the effect at low values of d or V of increasing α or η, rather than of curving the graphs of $\log_e i$ against d or V.

It is therefore essential, if α or η are to be found correctly, that the whole $\log_e i$ against d or V curve, both linear and curved parts or the linear part together with values of V_s and d_s, be considered as a whole. This point has already been made by Jones and Llewellyn-Jones[12] who give an analysis for the correct calculation of α from current-distance data. Independently the present authors[13] have developed an analogous analysis for use with current-voltage data. The equation uses three values of current and voltage (i_1, V_1), (i_2, V_2) and (i_3, V_3) whence it can be shown from equation (1) that:

$$f(\eta) \equiv i_1(i_3-i_2)\exp[\eta(V_3-V_1)] - i_2(i_3-i_1)\exp[\eta(V_3-V_2)] + i_3(i_2-i_1) = 0$$

where $i_3 > i_2 > i_1$ and $V_3 > V_2 > V_1$ (3)

Solution of this equation numerically using Newton's formula gives η. If any one of ω/α, i_0 and V_0 are known, the other two can be found; i_0 is the parameter usually found experimentally so that one can find ω/α and V_0 using:

$$\omega/\alpha = \frac{i_3 - i_2\exp[\eta(V_3-V_2)]}{i_3 i_2\{\exp[\eta(V_3-V_2)]-1\}}\cdot i_0$$

$$\exp[\eta(V-V_0)] = \frac{[1+(\omega/\alpha)]i}{i_0+(\omega/\alpha)\cdot i}$$

where (i, V) is any suitable current-voltage value.

It is worth noting that the above analysis to find η requires no value of i_0, V_0 or ω/α, but only that they remain unchanged during the determination of the current-voltage values. The value of ω/α is, however, proportional to i_0, so that an error in the value of i_0 due to back diffusion effects or other factors will affect ω/α but not η.

* Now at the Physics Department, University of Sheffield.

The correction of η described above is, of course, entirely one of correct calculation of results from the experimental data. However, there seems to be a further possible source of error not of this kind, which does not seem to have been reported elsewhere. During some work on the influence of the cathode work function on the sparking potentials in hydrogen, Davies and Fitch[14] have found that passing a current of the order of 10^{-7} A can lower the cathode work function considerably. It therefore seemed reasonable to examine whether the value of i_0 could be changed by passing a current of the order of 10^{-7} A. Increases of up to 6% in i_0 were indeed found, and this is about the order of magnitude of change expected from the work function results. Davies and Fitch concluded that the positive ions in the discharge are responsible for this effect. Thus, if voltages are used which put the current value on to the curved part of the $\log_e i$ against V curve, there will be a considerable density of positive ions, some of which will accumulate on the cathode surface under certain conditions. The resulting decrease in work function would cause i_0 to increase provided the ultra-violet source is not monochromatic. Hence in an indirect way the effective value of i_0 is dependent on i and so also will be ω/α, since the sparking potential was found to be lower after passing a current of the order of 10^{-7} A,[14] and hence ω/α must be larger. Therefore with both i_0 and ω/α possibly increased by the increase in prebreakdown current, the assumption of constant i_0 and ω/α may not be true. Hence the calculation of η will be falsified.

APPARATUS AND EXPERIMENTAL PROCEDURE

The first type of experimental tube (Fig. 1) used bulk metal electrodes of copper, shaped to reduce field distortion and

Fig. 1. The bulk-electrode experimental tube with glass vacuum jar removed

suitably mounted in a glass vacuum jar to give a plane parallel gap of variable separation from 0–5 mm. The electrodes each of 30 mm diameter were mounted in baked soapstone insulators on steel spiders, which in turn were mounted on steel bosses attached to two steel plates. The upper electrode was the anode and it contained a hole of 1 mm diameter in its centre. This was to allow ultra-violet light to fall almost normally on to the cathode below. The lower electrode was the cathode and this was mounted on a gearing system which could be operated from outside the tube through a vacuum seal. Thus the inter-electrode separation could be varied continuously and was measurable to about $\pm 1/300$ mm. The upper and lower steel plates were ground flat and were separated by a glass vacuum jar, 70 mm diameter and 200 mm long, with ground ends which were parallel to within 10^{-3} cm. A good vacuum joint could be made between the glass and the steel using Apiezon T grease. Electrical leads entered the tube through tungsten-glass seals. These were mounted on glass-to-copper seals which in turn were soldered into the appropriate steel plate. The upper plate also contained a glass-to-copper seal with a quartz window across it set at 15° to the vertical and 30 mm off-centre. This was to admit ultra-violet light, the angle being chosen so that the hole in the anode was illuminated. The pumping tube entered the bottom steel plate as also did an electrical lead to a cylindrical sheet-silver electrostatic screen (not shown in the photograph) which surrounded the electrodes. The vacuum system was of the conventional type using a rotary backing pump and oil diffusion pump. Two liquid air traps separated the pumps from the experimental tube.

Hydrogen was prepared by the electrolysis of barium hydroxide in distilled water, and purified by standing it over phosphorus pentoxide and then passing it through a heated palladium osmosis tube. The gas pressure was measured using an oil manometer containing Apiezon oil B, the density of which had been accurately determined. Small pressures were measured by viewing the oil columns with a cathetometer.

Voltage supplies for the experimental tube came from a bank of dry cell h.t. batteries, as these were found to be much the most stable source of voltage available. The voltage was measured using a calibrated resistance chain of 10 or 20 MΩ (five or ten independently calibrated 2 MΩ high-stability carbon resistances in series) and a potentiometer across a 30 kΩ wire-wound resistance at the bottom of the chain. Voltages could be determined to better than 0·1%, especially at higher voltages. The ionization currents were measured in the anode circuit (cathode at potentials negative with respect to earth) using a Ferranti type DBM4A double tetrode electrometer valve. The use of high input resistances of 10^{11} or 10^{12} Ω enabled currents of 10^{-13} A to be determined to within 2 or 3%. The source of ultra-violet light was a quartz mercury vapour lamp run off a constant voltage transformer. As there were greased ground joints in the tube, baking was impossible so that pumping over a long period was the only means of getting a reasonably good vacuum. In both this experimental tube and the evaporated film tubes, the vacuum pressures were measured using a Penning gauge. The experimental procedure was to isolate the tube and manometer from the pumps at a pressure of about 10^{-6} mm of mercury and then flush out with freshly prepared hydrogen. The tube was then filled with hydrogen at the desired pressure and current-distance values found by altering the applied voltage and electrode separation so as to keep E/p_0 constant. Different values of E/p_0 were used by varying the gas pressure (always reduced to 0° C).

The second type of experimental tube used the same voltage supply and current measuring circuit, but used a separate vacuum system. The vacuum system used for the bulk metal tube became the gas supply and gas pressure measuring system.

The evaporated film tubes were, as far as possible, of all

glass construction (Fig. 2). A structure of boro-silicate glass rod was made on which the anode was rigidly attached, together with a similar electrode on a yielding support made of crossed tungsten strips. This electrode, used for contact potential difference measurements and on to which gold was evaporated, is of no concern here. Below the anode was the cathode on a pivot so arranged that this electrode could be swung magnetically, using a ball bearing encased in glass

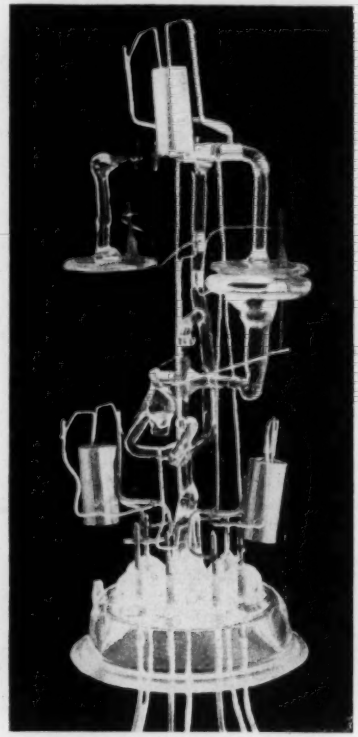

Fig. 2. The evaporated-film experimental tube prior to sealing in an envelope

attached beneath the cathode, either under the anode or vibrating electrode or held magnetically between them under its filament and bead. The electrodes were glass disks about 2 mm thick and 25 mm diameter, containing a short tungsten rod sealed through the disk perpendicular to the plane of the electrode and ground down flush with the electrode surface. This surface was also ground and then flame polished and the oxide removed from the tungsten by electro-polishing. The purpose of the tungsten was to provide electrical contact with the metal film evaporated on to the glass surface. As an additional precaution to ensure good contact, a small smear of Aquadag covered the tungsten.

Fixed below the two upper electrodes and above the lower electrode were tungsten wire filaments on which had been melted beads of copper, in a stream of hydrogen, while for the reference electrode gold had been used. These filaments were surrounded by nickel cylinders, the purpose of which was to direct the evaporated metal on to their respective glass surfaces. By passing a heavy current through these filaments the copper and gold could easily be evaporated on to the electrodes to give uniform gas-free surfaces, provided everything had been carefully outgassed. The whole electrode assembly was mounted on a C9 glass pinch (supplied by Siemens-Edison Swan Co. Ltd.) and sealed into a glass envelope. This envelope contained three side arms: one for pumping and a second to which was attached a Pyrex-quartz graded seal and a quartz window to admit ultra-violet light. This side arm was so arranged that the light shone obliquely at almost grazing incidence on to the centre of the cathode when in position under the anode. The third arm contained a tungsten-glass seal to make electrical contact to an Aquadag electrostatic screen painted and baked on to the inside of the envelope. Plane parallelism of the inter-electrode gap was ensured by placing a flat parallel-faced steel washer between the electrodes during assembly.

This type of experimental tube contained no bulk metal at all except for the three small nickel cylinders. These cylinders were eddy current heated to bright redness many times during pumping so that no contamination of the gas would result from this source. Likewise the metal beads on the filaments were melted several times during pumping so as to thoroughly outgas them. All the glassware in the tube was baked for many hours at 420° C. The vacuum system used was a backing pump and mercury diffusion pump with two liquid air traps, no stop cocks being used anywhere in the vacuum system. So as to exclude mercury vapour as completely as possible, a special manifold consisting of two breakers and constrictions in parallel was placed between the tube and second liquid air trap. Until a breaker was broken, using a steel ball bearing in glass, the tube remained unpumped. Hence, until the diffusion pump was running smoothly with its attendant liquid air traps, no mercury could diffuse into the experimental tube. The constriction was used to seal off the tube from the vacuum system after pumping. Seal-off pressures were always of the order of 10^{-7} mm of mercury. The experimental tube was joined to the vacuum system, used with the gas supply and oil manometer, through two palladium osmosis tubes in parallel. The gas pressure was measured using the oil manometer and, by heating the palladium tubes, pure hydrogen entered the experimental tube causing the pressure over the manometer to fall. When this ceased, the pressure over the manometer was equal to that in the experimental tube.

Because the electrode separation is fixed and constant, p_0 must be varied with applied voltage V to give constant E/p_0. This was done by removing some gas from the manometer and allowing the pressure to equalize across the heated palladium tubes. In this way current-voltage curves were obtained at constant E/p_0 values. Ample time—at least three hours—was always allowed for the pressure to equalize. Also, gas was always removed from the tube and never put in again after the initial filling up.

RESULTS AND DISCUSSION

(i) *Hydrogen.* The current-distance readings for the bulk-metal tube were obtained in the usual way, and the values of α and hence of α/p_0 were calculated using the simple equation neglecting secondary coefficient effects. Later, as already explained, the values of the sparking potential were used to

correct α/p_0 for ω/α contributions. As these sparking potential values were obtained some time after the α/p_0 values, the ω/α values so found are not necessarily the same as those pertinent to the α/p_0 determinations. Hence the correction is not very reliable quantitatively. However, it is interesting to find that the corrected α/p_0 values, when converted into η values, approach the evaporated film tube corrected values at higher values of E/p_0. While these bulk metal tube results are therefore not reliable, they show very clearly how important it is to calculate α/p_0 or η correctly from the current-distance or current-voltage data.

For the evaporated film tubes two separate tubes were made and used successfully, and the results given here are the average values. The current-voltage readings for these evaporated film tubes were obtained, as already explained, by varying the gas pressure p_0 and applied voltage V at constant electrode separation d so as to keep E/p_0 constant. For these results, the value of the input resistance for the electrometer was $10^8\ \Omega$ and the currents used varied from 4×10^{-11} to 10^{-8} A. This gave increased stability in the electrometer behaviour. Because of previous workers' discrepancies at higher values of E/p_0, two separate determinations of the current-voltage curves were done on the second experimental tube for $E/p_0 > 200$ V cm^{-1} mm^{-1} of mercury. The values for η from these two sets of results lie within the experimental error.

Initially the values of η were found graphically in the usual way using equation (2), but later they were recalculated using the above analysis [equation (3)]. Because of possible small fluctuations in i_0, the results were further analysed. Having found η and V_0 as above using three values of current and voltage, the whole current-voltage curve of ten to twelve points was fitted using the values of η, ω/α and V_0 to find the i_0 value effective for each value of i. The mean value of i_0 was then found and hence the mean square deviation of the i_0 values was calculated. Then the values of η and ω/α were varied slightly, the mean square deviation in i_0 recalculated and η and ω/α varied again until the mean square deviation was a minimum. These final values of η are the ones given here. The minimum r.m.s. deviation in i_0 was 2% or less, except for $E/p = 450$ and 500 V cm^{-1} mm^{-1} of mercury, where the r.m.s. deviations were 3 and 3½% respectively. Fig. 3 shows the curves of η against E/p_0 for both the corrected and uncorrected calculations, and for similar calculations on the bulk metal tube results. Table 1 gives the actual corrected evaporated film values for η for the E/p_0 range 40–500 V cm^{-1} mm^{-1} of mercury to an overall accuracy of about ±2%.

Table 1. *α/p_0 and η as a function of E/p_0 for hydrogen*
(p_0 is gas pressure reduced to 0° C)

E/p_0 (V cm^{-1} mm^{-1} Hg)	$\eta_c \times 10^2$, V^{-1}	α/p_0, cm^{-1} mm^{-1} Hg
40·0	0·395	0·158
50·0	0·633	0·317
60·0	0·837	0·502
70·0	0·993	0·695
85·0	1·16	0·986
100·0	1·26	1·26
125·0	1·33	1·66
150·0	1·33	2·00
175·0	1·27	2·22
200·0	1·19	2·38
250·0	1·08	2·70
300·0	0·990	2·97
350·0	0·884	3·09
400·0	0·804	3·22
450·0	0·743	3·34
500·0	0·691	3·46

Comparison with results by previous workers shows no agreement with any other results except for $E/p_0 \leqslant 100$ V cm^{-1} mm^{-1} of mercury, where agreement with Rose[9] is very good. Above $E/p_0 > 100$ V cm^{-1} mm^{-1} of mercury the *uncorrected* η values agree very well with Rose and Ayres,[5] but the *corrected* ones lie 10–15% lower. It will be seen that Jones and Llewellyn-Jones's[12] values lie lower still, but at present it is impossible to account for this unless the method of gas preparation is responsible. This seems unlikely, but is receiving further attention. With regard to Hale's results[6] one must, it seems, now conclude that they are incorrect.

Values of V_0 and ω/α were also found and these are shown in Fig. 4. The ω/α values show a very small variable value up to $E/p_0 \simeq 110$ V cm^{-1} mm^{-1} of mercury, and thereafter rise very rapidly and almost linearly to high values at

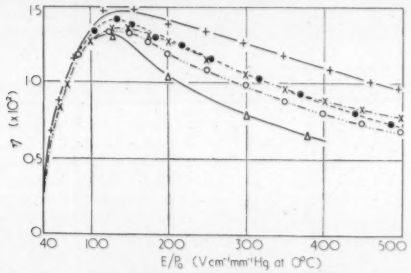

Fig. 3. η (in V^{-1}) as a function of E/p_0 in hydrogen
+ — + — + = bulk metal tube, uncorrected results
– – ● – – ● – = bulk metal tube, corrected results
× — · — · × = evaporated-film tube, uncorrected results—also Ayres[5] and Rose[9]
○ ·· — ·· ○ = evaporated-film tube, corrected results
—△——△ = Jones and Llewellyn-Jones[12]

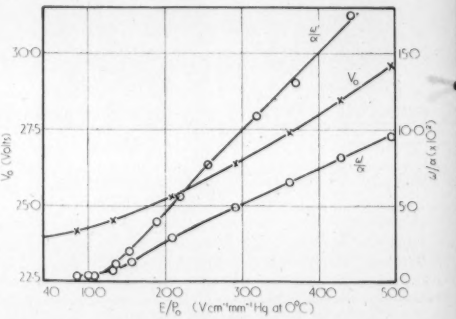

Fig. 4. V_0 (voltage correction) and ω/α as a function of E/p_0 in hydrogen. ω/α', bulk copper electrode; ω/α, copper film electrode
× —— × = V_0
○ —— ○ = ω/α

$E/p_0 \simeq 500$ V cm^{-1} mm^{-1} of mercury. Interpretation of such a curve without time lag data is quite impossible. The V_0 values lie between about 23 and 30 V rising steadily from the lower value to the higher one as E/p_0 is increased. Converted into values of d_0 for a standard pressure of 1 mm

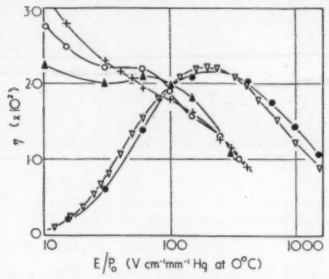

Fig. 5. η (in V^{-1}) as a function of E/p_0 in neon and argon

● = argon
▽ = argon (by Kruithof[3])
▲ = neon (sample 1)
○ = neon (sample 2)
× = neon (+0·1% argon, by Kruithof and Penning[2])

of mercury at 0° C, this means that d_0 decreases from about 2·4 mm at $E/p_0 = 100$ V cm^{-1} mm^{-1} of mercury to 0·6 mm at $E/p_0 = 500$ V cm^{-1} mm^{-1} of mercury. It would therefore seem that as the mean electron energy increases, the distance the avalanche must traverse before reaching a stationary distribution decreases for a fixed gas pressure.

(ii) *Neon and argon.* A further experimental tube, again using copper films, was used for a preliminary study of commercial spectroscopically pure neon and argon. The stepwise behaviour in the current-voltage curves for neon at low values of E/p_0 ($E/p_0 \simeq 10$ V cm^{-1} mm^{-1} of mercury) was very marked and was observable even at $E/p_0 = 60$ V cm^{-1} mm^{-1} of mercury. This is very similar to the behaviour found by Kruithof and Penning[2] for neon with small amounts of argon impurity. The values of η calculated from these curves using the above analysis show a steady decrease for E/p_0 from 6·0 to 350 V cm^{-1} mm^{-1} of mercury (see Fig. 5). Two different sets of results were obtained using two different gas samples from different bottles. The first set gave η values roughly corresponding to about 10^{-2}% argon impurity if compared with Kruithof and Penning's results; the second set gave slightly higher η values corresponding to about 5×10^{-2}% argon impurity.

The argon results (Table 2) covered the E/p_0 range of 15·0 to 1500 V cm^{-1} mm^{-1} of mercury. The η values, when compared with Kruithof's,[3] show that for E/p_0 below the maximum in η the present values are lower by about 12–16%, while for E/p_0 above the η maximum the present results lie higher by up to the same percentage. It is, however, too early to draw any conclusions from this result. Values of ω/α and V_0 were found as well. The ω/α values show a U-shaped curve when plotted against E/p_0. Theoretical estimates of the sparking potential using Townsend's criterion:

$$1 - \omega/\alpha\{\exp[\eta(V_s - V_0)] - 1\} = 0$$

agreed well with experimentally determined values for V_s at p_0d values above that corresponding to the minimum sparking potential.

CONCLUSIONS

The conclusions to be drawn from this work are threefold. Firstly, it is imperative to calculate the value of η from the full current-voltage curve, not graphically, as is usually done, but analytically. Only in this way can secondary coefficient effects be properly corrected for.

Secondly, because positive ions of hydrogen in hydrogen seem to alter the cathode work function when striking it under discharge conditions, the values of i_0 and ω/α may not remain constant at constant E/p_0, but may increase as the ionization current—and therefore the positive ion current—increases. This may falsify the values of η though the error will be small and may be less than the experimental error.

Thirdly, a new type of experimental tube has been designed and made to work successfully enabling ultra-high vacuum techniques to be used without much difficulty. Provided the gas purity is comparable, precision values of η can be obtained from these tubes. While the authors would like to claim that the η values in hydrogen given here are the best and most accurate so far determined, the discrepancy with Jones and Llewellyn-Jones's recent values is disturbing. Hence further experiments are being carried out using uranium hydride to purify the hydrogen and guard rings to improve the geometry of the tubes. It is hoped that this discrepancy can then be resolved.

Table 2. *η as a function of E/p_0 for argon*

E/p_0 V cm^{-1} mm^{-1} Hg	15	30	60	100	150	250	400	650	1000	1500
$\eta \times 10^2$ V^{-1}	0·218	0·608	1·39	1·99	2·08	2·19	1·99	1·75	1·43	1·155

ACKNOWLEDGEMENTS

The authors wish to thank Prof. F. A. Vick for extending to them the facilities of the Laboratory, and Siemens-Edison Swan Co. Ltd. for the gift of pinches and envelopes. They also wish to thank Mr. E. Roberts, who constructed the bulk-metal tube, and Mr. F. Rowerth and Mr. B. Bloor, who assisted in preparing the paper.

REFERENCES

(1) Townsend, J. S. *Electrons in Gases* (Oxford: University Press, 1915; London: Hutchinson, 1947).

(2) Kruithof, A. A., and Penning, F. M. *Physica*, **3**, p. 515 (1936); **4**, p. 430 (1937).

(3) Kruithof, A. A. *Physica*, **7**, p. 519 (1940).

(4) Townsend, J. S., and McCallum, S. P. *Phil. Mag.*, **17**, p. 678 (1934).

(5) Ayres, T. L. R. *Phil. Mag.*, **45**, p. 353 (1923).

(6) Hale, D. H. *Phys. Rev.*, **54**, p. 241 (1938); **55**, p. 815 (1939); **56**, p. 1199 (1939).

(7) Hopwood, W., Peacock, N. J., and Wilkes, A. *Proc. Phys. Soc.* (*London*) *A*, **235**, p. 334 (1956).

(8) Crompton, R. W., Dutton, J., and Haydon, S. C. *Proc. Phys. Soc.* (*London*) *B*, **69**, p. 2 (1956).
(9) Rose, D. J. *Phys. Rev.*, **104**, p. 273 (1956).
(10) de Bitetto, D. J., and Fisher, L. H. *Phys. Rev.*, **104**, p. 1213 (1956).
(11) Vanerin, L. J., and Brown, S. C. *Phys. Rev.*, **79**, p. 946 (1950).
(12) Jones, E., and Llewellyn-Jones, F. *Proc. Phys. Soc.* (*London*), **72**, p. 363 (1958).
(13) Milne, J. G. C. Ph.D. Thesis (University of Birmingham, May 1958).
(14) Davies, D. E., and Fitch, R. K. *Brit. J. Appl. Phys.* (in the press).

Permittivity of mixtures of zinc oxide and rubber

By N. H. Langton, M.Sc., Ph.D., A.M.Brit.I.R.E., A.Inst.P., and D. Matthews, F.N.C.R.T., D.P.I.,
The National College of Rubber Technology, Northern Polytechnic, London, N.7

[*Paper received* 29 *January*, 1959]

Measured values are given for the permittivities of a number of zinc oxide/rubber mixes at frequencies of 0·1, 1·0, and 10·0 Mc/s. The zinc oxide was of known particle size and shape, and the particle distribution in the rubber was examined with an electron microscope. The measured permittivities are compared with those calculated from the equations of Lichteneker,[2] Weiner,[6] and Bruggeman.[7] Values of Weiner's form factor are also calculated. It is shown that whilst the equations of Weiner and Bruggeman give satisfactory agreement, Lichteneker's equation gives permittivity values which are too low.

The problem of predicting the permittivity of two-phase mixtures has interested many workers in the past, and several equations have been derived for this purpose. Among these formulae, those of Maxwell[1] and Lichteneker[2] are well known and in fairly general use. In a recent paper, Pearce[3] has discussed a number of these equations and examined their validity using models and emulsions of oil and water. An important aspect of this subject is that most of the equations are based upon the assumption that the dispersed phase is in the form of small spherical particles of constant size, distributed in a specified manner throughout the continuous phase.

In this paper, the validity of a number of these formulae is examined when they are applied to practical mixtures of rubber and zinc oxide. The accuracy of the predicted permittivity value has been found by comparison with the measured value over a range of frequencies. The zinc oxide used throughout this work was of known particle size, shape and permittivity, and the distribution of the zinc oxide particles in the rubber phase has been investigated by electron microscopic examination.

Rubber Compounds

The mixtures used in these investigations consisted of rubber, together with the necessary vulcanizing ingredients, and a colloidal zinc oxide of high chemical purity [supplied by Amalgamated Oxides (1939) Ltd.]. The proportion of zinc oxide in the mixtures was varied from 3 to 30% by volume of the total. The effect of the vulcanizing ingredients on the permittivities of the mixtures can be ignored, since the same proportion based on the rubber was used in each compound. A base rubber compound, containing only rubber and vulcanizing ingredients with the addition of 0·3% by volume of zinc oxide, was made up in order to determine the permittivity of the vulcanized rubber phase. The zinc oxide in this base compound was necessary to carry out the vulcanization process, and was regarded as part of the base compound, a similar amount being allowed for in each of the mixtures.

Measurement of particle distribution. The distribution of the zinc oxide in the rubber mixes was examined using an electron microscope, sections being cut on an ultra-microtome. Details of the technique employed have been published recently in a paper by Langton and Stephens.[4] Photographs of sections obtained by this method were ruled with a grid giving squares of 0·5 μ side in the original section. A particle count was carried out over a field of a hundred of these squares, and the distribution of particles over the field was plotted as a histogram. Three theoretical distributions were calculated, these being of the binomial, Poisson, and Gaussian types respectively, and compared with the actual distribution. Fig. 1 shows the actual and theoretical distributions calculated for a compound containing 23·1% by volume of zinc oxide. It can be seen that the Gaussian distribution was the best fit to the actual distribution, a fact which was verified by means of a X^2 test. Comparisons

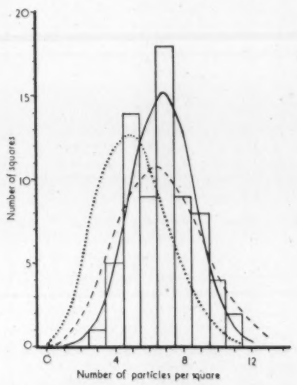

Fig. 1. Comparison of the actual particle distribution of a mix with three theoretical distributions
– – – – – = binomial distribution.
— — — = Poisson distribution.
——— = Gaussian distribution.

carried out for the other mixes also showed a Gaussian distribution of the zinc oxide particles in the rubber.

Preparation of rubber samples and method of measuring permittivity. The rubber compounds were vulcanized between steel plates in a hydraulic press to give flat sheets of approximately 4 mm thickness, from which disks of 1·5 in. diameter were cut with a punch. After standing for a period of 24 h at room temperature, the samples were carefully cleaned with ether on cotton-wool, and dried for 12 h in an oven at 35° C, followed by a further 12 h at 20° C in a desiccator.

The permittivity measurements were carried out with the aid of a circuit magnification meter, model TF 329E (by Marconi Instruments Ltd.), in conjunction with a dielectric loss test jig, type TJ 155 supplied by the same company. The specimen capacitor electrodes of the test jig were disks of 1·0 in. diameter. Subsidiary electrodes of the same size, cut from 0·001 in. aluminium foil, were applied to the rubber samples, using a smear of white Vaseline to obtain good adhesion. Great care was taken during this operation to avoid air bubbles between the electrodes and the rubber, which would give rise to errors in the measurements.

Permittivity measurements on rubber compounds. The results given in this section are restricted to measurements taken at frequencies of 0·1, 1·0, and 10·0 Mc/s, although measurements were made at several intermediate frequencies. All the results given were obtained from the average of four test samples, except in the case of the compounds containing 3·9 and 14·8% of zinc oxide, where only two samples were tested. The permittivity of the zinc oxide used throughout these experiments was measured by the authors using the method of mixtures, details being given elsewhere.[5] Table 1 gives the results of these permittivity measurements, the accuracy of measurement being ±2·5%.

Table 1. *Permittivities of rubber compounds*

*Percentage by volume of zinc oxide**	*Permittivity of mixture at frequency of* 0·1 *Mc/s*	1·0 *Mc/s*	10·0 *Mc/s*
0·0	3·07	2·99	2·85
3·9	3·32	3·26	3·18
4·7	3·23	3·18	3·01
9·1	3·35	3·35	3·24
13·0	3·62	3·54	3·54
14·8	3·76	3·74	3·55
16·7	3·88	3·81	3·73
20·0	4·08	3·94	3·77
23·1	4·18	4·18	4·01
29·6	4·58	4·49	4·40
100·0	10·4	10·4	10·2

* Colloidal zinc oxide supplied by Amalgamated Oxides (1939) Ltd.

THEORETICAL FORMULAE

Three formulae, put forward for calculating the permittivity of mixtures were investigated, these being Lichteneker's,[2] Weiner's,[6] and Bruggeman's[7] equations. Of these three, Lichteneker's equation was derived empirically, but is in fairly common use. Weiner's equation is a more general case of Maxwell's equation,[1] using a form factor to allow for particles of varying shape in the dispersed phase. The value of this form factor for ellipsoidal particles has been calculated by Fricke,[8] while Weiner gives values for spherical and cylindrical particles arranged in a lattice point pattern within the continuous phase. Bruggeman's equation assumes a random dispersion of spherical particles. In order to simplify the writing of these expressions, the following list of symbols is given.

ε_m = permittivity of the mixture.
ε_1 = permittivity of the continuous phase (rubber).
ε_2 = permittivity of the disperse phase (zinc oxide).
p_1 = proportion by volume of continuous phase.
p_2 = proportion by volume of disperse phase.
F = Weiner's form factor.

Lichteneker's equation. This equation can be written:

$$\log \varepsilon_m = p_1 \log \varepsilon_1 + p_2 \log \varepsilon_2 \qquad (1)$$

The permittivities of the different mixtures were calculated from the permittivities of the zinc oxide and rubber, which are given in Table 1, and compared with the measured values. Fig. 2 shows a comparison made at a frequency of 1 Mc/s,

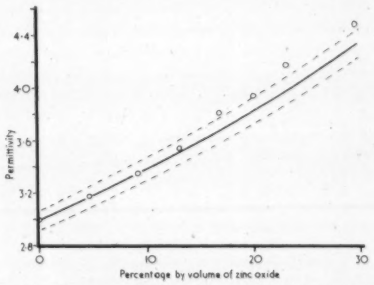

Fig. 2. Comparison between measured permittivities and those predicted from Lichteneker's equation
○ = experimental result.
——— = theoretical curve.
– – – – = limits of experimental error.

the calculated values being shown as a curve and the measured values as points. The effect of errors in the measurement of ε_1 and ε_2 on the calculated value of ε_m was taken into account by differentiation of the equation with respect to ε_1 and ε_2, and limits of experimental error are indicated.

It will be seen that as the percentage of zinc oxide in the mixtures is increased, the measured permittivity tends to be greater than that predicted by the equation, suggesting that Lichteneker's equation does not hold true for a Gaussian distribution of zinc oxide in rubber. A comparison between the calculated and measured permittivities, over a range of frequency, of two mixtures containing 4·7 and 29·6% by volume of zinc oxide respectively is given in Fig. 3, and demonstrates this point. The 4·7% zinc oxide compound has a measured permittivity quite close to the calculated value over the whole frequency range, whilst that of the 29·6% zinc oxide compound is higher than the calculated value over the whole frequency range.

Weiner's equation. This equation was derived for calculating the permittivity of a mixture of small particles in a lattice point distribution within a continuous phase, and can be written:

$$\varepsilon_m = \frac{\varepsilon_1\{\varepsilon_2 + F\varepsilon_1 + p_2F(\varepsilon_2 - \varepsilon_1)\}}{\varepsilon_2 + F\varepsilon_1 - p_2(\varepsilon_2 - \varepsilon_1)} \qquad (2)$$

A form factor F is introduced to deal with particles of different shapes. For spherical particles this has a value of 2, but with

asymmetric particles the value depends upon the shape and orientation. Fricke[8] has shown that for ellipsoidal particles aligned with their short axes parallel to the electric field, the form factor lies between 0 and 2. When the ellipsoids are aligned with their short axes perpendicular to the field, the form factor lies between 2 and infinity. In both cases the actual value is dependent upon the particle shape. If the particles are aligned in other ways the form factor will have any value, although where the particles are orientated at random the effect of particle orientation is balanced out, and the form factor is mainly dependent upon the particle shape. In the rubber/zinc oxide mixtures under investigation, a random orientation of the particles was observed.

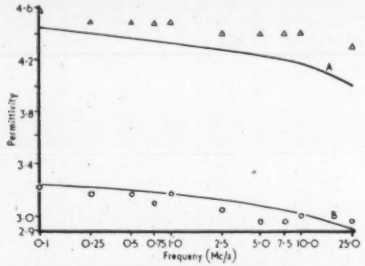

Fig. 3. Comparison between measured and calculated permittivities of two zinc oxide/rubber mixtures over a range of frequency, assuming Lichteneker's equation

Curve *A*, 29·6% zinc oxide compound; △ = experimental results.
Curve *B*, 4·7% zinc oxide compound; ○ = experimental results.

In order to calculate the permittivity of a mixture, using Weiner's equation, it is first necessary to determine the value of the form factor. By rearrangement of equation (2)

$$F = \frac{p_2\varepsilon_m(\varepsilon_2 - \varepsilon_1) - \varepsilon_2(\varepsilon_m - \varepsilon_1)}{\varepsilon_1\{(\varepsilon_m - \varepsilon_1) - p_2(\varepsilon_2 - \varepsilon_1)\}} \qquad (3)$$

Substituting the values for ε_1, ε_2 and ε_m given in Table 1, the form factors were calculated for the mixtures at the three frequencies and are given in Table 2. The scatter in these values and the limits of error, however, are too large to give very useful results. The effect of frequency upon the value of the form factor for two mixes, one containing 4·7% the other 29·6% by volume of zinc oxide, is shown in Figs. 4 and 5. In the case of the 4·7% zinc oxide mixture, there is a large amount of scatter which would be expected, owing to the large effect of errors at this percentage of zinc oxide. With the 29·6% zinc oxide mixture, however, the effect of errors is diminished, and a rise in the form factor value is observed as the frequency is increased. No explanation can be given for this phenomenon.

Table 2. *Form factor values at three frequencies*

Percentage by volume of zinc oxide	*Form factor at frequency of* 0·1 *Mc/s*	1·0 *Mc/s*	10·0 *Mc/s*
0·0	—	—	2·28
3·9	4·14	4·98	1·13
4·7	0·37	1·79	1·13
9·1	0·29	1·52	2·28
13·0	1·48	1·76	4·82
14·8	2·15	3·38	2·96
16·7	2·48	2·92	3·81
20·0	2·85	2·41	2·45
23·1	2·23	3·18	3·28
29·6	2·60	2·62	3·50
100·0	—	—	—
Average (graphical)	2·70	2·89	3·43

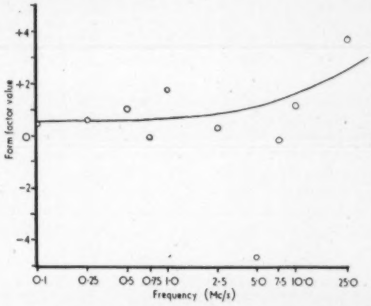

Fig. 4. Weiner's form factor over a range of frequency; 4·7% zinc oxide compound

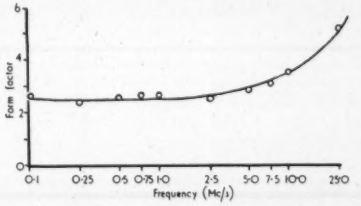

Fig. 5. Weiner's form factor over a range of frequency; 29·6% zinc oxide compound

The mean value of the form factor was calculated from the results obtained at a frequency of 1 Mc/s, and was found to be 2·9. From this result the permittivity of the mixture was calculated, and the results are compared with the measured permittivities in Fig. 6, similar results being obtained

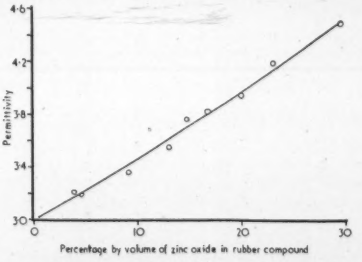

Fig. 6.—Comparison between experimental and theoretical permittivities of mixtures at 1·0 Mc/s; Weiner's equation, $F = 2{\cdot}9$

○ = experimental point.
——— = theoretical curve using F = 2·89.

at other frequencies. Good agreement is obtained between the actual and calculated permittivities of mixtures using Weiner's equation, once the value of the form factor has been found accurately.

Bruggeman's equation. This equation, which assumes a random distribution of spherical particles, has been found by Pearce[3] to give satisfactory results for practical mixtures, such as dispersions of water in oil, and has been tested for applicability to the present mixtures. It can be written:

$$(1 - p_2) = \frac{\epsilon_2 - \epsilon_m}{\epsilon_2 - \epsilon_1} \cdot \sqrt[3]{\frac{\epsilon_1}{\epsilon_m}} \qquad (4)$$

this being a cubic equation in ϵ_m. In his paper, Pearce assumes the permittivity of sea water to be infinite, because of its high conductivity, enabling the equation to be simplified to the form:

$$\epsilon_m = \epsilon_1(1 - p_2)^{-3} \qquad (5)$$

Neither component of the present mixtures has infinite permittivity however, and it is necessary to use a different approach. One possible method would be to solve the equation for ϵ_m, using Cardan's method, but in the present instance the value of $(1 - p_2)$ was calculated from the experimental measurements, using equation (4), and compared with the actual value obtained from the known constitution of the mixture. Fig. 7 shows this comparison made at

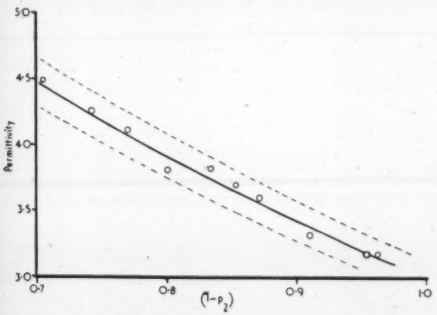

Fig. 7. Comparison between calculated values and experimental values of $(1 - p_2)$ at 1·0 Mc/s frequency

○ = experimental value.
——— = calculated value.
– – – – = limits of experimental error.

1 Mc/s frequency. The effect of errors in the permittivity measurements on the value of $(1 - p_2)$ was taken into account and upper and lower limits of experimental error are indicated in the figure. Similar results were obtained in comparisons at frequencies of 0·1 and 10·0 Mc/s. It can be seen that there is good agreement between the actual values of $(1 - p_2)$ and those calculated from Bruggeman's equation. The effect of frequency upon Bruggeman's equation is shown in Fig. 8, where the permittivities of two mixtures are plotted over a range of frequency. (These permittivity values were found graphically from the relationship between permittivity and the percentage of zinc oxide in the mixtures.) The equation is seen to fit the experimental results very well, except for the result at 25 Mc/s with the 29·6% zinc oxide mix, where the calculated permittivity is much smaller than the measured value.

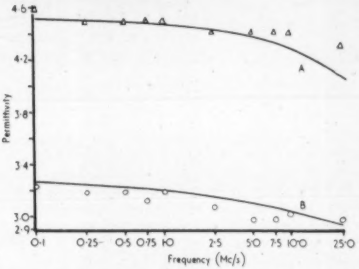

Fig. 8. Measured and calculated permittivities, from Bruggeman's equation, of two mixtures over a range of frequency

Curve A, 29·6% zinc oxide compound; △ = experimental results.
Curve B, 4·7% zinc oxide compound; ○ = experimental results.

CONCLUSIONS

It has been found that of the three equations which were investigated, those of Weiner and Bruggeman were most satisfactory for predicting the permittivity of mixtures of zinc oxide dispersed according to a Gaussian distribution in rubber. Lichteneker's equation, which is commonly used for this purpose, was found to give lower permittivity values than those found by experiment, the discrepancy increasing with increasing proportions of zinc oxide over the range of proportions investigated. The difficulty of obtaining an accurate value of Weiner's form factor for a particular system, and its apparent change with frequency, makes the use of Bruggeman's equation preferable for predicting the permittivity of a mixture. A drawback to Bruggeman's equation is that it is difficult to calculate ϵ_m, but on the other hand, it is fairly simple to calculate the value of $(1 - p_2)$ for a given value of ϵ_m, thus enabling the constitution of a mixture of specified permittivity to be calculated. It is to be noted that the agreement between the measured and calculated permittivities of the mixtures tends to deteriorate at the higher frequencies, due possibly to increased errors of measurement.

REFERENCES

(1) Clerk Maxwell, J. *Electricity and Magnetism*, 3rd. Ed., Vol. 1, p. 440 (Oxford: The Clarendon Press, 1904).
(2) Lichteneker, K. *Phys. Z.*, **27**, p. 115 (1926).
(3) Pearce, C. A. R. *Brit. J. Appl. Phys.*, **6**, p. 113 (1955).
(4) Langton, N. H., and Stephens, M. *Plastics*, **23**, p. 384 (1958).
(5) Langton, N. H., and Matthews, D. *Brit. J. Appl. Phys.*, **9**, p. 453 (1958).
(6) Weiner, O. *Abhandl. Math. Phys. Kl. Sachs Acad. Wiss. (Leipzig)*, **32**, p. 507 (1913).
(7) Bruggeman, D. A. G. *Ann. Phys. (Leipzig)*, **24**, p. 636 (1935).
(8) Fricke, H. *Physics*, **1**, p. 106 (1931).

Theory of operation and constructional principles of a high-precision spectroscopic spark source*

By Á. Bardócz, D.Eng., Hungarian Academy of Sciences, Central Research Institute of Physics, Budapest, Hungary

[*Paper first received* 8 *September*, 1958, *and in final form* 17 *March*, 1959]

For the production of time-resolved spark spectra, an electronically controlled source operating with a high precision in time is necessary. The high operational precision of the spark source with double controlling spark gaps is, on the one hand due to the spark gaps being electrically prestressed, and on the other hand to the transient wave arising at the breakdown of spark gaps. A further condition for the high operational precision in time is the adequate preionization of the spark gaps. A spark frequency higher than mains frequency may be realized by using a saturated iron-cored transformer to give complete separation of the charging and discharging processes. To illustrate time-resolved spectrochemical analysis, the separation of the background of the spark spectrum was carried out by means of a rotating disk placed before the slit of the spectrograph. Owing to the separation of the background the working curve obtained is a straight line even in the case of small percentage contents, and the sensitivity may be increased.

If, in spectroscopic work, the goal is first of all the production of line spectra, then discharges of relatively low energies are necessary for the spectrum excitation. But to obtain spectra with the aid of relatively low energy discharges, the light of many hundreds or many thousands discharges require to be integrated. The situation is a similar one if time-resolved spectra are produced with energies of such an order of magnitude. Although for the production of spectra not resolved in time, the scattering of the time between the individual discharges can be arbitrary, the situation is different in the case of time resolved spectra. The situation is particularly delicate if there is question of a time resolution of the order of magnitude of microseconds. In order to achieve useful time resolution, the time-resolved spectra should be placed precisely on each other on the spectrum plate, ensuring that the individual spark discharges succeed each other by a very high precision in time. Spark discharges can be produced with the high precision in question by electronically controlled, high-precision, spark sources. A high-precision spark source is such a spectroscopic source where the breakdown of sparks with respect to a given electric signal takes place with a time scattering of the order of magnitude of 10^{-7} s.

The circuit and the operational principle of the high-precision spectroscopic spark source introduced by the author has been described already.[1-6] The theory of operation of the source in question, however, has not been discussed hitherto and this is the purpose of the present paper. The constructional requirements are due to the operational theory of the spark source and the constructional fundamentals arising from these requirements are described. The high sparking frequency, exceeding that of the spark source described earlier,[1-6] results in a much more reliable and reproducible operation, so that it is possible to apply the improved source for time-resolved spectrochemical analytical purposes. The applicability of the improved source is shown with the aid of some time-resolved spectrochemical examples.

THE THEORY OF OPERATION OF THE SPARK SOURCE

In Fig. 1 the schematic circuit diagram of the electronically controlled, high-precision, spectroscopic spark source, as used by the author, is shown. This circuit and its operation have already been described in several papers[1-6] and will not be given here. The possibilities of applying the source illustrated in Fig. 1 to time-resolved spectroscopy has also been described earlier.[7, 8, 9]

In Fig. 1, C is the capacitor supplying the excitation energy, F is the analytical spark gap, S the symmetrical double controlling spark gap, V is an electron tube and R_1–R_4 are ohmic resistances.

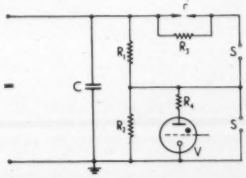

Fig. 1. Circuit diagram of the electronically controlled, high-precision, spectroscopic spark source

The discharge circuit, shown at the right-hand side of capacitor C in Fig. 1 has two very important features. One feature is that the system can be controlled by low-energy and low-voltage electric signals. It is thus possible to control the system by trigger generators, and there is also the possibility of control by light signals. The control by light signals is important from the point of view of time-resolved spectroscopy. The other feature of this part of the circuit is the high-precision operational accuracy, since relative to the controlling electric signal given on the grid of electron tube V, the breakdown of analytical spark gap F takes place with the small time scatter already mentioned.

It is shown, by theoretical considerations and experience, that the source of Fig. 1 will operate with the desired accuracy if the double controlling spark gaps S are electrically strongly prestressed while the signal to the grid of electron tube V is operating. If, during this time a positive voltage signal is applied to the grid of tube V, which is blocked by a negative bias, the upper half of S will break down with a very small time scatter. It is known from physics of gas discharges that strongly prestressed spark gaps break down in 10^{-7} to 10^{-8} s, if sudden voltage pulses are applied to them and the statistical time lag is of such an order of

* Investigations concerning light sources for spectrum analysis XIII.

magnitude. Thus the breakdown, with a small time scatter, of the upper half of double spark gap S would be explained. Experience proves, however, that the discharge circuit of Fig. 1 works with a time scatter of the order of magnitude of 10^{-7} s. In other words, this means that the breakdown of F and of the lower half of S takes place with the same time scatter. As against this, the breakdown of spark gap F and of the lower half of double spark gap S cannot be explained on the aforesaid basis. The breakdown with a small time scatter of spark gap F and the lower half of S can be explained in the following way.

As a consequence of the circuit data the breakdown of the upper half of S will be followed by the breakdown of F. Experience shows, for instance, that with a charging voltage of capacitor C of 20000 V, even with an analytical spark gap F of 8–10 mm, the high precision will still hold. From this it follows that across the spark gap F some additional voltage is applied over and above the static voltage on the terminals of capacitor C, which causes the breakdown to occur with a small time scatter. This additional voltage can only be the result of the wandering wave arising after the breakdown of the upper half of double spark gap S.

The breakdown of the upper half of S and F is followed by the breakdown of the lower half of S, because the voltage on it increases to nearly double its previous value. This increase in the voltage on S is not sufficient reason for the spark gap to break down with the known small time delay. For the breakdown to take place with a time scatter of 10^{-7} s order of magnitude, it must be assumed that it is caused by the wandering wave arising during the breaking down of F.

From the above it can be seen that the high-precision operation in time of the circuit of Fig. 1 is due to two circumstances. The one consists of the fact that the upper half of double spark gap S is electrically prestressed, and the voltage pulse applied to it results in a breakdown of small time scatter. The other circumstance is that the wandering wave arising at the breakdown of the upper half of S promotes the breaking down with a small time scatter of F, whereas the wandering wave arising at the breaking down of F acts favourably to the breakdown of the lower half of S.

It is, however, empirically shown that the electrical prestressing of the upper half of S and the wandering waves arising at the breakdown of F and the lower half of S are necessary, but are not sufficient to attain the high precision in time necessary for time-resolved spectroscopy. To attain the high precision in time it is also necessary that the spark gaps be preionized.

The decisive importance of the preionizing for the high-precision operation of source according to Fig. 1 can be demonstrated by a very simple experiment. Namely, if the sparking frequency is varied one will see that the higher the sparking frequency, the smaller the time scatter. Here it should be mentioned that the higher the sparking frequency, the greater the operational stability of the system. Thus, for a higher sparking frequency the system will be less sensitive to the dimensions of the spark gap S and also to other conditions.

The high sparking frequency is not only advantageous from the point of view of preionization, but also because for a higher sparking frequency the light yield of the source increases, and the sampling of the analytical electrode surfaces by the sparks is more uniform. This latter fact increases the reliability of spectrochemical analyses.

The spark source illustrated in Fig. 1 has, from a certain point of view, the same properties as any spark source provided with fixed controlling spark gaps. During the discharge of capacitor C the spark gaps F and S are practically short-circuited. Therefore, if during the discharge of capacitor C the supply voltage is still connected to the terminals of capacitor C, a continuous current will flow and capacitor C will not charge up. Therefore to make the system operate, the charging and discharging processes of capacitor C should be electrically completely separated from one another and, after the discharge, sufficient interval must be ensured for the spark gaps to deionize to the extent that no current will flow through them. On the other hand, this interval can be only of such a duration that the ionization necessary as a precondition of accurate operation be still present. The degree of ionization after an interval is, however, not related to the degree of ionization which is present directly after the discharge.

The electrical separation of the charging and discharging processes of capacitor C (Fig. 1) is easily attained if one is contented with a spark frequency corresponding to the mains frequency. In this case the circuit of Fig. 2 can be used.

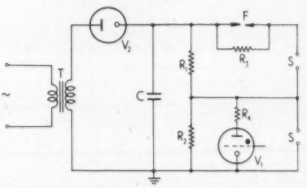

Fig. 2. Circuit diagram of the electronically controlled, high-precision, spectroscopic spark source. The sparking frequency per second is identical with the mains frequency

However, this solution is not satisfactory except at a relatively small sparking frequency, and it also has the drawback that, owing to the relatively long intervals between the individual sparks, it is not reliable.

THE BUILDING-UP OF THE NEW SPARK SOURCE

If the object is to attain a higher number of sparks per second than the mains frequency, while at the same time it is intended to separate the charging and discharging processes of the capacitor, there are serious difficulties to be taken into consideration. Although there is no objection in principle to charging up the capacitors C of Figs. 1 and 2 through controlled tubes, the arrangement is complex. Experience shows that the charging tube can be omitted, and the separation of the charging and discharging processes of capacitor C should be solved in another way.

The separation of the charging and discharging processes of capacitor C illustrated in Figs. 1 and 2 can be attained for a higher sparking frequency than the mains frequency by the application of special transformers. These transformers convert the mains voltage sine waves to voltage pulses of short duration. The capacitors illustrated in Figs. 1 and 2 are charged up by these voltage pulses. The essential fact is that between these short voltage pulses practically voltage-free intervals are present, during which time the spark gaps can deionize.

As described in the preceding paragraph, spark discharges can be produced at twice mains frequency with the source illustrated in Fig. 3, and charging and discharging processes are practically completely separated from one another. In Fig. 3 the part of the circuit on the right-hand side of

capacitor C is identical with the corresponding part of Figs. 1 and 2. A difference is to be found in the part to the left of capacitor C. Here T is a transformer of special design, the core carrying the secondary being designed in such a manner that it is saturated for a small field strength. Transformer T is usually provided with a shunt magnetic circuit having an air gap, as well as the magnetic circuit carrying the primaries and secondaries. The design in principle of such a transformer can also be seen in Fig. 3.

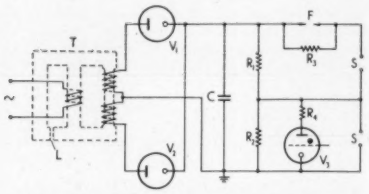

Fig. 3. Circuit diagram of the electronically controlled, high-precision, spectroscopic spark source. The sparking frequency per second is twice the mains frequency

The operational principle of transformer T of Fig. 3 is illustrated in Fig. 4, where curve a signifies the magneto-motive force of the primary, curve b the flux in the iron core of the secondary, curve c the secondary voltage, curve d the rectified voltage pulses, and curve e the voltage at the terminals of capacitor C of Fig. 3. Hence with the aid of the circuit illustrated in Fig. 3, voltage pulses of short duration at twice mains frequency can be produced, and the capacitor C charged and discharged correspondingly.

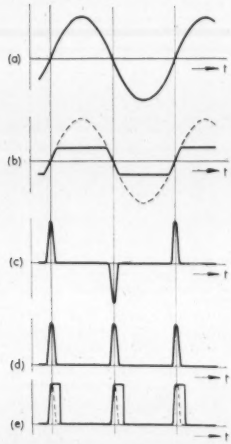

Fig. 4. Production of voltage pulses with the aid of a transformer of special design and the theoretical voltage curve at the terminals of capacitor C of Fig. 3

The effective voltage at the terminals of capacitor C of the spark source illustrated in Fig. 3, is shown by the cathode-ray oscillogram of Fig. 5. The sparking frequency is 100/s. Looking along the time base from left to right, the capacitor is charged up and then discharges suddenly. The voltage-free interval between the individual charging and discharging processes can easily be observed.

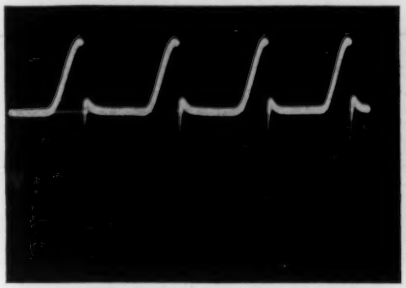

Fig. 5. Cathode-ray oscillogram showing the voltage at the terminals of the capacitor C of Fig. 3. $C = 0{\cdot}05\ \mu$F. Charging voltage = 20000 V

THE APPLICATION OF THE SOURCE FOR TIME-RESOLVED SPECTROCHEMICAL ANALYSIS

The spark source described here can be used for conventional spectroscopic work, but owing to its high operational precision is particularly suitable for the production of time-resolved spectra. The source can be applied for producing time-resolved spectra with the aid of rotating mirrors[5–8] or rotating disks.[10] In the present case the applicability to time-resolved spectroscopy is illustrated with the aid of the rotating disk. The disk, the layout of which is seen in Fig. 6, is placed directly before the slit S of the

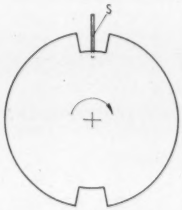

Fig. 6. Rotating disk placed before the slit of the spectrograph in order to screen out light arising from the initial period of the spark discharge

spectrograph. The phase of the disk is set so as to prevent the radiation arising from the initial part of the spark discharge entering the spectrograph. The amount screened can be electronically controlled. This problem will be dealt with in more detail elsewhere. One part of the slit of the spectrograph has been left free, so that in that part all the light arising from the spark discharge enters the spectrograph, and two spectra are produced; one containing the total radiation with the background, and the other containing radiation from the later time range of the spark discharge, which is usually background-free. In this way, exposures suitable for comparison purposes can be made. From one

of the spectra without screening the usual evaluation can be carried out, whereas from the other time-resolved spectrum one obtains a spectrum which essentially contains only arc lines without background. A set of spectra of this kind is illustrated in Fig. 7, which shows part of the spectrum of aluminium containing impurities with the lines manganese 2933, 2939 and 2949. For the upper spectrum photograph the phase of the rotating disk of Fig. 6 was set so that light emitted during the whole duration of spark discharges entered the spectrograph. In each succeeding spectrum about 4 μs more is cut from the initiation of the spark discharge. In each exposure only the half of the slit is screened by the rotating disk. In the double spectra, the upper spectra are identical with the first spectrum. From Fig. 7 it can be seen that the longer the screening from the start of the spark discharge, the greater is the extent the background vanishes.

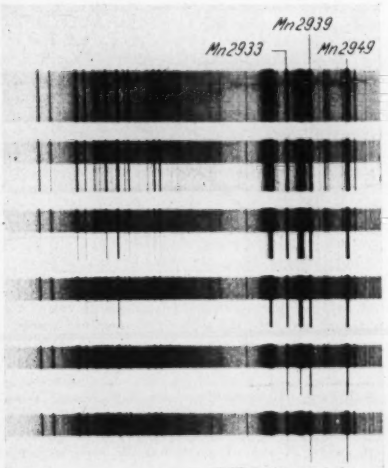

Fig. 7. Spectra resolved in time with the aid of the disk rotating before the slit of the spectrograph. In the upper spectrum and for the upper part of the double spectra the total light of the spark discharge enters the spectrograph. In each following lower spectrum an additional time of 4 μs has been screened from the spectrum

In order to see whether this electronically controlled, high-precision spark source and rotating disk were applicable for spectrochemical analyses, reproducibility tests and working curves have been made. In Table 1 the working conditions, and in Table 2 reproducibility results obtained with aluminium containing impurities, are illustrated.

The working curves made with the working conditions given in Table 1 are illustrated in Fig. 8 for the determination of manganese, copper, silicon and iron in aluminium. In each part of Fig. 8 there are two working curves. The lower one is based on the line-intensity ratios formed in the background-free, time-resolved spectrum. In these spectra about 14 μs was cut off from the beginning of the spark discharge. The second curve gives in the usual way the working curves to be obtained with spectra not resolved in time. In Fig. 8 $+Bg$ represents the spectrum with background, $-Bg$ the spectrum without background.

Table 1. *Spectrographic working conditions*

Capacitance value (C, Fig. 3)	0·01 μF
Charging voltage of C	20000 V
Self-inductance of discharge circuit	residual self-inductance of leads
Discharge frequency	100/s
Frequency of the discharge circuit	approximately 0·5 M Hz
Total duration of one discharge	approximately 45 μs
Analytical spark gap	3 mm
Form of electrodes	3 mm diameter cylindrical
Spectrograph	Hilger E 478 autocollimating
Spectrograph slit width	30 μ
Photographic emulsion	Agfa blau rapid
Exposure time	60 s
Pre-sparking time	60 s
Rotation of the screening disk	3000 rev/min
Screened out from the beginning of the spark discharge	approximately 14 μs
Developer	high-speed Kodak D 19
Developing	time 3 min
Developing	temperature 18° C

Table 2. *Reproducibility results for the determination of impurities of aluminium with the aid of time-resolved spark spectra*

The average deviation was obtained from ten measurements

Element	*Average deviation (%)*	*Lines used*	*Percentage of impurities in the sample*
Cu	2·58	Cu 3274/Al 3064	0·01
Mn	1·58	Mn 2949/Al 3064	0·115
Si	1·64	Si 2519/Al 3064	0·57
Mg	2·65	Mg 2791/Al 3064	0·11
Fe	1·76	Fe 2599/Al 3064	0·11
	Average 2·04		

The observation of Fig. 8 shows unambiguously that the working curves made with the aid of time-resolved spectra are better than those made in the usual way. For instance in Fig. 8, for the determination of manganese and copper below 0·01%, the usual working curves are of little use, whereas with time-resolved spectra the determination of even smaller percentages is possible.

The reproducibility obtained is summarized in Table 2. The results of this table show that analytical results, obtained by increasing the analytical sensitivity with the sources described here and with the time-resolved spectra produced with the aid of a rotating disk, may be favourably compared with the best other results.

REFERENCES

(1) Bardócz, Á. *Nature (London)*, **171**, p. 1156 (1953).
(2) Bardócz, Á. *Acta Phys. Hungar.*, **4**, p. 91 (1954).
(3) Bardócz, Á. *Spectrochim. Acta*, **7**, p. 307 (1955).
(4) Bardócz, Á. *Acta Tech. Hungar.*, **8**, p. 99 (1954).

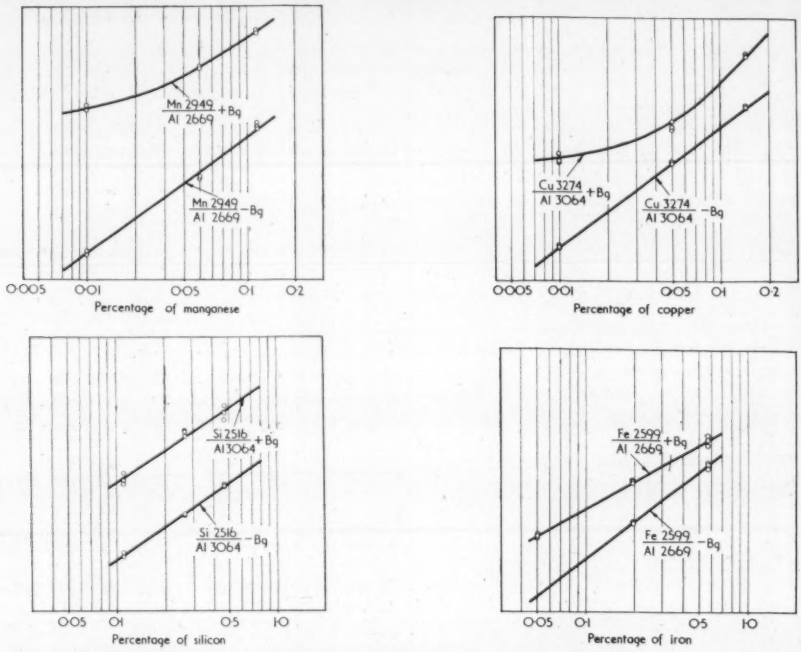
Mn 2949 / Al 2669 + Bg
Mn 2949 / Al 2669 − Bg
0·005 0·01 0·05 0·1 0·2
Percentage of manganese
Cu 3274 / Al 3064 + Bg
Cu 3274 / Al 3064 − Bg
0·005 0·01 0·05 0·1 0·2
Percentage of copper
Si 2516 / Al 3064 + Bg
Si 2516 / Al 3064 − Bg
0·05 0·1 0·5 1·0
Percentage of silicon
Fe 2599 / Al 2669 + Bg
Fe 2599 / Al 2669 − Bg
0·05 0·1 0·5 1·0
Percentage of iron

Fig. 8. Working curves for the determination of impurities in aluminium with the aid of time-resolved spectra. $+Bg$ indicates the working curve made from the background containing spectrum, $-Bg$ the curve from the background-free spectrum

(5) Bardócz, Á. *Appl. Spectrosc.*, **10**, p. 183 (1956).
(6) Bardócz, Á. *Z. Angew Phys.*, **9**, p. 82 (1957).
(7) Bardócz, Á., and Varsányi, F. *Z. Naturforsch.*, **10**a, p. 1031 (1955).
(8) Bardócz, Á., and Varsányi, F. *Nature* (*London*), **177**, p. 222 (1956).
(9) Bardócz, Á. *Appl. Spectrosc.*, **11**, p. 167 (1957).
(10) Bardócz, Á., and Tabeling, R. W. To be published.

Transient temperature rise due to a line source in a semi-infinite medium, with a radiation boundary condition at the interface

By H. Goldenberg, M.Sc., Electrical Research Association Laboratory, Leatherhead, Surrey

[*Paper received* 18 *December*, 1958]

The problem of the transient temperature rise due to a line source in a semi-infinite medium, with a radiation boundary condition at an interface parallel to the line source, is solved in the present paper. An approximate formula and an error bound are given for the deviation between this solution and the solution subject to an isothermal boundary condition at the interface. A condition is given for the validity of Neher's approximate formula for the steady-state temperature. In a typical example it is shown that the temperature rise above ambient at the surface of a buried cable differs negligibly when the two types of boundary condition are assumed valid at the earth's surface.

1. Introduction

In normal cable engineering practice the current rating of a cable laid direct in the ground is based on the simplifying assumption that the soil surface is an isothermal. This assumption is known to be an approximation, and its falseness can occasionally be seen when, under frost conditions, there is an absence of frost along a cable route. It is therefore a matter of importance to consider whether the current ratings are materially affected if a radiation boundary condition is assumed to hold at the soil surface in place of the less accurate isothermal condition.

No results appear to have been obtained for the transient

temperature rise due to a buried cable when a radiation boundary condition is assumed to hold at the soil surface, although the steady-state temperature rise under this condition has been studied by Neher.[1] Neher derived an approximate formula from a complex integral solution of the steady-state problem by Poritsky,[2] as the latter solution was not readily expressible in terms of tabulated functions. In the discussion on Neher's paper, Dwight pointed out that Neher's solution was inadequate, as it was based on the approximate sum of an infinite series, the convergence of which was unsatisfactory.

More recently the author has derived a method for the calculation of cyclic rating factors[3] to permit the calculation of the maximum applied current which, when in the form of a known daily repetitive cycle, gives rise to a specified maximum conductor temperature. These calculations have been based on the assumption that the soil surface is an isothermal, but the question has arisen as to what extent the transient behaviour at the cable surface is affected by the modified boundary condition at the soil surface. For the times of most interest, namely for two or more hours after the application of a load, the thermal capacity of the cable is negligible for British Standard cables, and the temperature rise may be considered as due to a line source at the cable centre. With the assumption that the temperature rise produced by the line source is proportional to the square of the applied current, the system is linear, and the fundamental problem for solution is the transient temperature rise due to a line source in a semi-infinite medium with a radiation boundary condition at the interface. This problem is solved in the present paper.

2. BASIC THEORY

The Green's function u_1 giving the temperature at time t at (x, y, z) due to a unit instantaneous point source at an earlier time τ at (x', y', z') in a semi-infinite medium of thermal diffusivity D, initially at zero temperature, and with radiation at the boundary $x = 0$, into a medium at zero temperature, namely $(\partial u_1/\partial x) = hu_1$ at $x = 0$, has been given by Carslaw and Jaeger.[4] The integration of u_1 with respect to z' from $z' = -\infty$ to $z' = +\infty$, followed by the integral of the result with respect to τ from $\tau = 0$ to $\tau = t$, then gives the temperature u at time t at (x, y, z) due to a unit continuous line source introduced at $t = 0$, where the line source passes through (x', y') and is parallel to the z axis, and where there is radiation at the boundary $x = 0$ into a medium at zero temperature. The temperature u is then given by:

$$u = \int_0^t \left(\frac{1}{4\pi Dt'}\left[\exp\left\{-\frac{(x-x')^2}{4Dt'}\right\} + \exp\left\{-\frac{(x+x')^2}{4Dt'}\right\}\right] \times \exp\left\{-\frac{(y-y')^2}{4Dt'}\right\} - \frac{h}{2(\pi Dt')^{1/2}}\operatorname{erfc}\left\{\frac{x+x'}{2(Dt')^{1/2}} + h(Dt')^{1/2}\right\} \times \exp\left\{h(x+x') + Dh^2t' - \frac{(y-y'^2)}{4Dt'}\right\}\right)dt'$$

where

$$(\partial u/\partial x) = hu \quad \text{at} \quad x = 0$$

and

$$\operatorname{erfc} X = (2/\sqrt{\pi})\int_X^\infty \exp(-v^2)dv \qquad (1)$$

Denote r_1 and r_2 as the distances from (x, y) to (x', y') and $(-x', y')$ respectively, so that:

$$r_1^2 = (x-x')^2 + (y-y')^2; \quad r_2^2 = (x+x')^2 + (y-y')^2$$

With the substitutions $X = h^2Dt'$ and $T = h^2Dt$, equation (1) then simplifies to:

$$u = \frac{1}{4\pi D}\{-Ei(-r_1^2/4Dt) - Ei(-r_2^2/4Dt)\} - \frac{1}{2\sqrt{\pi D}}\int_0^T \frac{dX}{X^{1/2}}\operatorname{erfc}\left\{\frac{h(x+x')}{2X^{1/2}} + X^{1/2}\right\} \times \exp\left[h(x+x') + X - \{h^2(y-y')^2/4X\}\right]$$

where

$$-Ei(-X) = \int_X^\infty \frac{\exp(-v)}{v}dv \qquad (2)$$

On integration by parts it may be shown that:

$$\operatorname{erfc} Y = \frac{1}{\sqrt{\pi}}\frac{\exp(-Y^2)}{Y} - \frac{1}{\sqrt{\pi}}\int_Y^\infty \frac{\exp(-y^2)}{y^2}dy$$

When this substitution is made in the final integral of equation (2), one obtains, after some manipulation

$$4\pi Du = -Ei(-r_1^2/4Dt) + Ei(-r_2^2/4Dt) - 2\exp(c)\,Ei\left\{-\left(\frac{r_2^2}{4Dt} + c\right)\right\} + \int_0^T \frac{dX}{\sqrt{X}}\left\{2\int_Y^\infty \frac{\exp(-y^2)}{y^2}dy\right\}\exp\{Y^2 - (h^2r_2^2/4X)\}$$

where

$$Y = \frac{h(x+x')}{2\sqrt{X}} + \sqrt{X} \quad \text{and} \quad c = hr_2^2/2(x+x') \qquad (3)$$

The solution to the identical heat conduction problem, but with the radiation boundary condition at $x = 0$ replaced by an isothermal boundary condition, is given when only the first two terms on the right-hand side of equation (3) are present.

The steady-state temperature distribution is obtained by letting $t \to \infty$ in equation (3), making use of the expansion

$$-Ei(-x) = -\gamma - lnx + \frac{x}{1.1!} - \frac{x^2}{2.2!} + \ldots,$$

where γ = Euler's constant = 0·5772 . . . , prior to taking the limiting value of the first two terms for u. One can then obtain

$$\underset{t\to\infty}{Lt}\, 4\pi D\, u = 2ln(r_2/r_1) - 2\exp(c)\,Ei(-c) + \int_0^\infty \frac{dX}{\sqrt{X}}\left\{2\int_Y^\infty \frac{\exp(-y^2)}{y^2}dy\right\}\exp\{Y^2 - (h^2r_2^2/4X)\} \qquad (4)$$

Only the first term of the right-hand side of equation (4) is present if the radiation boundary condition is replaced by an isothermal boundary condition.

An upper bound on the infinite integral in equation (4) can be obtained, on integration by parts, as

$$2\exp(Y^2)\int_Y^\infty \frac{\exp(-y^2)}{y^2}dy = \frac{1}{Y^3} - 3\exp(Y^2)\int_Y^\infty \frac{\exp(-y^2)}{y^4}dy < \frac{1}{Y^3}$$

so that the infinite integral in equation (4) is less than

$$\int_0^\infty \frac{dX}{\sqrt{X}}\frac{1}{Y^3}\exp(-h^2r_2^2/4X) \quad \text{where} \quad Y = \frac{h(x+x')}{2\sqrt{X}} + \sqrt{X}$$

The substitution $u = h^2r_2^2/4X$ in the latter integral, followed

by $w = u + c$, gives a more convenient form for the upper bound on the infinite integral, namely

$$\frac{4c^3 \exp(c)}{h^2 r_2^2} \int_c^\infty \frac{\exp(-w)}{w^3}\, dw = \frac{2c^3}{h^2 r_2^2}\left[\exp(c)\left\{-Ei(-c)\right\} - \frac{1}{c} + \frac{1}{c^2}\right] \quad (5)$$

A simpler but less accurate upper limit is obtained by replacing the denominator w^3 of the integrand by c^3, giving an upper bound to the infinite integral of $4/h^2 r_2^2$.

When the upper bound (5) on the infinite integral is negligible compared to $2ln(r_2/r_1) - 2\exp(c)Ei(-c)$, then the finite integral in equation (3), which is less than the infinite integral, can also be neglected, and the transient temperature u is given approximately by

$$u \simeq \frac{1}{4\pi D}\left[-Ei\left(\frac{-r_1^2}{4Dt}\right) + Ei\left(\frac{-r_2^2}{4Dt}\right) - 2\exp(c)Ei\left\{-\left(\frac{r_2^2}{4Dt} + c\right)\right\}\right] \quad (6)$$

while the steady-state temperature is given approximately by

$$u(\infty) = \frac{1}{2\pi D}\left\{ln\left(\frac{r_2}{r_1}\right) - 2\exp(c)\, Ei(-c)\right\} \quad (7)$$

When the upper bound (5) on the infinite integral is not negligible compared to $2ln(r_2/r_1) - 2\exp(c)Ei(-c)$, numerical integration may be applied directly to evaluate the integrals in equations (3) and (4), as

$$2\exp Y^2 \int_Y^\infty \frac{\exp(-y^2)}{y^2} dy = \frac{2}{Y} - \frac{4\,\mathrm{erfc}\, Y}{(2/\sqrt{\pi})\exp(-Y^2)} \sim \frac{1}{Y^3} - \frac{1.3}{2Y^5} + \frac{1.3.5}{2^2 Y^7} - \quad (8)$$

and extensive tables[5] exist for the functions erfc Y and $(2/\sqrt{\pi})\exp(-Y^2)$. For large values of c a further approximation can be obtained for the steady-state temperature $u(\infty)$, as

$$\exp(c)\{-Ei(-c)\} \sim \frac{1}{c} - \frac{1}{c^2} + \frac{2!}{c^3} - \frac{3!}{c^4} + \ldots,$$

giving

$$u(\infty) \simeq \frac{1}{2\pi D}\left\{ln\left(\frac{r_2}{r_1}\right) + \frac{1}{c}\right\} \quad (9)$$

as the infinite integral is then negligible for points in the vicinity of the line source.

Equation (9) has been used by Neher[1] to determine the steady-state temperature in the neighbourhood of a buried cable with a radiation boundary condition at the earth's surface. For greater accuracy Neher replaced the term $1/c$ in equation (9) by $0{\cdot}95/c$ in order to take account of higher inverse powers of c, but did not seem to realize the limitation on equation (9) for small values of c.

In the above calculation the temperature due to a unit continuous line source is the temperature due to a steady supply of heat at the rate $\rho\alpha$ heat units per unit length per unit time,[4] where ρ is the density and α the specific heat of the medium. When heat is supplied at the constant rate q heat units per unit length per unit time, each of the temperatures given by the above formulae should be multiplied by $q/\rho\alpha$, i.e. by Dgq, where g is the thermal resistivity of the medium.

3. EXAMPLE

A 3 in. diameter cable is laid direct in the ground at a depth of cable axis below ground surface of 36 in. The cable is under a steady load producing a cable loss of 0·75 W/cm from time $t = 0$. Find the steady-state temperature rise, and the ratio of transient to steady-state temperature rise, at the upper surface of the cable for subsequent times sufficiently large for the cable to be assumed as a line source at the cable centre. The soil constants can be assumed as follows: thermal resistivity $g = 60°$ C cm/W, thermal diffusivity $D = 0{\cdot}01$ cm^2/s and surface resistivity $\beta = 2000°$ C cm^2/W. (A conservative value given by Neher.[1])

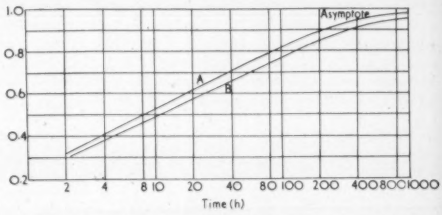

Ratio of transient to steady-state temperature rise at upper surface of cable

Curve *A*, ground surface assumed isothermal; curve *B*, ground surface resistivity included.

From the given soil constants $h = g/\beta = 0{\cdot}03$ cm^{-1}. From the geometrical configuration involved $r_2 = 70{\cdot}5$ in., $r_1 = 1{\cdot}5$ in. and $c = hr_2/2$. Therefore, $c = 2{\cdot}69$ and, from equation (4) and from the change of line source strength indicated in the last paragraph of Section 2,

$$4\pi u(\infty) = 60 \times 0{\cdot}75 \times (8{\cdot}27 + \text{infinite integral}).$$

An upper bound on the infinite integral is given by equation (5), and is 0·071, so that an error of less than 1% is obtained by neglecting the infinite integral. The steady-state temperature rise above ambient at the upper surface of the cable is therefore 29·6° C, with an error of less than 1%. When the soil surface is assumed isothermal this temperature rise is reduced by 2·0° C, i.e. by 7% of its value. The required ratio of transient to steady-state temperature rise at the upper surface of the cable is given by equations (6) and (7), and is plotted in the figure together with the corresponding ratio when the soil surface is regarded as an isothermal.

It will be observed that there is little difference between the transient curves or between the steady-state temperature rises, confirming the adequacy of the assumption that the soil surface is an isothermal in this case. For American cables the external cable diameter is frequently much greater than 3 in., and the validity of the isothermal assumption would need confirmation under the soil conditions in practice.

The steady-state temperature rise at the soil surface immediately above the cable can readily be shown to lie between 3·4 and 3·9° C, namely the values given by equation (4) when the infinite integral is (*a*) neglected and (*b*) replaced by its upper bound (5).

ACKNOWLEDGEMENT

The author wishes to express his thanks to the Director of the Electrical Research Association for permission to publish this paper.

REFERENCES

(1) NEHER, J. H. *Trans Amer. Inst. Elect. Engrs*, **68** (1), p. 9 (1949).
(2) PORITSKY, H. *Bull. Amer. Math. Soc.*, **43**, p. 873 (1937).
(3) GOLDENBERG, H. *Proc. Instn Elect. Engrs*, **104** (C), p. 154 (1957).
(4) CARSLAW, H. S., and JAEGER, J. C. *Conduction of Heat in Solids*, p. 308 (London: Oxford University Press, 1947).
(5) *Tables of Probability Functions*, **1** (New York: National Bureau of Standards, 1941).

Studies of the viscosity and sedimentation of suspensions

Part 5.—The viscosity of settling suspensions of spherical particles*

By D. R. OLIVER, Ph.D., and Prof. S. G. WARD, Ph.D., D.I.C., Department of Mining, University of Birmingham

[*Paper received 7 January*, 1959]

A description is given of a series of viscosity measurements on upward- and downward-settling suspensions of spherical particles, in which an efflux type capillary-tube viscometer was employed.

It is shown that the viscosity characteristics of settling suspensions are related to those of corresponding suspensions which do not settle, termed "stable suspensions." The degree of instability of the settling suspensions has a well-defined effect on the viscosity-concentration relationships. The measured values of the viscosity are shown to be modified by a form of wall effect, similar to that encountered during measurements on stable suspensions of spherical particles.(7) The magnitude of the wall effect, however, changes with the degree of instability of the suspensions, and in one case varies also with the volume concentration of solids present.

The final values of the relative viscosity, corrected for wall effect, are shown to be related to the volume concentration by a single type of equation, which is closely related to the one which applies to stable suspensions of spherical particles.(7)

The influence of concentration, particle size and particle shape on the viscosity of stable suspensions of solids in liquids has been investigated by a number of workers.(1–7) Little is known, however, about the viscosity characteristics of suspensions in which the solid phase settles, either upwards or downwards, in the absence of adequate agitation. An instrument suitable for measuring the viscosities of such suspensions has been described by DeVaney and Shelton,(5) who made a series of measurements on aqueous suspensions of irregularly-shaped mineral particles using a specially designed downward-flow type of capillary-tube viscometer, which they called a "consistometer". The behaviour of this instrument appeared to be satisfactory, but the results published do not allow effects due to particle settling and effects due to particle shape to be differentiated; the possibility of a wall effect was not taken into account.

In the work now described a suspended level, efflux type capillary-tube viscometer was used, the object of the investigation being to find the influence of the departure from stability of suspensions of spherical particles upon their relative viscosities.

SUSPENSIONS

The characteristics of the suspensions used are shown in Table 1. Suspensions 1, 2 and 3 were downward settling; suspension 4 was upward settling.

In order to inhibit flocculation, approximately 0·01% of a dispersing agent (Dispersol O.G., by Imperial Chemical Industries Ltd.) was added to all suspensions.

Table 1. *Characteristics of the suspensions used*

Suspension No.	*Material*	*Size range (μ)*	*Suspending liquid*	*Density of solid phase minus density of liquid phase (g/ml.)*
1	Kallodoc*	53–76	Water	0·196
2	Kallodoc	53–76	Ethyl alcohol and water	0·382
3	Glass	62–100	Glycerol and water	1·816
4	Kallodoc	53–76	Solution of lead nitrate in water	−0·209

* A methyl methacrylate polymer.

The efflux type capillary-tube viscometer. The viscosities of the suspensions were measured by means of the capillary-tube viscometer described in an earlier communication.(7) The greatest error in the measured relative viscosities was of the order 2%.

EXPERIMENTAL METHOD

The measurement of viscosity was carried out in a manner similar to that used for stable suspensions.(7) The original stirrer was found to homogenize the Kallodoc suspensions satisfactorily, but the suspensions of glass spheres tended to settle in the upper reservoir; this was prevented by the addition of two small vanes to the stirrer blade. In each case the viscosity of the dispersing liquid was measured under the same conditions of temperature and stirrer speed as those used for the suspension. Corrections of the type suggested by Vand(2) were not applied to the measured volume concentrations, which were obtained by drying and weighing the particles present in a typical sample of the suspension flowing through the capillary tube.

The viscosities of the suspensions were measured at intervals of concentration of approximately 5% in tubes of diameter 1 and 2 mm, except for suspensions of type No. 2, where

* Parts 1 and 2 of this paper, "The viscosity of suspensions of spherical particles" and "The viscosity and sedimentation of suspensions of rough powders" were published on pp. 286 and 325 of Vol. 1 (1950) of this *Journal*. Part 3, "The sedimentation of isometric and compact particles," was published on p. 83 of Vol. 6 (1955) of this *Journal*. Part 4, "Capillary-tube viscometry applied to stable suspensions of spherical particles," was published on p. 372 of Vol. 9 (1958) of this *Journal*.

the wider tube only was used. The measured viscosity of each suspension was divided by the viscosity of the dispersing liquid to give the apparent relative viscosity of the suspension appropriate to the size of the tube used.

It may be noted that, for settling suspensions, relative viscosities based on the use of dynamic viscosities η, differ from those based on kinematic viscosities η/ρ, where ρ is the density of the suspensions. This is due to the fact that both η and ρ are functions of the volume concentration of solids present. In the present work all relative viscosities mentioned are relative dynamic viscosities, whilst the density ρ of the suspension is taken as

$$\rho = c\rho_s + (1 - c)\rho_l \qquad (1)$$

where ρ_s = density of solid phase,
ρ_l = density of liquid phase,

and c = volume concentration of solid present.

RESULTS

(i) *Downward settling suspensions* (Nos. 1, 2 and 3). Measured values of the relative viscosity are given in Table 2, whilst values corrected for wall effect are listed in Table 3.

Table 2. *Measured values of the relative viscosity*

Suspension No.	1		2		3		4	
Capillary-tube diameter (mm)	1·0	2·0	2·0	1·0	2·0	1·0	2·0	
Volume concentration (%)								
5·0	1·13	1·15	1·14	1·13	1·16	1·09	1·09	
10·0	1·28	1·31	1·30	1·27	1·33	1·23	1·23	
15·0	1·45	1·52	1·50	1·42	1·51	1·42	1·42	
20·0	1·68	1·81	1·76	1·60	1·75	1·65	1·68	
25·0	1·98	2·22	2·13	1·85	2·08	1·97	2·06	
30·0	2·45	2·86	2·67	2·26	2·56	2·47	2·66	
35·0	3·27	3·85	3·62	3·27	3·36	3·32	3·70	
40·0	—	—	—	—	—	—	—	
Value of D/r	0·72		—	0·80		0·36		

Table 3. *Values of the relative viscosity corrected for wall effect*

Suspension No.	1		2		3		4	
Capillary-tube diameter (mm)	1·0	2·0	2·0	1·0	2·0	1·0	2·0	
Volume concentration (%)								
5·0	1·17	1·16	1·16	1·18	1·18	1·09	1·09	
10·0	1·36	1·36	1·34	1·39	1·39	1·25	1·24	
15·0	1·60	1·60	1·58	1·63	1·63	1·48	1·45	
20·0	1·95	1·96	1·91	1·96	1·96	1·76	1·74	
25·0	2·50	2·52	2·40	2·49	2·44	2·17	2·17	
30·0	3·52	3·51	3·22	3·67	3·27	2·87	2·89	
35·0	6·29	5·38	4·90	—	4·95	4·27	4·26	

For suspensions 1 and 2, the measured relative viscosities η_r were plotted against the volume concentration of the solid phase, as were the quantities $(1 - 1/\eta_r)$. Fig. 1 shows the plots of $(1 - 1/\eta_r)$ against volume concentration for suspensions of Kallodoc in water. These lines differ from the corresponding curves for stable suspensions in that they show curvature towards the concentration axis at values of the concentration below 10%, but are straight lines for concentrations between 10 and 30%. At higher concentrations curvature similar to that described in a previous communication[7] dealing with stable suspensions appears. The straight regions of the curves may be produced backwards to meet the $(1 - 1/\eta_r)$ axis at a positive point; a larger positive intercept is obtained from the results for suspensions of Kallodoc in an alcohol-water mixture.

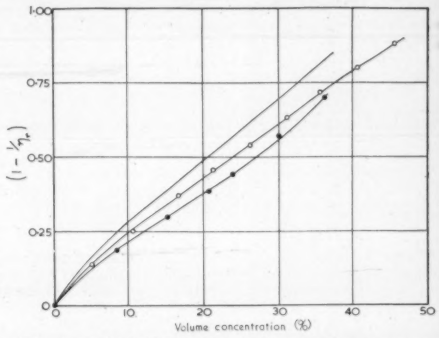

Fig. 1. Relationships between $(1 - 1/\eta_r)$ and volume concentration for suspensions of Kallodoc in water

——— = corrected viscosities.
○ = tube 2 mm diameter.
● = tube 1 mm diameter.

The separation of the lines appropriate to the 1 and 2 mm diameter tubes showed that a wall effect was present, the magnitude of which was comparable with that obtained for stable suspensions of spherical particles. The thickness D of Vand's hypothetical layer of pure liquid[2] was calculated for suspensions of type No. 1, using the method outlined in a previous paper.[7] For volume concentrations below 30% the value was steady and equal to $D = 0{\cdot}72\,r$, where r is the mean radius of the spherical particles. This may be compared with the corresponding value $D = 0{\cdot}70\,r$ obtained for stable suspensions of spherical particles.

The experimental values of the relative viscosity obtained for suspensions 1 and 2 were corrected for wall effect using the figure $D = 0{\cdot}72\,r$, giving corrected curves of the quantities $(1 - 1/\eta_r)$ against volume concentration which were of similar form to those obtained from the experimental quantities (Fig. 1). The equations of these curves and the values of the constants will be discussed at a later stage.

The results obtained for the more rapidly settling suspensions of glass spheres, No. 3, were plotted in similar manner to the above. Fig. 2 shows the relationships between the measured relative viscosities η_r and the volume concentration; Fig. 3 shows the corresponding curves for the quantities $(1 - 1/\eta_r)$. It is noteworthy that the curves in Fig. 3 show marked curvature at the lower concentrations and then become straight, whereas the curves in Fig. 2 are almost straight at the lower concentrations and then curve quite rapidly upwards. This behaviour is reminiscent of the graphs of DeVaney and Shelton[5] for unstable suspensions of irregularly shaped mineral particles.

The curves showed effects attributable to a wall layer, the thickness of which was calculated as $D = 0{\cdot}80\,r$ for volume concentrations below 25%. The final values of η_r and $(1 - 1/\eta_r)$, corrected for wall effect, are included in Figs. 2 and 3; the final relationship shown in Fig. 3 is of similar

form to that obtained for suspensions of types Nos. 1 and 2. On producing the linear section backwards, a positive intercept was obtained on the axis of $(1 - 1/\eta_r)$, the magnitude of which was greater than that obtained for either of the previous types of suspension.

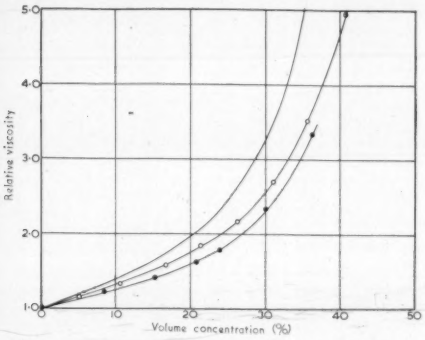

Fig. 2. Relationships between relative viscosity and volume concentration for suspensions of glass spheres in glycerol-water

——— = corrected viscosities.
○ = tube 2 mm diameter.
● = tube 1 mm diameter.

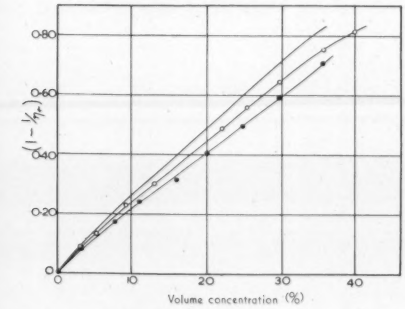

Fig. 3. Relationships between $(1 - 1/\eta_r)$ and volume concentration for suspensions of glass spheres in glycerol-water

——— = corrected viscosities.
○ = tube 2 mm diameter.
● = tube 1 mm diameter.

The values of K, the gradient of the straight line sections K_1, the intercept on the axis of $(1 - 1/\eta_r)$ and D/r are summarized for all four types of settling suspension in Table 4. The corresponding figures for stable suspensions having the same particle size[7] are added for comparison.

(ii) *Upward settling suspensions* (No. 4). Values of the measured relative viscosity η_r and the quantity $(1 - 1/\eta_r)$ were plotted against volume concentration, the latter curves being shown in Fig. 4. Straight lines were again produced over most of the concentration range, but there were two significant differences from the above-described results.

Table 4. *Values of K, K_1 and D/r for stable and settling suspensions of spherical particles*

Suspension No.	Density difference of solid and liquid phases $(\rho_s - \rho_l)$	$\frac{\rho_s - \rho_l}{\eta_0}$*	K	K_1	D/r
(3)	1·816	0·460	2·06	0·078	0·80
(2)	0·382	0·251	2·18	0·041	—
(1)	0·196	0·196	2·31	0·026	0·72
Stable	0·000	0·000	2·46	0·000	0·70
(4)	−0·209	−0·136	2·28	−0·030	0·36

* η_0 = viscosity of dispersing liquid.

Firstly, negative intercepts were obtained on the axis of $(1 - 1/\eta_r)$ when the linear parts of the graphs were produced backwards. Secondly, points obtained from measurements in the 1 and 2 mm diameter tubes respectively lay on the same line at concentrations of less than 15%. This indicated that the wall effect was insignificantly small over this range of concentrations.

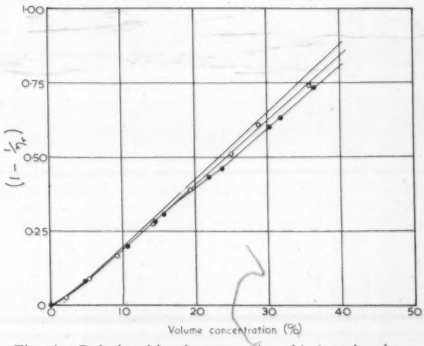

Fig. 4. Relationships between $(1 - 1/\eta_r)$ and volume concentration for suspensions of Kallodoc in lead nitrate solution

——— = corrected viscosities.
○ = tube 2 mm diameter.
● = tube 1 mm diameter.

In the range of concentration from 25 to 35%, the thickness of the wall layer was sensibly constant and equal to $D = 0{\cdot}36$ r. It therefore appears that, for viscosities measured in a downward-flow type of capillary-tube viscometer, the wall effect for upward-settling suspensions is very much smaller than that obtained from the other types of suspension.

The measured values of the relative viscosity obtained in the 2 mm diameter tube were corrected by using a value of D equal to $0{\cdot}36$ r, giving a final graph of $(1 - 1/\eta_r)$ against concentration which was straight between the concentrations of 5 and 35%. This line also gave a negative intercept when produced backwards to meet the axis of $(1 - 1/\eta_r)$ (Table 4).

DISCUSSION OF RESULTS

For each suspension examined in the present work, the relationship between the relative viscosity η_r and the volume concentration of the solid phase c may be represented by the equation

$$1 - 1/\eta_r = Kc + K_1 \qquad (2)$$

provided $0{\cdot}10 < c < 0{\cdot}30$. Values of the constants K and

K_1 are listed in Table 4. The quantity K_1 is either positive or negative according as the suspensions are downward or upward settling respectively. Equation (2) may be expanded to give η_r as

$$\eta_r = (1 + K_1) + (1 + 2K_1)Kc + (1 + 3K_1)K^2c^2 \ldots \quad (3)$$

with the same limitation on c. This equation reduces to that obtained for stable suspensions of spherical particles,[7, 8] when K_1 becomes zero. The formation of the intercept K_1 therefore appears to be a characteristic of a settling suspension of spherical particles.

For concentrations below 10%, the relative viscosity of downward-settling suspensions may be represented by the equation

$$\eta_r = 1 + K_2c \quad (4)$$

The constant K_2 is equivalent to the Einstein constant for stable suspensions of spherical particles (2·50), but the value now ranges from 3·00 for Kallodoc in water to 3·60 for the more unstable suspensions of glass spheres in a glycerol-water dispersing liquid. For upward-settling suspensions the above type of equation breaks down at concentrations below 2%, K_2 being as low as 1·2 for suspensions of type 4. Thus it appears that K_2 is very sensitive to changes in the stability of the suspensions; its value as a criterion is diminished, however, by difficulty of measurement, since the manner in which the curves are drawn near the origin markedly affects the value obtained.

The present work indicates that the magnitude of the intercept K_1 is closely related to the degree of instability of the suspension under examination. This is illustrated in Fig. 5, where K_1 is plotted against the quotient $(\rho_s - \rho_l)/\eta_0$, a quantity proportional to the settling rate of the suspensions,

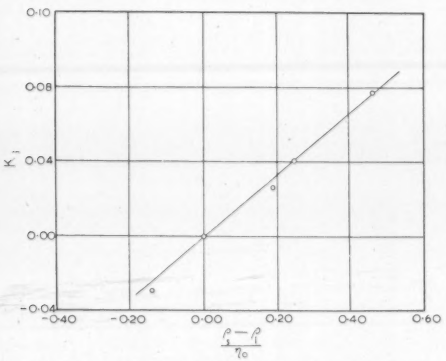

Fig. 5. Relationship between the intercept K_1 and the quotient $(\rho_s - \rho_l)/\eta_0$ for unstable suspensions of spherical particles

at constant concentration and particle size. An approximately linear relationship holds between these quantities for the suspensions used, but it should be pointed out that the line may not be capable of extrapolation to a point where it might include suspensions of dense mineral particles in water $\{(\rho_s - \rho_l)/\eta_0 \simeq 4{\cdot}0\}$, even assuming that such particles were approximately spherical. The equation of the line is

$$K_1 = 0{\cdot}33\{(\rho_s - \rho_l)/\eta_0\} \quad (5)$$

The gradient K of the straight-line sections of the graphs has a maximum value for stable suspensions, despite the fact that the wall correction factor is greater for downward-settling suspensions. Thus, at a volume concentration of 30%, stable suspensions of 53–76 μ spherical particles give higher relative viscosity than either upward- or downward-settling suspensions of the same concentration.

The thickness of the hypothetical layer of pure liquid at the tube wall changes with the degree of instability of the suspensions, particularly for those which are upward settling in character. The latter variation may be due to a tendency of the slowest moving spheres close to the wall to rise against the flow of liquid, thus reducing the effect of slippage flow at the tube wall. In a typical case, for which the velocity of flow at the centre of the tube was 48·3 cm/s the velocity at a point one particle radius distant from the walls was 0·3 cm/s, whereas the upward-settling velocity of the particles was about 0·03 cm/s. It is possible that this would affect the wall-layer thickness, for if the upward-settling velocity were equal to 0·3 cm/s the particles would be almost stationary on the tube walls, and a form of wall effect might be produced which was equivalent to a solid wall layer of thickness equal to twice the particle radius. The apparent thickness of this layer would decrease with increasing volume concentration of the solid phase, as inter-particle forces tended to move the stationary particles in a downward direction. Such forces may have been responsible for the changes of wall-layer thickness noted in the present work (Fig. 4), causing the effective thickness of a normal fluid layer to be increased at increased solids concentrations.

The results obtained using downward-settling suspensions may be compared with those obtained by DeVaney and Shelton[5] and by Vand.[2] The former workers' graphs of viscosity against specific gravity for settling mineral suspensions were linear at low specific gravities; the present work suggests that this linearity was caused by the unstable character of the suspensions and not by variations of the particle shape. Vand plotted values of the quantity $(1 - 1/\eta_r)$ against volume concentration for supposedly stable suspensions of glass spheres in a zinc iodide solution. The graphs did not yield straight lines passing through the origin, however, but curves very similar to those described above for downward-settling suspensions. In view of the fact that Nandi[9] was unable to obtain stable suspensions by Vand's method, it is probable that Vand's suspensions also were not truly stable.

CONCLUSIONS

The viscosities of settling suspensions of spherical particles may readily be measured by means of an efflux type capillary-tube viscometer. Each of the suspensions behaved as a Newtonian fluid in the range of solids concentration used.

Settling suspensions of spherical particles are characterized by graphs of the quantity $(1 - 1/\eta_r)$ against volume concentration, which are straight over a considerable part of their length; when the straight section is produced backwards, positive or negative intercepts are formed on the axis of $(1 - 1/\eta_r)$ according as the suspensions are downward or upward settling respectively. The gradient of the straight lines is always less than that of corresponding lines obtained from measurements using stable suspensions.

The magnitude of the wall effect changes with the degree of instability of the suspensions. For downward-settling suspensions, the change is small and there is no tendency for the wall-layer thickness to vary with the concentration (at concentrations below 30%). For upward-settling suspensions

the change appears to be more pronounced and the wall-layer thickness also shows some variation with volume concentration. It should be emphasized that these conclusions apply to viscosities measured in a downward-flow type of capillary-tube viscometer.

The final series of relative viscosities, corrected for wall effect, may be represented by the equation

$$\eta_r = (1 + K_1) + (1 + 2K_1)Kc + (1 + 3K_1)K^2c^2 \ldots$$

when $0{\cdot}10 < c < 0{\cdot}30$ and K_1 is positive for downward-settling suspensions and negative for upward-settling suspensions.

REFERENCES

(1) EIRICH, F., BUNZL, M., and MARGARETHA, H. *Kolloid, Z.*, **74**, p. 276 (1936).

(2) VAND, V. *J. Phys. Coll. Chem.*, **52**, p. 300 (1948).

(3) WARD, S. G., and WHITMORE, R. L. *Brit. J. Appl. Phys.*, **1**, p. 286 (1950).

(4) EVESON, G. F., Ph.D. Thesis (Birmingham University, 1950).

(5) DEVANEY, F., and SHELTON, S. *U.S. Bureau of Mines, R.I.* 3469 (*R*) (1940).

(6) PRYCE-JONES, J. *Proc. Univ. Durham Phil. Soc.*, **10**, p. 427 (1947).

(7) HIGGINBOTHAM, G. H., OLIVER, D. R., and WARD, S. G. *Brit. J. Appl. Phys.*, **9**, p. 372 (1958).

(8) OLIVER, D. R., and WARD, S. G. *Nature (London)*, **171**, p. 396 (1953).

(9) NANDI, H., M.Sc. Thesis (Birmingham University, 1949).

New method for the determination of grain or crystallite size from spotty diffraction rings

By K. W. ANDREWS, D.Sc., F.Inst.P., and W. JOHNSON, M.A., Research and Development Department, The United Steel Companies Limited, Rotherham

[*Paper first received* 15 *September*, 1958, *and in final form* 23 *March*, 1959]

In contrast to previously proposed methods for determining grain size from X-ray diffraction rings which employed back-reflexion photographs, the new method uses transmission photographs. The specimen is also oscillated through a known angle. Possible confusion between Laüe and Debye–Scherrer spots is therefore avoided, and adjustment of experimental conditions to give a suitable number of spots enables a wide range of grain sizes to be covered. The angular divergence of the X-ray beam can be eliminated and the volume of specimen irradiated accurately estimated. The effects of grain-size distribution on visibility and blackening of spots are considered and a graphical method is proposed which takes account of grains at the surface and within a specimen.

Methods for the determination of grain or crystal size by counting the number of spots on an X-ray powder diffraction ring have been described in the literature.[1–3] In connexion with their work on micro-beam cameras, Hirsch and Kellar[4] and Gay and Kelly[5] also used such a method and were able to determine grain sizes in the range 1–100 μ. Back-reflexion rings were used and therefore the problem arose as to the exact depth of penetration of the X-ray beam or otherwise the irradiated volume containing the grains which have contributed to the ring. Stephen and Barnes[1] attempted to resolve this difficulty by means of a procedure involving two exposures. This was further developed by Hirsch and Kellar[4] and later Hirsch[6] gave a full analysis of the effects of grain-size distribution and other factors which might affect the accuracy.

PRINCIPLE OF NEW METHOD

It is evident that there would be some advantage if the back-reflexion arrangement could be replaced when possible by a transmission method. In this case the total irradiated volume of specimen can very easily be calculated, although the specimen must be thin enough to avoid excessive absorption of the X-rays. The method considered in this paper is therefore based on the transmission case using low-angle diffraction lines. A second feature of this method is that the specimen is oscillated about an axis perpendicular to the X-rays through an angle of a few degrees. This oscillation conveys the following advantages:

(*a*) The removal of possible confusion of Laüe spots with Debye–Scherrer spots.

(*b*) By suitable choice of collimator diameter and angle of oscillation, the number of spots on the chosen ring is sufficient to represent a reasonable number of grains (unless preferred-orientation effects arise), but not large enough to give appreciable overlapping of spots.

(*c*) In calculating the probability of reflexion, it is required to know the angular divergence of the X-ray beam. This involves certain assumptions. In the transmission case with oscillation, any error in the divergence has a relatively smaller effect on the final result because of the addition of the oscillation angle. Furthermore, the divergence can be eliminated completely by carrying out two exposures with different angles of oscillation.

BASIC FORMULA

In accordance with previous treatments,[3] it can easily be shown that the number of spots in a diffraction ring Y is given by:

$$Y = \frac{ptA}{\bar{v}} \cdot P \qquad (1)$$

where A is the area irradiated; t, the thickness of specimen; p, the planar multiplicity factor; $\bar{v}$, the mean grain volume; and P, the probability of reflexion. The experimental variables are:

(*a*) Collimator diameter.
(*b*) The effective divergence (Δ).
(*c*) Angle of oscillation (ψ).
(*d*) Thickness of specimen t.

The first two of these affect the area A, whilst the second and

third determine P. A specific choice of collimator and camera set-up defines A which can be found experimentally for each case. The calculation of P requires separate consideration.

In Fig. 1, which is a stereographic projection of the transmission method, the specimen is at C, the centre of a sphere and the direction of the incident X-ray beam is XCO. Diffracted rays lie on a cone defined by the angle 2θ with

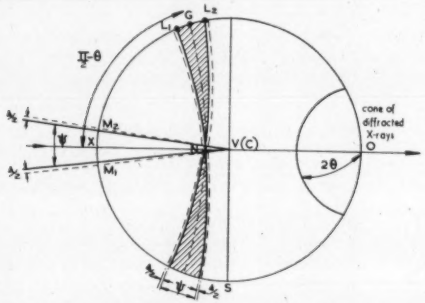

Fig. 1. Stereographic projection showing area swept out by circle of normals during oscillation. Additional area on either side of shaded area is caused by divergence of X-ray beam

CO. When diffraction occurs, the planes contributing must have normals CN tracing out a circle NG or, more exactly, a narrow band of angular width Δ (equal to the angular divergence). The angles NCX and GCX are both equal to $(\pi/2) - \theta$. By oscillating the specimen about the vertical axis VC, normals which lie on circles passing through N and through points between the limits L_1 and L_2 are brought into position of the circle NG.

Diffraction occurs when the normal to the plane meets this circle or a band $\Delta/2$ on either side of it. The total area of the sphere traced out by normals of all the possible planes that can contribute to the diffraction ring is represented by the shaded area (Fig. 1) together with the non-overlapping contributions of width $\Delta/2$ on either side.

To calculate P, the quantities represented in Fig. 2 are

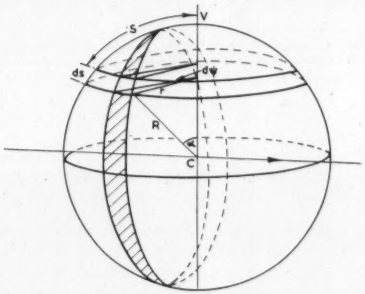

Fig. 2. Illustration of derivation of double lune-shaped area

required. The shaded area, the projection of which is shown in Fig. 1, is given by:

$$\iint r d\psi dS,$$

where r is the distance from an element of area to the vertical axis of the sphere CV. If R is the radius of this sphere, $r = R \sin \alpha$ and $dS = Rd\alpha$, where α is the angle subtended by r at the centre of the sphere.

Hence the shaded area is given by:

$$4 \int_{\pi/2}^{0} \int_{0}^{\psi} R^2 \sin \alpha . d\alpha . d\psi,$$

that is, by:

$$4R^2\psi \cos \theta.$$

The area of two belts of width $\Delta/2$ each is: $2\pi R^2 \Delta \cos \theta$. Therefore:

$$P = \frac{4R^2\psi \cos \theta + 2\pi R^2 \Delta \cos \theta}{4\pi R^2},$$

which reduces to:

$$P = \left(\frac{\psi}{\pi} + \frac{\Delta}{2}\right) \cos \theta. \tag{2}$$

Combination of the equations (1) and (2) gives:

$$Y = \frac{pt}{\bar{v}} A \left(\frac{\psi}{\pi} + \frac{\Delta}{2}\right) \cos \theta. \tag{3}$$

SIGNIFICANCE OF Δ AND $\bar{v}$ AND SOURCES OF ERROR

(i) *The divergence* Δ. Hirsch and Kellar[4] considered this quantity to consist of two parts, the first arising from the geometry of the experimental arrangement and the second from the wavelength spread of the radiation, crystal imperfection and size. The latter component cannot be calculated, but the experimental conditions are usually such that it can be eliminated or neglected. For the transmission case, it is much smaller than for the back-reflexion condition. The geometrical term requires further consideration, and it is by no means certain how precisely this can be calculated. The value required is an average of the angle—better described as a convergence angle—subtended at a grain within the irradiated area. X-rays arrive at such a grain from any point in the focal spot visible from that grain. This matter was discussed in detail by Schdanov[2] who gave a graphical method for finding the mean value. Hirsch and Kellar[3] used an average value calculated from a consideration of the energy passing through the pinhole collimator.

Instead of making such an estimate which is still only an approximation, the correct value of Δ can be found experimentally by taking exposures with the same sample at two different angles of oscillation with appropriate allowance for exposure to give equal blackening for spots of equal size. Thus:

$$Y_2 - Y_1 = \frac{ptA}{\bar{v}\pi} (\psi_2 - \psi_1) \cos \theta. \tag{4}$$

Equation (4) can thus be used to eliminate Δ, or values of Δ can be found from the two separate results. A number of such values can be used to give a mean Δ for a given experimental set-up and type of specimen.

If Δ is so determined with proportionate error of $\pm\epsilon$, the proportionate error in $\bar{v}$ is $\pm\Delta\pi\epsilon/(2\psi + \Delta\pi)$, the magnitude of which decreases as ψ increases. The error in linear dimension is one-third of this.

(ii) *The mean grain volume $\bar{v}$ and grain-size distribution.* The effect of distribution of grain volume for the back-reflexion case was considered by Hirsch. The present case can be approached in a similar manner, but there are significant differences. If the specimen is too thick relative to the absorption coefficient of the material, small grains on the side of the specimen facing the collimator may just fail to give visible spots, while the same sized grains on the opposite surface could give visible spots because of the somewhat smaller absorption path. Hence, in the most general case where an "infinite" range of grain sizes is assumed to be present, there will be grains too small to give visible spots throughout the specimen. For a given exposure time, the minimum volume of grain which can just be seen varies with position along the direction of the incident beam and is smallest on the side of the specimen away from the X-ray source. With correct exposure time, this will turn out to be negligible but the general effect of exposure and grain-size distribution can be considered as follows.

If B_0 is the minimum total blackening from a grain of volume v_1 which forms a spot too faint to be seen, then for a stationary specimen we have (Hirsch[6]):

$$B_0 = v_1 K T_0 I_0 \exp(-\mu x)$$

or a blackening per unit area on the film of:

$$\frac{v_1 K T_0 I_0 \exp(-\mu x)}{\delta^2}, \tag{5}$$

where δ is the part of the angular divergence caused by wavelength spread, crystal imperfection, etc.

When the specimen is oscillated through an angle ψ large compared with the divergence, then the blackening per unit area remains independent of ψ provided T_0 is increased to $T_0\psi/\delta$. (See Appendix II for comments on this.) In equation (5), x is the total path length, given by:

$$x = t \sec 2\theta + y(1 - \sec 2\theta) \tag{6}$$

and v_1 is the volume of a grain at depth y in the specimen.

If the grain-size distribution is $f(v)$ per unit volume, then the number of grains in a layer of thickness dy which can contribute spots is:

$$A dy \int_{v_1}^{\infty} f(v)dv,$$

and the total number of spots counted is therefore:

$$Y_c = pAP \int_{y=0}^{y=t} \int_{v_1}^{\infty} f(v)dv dy$$

which becomes:

$$Y_c = pAP \int_{y=0}^{y=t} \left\{ \int_0^{\infty} f(v)dv - \int_0^{v_1} f(v)dv \right\} dy.$$

Now, when all grains contribute, the maximum number of spots would be given by equation (1) and since, by definition:

$$\frac{1}{\bar{v}} = \int_0^{\infty} f(v)dv,$$

then:

$$Y = Y_c + pAP \int_0^t \int_0^{v_1} f(v)dv dy. \tag{7}$$

Differentiation of equations (5) and (6) and substitution for dy gives equation (7) in terms of v_1 as:

$$Y = Y_c + \frac{pAP}{\mu(1 - \sec 2\theta)} \int_{(v_1)_{y=0}}^{(v_1)_{y=t}} \frac{F(v_1)}{v_1} dv_1, \tag{8}$$

where $F(v_1) = \int_0^{v_1} f(v)dv$.

The function $f(v)$ or its integral $F(v)$ is not generally known. If it has a gaussian or some other standard form, the right-hand term could be calculated—if necessary, with the aid of tables or graphs. In practice, however, this term should be negligible if the exposure has been long enough and it ought to represent only a small correction to the number of counted spots. Hence, a simple test is to repeat the photograph at double the time T_1 which thus halves the volume v_1 for the same degree of blackening B_0. If no extra spots appear, the correction term is already negligible. Alternatively, an extrapolation method using different exposure ratios could be used to find Y.

(iii) *Surface grains and internal grains.* A further problem arises because some grains are cut by either surface and this gives a higher number of grains per unit volume than the true value. The error increases as the size of the grains increases compared with the thickness of the specimen. Hence, it is desirable to avoid the condition where the linear dimension of the grains approaches that of the specimen thickness. The approach to the treatment of this case is again similar to that of Hirsch, but a method is proposed for considering both surface and volume grains together in order to obtain the true mean volume $\bar{v}$ or linear dimension l, which equals $\bar{v}^{1/3}$.

A simplified picture shows that, for small cubic grains of length l, the mean number in a thickness t is $\{(t/l) + 1\}$, and the number per unit of irradiated surface area is A/l^2. Hence, instead of equation (1), the following should be written:

$$Y = \frac{pPA}{l^2}\left(\frac{t}{l} + 1\right).$$

The number of spots can thus be regarded as the sum of a volume term plus a surface term:

$$\frac{Y}{pPA} = \frac{t}{l^3} + \frac{1}{l^2}. \tag{9}$$

Similarly, equation (4) may be re-expressed as:

$$\frac{\pi}{pA \cos\theta}\left(\frac{Y_1 - Y_2}{\psi_1 - \psi_2}\right) = \frac{t}{l^3} + \frac{1}{l^2}. \tag{10}$$

There are several ways of finding the correct value of l.

(*a*) Equation (9) is a cubic equation and can be solved.

(*b*) It can also be solved by approximation, as follows:

A value of l which is too small should be obtained by the direct use of equations (3) or (4). This value is $(l - \delta l)$. Therefore:

$$l^3 - (l - \delta l)^3 = \frac{pPA}{Y}(t + 1) - \frac{pPA}{Y}t.$$

If the term in $(\delta l)^3$ is neglected, then:

$$l = \frac{1}{3(l - \delta l)} \frac{pPA}{Y}. \tag{11}$$

(*c*) A graphical method can also be used. In this case, the function (t/l^3) is plotted as abscissa with l as

ordinate, for a range of values of t. With the same origin and ordinate, the function $(1/l^2)$ is plotted in the opposite direction, starting from the origin. These two functions represent the separate components of surface and volume grains and their sum is the horizontal distance between the two curves. This horizontal therefore cuts the ordinate at the correct value of l (see Fig. 3).

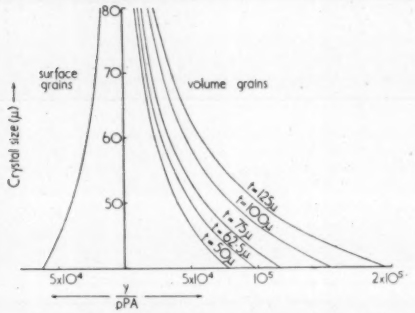

Fig. 3. Variations of Y/pAP with t/l^3 and $1/l^2$ for different values of t

EXPERIMENTAL APPLICATION

The various steps in the experimental application of the method are as follows:

(i) A is determined by direct exposure of a piece of film placed in the specimen holder for each collimator.
(ii) Δ is determined by application of equation (4) to results from suitably chosen samples.
(iii) From the values of Δ, ψ and A for a given experimental arrangement, values of PA, which equals $A\{(\psi/\pi) + (\Delta/2)\} \cos\theta$, can be plotted against θ.
(iv) The number of spots is counted on a photograph and divided by pPA. From this, the mean grain diameter can be found directly by use of the graphical method of Fig. 3 or by the approximation method.

Alternatively, if two exposures at different angles of oscillation are taken, Δ can be completely eliminated thus:

(i) Graphs of $P'A$, which equals $(A/\pi)(\psi_1 - \psi_2) \cos\theta$, against θ are prepared for the values of ψ_1, ψ_2 and A relevant to a given experimental arrangement.
(ii) The difference in the number of spots for two different angles of oscillation is determined and divided by $pP'A$, giving equation (10).
(iii) The mean grain diameter can be found from this as in paragraph (iv) above.

N.B.—For the films at two different angles, the exposure time should be proportional to the angle of oscillation to give equal blackening for the same spots. To test whether or not the whole of the grain-size distribution is contributing spots, exposures should also be doubled under identical experimental conditions to see if any more spots can be counted. A slight error is introduced by oscillating the specimen, as this affects the volume of specimen irradiated but, up to a symmetrical oscillation of 15° or so, the error is less than 1%.

ACKNOWLEDGEMENTS

The authors thank Mr. F. H. Saniter, Director of Research, United Steel Companies Limited, for permission to publish this paper. They would also like to express their indebtedness to Dr. P. B. Hirsch of the Cavendish Laboratory, Cambridge, for helpful discussion.

REFERENCES

(1) STEPHEN, R. A., and BARNES, R. T. *J. Inst. Metals*, **60**, p. 285 (1937).
(2) SCHDANOW, H. S. *Z. Kryst*, **90**, p. 82 (1935).
(3) HIRSCH, P. B., and KELLAR, J. N. *Acta Cryst*, **5**, p. 162 (1952).
(4) HIRSCH, P. B., and KELLAR, J. N. *Proc. Phys. Soc. (London) B*, **64**, p. 369 (1951).
(5) GAY, P., and KELLY, A. *Acta Cryst.*, **6**, p. 165 (1953).
(6) HIRSCH, P. B. *Brit. J. Appl. Phys.*, **5**, p. 257 (1954).
(7) HIRSCH, P. B. *Acta Cryst.*, **5**, p. 168 (1952).

APPENDIX 1

Examples of crystal size determination

(1) *Sintered MgO.* With 5° of oscillation, there was no appreciable increase in the number of spots with exposure times longer than 4 hours. The 10° oscillation exposure was given 8 hours. Other experimental conditions were a collimator diameter of 0·25 mm and a specimen thickness of 0·010 cm. Spots were counted on the (200) ring ($p = 6$), which has a value of θ of 21·6° for CoKα radiation.

Results.

5° oscillation: 190 spots
10° oscillation: 280 spots
} 90 difference

Hence, because:

$$PA = \frac{5A \cos\theta}{\pi} = 5{\cdot}4 \times 10^{-5},$$

Therefore:

$$\frac{Y}{pPA} = \frac{90}{6 \times 5{\cdot}4 \times 10^{-5}} = 2{\cdot}78 \times 10^{5},$$

which, from Fig. 3, gives l to be 35 μ. This compares well with a microscopical value of l of 33 μ.

(2) *Alloy steel (cooled from 1250° C).* The experimental conditions were a collimator diameter of $\frac{1}{16}$ in. and a specimen thickness of 0·005 cm. Spots were counted on the (110) ring ($p = 12$) which has a value of θ of 26·1° for CoKα radiation.

Results.

Stationary photograph: 23 spots } 20 difference
5° oscillation: 43 spots } 25 difference
10° oscillation: 68 spots } 18 difference
15° oscillation: 85 spots

This gives a mean value of 21 spots corresponding to 5° oscillation.

Hence, because:

$$PA = \frac{5A \cos\theta}{\pi} = 1{\cdot}64 \times 10^{-3},$$

for this collimator:

$$\bar{v} = \frac{PApt}{Y} = \frac{1{\cdot}64 \times 10^{-3} \times 12 \times 5}{21} \times 10^{-3},$$

$$= 4{\cdot}71 \times 10^{-6}.$$

Thus:

$$(l - \delta l) = 167\mu.$$

This gives δl to be 190 μ, or l to be 357 μ. Here, the very large grain size makes the approximation method invalid because surface grains play a more important part than the volume grains, the grain size being greater than the specimen thickness. Hence, the value of l must be derived from equation (9), whence $l = 320\,\mu$. Microscopically, l was determined as 350 μ, but with metallic specimens the presence of preferred orientation and twining can give results which are different from microscopical measurements.

(3) *Derivation of* Δ. From results given in Section (1) for MgO, 90 spots are equivalent to 5° oscillation and hence a stationary photograph should have (190 − 90) characteristic spots on the (200) ring. (An actual count of the stationary photograph was very difficult in this case because of confusion with Laüe spots.) Hence:

$$\frac{90}{100} = \frac{5 \times 2}{\pi\Delta}$$

which gives Δ to be 3·8°.

APPENDIX 2

The effect of oscillation on the blackening of a spot

The divergence Δ can be considered to consist of two parts, $d\theta$ arising from slit geometry and δ arising from wavelength spread, crystal imperfection particle size, etc., so that:

$$\Delta = d\theta + \delta.$$

The effect of δ is to replace each normal by a finite cone of small solid angle so that when the crystal is stationary, reflexion can occur only if the base of the cone lies wholly or partly within a belt of width $d\theta$. During oscillation, reflexion occurs continuously as the belt is traversed by the normals, but ceases when the cone of normals passes out of the belt. The effect of oscillation is therefore twofold; it spreads spots out into small streaks, and it reduces the time spent by the normal in a reflecting position, as ψ is usually five or ten times as large as Δ.

The effect of the oscillation on the blackening can be calculated as follows. If ρ is the angle between a normal and the axis of oscillation, and ϕ the angle between the plane containing the X-ray beam and the axis of oscillation and the plane containing the normal and the axis of oscillation, then $d\rho_\delta$ and $d\phi_\delta$ represent the values of the divergence in ρ and ϕ co-ordinates. To a good approximation, $d\phi_\delta = \delta/\sin\rho$ and $d\rho_\delta = \delta$.

During oscillation through an angle ψ, the normal moves as a constant-ρ curve and hence ψ is already measured in ϕ-co-ordinates. Now, as a normal moves through a band of width Δ along a constant-ρ curve, $d\phi_\delta$ is increased to $d\phi_\Delta$ whilst $d\rho_\delta$ remains constant.

The area of the spot on the film is therefore increased in the ratio $d\phi_\Delta/d\phi_\delta$, while the time for reflexion is decreased by the fraction $d\phi_\Delta/\psi$ of the total exposure time (if $\psi > d\phi_\Delta$). Hence, on oscillation, the blackening per unit area is decreased in the ratio $d\phi_\delta/\psi$ and therefore it would be necessary to increase the exposure time in the ratio $\psi/d\phi_\delta$ to keep the experimental conditions independent of ψ. Hence:

$$T_\psi = \frac{T_0\psi}{d\phi_\delta},$$

or

$$T_\psi = \frac{T_0\psi \sin\rho}{\delta}. \qquad (12)$$

The exposure time would thus be a function of ρ and vary for different points around the diffraction ring. This is clearly difficult to arrange, but an exposure time of $T_0\psi/\delta$ would give a minimum blackening per unit area (which is the determinative quantity for spot visibility) of B_0 divided by the spot area of:

$$\frac{v_1 K' T_0 \psi d\phi_\Delta I_0 \exp(-\mu x)}{\delta\psi d\phi_\Delta d\phi_\delta \sin\rho}$$

or

$$\frac{v_1 K' T_0 I_0 \exp(-\mu x).}{\delta^2 \sin\rho}$$

If a significant fraction of the grain-size distribution is less than v_1, then the dependence on ρ must be allowed for by counting spots only in a band near the equator, where ρ is approximately $\pi/2$, and $\sin\rho$ varies little. The minimum value of the blackening per unit area is then $\{v_1 K' T_0 I_0 \exp(-\mu x)\}/\delta^2$. Usually T_0 is chosen so that most of the grain-size distribution is included in the counting, and $T_0\psi/\delta$ is an adequate exposure for the oscillation case as all spots which appear on the stationary photographs will appear on the oscillation one. Clearly, for exposures at two different angles of oscillation the exposure ratio should be ψ_1/ψ_2.

Journal of Scientific Instruments

Contents of the July issue

ORIGINAL CONTRIBUTIONS

Papers

High-gain d.c. amplifier for biological purposes. By S. V. Hill.
Method for measuring the moisture content of air. By J. Higgins.
Integrating exposure meter for electron microscopy. By J. Cartwright and A. E. Bishop.
Photoelectric apparatus for measuring velocity. By A. C. Gray and S. Thomas.
High energy, high current synchrotron injector. By G. R. Davies and P. R. Chagnon.
Dielectric measurements on thin films by means of electrodes coated with irradiated silicone rubber. By W. P. Baker and F. B. Waddington.
Inductance bridge for sensitive displacement measurements over long periods. By D. Murray.
Relative energy calibration of electron accelerators. By E. Matsukawa and B. N. C. Agu.
7 kW plasma jet for laboratory use. By A. B. Osborn.

Laboratory and workshop notes

Two techniques for measuring the density of a porous solid by displacement of a liquid. By W. B. Jepson.
Extensometer for recording the slip of riveted joints under load. By S. A. V. Swanson.
Drift-free phase-sensitive detector. By E. A. Faulkner.
The attachment of fine fibres with electro-deposited metal. By D. W. Bassett and A. J. B. Robertson.
On the use of coarse gratings to find the refractive indices of a double refracting crystal. By G. M. Sreekantath and C. A. Verghese.
Location of white-light fringes in the Michelson interferometer. By P. Hariharan and R. G. Singh.
A dismountable vacuum joint for bakeable glass vacuum systems. By L. A. Green, H. T. Miles and A. C. Richardson.
Electrostatic vibrator with a highly stable centre of oscillation. By R. H. Bradsell.
Reinforced sulphur for insulators. By J. E. Crawford Stringer.
Capacitance-coupled cell for electrolytic conductivity measurements. By D. E. Bromley and P. T. Good.
Adaption of a Dick microscope for orientating crystal fragments. By J. E. T. Horne.
Indium extruder. By R. L. Simpkins.
Oil-cooled electromagnet coils. By F. D. Stacey.
Air-bubble micromanometer developed for outdoor use. By E. Kovačič.

Correspondence

New housing for the sensitive cup-contact anemometer, Mk. 1. From H. Charnock and F. E. Pierce.
Wire grating ultrasonic interferometer. From G. M. Sreekantath.
Shielded cathode X-ray tube. From A. H. McIlraith.

NOTES AND NEWS

New instruments, materials and tools
New books
Notes and comments

Transient response of direct current amplifier systems

By R. D. STUART, M.A., Ph.D., Grad.I.E.E., Admiralty Research Laboratory, Teddington

[*Paper received 6 February*, 1959]

The transient response of a direct current amplifier to a step function input current, is compared with its response to a spurious charge suddenly induced on the capacitance across the grid of the first valve. The behaviour of circuits consisting of simple RC networks is considered first, and this is then compared with the behaviour of a system containing an amplifier with feedback. It is shown that the problem of improving the signal-to-noise ratio for this case is one of filtering, and can be considered independently of any characteristics introduced into the system by feedback.

In a previous paper Sanders* has considered the transient response of an amplifier such as that shown in Fig. 1 when the capacity across the input terminals is appreciable. The signal input is the current I. A spurious input can arise due to a charge induced on the capacitor C_1. The behaviour of the amplifier to these two types of input is considered below.

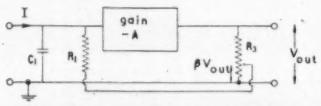

Fig. 1. D.C. amplifier with feedback

Consider first the simple circuit shown in Fig. 2, where C represents, for example, an ionization chamber. The ionization chamber produces the current which is of interest and this develops a voltage V across the resistance R which is subsequently amplified. Since the transient response is

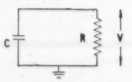

Fig. 2. Basic input circuit

under consideration, it is desirable to consider the response to changes in current, and a step function is a suitable input. The output is then given by

$$V_I = (IR)\{1 - \exp(-t/\tau)\} \tag{1}$$

If a charge Q is instantaneously placed on C, then the output is given by

$$V_Q = (Q/C)\exp(-t/\tau) \tag{2}$$

The ratio of the magnitudes of the response for the two cases is given by

$$IR/(Q/C) = (I/Q)CR \tag{3}$$

For given values of I and Q this ratio can be increased by increasing C or R. Both of these procedures, however, increase the time constant, and thereby make the response of the system to changes in wanted signal worse.

FREQUENCY SPECTRUM OF THE SIGNALS

The frequency spectrum of the signals given by equations (1) and (2) are quite different, and hence there is a possibility of differentiating between them by filtering. Normalizing the expressions and writing $\alpha = 1/\tau$ gives for the two cases,

$$V_I(t) = 1 - \exp(-\alpha t) \tag{4}$$

and

$$V_Q(t) = \exp(-\alpha t) \tag{5}$$

Equation (5) is readily Fourier analysed. The complex Fourier transform is given by

$$F(\omega) = \int_{-\infty}^{\infty} f(t)\exp(-j\omega t)dt$$

For the case represented by equation (5) one has

$$\begin{aligned} f(t) &= \exp(-\alpha t) \quad t > 0 \\ &= 0 \qquad\qquad t < 0 \end{aligned}$$

Hence

$$F(\omega) = \int_0^{\infty} \exp\{-(\alpha + j\omega)t\}dt = \frac{1}{\alpha + j\omega}$$

and

$$|F(\omega)| = 1/\sqrt{(\alpha^2 + \omega^2)} \tag{6}$$

The analysis of equation (4) is not quite so straightforward since, as defined, $\int_{-\infty}^{\infty} |f(t)|dt$ is not finite. To overcome this, define $f(t)$ as follows,

$$\begin{aligned} f(t) &= 1 - \exp(-\alpha t) \quad \text{for } 0 < t < T \\ &= 0 \qquad\qquad\qquad\quad \text{elsewhere.} \end{aligned}$$

and investigate the behaviour as $T \to \infty$. By this means it may be shown that

$$|F(\omega)| = \{\alpha/\omega\sqrt{(\alpha^2 + \omega^2)}\} \tag{7}$$

(For the details of carrying out this procedure see, for example, Goldman.†) Comparing now equations (6) and (7) it can be seen that the magnitudes of the spectral components of the two signals are equal when $\omega = \alpha$. Below this frequency the components of the wanted signal (7) are greater than those of the unwanted signal, and for higher frequencies they are smaller. Hence the wanted and unwanted signals can be separated to some extent by a low-pass filter, the cut-off frequency of which is given by $\omega_c = \alpha$.

FILTER OUTPUT

Consider a simple single-stage RC filter as shown in Fig. 3. The transfer impedance of this circuit is given by $1/(1 + pC'R')$ and, from the arguments given in the last section, make $C'R' = 1/\alpha = \tau$. The output of this filter for the two inputs

* SANDERS, J. H. *J. Sci. Instrum.*, **31**, p. 453 (1954).

† GOLDMAN, S. *Frequency Analysis, Modulation and Noise*, p. 124 (New York: McGraw-Hill Book Co. Inc., 1948).

described by equations (1) and (2) can be obtained by the Laplace transform method.

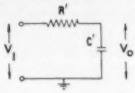

Fig. 3. Simple filter

Hence for equation (1)

$$\mathscr{L}(V_0)_I = (IR)\frac{1}{1+p\tau}\mathscr{L}\{1-\exp(-\alpha t)\}$$

$$= (IR)\frac{1}{p(1+p\tau)^2} \quad (8)$$

Therefore

$$(V_0)_I = (IR)\{1-\exp(-t/\tau)-(t/\tau)\exp(-t/\tau)\} \quad (9)$$

For equation (2)

$$\mathscr{L}(V_0)_Q = \left(\frac{Q}{C}\right)\frac{1}{1+p\tau}\mathscr{L}\{\exp(-\alpha t)\}$$

$$= \left(\frac{Q}{C}\right)\frac{1}{(1+p\tau)^2} \quad (10)$$

Therefore

$$(V_0)_Q = \left(\frac{Q}{C}\right)\frac{1}{\tau}t\exp(-t/\tau) \quad (11)$$

AMPLIFIER WITH FEEDBACK

Now return to the case of the amplifier shown in Fig. 1. It may be shown that for a step function current input the transform of the output voltage is given by

$$\mathscr{L}(V_I) = (IR)\frac{-A}{1+A\beta+pC_1R_1}\left(\frac{1}{p}\right) \quad (12)$$

Hence

$$V_I = -A\left(I\frac{R_1}{1+A\beta}\right)\left\{1-\exp\left(-t\Big/\frac{C_1R_1}{1+A\beta}\right)\right\}$$

Writing $C = C_1$ and $R = R_1/(1+A\beta)$,

$$V_I = -A(IR)\{1-\exp(-t/\tau)\} \quad (13)$$

For the unwanted signal case

$$\mathscr{L}(V_Q) = \left(\frac{Q}{C_1}\right)\frac{-AC_1R_1}{1+A\beta+pC_1R_1} \quad (14)$$

Hence

$$V_Q = -A\left(\frac{Q}{C_1}\right)\exp\left(-t\Big/\frac{C_1R_1}{1+A\beta}\right)$$

Again, writing $C = C_1$ and $R = R_1/(1+A\beta)$,

$$V_Q = -A(Q/C)\exp(-t/\tau) \quad (15)$$

It is seen that equations (13) and (15) are identical to equations (1) and (2) apart from the amplification factor $-A$.

Finally, consider the case treated by Sanders and shown in Fig. 4.

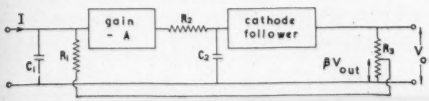

Fig. 4. Amplifier with simple filter incorporated

The equations for this case are obtained from equations (10) and (12) by considering A to be a function of frequency and replacing A by $A/(1+pC_2R_2)$ throughout. Putting $C_1R_1 = \tau_1$ and $C_2R_2 = \tau_2$ one has, for the current input case,

$$\mathscr{L}(V_0)_I = (IR_1)\frac{-A}{(1+p\tau_1)(1+p\tau_2)+A\beta}\left(\frac{1}{p}\right) \quad (16)$$

This can be made to correspond to equation (8) by choosing τ_1, τ_2 so that $\{(1+p\tau_1)(1+p\tau_2)+A\beta\}$ is a perfect square. Let

$$(1+p\tau_1)(1+p\tau_2)+A\beta = \tau_1\tau_2(p+\alpha)^2 \quad (17)$$

One then has

$$\mathscr{L}(V_0)_I = (IR_1)\{-A/\tau_1\tau_2(p+\alpha)^2p\}$$

Therefore

$$(V_0)_I = (IR_1)(-A/\alpha^2\tau_1\tau_2)\{1-\exp(-\alpha t)-\alpha t\exp(-\alpha t)\} \quad (18)$$

From equation (17)

$$\alpha^2 = (1+A\beta)/\tau_1\tau_2 \quad (19)$$

and

$$\alpha = (\tau_1+\tau_2)/2\tau_1\tau_2 \quad (20)$$

Hence, from equations (18) and (19),

$$(V_0)_I = -A\left(I\frac{R_1}{1+A\beta}\right)\{1-\exp(-\alpha t)-\alpha t\exp(-\alpha t)\} \quad (21)$$

Similarly, for the case of a spurious induced charge,

$$\mathscr{L}(V_0)_Q = \left(\frac{Q}{C_1}\right)\frac{-AC_1R_1}{(1+p\tau_1)(1+p\tau_2)+A\beta}$$

$$= \left(\frac{Q}{C_1}\right)\frac{-A}{\tau_2(p+\alpha)^2}$$

Therefore

$$(V_0)_Q = -A\left(\frac{Q}{C_1}\right)\frac{1}{\tau_2}t\exp(-\alpha t) \quad (22)$$

The variations of $(V_0)_I$ and $(V_0)_Q$ with time given by equations (21) and (22) can be made the same as the variations with time of $(V_0)_I$ and $(V_0)_Q$ given by equations (9) and (11) by making $\alpha = 1/\tau$; τ_1 and τ_2 will then be determined by equations (19) and (20). [Note that this means one cannot write $C = C_1$ and $R = R_1/(1+A\beta)$ in equations (21) and (22).] Equations (19) and (20) can now be written

$$\tau_1\tau_2 = \tau^2(1+A\beta) \quad (23)$$

$$\tau_1+\tau_2 = 2\tau_1\tau_2/\tau = 2\tau(1+A\beta) \quad (24)$$

Hence τ_1, τ_2 are the roots of the equation

$$x^2 - 2\tau(1+A\beta)+\tau^2(1+A\beta) = 0 \quad (25)$$

Therefore

$$x = \tau[(1+A\beta) \pm \sqrt{\{(1+A\beta)^2-(1+A\beta)\}}] \quad (26)$$

Since A and β are both considered positive (corresponding to negative feedback) $(1+A\beta) > 1$. Hence the expression under the square root sign is positive and less than $(1+A\beta)^2$. Both roots are therefore real and positive so that the conditions specified correspond to a physically realizable case.

Equations (21) and (22) can now be written

$$(V_0)_I = \left[-A\left(I\frac{R_1}{1+A\beta}\right)\right]\{1 - \exp(-t/\tau) - (t/\tau)\exp(-t/\tau)\} \quad (27)$$

$$(V_0)_Q = \left[-A\left(\frac{Q}{C_1}\right)\frac{1}{\tau_2}\right] t\exp(-t/\tau) \quad (28)$$

The ratio of the multiplying factors (the terms in square brackets) is given by

$$I\frac{R_1}{1+A\beta}\frac{C_1\tau_2}{Q} = \frac{I}{Q}\frac{\tau_1\tau_2}{1+A\beta} = \frac{I}{Q}\frac{1}{\alpha^2} = \frac{I}{Q}\tau^2 \quad (29)$$

This is identical to the ratio of the corresponding terms in equations (9) and (11). Hence apart from a scaling factor the response described by equations (27) and (28) is identical to that described by equations (9) and (11). The relationship between the parameters τ_1 and τ_2 in this circuit, given by the method of choice used above, is exactly the same as that suggested as optimum by Sanders.

ACKNOWLEDGEMENT

The author would like to thank Mr. T. G. Weale for checking the manuscript.

Measurement of fibre diameter variation by optical diffraction

By W. J. Onions, B.Sc., and B. Ellingham, B.Sc., Ph.D., A.Inst.P., Department of Textile Industries, University of Leeds

[*Paper first received* 17 *January*, 1958, *and in final form* 2 *February*, 1959]

A theory is developed relating the intensity of light diffracted at any given angle by a parallel array of opaque fibres of unequal diameters with the mean diameter and the coefficient of variation of fibre diameter. The ratio of the intensities of the first minimum and the first maximum is shown to depend upon the coefficient of variation of fibre diameter. This affords an opportunity of measuring fibre diameter variation. The possibilities and limitations of the method in practice are explored.

Starting with Thomas Young[1] in 1824 several workers[2–6] have used the principle of diffraction to measure the diameter of fibres or the size of small objects. Usually it has been assumed that the fibres are of uniform diameter and the mean has been found by measuring, in some way, the diffraction angle of the first minima.

One such instrument available to the writers was that devised by Ewles[7] in 1928. Experience has shown that using this instrument it is easier to locate the first minima for a relatively uniform specimen of man-made filaments than for a specimen of wool, the diffraction bands becoming more diffuse as the variation between the fibres in the specimen is increased. If the degree of diffusion of the diffraction pattern can be defined and measured it might afford a method of assessing the variation in fibre diameter of the specimen.

THEORY

Consider first the diffraction pattern produced by a single opaque fibre of diameter a. By Babinet's principle this pattern is the same as that produced by a slit of width a.

When the light is incident on the slit in a direction perpendicular to the plane of the slit, the expression for the intensity[8] at an angle θ may be written

$$I = A_0\{(a^2\sin^2 b)/b^2\} \quad (1)$$

where A_0 = a constant, a = width of slit, $b = (\pi a\sin\theta)/\lambda$, θ = angle of diffraction, and λ = wavelength of the light.

In a group of fibres, all approximately parallel to the slit, different fibre elements will generally vary in diameter and will simultaneously intercept different portions of the light beam. Applying Babinet's principle again the arrangement of fibres may be considered as replaced by a group of equivalent slits. The length axes of these slits are only approximately parallel to each other and are not uniformly spaced, so that there is no precise geometrical relationship between all elements of slit in the group. The group is regarded as a large number of parallel slits in random positions, each element or fibre acting independently of the other elements to form its own diffraction pattern of the source. These patterns may all be superimposed on one another, and to arrive at an expression for the intensity distribution due to the array of fibres, expression (1) must be summed for all the elements concerned.

If the number of fibres having a diameter between a and $a + da$ is represented by $p(a)da$, the intensity at an angle θ due to all the fibres in this diameter group will be given by

$$I_\theta = A_0\frac{a^2\sin^2 b}{b^2}\cdot p(a)da \quad (2)$$

The total intensity due to all the fibres in the specimen will be given by

$$I_{T,\theta} = \int_{a_1}^{a_2} A_0\frac{a^2\sin^2 b}{b^2}\cdot p(a)da \quad (3)$$

where a_1 and a_2 are the limits of the diameter range fo the specimens. This equation will be considered for different distribution functions.

Case 1. *Rectangular distribution*. In this case $p(a)da = kda$ between a_1 and a_2 where k is a constant.

The standard deviation σ is given by $\sigma^2 = (a_2 - a_1)^2/12$ and $f = \sigma/\bar{a} = (a_2 - a_1)/\bar{a}\sqrt{12}$ ($\bar{a}$ is the mean diameter). It can readily be shown that

$$I_{T,\theta} = \frac{B_0}{\phi^2}[1 - \cos\phi\sin\{\sqrt{(3)}f\phi\}/\sqrt{(3)}f\phi] \quad (4)$$

where $\phi = (2\pi\bar{a}\sin\theta)/\lambda$ and $B_0 = 2NA_0\bar{a}^2$, i.e. a constant independent of θ. N is the number of fibres in the specimen.

Case 2. *Triangular distribution.* For a symmetrical triangular distribution $p(a) = ma + c$

where $m = m_1$ and $c = -m_1 a_1$ from a_1 to $\bar{a}$
and $m = -m_1$ and $c = m_1 a_2$ from $\bar{a}$ to a_2
$f = (a_2 - a_1)/2\bar{a}\sqrt{(6)}$ and $m_1 = N/6f^2\bar{a}^2$

Hence it can be shown that

$$I_{T,\theta} = \frac{B_0}{\phi^2}[1 - \cos\phi\{1 - \cos\sqrt{(6)}f\phi\}/3f^2\phi^2] \qquad (5)$$

where B_0 and ϕ are defined as before.

Case 3. *Gaussian distribution.* For a Gaussian distribution of fibre diameter

$$p(a) = \frac{N}{\sigma\sqrt{(2\pi)}} \exp(-\tfrac{1}{2}z^2)$$

where $z = (a - \bar{a})/\sigma$

If infinite limits are assumed it is not difficult to show that

$$I_{T,\theta} = \frac{B_0}{\phi^2}\{1 - \cos\phi \,.\, \exp(-\tfrac{1}{2}f^2\phi^2)\} \qquad (6)$$

Thus for three hypothetical types of distribution the intensity for any value of ϕ, corresponding to $\bar{a}$ and θ, has been derived. Curves computed from the Gaussian relation are plotted in Fig. 1 for various assumed values of f.

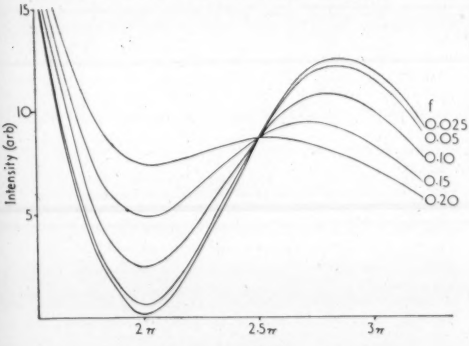

Fig. 1. Theoretical intensity curves for the Gaussian distribution

Intensity curves based on the other distributions are closely similar. It is reasonable to suppose that the distribution of diameter will, in practice, approach more closely to the Gaussian distribution than to the others, and it is upon this assumption that the further computations are based.

Positions of maximum and minimum intensity. The positions of maximum and minimum intensity are found from

$$dI_{T,\theta}/d\phi = 0$$

This gives the relation

$$(f^2\phi^2 + 2)\cos\phi + \phi\sin\phi = 2\exp(\tfrac{1}{2}f^2\phi^2) \qquad (7)$$

If $f = 0$ (i.e. all fibres are uniform in diameter) this is satisfied by $\sin\phi/2 = 0$ or by $\tan\phi/2 = \phi/2$ and, as should be expected, these are the positions of the minima and maxima produced by a single slit. For the case when $f \neq 0$ (the practical case) a graphical method has been used. The results of these computations are shown in Table 1.

Table 1. *Positions of first maxima and minima*

f	ϕ_{min} (rads)	ϕ_{max} (rads)	$\frac{\phi_{max}}{\phi_{min}}$
0·025	6·283	8·975	1·428
0·05	6·284	8·940	1·423
0·075	6·285	8·882	1·413
0·10	6·289	8·794	1·398
0·15	6·321	8·510	1·346
0·20	6·434	8·007	1·245
0·21	6·480	7·855	1·212
0·22	6·547	7·692	1·175
0·23	6·654	7·477	1·124
0·24	6·918	7·087	1·024

It will be seen from Table 1 and Fig. 1 that the position and the intensity of the minima and maxima are dependent upon f, the variation in diameter. The position of the first minimum changes from 2π to $2{\cdot}2\pi$ approximately, as f is increased from 0 to 0·24. Over the same range of f the position of the first maximum is changed from $2{\cdot}85\pi$ to approximately $2{\cdot}2\pi$.

By measuring ϕ_{max} and ϕ_{min} (or actually θ_{max} and θ_{min}) for any practical sample it should be possible from these curves to estimate the value of f for the particular sample. It is actually fairly simple to locate the minimum with the desired accuracy, but it is much more difficult to find the true peak of the somewhat flatter maximum. This makes the estimate of f from ϕ_{max}/ϕ_{min} rather inaccurate.

Values of $I_{2\pi}$ and $I_{3\pi}$. It will be noted that the position of the minimum does not move very much from $\phi = 2\pi$. If the minimum is located and taken as indicating $\phi = 2\pi$, the intensity could then be measured at a position corresponding to $\phi = 3\pi$ (i.e. at an angle 3/2 times that for minimum intensity).

The ratio of these intensities is then dependent only on f.

$$\frac{I_{\phi=2\pi}}{I_{\phi=3\pi}} = \frac{9\{1 - \exp(-2f^2\pi^2)\}}{4[1 - \exp\{-(9/2)\,.\,f^2\pi^2\}]} \qquad (8)$$

The values computed for this ratio are shown in Table 2.

Table 2. *Ratios of $I_{2\pi}$ and $I_{3\pi}$*

$I_{2\pi}/I_{3\pi}$	f	$I_{2\pi}/I_{3\pi}$
0	0	0·6761
0·02	0·0090	0·8591
0·04	0·0367	1·0510
0·06	0·0837	1·2398
0·08	0·1519	1·4184
0·10	0·2455	1·5788
0·12	0·3632	1·7185
0·14	0·5085	1·8356

In Table 1 it was noted that if f is greater than approximately 0·24 the positions of maximum and minimum coincide, i.e. there is no true maximum or minimum if f is greater than 0·24. In principle the ratio $I_{2\pi}/I_{3\pi}$ could be used for higher values of f provided the positions θ for $\phi = 2\pi$ and 3π are known. This is possible if $\bar{a}$ and λ are known beforehand.

The ratio $I_{2\pi}/I_{3\pi}$ has one marked disadvantage in that a small error in determining the position $\phi = 2\pi$, and therefore in $\phi = 3\pi$, produces a considerable error in the determination of $I_{3\pi}$, since intensity curves fall fairly steeply near $\phi = 3\pi$.

The ratio I_{min}/I_{max}. It would seem that the intensity of the maximum could be measured with greater accuracy than any

of the parameters previously discussed. Except at low values of f it would also seem possible to measure I_{min} accurately. Values of I_{min}/I_{max} have been calculated from equation (6) and the values of ϕ in Table 1. These are tabulated in Table 3.

Table 3. *Values of I_{min}/I_{max}*

	I_{min}/I_{max}		
f	*Gaussian*	*Triangular*	*Rectangular*
0·025	0·0130	0·0133	0·0134
0·05	0·0540	0·0543	0·0547
0·075	0·1190	0·1262	0·1278
0·10	0·2210	0·2320	0·2382
0·15	0·5170	0·5455	0·5807
0·20	0·8440	0·8974	0·9485
0·21	0·899		
0·22	0·944		
0·23	0·980		
0·24	1·000		

Although the ratio I_{min}/I_{max} is only useful in the range $f = 0$ to $f = 0{\cdot}24$, it was considered to be the most promising of the methods because a small error in the location of the maximum and minimum positions does not introduce an appreciable error into the measurement of the intensities and their ratio.

EXPERIMENTAL

Fig. 2 illustrates the general design of an instrument built to investigate the practical possibilities of fibre measurement by diffraction. Light from a sodium vapour lamp passes through a diffusing screen before reaching a horizontal slit.

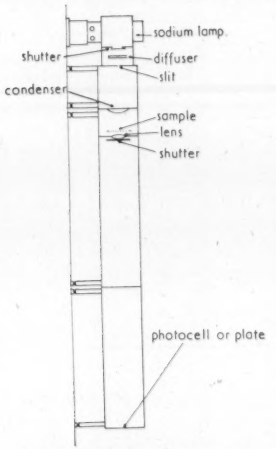

Fig. 2. The final eriometer

The light from the slit is formed into a parallel beam by a plano-convex lens of 140 mm focal length. Into this parallel beam and at right angles to it is inserted a plane sheet of fibres mounted parallel to the slit across a large aperture. The specimen is inserted close to a convex lens of focal length 900 mm. In the focal plane of the lens may be mounted as desired either a photocell assembly or a photographic plate.

Initially, a very sensitive Schwarz cell, supplied by Messrs. A. Hilger Ltd., was used, held in a vertical sliding mount attached to the moving edge of a vernier caliper. To protect the cell from the strong direct light of the central image an opaque stop was placed across the centre of the band system.

Because the slit itself and the optical system distribute some light in the focal plane, it was necessary to measure the background intensity and to subtract it from the total intensity produced by the fibres and the system. This is a drawback which has its most serious effects for specimens of high mean diameter and low variation.

When the cell developed defects and could not be replaced, photographic means were used to study the possibilities of the method. The opaque stop used in the centre for the photocell was replaced by an optical wedge with steps of known transmission. Two plates are exposed (one for the total and one for the background intensity without a sample), developed and photometered across the diffraction pattern at intervals of 0·2 mm. The centre of the plate is also photometered so that a scale of photometer reading against the density of the steps of the central transmission wedge is obtained. From this, equivalent wedge densities corresponding to the intensity at any point on the plate may be found (relative to the central beam). If the equivalent wedge density is D_1 at the position of the diffraction minimum and D_2 at the position of maximum total intensity, and d_1 and d_2 are the equivalent wedge densities at the corresponding points on the background plate, it is easily shown that $I_{min}/I_{max} = (10^{-D_1} - 10^{-d_1})/(10^{-D_2} - 10^{-d_2})$.

RESULTS AND DISCUSSION

Table 4 illustrates the accuracy and deficiencies of the method.

Table 4. *Fineness of fibres*

	By Microscope		*By Diffraction*	
Materia	*Mean* (μ)	f	*Mean* (μ)	f
Wire	51·0	0·027	51·1	0·063
Ardil	47·1	0·187	46·8	0·19
Nylon (black)	19·9	0·054	19·2	0·10

The mean fibre diameter, estimated from the position of the first minimum, gives close agreement with the mean derived from projection microscope measurements for fibres with a coefficient of variation (C.V.) below 20%. Estimation of f, the fractional C.V. of fibre diameter, is successfully made from I_{min}/I_{max} if f lies between 0·1 and 0·2, but difficulties arise in estimating low values of f, especially if the mean diameter is large. Thus even when corrections are made for spherical aberrations and the finite width of the slit, a specimen of wire of mean diameter 51 μ and $f = 0{\cdot}027$ is estimated by the diffraction method (from I_{min}/I_{max}) to have a value of $f = 0{\cdot}063$. This difficulty arises from the measurement of I_{min}, which for $f = 0{\cdot}025$ is very low. Since the background illumination in this region is of the same order of magnitude, the errors in measuring I_{min} become considerable. Nor is there any advantage in using ϕ_{max}/ϕ_{min}, which remains between 1·428 and 1·413 as f goes from 0·025 to 0·075.

Mounting the samples. Considerable attention has been given to this. It can readily be shown theoretically that errors of alinement even up to $\pm 6°$ produce a negligible effect on f. It is easy to mount the fibres within this tolerance in alinement, provided care is taken to straighten the fibres free of crimp.

Larger errors occur if the fibres are allowed to touch each other. For example, in a specimen of fibres having $f = 0{\cdot}05$, if 5% of the fibres are touching each other in pairs, the actual value of f for the specimen becomes 0·16. This it is which limits the number of fibres that can be mounted as a specimen, and rules out the use of short pieces of fibre mounted on a glass slide and alined by an alternating electric field. The fibre pieces tend to lie alongside each other, greatly modifying the distribution of diameter. Nor has the use of a high voltage to aline tufts of whole fibres proved any better, for the same reason. So far the most successful procedure has been to mount up to one hundred fibres one by one across a 2 in. mount with adhesive paper at each side. This is slow and limits the method.

An alternative procedure would be to mount fibre pieces with randomized directions in the same plane and to use this to diffract light from a point or circular aperture. It can readily be shown for the system of concentric rings, using the same symbols as before, that the intensity at an angle θ is given by

$$I_{T,\theta} = (C_0/\phi^3)\{1 - \cos\phi \,.\, \exp(-\tfrac{1}{2}f^2\phi^2)\} \qquad (9)$$

where C_0 involves the size of the aperture and the intensity of the illumination. Table 5 shows values of ϕ_{min}, ϕ_{max} and I_{min}/I_{max}.

Table 5. *Values for randomized pieces*

f	ϕ_{min} (rads)	ϕ_{max} (rads)	I_{min}/I_{max}
0·05	6·292	8·709	0·076
0·1	6·326	8·530	0·311
0·15	6·421	8·171	0·680
0·20	6·795	7·385	0·989
0·205	6·978	7·154	1·0
0·21	no min.	no max.	—

In the range $f = 0{\cdot}05$ to $f = 0{\cdot}20$, I_{min}/I_{max} depends almost linearly on f. Nevertheless, it will be seen that the system using randomized pieces is likely to be of more restricted application than the parallel fibre arrangements, especially for wool samples where f is seldom below 0·19. However, the randomized fibre method might be of interest for fibres other than wool.

Errors due to slit width and spherical aberration. In the theory it is assumed that the slit and its image are very fine. In the practical instrument the image of the slit is 1·5 mm wide, and this, at 900 mm from the lens, corresponds to a change of θ of $\pm 1{\cdot}5/(2 \times 900)$. The change in ϕ associated with a change $\delta\theta$ is $\delta\theta \times (2\pi\bar{a}\cos\theta)/\lambda$, which in practice becomes $\pm\pi\bar{a}/600\lambda$.

The intensities at the maximum and minimum positions, when the slit width is considered, may be found by taking the means of the intensities over the ranges $\phi_{max} \pm \delta\phi$ and $\phi_{min} \pm \delta\phi$. This was done graphically, by measuring the area beneath the intensity curves in the appropriate ranges, and from these new values of I_{min}/I_{max} were calculated for various values of $\bar{a}$ and f.

The second large source of error is due to the aberrations of the optical system, of which spherical aberration is the most important. Following the treatment described by Hardy and Perrin[9] it is possible to compute the position in the focal plane of the diffraction pattern produced by fibres at known distances from the optic axis. By considering diffraction patterns from thirty regions spaced equally across the holder, the sums of the intensities produced by each region near the maximum and minimum were found. Table 6 shows the values of I_{min}/I_{max} so computed for three values of mean diameter and four values of diameter variation, taking into account the finite size of the slit and the spherical abberations of the practical lens system.

Table 6. *Ratio I_{min}/I_{max}*

Coefficient of variation (%)	Mean diameter (μ) 50	30	20	Fine slit and no aberrations
2·5	0·060	0·029	0·020	0·013
5	0·109	0·075	0·064	0·054
10	0·277	0·240	0·230	0·221
20	0·874	0·853	0·848	0·844

Fig. 3 shows how the value of I_{min}/I_{max} varies with the C.V. for a sample of mean diameter 50 μ. The curve assuming an infinitely fine slit is shown together with the corrected

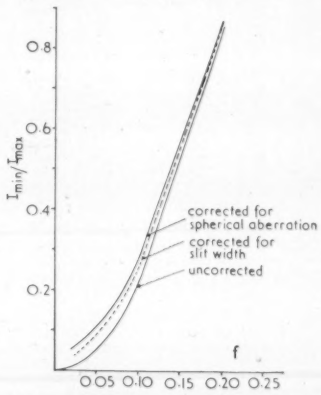

Fig. 3. Curves obtained with a sample with a mean diameter of 50 μ

curve allowing for the width of the slit and spherical aberration calculated separately as above. It will be seen that these factors are important when the coefficient of variation is small and the mean diameter large.

CONCLUSIONS

The method of diffraction may be used to measure the coefficient of variation of fibre diameter of a parallel array of fibres or of randomized pieces when this coefficient is between 10 and 20%. When the coefficient of variation is above 24% the band system for parallel fibres vanishes. The ring system for randomized pieces diffuses when the coefficient of variation is above 20%. Coefficients of variation from very uniform specimens (below 7·5%) have proved more difficult to estimate because of the difficulty of measuring accurately the intensity at the minima.

ACKNOWLEDGEMENTS

The authors are indebted to the Worshipful Company of Clothworkers of London for grants which have made it possible for one of them (B. E.) to take part in this research.

REFERENCES

(1) YOUNG, T. *Misc. Works*, 1855, **1**, p. 343 (1855).
(2) PIJPER, A. *Lancet*, **2**, p. 367 (1924).

(3) BERGANSIUS, F. L. *Pfluger's Archiv.*, **112**, p. 118 (1921).
(4) MILLAR, W. G. *Proc. Roy. Soc.* (*London*), *B*, **99**, p. 264 (1926).
(5) EMMONS, P. *Quart. J. Medicine*, **21**, p. 83 (1927).
(6) MCNICHOLAS, H. J., and CURTIS, H. J. *J. Res. Nat. Bur. Stand.*, **6**, pp. 717–34 (1931).
(7) EWLES, J. *J. Text. Sci.*, **2**, pp. 101–102 (1928).
(8) JENKINS, F. A., and WHITE, H. E. *Fundamentals of Physical Optics*, 1st ed., pp. 106 *et seq.* (New York: McGraw-Hill Book Co. Inc., 1937).
(9) HARDY, A. C., and PERRIN, F. H. *The Principles of optics*, 1st ed., pp. 86 *et seq.* (New York: McGraw-Hill Book Co. Inc., 1932). (For a more detailed account see *Nat. Bur. Stand. Sci. Paper* 461.)

Methods of cleaning glass by vapour degreasing and ultrasonically agitated solvents

By T. PUTNER, Grad.Inst.P., Research Laboratory, Edwards High Vacuum Ltd., Crawley, Sussex

[*Paper received* 19 *March*, 1959]

The production of clean glass surfaces for vacuum evaporation purposes has been studied using a number of different chemical cleaning techniques. The principal cleaning methods investigated were vapour degreasing, using a range of solvents, and high- and low-frequency ultrasonic agitation of an *iso*propyl alcohol bath. The cleanliness of glass surfaces after treatment was assessed from their coefficient of friction, wetting properties and adherence to vacuum deposited coatings. In terms of these properties vapour degreasing in pure *iso*propyl alcohol produced the cleanest surface. However, low-frequency ultrasonic agitation was the most effective method of removing gross surface contaminants. The cleaning of intricately shaped components is briefly discussed and it is shown that the gas pressure above the cleaning medium must be initially reduced to allow the solvent to enter cavities and thus provide maximum irradiation of the surface. Ultrasonic cleaning was found to be most effective when operated at low frequency (25 kc/s) with an undegassed fluid under atmospheric pressure.

A number of techniques have been advocated for preparing highly clean glass before depositing thin films on its surface by vacuum evaporation. Undoubtedly one of the most efficient methods of cleaning a glass surface is to immerse it in a glow discharge and much of the work on this subject has been reviewed by Holland.[1] Recent work done in this laboratory has shown that the most effective cleaning agency in the glow discharge is the bombardment of the glass surface by positive ions and high energy neutral molecules, whereas electron irradiation of the surface may give rise to the formation of contaminant films.[2] Glow discharge cleaning cannot remove gross contaminants from a surface, although uniform coatings of many molecular layers in thickness may be removed. Experiments were at first undertaken to determine the best chemical method of removing thick contaminant layers from glass surfaces before submitting them to glow discharge cleaning. However, in the course of these experiments it was found that under certain conditions clean glass surfaces could be prepared which were equal to those with a glow discharge.

Chemical methods of cleaning glass involving detergents, hydrocarbon solvents and acids are well described in the literature (see, for example, Strong[3]). Acid cleaning can be injurious to the surfaces of certain types of glasses and for this reason was not considered in these investigations. One of the simplest methods of cleaning glass is to wash the surface with a detergent and water followed by cleaning with cotton-wool steeped in a solvent such as *iso*propyl alcohol. Another and more effective process for removing molecular contamination from glass surfaces is by vapour degreasing in an alcohol vapour, a method which has become fairly well established in the lens-coating industry. Ultrasonic agitation of cleaning fluids has also been used successfully for removing gross contamination, e.g. rouge and pitch from the surfaces of optical components.[4] Each of the foregoing processes has been investigated to determine the standard of surface cleanliness it is capable of producing, and to find whether it can produce glass surfaces of comparative cleanliness to that obtained with ionic bombardment.

EXPERIMENTAL

The test glasses used in the experiments to be described were, with few exceptions, 2 mm thick uncoated lantern slides made of green soda-lime. The manner of employing the different cleaning processes are described below after a discussion of the techniques used for determining surface cleanliness.

(*a*) *Assessment of cleanliness*

There are various simple tests which can be used to find whether a glass surface is free from molecular contamination after treatment and these can be summarized as follows.

(i) *Breath figures and wetting.* The breath condensate formed on a clean glass surface exists as a uniform water layer because of the affinity of the clean glass for water. Such a breath figure has been termed "black" to differentiate it from the "grey" breath figure which is formed on contaminated glass and is due to the formation of minute water globules in the condensate (see, for example, Rayleigh,[5] Baker[6] and Fraser[7]). Similarly, a water droplet placed on a clean surface immediately flows outwards over the surface, whereas on a contaminated glass it forms a droplet with a measurable contact angle. Both the wettability and the type of breath figure were studied for the glass surfaces cleaned by the processes described in these experiments.

(ii) *Coefficient of friction.* A glass surface free from monomolecular contaminating layers has a high coefficient of friction (μ) to metals and glass as shown by Langmuir.[8] Values of the static coefficient of friction of about 0·8 have been obtained in this laboratory for glass on glass after the surface has been cleaned with Teepol and alcohol and bombarded in a glow discharge.[2] In the tests made in these experiments the static coefficient of friction (μ) was measured

in air, directly after cleaning, using a glass rider cut from ¼ in. thick plate, with a contact area of 2 × 5 cm. The rider was maintained in a clean state at all times by continuously degreasing it in *iso*propyl alcohol vapour. Values for the kinetic coefficient of friction were obtained by vibrating the specimen surface at 50 c/s during measurement.

(iii) *Thin film adhesion.* Evaporated metal films generally adhere more strongly to glass when the substrate has been thoroughly cleaned, so that the resistance shown by a metal film to stripping is a simple measure of the effectiveness of the pre-cleaning. This is particularly true for evaporated aluminium which was used in these experiments. The adhesion of the aluminium was tested by stripping the metal film with Sellotape pressed on to its surface.

(*b*) *Detergent washing and solvent cleaning method*

The test surface was first washed in a detergent (Teepol) and distilled water to remove heavy gross contaminants and then thoroughly rinsed and dried using a soft cloth. The glass was then polished with a soft absorbent cloth soaked in *iso*propyl alcohol. When the solvent had completely dried off the surface, a final polish was given with a Selvyt cloth. The results for the standard of cleanliness achieved are shown in Table 1, showing that the coefficient of friction (μ) of a surface cleaned with a detergent only is lower than one cleaned finally with a solvent. However, the values of μ obtained with both treatments rose to the same value after ion bombardment for 10 min at 3000 V and 500 mA in an 18 in. diameter bell jar. This shows that the solvent cleaning stage can be omitted provided the Teepol washed surface is glow-discharge cleaned.

Table 1. *Values for the static and kinetic coefficient of friction for glass surfaces cleaned by solvent and detergent cleaning methods*

Method of cleaning	*Coefficient of friction* Static	Kinetic
Vapour degreased in *iso*propyl alcohol	0·5–0·64	0·4–0·62
Vapour degreased in trichlorethylene	0·39	0·31
Vapour degreased in carbon tetrachloride	0·35	0·28
Teepol washed and polished	0·07	0·04
Teepol washed and h.t. discharge cleaned	0·8	0·6
Teepol washed, cleaned with alcohol and chalk, wiped with cotton-wool	0·33	0·27
Teepol washed, cleaned with alcohol, wiped with cotton-wool and h.t. discharge cleaned	0·8	—
Vapour degreased in *iso*propyl alcohol and h.t. discharge cleaned	0·8	0·6
Teepol washed, cleaned with alcohol and chalk, wiped with cotton-wool and flamed with gas flame	0·41	—

The value given for each cleaning method is a mean value resulting from several tests with that particular technique.

(*c*) *Vapour degreasing*

The vapour degreasing process was carried out in a large glass beaker, which was heated on an electric hot plate. The glass surfaces being cleaned were first washed in Teepol to remove heavy contamination. Three solvents were tested in sequence, namely carbon tetrachloride, trichlorethylene and *iso*propyl alcohol. The glass slides were suspended in the vapour for periods ranging from 15 s to 15 min. Maximum cleaning was achieved after an immersion period, which generally corresponded to the time taken for the condensing vapour to heat the glass to the temperature of the saturated vapour so that condensation ceased. Obviously the greater the thermal capacity of the specimen body the longer would be the time for which condensing vapour washes the exposed surface. If, however, the thermal capacity of the specimen is low, then it is possible for its surface to reach the temperature of the saturated vapour before the vapour has effected maximum cleaning. In the event of this it is necessary to immerse the specimen in the vapour a number of times. However, these tests indicated that effective cleaning can be obtained within a small time interval of about two minutes.

The highest value for the coefficient of friction obtained by vapour degreasing was 0·64 using *iso*propyl alcohol as the cleaning agent (see Table 1). Of the chemical cleaning methods investigated this technique gave a coefficient of friction nearest to that obtained by ion bombardment. Good results for the adhesion of evaporated aluminium were also obtained, as demonstrated in Fig. 1.

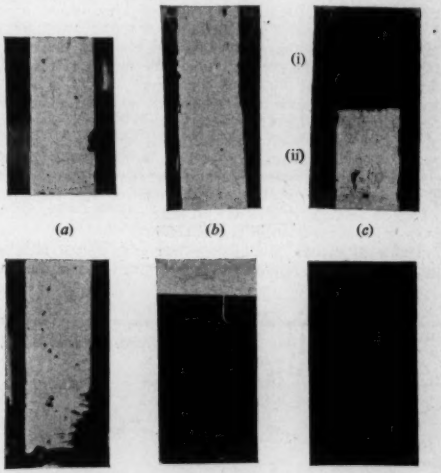

Fig. 1. Results of Sellotape stripping tests carried out on aluminium coatings deposited upon surfaces pre-cleaned by the following methods:

(*a*) Teepol washed and polished with soft cloth, no discharge cleaning; (*b*) vapour degreased then immersed in Teepol and water solution and allowed to dry, no discharge cleaning; (*c*) (i) vapour degreased, (ii) immersed in *iso*propyl alcohol and allowed to dry.

No discharge cleaning; (*d*) ultrasonically cleaned using high frequency agitation in *iso*propyl alcohol, no discharge cleaning; (*e*) vapour degreased in *iso*propyl alcohol, no discharge cleaning; (*f*) vapour degreased in *iso*propyl alcohol and discharge cleaned.

The results obtained with *iso*propyl were still maintained when the cleaning was carried out in a large stainless steel container suitable for cleaning 2 ft square glass plates with a steam-heated alcohol boiler. However, it was found necessary, especially when cleaning a relatively large specimen with high thermal capacity, to withdraw it slowly from the

vapour, allowing time for any condensate tears which may be still on the surface to evaporate off. When tears were left to dry off on the surface in air their marks or figures appeared after vacuum coating and in these regions the adhesion was always very poor.

Both carbon tetrachloride and trichorethylene produced low values for μ and poor film adhesion. The inferior results obtained with these two solvents are partly attributed to the loose whitish residue which appeared on the glass surface after vapour degreasing. If the deposit had been due to volatile impurities in the solvents then it should have re-evaporated from the glass when it became hot. The persistence of the deposit suggested that it was a chloride produced by reaction between the solvents and constituents in the glass surface.

(d) Ultrasonic cleaning methods

The use of both low- and high-frequency ultrasonic agitation of cleaning fluids for industrial purposes is discussed by Atherton[9] who considers the cleaning effect of cavitation in the agitated fluid. It is shown that the phenomenon, which is present at the lower frequencies (20 to 100 kc/s) will greatly assist the removal of gross particles from contaminated bodies. High cavitation energies can damage the surface of the article being cleaned and therefore the energy output of a low-frequency system must be carefully controlled. High energies can be used with high-frequency systems having frequencies of the order of 1 Mc/s, because the cleaning action is more gentle and free from cavitational bombardment of the irradiated surface. Noltingle and Neppiras[10] have investigated the problems of cavitation and its dependence on vibration frequency, internal pressure and the presence of nuclei of suitable size for its production.

There are certain conditions which arise by reducing the pressure above the liquid in agitation, which may or may not

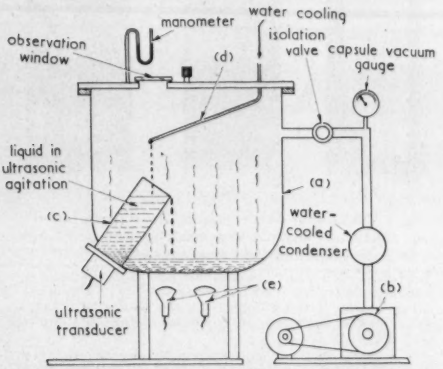

Fig. 2. Apparatus used for ultrasonic cleaning

be advantageous when cleaning surfaces.* The two main factors introduced are as follows:

(1) dissolved gases which provide suitable nuclei for cavitation centres are removed, and therefore cavitation effects may be reduced.[11]

(2) air trapped in deep holes in the surface of intricately shaped components may be removed, thereby permitting the solvent to cover completely the surface to be cleaned.

The influence of these two effects and the standard of cleaning obtainable with ultrasonics were observed using an apparatus constructed as shown in Fig. 2. With this system, cleaning could be conducted either at atmospheric or reduced pressures.

Ultrasonic cleaning apparatus

The vacuum chamber *a* was evacuated using a rotary pump *b* having a pumping speed of 450 l./min; the pump was fitted with air ballasting. The vessel *c* isolated the fluid in ultrasonic agitation from the solvent contained in the chamber. A condensing system *d* was fitted in the chamber lid to produce a continuous exchange of fluid by distillation from the chamber into the vessel *c* so that fluid was kept clean. For distillation the liquid was heated externally by two infra-red heaters *e*.

The ultrasonic power was provided by either a high-or low-frequency ultrasonic generator. The high-frequency unit operated at 1 Mc/s and had a 300 W output. A thin slice of barium titanate crystal was used as the transducer with an effective area of 4 × 8 cm. The low-frequency unit operated at 25 kc/s at an output of 250 W using a magneto-strictor for the transducer, the vibrating plate was approximately 10 cm in diameter. The transducer mountings were suitably constructed to fit into the vacuum system as shown in Figs. 3 and 4. In view of the effectiveness of *iso*propyl alcohol when used in vapour degreasing it was decided to restrict the ultrasonic tests to this fluid.

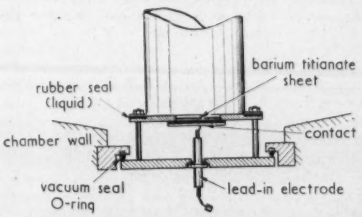

Fig. 3. High-frequency transducer (barium titanate crystal)

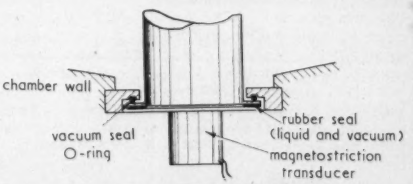

Fig. 4. Low-frequency transducer

Ultrasonic experiments

The cleaning liquid was degassed under a controlled pressure of between 30–50 mm of mercury, i.e. in the region

* An ultrasonic cleaning system, in which the fluid is agitated under reduced gas pressure, is manufactured by the Technochemie Co. of Switzerland.

of the saturated vapour pressure of the solvent at room temperature. Further degassing occurred when the liquid was ultrasonically agitated. In fact, when using the low-frequency agitation the boiling of the liquid was violent unless the generator was operated at reduced power. However, in the high-frequency case conditions were stable enough for carrying out cleaning tests using maximum power input. The slides were cleaned for periods of from fifteen seconds up to several minutes. After each operation the solvent was allowed to dry by evaporation to ensure that the final state of the surface was due to the ultrasonic cleaning, and not interfered with by wiping or polishing. Tables 2, 3 and Fig. 1 indicate the standard of cleanliness obtained using ultrasonics under these conditions.

Table 2. *Static and kinetic coefficient of friction results for ultrasonically cleaned glass surfaces*

	High-frequency cleaning		*Low-frequency cleaning*		
Time (s)	*Static*	*Kinetic*	*Static*	*Kinetic*	*Comments*
15–20	0·39	0·28	—	—	High-frequency generator run at full power, 300 W
30–45	0·39	0·27	—	—	
60	—	—	0·3	0·2	
120	0·4	0·27	0·28	0·2	Low-frequency generator run at half power, 125 W
5 min	0·37	0·25	0·3	0·2	

The values given are mean values resulting from many tests.

The highest value achieved for the static coefficient of friction was 0·4. It was not easy to explain why there should be a difference in the cleaning results between the vapour degreasing and ultrasonic cleaning methods. In the first technique the test surfaces were immersed in a very pure alcohol vapour and in the second the surfaces were immersed in the very pure distilled alcohol liquid itself. Both samples in their respective cleaning medium should then be exposed to equivalent surface contamination, if any. A number of theories were discussed but no conclusions were arrived at. Radiant heating of the glass surface to accelerate drying after removal from the fluid did not alter the results. However, h.t. discharge cleaning in a vacuum cleaned off the residual contamination responsible for the low friction values as shown by adhesion tests (see Fig. 1).

Table 3. *Wetting observations for different cleaning methods*

Method of cleaning	*Observation*
Ultrasonically cleaned in *iso*propyl alcohol using high frequency at reduced pressure	Only slight indication of wetting
Ultrasonically cleaned in *iso*propyl alcohol using low frequency at reduced pressure	Only very slight indication of wetting
Vapour degreasing in *iso*propyl alcohol	Surface wets
Discharge cleaned in correctly designed systems	Surface wets
Teepol washed and polished	No wetting
Vapour degreased in either carbon tetrachloride or trichlorethylene	Partial wetting

A series of tests were carried out on unwashed slides with both low- and high-frequency ultrasonic cleaning which showed that heavy contaminants, such as greasy finger prints, could be removed from a glass surface when exposed to ultrasonic agitation providing the fluid was at atmospheric

Table 4. *Removal of heavy dirt deposits*

The glass slides were heavily finger-printed with grease and dust. Two greases were used: Apiezon vacuum grease and ordinary lubricating oil.

Method of cleaning	*Cleaning ability*	*Comments*
Immersed in *iso*propyl alcohol for 2 min	No cleaning	Oil contamination only
Immersed in trichlorethylene for 2 min	No cleaning	Oil contamination only
Ultrasonically cleaned at atmosphere for 2 min in *iso*propyl alcohol. Using high-frequency transducer	Removed grease and dirt, but not the finger print impression	Oil contamination only
Ultrasonically cleaned at reduced pressure for 2 min in *iso*propyl alcohol using high-frequency transducer	Removed grease and dirt, but not the finger print impression	Oil contamination only
Ultrasonically cleaned at atmosphere for 2 min in *iso*propyl alcohol using low-frequency transducer	Removed both grease and dirt and completely removed finger print impression	Will clean oil prints off in ½ min
Ultrasonically cleaned at reduced pressure for 2 min in *iso*propyl alcohol using low-frequency transducer	Removed both grease and dirt and completely removed finger print impression	Will clean oil prints off in ½ min
Vapour degreased in *iso*propyl alcohol	Removed grease and dirt, but not finger print impression	—

Table 5. *Cleaning of enclosures using ultrasonic methods*

Closed ended tubes and capillaries	Ultrasonic cleaning at atmosphere using low-frequency transducer in *iso*propyl alcohol. Trapped gases not removed	Colloidal carbon (Dag)	No cleaning
Closed ended capillary	Ultrasonic cleaning at reduced pressure using low-frequency transducer in *iso*propyl alcohol	Colloidal carbon (Dag)	Partial cleaning after 4 min
Closed ended capillary	Low-frequency transducer in *iso*propyl alcohol. System pumped out to remove trapped air from capillary. Air admitted to system. Ultrasonic cleaning carried out at atmosphere in undegassed medium	Colloidal carbon (Dag)	Complete removal after approximately 4 min

The exact times required for removing a particular contaminant could not be obtained because of the variation in quantity of contamination from specimen to specimen in the many repeated runs.

pressure and agitated at a low frequency (see Table 4). These results show how cavitation is essential for removing gross contaminants. The effectiveness of the ultrasonic cleaning of enclosures was determined using glass capillary tubes 1·5 mm diameter × 2 cm long with closed ends. The inside surfaces were contaminated with colloidal carbon (Dag) or grease. The tests demonstrated that it is necessary to reduce the gas pressure above the cleaning medium to remove the trapped air from the holes and interstices to obtain maximum irradiation of all surfaces, but in order to achieve the most effective cleaning the liquid should again be in an undegassed state as shown in Table 5. This again shows the need for cavitation when removing gross contaminants. The standard of the cleaning obtained after the removal of the major contaminants could not be assessed, but it was assumed to be of similar order to that achieved on the flat glass surfaces.

CONCLUSIONS

The investigations show that vapour degreasing in *iso*propyl alcohol produces a higher standard of surface cleanliness than can be achieved with ultrasonic cleaning. The failure to obtain comparable results with ultrasonic agitation was not easy to explain as stated above. It was found that vapour degreasing in *iso*propyl alcohol could produce clean surfaces which were almost comparable to those obtained by discharge cleaning. However, this method was not found to be efficient in the removal of gross contamination and must therefore be used in combination with a detergent washing process. The vapour degreasing and ultrasonic methods are both suitable as pre-cleaning techniques for preparing glass supports for thin film deposition, provided discharge cleaning is used, especially in the ultrasonic case, in the final treatment.

It was shown that, to obtain uniform cleaning of intricately shaped surfaces when using ultrasonics, a vacuum system must be used in order that the pressure above the cleaning medium can be initially reduced to release trapped gases from enclosures. However, it was found that the fluid should be in an undegassed state and agitated at low frequency to obtain the most effective cleaning, demonstrating the importance of cavitation for the removal of gross contaminants.

ACKNOWLEDGEMENTS

Acknowledgements are made to Mullard Ltd. for the use of their ultrasonic generator equipment, to Mr. K. Day of Mullard Ltd. for his valuable assistance with the ultrasonic cleaning tests, to Mr. L. Holland for his guidance throughout the work, and to Mr. A. S. D. Barrett, Technical Director of Edwards High Vacuum Ltd., for permission to publish this paper.

REFERENCES

(1) HOLLAND, L. *Vacuum Deposition of Thin Films* (London: Chapman and Hall Ltd., 1958).
(2) HOLLAND, L. *Brit. J. Appl. Phys.*, **9**, pp. 410–415 (1958).
(3) STRONG, J. *Modern Physical Laboratory Practice* (London: Blackie, 1944).
(4) *Manufacturing Optician*, **11**, pp. 288–290 (1958).
(5) RAYLEIGH, LORD. *Nature* (*London*), **86**, p. 416 (1911).
(6) BAKER, T. J. *Phil. Mag.*, **44**, pp. 752–766 (1922).
(7) FRAZER, J. H. *Phys. Rev.*, **33**, p. 97 (1929).
(8) LANGMUIR, I. *J. Franklin Inst.*, **218**, p. 143 (1934).
(9) ATHERTON, L. *Brit. Commun. and Electronics*, March (1957).
(10) NOLTINGLE, B. E., and NEPPIRAS, E. A. *Proc. Phys. Soc.* (*London*) *B*, **63**, p. 674 (1950).
(11) NEPPIRAS, E. A. *Research*, **6**, p. 276 (1953).

Technique for determining the orientation of single crystals of bismuth

By D. T. J. HURLE, B.Sc., Grad.Inst.P., and S. WEINTROUB, M.A., F.Inst.P., Department of Physics, The University of Southampton

[*Paper received* 16 *January*, 1959]

Except in particular cases, neither X-rays nor light figures alone suffice to determine completely and unambiguously the orientation of a bismuth crystal rod. The technique described consists of a combination of the two. The light figure pattern is used to locate the (111) plane approximately in order to aline the rod relative to the X-ray beam before the back-reflexion Laue photograph is taken, and to assist in the interpretation of the stereographic projection. The modifications made to a Unicam single-crystal X-ray goniometer to enable the technique to be applied to rods of 6 mm diameter and 25 cm length are described.

The orientation of a metal single-crystal rod, that is the angles which the principal crystallographic axes make with the rod axis, may be determined either from back-reflexion Laue photographs of the crystal using X-rays or from the optical reflexion patterns, so called "light figures," obtained from the etched surface of the crystal. In the case of bismuth neither method may prove conclusive. However, by a careful combination of the two methods it has been found possible to determine completely and unambiguously the orientations of single-crystal rods of bismuth, about 6 mm in diameter and of lengths ranging up to 25 cm. The details of the technique and procedure are described in the next section. The technique is applicable both to crystals of high quality and to crystals exhibiting a gross macromosaic structure of the type described by Teghtsoonian and Chalmers.[1]

Bismuth is trigonal, and its primitive cell consists of a simple rhombohedron with an axial angle of 57° 14′. It is more useful, however, to characterize the structure by a face-centred rhombohedron formed from the primitive cell (see Salkovitz[2] and Vickers[3]), and in addition, this face-centred rhombohedron may be regarded as a face-centred cube which has been slightly deformed by extension along a diagonal until the axial angle becomes 87° 34′. The diagonal corresponds to the trigonal axis. Vickers[3] has published tables of the angles between the crystallographic directions and between the planes of the bismuth lattice, and he has discussed how back-reflexion Laue photographs of bismuth crystals can be interpreted. However, because of the near cubic symmetry of the bismuth lattice, it is not possible to obtain an unambiguous interpretation of the photographs of

defective crystals, or even of high quality crystals, unless the angles between the Laue spots or zones can be measured extremely accurately (to within $\frac{1}{2}^\circ$). To particularize, consider the "pseudo-cube" as the unit cell and describe the bismuth structure in terms of Miller indices assigned to this "pseudo-cube." The orientation of a single-crystal rod can then be specified by the angles which the trigonal axis [111] and the digonal axes ([10$\bar{1}$], [0$\bar{1}$1], [$\bar{1}$10]) make with the rod axis. Because of the near cubic nature of the bismuth lattice, it will not be possible, except for high quality crystals where sharp Laue spots are obtained, to differentiate by the X-ray method between the [111] and the $\langle 11\bar{1} \rangle$ directions.

In the light figure method, the orientation is determined by observation of the patterns formed by reflecting a convergent light beam at the etched surface of the crystal. Yamamoto and Watanabe,[4] who made a systematic study of the light figure patterns obtained from bismuth crystals treated with various chemical etchants, developed a technique whereby they could determine the orientation of any bismuth crystal from its light figures. Using an etchant of a 50% aqueous solution of a 1 : 2 mixture of hydrochloric acid and nitric acid, they obtained light figures corresponding to the planes (111), $\{uv\bar{w}\}$, $\{uvw\}$ and $\{uuw\}$. The $\{uv\bar{w}\}$, $\{uvw\}$ and $\{uuw\}$ planes are not of low index and the actual indices which can be assigned to them, namely: $\{44\bar{1}\}$, $\{55\bar{1}\}$, or $\{66\bar{1}\}$ for $\{uv\bar{w}\}$; $\{449\}$ or $\{337\}$ for $\{uvw\}$; and $\{\bar{1}15\}$ for $\{uuw\}$ are dependent to some extent on the etching conditions. The orientations were determined from the (111) and the $\{uv\bar{w}\}$ figures.

The light figure technique, as applied to bismuth, has been examined in some detail by Hart[5] and again more recently by the authors. It has been established that the technique is of use only for crystals for which the (111) light figure can be obtained directly. For other crystals the diffuseness and lack of an obvious centre of symmetry of the $\{uv\bar{w}\}$ figure, together with the uncertainty of their indices, make the technique at best an approximate one. However, since a light figure is obtained from the (111) and not from the $\{11\bar{1}\}$ planes, the (111) plane can be unambiguously identified.

THE TECHNIQUE AND APPARATUS

The basis of the authors' technique is to obtain the approximate position of the (111) plane prior to taking the Laue photograph so that the (111) position also can be plotted on the stereographic projection obtained from the photograph.

A Unicam type S25 single-crystal X-ray goniometer, used in conjunction with a Raymax type 60 X-ray set, was modified in order to accommodate a crystal rod. A Duralumin trough 26 cm long, in which the crystal was placed, was attached to the goniometer head and arranged horizontally with its axis parallel to, and exactly 3·00 cm from, the plane of the X-ray film. The approximate position of the (111) plane was determined before the X-ray photograph of the crystal was taken by replacing the X-ray collimator by a collimator of aperture of about 4 mm and with a flange at one end. The collimator was screwed into the camera from the side facing the crystal and the flange was used to hold a white hemicylindrical screen with its axis vertical. The axis intersected the front surface of the crystal at the point at which a convergent light beam, after passing through the collimator, was incident on the crystal. The goniometer position relative to the focal point of this beam was adjusted so that light reflected from the etched planes of the crystal was in focus on the screen in the horizontal plane containing the collimator. The intersection of this horizontal plane with the screen was marked and calibrated in degrees.

The crystal rod was rotated about its axis in the trough and the optical pattern observed. The two (111) light figures were located (180° apart) and the crystal was rotated until one of them was in the horizontal plane through the collimator. The approximate angular position of the (111) light figure relative to the rod axis was read from the calibrated screen. After the crystal had been alined in this way the screen and collimator were removed, the X-ray collimator was replaced and the Laue photograph taken. To ensure that the crystal did not move after alinement it was held fixed in the trough by two small phosphor bronze clips.

A stereographic projection of the zone axes was then plotted from the Laue photograph and the approximate position of the (111) plane normal marked on the projection. This lies on the line of the projection representing the rod axis, and at a distance from the centre of the projection equal to one-half the measured angular distance. The projection was then interpreted by the method suggested by Vickers.[3] The knowledge of the approximate position of the (111) plane normal helps considerably in indexing the zones, and entirely removes the ambiguity referred to earlier.

The above method served for crystals of orientation ψ (the angle between the rod and trigonal axes) greater than 45°, but for those crystals of ψ less than 45° the (111) light figure did not appear on the screen. However, for crystals of ψ between 45 and 30° the approximate position of the light figure was inferred from the pattern which was present. For crystals of ψ between 30 and 0° it was necessary to make the optical examination and take the Laue photograph with the crystal alined parallel to the incident beam, and then the light figure pattern did contain the (111) figure. To do this an additional modification to the goniometer was necessary.

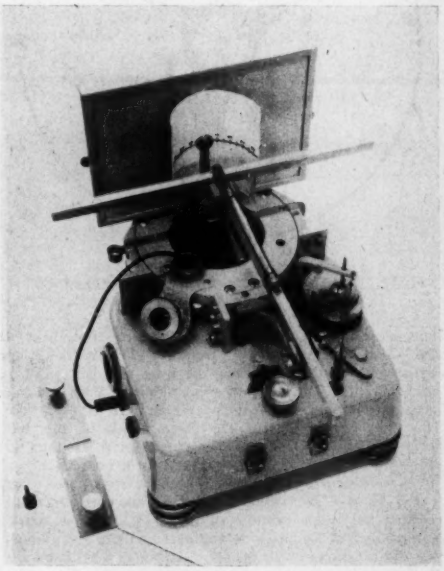

Fig. 1. Modified X-ray goniometer

A Duralumin trough similar to the first was mounted parallel to the collimator axis and supported at the camera end by a channel-section piece which fitted over the top rocking slide of the goniometer head. At the other end the trough was supported in a similar channel-section piece, held at the end of an arm which was screwed on to the goniometer in the position usually occupied by the tele-microscope. The trough could be raised or lowered vertically by means of a thumbscrew and moved laterally by two pinching screws in the supporting channel-section piece. The trough was alined optically with respect to the collimator by placing a hollow 6 mm diameter rod in the trough. The crystal-to-film distance was fixed at 3·00 cm by using a brass spacing piece. The modified goniometer with the crystal mounted in the "end on" position is shown in Fig. 1.

THE LIGHT FIGURES

A 50% aqueous solution of nitric acid was used as etchant since it produced the clearest (111) light figure. The crystal was etched for about thirty seconds. The etchant must then be slowly diluted before removal of the crystal, or the crystal surface will become covered with white hydrolyzed reaction products. Fig. 2 is a stereographic representation of the

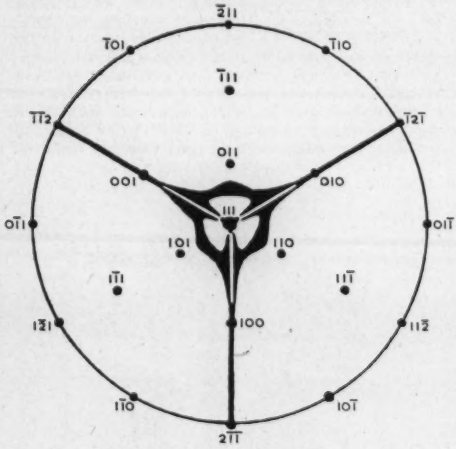

Fig. 2. Stereographic representation of the light figure pattern

light figure pattern. The pattern consists of three lines, at 120° to each other, radiating from the (111) spot. In the region near to the (111) spot the lines are dark (that is, defined by the light areas on either side of them), but they merge into lines of light at some distance from the (111) spot. The lines correspond to the three zones of the type $\{111\}$—$\{2\bar{1}1\}$—$\{100\}$—$\{2\bar{1}\bar{1}\}$. For crystals of ψ less than 45° only zone lines appear, and for crystals of ψ between 45 and 30° the position of the intersection of the zone lines, which is the (111) position, can be deduced approximately by extrapolating the visible portions of the lines. In their papers Yamamoto and Watanabe do not mention these lines, though they did experiment with the above etchant. The absence of the lines in their case may be due to the fact that bismuth of 99·95–99·99% purity was used, compared with zone-refined 99·9995% pure bismuth in the present work. A simple model was constructed in order to assist in the interpretation of the observed positions of the zone lines. It consists of three similar metal disks, intersecting along the diameter of a sphere and inclined at 60° to each other, which represent the three zones $\{\bar{2}11\}$—$\{\bar{1}11\}$—$\{111\}$—$\{100\}$—$\{2\bar{1}\bar{1}\}$, and their common diameter is the trigonal axis. A horizontal rod, which represents the crystal rod axis and is free to rotate about its own axis, is attached to the centre of the disks by a ball and socket joint. A vertical hemicylindrical cellophane screen of radius slightly larger than that of the disks is fixed with its axis passing through the centre of the disks. The disks are looked at through the screen and tilted until their trace on the screen is found to correspond to an observed optical pattern from a crystal rod. A very approximate determination of ψ can then be made.

DISCUSSION

The important advantage of the combined optical/X-ray technique is that it enables one to determine the complete orientation of any single-crystal rod of bismuth, and may be carried out for both crystals of high perfection and those which exhibit a gross macromosaic structure. The accuracy of the method depends on the X-ray measurements and does not depend on the accuracy with which the centre of symmetry of the (111) or $\{u\bar{u}\bar{v}\}$ light figures is determined. It is only necessary to know the (111) position approximately in order to distinguish it from the plane $\{11\bar{1}\}$ on the stereographic projection of the Laue photograph. Hence, the accuracy with which the orientation of near perfect crystals is determined is limited by the accuracy of the stereographic net, the Greninger chart and the alinement of the X-ray film in its holder. The accuracy in the present work is estimated as one degree, but it could be improved with care. In crystals which exhibit a gross macromosaic structure, the misorientation across the lineage boundaries may be a degree or two, and thus the orientation of the crystal cannot be specified more accurately than to within this limit.

In the light figure method sharp figures with well defined centres of symmetry are required for the greatest accuracy, and such figures are difficult to obtain, but with the combined optical/X-ray technique sharply defined figures are not essential and the etching conditions are therefore not critical. A critical comparison of the light figure and X-ray methods as applied to a number of metals, including bismuth, which differ in their crystallographic symmetry, has been made by Yamamoto and Watanabe[6] and an accuracy of 0·2° is claimed by them for bismuth crystals of all orientations when using the light figure method. However, both Hart[5] and the present authors have been unable to attain this high accuracy. In fact, Hart found that the light figure method was useful only for crystals of ψ between 90 and 60° for which the (111) spot is directly visible. In the range 90 to 80° the accuracy was 1° and in the range 80 to 60° was 2°.

Laue photographs of crystals of antimony, which has the same crystal symmetry as bismuth with an axial angle (for the face-centred rhombohedron) of only 10′ less than that of bismuth, are equally difficult to interpret, and thus the combined optical/X-ray technique might well be useful in determining the orientation of antimony crystals. However, antimony is very difficult to etch chemically. The reaction products on etching with nitric or hydrochloric acid solutions are hydrolyzed even when the etchant is carefully diluted, and a film is left on the crystal surface so that distinguishable light figures are not obtained. The authors have, however, observed a sharply defined optical pattern from unetched

antimony crystals which have been grown in contact with silica moulds. The pattern consisted of three lines similar to those observed in bismuth and corresponding to the same zones, with sharp spots on the lines corresponding to the planes {111}, {211}, {311}, {100}.

ACKNOWLEDGEMENTS

The authors are indebted to the University of Southampton for facilities provided and to Mullard Southampton Works for the antimony crystals. One of us (D. T. J. H.) is grateful to the D.S.I.R. for a maintenance allowance.

REFERENCES

(1) TEGHTSOONIAN, E., and CHALMERS, B. *Canad. J. Phys.*, **29**, p. 370 (1951); **30**, p. 388 (1952).
(2) SALKOVITZ, E. *J. Metals*, **8**, p. 176 (1956).
(3) VICKERS, W. *J. Metals*, **9**, p. 827 (1957).
(4) YAMAMOTO, M., and WATANABE, J. *Sci. Rep., Tôhoku Univ. A*, **4**, p. 127 (1952); **5**, p. 124, 135 (1953).
(5) HART, B. M.Sc. Thesis (University of Southampton, 1957).
(6) YAMAMOTO, M., and WATANABE, J. *Sci. Rep., Tôhoku Univ. A*, **9**, p. 24 (1957).

Transient temperatures attained in disk brakes

By T. P. NEWCOMB, M.Sc., A.Inst.P., Ferodo Ltd., Chapel-en-le-Frith, Stockport, Cheshire

[*Paper first received* 12 *January, and in final form* 17 *February*, 1959]

A solution is given to the problem of heat conduction in a composite solid consisting of three infinite slabs between parallel plane boundaries, when the two interfaces are subjected to a thermal flux which decreases linearly with time, whilst at the two outer plane surfaces there is no flow of heat. This solution is applied to the problem of determining the transient temperatures reached at the friction surfaces of a disk brake when a constant deceleration is produced during braking. Typical values of the temperature of the surface of a disk obtained by use of a radiation pyrometer with a rapid response are given, and comparisons made with the mean temperatures determined theoretically.

In a type of brake known as a disk brake two blocks of friction material known as "pads" are pressed against each side of a rotating annular ring of ferrous material, the latter being rigidly attached to the body, the motion of which requires to be retarded. If in a single brake application each pad exerts a constant frictional force, the rate of heat generation H at the friction surfaces decreases linearly with time t and $H = Q(1 - at)$ where Q and a are constants. Under these conditions, a first approximation to the determination of the temperatures associated with disk braking may be obtained by considering the problem of the linear flow of heat through a composite solid consisting of three infinite slabs between parallel boundaries, of which the two interfaces are subjected to a thermal flux which decreases linearly with time, whilst at the two outer boundaries there is no flow of heat. This heat problem is a generalization of one considered previously by the author,[1] and may be solved by the use of a Laplace transformation.

THE SOLUTION TO THE HEAT CONDUCTION PROBLEM

Consider the linear flow of heat in a composite solid consisting of three parallel-faced infinite slabs where $-d_1 < x < 0$ and $d_1 + d_2 > x > d_2$ represents the two outer slabs each with physical properties $K_1, \rho_1, c_1, k_1, v_1, v_3$, and $0 < x < d_2$ is the other medium with physical properties $K_2, \rho_2, c_2, k_2, v_2$. The quantities K, ρ, c, k, v with suffixes for whichever body is considered refer respectively to the thermal conductivity, density, specific heat, thermal diffusivity and the temperature rise at any point x in the medium concerned. At the surfaces of contact $x = 0$ and $x = d_2$ there exists a total flux $Q(1 - at)$, whilst at the other boundaries ($x = -d_1$ and $x = d_1 + d_2$) there is no flow of heat. Initially the composite body is at zero temperature. Using these boundary conditions and following the procedure outlined previously by Newcomb,[1] the equations giving the Laplace transform of the temperatures attained in the slabs reduce to

$$\bar{v}_1 = f(q_1, q_2) \sinh q_2 d_2 \cosh q_1(d_1 + x) \tag{1}$$

$$\bar{v}_2 = f(q_1, q_2)[\cosh q_1 d_1 \sinh q_2(d_2 - x) + \cosh q_1 d_1 \sinh q_2 x] \tag{2}$$

$$\bar{v}_3 = f(q_1, q_2) \sinh q_2 d_2 \cosh q_1(x - d_1 - d_2) \tag{3}$$

where

$$f(q_1, q_2) = \frac{Qk_2^{1/2}}{K_2}\left(\frac{1}{p^{3/2}} - \frac{a}{p^{5/2}}\right) \frac{1}{\cosh q_1 d_1 (\cosh q_2 d_2 - 1) + \sigma \sinh q_2 d_2 \sinh q_1 d_1} \tag{4}$$

and

$$q_1^2 = \frac{\rho}{k_1}, q_2^2 = \frac{\rho}{k_2}, \sigma = \frac{K_1}{K_2}\left(\frac{k_2}{k_1}\right)^{1/2} \tag{5}$$

In practice, the most important temperatures are those reached at the friction surfaces where $x = 0$ and $x = d_2$, and these are given by the equation

$$\bar{v} = \bar{v}_1 = \bar{v}_3 = \frac{Qk_2^{1/2}}{K_2}\left(\frac{1}{p^{3/2}} - \frac{a}{p^{5/2}}\right)\left[1\Big/\left(\tanh\frac{q_2 d_2}{2} + \sigma \tanh q_1 d_1\right)\right] \tag{6}$$

If in this relationship one expresses

$$\tanh(q_2 d_2/2) + \sigma \tanh q_1 d_1$$

in terms of negative exponentials and expands by the binomial theorem, a converging series of negative exponential terms is obtained. These expressions can be inverted from a table of Laplace transforms[2] and the first few terms of v then reduce to

$$\begin{aligned} v = \frac{Qk_2^{1/2}}{K_2(1+\sigma)}\Big\{ & \frac{2t^{1/2}}{\pi^{1/2}}\left(1 - \frac{2}{3}at\right) + \frac{4t^{1/2}}{(1+\sigma)}\left[i\operatorname{erfc} 2\lambda_2 - \right. \\ & - \sigma i \operatorname{erfc} 2\lambda_1 - 4at(i^3 \operatorname{erfc} 2\lambda_2 - \sigma i^3 \operatorname{erfc} 2\lambda_1)] \\ & + 2(1 - 2A^2)t^{1/2}[i \operatorname{erfc} 2(\lambda_1 + \lambda_2) - \\ & - 4ati^3 \operatorname{erfc} 2(\lambda_1 + \lambda_2)] \\ & + 4Bt^{1/2}[i \operatorname{erfc} 4\lambda_2 - \sigma i \operatorname{erfc} 4\lambda_1 - \\ & - 4at(i^3 \operatorname{erfc} 4\lambda_2 - \sigma i^3 \operatorname{erfc} 4\lambda_1)] \\ & + 2(1 + 3A - A^2)t^{1/2}[i \operatorname{erfc} 2(2\lambda_2 + \lambda_1) - \\ & - 4\, ati^3 \operatorname{erfc} 2\,(2\lambda_2 + \lambda_1)] \\ & + 2(1 - 3A - A^2)t^{1/2}[i \operatorname{erfc} 2(\lambda_2 + 2\lambda_1) - \\ & - 4ati^3 \operatorname{erfc} 2\,(\lambda_2 + 2\lambda_1)] \\ & \left. + 4Ct^{1/2}[i \operatorname{erfc} 6\lambda_2 - 4ati^3 \operatorname{erfc} 6\lambda_1] + \ldots \right\} \end{aligned} \tag{7}$$

where $\lambda_2 = \dfrac{d_2}{4(k_2 t)^{1/2}} \quad \lambda_1 = \dfrac{d_1}{2(k_1 t)^{1/2}}$

$$A = \frac{1-\sigma}{1+\sigma} \quad B = \frac{1-\sigma}{(1+\sigma)^2} \quad C = \frac{(1-\sigma)^2}{(1+\sigma)^3}$$

and $i^n \operatorname{erfc} x = \int_x^\infty i^{n-1} \operatorname{erfc} y\,dy (n = 1, 2, 3 \ldots)$

with $i^0 \operatorname{erfc} x = \operatorname{erfc} x = \dfrac{2}{\pi^{1/2}} \int_x^\infty \exp(-y^2) dy$

The function $i^n \operatorname{erfc} x$ for various values of n and x has been considered by Hartree,[3] the results being given in tabular form (see also Carslaw and Jaeger[2] Appendix II).

The above series for determining the temperature at the friction surfaces is rapidly convergent, and in practice only three or four terms are needed for values of λ normally encountered.

APPLICATION OF THEORY

If a disk brake pad of area A_1 slides against a rotating cast iron annulus and sweeps out an area A_2 (where $A_2 > A_1$), then the ratio of H_2 to H_1, where H_1 and H_2 are the net instantaneous energies entering the pad and disk respectively, is given by A_2Q_2/A_1Q_1. This ratio is to a first approximation $(A_2K_2/A_1K_1)(k_1/k_2)^{1/2}$ which is of the order 90 : 1 in a typical disk brake where $K_1 = 2{\cdot}9 \times 10^{-3}$ cal cm^{-1} s^{-1} °C^{-1}, $k_1 = 6{\cdot}28 \times 10^{-3}$ cm^2/s, $d_1 = 1{\cdot}1$ cm and $K_2 = 1{\cdot}1 \times 10^{-1}$ cal cm^{-1} s^{-1} °C^{-1}, $k_2 = 1{\cdot}1 \times 10^{-1}$ cm^2/s, $d_2 = 1{\cdot}27$ cm and $A_2 = 400$ cm^2 and $A_1 = 4{\cdot}5$ cm^2. Hence, if the initial speed of the disk is u cm/s and during braking a constant linear deceleration of f cm/s^2 is produced, then the instantaneous energy H generated at the friction surface is $H = (Fu/A_2J)[1 - (ft/u)] = Q(1 - at)$ where F is the frictional force acting at the interface of annulus and one pad; J is the mechanical equivalent of heat taken as $4{\cdot}18 \times 10^7$ erg/cal; $Q = Fu/AJ$; $a = f/u$. Thus since F and f can be measured during the brake application, the quantities Q and a can be determined from the above equations.

Experimental results have been obtained with a brake possessing the above physical quantities and a comparison made with temperatures determined from equation (7). Temperature measurements were made by using a commercial infra-red radiation pyrometer which can measure temperatures in the range 150–1200° C. The infra-red sensitive element is a lead sulphide cell, which is placed behind a rotating chopper disk in such a manner that it is irradiated alternately by the hot surface and by a tungsten filament comparison lamp. An alternating voltage is thus produced across the cell, the value of which is zero if the quantity of radiation from the sources is the same. A control circuit adjusts the lamp current and ensures that the alternating voltage of the cell is kept at a minimum, and it is the lamp current, which is indicated on a meter, that is a function of the surface temperature. Thus the cell is used as a null-detector and any drift in its sensitivity is unimportant.

Further details concerning the pyrometer are given by Birnstingl.[4] The pyrometer does not measure temperature directly; it measures the amount of infra-red radiation falling on the cell, and the scale reading depends on the emissivity of the surface, the size of aperture fitted, the extension of the lens tube and the distance to the pyrometer. The pyrometer was calibrated by viewing the disk when the latter was at a known temperature and in the same surface condition as during braking. Surface temperature measurements were taken on the disk just after the trailing edge of the pad for brake applications of 10 and 16 s duration from initial speeds of 2180 cm/s, thereby resulting in values of Q of 54·2 cal/s and 35·08 cal/s respectively. The transients were traced on a recorder connected to the pyrometer amplifier and the curves obtained together with the theoretical values of the surface temperature, are shown in the figure. These curves agree to the order of 15%, but this figure should be reduced if cooling losses were taken into account.

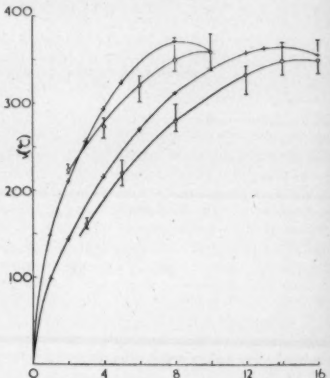

Typical curves of transient temperature at the surface of a disk during braking

+ = calculated values;

○ = mean experimental values; the range of values is also shown.

ACKNOWLEDGEMENTS

The author wishes to thank Dr. R. T. Spurr of the Research Division of Ferodo Ltd. for assistance and criticism, and the directors of Ferodo Ltd. for permission to publish this paper.

REFERENCES

(1) Newcomb, T. P. *Brit. J. Appl. Phys.*, **10**, p. 204 (1959).
(2) Carslaw, H. S., and Jaeger, J. C. *Conduction of Heat in Solids*, 1st Ed., Appendix V (Oxford: Clarendon Press, 1947).
(3) Hartree, D. R. *Mem. Manchester Lit. Phil. Soc.*, **80**, p. 85 (1935).
(4) Birnstingl, D. W. *Electronic Engng*, **30**, p. 189 (1958).

THIS JOURNAL is produced monthly by The Institute of Physics, in London. It deals with all branches of applied physics (including theory and technique). All rights reserved. Responsibility for the statements contained herein attaches only to the writers.
EDITORIAL MATTER. Communications concerning editorial matter should be addressed to the Editor, The Institute of Physics, 47 Belgrave Square, London, S.W.1. (*Telephone:* Belgravia 6111.) Prospective authors are invited to prepare their scripts in accordance with the *Notes for Authors*. (Price 3*s*. 6*d*. including postage.)
REPRODUCTION. The Institute of Physics is a signatory to The Royal Society's Fair Copying Declaration. Details may be obtained upon application from The Royal Society, London, W.1.
ADVERTISEMENTS. Communications concerning advertisements should be addressed to the agents, Messrs. George Jackson (Fleet St.) Ltd., Cliffords Inn, Fleet Street, London, E.C.4. (*Telephone:* Holborn 3611–2.)
CLAIMS FOR MISSING JOURNALS. Claims from regular subscribers to this *Journal* for missing numbers will only be considered if received within 60 days of the date of mailing plus normal outward time of transit and time for lodging the claim. Losses attributable to failure to notify a change of address or to similar omissions will not be considered.
SUBSCRIPTION RATES. A new volume commences each January. The charge is £6 per volume ($17 U.S.A.), including index (post paid), payable in advance. Single parts, so far as available, may be purchased at 12*s*. 6*d*. each ($1.75 U.S.A.), post paid, cash with order. Orders should be sent to The Institute of Physics, 47 Belgrave Square, London, S.W.1, or to any bookseller.

Differential scattering cross-section of atoms to medium energy electrons at small angles

By M. E. Haine, M.Sc., F.Inst.P., and A. W. Agar, B.Sc., F.Inst.P., Associated Electrical Industries Ltd., Aldermaston, Berks

[*Paper first received* 13 *November*, 1958, *and in final form* 4 *March*, 1959]

The differential scattering cross-section of a range of atoms has been determined experimentally for angles between 10^{-2} and 10^{-3} rad. The results are in reasonably good agreement with the theory of Lenz.

Contrast in the electron microscope results from elastic and inelastic scattering of the electrons. Since the microscope aperture angle is usually in the region $0{\cdot}002^{c}$–$0{\cdot}01^{c}$, scattering at small angles is important. In a recent paper Haine[1] has evaluated the contrast by separating the effects of elastic and inelastic scattering, the former giving mainly phase contrast and the latter an amplitude or "in phase" contrast, which is partly offset by the arrival of the inelastically scattered electrons, defocused by the chromatic aberration of the objective lens. To evaluate the final contrast, knowledge of the differential scattering cross-sections is required as well as the distribution of energy loss in the inelastic processes. Lenz[2] has modified previous scattering theories to give a more accurate assessment of the differential cross-sections at small angles both for elastic and inelastic processes. His results show large departures from previously computed results, based on earlier work such as that by Bullard and Massey.[3] It is clearly very desirable that further experimental measurements should be made to ascertain the validity or otherwise of Lenz's predictions.

At the small angles of interest, the inelastic scattering is so much stronger than the elastic that the measurement of the elastic component becomes exceedingly difficult. By the same token, however, a measurement of the total scatter does not differ much from the inelastic scatter at small angles, and some of Lenz's predictions can be experimentally verified.

The total cross-section for chromium was measured by Biberman and others[4] and agrees closely with Lenz's theory over the angular range 3×10^{-4} to 10^{-2} rad, and with some divergence to 3×10^{-2} rad. These measurements were made in a slightly modified electron microscope. Leonhard[5,6] using a spectrometer due to Mollenstedt,[7] measured the elastic and inelastic cross-sections for beryllium, aluminium and gold, and his results also agree fairly well over the range 5×10^{-4} to 10^{-2} rad. This paper describes further measurements for carbon, aluminium, copper, silver and gold.

The scattering calculations are based on single atoms, and the only experimental checks so far envisaged have been made with thin films of the material under investigation. It is desirable to find out how nearly the differential cross-sections deduced from such experiments agree with the calculations, since this would indicate the extent to which coupling between atomic fields affects the scattering. The experiments must, of course, be carried out on films appreciably thinner than the "transparency thickness" (defined by von Borries as the mass thickness in which, on the average, every incident electron is scattered once elastically). This should avoid conditions under which plural scattering would be expected. In fact, however, owing to the statistical nature of the collisions, some electrons will suffer more than one collision in extremely thin films, with resulting divergence from theories based on idealized single scattering.

EXPERIMENTAL ARRANGEMENT

Biberman and his co-workers illuminated a small area of a specimen in an electron microscope, and recorded the scatter intensity distribution on a photographic plate at a considerable distance from the specimen. This necessitated the removal of the projector lens pole-pieces and various screens and apertures within the instrument. Consideration of Fig. 1 will show that any electron scattered through a particular angle in any given plane from a specimen will be brought to a focus at a point in the back focal plane of the objective. Thus the back focal plane contains the angular scatter distribution, and this image can be projected on to the final screen or the photographic plate by the projector lens system, as for the recording of diffraction patterns in the microscope.[8] The instrument can thus be used without any modification from the normal operating conditions.

The work of Digby, Firth and Hercock[9] showed that the blackening density of some photographic plates was linearly related to the charge density falling upon them from the electron beam. Thus, for Ilford thin film half-tone plates, the density exposure relationship is certainly linear between blackening densities of 0·2 and 1·0. A scatter pattern recorded photographically contains a much wider range of densities than this, and it is therefore necessary to employ a range of exposures, so as to be able to measure all parts of the pattern within this range of linear response.

A typical scatter pattern for a thin silver film and the results

Conference on developments in the production of high vacua

Owing to the recent dispute in the printing industry, the summarized proceedings of the above conference, which was scheduled to be published in this issue, will not now be published until September.

of microphotometer measurements of photographic density are shown in Figs. 2 and 3.

It was found to be possible to cover the required range of angles from 5×10^{-4} to 3×10^{-2} rad with a series of six exposures. The overlap of the densitometer readings in the linear response region from successive exposures of the scatter pattern permitted the construction of a density/angle curve referred to the longest exposure used. The only exposure required to be known accurately, therefore, was the longest one (except for experiments where the contamination rate is to be measured, as described below).

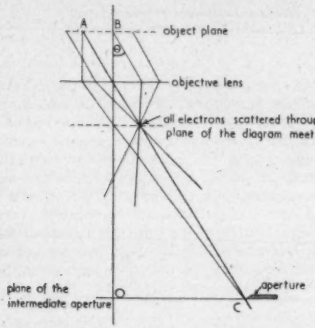

Fig. 1. Collection of scatter pattern and definition of scattering area. An aperture of radius OC defines an area at the object, radius AB, from which area alone are scattered electrons collected

The electron intensity incident on the scattering foil was also measured photographically. The illumination was allowed to fall through a hole in the scattering film and on to the photographic plate, at a known magnification, the exposure being timed.

The differential scattering cross-section could then be deduced as follows.

Let d = thickness of scattering film
a = area of film from which scattered electrons are collected
M_2 = magnification between back focal plane of objective lens and photographic plate
t_2 = exposure time of scatter pattern (effective)
D_r = photographic density of scatter pattern at radius r from its centre on the plate (angle θ)
f = focal length of objective lens
D_1 = photographic density of calibration patch
M_1 = magnification from object plane to photographic plate
t_1 = exposure time for calibration patch

Let A' be the area in the back focal plane of the objective, in which the electrons scattered through angle θ are measured. Then, number of electrons scattered through

$$\theta = (K \,.\, D_r \,.\, A' \,.\, M_2^2)/t_2$$

where K is the constant of proportionality between photographic density and the number of incident electrons per square centimetre in the linear response region.

Therefore, number of electrons scattered through θ into unit solid angle equals

$$\frac{K \,.\, D_r \,.\, A' \,.\, M_2^2}{t_2} \cdot \frac{f^2}{A'}$$

Number of incident electrons per unit area equals

$$(K \,.\, D_1 M_1^2)/t_1$$

Therefore

$$\frac{\text{No. of electrons scattered into unit solid angle through } \theta}{\text{No. incident per unit area}} = \frac{D_r \,.\, M_2^2 f^2 t_1}{D_1 M_1^2 t_2} \quad (1)$$

If there are n scattering atoms per unit area of the film, the total differential cross-section for elastic plus inelastic scattering is:

$$(I_\theta + I'_\theta) = \frac{D_r \,.\, M_2^2 f^2 t_1}{D_1 M_1^2 t_2} \cdot \frac{1}{n \,.\, a} \quad (2)$$

provided that the scattering due to each atom in the films remains independent of the presence of the other atoms. If, for the scattering material,

density $= \gamma$
atomic weight $= A$
mass of hydrogen atom $= M_0$
γ/AM_0 = number of atoms per unit volume $= n/d$

Hence

$$I_\theta + I'_\theta = \frac{D_r \,.\, M_2^2 f^2 t_1}{D_1 M_1^2 t_2} \cdot \frac{AM_0}{\gamma \,.\, d \,.\, a} \quad (3)$$

Thus, the total differential cross-section can be obtained very simply from the measurements of photographic density and the exposure times, knowing the various instrumental constants and the properties of the scattering material. It will be noted that the cross-section is inversely dependent on the measured thickness of the scattering film. This is usually the least certain of the measurements (it was specifically mentioned as a possible error by Leonhard), and could easily account for discrepancies in the results of different experimenters.

In order to keep the densities D_1 and D_r in the linear response range, and the exposure times long enough to measure easily with reasonable accuracy, the incident beam intensity had to be kept low. This was, in any case, desirable in order to reduce the rate of contamination of the specimen. In practice, the condenser lenses were switched off and the gun operated rather inefficiently in order to obtain suitable illumination conditions.

A 50 μ aperture was placed just above the specimen to screen all areas from the electron beam, except those being viewed. It was thus possible to complete the alinement and adjustment of the microscope without contamination of the area of the specimen to be used for the measurements. The area from which the scattered electrons were collected was defined by an intermediate aperture just above the first projector lens. The area so defined was 5 μ^2.

EXPERIMENTAL PROCEDURE

Earlier workers[4,5] had mentioned the possible errors arising from the layer of contamination building up on the film under examination during the course of the experiment. The first experiments in this investigation were therefore confined to carbon films, since any additional layer would then be of the same material. Since, for thin films, the cross-section should remain constant, the photographic density D_r

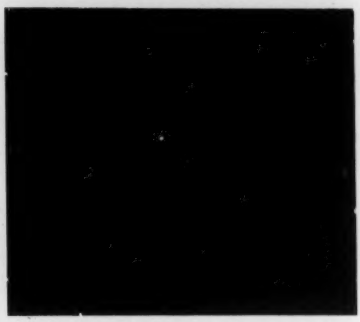

(*a*)

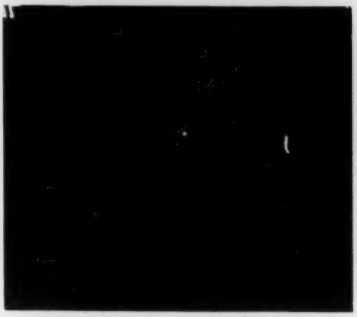

(*b*)

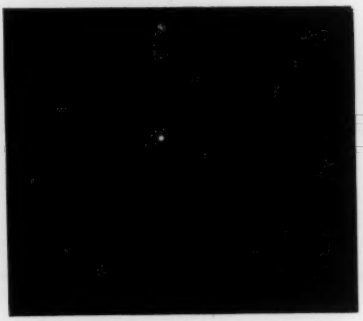

(*c*)

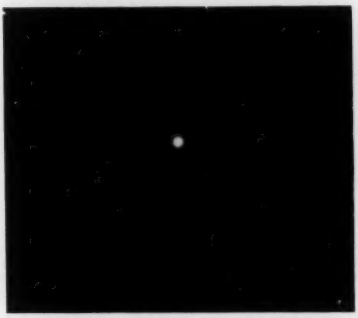

(*d*)

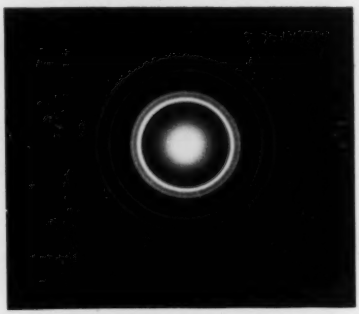

(*e*)

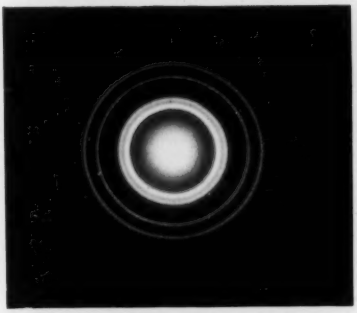

(*f*)

Fig. 2. Scatter patterns recorded from a 30 Å silver film on carbon with exposures of: (*a*) 1 s; (*b*) 2 s; (*c*) 4 s; (*d*) 8 s; (*e*) 20 s; (*f*) 60 s

at a given radius from the centre of the scatter pattern will be directly proportional to the total thickness of carbon film plus contamination, other experimental conditions being constant.

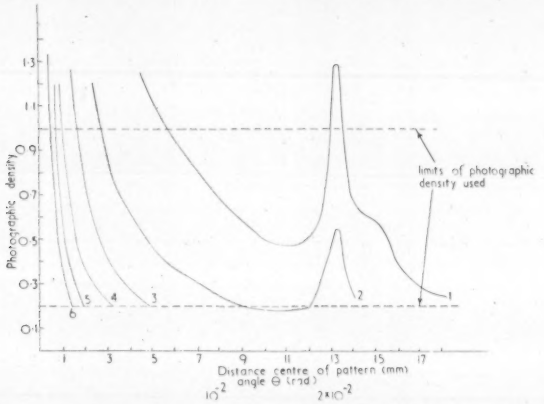

Fig. 3. Microphotometer measurements of scatter pattern from 60 Å silver film on carbon support

Plate exposures: curve (1), 60 s; curve (2), 20 s; curve (3), 8 s; curve (4), 4 s; curve (5), 2 s; curve (6), 1 s.

The following routine was therefore established for the photography of patterns.

(i) The electron beam was arranged to pass through a hole in the film, the magnification of the instrument was set to 10 000 ×, and the patch of illumination was photographed.
(ii) A clean area of film was selected, and the illumination patch again photographed.
(iii) The first projector lens was re-focused to project the scatter pattern into the focal plane of the second projector. The scatter pattern was photographed at exposures of 4, 20, 1, 2, 8 and 60 s.
(iv) The calibration patch (through the film) was again photographed.
(v) The beam was left on the specimen for 10 min from the time of the first exposure under (iii) above.
(vi) The scatter pattern was again photographed at exposures of 4 and 20 s.
(vii) The illumination patch was photographed at × 10 000 (through the film).
(viii) The illumination patch was photographed at × 10 000 (through a hole in the film).

Operations (i) and (viii) are required for determining the incident electron intensity. The calibrations (ii) and (iv) enable the incident intensity to be checked immediately before and after the recording of the scatter patterns, but without the necessity of moving the illumination through a hole again. This guards against any drift of incident intensity during the recording of the patterns. The exposure times used under (iii) were found by experiment to give the required overlap for transposition of densities. It is obviously desirable to record as many as possible of the exposures quickly, to minimize the effects of contamination, and therefore to start with the shortest exposures first. However, the shortest exposures are not measurable accurately enough in the standard instrument for use in the calibration of the contamination rate, and the 4 and 20 s exposures were used for this purpose. The 4 s exposure was included as a precaution against very high contamination rates, but in practice the rates were low enough to justify using only the 20 s exposures for contamination calculations.

The rate of contamination under the illuminating conditions used in the experiments was found to be of the order of 3 Å/min. This agreed well with the figure calculated from the data of Ennos.[10] Since the series of exposures of the scatter pattern could usually be recorded within 3 min of the beam first striking the portion of the film under investigation, it was only necessary to apply a correction for contamination build-up for films of carbon less than 100 Å thick, for an accuracy of 10%. For films of higher atomic number, no correction for contamination rate was necessary.

EFFECT OF FILM THICKNESS

In an effort to determine the thickness of scattering material at which plural scattering started to be important, it was decided to examine carbon films of a range of thicknesses. It was expected that the very thin films would all have something near the theoretically calculated cross-section, and that as the thickness approached the transparency thickness the agreement would start to fall off. In view of the need to know the thickness of large numbers of films, some way of avoiding the need for measurement by multiple beam interferometry was sought. It was found that the optical density of the carbon films, as measured on a simple densitometer, bore a simple relation to the film thickness. The accuracy of such measurements was estimated as better than ± 10% by Agar.[11] Densitometer measurements are very quickly and easily made without destruction of the film or the need for coating with silver, and thus a suitable film thickness could be selected with a minimum of trouble. Scattering measurements with 50 keV electrons were made on carbon films of thicknesses (as determined by their density) 30, 45, 55, 75, 90, 110, 190, 290 and 740 Å. For the thinnest films, the scatter intensity, based on single scattering, would be expected

to be proportional to the film thickness and the calculated cross-section should therefore be unchanged for these films. In fact, the results are as shown in Fig. 4, and there seems to be a definite correlation of cross-section with film thickness. The thinnest film (30 Å) examined gave a result in very good agreement with theoretical prediction. It is interesting to note that the experimentally determined cross-section for this film, and for the 45 Å film, lies above the theoretical value between the scatter angles of about 7×10^{-3} and 2×10^{-2} rad. This is very similar to the effect demonstrated by Lenz when comparing Biberman's results for chromium with his theoretical curve.

It is difficult to explain the discrepancy, which was found consistently with repeated experiments, in the results for very thin films. Some of the films were prepared from spectroscopically pure carbon and some from carbon of 99·7% purity from a different supplier. The results for the 45 and 75 Å films were obtained on later experiments to check the thickness dependence and they fell very convincingly into the earlier pattern of results. It has recently been suggested by Cosslett and Cosslett[12] that the method of measuring film thickness by optical density measurements may be unreliable. For the purposes of this paper, however, it will only be remarked that even if one accepts these authors' thickness calibration (their curve *B*) of films prepared in connexion with this scattering study, the variation of scattering cross-section with film thickness remains (Table 1).

This could explain the thickness dependence of the scattering cross-section, because only the thinnest film would then be less than the transparency thickness. However, acceptance of these figures for film thickness would bring the cross-section for carbon materially below those for other elements examined (see section below and Table 3). The authors, therefore, prefer the thickness values here determined.

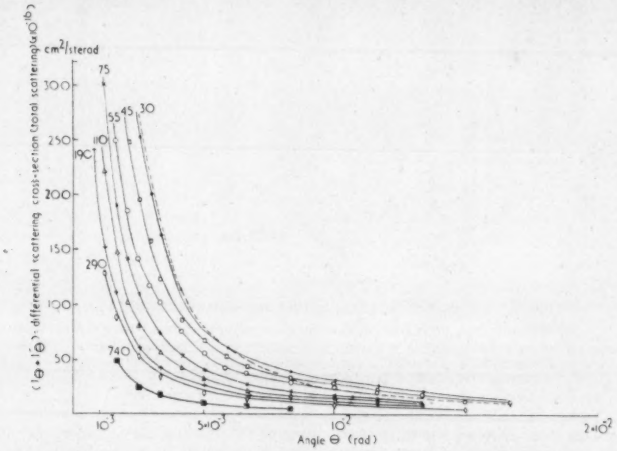

Fig. 4. Differential scattering cross-section for carbon films of differing thickness at 50 kV
Carbon film thickness: • = 30 Å; □ = 45 Å; ○ = 55 Å; × = 75 Å; △ = 110 Å; + = 190 Å; ◇ = 290 Å; ■ = 740 Å.
– – – – = theoretical curve for single scattering (total).

Table 1. *Cross-section for carbon at 50 kV and* $\theta = 5 \times 10^{-3}$ *rad*

Carbon film thickness (Å)		$(I_\theta + I'_\theta) \times 10^{-16}$ *(cm²/sterad)*	
Agar	*Cosslett and Cosslett Curve B*	*Agar*	*Cosslett and Cosslett*
30	60	79	40
45	100	67	30
55	128	57	24
75	155	40	19·5
110	210	32	16·8

EFFECT OF ATOMIC NUMBER OF SCATTERING MATERIAL

As shown by Haine,[3] it is to be expected that the inelastic cross-section is independent of atomic number. The scattering from a series of films of different materials at 50 kV was therefore determined in the manner described above for carbon films. The thicknesses were measured by the multiple beam interferometer method. Some of the thicker metal films were self-supporting, but the thinner films had to be mounted on very thin carbon films of known thickness, and a correction applied for the scattering due to the carbon. The results from these different materials are summarized in Fig. 5. It will be seen that the differential scattering cross-section at angles below about 10^{-2} is independent of the atomic number of the scattering material for thin films, in agreement with the theoretical prediction. Some of the results obtained by Leonhard and by Biberman are also shown in Fig. 5 for comparison purposes. The theoretical curve dotted in Fig. 5 is the sum of the elastic and inelastic differential cross-sections for silver. For angles below 10^{-2} rad, the contribution of the elastic scattering is small, compared with the inelastic component; the disparity between the experimental and theoretical curves at larger angles is accounted for by the dependence of elastic scattering on atomic number. The results showing the greatest difference

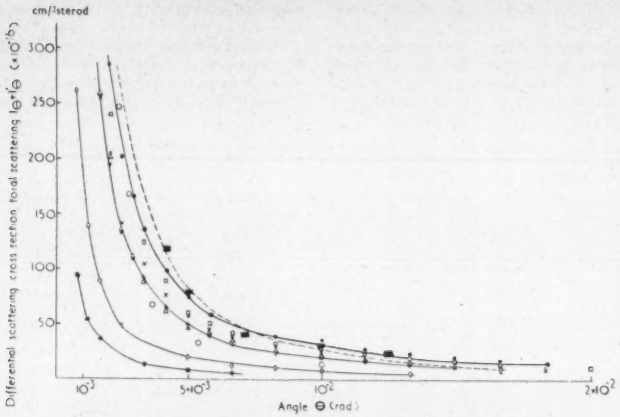

Fig. 5. Differential scattering for different materials at 50 kV

In order to avoid confusion, the curves for carbon, aluminium and copper 50 Å have not been drawn in.
● = silver 60 Å (corrected for carbon support); × = carbon 55 Å (corrected for contamination); + = gold 80 Å (corrected for carbon support); □ = aluminium 90 Å (corrected for carbon support); △ = copper 50 Å (corrected for carbon support); ◇ = silver 180 Å; * = copper 350 Å; ■ = chromium (after Biberman) 60 kV; ○ = gold (after Leonhard).
– – – – = theoretical (elastic + inelastic) for silver (after Lenz).

from the theoretical curve are those obtained with the thicker scattering films, and are, in general, films which are thicker than the transparency thickness for the material. Table 2 shows the transparency thicknesses for the materials used, and the proportion of this thickness for the different scattering films.

Table 2. *Transparency thicknesses (for elastic and inelastic scattering) of materials examined, and thickness used*

Material	*Atomic number Z*	*Transparency thickness (calculated for Lenz data) (Å)*	*Thickness examined (Å)*	*Ratio of thickness to transparency thickness*
Carbon	6	90	30	0·33
			45	0·5
			55	0·61
			75	0·83
			110	1·2
			190	2·1
			290	3·2
			740	8·2
Aluminium	13	125	90	0·72
			120	0·96
Copper	29	56	50	0·89
			350	6·2
Silver	47	57	60	1·05
			180	3·15
Gold	79	38	80	2·1

It will be noted that the thinner films of the various scattering materials (except silver) give a cross-section only 60–70% of that predicted theoretically. The values of the cross-section for the scatter angle 5×10^{-3} rad are given in Table 3.

It is perhaps remarkable that a film of gold with a thickness of 2·1 times the transparency thickness should give a cross-section so well in agreement with the thin films of other elements. No good reason for this can be advanced. A study of the figures in Table 3 seems to reinforce the acceptance of the values of carbon film thickness obtained from the authors' calibration, as use of Cosslett's figures would introduce a considerable discrepancy between the results for carbon and all other elements used.

Table 3. *Total scattering cross-section at $\theta = 5 \times 10^{-3}$ rad for different elements (50 kV)*

	$(I_\theta + I'_\theta) \times 10^{-16}$ (cm²/sterad)
Theoretical value	80
Silver 60 Å film	74
Aluminium 90 Å	59
Gold 80 Å	56
Carbon 55 Å	57
Copper 50 Å	49
Aluminium 120 Å	44
Chromium (after Biberman)	78
Gold (after Leonhard)	33

EFFECT OF ACCELERATING VOLTAGE

A thin film of carbon of thickness 90 Å was examined at electron accelerating voltages of 50, 75 and 100 kV. After correcting for the different magnifications of the diffraction patterns, the differential cross-section was calculated in each case. This value was multiplied by the accelerating voltage used and the results are plotted on one curve in Fig. 6. The results for all three voltages are seen to lie very close to the same curve, and this shows that the cross-section is inversely proportional to accelerating voltage, as predicted [Haine,[1] equation (17)].

CONCLUSIONS

The differential scattering cross-section of different elements can be determined by experiments in an unmodified

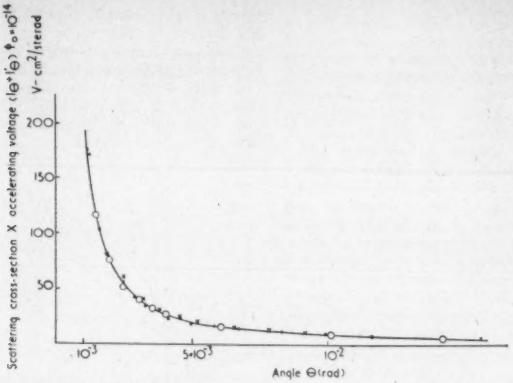

Fig. 6. Effect of accelerating voltage on electron scattering
● = 50 kV;
○ = 75 kV;
× = 100 kV.

electron microscope. The variation with scatter angle follows the form of the curve predicted by Lenz, and the cross-section appears to be independent of the atomic number of the scattering material and inversely proportional to the accelerating voltage. A dependence of cross-section for film thicknesses less than the transparency thickness in the case of carbon was not explained.

At angles below 10^{-2} rad (where inelastic scattering is dominant) the mean scattering cross-section for films near the transparency thickness for the material of the film seems to be materially less than that predicted.

REFERENCES

(1) HAINE, M. E. *J. Sci. Instrum.*, **34**, p. 9 (1957).
(2) LENZ, F. *Z. Naturforsch.*, **9a**, p. 185 (1954).
(3) BULLARD, E. C., and MASSEY, H. S. W. *Proc. Cambridge Phil. Soc.*, **26**, p. 556 (1930).
(4) BIBERMAN, L. M., WTOROW, E. N., KOVNER, I. A., SUCHKIN, N. G., and JAVORSKI, B. M. *C.R. Akad. Sci. URSS.*, **69**, p. 519 (1949).
(5) LEONHARD, F. *Z. Naturforsch*, **9a**, p. 727 (1954).
(6) LEONHARD, F. *Z. Naturforsch*, **9a**, p. 1019 (1954).
(7) MOLLENSTEDT, G. *Optik*, **5**, p. 499 (1949).
(8) HAINE, M. E., PAGE, R. S., and GARFITT, R. G. *J. Appl. Phys.*, **21**, p. 173 (1950).
(9) DIGBY, N. G., FIRTH, K., and HERCOCK, R. J. *J. Photogr. Sci.*, **1**, p. 194 (1953).
(10) ENNOS, A. E. *Brit. J. Appl. Phys.*, **4**, p. 101 (1953).
(11) AGAR, A. W. *Brit. J. Appl. Phys.*, **3**, p. 35 (1952).
(12) COSSLETT, ANNA and COSSLETT, V. E. *Brit. J. Appl. Phys.*, **8**, p. 374 (1957).

Electric stress and heat transfer

By P. H. G. ALLEN, B.Sc.(Eng.), A.K.C., A.M.I.Mech.E., A.M.I.E.E., The British Thomson-Houston Co. Ltd., Rugby

[*Paper first received* 19 *January, and in final form* 9 *April*, 1959]

Apparent contradictions in published reports of the effect of electric stress on heat transfer in fluids have been resolved by small-scale experiments and by reanalysis of available data. The effect of deliberately mixed unidirectional and alternating stress has been investigated for the first time. While alternating stress increases heat transfer in its presence, purely unidirectional stress inhibits it, while "mixed" stress may have either effect according to the magnitude of its components.

LIST OF SYMBOLS

Nu = Nusselt number for heat transfer $= ql/k\Delta\theta$
Pr = Prandtl number for heat transfer fluid $= c\nu/k$
El = characteristic electric number for heat transfer in the presence of electric stress $= \frac{dK}{d\theta}\Delta\theta l^2E^2/\nu^2\rho$
q = heat transfer per unit area
l = a reference length
$\Delta\theta$ = a reference temperature interval
E = a reference electric field strength
k = thermal conductivity for heat transfer fluid
c = specific heat per unit volume for heat transfer fluid
ν = kinematic viscosity for heat transfer fluid
$\frac{dK}{d\theta}$ = rate of change of permittivity K with temperature θ, for heat transfer fluid
ρ = density, heat transfer fluid
σ = space charge per unit volume
D = electric displacement
R = resistance of fine wire ($= R_a$ at bulk temperature of ambient fluid)
v = potential drop along fine wire
i = current in fine wire

ΔNu, Δq, $\Delta(\Delta\theta)$, ΔR and Δi are small changes in Nu, q, $\Delta\theta$, R and i, respectively.

INTRODUCTION

The connexion between thermal and electrical phenomena in fluid dielectrics has been established for about 25 years. In 1947, Kronig and Schwartz[1] gave a dimensionless correlation of available data on improved heat transfer to gases due to the presence of electric stress. Ahsmann and Kronig[2] later applied this to their own observations of the effect of rectangular waveform stress alternating at 40 c/s using several organic liquids. Mascarenhas and others[3, 4] studied such effects in fatty acids. The present work follows reports[5, 6] of the effect in transformer oil. Schmidt and Leidenfrost[5] claimed that, as for other organic liquids tested, its thermal conductivity was increased by unidirectional stress and in this way they improved very greatly the performance of a simple oil-to-water heat exchanger. Weber and Halsey[6] studied the improved heat transfer due to stress varying sinusoidally at 60 c/s. Both publications included pictorial evidence of liquid motion obtained by "Schlieren" technique. The need for further experiment arose from the fact that, unlike Schmidt and Leidenfrost,[5] Ahsmann and Kronig[2] observed heat transfer inhibition by unidirectional stress.

EXPERIMENTAL ARRANGEMENTS

A simple apparatus of the type used by Ahsmann and Kronig[2] was employed. It consisted of a fine thermo-pure platinum wire suspended vertically along the axis of a tube immersed in the liquid under investigation and forming, electrically, one arm of a Wheatstone bridge. Fig. 1 gives details of the test cell formed by the wire and tube and Fig. 2 shows the electrical circuit. The bridge current heated the wire and suitable voltages V applied between wire and tube produced electric stress in the liquid at the wire surface. The effect of this on heat transfer there was indicated by changes in the wire resistance. Galvanometer G was used to balance both the bridge and the potentiometer used to measure the wire current.

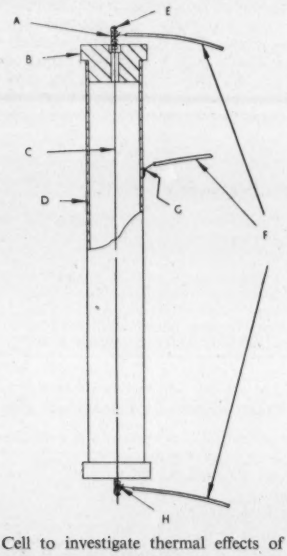

Fig. 1. Cell to investigate thermal effects of electric stress

A, light spring; *B*, Perspex cap drilled for wire and counterbored for spring; *C*, 0·001 in. diameter platinum wire; *D*, $\frac{3}{8}$ in. inside diameter brass tube; *E*, platinum wire soldered to spring; *F*, connections to circuit; *G*, connection soldered to tube; *H*, connection soldered to spring.

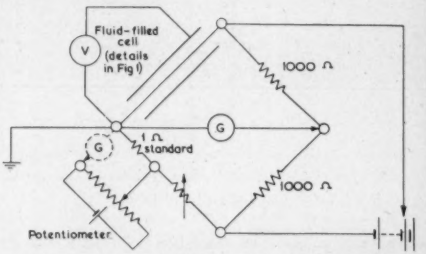

Fig. 2. Circuit to investigate thermal effect of electric stress

It is shown in the Appendix that at constant bridge supply volts small changes, ΔR and ΔNu respectively, in wire resistance R and Nusselt number Nu for heat transfer at the wire surface, are related by

$$\Delta Nu/Nu = -\Delta R(2 - R_a/R)/(R - R_a) \qquad (1)$$

In the Kronig and Schwartz correlation,[1] ΔNu is related to the product of fluid Prandtl number Pr and a new dimensionless quantity, the characteristic electric number El, which, for liquids, can be defined as

$$El = \frac{dK}{d\theta}\Delta\theta l^2 E^2/\nu^2\rho \qquad (2)$$

fluid properties being evaluated at the temperature of the heat transfer surface. Thus

$$\Delta Nu = f(El \,.\, Pr) \qquad (3)$$

Following Ahsmann and Kronig,[2] the present work takes the wire diameter as the system reference length l and the wire rise above the bulk of the fluid as $\Delta\theta$, the reference temperature interval.

EXPERIMENTAL PROGRAMME

(1) *The effect of polarity change.* Using series-connected dry batteries as the source of voltage V, unidirectional stresses of either polarity up to 84 000 V/cm were produced at the wire surface. For the present, it is sufficient to note that in all cases heat transfer was inhibited. On removing the stress, normal conditions were restored, but when polarity was reversed, a transient increase in heat transfer occurred. As ΔNu can be related directly to ΔR [equation (1)] and the deflexion of galvanometer G can be calibrated in terms of ΔR, detailed study of such transient states was possible as shown in Fig. 3. As might be expected, manual polarity reversal of sufficient rapidity gave a continuous heat transfer increase since it represents crudely an alternating stress condition. Evidently, unidirectional and alternating stress have very different thermal effects.

(2) *Correlated results.* Tests were made with two samples of the same grade of transformer oil under both unidirectional and sinusoidally alternating (50 c/s) stress conditions. Figs. 4 and 5 give logarithmic graphs of ΔNu (negative for unidirectional, positive for alternating, stress) against $El \,.\, Pr$ at Nu values of the order of 0·4. A mean line drawn for the results of Ahsmann and Kronig[2] is given for comparison.

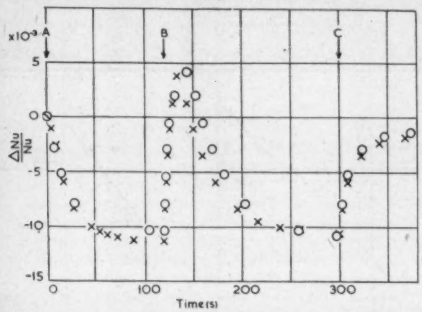

Fig. 3. Transient thermal response to unidirectional stress

○ Zero to positive at *A*, positive to negative at *B*, negative to zero at *C*
× Zero to negative at *A*, negative to positive at *B*, positive to zero at *C*
} Cylinder voltage changes

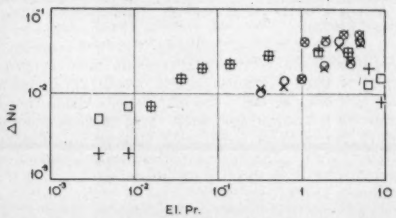

Fig. 4. Correlation of results for unidirectional stress

Sample A ○ } cylinder positive × } cylinder negative
Sample B + } □ }

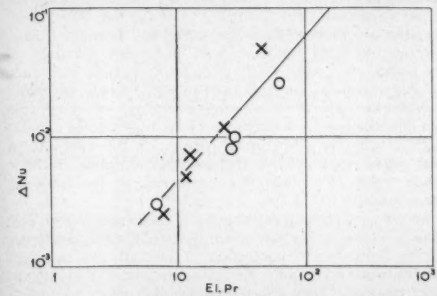

Fig. 5. Thermal effect of 50 c/s sinusoidal electric stress in transformer oil

○ Sample A × Sample B
—— Results of Ahsmann and Kronig[2] for 40 c/s rectangular stress.

While the alternating stress results show good repeatability between samples and linearity of points graphed, those for unidirectional stress depart from linearity. Ahsmann and Kronig[2] considered the inhibitive effect as probably due to a thin layer of gas forming on the wire. Differences in dissolved gas content could thus give bad repeatability between samples while gas ionization at higher stresses could lead to the "saturation" and ultimate decrease of the inhibitive effect.

(3) *The effect of "mixed" stress.* The discrepancy between the results of Schmidt and Leidenfrost[5] and those of Ahsmann and Kronig[2] and the present work has yet to be explained. However, published details of the Schmidt and Leidenfrost apparatus suggest the presence in their high voltage supply of a considerable proportion of "ripple", i.e. alternating component superposed on unidirectional. This is more than probable in the work of Mascarenhas and others[3, 4] also. Such an effect was simulated in the present work by supplying a variable amplitude alternating voltage, isolated from earth, across a resistor connected between the dry batteries and the outside of the test cell. This arrangement gave the results shown in Fig. 6. Firstly, heat transfer

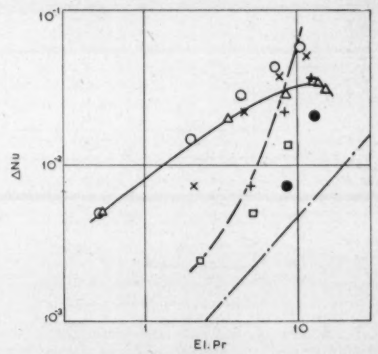

Fig. 6. Correlation of results for mixed stress with cylinder positive to wire

Unidirectional stress at wire surface: ○ 70 kV/cm, × 56 kV/cm, + 42 kV/cm, □ 28 kV/cm, • 14 kV/cm
Points of zero net effect △
Line of zero net effect ——
Alternating stress results from Fig. 5 —— · ——
Constant harmonic content —— ——

with purely unidirectional stress (tube positive to wire) was established at a datum value of Nu (again, about 0·4). Deviations, ΔNu, were then measured for a number of values of superposed alternating stress and log ΔNu plotted against log $El \,.\, Pr$ with El calculated for the peak value of alternating stress. This procedure was repeated at different initial unidirectional stresses. In each case, also, at a certain value of ΔNu due to alternating stress, the deviation due to purely unidirectional stress was neutralized. The "line of zero net effect" thus obtained divided the results into two

regions, an upper one in which the overall effect is one of improved heat transfer, and a lower one in which inhibition occurs. A similar graph was obtained when the tube was kept negative to the wire.

From these results, the inhibition caused at the higher unidirectional stresses is seen to be more readily reversed by the opposite effect of simultaneous alternation. The results of Schmidt and Leidenfrost[5] can thus be explained as due to the "ripple" in their high voltage supply and this possibility is discussed further in the next section.

CORRELATION OF AVAILABLE DATA

Schmidt and Leidenfrost's data[5] for improved performance of a simple annular counterflow oil-to-water heat exchanger was re-examined in the light of these results. Published data, given in Fig. 7, are for overall heat-exchanger

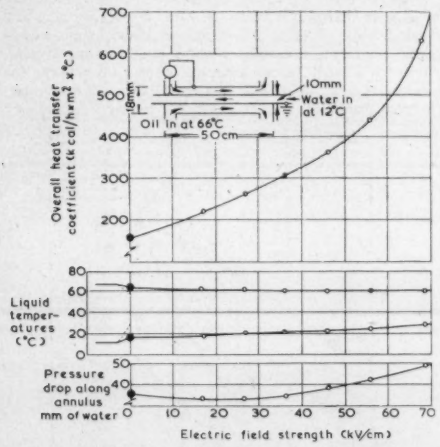

Fig. 7. Results of Schmidt and Leidenfrost[5] for electrically stressed transformer oil in an annular heat exchanger

Mean flow velocities: oil, 0·135 m/s; water, 0·11 m/s.

performance and to apply the Kronig and Schwartz correlation, Nusselt numbers for the oil side only must be derived. The water flow is in the laminar regime and, assuming the water tube to have 1 mm thick walls, published data[7] can be used to calculate water-side heat transfer coefficients. On the oil side, the annular clearance of 4 mm is taken as the system reference length. In calculating *El* values, the nominal unidirectional stress has been used and as this is a constant multiple of its percentage harmonic content, plotted values of *El* bear a constant relationship to the true value due to alternating stress only. This has no effect on the shape of a logarithmic graph, but makes the results useless for practical application. These results are shown as circles on Fig. 8. They lie on a line which compares very closely with one drawn on Fig. 6 through points having a common ratio of alternating to unidirectional stress, i.e. constant percentage harmonic.

Although Weber and Halsey[6] mention the Kronig and Schwartz correlation, they use a much more complex one to present their experimental data. By using Rogowski electrodes of effective diameter 1 in. at spacings of 0·2, 0·4 and 0·8 in., three different geometrical arrangements were

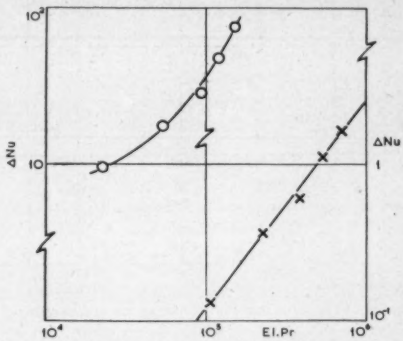

Fig. 8. Application of Kronig and Schwartz[1] correlation method to available data

○ Results of Schmidt and Leidenfrost[5] for mixed stress in 4 mm annulus.
× Results of Weber and Halsey[6] for 60 c/s sinusoidal stress in 0·2 in. gap.

employed but their correlation allowed for this. However, assuming a bulk oil temperature of about 20° C, points plotted as crosses in Fig. 8 for one of these geometries, in this case the 0·2 in. gap (gap width being taken as reference length *l*), give a linear relationship between logarithms of ΔNu and $El \,.\, Pr$. This has the characteristic slope shown for purely alternating stress in the present work and in that of Ahsmann and Kronig.[2]

DISCUSSION OF RESULTS

Calculations of the heat dissipation due to the small currents flowing between outer cylinder and wire show this to be no greater than about 0·1% of Δq (see Appendix). Its effect on observations is thus negligible. Further, if these currents interfered noticeably with the correct operation of the bridge, their effect would change with polarity and pairs of observations of the type given in Fig. 3 would not show coincidence. The small capacitance (about 3 pF) of the test cell and relatively low resistance of the high voltage supply, together with the low thermal capacity of the wire, ensure that system electrical and thermal time constants are of a much lower order than those exhibited by the transient phenomena of Fig. 3.

So far as a physical explanation is concerned, Weber and Halsey[6] have shown that one of the non-conservative forces in the fluid due to interaction of thermal and electrical gradients acts towards the thermal source and thus suppresses heat transfer. They concluded that this effect was small compared with improved heat transfer due to the motion of free charges in the dielectric under the influence of the alternating field. These charges can arise in at least two ways. Recent work[8] indicates suspended impurities as causing free charges, even in the "purest" liquids. In addition, if a

unidirectional field of strength E is present in a thermal field, space charge σ per unit volume is generated by the change of permittivity with temperature

$$\sigma = \nabla . D = \nabla . (KE) = E\nabla . K + K\nabla . E$$
$$= E\frac{dK}{d\theta}\nabla . \theta \qquad (4)$$

which would explain the increased effectiveness of alternating stress at high unidirectional stresses.

CONCLUSIONS

The present work confirms that alternating electric stress increases heat transfer in its presence, but indicates that previous work using unidirectional stress has lead to erroneous conclusions due to "ripple" in the high voltage supplies. Owing to difficulties in smoothing these, apparatus was used requiring moderate supply voltages readily obtainable from dry cells. When the effects of both mixed and purely alternating stress using this apparatus are compared with results from apparatus with much more uniform field configurations, the correspondence of slopes of the correlation graphs confirms the validity of the simple apparatus for qualitative investigations despite the inhomogeneity of its electric and thermal fields. The intention has been to clarify the nature of the effect rather than to seek an explanation. However, as all experimental work has so far overlooked the difference between the effects of unidirectional and "mixed" (simultaneous unidirectional and alternating) stress, theoretical deductions[9] from it are open to criticism, and a possible alternative explanation has been offered.

The phenomena discussed have important practical applications. Industrial frequency a.c. supplies can evidently be used, without rectification, to improve heat transfer in equipment handling oil and many organic chemicals. In high voltage equipment, such as transformers, those designs (e.g. the layer type of transformer winding) which subject the heat transfer surfaces to high electric stress can be expected to show an advantage under operational conditions and "thermal image" devices used to monitor their effective service rating must make allowance for this.[10] Conversely, the inhibitive effect of unidirectional stress due to stray electrostatic charge build-up must be taken into account, e.g. in the operation of steady-state thermal conductivity apparatus.[11]

ACKNOWLEDGEMENTS

The work described is part of that carried out under an Engineering Research Fellowship of the British Thomson-Houston Co. and thanks for permission to publish are expressed to the Directors (in particular Mr. G. S. C. Lucas, who drew attention to the problem) and to the Manager, Transformer Engineering Department.

APPENDIX

The Nusselt number is defined as

$$Nu = ql/k\Delta\theta \qquad (5)$$

Any small change, ΔNu, is due to changes in q and $\Delta\theta$ only, so that

$$Nu + \Delta Nu = ql/k\Delta\theta + (l/k)\{\Delta(q/\Delta\theta)\} \qquad (6)$$

and

$$\Delta Nu/Nu = \Delta(q/\Delta\theta)/(q/\Delta\theta) \qquad (7)$$

For small changes

$$\Delta(q/\Delta\theta) = (q/\Delta\theta)\{(\Delta q/q - \Delta(\Delta\theta)/\Delta\theta\} \qquad (8$$

whence, substituting in (7),

$$\Delta Nu/Nu = \Delta q/q - \{\Delta(\Delta\theta)\}/\Delta\theta \qquad (9)$$

At constant bridge supply volts, the potential drop v along the wire, resistance R, is also constant. For current i in the wire, q is proportional to vi, so that

$$\Delta q/q = \Delta i/i \qquad (10)$$

and since the product of i and R is equal to v (constant)

$$\Delta i/i = -\Delta R/R \qquad (11)$$

Again, by resistance thermometry

$$\Delta(\Delta\theta)/\Delta\theta = \Delta R/(R - R_a) \qquad (12)$$

Substituting (11) in (10) and (10) and (12) in (9)

$$\Delta Nu/Nu = -\{2\Delta R - R_a(\Delta R/R)\}/(R - R_a)$$
$$= -\Delta R(2 - R_a/R)/(R - R_a) \qquad (1)$$

REFERENCES

(1) KRONIG, R., and SCHWARTZ, N. *Appl. sci. Res. A*, **1**, p. 35 (1947).

(2) AHSMANN, G., and KRONIG, R. *Appl. sci. Res. A*, **2**, p. 235 (1950); *erratum*: **3**, p. 83 (1951).

(3) MASCARENHAS, S., MASCARENHAS, Y., FERREIRA DE SOUZA, M., and RABELLO, R. F. *Anais da Academia Brasileira de Ciências*, **28**, p. 95 (1956).

(4) MASCARENHAS, S. *Anais da Academia Brasileira de Ciências*, **28**, p. 99 (1956).

(5) SCHMIDT, E., and LEIDENFROST, W. *Forschung auf dem Gebiete des Ingenieurwesens*, **19**, p. 65 (1953).

(6) WEBER, K. H., and HALSEY, G. H. *Heat Transfer and Fluid Mechanics Institute*, University of Southern California, Los Angeles, p. 97 (1953).

(7) MCADAMS, W. H. *Heat Transmission*, 2nd ed., p. 189 (London: McGraw-Hill Publishing Co. Ltd., 1951).

(8) AUER, P. L., and SHARBAUGH, A. H. *Gen. Elect. Rev.*, **61**, No. 4, p. 37 (July 1958).

(9) MASCARENHAS, S. *Il Nuovo Cimento*, **5**, p. 1118 (1957).

(10) Brit. Pat. Appl. No. 13861/56.

(11) ALLEN, P. H. G. *A.S.M.E. Symposium on Thermal Properties*, p. 350 (1959).

Spectrum display comparator

By W. J. Price, B.Sc., A.C.T.(Birm.), Magnesium Elektron Ltd., Manchester

[*Paper first received* 10 *December*, 1958, *and in final form* 3 *April*, 1959]

This instrument for evaluation in photographic spectroscopy is a projection-comparator provided with means for displaying a density profile of part of the spectrum. The design allows the projected spectrum images to remain stationary for examination while the density profile is displayed simultaneously on a cathode-ray tube. Applications to both qualitative and quantitative spectrography are outlined.

In the derivation of analytical results from photographed spectra, the methods employed may be classified as either "visual" or "photometric". Visual methods call for the use of spectrum viewers, comparators or projectors, and the accuracy obtained is generally not better than $\pm 25\%$ although, with special techniques (for example, using the log sector[1]), better accuracy is obtained. Considerably increased accuracy is obtained over a larger part of the density range by using photometric density measurements and, under ideal conditions, coefficients of variation down to about 1 or 2% are common. The limiting value is a property of the photographic emulsion itself. Ideal conditions include high line-to-background ratio and the use of highly homogeneous samples, but in trace-element analysis the former condition is very rarely realized. Furthermore, at optical densities below about 0·05, the accuracy of evaluation methods employing the conventional densitometer rapidly decreases. Much better accuracy in the low-density range has been claimed for the recording photometer and cathode-ray display photometer, and the reasons are given in a later section.

Instruments for spectrum evaluation

Function	*Examination of single spectrum*	*Comparison of two spectra (e.g. standard and unknown)*
Visual examination through eyepiece	Spectrum viewer	Judd Lewis comparator
Visual examination on screen	Spectrum projector	Projection comparator
Measurement of optical density	Microphotometers or densitometers	
Visual examination and density measurement	Projector photometers	Comparator-photometers
Instrument recording density profile	Recording photometers	Recording comparator-photometer
Instrument displaying density profile instantaneously	Display photometer	Display comparator (Subject of present paper)

The instruments used in spectrum evaluation may be listed as in the table. All the instruments, with the exception of those entered under the last function (that is, giving instantaneous density profile), are fully described either in standard text books on emission spectroscopy or in the advertisement pages of the appropriate scientific journals.

Two types of cathode-ray tube display photometer have been described:

(i) The Fürth[2] and Fürth–Oliphant[3] microphotometers, designed to give a trace with a frequency of 50 c/s.

(ii) The cathode-ray photometer of Davis and Webb,[4] which gives a trace at much lower frequency on a long-afterglow tube.

The advantages of the latter instrument over the former appear to be higher mechanical stability (and hence better definition and resolution of trace), simplicity and ease of conversion of a standard microphotometer. It recently became evident that a display photometer would be of considerable value for certain of the determinations undertaken in our spectrographic laboratory. It also seemed likely that its usefulness could be enhanced by combining it in a single instrument with a spectrum projection comparator. Such an instrument has now been built,* and will be referred to henceforth as the "display comparator". Its relationship to the other instruments is shown in the table.

DESCRIPTION OF THE DISPLAY COMPARATOR

The specific function of this instrument is to exhibit a profile of the central part of a section of spectrum while the section is projected as a stationary observable image on a viewing screen in juxtaposition with another (reference) spectrum. The method of achieving this is shown by the diagrams. Fig. 1 shows the projection comparator, a conventional arrangement whereby the spectra at A and B are projected upwards on to the mirrors at M and thence vertically downwards to a focus on the screen S. Magnification at S is 20 times. Fig. 2 shows the front view of the projection comparator and the scanning arrangement. To the screen S is imparted a slow lateral reciprocating motion (about 12 cycles per minute) by the motor E and connecting

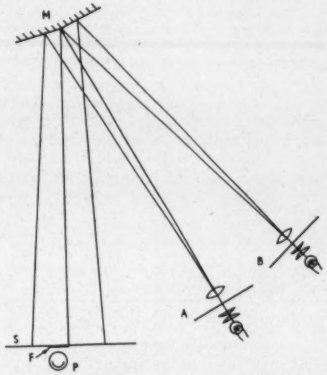

Fig. 1. Diagram of projection comparator

* Brit. Pat. Spec. No. 792, 423 (March 1958).

rod *C*. A slit *F* is incorporated in the screen and attached immediately below the slit is a photocell *P*. The cathode-ray tube is disposed to the right of the comparator, together with its associated electronic equipment. The Y-plates are fed via amplifiers by the photocell *P*, and the X-plates by a time-base consisting of a sliding contact, fixed to the screen, moving over a stationary resistance wire *W*.

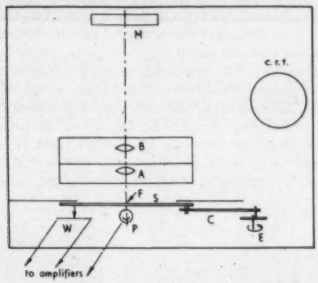

Fig. 2. Front view of projection comparator

The details of the electronic equipment and circuitry as given for the display photometer[4] apply without exception to the present instrument. Special details relating to the present instrument are:

Projection lamps—6 V, 48 W pre-focus lamps connected in series, fed from a 12 V car battery;

Projection lenses—Wray f1·35, 1·5 in.;

Plateholders—Plates are capable of lateral movement in two directions, and of rotational adjustment, thus having all the facilities of a conventional comparator;

Mirrors—Optically flat, front surface aluminized;

Screen—An area, 10 × 15 in. always visible. Lateral movement 1 in. The slit, 200 μ × 1 in. (max. adjustable) set slightly forward of the geometrical centre of screen.

Photocell—Gas-filled, Cintel type GS16. Output connexions *via* graphite-covered coaxial cable to prevent static charge building up through movement;

Slide wire—40% silver palladium (0·0025 in. diam., 3 Ω per in.). Connexion to sliding contact through special coaxial cable as for photocell;

Reciprocating-drive motor—Double-reduction drive giving 12 cycles per minute, vibrationless.

APPLICATIONS

The main applications of cathode-ray tube display photometry, as shown by Garton and Webb,[5] are:

(1) Quantitative analysis—particularly for trace elements in a matrix giving rise to a complex spectrum;
(2) Determination of limit of detection;
(3) Determination of blank values in "synthetic" standard materials;
(4) Qualitative analysis.

It is now desired to discuss the method by which quantitative results can be derived with this or any other display unit, and then to show how the combination of comparator and display photometer has some special advantages over the individual instruments, particularly in the first and last of these applications.

QUANTITATIVE ANALYSIS WITH THE DISPLAY UNIT

Provided that the beam deflexion is proportional to the amount of light falling on the photocell, the height of deflexion h of a spectrum line, as measured from the zero level given by the uninterrupted photometer light beam, is proportional to $(i_0 - i)/i_0$, that is to the *absorptance* of the photographic image of the spectrum line, where i_0 is the intensity of the beam incident upon the plate and i is the intensity of light transmitted by the line (see Fig. 3). The term *absorptance* is adopted by analogy with the terminology of absorption spectroscopy[6] because optical *density*, which is a logarithmic function, cannot be used here.

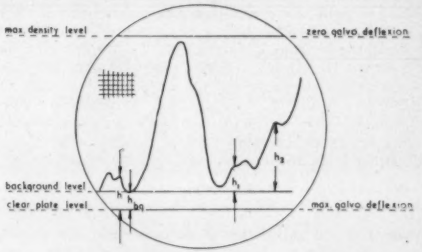

Fig. 3. Spectrum profile, iron-free zirconium

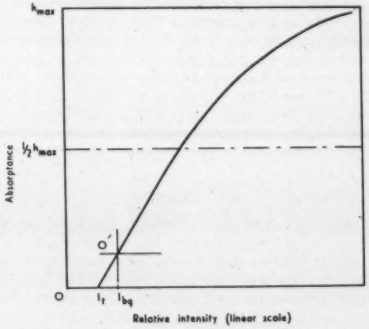

Fig. 4. Variation of absorptance with relative intensity

If the absorptance value is plotted against relative intensity in the plate-calibration pattern, a linear graph (see Fig. 4) is obtained over about half of the full absorptance range (corresponding to the range from maximum galvanometer deflexion to half maximum galvanometer deflexion of a conventional densitometer. Hence, provided $h > \frac{1}{2}h_{max}$,

$$h = m(I - I_t),$$

where I_t is the threshold intensity of the emulsion, and m is a constant related to emulsion speed. When the intensity of a spectrum line is being considered,

$$I = I_l + I_{bg},$$

where l and bg refer to line and background respectively. Therefore,

$$h = m(I_l + I_{bg} - I_t).$$

Provided that $I_{bg} > I_t$, the working origin can be shifted to some point O' on the calibration curve corresponding to the reference point (generally at background level) on the profile. With O' as origin, $h_1 = mI_1$, and for another line subject to the same value of m and measured from the same reference point, $h_2 = mI_2$, so that $h_1/h_2 = I_1/I_2$. This relationship will, therefore, apply in particular when the two lines are on the same plate and near enough to each other to be in a region of the same plate characteristic.

If h_1 is the height of a line profile of a trace element, and h_2 is the height of a line profile of an internal standard element, the ratio h_1/h_2 must be a linear function of the concentration C of the trace element. This final result is independent of the emulsion characteristics I_t and m. It should be pointed out that this linear relationship is a result, not of the method of display photometry, but of the units in which the variables are expressed. The display photometer and display comparator measure readily in these units under all conditions, whereas the practicability of making these measurements on the conventional densitometer depends very much upon the type of spectrum under examination.

It can readily be shown, in a manner similar to the derivation given above, that, for a normal densitometer,

$$\frac{d_{bg} - d_i}{d_{bg} - d_s} \propto C_i$$

where d is the galvanometer deflexion and the subscripts denote as follows: bg, background; i, impurity line; s, internal standard line. This relationship is independent of plate characteristics and densitometer sensitivity setting, and is subject only to the limitation that the absorptance value of the line should be *not greater* than approximately one-half. This method of evaluation is therefore complementary to the more conventional systems of densitometry, for example, intensity calibration by log sector or other methods,[7] or deflexion-ratio methods[8, 9] in which absorptance values should be *not less* than about one-half.

SPECIAL APPLICATIONS OF THE DISPLAY COMPARATOR

As stated above, this method of evaluation can be carried out with a normal densitometer, but it is particularly convenient to use with the profile display instruments. In certain circumstances, however, the special facilities of the display comparator become almost essential for accurate and reliable analysis.

(i) *An impurity line occurring in a region devoid of suitable reference lines.* In the magnesium spectrum, for example, there are many instances of impurity lines occurring sufficiently far away from reference lines as to appear completely isolated on the microphotometer screen. While this could be handled on a microphotometer by the expedient of recording a standard spectrum on the same plate, the procedure is often inconvenient and is not sufficiently exact if there are a large number of spectra to be examined (on a long "routine" plate, for instance). With the display comparator, it is a simple matter to aline the sample spectrum with standard spectra on a separate reference plate. Both are then moved into the correct scanning position as indicated by the reference plate. The alinement operation is performed when the internal standard line is being measured. To measure a series of spectra in this way is much faster than with a microphotometer, and the identity of the line being measured is assured beyond doubt.

If, for any reason, the reference line cannot be used as internal standard, the background adjacent to the analysis line can be used instead. The alinement is checked as above when necessary, and alternate scans are made over the spectrum and clear plate.

The long after-glow allows both background and analysis line heights to be read off at once. The height ratio h/h_{bg} in Fig. 3 is still a linear function of the concentration of the element concerned, because the working origin, as shown in Fig. 4, is moved to I_t. For the ratio h/h_{bg} to be reproducible, however, it is necessary for the background intensity value in any given instance either to be constant, or to be large in comparison with the threshold intensity value of the plate. For this reason, background intensities, when used as an internal standard, should have absorptance values of at least 0·2, corresponding to a microphotometer galvanometer reading of 40 cm or less with 50 cm clear plate.

An illustrative working curve is given in Fig. 5, which shows the determination of traces of cadmium in high-purity

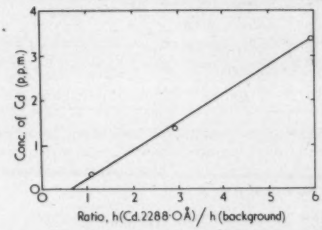

Fig. 5. Working curve for determination of concentration of cadmium impurity in magnesium

magnesium metal using Cd 2288·0 Å and background as internal standard. It shows good linearity and sensitivity down to cadmium concentrations of the order of one-tenth of a part per million. The determination is carried out using a controlled arc-type of discharge, point-to-plane sample-electrode technique, and a Hilger medium spectrograph.

(ii) *A spectrum region very thickly populated with lines of the base element and other impurities.* It is often essential to view the spectrum under examination in juxtaposition with a reference spectrum to ensure that the line being measured has been correctly identified in the presence of other impurity and interfering lines. Under such conditions, normal photometry may be difficult or, if the line sought appears as a point of inflexion rather than a maximum, it may be impossible. A means of alining and profiling then becomes essential.

A typical analysis in such circumstances is the determination of traces of hafnium in zirconium with the possible interference from the presence of iron at various concentrations as an impurity. This determination is performed by the porous-graphite cup solution technique,[10] using simple condensed-spark excitation and a Hilger large-quartz spectrograph. Fig. 3 shows the spectrum profile free from iron in the 2641 Å region. The point of inflexion h_1 represents Hf 2641 Å at about 20 parts per million, and h_2 is the zirconium peak Zr 2643 Å normally used as internal standard. The small peak between h_1 and h_2 is the source of interference with the hafnium line, and, although not listed by Harrison,[11] it is probably a weak zirconium line. Equality between Hf 2641 Å and the interference peak occurs at a concentration of about 60 p.p.m. of hafnium in zirconium. At this

level, the working curve drawn from normal microphotometric data becomes horizontal and the lower limit of detection by such methods is, therefore, about 100 p.p.m.

With the display comparator, the height ratio h_1/h_2 is comparatively easy to evaluate at much lower concentrations of hafnium. When iron is present, further small interference humps appear to modify the shape of the troughs on both sides of h_1 (see Fig. 6) and this may make it very difficult to

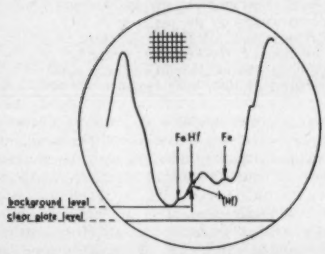

Fig. 6. Spectrum profile, zirconium with iron present

recognize the hafnium point of inflexion. It then becomes essential to check the alinement by means of the comparator facilities. Under such very adverse circumstances, it is probably better to estimate the height of the point of inflexion above the interfering line profile. Residual blank values can then be determined from the profile as shown in Fig. 6, and the working graph must pass through the origin. Fig. 7 is the resulting working curve for the example given. This shows that good sensitivity is obtainable down to hafnium contents of about 20 p.p.m. even in the presence of small amounts of iron.

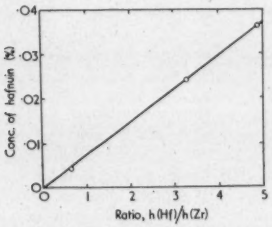

Fig. 7. Working curve for determination of concentration of hafnium impurity in zirconium

(iii) *Qualitative analysis.* In quantitative work with the display comparator, the projection comparator section has been shown to be an almost essential adjunct to the display unit. In qualitative analysis, the display unit is often an equally important complement to the comparator. Garton and Webb[5] show how to interpolate the wavelength of an unknown line. Conversely, the display unit can also be used to reveal, at positions predetermined with the comparator, the presence of lines of low intensity which are not apparent on the viewing screen to the unaided eye, either because of the interference effect of other closely situated lines, or because of their very faintness. Fig. 6 might represent, by way of an example, the profile of a zirconium spectrum in which it is desired to detect hafnium in the presence of other impurities. In this type of spectrum, the hafnium line is by no means apparent, even in the enlarged spectrum image. It would be detected only on the screen of the cathode-ray tube as a point of inflexion and identified by reference to the position of the line in a standard spectrum.

SUMMARY

An instrument has been built to combine the functions of a spectrum projector comparator and cathode-ray display photometer. This combination instrument, known as the "Display Comparator", possesses several important advantages over these individual instruments in the derivation of both qualitative and quantitative results in emission spectrography. Its most important function is the determination of trace elements under adverse spectral conditions.

ACKNOWLEDGEMENTS

The author is indebted to Mr. E. W. H. Selwyn of Kodak Research Laboratories and also to Mr. J. H. Dowell of Hilger and Watts Ltd., for advice concerning the optical system of this instrument. Thanks are sincerely accorded to the Chairman and Board of Directors of Magnesium Elektron Limited for permission to publish this report.

REFERENCES

(1) METSON, G. H. *Post Office Engineering Journal*, **25**, p. 143 (1932).

(2) FÜRTH, R. *Proc. Phys. Soc.* (*London*), **55**, p. 34 (1943).

(3) FÜRTH, R., and OLIPHANT, W. D. *J. Sci. Instrum.*, **25**, p. 289 (1948).

(4) DAVIS, H. M., and WEBB, R. J. *Spectrochim. Acta*, **4**, p. 13 (1950).

(5) GARTON, F. W. J., and WEBB, R. J. *Colloq. Intern. Spectrog., Strasbourg*, p. 127 (1950).

(6) MELLON, M. G. (Editor). *Analytical Absorption Spectroscopy* (London: Chapman and Hall, 1950) p. 193.

(7) BRODE, W. R. *Chemical Spectroscopy* (New York: Wiley, 1943), Chap. V.

(8) ARGYLE, A., and PRICE, W. J. *J. Soc. Chem. Ind.*, **67**, p. 187 (1948).

(9) PRICE, W. J. *Spectrochim. Acta*, **5**, p. 278 (1952).

(10) FELDMAN, C. *Anal. Chem.*, **21**, p. 1211 (1949).

(11) HARRISON, G. R. *M.I.T. Wavelength Tables* (New York: Wiley, 1939).

Microwave method of investigating the afterglows of pulsed gaseous discharges

By M. C. Sexton, M.Sc., Ph.D., J. J. Lennon, B.Sc., and M. J. Mulcahy, B.Sc., Department of Electrical Engineering, The University of Liverpool

[*Paper first received* 30 *January, and in final form* 1 *April*, 1959]

An apparatus suitable for recording the decrease of electron density in the afterglows of pulsed microwave discharges at 3 and 10 cm wavelengths is described. This employs the well-known method of measuring the frequency shift induced in a resonant cavity by the presence of free electrons, but a new method of detecting the resonant reflexions using a hybrid T-junction is employed. Modifications to the frequency-modulation method of probing the afterglow, which are particularly suitable for the analysis of slowly decaying plasmas, are described. An account is also given of a vacuum system suitable for handling high purity gases.

Microwave techniques have been extensively employed in recent years for investigating the electron density decay in pulsed discharge afterglows.[1] The usual method consists of energizing a discharge within a resonant cavity, and using the known linear relationship between the cavity frequency shift and the electron concentration to measure the changing density during the afterglow. This relationship is of the form

$$\frac{\Delta\omega}{\omega_0} = \frac{\bar{n}e^2}{m\omega_0^2} C \qquad (1)$$

where e and m are the electron charge and mass respectively; ω_0 is the cavity resonant frequency in the absence of electrons; $\Delta\omega$ is the change in cavity resonance brought about by the presence of an average electron concentration $\bar{n}$ per cm^3 and C is the constant depending on the electron spatial distribution and the geometry of the system.

Important factors adversely affecting the linearity of equation (1) are relatively high electron densities (approximately 10^{10} electrons per cm^3) and time-varying electron spatial distributions. However, by delaying measurements for a sufficiently long time after cessation of the discharge pulse, the distribution should be either essentially uniform or at least well defined.

The technique initially used by Biondi and Brown[2] and later modified by Biondi[3] was as follows: a high-powered magnetron produced the pulsed discharge in a quartz tube enclosed by a 10 cm cylindrical cavity. The gradual approach of the cavity resonance to that of the "empty" cavity during the afterglow was measured by probing the cavity at various times with a low-powered signal from a tunable klystron. The resonant reflexions were then picked up with a directional coupler and displayed on an oscilloscope by means of a crystal rectifier and high-gain (approximately 10^6) video amplifier. Frequency modulation was employed in the late afterglow to maintain the sharp response when the frequency shift was within 10 kc/s of the "empty" resonance. The more recent 3 cm apparatus used by Oskam[4] employed a high-powered pulsed klystron to fire the discharge, and directional isolators to eliminate undesirable reflexion effects. The cavity resonance was detected by the method of Biondi and Brown.

This paper describes the microwave and associated high vacuum gas-handling techniques which have been developed and used for afterglow measurements at 3 and 10 cm wavelengths for some years past in Liverpool.

THE EXPERIMENTAL METHOD

Generation of the pulsed discharge. A simplified block diagram of the apparatus is shown in Fig. 1. The gas is ionized in a manner similar to that described by Biondi.[3] The magnetron power output is controlled by water-cooled attenuators or by varying the height of the modulator h.t. pulse. Frequency pulling is minimized by dividing the power between a matched load and the cavity, and maximum power is coupled into the cavity line by adjusting the matching piston. In the present apparatus this power is monitored continuously with a thermistor unit before entering the cavity, by tapping off a known small fraction with a directional coupler of 17 dB attenuation. The voltage standing-wave ratio may also be measured on this section of the line by replacing the coupler with a thermocouple wattmeter situated on a slotted section of the waveguide. The maximum peak power available from the 3 cm type

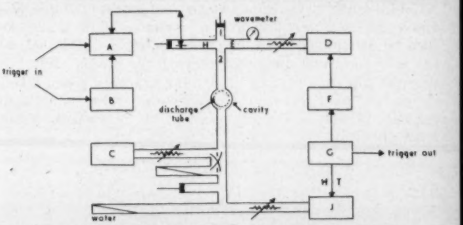

Fig. 1. Simplified block diagram of the apparatus

A, cathode-ray oscilloscope; *B*, time marker; *C*, thermistor; *D*, klystron; *F*, sawtooth generator; *G*, modulator; *J*, magnetron.

725A magnetron is 40 kW with a 1 μs pulse duration, whereas up to 450 kW is obtainable from the 10 cm type CV1481 magnetron with pulse durations of 0·6 and 1·9 μs.

The resonant cavities. High Q resonant cavities are desirable for this work to enable relatively low electron densities (approximately 10^8 electrons per cm^3) to be accurately measured. The TM_{010} mode was adopted for both wavelengths, ensuring an axial E-field for the gas breakdown. The cavities were assembled with an axial split (parallel to the current flow) and soldered end-plates.

An electro-forming method was used in shaping the 3 cm cavity to reduce surface irregularities. As noted by Biondi,[3] a compromise between maintaining a high Q and absorbing sufficient power, both for discharge stability and probing signal (see below), must be struck when determining the optimum size of the coupling irises. In the present work an iris diameter of 0·64 cm was found to be very satisfactory for a 3 cm cavity of diameter 2·1 cm and height 3·77 cm. This led to a Q of 3100 at a frequency of 9430 Mc/s when loaded with a cylindrical quartz discharge tube of diameter 1·5 cm and length 3·0 cm. The insertion of the quartz at

this frequency gave rise to the considerable reduction of 1500 Mc/s from the theoretical value. For the 10 cm apparatus a 1·27 cm diameter coupling iris in a cavity 7·35 cm diameter and 6·1 cm high resulted in a Q of 3000 at 3006 Mc/s, when loaded with a discharge tube of the same dimensions as used for the 3 cm cavity. The departure from the theoretical frequency was only 140 Mc/s at this frequency.

The measurement of frequency. A klystron supplies the low-powered signal for probing the cavity during the afterglow. Valve types 723A/B and CV35 are in use at 3 and 10 cm respectively. The gradual approach of the frequency to that of the "empty" cavity during the afterglow period is then measured by recording the power reflected at the different frequencies. Fig. 1 illustrates the method adopted. Following the technique of Biondi,[3] frequency modulation of the klystron output with a sawtooth generator maintains a sharp reflected signal in the late afterglow when the frequency is approaching that of the "empty" cavity. It was then found that the klystron power output varied from zero, through a maximum and back to zero over the modulation range, making it difficult to identify the signal due to the cavity resonance. However the removal of the modulation envelope, using the hybrid T-junction arrangement shown in Fig. 1, is considered to be a substantial improvement over the original method of Biondi and Brown. The klystron power transmitted through the *E*-plane arm will divide equally between side-arms 1 and 2, if the latter are of equal electrical length and are terminated identically. The waves reflected from the side-arm terminations will arrive back at the junction equal in magnitude but 180° out of phase and will, therefore, completely cancel, with no power being propagated into the *H*-plane arm. Thus if, as shown in Fig. 1, the cavity terminates side-arm 2 and side-arm 1 is closed by a correctly adjusted reflecting piston, the modulation envelope arriving from the *E*-plane arm will be reflected equally from the terminations of 1 and 2, except for the small amount of power absorbed by the cavity at resonance. Since the signals arrive back out of phase and cancel, the cavity reflexion *alone* is fed into the *H*-plane arm leading to the oscilloscope *via* the crystal rectifier termination.

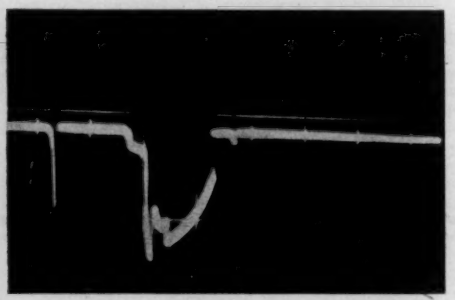

(*a*)

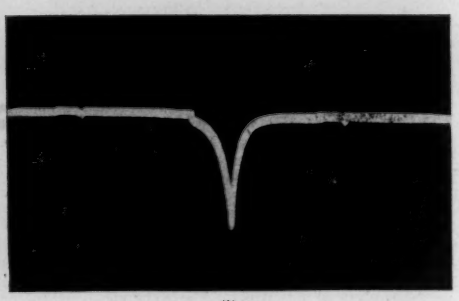

(*b*)

Fig. 2. (*a*) The signal reflected from the cavity at resonance partially obscured by the klystron modulation envelope. (*b*) The same signal reflected from the cavity at resonance, following removal of the klystron modulation envelope by using the hybrid T-junction. (10 cm apparatus)

To illustrate this process, Fig. 2(*a*) shows the cavity resonance partially obscured by the modulation envelope, whereas Fig. 2(*b*) indicates the successful removal of the envelope by adjustment of the T-junction, leaving the cavity resonance undisturbed for accurate frequency measurements. Amplifier requirements then become less stringent since the omission of the directional coupler leaves the resonant reflexion without appreciable attenuation. Thus a probing signal of the order of a few microwatts may be readily amplified, ensuring minimum perturbation of the thermal electrons.

Two methods of analysing the afterglow with this technique are employed. One of these consists of sweeping the klystron frequency with the sawtooth generator a convenient number of times during the measuring period, enabling several different frequencies to be noted simultaneously with time. Figs. 3(*a*) and 3(*b*) illustrate this process without and with a discharge respectively. The broader "spikes" represent the resonant minima corresponding to the repetition rate of the modulation, whereas the sharper dips result from the fast flyback of the sawtooth voltage. In Fig. 3(*a*) the wavemeter "pip" appears as a bright spot at a constant height above the resonant minima (about one-fifth of the way up) indicating a time-independent cavity frequency, whereas, in Fig. 3(*b*), the height of this "pip" above the minima increases with time, showing the decrease of frequency in the afterglow of an argon discharge. The wavemeter is fitted with a high reduction drive ensuring an accuracy of $\pm 1 \cdot 5$ kc/s.

Alternatively, a variable delay unit, which may be inserted between the modulator and sawtooth generator, enables the latter to be triggered and hence the cavity resonance to be recorded at any desired time in the afterglow. The oscilloscope traces of Figs. 2(*a*) and 2(*b*) were obtained in this manner. The "spike" to the left of the modulation envelope in Fig. 2(*a*) is due to the sawtooth flyback.

It is clear that either of the techniques referred to above is particularly suitable for electron density measurements in relatively slowly decaying plasmas, where the entire decay picture over a long time interval may be instantly observed without the necessity of retuning the klystron.

Synchronization of events. A master trigger in the modulator unit synchronizes the various events, including a time-marker for calibrating the oscilloscope trace. Satisfactory afterglows have been obtained with pulse repetition frequencies of 100 and 200 pulses per second. In adapting the conventional radar modulators to these low pulse frequencies, resistance charging of the artificial lines proved to be more flexible than the choke input type.

The vacuum system. Considerable care was taken to ensure high purity gas samples, as an impurity content of

greater than approximately 1 part in 10^7 leads to serious errors in recombination and diffusion measurements in rare gases. Accordingly, the vacuum system was constructed with all-metal valves of the Alpert type,[5] employing a screw mechanism to drive a stainless steel plunger into a copper seating. The valves are bolted to a rigid framework with U-bends in the glass work to reduce strain, thereby enabling the whole system to be effectively outgassed.

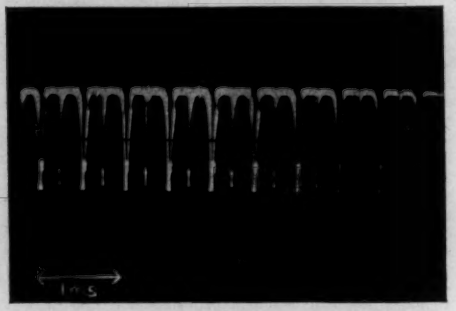

(*a*)

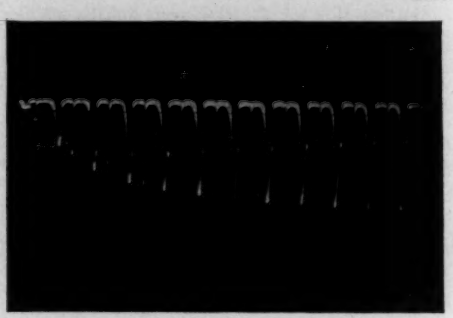

(*b*)

Fig. 3. (*a*) The constant-frequency signals reflected from the cavity with no discharge. (*b*) The variation of cavity frequency following a pulsed discharge in 10 mm argon. (3 cm apparatus)

Valve designs obtained through the courtesy of the Services Electronics Research Laboratory (Baldock) and Mullard Research Laboratories (Salfords) have been used with equal success. A $\frac{1}{2}$ in. diameter seating annulus in the former valve facilitates relatively high pumping speeds, and connexions are made to the kodial glass system with kovar seals. The Mullard valve uses OFHC copper-kodial seals and employs a differential screw mechanism for fine control of the gas flow. Residual pressures attainable with systems incorporating these valves lie between 10^{-8}–10^{-9} mm of mercury, using ionization gauge pumping, with a holding pressure of approximately 5×10^{-8} mm on closing-off the pumps.

The experimental gas pressure is measured by a null method similar to that described by Danby and Cook.[6] A brass tombac bellows is enclosed in a vacuum-tight container with the inside of the bellows connected to the vacuum system, and the outside (i.e. the container) to a McLeod gauge. Pressure measurement is effected by equating the gas pressure inside the bellows to the McLeod pressure outside by noting the change in resonance produced in a tuned circuit when the capacitance alters between the top of the bellows and a fixed plate. This arrangement enables pressures down to 0·5 mm of mercury to be accurately measured.

The gas samples are spectroscopically pure. Before taking readings a continuous discharge is run until a reproducible afterglow is observed, as this has proved to be the only effective method of eliminating impurities occluded in the discharge tube walls. The short pulse durations are advantageous in keeping this type of contamination within reasonable limits.[7]

PRELIMINARY RESULTS

Fig. 4 shows the decline of electron density in 0·55 mm argon following a 50 kW (peak) discharge of 0·9 μs duration. The range of density covered, from $1{\cdot}3 \times 10^9$ to $3{\cdot}0 \times 10^7$ electrons per cm^3, represents the limits within which measurements may be taken using the frequency modulation method, without retuning the klystron. The linearity of the $\log_e n$ *versus* t plot indicates loss of electrons by a diffusion mechanism. This result was obtained with the 10 cm apparatus. Initial measurements at 3 cm which have been published[8] show good agreement with previous studies.

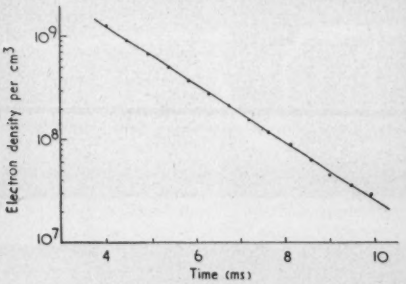

Fig. 4. The decline of electron density following a pulsed discharge in 0·55 mm argon. (10 cm apparatus)

The maximum probing signal power permissible to avoid appreciable temperature effects in the thermal afterglow has been investigated and will be reported later. Some work is currently in progress on the measurement of electron attachment cross-sections in oxygen afterglows.

ACKNOWLEDGEMENTS

The authors are indebted to Prof. J. D. Craggs for his active interest in the progress of this work and for advice in the preparation of this paper. The technical assistance of Mr. W. E. Austin and Mr. T. Rice is acknowledged. Thanks are also extended to Dr. M. A. Biondi (Westinghouse) for the design of a 10 cm cavity and to the Services Electronics Research Laboratory (Baldock) and Mullard Research Laboratories (Salfords) for the designs of the vacuum valves.

Acknowledgement is made to the Admiralty for permission to publish this paper.

REFERENCES

(1) GOLDSTEIN, L. *Advances in Electronics and Electron Physics*, **7**, p. 399 (New York: Academic Press Inc., 1955).

(2) BIONDI, M. A., and BROWN, S. C. *Phys. Rev.*, **75**, p. 1700 (1949).

(3) BIONDI, M. A. *Rev. Sci. Instrum.*, **22**, p. 500 (1951).

(4) OSKAM, H. J. *Philips Res. Rep.*, **13**, p. 419 (1958).

(5) ALPERT, D. *J. Appl. Phys.*, **24**, p. 860 (1953).

(6) COOK, D. B., and DANBY, C. J. *J. Sci. Instrum.*, **30**, p. 238 (1953).

(7) PERSSON, K. B., and BROWN, S. C. *Phys. Rev.*, **100**, p. 729 (1955).

(8) SEXTON, M. C., and CRAGGS, J. D. *J. Elect. and Control*, **4**, p. 493 (1958).

Reversible poisoning by sulphur, oxygen and other gases of oxide-coated cathodes at high temperatures

By N. A. SURPLICE, B.Sc., Ph.D., Physics Department, University College of North Staffordshire, Keele, Staffs.

[*Paper first received* 1 *January, and in its final form* 11 *March*, 1959]

A simple mass spectrometer has been used to select and study the behaviour of the negative ions of sulphur and oxygen emitted by oxide-coated cathodes on recovery from the poisoning of their electron emission by these agents over the temperature range 1075–1300° K. Only the atomic ions were observed, and the behaviour of the $^{32}S^-$ ion emitted on recovery from sulphur poisoning was similar to that of the $^{16}O^-$ ion emitted on recovery from oxygen poisoning. The ion $^{13}CH^-$ also had a slight poisoning effect. Measurements of the energy distributions of these ions showed that, during recovery, many more of them were sputtered off the top surface of the cathode than were evaporated from its pores. These results support the hypothesis that high-temperature reversible poisoning is caused by the adsorption of negative ions on the internal and external surfaces of the porous oxide-coating.

The effect of certain residual gases and vapours in reducing the electron emission of oxide-coated cathodes in valves is known as poisoning. The poisoning effect of controlled leaks of oxygen or other gas in molecular form has been studied by Herrmann and Krieg[1] and by Wagener.[2] The effect of liberating the poison in atomic form by the thermal decomposition of a chemical compound in vacuum, as occurs in practice, has been studied for chlorine by Hamaker, Bruining, and Aten[3] and by Vick and Walley,[4] and for oxygen by Metson,[5] Shepherd,[6] and Higginson.[7] Only Higginson has studied the effect of sulphur, though this has been mentioned as a practical nuisance by Stahl[8] and Penotet.[9] Most investigations have been simply of the poisoning and recovery of the electron emission,[1, 2, 3, 5] rather fewer of the conductivity as well,[6, 7] or of the ions emitted by the cathode on its recovery.[4, 6] In the experiments described below, the poison was liberated by thermal decomposition in vacuum, and a simple mass spectrometer was used to select and study the negative ions $^{32}S^-$, $^{16}O^-$ and $^{13}CH^-$ emitted by the cathode during its recovery from the poisoning.

APPARATUS

The mass spectrometers had glass envelopes and were similar to those described by Shepherd[6] by Grattidge and Shepherd.[10] They used a 90° sector magnetic analyser placed symmetrically between the source and exit slit, with simple first-order direction focusing, and the mass spectra were scanned by varying the magnetic field. The negative ion current to the collector was measured with a d.c. amplifier using an electrometer valve type DBM4A (by Ferranti). The energy distribution of any particular ion could be found by measuring its current to the collector against a retarding potential; this retarding potential was applied directly between the collector and cathode because preliminary experiments showed that applying it to a separate slotted retarder did not give sufficiently accurate energy measurements. This potential could be varied over a pre-set range by means of a potentiometer driven by a synchronous motor and a timing gear on the potentiometer shaft triggered electrical signals at each of which the ion current to the collector could be recorded for a known retarding potential. The variation of retarding potential was spread over two minutes because of the long period (6 s) of the galvanometer which measured the output of the d.c. amplifier.

Each cathode had a base of O-nickel 0·04 cm^2 in area which had been cleaned by heating it to redness in a hydrogen furnace, and was sprayed with a coating of mixed barium and strontium carbonates about 0·005 cm thick, using the same mixture as Higginson.[7] Its temperature was measured with a nickel–tungsten thermocouple. The controllable source of poison was an alumina-coated tungsten filament on which was painted either barium peroxide or molybdenum disulphide[7] mixed with amyl acetate and a little collodion to act as binder. Oxygen and sulphur respectively were released when the filament was subsequently heated. The electron gun was mounted on a ceramic frame and a nickel sleeve on its anode alined it with the deflexion chamber, but did not fix it permanently there, and so the entire gun was changed each time that the cathode was changed. This arrangement is shown in Fig. 1.

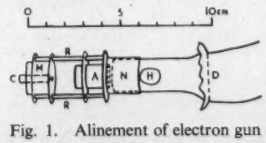

Fig. 1. Alinement of electron gun

A, anode; *C*, cathode; *D*, deflexion chamber; *H*, hole for gas flow from *D*; *M*, modulator; *N*, nickel sleeve; *R*, ceramic rods.

The usual techniques of cleaning the glass in acid and in distilled water and of heating each electrode to redness in a hydrogen furnace before the tube was assembled and sealed to the vacuum system were used. Each tube was baked and

its electrodes were eddy-current heated to redness both before and after the breakdown of the cathode carbonates to oxides, and the poisoning filament was also heated to drive off adsorbed gases. During the heatings of the electrodes and of the poisoning filament, the cathode was kept at 1175° K to help it resist any unintentional poisoning. The cathode was activated by heating it for two minutes at 1325° K. Then the tube was sealed off with the cathode at 1175° K and barium getters were fired. All the apparatus was screened by an earthed steel cupboard, and all its electrical supplies were d.c. supplies.

INSTRUMENTAL EFFECTS

Some instrumental effects were studied to ensure that they would not unduly influence the main experiment. The heights of the ion peaks were found to be proportional to their areas over the full range of observable peak heights, and therefore gave a satisfactory measure of the ion currents. However, the following two effects limited the instrument to comparative rather than absolute measurements. As the retarding potential was increased to allow only ions of the higher energies to pass to the collector, it was inevitable that these ions also had higher momenta than the average and that consequently they needed a slightly stronger magnetic field to focus them in the same place. For technical simplicity the magnetic field was kept constant, and this caused the position of the ion peak to move by about a quarter of its half-width during a full measurement of the energy distribution of the ions and made the apparent current of high-energy ions about 25% low. In contrast to this, the slow response of the galvanometer to changes of current exaggerated the high-energy currents when the motor-driven potentiometer was used to change the retarding potential from positive to negative. The degree of exaggeration depended markedly on the shape of the energy distribution plot, being very high for a plot with a sharp cut-off, such as for electrons, but only about 10% of the high-energy current for a plot with a gradual cut-off, such as for oxygen ions. This effect is shown in Fig. 2, comparing energy distributions

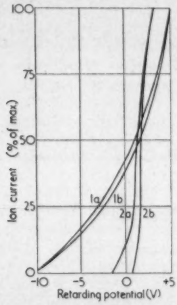

Fig. 2. Exaggeration of high-energy currents

1*a*, continuous variation of retarding potential for $^{16}O^-$ ions; 1*b*, discontinuous variation of retarding potential for $^{16}O^-$ ions; 2*a*, continuous variation of retarding potential for electrons; 2*b*, discontinuous variation of retarding potential for electrons.

measured (*a*) by varying the retarding potential continuously by the motor-driven potentiometer with those obtained (*b*) by the discontinuous method of measuring the steady currents for various steady retarding voltages. The random error in the integral energy-distribution measurements taken with the motor-driven potentiometer was estimated from a series of consecutive plots for the same steady ion peak and was found to have a standard deviation of 2½%.

EXPERIMENTAL RESULTS

The mass spectra. The mass spectra were calibrated using the chlorine negative ions $^{35}Cl^-$ and $^{37}Cl^-$ and were checked with $^{16}O^-$ from the poisoning filament. They were qualitatively similar to those found by Vick and Walley[4] and by Grattidge and Shepherd,[10] who had used similar apparatus made from 1947 Hysil glass, but the chlorine-ion currents to the collector in the present 1958 Pyrex glass apparatus were only of the order of 10^{-13} A instead of 10^{-11} A. At cathode temperatures from 1075 to 1300° K the oxygen $^{16}O^-$ and sulphur $^{32}S^-$ ion currents measured five minutes after poisoning with the appropriate agent were from 10^{-13} to 3×10^{-12} A, and the $^{13}CH^-$ peak was of similar size. The $^{13}CH^-$ ion was seen only after the poisoning filament had been heated, and the molecular ion $^{32}O^-$ was seen only after the cathode had been run for about 48 hours. The $^{28}CO^-$ ion was observed as a small peak of about 10^{-13} A, but the $^{44}CO_2^-$ ion was not seen at all.

The energy distributions of the ions. The energy distribution of each type of ion was found by the retarding-potential method. For most types of ion, the current cuts off quite suddenly at a retarding potential which is a few volts positive with respect to the cathode, just as it did for electrons, showing that the energies of the ions varied, but little from

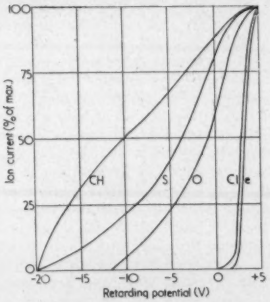

Fig. 3. Typical energy-distribution curves for $^{13}CH^-$, $^{32}S^-$, $^{16}O^-$, $^{35}Cl^-$ and electrons

that given to them by the electron gun. This cut off was at one or two volts above the cathode potential because of the voltage drop in the oxide coating and contact potential difference between the cathode and retarder,[6] and was not quite sharp because the cathode was slightly convex rather than exactly planar. By contrast, the ion currents of $^{16}O^-$, $^{32}S^-$, and $^{13}CH^-$ decreased only gradually with increasing retarding potential thus showing that a large proportion of these ions had energies greater than that given them by the electron gun alone. This extra energy presumably came from positive ion bombardment sputtering off O, S, or CH from the cathode.[11, 12] For one cathode, a small proportion of the ions of mass number 26 ($C_2H_2^-$ or CN^-) also had excess energies, which is not unreasonable in view of the evidence that this radical comes from the cathode binder.[4, 10] Typical energy distribution curves of both types are shown in Fig. 3. The energy distributions of all ions changed slightly, slowly, and in a random fashion with time; only those of $^{16}O^-$, $^{32}S^-$ and perhaps $^{13}CH^-$ were found to change in any different manner when the cathode was recovering from poisoning.

The emission of negative ions of sulphur and oxygen during recovery from poisoning. Separate mass spectrometers were used to study sulphur and oxygen poisoning, so that no tube was contaminated with both poisons. The potential difference between the cathode and the modulator was kept at 9 V, which was less than the ionization potentials of sulphur, oxygen, and all likely residual gases. Poisoning and recovery cycles were studied at temperatures between 1075 and 1300° K and could be repeated indefinitely without any permanent effect on the electron emission of the cathodes. The only ions of sulphur or oxygen detected during recovery of the cathodes were the atomic ones $^{32}S^-$ and $^{16}O^-$. The molecular oxygen ion was not detected at all[6]; the molecular ion of sulphur was beyond the range of the mass spectrometer but, from analogy, was unlikely to be emitted, so for simplicity S^- and O^- are used to denote the atomic ions. The total current of S^- or O^- decreased as the cathode recovered and equilibrium was reached most rapidly at the highest temperature.

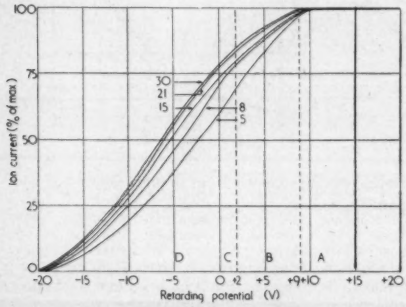

Fig. 4. Variation of energy distribution of S^- ions emitted during recovery from sulphur poisoning at 1175° K

(Numbers on curves indicate time in minutes after poisoning.)

The energy distribution of the S^- or O^- ions was measured every few minutes during the recovery of the cathodes and each distribution was corrected for the decrease of ion current during the two minutes needed to cover the full range of retarding potential by the motor-driven potentiometer. In Fig. 4, a typical series of such measurements showing percentages of S^- current is plotted against retarding potential: similar results for O^- confirmed some previous work.[6] Ions formed between the anode and the modulator are shown by Part A and those formed between the modulator and the cathode by Part B. It can be seen that at the beginning there was a large percentage of these low-energy ions formed from the cloud of sulphur vapour which had been released in front of the cathode, and this decreased as the vapour was cleaned up by the getters, the electrodes, and the glass. The sections of the curves giving information about the cathode are Parts C and D which show in turn the ions evaporated from its pores and the ions which were given extra energy by being sputtered off its surface. The ordinates and the slopes of the curves show that, as the cathode recovered, an increasing percentage of ions had these high energies, and their most probable energy increased until it was about 8 V more than was given by the electron gun alone.

More information was obtained by studying changes in the actual currents of high-energy ions emitted during recovery of the cathodes. In Fig. 5 these changes are shown for a particular cathode studied during three consecutive cycles of sulphur poisoning and recovery at different temperatures. These results show that during recovery both the current of sputtered ions and the current of evaporated ions decreased, and that this decrease was most rapid during the first few minutes. After about an hour (depending on the temperature), these currents remained constant within the limits of random experimental error and were about the same as they had been at the end of recovery from the previous poisoning. They were not expected to be exactly the same as before because the environment of the cathode was changed by each release of poison. At the lowest temperature, least sulphur was needed to poison the cathode to the same extent so the initial current of sulphur ions was also the smallest. Although the current appeared to reach equilibrium

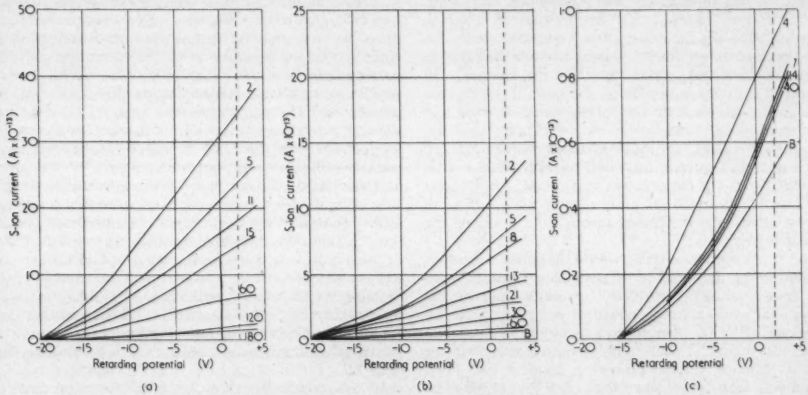

Fig. 5. Variation of current of high-energy S^- ions emitted by cathode recovering from sulphur poisoning at temperatures of (*a*) 1300° K; (*b*) 1175° K; (*c*) 1075° K

(Numbers on curves indicate time in minutes after poisoning. Curve B was obtained before poisoning.)

most rapidly at the lowest temperature, this was only because the d.c. amplifier could not detect changes of less than 10^{-15} A, and this limit was reached most rapidly when the initial currents were smallest. Results similar to these were obtained from a study of the high energy O^- ions emitted during recovery from oxygen poisoning, and also from calculations based on Shepherd's[6] result for oxygen poisoning (Thesis 1951).

Raising the temperature of cathodes during their recovery caused a rapid but brief rise in the S^- ion current. An example of this is shown in Fig. 6: this cathode was poisoned on the poisoning filament. The corresponding positive ion CH^+ is present, though not abundant, in the cracking patterns of several organic compounds.[13] The $^{13}CH^-$ ion seems only once to have been detected from an oxide-coated cathode under normal conditions,[14] but it is energetically possible to form it there from the neutral radical because its electron affinity is greater than 1·2 eV.

A separate poisoning experiment was carried out with the tungsten poisoning filament coated only with alumina powder and the usual binder. This was found to poison the emission slightly, but to a far less extent than either oxygen or sulphur.

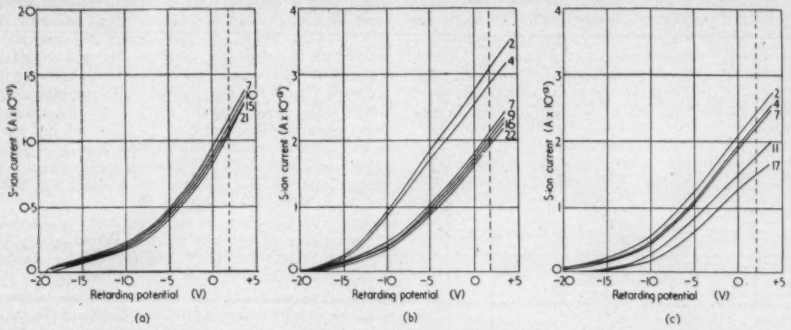

Fig. 6. Effect on S^- ion current of raising cathode temperature during recovery from sulphur poisoning

(*a*) Recovery at 1075° K. Numbers on curves indicate time in minutes after poisoning;
(*b*) and (*c*) Temperature raised to 1175 and 1300° K respectively. Numbers on curves indicate time in minutes after raising temperature.

with sulphur at 1075° K to 10% of its electron emission and allowed to recover to 50%, by which time the changes in the high-energy S^- ion current had become too small to be resolved satisfactorily. Its temperature was raised to 1175° K, which caused the high-energy S^- current to rise suddenly and then fall again to reach a new equilibrium value in about twenty minutes. Meanwhile, the electron current had risen steadily until it had reached its new equilibrium value after about ten minutes. Raising the temperature to 1300° K had a similar effect on the electron emission, but much less effect than previously on the S^- current because the cathode had by that time already ejected most of the sulphur. In experiments at constant temperature, the ratio of the current evaporated from the cathode to that sputtered from it had decreased steadily with time, but in this experiment, when the temperature was raised, the ratio dropped suddenly from 0·3 to 0·1 and then quickly increased again to 0·25. This suggests that, when the temperature was raised, the S^- ions were temporarily sputtered off more rapidly than they were replaced by others which diffused through the pores of the cathode coating.

All these results were unaffected, within the limits of random experimental error, by degrees of poisoning from 50% to 90%, by anode voltages from 600 V to 900 V, and by the range over which the retarding potential was varied.

The emission of $^{13}CH^-$ ions during recovery from poisoning. An ion of mass number 13 invariably appeared after, but not until, an oxygen- or sulphur-poisoning filament had been heated and was most prominent for the first few heatings of the filament. This peak was clearly resolved from the small $^{12}C^-$ peak, and was presumably $^{13}CH^-$ formed from the breakdown of the binder $\{CH_3COOC_5H_{11}$ and $(C_6H_7O_5NO_2)_n\}$. For example, with the cathode at 1200° K the tungsten filament had to be kept hot for over a minute to reduce the cathode emission to 80% of its initial value, whereas oxygen or sulphur would have reduced it to that in about a second. This poisoning filament had been given the usual preliminary heating before the tube had been sealed off, and the poisoning experiments were repeated six times with it, so the poisoning was most unlikely to have been caused by any adsorbed gas which had escaped detection. The energy distribution of the CH^- ion showed that it was produced more from a surface layer on the cathode and less from the interior of the coating than were the S^- and O^- ions. When the cathode was recovering from sulphur or oxygen poisoning, the percentage of CH^- current plotted against retarding potential showed a tendency to vary in a manner similar to, though less pronounced than, the S^- or O^- ions, but the actual current of high-energy ions varied much less and there was not conclusive evidence that it always decreased steadily with time. The evidence suggested that, for the first few poisonings, CH^- behaved in a way similar to, though much less effective than S^- and O^-, but later on there was so little binder left on the filament that the partial layer of CH^- on the cathode surface was being replaced by oxygen after oxygen poisoning or sulphur after sulphur poisoning. A sudden rise of cathode temperature had an effect on CH^- similar to that described for S^-, causing the current of high-energy ions at first to increase but then to fall again to a new equilibrium value (Fig. 7).

It was concluded that the breakdown products of the binder and CH^- in particular played so small a part in the poisoning of the cathode that there was no need to use a different type of binder on the poisoning filaments. Radicals

such as CH^- would presumably be a product of the breakdown of the cathode (from carbonates suspended in amyl acetate to oxides of alkaline earth metals), but should scarcely affect the subsequent performance of the cathode because most of these mild poisons would be pumped off before the cathode was activated.

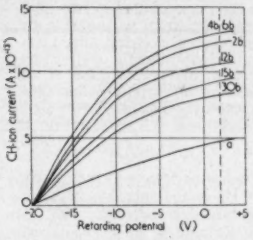

Fig. 7. Effect on CH^--ion current of raising cathode temperature

Curve (*a*) is current for cathode at 1075° K.
Curves (*b*) are for currents at times, in minutes, indicated on curves after cathode temperature had been quickly raised to 1300° K.

DISCUSSION

The oxide cathode consists of many small crystals deposited on a base to form a powdery coating whose pores play an important part in its electrical properties.[17] These experiments have shown that oxide cathodes recovering from poisoning by sulphur or oxygen at temperatures from 1075 to 1300° K, emit negative atomic ions of the poison. Some of these ions are evaporated from the pores of the coating, but most seem to be sputtered off the cathode by positive-ion bombardment, and the negative-ion current decreases as the cathode recovers. This suggests that a poisoned cathode has negative ions on its top and interior surfaces and that, when it recovers, these ions are removed until dynamic equilibrium is reached with the surroundings.

The cathode is very irregular on the atomic scale and has points and ridges on it which are predominantly responsible for its electron emission,[15] so any negative ions on these sites will raise the work function and thus decrease the electron emission. These same sites are also the places where atoms of sulphur or oxygen which strike the cathode will be preferentially held by chemisorption. Such chemisorbed atoms can each obtain an electron from a donor in the cathode and become singly charged negative ions because their electron affinities are all greater than the mean emissive work function of the cathode (1·2 eV); negative ions of the halogens could be formed in the same way. Wagener[15] has shown that the formation of singly charged oxygen ions from oxygen molecules on the coating is also energetically possible, but that the formation of the doubly charged negative ion is unlikely unless positive ions strike the cathode. Repeating these calculations with the most recent result for the electron affinity of oxygen[16] confirms that singly charged negative ions can be formed from the molecule provided its adsorption energy is not less than 2·25 eV (56·5 kcal.mole^{-1}), but that to form a doubly charged negative ion would need about 8·5 eV (212 kcal.mole^{-1}), which is far too high for an adsorption energy and would have to be provided mainly by positive ions. It has also been suggested[15] that reversible poisoning might be caused by O^- entering the lattice because it would be so much easier to dislodge this than to dislodge O^{--}. However, such an O^- ion in the lattice would introduce a positive hole into the filled band of the crystal and this would quickly be filled by an electron from a donor level, thus changing the O^- ion to O^{--}. There is a similar argument against S^- being in the lattice, but a halogen negative ion would stay singly charged and the resulting positive hole would remain until the cathode recovered, and would affect its conductivity in a manner that has not been observed.[3]

There are therefore both experimental and theoretical grounds for suggesting that high-temperature reversible poisoning is caused by the adsorption of negative ions on the internal and external surfaces of the porous oxide coating. The part played by positive ions in the recovery process is the subject of a further investigation in this laboratory.

ACKNOWLEDGEMENTS

The author thanks Prof. F. A. Vick for suggesting this problem, providing the laboratory facilities, and discussing the results; and Prof. N. F. Mott for a discussion during a visit to Keele. He thanks Mr. H. Stewart (Scientific Glass Blowing Co. Ltd.) for making the mass spectrometer envelopes, Siemens-Edison-Swan Ltd. for the gift of valve stems, and Ferranti Ltd. for the gift of electron guns.

REFERENCES

(1) Herrmann, G., and Krieg, O. *Ann. Phys.* (*Leipzig*), **6(4)**, p. 30 (1949).

(2) Wagener, S. *Proc. Phys. Soc.* (*London*), **B67**, p. 369 (1954).

(3) Hamaker, H. C., Bruining, H., and Aten, A. H. W. *Philips Res. Rep.*, **2**, p. 171 (1947).

(4) Vick, F. A., and Walley, C. A. *Proc. Phys. Soc.* (*London*), **B67**, p. 169 (1954).

(5) Metson, G. H. *Nature* (*London*), **164**, p. 540 (1949).

(6) Shepherd, A. A. *Brit. J. Appl. Phys.*, **4**, p. 70 (1953).

(7) Higginson, G. S. *Brit. J. Appl. Phys.*, **8**, p. 148 (1957).

(8) Stahl, H. A. *Appl. Sci. Res.*, **B1**, p. 397 (1950).

(9) Penotet, H. *Vide*, **10**, p. 362 (1955).

(10) Grattidge, W., and Shepherd, A. A. *Proc. Phys. Soc.* (*London*), **B67**, p. 177 (1954).

(11) Sloane, R. H., and Press, R. *Proc. Roy. Soc.*, **A168**, p. 872 (1938).

(12) Arnot, F. L., and Beckett, C. *Proc. Roy. Soc.*, **A168**, p. 103 (1938).

(13) Barnard, G. P. *Modern Mass Spectrometry* (London: Institute of Physics, 1953).

(14) Sloane, R. H., and Watt, C. S. *Proc. Phys. Soc.* (*London*), **61**, p. 217 (1948).

(15) Herrmann, G., and Wagener, S. *The Oxide Coated Cathode*. Vol. 2 (London: Chapman and Hall Ltd., 1951).

(16) Branscombe, L. M. *Advances in Electronics and Electron Physics*, **9**, p. 43 (1957).

(17) Loosjes, R., and Vink, H. J. *Philips Res. Rep.*, **4**, p. 449 (1949).

Bistable behaviour of the Bayard-Alpert ionization gauge

By G. Carter, B.Sc., Grad.Inst.P., and J. H. Leck, M.Eng., A.Inst.P., A.M.I.E.E., Dept of Electrical Engineering, University of Liverpool

[*Paper first received* 9 *January, and in final form* 12 *March*, 1959]

It has been observed that the Bayard–Alpert ionization gauge can possess either of two completely independent and stable modes of operation. The difference appears as variations in the pressure sensitivity of the gauge and complementary changes in the electrical adsorption characteristics of different gases. This bistable behaviour has been consistently observed on three different gauges and is attributed to the electrical charging of the inner surfaces of the gauges as a result of secondary-emission processes. Confirmation of this hypothesis has been made with a metal-screened gauge in which it was possible to control the discharge.

INTRODUCTION

The phenomenon of variable ionization-gauge sensitivity described in this paper was discovered during an investigation of the adsorption characteristics of the inert gases on to glass surfaces. The main purpose of that work was to observe adsorption phenomena on the glass envelopes of Bayard-Alpert ionization gauges. It was necessary to keep a close check upon the sensitivity of these gauges during the whole period of the work because this was an experimental parameter. In each of the three series of experiments that were carried out, the test gauge was found to possess two independent values of sensitivity which differed from each other by a factor of three. Each gauge exhibited two distinct and stable modes of operation. There is evidence to suggest that two stable modes are possible because of changes in the electrical potential of the glass envelope. The object of this paper is to describe the experimental observations of the changes in gauge sensitivity and to present evidence for ascribing the phenomenon to an electrical effect at the glass surface. A preliminary and brief account of these experiments was given in a paper[1] of much wider scope, entitled "Adsorption and Desorption of Positive Ions on Glass and Metal Surfaces" at the First International Congress of Vacuum Techniques held at Namur in June 1957.

APPARATUS

A small all-glass vacuum system was used for the adsorption experiments. It consisted essentially of a Bayard–Alpert ionization gauge evacuated by a three-stage mercury diffusion pump, together with three vapour traps of conventional design. The first trap (that is, the one nearest the diffusion pump) contained a solid carbon-dioxide/acetone freezing mixture, and the other two traps contained liquid nitrogen. A second Bayard–Alpert gauge was included between the two liquid-nitrogen traps in order to record the desorption transient from the test gauge. The traps and the ionization gauges could be heated to a temperature in excess of 300° C by means of a detachable electric furnace and, in addition, the experimental gauge could be heated to 450° C by a second smaller furnace, this furnace being carefully constructed to ensure uniform heating of the glass envelope. The ultimate pressure in this system was easily reduced to better than 10^{-9} mm Hg, equivalent nitrogen pressure, as measured by either gauge.

An auxiliary vacuum reservoir, connected to the main system by a silicon–carbide porous plug, enabled gas to be admitted at a controlled and known rate. Thus, as both the rate of flow of gas and the effective conductance of the vacuum system were known, both gauges could be calibrated.

EXPERIMENTAL PROCEDURE AND RESULTS

As soon as a low pressure had been reached (that is, less than 10^{-9} mm Hg as indicated by the auxiliary gauge) the test gauge was heated to more than 400° C for a period of approximately 30 minutes, its filament being switched on while the gauge was at its highest temperature. When the temperature had fallen to 30° C, gas (neon, argon, or krypton) was passed through the system at a pressure of 10^{-5} mm Hg for a given time. After this flow had been stopped, the test gauge was switched off and re-heated to 400° C. Careful measurements were made with the auxiliary gauge during this baking in order to detect any desorption. This experiment was repeated a number of times while only the duration of the gas flow and the electron current in the test gauge were varied. The sensitivity of both gauges was checked for the particular gas being used at least once during each experiment.

Altogether, three series of experiments of the above type were made using different gauges which were all of the same design and had the same type of boro-silicate glass envelopes. The geometric configuration of the electrodes in these gauges was the same as that described originally by Bayard and Alpert,[2] that is, the inverted-triode construction. The design details differed somewhat however from the original because such rigid vacuum requirements were not imposed upon the present work and it was consequently found convenient to construct the electrodes from stouter material. All the electrodes were about 6 cm long and were supported by tungsten leads sealed through the glass at the well of a re-entrant type pinch. The two filaments of 0·07 mm diameter tungsten were situated roughly mid-way between the walls and the helical electron collector. The electron collector was made from 0·5 mm diameter nickel wire and the diameter and pitch of the helical turns were, respectively, 2·0 and 0·8 cm. The ion collector, a 0·5 mm diameter nickel rod, was located at the central axis of the tube.

In each series of experiments, the test gauge behaved in an unpredictable manner. It was observed to give one of two values of sensitivity, either a value close to that of the auxiliary gauge, or one about 60% lower, all measurements being grouped around these two figures to within the limits of experimental error. The sensitivity of the auxiliary gauge remained constant throughout. The pattern of behaviour was the same in each series of experiments. In the early measurements, the sensitivity of the test gauge was mostly low (designated "Mode A Operation" below), but later, after about 15 experiments had been performed, the higher sensitivity (designated "Mode B Operation") predominated. A typical set of results is shown in the table which gives the sensitivity of both gauges measured over a period of eight weeks. The estimated inaccuracies in measuring sensitivity

were ±10% and these resulted chiefly from the errors inherent in calculating the gas flow into the system from the auxiliary reservoir.

It was found possible on several occasions to switch from Mode A to Mode B operation (that is, from the low to the high sensitivity) by increasing the electron current in the test gauge. This was carried out for the experiments numbered 12 and 17 in the table. In each of these, the positive ion current initially increased linearly with electron current but, at some critical point, it increased sharply, so putting the operating point on the higher characteristic. This higher mode persisted for as long as the gauge remained operating, irrespective of any changes in emission. The critical electron current fell progressively from 2·5 to 1 mA for experiments 9 to 17 respectively.

Ionization-gauge sensitivities measured over a period of eight weeks

Experiment No.	Sensitivity for argon (μA . mA⁻¹μ⁻¹) Test gauge	Mode of operation (A or B)	Auxiliary gauge
1	14·4	B	—
2	13·7	B	—
3	13·7	B	—
4	4·1	A	10·6
5	3·6	A	9·8
6	3·8	A	10·5
7	3·5	A	10·1
8	3·9	A	10·4
9	14·1	B	10·4
10	3·4	A	9·5
11	13·8	B	10·0
12	3·3	A	9·5
12	12·9	B	9·5
13	13·5	B	9·6
14	13·0	B	9·7
15	12·8	B	9·7
16	12·5	B	9·2
17	3·8	A	9·3
17	14·0	B	9·9
18	13·9	B	9·7
19	13·9	B	10·2
20	13·8	B	10·1
21	14·4	B	10·7
22	13·9	B	10·5
23	14·1	B	10·4
24	14·2	B	10·5

Test gauge sensitivity mean value, mode A = 3·6
Test gauge sensitivity mean value, mode B = 13·7
Auxiliary gauge sensitivity mean value = 10

(All measurements made with an electron current of 1 mA.)

The results from the desorption experiments also showed evidence of two modes of operation of the ionization gauge. This is illustrated in Fig. 1, where the total quantity of gas desorbed from the glass walls during the heating cycle is plotted as a function of the number of ions formed in the previous discharge. Clearly, these experimental points fall on two separate curves, and it should be noted that the higher adsorption corresponds to the higher observed sensitivity. Similar results were obtained in all three series of experiments.

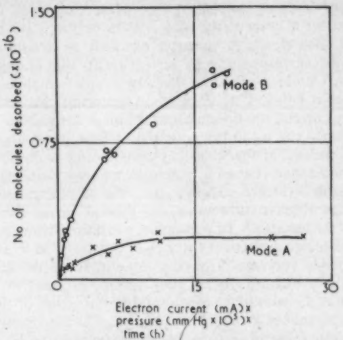

Fig. 1. Number of gas molecules desorbed from the glass wall shown as a function of the number of positive ions formed in the previous discharge for both Mode A and Mode B operation

DISCUSSION

Because the electrical potential of the glass envelope was the only important parameter not under control or measurement during this series of experiments, it is reasonable to ascribe the effects which were observed to this parameter. In the Bayard–Alpert type of ionization gauge, the discharge is exposed to the glass envelope and can therefore be influenced by the wall potential. An estimate of this potential can be made as follows:

The dynatron characteristics shown in Fig. 2 represent the flow of current to a conducting probe as a function of its potential with respect to the cathode of the discharge. Starting at zero voltage, this current first increases with voltage as electrons are drawn from the discharge. Beyond some point, however, the effective current falls with increasing voltage because of the loss of secondary electrons (emitted from the probe by primary bombardment) to the anode. At

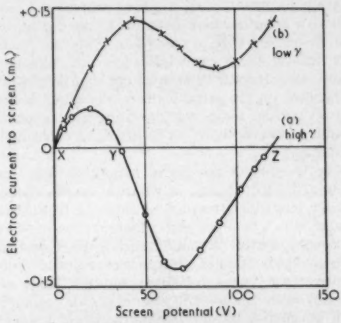

Fig. 2. Dynatron characteristics

still higher voltages, these secondary electrons are drawn back to the probe, and hence the current again rises. Curve (*a*) represents the characteristics obtained with a probe of high secondary-emission coefficient (γ), while Curve (*b*) is that obtained for a lower value of γ. If the probe is electrically isolated, then clearly its potential can only be in equilibrium at a value corresponding to zero current, that is, at *X*, *Y* or *Z* on Curve (*a*), Fig. 2. Because a small change in the potential at either *X* or *Z* causes a restoring change in the charging current, the potentials at *X* and *Z* are stable. However, a small change in the potential at *Y* results in an accentuating change in the charging current and a consequent, similarly directed change in potential, making *Y* unstable.

Available evidence suggests that the secondary-emission properties of glass surfaces are, in general terms, similar to those of the metals.[3] In particular, γ is normally in excess of unity for incident-electron energies in the range 50 to 500 eV, but depends very much on the cleanliness of the surface. Thus, like a metal probe, a glass surface exposed to a discharge has the possibility of stabilization at either of the two distinct potentials *X* or *Z*.* As the glass is thoroughly outgassed, the value of γ falls, in all probability to less than unity for the whole range of incident-electron energies.[4] Thus, while stabilization at either potential is possible in the earlier part of any work [analogous to operation on Curve (*a*), Fig. 2], the lower potential may be the only one possible for a large fraction of the surface [Curve (*b*)] in later experiments. Any transition from *X* to *Z* is likely to be quite sudden and the resulting change in electric field sufficient to alter drastically the gauge sensitivity.

In gauge operation, a part of the recorded current to the electron collector is that arising from secondary emission from the glass. If the walls are at the higher voltage, these electrons are accelerated only through a small potential difference and therefore contribute little to the ionization. Furthermore, the effective ionizing paths of the primary electrons are reduced by the positive potential at the walls because the electrons move directly to the walls instead of oscillating about the electron collector. (Nottingham[5] has reported an increase in sensitivity of a modified Bayard–Alpert gauge by maintaining a screen around the electrode structure at a large negative potential.) At the same time, the positive ions are able to reach a much larger fraction of the glass surface, which obviously allows an increase in the adsorption rate. It must be pointed out that the positive-ion current incident on the gauge walls is very much lower than the electron current under the operating experimental conditions and, consequently, plays little part in determining the glass potential.

Evidence to support the above hypothesis was obtained with a Bayard–Alpert gauge in which a metal cylinder surrounded the electrode structure, shielding it from the glass. This gauge was operated and calibrated on a small oil diffusion pump system without freezing traps or adequate baking so giving an ultimate pressure in excess of 10^{-6} mm Hg. The sensitivity was found to be increased by a factor of three without any modification of the electrode geometry or potential, but merely by introducing the shield. This nickel cylinder exhibited the dynatron characteristic, the curves in Fig. 2 being, in fact, obtained with this system. When the gauge was first switched on—after only a short pumping period and without any baking—Curve (*a*) of Fig. 2 was obtained. Gradually, a slow change over a period of about one hour took place to Curve (*b*) (presumably as the nickel surfaces were cleaned by heating induced from the filament). After reaching this stable state, the gauge was switched off for 24 hours, when it again exhibited a characteristic closely following Curve (*a*) in Fig. 2. The shield was then isolated from earth and its potential measured with an electrometer. Initially this remained steady at 110 V above the filament voltage, but after 30 minutes it switched suddenly to within 5 V of filament potential. A characteristic similar to Curve (*b*) was now observed. In subsequent experiments, it was often found that the change in potential could be induced by increasing the gauge emission by a factor of two or three. The change in sensitivity was not by more than 30% at this switch in potential. This, however, was not unexpected, for even at the high potential the gauge had a high sensitivity which at no time could be reduced to that of Mode A.

* The existence of two stable operating potentials of the glass envelope was well known in large radio transmitting valves of early design, and was introduced to explain the so-called "Schalt effect" many years ago.[6]

CONCLUSIONS

The observations on the bistable behaviour of the Bayard–Alpert gauge reported here are too readily reproducible to be explained by observational errors or some other intermittently operating effect, for not only could a cross check on the sensitivity be made with the auxiliary gauge, but both sensitivity and desorption exhibited evidence of a double mode of operation, each factor being always complementary to the other. The changes in sensitivity and adsorbed quantity have been ascribed to the fact that the glass wall potential can assume either of two equilibrium values. The reason why adsorbed quantity should depend upon wall potential is apparent in that one would expect more or less adsorption depending upon the incident-ion energy at the walls and consequent "sticking Probability". The sensitivity of the gauge can be influenced by the wall potential by several mechanisms. Firstly, the effective ionizing path of primary electrons can be reduced by a positive potential at the walls by virtue of the fact that they move directly to the walls rather than oscillate about the electron collector helix. Secondly, the ionizing efficiency of secondary electrons, which contribute to the measured electron current, is low because of their low energy, and consequently they contribute little to the ion current and a reduction in sensitivity therefore results.

The hypothesis that the bistable behaviour is a result of two possible wall potentials is supported by the observations made on a metal shielded gauge. Although in these latter experiments no change in sensitivity was evident, this is not altogether surprising because the shield potential was never higher than 110 V, under which conditions, secondary electrons could be expected to contribute a large amount to the observed sensitivity. There would thus seem to be adequate evidence for assigning the behaviour of the gauge to surface charge. In order to overcome this instability it would seem advisable either to deposit an equipotential surface of low secondary emission upon the glass walls, or to arrange a further grid within the envelope to shield the walls from the discharge.

ACKNOWLEDGEMENTS

The authors would like to thank Professor J. D. Craggs for the continuous interest he has shown in this work. An acknowledgement is also made to the Admiralty for permission to publish this paper.

REFERENCES

(1) LECK, J. H., and CARTER, G. (London: Pergamon Press.) To be published.
(2) BAYARD, R. T., and ALPERT, D. *Review of Scientific Instruments*, **21**, p. 571 (1950).
(3) STEVELS, J. M. *H. der Physik.*, **20**, p. 350 (Springer-Verlag, Berlin, 1957).
(4) SCHWARZ, H. *Z. F. Physik.*, **117**, p. 23 (1940).
(5) NOTTINGHAM, W. B. Committee on Vacuum Techniques. *Vacuum Symposium Transactions*, p. 76 (London: Pergamon Press, 1954).
(6) BRUINING, H. *Physics and Applications of Secondary Electron Emission* (London: Pergamon Press, 1954).

Pick-up of copper and duralumin on bonded tungsten carbide

By J. GOLDEN, B.Sc., Ph.D., and G. W. ROWE, M.A., Ph.D., Tube Investments Research Laboratories, Hinxton Hall, Cambridge

[*Paper received* 23 *March*, 1959]

Experiments have been made using radioactive copper and duralumin to study their pick-up on cobalt-bonded tungsten carbide. Both copper and duralumin adhere to the carbide surface, forming a thin layer or "shoe" of transferred metal, the amount of which increases during the first few millimetres of contact and then reaches a constant value. The eventual size of the copper shoe, and the distance required to pick it up, both increase with the roughness of the carbide surface. Once the shoe has been acquired, a dynamic equilibrium is established between it and the track, with copper transferring steadily to and from the shoe on the carbide. Duralumin also shows a rapid initial pick-up, but the shoe subsequently remains static and does not steadily exchange. Fragments do, however, break off occasionally as sliding proceeds. Auto-radiographs show that the transfer of tungsten carbide to copper occurs smoothly while the transfer of carbide to duralumin is erratic. It is suggested that the pick-up and wear processes are closely associated.

INTRODUCTION

Earlier experiments on wear have shown that the transfer of bonded tungsten carbide to other metals can be studied in detail by radio-tracer techniques.(1) It is found that, provided the surfaces are smooth and uniform, steady wear is obtained on copper, mild steel and stainless steel during single-traverse sliding.(2) The wear pattern is, however, different on aluminium alloys where the tungsten carbide is transferred in irregular snatches.

The other aspect of wear, transfer of the copper or other block material to the carbide slider, is also important. The present experiments use radioactive copper and duralumin to study the quantitative pick-up on to carbide specimens in different conditions. It is found that the amount of pick-up first increases with sliding distance on copper and then remains constant. If the slider is subsequently transferred to an inactive copper block, the removal of the copper pick-up can also be studied, and it is found to follow a similar pattern. This suggests that there is a dynamic equilibrium, with copper being picked up and put down throughout the sliding. This does not appear to occur with duralumin, which transfers in a much more intermittent manner. The difference between carbide transfer on copper and on duralumin is reflected in their pick-up behaviour.

APPARATUS AND TECHNIQUE

A modified form of the Bowden–Leben apparatus was used for these experiments. Fig. 1 shows the arrangement for the present work. An inactive tungsten carbide hemisphere *A* is pressed on to an active copper slip *B* which is waxed to a copper block ($1 \times 1\frac{1}{2} \times \frac{1}{4}$ in.). The carriage holding the block is then moved along a short distance to make a sliding track under the load applied by a weight *W*. When a sufficient distance has been traversed, the slider is lifted off the active copper slip and the carriage is moved further until an inactive block is beneath the slider. The active copper picked up from the first slip *B* is then deposited on an identical sliding track on the inactive block *C*, which is subsequently auto-radiographed. The tip holder is so arranged that it can be removed complete with tip for examination in the Geiger-counter jig and then replaced in exactly the same place. It is found that careful machining of the holder guides will allow the pick-up shoes to superpose within about 2–3%.

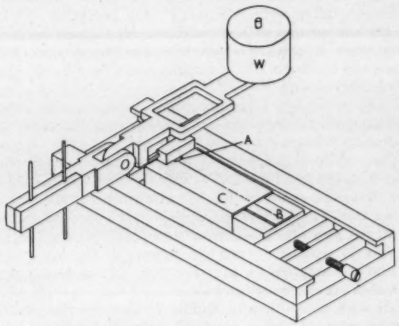

Fig. 1. Diagrammatic sketch of experimental arrangement

A small hemispherical tungsten carbide tip *A* is first slid under 2·2 kω load *W*, on a radioactive copper plate *B* and the pick-up is assessed. When the equilibrium amount of copper has been picked up, sliding is recommenced on inactive copper *C* and the loss of pick-up is followed.

Irradiation data. The slip of copper ($2 \times 1 \times 0{\cdot}06$ cm) was irradiated for two days in a flux of 10^{12} neutrons/cm^2/s. Sufficient ^{64}Cu (the half-life of which was 12·8 h) was generated to enable two days' work to be completed with

each sample. At pile exit, the activation level was approximately 650 mc/gm. Experimental work began five hours later. A similar slip of duralumin was activated under the same conditions. As well as aluminium, this contained approximately 4% copper, and 0·4% of each of the following: manganese, magnesium, silicon and iron. After an initially faster decay because of ^{56}Mn (half-life 2·58 h), the decay of the duralumin specimen was the same as that of the copper. Because of the low neutron-excitation cross-section of aluminium and the very short half-life of ^{28}Al that is produced (2·27 min), the level of activation of the duralumin was, of course, considerably less than that of the copper, but it nevertheless enabled pick-up to be detected with fair accuracy. With the most efficient counting geometry at the beginning of the work, the following counting rates were obtainable: 480 ± 7 counts per second per microgram of copper, 14·8 ± 1 counts per second per microgram of duralumin.

Assessment of radioactivities was carried out using a Geiger counter with a thin end-window (type MX108, by Mullard Ltd.), feeding a ratemeter (type 550, by Isotope Developments Ltd). This system enabled many estimations to be made within a fairly short time. A time constant of 10 seconds was used for most of the copper results, and a time constant of 100 seconds for some of the duralumin results and the background determinations.

Specimen preparation. The carbide tips were prepared either by polishing with diamond paste on Selvyt or by such polishing followed by alkaline-ferricyanide etching and water washing. This etchant consisted of equal volumes of 10% sodium-hydroxide solution and 30% potassium-ferricyanide solution, in which a tip was etched by immersion for two minutes at room temperature (cold etch) or at 60° C (hot etch).

The slips of metal were prepared before irradiation by abrasion with silicon-carbide papers under a flood of methanol, ending with 4/0 paper. On reception from the pile, the slip of copper was waxed to its support block and it was then leached with 1 : 1 hydrochloric acid, water-washed and air-dried. This technique has been found to give reproducible results.[3]

Sliding procedure. The technique adopted was first to make contact between the carbide tip and the radioactive metal under a known static load. The tip was then removed and the pick-up of radioactivity was assessed. It was replaced in the stick-slip machine and as short a track as possible was made, followed again by further assessment of the pick-up. Further tracks of increasing length were made until the pick-up reached a steady value. The carbide tip plus pick-up was then loaded against an inactive surface of the same metal, removed and assessed for radioactivity. It was then replaced and a short track made, and so on.

Tests with discontinuous sliding in this manner gave full counting data on the pick-up of metal and its subsequent behaviour. Tests were also carried out when contact between the two members was continuous over the whole length of track. When this was done, the length of track on the radioactive specimen had to be sufficient to establish the constant value of pick-up found from the discontinuous tests. The continuous track of tip plus radioactive pick-up on the inactive metal was examined by taking an auto-radiograph. The inactive metal block bearing the radioactive tracks was pressed close to an Industrial B X-ray film (by Ilford) in a light-tight box. After a suitable exposure, the film was developed, fixed, washed and prints were made. The film itself is blackened by the radioactivity, so the active regions appear white in the print. To obtain quantitative information from an auto-radiograph, it was examined by a Joyce–Loebl recording micro-densitometer.

RESULTS

Pick-up of copper on polished carbide. The following specimens of different tungsten carbide materials were used:

(*a*) medium grain size (1–2 μ) with 6% cobalt bonding;
(*b*) very coarse grain size (3–5 μ) with 6% cobalt; and
(*c*) coarse grain size (2–4 μ) with 20% cobalt.

They were carefully polished with diamond paste on a Selvyt cloth and then washed and dried. All gave the same results. A small amount of copper was picked up over a short sliding distance (1–2 mm) and the amount remained unchanged after further sliding. The accuracy of measurement is about 0·01 μg, so it is not possible to make valid deductions, except to affirm that some copper was detectable and that it was less than 0·02 μg. If the copper is uniformly distributed over the contact area, this sets an upper limit of about 0·06 μ to the thickness. An examination with a surface profilometer suggests that the average roughness of the polished surface is about 0·002 μ (0·1 μ in). However, a small local concentration of copper could easily account for the total amount.

Transfer of copper on etched carbide. The other standard treatment adopted in the earlier wear experiments is to immerse the carbide, after polishing, in hot alkaline ferricyanide for two minutes. This completely removes the polish layer and etches the surface, leaving the carbide grains clearly visible. A final washing in hot water gives a reproducible condition.

(*a*) Pick-up of a copper "shoe"

The experiments were then carried out as described above, first making short sliding tracks on active copper and then counting the tip to determine the amount of copper picked up after different successive sliding distances. The results obtained with 6% cobalt, medium grain size, tips are shown in Fig. 2(*a*) It will be seen that the amount of copper picked

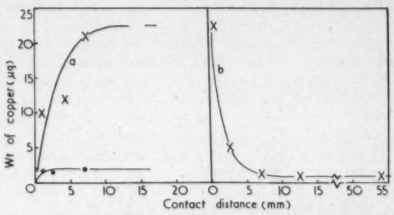

Fig. 2. Transfer of copper during dry sliding

(*a*) Pick-up from copper block to tungsten carbide slide. ○, lightly edged carbide (10 times actual size); ×, heavily etched carbide.
(*b*) Deposited of the copper "slide" from carbide slider on to a fresh copper block.

up increases fairly smoothly over the first few millimetres and then reaches a steady value, which is at least a thousand times as great as the amount found on the polished slider. The surface roughness is increased by a factor of about a hundred by etching. A typical average value for the centre line average (c.l.a.) of the etched specimens is 0·2 μ (10 μ in.).

(*b*) Redeposition of the "shoe" on fresh copper

The etched carbide tip was transferred to an inactive copper block after acquiring its active copper shoe, so that the persistence or removal of the pick-up could be studied. Exactly the same procedure was followed, the tip being counted after each short sliding track. The results given in Fig. 2(*b*) show that the pick-up is removed rapidly; after a few millimetres, only a very small amount is left. It is probable that this residual quantity represents the experimental error inherent in re-alining the slider on the second copper block. Unless the contact areas are identical, a small fraction of the original copper pick-up may not be touched by the fresh copper.

These results were obtained by studying the two processes separately, but this was simply for experimental reasons. Both will normally occur simultaneously—indeed inactive copper was, of course, being picked up while the active copper was removed in our experiments. There is thus a continuous transference, copper being taken from the block to the tip while an equivalent amount is redeposited, the total shoe at a given moment remaining very nearly constant.

It will be recognized that the counting measurements entailed removing the slider from its track. This could disturb

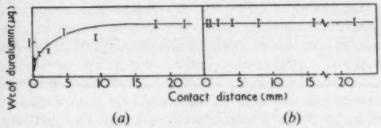

(*a*) (*b*)

Fig. 3. Transfer of duralumin during dry sliding

(*a*) Pick-up from duralumin block to tungsten carbide slider.
(*b*) Behaviour of duralumin "shoe", when carbide is slid over fresh duralumin.

the quantitative results by tearing the copper, but it is possible to examine the uninterrupted process of putting radioactive copper down from slider to block by taking an auto-radiograph of the track. Fig. 4(*a*) shows a print from such an auto-radiograph, in which it will be seen that the amount of deposited activity falls smoothly as sliding proceeds, thus bearing out the counting results of Fig. 2(*a*). For comparison a print of the auto-radiograph of a cotton thread bearing $1{\cdot}7 \times 10^{-3}$ μg/mm is shown in Fig. 4(*c*).

(*c*) Deposition of the copper "shoe" on steel

When the slider with its active copper shoe is subsequently run on steel instead of copper, the auto-radiograph is similar [Fig. 4(*b*)]. It may, however, be significant that localized put-down is found on the steel after relatively long sliding distances, suggesting that the transfer process is less steady. The detailed behaviour of steels will be examined later.

Transfer of copper on lightly-etched carbide

(*a*) Pick-up of copper shoe

It is possible that the very marked increase in the pick-up on the etched slider is associated with the increase in roughness, though the surfaces are still smooth by ordinary standards (5–10 μ in. c.l.a. for the heavily etched carbide). Further carbide sliders were polished and then very lightly etched (in cold alkaline ferricyanide) so that the carbide grains were just clearly visible. The surface roughness (0·005 μ or 0·2 μ in.) was only slightly greater than that of the polished slider, but the pick-up was about ten times as much as was found on the polished tip. As may be seen from Fig. 2(*a*), however, it was still very much less than on the heavily etched slider. (The ordinate scale has been increased by a factor ten to make the lightly etched results visible on the graph.) The track closely resembled that left by the polished tip and the pick-up increased only slightly

Table 1. *Pick-up of copper on lightly etched tungsten carbide*

A—6% cobalt, medium grain; 2·2 kg load

Sliding distance on	contact				
active copper	only	0·7	2·5	7·2	mm
Copper picked up	0·10	0·14	0·12	0·15	μg

B—20% cobalt, coarse grain; 4·4 kg load

Sliding distance on	contact				
active copper	only	1·25	3·6	6·6	mm
Copper picked up	0·07	0·31	0·31	0·33	μg

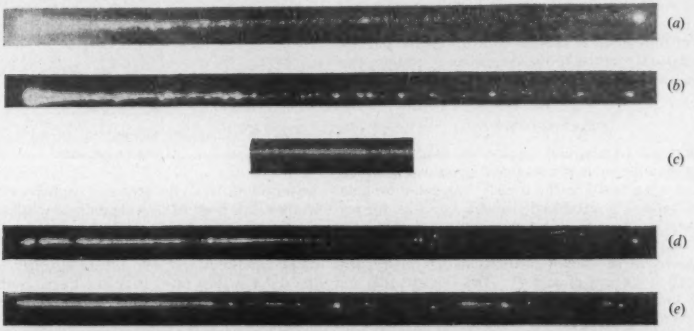

Fig. 4. Auto-radiographic prints (white regions indicate radioactive material)

(*a*) Transfer of picked-up radioactive copper from fully etched tungsten carbide to inactive copper.
(*b*) As for (*a*) but transferred to mild steel.
(*c*) Piece of cotton thread carrying $1{\cdot}7 \times 10^{-3}$ μg copper per mm length.
(*d*) Transfer of picked-up radioactive copper from semi-polished tungsten carbide to inactive copper (discontinuous track).
(*e*) As for (*d*) but transferred to mild steel (continuous track).

after the first contact (Table 1). The standard deviation for these counting results is about $\pm 0{\cdot}01\ \mu g$. It will be seen that the equilibrium amount of copper pick-up is roughly proportional to the load, and hence to the contact area.

(*b*) Deposition of copper "shoe"

After the copper pick-up experiments recorded above, the lightly-etched slider with its picked-up copper was run for successive short distances on an inactive copper block. The auto-radiograph obtained [Fig. 4(*d*)] shows that the shoe was steadily deposited. The deposition of the copper shoe on a steel block [Fig. 4(*e*)] is similar to that on copper, but some active copper fragments are found after longer distances on steel.

Transfer of duralumin

(*a*) Pick-up of duralumin "shoe"

Experiments of the same type were then performed with a tungsten carbide slider on radioactive duralumin. The results shown in Table 2 were obtained at a load of 2·8 kg with 11% cobalt, coarse-grained tungsten carbide which had been etched in hot alkaline ferricyanide, but are typical of all the sliders and conditions. It can be seen also from Fig. 3(*a*), obtained with a lightly-etched 6% cobalt fine-grain carbide specimen, that the amount of duralumin increases rapidly during the early part of the sliding, and then reaches a fairly constant, but rather erratic, value.

Table 2. *Pick-up of duralumin on carbide*

Contact distance on active dural	0·5	1·9	4·3	12·7	mm
Duralumin picked up	0·5	0·8	1·0	0·8	μg

(*b*) Deposition of the duralumin "shoe"

The carbide sliders with their equilibrium shoes of duralumin were then slid over a block of inactive duralumin. It was found that even after 30 mm of sliding, little reduction of the original shoe could be detected although the results were rather erratic [Fig. 3(*b*)]. As with the duralumin pick-up, it appeared that variation of the grain size or cobalt content of the slider made practically no difference to the result. 1 μg evenly distributed over the contact area would correspond to a layer about 5 μ (200 μ in.) thick. It appears that a film of duralumin is rapidly built up on the carbide slider, and that, in contrast to the behaviour of copper, this film then persists without change during subsequent sliding.

DISCUSSION

The experiments with etched tungsten-carbide sliding on copper show that copper is continuously being picked up on the slider and redeposited in the track. The counting data show that a balance is produced between these competing processes such that the total amount of copper carried with the slider at any moment remains constant. The weight of this shoe appears to be roughly proportional to the applied load and hence to the area of contact. This suggests that the thickness of the shoe remains constant and approximately independent of load for given sliding conditions. However, the thickness is strongly dependent upon the surface state of the tungsten carbide.

If the carbide is highly polished very little copper is picked up; indeed it may well be that the small positive result obtained can be accounted for by imperfections in the polish. When the surface is lightly etched to expose the grains, a marked increase in the quantity of copper pick-up is found. The amount ($0{\cdot}3\ \mu g$) is equivalent to a uniform layer about 1 μ thick on the surface of the carbide in contact with the copper. This is appreciably greater than the average roughness of the lightly-etched carbide, $0{\cdot}01\ \mu$ ($0{\cdot}4\ \mu$ in.). If the surface is made rougher still by hot etching, the amount of copper pick-up is further increased by a large factor, to about 25 μ, depending on the precise conditions. The surface roughness is increased to $0{\cdot}2\ \mu$, so the copper shoe is still many times thicker than would be required to fill the surface roughness. It should, however, be pointed out that the c.l.a. figure can be misleading since obviously many peaks will extend well above this level. Further detailed work on the exact relationship between the roughness of the carbide and the thickness of the copper shoe is still needed, but the present work shows clearly that the roughness of the surface is an important factor.

When the carbide with its active copper shoe is then run over inactive copper the shoe is transferred in a continuous way to the fresh copper. Nevertheless, it can be seen that a shoe is still present after long sliding on the inactive block, which means that the original shoe has been entirely replaced, not simply removed, as it might have been, for example, by a general attrition and smoothing of the carbide. This conclusion is supported by the picked-up active shoe remaining constant in amount during long sliding on active copper. There is, of course, no physical difference between the active and inactive copper which contributes to the process; the activity merely enables us to follow the transfer in detail in both directions and thus to see that, once a shoe has been picked up, a dynamic equilibrium is established between it and the copper in the sliding track, such that the shoe is almost completely replaced every few millimetres, or sometimes centimetres, of sliding.

A possible explanation of this behaviour is that the roughened carbide tip acts on a microscopic scale somewhat like a file (see Fig. 5). The hard grains, like the teeth of a file,

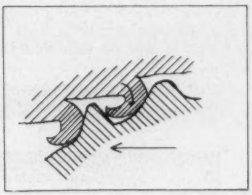

Fig. 5. Diagram suggesting possible details of the transfer process

will machine small quantities of copper away from the block as they slide past. This will continue until the spaces between the teeth are filled but, in contrast to actual filing, the copper cannot then escape. The copper machined off will be in a clean condition and will adhere strongly to the slider. If the slider is then lifted from the track, copper will be found attached to it. In general, the amount of this copper will not be equal to the copper shoe moving along with the tip, but the two will be related: when one reaches a steady value, so will the other. If sliding proceeds beyond the stage at which the spaces or pockets are filled, the total "shoe" cannot increase. The copper filling the pockets will now have come into contact with the block again and will adhere to it, so being carried forward across the mouth of the pocket, some

of it passing into the next one. Meanwhile, some of the fresh copper will be machined off and start a transit round the pocket, so that eventually the first shoe is replaced.

This suggestion is very tentative, but it does explain a number of features. In the first place, we can see that a shoe builds up [as in Fig. 2(*a*)] to a constant value, and that, subsequently, it may be transferred back to the copper and completely replaced. In the second, the total amount of carbide pocket surfaces as easily as the copper does. Occasionally a fairly large fragment will be broken away from the pick-up but there is no evidence of the smooth deposition found with copper.

A contrast between the behaviour of copper and of aluminium can also be seen in wear tests. The auto-radiograph prints (in Fig. 6) show that the tracks left on copper are uniformly covered with tungsten carbide while

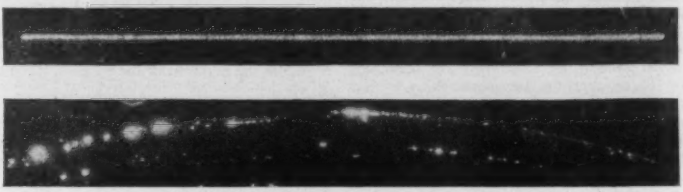

Fig. 6. Auto-radiographic prints

(*a*) Radioactive tungsten carbide wear deposit on inactive copper (times 8).
(*b*) Radioactive tungsten carbide wear deposited on inactive aluminium (curved tracks from spiral wear machine) (times 2).

copper shoe will be related to the pocket shape and size. It may well be greater than the simple picture suggests because the deformed copper filling the pockets will have been hardened, so that subsequent fracture occurs away from the geometrically predicted line, thus carrying more copper than is needed just to fill the pockets. The rate of equilibration of the filled pockets and the fresh copper will, in general, be expected to differ from the rate of initial filling of the pockets. The time to fill the pockets will also clearly depend on the roughness, as if found in Fig. 2(*a*).

The results of the experiments on duralumin show a modified pattern of behaviour. Here, the pick-up increases as before to a constant value, but when the slider is removed and slid over inactive duralumin, it is found that the shoe remains unchanged. Now it is known that aluminium and duralumin are very easily pressure-welded and that, once the oxide skin is broken, the friction is very high. Thus it may be that the duralumin pick-up is unable to slide over the those on aluminium show scattered deposits of small fragments. This suggests that the two processes—transfer of metal to and from the carbide, and wear of carbide—are closely associated.

ACKNOWLEDGEMENTS

We should like to thank the Chairman of Tube Investments Ltd. for permission to publish these results, Dr. T. P. Hughes for valuable discussions, and Mrs. B. J. Francis and Mr. T. A. Nunn for their help.

REFERENCES

(1) GOLDEN, J., and ROWE, G. W. U.N.E.S.C.O. Radio-isotope Conference, Paris, September 1957.
(2) GOLDEN, J., and ROWE, G. W. *Brit. J. Appl. Phys.*, **9**, p. 120 (1958).
(3) *Wear*, **1**, p. 491 (1957–58).

Theoretical evaluation of capillary viscometers for the measurement of the viscosity of suspensions of spheres

By A. D. MAUDE, B.Sc., Ph.D., A.Inst.P., Liverpool College of Technology

[*Paper received* 1 *April*, 1959]

The effect of the presence of stable, equi-sized spheres suspended at low concentration in a Newtonian fluid on the viscosity when measured in a capillary-tube viscometer is compared with that in an idealized viscometer. The result of the curvature of the velocity profile is found, and that of mechanical interaction with the tube wall is evaluated. Reynolds' number, tube length and the quantity flowing before a steady state is established are also considered, as is the effect of the presence of the rigid wall on the perturbation velocity fields.

These theoretical results are compared with published data, and it is concluded that some other factor, beside those considered, must be operating.

1. INTRODUCTION

Since Einstein's famous papers[1] on the viscosity of dilute suspensions of stable non-interacting spheres, the number of experimental and theoretical formulae relating the viscosity of a suspension to its concentration has increased at an alarming rate. For theoretical purposes, an idealized viscometer is usually envisaged, which consists of two infinite sheets, separated by a distance which is large in comparison with the size of the suspension particle, containing the suspension between them and moving parallel to each other at a constant velocity. Such an idealized system is best realized in practice by the use of a coaxial rotating-cylinder

viscometer, the distance between the cylinders being small compared with the cylinder radii, but large compared with the particle diameter. For experimental work, however, this is seldom the most convenient type of viscometer. Rising-sphere and capillary-tube viscometers have also been used, and in these instruments the idealized conditions postulated in theoretical discussions are far from being realized. Doubt has been cast on the extent to which the theoretical expressions for viscosity are applicable in the various more usual viscometers, and it is the purpose of this paper to investigate this problem in connexion with a capillary-tube viscometer.

In the work which follows, inertial effects are neglected, except in Section 8, so that the linearized form of the Navier–Stokes equations is taken to represent the equation of a fluid motion. No attempt is made to deal with any but suspensions of equi-sized spheres which do not tend to settle (or float) and which possess no attractive (floculating) forces between them.

The term concentration c is taken to refer to the number of sphere centres present in unit volume multiplied by the volume of a single sphere. This is the usual volume concentration for a bulk of suspension, but it is now also defined for layers the thickness of which is less than a particle diameter.

It has been found more convenient to deal with fluidities rather than viscosities throughout.

2. IDEALIZED VISCOMETER

For a single rigid sphere, radius a, placed in a liquid between the plates of the idealized viscometer described above, if the fluid is of fluidity μ_0 (which is the reciprocal of the viscosity), the equations of motion of the fluid will be:

$$\text{curl curl } v = -\mu_0 \text{ grad } p, \tag{1a}$$

$$\text{div } v = 0, \tag{1b}$$

where v and p are the fluid velocity and pressure.

If the walls of the viscometer are planes $y =$ constant, and the fluid velocity v_x before the addition of the spheres is ρy, then the addition of a single sphere with its centre at the origin produces[2] a perturbation velocity field of:

$$v_x = \rho \cdot \frac{5}{2} \cdot \frac{a^3 x^2 y}{r^5}\left(1 - \frac{a^2}{r^2}\right) - \rho \cdot \frac{1}{2} \cdot \frac{a^5 y}{r^5}, \tag{2a}$$

$$v_y = \rho \cdot \frac{5}{2} \cdot \frac{a^3 x y^2}{r^5}\left(1 - \frac{a^2}{r^2}\right) - \rho \cdot \frac{1}{2} \cdot \frac{a^5 x}{r^5}, \tag{2b}$$

$$v_z = \rho \cdot \frac{5}{2} \cdot \frac{a^3 xyz}{r^5}\left(1 - \frac{a^2}{r^2}\right), \tag{2c}$$

where $$r^2 = x^2 + y^2 + z^2.$$

The boundary conditions at the wall of the viscometer are now no longer satisfied. A second-order perturbation-velocity field which restores the boundary condition exactly can be calculated, and the effect of such a field is what will be called a *wall effect* and will be considered below. It may easily be shown that equations (2*a*), (2*b*) and (2*c*) represent no traction on the viscometer wall, and produce no change in the average values of v_y and v_z at the wall. The average value of v_x is, however, altered. An evaluation of $\iint v_x dydz$ over any plane $y =$ constant gives $-5\rho\left(\frac{4}{3}\pi a^3\right)/4$ for $y > 0$ and $+5\rho\left(\frac{4}{3}\pi a^3\right)/4$ for $y < 0$.

If a large number of spheres is present, each one will increase the integral by the same amount. If the viscometer walls are separated by a distance l, then for a large area A' the average decrease in v_x on each wall caused by n spheres will be:

$$\frac{1}{A'} \Sigma \iint v_x dxdz = n\rho\left(\frac{4}{3}\pi a^3\right) 5/(4A'),$$

or

$$\frac{1}{A'} \Sigma \iint v_x dxdz = 5\rho lc/4, \tag{3}$$

so that the rate of shear will be decreased by $5\rho c/2$.

Before the addition of the spheres, the fluidity was:

$$\mu_0 = A'\rho/F',$$

where F' is the traction force on the wall of the viscometer. After the addition of the spheres, the apparent fluidity becomes:

$$\mu = (1 - 5c/2)A'\rho/F'.$$

Therefore

$$\mu = \mu_0(1 - 2{\cdot}5c). \tag{4}$$

So far, the interaction of the spheres has been neglected. The existence of the first-order perturbation field of one sphere, given by equation (2), results in the boundary conditions on the surface of other spheres no longer being satisfied. It would be possible to calculate a second-order perturbation field to remedy this, and it might change v_x. It is apparent that such a change would produce a term in c^2 in equation (4). An iterative process would produce more exact solutions higher order perturbation fields producing terms in higher powers of c. It has been observed empirically,[3] however, that an equation similar to equation (4) is obeyed for values of c as high as 0·3, so that the terms in higher powers of c must be very small. Theoretical grounds for the belief that they are, in fact, zero will be presented elsewhere. For this reason, higher orders of perturbation fields will not be taken, and this practice will be followed throughout this paper.

Empirical evidence can be used to justify the neglect of the wall effect, for experiments on suspensions in rotating-cylinder viscometers have failed to show any change of measured viscosity with gap width, which such a wall effect would produce.[4, 5]

3. VELOCITY PROFILE IN A CAPILLARY TUBE VISCOMETER

For a tube whose axis is taken as the x-axis of a system of rectangular co-ordinates, if a sphere, radius a, is placed at the points $y = b$, $x = 0$, $z = 0$, in the parabolic velocity profile, then, before the addition of the sphere, the velocity would be:

$$v_x = \alpha(R^2 - y^2 - z^2), \tag{5a}$$

$$v_y = v_z = 0, \tag{5b}$$

where R is the tube radius and α equals $\delta P\mu_0/4l'$, according to Poisseuille's Law (δP is the pressure drop along a length l' and μ_0 equals the fluidity).

If the origin is moved to (0, b, 0), equations (5*a*) and (5*b*) become:

$$v_x/\alpha = (R^2 - b^2) - (y^2 + z^2) - 2by,$$

$$v_y = v_z = 0.$$

It is seen that the velocity distribution before the addition of the sphere can be split into three components: a constant velocity $(R^2 - b^2)$, which requires no perturbation velocity

if the sphere centre moves with this velocity; a parabolic-velocity profile, with the sphere on the axis of the parabola; and a uniform shear. Because of the linear nature of the flow equations, the perturbation velocity caused by each component can be evaluated separately, and the results of them on the measured fluidity can be summed.

4. PERTURBATION CAUSED BY SHEAR COMPONENT

A sphere placed in a sheared fluid will cause a perturbation velocity given by equations (2), and in this case, ρ equals $-2b\alpha$. Integration of $\int v_x dA$ over the area of a cylindrical surface concentric with the capillary tube axis, radius r, gives:

$$\int v_x dA = 0, \text{ for } r > b, \tag{6a}$$

$$\int v_x dA = 5\left(\tfrac{4}{3}\pi a^3\right)\rho r/(2b), \text{ for } r < b. \tag{6b}$$

This shows that the velocity of the tube wall is unaffected, and that there is no change of rate of flow through the tube outside a radius b, caused by spheres, centres of which lie at a distance b from the tube axis.

Integration over the volume of the cylinder radius b gives:

$$\int v_x dV = 5\left(\tfrac{4}{3}\pi a^3\right)\rho b/4. \tag{7}$$

Each sphere contributes this amount to the total integral, and the change of the volume rate of flow Q can be found directly. The reduction of Q because of a concentration c of sphere centres in the annulus b to $(b - db)$ can thus be shown to be $5\pi\alpha c b^3 db$. If terms in $(db)^2$ are neglected, it can also be shown that the effect of decreasing the fluidity of the annulus b to $(b - db)$ in a capillary tube from μ_0 to $\mu_0(1 - \beta)$ is to reduce the volume rate of flow by $2\pi\alpha\beta b^3 db$. That is, the effect on the volume rate of flow of the spheres in this annulus is the same as the effect of reducing the fluidity from μ_0 to $\mu_0(1 - 2{\cdot}5c)$. Thus, as would be expected, the shear component of the velocity produces a result in accordance with equation (4).

5. PERTURBATION CAUSED BY THE PARABOLIC COMPONENTS

A sphere held stationary in a parabolic velocity distribution $v_x = -\alpha(y^2 + z^2)$ will cause a perturbation velocity given[6] by:

$$-v_x/\alpha = \left(-\frac{a^3}{r} + 2\frac{a^5}{r^3} - \frac{a^7}{r^5}\right) + \frac{1}{2}\left(\frac{a^3}{r} - 13\frac{a^5}{r^3} + 10\frac{a^7}{r^5}\right)\frac{(y^2+z^2)}{r^2} + \frac{35}{8}\left(\frac{a^5}{r^3} - \frac{a^7}{r^5}\right)\frac{(y^2+z^2)^2}{r^4} \tag{8a}$$

$$-v_y/\alpha = \frac{1}{2}\left(-\frac{a^3}{r} + 6\frac{a^5}{r^3} - 5\frac{a^7}{r^5}\right)\frac{xy}{r^2} - \frac{35}{8}\left(\frac{a^5}{r^3} - \frac{a^7}{r^5}\right)\frac{xy(y^2+z^2)}{r^4} \tag{8b}$$

$$-v_z/\alpha = \frac{1}{2}\left(-\frac{a^3}{r} + 6\frac{a^5}{r^3} - 5\frac{a^7}{r^5}\right)\frac{xz}{r^2} - \frac{35}{8}\left(\frac{a^5}{r^3} - \frac{a^7}{r^5}\right)\frac{xz(y^2+z^2)}{r^4}. \tag{8c}$$

According to Faxen's theorum,[7] the force on a sphere in an infinite fluid is:

$$6\pi a v_0/\mu_0 + \pi a^3 (\text{grad } p)_0 \tag{9}$$

where v_0 and $(\text{grad } p)_0$ are the velocity and pressure gradient at the position of the sphere centre before the perturbation velocity is added. In the present case, the force on the sphere must be zero, so that the sphere must move with a velocity of $-\frac{1}{4}a^2\alpha$ relative to the fluid at a distance b from the tube axis. This further movement will set up a perturbation velocity given by Stokes' equation for the steady movement of a sphere in an infinite fluid. The addition of this to equations (8*a*), (8*b*) and (8*c*) gives the complete perturbation velocity resulting from the parabolic component of the velocity, that is:

$$-v_x/\alpha = \left(\frac{5}{3}\frac{a^5}{r^3} - \frac{a^7}{r^5}\right) - \left(6\frac{a^5}{r^3} - 5\frac{a^7}{r^5}\right)\frac{(y^2+z^2)}{r^2} + \frac{35}{8}\left(\frac{a^5}{r^3} - \frac{a^7}{r^5}\right)\frac{(y^2+z^2)^2}{r^4}, \tag{10a}$$

$$-v_y/\alpha = -\frac{1}{2}\left(\frac{a^3}{r} - \frac{a^5}{r^3}\right)\frac{xy}{r^2} + \frac{xy(y^2+z^2)^{1/2}}{r^3}\left\{\frac{1}{2}\left(\frac{a^3}{r} - 6\frac{a^5}{r^3} + 5\frac{a^7}{r^5}\right) + \frac{35}{8}\left(\frac{a^5}{r^3} - \frac{a^7}{r^5}\right)\frac{(y^2+z^2)}{r^2}\right\} \tag{10b}$$

$$-v_z/\alpha = -\frac{1}{2}\left(\frac{a^3}{r} - \frac{a^5}{r^3}\right)\frac{xz}{r^2} + \frac{xz(y^2+z^2)^{1/2}}{r^3}\left\{\frac{1}{2}\left(\frac{a^3}{r} - 6\frac{a^5}{r^3} + 5\frac{a^7}{r^5}\right) + \frac{35}{8}\left(\frac{a^5}{r^3} - \frac{a^7}{r^5}\right)\frac{(y^2+z^2)}{r^2}\right\} \tag{10c}$$

An integration of equation (10*a*) over the area of the tube wall shows that this perturbation does not affect the velocity of the tube itself. The pressure drop from $x = -\infty$ to $x = +\infty$ is unaltered, and the volume integral of equation (10*a*) over all space except the sphere volume also gives a zero result. It follows that the perturbation velocity caused by the addition of a sphere to the parabolic portion of the velocity does not affect the average velocity at which the fluid moves. However, because of the discontinuity at the origin in equations (10*a*), (10*b*) and (10*c*), the sphere moves at a velocity which is different from the average velocity of the fluid which previously occupied its position. Thus, equation (10*a*) implies that, whilst the pressure drop and rate of flow of fluid is unaltered, the rate of flow of suspension is reduced because of the lower velocity of the spheres themselves.

Using this to evaluate the change of the rate of flow, we find Q is reduced by $4\pi R^2\alpha a^2\bar{c}/15$, where $\bar{c}$ is the average concentration within the tube. The measured fluidity is thus reduced by $8\mu_0(a/R)^2\bar{c}/15$.

If this result is combined with that of the previous section, and if it is assumed that $\bar{c} = c$, then:

$$\mu = \mu_0\{1 - 2{\cdot}5c(1 + 16a^2/75R^2)\}. \tag{11}$$

It seems that the effect is such that an error of $\frac{1}{3}\%$ will be made in the determination of Einstein's constant of 2·5 when the ratio of tube to particle radius is eight to one.

Simha[8] performed a calculation similar to that given

above, but he concluded that the parabolic component of the original flow did not affect the measured viscosity of a suspension of spheres at low concentration in capillary flow. This is in direct contradiction to the results obtained above, and it is felt that an error was made in Simha's work. Simha calculated the increase in the rate of dissipation of energy resulting from the addition of a single sphere, and assumed that this was proportional to the increase of viscosity. This method is only valid, however, if the rate of flow has remained unchanged. An examination of the expression for v_x (using the present notation) in the perturbation velocity given by Simha shows that it implies that the volume rate of flow is a function of the reciprocal of the length of tube considered. While this does, in fact, give no change of rate of flow for an infinitely long tube, such a tube gives zero concentration. If the concentration is maintained constant by increasing the number of spheres present in proportion to the tube length, the change of rate of flow caused by the introduction of the spheres remains finite, so that the method used for calculating the increase of viscosity is inadmissible.

It is possible to show, without exact analysis, that Simha's conclusion must be wrong because it implies that spheres placed on the tube axis, where the rate of shear is zero, would not affect the rate of dissipation of energy for a constant rate of flow. This is incompatible with the well-known result[12] that the flow distributes itself so that the rate of dissipation of energy is a minimum, implying that the rate of dissipation of energy of the original plus the perturbation flow must be greater than for the original flow alone.

6. CHANGE OF CONCENTRATION

It is well recognized[9, 10, 11] that, if the particle of a suspension travels through a tube at a rate which is on the average greater than that of the fluid, the concentration will fall below that in the feeding vessel and, conversely, if the solid velocity is less, the concentration will be increased.

If U is the velocity of both spheres and fluid in a region where they move at the same rate, v_b and v_s are the velocities of the fluid and spheres respectively, and c_1 and c_2 are the concentrations in the region where the velocities are the same and where they are different respectively, then, if the volume rates of flow of spheres in the two regions are equated:

$$Uc_1 = v_s c_2.$$

If the volume rates of flow of fluid are equated, then:

$$U(1 - c_1) = v_b(1 - c_2).$$

Therefore

$$v_s/v_b = \frac{c_1}{(1 - c_1)} \cdot \frac{(1 - c_2)}{c_2}. \qquad (12)$$

The relative velocity between fluid and spheres caused by the pressure gradient, cannot alter the concentration in the body of the suspension however. The velocity of the spheres may be looked upon as the result of a velocity field consisting of two parts, one proportional to the original fluid velocity at the sphere centre, and the other proportional to the pressure gradient there—see equation (9). In the slow viscous flow of an incompressible fluid, both the velocity and the pressure gradient have zero divergence, so that the resultant velocity field for the spheres must be non-divergent. Thus, in the bulk of the suspension, if the concentration is uniform at any one time, it will remain uniform. This does not, in general, hold near to a wall or surface where the concentration contains a discontinuity, but it will hold for the walls of the tube because there will be no component of velocity or pressure gradient perpendicular to them.

It is necessary to consider the fate of spheres, centres of which lie on stream lines which pass from the feeding vessel into the tube, and pass down the tube, very close to the wall. Because a sphere centre cannot approach closer to the wall than a distance a, the spheres must be pushed inwards and roll down the tube in contact with the wall. If the velocities of the spheres and fluid in the annulus $(R - a)$ to R are that found in Sections 4 and 5, then with no displacement:

$$v_s = \alpha a(R - 7a/6),$$
$$v_b = \alpha a(R - a/2).$$

Because of the displacement, however:

$$v_s = \alpha a(2R - 5a/3),$$
$$v_b = \alpha a(R - a/2).$$

An elementary calculation similar to that by which equation (12) was obtained gives the number of spheres per unit length in contact with the wall as:

$$\frac{3c(R - 7a/6)(2R - a)}{4a^2\{(2R - 5a/3) - c(R - a/2)\}},$$

so that the consequent reduction in Q attributable to the shear component is:

$$\frac{5\pi c\alpha a(R - 7a/6)(2R - a)(R - a)^2}{2\{(2R - 5a/3) - c(R - a/2)\}},$$

instead of:

$$5\pi c\alpha a(2R - a)(2R^2 - 2Ra + a^2)/4,$$

which would have been obtained if the effect of the displacement had been neglected. The difference between these gives the change in equation (11) which results.

The effect on the result of Section 5 is to make $\bar{c}$ no longer equal to c. It can be shown in a manner similar to that used to obtain equation (12) that:

$$\bar{c} = c\left\{\left(1 - \frac{a}{R}\right)^2 + \frac{\left(1 - \frac{7a}{6R}\right)\left(2 - \frac{a}{R}\right)\frac{a}{R}}{\left(2 - \frac{5a}{3R}\right) - c\left(1 - \frac{a}{2R}\right)}\right\} \qquad (13)$$

For low concentration, where powers of c higher than the first may be neglected, all the results obtained so far may be expressed as:

$$\mu_r = \frac{\mu}{\mu_0} = 1 - 2{\cdot}5cF\left(\frac{a}{R}\right) \qquad (14a)$$

or

$$\mu_r = 1 - 2{\cdot}5c\left\{1 - 2\frac{a}{R} + \frac{166}{75}\left(\frac{a}{R}\right)^2 - \ldots\right\} \qquad (14b)$$

This section gives a fuller examination of the result obtained approximately in an earlier paper.[10]

7. ESTABLISHING A STEADY STATE

When a suspension enters an empty capillary tube, the mechanical displacement of the spheres near to the wall causes them to travel faster than the corresponding liquid. This relative movement implies that spheres will arrive at the front end of the column of suspension and will accumulate there. The decrease of concentration at the leading edge resulting from the relative movement caused by the pressure gradient is generally small in comparison with this, and it is

easy to observe the formation of the plug of high concentration as a suspension is sucked up into a tube if the particles are an appreciable fraction of the tube diameter.

During the time when the suspension is first filling the tube, the liquid which arrives near to the wall comes from this initial region of high concentration, and is consequently of a higher concentration than when it comes directly from the inlet vessel. It is only when all the spheres in contact with the wall have arrived at their positions by rolling down the wall from the tube entrance that a steady state is established. This state will be reached when the first sphere to begin to roll down the wall has reached the tube exit. It will travel at a velocity $\alpha a(2R - 5a/3)$ so that a length l'' will have reached the equilibrium condition when a volume $3\pi\mu_r R^4 l''/a(12R - 10a)$, which equals approximately $(\mu_r R/4a)$ times the volume of the tube, has entered the tube. It is necessary that this volume of liquid is allowed to pass into the tube before measurements of the rate of flow are made if the initial disturbance is to have no effect on the result.

8. INERTIAL EFFECT

Some workers believe that suspension spheres will tend to migrate towards the axis of a capillary-tube viscometer.[13, 14] It may easily be shown that this cannot primarily be caused by viscous forces, as the linearized Navier–Stokes equations are reversible with respect to time. That is, reversing the direction of flow along the tube will result in a reversal of all motions, and as a sphere cannot tend to migrate both inwards and outwards, there can be no tendency for radial motion to occur. Inertial forces might, however, cause such an inward radial motion. If this were the case, the measured viscosity would depend upon Reynolds' number, because such a movement would reduce the concentration near to the wall only when the terms containing density in the Navier–Stokes equations were no longer negligible.

9. WALL EFFECT

Vand[2] has made an attempt to evaluate theoretically the wall effect in an idealized viscometer. He used the method of images to find a perturbation-velocity field which was equal and opposite to the tangential velocity of the first-order perturbation velocity of a sphere in a sheared fluid. He obtained a result which was independent of the distance of the sphere from the wall and which was equivalent to the existence of a layer of pure fluid (rather than suspension) of a thickness $1{\cdot}3a$ adjacent to the wall.

This method of calculating the wall effect is suspect because it neglects the velocity components normal to the wall. If a negative image were used (that is, one in which the image sphere is sheared in the opposite direction to the real sphere) the normal component of the velocity at the wall will be reduced to zero, but the use of such an image would have exactly the opposite effect to that described by Vand. The two images together would produce no wall effect, and no correction for the presence of the wall. This suggests that the effect of the normal component is of equal importance to that of the tangential component at the wall, and Vand's conclusion is incorrect. This conclusion is supported by the experimental result in rotating-cylinder viscometers[4, 5] in which no change of measured viscosity with gap width has been observed.

It is, in fact, possible to show that the wall effect at very low concentration cannot decrease the measured viscosity in an idealized viscometer. If the separation of the plates is increased from l to $(l + \delta l)$, the velocity of the plates being adjusted so that the average rate of shear $\bar{\rho}$ remains constant, the rate of dissipation of energy cannot be greater than that in the original velocity field and the layer of thickness δl sheared at a rate $\bar{\rho}$ (from the theory of the minimum rate of dissipation of energy[12]). If the viscosity is now expanded as a power series in concentration, and if powers of order higher than the first are neglected, then:

$$\frac{1}{\mu} = \frac{1}{\mu_0}\Big\{1 + c\phi(l)\Big\},$$

where the possibility of a wall effect has been taken into account by the inclusion of $\phi(l)$, which is some unknown function of l. The rate of dissipation of energy in the original velocity field, the layer of thickness δl and the final arrangement are $A'l\bar{\rho}\{1 + c\phi(l)\}/\mu_0$, $A'\delta l\bar{\rho}/\mu_0$ and

$$A'(l + \delta l)\bar{\rho}\{1 + (c + \delta c)\phi(l + \delta l)\}/\mu_0$$

respectively. If there is a volume V' of particles present, $c = V'/(A'l)$, and $c + \delta c = V'/A'(l + \delta l)$, so that the statement concerning the rates of dissipation of energy becomes:

$$\frac{A'l\bar{\rho}\{1 + c\phi(l)\}}{\mu_0} + \frac{A'\delta l\bar{\rho}}{\mu_0} > > \frac{A'(l + \delta l)\bar{\rho}\{1 + (c + \delta c)\phi(l + \delta l)\}}{\mu_0}.$$

Therefore

$$\phi(l) > \phi(l + \delta l).$$

Thus, to the first power of c, the viscosity can only increase as the distance between the plates of the viscometer is reduced.

In general it can be said that, if the extra rate of energy dissipation, resulting from the perturbation-velocity field of the sphere, is a constant value independent of the presence of other spheres or of the nearness of a viscometer wall, a fluidity-concentration relationship of the form $\mu^{-1} = \mu_0^{-1}(1 + Kc)$ is found. An increase in the rate of energy dissipation per sphere increases K. By reasoning similar to that given above, the excess rate of dissipation of energy resulting from the presence of a sphere at a certain distance from the tube axis, can only be increased by taking into account the perturbation velocity caused by the tube wall. For these reasons, the idea that some hydrodynamical interaction between sphere perturbation velocity and the tube wall (at very low concentrations) may lead to a reduced viscosity must be rejected. An increased viscosity could, of course, be produced.

Dix and Scott-Blair[15] have also produced an explanation for the change of measured viscosity with tube radius, in which the integral in the usual derivation of Poiseuille's law is replaced by a summation. It has been found impossible to relate their approach, which is adapted to high concentrations or continuous media, to the present analysis which deals with low concentrations of spheres. If their theory is correct, it must reduce to that given above for the simple case, and it need not be considered separately.

10. COMPARISON WITH EXPERIMENT

The theory presented above may be compared with the results of the careful experimental work of Higginbotham, Oliver and Ward.[16] If their results are expressed in the form given in equation (14a), $F(a/R)$ appears to be independent of concentration within the limits of experimental variation, except for the largest value of a/R. Results at 5% concentration and less do not give sufficiently accurate values of $F(a/R)$ for comparison of experiment and theory, so that values of this function have been calculated from the

experimental results for concentrations from 7·5–20%. These results are shown in the Fig. 1, together with the curve from equation (14*b*). It will be seen that the experimental results fit the equation:

$$F(a/R) = 1 - 4a/R + 10(a/R)^2, \qquad (15)$$

which differs appreciably from the theoretical curve.

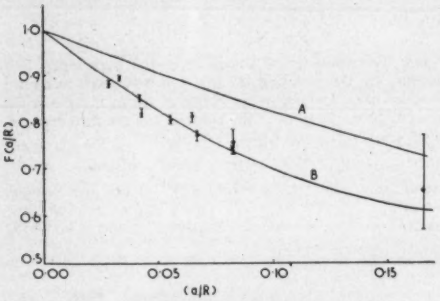

Graph of $F(a/R)$ as defined in equation (14*a*)

Curve *A*—curve of equation (14*b*), constituting the result of theory presented here. Curve *B*—curve of equation (15), constituting a parabola with coefficients expressed to one significant figure only, and chosen to fit the experimental results. The vertical lines represent the spread of the experimental results, the central point being an average value.

The experimental results were found to be independent of Reynolds' number, so that inertial effects described in Section 8 cannot have occurred. A wall effect, if present, would increase the viscosity and move the theoretical curve further from the experimental points. If insufficient time had been allowed for a steady state to be established, this too would make the agreement between theory and experiment worse.

It must be concluded that some other effect, not considered here, has occurred. It seems possible that this effect resulted in an inward displacement of spheres at the tube entrance, and a consequent reduction of concentration within the tube. Experimental results on the effect of changing the shape of the tube entrance would be of interest.

11. CONCLUSION

After careful consideration of the possible differences between the flow of a suspension of spheres within an idealized viscometer and that in a capillary-tube viscometer, it has been found that the experimental results of Higginbotham, Oliver and Ward can only partially be explained. Some further mechanism seems necessary before full agreement between experiment and theory can be obtained.

REFERENCES

(1) EINSTEIN, A. *Ann. Phys.* (*Leipzig*), **19**, p. 289 (1906); **35**, p. 591 (1911).
(2) VAND, V. *J. Phys. Coll. Chem.*, **52**, pp. 277, 300 (1948).
(3) OLIVER, D. R., and WARD, S. G. *Nature* (*London*), **171**, p. 396 (1953).
(4) EVESON, G. F., WHITMORE, R. L., and WARD, S. G. *Nature* (*London*), **166**, p. 1074 (1950).
(5) SWEENY, K. H., and GECKLER, R. D. *J. Appl. Phys.*, **25**, p. 1135 (1954).
(6) HASIMOTO, H. *J. Phys. Soc.* (*Japan*), **2**, p. 793 (1956).
(7) PÈRÈS, J. *Compt. rend.*, **188**, p. 310 (1929).
(8) SIMHA, R. *Kolloid Z.*, **76**, p. 16 (1936).
(9) WORSTER, R. C. *Proceedings of a colloquium on the hydraulic transport of coal*, held by the National Coal Board, London, November 1952.
(10) MAUDE, A. D., and WHITMORE, R. L. *Brit. J. Appl. Phys.*, **7**, p. 98 (1956).
(11) FAHRAEUS, R., and LINDQUIST, T. *Am. J. Physiol.*, **96**, p. 562 (1931).
(12) LAMB, H. *Hydrodynamics*, 6th Ed., par. 344 (New York: Dover Publications, 1945).
(13) JEFFERY, G. B. *Proc. Roy. Soc. A*, **102**, p. 161 (1923).
(14) STARKEY, T. V. *Brit. J. Appl. Phys.*, **7**, p. 52 (1956).
(15) DIX, F. J., and SCOTT-BLAIR, G. W. *J. Appl. Phys.*, **11**, p. 574 (1940).
(16) HIGGINBOTHAM, G. H., OLIVER, D. R., and WARD, S. G. *Brit. J. Appl. Phys.*, **9**, p. 372 (1958).

Measurement of the quantum efficiency of a proportional counter using X-rays

By A. E. KISS, B.Sc., A.Inst.P., and N. PATLA, M.Sc., Sir John Cass College, London

[*Paper received* 19 *March*, 1959]

The variation of quantum efficiency with X-ray wavelength and beam direction is investigated in the range 0·2–2·3 Å. Measurement, in the same range, of the absorption coefficient for the counter-window material (Pyrex) is described. The counter used shows a maximum efficiency of about 70% at 1·4 Å., decreasing on either side of this wavelength. Proper choice of beam direction within the counter is required if a useful efficiency is to be obtained at the shorter wavelengths. The effects of counter geometry and construction, scattering processes and fluorescence on the quantum efficiency are briefly discussed.

Historically, ionization chambers were the first quantitative detecting devices used for X-rays.[1] They have been largely superseded by Geiger–Muller counters[2–7] and, more recently, proportional counters,[8–11] especially where speed of operation is important.

The design and construction of both forms of counter and associated apparatus have advanced sufficiently to provide reasonable stability over short experimental periods and adequate signal-to-noise ratio in response to single X-ray photons. Because of the inherently small gas amplification in the proportional-counter discharge, however, the voltage pulses developed are small relative to those in a Geiger counter, and a high-gain stable amplifier is required to prepare these pulses for scaling. This additional complexity of the proportional-counter equipment is amply justified by the shorter resolving time and the possibility, first discussed by Lang,[9] of wavelength discrimination.[12, 13]

Providing the entire energy (E) of an X-ray photon is converted into the kinetic energy of a photo-electron ejected from a gas atom, the total charge generated in the subsequent

discharge will be proportional to E, and thus the voltage pulse developed will be inversely proportional to wavelength. These statements depend, in turn, on the experimental fact[14] that the average energy expended by the photo-electron in successive ionizing collisions with the gas atoms is constant, and that the binding energy is small compared with E.

The noise generated by the high-gain counting system imposes an upper limit to the wavelength of X-rays with which the proportional counter may be used. In the present experiments, the amplitude of the counter pulses from X-rays of wavelength greater than about 4 Å was less than the noise level.

As the field of application of the proportional counter is greatly extended by the property of wavelength discrimination, the efficiency of the device in the wavelength range for which it may be used becomes important and forms the subject of this paper.

Proportional counters for use with X-rays. Although no proportional counter suitable for use with X-rays is at present available on a commercial scale, the constructional details and application of both sealed[15–17] and continuous flow[18] counters as well as design criteria for improved wavelength resolution[19] have been discussed. The proportional counter (type PX28B) used in the present experiments and developed by 20th Century Electronics Ltd. was constructed as follows (Fig. 1):

Overall length, 20 cm;
External diameter, 2·3 cm;
Length between diagonally opposed bubble-glass windows, 9·0 cm;
Windows of Pyrex, 7–10 mg/cm^2; diameter, 1 cm;
Filling, 97·5% argon, 2·5% carbon dioxide as stabiliser, to a total pressure of 1 atmosphere;
Anode, 0·1 mm tungsten wire;
Cathode, Aquadag coating on the glass wall;
Working voltage, V_w, 1400 V.

The gas mixture was chosen because of its linearity in energy response and high stability.[20]

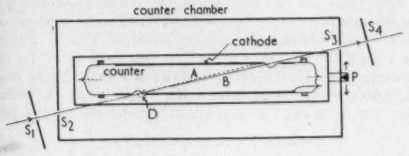

Fig. 1. Proportional counter, chamber and apertures

Quantum efficiency η. At any particular X-ray wavelength, η may be defined as the ratio of the number of counts recorded to the number of quanta incident upon the counter, and is expected to be greatest if the photons remaining after passage of the beam through the gas, strike the cathode surface and eject photo-electrons, or are scattered back into the sensitive volume of the counter. The quantum efficiency of the present counter has been determined for two specified X-ray beam directions: (i) entrance window in Fig. 1 to exit window (B), and (ii) entrance window to cathode surface adjacent to exit window (A), and is generally larger in (ii) as a result of the secondary processes at the cathode. End effects and dead volume are reduced to a small value by arranging the windows near the ends of the cathode coating, thus confining the beam to the central uniform region of the counter. The monochromatic and collimated beam passes through the entrance window at a small angle to the counter axis, thereby traversing a long absorption path. If the X-rays enter the counter through the cathode coating near the entrance window, a slightly greater, but rather unstable, counting rate is obtained.

THE MEASUREMENT OF QUANTUM EFFICIENCY

Theory. The X-ray beam is assumed to be so collimated that its cross-section within the proportional counter is always less than the projected cross-section of the windows. If a one-to-one correspondence between the number of counts recorded and the number of photons absorbed is assumed, the fraction f of photons absorbed from the primary beam will be:

$$f = n_1/n = 1 - e^{-\mu l} \qquad (1)$$

where n_1 is the number of counts per second recorded when the beam passes only through the gas (that is, from window to window); n is the number of photons per second incident on the gas after passage of the beam through the window; μ is the linear absorption coefficient of the gas at the wavelength used,[14] and l = the path length of beam in gas. The value of n may thus be found from the experimental value of n_1. The number of photons N arriving per second at the counter window is then deduced, by application of a correction for the absorption of the window.

When the beam is directed to fall on the cathode coating near the exit window, a new counting rate n_2, generally greater than n_1, is obtained. The quantum efficiency of the counter for this setting is n_2/N.

Experimental arrangement. The K_α radiation from the targets used was obtained by Bragg reflexion from a large plane calcite crystal. The very sharp reflexion gives adequate collimation in the horizontal plane and the apertures S_1 and S_2 each of diameter 1 mm were used to limit the cross-section of the beam within the counter (Fig. 1).

The proportional counter was mounted on a pivoted block within a metal chamber in the end walls of which the apertures S_2 and S_3 were drilled. To avoid mechanical disturbance, the counter supports were lined with soft polythene and the tube held down with rubber bands. To align the counter windows with S_2S_3, a line was scribed in the chamber vertically below and parallel to S_2S_3, above which the counter windows could be set at the proper height.

The counter cradle was pivoted (D) immediately below the entrance window so that the beam entered this window regardless of the angular setting of the counter, the settings A and B being indicated by a calibrated pointer (P) moving over a fixed external scale.

Alignment. An auxiliary aperture S_4 and Geiger counter were used to find the direction of the K_α Bragg reflexion. The empty counter chamber was then placed in position on an adjustable turntable and the apertures S_2 and S_3 aligned with S_1 and S_4 by means of a small light source. Because of a thin Aquadag coating over the counter windows, optical alinement of the counter with S_2 and S_3 was not possible, and the procedure referred to above was used, when the counter was inserted.

MEASUREMENTS

The K_α radiations available were those from cobalt, chromium, copper, molybdenum and tungsten, covering a range of wavelengths from 0·2 to 2·28 Å. At each wavelength, the counting rates were determined for (i) window to window path (n_1), and (ii) window to cathode (n_2) and are shown in Table 2.

Pulse-counting system.[13] The pulses from the proportional counter were amplified by a two-stage head amplifier mounted near the counter and then passed *via* a cathode follower and screened cable to further stages of amplification situated near the scaling unit. The maximum overall gain available was about 10^6. The amplified pulses were fed into a diode pulse-height discriminator so constructed that all pulses below any predetermined level could be suppressed. This essential stage permits noise pulses to be removed prior to counting. The noise level at the discriminator, at the amplification used, was about 4 V. To record only those pulses caused by X-rays, the discriminator bias was adjusted to reject pulses below 4·5 V. This level corresponded to counter pulses from photons of energy 3100 eV (4 Å). It was not possible, therefore, to distinguish pulses from X-rays of wavelength greater than 4 Å. Special attention must be directed to the design of the input stage of the amplifier and to filtering the e.h.t. supply to the counter if longer wavelengths are to be recorded. Finally, the selected pulses were passed into a Dynatron scaling unit and counting rates obtained by timing the counts indicated on a mechanical register.

Statistical accuracy. The counting rates shown in Table 2 are normalized to an interval of one second for simplicity, but each is the mean of ten separate samples of 1000 counts. The standard deviation of the mean is mainly an indication of the fluctuations of the beam intensity of the X-ray tube. These have been investigated using a monitor system[13] and, provided a warming-up period is allowed for the whole apparatus, amount to about ±1% over the periods of these experiments.

Correction for window absorption. The linear absorption coefficient μ of Pyrex glass was measured at each of the wavelengths employed in the main experiments, using a thin slip of the same thickness as the counter window. Fragments of a large bubble were examined in sodium light and a specimen of reasonably uniform thickness of mean areal density 9 mg/cm^2 was selected. The actual thickness was then measured at many points by means of a dial gauge calibrated in 0·0001 in. (Fig. 2). A region of about 1 mm^2 was then selected over which the thickness d was 0·0043 ± 0·000 12 cm. This specimen, mounted over a hole in a hardboard slide, was then inserted in the pivoted holder shown in Fig. 3, attached to the front of an end-window Geiger-

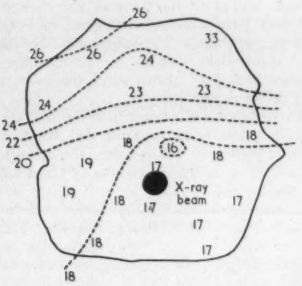

Fig. 2. Thickness contours of Pyrex glass specimen (10^{-4} in. units)

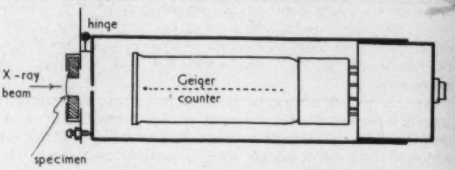

Fig. 3. Absorption measurement Geiger counter chamber and pivoted specimen holder

counter chamber. The area selected for the experiment was carefully registered with the circular entrance window of the chamber. The smoothly pivoted holder ensured that the specimen could be placed in exactly the same position for each absorption measurement and removed rapidly without disturbing the system.

Observations were then made at each wavelength of the counting rates p_1 and p_2 with and without the specimen respectively, and the linear absorption coefficient calculated from the relationship:

$$\mu = \{ln(p_2/p_1)\}/d.$$

The readings and results are shown in Table 1.

Table 1. *The linear absorption coefficient of Pyrex glass*

Wavelength	0·208	0·708	1·54	1·78	2·28	Å
p_1	62·0	38·6	21·2	40·5	30·9	s^{-1}
p_2	62·0	40·2	28·3	62·1	74·5	s^{-1}
μ	0	9·10	67·0	99·9	204·0	cm^{-1}

As a check on this experiment, the constants A and n of the relation $\mu = A\lambda^n$, where λ is the wavelength in Angstrom units, were determined from a graph of $\log_{10}\mu$ against $\log_{10}\lambda$ plotted in Fig. 4. For the specimen used, the law becomes $\mu = 21{\cdot}9\,\lambda^{2{\cdot}62}$ cm^{-1}, to within about 3%, the main limitation being uncertainty in the value of d. A thicker specimen is needed for accuracy at the shorter wavelengths.

THE QUANTUM EFFICIENCY

The quantum efficiency of the proportional counter at each wavelength used is given in Table 2 and shown graphically in Fig. 5. As the areal density (9·5 mg/cm^2) of the Pyrex specimen used in the absorption measurements was within the range quoted by the makers for the windows of the

Table 2. *Observations and quantum efficiency*

Wavelength	0·208	0·708	1·54	1·78	2·28	Å
μ Argon	0·000 82	0·021	0·189	0·290	0·568	cm^{-1}
$f(=1-e^{-\mu l})$	0·007 4	0·175	0·817	0·926	0·994	—
n_1	6·0 ± 0·6	41·9 ± 0·5	82 ± 0·3	55·0 ± 0·2	32·0 ± 0·4	s^{-1}
$n\,(=n_1/f)$	811	239	100	60·0	32·2	s^{-1}
Absorption in window	—	3·95	25·0	34·8	58·5	%
N	811	249	133·9	92·0	77·5	photons/s
n_2	93 ± 0·8	81·4 ± 0·8	91 ± 0·3	58·0 ± 0·2	32·0 ± 0·5	s^{-1}
Quantum efficiency η_1 $(=100\,n_1/N)$	0·74	16·8	61·3	59·8	41·3	%
Quantum efficiency η_2 $(=100\,n_2/N)$	11·5	32·6	67·9	63·1	41·3	%

counter, the correction for this absorption was obtained simply from the fractional loss computed directly from Table 1. The value of μ for argon[14] is that for a pressure of one atmosphere, a small correction for the carbon dioxide present being neglected.

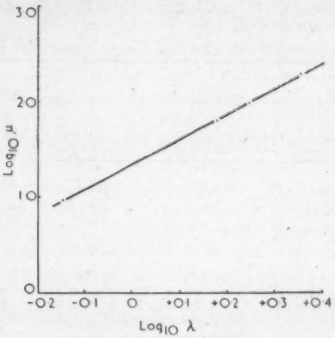

Fig. 4. Variation of linear absorption coefficient of Pyrex with wavelength

DISCUSSION

For the particular counter used, the maximum efficiency occurs near the CuK_α wavelength. The position of the maximum is mainly governed by the nature of the windows. The general form of the curves in Fig. 5 is to be expected from the opposing effects of window material and gas filling

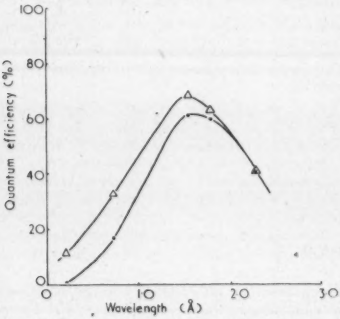

Fig. 5. Variation of quantum efficiency with X-ray wavelength

window-window path (B)
window-cathode path (A)

respectively. At short wavelengths the windows, being relatively transparent, admit the whole beam but, at these wavelengths, the gas absorbs little, so that the counting rate and efficiency are low (Fig. 6). At long wavelengths, the windows absorb the beam before entry to the gas and, although the remaining beam is almost entirely absorbed, the efficiency is again low. Thinner windows would admit more of the less energetic X-ray photons, and the peak would move to longer wavelengths.

It is further evident from the graphs that the beam path must be as long as possible and fall upon the cathode if an appreciable efficiency is to be obtained at the shorter wavelengths. For instance, for the MoK_α rays at 0·71 Å, the efficiency is doubled for the window-to-cathode path, while at 0·21 Å a fourteen-fold improvement is shown.

For any particular design there is a wavelength above which little advantage can be obtained by secondary processes at the cathode. This is seen in Table 2 to correspond to about 95% absorption of the beam entering the gas, that is, f equals 0·95. Because $(1 - e^{-\mu l})$ equals 0·95, where l is the path length in the gas, μ equals $3{\cdot}00/l\ \text{cm}^{-1}$, and the wavelength limit is that at which the gas has this value of μ (obtainable from tables).

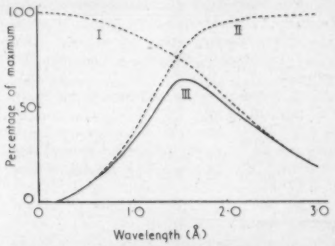

Fig. 6. Curves relating quantum efficiency (III), window transmission (I) and gas absorption (II), each expressed as a percentage of its maximum value

At the shorter wavelengths, improvement of efficiency by increasing the gas pressure is limited because of the higher working potentials then required and the thickening of the windows to withstand the pressure difference. Longer path lengths and an improved system for scattering the unabsorbed beam back into the counter, or a more efficient photoelectron production at the cathode, would assist in this respect.

Absolute value of quantum efficiency. While the above experiments have been conducted with due regard to statistical accuracy, further consideration suggests that the results for the counter are only to be regarded as a reasonable guide to its quantum efficiency.

First, for the quantum efficiency measurements made, the diagonally opposed window arrangement of this counter is not very satisfactory. At the small oblique angles of incidence required, the actual thickness of window material traversed by the beam is uncertain. Furthermore, without destroying the tube, the window thickness is only known to lie within the range 7–10 mg/cm^2. This uncertainty is most important at the longer wavelengths used.

Second, a one-to-one correspondence between photon absorption and counts is assumed. This neglects photons lost by scattering which either (as in the "classical" case) do not give rise to an initial photoelectron, or (as may occur in Compton scattering) produce a recoil electron of too small an energy to provide a pulse large enough to be detected above the noise level of the detecting system.

An elementary calculation based on the data given by Compton and Allison[14] shows that, for argon at one atmosphere and in the wavelength range 0·2–2·2 Å, the fraction scattered classically is of the order of 10^{-3} per cm^3. Thus, the fraction lost in this way from the 1 mm diameter beam of length 9 cm is only one part in 10^4 and may, therefore, be neglected.

The effect of Compton scattering, important below about 0·7 Å, is more difficult to assess, and depends on whether or not the recoil electron has enough energy to generate sufficient initial charge. Previous work on the Compton effect in argon[14] shows that the ratio of the number (N_r) of recoil electrons to the number (N_p) of photoelectrons is about 1 at 0·2 Å, the recoil electrons having energies up to 16000 eV. Most of these will therefore be recorded. At 0·4 Å, the ratio N_r/N_p falls to about 0·1, but the maximum recoil energies are then about 3000 eV. The majority would not be recorded in the present experiment. At 0·7 Å, although none of the recoil electrons could be expected to produce detectable pulses, the ratio N_r/N_p has fallen to 0·01 and above this wavelength the losses may be neglected. Some mitigation of these losses may be effected if the scattered photons eject photoelectrons from the cathode. It appears, therefore, that the quantum efficiency in the range 0·2–0·7 Å may be optimistic.

Third, the stimulation of fluorescence in the argon atom, requiring at most an energy of 3200 eV is accompanied, at 2·25 Å, by a few ejected electrons of energy less than 3000 eV which would not be recorded. If the noise level were lower and the resolving time of the whole apparatus very short, reabsorption of the fluorescent radiation could result in more than one pulse for each incident photon, especially if the Auger electrons could be recorded.

Fourth, a small correction should be made for those electrons which strike the cathode before they have had an opportunity to develop sufficient ionization. The path length of photoelectrons in argon at 1 atmosphere from a beam of wavelength 0·6 Å is about 0·7 cm.[14] Those ejected near the entrance window and close to the cathode may not therefore be recorded. This effect has been shown to be small with normal counter geometry.[11]

ACKNOWLEDGEMENTS

The research described in this paper was carried out at Sir John Cass College, London. The authors wish to thank Mr. R. H. Humphry, Head of the Department of Physics, for his interest and encouragement.

REFERENCES

(1) BRAGG, W. H., and BRAGG, W. L. *X-rays and crystal structure* (London: G. Bell and Sons Ltd., 1915).
(2) HUPPERTSBERG, A. *Z. Phys.*, **75**, p. 231 (1932).
(3) LOCHER, G. L., and LEGALLEY, D. P. *Phys. Rev.*, **46**, p. 1047 (1934).
(4) LEGALLEY, D. P. *Rev. Sci. Instrum.*, **6**, p. 279 (1935).
(5) MILLER, R. D. *Phys. Rev.*, **51**, p. 959 (1935).
(6) DAVEY, W. P., and BELL, P. H. *Phys. Rev.*, **58**, p. 198 (1940).
(7) SULLIVAN, H. M. *Rev. Sci. Instrum.*, **11**, p. 356 (1940).
(8) TROST, A. *Z. Angew. Phys.*, **2**, p. 286 (1950).
(9) LANG, A. R. *Nature* [*London*], **168**, p. 907 (1951).
(10) ARNDT, U. W., and RILEY, D. P. *Proc. Phys. Soc.* [*London*], *A***65**, p. 74 (1952).
(11) SKERTCHLY, A. R. B. *J. Sci. Instrum.*, **33**, p. 209 (1956).
(12) LANG, A. R. *Proc. Phys. Soc.* [*London*], *A***65**, p. 372 (1952).
(13) PATLA, N. *M.Sc. Thesis*, University of London (1958).
(14) COMPTON, A. H., and ALLISON, S. K. *X-rays in theory and experiment* (London: Macmillan and Co. Ltd., 1935).
(15) BERNSTEIN, W., BREWER, H. G., and RUBINSON, W. *Nucleonics*, **6**, p. 39 (1950).
(16) CURRAN, S. C., ANGUS, J., and COCKROFT, A. L. *Nature* [*London*], **162**, p. 302 (1948); *Phil. Mag.*, **40**, p. 36 (1949).
(17) ROSSI, R. B., and STAUB, H. H. *Ionisation chambers and counters* (New York: McGraw-Hill, 1949).
(18) ARNDT, U. W., COATES, W. A., and CRATHORN, A. R. *Proc. Phys. Soc.* [*London*], *B***67**, p. 357 (1954).
(19) WEST, D., and ROTHWELL, P. *Phil. Mag.*, **41**, p. 873 (1950).
(20) PARRY, J. K., RATHGEVER, H. D., and ROUSE, J. L. *Proc. Phys. Soc.* [*London*], *A***66**, p. 541 (1953).

Correspondence

Reaction of indium solder with mercury telluride

During our investigation of mercury telluride,* it was noticed that a reaction occurred between the mercury telluride and the indium used to solder electrical contacts on to specimens; we report here some preliminary observations on this reaction. We also note that tin can be used as a satisfactory solder for contacts to specimens of mercury telluride.

When mercury telluride was "tinned" with indium solder or pure indium, mercury was displaced from the mercury telluride. The reaction was quite slow and its progress was easily observed by the sharp demarcation line between the black lustrous mercury telluride and the dull grey product; the progress of the reaction, about 2 mm/day, is illustrated in Fig. 1. The demarcation line was not usually a straight line across the specimen, as the reaction was appreciably retarded by grain boundaries and faults in the material. The product usually held together in the form of the specimen, but on examination proved to be an extremely fine powder interspersed with rivulets of mercury and slight agitation was sufficient to break this. The nature of the grey powder was

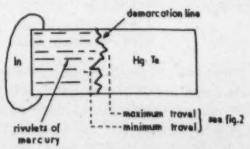

Fig. 1. Progress of the reaction

* LAWSON, NIELSEN and YOUNG. *J. Phys. Chem. Solids*, **9**, p. 325 (1959).

not determined, and an X-ray powder photograph showed a complex pattern of lines and much background haze. The indium solder soon became a liquid amalgam.

It was noticed that occasionally there was no reaction between the indium and the mercury telluride, or that there was a lag time before reaction occurred. This was almost certainly due to poor contact between the two materials and was not observed when freshly etched specimens were used.

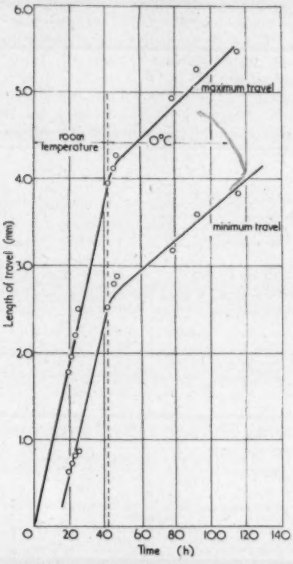

Fig. 2. Rate of reaction for experiment 16, crystal No. 4: the specimen was not etched and was maintained at room temperature for 42 h and subsequently at 0° C

Woods metal, gallium, lead, bismuth and tin were also used as solders, but no reaction was observed between these and mercury telluride; the first three of these solders, however, gave very poor contacts. Also no reaction was observed when indium was soldered to mercury selenide or to mercury selenide doped with phosphorus or arsenic.

The rate of the reaction was measured from the rate of movement of the maximum and minimum points of the demarcation line (Fig. 1). The rate showed some variation from specimen to specimen but this could probably be attributed to variations in the numbers of grain boundaries and other defects. The rate proved to be independent of time but was markedly affected by temperature. This was demonstrated by allowing the reaction to proceed to a steady state at room temperature and then altering the temperature. The results of a typical experiment are shown in Fig. 2. The rate at 43° C was found to be only slightly greater than that at room temperature, but the room temperature rate was about three times that at 0° C; at −183° C and 100° C the rate was zero. It is possible that oxidation prevents reaction at the higher temperatures. Some typical results are given in the Table.

Some typical experimental results

Experiment	*Crystal*	*Dimensions (mm)*	*Rate of reaction (mm/h × 10²)* R.T.	0° C	43° C	100° C
5	2	8·0 × 2·2 × 1·7	6·5			
7	2	9·0 × 2·0 × 1·8	6·0			
7	4	7·6 × 2·1 × 2·0	5·5			
7	3	6·27 × 1·8 × 1·6	7·6			
10	1	9·0 × 2·2 × 2·0	9·3			0
10	2	6·3 × 3·0 × 2·1	7·7			0
10	3	6·8 × 2·7 × 1·9	12·0			0
10	4	8·3 × 2·8 × 1·2	8·5			0
14	2	9·6 × 2·9 × 1·6	8·9		9·6	
14	4	9·5 × 2·2 × 1·5	9·0		10·2	
16	1	6·8 × 2·2 × 1·9	9·0	3·3		
16	3	4·9 × 2·7 × 2·0	3·1	1·0		
16	4	6·5 × 2·8 × 1·2	9·0	2·3		

There was also some indication that the rate was affected by passing a current through the specimen, the rate at the positive end tending to increase and that at the negative end to decrease, and it is of interest to note that a specimen such as shown in Fig. 1 behaved as an electrolytic cell developing $4{\cdot}4 \times 10^{-4}$ V. Also the resistance of the specimen did not change appreciably during the reaction; after complete reaction a specimen 10·3 × 2·5 × 2·5 mm had a resistance of 0·185 Ω.

Royal Radar Establishment,
Gt. Malvern, Worcs.

S. NIELSEN
[1 *April*, 1959]

NOTES AND NEWS

Notes and comments

The printing dispute

The delay in the publication of this, and the preceding, issue of the *British Journal of Applied Physics* has been occasioned by the recent dispute in the printing industry. The editor regrets any inconvenience caused to readers and authors and every effort is being made to return to normal publication dates as soon as possible.

Elections to The Institute of Physics

The following elections have been made by the Board of The Institute of Physics:—

Fellows: A. Ashmore, G. B. Banks, W. W. H. Clarke, R. P. Chasmar, W. H. Lunning, C. H. Vincent, O. M. White, R. L. Whitemore.

Associates: F. R. Bareham, A. Bent, J. R. Brown, R. H. Caplen, P. J. Coppen, D. Dasgupta, I. D. Dodd, S. H. Dunlop, L. W. Eales, S. Edwards, I. C. Fricker, A. H. Gabriel, R. E. Gee, O. G. Griffin, A. H. Hayward, W. S. E. Hickson, D. L. Lewis, I. D. Lewis, J. K. Monaghan, D. E. Morgan, M. J. Morshead, S. A. F. Murrell, A. Owen, D. H. Page, G. J. Parish, J. L. Petrie, H. A. J. Prentice, B. K. Ridley, G. W. Roderick, E. C. Rogers, S. D. Rosenbaum, A. A. Runki, E. W. Simpson, G. D. Smith, N. W. W. Smith, W. R. Thomas, G. O. Walker, R. L. B. Wall, E. H. Ward.

Twenty-four Graduates and thirty Students were also elected.

ICSU review (International Council of Scientific Unions)

The international organization of science through National Scientific Academies or National Research Councils is not as well known among scientists as it should be. Indeed, it is often one of the Unions affiliated to this Council that initiates and organizes international conferences on particular branches of science, and in this respect the International Union of Pure and Applied Physics and the International Union of Crystallography have been active. World-wide experiments are also arranged, of which the most notable example has been the recent International Geophysical Year. There are 13 Unions under the Council and 45 countries are in this scheme.

The Bureau of the ICSU has for some time been conscious that the members of the ICSU, both national and scientific, were not being adequately informed concerning the affairs of the ICSU, and that this lack of information was detrimental to the continuing growth of the ICSU. The Unions, moreover, receive little information about each other's activities.

To help to remedy this situation a new quarterly entitled the *ICSU Review* is being published for the Council by the Elsevier Publishing Company of Amsterdam under the general editorship of Sir Harold Spencer Jones. The first issue contains the following contributions: "What does ICSU stand for?" by Alexander von Muralt; "International collaboration in science," by L. V. Berkner; "The international geophysical year," by Sydney Chapman; "International co-operation in the marine sciences," by R. Revelle; "Some aspects of the origins of life considered in the light of the Moscow International Symposium," by N. W. Pirie. In addition there are notes and announcements of recent and forthcoming events.

The subscription price is 30*s.* or $4.50 or f.16 per volume (including postage) or the equivalent in other currencies.

Review of the Proceedings of the Geneva Conference

The *Journal of the British Nuclear Energy Conference* is to publish a list of the contents of each volume of the Proceedings of the Geneva Conference as it becomes known. The library of the Institution of Civil Engineers will have a complete set of the Proceedings which will be held for the use of members of the constituent societies of the British Nuclear Energy Conference. Other constituent societies will retain for their libraries only those volumes which will be of particular interest to their members but they will be willing for members of the constituent societies to consult those volumes should they so wish. Members of The Institute of Physics may obtain details from the Secretary at 47 Belgrave Square, London, S.W.1.

Errata

On p. 225 of the May issue of this *Journal* the address of Dr. K. Little should have been British Nylon Spinners Ltd., Pontypool, Monmouthshire, and not Coventry as printed.

In the paper by E. R. Wooding and D. R. Lintin entitled "An investigation of the ignition of a gas by an electric spark" which appeared on p. 159 of the April issue of this *Journal* the correct orientation of the dissected shadowgram (Fig. 11) should be obtained by rotating the figure counter clockwise through 90°.

Journal of Scientific Instruments

Contents of the August issue

ORIGINAL CONTRIBUTIONS

Papers

Differential microdensitometer. By A. H. Cook and R. G. Hitchins.
Solarimeter for field use. By J. L. Monteith.
Improved equipment for the measurement of interfacial potentials. By C. D. Kinloch and A. I. McMullen.
Electron-optical design of an X-ray micro-analyser. By T. Mulvey.
Spinner-magnetometer for thermal demagnetization experiments on rocks. By F. D. Stacey.
Weight-in-air basis of adjustment of precision weights. By P. H. Bigg.
Time-controlled unit-function, constant-voltage generator. By Y. Ettinger and H. Edels.
Measurement of systematic track distortion in a propane bubble chamber. By W. H. Evans, D. W. Hadley, T. D. N. Morgan, P. R. Williams and A. Kirk.

Laboratory and workshop notes

Apparatus for tilting extraction replicas through large angles in the electron microscope. By G. R. Booker and J. Norbury.
Use of a photomultiplier in the flame photometric analysis of substances with emission bands in the red. By E. J. Harris.
Power unit for welding fine wires. By J. D. Hill.
Device for admitting gas at constant rate to vacuum apparatus. By A. D. Osborne.
Method of etching germanium to precise limits. By B. T. Scofield.
Notes on three kinematic constraints. By O. P. T. Kantorowicz.
Automatic constant level device for liquid air. By I. Flinn and P. Moore.
Pump for circulating gases. By J. Hume.
Collection of chromatographic fractions in a mass spectrometer sample system. By J. H. Beynon, R. A. Saunders and A. E. Williams.
Cap-and-cup mercury vacuum seal. By A. J. Gaunt and R. A. Redford.
Comparator for X-ray spectrum films. By C. F. Smith.
New absolute wedge-calibration method for the Dobson ozone spectrophotometer. By J. P. Funk.

Correspondence

Simple method for finding the ratio of surface tension to viscosity of a liquid. From G. M. Sreekantath, N. Rajaram and C. K. Ponnappan.

NOTES AND NEWS

Notes and comments

THIS JOURNAL is produced monthly by The Institute of Physics, in London. It deals with all branches of applied physics (including theory and technique).
All rights reserved.
Responsibility for the statements contained herein attaches only to the writers.

EDITORIAL MATTER. Communications concerning editorial matter should be addressed to the Editor, The Institute of Physics, 47 Belgrave Square, London, S.W.1. (*Telephone:* Belgravia 6111.) Prospective authors are invited to prepare their scripts in accordance with the *Notes for Authors.* (Price 3*s.* 6*d.* including postage.)

REPRODUCTION. The Institute of Physics is a signatory to The Royal Society's Fair Copying Declaration. Details may be obtained upon application from The Royal Society, London, W.1.

ADVERTISEMENTS. Communications concerning advertisements should be addressed to the agents, Messrs. George Jackson (Fleet St.) Ltd., Cliffords Inn, Fleet Street, London, E.C.4. (*Telephone:* Holborn 3611–2.)

CLAIMS FOR MISSING JOURNALS. Claims from regular subscribers to this *Journal* for missing numbers will only be considered if received within 60 days of the date of mailing plus normal outward time of transit and time for lodging the claim. Losses attributable to failure to notify a change of address or to similar omissions will not be considered.

SUBSCRIPTION RATES. A new volume commences each January. The charge is £6 per volume ($17 U.S.A.), including index (post paid), payable in advance. Single parts, so far as available, may be purchased at 12*s.* 6*d.* each ($1.75 U.S.A.), post paid, cash with order. Orders should be sent to The Institute of Physics, 47 Belgrave Square, London, S.W.1, or to any bookseller.

CONFERENCE REPORT

Summarized proceedings of a symposium on current developments in the production of high vacua—London, April 1959

At a symposium organized by The Institute of Physics and held in London, on 17 April, 1959, the first session was devoted to getter-ion and ion-sorption pumps, the second to the production of high vacua in large equipment, and the third to short contributions on the analysis of residual gases in kinetic vacuum systems. A summarized account is given below.

PRINCIPLES OF CHEMICAL AND IONIC PUMPING

The symposium was opened by Mr. R. N. BLOOMER (Siemens Edison Swan Ltd., Harlow, Essex), with a paper on "General principles of chemical and ionic pumping in kinetic vacuum systems". Differences between physical and chemical sorption were emphasized. In physical adsorption, a molecule approaching a metal surface undergoes a fall of potential energy of about 0·1 eV (so-called heat of binding by Van der Waals's forces) when it is still about a molecular diameter away from the electronic surface of the metal, and the sorption is rapid and common because no potential barrier to the binding exists. In contrast, when a molecule is chemically absorbed its potential energy falls by a few eV (so-called heat of absorption) when the nuclei of the atoms or ions of the gas are within atomic radii of the metal surface, but before they can reach such positions, the constituents of the molecule may have to surmount a potential barrier (the so-called activation energy for chemisorption). Physically, this activation energy is needed to dissociate the molecule into atoms. Chemisorption may hence be expected to be a specific property of some surfaces only and to be a slower process than Van der Waals's absorption. Again, chemisorption would be expected to be accelerated by extraneous dissociation or ionization of the molecules. In fact, chemisorption is rapid and dissociation occurs at the metal surface itself and extraneous ionization is no help.

To distinguish chemical from ionic pumping, the word "chemical" is used to describe exchanges of electrons between reacting atoms that occur through the thermal energy of the constituents whilst the term "ionic" is used to describe the removal from the vapour phase of ionized and excited molecular fragments. Thus, chemical clean-up of gas arises from natural affinities whereas ionic clean-up has to be induced. Yet indications in contemporary literature on getter-ion pumps are that ionizing discharges are run near chemically active materials in the belief that thereby unnatural chemical reactions may be induced or the kinetics of natural ones improved. These possibilities are unlikely for the reasons given.

The condensation coefficient (ratio of number of molecules sticking to number incident on a surface in unit time) and the heat of adsorption are independent of one another. For example, barium and oxygen react exothermally yet a pure barium film can be prepared which does not take up oxygen until after about 15 min; thereafter the film takes up oxygen normally.

The physical processes in chemical and ionic clean-up are quite different. The latter can occur because ions are smaller than atoms and can be shot into interstitial lattice positions at the surface and there acquire electrons from some donor site or the conduction band and so become too large to move out again. A notable and apparent exception is the case of the nitrogen molecule for which excitation to a comparatively long-lived metastable state at an energy of about 9 eV enhances the pumping action. Lukirskey and Ptizn discovered this using magnesium getters; it has been shown to occur with barium getters also.

The adsorption at a metal surface of the molecules of one kind of gas in a mixture of gases can be greatly influenced by the partial pressure of the other. In a getter-ion pump the metal film must act as a sink to many kinds of gas and can never be clean. Hence, condensation coefficients estimated from the measured pumping speeds of getters may be only a fraction of their true values (Wagener[1]). However, if the measurement of the pumping speed of getter-ion pumps is thereby influenced it can be demonstrated by experiments with a range of values of getter film area.

False values of condensation coefficients can also be obtained for complicated molecules. Stout and Gibbons found that titanium films remove carbon from incident methane and release hydrogen. Similar behaviour is found for benzene and toluene. Gettering may therefore result in a pressure increase and not the expected decrease.

In getter-ion pumps, a variety of surface reactions may occur. Divatia, Davis and Herb[2] and Cloud, Beckman and Trump[3] have reported on the reaction of oxygen with films of titanium and barium respectively. Bloomer's experiments show that, at room temperature, titanium takes up the first monolayer of oxygen rapidly but subsequent monolayers at a much decreased rate. In all, about four monolayers are adsorbed. Barium, however, takes up about 30 layers of oxygen at a constant rate until a protective oxide film (thickness 70 Å) is formed. Thus, with titanium and oxygen, the behaviour is reminiscent of that of oxygen on tungsten, investigated by Becker.[4] There is a heat of sorption (binding energy about 4 eV) typical of chemisorption during the formation of the first monolayer and first valence bonds between oxygen and the metal are formed. For further sorption, the binding energy decreases rapidly; only second (at 2 eV) or third valence bonds with the metal are possible. The kinetics of this build-up of oxygen concentration at the surface are probably those given by Gomer[5] for various gases on tungsten. For oxygen on tungsten at 30° to 70° K, physical adsorption and chemisorption co-operate. The chemisorbed oxygen is fixed at particular lattice sites but that which is physically absorbed onto the gas already chemisorbed is mobile and moves to the edge of the raft of chemisorbed oxygen there to be itself chemisorbed. At too low a temperature, the physically adsorbed gas is immobile; at too high a temperature, it evaporates before it can migrate over the surface. At about 500° C, growth of a chemisorbed layer occurs by migration radially from one trap site to the next, requiring an activation energy of about 1 eV and decreasing slightly as the traps are filled (a process which also explains the variation of the condensation coefficient of oxygen on

barium at room temperature during the deposition of the first monolayer[6]). That the process for oxygen on tungsten is also significant for titanium is likely since Wagener[7] has shown that tungsten and titanium behave similarly as getters.

By contrast, the reaction of oxygen with barium is understandable from Mott's theory of oxidation. Barium ions move through the growing oxide *via* interstitial lattice positions until a thickness is reached for which the field across the oxide is too weak for electron transfer by field emission.

To increase the capacity of titanium for oxygen, cooling the deposited film would seem to be advantageous; by contrast, barium films should be heated so that thermionic emission of electrons can occur across otherwise thin protective oxide layers. Again, as these reactions proceed by interstitial diffusion, numerous lattice defects are beneficial; hence it should help to evaporate some foreign atoms of different size from barium atoms to increase the condensation coefficient. Certainly, the condensation coefficient is increased by having a substrate with a high density of lattice defects.

Further basic studies of the Penning type of ion pump are required. Is the sputtered metal useful because it can sorb gas, or does gas react with metal electrodes cleaned by sputtering off oxides and the like? Merely exposing fresh titanium by abrasion[8] enables the gas pressure to be reduced. Improved ion pump performance can only result from detailed study of the atomic processes involved.

Getter-ion pumps. The second paper in this session entitled "The design and use of getter-ion pumps", was read by Mr. L. HOLLAND (Edwards High Vacuum Ltd., Crawley, Sussex). He opened his lecture with an account of the various types of ion-pump and getter-ion pump on the lines of his recent review.[9] It was emphasized that titanium is a most promising gettering material because of its availability, volatility and chemical reactivity. Fig. 1 illustrates the effect on the pumping speed of a fresh titanium film in a Penning type getter-ion pump.[10]

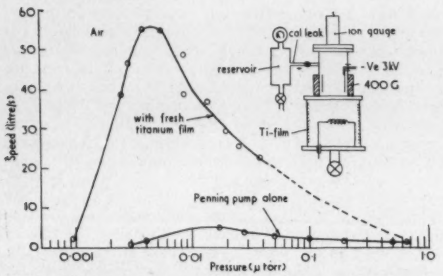

Fig. 1. Speed against pressure curves for a Penning type getter-ion pump

The Herb-type of titanium evapor-ion pump[11] is limited in its operation because the titanium evaporant reacts with its Tantalloy or carbon support. The problem of providing a design with a speed of about 1000 litre/s at 10^{-5} torr or below is primarily that of developing a new type of titanium vapour source.

A new getter-ion pump was described (a model was exhibited) in which it is possible to evaporate titanium continuously at high rates and for extended periods. The pump consists of a water-cooled stainless steel chamber (30 cm diam. by 60 cm height; joints argon-arc welded) in which there is mounted the evaporation source, the electrodes of an ionization pump and a hot cathode for degassing the pump components by electron bombardment. The titanium wire is fed downwards into the pump body through a bellows by a cam on a variable speed electric motor. Within the pump it passes down an inclined plane on a copper block anode so that its tip is melted to a globule and evaporated as it enters the electron beam from a heated tungsten filament (Fig. 2). If the wire feed is obstructed when the metal

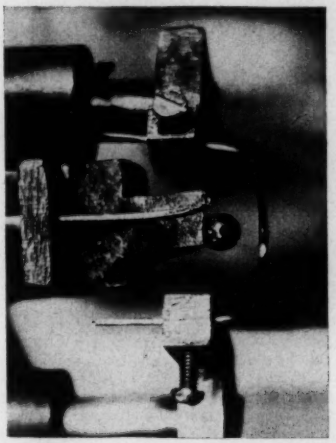

Fig. 2. Evaporation source showing copper block, bead and filament for electron bombardment

globule freezes to the anode, the wire may bend sideways and continue to enter the electron beam and the globule continues to grow. The useful life of this vapour source is limited only by that of the cathode filament which is several thousand hours at 10^{-5} torr or below.

The ionization pump consists of two grids (9 cm and 20 cm diam. respectively) in the form of tungsten wires hanging vertically from stainless steel bands and placed coaxially around the evaporation filaments. Electrons are accelerated to these positive grids and the positive ions formed are transported to the metal inner walls of the pump chamber which is at a negative potential.

The use of glass-to-metal and ceramic-to-metal seals for the electrical lead-ins, and aluminium wire gaskets[12] enables this pump to be baked-out at up to 500° C.

To operate the pump it is first degassed by heating to about 400° C by bombardment with electrons from a special cathode filament. When the pressure during pre-pumping falls to 10^{-4} torr, heating is stopped and the pump chamber water-cooled. When the pressure has been reduced to 10^{-5} torr by a small diffusion pump, evaporation of the titanium is begun. Initial outgassing of the filament and the titanium wire usually causes a pressure rise to about 5×10^{-5} torr; on subsequent fall to 10^{-5} torr, the cathode is earthed so that positive ions may be transported to the pump wall. An ultimate of 10^{-7} torr (10^{-8} torr has recently been attained) is possible by alternate evaporation and use of the ionization pump, either with the getter-ion pump isolated

from the diffusion pump or with the vacuum valve to the diffusion pump still open.

Pumping speeds recorded for various gases are shown in Table 1.

Table 1. *Pumping speed of titanium droplet pump measuring during continuous titanium evaporation at a rate of* 40 *mg/min*

Gas	Pumping speed (litre/s)			
	Isolated at 10^{-5} *torr*	*With diffusion pump*	*Isolated at* 10^{-6} *torr*	*With diffusion pump*
Air	240	530	110	300
Oxygen	1200	2300	700	1600
Nitrogen	1700	2500	450	1550
Hydrogen	1400	1500	500	800

The pumping speed is greatly increased by the diffusion pump although this has an effective speed of only 10 litre/s. This is probably due to the removal from the getter-ion pump by the diffusion pump of a gas component which poisons

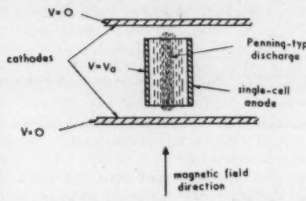

Fig. 3. Cross-sectional side view of a single cell VacIon pump

the getter film. Klopfer and Ermrich[13] show that methane is formed during the evaporation of titanium in a glass pump because of reaction between the hydrogen and carbon present in titanium. Unsaturated molecules produced on dissociation and polymerization of such hydrocarbons have a high affinity for clean metal surfaces which would reduce the rate of adsorption and diffusion of the gas to be pumped.

Dr. N. W. Robinson (Mullard Research Laboratories, Salfords, Surrey) opened the discussion with a short contribution on the use of small glass getter-ion pumps in the maintenance of high vacua in electron tubes. Two types of pump described were (1) a Bayard–Alpert ionization gauge containing an auxiliary filament bearing titanium; (2) a Penning type ionization gauge in which the anode loop consists of titanium and tungsten wires interwoven and the cathodes are formed by the evaporation of the titanium on to the walls of tube to make contact with an electrode in the side wall.

Both pumps are used for pumping single large electron tubes, sealed-off and then discarded. Pumping speeds are about 3 to 4 times faster than a Bayard–Alpert ionization gauge alone. A volume of 0·5 litre can be pumped to 10^{-10} torr in 2 or 3 hours if the system has been thoroughly outgassed.

Residual gases at 10^{-9} torr after pumping with these getter-ion pumps are primarily hydrogen and helium. The former results from the formation of unstable pseudo-hydrides of titanium.

Dr. R. L. Jepsen (Varian Associates, Palo Alto, California) then described the VacIon pump. The single-cell type (Fig. 3) is based on the Penning gauge. A cylindrical anode is set up between a pair of titanium cathode plates and an axial magnetic field is used to confine the electrons in the cold discharge to oscillatory paths between the cathodes. Positive ions impinging on the cathodes cause atoms of titanium to be sputtered on to the anode. At the anode, freshly sputtered titanium from the cathodes may combine chemically with active gases such as oxygen and nitrogen. Many other processes also occur in the discharge: dissociation, excitation, attachment of positive ions to the cathodes, sputtering of previously buried gas atoms, sputtering of cathode material from one cathode to another. Some of these processes have a considerable effect on the pumping action. It is believed that most of the permanent gas take-up occurs at the anode.

Typical variations of speed with magnetic field for two different anode voltages are shown in Fig. 4. The speed is about 2 litre/s at 3000 G and 10 kV.

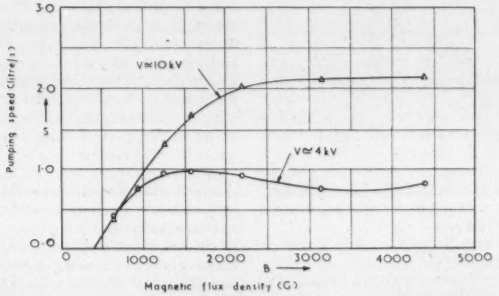

Fig. 4. Typical variations of speed (single cell) with magnetic field for two values of anode voltage

(Cathodes of titanium. Cathode spacing ≃1·4 in.; anode length ≃0·9 in.; anode diam. ≃0·5 in.; pressure ≃1–5 × 10^{-5} torr.)

A medium size multi-cell VacIon pump (Fig. 5) of nominal speed for air of 250 litre/s has a speed essentially independent of pressure over the range from about 5 × 10^{-8} to 10^{-5} torr. The speeds recorded for various gases are given in Table 2.

The fact that air is pumped faster than its major constituents shows that these gases are not pumped independently;

the speed for a particular gas depends on the type and amount of other gases present.

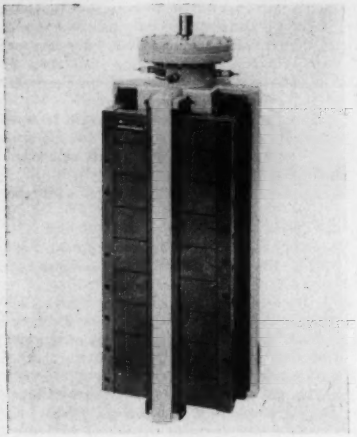

Fig. 5. View of 250 litre/s VacIon pump

Table 2. *Speeds for various gases for the multi-cell VacIon pump*

Gas	*Speed in litre/s*
Hydrogen	850
Deuterium	590
Air	280
Nitrogen	260
Carbon dioxide	230
Oxygen	155
Helium	30

The two-gauge method of measuring pumping speed was described and the practical advantages of this type of pump were pointed out.

As these pumps are clean and oil-free it was aimed to provide also oil-free backing. Two possibilities are (1) to cool an appendage attached to the system with liquid helium;[14] (2) to use activated charcoal cooled with liquid nitrogen. A given volume of activated charcoal can exhaust about 10 times its own volume of air to reduce the pressure to about 10^{-2} torr in a few minutes.[15]

The possibility of building very high speed pumps (10^5 or even 10^6 litre/s) was discussed briefly. To use a very large number of cells to obtain higher speeds, problems of adequate gas access arise. Schematic pump designs have cathode-anode cell sections of radial depth ω around a tube of inner bore diameter d and length L. The spacing from one section to the next (measured along the inner bore) is λ. ω, λ and L/d are kept constant, independently of the desired speed. For a constant value of ω the "radial" conductance effects are unchanged. With ω and λ fixed, similar cathode-anode sections and magnets are useable for pumps of various sizes. The major gas conductance problem is then that of the tube itself.

A short paper by Messrs L. G. CARPENTER and W. N. MAIR (Royal Aircraft Establishment, Farnborough, Hants.), read by Mr. Carpenter, dealt with the sorption by titanium of oxygen and nitrogen at low pressures. Titanium exists in the high temperature β-phase (body-centred cubic) and the low temperature α-phase (hexagonal) with a transition temperature of 880° C. The sorption of oxygen by titanium raises the transition temperature, i.e. stabilizes the α-phase. The apparatus used to study by a continuous flow technique gas sorption on a 0·5 mm diameter titanium wire (or strip filament) has been described elsewhere.[16] The titanium wire was operated at constant power and the optical temperature observed so that phase changes resulting from oxygen sorption leading to optical emissivity changes could be followed. The gas take-up was measured in terms of the electrical resistance of the titanium. X-ray diffraction measurements were made both on slowly cooled filaments and on filaments suddenly quenched in mercury so that phase changes due to oxygen sorption could be followed; metallographic studies by light microscope were also made on sections of quenched filaments.

If η is defined as the number of molecules sorbed by a given area of hot titanium divided by the number of molecules incident in a given time, the experiments show that, for oxygen, η increases with temperature and appears to be asymptotic to a value rather less than one, perhaps because there are some orientations of the oxygen molecule to the metal surface which prevent sorption however high the temperature may be. An Arrhenius plot of the data for oxygen does not yield a significant result: the activation energies range from about 1 to 3 kcal/mole. For nitrogen, an Arrhenius plot appears significant; the curve is in two portions, the higher temperature part has a slope of about 40 kcal/mole and the lower part about 18 kcal/mole. The discontinuity in the curve appears at the transition temperature at about 880° C.

At about 1000° C, for oxygen η is nearly one; for nitrogen η is about 10^{-3}.

The dual sorption modes of Bayard–Alpert ionization gauges. Mr. G. CARTER (University of Liverpool) contributed to the discussion by referring to his recent work which establishes that the ion pumping speed for some noble gases in Bayard–Alpert gauges has two distinctly different values and, correspondingly, the gauge has two different pressure sensitivities. These phenomena are ascribed to changes of the electric potential of the glass envelope. The gauge is initially evacuated to 10^{-9} torr or below by means of a diffusion pump with liquid nitrogen trap. Admitted pure gas is then pumped at a constant rate so that the pressure is approximately 10^{-5} torr. The gauge is then operated for a specified time, the test gas removed and the pressure of 10^{-9} torr restored. Heating to 400° C then re-evolves gas pumped to the gauge walls during the ionization; the quantity of gas so desorbed is evaluated by observing the pressure transients (which are approximately proportional to the desorption rate) recorded at an auxiliary Bayard–Alpert gauge and a mass spectrometer and integrating these transients over the period of desorption. Fig. 6 shows the quantity of argon sorbed (or rather subsequently desorbed) *versus* the ionization produced in the gauge, which is taken as proportional to the product of the electron current, time of operation of the discharge and the gas pressure. For a specific value of the ionization, *two* distinct quantities of gas may be sorbed at the walls, one quantity about five times the other. Furthermore, the gauge has two different pumping speeds and it is found that when the higher gas quantity is sorbed the gauge pressure

sensitivity is about five times larger than when the smaller quantity is sorbed.

The likely explanation is that the inner glass wall of the gauge can acquire either of two distinct potentials. Secondary electron emission at the glass results in this potential becoming stabilized either at about that of the cathode or that of the positive grid. At either of these stable values, the glass receives no net charging current.[17] At cathode potential, more positive ions of higher mean energy strike the walls and are sorbed than at grid potential. The gauge sensitivity is similarly affected by the change of field distribution.

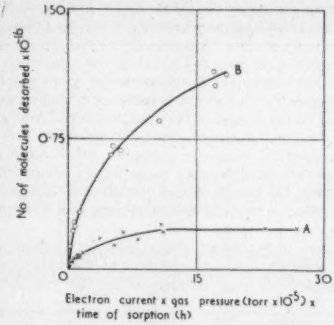

Fig. 6. Sorption of gas by a Bayard–Alpert gauge

Similar results were obtained for the Comsa and Musa[18] type of ion pump for which the change of the glass wall potential was determined directly by a capacitance technique and an electrostatic voltmeter.

Mr. M. W. ROBERTS (National Chemical Laboratory, Teddington, Middlesex) reported his recent investigation with Dr. F. C. TOMPKINS of the kinetics of the interaction of nitrogen with evaporated calcium films. The activation energy of the process was found to increase linearly with the nitride thickness, suggesting that the Mott–Cabrera theory [*Rep. Prog. Phys.*, **12**, p. 163 (1948)] is valid, i.e. the rate was controlled by the diffusion of Ca^{++} ions under the influence of the field existing at the metal-nitride interface. A critical temperature deduced on the basis of the theory was in excellent agreement with that found experimentally.

By means of physical adsorption techniques, namely, the adsorption of krypton at −195° C, the stability of evaporated iron films has been investigated. Films deposited at −195° C and then allowed to "anneal" at room temperature at a pressure below 10^{-6} torr decrease in area by about one-third in 5 h. The subsequent decrease is smaller. The activation energy of this "sintering" or "annealing" process is around 2–3 kcal/mole^{-1}, suggesting that the process is one of diffusion of clusters of vacancies [Cottrell: *Symposium on Vacancies and other Point Defects in Metals and Alloys.* Monograph No. 23 (London: Institute of Metals (1957)] which coalesce causing a shrinkage of the surface as observed experimentally.

PROBLEMS IN THE PRODUCTION OF HIGH VACUA IN LARGE EQUIPMENT

Mr. J. BLEARS (Metropolitan-Vickers Electrical Co. Ltd., Manchester) opened the afternoon session with a lecture in which he stressed the necessity for further quantitative study of factors which control and limit the ultimate pressures attainable in a vacuum system.

Three examples were considered. The first showed that with a well designed baffle system the oil vapour pressure and rate of adsorption on the fine side are consistent with values calculable from the rate of evaporation of liquid from the baffle; consequently, jet design has only a minor effect on the contamination of the fine side due to back-streaming when such baffles are used (see Table 3).

Table 3. 14 *in. oil diffusion pump with Apiezon C oil and refrigerated baffle operating at* −12° *C*

	6-day total g	g/s	g/cm²/s
Observed back-streaming rate	10^{3}	2×10^{-3}	2×10^{-6}
Calculated maximum escape due to vapour/vapour collisions within baffle	5×10^{-11}	10^{-16}	10^{-19}
Rate of evaporation from wet baffle at vapour pressure of 5×10^{-10} torr	$2{\cdot}5 \times 10^{-2}$	5×10^{-8}	5×10^{-11}
Integrated quantity of vapour desorbed from vessel and recondensed on baffle	$1{\cdot}3 \times 10^{-2}$	$2{\cdot}5 \times 10^{-8}$	$2{\cdot}5 \times 10^{-11}$

The second example showed that it is possible to predict the partial pressure due to the outgassing of materials in large systems by scaling from data obtained in small-scale experiments. The appropriate equation is

$$SP_t = \Sigma k_t A$$

where S is the pumping speed, P_t the partial pressure at time t, k_t the outgassing rate per unit area of the material (measured in the small scale experiment) and A the area of the material. In illustration of this point computed and measured outgassing curves for a proton linear accelerator were given (Fig. 7). Calculations on the vacuum system of

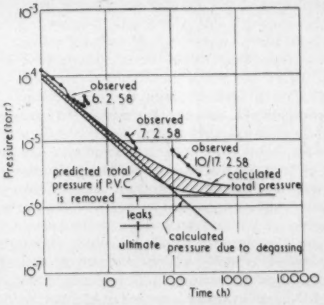

Fig. 7. Calculated and measured pressures in the Harwell proton linear accelerator

ZETA have been considered in this way (appropriate graphs were shown) whilst, at the other end of the range of sizes of equipment, the effect of using an O-ring attached to a vacuum gauge can be assessed. A plea was made for further experimental work on the outgassing rates of various constructional materials used in vacuum systems.

Thirdly, an experiment was described showing that when a 4 MeV electron accelerator is started up the transient pressure rise which is almost always observed (appropriate graphs were shown) may be due to carbon monoxide and not to the removal of surface adsorbates such as oil vapour and water. More experimental evidence is required but it seems possible that the carbon monoxide is a reaction product from the hydrocarbon and water adsorbates under the influence of ionizing particles.

Mr. S. H. Cross (Atomic Energy Research Establishment, Harwell, Berks.) described the vacuum system of the 7 GeV proton-synchrotron at Harwell. After an outline of the principle of the proton-synchrotron, it was emphasized that, as the accelerating potential on the r.f. cavity is about 7 kV, in order to reach 7 GeV, the protons must circulate around the machine 10^6 times (i.e. travel 10^5 miles). The scattering effect of residual gas molecules is therefore of major importance; this effect varies inversely with the energy of the protons so the most serious loss is soon after proton injection. Theoretical curves show the relative proportion of protons surviving the acceleration cycle for a given pressure P_0, where the initial amplitude of oscillation of the particles is α, against the semi-aperture A for two values of α/A, and similar curves for $\frac{1}{3}P_0$ and $3P_0$. The steepness of the curves shows that an aperture is chosen for 90% survival of protons; a small reduction in aperture or a slight increase in pressure will result in the loss of nearly all the protons in the beam. The Harwell machine is designed for a vertical aperture of 9 in. and a pressure of 10^{-6} torr. The first steps in designing the machine are hence possible. The need for uniformity of access to the machine has led to the decision to extend the vessel beyond the magnet throat to form a pumping chamber. Calculation shows that it is impossible to achieve the required average pressure with a single pump in view of the assessed outgassing rates. Five 24 in. pumps to each octant of the machine will be used, i.e. 40 pumps in all, each with a baffled speed of 5000 to 6000 litre/s. Each pumping station is to consist of an oil diffusion pump with a mildly refrigerated chevron baffle and a sliding gate valve backed by an oil ejector pump and a small mechanical pump. Roughing will be by eight separate units each comprising a 30 c.f.m. rotary pump backing a 200 c.f.m. Roots pump and includes a refrigerated oil trap. Fully automatic control is to be used except for manually operated high vacuum valves. A fault in the main vessel leads to closure of all high vacuum valves automatically.

As the magnetic field rises from 0·3 to 14 kG in 0·7 s, the maximum permissible amount of metal in the vacuum vessel is limited to stainless steel ribbon not more than 0·002 in. thick and about 3 in. wide. Ceramics and glass are attractive electrically but poor mechanically. The polyesters and the epoxies used as binding media for glass fibres produce laminates of high mechanical strength. The epoxies are considered to meet most nearly the requirements.

Hardeners for the resin which have been investigated are aliphatic amines, aromatic amines and anhydrides. The last two are superior in vacuum and radiation resistant properties and the anhydrides are preferable but need longer curing times. The vacuum properties of the epoxy resins at various temperatures were investigated by the Knudsen effusion method. Typical results were shown. Outgassing would seem to be more due to a diffusion process rather than vapour pressure effects. Gas evolution rate studies on cast resins and glass fibre laminates made with similar resins at different laminating pressures show that significant improvement results from the use of pressure laminates. An epoxy resin plasticized with di-butyl phthalate gave a lower residual pressure than either the unplasticized resin or the plasticizer. An optimum amount of plasticizer was therefore found which gives the least residual pressure. Mass spectrometer tests on resins showed that only water vapour was evolved; the plasticizer may therefore serve to block the epoxy lattice up to a point where excess plasticizer begins to be desorbed.

A double walled vacuum vessel was finally chosen. The epoxy resin glass fibre laminate ($\frac{1}{8}$ in. thick) outer vessel contains the magnet pole tips which provide the mechanical support. The inner vessel (wall thickness: $\frac{1}{4}$ in.) is inserted between the pole tips and the single-walled header vessel is brought up to the flanges of the inner and outer vessels. To accommodate manufacturing tolerances in these 50 ft long vessels, a specially moulded elastomer seal is used. The inner vessel will be lined with metal foil to prevent charge accumulation and also to reduce the effective exposed area of epoxy resin, so bringing the outgassing rate down to the design figure.

Advantages of this vessel construction are an outer vessel protected somewhat against radiation by the magnet poles, an inner vessel only lightly stressed and so less susceptible to radiation degradation of its mechanical properties and a larger beam aperture than is possible with a single-walled vessel. If the inner vessel has to be changed, no disturbance of the accurately set magnets is necessary. To prevent collapse of the inner vessel, the speed of pumping is restricted at the higher pressures so that there is no excess pressure in the outer vessel until a pressure of 1 torr is attained.

Leak testing on the construction site before installation will be with helium mass spectrometers and palladium barrier leak detectors.

Mr. B. D. Power (Edwards High Vacuum Ltd., Crawley, Sussex) opened the discussion with a contribution entitled "Characteristics of some pumps with experimental results". He reported that a typical pumping system under construction for the 7 GeV proton-synchrotron contained a gate valve with neoprene for the plate and shaft seals and vacuum grease lubrication, a chevron baffle at −25° C and a four-stage pump with three stages of fractionation and a side-jet to eject volatiles. A vapour booster backing the diffusion pump permits the use of a small mechanical backing pump. The ultimate pressure provided is below 5×10^{-8} torr with an overall speed of about 5000 litre/s.

To use such pumping equipment to produce ultra-high vacua in a bakeable system, the valve is replaced by a liquid air trap of the non-creep type and all gasketing must be metal. Large size all-metal bakeable valves are not yet available but are being developed. By baking the trap and the system but not the pump, and *without* the use of a refrigerated baffle, blank-off pressures below 10^{-10} torr have been achieved with a 6 in. pump (speed about 600 litre/s), and there seems no reason why larger models should behave differently. The pump fluid was silicone 704. Apiezon C gave a higher pressure possibly due to decomposition of the fluid in the pump boiler. This may prove that hydrocarbon oil is more prone to yield permanent gases as direct products of first decomposition whereas silicone 704 tends to form vapours which are trapped or ejected from the pump before they can decompose further.

For the linear accelerator which injects protons into the proton-synchroton, mercury diffusion pumps were selected because of fears about the possible effects of oil vapour in the system, though neoprene and hydrocarbon grease in the isolation valves were accepted. A mercury pump with a one-collision liquid air trap can produce a blank-off pressure of about 5×10^{-8} torr without baking but loss of mercury by distillation on to the cold trap results in a 9 in. pump losing its fluid charge in about 5 d. A refrigerated baffle between the pump and trap is therefore provided to condense most of the mercury so that it drips back into the pump; the system could then run for about a year. The baffle plus trap reduces the speed of a 10000 litre/s pump to only 2000–3000 litre/s but, against this, the trap has a very high speed for condensable vapours.

To attain ultra-high vacua in a bakeable system, at least two liquid air traps are necessary because a single-collision trap will not reliably stop all mercury vapour and, moreover, it is best to bake the system before cooling the trap nearest to it. With such metal systems, 10^{-10} torr and below should be obtainable. As the bake-out is necessary, the cold trap does not now provide any compensation for the loss of speed due to the necessary traps and baffle.

Pressures below 10^{-10} torr with really large-scale systems would appear to be readily obtainable with both oil and mercury pumps, the former being less complex but the latter may eventually prove superior as there is a danger of organic contamination and oil decomposition with the oil pumps.

Mr. R. S. BARTON (Atomic Energy Research Establishment, Harwell, Berks.) stressed that it is essential to understand further the influence of constructional materials on ultimate pressures in accelerators and thermonuclear machines. Data was obtained with a glass volume and attached ionization gauge pumped by an oil diffusion pump with liquid nitrogen trap. A sample tube with its own ionization gauge could be isolated from the main volume by a blanking-off plate containing a central orifice with a conductance of 1 litre/s for nitrogen. The bulk of the gas from the sample and tube is first pumped off with the blanking-off plate withdrawn. This plate is then inserted and the temperature of the sample (a small electric oven is used around the sample tube) cycled in stages for some days until plots of pressure against temperature are repeatable.

An improved system made of stainless steel and glass, the whole of which was bakeable under vacuum (ultimate for clean system: 2×10^{-9} torr), was illustrated. Results were shown for polystyrene and also a series of curves of log pressure against 1000/abs. temp. for a number of materials. Table 4 shows the approximate pressure (equivalent nitrogen) resulting from particular materials in the system, the equation $\log P = A - B/T$ being assumed. These pressures are loosely referred to as vapour pressures; this may not be true as dissociation and outgassing may contribute, but the curves resemble those of a vapour.

Table 4. *Approximate vapour pressures and rates of evaporation of various plastic and similar materials*

Material	*Vapour pressure in torr at 293° K*	*Rate of evaporation Litres μ s^{-1} cm^{-2} at 293° K*	*A*	*B*	*Highest safe temperature (°C)*
Nylon 51	$3{\cdot}0 \times 10^{-8}$	$34{\cdot}95 \times 10^{-5}$	0·89	2470	120
Nylon 31	$1{\cdot}6 \times 10^{-9}$	$18{\cdot}63 \times 10^{-6}$	3·376	3572	120
Nylon B100M	$3{\cdot}7 \times 10^{-8}$	$43{\cdot}1 \times 10^{-5}$	0·318	2273	
Perspex	$1{\cdot}2 \times 10^{-9}$	$14{\cdot}0 \times 10^{-6}$	6·426	4495	90 approx.*
Polyvinyltoluene	$1{\cdot}9 \times 10^{-11}$	$22{\cdot}1 \times 10^{-8}$	17·0	8132	75 approx.†
X-ray film type					
Industrial G	$2{\cdot}2 \times 10^{-8}$	$25{\cdot}6 \times 10^{-5}$	1·684	2739	
Polystyrene	$7{\cdot}6 \times 10^{-11}$	$88{\cdot}5 \times 10^{-8}$	8·066	5334	80
Polythene	$7{\cdot}3 \times 10^{-7}$	$85{\cdot}0 \times 10^{-4}$	−0·93	1527	
Rubber type P.B.60	$1{\cdot}0 \times 10^{-6}$	$11{\cdot}65 \times 10^{-3}$	9·225	4465	
Natural rubber					
J.1260 (AERE 337)	$6{\cdot}3 \times 10^{-8}$	$73{\cdot}4 \times 10^{-5}$	6·575	4041	
P.V.C. (Polyvinylchloride)	$5{\cdot}5 \times 10^{-6}$	64×10^{-8}	1·626	2020	
P.T.F.E.	$1{\cdot}6 \times 10^{-11}$	$18{\cdot}6 \times 10^{-8}$	−2·226	2513	
Mycalex	$2{\cdot}0 \times 10^{-18}$	$23{\cdot}3 \times 10^{-15}$	11·96	8696	400

* Softens at about 100° C.

† Softens at about 80° C.

THE ANALYSIS OF RESIDUAL GASES IN KINETIC VACUUM SYSTEMS

Mr. N. T. GALLAGHER (Leybold Vacuum Sales Ltd., London) first reviewed briefly the principle of the working, construction and advantages of the omegatron as a gas analyser and leak-detector. The Leybold omegatron (E. Leybold's Nachfolger, Cologne) was described in detail with illustrations of the head, the circuit diagram and the pumping system used. Platinum–iridium alloy electrodes were used with advantages of ready degassing (on eddy-current heating to about 900° C) and operation stability. As compared with previous instruments, the Leybold omegatron has a simpler operating circuit with the shield box, ion collector, lower r.f. plate and coaxial shielding cylinder around the lead from the ion collector all at earth potential. A trapping potential of 0·1 to 0·6 V is applied to the shield box walls; its optimum value decreases as the ion mass number increases and is more critical at the higher pressures (T. A. Giorgi, *private communication*).

Illustrations were shown of spectra obtained in the research laboratories of the parent company for (*a*) probe gases with mass numbers in the range from nitrogen (28) to xenon (132); (*b*) Diffelen as the pumping fluid and a baffle temperature of 13° C; (*c*) for various pumping fluids. In relation to (*c*), for Narcoil 40, hydrocarbons of high mass numbers are well represented but these almost disappear if the baffle temperature is reduced to −40° C; the lower baffle temperature has little effect on the line at mass 28 but for the lines corresponding to water and the lighter hydrocarbons, the reduction is by a factor of 2 approximately. The same effect is shown with

Diffelen and Diffelen V. Whereas the line at mass number 148 can be interpreted as due to hydrocarbons with 11 or 12 carbon atoms in the molecule, there is also the possibility for Narcoil 40 that this line is due to phthalic anhydride, $C_6H_4(CO)_2O$ ($m = 148{\cdot}11$). With Diffelen V, hydrocarbons are completely absent at the lower baffle temperature. Even at 13° C, the vapour pressure of Diffelen V is lower than that of Diffelen by a factor of about 3. The spectrum for Apiezon C shows that at 13° C it is preferable to Diffelen V but at −40° C there is little to choose between the two oils. For silicone 703, a range of hydrocarbons of masses 43 to 131 is shown with only a slight reduction at the lower baffle temperature.

The results were surveyed of Reich and Nöller[19] on the use of an omegatron to analyse the residual gases in a system pumped by a small glass titanium getter-ion pump. The system was first evacuated to 10^{-2} torr by a mechanical pump, sealed, and the getter-ion pump operated. In several hours, the pressure dropped to 5×10^{-7} torr. On switching off the ionization, the pressure rose in 16 h to 2×10^{-5} torr. Omegatron analysis then showed small peaks for hydrogen, helium, water and argon and considerably larger peaks in the region of mass numbers 15 to 28, attributed to methane and ethane formed in reactions between hydrogen- and carbon-containing gases on the getter layer. On restarting the ionization, the pressure dropped to 5×10^{-9} torr after several hours and was determined equally by helium, argon and methane. On switching off again, the partial pressure of methane rose again; propane peaks were also identified.

Spectra obtained using a mercury diffusion pump with liquid air trap showed that mercury vapour is almost completely absent, and no hydrocarbons were recorded, a result at variance with those of other workers.[20, 21] The sensitivity of the omegatron was reported to be greater than that of a conventional mass spectrometer and only slightly less than that of the more recent trochoidal mass spectrometer.[22]

Mr. A. O. Edmunds (20th Century Electronics Ltd., Croydon, Surrey) read a short paper entitled "The application of miniature mass spectrometers to leak detection and analysis" in which he described two instruments. The first is a 180° mass spectrometer with an orbit radius of 12·5 mm, developed for helium probing but useful for mass numbers up to 40 and with which it is possible to distinguish between real and virtual leaks by observing water vapour and nitrogen peaks. The complete instrument contains the mass spectrometer head, ionization and Pirani gauges to enable leak detection to be carried out over a wide range of pressures. A loudspeaker is incorporated to give an audio output of variable pitch proportional to the mass spectrometer ion current. For helium, partial pressures of 10^{-11} torr can be measured.

The second instrument is a 180° mass spectrometer with an orbit radius of 11 cm[23] and has cathode-ray tube display, arranged by superimposing a saw-tooth sweep voltage on the ion accelerating voltage and a voltage proportional to this sweep applied to the horizontal plates of the cathode-ray tube, the ion collector voltage pulses being amplified and fed to the vertical plates. The smaller peaks can be additionally amplified and the time base extended so that small sections of the mass spectra may be examined more accurately. A reference pulse of fixed amplitude can also be displayed to allow the relative amplitudes of peaks to be measured by adjusting each in turn to the same height as the reference pulse and noting readings on a calibrated attenuator.

Applications of this second instrument have been (1) to check the isotopic abundance ratios of CO enriched with ^{13}C; (2) checking the concentration of argon in the ^{13}C distillation plant; (3) analysis of residual gases in vacuum furnaces; (4) measurement of efficiency of various types of gas sorption systems, e.g. cooled charcoal, zirconium and titanium.

Mr. B. N. Green (Metropolitan-Vickers Electrical Co. Ltd., Trafford Park, Manchester) described a 180° mass spectrometer of 2 in. radius conceived as an instrument to be built into the vacuum system to be studied (Fig. 8). Ions

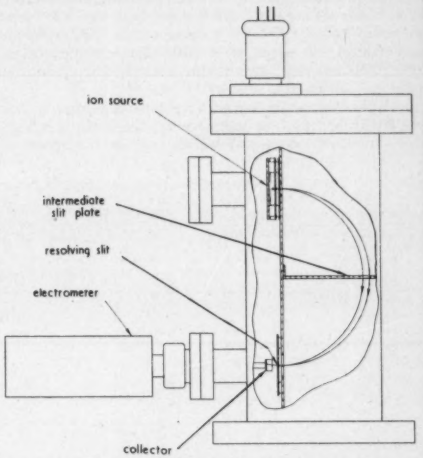

Fig. 8. 2 in. radius 180° mass spectrometer

are produced in the source by a $0{\cdot}005 \times 0{\cdot}04$ in. ribbon of 70 eV electrons directed perpendicular to the diagram and are focused and accelerated by a two-slit lens system. The resolving slit is $0{\cdot}5 \times 0{\cdot}02$ in. and the angle of the divergent beam is limited to 4° by an intermediate slit. The ionization region is made as open as possible, the conductance of the apertures in the ionization region being 6 litre/s. The mass spectrum is voltage scanned (40 to 2000 V, i.e. mass 2 to 100) and the magnetic field of 2000 oersted is provided by a permanent magnet with semi-circular pole-pieces. The mass spectrometer tube is constructed of stainless steel with gold wire (0·02 in. diam.) sealed demountable joints and ceramic-to-metal seals for electrical lead-ins. The resolving power is approximately 50 and the sensitivity to most gases commonly encountered in high vacuum systems is about 3×10^{-5} amp/torr at 50 μA electron current.

The partial pressures of the residual gases is given in Table 5 for a baked kinetic system comprising an oil diffusion pump, liquid nitrogen trap, large metal isolation valve and a small metal gas-metering valve. Only hydrogen, nitrogen and argon are definitely detected. The last two are due, in part, to

Table 5. *Composition of residuql gases at ion gauge pressure of* $7{\cdot}5 \times 10^{-9}$ *torr*

Gas	H_2	H_2O	N_2	CO	O_2	A	CO_2	*hydrocarbons*
Pressure (in 10^{-11} torr)	60	<3	700	<70	<4	25	<3	<3

known air leaks on the ceramic-to-metal seals; oxygen is absent presumably due to reaction with the walls of the freshly baked system. The hydrogen appears to come from the walls of the system above the isolation valve; thermal decomposition of the Apiezon B pump oil does not appear to be a major source of hydrogen, indeed, the hydrogen pressure increases, not decreases, on isolating the diffusion pump.

Dr. N. W. ROBINSON (Mullard Research Laboratories, Salfords, Surrey) pointed out that it is almost impossible to remove entirely the desorption of water vapour from glass even though bake-out is carried out at high temperature for long periods. Improvement can be effected by deposited metallic films to "seal up" the glass surface. Bulbs were constructed with two planar electrodes of various metals about 1 cm apart. One of these tubes was mounted on one inlet to a mass spectrometer and a similar plain glass bulb mounted on a second inlet. Both bulbs were heated to 450° C for an hour and the gas evolution measured at intervals. The bulbs were then cooled. Neon was introduced into the bulb containing electrodes and a thin metallic film sputtered all over the glass. The neon was removed and both bulbs reheated to 450° C and the gas evolution measured. The evolution from the plain glass bulb was diminished in the ratio r and that from the bulb with a sputtered film by the ratio s. The figure of merit of the film was then given as $M = s/r$. The metals could then be placed in the following order: magnesium, molybdenum, aluminium, zirconium, nickel, Fernico, with $M < 1$ and gold and copper with $M > 1$. The first three metals give $M \simeq 0{\cdot}01$ at temperatures up to 450° C. The mechanism seems to be a combination of gettering and sealing by the metal of the glass surface.

The Polytechnic,
Regent Street,
London.

J. YARWOOD

REFERENCES

(1) WAGENER, S. *J. Phys. Chem.*, **60**, p. 567 (1956).
(2) DIVATIA, A. S., DAVIS, R. H., and HERB, R. G. *Phys. Rev.*, **93**, p. 926 (1953).
(3) CLOUD, R. W., BECKMAN, L., and TRUMP, J. G. *Rev. Sci. Instrum.*, **28**, p. 889 (1957).
(4) BECKER, J. A. *See*, for example, *Advances in Catalysis*, **8** (New York: Academic Press Inc., 1955).
(5) GOMER, R. *Second International Conference on Surface Activity*, **2**, p. 236 (London: Butterworths Scientific Publications, 1957).
(6) BLOOMER, R. N. *Brit. J. Appl. Phys.*, **8**, p. 321 (1957).
(7) WAGENER, S. *J. Phys. Chem.*, **61**, p. 267 (1957).
(8) HAINE, M. E., FRANCIS, E. W. R., and BLOOMER, R. N. *Nature* (*London*), **182**, p. 931 (1958).
(9) HOLLAND, L. *J. Sci. Instrum.*, **36**, p. 105 (1959).
(10) HOLLAND, L., and TATE-HARTE, T. To be published.
(11) HERB, R. G., DAVIS, R. H., DIVATIA, A. S., and SAXON, D. *Phys. Rev.*, **89**, p. 897 (1953).
(12) HOLDEN, J. T., HOLLAND, L., and LAURENSON, L. *J. Sci. Instrum.*, **36**, p. 281 (1959).
(13) KLOPFER, A., and ERMRICH, W. *First International Congress on Vacuum Techniques, Namur* 1958 (London: Pergamon Press). To be published.
(14) AMES, I., CHRISTENSEN, R. L., and TEALE, J. *Rev. Sci. Instrum.*, **29**, p. 736 (1958).
(15) JEPSEN, R. L., MERCER, S. L., and CALLAGHAN, M. J. *Rev. Sci. Instrum.* To be published.
(16) CARPENTER, L. G., and MAIR, W. N. *J. Sci. Instrum.*, **34**, p. 110 (1957).
(17) BRUINING, H. *Physics and Applications of Secondary Electron Emission* (London: Pergamon Press, 1954).
(18) COMSA, G., and MUSA, G. *J. Sci. Instrum.*, **34**, p. 291 (1957).
(19) REICH, G., and NÖLLER, H. G. *Fourth National Symposium of Vacuum Technology*, 1957, p. 97 (London: Pergamon Press, 1958).
(20) BLEARS, J. *J. Sci. Instrum., Suppl. No.* 1, p. 36 (1951).
(21) MCNARRY, N. R. *National Research Council of Canada*, Report No. NRC 4259 (December 1956).
(22) KORNELSEN, E. V. *Bulletin of National Research Council of Canada*, **8**, No. 4, p. 1 (1958).
(23) COOKE-YARBOROUGH, E. H., and RUSSELL, M. C. B. *J. Sci. Instrum.*, **30**, p. 474 (1953).

SPECIAL ARTICLE

Dense electron beams

By B. MELTZER, F.Inst.P., Engineering Department, University of Edinburgh

The industrial context of electron beam design is sketched. The theoretical assumptions of classical trajectory behaviour and laminarity are discussed. Langmuir's diode analyses, Pierce's design method and Brillouin's magnetic collimation are described, as well as recent studies of the Pierce–Cauchy problem and self-magnetic effects in simple beams. Summaries are given of the conservation principles of beam dynamics, use of the action function in analysis and design, the position as regards computation, and some recent progress.

The electron device industry would commonly be regarded as one of the most scientific in existence. This is true in the sense that it stems from quite recent brilliant discoveries of physics, but in respect of the methods used in it the claim is not well founded. Those who work in it know well the predominant cut-and-try approach to design, the "engineering formulae" which disagree unsystematically with actual performance but continue to be used, the "black magic" recipes like those for thermionic or photoelectric activation, the neglect—in so-called "research"—of such phenomena appearing in devices as were not bargained for. The reasons for this state of affairs, and its effect on quality and cost of product as well as morale of scientists in the industry, are well worth study, but attention is drawn to it only to provide the backcloth to developments described below.

The nub of any electron device is the electron beam itself, and if one considers a typical one, say that of a cathode-ray tube (see Fig. 1), an important distinction appears. Over most of its length the motion of the electrons is controlled practically entirely by electric or magnetic forces imposed from outside the beam by electrodes, magnets or coils of current. But there are at least three places where forces due

to the beam itself may be dominant or effective. For the strongly focused spot S on the viewing screen is an image of the "cross-over" C, C being a small region of intense concentration of electrons; at S and C effects of electrostatic repulsion of the electrons on each other are to be expected; also near the thermionic cathode K, the concentration of electrons is high because their speeds are low and, in fact, it is the repelling forces they collectively exert at the cathode

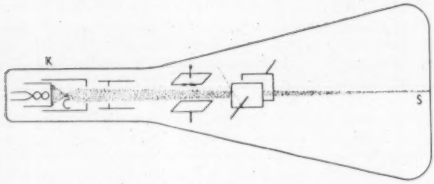

Fig. 1. Dense regions in the electron beam in a cathode-ray tube

K, cathode; C, cross-over; S, focused spot.

which determine what proportion of the thermionically available electrons actually get into the beam. Over part of the beam, then, one is concerned with single-electron dynamics, since as far as each electron is concerned the rest of the beam may just as well be absent; but at these special and important places one is concerned with beam dynamics. Similarly, in other devices, e.g. a high-energy electron accelerator, the magnetic forces between the moving electrons may play a dominant role, although these will usually be attractive rather than repulsive. Since internal forces exist in all beams, the distinction between non-dense and dense beams is a relative and conventional one, but still useful. For instance, most of the highly-developed science of *electron optics*,[1-5] with such marvels to its credit as microscopes of a few Ångströms resolution, is based on single-electron dynamics or the theory of non-dense beams. On the other hand, many of the bad design methods used on electron tubes are ascribable to the illegitimate use of this theory for dense beams. That this is partly recognized in the industry is attested by the frequency with which the failure of a device to give its predicted performance is shrugged away with the comment, "It must be due to space-charge!": a safe one, being usually accompanied by general ignorance of what the effects of the latter are likely to be. The study of dense beams, while far less developed than that of electron optics, has in the last decade or two been much stimulated by the need for highly-concentrated beams in microwave tubes like the klystron and travelling-wave-tube. It is significant that the only English text devoted to the subject[6] is by a scientist prominent in this field.

THEORETICAL ASSUMPTIONS AND REAL BEAMS

It is assumed that the force $\boldsymbol{F}$ acting on an electron has the Lorentz value

$$\boldsymbol{F} = -e(\boldsymbol{E} + \boldsymbol{v} \times \boldsymbol{B}),$$

where $\boldsymbol{E}$ the electric field and $\boldsymbol{B}$ the magnetic flux density satisfy Maxwell's four partial differential equations of the electromagnetic field. (The electric charge of the electron is $-e$ and $\boldsymbol{v}$ is its velocity.) These assumptions combined with Newton's law of motion for ordinary and Einstein's for light-comparable speeds, form the axiomatic basis of high-vacuum beam analysis and design.

Applicability of the theory is therefore limited. If the field varies significantly in a distance comparable with the de Broglie wavelength $\lambda = h/p$ (where h = Planck's constant, and p = momentum of electron) the particle's behaviour cannot be described in trajectory terms at all,[1] but only in terms of a probability wave-function. The electron has inherent angular momentum and magnetic moment,[7] the effects of which are also non-classical. Furthermore, in any electron device there are residual gas molecules with which the beam will interact, and the interaction is described in terms of scattering cross-sections calculable by quantum theory[7] and not of well-determined particle trajectories. Fortunately, in most modern applications, these effects may probably be ignored. It is true that λ sets the limit of resolution in the electron microscope, but generally λ is far too small to upset the trajectory approximation. Apparently, also, electron concentrations would have to be far higher than those in present-day devices before spin and magnetic moment effects would show, and the degree of vacuum attained as a matter of routine is sufficiently high in most cases to justify neglect of gas interactions. Some work[8, 9] has, however, been done on the analysis of these effects in dense beams. Apropos of the quantal effects, it is interesting to note that a usable quantum theory of dense beams has—to the author's knowledge—not yet even been broached.

Most work in this field has, further, assumed that the beam is laminar, i.e. that streams of electrons do not cross each other's paths, in which case a unique velocity vector represents the motion at any point at any time. Most work has also assumed that the force exerted on a single electron by the rest of the beam is the same as if the latter did not consist of discrete particles, but of a continuum of electrically charged matter with charge-to-mass ratio of $-e/m$. The theory based on these additional assumptions will be termed "electron-hydrodynamics". It should therefore not be applied, for example, to the "cross-over" in a cathode-ray tube, if the electrons do really cross over there; it also fails to take into account the effects of single or multiple electron encounters. General theories in which these assumptions are not made have been presented,[10, 11] but have not so far proved usable.

Certainly some of the phenomena encountered in experimental work do not appear to fit in with the laminar continuous fluid picture; phenomena such as hollowness in beams, extremely odd variations of current density across the beam, anomalous velocity distributions, unplanned oscillations and so on. A striking example is the multiple-

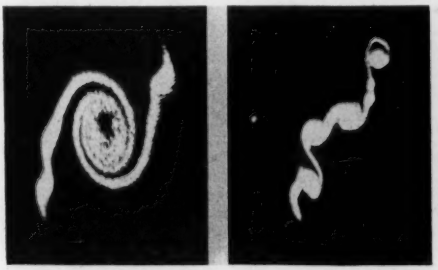

(*a*) (*b*)

Fig. 2. Two examples of observed beam cross-sections (Webster, G. E. Research Lab., Schenectady)

swirl and spiral structures Webster[12] found (see Fig. 2) in a fairly conventionally produced beam. One may therefore ask whether electron-hydrodynamics is worth studying at all. It is, for three reasons: Unless it is studied—and very few cases had been worked out until recently—one will not know whether and when it is applicable. Secondly, it is often technically advantageous for control purposes to have laminar flow. Thirdly, it constitutes—together with hydrodynamics, aerodynamics, magneto-hydrodynamics and other disciplines—one of the most challenging and important fields of applied mathematics: non-linear partial differential equations, the solutions and properties of which—so important in engineering applications—have only begun to be explored.[13]

SOME MAJOR ADVANCES

Langmuir's explanation[14] in 1913 of why the current in a thermionic vacuum diode with metallic cathode does not increase indefinitely with increase of cathode temperature, was the beginning of the subject: there comes a stage at which the extracting field at the cathode due to positive charge on the anode is balanced by the repulsive field due to the electrons in the space between cathode and anode. Merely making more electrons thermionically available at the cathode should not then further increase this *space-charge-limited* current. Neglecting initial velocities and magnetic forces, Langmuir analysed the one-dimensional case of a planar diode; he showed that this current was proportional to the three-halves power of the anode potential—a result generally true[15] for other geometries, too, the constant of proportionality being termed the *perveance*—and that the potential along the beam varies as the four-thirds power of distance from cathode. Langmuir and Blodgett[16, 17] also analysed the one-dimensional cases of cylindrical and spherical diodes, obtaining results by numerical computation because of the difficulty of the differential equations involved. A number of investigators including Langmuir[18] analysed also, for the planar case, the effects of initial electron velocities. The most important is formation of a potential barrier in the beam near the cathode. Although its height is small, of the order of the average thermal energy of the electrons expressed in electron-volts, it was later shown[19] to be of importance in determining the magnitude of current fluctuations or "noise" in electron tubes.

These results were used in the design of the spate of new devices which came out of the electronics industry in the succeeding decades: diodes, triodes, tetrodes, etc., of many different kinds. But the uses made were more often than not illegitimate. "Engineering formulae" proliferated not only in the files of industrial firms but into academic text-books, some—such as those for "cut-off amplification factor" of a triode—having a scientific basis, but others none. It is noteworthy, for example, that the first and only analyses of any triode whatsoever on Langmuir's lines were carried out only very recently.[20, 21] The next important advance came as late as 1940 in Pierce's proposal[22, 23] of a rational method of electron gun design. The principle is illustrated in Fig. 3. Consider Langmuir's space-charge-limited flow of constant current-density and infinite cross-section in a planar diode [Fig. 3(*a*)]. If one selects a slice of this flow and imagines all the electrons outside it removed, this beam would diverge owing to the forces of space-charge repulsion, *unless* one could design an electrostatic field outside the beam which would provide along the boundary of the beam precisely the same electric field that existed there in the infinite diode. In this case one merely needs to provide the correct four-thirds power variation of potential along the boundary. Design is thus reduced to electrostatics: one has to find that solution of Laplace's equation for the potential, $\nabla^2 V = 0$ which reduces to the correct potential at the boundary.

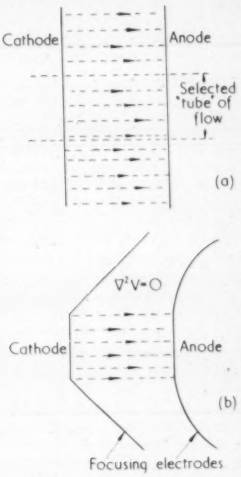

Fig. 3. Principle of Pierce's method of beam design

(*a*) Langmuir flow; (*b*) Pierce beam

Then one selects two equipotentials of this field, such as the zero and anode ones, and shapes electrodes to fit them. An entirely new "look" of electron gun results [see Fig. 3(*b*)]. More important in applications than a collimated beam of this sort is a converging beam: this too can similarly be designed by starting from the Langmuir–Blodgett flow from an outer spherical cathode to an inner concentric anode and carving out of it a conical shaped sector. Such guns are much used in high-powered klystrons, for example. Like other important technical advances, Pierce's method raised many new problems. He had considered only beams with rectilinear trajectories, but when the boundaries are curved the normal derivative of potential on the beam boundary is not zero and must be taken into account. The electrostatics of the electrode design may be worked out by analytic methods,[22, 24–26] analogues like the electrolytic tank[22, 27] or computation.[28, 29] Another problem is the effect of an anode-aperture,[30] which is required to let the beam through for use in applications; it may be large in high-perveance guns. Attention should also be drawn to an empirically found improvement involving an ellipsoidal cathode.[31]

Pierce's idea is of importance because it has laid down—for the foreseeable future—the rational procedure for designing a dense beam. It has so far been applied mainly to electrostatically controlled beams, but this limitation is not inherent.

Another important advance was made by Brillouin[32] in magnetic control. In applications, e.g. travelling-wave-tubes, one may require to keep a beam parallel over a considerable length. Brillouin pointed out that the electrostatic forces of repulsion could, in principle, be exactly balanced by the Lorentz magnetic force due to a parallel magnetic field, provided the electrons had a transverse as well as forward component of speed. When this is achieved the whole beam

advances in rotatory screw-fashion. It turns out that the conservation of angular momentum requires that the cathode source of the beam be magnetically shielded. The method is applicable to hollow as well as "solid" beams. Again a number of new problems arise. How does one best shield the cathode and impart the initial transverse component of velocity to the electrons?[33] Another problem[33] is to account for the fact that Brillouin beams generally require a rather larger magnetic field than the theory predicts. Also further developments of the method[34, 35] have taken place.

SOME SPECIAL ASPECTS

The design of Pierce guns would appear to be a straightforward matter, but there is an inherent instability involved which is interesting. One is concerned with what is known in mathematics as a Cauchy problem.[36] The usual situation in electrostatics, known as the Dirichlet problem, is: given the potential V on a closed surface, find the solution of $\nabla^2 V = 0$ inside. But the Cauchy problem is: given on a surface (*not* closed in general) both V *and* its normal derivative $\partial V/\partial n$, find the solution of $\nabla^2 V = 0$ outside. It can be proved, and is plausible on physical grounds, that the Cauchy problem is in general soluble only in a restricted sense.[25, 36, 37] For example, consider a perfectly conducting plate kept at zero potential, and a number of isolated concentrations of charge distributed in its neighbourhood. These will induce charges on the plate, the charge density at any point on its surface being equal—apart from a constant factor—to the value of $\partial V/\partial n$ there. If now one forgets about how the field was produced, and treat $V = 0$ and these values of $\partial V/\partial n$ as the Cauchy surface data, what solution is one likely to get? The physical potential field one started with obviously does not satisfy $\nabla^2 V = 0$ everywhere outside the plate, since it holds only where no charge is present: in the charged regions $\nabla^2 V = -\rho/\epsilon_0$, ρ being the charge per unit volume and ϵ_0 the permittivity of vacuum. But if these regions are *excluded*, the physical field will be the correct solution.

However, in a region where a solution exists it is an unstable one, in the sense of being extremely sensitive to small changes in the surface data. Take, for example, the two-dimensional Cauchy problem (in ordinary rectangular co-ordinates): On $y = 0$, $V = 0$, $\partial V/\partial y = (1/a)\sin ax$; find V for $y \geqslant 0$. Laplace's equation is

$$(\partial^2 V/\partial x^2) + (\partial^2 V/\partial y^2) + (\partial^2 V/\partial z^2) = 0$$

and it is easily verified that the solution is

$$V = (1/a^2)\sin ax \sinh ay,$$

Now $\sinh ay$ increases far faster than a^2; so if larger and larger values of a are considered, i.e. smaller and smaller values of the surface data, the potential outside the surface shows larger and larger oscillations! When the attempt is made to calculate Pierce electrodes by ordinary finite-difference methods, with or without digital computers,[28, 38, 39] precisely such violent oscillations are found in the results, leading to fantastic electrode shapes. This is an example of breakdown of one of the clichés of physical intuition, so brilliantly discussed by Birkhoff,[13] namely, that "small causes always produce small effects". Further work[26, 40] has shown that the instability may be avoided by using convergent series expansions for the data or by converting the problem into Dirichlet form. From the practical point of view, the instability has its advantages, since it may mean that constructionally simpler shapes of Pierce electrode than the correct ones may be used without greatly affecting the gun performance.

Another unexpected feature of Langmuir and Pierce beams appears when they have high speeds, as in high-power klystrons being developed today.[41] The magnetic attraction between moving electrons increases with increase of speed, hence beam magnetic forces[42–44] need to be considered. Take firstly the infinite planar diode. Let J be the Langmuir uniform current density in it, depending only on the anode potential and distance, and consider any cylindrical tube of flow of radius r in it. Since there is a finite current $\pi r^2 J$ in it, there must—by Ampere's law—be a tangential transverse magnetic field H around it, given by $2\pi rH = \pi r^2 J$, H being constant because of the symmetry. Thus $H = \frac{1}{2}rJ$, and so the magnetic field increases without limit as r is increased! This cannot be so, since a *uniform* beam has been postulated. Thus, even at low speeds, a Langmuir parallel beam is in *principle* impossible. What this means for Pierce guns is that for a given anode potential and distance the electrostatic design is only valid for practical purposes over a certain range of beam radius: for larger beams the magnetic forces would "pinch in" the beam. The higher the speeds, the smaller the range; for speeds not comparable with that of light, the design is valid provided $r/a \ll 6c^2/v^2$, v being the speed at anode, c the speed of light and a the anode-cathode distance. For speeds comparable with that of light, one finds, for instance, that $r/a \ll 5{\cdot}6$ for an anode potential of 511 kV. A further interesting question of principle is this: by a similar use of Ampere's law one can show that the symmetrical radial flow between cylinders or spheres postulated by Langmuir and Blodgett is impossible. An asymmetrical flow would, however, seem to imply that vacuum is not isotropic with regard to electricity; but this is not so, since for the *steady* electric current considered there must be provided a return path, say from the outer to the inner sphere, and this will be the cause of asymmetry. If, however, one has, say, a transient current due to suddenly releasing a uniform spherical shell of electrons at the inner sphere, then the flow *would* be symmetrical: there is now a displacement current which exactly balances the convection current so that the self-magnetic field is zero. One could, in fact, deduce the existence of Maxwell's displacement current as a requirement of the isotropy of vacuum!

ELECTRON-HYDRODYNAMICS AND CONSERVATION PRINCIPLES

Rational beam design is impossible without beam analysis. The rate of change of mechanical momentum of an electron is given by the Lorentz force, so its motion is governed by

$$\frac{d}{dt}\left\{\frac{m\boldsymbol{v}}{(1 - v^2/c^2)^{1/2}}\right\} = -e(\boldsymbol{E} + \boldsymbol{v} \times \boldsymbol{B})$$

For speeds not comparable with the speed of light, this reduces—to high accuracy—to Newton's law

$$m(d/dt)\,\boldsymbol{v} = -e(\boldsymbol{E} + \boldsymbol{v} \times \boldsymbol{B})$$

Furthermore, $\boldsymbol{E}$ and $\boldsymbol{B}$ in the beam are themselves governed by the four laws expressed in Maxwell's equations:

Ampere–Maxwell theorem:	$\text{curl}\,\boldsymbol{B} = (1/c^2)(\partial \boldsymbol{E}/\partial t) + \mu_0 \rho \boldsymbol{v}$
Electromagnetic induction:	$\text{curl}\,\boldsymbol{E} = -\partial \boldsymbol{B}/\partial t$
Gauss's theorem:	$\text{div}\,\boldsymbol{E} = \rho/\epsilon_0$
Gauss's theorem:	$\text{div}\,\boldsymbol{B} = 0$

Here ρ is the charge density, $\rho\boldsymbol{v}$ the current density and $\epsilon_0(\partial E/\partial t)$ the displacement current density (μ_0 is the magnetic permeability of vacuum); $\boldsymbol{E}$ and $\boldsymbol{B}$ can always be derived[45] from an electrostatic scalar potential V and magnetic vector

potential $\boldsymbol{A}$, themselves depending on charge and current distributions respectively, by the relations

$$\boldsymbol{B} = \text{curl } \boldsymbol{A}$$
$$\boldsymbol{E} = -\text{ grad } V - (\partial \boldsymbol{A}/\partial t)$$

From these laws the following conservation principles, useful in beam analysis, can be derived.

Conservation of charge. $\text{div } \rho \boldsymbol{v} + (\partial \rho/\partial t) = 0$.

Conservation of energy. For conservative fields (V and $\boldsymbol{A}$ time-independent), on any electron trajectory,

$$\frac{mc^2}{(1 - v^2/c^2)^{1/2}} - eV = \text{constant}$$

For non-relativistic speeds,

$$\tfrac{1}{2}mv^2 - eV = \text{constant}$$

Lagrange invariant.[46] Consider any closed curve C going through a particular set of electrons in a beam. In the course of the motion, the line-integral

$$\int_c (\boldsymbol{p} - e\boldsymbol{A})d\boldsymbol{l} = \text{constant}$$

where $\boldsymbol{p}$ is the mechanical momentum. A special case is:

Kelvin's circulation theorem[47] of hydrodynamics. For non-relativistic speeds and no magnetic field ($\boldsymbol{A} = 0$)

$$\int_c \boldsymbol{v}\, d\boldsymbol{l} = \text{constant}$$

Busch's theorem[2] is also a special case.

Liouville invariant.[48, 49] This has a useful meaning only for non-laminar flows, in which there is a quasi-continuous *distribution* of velocities at any point. If one considers each beam electron represented by a point in a six-dimensional phase space, of which the co-ordinates are the three position co-ordinates x, y, z and the three corresponding momenta p_x, p_y and p_z, then the volume of this space occupied by the representative points of any particular group of neighbouring electrons

$$\int\int\int\int\int\int dx\, dy\, dz\, dp_x\, dp_y\, dp_z = \text{constant}$$

in the course of the motion.

Some instances of the use made of these principles are the following: The Langmuir[14, 16, 17] calculations were based on the conservation of charge and energy, and Gauss's theorem for $\boldsymbol{E}$, while $\boldsymbol{B}$ was neglected. A good deal of electron optical design[4] is based on the Lagrange invariant, and the theory of axisymmetrical electron lenses,[2] in particular, is based on Busch's theorem. The treatment of the propagation of electromagnetic and "space-charge" waves[50] along beams, in a linear approximation, is usually based directly on Maxwell's equations and Newton's law of motion. Study of the effects[51, 52] of a statistical distribution of initial electron velocities has mainly made use of the Liouville invariant: the absolute limit which cathode temperature sets to the degree of focusing of a dense or non-dense beam was thus determined, for example.

STATIONARY, NON-MAGNETIC, NON-RELATIVISTIC BEAMS

In illustration of typical features, difficulties and possible approaches to the subject of beam analysis, consider now a particular branch of electron-hydrodynamics: the study of stationary (time-independent) beams, having no external and negligible internal magnetic field and non-relativistic speeds: in fact the immediate generalization of the Langmuir theory. Since the velocity is a function of position only, Newton's law of motion can be put in the time-independent form:

$$m(\boldsymbol{v} \,.\, \nabla)\boldsymbol{v} = -e\boldsymbol{E}$$

In addition, it is convenient to take as other basic equations, the conservation of charge

$$\text{div } \rho \boldsymbol{v} = 0$$

Gauss's theorem

$$\text{div } \boldsymbol{E} = \rho/\epsilon_0$$

and

$$\text{curl } \boldsymbol{E} = 0$$

It follows that for $\boldsymbol{v}$ to represent a possible beam

$$\text{div } [\boldsymbol{v} \text{ div } \{(\boldsymbol{v} \,.\, \nabla)\boldsymbol{v}\}] = 0$$

and

$$\text{curl } \{(\boldsymbol{v} \,.\, \nabla)\boldsymbol{v}\} = 0$$

Thus four, non-linear, simultaneous partial differential equations in three unknowns, one of third and three of second order, have to be satisfied! Fortunately, in most applications, a further considerable simplification is possible. The beam issues with assumed zero initial velocities from a cathode of constant potential, hence all electrons have the same energy: beams for which this is the case are known as "normal" beams. For normal beams it can be shown[53] that $(\boldsymbol{v} \,.\, \nabla)\boldsymbol{v} = \text{grad } (\frac{1}{2}\boldsymbol{v}^2)$, hence the vector equation above is automatically satisfied, and one is left with a *single* scalar equation

$$\text{div } \{\boldsymbol{v} \text{ div grad } (\boldsymbol{v}^2)\} = 0$$

which expresses the conservation of charge.

This is still a mathematically formidable entity: a non-linear, third-order partial differential equation in three unknowns.

A further fact, however, is helpful. From Kelvin's circulation theorem it can be shown[54, 55] that a beam with zero initial velocities is irrotational, i.e. $\text{curl } \boldsymbol{v} = 0$. Therefore

$$\boldsymbol{v} = \text{grad } W$$

where W is some scalar function of position, known as the "action function" (the velocity-potential of hydrodynamics). If this be substituted, one finally has a fourth-order non-linear partial differential equation in *one* unknown W.[54] Once a solution has been found, the potential, current density, and trajectories of the beam are given by

$$V = \tfrac{1}{2}(m/e)\boldsymbol{v}^2$$
$$\boldsymbol{J} = -(m\epsilon_0/2e)\boldsymbol{v} \text{ div grad } (\boldsymbol{v}^2)$$
$$dx/v_x = dy/v_y = dz/v_z$$

THE USE OF THE ACTION FUNCTION

In recent years, mostly with the aid of the action function, some new kinds of dense beams have been discussed and analysed, e.g. hyperbolic-path beams,[53] space-charge limited beams between inclined plane cathode and anode,[55, 56] along circular-paths,[24, 26, 57–59] along equiangular spirals,[60] spatially periodic beams,[60] hollow beams,[61] beams from conical cathodes,[62] etc., as well as others referred to above. Proposals have been made on possible uses in connexion with diode tolerances[56] in "slalom" focusing,[24, 60] in circular accelerators,[57] for guns of improved perveance,[62, 63] etc. The methods used for solving the equation for the action function have included separation of variables, the use of special co-ordinate systems and perturbation of known solutions and co-ordinate systems. An example, that of a space-charge-limited circular beam,[24] is shown in Fig. 4, together with its associated Pierce electrodes. It must be admitted that no very powerful *general* analytic method of solution has yet been found.

The action function approach is very suitable in design. Suppose (see Fig. 5) one is looking for a beam of a certain shape with a proposed set of trajectories. The surfaces of constant action will be the surfaces at right angles to the trajectories and—if plotted for constant increments of action—will be most closely packed at the high-energy end of the beam. Now one may introduce a co-ordinate system, one set of co-ordinate surfaces of which coincides with the proposed action surfaces. The action function W would be a function only of this one co-ordinate, say x_1, and the differential equation for it[57] will involve derivatives with respect to x_1 only, though their coefficients may involve the other two co-ordinates x_2 and x_3. If a solution is possible, one has a possible beam; if not, and one had started with a good guess, a first-order perturbation of the action surfaces and co-ordinate system[62] may then make it so. The last step is to design the Pierce electrodes for a finite portion of the beam. In this way, too,[64, 65, 66] a pair of sufficient metric conditions for a possible beam have been found.

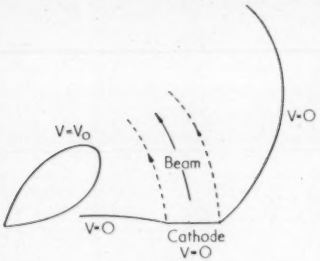

Fig. 4. Pierce electrodes for circular beam (after Lomax)

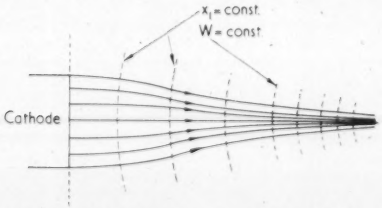

Fig. 5. Action function approach in beam design

Co-ordinate surfaces:

$x_1(x, y, z) = \text{const.}$ action surfaces
$x_2(x, y, z) = \text{const.}$ orthogonal to
$x_3(x, y, z) = \text{const.}$ action surfaces

The converse problem of analysis of the beam in a given electrode structure presents some challenging difficulties. Consider, for instance, a negatively-biased space-charge-limited triode of planar structure shown in Fig. 6. Considered as a boundary-value problem, it cannot have a single solution in terms of analytic functions. For it is a property of analytic functions, which include most of the functions commonly used in engineering and physics, like algebraic, trigonometrical or Bessel functions, that if they are zero over a finite region they are zero everywhere. Now the current density, for example, must be zero between the zero equipotential and the modulator, therefore if it were an analytic function of position it would be zero in the beam too, which is absurd. A possible approach may be to work with more general classes of functions, e.g. functions not completely regular like analytic functions, but with certain degrees of regularity, as discussed by Hadamard.[36] The question of how one defines the action function *outside* a beam is a subtle and interesting one too.[46, 67]

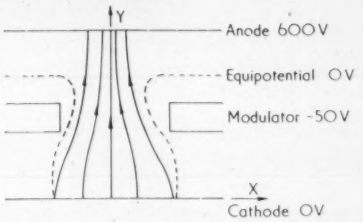

Fig. 6. Beam analysis of space-charge-limited triode

THE USE OF COMPUTERS

During the last war, magnetron problems stimulated Hartree and his co-workers to apply their method of the self-consistent field, so successful in the calculation of atomic wave functions,[68] to dense beams. In this method, applied say to the triode problem discussed above, one would first make some guess at the potential V, then calculate the trajectories in this field, find the resulting distribution of charge ρ, and find a new potential field V satisfying Poisson's equation $\nabla^2 V = -\rho/\epsilon_0$. The new V is now used and this computing process is iterated until the change of field in successive steps is negligible. The method appears to be very slowly convergent and not many solutions were obtained.

Fig. 7. Network analogue units

(*a*) Potential network

$$\frac{V_1 - V_0}{R} + \frac{V_2 - V_0}{R} + \frac{V_3 - V_0}{R} + \frac{V_4 - V_0}{R} + \frac{\rho_0 h^2}{K\epsilon_0 R} = 0$$

where injected current $I_0 = \rho_0 h^2/K\epsilon_0 R$.

(*b*) Action network

$$\frac{W_1 - W_0}{1/(\rho_1 + \rho_0)} + \frac{W_2 - W_0}{1/(\rho_2 + \rho_0)} + \frac{W_3 - W_0}{1/(\rho_3 + \rho_0)} + \frac{W_4 - W_0}{1/(\rho_4 + \rho_0)} = 0$$

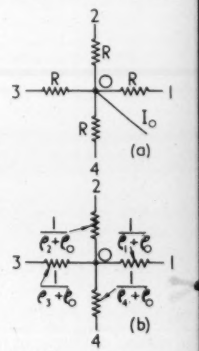

A similar method,[69] using an electrolytic tank with floor of variable shape to solve Poisson's equation, and other electrolytic tank methods[70, 71] have been proposed. It may be that calculating the action function rather than the trajectories may speed the convergence. This might be achieved[72] by using two network analogues,[73] one for solving Poisson's equation for the potential V, and the other for finding the action function W. In the two-dimensional case (see Fig. 7), for example, the governing equations are

$$\frac{\partial^2 V}{\partial x^2} + \frac{\partial^2 V}{\partial y^2} = -\rho/\epsilon_0$$

$$\frac{\partial}{\partial x}\left(\rho\frac{\partial W}{\partial x}\right) + \frac{\partial}{\partial y}\left(\rho\frac{\partial W}{\partial y}\right) = 0$$

while action and potential are connected by the energy relation

$$V = m/2e\,(\text{grad } W)^2$$

Digital computers should eventually prove the most useful aid, but—in this country at any rate—they are still rather too limited in respect of both storage capacity and speed,[74] to deal easily, by the iterative methods today available, with multi-dimensional problems. As ancillaries in other methods they can, of course, be very helpful already, but it is probable that their general usefulness will advance only hand in hand with the mathematical development of this subject.

REFERENCES

(1) DE BROGLIE, L. *Optique electronique et corpusculaire* (Paris: Herrman, 1950).
(2) COSLETT, V. E. *Introduction to electron optics* (Oxford: Clarendon Press, 1946).
(3) KLEMPERER, O. *Electron optics* (Cambridge: Cambridge University Press, 1953).
(4) STURROCK, P. A. *Static and dynamic electron optics* (Cambridge: Cambridge University Press, 1955).
(5) GLASER, W. *Grundlagen der Elektronenoptik* (Vienna: Springer Verlag, 1952).
(6) PIERCE, J. R. *Theory and design of electron beams* (New York: D. Van Nostrand Co. Inc., 1949).
(7) SCHIFF, L. I. *Quantum mechanics* (New York: McGraw-Hill Book Co., 1949).
(8) BARFORD, N. C. *J. Electronics and Control*, **3**, p. 63 (1957).
(9) SENISE, J. T. *J. Appl. Phys.*, **29**, p. 839 (1958).
(10) BUTCHER, P. N. *Phil. Mag.*, **44**, p. 971 (1953).
(11) GABOR, D. Unpublished lectures.
(12) WEBSTER, H. F. *J. Appl. Phys.*, **28**, p. 1388 (1957).
(13) BIRKHOFF, G. *Hydrodynamics* (New York: Dover Publications Inc., 1955).
(14) LANGMUIR, I. *Phys. Rev.*, **2**, p. 450 (1913).
(15) IVEY, H. F. *Advances in Electronics*, **6**, p. 137 (New York: Academic Press Inc., 1954).
(16) LANGMUIR, I., and BLODGETT, K. B. *Phys. Rev.*, **22**, p. 347 (1923).
(17) LANGMUIR, I., and BLODGETT, K. B. *Phys. Rev.*, **24**, p. 49 (1924).
(18) LANGMUIR, I. *Phys. Rev.*, **21**, p. 419 (1923).
(19) NORTH, D. O., HARRIS, W. A., and THOMSON, B. J. *R.C.A. Rev.*, **3**, p. 463 (1940).
(20) BUNEMAN, O. Unpublished work.
(21) STUART, G. A., and MELTZER, B. *J. Electronics and Control*, **3**, p. 51 (1957).
(22) PIERCE, J. R. *J. Appl. Phys.*, **11**, p. 548 (1940).
(23) FIELD, L. *Rev. Mod. Phys.*, **18**, p. 353 (1946).
(24) LOMAX, R. J. *J. Electronics and Control*, **3**, p. 367 (1957).
(25) KIRSTEIN, P. T. *Proc. Inst. Radio Engrs*, **46**, p. 1716 (1958).
(26) RADLEY, D. E. *J. Electronics and Control*, **4**, p. 125 (1958).
(27) COOK, E. J. *Proc. Inst. Radio Engrs*, **46**, p. 497 (1958).
(28) BREWER, G. R. *J. Appl. Phys.*, **28**, p. 634 (1957).
(29) SUGAI, I. *Proc. Inst. Radio Engrs*, **47**, p. 87 (1959).
(30) STUART, G. A., and MELTZER, B. *Proc. Instn Elect. Engrs*, *B*, **105**, p. 928 (1959).
(31) HEIL, O., and EBERS, J. J. *Proc. Inst. Radio Engrs*, **38**, p. 645 (1950).
(32) BRILLOUIN, L. *Phys. Rev.*, **67**, p. 260 (1945).
(33) SÜSSKIND, C. *Advances in Electronics*, **8**, p. 363 (New York: Academic Press Inc., 1956).
(34) WANG, C. C. *Proc. Inst. Radio Engrs*, **38**, p. 135 (1950).
(35) HARRIS, L. A. *Proc. Inst. Radio Engrs*, **40**, p. 700 (1952).
(36) HADAMARD, J. *Lectures on Cauchy's problem in linear partial differential equations* (New York: Dover Publications Inc., 1952).
(37) KIRSTEIN, P. T. *J. Electronics and Control*, **5**, p. 163 (1958).
(38) HECHTEL, R. *Telefunken Ztg*, **28**, p. 222 (1955).
(39) BERZ, F. *Phil. Mag.*, **41**, p. 209 (1950).
(40) BORRIE, J. A., and MELTZER, B. Unpublished work.
(41) CHODOROW, M., GINZTON, E. L., NEILSEN, I. R., and SONKIN, S. *Proc. Inst. Radio Engrs*, **41**, p. 1584 (1953).
(42) MELTZER, B. *J. Electronics and Control*, **4**, p. 350 (1958).
(43) MELTZER, B. *Nature* (*London*), **181**, p. 1332 (1958).
(44) LUCAS, A. R. *J. Electronics and Control*, **5**, p. 245 (1958).
(45) STRATTON, J. A. *Electromagnetic theory* (New York: McGraw-Hill Book Co., 1941).
(46) GABOR, D. *Proc. Inst. Radio Engrs*, **33**, p. 792 (1945).
(47) MILNE-THOMSON, L. M. *Theoretical hydrodynamics* (London: MacMillan and Co. Ltd., 1949).
(48) FOWLER, R. H. *Statistical mechanics* (Cambridge: Cambridge University Press, 1936).
(49) KHINCHIN, A. I. *Statistical mechanics* (New York: Dover Publications Inc., 1949).
(50) BECK, A. W. *Space-charge waves* (London: Pergamon Press Ltd., 1958).
(51) PIERCE, J. R. *J. Appl. Phys.*, **10**, p. 715 (1939).
(52) MELTZER, B. *J. Electronics and Control*, **3**, p. 355 (1957).
(53) MELTZER, B. *Proc. Phys. Soc.* (*London*) *B*, **62**, pp. 431, 813 (1949).
(54) SPANGENBERG, K. *J. Franklin Inst.*, **232**, p. 365 (1941).
(55) WALKER, G. B. *Proc. Phys. Soc.* (*London*) *B*, **63**, p. 1017 (1950).
(56) IVEY, H. F. *J. Appl. Phys.*, **23**, p. 240 (1952); **24**, p. 227 (1953).
(57) MELTZER, B. *J. Electronics*, **2**, p. 118 (1956).
(58) MAYO, B. J. Unpublished work.
(59) WATERS, W. E. *J. Appl. Phys.*, **30**, p. 368 (1959).
(60) KIRSTEIN, P. T. *J. Electronics and Control*, **4**, p. 425 (1958).
(61) KIRSTEIN, P. T. *J. Electronics and Control*, **5**, p. 33 (1958).
(62) KIRSTEIN, P. T. Unpublished work.
(63) WATERS, W. E. Unpublished work.
(64) LUCAS, A. R., MELTZER, B., and STUART, G. A. *J. Electronics and Control*, **4**, p. 160 (1958).
(65) MELTZER, B., and LUCAS, A. R. *J. Electronics and Control*, **4**, p. 454 (1958).
(66) KIRSTEIN, P. T. *J. Electronics and Control*, **4**, p. 457 (1958).
(67) LUCAS, A. R. Unpublished work.
(68) SEITZ, F. *The modern theory of solids* (New York: McGraw-Hill Book Co., 1940).
(69) MUSSON-GENON, R. *Onde Elect.*, **28**, p. 236 (1948).
(70) DAVIES, D. H., and SANDER, K. F. *J. Electronics and Control*, **5**, p. 114 (1958).
(71) PICQUENDAR, J. E., CAHEN, O., and LAPOSTOLLE, P. *Les effects de la charge d'espace dans les canons a electrons* (Paris: Compagnie Francais de Thomas Houston, 1956).
(72) LUCAS, A. R. *Postgraduate Diploma Thesis E.D.R.* 33 (University of Edinburgh, 1956).
(73) LIEBMANN, G. *Advances in Electronics*, **2**, p. 101 (New York: Academic Press Inc., 1950).
(74) MELTZER, B., and BROWN, I. F. *Nature* (*London*), **181**, p. 1384 (1958).

Bulb breaking correction for heats of wetting determinations

By R. C. GALLAVAN, Rothamsted Experimental Station, Harpenden, Herts

[*Paper first received* 13 *March, and in final form* 1 *June*, 1959]

Some factors affecting the heat generated when an evacuated glass bulb is broken in water at 25° C have been studied using a calorimeter of high sensitivity. The importance of the gaseous content of the water in the calorimeter is illustrated by deliberate variation of the carbon dioxide content. By careful control of factors discussed, heats of breaking have been measured that are reproducible to $\pm 0{\cdot}005$ J of the mean value.

INTRODUCTION

In heat of wetting experiments where the observed heat is less than a Joule, the bulb breaking correction becomes very important, and following the work of others an effort was made to obtain much smaller variations in bulb breaking heats. A method has now been evolved for obtaining heats which are reproducible to $\pm 0{\cdot}005$ J of the mean value for evacuated glass bulbs broken in water. It is particularly suitable for "absolute" surface area measurements using the method described by Harkins and Jura,[1] and for the heat of wetting of materials that do not need to be highly dispersed to obtain rapid wetting.

When an evacuated bulb is shattered in water the observed heat is the result of several superimposed effects. Some of these have been discussed by other workers in the light of their experimental requirements. Heats of $0{\cdot}3 \pm 0{\cdot}1$ J were reported by Zettlemoyer and others[2] for their blank bulbs. Bartell and Suggitt[3] carried out a number of experiments using evacuated bulbs having an average volume of 17·2 ml. These bulbs gave high heats, 3·05 J, with rather poor reproducibility $\pm 0{\cdot}29$ J. Guderjahn and others[4] were able to show by experiments with evacuated bulbs of varying volumes that most of the observed heat was due to the pressure-volume effect if the glass bulbs were well annealed. The heats they measured had a mean deviation of $\pm 0{\cdot}07$ J. It was interesting to note that when using metal bulbs with foil end-windows they still observed variations from the pressure-volume effect. This tended to indicate some effect other than varying stresses and breaking energy associated with glass bulbs. A large number of experiments in this laboratory showed heats of $0{\cdot}25 \pm 0{\cdot}05$ J for evacuated bulbs of 3 ml. volume that were shattered in water at 25° C. There were, however, occasional heats as high as 0·44 J and as low as 0·15 J and the object of this work was to explain these results and if possible develop a method whereby reproducible heats with a closer tolerance could be measured.

APPARATUS

The calorimeter used for this work has been previously described in detail by Greene-Kelly and Gallavan.[5] A simple modification was made to the breaker mechanism to take the new type of bulb stem shown in the figure. To measure the small heats evolved, it was necessary to increase the sensitivity of the apparatus from 3·5 cm/J to 13·0 cm/J. This was done by incorporating a Tinsley photocell galvanometer amplifier in the bridge circuit. The stability of the circuit was maintained by reducing the current through the thermistor.

The bulbs used for all the experiments were of commercial mould-blown lead glass (annealed) having a volume of approximately 3 ml. and stems of 7 mm diameter tube with 1 mm wall thickness. The stems were supplied 2·5 cm long for sealing the bulbs on to the vacuum apparatus. All the bulbs were evacuated to less than 10^{-3} mm Hg unless otherwise stated.

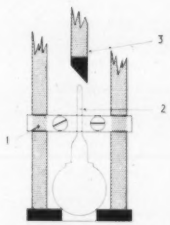

Modification to the original breaking mechanism of the micro-calorimeter[5] to hold the new type of bulb and to break its stem only

(1) Perspex half clamp gripping Tufnol rods and holding the bulb stem;

(2) Scratch, made with a glass knife before loading into the calorimeter;

(3) Tufnol rod with polished brass end at an angle of 45°. The thumb-screw of the original breaker was dispensed with as a light pressure on top of the rod was sufficient to break the thin bulb stem at the scratch.

RESULTS

The occasional high heats that had been observed in the earlier experiments were thought to be due to the unpredictable energy required to shatter the bulbs, and the varying strain energy released from the glass on being shattered. To eliminate or reduce these effects the stems of the bulbs were drawn out as shown in the figure. In this way it was possible to break the stems, where they were scratched with a glass knife, with the minimum of energy and leave the bulbs intact. Bulbs that were sealed at atmospheric pressure at about 60% relative humidity gave no detectable heat of breaking even when the stems were deliberately thickened and no scratch was made to help the fracture.

Experiments were then carried out on a number of evacuated bulbs. Occasional high heats were no longer observed and it was concluded that the shattering of the glass (which had given a heat of approximately 0·15 J[5] in previous experiments) was an unsuitable method for obtaining results of very close tolerance. Varying the capillary bore of the bulb stem from 1·5 to 0·5 mm had no measurable effect on the heat evolved by evacuated bulbs.

To investigate the cause of the occasional low heats it was necessary to observe the effect of breaking an evacuated bulb in the calorimeter and to do this a beaker was substituted for the Dewar flask. When the bulbs were shattered many small bubbles were formed and escaped from the water. When the stems were broken by the new method the bubbles were sucked into the bulb and remained entrapped. These bubbles were thought to be gas removed from the water by the sudden pressure change when the stem was broken. Using carbon dioxide to vary the gaseous content of the water it was possible to alter the bubble volume considerably. Water saturated with carbon dioxide (pH 4·1) gave a bubble of 0·5 ml., equivalent to a negative heat of −0·44 J as calculated from heat of solution of carbon dioxide published by Bichowsky and Rossini.[6] This large heat was not observed experimentally, however, as even when the water was loaded at pH 4·1 it had to be stirred in the calorimeter for about 18 h before temperature equilibrium conditions were reached that were suitable for the experiment. The value obtained for such an experiment was +0·07 J which, allowing for an estimated pressure-volume value of +0·32 J was approximately −0·25 J for the heat of desolution of the gas in the bubble (estimated bubble size 0·26 ml.). Successive daily determinations showed that the same water required several days to attain a point where a reproducible heat of breaking value could be obtained. When this value was obtained, the results were reproducible at 0·235 ± 0·005 J. The volumes of the bubbles determined in the bulbs at this stage were 0·16 ml. and gave a value of −0·09 J for the de-solution of the gas. The value calculated from the published data[6] is −0·14 J which is of the same order.

In heat of wetting experiments it is usually necessary to change the water in the calorimeter for each run. It was apparent from the experimental results that the gaseous composition of the water must be reproducible. The pH values of distilled water from various sources in the laboratory varied from 4·1 to 5·6 according to the time elapsed since distillation, and the laboratory environment. This variation could not be tolerated nor was it convenient to wait for the water to reach the condition where it gave the heat of breaking value of 0·235 J. Therefore 6 l. of freshly distilled water was stirred in a large aspirator, in the same room, and with the same contact with the atmosphere as the water had in the calorimeter. This water reached a pH value of between 5·6 and 6·1 after several days and was sufficient for about 20 experiments. Heat of breaking experiments gave a reproducible value of 0·205 ± 0·005 J when this water was changed for each experiment. If the water was not changed this value continued to rise until it reached 0·235 J, the pH then being 6·4.

It should be emphasized at this point that the water in the calorimeter should always be at equilibrium with atmospheric pressure. This was illustrated when large negative heats of breaking were observed in some earlier experiments after modifications to the calorimeter. The use of a new type of cement for sealing the thermistor and the heater leads had led to the calorimeter being virtually sealed from the atmosphere except for a variable leakage through the oil film on the stirrer shaft and breaker rod. The observed heats of breaking which were as low as −0·30 J were then due to a pressure-volume effect *and* a negative heat due to the evaporation of water when the bulb was broken. To overcome this difficulty a small hole was drilled in the calorimeter cover to provide a fixed leak by way of the chamber above it to atmospheric pressure. Care was taken to ensure that the air sucked into the calorimeter at 25° C was saturated with water vapour. Guderjahn and others[4] were able to maintain pressure equilibrium by leakage down the stirrer shaft and so did not experience this trouble.

To check the effect of different bulb volumes, bulbs were filled with different amounts of Ceresin Wax and then evacuated. Heat of breaking varied in proportion to the weight of water taken into the bulb if a correction was applied for the heat of wetting of the Ceresin Wax. This was determined by nearly filling a bulb with Ceresin Wax, evacuating it and then saturating it with water vapour. The observed heat of breaking was +0·08 J which, after applying a correction for the water taken into the bulb, and the heat of condensation of the water vapour, was evaluated as 0·011 J/gm of Ceresin Wax. The calculated value for a 3 ml. bulb full of water vapour was the sum of the observed heat of breaking of an evacuated bulb and the heat of condensation of the water vapour, i.e. 0·23 + 0·17 = 0·40 J. The experimentally determined heat of 0·36 J was in fairly good agreement.

No allowance has been made in this work for the effects of other gases in the water. Evacuated bulbs broken in water that had been aerated overnight contained very small bubbles and gave a heat of breaking of 0·31 J. Evacuated bulbs broken in water enriched overnight with nitrogen contained very small bubbles and gave a heat of breaking of 0·25 J. These values are of the order expected from water having a very low carbon dioxide content.

ACKNOWLEDGEMENT

This work was a part of a programme of work on the surface properties of clay minerals under the direction of Dr. R. Greene-Kelly to whom the author is indebted for advice and guidance.

REFERENCES

(1) HARKINS, W. D., and JURA, G. *J. Amer. Chem. Soc.*, **66**, pp. 919, 1362 (1944).

(2) ZETTLEMOYER, A. C., YOUNG, G. J., CHESSICK, J. J., and HEALEY, F. H. *J. Phys. Chem.*, **57**, p. 649 (1953).

(3) BARTELL, F. E., and SUGGITT, R. M. *J. Phys. Chem.*, **58**, p. 36 (1954).

(4) GUDERJAHN, C. A., PAYNTER, D. A., BERGHAUSEN, P. E., and GOOD, R. J. *J. Chem. Phys.*, **28**, p. 520 (1958).

(5) GREENE-KELLY, R., and GALLAVAN, R. C. *Clay Min. Bull.*, **3**, p. 167 (1957).

(6) BICHOWSKY, F. R., and ROSSINI, F. D. *Thermo-Chemistry of Chemical Substances* (New York: Reinhold Publishing Corp., 1936).

Application of delayed feedback in electronic circuits

By Zs. NÁRAY, Department of Physics, The University of Zürich, Switzerland*

[*Paper first received* 13 *February, and in final form* 1 *April*, 1959]

By the use of suitable delayed feedback (d.f.b.) from the output terminals of a four- (or two-) pole network to the input, a great variety of different signals can be generated, the shape of which is determined by the characteristics of the four- (or two-) pole network, the d.f.b. loop and, under certain conditions, by the shape and duration of the trigger signal which is needed to set the d.f.b. system in operation. Two simple applications of delayed feedback in electronic circuits (where the loop gain is real and equal to or less than unity) are given:

(*a*) The output of a phase-inverting amplifier (amplification, $-g$) is fed by a delay line (delay time τ) to the input of the amplifier. If $|g|v \simeq 1$ (where v is the loss in the d.f.b. loop), periodic signals of frequency $f \simeq 1/2\tau$ are generated.

(*b*) If, in the same arrangement as (*a*), $|g|v < 1$, an output signal is produced only if a trigger signal is fed into the d.f.b. loop; that is, the circuit works as a triggered oscillator of frequency $f \simeq 1/2\tau$. Because of mixing (additive or multiplicative) between the trigger signal of duration T and the d.f.b. signal, the shape of the output signal depends on the value T/τ.

By investigation of the output signal with a frequency meter or oscilloscope, the delay time of an unknown element (e.g., delay line amplifier) connected in the feedback loop can be measured. The d.f.b. oscillators have a frequency stability of about 10^{-5}/h.

GENERAL DELAYED FEEDBACK CIRCUIT

By connecting the output terminals of a four-pole or two-pole network P (which generally can be active or passive, and electrical, electronic, mechanical, etc.) by means of a delay element D (delay time τ), amplifier A (gain g), forming element F, and mixer M to the input terminals (see Fig. 1), signals with a shape determined by the characteristics of the delayed-feedback (d.f.b.) loop can be generated. A part

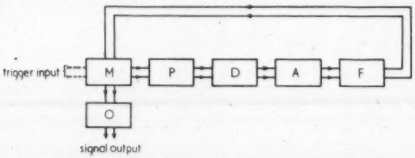

Fig. 1. Block diagram of a delayed feedback loop

M, mixer; *P*, 4-pole network; *D*, delay element; *A*, amplifier; *F*, forming element; *O*, output element.

The output of the element *P* is connected to the input by means of the elements *D*, *A*, *F* and *M*. Part of the d.f.b. signal can be taken at the output element *O*.

of this d.f.b. signal appears on the output element O, which, depending on the actual circuit, is connected either to the mixer M or to another suitable point of the d.f.b. loop. The role of the elements D, A, M and O is obvious. It should be mentioned that in the following it is assumed that these elements have ideal characteristics (that is, the amplifier has an infinite band width, etc.). The forming network can serve, if needed, to alter the shape or duration of the feedback signal. If such forming is not needed, F can compensate for the deviations from the ideal of the elements D, A, M and O mentioned above, which occur in practice. Under certain circumstances (for example, if the product of the gain g and total loss v in the closed d.f.b. loop is $|g|v < 1$) the d.f.b. system works only if a trigger signal is fed into the closed loop. This can be achieved, for example, by feeding the trigger signal to the mixer M. In this case, the trigger pulse sets the d.f.b. system into operation for a time given by the characteristics of d.f.b. loop and the trigger signal itself.

In the simplest cases (that is, when the conditions given below hold), the d.f.b. signal can be characterized by the three quantities, G, τ and T. The conditions are: the characteristics of the d.f.b. loop can be considered ideal; P is linear; the mode of mixing given; and the trigger pulse is a square wave of duration T, starting at $t = 0$. If additive mixing is used, the d.f.b. signal is given by:

$$E(t) = E_0 \sum_{n=0}^{\infty} G^n\{u[t - n\tau] - u[t - (T + n\tau)]\}. \quad (1)$$

where u denotes the unit step function

$$u[x] = 1, \quad \text{if} \quad x \geqslant 0, \qquad \text{and}$$
$$u[x] = 0, \quad \text{if} \quad x < 0.$$

$G = gv$ is the resulting gain in the closed d.f.b. loop and E_0 is the amplitude of the trigger pulse. With multiplicative mixing, the expression corresponding to (1) is:

$$E(t) = E_0 \prod_{n=0}^{\infty} G^n\{u[t - n\tau] - u[t - (T + n\tau)]\}.$$

It will be shown later that, by choosing suitable feedback loops, the form of the d.f.b. signal can be made very different even in the simplest case described by equation (1). A detailed analysis[3] shows that, in the general case of synthesizing a system from N circuits of the form represented in Fig. 1 completed by gates and programme elements which, according to a given programme, set the individual d.f.b. circuits in operation, a great variety of output signals can be generated.

As can be seen from the previous sections, a general d.f.b. circuit may serve first of all as a generator of complicated functions (for example, for computers). The present paper does not deal with this general aspect and restricts itself to giving some applications of the simplest form of delayed feedback—inasmuch as it treats only circuits in which the loop gain G is real and $|G| \leqslant 1$ and the output signals of which can be described by equation (1)—for use in the field of electronic measuring technique. The applications treated are:

(i) an oscillator for production of periodic signals,
(ii) a triggered oscillator.

* On leave from the Central Research Institute of Physics of the Hungarian Academy of Sciences, Budapest.

GENERATION OF PERIODIC SIGNALS

If, in the block diagram of Fig. 1, the element P is itself a phase-inverting amplifier (amplification, $-g$), the element A can be neglected. Such a simplified d.f.b. loop can be realized by the circuit shown in Fig. 2, which consists of a

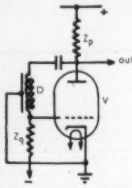

Fig. 2. D.F.B. oscillator for generating periodic signals

The frequency is given by $f \simeq 1/2\tau$, where τ is the delay time of the delay element D.

vacuum-valve amplifier (in the figure, simply an amplifier valve, V) and a cable or delay line D, feeding the output signal of the amplifier back to the input. The mixing element is the grid impedance Z_g, which can also serve as matching impedance for the delay element while matching at the other end of the delay element can be provided by the load impedance Z_p. If the gain of the amplifier valve is adjusted, by means of the screen grid potential, for example, so that

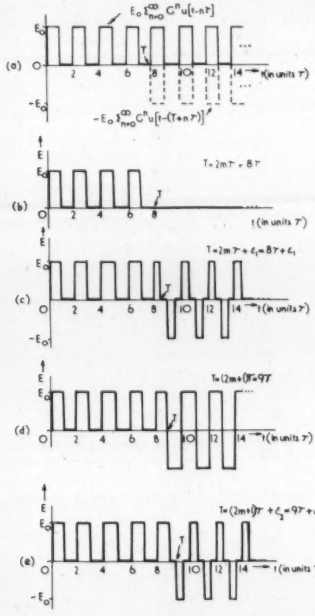

Fig. 3. Determination of the d.f.b. signal by equation (1) if $G = -1$

Curve (*a*) is a representation of the two sums of equation (1), assuming that $T = 2m\tau$ (m an integer). The d.f.b. signals for $T = 2m\tau$, $T = 2m\tau + \epsilon_1$, $T = (2m+1)\tau$ and $T = (2m+1)\tau + \epsilon_2$ are represented by the graphs (*b*), (*c*), (*d*) and (*e*) respectively.

$|g|v \gtrsim 1$, the circuit furnishes at the output a periodic signal of frequency $\simeq 1/2\tau$. As the characteristic impedance Z_0 of cables and delay lines of usual design is generally less than 1 kΩ (even with high specific delay) the output impedance of the anode (or grid) circuit is low.

For the explanation of the operation of the circuit of Fig. 1, it is useful to determine the output signal by means of equation (1), by setting $G = -1$ and by assuming for the moment that the operation of the circuit is started by a square-wave trigger pulse of duration T. In Fig. 3, some output signals calculated from equation (1) are shown. In Fig. 3(*a*), on the assumption that $T = 2m\tau$ (where m is an integer), the two sums of equation (1) are separately represented, the first sum by a full-line curve, the second by a dotted-line curve. The difference E of the two sums—which is really the d.f.b. signal—is shown in Fig. 3(*b*). Figs. 3(*c*), 3(*d*) and 3(*e*) show the output signal for $T = 2m\tau + \epsilon_1$, $T = (2m+1)\tau$ and $T = (2m+1)\tau + \epsilon_2$, respectively, where $0 < \epsilon_1 < \tau$ and $0 < \epsilon_2 < \tau$. If the case represented in Fig. 3(*b*) is neglected, it can be seen that the frequency* of the periodic output signal is always the same, namely $1/2\tau$, but the shape depends very much on the duration of the trigger pulse. The output signal shows, in the region $0 < t < T$, a transient form (which can be used for function generation) and then turns into a periodic time function.

In the real circuit shown in Fig. 2, no external trigger pulse is needed to set the circuit in operation because instability in the anode current produces such triggering (which reaches the grid after a time τ, and gives rise to an anode signal of opposite sign) across the load. As the oscillator shown in Fig. 2 uses a passive delay element for feeding the output signal back in correct phase to the input of the phase-inverting amplifier, it can be regarded as a form of phase-shift oscillator.[1, 2] It should be mentioned, however, that because of the use of a delay line as phase-shift element, the required gain of the amplifier is considerably less than in the usual phase-shift oscillator, where a gain of about 30 is needed. An arrangement using an artificial transmission line as delay element is shown by Stewart.[4]

Furthermore, if a continuous sequence of output signals is used in Fig. 2, the assumptions used in deriving equation (1) are no longer justified, because each pulse of the d.f.b. signal passes through the amplifier and delay line an infinite number of times. Even with elements of wide band width, the output signal deviates from that shown in Fig. 3 and approaches more or less a sinusoidal signal with the frequency $1/2\tau$, the amplitude of which is given by the real characteristics of the d.f.b. loop and the nonlinearities of the system or, otherwise, by the forming element F. In Fig. 4, an oscillogram of the

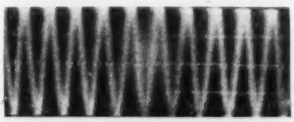

Fig. 4. Oscillogram of an output signal of a d.f.b. oscillator

$f = 50$ Mc/s. The delay element is a cable, type RG7/U 240 cm long.

output signal of a 50 Mc/s d.f.b. oscillator is given in which cable of the type RG7/U is used as delay element.

* If the signal is not sinusoidal, f denotes the fundamental frequency.

Advantage can be taken of the fact that the shape of the output signal depends on the value T/τ if, for example, the d.f.b. loop is interrupted by means of a gate until an external trigger pulse is applied. If the trigger pulse with a duration corresponding to the shape wanted is applied and the gate in the d.f.b. loop is closed at the same time, a periodic signal of given shape is produced.

It must be mentioned that the simple expression for the frequency ($f = 1/2\tau$) is valid only if $\tau \gg \tau_0$, that is, if the delay in the delay element is long compared with the transit time τ_0 in the elements A, F and M and/or the anode or grid time constant. This condition is generally satisfied up to frequencies of about 10 Mc/s. At higher frequencies, the influence of the time constants and the transit time on the frequency of the output signal can be simply taken into consideration. Fig. 5 shows the variation of delay time and frequency with the length l of a cable, type RG65/U. The propagation velocity of electromagnetic waves in the cable can be calculated by the expression $c' = l/\tau = 2lf$.

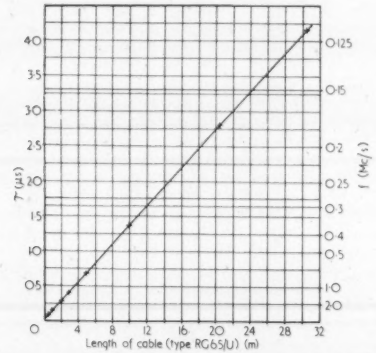

Fig. 5. Frequency of a d.f.b. oscillator plotted against length of cable, type RG65/U, used as delay element

The calculated propagation velocity of electromagnetic waves in the cable is $c' = 7{\cdot}2 \cdot 10^8$ cm/s from the measured curve.

An advantage in principle of a d.f.b. oscillator is that the frequency can be traced to the propagation velocity of electromagnetic radiation. With a knowledge of the dielectric constant and permeability of the medium (for example, cable), the frequency can be determined (if $\tau \gg \tau_0$) from the velocity of light and a measurement of a length. A feature of more practical character is the possibility of building a decadic frequency generator by splitting the delay element into units connected in series having delay times of τ', $10^{-1}\tau'$, $10^{-2}\tau' \ldots$, which can be adjusted in suitably choosen steps of its total delay. In this way, high frequency-reading accuracy and comfort are obtained. A similar advantage is the possibility of using cables with standard connectors and with precisely adjusted lengths, corresponding to the frequencies most often needed. The d.f.b. oscillator has a fairly high stability (about 10^{-5}/h), which can certainly be increased by special stabilization of the supply voltages.

Another application of the d.f.b. oscillator provides for measurement of delay times of passive (for example, cables, delay lines, etc.) or active (amplifier, etc.) elements. This measurement can be achieved by reversing the action of the d.f.b. oscillator described above. Instead of calculating frequency from the known delay time of the delay element, the frequency of the output signal is measured and the delay time of the unknown element used as delay element D is calculated. In this way, delay times of passive elements can be measured accurately and quickly by first measuring the frequency f_1 of the d.f.b. signal (using, for example, a short cable with delay $\tau \gg \tau_0$) and then by connecting the unknown element in the d.f.b. loop and measuring the frequency f_2. The delay time τ_u of the unknown element can then be calculated from the expression:

$$\tau_u = \tfrac{1}{2}\left(\frac{1}{f_2} - \frac{1}{f_1}\right).$$

TRIGGERED D.F.B. OSCILLATOR

If the circuit described in the previous section is used with a reduced gain ($|g|v < 1$), an external trigger signal is needed to set the circuit into operation. This trigger signal should be fed into the d.f.b. loop by means of a mixer. The load or grid impedance could be directly used as mixer, but it is advantageous to avoid altering the values of these impedances by the loading effects of the trigger source. This can be achieved, for example, by the circuit shown in Fig. 6, in

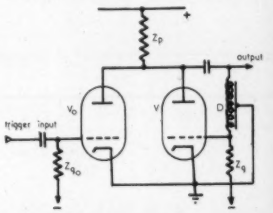

Fig. 6. Triggered oscillator

The trigger signal is fed in by means of the valve V_0 in the d.f.b. loop built up by the amplifier V and the delay element D.

which the valve V_0 feeds the trigger signal to the load impedance Z_p which functions as an additive mixer for the trigger and d.f.b. signal. The latter is started by the action of the trigger signal in the d.f.b. loop formed by the amplifier V and the delay element D.

When a square-wave trigger pulse of duration T is applied to the input impedance Z_{g0}, if the system is built up from the valve V_0 and Z_p is ideal, the shape of the output signal can be again calculated, by setting $G' = -G$, $(0 < G' < 1)$ in equation (1). The results of this calculation are given in Fig. 7. The shape of the d.f.b. signal depends not only on the value of the T/τ parameter as in case (*a*), but also on the resulting gain (or, strictly, attenuation) of the circuit. If the amplitude of the subsequent individual pulses (formed by addition of the d.f.b. and trigger signals at the impedance Z_p, and delayed with respect to each other by τ) decreases to a negligible value in comparison with the trigger-pulse amplitude before the end ($t = T$) of the trigger pulse in Fig. 7(*a*) (that is, if $|(G')^{T/\tau}| \ll 1$), pulses of duration τ and of decreasing amplitude appear after the leading and tailing edges of the trigger signal, while the part before the end is flat. The amplitude E'' of this part can be calculated using equation (1), and gives:

$$E'' = \frac{E_0}{1 + G'}. \qquad (2)$$

If $|(G')^{T/\tau}|$ is only slightly less than one, the shape of the output pulse will vary with the value of T/τ. For example, if T equals $(2m\tau + \epsilon_1)$, and $|(G')^{T/\tau}|$ is about one-third, then a waveform of the type shown in Fig. 7(*b*) will be obtained. For comparison, oscillograms of output signals

taken with circumstances corresponding to those of Figs. 7(*a*) and 7(*b*) are shown in Figs. 8(*a*) and 8(*b*) respectively.

As can be seen from the figures, this d.f.b. circuit can be used as a triggered oscillator. The jitter of a triggered oscillator of this type is small even at higher frequencies, and the duration of the oscillation can be easily controlled to meet particular requirements.

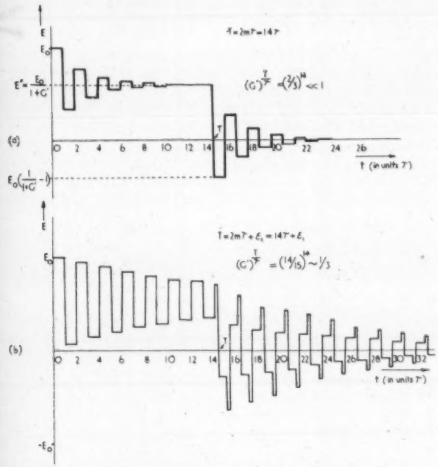

Fig. 7. Determination of the d.f.b. signal by equation (1) if $G' < 1$

Curve (*a*) represents the d.f.b. signal if $T = 2m\tau = 14\tau$ and $G' = \frac{1}{3}$. The case where $T = 2m\tau + \epsilon_1$ and $G' = \frac{14}{15}$ is represented by the graph (*b*).

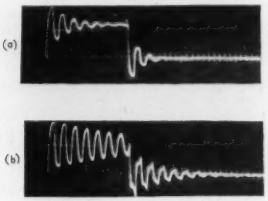

Fig. 8. Oscillograms of output signals of a triggered oscillator taken at settings corresponding to curves shown in Fig. 7

The output signals for $T = 46\ \mu s$ and $T = 47\ \mu s$ are represented by (*a*) and (*b*) respectively.

As with the circuit described in the previous section, this circuit can also be used in a reversed way, that is, not for generation of a signal by means of circuit elements of known parameters, but for investigation of the signal to determine the parameters of unknown elements connected in the d.f.b. loop. While the first circuit offered only the possibility of measuring delay times (or propagation velocities) and, by investigation of the shape of the periodic signal, of drawing conclusions about the value of T/τ, the second circuit is more generally applicable in the field of measuring techniques, and some possible applications are briefly reviewed.

Measurement of the value of T. Using a cable of delay time τ (which can be checked simply by increasing the amplification of the amplifier V until periodic signals are generated, and then measuring the frequency) and adjusting the gain of the circuit until a pattern similar to Fig. 7(*b*) appears on the oscilloscope, one can measure T directly in units of τ. The sign of the first narrow signal can be used for interpolation. (This narrow signal can sometimes be used as an error signal, for example, if the length of a pulse has to be stabilized.)

Measurement of gain and gain stability. The measurement of gain and the investigation of gain stability (in time or in dependence of supply voltage, etc.) by choosing an adjustment which gives a pattern like Fig. 7(*a*) is also possible. For more accurate measurements, the determination of the ratio:

$$\frac{E\{(i+1)\tau\}}{E(i\tau)} = \frac{1+G'}{1+(G')^i} - G'$$

(which is independent of E_0) can be used, while for less accurate measurements equation (2) suffices.

As a final example of the application of the simple d.f.b. circuits treated in this paper, the circuit shown in Fig. 6 is triggered with a periodic signal. The frequency components of the periodic signal for which a relation:

$$f_k = \frac{2m+1}{2\tau}$$

holds are amplified, while the other components are suppressed. Fig. 9 shows the output signal amplitude plotted against input frequency.

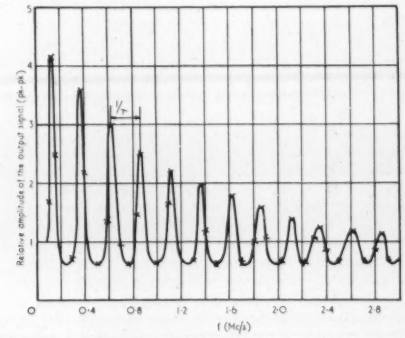

Fig. 9. Amplitude of the output signal plotted against the frequency of the constant amplitude sinusoidal signal fed to the trigger input

ACKNOWLEDGEMENTS

The author wishes to thank Prof. H. Staub for having provided the facilities which made this work possible, and Dr. H. Loeliger, Dr. R. McAllister and Dr. W. Tschopp for valuable discussions.

REFERENCES

(1) GINZTON, E. L., and HOLLINGSWORTH, L. M. *Proc. I.R.E.*, **29**, p. 43 (1941).
(2) KUNDE, W. W. *Electronics*, **16** (No. 11), p. 132 (1943).
(3) NÁRAY, Zs. In preparation.
(4) STEWART, J. L. *Proc. I.R.E.*, **43**, p. 589 (1955).

Dielectric properties of water/alumina

By J. L. Wood, M.A., Ph.D., Department of Chemistry, Sir John Cass College, Jewry Street, London, E.C.3

[*Paper first received* 4 *March, and in final form* 14 *April*, 1959]

The real and imaginary components of the dielectric constant of activated alumina powder containing various quantities of water have been measured at temperatures from 0–29·8° C, and at frequencies from 40 c/s to 100 Mc/s. The loss observed in this frequency range is ascribed to a Wagner-type mechanism. No discontinuity in the dielectric properties of the medium was observed.

INTRODUCTION

The losses in dielectric media which occur whenever the polarization lags behind the applied field can arise from a variety of molecular processes. The low-frequency losses observed in solids can be caused by the heterogeneity of the material (Wagner type), or by the slow re-orientation of the molecular dipoles (Debye type). Because the frequency-dependence of the loss is the same in both cases, the cause must be determined by the influence of such factors as temperature and composition. In this way, it is established that the losses observed in water/alumina gel are due to the Wagner-type mechanism.

EXPERIMENTAL METHOD

A capacitor, formed of five coaxial brass cylinders separated by Pyrex-glass spacers, was filled with chromatographic alumina, type "H" (by Peter Spence), which had been carefully neutralized and dried. The surface area[1] of the alumina after this treatment was 130 m^2/g.

In the experiments conducted at constant temperature (29·8° C), the capacitor was suspended in an evacuated container, and connexion made to another container at a lower temperature filled with water. The water-vapour pressure over the sample, determined by the choice of the lower temperature, was measured with a manometer. The weight of water taken up by unit weight of alumina was found from the extension of a silica spring carrying a small bucket containing further alumina, suspended beside the capacitor. The alumina was degassed at 115° C for five days before the addition of water.

In the other experiments reported, the capacitor was suspended in humidity bottles maintained at constant temperature. Saturated solutions of the salts recommended by Wexler and Brombacher[2] were used to provide the required humidity. The quantity of water incorporated in the alumina was not measured in these experiments.

At frequencies below 30 kc/s, the parallel capacitance C_p and resistance R_p of the capacitor were measured on a bridge similar to that described by Hague.[3] At higher frequencies, a radio-frequency bridge (by Pye) was used. The measured capacity of the empty capacitor was corrected for the area occupied by the spacers to obtain the available capacity C_0.

RESULTS

Addition of water at constant temperature. Fig. 1(*a*) shows Cole-and-Cole plots for various amounts of water added to the alumina. In these, the real component ϵ'_ω (which equals C_p/C_0) of the dielectric constant is plotted against the imaginary component ϵ''_ω (which equals $1/\omega R_p C_0$), over the frequency range employed. Except at very low frequencies, where deviations resulting from leakage occur, the curves are circular arcs, identical except that the frequency at which ϵ''_ω reaches a maximum increases as water is added to the alumina.

Effect of increasing temperature. Fig. 1(*b*) shows Cole-and-Cole plots at a single relative humidity (0·85) for various temperatures between 0 and 25° C. With the possible exception of the one for the lowest temperature, all the curves are identical, except that the frequency (f_{max}) at which ϵ''_ω is a maximum increases with temperature. The

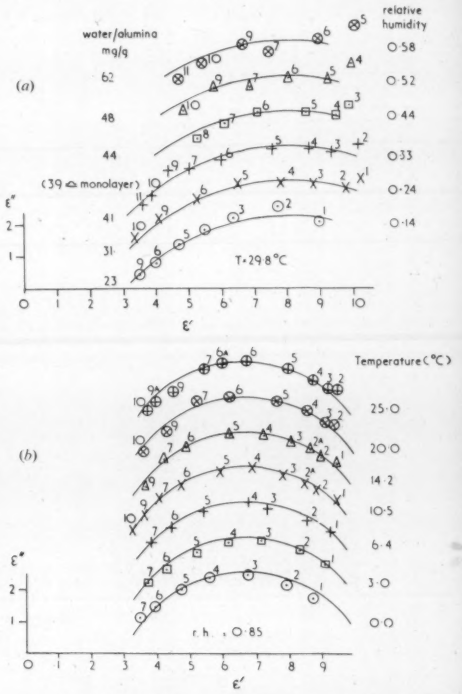

Fig. 1. Losses of water/alumina gel for (*a*) various amounts of added water and (*b*) various temperatures

The ϵ'' scale is moved up an equal distance for each successive curve, so that the same circular arc is drawn throughout Fig. 1(*a*). Similarly in Fig. 1(*b*).

Key

1 = 100 c/s	4 = 1 kc/s	7 = 10 kc/s	10 = 100 kc/s	
2 = 200 c/s	5 = 2 kc/s	8 = 16 kc/s	11 = 300 kc/s	
2*a* = 300 c/s	6 = 5 kc/s	9 = 30 kc/s		
3 = 500 c/s	6*a* = 8 kc/s	9*a* = 60 kc/s		

linearity of a plot of log (f_{max}) against $1/T$ indicates the usual relationship for an activated process:

$$2\pi f_{max} = \omega_{max} = (kT/h) \cdot e^{\Delta S/R} \cdot e^{-\Delta E/RT} \qquad (1)$$

The value of the entropy of activation ΔS is -12 e.u./mole, and the value of the energy of activation ΔE is 15·8 kcal/mole. The difference between the position of this plot and that obtained in the first series of experiments probably arises from the refilling of the capacitor between the series.

DISCUSSION

Dielectric relaxation. The application of a periodic field $E_\omega = (E_\omega)_0 e^{i\omega t}$ to a dielectric results in a periodic displacement $D\omega = (\epsilon'_\omega + i\epsilon''_\omega)E_\omega$. If the displacement decays exponentially when the field is removed, that is if:

$$D(t + t_0) = kE(t)e^{-t_0/\tau} \qquad (2)$$

where τ is a relaxation time, then it may be shown[4] that the frequency dependence of the real and imaginary components ϵ'_ω and ϵ''_ω of the dielectric constant are given by:

$$\epsilon'_\omega = \epsilon'_\infty + (\epsilon'_0 - \epsilon'_\infty)/(1 + \omega^2\tau^2) \qquad (3a)$$

$$\epsilon''_\omega = (\epsilon'_0 - \epsilon'_\infty)\omega\tau/(1 + \omega^2\tau^2) \qquad (3b)$$

The suffixes refer to the frequency at which ϵ' and ϵ'' are measured. The plot of ϵ''_ω against ϵ'_ω is a semicircle passing through the origin, and with centre on the $\epsilon''_\omega = 0$ axis. The radius of the circle is determined by $\epsilon'_0 - \epsilon'_\infty$ alone, while τ determines the frequency corresponding to any point on the curve. The form of the relationship between ϵ'_ω and ϵ''_ω is quite independent of the molecular process causing the displacement, provided this decays exponentially, but the process does serve to fix the size of the two parameters τ and $\epsilon'_0 - \epsilon'_\infty$.

Wagner loss. This arises from any region in a dielectric having a time constant (capacitance × resistance) differing from that of the surroundings. The dielectric properties of the medium as a whole follow equations (1) to (3) above. The influence of the shape of conducting spheroids set in an insulating matrix on the parameters τ and $\epsilon'_0 - \epsilon'_\infty$ has been considered by Sillars[5] who obtained:

$$\tau = [\epsilon'_1(n - 1) + \epsilon'_2]/4\pi\sigma_2 \qquad (4a)$$

$$\epsilon'_0 - \epsilon'_\infty = n^2(\epsilon'_1)^2 q_2/[\epsilon'_1(n - 1) + \epsilon'_2] \qquad (4b)$$

Suffix "1" refers to the matrix, the conductivity σ_1 of which is taken to be negligible, and suffix "2" to the heterogeneous region of volume fraction q_2. The expressions ϵ'_1 and ϵ'_2 are the real components of the dielectric constant of 1 and 2, measured at zero frequency, and n is a shape factor, equal to unity for thin plates normal to the field, and to three for spheres.

The addition of water. Equations (4*a*) and (4*b*) may be applied to the water/alumina dielectric by taking the gas phase (about 70% by volume) as the insulating matrix 1, and the alumina particles with their added water as the conducting regions 2. The position of the centre of the Cole-and-Cole plots, below the $\epsilon''_\omega = 0$ axis, indicates a spread in the relaxation times,[6] and also, probably, in the $\epsilon'_0 - \epsilon'_\infty$ values, as would be expected for powder particles varying in shape and conductivity.

As water is added to the alumina, the radius of the loss curve does not change. The shape factor n and the volume fraction q_2 of the powder particles remain constant, and ϵ'_1, which refers to the gas phase, will not change markedly from 1. However, ϵ'_2 will increase considerably as water is added, measurements at 100 kc/s indicating that ϵ'_2 increases from about 8 to 18 when 6·2% water is added to the alumina. Accordingly n must be large for $\epsilon'_0 - \epsilon'_\infty$ to remain constant. An independent estimate of n obtained by substituting numerical values in equation (4) also gives a large value. Thus if $\epsilon'_0 - \epsilon'_\infty$, (equals $2\epsilon''_{max}$), is taken as 4, ϵ'_1 as 1, q_2 as 0·3, and ϵ'_2 as 8, then n is approximately 18, which corresponds to an ellipsoid with axis ratio of about 5.[5] This could come from a model in which conduction paths crossed several particles, as shown in Fig. 2. Reference to equation

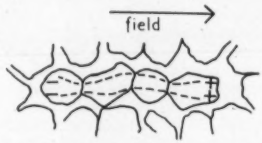

Fig. 2. Possible conduction path in water/alumina gel

(4) shows that, with a distribution in the values of n, those regions with large values of n will predominate in the loss. It would seem that the similar observations of Heukelom and van Reijen[7] for polar liquids/silica gel may be explained in this manner.

The marked decrease in τ as water is added to the alumina results from the rise in the conductivity σ_2 greatly outweighing the smaller increase in $[\epsilon'_1(n - 1) + \epsilon'_2]$ so that, to a fair approximation, σ_2 is proportional to $1/\tau$. Fig. 3 shows that a plot of log (f_{max}) against q_w (the quantity of added water), is linear, implying that:

$$\log \sigma_2 = kq_w + \text{const.}$$

The same logarithmic relation has been found by Kawasaki[8] for the conductivity of water films on various solids, including glass.

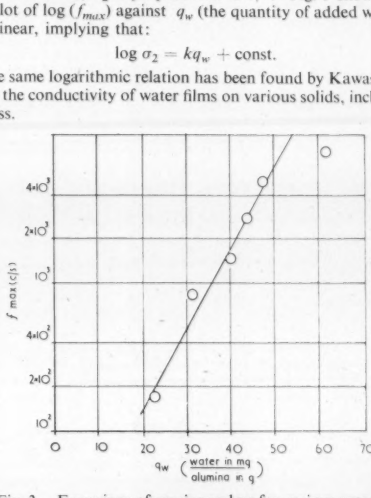

Fig. 3. Frequency of maximum loss for various amounts of added water

Temperature dependence. The observation that the Cole-and-Cole plots are unchanged on increasing the temperature, except that the frequency at which ϵ''_ω is a maximum rises, may be interpreted as a consequence of an increase in the conductivity σ_2. The fairly high value of the activation energy (15·8 kcal/mole) suggests that charge is transferred by a Grotthus chain, rather than by a diffusion

process comparable with electrolytic conduction. Confirmation of this is provided by an estimate of the number of layers of water on the alumina surface. If it is assumed that a water molecule occupies 10 Å^2 of the surface accessible to nitrogen sorption, the coverage is calculated to rise from less than a monolayer at the lowest relative humidity, to about 4 monolayers at 85% relative humidity. Electrolytic conduction would not be expected with less than a monolayer on the surface, and the absence of any discontinuity in the dielectric properties in the range of conditions explored suggests that even at 85% relative humidity, where the temperature dependence was measured, the same mechanism of conduction is operative.

Alternative Debye mechanism. Although the alternative Debye-type mechanism has been invoked by Rolland and Bernard[9] to account for the low-frequency losses of a water/silica gel dielectric, this possibility is ruled out, at least in the present case, by the following considerations.

(i) The magnitude of $\epsilon_0' - \epsilon_\infty'$ is found to be independent of the quantity of water added. If the losses resulted from a Debye-type mechanism, $\epsilon_0' - \epsilon_\infty'$ would be proportional to the quantity of water added.

(ii) The real dielectric constant of the added water, calculated on a basis of simple proportion, may exceed a value of 200. Such high values are not found in the absence of a Wagner loss, the values measured at frequencies where the Wagner loss is negligible not differing greatly from those for the bulk liquid.

(iii) The relaxation times observed are much greater than those of water or even ice (at 0° C). To account for this on the Debye mechanism would require the water dipoles to be much more rigidly oriented on the surface than in the solid.

CONCLUSION

The low-frequency loss region of a water/alumina dielectric is attributable to a Wagner mechanism arising from the conduction of the particles. A similar conclusion has been reached by Heukelom and van Reijen[7] for the system water/silica gel. The relaxation time provides a measure of the conductivity of the particles, which, over the whole range of humidity up to 85%, appears to arise from a charge-transfer mechanism, rather than from the bodily movement of ions which is responsible for conduction in the bulk liquid.

ACKNOWLEDGEMENTS

It is a pleasure to acknowledge the help given by Messrs. Peter Spence and Co. who provided samples of alumina, by Mr. A. S. Joy for the determination of the surface area of the alumina, and by Dr. C. J. L. Booker in the construction of apparatus. I am also grateful to the Central Research Fund of the University of London for a grant for the purchase of apparatus.

REFERENCES

(1) Joy, A. S. Private Communication, Fuel Research Station, D.S.I.R. London, S.W.10.

(2) Wexler, A., and Brombacher, W. G. *Nat. Bur. Stand.*, Circular 512 (1951).

(3) Hague, B. *A.C. Bridge Methods*, 4th Ed., pp. 329, 335 (London: Sir Isaac Pitman and Sons Ltd., 1938).

(4) Fröhlich, H. *Theory of Dielectrics* (London: Oxford University Press, 1949).

(5) Sillars, R. W. *Proc. Instn. Elect. Engrs*, **80**, p. 378 (1937).

(6) Yager, W. A. *Physics*, **7**, p. 434 (1936).

(7) Heukelom, W., and van Reijen, L. L. *J. Chim. Phys.*, **51**, p. 632 (1954).

(8) Kawasaki, K. *Bull. Electrotech. Lab., Tokyo*, **19**, p. 825 (1955).

(9) Rolland, M. T., and Bernard, R. *Compt. Rend.*, **232**, p. 1098 (1951).

Powder technique for the empirical determination of absorption corrections

By H. A. Richard Wegener, Tung-Sol Electric Laboratory, Bloomfield, New Jersey

[*Paper received* 12 *March*, 1959]

The X-ray absorption factors necessary in the accurate determination of intensities in X-ray diffraction structure analyses can be obtained empirically by an analog technique. This is accomplished by replacing the single crystal in its camera by a powder specimen of the same shape, macroscopic orientation and absorption properties, and recording the pattern as the camera goes through the same motions as performed before with the single crystal. The patterns arising in conjunction with different cameras are described, the correction factors necessary are pointed out, and the technique of finding relative and absolute absorption factors with the help of a pattern having calculable absorption factors is elucidated. In the appendix, the correction factors peculiar to this technique are derived analytically.

In the determination of the intensity of reflexions arising from X-ray diffraction, it has long been established that the intensity of the diffracted beam is proportional to the integral of $\exp(-\mu x)dV$. The integration of this expression has been found difficult because of the form x takes as a function of the cross-section of the incident beam, the shape of the specimen, and its orientation with respect to the incident and reflected beam. The problem was solved explicitly for a parallel-plate specimen for any orientation of incident and reflected beam by James *et al.*[1] Absorption factors for a sphere were calculated with the help of approximations by Evans and Ekstein.[2] For reflexions having their zone axis parallel to the axis of a cylindrical specimen, the absorption factors were calculated by Bradley.[3] Other cases can be treated by approximations summarized by Howells[4] and Rogers and Moffet.[5] In practice, it is often difficult and laborious to approximate the special conditions of shape and orientation, or to assess the accuracy of the approximations used.

It may be profitable therefore, at least in some cases, to exchange the difficulties mentioned before for those encountered in the calculation and measurement of powder-line intensities. The main problems that come to mind in this connexion are the existence of the micro-absorption factor

(Taylor[6, 7]) and the danger of preferred orientation. If these problems can be avoided or accounted for, the following approach is useful (especially for cylindrical specimens). After single crystal data have been taken, the specimen is replaced in its camera by a powder specimen of the same shape and orientation in the goniometer. This powder specimen should ideally consist of the same substance as the single crystal, otherwise it should have the same effective absorption coefficient, or, for cylindrical specimens, the same μr-value. An exposure is then taken as if the powder specimen were the same as that used in the previous single-crystal photograph. The diffraction diagram obtained in this manner will show, after a suitable reduction of the data, the change of the absorption factor along each line of constant Bragg angle. After this, another exposure is taken with the powder specimen in an orientation for which absorption factors have been tabulated (for cylindrical specimens the axis should be exactly normal to the X-ray beam), or for which the correction can be calculated easily. This second exposure will be used to normalize the intensities of lines having different Bragg angles. If this exposure time has a known proportion to that of the first photograph, the absolute values of the absorption factors can be calculated. If it is considered impossible or unnecessary to know that exposure relationship, the relative ideal intensities of the powder lines of different Bragg angles will be sufficient to facilitate the calculation of the relative absorption corrections for a given experimental arrangement. The use of relative intensities eliminates the necessity of applying polarization and geometrical-powder corrections, although corrections arising from the peculiarities of this technique in conjunction with the camera used cannot be avoided. The absorption factors determined for a particular spot on the powder diagram obtained by this technique can then be directly applied to a single-crystal reflexion having the same film co-ordinates.

The diffraction photographs obtained by this method will have patterns that are characteristic of the geometry and the movements of the camera, and especially the screens used. For a simple rotation or oscillation camera, the diagram will consist of concentric ovals (the traces of the intersections of the concentric cones of reflected radiation with the cylindrical film, cone axis and cylinder axis being at right-angles to one another). The sole correction factor that has to be applied, apart from the normalization procedure outlined before, arises from the diminution of the powder-ring intensity as the inverse function of distance. The correct absorption factors in a rotation diagram can be obtained only for cylindrical specimens parallel with the axis of the camera. For other orientations, the intensities will be averaged out to give effectively the same result as if the specimen had been alined parallel. In an oscillation diagram, the averaging process will extend only over the oscillation range, so that this would probably yield acceptable results.

The powder-analog technique appears to be well suited for work with the Weissenberg camera. The diagram obtained with the layer-line screen in place will be a set of parallel lines. Their spacing is determined by the intersection of the layer-line screen with the concentric ovals found on the rotation photographs. Normalization of the different lines is achieved again by a second exposure with the specimen in a convenient orientation. There are three corrections that have to be applied. The first is the same inverse distance correction as that for the rotation camera. The second accounts for the fact that the section of the oval permitted to reach the film by the slot in the layer line screen becomes longer and longer as z approaches $R \tan 2\theta$. The third arises from the change of the effective width of the screen slot as a function of distance. These correction factors are calculated in the appendix. They might be compensated for by the proper shaping of the screen slot. If a Geiger counter is used, no correction will be necessary, provided the proper geometry is employed. The counter tube should be mounted on a two-circle goniometer, with the axis of the independent circle parallel and coincident with the incident X-ray beam, and the axis of the dependent circle at right-angles to the independent circle. The (imaginary) point of intersection of both axes should lie at the centre of the irradiated portion of the crystal.

In the precession camera, the diagram obtained by this technique will consist of concentric rings, with the innermost and outermost rings more sharply defined than those in between. The origin of this pattern can be envisioned in the following manner. Although the specimen is in constant motion, the rays reflected from the powder will always form the same concentric cones around the incident beam. The film is inclined to the incident beam, its normal reproducing the precession angle with respect to the incident beam. At any one moment, and in the absence of a screen, the diagram would consist of concentric ellipses. This is attributable to the intersection of a circular cone with a plane inclined to the cone axis. The layer-line screen, however, prevents most of the reflected radiation from reaching the film. Only those portions that are equivalent to single-crystal planes fulfilling the reflexion conditions are allowed to pass. Because the film is inclined to the incident beam always at the same angle, and the annular screen is always in the same position with respect to the film normal, the elliptical trace of each powder-reflexion cone is always intersected in the same place. As film and screen go through their precessional motion, these sections are recorded as concentric circles on the film, usually making a small angle with the tangent of the recorded circle. Of the correction factors that have to be applied, one has its origin in the different lengths of the sections of the ellipses as a function of the Bragg angle, and the other serves to correct for the speed at different points of the annulus as a function of its radius which, in turn, affects the exposure time of each elliptical section. Compensation of these correction factors could also be achieved by shaping the screen slot. The calibration photograph, best taken in a powder camera, can only be used to establish the relative intensities of lines having different Bragg angles. Absolute absorption factors cannot be established with the help of the Bradley corrections because there is no positional configuration in the precession camera which corresponds to the normal beam geometry for which these corrections are applicable.

In the appendix, the correction factors necessary for reducing the data are derived analytically. These same correction factors may be determined empirically also. This can be achieved by using a spherical specimen for the determination of the particular analog pattern. Application of the known spherical absorption factors (Evans and Ekstein[2]) to the normalized intensities will yield the factors for the screen correction. Even this calculation can be avoided if a standard pattern is taken with the spherical specimen, and the ratio of the intensity of the standard pattern to that of the analog technique is determined at equivalent points.

APPENDIX

Calculation of correction factors

Rotation and oscillation camera. Only an inverse-square-law correction is necessary, which arises from the increasing

distance of the film from the crystal as a function of z, the distance from the crystal along the cylinder axis. The measurement of the intensities requires a photometer with finite slit width and effectively infinite slit height. The long dimension of the slit should be parallel to the normal of the arc at the point where the measurement is taken. In this case, the maximum transmission reading is obtained. Because the slit is infinite in one dimension the inverse-square law becomes an inverse-distance law in this application. The correction factor C_1 is taken relative to the radius of the camera cylinder R, so that C_1 equals D/R where D is the distance between the crystal and the measured spot on the film. Every distance D can be resolved into rectangular components R and z. Then:

$$D = (R^2 + z^2)^{1/2} \quad \text{and} \quad C_1 = (1 + z^2/R^2)^{1/2} \qquad (1)$$

Weissenberg camera. Three correction factors have to be applied to the powder patterns obtained in the Weissenberg camera. The first C_1 is the same inverse-distance correction as that found for the rotation camera. The second factor C_2 is best defined as the ratio of the arc length L_z for the slot at z to the arc length L_0 for the slot at $z = 0$ so that C_2 equals L_0/L_z.

L_z is derived by considering the intersection of the surface of a cone, its apex half-angle being 2θ, with the surface of a right circular cylinder (in Cartesian co-ordinates). The axis of the cone is at right-angles to that of the cylinder. One of the resulting two equations is eliminated by considering the film (the surface of the cylinder) flattened out. This is equivalent to setting one variable equal to zero and replacing another by its arc y. The trace of the powder line on the film is thus given by the equation:

$$R^2 \sin^2 ny = R^2 \sin^2 2\theta - z^2 \cos^2 2\theta$$

where z is the direction parallel to the cylinder axis, y the direction normal to it, and n is equal to $180/\pi R$. Application of the standard technique for calculating arc lengths results in an integral the solution of which is not known to the author. An approximation is however possible by working with the differential. Because this is equivalent to using the chord of the arc, the approximation becomes poorer as z and Δz increase. C_2 is equal to L_0/L_z, which is approximately equal to $\Delta s/\Delta z$. Thus:

$$C_2 = \left\{ \frac{n^2(R^2 + z^2)(R^2 \sin^2 2\theta - z^2 \cos^2 2\theta)}{z^2 \cos^2 2\theta + n^2(R^2 + z^2)(R^2 \sin^2 2\theta - z^2 \cos^2 2\theta)} \right\}^{1/2} \qquad (2)$$

The correction factor C_3 is derived with the help of Fig. 1:

$$C_3 = \Delta z_0/\Delta z = Rw/(Rw - zh)$$

where $z_0 = z$ at $z = 0$, w is the slot width of screen, and h is the thickness of screen.

Inspection of C_1. C_2 and C_3 reveals that C_1 and C_3 depend on z only, that is, on the setting of the layer-line screen. That value is fixed for each exposure, so that these factors need not be applied if correlation of several levels is unnecessary or impractical by this method. It is unfortunate that C_2 becomes less accurate as the ordinate of the arc on the film decreases. At this moment, it appears that there is little that can be done about it because even if the line integral were solved by some means, the finite width and varying distribution of density over it will complicate the mathematical treatment of this problem further as the tangent to the powder line becomes normal to the z-axis.

Precession camera. The inverse-distance correction necessary in the cylindrical camera does not have to be applied. All the radiation the screen permits to fall on the film lies along a circular cone the axis of which is normal to the film, so that all recorded rays travel the same distance. A new correction that arises from the movement of the screen around the centre of the film is required. The speed at each point of the circular screen slot increases as its distance

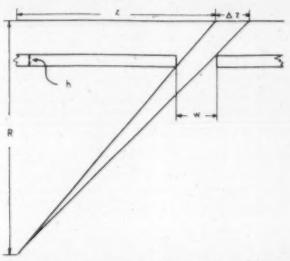

Fig. 1. Geometrical relationships of quantities involved in correction factor C_3

from the centre. This is equivalent to a proportional decrease in exposure time at that point. If the screen were a sector wheel the arc a at constant sector angle would be equal to $\psi\pi r_i/180$. Because all intensities are corrected to conform to a standard arc length a_s a_i is equal to $a_s r_i/r_s$, that is, the correction factor to be applied would be proportional to r_i. The other correction required has its origin again in the different lengths of arc that the screen permits to be recorded on the film. These sections are part of the circumference of an ellipse. This ellipse arises from the intersection of the cone of radiation of constant Bragg angle with the plane of the film which is inclined to the cone axis by the angle $(90 - \bar{\mu})$. The sections of the ellipse are bounded by its

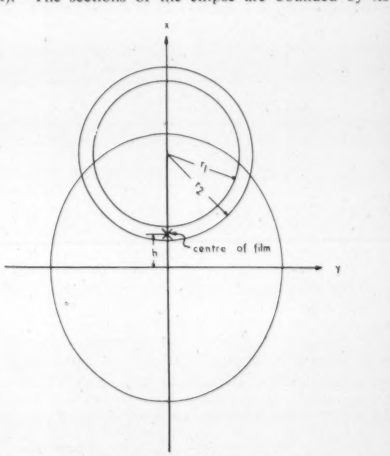

Fig. 2. Location of the centre of the film with respect to the co-ordinates of the ellipse formed by the projection of a cone of half apex angle 2θ on the inclined film of the precession camera

intersection with the two concentric circles of the screen. It is difficult to normalize these correction factors right from the outset. This can still be done once a set of values has been calculated.

The problem of the screen correction factor is to formulate the equation for the ellipse to bring it into the standard form which facilitates the evaluation of the arc length as an elliptic integral and to determine the limits of the integral. The standard form for the arc S of an ellipse can be given as (Reddick and Miller[8])

$$S = a\{E(\phi_2, k) - E(\phi_1, k)\} \quad (3)$$

where

$$E(\phi, k) \equiv \int_0^{\phi} (1 - k^2 \sin^2 \phi)^{1/2} d\phi \quad (4)$$

$$\phi_1 = \sin^{-1}(x_1/a), \quad (5)$$

$$x_1 = -(1/k^2)[-l \pm \{l^2 - k^2(b^2 + l^2 - r_1^2)\}^{1/2}] \quad (6)$$

The value of the function $E(\phi, k)$ is tabulated in Peirce's Tables as a function of ϕ and k. These two values depend on the constants following. They arise in the transformations of variables required to bring the ellipse into the form given, and also from the intersection of the ellipse of the powder line with the circle of the screen (see Fig. 2):

$$a = F \tan 2\theta \cos \bar{\mu}/(1 - \sin^2 \bar{\mu} \sec^2 2\theta),$$
$$b = F \tan 2\theta \cos \bar{\mu}/(1 - \sin^2 \bar{\mu} \sec^2 2\theta)^{1/2}$$
$$h = F \tan^2 2\theta \sin \bar{\mu}/(1 - \sin^2 \bar{\mu} \sec^2 2\theta),$$

where F is the film-to-crystal distance, $\bar{\mu}$ the precession angle, θ the Bragg angle of powder line, r_2 the radius of projection on film of outer ring bounding screen slot, and k^2 is equal to $(a^2 - b^2)/a^2$ and l equals $(h + r)$, where r is r_1, or r_2, or $\{r_1 + (r_1 + r_2)/2\}$, depending on how the screen is situated with respect to the centre of the film. If r_1 is identical with $\rho_1 - \Delta_1/2)$ and r_2 is identical with $\rho_2 + \Delta_2/2)$, where ρ is the radius of a ring bounding the screen slot annulus as projected on to the film from an ideal point source, and Δ is the increment added because of a finite extension of the source, then $r_1 = R_1 F/f$ and $r_2 = R_2 F/f$, where R_1 and R_2 are the inner and outer radii of the screen annulus, and f is the distance between crystal and screen.

REFERENCES

(1) James, R. W. *Proc. Roy. Soc.*, **153***A*, p. 230 (1935).
(2) Evans, H. T., and Ekstein, M. *Acta Cryst.*, **5**, p. 540 (1952).
(3) Bradley, A. J. *Proc. Phys. Soc. (London)*, **47**, p. 879 (1935).
(4) Howells, R. G. *Acta Cryst.*, **3**, p. 366 (1950).
(5) Rogers, P. and Moffet, R. H.. *Acta Cryst.*, **9**, p. 1037 (1956).
(6) Taylor, A. *Phil. Mag.*, **35**, p. 215 (1944).
(7) Taylor, A. *Introduction to X-Ray Metallography*, p. 350 (London: Chapman and Hall, 1945).
(8) Reddick, H. W. and Miller, F. H.. *Advanced Mathematics for Engineers*, p. 116 (New York: John Wiley and Sons, 1938).

Cathode emission measurements in low pressure discharges

By Miss A. D. Forster-Brown, B.Sc., Grad.Inst.P., and M. A. Cayless, B.Sc., A.R.C.S., A.Inst.P.,
The British Thomson–Houston Group Research Laboratory, Rugby

[*Paper received* 8 *April*, 1959]

A method described in an earlier paper[1] for measuring the zero field emission from hot cathodes in discharges is compared with that of the probe methods described by C. G. Found.[2] Good agreement is obtained, thus supporting the interpretation of the measured characteristics. It is shown how this method may be applied to measure the emission from cathodes in ordinary long discharge tubes, such as fluorescent lamps, without the necessity for inserting probes or interfering with the construction of the tubes or electrodes in any way.

In a previous paper (Cayless[1]), a method has been described of measuring the zero-field electron emission of oxide-coated cathodes in discharges in a few millimetres pressure of a rare gas. This consists of identifying the point at which the field at the cathode is zero when either: (*a*) the discharge current is varied whilst the temperature of the cathode is kept constant, or (*b*) the temperature of the cathode is changed whilst a constant discharge current is drawn. At this point the arc current is closely related to the thermionic emission of the cathode and is called the zero-field emission. This zero-field point can be identified either by measuring the electrical characteristics of the discharge, or by observing the change in the visual form of the discharge.[1]

Found[2] has described a method of determining the zero-field point using a negative probe in front of the cathode. When the arc current is increased beyond the zero-field current, the ion current to this probe increases more rapidly than before and this break in the characteristic enables the point to be identified. Found worked mainly in discharges at pressures well below 1 mm of mercury, and satisfactory results were initially unobtainable using this method at pressures over 1 mm, mainly because of the non-uniform nature of the plasma at currents below the zero-field point, resulting in the "ball of fire" mode of discharge which gives rise to further irregularities in the probe characteristic which mask the discontinuity. It has since been found that a suitably designed small wire probe can be used to give a characteristic which clearly shows the transition point, and a satisfactory correlation has been obtained between emission measurements made in this way and by the technique described in the previous paper. Because the evidence for the correctness of the latter method is mainly indirect, this provides valuable corroboration.

MEASUREMENTS

The circuit is shown in Fig. 1. The probe is maintained at a potential of 36 V negative to the anode, in a region of reasonably saturated positive-ion current (at pressures above 1 mm complete saturation is never obtained, the current

increasing slowly with voltage until a glow discharge forms). The cathodes used consisted of sintered rods of a mixture of 40% by weight of $3BaO . Al_2O_3$ and 60% molybdenum powder, these being currently under investigation. These were about 1·5 mm in diameter and 10 mm long and were heated by the direct passage of an alternating current. The cross-cathode potential was always less than 0·2 V. Tantalum anodes 15 mm square were mounted 1 cm from the cathodes and parallel with them. The discharge tubes (3·5 cm in diameter) were processed in the usual way and sealed off with a pressure of 3 mm argon and a drop of mercury.

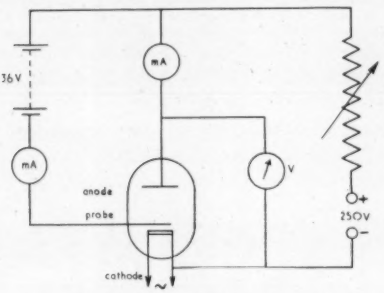

Fig. 1. Circuit of the apparatus

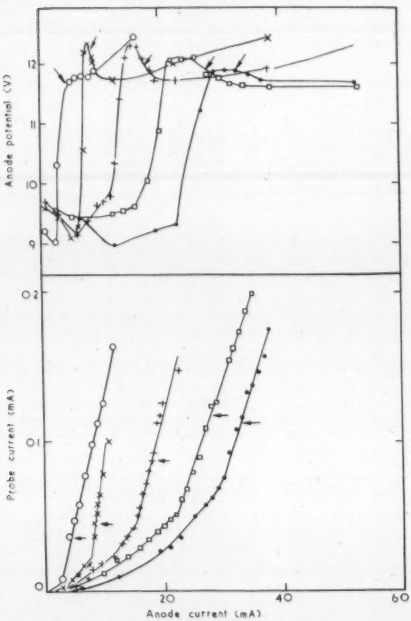

Fig. 2. Anode characteristics (above) and negative probe characteristics (below) for cathode temperatures of 908, 952, 998, 1040 and 1087° C for curves 1 to 5 respectively

The arrows indicate the visible change in the negative glow.

Fig. 2 shows, in the upper half, anode potential plotted against anode current at various cathode temperatures, and the corresponding probe characteristics in the lower half. The latter show clear discontinuities in slope which occur at almost the same currents as those at which the former reach the top of their rather sharp increase in potential. These are the zero-field points and are plotted as functions of temperature in Fig. 3. It is seen that the two types of characteristic yield almost the same emission curve. (Note that these characteristics are necessarily plotted on a linear current scale, whereas those in the earlier paper[1] are on a logarithmic scale.) The curvature in the lower part of the probe characteristics is caused by the formation of the "ball of fire" mode of discharge. At lower pressures this does not occur and the characteristics are linear, as observed by Found.

Also shown in Figs. 2 and 3 are the points at which the visible glow changes from the retarding- to the accelerating-field Langmuir form, the plasma suddenly shrinking on to

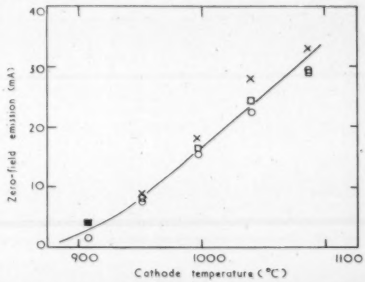

Fig. 3. Zero-field emission as a function of cathode temperature from constant temperature measurements

○ from probe characteristics.
□ from anode characteristics.
× from observations of the form of the negative glow.

the cathode, with disappearance of the dark space. This change is seen to occur at slightly higher currents than the zero-field currents determined from the characteristics of Fig. 2, but the occurrence appears to be fortuitous because, on another occasion, shown in Fig. 4, it does not occur. (The cathode had been activated somewhat between the observations shown in Figs. 3 and 4.)

It is often more convenient to maintain a constant arc current and to vary the cathode temperature in making measurements. As the temperature is decreased, a sudden increase in the anode-to-cathode potential occurs together with a corresponding increase in the positive-ion current to the probe and a change in the appearance of the glow from the retarding- to the accelerating-field form. A corresponding set of observations obtained in this way is included in Fig. 4.

It is seen that, in this case, the anode potential begins to increase at a rather higher cathode temperature than the other changes as the cathode is cooled. The zero-field point is, in fact, not reached in some cases until the voltage reaches a

maximum, as with the constant-temperature characteristics. This maximum is rather vague in most cases, however, and not suitable for use as a criterion.

The start of the rise in anode potential appears to be associated with the change from the "ball of fire" mode to the retarding-field Langmuir mode.[1] This should occur when the arc current is about one-half the cathode emission current.[3] Fig. 4 shows that this is approximately so.

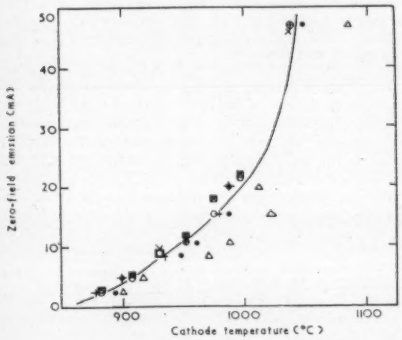

Fig. 4. Zero-field emission as a function of temperature

- ○ from constant temperature probe characteristics.
- □ from constant temperature anode characteristics.
- × from observations of the form of the negative glow at constant temperature.
- • from constant anode current probe characteristics.
- △ from constant current anode characteristics.
- \+ from observations of the form of the negative glow at constant anode current.

In making measurements at constant arc current, therefore, it is usually more reliable to use the visual change in the appearance of the discharge, rather than the electrical characteristics, which are sometimes rather difficult to interpret. (The situation is not often as clear as that shown in Figs. 5 and 6 of the previous paper.[1])

EMISSION MEASUREMENT IN POSITIVE COLUMN DISCHARGES

Discharges have been discussed in which the anode is placed near enough to the cathode to prevent the formation of a positive column. In discharge tubes in which this is not so, it becomes difficult to use the form of the electrical characteristics to detect the zero-field point. The phenomena at the cathode and in the negative-glow region are exactly the same as with short arcs, but the effect of changes in the length of the positive column and in its potential gradient are superposed and, except in particularly favourable cases, the position of the zero-field point cannot be located on the characteristics.

The changes in the visual appearance of the negative glow, however, are still present and can be used to measure the zero-field emission of the cathode. In addition, it is observed that when the discharge changes from a retarding- to an accelerating-field Langmuir mode, with the consequent shrinking of the negative glow, the head of the positive column retreats from the cathode. This occurs because of the additional supply of energetic positive ions from the more highly excited glow, which enables the Faraday dark space to persist further up the tube without the need for further ionization. The movement of the positive-column head occurs quite suddenly and can be used to identify the zero-field point when details of the negative glow itself cannot be seen, as for example, with fluorescent lamps. When fluorescent lamps are run on direct currents of the order of 1 to 100 mA for the purpose of measuring cathode emission, the movement (about 3 cm) of the column head is clearly visible through the phosphor coating. In this way, measurements of the cathode emission have been made on complete, normal production fluorescent lamps, a measurement hitherto only possible when the lamp was altered in some way by inserting a probe or auxiliary electrode, for example, or removing the powder. Such alterations invariably result in a lamp with altered characteristics.

DISCUSSION

It has been shown that zero-field emission measurements made by observing the voltage-current characteristics and the appearance of the negative glow agree satisfactorily with those made by the probe method of C. G. Found. A certain amount of experimental scatter is observed, as shown in Figs. 3 and 4, but except when measurements are obtained from constant-temperature anode characteristics (discussed above), this is satisfactorily small for measurements of this sort. Under any given circumstances, it may be difficult to locate the zero-field point using one of the criteria described because of overlapping or rounding of parts of the characteristics, for example, but it is usually possible to find one of the other criteria satisfactory.

Undoubtedly the explanation given in the earlier paper[1] of the visible change in the negative glow accompanying the transition from the retarding- to the accelerating-field Langmuir mode is over simplified. What is actually observed is a change from a negative-glow plasma commensurate in size with the anode-to-cathode spacing in the retarding-field mode to one much more closely confined to the cathode surface in the accelerating-field mode. This is at a much higher electron temperature and is able to supply a higher proportion of positive ions and other excited particles both to the cathode and to the remainder of the discharge.[4] This is evident for a neon discharge, for example, where the colour changes suddenly from red to yellow at the point as the degree of excitation is increased.

ACKNOWLEDGEMENTS

The authors would like to thank their colleagues at the Research Laboratories of the British Thomson-Houston Co. Ltd., and elsewhere, with whom they have had valuable discussions during the course of this work.

REFERENCES

(1) CAYLESS, M. A. *Brit. J. Appl. Phys.*, **8**, p. 331 (1957).

(2) FOUND, C. G. *Phys. Rev.*, **45**, p. 519 (1934).

(3) JOHNSON, E. O., and WEBSTER, W. M. *R.C.A. Rev.*, **16**, p. 82 (1955).

(4) CAYLESS, M. A. *J. Electronics. and Control*, **4**, p. 237 (1958).

Use of an integrating sphere to distinguish between absorption and scattering in solids

By J. A. Bastin, B.A., Ph.D., E. W. J. Mitchell, M.Sc., Ph.D., A.Inst.P., and J. Whitehouse, B.Sc.,
Physics Research Laboratory, The University, Reading

[*Paper first received* 15 *April, and in final form* 25 *May*, 1959]

In transmission measurements on plane-parallel specimens, light might be lost by absorption or scattering. A method is described in which measurements are made with the same plane-parallel specimen in an integrating sphere. Comparison of the two sets of results allows a quantitative distinction to be made between absorption and scattering. The method is illustrated by some measurements on quartz and diamond.

INTRODUCTION

Optical absorption spectra are usually measured by determining the fraction of the incident intensity which is transmitted through a plane-parallel specimen. When scattering centres are present light is removed from the "straight-through" beam and this loss of light, in the simple experiment, is indistinguishable from the loss by absorption. In some cases (for example, the transmission of light through sodium chloride containing colloidal sodium) a scattering process can give rise to a minimum in a transmission curve. Whether or not such a minimum occurs depends on the size of the scattering particle relative to the wavelength of the light being used.(1)

In a recent paper Compton(2) has discussed the means available for deciding whether a transmission minimum arises from a true absorption process, or from a scattering process. The surest method (No. 1 in Compton's paper) is to measure the spectrum of a part of the scattered light—for example, that scattered at right-angles to the incident beam. However, the intensities scattered into the small solid angles involved in such experiments are usually weak, and the sizes of specimen commonly available are often not sufficient to prevent light scattered by surface irregularities from reaching the detector.

It is desirable in practice to have some other means of deciding whether scattering or absorption is causing a given transmission minimum. Compton(2) considers two other properties which have been used to help to distinguish the two possibilities in experiments on the alkali halides. The properties are:

(1) The effect of temperature on band width.
(2) The bleaching of "absorption" at all wavelengths in a band when illuminated by light having a wavelength spread which is narrow compared with the band width.

The evidence from these properties is not, in general, conclusive. One can readily suggest models of *absorption* centres which lead to a broad, temperature-independent absorption band which does not show any optical bleaching. According to the criteria described by Compton, these properties would be considered as evidence in favour of *scattering* centres.

We have encountered the need for distinguishing absorption from scattering in experiments on the optical properties of diamond and quartz. In this paper a method is described in which a small integrating sphere is used to prevent the loss of scattered light. The experimental arrangement can easily be adapted for use with any spectrophotometer.

PRINCIPLE OF THE METHOD

The method utilizes the well-known properties of an integrating sphere.(3) In the present application, a parallel beam of light is considered having an intensity I_0 and a cross-sectional area a_i. The light enters an integrating sphere through an aperture of area a_e and falls on the specimen to be investigated, which is in position S (Fig. 1). This is in contrast to the usual arrangement in which the specimen is at the surface of the sphere.(3)

In the discussion below it is assumed that the inner surface of the integrating sphere is a perfect diffuse reflector and that

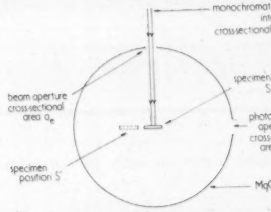

Fig. 1. Schematic diagram of integrating sphere

the diameter of the sphere is very much greater than the dimensions of the beam and detector apertures. The energy density (u) of radiation in the sphere can then be considered to be uniform and is determined by the steady-state balance between light entering and leaving the sphere. It is also assumed that none of the multiply reflected beams is lost from the sphere by retracing the path of the incident light. This condition is achieved by setting the specimen slightly off normal to the beam.

A photoelectric cell or photomultiplier may be used as the detector and the photosensitive surface will, in general, be some distance from the inner surface of the integrating sphere. It is clearly desirable to keep this distance to a minimum. As a result only a fraction of the energy lost per second through the detector aperture (area a_d) will in fact be recorded by the detector, and we shall call this fraction g.

First case. It is assumed first that the specimen only scatters light. For a specimen in position S the steady-state energy balance is:

$$a_i I_0 = \tfrac{1}{4} u c (a_e + a_d),$$

so that

$$u = \frac{4 a_i I_0}{c(a_e + a_d)}, \qquad (1)$$

where c is the velocity of light. Because no light is absorbed by the specimen at S, the steady-state energy density of light in the sphere is the same when the specimen is out of beam at S'. The energy incident on the detector will thus be $guca_d/4$ in both cases so that the ratio $I_s/I_{s'}$ of intensities recorded by the detector will be unity.

In the straightforward transmission experiment (no integrating sphere), taking multiple reflexions into account, we measure:

$$\frac{I_T}{I_0} = \frac{(1-R)^2 e^{-\sigma d}}{1 - R^2 e^{-2\sigma d}}, \tag{2}$$

where σ is the coefficient of scattering, d is the specimen thickness, I_0 and I_T are the incident and transmitted intensities, and R is the reflexion coefficient of the specimen at normal incidence. From this equation σ may be determined.

The maximum value of equation (2) is:

$$\left(\frac{I_T}{I_0}\right)_{max} = \frac{1-R}{1+R}, \tag{3}$$

and this occurs when σ is zero. The conditions for *scattering only* to be present are thus:

(*a*) the ratio of intensities measured with the integrating sphere must be unity.

(*b*) $\frac{I_T}{I_0}$ must be less than $\frac{1-R}{1+R}$ for the direct-transmission measurement.

Second case. The case when there is absorption but no scattering is now considered. In the position S the term A is defined as the fraction of normally incident light which is lost by absorption in the specimen, and A' as the fraction of isotropic incident radiation which is absorbed when the specimen is in any position in the sphere. In the position S the steady-state energy balance is:

$$a_i I_0 = \tfrac{1}{4} u c (a_e + a_d + A' a_s) + A a_i I_0,$$

where a_s is the total surface area of the plane parallel specimen. Thus:

$$u = \frac{4 a_i I_0 (1 - A)}{c(a_e + a_d + A' a_s)},$$

so that the detector records the expression:

$$\frac{I_0 a_i a_d g (1 - A)}{(a_e + a_d + A' a_s)}.$$

In the position S'

$$a_i I_0 = \tfrac{1}{4} u c (a_e + a_d + A' a_s),$$

and consequently the detector records

$$\frac{I_0 a_i a_d g}{(a_e + a_d + A' a_s)}.$$

The ratio of the intensities recorded by the detector is, therefore:

$$\frac{I_s}{I_{s'}} = 1 - A. \tag{4}$$

If μ is the absorption coefficient then, for near normal incidence,

$$A = (1 - R) - \frac{(1-R)^2 e^{-\mu d}}{1 - R e^{-\mu d}},$$

and

$$\frac{I_s}{I_{s'}} = \frac{R - R^2 e^{-\mu d} + (1-R)^2 e^{-\mu d}}{1 - R e^{-\mu d}}. \tag{5}$$

It will be seen from equation (5) that

$$\frac{I_s}{I_{s'}} = 1 \quad \text{for} \quad \mu = 0$$

and

$$\frac{I_s}{I_{s'}} = R \quad \text{for} \quad \mu \to \infty.$$

Between these extreme conditions, μ can be calculated from the measured values of $I_s/I_{s'}$ if the normal-incidence reflexion coefficient is known. In the straightforward transmission experiment, the following is measured:

$$\frac{I_T}{I_0} = \frac{(1-R)^2 e^{-\mu d}}{1 - R^2 e^{-2\mu d}}, \tag{6}$$

from which μ may again be determined. If a specimen contains absorption centres only, it is thus necessary that the values of μ determined from equations (5) and (6) should be identical. At the end of this section, it is shown that this condition is also sufficient to demonstrate the absence of scattering centres in an absorbing specimen.

Third case. Finally, the case when the specimen both scatters and absorbs light is considered. A "total light-removal coefficient" (Σ) is defined such that, in a transmission measurement in which the detector records only light travelling in the direction of the incident beam, instead of equation (6), the following applies:

$$\frac{I_T}{I_0} = \frac{(1-R)^2 e^{-\Sigma d}}{1 - R^2 e^{-2\Sigma d}}. \tag{7}$$

The coefficient Σ takes into account the fact that light is being removed from the beam by scattering and absorption so that Σ equals $(\mu + \sigma)$. Clearly, as defined, Σ is an ideal coefficient, but good approximations to it can be obtained in ordinary spectrophotometers by making the detector-to-specimen distance as large as possible and by a suitable choice of beam-defining apertures. When scattering occurs, Σ as measured in a transmission experiment will always be greater than the unknown μ, the true absorption coefficient.

Without specific assumptions about the probability of scattering in different directions, it is not possible in general to calculate exactly the ratio $I_s/I_{s'}$ which would be recorded using the integrating sphere. Instead, an exact criterion is obtained for detecting the presence of scattering centres in a specimen which also absorbs. In addition some limiting cases are considered when both μ and σ can be determined approximately.

In the position S, light of intensity I_0 falls on the specimen and some fraction of this will emerge without having been either scattered or absorbed. This light will make some contribution I_{s1} to the intensity recorded by the detector, and there will be a further contribution I_{s2} resulting from light which is scattered from the specimen. The ratio $I_{s1}/I_{s'}$ can be derived in the same way as $I_s/I_{s'}$ in equation (5), except that in this case μ is replaced by Σ. Thus

$$\frac{I_{s1}}{I_{s'}} = \frac{R - R^2 e^{-\Sigma d} + (1-R)^2 e^{-\Sigma d}}{1 - R e^{-\Sigma d}}. \tag{8}$$

The ratio of the intensities recorded by the detector will be

$$\frac{I_s}{I_{s'}} = \frac{I_{s1} + I_{s2}}{I_{s'}},$$

so that

$$\frac{I_s}{I_{s'}} > \frac{I_{s1}}{I_{s'}}.$$

This response ratio can be written as

$$\frac{I_s}{I_{s'}} = \frac{R - R^2 e^{-\phi d} + (1-R)^2 e^{-\phi d}}{1 - R e^{-\phi d}}, \tag{9}$$

which serves to define an effective coefficient ϕ.

It may readily be shown from equations (8) and (9) that Σ decreases monotonically with increasing $I_{s1}/I_{s'}$ and that ϕ changes in the same way with $I_s/I_{s'}$. Because these equations are identical in form and $I_s/I_{s'}$ is greater than $_{s1}/I_{s'}I$, it follows that Σ is greater than ϕ. The condition for scattering centres to be present is thus: $\Sigma > \phi$, Σ having been calculated from equation (7) and ϕ from equation (9).

Summarized principles

	Integrating sphere	*Transmission measurement*	*Distinguishing criteria*
Scattering centres only	$\frac{I_s}{I_{s'}} = 1$	$\frac{I_T}{I_0} = \frac{(1-R)^2e^{-\sigma d}}{1-R^2e^{-2\sigma d}}$ measures σ	$\frac{I_T}{I_0} < \frac{1-R}{1+R}$ and $\frac{I_s}{I_{s'}} = 1$
Absorption centres only	$\frac{I_s}{I_{s'}} = \frac{R - R^2e^{-\mu d} + (1-R)^2e^{-\mu d}}{1 - Re^{-\mu d}}$ measures μ	$\frac{I_T}{I_0} = \frac{(1-R)^2e^{-\mu d}}{1-R^2e^{-2\mu d}}$ measures μ	Values of μ determined both from integrating-sphere and spectrophotometer measurements are identical
Absorption and scattering centres overlapping spectra	$\frac{I_s}{I_{s'}} \simeq \frac{R - R^2e^{-\phi d} + (1-R)^2e^{-\phi d}}{1 - Re^{-\phi d}}$ determines μ approximately if $\bar{d} \simeq d$	$\frac{I_T}{I_0} = \frac{(1-R)^2e^{-\Sigma d}}{1-R^2e^{-2\Sigma d}}$ measures $\Sigma = \mu + \sigma$	$\Sigma > \phi$ and $\frac{I_s}{I_{s'}} < 1$

In the particular case when the average path length ($\bar{d}$) of scattered light in the specimen is approximately equal to the specimen thickness, an approximate value of μ can be determined from the integrating sphere. This value can be used with the value of ($\mu + \sigma$) from the spectrophotometer to determine σ. The average path length $\bar{d}$ will be approximately equal to d if μd and σd are both small compared with unity. Then the two processes can be considered independently because the chance of a photon being both scattered and absorbed is negligible. The average path length $\bar{d}$ may also be approximately equal to d for some larger (but not too large) values of σd, provided that μd is small.

Only in the absence of scattering, when I_{s2} is zero, are equations (7) and (9) the same as equations (5) and (6) respectively. It follows that only in this case will the values of the coefficient calculated from equations (5) and (6) or equations (7) and (9) be equal. The condition given in the second case above is thus both necessary and sufficient for absorption only to be present.

The results of this section are summarized in the table.

EXPERIMENTAL DETAILS

A diagram of the experimental arrangement is shown in Fig. 2. The sphere was constructed from two hollow hemispheres of diameter 10 cm, which were machined in an aluminium cylinder of diameter 12 cm. Three ports were provided to the interior of the sphere, port *A* allowing light to enter the sphere, port *B* providing a support for the specimen and port *C* allowing light to reach the detector. The axes of these holes passed through the centre of the sphere. The surface of the integrating sphere was coated with 1·5–2·0 mm of magnesium oxide which was formed by burning magnesium ribbon inside the sphere. Magnesium was fed in through one of the ports, the three ports providing an adequate supply of air for combustion.

The cylinder was bevelled on one side so that a photodetector could be attached with its photosensitive surface within 0·8 cm of the surface of the sphere. A 13-stage photomultiplier, type 9502B (by E.M.I. Ltd.) having an antimony–caesium photosensitive surface was used as detector. By including the fluorescent screen (*F*) the useful range of the photomultiplier was extended on the low-wavelength side to 2200 Å, the normal range being 9000–3000 Å. The screen was made by depositing willemite from an aqueous suspension on to a glass disk, the deposit being sufficiently thin to allow a large enough proportion of incident visible and near-ultraviolet light to reach the detector. Below 3000 Å, the detector recorded primarily ultraviolet-excited visible emission. The current between the final dynode and anode of the photomultiplier was measured by a galvanometer having a sensitivity corresponding to $4{\cdot}02 \times 10^{-9}$ A/mm. Usually the voltage across the resistance chain, from which individual dynode voltages were obtained, was adjusted so that the intensity $I_{s'}$ corresponded to 200 mm (100 scale divisions). The quantity ($100\,I_s/I_{s'}$) could then be read directly when the specimen was moved to *S*.

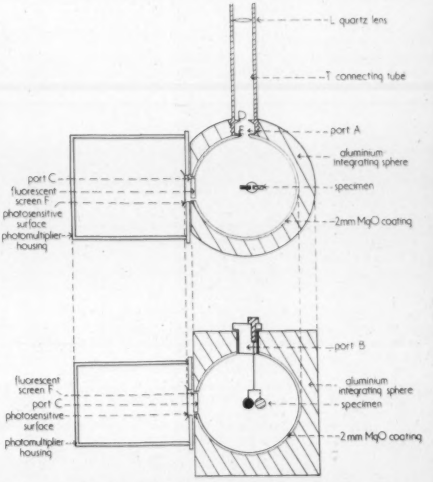

Fig. 2. Experimental arrangement of integrating sphere

Throughout the wavelength range, the monochromator

and lamps of a "Uvispek" spectrophotometer (by Hilger) were used as source. The slightly diverging beam from the monochromator was made slightly converging by the quartz lens L and the image of the monochromator slit at the centre of the sphere was about 1 mm wide and a maximum of 5 mm high. A variable-height stop attached to the monochromator exit slit was used to vary the height of the final image. The internal surfaces of the port A and the connecting tube (T) were painted with lamp black and knife-edge stops were placed at D and E.

Port B contained a plug through which a silver-steel spindle passed eccentrically. By rotating the spindle-head the specimen, which was attached to the other end of the spindle, could be put in either position S or S'.

The theory outlined in the previous section refers to an ideal integrating sphere. The basic requirement is that the energy density should be constant throughout the enclosure, and the extent to which this is true for the integrating sphere described in this section is now examined. For the condition to be satisfied it is required that the average distance travelled by a ray in the sphere before absorption should be much greater than the diameter, or that the mean absorption fraction ($\bar{a}_\lambda$), taken over all surfaces in the sphere, should be much less than one. If the surface of the sphere is a perfect diffuse reflector ($R_\lambda = 1$) this condition may always be satisfied by using a large enough sphere.

For the sphere used here, the conditions were:

(1) Magnesium oxide, 300 cm^2; $a_\lambda = 0{\cdot}04$.[4]
(2) Detector and entrance ports, 2 cm^2; a_λ not known (assumed to be unity).
(3) Specimen and mounting, 2 cm^2; a_λ not known (assumed to be unity).

Thus, in the worst case, $\bar{a}_\lambda$ is approximately equal to 0·05, so that the condition for uniform energy density is valid. It will also be seen that the main factor limiting $\bar{a}_\lambda$ is a_λ for magnesium oxide, and that decreasing the specimen or port sizes will not have a significant effect.

RESULTS

In this section the results are presented of two sets of experiments in which the method described above has been used. These results are given as examples of the application of the method and no detailed discussion of the nature of the centres involved will be given in this paper.

Quartz. Some specimens of synthetic quartz show a considerable "milkiness" after heating above 700° C. One class of specimen also appeared yellow, and there was a well-resolved minimum in the transmission curve at 3·0 eV. It was of interest to know whether the transmission minimum, which appeared to be superposed on the background scattering, was an absorption or scattering feature.

Integrating-sphere and transmission measurements have been made and the results for a typical specimen are shown in Fig. 3. These results show that, over the greater part of the wavelength range investigated, the third case above applies, so that both scattering and absorption are present in the specimen. Assuming that the average path length is of the order of d, values of μ and σ are calculated, and these curves are shown in Fig. 3. Independently of this assumption, however, the measurements establish that the monotonic decrease of transmission with photon energy—which occurs in all specimens—arises mainly from a scattering process, whereas the 3·0 eV peak is mainly, if not entirely, absorption.

Diamond. The absorption edge of type II*a* diamonds possesses an apparent absorption tail extending from the edge (2250 Å) into the visible part of the spectrum.[5] Clark, Ditchburn and Dyer[6] found that the tail could be enhanced by irradiation and heat treatment. They suggested that the

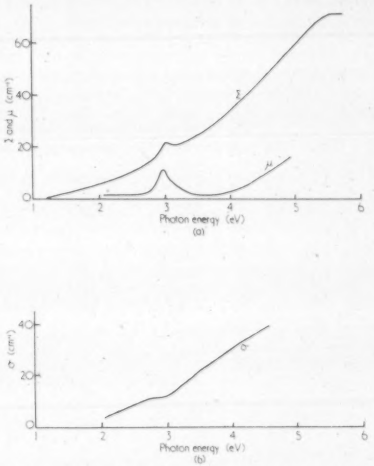

Fig. 3. Integrating-sphere and transmission measurements for heated synthetic quartz (specimen III$_4$)

(*a*) Σ from spectrophotometer results calculated from equation (7) and μ from integrating-sphere results calculated from equation (5).
(*b*) σ calculated as the difference ($\Sigma - \mu$).

effect might be associated with some large-scale imperfection in the diamond structure. Wedepohl[7] showed that the wavelength dependence of this apparent absorption was as $\lambda^{-3{\cdot}6}$. As a result of this he pointed out that most of the tail might arise from a Rayleigh scattering effect (λ^{-4}). The deviation was considered to be associated with either a small absorption contribution or a real particle-size deviation from the Rayleigh law.

Spectrophotometer and integrating-sphere measurements on a similar specimen (D. 80) have been made. From equations (5) and (6), the results of these experiments give the same values of μ within the limits of experimental error. These results, which are shown in Fig. 4, thus satisfy the criterion for the second case (above), so that the apparent

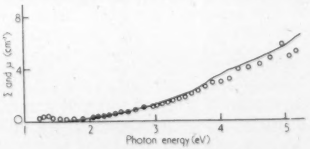

Fig. 4. Integrating-sphere and spectrophotometer results for diamond type II*a* (specimen D. 80)

Continuous curve gives Σ from spectrophotometer measurements.
Circles give μ from integrating-sphere measurements.

absorption tail is real. The similarity of the wavelength dependence with that required for Rayleigh scattering is therefore fortuitous.

ACKNOWLEDGEMENTS

We should like to thank Dr. J. Goulden of the N.I.R.D., Shinfield, for lending us an integrating sphere on which our design was subsequently based. We are grateful to Prof. R. W. Ditchburn for his interest, to Dr. C. D. Clark for providing them with a diamond for the experiment, and to Mr. L. A. Thomas and Mr. C. S. Brown of the G.E.C. Research Laboratory, Wembley, for providing the quartz specimens. J. A. B. wishes to acknowledge financial support from A.E.R.E., Harwell, and J. W. a maintenance grant from the D.S.I.R.

REFERENCES

(1) Scott, A. B., Smith, W. A., and Thompson, M. A. *J. Phys. Chem.*, **57**, p. 757 (1953).

(2) Compton, W. D. *Phys. Rev.*, **107**, p. 1271 (1957).

(3) Jacquez, J. A., McKeehan, W., Huss, J., Dimitroff, J. M., and Kuppenheim, H. F. *J. Opt. Soc. Amer.*, **45**, p. 971 (1955).

Wright, W. F. *Rev. Sci. Inst.*, **28**, p. 129 (1957).

Jacquez, J. A., and Kuppenheim, H. F. *J. Opt. Soc. Amer.*, **45**, p. 460 (1955).

(4) Tellex, P. A., and Waldron, J. R. *J. Opt. Soc. Amer.*, **45**, p. 19 (1955).

Middleton, W. E. K., and Saunders, C. L. *J. Opt. Soc. Amer.*, **41**, p. 419 (1951).

(5) Clark, C. D., Ditchburn, R. W., and Dyer, H. B. *Proc. Roy. Soc. A*, **234**, p. 363 (1956).

(6) Clark, C. D., Ditchburn, R. W., and Dyer, H. B. *Proc. Roy. Soc. A*, **237**, p. 75 (1956).

(7) Wedepohl, P. T. Ph.D. Thesis, University of Reading (1958).

Attenuation of light by wood smoke

By W. W. Foster, B. Sc., A.Inst.P., Ph.D.,* Torry Research Station, Department of Scientific and Industrial Research

[*Paper first received* 10 *November*, 1958, *and in final form* 8 *June*, 1959]

On the basis of experimental observations of the optical properties of wood smoke particles in bulk and in their natural form as spherical droplets, it is shown theoretically that the attenuation of light by wood smoke results mainly from scattering by the droplets, the effects of absorption being negligible. Other experimental observations on the effective optical density of wood smoke up to high mass concentrations lead to a calculation of the mean effective radius of the wood smoke particles. The Lambert–Beer law appears to hold over the whole experimental range, in accordance with a theoretical estimate of its limits of validity for the conditions used.

LIST OF SYMBOLS

Except where stated otherwise, the units are c.g.s. throughout.

a = radius of spherical aerosol particle

A = energy of wavelength λ absorbed by spherical particle per unit time divided by the energy incident per unit time on the projected area of the sphere = absorption cross-section area

$B = 3cs/4xd$

c = mass concentration of aerosol

C_0 = output of receiver corresponding to incident light intensity I_0

d = density of aerosol particle

i_0, i = initial and final intensities of light passing through aerosol material in bulk

I_0, I = initial and final intensities of light passing through aerosol

k = absorption index of material of aerosol particles

$K_e = \dfrac{S+A}{\pi a^2}$, extinction area coefficient

$K_s = \dfrac{S}{\pi a^2}$, scattering area coefficient

$\bar{K}_e$, $\bar{K}_s$ = effective extinction area and scattering area coefficients

l = length of light path in aerosol material in bulk

λ, $\bar{\lambda}$ = wavelength and effective wavelength of light in medium surrounding aerosol particles

m = refractive index of material of aerosol particles relative to the surrounding medium

s = length of light path in aerosol

S = energy of wavelength λ scattered by spherical particle per unit time divided by the energy incident per unit time on the projected area of the sphere = scattering cross-section area

$x = 2\pi a/\lambda$

INTRODUCTION

Colouring, flavouring and preservative agents may be deposited on a foodstuff by exposing it to wood smoke. In industrial practice it is difficult to control the process as there is no way of estimating continuously the quantity of smoke deposited. However, the process may be monitored indirectly by measuring the optical density of the smoke as the rate of deposition of smoke appears to be directly proportional to the optical density. During studies of smoke deposition,[1] therefore, the factors involved in measuring the optical density of wood smoke were investigated.

When wood is heated, distillation and degradation occur and the chemical structure and quantities of the products depend on a number of factors including the type of wood used and the temperature-time conditions. On cooling, some of the vapours condense on nuclei and eventually minute visible particles develop. For smoke generated by violently agitating oakwood sawdust in a blast of air at 314 $\pm$ 2° C[1, 2] and for smoke generated by burning the sawdust in a bed in which the temperature ranged from about 20° C to about 800° C, as in the experiments to be described, the vapours are apparently transparent and it is the particles which give rise to the attenuation of visible light. This is likely to be the case for all industrial wood smokes.

* Member of the staff of the Herring Industry Board.

For suspensions of materials whose light scattering and absorbing power is dependent on the wavelength of light, the Lambert–Beer law is usually not obeyed when the radiant energy is distributed throughout a broad wavelength band.[3] The present work shows that the Lambert–Beer law appears to hold for wood smoke even when unfiltered light from a tungsten lamp is used in measuring the optical density.

THEORY

The light scattering and absorbing properties of a particle are dependent on its size, shape, internal structure and on the relative refractive and absorption indices of the particle and the surrounding medium. Light microscope examination of the structure of wood smoke particles[1] indicates that they are spherical tarry droplets that all have the same density irrespective of their size. The density of these particles, determined by measurements on the bulk material, was $1{\cdot}30 \pm 0{\cdot}02$ g/cm^3. To determine the optical density of such particles in suspension in air it is necessary to know the amount of light which is absorbed and scattered by the particles and the angular distribution of intensity of the scattered light. The optical properties of homogeneous spherical particles have been worked out principally by Rayleigh[4] for dielectric spheres much smaller than the wavelength of light in the surrounding medium λ and by Mie[5] for particles of all sizes. For a spherical dielectric particle of refractive index m, whose radius $a \ll \lambda$, the energy scattered per unit time divided by the energy incident per unit time on the projected area of the sphere (the scattering cross-section area) is given by the expression

$$S = \frac{8\pi a^2}{3}\left(\frac{m^2-1}{m^2+2}\right)x^4 \qquad (1)$$

where $x = \dfrac{2\pi a}{\lambda}$ and λ = wavelength of light in the medium surrounding the particle. In the case of wood smoke the medium consists of air containing a small proportion of smoke vapours and the error will be negligibly small when it is assumed that λ is the same as that in air.

The Mie theory shows that when $a \simeq \lambda$, the scattering cross-section area is a complicated function of x and of xm. When a particle absorbs light, S is replaced by $S + A$, the total energy scattered and absorbed per unit time divided by the energy incident per unit time on the projected area of the sphere (the extinction cross-section area), and m is replaced by $m(1 - jk)$ where k is the absorption index of the material of the particle defined in the equation.[6]

$$k = \frac{2{\cdot}303\lambda}{4\pi ml} \cdot \log_{10}\frac{i_0}{i} \qquad (2)$$

where i_0 and i are the initial and final intensities of light passing a distance l through the bulk material and λ/m is the wavelength of light in the bulk material. The determination of m and k will be described later.

The Rayleigh and Mie theories discuss the optical properties of a single particle in an infinite medium or of a number of particles in an infinitely dilute suspension. Provided that the mean particle spacing is large compared with λ[7] and that the particles are randomly arrayed, the scattering is incoherent and the scattering terms for each particle are additive. Interaction does not occur when the particle spacing is greater than about $100a$.[8] Multiple re-scattering might also occur in suspensions but as pointed out by Mie[5] the effect can be neglected if it can be shown experimentally that the optical density is proportional to the mass concentration of the suspension.

When a beam of monochromatic light of initial intensity I_0 passes a distance s through a sufficiently disperse suspension of spherical particles of radius a, density d and mass concentration c, the final intensity I is defined in the equation

$$I = I_0 e^{-K_e B} \qquad (3)$$

where $B = \dfrac{3cs}{4ad}$ and $K_e = \dfrac{S + A}{\pi a^2}$, the extinction area coefficient.

When the particle only scatters light, K_e becomes $K_s\left(= \dfrac{S}{\pi a^2}\right)$, the scattering area coefficient. The optical density is

$$\log_{10}\frac{I_0}{I} = \frac{K_e B}{2{\cdot}303} \qquad (4)$$

The measured value of the light intensity at any particular wavelength is dependent on the intensity of the light emitted and on the sensitivity of the receiver. For monochromatic light the measured optical density is independent of the emitted light intensity and the receiver sensitivity provided that the receiver output is proportional to the light intensity. In the present experiments the photocell current was proportional to the intensity of light falling on the photocell. The light used was not monochromatic, however, and the emitted light intensity and the sensitivity of the receiver varied with wavelength. In a case such as this the optical density of any given aerosol may be markedly dependent on the spectral response of the emitter-receiver combination as well as on the variation of the extinction area coefficient with wavelength, i.e. effective optical density

$$\left.\begin{aligned} &= \log_{10}\left(\frac{\int C_0 d\lambda}{\int C_0 e^{-\bar{K}_e B} d\lambda}\right) \\ &= \frac{\bar{K}_e B}{2{\cdot}303} \end{aligned}\right\} \qquad (5)$$

where C_0 is the output of the receiver when light of wavelength λ and intensity I_0 falls on it, and $\bar{K}_e$ is the effective extinction area coefficient. K_s and $\bar{K}_s$ are applicable when the particle only scatters light. When both C_0 and K_e vary with λ, $\bar{K}_e$ as defined by equation (5) may vary somewhat with B (i.e. the Lambert–Beer law will not be strictly true) but provided $K_e B$ and $\bar{K}_e B$ are both sufficiently small, it is readily shown that $\bar{K}_e$ reduces to the constant value $\bar{K}_e = \dfrac{\int C_0 K_e d\lambda}{\int C_0 d\lambda}$.

APPARATUS AND EXPERIMENTS

Measurement of optical density and mass concentration. The optical density of wood smoke was measured by a double beam method[9] using a common source of unfiltered light from a tungsten lamp. In this instrument, the intensity of one of the beams passing through a compensating aperture in a reference column is compared with that of the other beam passing through both the smoke and a neutral density annular optical wedge. The attenuated beams fall on to selenium barrier-layer photocells which are connected in opposition across the input of an amplifier and the signal is reduced to zero by means of a servo motor driving the optical wedge. Optical density is indicated by a recording pen coupled to the wedge drive mechanism. Each photocell is shunted by a 500 Ω resistor and each output is about 2 μA. This current is well below the region in which the photocell output ceases to be directly proportional to the intensity of the illuminating light.

The relationship between the optical density and the mass

concentration of the wood smoke was determined using the apparatus shown diagrammatically in Fig. 1. Smoke from the generator, cleared of entrained sawdust by the cyclone, was directed by variable-speed centrifugal fans either into a box of capacity about 50 l. or to waste, the optical density of the smoke inside the box being controlled by the manipulation of stopcocks. The mass concentration was determined from the weight of particles electrically precipitated from a known volume of smoke, metered by the pressure drop across

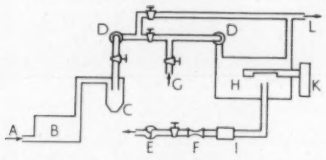

Fig. 1. Apparatus for optical and gravimetric density measurements

A, air inlet; *B*, smoke generator; *C*, cyclone; *D*, fan; *E*, sampling pump; *F*, flowmeter; *G*, air inlet; *H*, smoke box; *I*, electrical precipitator; *K*, smokemeter; *L*, smoke outlet.

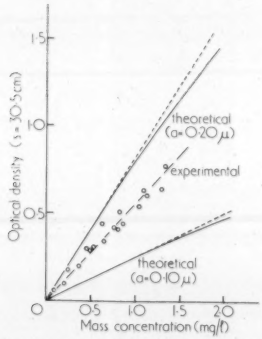

Fig. 2. Relationship between optical density and mass concentration of the particle phase of wood smoke

– – – – – extrapolation of linear portion of theoretical curve.

a calibrated venturi orifice. A typical set of results is presented in Fig. 2.

Spectral response of emitter-receiver combination. Using a Unicam U.V. spectrophotometer the spectral response was found by measuring the current from a barrier layer photocell through a galvanometer of internal resistance 1800 Ω, the light source being a 24 V 6 W single filament festoon lamp—the same combination as that in the optical density meter. It was unnecessary to have the same resistance in the photocell circuit as that in the optical density meter (500 Ω) as the current from such a photocell is independent of resistance in this range at the low light intensities obtaining in the meter. Results are presented in Table 1.

Measurement of m and k. The refractive index of wood smoke tar has been found using a method based on the transmission of light[1] but the tar absorbs blue and red light so strongly that such a method is unsuitable for measuring its dispersion. The refractive index was therefore measured by the method of total internal reflexion inside a glass prism[10] for red, green and blue light from a tungsten lamp using Kodak Wratten filters 29, 61 and 49. Filter 29 transmits most of the visible light of wavelength greater than about 0·62 μ while the transmission curves of filters 61 and 49 peak at 0·53 μ and 0·45 μ, the half widths being 0·06 μ and 0·04 μ respectively.

Table 1. *Spectral response of tungsten lamp–barrier layer photocell combination*

Wavelength λ (μ)	*Photocell output, C_0 (arbitrary units)*	*Wavelength λ* (μ)	*Photocell output, C_0 (arbitrary units)*
0·36	6	0·62	98
0·38	9	0·64	90
0·40	12	0·66	60
0·42	18	0·68	37
0·44	26	0·70	30
0·46	36	0·72	24
0·48	44	0·74	20
0·50	53	0·76	17
0·52	63	0·78	14
0·54	73	0·80	13
0·56	84	0·82	10
0·58	95	0·84	8
0·60	100		

The refractive index was 1·528 for red light, 1·534 for green light and 1·538 for blue light. These results lie within the range of those found using transmitted light.[1] Although these measurements do not cover the range of wavelengths to which the photocell is sensitive they show that there is no sharp increase of refractive index towards the ultra-violet end of the spectrum. It has therefore been assumed that m is constant for $0{\cdot}36\ \mu < \lambda < 0{\cdot}84\ \mu$ in order to simplify subsequent calculations.

The absorption index k was determined from equation (2) using the Unicam U.V. spectrophotometer to measure $\log_{10} i_0/i$ for wood smoke tar. k increased markedly towards the ultra-violet end of the spectrum and for this region a film of tar, thin and uniform enough to transmit sufficient light for measurements, could not be made. The tar was therefore completely dissolved in acetone and the effective thickness of the layer reduced. Results of these measurements are given in Table 2.

Table 2. *Variation of absorption index k with wavelength*

Wavelength λ (μ)	*Absorption index (k)*	*Wavelength λ* (μ)	*Absorption index (k)*
0·35	0·017	0·54	0·000 62
0·36	0·013	0·58	0·000 41
0·37	0·0097	0·62	0·000 30
0·38	0·0078	0·66	0·000 24
0·39	0·0064	0·70	0·000 29
0·40	0·0053	0·74	0·000 55
0·42	0·0038	0·78	0·001 1
0·44	0·0027	0·82	0·001 4
0·46	0·0019	0·86	0·001 7
0·48	0·0014	0·90	0·001 8
0·50	0·0011		

DISCUSSION

The optical properties of wood smoke particles and aerosols are calculated in the following sections, using the experimentally determined values of m and k given above

and assuming that the spectral response of the emitter-receiver combination is the same as that noted in Table 1.

Absorption and scattering of light by wood smoke particles. Measurements[1] on the deposition of unipolar charged wood smokes indicate that the average radius of the particles is about 0·1 μ. In determining the relative contributions of light absorption and scattering to light attenuation by wood smokes, the effective scattering area and extinction area coefficients $\bar{K}_s$ and $\bar{K}_e$ were therefore calculated for monodisperse aerosols of this order of size. Lowan's tables[11] were used since these give values of K_s for spherical particles of refractive index in the range 1·44 to 1·55 and functions for calculating K_e for particles of small absorption index up to about 0·1. Since k for wood smokes varies considerably with λ, values of K_e and K_s were first plotted against particle radius for a number of wavelengths in the range $0{\cdot}36\ \mu < \lambda < 0{\cdot}84\ \mu$; K_s and K_e were then plotted against λ for particles of radius 0·05 μ, 0·07 μ and 0·10 μ. Lowan's tables do not extend below $x = 0{\cdot}5$, but in these calculations it was necessary to know K_s and K_e down to $x = 0{\cdot}37$. The Rayleigh formula [equation (1)] was used to find K_s for $x < 0{\cdot}5$; corresponding values of K_e were found by extrapolating the curve for K_e obtained from Lowan's tables for $x > 0{\cdot}5$. The curves for K_s and K_e show no tendency to diverge markedly in the region $x = 0{\cdot}5$ and it is therefore considered that this method of finding approximate values of K_e for $x > 0{\cdot}37$ is justified.

In finding the effective scattering area and extinction area coefficients $\bar{K}_s$ and $\bar{K}_e$ for a monodisperse aerosol using a tungsten lamp-selenium barrier-layer photocell combination, the effective optical density was determined by stepwise integration of the terms given in equation (5) using values of C_0 given in Table 1 and the values of K_s and K_e found as described above. In a typical calculation it was assumed that $B(=3cs/4ad) = 1{\cdot}0$, since this is within the range of values of B for the wood smokes used in experiments. It was found that the difference between $\bar{K}_e$ and $\bar{K}_s$, expressed as a percentage of $\bar{K}_e$, was 7·5, 3 and 1% for monodisperse smokes whose particles had radii 0·05, 0·07 and 0·10 μ respectively. Thus, the effects of light absorption decrease as the particle radius increases and it is considered that they may be neglected for $a \gtrsim 0{\cdot}10\ \mu$. The attenuation of a beam of light in wood smokes containing particles of radius greater than about 0·10 μ is therefore mainly due to light scattering.

Relationship between optical density and mass concentration. To determine whether the Lambert–Beer law might be expected to be valid for hypothetical monodisperse wood smokes of particle radius 0·05, 0·10 and 0·20 μ, equation (5) was used to calculate effective optical densities over a range of values of B likely to be encountered in practice. Corresponding values of $\bar{K}_s$ were calculated and effective wavelengths $\bar{\lambda}$ were found from the relationship between K_s and λ. These results are presented in Table 3. It should be noted that $\bar{K}_s$ is directly proportional to the ratio of the effective optical density to the mass concentration [equation (5)] and that any variation in $\bar{K}_s$ with B indicates departure from the Lambert–Beer law. According to Table 3 $\bar{K}_s$ decreases as B increases, showing that at the higher values of B the Lambert–Beer law would not be expected to be valid. Furthermore, this departure is greater, the greater the particle radius. To illustrate this point, and to enable comparison of theoretical and experimental results, values of optical density and mass concentration, taken from Table 3 for aerosols of radii 0·10 and 0·20 μ, are plotted in Fig. 2. It appears from Fig. 2 that within the range of mass concentrations for the experimental wood smokes used, which reached much higher values than those normally obtaining in industry, the departure from the Lambert–Beer law is small enough to be ignored; and that this experimental observation is borne out by the theoretical calculations. It should be noted also that the average particle radius of these smokes appears to lie between 0·10 and 0·20 μ.

Table 3. *Optical constants of wood smoke particles*

$B\left(=\frac{3cs^*}{4ad}\right)$ (c.g.s. units)	Mass concentration c (mg/l)	Effective optical density	$\bar{K}_s$	$\bar{\lambda}$ μ
Particle radius, a, = 0·05 μ				
0·5	0·142	0·0057	0·0262	0·544
1·0	0·284	0·0114	0·0262	0·544
3·0	0·853	0·034	0·0261	0·544
5·0	1·42	0·056	0·0258	0·545
10·0	2·84	0·107	0·0247	0·547
Particle radius, a, = 0·10 μ				
0·23	0·131	0·0354	0·354	0·560
1·0	0·569	0·149	0·344	0·563
1·5	0·853	0·219	0·336	0·567
2·5	1·42	0·350	0·322	0·573
3·0	1·71	0·412	0·316	0·578
5·0	2·84	0·643	0·296	0·584
Particle radius, a, = 0·20 μ				
0·05	0·057	0·049	2·25	0·582
0·115	0·131	0·112	2·24	0·583
0·25	0·284	0·240	2·21	0·589
0·50	0·569	0·470	2·16	0·597
0·75	0·853	0·689	2·12	0·605
1·20	1·36	1·06	2·04	0·620
1·50	1·71	1·30	1·99	0·626
2·00	2·27	1·66	1·91	0·640
2·50	2·84	1·97	1·81	0·653

* $s = 30{\cdot}5$ cm; $d = 1{\cdot}30$ g/cm^3.

Since K_s is calculated for the total amount of light scattered by a particle, equation (4) is valid only if no scattered light enters the receiver. This would be so only if the illuminating beam were parallel and the receiver subtended zero angle at the aerosol. In the recording optical density meter used in this work the illuminating light is nearly parallel and the maximum angle subtended by the photocell is 5 deg. Calculations by Lothian and Chappell[12] show that with this angle the error in the measured value of K_s would be less than about 1% for $m = 1{\cdot}33$ and $x = 3{\cdot}0$. About the same result would be obtained for wood smoke, for which $m = 1{\cdot}53$ and $x \gtrsim 3{\cdot}0$ since Lowan's tables[11] show that the angular scattering curves for $x = 3{\cdot}0$ are almost the same shape over the range $m = 1{\cdot}33$ to 1·55, and that the total proportion of total light which is scattered forward (into the receiver) decreases as x decreases. It is considered that such an error of less than 1% is negligible.

Primary scattered light initially bound for the receiver could be diverted from it subsequently as a result of multiple re-scattering by other particles. If this occurred, the measured optical density would approach the theoretical maximum given by equation (4). According to the discussion in the previous paragraph, the increase in the optical density could not be more than about 1%. It appears, therefore, that any effect due to multiple re-scattering of light away from the receiver would be negligible. Multiple re-scattering of light into the receiver would result in a lower apparent optical

density measurement and a departure from the Lambert–Beer law in the same direction as that due to the spectral response of the tungsten lamp–selenium barrier-layer photocell combination. Since the experimental relationship between optical density and mass concentration appears to be linear, it is considered that such effects of multiple re-scattering can be ignored.

Average radius of wood smoke particles. It appears from Fig. 2 that the average radius of wood smoke particles is between 0·10 and 0·20 μ. According to Table 3, $\bar{\lambda}$ in this region is between 0·56 and 0·59 μ. Assuming $\bar{\lambda} = 0{\cdot}58\ \mu$ and, since the Lambert–Beer law applies, assuming $\bar{K}_s = K_s$, $\frac{K_s.s}{3{\cdot}07ad}$ (the optical density per unit mass concentration) was plotted against the particle radius. The average particle radius of the wood smokes used was found from this plot, knowing the optical density per unit mass concentration from the slope of the line through the experimental points in Fig. 2. Two values of particle radius were obtained—0·148 and 0·472 μ—since the relationship between K_s and a peaks at about 0·35 μ.[11] From the measurements so far described it would not be possible to decide which value of a is correct. However, it was observed that after transmission through wood smoke, initially white light was reddish in colour, indicating that the average particle radius lay in the region where the amount of light scattered increased with decreasing wavelength, i.e. on the rising section of the curve relating K_s and a. This was in the region containing the lower value of a, the higher value of a being on the falling section of the curve where transmitted light would be bluish in colour. It was concluded that the average particle radius of the wood smoke examined, measured in this way, was 0·148 μ.

ACKNOWLEDGEMENT

The work described was carried out at Torry Research Station of the Department of Scientific and Industrial Research by staff of the Herring Industry Board as a part of the programme of the Board and the Department. The author is indebted to Dr. A. C. Jason for advice in the course of this work.

Crown Copyright Reserved.

REFERENCES

(1) FOSTER, W. W. Ph.D. thesis, Univ. of Aberdeen (1957).
(2) NICOL, D. L. Brit. Pat. No. 781,591 (Sept. 1954); *Dep. sci. industr. Res., Lond., Food Investig. Bd. Repts.*, p. 41 (1954), p. 31 (1955).
(3) *The Science of Color*, p. 184 (New York: Thomas Y. Crowell and Co., 1953).
(4) RAYLEIGH, J. W. S. *Phil. Mag.*, **41,** 4th Series, pp. 107, 274, 447 (1871); *Phil. Mag.*, **12,** 5th Series, p. 81 (1881).
(5) MIE, G. *Ann. Phys. (Leipzig)*, **25,** p. 377 (1908).
(6) BÖTTCHER, C. J. F. *Theory of Electric Polarization*, pp. 235–8 (London: Elsevier Publishing Co., 1952).
(7) HOUGHTON, H. G., and CHALKER, W. R. *J. Opt. Soc. Amer.*, **39,** p. 955 (1949).
(8) SINCLAIR, D. *Optical Properties of Aerosols*, p. 84 of *Handbook on Aerosols* (Washington, D.C.: U.S. Atomic Energy Commission, 1950).
(9) JASON, A. C. *Process Control and Automation*, **3,** p. 61 (1956).
(10) WORSNOP, B. L., and FLINT, H. T. *Advanced Practical Physics*, p. 282 (London: Methuen and Co. Ltd., 1951).
(11) LOWAN, A. N. *Tables of Scattering Functions for Spherical Particles.* National Bureau of Standards Applied Mathematics, Series 4 (Washington, D.C.: U.S. Government Printing Office, 1949).
(12) LOTHIAN, G. F., and CHAPPELL, F. P. *J. Appl. Chem.*, **1,** p. 475 (1951).

The X-ray scanning microanalyser

By P. DUNCUMB, M.A., Ph.D., Grad.Inst.P., Cavendish Laboratory, Cambridge

[*Paper received* 8 *April*, 1959]

The chemical microanalysis of a surface by the Castaing technique is carried out by exciting characteristic X-ray emission from a selected point, located optically under a stationary electron beam about 1 μ in diameter. In many cases, the speed of working is greatly increased by the use of a scanning technique, which enables the surface distribution of a given element to be presented visually as an image on a cathode-ray tube screen. For quantitative analysis of a selected feature, accurate positioning of the beam may be carried out by reference to this image, or to a similar image showing topographical detail. The method has been applied to elements of atomic number 12 and above, in metallurgical, biological and mineralogical specimens.

The paper deals with the principle, theory and design of an X-ray scanning microanalyser, and typical applications are illustrated by two examples.

INTRODUCTION

The possibility of chemical analysis of an unknown substance by a study of its characteristic X-ray spectrum was first investigated over 30 years ago by several workers, notably von Hevesy.[1] Two methods of excitation are possible: direct bombardment of the specimen with an electron beam, or irradiation with X-rays of energy sufficient to cause fluorescence. Since the early work, the fluorescence method has been developed to a stage where it is now used for routine control measurements; it has the advantages that a standard sealed-off X-ray tube can be used, and that the specimen can be in air. In contrast, the use of an electron beam to cause direct emission, hereafter called the emission method, has received little attention until comparatively recently. Developments of electron-optical techniques have now made it possible to focus a beam of electrons into a probe of 1 μ diameter or less, and so to carry out the analysis of a correspondingly small region of the specimen surface, which is not at present practicable by the fluorescence method. The emission method thus finds its main application in the microanalysis of surfaces, and can be applied not only to metals but also to biological and mineralogical specimens. In combination with the scanning technique to be described, it gives a rapid means of obtaining both the concentration of a given

element at a selected point, and its distribution over the surface.

The technique of X-ray emission microanalysis using a static electron probe was initiated in France by Castaing[2, 3] and has been taken up in Russia,[4] England[5] and America.[6, 7] The specimen is positioned under the electron probe by means of an optical microscope, the smallest region which can be analysed being limited by the penetration of electrons into the surface; this is in the region of 1 to 3 μ at the beam voltage of 20 to 30 kV at present used, depending on the density of the target. X-rays emitted from the irradiated volume are then analysed with a crystal spectrometer, and, to a first approximation, the concentration of an element is proportional to the intensity of its characteristic line emission. Calibration is effected by comparison with a pure sample of each element; a relative accuracy of 1% in the determination of high concentrations is possible in favourable cases, with a minimum detectable concentration of less than 0·1%. Owing to the experimental difficulties of dispersing and detecting X-rays of wavelength longer than a few Ångström units without considerable loss of intensity, the method cannot at present be easily applied to elements lower in atomic number than about chlorine ($Z = 17$, Cl $K\alpha = 4{\cdot}7$ Å). However, the use of a vacuum spectrometer with mica crystal extends the range to about magnesium ($Z = 12$, Mg $K\alpha = 9{\cdot}9$ Å) as shown by Castaing and Descamps,[8] and, with a proportional counter alone, Dolby[9] has shown that special pulse analysis methods could be used to obtain useful information down to carbon ($Z = 6$, C $K\alpha = 44$ Å).

If the electron probe is scanned over the specimen, information can be rapidly obtained about the surface distribution of an element, but considerations of X-ray intensity which are discussed later, now become more important. The X-ray scanning microanalyser[10, 11, 12] therefore embodies an efficient electron-optical system, which is based on principles determined by Cosslett and Nixon[13] for the point-projection X-ray microscope; the method of deflecting the electron probe follows that developed by Smith[14] in the scanning electron microscope.[15, 16]

PRINCIPLE

In the present equipment, shown schematically in Fig. 1, the electron probe is focused by two magnetic lenses on to the specimen at the bottom of the column, and scanned over the surface by deflexion coils between the lenses. X-rays emerge through a port on the right of the objective lens, and characteristic radiation of a particular wavelength may be selected either with the crystal spectrometer or with proportional counter and pulse analyser. The amplified signal modulates the beam of a cathode-ray tube scanned in synchronism with the probe, which thus displays the surface distribution of the corresponding element. Alternatively, with the scintillation counter on the left, back-scattered electrons may be collected to form an image of the surface topography of the same area, as in the scanning electron microscope. The resolution of the X-ray image is limited by electron penetration as before to about 1 μ; that of the electron image is somewhat better and a value as low as 200 Å has been obtained in the scanning electron microscope of Smith and Oatley.[16] The maximum area of scan is at present limited to $400 \times 400\ \mu$, owing to the off-axis aberrations of the objective lens.

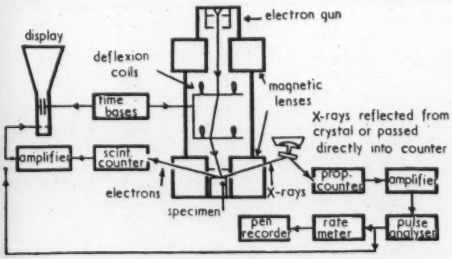

Fig. 1. Block diagram of the X-ray scanning microanalyser

After an electron or X-ray image has been obtained, the scan may be stopped and the electron probe accurately located on a particular feature in the surface by adjusting the position of the display tube spot on the image, which is retained for several seconds on a screen of long persistence. Quantitative analysis may then be carried out in the same way as with the static probe instrument, and a similar accuracy and detection sensitivity are obtainable. With the present air spectrometer, the lightest element detectable is chlorine, but a vacuum spectrometer capable of going down to magnesium has been successfully tested.

The main advantages of the scanning technique are thus the following. The distribution of a particular element can be obtained much more rapidly than in a point-by-point analysis using a static electron probe. Secondly, the accuracy of focusing and locating the electron beam is not limited by the resolution of an optical microscope, and errors due to interaction of stray lens field with a ferromagnetic specimen are eliminated. The importance of both these features is demonstrated later, but first, attention will be given to the statistical limitations to image quality, as governed by the intensity of characteristic X-ray emission.

THEORETICAL CONSIDERATIONS

Since the X-ray image is built up by collection of a limited number of quanta, it is necessary to consider the effect of statistical fluctuations in the number falling in each image point. If the fluctuation is sufficient to produce a visible change in brightness, the image will have a grainy appearance and is said to contain noise. To avoid this the number representing each image point must exceed a certain minimum. McMullan,[15] and Smith and Oatley[16] have used the theory developed by Rose[17] to calculate the corresponding effect in the scanning electron microscope, but quantum noise assumes greater importance in the present case owing to the low efficiency of X-ray production and to the small fraction collected.

If m is the number of quanta/image point and δm is the variation in m which produces the minimum visible change in brightness, then the r.m.s. fluctuation $m^{1/2}$ is related to δm by a constant k in such a way that $m^{1/2} \leqslant \delta m/k$ for a noise-free image. Rose has given the value of k as about 4. Assuming that the brightness is proportional to m, the minimum relative change in brightness which can be detected by the eye, i.e. the threshold contrast is $c = \delta m/m$. Thus, in the limiting case where noise is just visible $c = k/m^{1/2}$ and $m = (k/c)^2$. If the image is composed of N^2 image points built up in a time T, then the minimum counting rate required is

$$n = \frac{N^2 m}{T} = \frac{N^2 k^2}{Tc^2} \qquad (1)$$

For typical conditions of viewing the display screen, $N = 300$ lines, $T = 5$ s and $c = 15\%$, so that $n = 1{\cdot}3 \times 10^7$ s. In recording the image photographically, however, the final print is usually viewed at considerably greater brightness so that the threshold contrast of the eye may be reduced to a few per cent. An exposure time of several minutes is then required with the same count rate and more information is thereby obtained on the print than was visible on the display screen.

It is at once clear that the count rate required for a noise-free image is too high with normal counting equipment for the pulses to remain discrete, but if no pulse height discrimination is to be made, this is immaterial. A noise-free image can thus be obtained using a scintillation counter to detect X-rays of all wavelengths, followed by an amplifier fast enough only to respond to the variation between adjacent image points. An approximate check of the noise criterion has been made in this way, but in practice more importance attaches to being able to form the image with a selected emission line. It would be possible to precede the scintillation counter with a crystal monochromator, but the emitted X-ray intensity would then have to be inconveniently high, owing to the loss in reflexion at the crystal and to the smaller solid angle of collected X-rays. One must therefore accept, at present, the disadvantage that the visible image cannot be noise-free, but this consequence of a lower count rate is partly offset by being able to make use of the energy resolving property of a proportional counter. A characteristic line may be selected either with a crystal monochromator in front of the counter or with a pulse height analyser; the relative advantages of each method will be discussed later.

The maximum count rate of a proportional counter without deterioration of the energy resolution is in the region of 5×10^4 s. At first sight, this large deficiency in the rate compared with 10^7 s required for a noise-free image might be expected to impair image quality beyond the point where useful information can be obtained, especially when it is realized that it would involve only about 3 quanta/image point with the viewing conditions above. That this is not so, however, is illustrated in Fig. 2 which shows the progressive increase of noise in the image as the count rate is reduced. The specimen was a 200 mesh/in. copper grid; Cu $K\alpha$ radiation was selected with the crystal monochromator so that the superimposed silver grid appears dark. Even at the lowest count rate of 500 counts/s, which is nearly 30 000 times lower than the rate required for a noise-free image, the form of the copper grid is plainly visible, though little can be said about detail in the surface. As pointed out by Rose the eye integrates, over a certain area, the information presented to it, so that the effective size of image point is increased to an extent determined by the threshold contrast required. Thus it is often practicable to establish the form of large features in the specimen, and then to narrow down the scan to examine regions of particular interest in greater detail. For this reason it is advantageous to be able to scan the electron probe over as large an area in the surface as possible, though in practice lens aberrations limit this to about $\frac{1}{2}$ mm square.

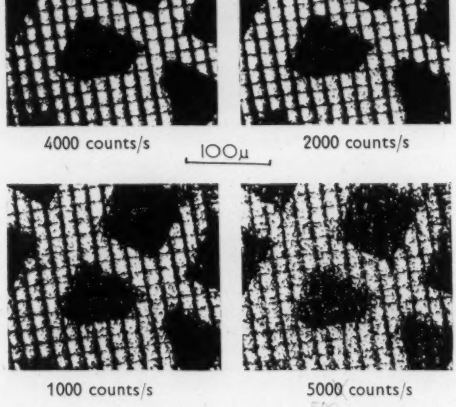

Fig. 2. X-ray scanning image, with Cu $K\alpha$ radiation selected, of 200 mesh/in. copper grid and superimposed silver grid, showing increase in graininess as count rate is reduced. Exposure 2 min

So far the discussion has been entirely concerned with the count rate required to form the image. It is now necessary to determine how small the emitting region of the specimen can be for a given count rate to be recorded. To do this, the count rate must first be related to the accelerating voltage and probe current.

Early experimental work, reviewed by Compton and Allison,[18] showed that the total number of characteristic quanta generated per second, or the quantum intensity n_e, varied with the accelerating voltage V according to the power law

$$n_e \propto (V - V_k)^p$$

where V_k is the excitation voltage for K ionization. For $V/V_k < 4$, p was found to lie in the region of 1·6 to 1·7; measurements on Cu $K\alpha$ radiation in the present apparatus confirm that p is close to 1·7. Since the quantum intensity is linearly related to the probe current i, the expression may be rewritten

$$n_e = Ai(U - 1)^{1{\cdot}7}$$

where A is constant for a particular target element, and U is the excitation ratio V/V_k. Little information is available to give a reliable value of A. Stoddard[19] has related empirically the intensities of characteristic and continuous radiation for certain elements, and, from an expression given by Compton and Allison[18] for the continuous intensity, A is found to be $2{\cdot}2 \times 10^{15}$ for copper with i in amps. In addition, p again comes out to be 1·7. This value of A is in close agreement with measurements made by Braxton, Baez and Kirkpatrick[20] at 15·5 kV and by Worthington and Tomlin[21] at 30 kV, and will therefore be used in the following argument. It may, however, be somewhat low, since experiments by Dyson[22] and theoretical calculations by Worthington and Tomlin suggest values 1·6 and 2·0 times greater respectively. On the other hand, the emitted intensity may be reduced by absorption within the target; this has not been taken into account but is negligible in the case of copper provided the emergent angle is sufficiently high. If the overall efficiency of the detecting system is f, then the count rate

$$n = fn_e = fAi(U - 1)^{1{\cdot}7} \qquad (2)$$

f is determined by design considerations, and the maximum current i which can be delivered into a probe of given

Gaussian-optical diameter is limited by the emission of the electron gun.

Langmuir[23] has related theoretically the axial current density j_a at an image of the cross-over of an electron gun to the current density j_c at the cathode. With an aberration-free optical system

$$j_a = j_c\left(1 + \frac{V}{V_e}\right)\sin^2\alpha$$

where V_e is the most probable energy of electron emission at the cathode. Since $V \gg V_e$ and $\sin\alpha \simeq \alpha$, the semi-angle of the electron beam at the image of the cross-over, then

$$j_a = j_c\frac{V}{V_e}\alpha^2$$

Haine and Einstein[24] have shown that the theoretical current density can be closely approached in practice, with the normal type of tungsten filament gun operated with j_c in the region of 2 A/cm^2. They have also checked Langmuir's prediction that, away from the axis, the current density falls off according to a Gaussian distribution. With these assumptions Smith[14] has given an expression for the total current i that can be delivered into a probe of Gaussian-optical diameter d_0 as

$$i = 0{\cdot}62j_c\frac{V}{V_e}\alpha^2\pi\frac{d_0^2}{4} \qquad (3)$$

where the factor 0·62 is consistent with the definition of d_0 as the diameter at which the current density has fallen to 1/5 of that on the axis.

Nixon[25] has discussed the optics of a two-lens probe-forming system, and has shown how d_0 may be controlled by the strength of the condenser lens. The diameter of the X-ray source is greater than d_0, due to spherical aberration in the objective lens and to lateral diffusion of the electrons in the specimen. Spherical aberration causes a point in the Gaussian-optical image to be spread into a disk of confusion, and the bundle of rays representing this point has a minimum diameter

$$d_s = \tfrac{1}{2}C_s\alpha^3 \qquad (4)$$

where C_s is the spherical aberration coefficient of the objective lens and α is the semi-angular aperture of the probe. C_s is made as small as possible by suitable design of the objective lens, and may be calculated from data by Liebmann[26]; d_s then depends only on the choice of α.

The enlargement of the probe due to lateral diffusion of electrons in the specimen may be estimated from the Thomson–Whiddington law[18] which states that

$$V^2 - V_1^2 \propto \rho x$$

where V_1 is the electron energy at depth x in a target of density ρ. The constant of proportionality has been determined by Terrill[18] and later work, reviewed by Dyson,[22] has shown that, except possibly for elements of high atomic number, this is not far in error for energies of from 5 to 30 keV. Assuming that some electrons are scattered laterally at the surface and retarded according to the same law, X-rays of energy greater than eV_1 come from a hemisphere of radius x. Cosslett[27] has suggested, and experience with the X-ray projection microscope has shown, that the effective volume of X-ray emission is somewhat smaller, and it is proposed to take the diameter d_p of the "disk of confusion" due to electron diffusion as equal to x. Thus, for characteristic X-ray emission of energy eV_k,

$$d_p = \frac{KV_k^2(U^2 - 1)}{\rho} \qquad (5)$$

where, from Terrill, K is equal to $2{\cdot}5 \times 10^{-12}$ with d_p in centimetres and V_k in volts.

Although the aberrations cannot strictly be regarded as imposing a Gaussian spread on each point in the electron probe, it is a better approximation to assume this rather than a linear spread. The diameter d of the X-ray source is therefore obtained by adding the aberrations in quadrature, so that

$$d^2 = d_0^2 + d_s^2 + d_p^2$$

d_0 may be expressed in terms of n from equations (2) and (3), which yield

$$n = 0{\cdot}50fAj_c\frac{V_k}{V_e}\alpha^2U(U-1)^{1{\cdot}7}d_0^2 \qquad (6)$$

d_s and d_p are given by equations (4) and (5), so that

$$d^2 = \frac{2{\cdot}0V_e}{fAj_cV_k}\frac{n}{\alpha^2U(U-1)^{1{\cdot}7}} + \frac{1}{4}C_s^2\alpha^6 + \frac{K^2V_k^4}{\rho^2}(U^2-1)^2$$

For a given count rate, α and U are set to make d a minimum, that is, to give the best resolving power for the instrument. Differentiation with respect to α and to U shows that this occurs when

$$d = 1{\cdot}5d_0 = 2{\cdot}5d_s = 1{\cdot}6d_p$$

The optimum values of α and U, obtained from equations (4) and (5), are

$$\alpha = \left(\frac{2}{C_s}\cdot\frac{d}{2{\cdot}5}\right)^{1/3}$$

$$U = \left(\frac{\rho}{KV_k^2}\cdot\frac{d}{1{\cdot}6} + 1\right)^{1/2}$$

Finally, the insertion of these optimum values in equation (6), with the approximation that $U(U-1)^{1{\cdot}7} = 0{\cdot}29(U^2-1)^{1{\cdot}7}$ within 10% for $1 < U < 4$, gives the count rate n in terms of the minimum X-ray source diameter d

$$n = 0{\cdot}026fAj_c\frac{V_k}{V_e}C_s^{-2/3}\left(\frac{\rho}{KV_k^2}\right)^{1{\cdot}7}d^{4{\cdot}37}$$

Thus, under optimum conditions, the count rate varies somewhat more rapidly than the fourth power of the X-ray source diameter. The absolute value for a source diameter of, say, 1 μ may be obtained by inserting the following typical values

$A = 2{\cdot}2 \times 10^{15}$	$C_s = 0{\cdot}4$ cm
$j_c = 2$ A/cm^2	$\rho = 8{\cdot}9$ g/cm^3
$V_k = 9$ kV	$K = 2{\cdot}5 \times 10^{-12}$
$V_e = 0{\cdot}25$ V	

whence $n = 1{\cdot}9 \times 10^9 f$ counts/s.

The collection efficiency f varies greatly with the type of spectrometer; with a typical curved lithium fluoride crystal and argon proportional counter, as used in the present instrument, the crystal accepts a beam $1{\cdot}3^\circ \times 5{\cdot}9^\circ$. The reflexion efficiency is in the region of 5%, though higher values may be obtainable with careful selection of the crystal, and the efficiency of the counter for Cu $K\alpha$ is about 60%. Thus $f = 5{\cdot}5 \times 10^{-6}$ and the count rate n comes out to be about 10^4/s, which is sufficient for a useful if not noise-free image. To give the optimum conditions for a 1 μ X-ray source in copper, α must be $5{\cdot}9 \times 10^{-2}$, $V = 17{\cdot}4$ kV, and $i = 1{\cdot}1$ μA. Such a performance can be realized in practice, though it is convenient where possible to work under somewhat relaxed conditions with an accelerating voltage of about 25 kV and correspondingly lower probe current. The source diameter is not greatly increased, and lens and gun adjustments are more easily carried out.

Wittry[28] has recently considered the optimum conditions

For typical conditions of viewing the display screen, $N = 300$ lines, $T = 5$ s and $c = 15\%$, so that $n = 1{\cdot}3 \times 10^7$ s. In recording the image photographically, however, the final print is usually viewed at considerably greater brightness so that the threshold contrast of the eye may be reduced to a few per cent. An exposure time of several minutes is then required with the same count rate and more information is thereby obtained on the print than was visible on the display screen.

It is at once clear that the count rate required for a noise-free image is too high with normal counting equipment for the pulses to remain discrete, but if no pulse height discrimination is to be made, this is immaterial. A noise-free image can thus be obtained using a scintillation counter to detect X-rays of all wavelengths, followed by an amplifier fast enough only to respond to the variation between adjacent image points. An approximate check of the noise criterion has been made in this way, but in practice more importance attaches to being able to form the image with a selected emission line. It would be possible to precede the scintillation counter with a crystal monochromator, but the emitted X-ray intensity would then have to be inconveniently high, owing to the loss in reflexion at the crystal and to the smaller solid angle of collected X-rays. One must therefore accept, at present, the disadvantage that the visible image cannot be noise-free, but this consequence of a lower count rate is partly offset by being able to make use of the energy resolving property of a proportional counter. A characteristic line may be selected either with a crystal monochromator in front of the counter or with a pulse height analyser; the relative advantages of each method will be discussed later.

The maximum count rate of a proportional counter without deterioration of the energy resolution is in the region of 5×10^4 s. At first sight, this large deficiency in the rate compared with 10^7 s required for a noise-free image might be expected to impair image quality beyond the point where useful information can be obtained, especially when it is realized that it would involve only about 3 quanta/image point with the viewing conditions above. That this is not so, however, is illustrated in Fig. 2 which shows the progressive increase of noise in the image as the count rate is reduced. The specimen was a 200 mesh/in. copper grid; Cu $K\alpha$ radiation was selected with the crystal monochromator so that the superimposed silver grid appears dark. Even at the lowest count rate of 500 counts/s, which is nearly 30 000 times lower than the rate required for a noise-free image, the form of the copper grid is plainly visible, though little can be said about detail in the surface. As pointed out by Rose the eye integrates, over a certain area, the information presented to it, so that the effective size of image point is increased to an extent determined by the threshold contrast required. Thus it is often practicable to establish the form of large features in the specimen, and then to narrow down the scan to examine regions of particular interest in greater detail. For this reason it is advantageous to be able to scan the electron probe over as large an area in the surface as possible, though in practice lens aberrations limit this to about $\frac{1}{4}$ mm square.

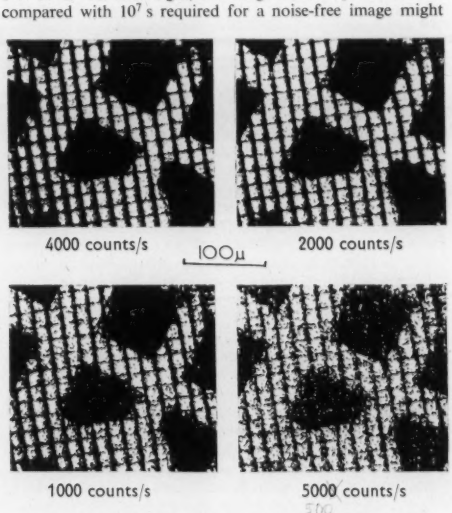

Fig. 2. X-ray scanning image, with Cu $K\alpha$ radiation selected, of 200 mesh/in. copper grid and superimposed silver grid, showing increase in graininess as count rate is reduced. Exposure 2 min

So far the discussion has been entirely concerned with the count rate required to form the image. It is now necessary to determine how small the emitting region of the specimen can be for a given count rate to be recorded. To do this, the count rate must first be related to the accelerating voltage and probe current.

Early experimental work, reviewed by Compton and Allison,[18] showed that the total number of characteristic quanta generated per second, or the quantum intensity n_e, varied with the accelerating voltage V according to the power law

$$n_e \propto (V - V_k)^p$$

where V_k is the excitation voltage for K ionization. For $V/V_k < 4$, p was found to lie in the region of $1{\cdot}6$ to $1{\cdot}7$; measurements on Cu $K\alpha$ radiation in the present apparatus confirm that p is close to $1{\cdot}7$. Since the quantum intensity is linearly related to the probe current i, the expression may be rewritten

$$n_e = Ai(U - 1)^{1{\cdot}7}$$

where A is constant for a particular target element, and U is the excitation ratio V/V_k. Little information is available to give a reliable value of A. Stoddard[19] has related empirically the intensities of characteristic and continuous radiation for certain elements, and, from an expression given by Compton and Allison[18] for the continuous intensity, A is found to be $2{\cdot}2 \times 10^{15}$ for copper with i in amps. In addition, p again comes out to be $1{\cdot}7$. This value of A is in close agreement with measurements made by Braxton, Baez and Kirkpatrick[20] at 15·5 kV and by Worthington and Tomlin[21] at 30 kV, and will therefore be used in the following argument. It may, however, be somewhat low, since experiments by Dyson[22] and theoretical calculations by Worthington and Tomlin suggest values $1{\cdot}6$ and $2{\cdot}0$ times greater respectively. On the other hand, the emitted intensity may be reduced by absorption within the target; this has not been taken into account but is negligible in the case of copper provided the emergent angle is sufficiently high. If the overall efficiency of the detecting system is f, then the count rate

$$n = fn_e = fAi(U - 1)^{1{\cdot}7} \qquad (2)$$

f is determined by design considerations, and the maximum current i which can be delivered into a probe of given

Gaussian-optical diameter is limited by the emission of the electron gun.

Langmuir[23] has related theoretically the axial current density j_a at an image of the cross-over of an electron gun to the current density j_c at the cathode. With an aberration-free optical system

$$j_a = j_c\left(1 + \frac{V}{V_e}\right)\sin^2\alpha$$

where V_e is the most probable energy of electron emission at the cathode. Since $V \gg V_e$ and $\sin\alpha \simeq \alpha$, the semi-angle of the electron beam at the image of the cross-over, then

$$j_a = j_c\frac{V}{V_e}\alpha^2$$

Haine and Einstein[24] have shown that the theoretical current density can be closely approached in practice, with the normal type of tungsten filament gun operated with j_c in the region of 2 A/cm^2. They have also checked Langmuir's prediction that, away from the axis, the current density falls off according to a Gaussian distribution. With these assumptions Smith[14] has given an expression for the total current i that can be delivered into a probe of Gaussian-optical diameter d_0 as

$$i = 0{\cdot}62j_c\frac{V}{V_e}\alpha^2\pi\frac{d_0^2}{4} \tag{3}$$

where the factor 0·62 is consistent with the definition of d_0 as the diameter at which the current density has fallen to 1/5 of that on the axis.

Nixon[25] has discussed the optics of a two-lens probe-forming system, and has shown how d_0 may be controlled by the strength of the condenser lens. The diameter of the X-ray source is greater than d_0, due to spherical aberration in the objective lens and to lateral diffusion of the electrons in the specimen. Spherical aberration causes a point in the Gaussian-optical image to be spread into a disk of confusion, and the bundle of rays representing this point has a minimum diameter

$$d_s = \tfrac{1}{2}C_s\alpha^3 \tag{4}$$

where C_s is the spherical aberration coefficient of the objective lens and α is the semi-angular aperture of the probe. C_s is made as small as possible by suitable design of the objective lens, and may be calculated from data by Liebmann[26]; d_s then depends only on the choice of α.

The enlargement of the probe due to lateral diffusion of electrons in the specimen may be estimated from the Thomson–Whiddington law[18] which states that

$$V^2 - V_1^2 \propto \rho x$$

where V_1 is the electron energy at depth x in a target of density ρ. The constant of proportionality has been determined by Terrill[18] and later work, reviewed by Dyson,[22] has shown that, except possibly for elements of high atomic number, this is not far in error for energies of from 5 to 30 keV. Assuming that some electrons are scattered laterally at the surface and retarded according to the same law, X-rays of energy greater than eV_1 come from a hemisphere of radius x. Cosslett[27] has suggested, and experience with the X-ray projection microscope has shown, that the effective volume of X-ray emission is somewhat smaller, and it is proposed to take the diameter d_p of the "disk of confusion" due to electron diffusion as equal to x. Thus, for characteristic X-ray emission of energy eV_k,

$$d_p = \frac{KV_k^2(U^2 - 1)}{\rho} \tag{5}$$

where, from Terrill, K is equal to $2{\cdot}5 \times 10^{-12}$ with d_p in centimetres and V_k in volts.

Although the aberrations cannot strictly be regarded as imposing a Gaussian spread on each point in the electron probe, it is a better approximation to assume this rather than a linear spread. The diameter d of the X-ray source is therefore obtained by adding the aberrations in quadrature, so that

$$d^2 = d_0^2 + d_s^{2\prime} + d_p^2$$

d_0 may be expressed in terms of n from equations (2) and (3), which yield

$$n = 0{\cdot}50fAj_c\frac{V_k}{V_e}\alpha^2U(U-1)^{1\cdot7}d_0^2 \tag{6}$$

d_s and d_p are given by equations (4) and (5), so that

$$d^2 = \frac{2{\cdot}0V_e}{fAj_cV_k}\frac{n}{\alpha^2U(U-1)^{1\cdot7}} + \frac{1}{4}C_s^2\alpha^6 + \frac{K^2V_k^4}{\rho^2}(U^2-1)^2$$

For a given count rate, α and U are set to make d a minimum, that is, to give the best resolving power for the instrument. Differentiation with respect to α and to U shows that this occurs when

$$d = 1{\cdot}5d_0 = 2{\cdot}5d_s = 1{\cdot}6d_p$$

The optimum values of α and U, obtained from equations (4) and (5), are

$$\alpha = \left(\frac{2}{C_s}\cdot\frac{d}{2{\cdot}5}\right)^{1/3}$$

$$U = \left(\frac{\rho}{KV_k^2}\cdot\frac{d}{1{\cdot}6} + 1\right)^{1/2}$$

Finally, the insertion of these optimum values in equation (6), with the approximation that $U(U-1)^{1\cdot7} = 0{\cdot}29(U^2-1)^{1\cdot7}$ within 10% for $1 < U < 4$, gives the count rate n in terms of the minimum X-ray source diameter d

$$n = 0{\cdot}026fAj_c\frac{V_k}{V_e}C_s^{-2/3}\left(\frac{\rho}{KV_k^2}\right)^{1\cdot7}d^{4\cdot37}$$

Thus, under optimum conditions, the count rate varies somewhat more rapidly than the fourth power of the X-ray source diameter. The absolute value for a source diameter of, say, 1 μ may be obtained by inserting the following typical values

$A = 2{\cdot}2 \times 10^{15}$ $\qquad$ $C_s = 0{\cdot}4$ cm
$j_c = 2$ A/cm^2 $\qquad$ $\rho = 8{\cdot}9$ g/cm^3
$V_k = 9$ kV $\qquad$ $K = 2{\cdot}5 \times 10^{-12}$
$V_e = 0{\cdot}25$ V

whence $n = 1{\cdot}9 \times 10^9 f$ counts/s.

The collection efficiency f varies greatly with the type of spectrometer; with a typical curved lithium fluoride crystal and argon proportional counter, as used in the present instrument, the crystal accepts a beam $1{\cdot}3^\circ \times 5{\cdot}9^\circ$. The reflexion efficiency is in the region of 5%, though higher values may be obtainable with careful selection of the crystal, and the efficiency of the counter for Cu $K\alpha$ is about 60%. Thus $f = 5{\cdot}5 \times 10^{-6}$ and the count rate n comes out to be about 10^4/s, which is sufficient for a useful if not noise-free image. To give the optimum conditions for a 1 μ X-ray source in copper, α must be $5{\cdot}9 \times 10^{-2}$, $V = 17{\cdot}4$ kV, and $i = 1{\cdot}1$ μA. Such a performance can be realized in practice, though it is convenient where possible to work under somewhat relaxed conditions with an accelerating voltage of about 25 kV and correspondingly lower probe current. The source diameter is not greatly increased, and lens and gun adjustments are more easily carried out.

Wittry[28] has recently considered the optimum conditions

for a point source of X-rays, and, with somewhat different assumptions, has arrived at similar figures. The treatment above is, however, more easily applicable to the scanning microanalyser. It should be emphasized that, with the data available it can only be approximate and has only been evaluated for a target of one element; nevertheless it indicates in general how the optimum conditions are to be chosen and the theoretical predictions are not far from those pertaining in practice.

One other theoretical aspect should be considered: the heat dissipation in the target. With a homogeneous target thick compared with the penetration of the electron beam, the isothermals are approximately hemispherical and the heat flow E is given by

$$E = \frac{2\pi\lambda(T_r - T_R)}{1/r - 1/R}$$

where λ is the thermal conductivity, T_r and T_R are the temperatures at the radius r of the X-ray source and R of the specimen holder. Since $R \gg r$ and $r = \frac{1}{2}d$, this reduces to

$$E = iV = \pi\lambda d(T_r - T_R)$$

The temperature within the source is greater than T_r by an amount $\sim 0{\cdot}1(T_r - T_R)$ which will be neglected. Thus the temperature rise in the specimen may be calculated for any combination of probe current and accelerating voltage. In the conditions assumed above with $\lambda = 0{\cdot}9$ cal cm^{-2} s^{-1} per deg C, the temperature rise in a copper target is thus about 16° C, which is not serious. For some materials, however, the thermal conductivity is lower by a factor of 1000, so that the probe current must be considerably reduced to avoid damage. In this case the count rate may be too low for satisfactory image formation using a crystal monochromator, and wavelength selection must be made instead with the proportional counter and pulse analyser. The removal of reflexion loss at the crystal increases the count rate by a factor of 20. The proportional counter is also useful in the preliminary investigation of a surface, where the presence of a strong characteristic line can be immediately recognized on a pulse monitoring oscilloscope. Provision must thus be made in the design of the spectrometer, for removal of the crystal to allow X-rays to pass straight into the counter, and this and other features in the design will now be considered.

APPARATUS

An RCA–EMB electron microscope provided a convenient starting point for the electron-optical system, since power supplies, vacuum system, gun and condenser lens could be used with little or no modification; the most noteworthy change was to alter the gun to conform to the design considered by Haine and Einstein,[24] with provision for filament centring during operation. The main consideration in the design of the objective lens was the requirement that the spherical aberration, and hence the focal length, should be as small as possible; at the same time X-rays must be collected at a large angle to the specimen surface to reduce absorption of the emergent beam. These conditions are satisfied in the present lens,[29] which was designed from the data of Liebmann[26] to have a focal length of 0·4 cm with a spherical aberration coefficient also of 0·4 cm. X-rays are collected through the polepiece gap at 20° to the specimen surface, which is set normal to the axis of the column to avoid defocusing of the probe at the edges of the scan. The deflexion coils are situated before the lens, and consist of two sets balanced in opposition so that the deflected beam always passes through the lens aperture (Fig. 1). The specimen, which is 1/8 in. in diameter, is insulated from the lens to permit measurement of the incident current, and can be moved and rotated during operation.

In many applications, it was found that more than sufficient X-ray intensity was available with this lens, and an alternative objective lens has been successfully tested, which brings the electron beam to a focus outside the lens. The spherical aberration coefficient is somewhat increased, but larger specimens can be accommodated and readily interchanged with pure elements for calibration without breaking the vacuum. Both these features are of significant advantage in a general purpose instrument. A simplified sectional diagram of this lens is shown in Fig. 3. The pole-

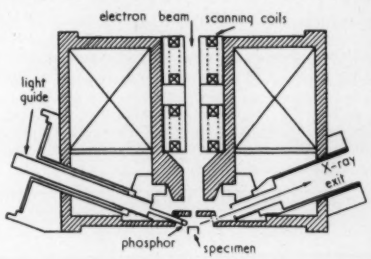

Fig. 3. Simplified diagram of objective lens for large specimens

piece is of the pinhole type,[30] and X-rays are collected at an angle of 20° to the specimen surface through the lens casing. A similar port on the left permits the introduction of a phosphor for sampling the intensity of scattered electrons, the light being conveyed by a Perspex rod to the photomultiplier mounted outside the lens. The deflexion coils consist of two balanced sets as before, housed in the wide upper bore of the lens to form one compact unit.

The main features of the scanning electronics are determined by the requirement that the spot on the display tube must be used to position the electron probe on the specimen. This means that the movement of the spot must at all times be locked to that of the probe, and that the screen of the display tube must retain the image sufficiently long to carry out the positioning after the scan is switched off. A long persistence screen is in any case desirable to reduce the effect of quantum noise. A simple electrostatic cathode-ray tube is adequate, which resolves about 300 lines across an image 8 cm square and has a useful persistence of about 20 s. The spot is scanned by line and frame sawtooth generators which also supply current to the probe-deflecting coils, the inductance of which sets the maximum convenient line frequency at about 150 lines/s. The frame frequency is thus about 0·5 frames/s and several scans are required for the afterglow to build up to maximum brightness. To match these scanning speeds, the scintillation counter amplifier, which provides a gain of 100, has a frequency response from 3 c/s to 25 kc/s. The d.c. level is reset before each line by a clamping pulse applied to the grid of the display tube; this is generated by switching off the electron probe during flyback, by means of an extra winding on one set of deflexion coils to deflect the beam off the lens aperture. No d.c. restoration is necessary with X-ray image formation since each quantum produces a discrete pulse at the grid of the display tube.

The crystal spectrometer is shown diagrammatically in Fig. 4. The crystal, which is lithium fluoride, is mounted on a goniometer head just outside a hydrogen tube leading from the centre of the lens. An argon-flow proportional counter collects the diffracted X-ray beam through a Melinex window, which is sufficiently close to the crystal to accept X-rays reflected over a wide range of Bragg angles without moving

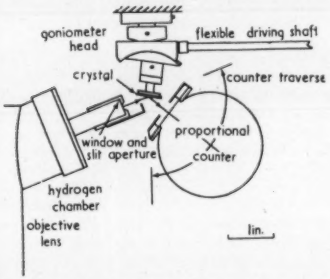

Fig. 4. X-ray spectrometer with short air path; X-rays may be reflected off curved crystal or passed direct into proportional counter

the counter; this simple arrangement has the disadvantage of increasing the background of scattered radiation but enables the path length of X-rays in air to be as low as 3 cm. The spectrometer was initially intended for use with a flat crystal and narrow entrance slit, but it was subsequently found beneficial to use a curved crystal to reflect a considerably wider pencil of X-rays, even though Rowland circle focusing conditions could only be obeyed at one Bragg angle setting. The reflexion of lithium fluoride was found to be sufficiently broad that a certain amount of defocusing was possible without adversely affecting the X-ray intensity. In this way, a range of 10 to 60° in Bragg angle could be covered with only three lithium fluoride crystals curved to appropriate radii. Typical working conditions of 25 kV accelerating voltage and 0·1 μA probe current gave a count rate of 10^4/s of Fe $K\alpha$ from a specimen of pure iron, with a background about 2% of the peak height. For analysis of the X-ray emission with the proportional counter and pulse analyser, the crystal may be removed and the counter moved into the direct X-ray beam.

The pulses from the proportional counter, which are of height approximately proportional to the X-ray quantum energy, are analysed by conventional techniques, the electronics consisting of amplifier, pulse height analyser, ratemeter and pen recorder. The pulse height analyser is normally used only when X-rays are collected by the counter directly, but is sometimes useful in conjunction with the crystal to reduce the background of scattered radiation of different wavelength. The overall dead-time of the system is 5 μs, and square pulses of this length are used to form the X-ray image on the display tube. The apparatus is capable of 1% accuracy in intensity measurements provided the statistical error is made negligible by using a sufficiently long counting time.

QUANTITATIVE MICROANALYSIS

For quantitative work, certain precautions are necessary to ensure accurate measurement of characteristic line intensity. A major cause of error is instability in the X-ray output due to build-up of carbon contamination on the specimen under the impact of the electron beam. This depends upon the pumping conditions in the neighbourhood of the specimen, and in the present lens can cause a 10% reduction in characteristic intensity over a period of a few minutes, due to the retardation of electrons before reaching the specimen. It was found, however, that this could be almost entirely overcome by the introduction of a copper rod close to the specimen, the other end of which is cooled by immersion in liquid air outside the vacuum. The total current leaving the electron gun is stabilized by the use of auto-bias, but some instability can appear in the probe current due to mechanical drift of the filament in the grid aperture causing movement of the beam off the lens aperture. This is overcome by occasionally recentring the filament during operation, and it is then possible to maintain the X-ray emission constant to 1% over periods of an hour or more.

Errors in the interpretation of the experimental results have been fully discussed by Castaing and Descamps.[31, 8] These arise mainly from absorption of the X-ray beam leaving the specimen and from fluorescence radiation excited in the matrix surrounding the region of analysis. Often these corrections are negligible, as in the case of a Cu–Zn alloy, where each element is transparent to the radiation from the other. On the other hand, in the unfavourable case of a 60% Fe, 40% Cr alloy where Fe $K\alpha$ radiation is strongly absorbed by the chromium causing fluorescence, the apparent composition would be 47% Fe, 44% Cr. This is for an emergent angle of 20° and an accelerating voltage of 25 kV; the absorption effect is reduced by an increase in emergent angle and a decrease in accelerating voltage. Further departure from the simple law of proportionality of characteristic intensity to concentration occurs when an alloy of two elements of widely different atomic number is analysed. In cases where corrections are not easily calculable it is often preferable to make up a calibration sample of known composition close to that of the specimen rather than to attempt

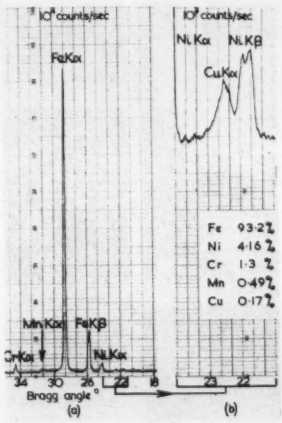

Fig. 5. X-ray emission spectrum from steel of given composition

(*a*) Complete spectrum.
(*b*) Part of spectrum at greater sensitivity to show Cu Kα peak.

comparison with a pure element. It is also important to prepare a smooth surface on the specimen so that the absorption of the emergent beam is accurately reproducible.

A typical spectrum, obtained from a steel of known composition, is shown in Fig. 5. Analysis was made of all the elements listed, the known concentrations of which are given, and results agreed to within experimental error; for the iron this was about $\pm 1\%$ and for the low concentration elements about $\pm 0{\cdot}1\%$. The amount of copper was $0{\cdot}17\%$, and although the Cu $K\alpha$ peak is not visible in (*a*), it can be readily detected by increasing the probe current and by plotting the spectrum more slowly to reduce background fluctuations. The result of doing this is shown in (*b*), which was plotted at $\frac{1}{4}°$/min with a probe current of 1 μA, about the maximum for a 1 μ probe. If these conditions are taken to represent the most sensitive convenient in practice, the minimum detectable concentration of copper over a volume of 1 μ^3, may be estimated at $0{\cdot}05\%$ which represents a mass sensitivity of better than 10^{-14} g. Although there are methods of analysis with a better concentration sensitivity than the X-ray emission method, there are none with better mass sensitivity. For this reason, the emission method is often the only way of analysing small masses of material, as, for example, in inclusion and segregation problems.

APPLICATIONS

Specimens of many types have been examined in the X-ray scanning microanalyser; with a separate instrument Long[32] has explored some of the mineralogical applications. The main advantages of the method can be illustrated by two examples. The first is a study of a mild steel, which had shown a tendency to crack during hot working. The cause was believed to be the segregation of copper and nickel impurities at the surface, but no direct evidence was available to support this, and the extent of segregation was not known. An optical micrograph of a section cut normal to the surface is given in Fig. 6(*a*), and shows a cavity typical of many associated with larger cracks. The same field was examined in the scanning microanalyser, first as a scattered electron image [Fig. 6(*b*)] and then by selection of Fe $K\alpha$, Ni $K\alpha$ and Cu $K\alpha$ radiations [Fig.6(*c*), (*d*), (*e*)]. These clearly demonstrate the presence of a layer surrounding the cavity rich in copper and nickel, and from the image on the display tube, it was possible to select the point of maximum segregation and carry out a quantitative analysis. The result indicated that, in regions a few microns across, the copper and nickel concentration was increased from the bulk average of $0{\cdot}2\%$ of each element to about 30%. An alloy was thus formed which was molten at the temperature of hot working and therefore had little cohesive strength. The result is described in greater detail elsewhere.[33] The points of maximum segregation could have been found with a static probe analyser only by a prolonged point-by-point analysis.

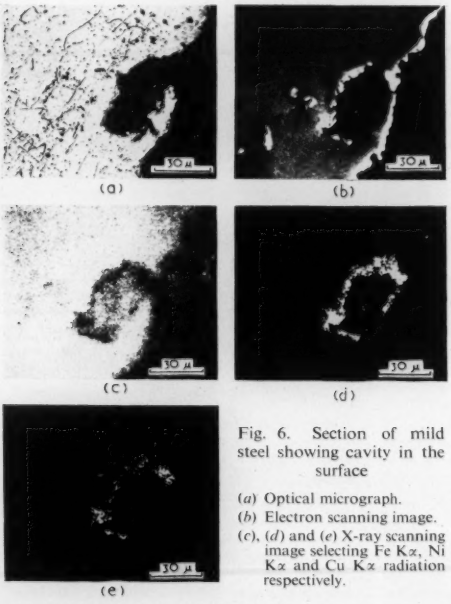

Fig. 6. Section of mild steel showing cavity in the surface

(*a*) Optical micrograph.
(*b*) Electron scanning image.
(*c*), (*d*) and (*e*) X-ray scanning image selecting Fe Kα, Ni Kα and Cu Kα radiation respectively.

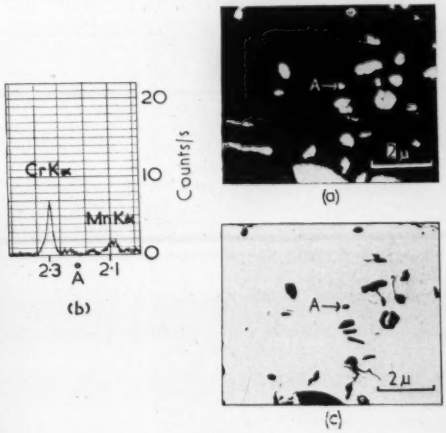

Fig. 7. Carbide particles in extraction replica from steel

(*a*) Electron scanning image.
(*b*) X-ray spectrum from particle *A*.
(*c*) Normal electron micrograph showing *A* to be about 3000 Å diameter.

The second advantage of the scanning method, that of accurate location, is shown particularly in the study of carbon film extraction replicas. In this case, the particles may be well below 1 μ in size, so that a large fraction of the incident electrons are transmitted, and the effect of lateral diffusion is reduced. A smaller X-ray source can then be obtained, as demonstrated by Nixon[34] and the resolution of the microanalyser is correspondingly improved. This is illustrated with an extraction replica taken from an intergranular fracture surface of steel. Fig 7(*a*) shows the electron scanning image of carbide particles on the carbon film, and Fig. 7(*b*) is the X-ray emission spectrum plotted from a

selected particle *A*, which is seen to contain chromium and manganese. The diameter of *A* is found from the normal electron micrograph of the same field [Fig. 7(c)] to be about 3000 Å. It is thus possible to analyse, at least qualitatively, individual particles on or below the limit of resolving power of the optical microscope, and a wide range of applications in conjunction with the electron microscope is foreseen.

CONCLUSIONS

The present work has illustrated the main advantages of the X-ray scanning microanalyser which are: image formation with a selected emission line to show the surface distribution of an element, and accurate positioning of the electron probe on a selected feature in the specimen for detailed analysis. Against the scanning method is to be set its complication, which lies mainly in the electronics. In view of the amount of equipment required by both static and scanning methods for analysis and for power supplies to the column, however, the electronics associated with the scanning forms a relatively small part of the total, and has proved satisfactory and reliable.

Further development of the instrument was thus indicated and two separate lines are being followed. Firstly, the need was felt for an instrument to be given over entirely to the many possible applications of the method, with facilities for the rapid examination of a large number of specimens. Such a machine was required by the Tube Investments Research Laboratories for metallurgical applications, and has now been constructed there.[35] It embodies the second type of objective lens described above and a specimen chamber with facilities for interchange, traverse and optical viewing of the specimen without breaking the vacuum. A vacuum spectrometer with sealed-off proportional counter permits the analysis of elements of atomic number 12 (Mg) and above.

The second line of development is towards better resolution, for thick specimens as well as for specimens thinner than the depth of electron penetration. This necessitates the use of a lower accelerating voltage which in turn reduces the available X-ray intensity; theoretical considerations given above for a thick specimen indicate that the characteristic intensity varies roughly as the fourth power of the resolution. The greatest room for improvement lies in the detecting system, since the normal type of crystal spectrometer makes use of only about 10^{-5} of the emitted quanta. With a proportional counter close to the specimen it should be possible to improve the efficiency to about 10^{-1}, but this has the disadvantage of poorer energy resolution. Unless an improved proportional counter becomes available, therefore, it is likely that a better resolution will be achieved through the use of proportional counter alone for X-ray image formation, together with a crystal spectrometer for static probe analysis. Further work is now being carried out along these lines to establish the practical resolution limit for a wide range of elements.

ACKNOWLEDGEMENTS

The author is indebted to Dr. V. E. Cosslett and other members of the Laboratory for many helpful discussions, and to the Department of Scientific and Industrial Research for two awards. The steel specimen was kindly provided by Dr. D. A. Melford of Tube Investments Research Laboratories, and the extraction replica by Dr. R. G. Ward of Sheffield University.

REFERENCES

(1) Hevesy, G. von. *Chemical analysis by X-rays and its applications* (New York: McGraw-Hill Book Co. Inc., 1932).
(2) Castaing, R., and Guinier, A. *Proceedings of Conference on Electron Microscopy, Delft* (1949).
(3) Castaing, R. *Thesis* (Paris University, O.N.E.R.A. publ. No. 55, 1951).
(4) Borovskii, I. B. *Problemy Metallurgii, Moscow*, p. 135 (1953).
(5) Mulvey, T. *J. Sci. Instrum.*, **36**, p. 350 (1959).
(6) Birks, L. S. and Brooks, E. J. *Rev. Sci. Instrum.*, **28**, p. 709 (1957).
(7) Wittry, D. B. *Thesis* (California Institute of Technology, 1957).
(8) Castaing, R., and Descamps, J. *La Recherche Aeronautique*, **63**, p. 41 (1958).
(9) Dolby, R. *Proc. Phys. Soc. (London)*, **73**, p. 81 (1959)
(10) Cosslett, V. E., and Duncumb, P. *Nature (London)*, **177**, p. 1172 (1956).
(11) Duncumb, P., and Cosslett, V. E. *Proceedings of Conference on X-ray Microscopy and Microradiography*, pp. 374, 617 (New York: Academic Press Inc., 1957).
(12) Duncumb, P. *Thesis* (Cambridge University, 1957).
(13) Cosslett, V. E., and Nixon, W. C. *J. Appl. Phys.*, **24**, p. 616 (1953).
(14) Smith, K. C. A. *Thesis* (Cambridge University, 1956).
(15) McMullan, D. *Proc. Instn Elect. Engrs*, **100**, Part II, p. 245 (1953).
(16) Smith, K. C. A., and Oatley, C. W. *Brit. J. Appl. Phys.*, **6**, p. 391 (1955).
(17) Rose, A. *Advances in Electronics*, **1**, p. 131 (New York: Academic Press Inc., 1948).
(18) Compton, A. H., and Allison, S. K. *X-rays in Theory and Experiment*, pp. 76–90 (London: Macmillan and Co. Ltd., 1935).
(19) Stoddard, K. B. *Phys. Rev.*, **46**, p. 837 (1934).
(20) Braxton, W. L., Baez, A. V., and Kirkpatrick, P. *Phys. Rev.*, **68**, p. 106 (1945).
(21) Worthington, C. R., and Tomlin, S. G. *Proc. Phys. Soc. (London) A*, **69**, p. 401 (1956).
(22) Dyson, N. A. *Thesis* (Cambridge University, 1956).
(23) Langmuir, D. B. *Proc. Instn Radio Engrs*, **25**, p. 977 (1937).
(24) Haine, M. E., and Einstein, P. A. *Brit. J. Appl. Phys.*, **3**, p. 40 (1952).
(25) Nixon, W. C. *Thesis* (Cambridge University, 1952).
(26) Liebmann, G. *Proc. Phys. Soc. (London) B*, **68**, p. 737 (1955).
(27) Cosslett, V. E. *Proceedings of Conference on Electron Microscopy, London*, p. 311 (1954).
(28) Wittry, D. B. *J. Appl. Phys.*, **29**, p. 1543 (1958).
(29) Cosslett, V. E., and Duncumb, P. *Proceeding of Conference on Electron Microscopy, Stockholm*, 1956, p. 12.
(30) Liebmann, G. *Proc. Phys. Soc. (London) B*, **68**, p. 682 (1955).
(31) Castaing, R., and Descamps, J. *J. Phys. Radium*, **16**, p. 304 (1955).
(32) Long, J. V. P. *Thesis* (Cambridge University, 1959).
(33) Melford, D. A., and Duncumb, P. *Metallurgia, Manchr.*, **57**, p. 159 (1958).
(34) Nixon, W. C. *Proc. Roy. Soc. A*, **232**, p. 475 (1955).
(35) Duncumb, P., and Melford, D. A. *Proceedings of Symposium on X-ray Microscopy and Microanalysis, Stockholm*, 1959.

Correspondence

Dimensions of microscope eyepiece graticules

For the microscopical counting of dust particles it is customary to use a reference graticule in the eyepiece. For the purposes of the National Coal Board routine dust sampling programme, in which dust concentrations in the size ranges 1 to 5 μ for coal and 0·5 to 5 μ for rock are measured, the "globe and circle" graticule illustrated was designed.* So that this graticule could be used effectively with positive (Ramsden) eyepieces and negative (Huygenian) eyepieces, it was manufactured in two sizes, with reference grid lengths of 4·0 mm and 3·5 mm respectively. Using 2 mm oil immersion objectives, the grid length is made, by

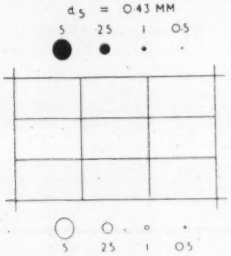

M.R.E. 043 eyepiece graticule for use with positive eyepieces

adjustment of tubelength, to be equal to 50 μ in the object plane.

Later work has indicated that, with the 4·0 mm graticule, in some instances the microscope tubelength could not be reduced sufficiently to give the desired primary magnification. It was therefore recommended that the grid lengths should be 4·3 mm for positive eyepieces and, for a similar reason, 3·3 mm for negative eyepieces. At the same time tolerances for the sizes of the graticules were specified as follows:

Taking the grid length as 50 units

the grid height should be 30 $\pm$ 0·3 units (1% tolerance)
the diameter of the 5 circles should be
5 $\pm$ 0·125 units (2·5%)
the diameter of the 2·5 circles should be
2·5 $\pm$ 0·0625 units (2·5%)
the diameter of the 1 circles should be
1 $\pm$ 0·025 units (2·5%)
and the diameter of the 0·5 circles should be
0·5 $\pm$ 0·0125 units (2·5%)

with the conditions that (*a*) the diameter of a globe or solid circle is measured to the outside edge, (*b*) the diameter of a hollow circle is measured between centres of the black line, and (*c*) the line width in the finished graticule should not exceed 10 μ.

As far as the author is aware, there is at present no standard for the accuracy of microscope eyepiece graticules, and indeed, some of those marketed, of various designs, show large discrepancies from their stated relative sizes. Although the 2·5% tolerance allowed represents 1 μ on the actual diameter of the smallest globe and circle in the graticule illustrated, experience with manufacturers indicates that such accuracy is obtainable and can be maintained in manufacture.

This letter refers to work carried out as part of the research programme of the Scientific Department of the National Coal Board and is published by permission of the Director General of Research.

Mining Research Establishment,
Isleworth, Middlesex.

R. J. HAMILTON
[20 *May*, 1959]

* HAMILTON, R. J., HOLDSWORTH, J. F., and WALTON, W. H. *Brit. J. Appl. Phys.*, Suppl. No. 3, p. S 101 (1954).

Absolute measurement of light intensities

In almost every published paper on, for example, photoelectric phenomenon, light intensity is measured relatively. This usually means that the data is not directly useful and one finds it difficult to understand why at least approximate absolute measurements are not made. Editors of scientific journals might do a service to science by trying to persuade scientific workers to measure light intensity absolutely and, perhaps, referees could be asked to criticize papers on this point. It might also be possible for The Institute of Physics to get in touch with the Laboratories pointing out this deficiency in the hope that this will persuade them to equip themselves for absolute measurement of this all-important quantity. If this worked a crusade might well be started in the U.S.A.

Siemens Edison Swan Ltd.,
Research Laboratory,
Harlow, Essex.

M. E. HAINE
[9 *March*, 1959]

Mr. Haine makes a good point in his letter. Authors too frequently do not give light intensities, or radiation intensities, in absolute terms. Our experience at this Laboratory suggests that one or more of the following reasons usually account for this: (1) unfamiliarity with the photometric units, although the definitions and the concepts behind them are quite simple; (2) unfamiliarity with the rather sensitive techniques of measuring radiation with a calibrated radiation thermopile, or inability to use them because the laboratory environment is not quiet enough; and (3) the temptation, for the sake of quick results, to study photoelectric devices, biological organisms, and so on, in terms of "white-light" response, only to find at a later stage that data necessary for interpreting the results absolutely in terms of the spectral response, of the device or organism, and the spectral energy content of the light, have been overlooked.

We get the impression that lack of knowledge of the subject is the real root of the trouble, not firstly lack of equipment. In any case, I think that more prominence should be given to the measurement of light and radiation in normal physics courses. The subject can provide many very instructive practical experiments with the aid of little more than a photocell, a simple radiation thermopile, and a negative-feedback galvanometer amplifier. The construction of the last two items—given a couple of suitable galvanometers—is well within the capability of a first year man, and in itself affords an introduction to several principles in the fields of optics, radiation and electronics. At the same time, Mr. Haine's suggestion seems well worth considering as an immediate step. The desirability of some such steps is confirmed by the constant stream of enquiries, dealt with at

this Laboratory, on how to make use of the standard measurements which we offer in this field. Perhaps others of your readers could also give their views on the suggestion.

It may be appropriate to recall that the present accepted definitions of the units of light—the candela and the lumen—afford a strict tie-up between photometric and radiometric quantities. As an example, if E_λ is the spectral energy distribution in a radiation, so that the total radiant energy in it is $\int_0^\infty E_\lambda d\lambda$ watts, then the total light in it is $680 \int_0^\infty E_\lambda V_\lambda d\lambda$ lumens, where V_λ is the "visibility function" as internationally agreed. Conversely, if the total light is known in lumens, and the shape of the distribution E_λ is known on a purely relative scale, a simple calculation suffices to find E_λ on the absolute scale.

We are working towards placing the realization of the units of light, as well as the regular photometric comparisons, on an all-radiometric basis, using this relationship, and hope to publish a fuller account of the basic principles and the methods in due course.

Radiometry and Standards Section,
Light Division,
National Physical Laboratory,
Teddington, Middlesex.

J. S. PRESTON
[7 *May*, 1959]

Controlling the habit of potassium cobalticyanide crystals

Potassium cobalticyanide, $K_3C_0(CN)_6$, crystals, doped with a small percentage of potassium chromicyanide, have been used in Masers and for various microwave studies. Such crystals may be grown from aqueous solution by standard techniques, although large crystals are very much more difficult to grow than, for example, the alums. Large flawless crystals have, however, been grown in these laboratories by a dropping-temperature method under carefully controlled conditions in an apparatus developed by Heritage and Plant.*

This note draws attention to some of the factors affecting the habit of potassium cobalticyanide crystals and to a method of obtaining crystals with a habit suitable for Maser applications.

These extremes of crystal habit that we have obtained are illustrated in Figs. 1 and 2.

Small crystals of cobalticyanide, grown by allowing a freshly prepared saturated solution to evaporate in a petri dish, usually take the form shown in Fig. 1(*a*). Use of these crystals as seeds in a larger apparatus usually produces crystals of the form shown in Fig. 1(*b*). Experiments have indicated that the capping over of the *a* face by *m* faces and the elongation along the *c* axis are associated with impurities. Such impurities may arise from the decomposition of the cobalticyanide or from extraneous sources. Thus exposing a solution of cobalticyanide to light for several days or to prolonged boiling may produce crystals of the form shown in Fig. 1(*b*), as may additions of various impurities, especially salts of divalent ions. It may be mentioned, too, that solutions of the chromicyanide are even more labile and may decompose rapidly at temperatures above 50° C.

Large crystals of the form shown in Fig. 1(*a*) can therefore be produced if the solutions are pure and not unduly exposed to light or heat. We have found that commercial cobalticyanide (as supplied by British Drug Houses Ltd.) can be sufficiently purified by two recrystallizations from water.

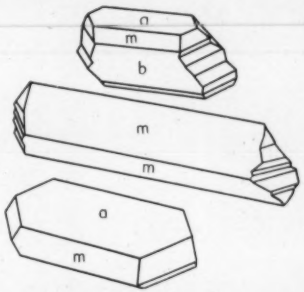

Fig. 1. Extremes of habit obtained with potassium cobalticyanide crystals

We have also observed that a solution of cobalticyanide containing 0·1% potassium sulphate crystallizes with a habit of the form shown in Fig. 1(*c*). Such crystals with large *b* faces are very suitable for certain Maser applications, and the introduction of 0·5% chromicyanide does not affect the habit.

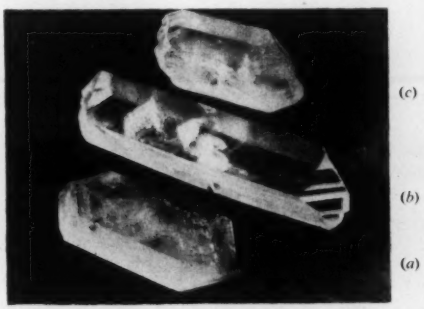

Fig. 2. Photograph of crystals showing habit as illustrated in Fig. 1. Crystal (*b*) was grown using more carefully controlled temperatures and shows less flow than (*a*) or (*c*): (*b*) is 9 cm long

Fig. 2 is a photograph of crystals showing the three extremes of habit which have been grown here. The crystals are flawed owing to temperature fluctuation during growth. The crystals also show much twinning along the *a* plane, and the extent of this seems to depend on temperature fluctuations and impurity concentrations.

Royal Radar Establishment,
Malvern,
Worcs.

A. E. RENNIE
S. NIELSEN
[1 *April*, 1959]

* HERITAGE and PLANT. R.R.E. Memo 1608.

Notes and comments

Elections to The Institute of Physics

The following elections have been made by the Board of The Institute of Physics:—

Fellows: J. C. Bell, S. I. Evans, C. G. Giles, A. E. Hawkins, C. A. Haywood, G. W. Nederbragt, R. L. Russell, C. A. Wass, A. E. Widdowson.

Associates: L. R. Beynon, I. R. Birss, G. S. Bogle, E. F. Bradley, J. C. Castle, C. R. Coleman, C. K. Coogan, J. W. Crawford, J. Dawber, K. M. Derrick, J. H. Dickson, S. N. Dutta, W. T. Eeles, B. Ellingham, K. Goldman, P. H. Herman, E. J. Higham, I. C. Hinckfuss, B. J. Hopkins, N. A. Khan, J. S. Johnston, A. B. Lewis, B. W. Lowthian, M. W. McElhinny, I. J. Macaulay, G. Maidanik, J. Marshall, W. W. Mason, C. S. Metcalfe, J. Morrison, D. F. Cakeshott, J. S. Orr, C. A. Padgham, N. Peacock, D. J. L. Pendleton, J. A. Rausell-Colom, V. M. Rout, J. Scobie, B. Scott, A. J. G. Shaw, J. R. Shepanskie, D. J. Silverleaf, L. Singh, J. Spector, G. M. Sreekantath, P. P. Starling, N. A. Surplice, J. D. Taylor, B. A. Tozer, G. G. Twidle, N. J. Wadsworth, G. White, G. C. Ziman.

Twenty-nine Graduates, fourteen Students and four Subscribers were also elected.

Powder metallurgy

In 1957 The Iron and Steel Institute and The Institute of Metals founded a Powder Metallurgy Joint Group having an official organ called *Powder metallurgy* which initially is to be published twice yearly, at an annual subscription of 25*s.* including postage.

The first issue is a double one running to 272 octavo pages. It contains the inaugural lecture of the group on "Recent developments in powder metallurgy" by Ivor Jenkins; the papers and discussion presented at the Symposium on "Developments in the production and quality of metal powders"; the papers and discussion presented at an informal meeting on "Developments in the practice of compacting and sintering", and the papers presented at the Symposium on "The powder metallurgy of metal–ceramic materials".

Correspondence regarding the Group and this new publication should be sent to the Secretary of the Group at 17 Belgrave Square, London, S.W.1.

The Journal of Mechanical Engineering Science

We have received the first issue of *The Journal of Mechanical Engineering Science*, a new periodical published by The Institution of Mechanical Engineers in London. This well-produced issue is in the same format as the *Proceedings* of that Institution and is to appear four times a year. The titles of the papers in the issue before us are: Stress concentration factors under dynamic loading conditions; A numerical solution to the elasto-hydrodynamic problem; A refinement in the calculation of the characteristics of shrink-fitted assembly; Instability and steady state coupled motions in vibration isolating suspensions; Determination of the viscosity of steam at super-critical pressures; The effect of hydrostatic pressure on the direct-stress fatigue strength of an alloy steel: The vibration of rotating shafts; The vibration and balancing of an unbalanced flexible rotor; The receptances of uniform and non-uniform rotating shafts.

The subscription rate is £3 p.a. including postage. Further details may be obtained from the Institution, 1 Birdcage Walk, Westminster, London, S.W.1.

Erratum

In the paper entitled "Studies of the viscosity and sedimentation of suspensions. Part V. The viscosity of settling suspensions of spherical particles", by D. R. Oliver and S. G. Ward, which appeared on p. 317 of the July issue of this *Journal*, the curves shown in Figs. 1 and 3 have been interchanged. For Fig. 1, therefore, see the curves entitled "Fig. 3", and *vice-versa*.

Journal of Scientific Instruments

Contents of the September issue

ORIGINAL CONTRIBUTIONS

Papers

Photoelectric double-slit interferometer for investigation of transparent thin solid films. By Lee Sang Soo.

Sensitive recording magnetic fluxmeter. By P. Lerond and Å. Thulin.

Use of electric-current shims in the cyclotron. By J. H. Fremlin, W. Hardy and H. R. Shaylor.

Use of scintillation counters in single crystal X-ray diffractometry. By P. J. Black and J. B. Forsyth.

Method of amplitude control of a.c. signals. By J. B. Cornwall.

Sensitive detector of γ-radiation in liquid or gaseous effluents. By J. G. Mitchell.

New type of search coil for metal-pipe location. By J. A. Phillips.

Vibration amplitude meter using moiré-fringe technique. By T. W. Aitchison, J. W. Bruce and D. S. Winning.

Grating spectrophotometer for the Schumann ultra-violet range. By F. J. P. Clarke, and W. R. S. Garton.

Laboratory and workshop notes

Quick method of computing the transmission of zinc sulphide-magnesium fluoride multilayer filters. By J. E. Knowles.

Rubber-jawed chuck for holding silicon crystals. By G. W. Green.

Simple d.c. amplifier for measuring very small currents. By G. Elliott and J. A. Ridley.

Stabilized direct-current supply suitable for energizing electromagnets. By D. C. Doughty and D. G. Wenham.

NOTES AND NEWS

New instruments, materials and tools.

THIS JOURNAL is produced monthly by The Institute of Physics, in London. It deals with all branches of applied physics (including theory and technique). All rights reserved. Responsibility for the statements contained herein attaches only to the writers.

EDITORIAL MATTER. Communications concerning editorial matter should be addressed to the Editor, The Institute of Physics, 47 Belgrave Square, London, S.W.1. (*Telephone:* Belgravia 6111.) Prospective authors are invited to prepare their scripts in accordance with the *Notes for Authors*. (Price 3*s.* 6*d.* including postage.)

REPRODUCTION. The Institute of Physics is a signatory to The Royal Society's Fair Copying Declaration. Details may be obtained upon application from The Royal Society, London, W.1.

ADVERTISEMENTS. Communications concerning advertisements should be addressed to the agents, Messrs. George Jackson (Fleet St.) Ltd., Cliffords Inn, Fleet Street, London, E.C.4. (*Telephone:* Holborn 3611–2.)

CLAIMS FOR MISSING JOURNALS. Claims from regular subscribers to this *Journal* for missing numbers will only be considered if received within 60 days of the date of mailing plus normal outward time of transit and time for lodging the claim. Losses attributable to failure to notify a change of address or to similar omissions will not be considered.

SUBSCRIPTION RATES. A new volume commences each January. The charge is £6 per volume ($17 U.S.A.), including index (post paid), payable in advance. Single parts, so far as available, may be purchased at 12*s.* 6*d.* each ($1.75 U.S.A.), post paid, cash with order. Orders should be sent to The Institute of Physics, 47 Belgrave Square, London, S.W.1, or to any bookseller.

Nuclear magnetic resonance in solids*

By E. R. ANDREW, Physics Department, University College of North Wales, Bangor, Caernarvonshire

The basic principles of nuclear magnetic resonance are discussed in elementary terms and an outline is given of the apparatus needed to detect the phenomenon. After brief reference to other uses, the application of nuclear magnetic resonance to solids is discussed in more detail. An account is given of the various interactions which generate the resonance spectrum and of associated spin-lattice relaxation mechanisms.

1. INTRODUCTION

Nuclear magnetic resonance is a branch of spectroscopy lying in the radio-frequency region of the electromagnetic spectrum, generally between 1 and 100 Mc/s. The phenomenon is concerned with the resonant absorption of energy by atomic nuclei when they are placed in a strong magnetic field and subjected also to a radio-frequency field. The spectrum of absorption occurs in the vicinity of the Larmor frequency of classical precession of the nuclei, and may be observed in matter in any of its ordinary forms, solid, liquid or gas. The first successful experiments were carried out in 1945.[1, 2] Since then there have been important applications to the measurement of nuclear properties, to the precise measurement of magnetic fields, to solid-state physics, in chemical analysis and in numerous other scientific fields.

Nuclear magnetic resonance is often abbreviated nmr, and alternative names are nuclear spin resonance (nsr) and nuclear induction.

2. BASIC PRINCIPLES

The phenomenon of nuclear magnetic resonance is necessarily confined to nuclei which have a magnetic moment and a spin angular momentum. Well over a hundred stable or long-lived nuclei satisfy this condition, but several important nuclei, for example ^{12}C, ^{16}O and ^{32}S, are excluded.

For simplicity, consider first the behaviour of a single proton. Its spin angular momentum is $\frac{1}{2}\hbar$, where $\hbar$ is $h/2\pi$, and h is Planck's constant. When placed in a magnetic field H_0 the proton may either be observed in a configuration parallel to the field with potential energy $-\mu H_0$, where μ is the magnetic moment of the proton, or in a configuration antiparallel to the field with energy $+\mu H_0$. These two configurations correspond to the two possible values $\pm\frac{1}{2}$ of the nuclear magnetic quantum number m. The two possible energy states are shown in Fig. 1(*a*).

If now the proton is also subjected to a radio-frequency field of such a frequency as to satisfy the relation

$$h\nu = 2\mu H_0 \qquad (1)$$

then it may absorb a quantum of energy if in the lower state, or it may be stimulated to emit a quantum if in the upper state. It is this resonant exchange of energy, between the nucleus and the electromagnetic field, in the presence of a steady magnetic field that gives the phenomenon its name. The resonant frequency is clearly proportional to the field strength H_0; for protons in a field of 10 000 G the resonance frequency given by equation (1) is 42·6 Mc/s.

Now suppose that one has a large assembly of protons such as one finds in 1 cm^3 of water, or ice, or paraffin or indeed of any material containing hydrogen. When placed in a magnetic field H_0 the nuclei distribute themselves among the two energy levels, with rather more of them in the lower level than in the upper. The ratio of the populations of the two levels is given by the Boltzmann factor

$$\exp(2\mu H_0/kT) \simeq 1 + (2\mu H_0/kT) \qquad (2)$$

where T is the temperature of the assembly. In a field of 10 000 G at room temperature the value of $2\mu H_0/kT$ is

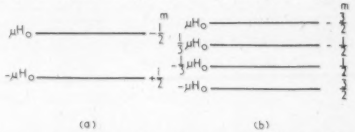

Fig. 1. (*a*) The two energy levels of a nucleus, such as a proton, which has spin number $I = \frac{1}{2}$, when placed in a magnetic field H_0. (*b*) The four equally-spaced energy levels of a nucleus such as ^{23}Na which has spin number $I = 3/2$, when placed in a magnetic field H_0

In both diagrams μ is the magnetic moment of the nucleus. Nuclear magnetic resonance occurs when electromagnetic radiation is applied which has the correct frequency to induce transitions between adjacent levels.

7×10^{-6}; the excess of population in the lower level is, in fact, always small in practice. The application of resonant electromagnetic radiation causes transitions between the two energy levels, and since the transition probabilities for absorption and for stimulated emission are equal, there is a small net absorption of energy by the nuclei from the electromagnetic field. By measuring this small absorption of energy, or some effect related to it, the nuclear magnetic resonance phenomenon is detected.

The continued absorption of electromagnetic energy tends to equalize the populations of the levels, raising the effective temperature of the nuclear assembly, and leading to a condition known as *saturation*. This tendency towards equalization of population is opposed by interactions between the nuclei and the thermal motions of the lattice of atoms in which they are embedded; these interactions tend to restore the temperature of the nuclear assembly to that of the lattice and to maintain the proper difference in population. This process is called *spin-lattice relaxation*, a name which is applied generally, even though in liquids and gases there is no lattice in the crystallographic sense.

If after saturation a nuclear assembly is allowed to return to equilibrium with the lattice, it does so in an exponential manner, and the time-constant is called the *spin-lattice relaxation time*. Experimentally these times are found from

* Based on a lecture given to the Yorkshire Branch of The Institute of Physics in Leeds on 16 October, 1957.

10^{-5} to 10^{5} s. One of the longest relaxation times recorded is 10 h for ^{29}Si in fused silica.[3]

Whereas a proton has just two energy levels available to it when placed in a magnetic field, a general nucleus having spin number I, and therefore spin angular momentum $I\hbar$, may be found in any of the $(2I + 1)$ equally-spaced energy levels shown in Fig. 1(*b*). The levels correspond to the $(2I + 1)$ values of the nuclear magnetic quantum number m in the sequence $-I, -I+1, \ldots, I$. The maximum and minimum values of energy $\pm\mu H_0$ correspond respectively to the greatest degree of antiparallel and parallel alinement of the nuclear magnetic moment with the magnetic field. The interval of energy between successive levels is clearly $\mu H_0/I$. If transitions are to be induced between adjacent levels, the frequency of the electromagnetic radiation must therefore satisfy the relation

$$h\nu = \mu H_0/I \qquad (3)$$

which reduces to equation (1) for $I = \frac{1}{2}$. The angular frequency of the radiation is thus

$$\omega = 2\pi\nu = (\mu/I\hbar)H_0 = \gamma H_0 \qquad (4)$$

where γ, which has been written for $\mu/I\hbar$, is the ratio of the magnetic moment of the nucleus to its spin angular momentum, and is commonly called the nuclear gyromagnetic ratio. The angular frequency in equation (4) is seen to be identical with the classical frequency of precession of a rotating magnet in a magnetic field given by Larmor's theorem. This classical frequency represents the natural internal mode of the system with which the externally applied electromagnetic vibration is in synchronism at resonance. Indeed, for many purposes, the phenomenon can be described in terms of a resonant forced precession of the nucleus.

3. APPARATUS

The basic apparatus is straightforward. A specimen of volume about 1 cm^3 containing the nuclei of interest is taken; if it is in the form of a liquid or a powder it is enclosed in a glass phial. A small coil of some ten turns is wound on the specimen, and it is then inserted between the poles of a magnet which provides a strong, stable and uniform magnetic field H_0 (see Fig. 2). A radio-frequency voltage is applied to the coil at the nmr frequency. The nuclei now absorb energy from the electromagnetic field within the coil. This absorption of energy may be detected in a number of ways. The specimen coil may be placed in an arm of a radio-frequency bridge; the additional resistive loss in the coil caused by the absorption of energy displaces the balance of the bridge. Alternatively, the specimen coil may be the inductance of the tuned circuit of an oscillator. The additional resistive loss at resonance reduces the amplitude of the oscillations and is revealed after detection. Details of these and other circuits are given elsewhere.[4] The magnetic field is swept cyclically through the resonance condition by passing current at a low frequency through an auxiliary coil mounted on the magnet pole. The change in output from the detector at each traverse of the resonance condition is displayed on an oscillograph or a pen recorder.

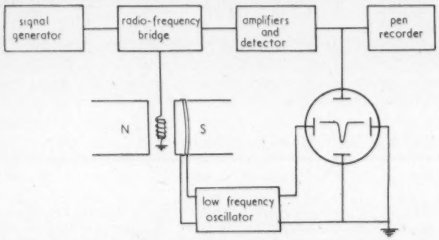

Fig. 2. Schematic arrangement of one method of detecting nuclear magnetic resonance. The crystal is mounted in a small coil between the poles of a magnet. When current at the resonance frequency energizes the coil the absorption of energy by the nuclei causes an additional loss in the coil. The field of the magnet is swept cyclically through the resonance condition. The balance of the bridge, into which the coil is connected, is displaced at each traverse of the resonance condition and, after amplification, is displayed on an oscillograph or a pen recorder

The steady magnetic field may be provided by either an electromagnet or a permanent magnet. Field strengths between 3 and 15 kG are normally used, the range 5 to 10 kG being most common. Since the resonance condition is usually sharp, accurate work demands a very uniform and stable field. For work with solid specimens a uniformity of a few parts in 10^5 over the specimen volume generally suffices. A typical experimental arrangement is shown in Fig. 3.

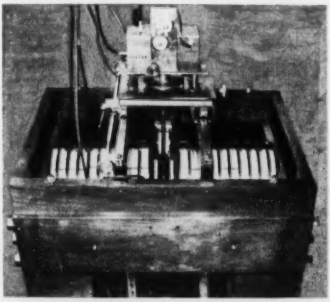

Fig. 3. An apparatus used in Bangor for nuclear magnetic resonance work on solids. The permanent magnet has a symmetrical yoke set horizontally, giving vertical access to the gap. A spectrometer of the marginal oscillator type is mounted above the magnet. The crystal is mounted inside a small coil at the lower end of the coaxial tube running vertically downwards from the spectrometer into the magnet gap. The apparatus is shown set up for the spinning crystal experiment mentioned in Section 5(*a*); a photoelectric rotation ratemeter is mounted at the rear of the gap.

The magnet provides a field of 6300 G between pole faces $6\frac{1}{2}$ in. diameter. The 2 in. gap facilitates experiments at low temperatures. Over a volume of 1 cm^3 the field is uniform within 50 mG, which is ample for most solid-state work. Magnetization was effected from the laboratory battery using the 5000 turns of copper wire wound on each of the Alcomax III pole-pieces (supplied by Swift Levick Ltd.). The magnet was designed by Dr. R. G. Eades and the author, and assembled by J. H. Humphreys and Sons Ltd. of Oldham who made the yoke and other large parts. The weight is about 2 tons and the cost was £1330

4. SOME GENERAL APPLICATIONS

Nuclear magnetic resonance has many applications which lie outside the main theme of this article. The magnetic moment of a nucleus may be determined by measuring its resonance frequency in a known magnetic field and applying equation (3). Over eighty nuclear magnetic moments have been measured with precision by this means.[4, 5, 6] The sign of the magnetic moment and the spin number I may also be determined. Again using equation (3), the strength of a magnetic field may be determined by measuring the resonance frequency of a nucleus of known magnetic moment in the unknown field; an absolute accuracy of a few parts in 10^5 is readily obtained, while the still higher relative accuracy facilitates the exploration of the field uniformity. The method can be adapted to the measurement of quite low fields such as the earth's field.[7, 8] Measurements of this kind have been used in geophysical prospecting[9] and in archeological surveys;[10] moreover, it is intended to use them in earth satellites[11] to measure the magnetic field in the satellite's track. The sharpness of the resonance line from a liquid specimen has been exploited to provide the control element of the field stabilizer of an electromagnet.[12] The intensity of the resonance is proportional to the number of resonant nuclei in the specimen and can provide a measure of the relative abundance of isotopes in the specimen.[13] The strength of the proton resonance signal from a specimen can be used as a measure of its moisture content.

5. SOLIDS

The nmr absorption lines from solids usually have a width of the order of 1 to 100 kc/s when expressed in terms of frequency, or of the order of 1 to 100 G in terms of field. In contrast to this the absorption lines from liquids are usually a thousand times narrower. In both cases, when examined in detail, the resonance line is often found to display a fine structure, the structure of the narrower liquid lines being correspondingly finer. It is therefore proper to refer to the detailed shape of the resonance absorption as a spectrum. The structure of the spectrum from a single crystal depends upon the orientation of the crystal; much detail is therefore lost when dealing with polycrystalline specimens, since the observed spectrum is the integrated resonance shape from all the crystal grains of various orientations.

Some of the more important sources of spectral broadening are considered in turn in the following sections. Many of the interactions concerned also provide mechanisms for spin-lattice relaxation and these are considered at the same time. A full nmr examination of any solid will normally embrace the measurement of its spectrum and of its spin-lattice relaxation time over a wide range of temperature.

(*a*) *Magnetic dipolar interaction between nuclei.* Each nucleus in a solid specimen experiences not only the steady field H_0 applied by the laboratory magnet, but also a local field, of the order of several gauss, generated by all the other magnetic nuclei in the specimen. This local field does not have the same value on all nuclear sites; different nuclei therefore experience different resultant field strengths and their resonances occur at different frequencies.

This source of spectral broadening occurs for all solids, though in some cases it is dwarfed by other mechanisms. However, for light nuclei with spin number $\frac{1}{2}$ in non-metallic solids it is the only significant source of broadening. In particular, the magnetic resonance spectrum of protons in diamagnetic solids is almost entirely due to this mechanism.

The proton magnetic resonance spectrum from a crystalline hydrate provides an excellent illustration. In Fig. 4(*a*) are depicted the two protons A and B of a water molecule in a hydrated crystal. Looked at from the standpoint of elementary magnetostatics, the field experienced by proton A is $H_0 \pm H_{local}$, where H_{local} is the local field component at A due to the magnetic moment μ of proton B, and is given by

$$H_{local} = (\mu/d^3)(3\cos^2\theta - 1). \qquad (5)$$

The sign $\pm$ reflects the fact that proton B may be oriented either parallel or antiparallel with respect to the applied field H_0. The resonance spectrum should therefore consist of a doublet, and this is well illustrated by the proton spectrum

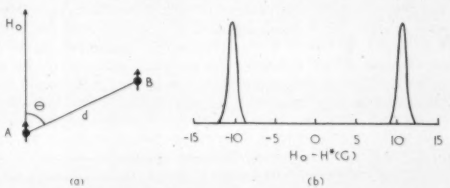

Fig. 4. (*a*) A and B are the two protons in one water molecule of a hydrated crystal placed in a uniform magnetic field H_0. (*b*) Proton magnetic resonance spectrum of a single crystal of barium chlorate monohydrate $Ba(ClO_3)_2 . H_2O$; $H^* = h\nu/2\mu$, where ν is the constant frequency of resonance. [Based on a recorded spectrum kindly provided by Prof. R. D. Spence[14]]

of a single crystal of $Ba(ClO_3)_2 . H_2O$,[14] shown in Fig. 4(*b*). The separation of the doublet lines should, from equation (5), be $2H_{local}$. However, for a proper quantum-mechanical solution of this problem the Hamiltonian of the two nuclei, including their dipolar interaction, must be written down and the energy levels found by perturbation procedure.[15] When nuclei A and B are not identical the classical expression (5) turns out to be correct, but when they are identical, as in the present problem, the contribution of off-diagonal matrix elements increases the effective local field by a factor 3/2. The separation of the doublet lines is therefore $3\mu d^{-3}(3\cos^2\theta - 1)$. If the angular setting of the crystal is altered, the doublet separation changes, following the angular factor $(3\cos^2\theta - 1)$. From the variation of doublet separation with angle, the orientation of the proton pairs in the crystal is found. The maximum doublet separation, $6\mu d^{-3}$ (when $\theta = 0$), enables the proton–proton separation in the water molecule to be found. With this information it is often possible to infer the positions of the protons in the crystal lattice, and thus complete the determination of the crystal structure. Since the field of a dipole falls as the inverse cube of distance, the other protons in the crystal make only a small contribution to the local field and their effect is to broaden the two lines of the doublet.

In general, the dipolar-broadened nmr spectrum of a solid provides a valuable structural tool supplementing crystallographic information provided by other methods. The interpretation is not always as clear-cut as in the example just given. The spectrum may be calculated for groups of three and, in some cases, of four nuclei and is found to be complex. In still more complicated situations the mean

square width of the spectrum provides a useful characteristic amenable to calculation which can be used to derive crystallographic information. In this way it has been possible to show that in crystalline urea the molecules are plane,[16] that an equilateral oxonium ion exists in certain acid hydrates,[17, 18] and that in solid $CHCl_2CHCl_2$ the molecules are in the gauche-form,[19] to mention just three examples.

When the temperature of a crystal is raised it is sometimes found that its spectrum becomes narrower. For example, the dipolar-broadened proton spectrum of solid benzene decreases from a width of about 9 G at low temperatures to about 3 G above 120° K.[20] This is caused by the random rotation of the benzene molecules about their six-fold symmetry axes. The local field which each proton experiences is no longer constant since its neighbours are moving; the mean local field is now smaller, and the spectrum is therefore narrower. In this way molecular motion has been discovered and studied in a great many solids and polymers. The fluctuating part of the local magnetic field produces side-spectra on either side of the narrowed spectrum, but in practice these are too weak to be observed. Their existence has, however, recently been demonstrated[21] by rotating a crystal at high speed. In this way molecular motion is simulated, but with the important difference that all the molecules now rotate with the same angular velocity.

The more general the nature of the molecular motion the greater is the reduction of spectral width. When solid cyclohexane[22] is heated from a low temperature the molecules begin to rotate about their trigonal axes, causing a reduction of spectral width from 16 to 6 G. At 186° K a change of crystal structure enables the molecules to rotate isotropically about fixed centres, causing a further narrowing to 3 G. Above 230° K the molecules diffuse through the solid; the mean local field becomes very small and the spectrum very narrow. One can see now why the spectrum from a liquid specimen is so very much narrower than that from a solid. The rapid random rotation and diffusion of molecules in a liquid averages the local magnetic field to an extremely small value. Self-diffusion in a number of solids, molecular, ionic and metallic, has been studied through the spectral narrowing which it causes.

The fluctuating local magnetic field caused by molecular motion induces nuclear transitions and thus promotes spin-lattice relaxation. The efficiency of this relaxation mechanism depends upon the intensity of the Fourier spectrum of the fluctuating field at the Larmor frequency; this in turn depends upon the correlation time τ of the random motion and is greatest when $1/\tau$ is of the order of the Larmor frequency. The correlation time in its turn is dependent on the temperature. From a study of the variation of relaxation time with temperature, the temperature-variation of τ may be found. A simple exponential law of the form

$$\tau = \tau_0 \exp(V/RT) \qquad (6)$$

is found to be obeyed over a wide range of values of τ from 10^{-4} to 10^{-10} s in ammonium chloride and ammonium bromide[23] and in solid benzene.[20] From a plot of $\log \tau$ against $1/T$ the activation energy of the molecular re-orientation process is found, and has the values 4·7, 3·4 and 3·7 kcal/mol respectively for the three solids just mentioned.

(*b*) *Chemical shift.* It has so far been implicitly assumed that the resonant nuclei experience without modification the field applied by the laboratory magnet. In fact, however, the field is modified by the magnetization it produces in the molecular electron clouds surrounding the nuclei. If H_b is the field in the bulk of the specimen, the field actually experienced by the nuclei may be written

$$H_0 = H_b(1 - \sigma) \qquad (7)$$

where the constant σ is characteristic of the electronic environment of the nuclei. The displacement of resonance produced by the additional field σH_b is clearly proportional to the strength of the applied field and is called the *chemical shift*. The shift differs from one chemical compound to the next since the electronic environment is not the same in each. Indeed, in the same compound the electronic environment of all nuclei may not be the same. For example, the ethyl alcohol molecule has three protons in a methyl group, two in a methylene group and one in a hydroxyl group. The proton resonance spectrum of liquid ethyl alcohol is found to have three distinct peaks of relative intensity 3 : 2 : 1. The nmr spectrum of an organic liquid is thus characteristic of its molecular structure and finds great use in chemical analysis and identification. For protons the values of σ are small, of the order of 10^{-5}. The separation of the outer peaks in ethyl alcohol is only 50 mG in an applied field of 10 kG. The constant σ is greater for heavier nuclei since they have larger numbers of electrons surrounding them, and can be as large as 10^{-2}.

The chemical shift can lead to a broadening of the spectrum from solid specimens. Any compound which, like ethyl alcohol, displays a chemically-shifted fine structure in the liquid state, must show a comparable spread of resonance frequencies in the solid state also. For protons, however, this breadth is entirely masked by the much larger dipolar interactions discussed in the previous section. For heavier nuclei with larger values of σ, the broadening due to this cause could be appreciable.

There is a second way in which the chemical shift can lead to spectral broadening. If the site of a nucleus is of low symmetry the shift constant σ is anisotropic. This has been clearly shown[24] for the ^{13}C resonance in calcite; in a field of 8 kG the resonance moves over a range of 0·6 G, corresponding to a variation in σ of $7{\cdot}5 \times 10^{-5}$, when the crystal is turned about an axis normal to the trigonal axis. As ^{13}C has low abundance the dipolar broadening in this crystal is particularly small, about 0·005 G. If a polycrystalline specimen of calcite were taken, the resonances of the individual crystal grains would extend over 0·75 G in a field of 10 kG, and the spectrum would have a breadth more than a hundred times that of the single crystal. For heavy elements the effect is greater, and a breadth of the order of 5 G for the ^{205}Tl resonance in powdered thallium oxide, which is rich in the isotope, is ascribed to this cause;[25] the dipolar broadening is some five times smaller. However, for protons this source of broadening is negligibly small in solids.

In a liquid, the rapid reorientation of the molecules causes σ to run rapidly through any anisotropic range of values which it may have. The shift field $H_b\sigma$ thus fluctuates and the resonance occurs at the field strength $H_b(1 - \bar{\sigma})$, where $\bar{\sigma}$ is the mean value of σ; there is thus no anisotropy broadening in liquids. Like the fluctuating dipolar field considered in the last section, the fluctuating shift field provides a means of spin-lattice relaxation in liquids; the relative magnitudes of these two fields determines which mechanism is the more effective. For protons the shift field is normally too small to compete, but for ^{13}C and ^{19}F it is large enough for relaxation through its anisotropy to be significant.[26, 27] In solids and polymers too, this mechanism of relaxation is likely to be of importance for these or heavier nuclei, if they are found in positions of low symmetry in reorienting molecules and groups.

(*c*) *Knight shift.* For metals also there is a resonance shift, similar to the chemical shift for non-metals; it is called the Knight shift after its discoverer.[28] The paramagnetic susceptibility of the conduction electrons increases the magnetic field experienced by the nuclei to a value greater than the applied field. The consequent increase in resonance frequency is only a few parts in 10^4 for light metals, but rises to several per cent for heavy metals.

In non-cubic metals the Knight shift is anisotropic. Since most work is done on finely powdered metal in order to combat the skin effect, this anisotropy leads to a broadening of the resonance spectrum. In white tin, for example, which has tetragonal symmetry, the anisotropy is the main cause of spectral breadth,[29] amounting to about 5 G in an applied field of 10 kG.

The fluctuating local magnetic field caused by the conduction electrons provides a means of spin-lattice relaxation. The Knight shift and the relaxation time are therefore closely related to each other. A study of these two quantities gives information about the electron spin paramagnetism and the electronic states of metals, including superconductors.

(*d*) *Electron-coupled spin-spin interactions.* In the previous section it was seen that the chemical shift causes the proton magnetic resonance spectrum of liquid ethyl alcohol to consist of three distinct peaks. When these peaks are examined under still higher resolution, it is found that each has a still finer structure. This sub-structure arises from an indirect interaction between the protons in one group with those in an adjacent group. It is found generally in organic liquids; their proton spectra thus become their characteristic "fingerprints", and are of great value to the chemist for structural and analytical investigations. Unlike the chemical shift separations, which are proportional to the applied field H_0, these finer splittings are independent of H_0 to a first-order.

The interaction may be most simply illustrated by the molecule HD. The magnetic moment of the proton slightly polarizes the molecular electrons, which in turn slightly alter the magnetic field experienced by the deuteron. Since the proton can have either of two orientations in the applied field, the extra field experienced by the deuteron can have either of two values and the deuteron resonance is a doublet. The deuteron similarly influences the proton resonance, but since the deuteron's spin number $I = 1$, it has three permitted orientations and the proton resonance is a triplet. This splitting is always small for hydrogen, amounting to 43 c/s for HD.[30] For heavy atoms the interaction is stronger.

Unlike the direct dipolar interaction these indirect electron-coupled interactions are not obliterated by rapid molecular reorientation in a liquid, and therefore, although small for hydrogen, they are revealed in high-resolution studies. In the solid state, however, the resonance spectrum for protons is determined by the very much stronger static dipolar interactions. On the other hand, for heavier nuclei the indirect interaction can be more important than the direct dipolar interaction. Thus in metallic thallium[25] the spectral widths of the order of 25 kc/s (or 10 G) for ^{203}Tl and ^{205}Tl (both $I = \frac{1}{2}$) are ascribed mainly to the indirect interaction; the anisotropy of Knight shift also contributes significantly especially in strong applied fields, but the direct dipolar interaction plays only a minor role in this case. The indirect interaction also provides the main source of spectral broadening in metallic silver,[31] and in the semiconductors InSb and GaSb.[32]

In section 5(*a*) the application of dipolar-broadened spectra to the determination of structural parameters was discussed, and it should be noticed that this application is limited to cases in which broadening due to the electron-coupled spin interactions and to chemical shift anisotropy are small compared with the direct dipolar broadening. It is therefore fortunate that for the nucleus of most structural interest, namely the proton, this condition is satisfied. It is also reassuring to note that there is excellent agreement between the mean square width of the carefully measured ^{19}F spectra for a single crystal of calcium fluoride with that calculated on the assumption that the broadening is entirely due to direct dipolar interaction.[33]

(*e*) *Quadrupole interactions.* Nuclei which have $I > \frac{1}{2}$ possess an electric quadrupole moment which interacts with the crystalline electric field and can provide a much stronger source of spectral broadening for these nuclei than the other interactions so far mentioned. Nuclei may be regarded as ellipsoidal distributions of positive electric charge. They therefore have no electric dipole moment, and the electric quadrupole moment is a measure of the departure of the charge distribution from spherical shape. The quadrupole moment is positive for a prolate distribution and negative for an oblate distribution; for $I = 0$ or $\frac{1}{2}$ the quadrupole moment is always zero.

From elementary electrostatics, it is known that the energy of an electric charge is given by the product of the charge and the electric potential at its site; also the energy of an electric dipole is given by the product of the dipole moment and the first derivative of the potential, namely the electric field, both of which are vectors; in the same sequence the energy of an electric quadrupole is given by the product of the quadrupole moment with the second derivative of the potential, namely the electric-field gradient, both of which are tensors of second rank.

If, therefore, a nucleus with $I > \frac{1}{2}$ is situated in a crystal at a point where there is a finite electric-field gradient, its energy is affected by the electric field to an extent dependent upon its orientation, and therefore upon its magnetic quantum number m. The energy levels are perturbed as indicated in Fig. 5, which refers to a nucleus having $I = 3/2$. The spacings between adjacent levels are now all unequal.

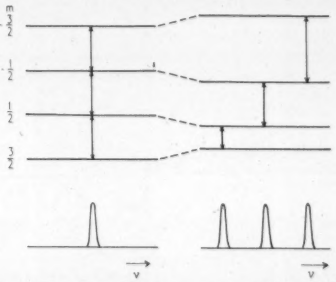

Fig. 5. A nucleus of spin number 3/2, placed in a magnetic field, has the four equally-spaced energy levels indicated on the left of the diagram. The spectrum, shown below, consists of a single line broadened by magnetic interactions. If the nucleus is also subjected to an electric field gradient the levels are perturbed as shown on the right of the diagram, the spacing between the levels now being all unequal. The spectrum, shown below, now consists of three lines, usually well resolved in a single crystal

If a single crystal contains nuclei, all of which are subjected to the same electric environment, the nuclear magnetic resonance spectrum therefore consists of three lines instead of one, and the separation of the lines is a measure of the product of the nuclear quadrupole moment and the electric-field gradient. For general values of I there are $2I$ lines in the spectrum. This provides one method for measuring I.

Nuclei which reside on lattice sites having cubic symmetry are not subjected to an electric-field gradient, and their quadrupole moments do not therefore split their spectrum. At sites devoid of cubic symmetry the field gradient reflects the symmetry of the site. If the nuclear sites have three-, four- or six-fold symmetry, one of the principal axes of the field-gradient tensor lies along this symmetry axis, and the tensor is symmetric about this axis. Thus for sodium nitrate, the three lines of the ^{23}Na spectrum do not move if the crystal is rotated about its triad axis, since each sodium nucleus lies on the triad axis of the rhombohedral unit cell. On the other hand, if the crystal is rotated about an axis perpendicular to the triad axis, the lines move with 180° periodicity. If the nuclear sites do not have even axial symmetry, the spectrum alters when the crystal is rotated about any crystal axis.

It is therefore possible: (i) to obtain information concerning the symmetry of the nuclear sites from the angular dependence of the quadrupole-split spectrum; (ii) to determine the crystallographic direction of the principal axes of the field-gradient tensor; (iii) in the absence of axial symmetry to find the degree of asymmetry of the field gradient; (iv) to determine the number of non-equivalent nuclear sites in the crystal; (v) to determine quite simply and non-destructively, for even a rough or opaque specimen, whether it is a single crystal; and (vi) from the magnitude of the splitting to find the quadrupole coupling constant e^2Qq/h, where eQ is the quadrupole moment, Q having the dimensions of an area, and eq is a measure of the electric field gradient. The coupling constant yields a value for q if Q is known from other studies. The parameter q may then be used to test recent calculations of the crystalline electric field.[34] Alternatively, if Q is not known a value for it may be found using the calculated field gradient.

The separation of the spectral lines is almost always much greater than the spectral broadening encountered in sections 5(*a*), (*b*), (*c*) and (*d*). For example, for ^{23}Na in sodium nitrate, the maximum separation between the outer lines is 334 kc/s at room temperature,[35] or 300 G in terms of magnetic field. This is typical of the splitting in an ionic crystal. If the atoms containing the resonant nuclei are covalently bound, the electric-field gradient may be a hundred times or more larger than in ionic crystals. The quadrupole interaction is then no longer the small perturbation depicted in Fig. 5; it may produce level splittings of 10 Mc/s or more even without application of a magnetic field. Transitions between energy levels split by the quadrupole interaction alone are described as pure quadrupole resonance.

There is usually no marked change in the quadrupole-split spectrum when the temperature of a crystal is changed. The mean electric-field gradient decreases by perhaps a few per cent for a rise of 100° C on account of lattice expansion and increased vibrational amplitudes. However, a more rapid temperature variation is occasionally produced by ionic or molecular motion and thus provides a means of studying the motion.[36, 37, 38]

While normally there is no splitting of the spectrum if the nuclei are found on sites having cubic symmetry, it can nevertheless arise if the crystalline arrangement is not perfect. For example, the sodium sites in a sodium chloride crystal may lose their perfect cubic symmetry if there are foreign atoms in the crystal, or if the crystal is strained or if it is exposed to high-energy radiations. The electric-field gradients experienced by the nuclei in such cases are not all the same. The spectrum therefore consists of a central line and a diffuse band of satellites on either side. Only the central line is likely to be observed, and its intensity is 0·4 of that for a perfect crystal, the whole spectrum of which is concentrated in the central line. [The value 0·4 is the fractional intensity for the example of $I = 3/2$. In the general case the fractional intensity is readily shown to be $3(2I + 1)/8I(I + 1)$.] Even the central line becomes weaker and broader if there is a high density of defects, on account of second-order effects. A study of the spectrum thus provides a measure of the degree of imperfection of solids, and has been applied also to the study of disorder in alloys.

Lattice vibrations cause the electric field gradient experienced by each nucleus to fluctuate. The fluctuating gradient can, by interacting with the nuclear quadrupole moment, cause transitions between the nuclear energy levels and thus effect a transfer of energy between the nuclear spin system and the lattice. In a number of crystals it has been shown that this interaction provides the operative spin-lattice relaxation mechanism. Even in cubic crystals this mechanism can operate since the lattice vibrations produce a fluctuating distortion from cubic symmetry.

(*f*) *Paramagnetic centres.* Unpaired electrons, whether in the form of paramagnetic ions or otherwise, can have a marked effect on both the spectrum and the spin-lattice relaxation time of a solid. In a hydrated paramagnetic salt the paramagnetic ions generate a local magnetic field which displaces the proton resonance frequencies. The protons may be regarded as small magnetic indicators dispersed throughout the unit cell, which by their individual resonance frequencies register the local field of the paramagnetic ions at various points in the cell. The magnetic moments of the ions are continually changing their orientation by exchanging energy with each other and the lattice. The large local field of the ions is therefore rapidly fluctuating, and the displacement of the proton resonance frequencies is a measure of its time-average. The average value of the ionic magnetic moment is not zero, since the separation of the ion's energy levels in an applied field of several kilogauss is not small compared with kT. The average value of the ionic moment follows Curie's law in first approximation, and the average local field is therefore inversely proportional to the absolute temperature. In a typical case the local field may be of the order of a Gauss at room temperature, and of the order of several hundred Gauss at 1° K. The ten different protons in the unit cell of $CuSO_4 . 5H_2O$ lead to ten lines in the proton spectrum of a single crystal, spread over some 700 G at 1° K.[39] The low-temperature behaviour of the proton resonance spectrum of $CuCl_2 . 2H_2O$ gives information concerning its antiferromagnetic properties.[40]

In MnF_2 and other iron group fluorides, there is an overlap of the magnetic electrons of the paramagnetic ion on to the fluorine nuclei on account of a partial covalent binding between the atoms. The effective internal fields at the ^{19}F sites arising from this coupling produce a much larger resonance shift than for the hydrates.[41]

The strong, rapidly fluctuating, local field in paramagnetic crystals causes transitions among the nuclear energy levels and provides a strong mechanism for spin-lattice relaxation. Relaxation times are usually 10^{-3} s or less.

The presence of small concentrations of paramagnetic

centres, either as impurities or through defects, can provide the main source of spin-lattice relaxation for crystals which are otherwise diamagnetic. Nuclei in diamagnetic ionic crystals often find it difficult to relax. For example, the ^{19}F relaxation time in a good crystal of lithium fluoride is usually several minutes at room temperature. These nuclei have no quadrupole moment since $I = \frac{1}{2}$, and therefore they cannot relax by the quadrupolar process [Section 5(*d*)]. Magnetic relaxation brought about by nuclear motion [Section 5(*a*)] is not available, since there is no nuclear motion other than lattice vibrations and these are insufficiently effective. However, the fluctuating field of a paramagnetic impurity centre can relax nearby nuclei. Although its influence may not extend directly to more remote nuclei, excess energy from remoter nuclei can diffuse towards the absorbing centres by successive exchanges of energy between neighbouring nuclei.[42] For nuclei having $I > \frac{1}{2}$, this process and the quadrupolar process are both available for relaxation in ionic crystals; in natural mineral crystals the magnetic process is usually the more effective, whereas in pure synthetic crystals the quadrupolar process usually dominates.[43]

(*g*) *Relaxation broadening.* If the spin-lattice relaxation time T_1 is short, the relaxation process itself can be an important source of spectral broadening. The average lifetime of a nucleus in a given energy state is of the order of T_1; the uncertainty in the energy on this account is therefore of the order of h/T_1, and the resonance frequency is uncertain to an extent of the order of $1/(2\pi T_1)$. This source of line broadening is negligible for solids unless T_1 is appreciably less than a second. However, when T_1 is of the order of 10^{-4} s the spectrum can be entirely dominated by this mechanism; certain metals[44] provide examples of this behaviour. The relaxation-broadened line has the characteristic Lorentzian shape, with wide, slowly converging skirts, that is encountered in collision-broadening of atomic spectral lines.

BIBLIOGRAPHY

ANDREW, E. R. *Nuclear Magnetic Resonance* (London: Cambridge University Press, 1955).

PAKE, G. E. *Amer. J. Phys.*, **18,** pp. 438, 473 (1950).

PAKE, G. E. *Solid State Physics*, **2,** p. 1 (1956).

SAHA, A. K., and DAS, T. P. *Theory and Applications of Nuclear Induction* (Calcutta: Saha Institute of Nuclear Physics, 1957).

SLICHTER, W. P. *Advances in Polymer Sci.*, **1,** p. 35 (1958).

REFERENCES

(1) PURCELL, E. M., TORREY, H. C., and POUND, R. V. *Phys. Rev.*, **69,** p. 37 (1946).

(2) BLOCH, F., HANSEN, W. W., and PACKARD, M. E. *Phys. Rev.*, **69,** p. 127 (1946).

(3) HOLZMAN, G. R., ANDERSON, J. H., and KOTH, W. *Phys. Rev.*, **98,** p. 542 (1955).

(4) ANDREW, E. R. *Nuclear Magnetic Resonance* (London: Cambridge University Press, 1955).

(5) RAMSEY, N. F. *Nuclear Moments* (New York: John Wiley and Sons Inc., 1953).

(6) KOPFERMANN, H. *Nuclear Moments*, English translation by E. E. Schneider (New York: Academic Press Inc., 1958).

(7) PACKARD, M. E., and VARIAN, R. *Phys. Rev.*, **93,** p. 941 (1954).

(8) WATERS, G. S., and FRANCIS, P. D. *J. Sci. Instrum.*, **35,** p. 88 (1958).

(9) GIMLETT, J. I., HUNTER, K. E., and WHITTAKER, J. C. *Engineering and Mining J.*, **158,** p. 88 (1957).

(10) HALL, E. T. *Physical Society Year Book*, p. 22 (1958).

(11) BLOOM, A. L., and JOHNSON, L. E. *Electronic Industr.* (August 1957).

(12) PACKARD, M. E. *Rev. Sci. Instrum.*, **19,** p. 435 (1948).

(13) MITCHELL, A. M. J., and PHILLIPS, G. *Brit. J. Appl. Phys.*, **7,** p. 67 (1956).

(14) SPENCE, R. D. *J. Chem. Phys.*, **23,** p. 1166 (1955).

(15) PAKE, G. E. *J. Chem. Phys.*, **16,** p. 327 (1948).

(16) ANDREW, E. R., and HYNDMAN, D. *Disc. Faraday Soc.*, **19,** p. 195 (1955).

(17) RICHARDS, R. E., and SMITH, J. A. S. *Trans Faraday Soc.*, **47,** p. 1261 (1951).

(18) ANDREW, E. R., and BERSOHN, R. *J. Chem. Phys.*, **18,** p. 159; **20,** p. 924 (1950).
ANDREW, E. R., and FINCH, N. D. *Proc. Phys. Soc. (London)*, **70,** p. 980 (1957).

(19) TAKEDA, M., and GUTOWSKY, H. S. *J. Chem. Phys.*, **26,** p. 577 (1957).

(20) ANDREW, E. R., and EADES, R. G. *Proc. Roy. Soc. A*, **218,** p. 537 (1953).

(21) ANDREW, E. R., BRADBURY, A., and EADES, R. G. *Nature (London)*, **182,** p. 1659 (1958).

(22) ANDREW, E. R., and EADES, R. G. *Proc. Roy. Soc. A*, **216,** p. 398 (1953).

(23) SACHS, A. M., and TURNER, E., quoted by PURCELL, E. M. *Physica*, **17,** p. 282 (1951).

(24) LAUTERBUR, P. C. *Phys. Rev. Letters*, **1,** p. 343 (1958).

(25) BLOEMBERGEN, N., and ROWLAND, T. J. *Phys. Rev.*, **97,** p. 1679 (1955).

(26) MCCONNELL, H. M., and HOLM, C. H. *J. Chem. Phys.*, **28,** p. 749 (1958).

(27) GUTOWSKY, H. S., and WOESSNER, D. E. *Phys. Rev.*, **104,** p. 843 (1956).

(28) KNIGHT, W. D. *Solid State Physics*, **2,** p. 93 (1956).

(29) BLOEMBERGEN, N., and ROWLAND, T. J. *Acta Metallurgica*, **1,** p. 731 (1953).

(30) CARR, H. Y., and PURCELL, E. M. *Phys. Rev.*, **88,** p. 415 (1952).

(31) RUDERMAN, M. A., and KITTEL, C. *Phys. Rev.*, **96,** p. 99 (1954).

(32) SHULMAN, R. G., MAYS, J. M., and MCCALL, D. W. *Phys. Rev.*, **100,** p. 692 (1955).

(33) BRUCE, C. R. *Phys. Rev.*, **107,** p. 43 (1957).

(34) BERSOHN, R. *J. Chem. Phys.*, **29,** p. 326 (1958).

(35) POUND, R. V. *Phys. Rev.*, **79,** p. 685 (1950).

(36) ITOH, J., and YAMAGATA, Y. *J. Chem. Phys.*, **24,** p. 621 (1956).

(37) KETUDAT, S., and POUND, R. V. *J. Chem. Phys.*, **26,** p. 708 (1957).

(38) EADES, R. G., HUGHES, D. G., and ANDREW, E. R. *Proc. Phys. Soc. (London)*, **71,** p. 1019 (1958).

(39) POULIS, N. J. *Physica*, **17,** p. 392 (1951).

(40) POULIS, N. J., and HARDEMAN, G. E. G. *Physica*, **18,** pp. 201, 315 (1952).

(41) SHULMAN, R. G., and JACCARINO, V. *Phys. Rev.*, **108,** p. 1219 (1957).
JACCARINO, V., SHULMAN, R. G., and STOUT, J. W. *Phys. Rev.*, **106,** p. 602 (1957).
BAKER, J. M., and HAYES, W. *Phys. Rev.*, **106,** p. 603 (1957).

(42) BLOEMBERGEN, N. *Physica*, **15,** p. 386 (1949).

(43) ANDREW, E. R., and SWANSON, K. M. (to be published).

(44) GUTOWSKY, H. S., and MCGARVEY, B. R. *J. Chem. Phys.*, **20,** p. 1472 (1952).

Summarized proceedings of a conference on precipitation in alloys and on metal structures—London, November 1958

A joint conference of the X-ray Analysis and Electron Microscopy Groups of The Institute of Physics was held in London, on 28 November, 1958. The subject of the conference was precipitation in alloys. On the following day the X-ray Analysis Group discussed metal structures.

PRECIPITATION IN ALLOYS

The joint conference was under the Chairmanship of Prof. F. G. Cox (School of Chemistry, University of Leeds) and the first paper was given by Prof. A. GUINIER (Conservatoire des Arts et Métiers, Paris) who discussed the structure of age-hardened alloys in the pre-precipitation stage. This stage was marked by the formation in the matrix of the alloy of small zones of segregation. The properties of these zones and the conditions under which they formed were principally determined by their coherency with the matrix. Zones had been studied by the X-ray scattering produced outside the normal Bragg reflecting positions, but the interpretation of the results was difficult because the composition of the zones was unknown and they did not possess a regular crystalline structure. The problem had been solved quantitatively for certain alloys such as the G.P. zones in Al–Cu and the spherical zones of Al–Ag and Al–Zn. The structure of zones in the ternary alloys had not yet been established. For Al–Mg–Si, the zone was certainly elongated along the ⟨100⟩ axis of the matrix, its length was several hundred Ångstrom units but its diameter was unknown. The cluster was formed by rows of atoms which maintained a linear periodicity along the ⟨100⟩ axis of Al but which were irregularly displaced laterally. In Al–Mg–Zn, the zones contained atoms of Mg and Zn which displayed partial order. Gerold had tried to interpret the diffraction patterns using a simple model of a superstructure derived from an Al lattice. The observations of Graf had shown that the superstructure was certainly more complex than in this model and that the ordering was very imperfect. Before testing various models, the complete reciprocal lattice of the zone should be established. The shape and structure of the zones were determined by (i) the relative size of the atoms of the matrix and the additions, and (ii) the bonding between the segregated atoms which might differ from the metallic bond, especially in ternary alloys. In Al–Mg–Si, chains of $SiMg_2$ of ionic character were formed in the matrix, while in Al–Mg–Zn, $ZnMg_2$ formed the nucleus. As neither linear nor planar epitaxial growth was possible, the zones, except for the nucleus, developed very nearly isotropically. Structures having properties intermediate to those of the zones and the precipitates had also been found and were typified by the G.P. [2] zone in Al–Cu. In Al–Zn–Mg, the corresponding phase is the η' phase and the structure was derived from the superstructure of the matrix. The grains always remained very small and cohered well with the matrix. Up to now, a qualitative description only of the reciprocal space of these imperfect crystals had usually been available. More quantitative data would be of great interest to throw further light on the age-hardening process which played such an important role in metallurgical problems.

Dr. J. NUTTING (Metallurgy Department, University of Cambridge) said that the results of electron microscope studies of precipitation in aluminium alloys were in good agreement with those of X-ray diffraction studies. However, studies of zone formation with the oxide replica technique, which had been invaluable in past studies of well-defined precipitates, produced anomalous results which conflicted with the X-ray diffraction results.

This conflict was resolved with the advent of the thin foil technique.[1] These foils must be less than 1000 Å thick and, when viewed in the electron microscope, can show up precipitates as well as dislocations.[2] Surprisingly, the G.P. [1] zone of copper segregation in the Al 4% Cu alloy, which is only 1 atom thick, can also be detected, though this thickness is well below the resolving limit of the microscope (Fig. 1, p. 447). The G.P. [2] zones, which are thicker and longer, can be resolved easily. These zones are coherent with the matrix and, associated with them, are regions of dark and light contrast, which are attributed to distortion of the matrix by coherency stresses.

As the precipitate grows it cannot remain coherent, and an array of dislocations can be seen surrounding it to accommodate the strain. Since the precipitate and the matrix are in the same orientation and their lattice parameters differ, moiré fringes should be visible between them under favourable conditions.[3] Fig. 2 (p. 447) shows these fringes in the [220] direction and the extra half-fringes due to the dislocations can also be seen.

Dr. Nutting then gave a brief outline of ageing studies on some other aluminium alloys.

Aluminium zinc. Since the zinc and aluminium atoms are approximately the same size, the matrix is not strained during zone formation and only preferential scatter contrast occurs. The first zones seen are dots about 25 Å diameter which grow into spheres as ageing proceeds.

Aluminium silver. The first zones of silver segregation are about 50 Å diameter. Subsequent ageing precipitates the γ' phase on stacking faults on the {111} planes. Stacking faults are abnormal in aluminium, but are induced by the presence of the silver.

Aluminium magnesium zinc. The zones of segregation are both spherical and plate-like, the plates forming at the grain boundaries. An associated denuded region can be seen which plays a vital part in explaining the early failure of this material under conditions of stress corrosion.

Dr. Nutting discussed possible causes of the observed pattern of distribution of precipitates and their effect on the movement of dislocations through the matrix. Patterns such as Fig. 3 (p. 447), together with pictures of similar patterns of dislocation (Fig. 4, p. 448), suggest that precipitates nucleate on dislocations. This conclusion is strengthened by measurement of relative distribution densities of precipitates and dislocations.

Oxide replica studies of the interaction of slip lines and precipitates suggested that the slip lines passed through the

particles, rather than round them as the theories suggested. These phenomena can be observed dynamically in the electron microscope when thin foils are strained by heating. The dislocations move and can be seen to pass through precipitates, thus confirming the results of the earlier work.

Miss J. M. Silcock (Fulmer Research Institute, Stoke Poges, Bucks) described some X-ray studies of precipitation in aluminium alloys. The aim of the research was to study the effects of trace elements, quenching rate and deformation on the age-hardening sequence in alloys based on Al–Cu. The additives used were Cd, In, Sn, Li and Mg. In the Al–Cu–Mg system, alloys which formed either S or $S + T$ phases after long ageing times at low temperatures showed the same type of zone, the G.P.B. zone. Alloys with a higher Cu to Mg ratio formed a mixture of G.P. [1], characteristic of Al–Cu, and G.P.B. zones. The G.P.B. zones were rods parallel to the $\langle 100 \rangle$ direction of the Al matrix and varied in length from 20 to 100 Å with a diameter of approximately 10 atoms. The length of the G.P.B. rod was decreased by either increasing the Mg content or by rapid quenching. At higher ageing temperatures (220 to 260° C) a phase was obtained called G.P.B.* which had a superstructure in the plane perpendicular to the G.P.B. rod axis and was more stable in the higher Cu alloys; this indicated that the composition had a Cu : Mg ratio nearer 2 : 1 than 1 : 1. A large number of precipitates were nucleated by deformation and were oriented in a manner which could generally be related to the primary slip directions. The nucleii for θ' were thought to be the edges of stacking faults which had a structure similar to θ'.

The results from experiments at different quenching rates and from reversion treatments indicated that G.P. [1] formation was accelerated by an excess of quenched-in mobile vacancies, but that the dislocation rings or spirals, shown recently by Hirsch and others[4] to be present in severely quenched crystals, act as θ' nucleii. The variations in the rate of zone formation in the Al–Cu alloys which could be explained by the vacancy concept were: (i) high rates of G.P. [1] formation given by a high quenching rate or Mg additions, and (ii) low rates of G.P. [1] formation obtained after reversion or elongation at room temperatures of fast quenched alloys and Cd additions. Deformation generally increased the rate of formation of precipitates and was particularly effective if the atomic arrangement at a dislocation array was similar to the precipitate. Increased rates of θ' formation were also obtained by Li and Mg additions. Cd, In and Sn were the most effective nucleators because they decreased the surface energy of the particles and increased their coherency. They also reduced the rate of platelet growth so that the mechanical properties were much improved. Both Li and deformation interfere with nucleation by Cd, In or Sn; Cd apparently having an affinity for Li. Dislocations trapped the Cd atoms and only the normal "dislocation nucleii" were then operative.

In his paper on precipitation in steels, Prof. R. W. K. Honeycombe (Metallurgy Department, University of Sheffield) drew attention to a recent two-day conference on precipitation[5] and said he could only attempt to high-light recent developments in this field.

He started with a brief study of the iron carbon alloys, described the transformation, on quenching, of austenite to martensite, and discussed the decomposition of the martensite on subsequent tempering. Tempering between 50 and 200° C causes precipitation of a coherent hexagonal carbide, $Fe_{2.4}C$ which transforms, apparently in position, between 200 and 300° C to cementite, Fe_3C, forming a Widmanstätten structure within the martensite needles. Higher temperatures cause spherodization and general softening.

Addition of alloying elements modifies these simple reactions, and iron carbide is eventually replaced by alloy carbides. This arrests the softening of the material and frequently gives rise to the familiar secondary hardening peak. The transformation from Fe_3C to the alloy carbide can occur in two ways:

(i) transformation in position by diffusion of alloying elements into the cementite. This has already been observed in pearlitic structures (Fig. 5, p. 448)[6];

(ii) separate nucleation of alloy carbides which grow at the expense of the cementite.

Studies of the onset of secondary hardening in relation to the state of formation of the carbides have been made by Kuo[7] using carbide extracts. Smith and Nutting[8] and Seal and Honeycombe,[9] using extraction replicas, have been able to correlate the occurrence of fine dispersions of alloy carbides with the secondary hardening peaks.

The fundamental tempering reactions are best studied with steels containing only one carbide-forming element. It is found that all the effective carbides have similar dimensions: 15–30 Å thick, 100–250 Å long rods or platelets. For example, a steel containing 3–4% Mo, 0·2% C reaches peak hardness after tempering for approximately 1000 h at 500° C (Fig. 6). Extraction replicas at this stage show a

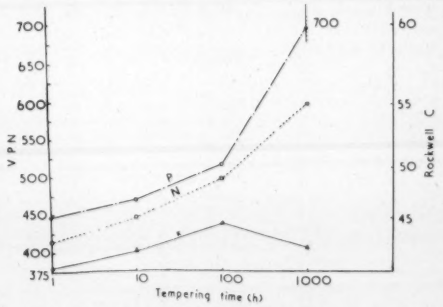

Fig. 6. Tempering curves for molybdenum steels. Tempering temperature 500° C

Steel K, 0·23% carbon, 0·99% molybdenum. Steel N, 0·19% carbon, 3·61% molybdenum. Steel P, 0·20% carbon, 3·83% molybdenum, 0·22% tantalum.

random dispersion of small rods (Fig. 7, p. 448) which are thought to be coherent with the matrix. Electron diffraction patterns from these are difficult to interpret but suggest a structure intermediate between the matrix and Mo_2C.

After 500 h at 600° C, a clear Mo_2C pattern is obtained; the Widmanstätten nature of the precipitate is seen and the non-coherent M_6C carbide nucleates. This grows rapidly and at 700° C eventually replaces the Mo_2C, but does not retard the softening of the steel.

In more complicated steels, the possibility exists of solid solution of other elements in alloy carbides, the formulae of which are thus very nominal. The actual carbide composition will vary significantly during tempering and minor alloying additions [e.g. 0·22% Ta to the above steel (Fig. 6)] can have considerable influence on ageing behaviour. Con-

siderable improvements in mechanical properties can thus be obtained by controlled alloy additions.

In stainless and high-temperature, creep-resisting steels the face-centred cubic form of iron is stabilized at room temperature by the addition of elements such as Ni and Mn. Up to 800° C, however, the solubility of carbon in this material is still very low, and therefore quenching and tempering treatments often result in precipitation hardening.

The primary carbide encountered is $Cr_{23}C_6$. This can adopt a great variety of forms (Figs. 8 and 9, p. 449) and grows preferentially at grain boundaries, giving rise to an associated chromium-depleted zone (Fig. 10, p. 449) where intergranular corrosion can occur.

Precipitation of $Cr_{23}C_6$ can be induced within the grains by deformation. It will then form at coherent twin boundaries[10] and also at the intersection of slip bands.[11]

Addition of elements such as Ti, Nb, etc., with a strong affinity for carbon produces a variety of new phases at the expense of the $Cr_{23}C_6$. Heat treatment can thus be used to produce a fine dispersion of alloy carbides within the grains with consequent improvement of the mechanical properties.

Dr.Ir. T. J. TIEDEMA (Laboratory of Physical Chemistry, Technical University, Delft) discussed results obtained in his laboratory on precipitation in supersaturated Au–Pt alloys. According to Borelius, the rate of precipitation in systems with limited solid solubility was dependent on the spinodal curve, which was the locus of the points of inflexion of the curve of free energy G *versus* composition x for all temperatures [Fig. 11(*a*), (*b*)]. In the concentration range between

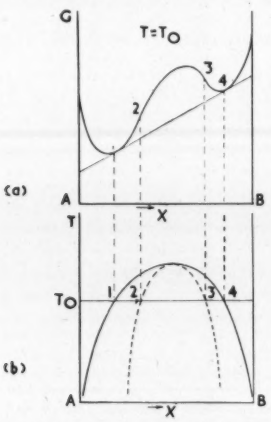

Fig. 11. (*a*) Free energy *versus* composition for temperature T_0. (*b*) Solubility curve and spinodal curve (dotted) for a system with limited solubility

the solubility limit and the spinodal curve where $\partial^2 G/\partial x^2 > 0$, supersaturated alloys would decompose at a slower rate than in the composition range where $\partial^2 G/\partial x^2 < 0$. When $\partial^2 G/\partial x^2 < 0$ "uphill diffusion" was the governing process, and in the Au–Pt alloy examined by Mr. L. J. van der Toorn, this led to the formation, in the pre-precipitation range, of alternating Au-rich and Pt-rich regions, which caused side bands in rotating crystal photographs [Fig. 12(*a*), (*b*), p. 449]. In alloys in the range for which $\partial^2 G/\partial x^2 > 0$, the matrix changed gradually to its equilibrium position, indicated on the X-ray photographs by a continuous displacement of the reflexions.

Miss M. K. B. DAY (Research Laboratories, British Aluminium Co.) suggested that the thin foil technique, in spite of its success, was not yet suitable for quantitative work on practical alloys, for which purpose the constant thickness oxide replica is invaluable.

Miss Day described how the type of fracture of an aged Al–Mg–Zn alloy changes with increasing alloy content. Since precipitation occurs preferentially at the grain boundaries, low alloying concentrations produce little general precipitation and fracture is partially trans-crystalline.

With higher alloying additions, precipitation within the grains occurs and fracture takes place in the denuded grain boundary zone which now appears. Increasing the alloying additions narrows this zone and the fracture changes to the bright intercrystalline type.

There was some discussion of the effects of condensation of excess vacancies quenched-in from high temperatures, which are, in many ways, similar to precipitation effects. Dr. M. J. WHELAN (Cavendish Laboratory, University of Cambridge), reported observations of the helices produced when vacancies condense on to the many screw dislocations which appear in aluminium 4% copper alloy.[12] The axes of these helices are in the [110] direction and they range from 500–1000 Å in diameter.

Dr. R. E. SMALLMAN (Metallurgy Department, University of Birmingham), pointed out that "precipitation hardening" effects can occur in pure metals due to aggregation of vacancies.[4, 13] These aggregates collapse into dislocation loops, the form of which depends on the stacking fault energy of the metal. In aluminium, copper and nickel the loops are prismatic (Fig. 13, p. 449), but silver shows both loops and tetrahedral defects, similar to those in gold described by Hirsch.

Dr. P. B. HIRSCH (Cavendish Laboratory, University of Cambridge), explained the form of these defects from energy considerations. Collapse of vacancies on a (111) plane, by movement of atoms normal to that plane, results in a Frank sessile dislocation loop surrounding a stacking fault.[14] In aluminium, which has a high stacking fault energy, the fault is removed by shear on the (111) plane, giving a complete prismatic loop.[15] In gold, tetrahedra of stacking faults are found, the sides of which are parallel to the (111) planes. It can be shown that this is consistent with accepted values of the stacking fault energy of gold.

One of the highlights of the conference was a cinematograph film shown by Dr. G. THOMAS (Metallurgy Department, University of Cambridge), demonstrating solution and precipitation of the $CuAl_2$ phase in aluminium copper alloy. A thin foil was mounted on a heating stage,[16] and solution treatment, and quenching and ageing, were carried out inside the microscope. It was thus possible to watch all the stages of nucleation and precipitate growth and solution, and grain boundary migration.

Another technique for heat-treating metal foils in position in the microscope was described by Mr. K. F. HALE (Metallurgy Division, National Physical Laboratory, Teddington). The electron spot is used as the heat source and considerable increases in temperature can be obtained with increase in spot size beyond 5 μ.

Dr. T. MANENC (ONERA, Chatillon-sous-Bagneux, France) reported that if a Ni 10% Ti alloy is solution treated and aged at 800° C for 1 h, a coherent phase intermediate between the matrix and the hexagonal Ni_3Ti is formed.

This has a slightly deformed face-centred cubic habit and appears to follow the [100] directions.

On ageing for 16 h, the precipitates grow and are grouped on planes parallel to the (100) planes. After 64 h, this grouping is even more pronounced and can be confirmed by studying replicas from the (111) plane.

Mme. A. R. WEILL (Marine Nationale, Paris) reported some results of Jacquet[17] on aluminium 4% copper, homogenized, quenched and annealed for 15 min at 250° C. The resulting patterns of precipitation on grain boundaries, slip lines and bands, and dislocations are best studied in the interference light microscope, or in the electron microscope at low magnification. Some patterns are seen to be connected with such mechanisms as half and whole Frank-Reed sources.

An important extension of the thin foil technique was announced by Mr. P. M. KELLY (Metallurgy Department, University of Cambridge), who has prepared thin steel foils by a jet electrolytic machining technique. Slides were shown of a quenched 0·98% carbon steel, which showed fine striations across the martensite needles (Fig. 14, p. 450) and of a quenched and tempered 0·14% carbon steel; a Widmanstätten precipitation is normally seen, but tempering at low temperatures produces some deviations from this pattern (Fig. 15, p. 450).

Mr. K. THOMAS (Metallurgy Division, National Physical Laboratory, Teddington) described a modification to the electrolytic thinning technique for foils. The specimen is polished either from one side only or on alternate sides, until a foil is obtained from the desired level of the bulk specimen. In this way, the effect of the free surface on quenching and tempering behaviour is being studied. This effect may be substantial and it is desirable that details are always given of quenching treatment.

Mr. R. S. BARNES (United Kingdom Atomic Energy Authority, Harwell) described "precipitation" effects obtained by heating a copper α-particle target. Vacancies are generated at the grain boundaries and migrate inwards, permitting the precipitation of helium bubbles. The process is limited by the supply of vacancies, which are replaced by copper atoms, resulting in a bubble-free zone near the grain boundary (Fig. 16, p. 451).

Dr. SMALLMAN has studied the aluminium 20% silver alloy. He demonstrated, from Geiger counter traces across small-angle X-ray diffraction haloes, the rapidity of clustering of silver atoms on warming up to room temperature from a $-45°$ C quench. This high rate of precipitation is explained as the result of vacancies introduced during quenching, and the high concentration required (10^{-3} to 10^{-4}) is confirmed from counts in the electron microscope of dislocation loops formed by the collapse of disks of aggregated vacancies.[4]

Dr. T. Ll. RICHARDS (I.C.I. Ltd., Kynoch Works, Birmingham) sought a reason for the different forms of precipitate appearing in a well-defined temperature range. He quoted, as a possible explanation, recent work by Borelius,[18] who found four peaks of heat evolution during ageing of quenched alloys at different temperatures. This effect was attributed to release of elastic strain.

METAL STRUCTURES

The X-ray Analysis Group's Conference was also under Prof. Cox's chairmanship and was opened by Dr. A. R. LANG (Harvard University, Cambridge, Mass.), who presented a paper on the study of individual dislocations in crystals by X-ray diffraction. Dislocations had been observed in the interior of crystals by X-ray diffraction[19] using the method of "section topographs"[20] and of "projection topographs".[21] The latter method gave an X-ray diffraction image that showed a projection of a slice of crystal and the imperfections within it. Stereo-pairs of projection topographs could be prepared from the pair of reflexions (hkl) and $(\bar{h}\bar{k}\bar{l})$. From the variation of the visibility of a dislocation with the orientation of the X-ray reflecting plane the direction of the Burgers vector could be found. Dislocations had been studied by X-rays in diamond, silicon (Fig. 17, p. 451), germanium, lithium fluoride (Fig. 18, p. 451), sodium chloride, silver chloride, magnesium oxide, quartz, calcite and aluminium (Fig. 19, p. 451). Experiments indicated that individual crystals could be observed in any crystal provided that they were the principal imperfections present and that their density was fairly low (less than 10^6 to 10^7 lines per square centimetre).

Dislocations could be seen with good contrast when the product of the linear absorption coefficient μ and slice thickness t was of the order of unity or less. If $\mu t > 1$, the contrast was reversed owing to the Bormann effect. The methods were being applied to studies of the early stages of plastic deformation and to the origin of dislocations. Inclusions, precipitates and small variations in lattice parameter might also be studied with these diffraction methods.

Dr. M. J. WHELAN, commenting on Dr. Lang's work, pointed out that Hirsch, Howie and Whelan[22] had applied a kinematical theory to the problem of electron optical contrast at a dislocation in a thin metal foil. The results showed that contrast occurred on one side of the dislocation and that it vanished if $\mathbf{g} \cdot \mathbf{b} = 0$, where $\mathbf{b}$ is the Burgers vector and $\mathbf{g}$ the reciprocal lattice vector. This condition implied that the strain field of the dislocation had no component displacement normal to the reflecting planes.

Dr. T. Ll. RICHARDS suggested that although a tangle of dislocations was formed even after a small degree of strain, the situation was not without hope of resolution if it were remembered that in polycrystalline aggregates, deformation must occur as if it were homogeneous. Tensile tests on cube texture copper strip fully supported this view.[23]

Dr. A. N. MAY (Crystal Structures Ltd., Cambridge) described his work on the diffraction of X-rays by an aluminium crystal. The experiments were made with the object of comparing the distribution of intensity from distorted and undistorted crystals, in the immediate neighbourhood of the Bragg reflexion, as a means of investigating the mechanism of distortion. Large-grained specimens of spectroscopically pure aluminium rods were mounted in an X-ray diffractometer and examined with $CuK\alpha_1$ radiation. By the use of carefully constructed slides, selected areas of the specimen, 0·1 mm square, could be irradiated and the intensity of the reflected radiation was measured with a Geiger counter in front of which was a fine slit. The angle made by the counter and the direct beam ϕ was plotted against the counting rate, with the crystal in the reflecting positions, and yielded an asymetrical curve having a pronounced tail on the small ϕ side. This effect was ascribed in part to the penetration of X-rays into the specimen in a manner which was readily calculated and which agreed with observation. If i was the glancing angle of incidence on the crystal, then a rocking curve obtained for a given value of ϕ showed a peak at $i = i_m$ where the Bragg condition was fulfilled. At some points, where lattice distortion was heavy, a double peak was obtained on the rocking curve and the two values of i_m varied with ϕ. In one case, one peak from a (220) reflexion could be accounted for by geometrical effects due to the penetration of the radiation into

the specimen, but the other peak resulted from a considerable distortion of the lattice giving an extension of the diffraction pattern in reciprocal space. By plotting contour lines of constant counting rate it was found that the peak corresponded to an extension of the central maximum along a line nearly normal to the crystal surface. If, with the limited data available, it were assumed that the extension was in the form of a spike, then this might originate from a region approximately 10^{-4} mm thick. Ten irregularly spaced planes of disturbance parallel to the surface acted as the source of the spike.

Dr. May also presented a paper by Dr. WOOSTER (Crystal Structures Ltd., Cambridge) which was concerned with the study of S-lines in X-ray photographs. These photographs were taken with a stationary crystal set at 2 to 3° away from the Bragg position. At the place where Bragg reflexion would occur there appeared an S-line after the crystal had been subjected to alternating stress. The S-line followed a constant θ-curve, was very strong on the equator (for equatorial Bragg reflexions) but diminished rapidly in intensity away from the equator. The camera consisted of a modified type S-25 Unicam oscillation goniometer. The specimen, an aluminium crystal, was set in turn by a cam at 1°, 1° 45′ and 2° 45′ away from the Bragg position, the film being moved by a second cam to prevent overlap of the diffraction patterns. Fig. 20 shows the intensity contours of the S-lines and their associated Laue spots. If I is the peak intensity of the S-line and S is its distance from the reciprocal lattice point, then the results indicated that $I \propto S^{2.9}$.

In most photographs the maximum of the S-line was on the equator, but in one case the peak made an angle of 28° with the equator. Three sets of parallel striations were visible in a fatigued specimen and these were found to lie in directions corresponding to the intersection of the {111} glide planes with the surface.

Small-angle scattering from cold-worked, fatigued and irradiated metals had been studied by Dr. H. H. ATKINSON (Cavendish Laboratory, University of Cambridge). Experiments[24] had been carried out on the scattering of X-rays (wavelength 1·54 Å) at angles between 1½ and 15° from cold-worked and fatigued single grains of aluminium and polycrystalline copper. The results showed that almost all the observed scattering was due to double Bragg reflexions,[25] recognized by the geometrical relationship between the once- and twice-reflected beams. No evidence had been found for surface scattering. Experiments[26] on scattering at angles greater than 50′ from polycrystalline copper showed that there was an increase in scattering at small angles when the recrystallized metal was bombarded with fast neutrons; the objected effects (Fig. 21, p. 452), which were explained in terms of double Bragg reflexions and also possibly of "true" small-angle scattering, suggested that either small coherent regions (of diameter approximately 100 Å) or severe strains were present in the irradiated metal.

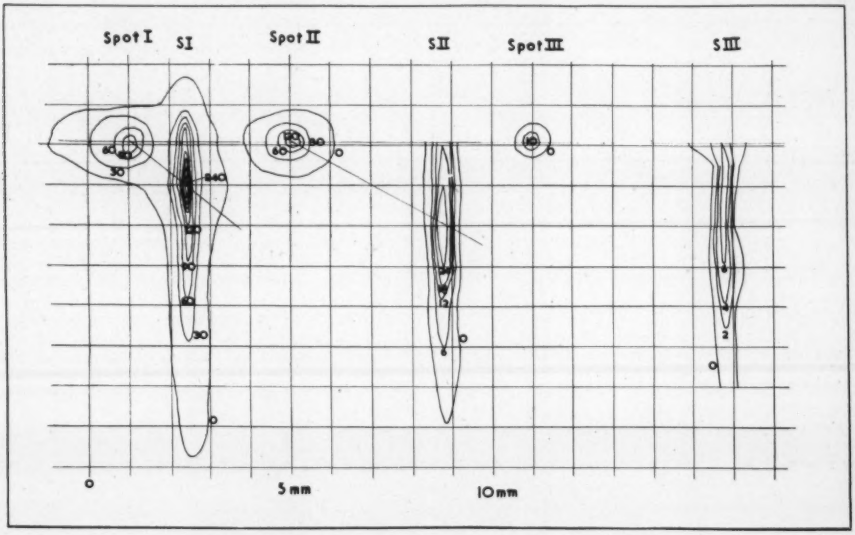

Fig. 20. Intensity contours of S-lines and their associated Laue spots

Double Bragg reflexions had been eliminated in experiments[24, 27] on cold-worked and fatigued aluminium and copper using neutrons of wavelength greater than the Bragg "cut-off" wavelength of the specimens. The results showed that the magnitude of the "true" small-angle scattering was not more than about 1% of that due to double reflexions observed in the X-ray experiments. Dislocation densities estimated from these results, using the theory of Atkinson and Hirsch[28] were consistent with currently accepted values. Hence there was now no evidence, as the result of small-angle scattering experiments, for the existence of cavities in cold-worked or fatigued metals.

Mr. K. THOMAS (Metallurgy Division, National Physical Laboratory, Teddington) pointed out that geometrically, low-angle X-rays streaks obtained from deformed metals could be accounted for by oriented cavities. Conclusive proof that they were, in fact, caused by double Bragg scattering was given by the radical changes in pattern obtained on irradiating single crystals in the same or chosen orientations with both CuK and CoK radiations.[29, 30] Streaks showing structure (Fig. 22, p. 452) has been obtained from fatigued single crystals and this was interpreted as being due to a non-homogeneous subgrain formation.

Dr. H. J. MILLEDGE (University College, London) described her work with Prof. E. ALEXANDER on a new X-ray study of gallium. Molybdenum radiation had been used to obtain rotation photographs, at room temperature, of a 0·1 mm radius sphere of very pure gallium. Absorption corrections had been applied and approximately 150 three-dimensional reflexions were available to determine the two positional parameters and the thermal vibrations. Preliminary analysis of this part of the data led to atomic positions virtually indistinguishable from those due to Bradley[31] but to surprisingly low values of the temperature factor, considering that the crystal was within 10° of the melting point. This might imply inadequate absorption corrections, a possibility which was supported by a comparison of intensities at 290 and 90° K obtained from a larger sphere with CuKα radiation. Preliminary examination of the expansion coefficients indicated that they were more consistent with other physical properties than the values obtained previously. The effect of using new theoretical *f*-curves for gallium was also being explored.

Prof. H. LIPSON (College of Science and Technology, Manchester) recalled that originally the structure of Ga was thought to be tetragonal, although some weaker reflexions could not be accounted for. Dr. A. J. Bradley[31] showed that the high-angle reflexions were split and deduced that the structure was orthorhombic, the agreement being entirely satisfactory for 1930. The result was not, however, in accord with Hume-Rothery's 8-N rule!* Dr. J. W. JEFFERY (Birkbeck College, London) emphasized the importance of correcting for absorption in non-spherical crystals. In the case of a square prism of Ga of side equal to the diameter of the sphere used by Prof. Alexander, the intensity of a reflexion with $2\theta = 90°$ and incident and reflected beams symmetrical about a side of the square would have an absorption correction about 25% less than that for a similar reflexion about a diagonal. If a prismatic crystal were treated as though it were cylindrical, such shape effects were equivalent to more or less random errors in the intensity measurements.

Mr. W. J. KITCHINGMAN (Metallurgy Department, Manchester College of Science and Technology) presented a joint paper with Dr. H. T. HALL and Mr. J. I. BUCKLEY on a transformation induced by cold work in the ζ phase of the alloy AgZn. These alloys around the composition 50 atomic % existed above the temperatures 258 to 274° C as a disordered body-centred cubic structure, the β phase. Below these temperatures the β phase transformed to the ζ phase which is a complex hexagonal structure. On quenching the β phase an ordered body-centred cubic structure of the CsCl type was obtained, the β' phase. The ζ phase transformed in five days to the β' phase after cold-working at room temperature. The lattice parameter was $3{\cdot}1552 \mp 0{\cdot}0003$ Å at 20° C for an alloy of 49·98 atomic % Ag, which agreed with that of the β' phase obtained by quenching. Edmunds[32] had shown that the β and ζ structures were closely related. The first Brillouin zone of the β-phase was bounded by {110} zone faces. These corresponded to the {30.0} and {11.1} zone faces in the hexagonal structure. The (11.1) and (30.0) were the first strong reflexions in the ζ phase powder photograph. The first Brillouin zone for the ζ phase was thus bounded by {11.1} and {30.0} zone faces. It was similar to that of the β phase save that the {11.1} faces had approached the origin in K space whilst the {30.0} faces moved away from it, as if a shearing distortion of the β zone had taken place. The Brillouin zone of the β phase was shown in Fig. 23(*a*) and that of the ζ phase in Fig. 23(*b*). These effects could be

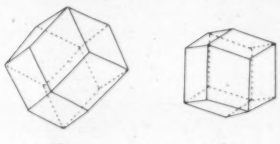

Fig. 23. (*a*) First Brillouin zone of the β phase. (*b*) First Brillouin zone of the ζ phase

explained by Goodenough's[33] theory. The transformation of ζ to β' which occurred on cold work suggested that the ζ structure might take up some energy of cold work by changing the Brillouin zone structure to that of the β phase. The β phase could not exist in the disordered state at room temperature and subsequently ordered. The transformation thus proceeded in two stages ζ to β', followed by β to β'.

Dr. R. W. CAHN (Department of Metallurgy, University of Birmingham) read a joint paper with Dr. A. LAWLEY and Mr. R. FEDER on order-disorder effects in alloys. The equilibrium relations of the iron-rich solid solutions of the Fe–Al system had been studied by X-ray diffractometry at high temperatures. Alloys containing between 23 and 25 atomic % Al were found by measurement of intensities of superlattice lines at high temperature to change directly from the Fe_3Al superlattice to complete disorder at 540° C. In alloys with Al content exceeding 25 atomic %, Fe_3Al-type order changed to FeAl-type order at approximately 540° C. This disagreed with the lattice parameter data[34] which suggested that the discontinuity should occur at 23 atomic % Al. The disagreement might be due to the influence of a magnetic field during annealing or to compositional changes due to filing. Preliminary tests on an alloy containing 20·5 atomic % Al clearly showed that appreciable ordering did not occur in the absence of a magnetic field, but the effect of the field on more concentrated alloys was not yet certain.

The state of order at a given temperature was also found to be sensitive to the thermal history. Rapid cooling in the vicinity of the critical temperature reduced the degree of order at the lower temperatures. This was believed to be due to the incidence of directional short range order which arose from the presence of internal ferromagnetic moments. Thermal history, state of sample dispersion and external magnetic fields could all affect the state of order.

The structural studies had been related to resistivity and creep resistance. Resistivity data confirmed the relation between order and thermal history, while creep rates at a

* HUME-ROTHERY, W. *The structure of metals and alloys*, p. 23 (London: Institute of Metals).

given stress changed rapidly near the critical temperatures at which order disappeared. Under certain circumstances the alloy, while under stress, oscillated between two states of order which gave rise to oscillatory creep (Fig. 24).

In discussing Dr. Cahn's paper, Dr. H. D. MEGAW (Cavendish Laboratory, University of Cambridge) pointed out that the effects of directional short-range order threw light on the relations between magnetic materials and ferroelectrics. In magnetic materials these effects were small compared with those of long-range forces but in ferroelectrics the reverse was true. Even for ferromagnetics it now

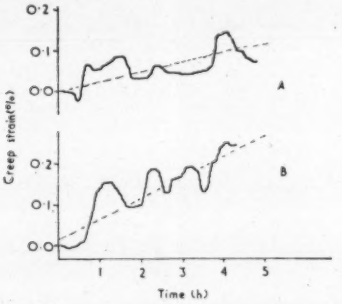

Fig. 24. Oscillatory creep in two iron aluminium alloys

Curve *A*, specimen No. 7, 24·8% aluminium, 557° C, 6·50 tons per square in. Curve *B*, specimen No. 3, 25·5% aluminium, 581° C, 5·50 tons per square in.

appeared that the nature of the structure arising from directional short-range order should be considered. Dr. Megaw made a plea that partly-ordered systems should be described in terms of the true cell of the ordered case—the "superlattice" cell (a word which had introduced a great deal of misunderstanding), so that established methods of three-dimensional crystal geometry could be applied.

In a further comment on Dr. Cahn's paper, Dr. H. J. GOLDSCHMIDT (B.S.A. Group Research Centre, Birmingham) recalled that a spurious face-centred cubic phase occurred in the Fe_3Al superlattice region and asked Dr. Cahn whether more was now known about this effect. In general, it seemed preferable to represent a superlattice boundary not as a line but as a zone of finite width because of the appreciable smearing of the free energy curves around the intersection. Dr. Cahn's effects afforded a splendid example of this.

In his reply, Dr. Cahn stated that the phase referred to had been studied by Taylor and Jones[34] who concluded that it nucleated as a double Fe–Al carbide in epitaxial relation to the body-centred cubic matrix and then continued to grow without participation of carbon. Dr. Cahn had also observed this phase micrographically and by X-ray diffraction, but only when the material had been strained by cold work or by quenching from 1200° C. Subsequent tempering at 500–600° C then produced the face-centred cubic phase.

In his closing words, Prof. E. G. Cox, Chairman of the X-ray Analysis Group, thanked everyone for helping to make the Conference such a success and remarked on the pleasure given to him by the participation of the Electron Microscopy Group.

A. FRANKS
R. S. M. REVELL

REFERENCES

(1) NICHOLSON, R. B., THOMAS, G., and NUTTING, J. *Brit. J. Appl. Phys.*, **9**, p. 25 (1958).
(2) HIRSCH, P. B., HORNE, R. W., and WHELAN, M. J. *Phil. Mag.*, **1**, p. 677 (1956).
(3) MENTER, J. W. *Proc. Roy. Soc. A*, **236**, p. 119 (1956).
(4) HIRSCH, P. B., SILCOX, J., SMALLMAN, R. E., and WESTMACOTT, K. H. *Phil. Mag.*, **3**, p. 897 (1958).
(5) *Proceedings of a Conference on Precipitation Processes in Steels, Sheffield*, 2–4 July, 1958. (The Iron and Steel Institute, to be published.)
(6) WEBER, F., and KOCH, W. *Stahl u. Eisen*, **74**, p. 989 (1954).
(7) KUO, K. *J. Iron Steel Inst.*, **184** (3), p. 258 (1956).
(8) SMITH, E., and NUTTING, J. *J. Iron Steel Inst.*, **187** (4), p. 314 (1957).
(9) SEAL, A. K., and HONEYCOMBE, R. W. K. *J. Iron Steel Inst.*, **188** (1), p. 9 (1958).
(10) HATWELL, H., and BERGHEZAN, A. Ref. 5, paper No. 5.
(11) YOUNG, B. M. Met. Thesis (University of Sheffield, 1958).
(12) WEETERMAN, J. *Phys. Rev.*, **107**, p. 1259 (1958).
(13) SILCOX, J., and HIRSCH, P. B. *Phil. Mag.*, **4**, p. 72 (1959).
(14) FRANK, F. C. *Proc. Phys. Soc.* (*London*) *A*, **62**, p. 202 (1949).
(15) KUHLMANN-WILSDORF, D. *Phil. Mag.*, **3**, p. 125 (1958).
(16) WHELAN, M. J. *Brit. J. Appl. Phys.*, **9**, p. 306 (1958).
(17) JACQUET, P. A., WEILL, A. R., and CALVET, J. *C.R. Acad. Sci.* (*Paris*), **247**, p. 1001 (1958).
(18) BORELIUS, G. *N.P.L. Symposium on Physical Chemistry of Metal Solutions and Intermetallic Compounds*, 1958 (London: H.M. Stationery Office).
(19) LANG, A. R. *J. Appl. Phys.*, **29**, p. 597 (1958).
(20) LANG, A. R. *Acta Met.*, **5**, p. 358 (1957).
(21) LANG, A. R. *Acta Cryst.*, **12**, p. 249 (1959).
(22) HIRSCH, P. B., HOWIE, A., and WHELAN, M. J. *Proceedings of the Fourth International Conference on Electron Microscopy, Berlin* (1958). (Heidelberg: Springer Verlag.)
(23) *The British Society of Rheology Conference "Flow, Fatigue and Failure", Leeds* (January 1959).
(24) ATKINSON, H. H. *Phil. Mag.*, **3**, p. 476 (1958); *J. Appl. Phys.*, **30**, p. 637 (1959).
(25) BEEMAN, W. W., KAESBERG, P., ANDREGG, J. N., and WEBB, M. B. *Hand. Physik*, **32**, p. 440 (1957).
(26) ATKINSON, H. H., SMALLMAN, R. E., and WESTMACOTT, K. H. *J. Appl. Phys.*, **30**, p. 646 (1959).
(27) ATKINSON, H. H., and LOWDE, R. D. *Phil. Mag.*, **2**, p. 589 (1957).
(28) ATKINSON, H. H., and HIRSCH, P. B. *Phil. Mag.*, **3**, pp. 213, 862 (1958).
(29) FRANKS, A., and THOMAS, K. *Proc. Phys. Soc.* (*London*), **71**, p. 861 (1958).
(30) THOMAS, K., and FRANKS, A. *J. Appl. Phys.*, **30**, p. 649 (1959).
(31) BRADLEY, A. J. *Z. Krist.*, **91a**, p. 302 (1935).
(32) EDMUNDS, I. G., and QRASHI, M. *Acta Cryst.*, **4**, p. 417 (1951).
(33) GOODENOUGH, J. *Phys. Rev.*, **43**, p. 105 (1953).
(34) TAYLOR, A., and JONES, M. *J. Phys. Chem. Solids*, **6**, p. 16 (1958).

Interferometric measurement of small angular displacements

By P. Hariharan, Ph.D., A.Inst.P., and D. Sen, M.Sc., Ph.D., National Physical Laboratory of India, New Delhi, India

[*Paper first received* 25 *May, and in final form* 15 *June*, 1959]

A modified three-beam interferometer is described for the measurement of small angular displacements. The instrument is extremely sensitive to angular displacements in a specified plane and is capable of a high degree of accuracy. In addition it is easy to handle and quite stable, since it is relatively insensitive to angular displacements in any other plane and is also completely unaffected by a linear translation of the detecting element.

While several methods have been described for the interferometric measurement of small angular displacements, one of the most elegant techniques utilizes the change in optical path produced by the rotation of a thick plane-parallel plate traversed by one of the interfering beams.[1] The sensitivity that can be obtained with this method naturally depends on the accuracy with which the fractional fringe shift can be estimated, and this is usually limited to about 1/30 of the fringe spacing in the case of two-beam interference by the sinusoidal intensity distribution in the fringe pattern. One method of attaining higher precision which has been suggested is the use of multiple-beam fringes.[2] However, this has the drawback that the aperture of the system must be made quite large to transmit a sufficient number of the higher order beams formed by multiple reflexions in the plate. An alternative method of obtaining greater accuracy, which avoids this difficulty and which has been utilized in the instrument described in the present paper, is to make use of the principle of three-beam interference for estimating the fractional fringe order.[3]

OPTICAL SYSTEM

The arrangement of the optical system, which is derived from that used in a three-beam interferometer described in an earlier paper,[4] is shown in Fig. 1.

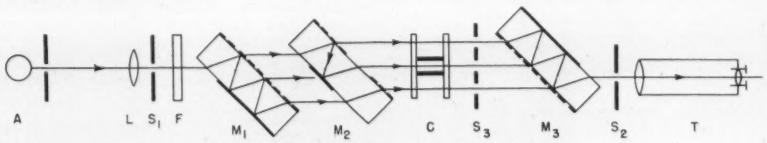

Fig. 1. Schematic diagram of the interferometer

A, source; *L*, condensing lens; *F*, monochromatic filter; M_1, M_2, M_3, beam dividing mirrors; S_1, S_2, S_3, stops; *C*, compensating cell; T_1, telescope.

The three beam-dividing plates M_1, M_2, M_3 are identical, optical glass blocks whose faces have been worked plane and parallel. One of these, M_2, is the moving element, while the other two are nominally stationary. The inner faces of M_1 and M_3 are coated with a $\lambda/4$ oxide film of high refractive index, which has a reflexion coefficient of about 50%, while the right-hand face of M_2 (with the exception of a narrow, vertical strip in the middle, which is left clear) is coated with a semi-transparent film of aluminium whose reflectivity is about 50%. Part of the outer faces of M_1 and M_3 and a narrow, vertical strip on the left face of M_2 (shown by thick lines in the diagram), are coated with an opaque, fully reflecting film of aluminium. Two stops S_1 and S_2 define the incoming and outgoing beams.

As will be seen from the figure, three beams are formed by multiple reflexion at M_1, but the middle one is blocked off by the opaque aluminized strip on M_2. Its place is taken by the beam formed by the division of the first beam at the semi-reflecting surface of M_2, which is reflected forward from the other face of the aluminized strip. After passing through a stop S_3, this beam and the two outer ones are recombined by reflexion at M_3. The fringe system formed by these three beams is viewed through a low power telescope *T*.

THEORY OF THE INTERFEROMETER

As has been previously pointed out,[3] the intensity distribution in the fringe system formed in a three-beam interferometer can be easily visualized by considering the amplitude at any point in the pattern as the resultant of the amplitudes arising from the fringe system formed by the two outer beams and the coherent background due to the middle beam.

If we assume that the reflexion and transmission coefficients of the inner faces of M_1 and M_3 are r_1 and t_1, respectively, while those of the semi-reflecting coating on the right-hand face of M_2 are r_2 and t_2, it is easily seen that the intensities of the two outer beams are equal to one another and are given by the expression

$$I_0 = IR^2t_1^2t_2r_1^2 \qquad (1)$$

where I is the intensity of the beam incident on M_1, and R is the reflexion coefficient of the opaque aluminium coating. The intensity of the middle beam, on the other hand, is given by the expression

$$I_M = IR^2t_1^2r_1r_2 \qquad (2)$$

If we ignore the effects of the phase coherence factors of the beams, the intensity distribution in the interference pattern will then be given by the relation[5]

$$I(x, \phi) = 2I_0\{1 + \cos(2\pi x/a)\} + I_M + 4(I_0I_M)^{1/2}\cos(\pi x/a)\cos\phi \qquad (3)$$

where x is the distance from the centre of the pattern, a is the fringe spacing and ϕ is the phase difference between the central beam and the two outer beams. When the central beam is either in phase or out of phase with the outer beams, its effect is to alternately weaken and reinforce the fringes, while all the fringes have the same intensity when the phase difference between the central beam and the outer beam is equal to $\pi/2$. In the latter case, a very small change in the

phase of the central beam results in an appreciable difference in brightness between adjacent fringes. Consequently, this criterion can be used as a very sensitive null-setting, in conjunction with a suitable compensator such as an auxiliary gas cell, to measure small changes in the angular position of the plate M_2.

ADJUSTMENT

The preliminary adjustment of the interferometer can be conveniently carried out in two steps. In the first instance, the central beam is blocked out, and the two plates M_1, M_2 are set parallel to one another so that a single fringe covers the whole field. After this, one of the outer beams is blocked out, and M_2 is set parallel to M_3 in the same manner. Three-beam fringes are then obtained by tilting M_3 about an axis in the plane of the paper (see Fig. 1). Any residual non-uniformity in the fringe pattern is removed by a final, slight adjustment of M_1.

SENSITIVITY

It is easily seen from Fig. 2 that the optical path difference P between two rays formed by the division of a single ray by reflexion within a tilted plane-parallel plate of thickness d is given by the relation

$$\begin{aligned} P &= BC + CD - BE \\ &= 2nd \cos r \end{aligned} \tag{4}$$

where n is the refractive index of the material of the plate, and r is the angle of refraction of the beam within the plate. The change in this path difference produced by a small rotation of the plate is then, obviously,

$$\begin{aligned} dP &= -2nd \sin r dr \\ &= -2d \tan r \cos i di \end{aligned} \tag{5}$$

where i is the angle of incidence of the beam on the plate.

Fig. 2. Path difference introduced by reflexion in a plane-parallel plate

The angular displacement of M_2 corresponding to a change in the optical path difference of one wavelength ($\lambda = 5500$ Å) for a 2·5 cm thick plate having a refractive index of 1·5 has been calculated for various values of the angle of incidence and is given in the table. It is apparent that the sensitivity is a maximum for an angle of incidence approximately equal to 50°. The exact value of this angle can be obtained by differentiating equation (5) and is defined by the relation

$$\sin^2 i = n^2 - n(n^2 - 1)^{1/2} \tag{6}$$

In addition, it is easily seen from equation (4) that the sensitivity in a given plane drops to zero when the angle of incidence in that plane is zero. It follows, therefore, that for small tilts of M_2 about any axis, the change in path difference is proportional only to the resolved component of the tilt in the plane of the paper (see Fig. 1).

*Change in tilt corresponding to a change in optical path of one wavelength** ($\lambda = 5500$ Å)

i (degrees)	Δi (seconds)
20	10·1
30	7·3
40	6·2
50	5·7
60	6·3
70	8·1

* For a 2·5 cm thick glass plate of refractive index, $n = 1·5$.

The other factor upon which the overall sensitivity depends is the accuracy with which the fractional fringe order can be estimated. Obviously, this depends upon the relative difference in intensity ΔI of the alternate fringes caused by a small change $\Delta\phi$ in the phase of the middle beam from the value for equality of illumination. It can be shown[3] that this is given by the expression

$$\Delta I = 8\{(I_0 I_M)^{1/2}/(4I_0 + I_M)\}\Delta\phi \tag{7}$$

where I_0 and I_M are the intensities of the outer beams and the middle beam, respectively. This expression has its maximum value when $I_M = 4I_0$. Optimum sensitivity should therefore be obtained, theoretically, when $(r_2/r_1 t_2) = 4$. This condition can be realized fairly easily, in practice, by using a semi-reflecting aluminium film on M_2 having a reflexion coefficient $r_2 = 0·5$ and a transmission coefficient t_2 approximately equal to 0·25. Measurements under these conditions showed that settings could be repeated to better than $\lambda/250$, which would correspond (see the table) to an angular displacement of M_2 of about 0·02 s.

A limit is set to the maximum permissible angular displacement of M_2 by the lateral shift of the middle beam which, beyond a certain point, results in distortion of the fringe pattern. It can be shown that this is zero, to a first approximation, when the angle of incidence is that corresponding to maximum sensitivity [see equation (6)]. Hence, for the widest useful range, the angle of incidence should be made equal to this value. However, in practice, this adjustment is not too critical, since for angles of incidence within about 5° of the optimum value, angular deviations of M_2 of the order of 5 min (corresponding to a path difference of about 50 wavelengths) can be measured without any loss of accuracy on this account.

CONCLUSIONS

The interferometer described is particularly suited to the measurement of small angular displacements with a very high degree of accuracy. It also has the basic advantage that the readings are sensitive to tilt in only one plane and are completely unaffected by a linear translation of the measuring element. Several applications of this instrument in the laboratory can be easily visualized.

ACKNOWLEDGEMENT

The authors wish to express their thanks to the Director, National Physical Laboratory of India, for permission to publish this paper.

REFERENCES

(1) Brillouin, M. *C.R. Acad. Sci.* (*Paris*), **137**, p. 786 (1903).
(2) Cagnet, M. *Rev. Opt.*, **33**, p. 229 (1954).
(3) Zernike, F. *J. Opt. Soc. Amer.*, **40**, p. 326 (1950).
(4) Hariharan, P., and Sen, D. *J. Sci. Instrum.*, **36**, p. 70 (1959).
(5) Vittoz, B. *Helv. Phys. Acta*, **26**, p. 400 (1953).

Summarized proceedings of a conference on precipitation in alloys and on metal structures—London, November 1958

By A. Franks and R. S. M. Revell

See pages 438–444

Fig. 1. Thin foil aluminium 4% copper aged 16 h at 130° C showing G.P. [1] zones (× 1 000 000)

Fig. 2. Thin foil of aluminium 4% copper aged 2 days at 200° C showing moiré fringes between θ' precipitate and the matrix. Note the dislocations showing in the fringe pattern (× 80 000)

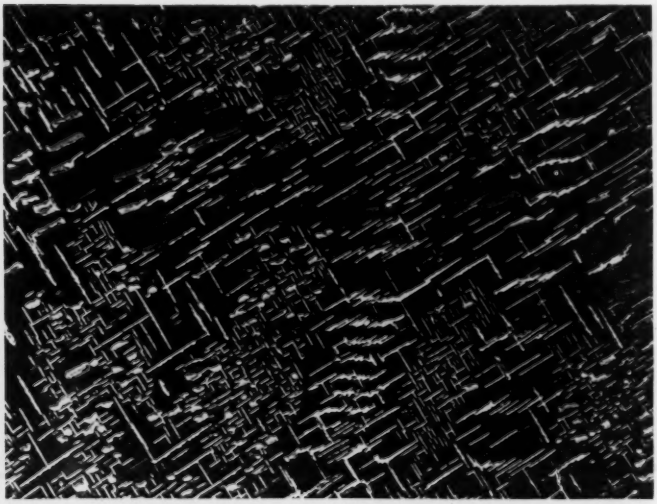

Fig. 3. Oxide replica of aluminium 4% copper aged 100 h at 200° C showing θ' precipitates on dislocations (× 20 000)

Fig. 4. Thin foil of aluminium 4% copper as quenched showing dislocation spirals (×40000)

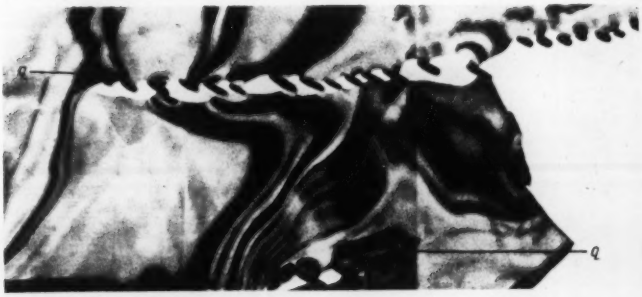

Fig. 5. Transformation to Cr_7C_3 in cementite plates (×25000)

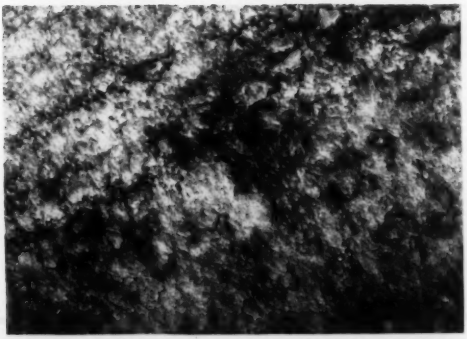

Fig. 7. Steel containing 3·6% molybdenum and 0·19% carbon tempered 1000 h at 500 C. A fine dispersion of carbide particles is visible. Carbon extraction replica (×100000)

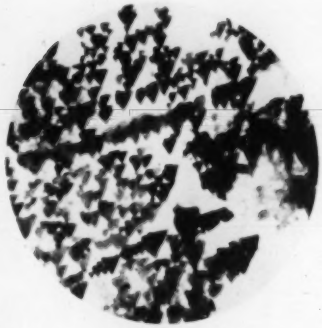

Figs. 8 and 9. Different forms of $Cr_{23}C_6$ precipitated at the grain boundaries of an 18/8 stainless steel during tempering. Carbon extraction replica. (Fig. 8, × 7500; Fig. 9, × 21 000)

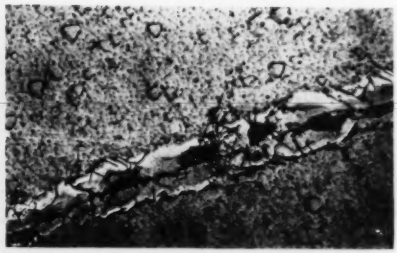

Fig. 10. Precipitation of $Cr_{23}C_6$ at a grain boundary in an 18/10 stainless steel. A thin chromium depleted layer can be seen. Carbon extraction replica (× 20 000)

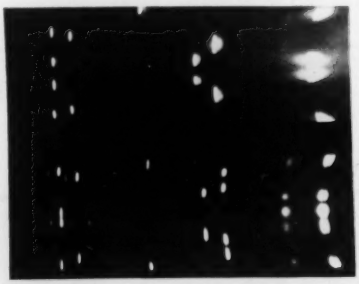

Fig. 12. Rotating crystal photograph of a gold–platinum single crystal (13·5% gold) ($\partial^2 b/\partial x_2 < 0$)

(*a*) Aged at 700 for 2 min showing side bands.
(*b*) Aged at 700 for 84 h showing final phases.

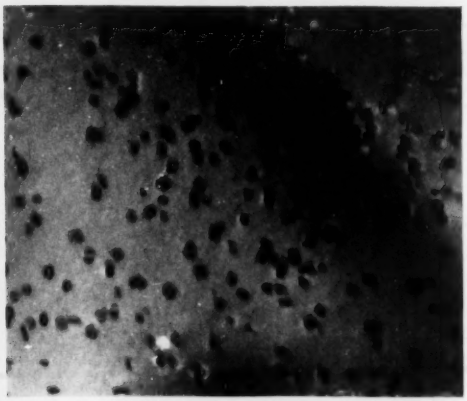

Fig. 13. Prismatic dislocation loops in aluminium quenched from 630 C (× 40 000)

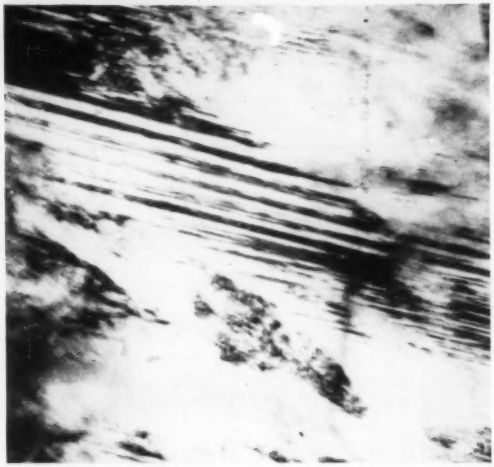

Fig. 14. Thin foil of a water quenched 0·98% carbon steel showing striations in a single martensite needle (× 80000)

Fig. 15. Thin foil of a water quenched 0·14% carbon steel tempered 1 h at 100 C showing Widmanstätten precipitate of cementite (× 80000)

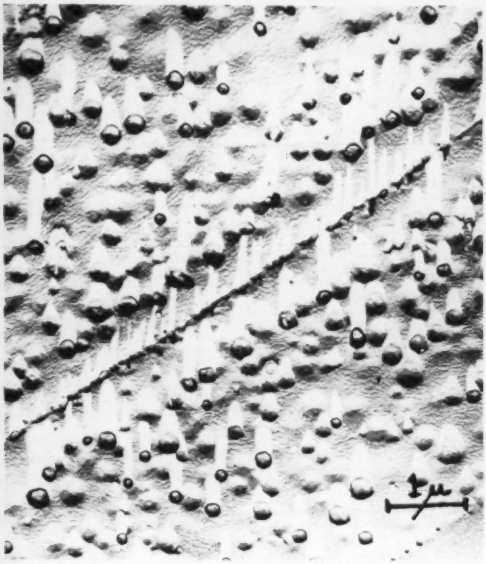

Fig. 16. Shadow-cast replica of a copper α-particle target showing helium bubbles which have been precipitated on heating (× 6750)

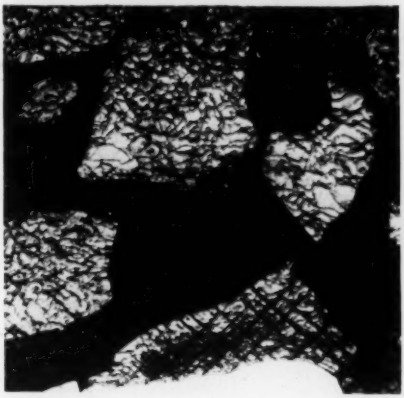

Fig. 18. Dislocations in lithium fluoride. (200) reflexion, AgKα radiation, specimen thickness 0·35 mm, area of field 4 × 4 mm

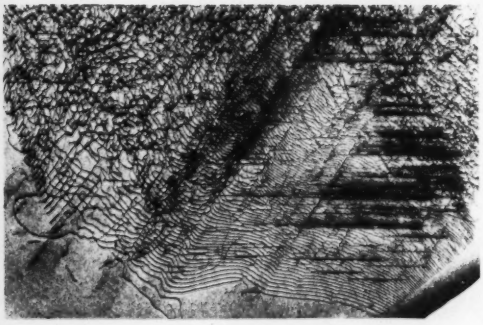

Fig. 17. Dislocations in silicon. (111) reflexion, AgKα radiation. Specimen thickness 1·25 mm, area of field 12 × 8 mm

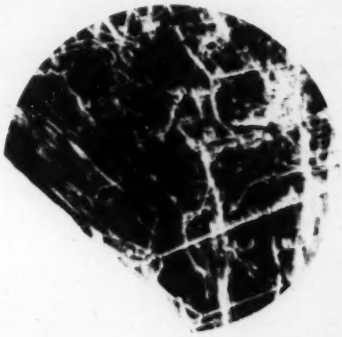

Fig. 19. Dislocations in aluminium. (111) reflexion, AgKα radiation, specimen thickness 0·1 mm, diameter of field 1 mm. This is a direct print from the X-ray photograph

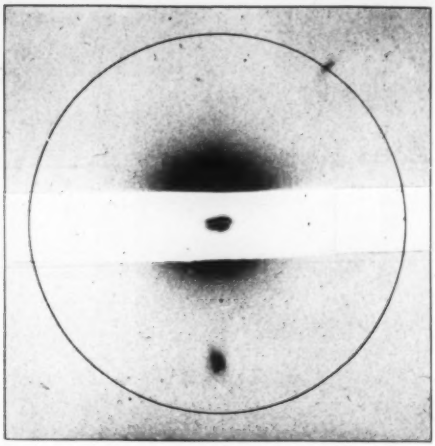

Fig. 21. Small angle scattering from polycrystalline copper foil irradiated with fast neutrons. The rectangular beam stop obscures angles less than 50′. The circle is drawn at a scattering angle of 5

Fig. 22. Low angle scattering streak from a single crystal of fatigued copper, showing structure

Refrigeration of a superconducting memory for a computer

By A. C. Rose-Innes, M.A., D.Phil., Services Electronics Research Laboratory, Baldock, Herts.

[*Paper first received* 13 *March, and in final form* 12 *May*, 1959]

An estimate is made of the refrigeration, in terms of consumption of liquid helium, required to maintain at low temperature a memory of superconducting cells. Using commercially available cable, the major source of heat is thermal conduction down the leads to the memory. If a cable of low thermal conductivity is used, a memory of one million cells should not consume more than about 2 l. of liquid helium per hour. In an appendix, the optimum size for copper electrical leads running directly from room temperature to liquid helium is calculated.

1. Introduction

In this article an estimate is made of the refrigeration required to maintain at low temperature a memory made up of superconducting storage cells.

At present, the type of cell which appears to be most advanced is that described by Crowe.* In this cell, binary digits are represented by the two opposite directions of circulation of persistent currents around holes in a thin superconducting film. The form that a memory might take is now considered. A random-access memory built in a matrix with coincident current selection, such as is common with ferrite cores, is considered, and it is supposed that only the memory itself is at low temperatures and that the switching and selection circuits are not refrigerated.

Let N be the total number of cells in the memory, and suppose that each cell stores one bit of information; let the number of binary digits in a word be n, and let v be the maximum frequency at which an individual cell can be switched. Such a memory will consist of n digit-planes each containing N/n cells, arranged as shown in Fig. 1. A "word" is selected by sending coincident pulses down the appropriate X- and Y-leads (for example, x_i, y_j), when the cells at location $x_i\ y_j$ in each digit-plane will be operated. Each digit-plane will also require a "read out" lead and an "inhibit" lead. It can be seen that the number of leads N_L to the memory will be:

$$N_L = 2\{2(N/n)^{1/2} + 2n\} \qquad (1)$$

where $2(N/n)^{1/2}$ is the number of X- and Y-leads coming to the first digit-plane, and $2n$ represents the n pairs of inhibit and read-out leads. The factor 2 outside the bracket occurs

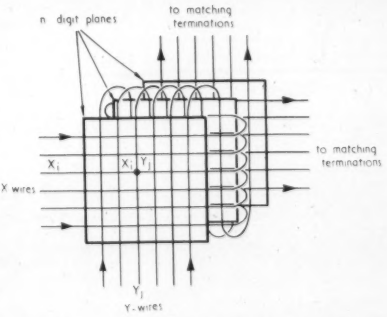

Form of a random-access memory. (The "readout" and "inhibit" leads to each digit-plane are not shown)

* Crowe, J. W. *I.B.M.J. of Research and Development*, **1**, p. 295 (1957).

because each lead, which will probably be a coaxial cable, may have to be terminated by its matching resistance, and it will be more favourable to have the power in these resistors dissipated outside the low-temperature enclosure. Hence the wires, after passing through the memory, will go out again, thus doubling the number of leads.

Typical values, which will be assumed throughout this article, are $N = 10^6$ bits, $n = 50$ bits. For these, equation (1) gives N_L to be 760. The digit-planes can probably be constructed so that there is $\frac{1}{8}$ in. between cells, giving 64 cells/in^2. If $\frac{1}{4}$ in. is allowed between digit-planes, which seems a reasonable figure, a density of 512 cells/in.^{3} is achieved. Hence a memory of 10^6 cells will occupy about one cubic foot. Presumably the memory will be contained in a metal Dewar vessel and will be cooled by liquid helium. The dimensions estimated in this paragraph are quite reasonable for such a system.

2. REFRIGERATION

The refrigeration must remove heat conducted down the leads to the memory and also heat generated by the operation of the cells. The principal sources of heat are:

(1) Thermal conduction down the leads to the memory;
(2) Joule heating by the electric currents flowing in these leads;
(3) Power dissipated by the operation of the cells;
(4) Inherent heat leaks in the Dewar vessel system.

With regard to (4), a typical metal helium storage Dewar vessel shielded by liquid nitrogen, only loses 10 ml. of liquid helium per hour by evaporation due to heat leaks and, as will be seen below, this is so much smaller than the losses due to the other three causes, that it can be ignored. We now consider these sources of heat separately.

2.1. *Heat conduction down the leads.* The memory will most likely be immersed in liquid helium, and it would be convenient to have the leads to it running directly down from room temperature. In order to maintain the shape of short switching pulses, some kind of transmission line may have to be used, and this should probably be in coaxial form in order to prevent interaction between the leads. In what follows, the leads will be considered to be coaxial, because this is the form which will conduct most heat, other kinds of lead being more favourable from the refrigeration aspect.

In a lead, nearly all the heat will be conducted down the metal conductor and heat conducted down the insulation can be neglected. If a is the cross-sectional area of the metal conductors in one lead, the liquid helium Q_c boiled off by thermal conduction down the N_L leads may be written:

$$Q_c = N_L K a \qquad (2)$$

where K is a constant which includes the average thermal conductivity of the metal. The value of K is more easily measured than calculated (see § 2.4).

2.2. *Joule heating by the switching pulses.* The switching pulses will give rise to Joule heating in the leads to the memory. The amplitude of these current pulses will be about the same as the critical current, i_c, of the cell. If R is the resistance of one lead, the maximum rate of Joule-heat production (that is, assuming continual switching) will be $2ni_c^2R$ watts. The factor 2 occurs because each current pulse goes in along one lead and out along another.

This heat will be distributed along the whole length of the lead. Now, a considerable part of each lead will not be immersed in the liquid helium and will heat the outflowing gas. If the gas coming out of the Dewar vessel is at room temperature (as it should be in an efficient system), the heat generated in the wire has been used to increase the enthalpy of the helium from the value of the liquid at 4·2° K to the value of the gas at room temperature. If the increase in enthalpy of unit volume of liquid helium when it is vaporized and raised to room temperature is ΔH, the liquid Q_J heated by the Joule heating in all the wires will be

$$Q = 2ni_c^2R/\Delta H = 0{\cdot}43R \text{ l./h.} \qquad (3)$$

This is the maximum possible consumption, as it assumes that the memory is switched at the maximum rate of a fifty-digit word every cycle. The actual consumption of liquid helium because of Joule heating will be much less than this.

2.3. *Heat generated by operation of the cells.* The energy stored in a cell is $\frac{1}{2}Li_c^2$, where L is the inductance of the cell, and, on switching from one state to another, about this amount of energy will be dissipated as heat. If there are n binary digits in a word, then, on an average, $\frac{1}{2}n$ cells will switch over at each operation of the memory and $\frac{1}{2}n \times \frac{1}{2}Li_c^2$ of heat will be generated. Let the maximum repetition rate of cell operation be ν, then the *maximum* power P generated will be given by:

$$P = \nu n L i_c^2/4 \qquad (4)$$

Typical values for cells constructed in this laboratory* are $\nu \simeq 10^7$ c/s, $L \simeq 4 \times 10^{-9}$ H, $i_c = \frac{1}{2}$A. If $n = 50$ bits, then $P \simeq 500$ J/h. The helium boiled off by this source of heat is a small fraction of the total, so that the assumption made above that the outcoming gas will be at room temperature is not materially affected. The additional amount of helium Q_{op} consumed by the operation of the cells is: $Q_{op} = P/\Delta H$ which becomes

$$Q_{op} = 2{\cdot}4 \times 10^{-3} \text{ l./h} \qquad (5)$$

2.4. *Total consumption of liquid helium.* The total consumption of liquid helium will be:

$$Q = Q_c + Q_J + Q_{op}$$

which, from equations (2), (3) and (5), becomes:

$$Q = N_L K a + 0{\cdot}43R + 2{\cdot}4 \times 10^{-3} \text{ l./h.}$$

Both the thermal conduction constant K and the resistance R depend on the particular kind of cable used for the leads. The smallest coxial cable which appears to be available commercially (Fortiphone sub-miniature twin-screened nylon cable) has the following characteristics. The outer braiding consists of forty-eight 45 s.w.g. copper wires, and has an outside diameter of about 1·2 mm; the centre conductor consists of two 43 s.w.g. copper wires twisted together. The total cross-sectional area of copper is about 2×10^{-3} cm^2. The insulation is nylon and the characteristic impedance was found to be 70 Ω. We have measured the rate at which liquid helium is boiled off by such a cable and find that a single cable 70 cm long running from room temperature to liquid helium boils off 0·01 litres an hour. The d.c. resistance of the cable under these conditions was 1 Ω. If this cable were to be used, the helium consumed by thermal conduction down the 760 leads would be much larger than that consumed by Joule heating and by operation of the cells, and would amount to 7·6 l/h. This is about the maximum output of a standard Arthur D. Little Collins' helium-liquifier, and for a practical system the helium consumption should be less than this. However, the properties of the

* RHODERICK, E. H. *Brit. J. Appl. Phys.*, **10**, p. 193 (1959).

cable could be much improved quite simply. In a coaxial cable most of the electrical resistance is due to the central conductor, whereas most of the heat conduction is along the outer sheath. If, therefore, the outer conductor were to be made of some suitable alloy, say nickel silver, instead of copper, its thermal conduction would be reduced by a factor of about 100 (table), and most of the heat conduction would be down the thin central copper conductor. The electrical resistance would only be increased by a factor of about 3. The rate of evaporation of liquid helium by heat conducted down one such cable would be about 8×10^{-4} l./h, so for 760 leads the consumption would be approximately 0·6 l./h. The resistance of each cable would be about 3 Ω. With these values, the total consumption of liquid helium would be:

$$Q < Q_c + Q_J + Q_{op} = 0{\cdot}6 + 1{\cdot}2 + 2{\cdot}4 \times 10^{-3} Q < 2 \text{ l./h}.$$

Some low temperature data

Density of liquid helium at 4·2 K: $\rho_l = 0{\cdot}13$ gm/ml.

Density of helium gas at N.T.P.: $\rho_g = 0{\cdot}18 \times 10^{-3}$ gm/ml.

Latent heat of vaporization of helium at 4·2 K: $\lambda = 2{\cdot}6 \times 10^3$ J/l.

Increase of enthalpy on converting 1 l. of liquid helium to gas at N.T.P.: $\Delta H = 2{\cdot}1 \times 10^5$ J/l of liquid.

Thermal conduction of copper. A wire 70 cm long running from room temperature into liquid helium boils off 5·2 l./h per cm² cross-section.

Thermal conduction of CuNi alloy (55/45 CuNi, "Ferry"). A wire as above boils off 3×10^{-2} l./h per cm².

This amount should be quite within the capability of a helium liquifier and suggests that, from a refrigeration aspect, a superconducting memory of this kind is a practical proposition. In any case, the consumption will be considerably less than this because Q_J, which is the biggest fraction, will be less in value, as the memory will not be operated on every possible cycle.

3. MISCELLANEOUS CONSIDERATIONS

Atmospheric pressure can vary over a range of about ±5 cm of mercury and this would produce a variation from about 4·1 to 4·3 K in the temperature of liquid helium. For cells made from lead films this variation should be insignificant. A difficulty could arise from bubbles forming on the surface of the digit-planes. The random movement of these bubbles across the cells can give rise to irregular operation. This has been observed in the case of single experimental cells. There are two ways to overcome this. Firstly, one could operate the memory above the surface of the liquid helium, cooling taking place through the gas, but the heat transfer from the memory into the gas would be rather poor and would probably result in slow temperature variations over the memory. Secondly, one could immerse the memory in helium II in which no bubbling takes place. This would mean lowering the temperature of the liquid helium to 2·2 K by reducing the pressure over the helium to about 40 mm of mercury. If the helium is evaporating at the rate of 2 litres of liquid per hour, the pump would have to have a speed of 23 l./min at a pressure of 40 mm of mercury, which is easily within the capacity of an ordinary laboratory rotary pump.

4. CONCLUSION

It seems that, from the refrigeration aspect, a superconducting random-access memory is a practical proposition. The hypothetical memory considered, with a capcity of a million binary digits, would not use more than two litres of liquid helium per hour, and its actual consumption would probably be considerably less. In this simple form, the leads run directly from room temperature. Refinements in design, such as running the leads from a liquid nitrogen bath, could reduce the helium consumption yet further, if necessary.

There are, of course, other arrangements of a random-access memory than the one considered here, and some of these may be more suitable for very high-speed operation; for instance, from "time-of-flight" considerations. Calculations similar to those in this article will apply to such systems.

APPENDIX

Optimum size for electrical leads running to liquid helium

Consider a wire of cross-section a cm². When a wire runs from room temperature to liquid helium, the amount of helium q_c evaporated per hour by thermal conduction (see § 2.1) is:

$$q_c = Ka \tag{6}$$

where K is a "conduction constant". If the wire carries a current i, the amount of helium q_J heated per hour by Joule heating (see § 2.2) is:

$$q_J = \frac{3600 i^2 R}{\Delta H}, \tag{7}$$

where R is the total resistance of wire. Now:

$$R = \frac{l}{\sigma a}, \tag{8}$$

where σ is the mean conductivity and l the length of the wire. Thus

$$q_J = \frac{l}{\sigma}\left(\frac{3600}{\Delta H}\right)\frac{i^2}{a}. \tag{9}$$

The total amount of helium q heated by a single wire is:

$$q = q_c + q_J = Ka + \frac{l}{\sigma}\left(\frac{3600}{\Delta H}\right)\frac{i^2}{a}. \tag{10}$$

For a minimum, $\partial q/\partial a$ is zero, so the optimum value a_{opt} for the area is:

$$a_{opt} = i\left\{\frac{1}{K}\left(\frac{3600}{\Delta H}\right)\frac{l}{\sigma}\right\}^{1/2}. \tag{11}$$

Experimentally (table), we have found that a copper conductor 70 cm long boils off 5·2 l. of liquid helium per hour per square-centimetre of cross-sectional area (with the condition of § 2.2. that the emerging gas is at room temperature); and that the electrical conductance is $2{\cdot}4 \times 10^4$ mho/cm². That is:

$$K = 5{\cdot}2 \text{ l./h} \quad \text{and} \quad \frac{l}{\sigma} = 4{\cdot}2 \times 10^{-5} \Omega \text{ cm}. \tag{12}$$

With these values, and a value of ΔH of $2{\cdot}1 \times 10^5$ J/l., the optimum value of cross-sectional area [equation (11)] is:

$$a_{opt} = 3{\cdot}7 \times 10^{-4} i \text{ cm}^2$$

ACKNOWLEDGEMENTS

I wish to thank Drs. O. Simpson and E. H. Rhoderick of this laboratory, and Dr. D. Wheeler of the Mathematical Laboratory, Cambridge, for their helpful advice and criticism. Acknowledgement is made to the Admiralty for permission to publish this paper.

Study of gas-lubricated, hydrodynamic, full journal bearings

By S. WHITLEY, M.A., D.Phil., and C. BETTS, B.Sc., United Kingdom Atomic Energy Authority (Industrial Group), Research and Development Branch, Capenhurst Works, Chester

[*Paper first received* 1 *December*, 1958, *and in final form* 10 *April*, 1959]

The two most important characteristics of gas-lubricated, full journal bearings are load-carrying capacity and half-speed whirl. In this paper these two characteristics have been investigated. The gases used as lubricants were mainly hydrogen, nitrogen and neon, giving a large viscosity variation; argon and carbon dioxide were also used to investigate the effect of the ratio of specific heats (γ). The bearings used were plain cylinders with a longitudinal groove cut into the upper surface of each bearing, extending over half the bearing length. It had been shown previously that this groove improved the half-speed whirl characteristics, and tests on bearings without the groove, included in the paper, demonstrate that the groove does not affect the load capacity.

The parameters investigated are bearing length, diameter, clearance, rotational velocity, ambient pressure, and the gas viscosity and ratio of specific heats. It is shown that, in general, the existing theories of load performance for compressible lubricants, operating in isothermal conditions, give a satisfactory correlation with the experimental results. The half-speed whirl results are not related to a complete analytical theory, but useful stability criteria are established.

LIST OF SYMBOLS

b = gland width (slave bearings) (cm)
c = radial clearance (cm)
d = shaft diameter (cm)
e = eccentricity (cm)
h = gap between shaft and bearing at any point around the periphery (cm)
I = transverse moment of inertia (g cm^2)
L = bearing separation (cm)
l = bearing length (cm)
N = rotational speed (rev/min)
N_w = threshold speed of half-speed whirl (rev/min)
n = eccentricity ratio ($=e/c$)
P = specific load (kg/cm^2)
p_1, p_2 = pressures at slave bearing annuli (dyn/cm^2)
p_0 = atmospheric pressure (dyn/cm^2)
p_a = ambient pressure (kg/cm^2)
p = gas film pressure at gap h (dyn/cm^2)
r = shaft radius (cm)
T = absolute temperature (° K)
T_0 = 273° K
U = surface velocity of journal (cm/s)
U_0 = surface velocity of bearing (cm/s)
V_1 = journal velocity perpendicular to line of centres
W = total static load on bearing (kg)
β = attitude angle (deg)
λ = dimensionless group $= 12\pi \dfrac{\eta N}{p_a}\left(\dfrac{r}{c}\right)^2$
η = lubricant viscosity (P)
θ = arbitrary angle defining h
ρ = gas density (g/cm^3)
ω = rotational frequency (rad/s)

INTRODUCTION

The idea of using a gas as a lubricant for hydrodynamic bearings is now well established. Kingsbury[1] was the first to conduct experiments in gas lubrication; his experimental results were explained theoretically by Harrison[2] in 1913. More recently Katto and Soda[3] derived an approximate theory of gas lubrication, based on Harrison's work, which gave an analytical expression for the load-carrying capacity of full journal bearings. This theory is based on isothermal conditions in the gas film, and infinitely long bearings (i.e. end leakage is neglected). Ford, Harris and Pantall[4] compared their results on the load-carrying capacity of plain journal bearings with this theory. They found that, under certain conditions, load-carrying capacities in excess of the predictions from the theory by Katto and Soda were obtained. To determine whether this effect was caused by adiabatic conditions in the gas film, Ford, Harris and Pantall used gases with values of the ratio of specific heats (γ) ranging from 1·11 to 1·67. They showed that γ had no effect on load capacity, and in fact the maximum spread of results obtained was 15%, whereas for adiabatic conditions a spread of 40% would have been observed. They therefore concluded that conditions were isothermal, and the discrepancy remained unexplained.

Despite this, the results of Ford and his co-workers can be fitted to a theoretical curve based on the finite bearing theory of Ausman,[5] if it is assumed that the gas obeys the law $pV^{1.4}$ = constant. Because of this, Ausman, by considering only the cases of hydrogen, helium and air (γ ranging from 1·4 to 1·6) concludes that conditions must be adiabatic. However, if the result for dimethyl ether ($\gamma = 1{\cdot}11$) is taken into account, this conclusion is clearly invalidated.

The second important characteristic of full journal bearings is half-speed whirl, briefly mentioned by Ford and others.[4] This phenomenon consists of a precession of the bearing axis about the shaft axis at half the shaft rotational speed. This unstable condition, at which the ability of the gas film to support the load disappears, occurs when certain threshold conditions of the bearing parameters are exceeded. When this happens, there is a sharp transition from stable to unstable conditions, and half-speed whirling begins. The amplitude of the whirl increases rapidly until rubbing contact occurs between bearing and shaft surfaces. In the experimental investigations it is convenient to quote the threshold speed at which the whirl commences for constant values of other parameters.

Earlier work at these laboratories showed that this threshold speed for plain journal bearings depends not only on the usual bearing parameters, but also on the angular position of the bearing relative to the direction of the load. It was thought that, although the bearings were straight and round to an accuracy of 5% of the clearance, the variation in whirl speed was caused by some geometrical inaccuracy which could not be detected but which destroyed the axial symmetry of the bearing. This interpretation was verified by showing that a bearing containing an axial slot (see Fig. 1) gave a similar but magnified effect.

On rotating the bearing relative to the load line, the whirl

threshold speed gave a cyclic variation with orientation, with the maximum when the slot was at the top of the bearing, i.e. opposing the load, and the minimum when the slot was at the bottom. Not only does the axial slot increase the whirl speed when placed at the top of the bearing, but it also enables reproducible results to be obtained.

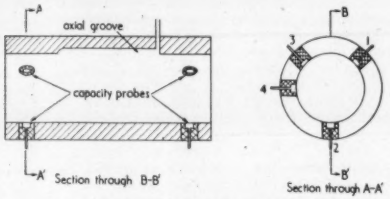

Fig. 1. Test bearing

The present paper gives the results of a systematic investigation of both the load-carrying capacity and the half-speed whirl characteristics of the full journal bearing. For the reasons stated above, most of the bearings used had an axial slot of half the length of the bearing cut into the bearing surface.

In order to show that this slot had no effect on load capacity, some tests were done on plain bearings. This was particularly important since the tests on the slotted bearings showed isothermal conditions, and did not exhibit the anomalous behaviour of the results given by Ford and others.[4] In fact, the plain bearings tested have behaved identically with the slotted bearings.

EXPERIMENTAL APPARATUS

Three test rigs were used for the experiments, one each for investigating 5·08, 10·16 and 17·78 cm diameter bearings. The 5·08 and 17·78 cm rigs were similar, but the 5·08 cm rig was more complicated to enable various test gases to be used.

5·08 *cm diameter test rig*. Fig. 2 is a schematic diagram of the test rig. One major requirement was that the test

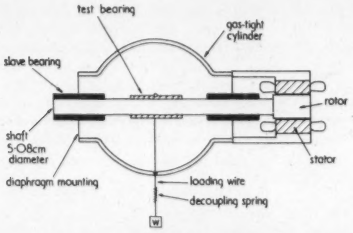

Fig. 2. 5·08 cm diameter test rig

bearings should be contained within a gas-tight box, so that test gases giving a wide range of viscosity could be used. The gases chosen were hydrogen, nitrogen and neon, which have viscosities of 88, 173 and 311 μP, respectively. Most other gases lie within this range. For the tests on the plain bearings, carbon dioxide ($\gamma = 1{\cdot}30$) and argon ($\gamma = 1{\cdot}67$) were used in order to give as wide a range of γ as possible without a large change in viscosity; this was to test whether conditions were adiabatic or isothermal.

The shaft was supported by two gas-lubricated "slave" bearings and driven by a squirrel-cage induction motor. The rotor was mounted directly on the shaft and situated outside the slave bearings so that the motor was not immersed in the test gas. The speed could be varied between 3000 and 20 000 rev/min by means of a variable-frequency supply.

The test bearings were mounted in the centre of the shaft and loaded by standard weights suspended on a wire which included a decoupling spring. Measurements of vibration and clearance between the test bearing and the rotating shaft were made using capacity probes set in the bearing wall.

The gas-lubricated slave bearings, as well as supporting the shaft, were used as seals to prevent the test gas from leaking out of, and air from leaking into, the test chamber. For their support duty, they each had to carry approximately half the load of the test bearing without half-speed whirling during the test. To ensure this a low clearance is required, and was chosen at 12·5 μ diametral; this is also suitable for efficient sealing characteristics.

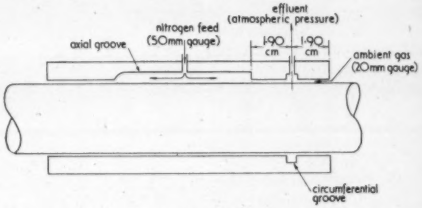

Fig. 3. Slave bearing

Fig. 3 is a diagram of the slave bearings. In addition to the axial groove common to the test bearings, there is a circumferential groove between the axial slot and the test chamber. During operation, this circumferential groove is connected *via* an effluent line to atmosphere while the axial slot is maintained at 50 mm of mercury gauge using nitrogen, and the test chamber is maintained at 20 mm of mercury gauge. Thus nitrogen flows inwards from the axial slot and test gas flows outwards from the test chamber, and both are discharged to atmosphere *via* the circumferential groove. The gas flows in the seal can be calculated approximately by assuming that the shaft is concentric in the slave bearings; the flow is then given by:

$$Q = \frac{\pi(p_1^2 - p_2^2)T_0 c^3 r}{12\eta P_0 T b} \text{ (cm}^3\text{/s) at N.T.P.}$$

For the dimensions of seal used, the flow of nitrogen from the axial slot is 4 cm^3/min at N.T.P. and the out-leakage of test gas is 0·9, 1·6 or 3·1 cm^3/min at N.T.P., depending on whether the test gas is neon, nitrogen or hydrogen.

10·16 *cm and* 17·78 *cm diameter test rigs*. The two rigs designed for investigating 10·16 and 17·78 cm diameter gas bearings are similar except for size. They were designed to operate in air only and to accommodate bearings with a length/diameter ratio of up to three in the case of the smaller rig and up to two in the larger rig. A diagram and photograph of the larger rig are given in Figs. 4 and 5 respectively.

In principle the rigs are the same as the 5·08 cm one; to avoid using a long heavy shaft, however, the shaft has been made hollow and the slave bearings have been positioned inside it. To give more load-carrying capacity they were of

the hydrostatic type. The shaft was again driven by a squirrel-cage induction motor with the rotor mounted on the end of the shaft. Because of the higher static loads required for these bigger bearings, the static loading system employed a 5 : 1 lever device in the 17·78 cm rig, while a pulley system was used in the 10·16 cm rig.

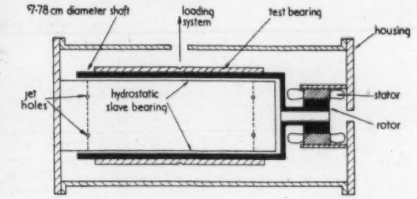

Fig. 4. Schematic diagram of 17·78 cm diameter test rig

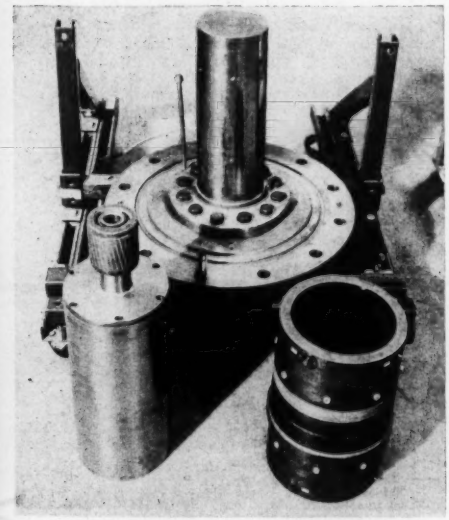

Fig. 5. Components of 17·78 cm diameter test rig

The internal hydrostatic bearings consisted of a hollow cylinder slightly longer than the rotating shaft which is supported on it. At both ends of the cylinder, in the position shown in Figs. 4 and 5, was a ring of eight holes around the circumference. The holes were designed for sonic flow conditions and were connected to a high-pressure (6 kg/cm^2 abs) compressed-air supply. The load capacity of this hydrostatic slave bearing was much higher than that of the hydrodynamic bearing being tested.

Test bearings. The test bearings were geometrically similar. The 5·08 cm diameter bearings were of length/diameter ratios of 1, 1·5, 2, 3 and 4·5 respectively (Fig. 1), the grooved ones having an axial slot (0·15 cm wide and deep) of half the length of the bearing. They were made of either phosphor-bronze or Stellite grade 4 (by Deloro Stellite, Ltd.) and finished honed to an accuracy, both round and straight, of 3 μ. A special bearing 10·16 cm long was made, of mass 2·84 kg but of variable transverse inertia.

The 10·16 and 17·78 cm diameter bearing were made of Meehanite (by International Meehanite Metal Co., Ltd.) and had length/diameter ratios of 2 and outside diameters of 1·21 times the inside diameter.

All bearings were fitted with either one or four capacity probes (nos. 1–4 in Fig. 1) at each end, depending on whether only vibrations or vibrations and load-carrying capacity were being investigated.

EXPERIMENTAL TECHNIQUE AND RESULTS

The physical measurements made in each test were shaft rotational speed, load on test bearing, relative position of shaft and bearing and detection of any vibrations of the bearing. The speed was measured with a stroboscope and standard weights were used for loading. The last two of the measurements were made using the capacity probes fitted to the bearings, in the following manner.

Before each test, a surface profile chart of each probe showing its position relative to the bearing surface was obtained using a Talysurf instrument. In general the probes were slightly recessed, but by less than 3 μ. In addition, the stray capacity of the probes and connecting coaxial cable was measured—this was usually a few picofarads.

During test, the capacity of each probe relative to the shaft was measured and the gap at that point calculated from the formula for a parallel-plate capacity (the diameter/gap ratio of the probe is approximately 500 and so end effects are negligible). Making allowance for the recessed position of the probes, it is possible to calculate the exact relative position of shaft centre and bearing centre. The average value of the gaps also gives the radial clearance of the bearing. This is particularly important in the 17·78 cm bearings, where there is a considerable amount of centrifugal expansion of the shaft, causing a decrease in clearance with speed. In all cases, however, the gaps measured by the capacity probes agree with the measurements taken during manufacture using Solex equipment, provided that allowance is made for temperature and centrifugal expansions. The results of this work on load-carrying capacity are summarized in Tables 1 and 2.

The capacity probes were also used to detect and measure vibrations. For this, they were made part of the capacity of the tank circuit of an oscillator, so that any vibrations would modulate the frequency of the oscillator. After using a discriminator to convert this to an amplitude-modulated signal, the output was fed to an oscilloscope. From the oscilloscope reading both the amplitude and frequency of any vibration can be measured, and in particular, the onset of half-speed whirl detected. The general method adopted to measure the threshold of whirl was to set the various parameters at their desired value, and then to increase the shaft speed slowly until half-speed whirl started. The half-speed whirl measured in these tests was always conical, as shown by the phase of vibration at the various probes.

The results on half-speed whirl are given in Figs. 6, 7 and 8 and in Table 3. The result for the 5·08 cm diameter bearings in Table 3 were actually measured on bearings of larger inertia, and corrected for, as explained later.

All of these whirl results were taken at an ambient pressure of one atmosphere. The effect of ambient pressure was measured on a bearing of diameter 5·08 cm, length 10·16 cm

Table 1. *Results on load-capacity for grooved bearings*

Speed (rev/min) × 10^3	Lubricant	Radial clearance (μ)	Length to diameter ratio	Ambient pressure (kg/cm²)	λ	n =	0·1	0·2	0·3	0·4	0·5	0·6	0·7	0·8
						Measured load W (kg)								
3	Nitrogen	40·7	3	1·033	0·124		—	—	—	—	—	5	7·25	11·3
						Attitude angle β (deg)	—	—	—	—	—	76	70	61
6	Nitrogen	40·7	3	1·033	0·248	W	—	—	—	5	7·7	10·9	14·1	18·6
						β	—	—	—	70	70	70	66	60
6	Nitrogen	30·5	3	1·033	0·44	W	—	4·1	6·8	10	14·1	19·5	—	—
						β	—	75	75	75	70	58	—	—
3	Nitrogen	21·0	3	1·033	0·466	W	2·04	4·54	7·25	10·4	14·0	18·6	24·5	31·8
						β	70	72	72	70	66	62	56	50
9	Nitrogen	40·7	3	1·033	0·372	W	—	—	—	6·8	10·4	14·7	20·2	28·1
						β	—	—	—	70	68	65	61	54
6	Nitrogen	21·0	3	1·033	0·935	W	2·7	7·7	13·6	20·4	29·5	39·0	—	—
						β	65	65	62	59	54	48	—	—
9	Nitrogen	21·0	3	1·033	1·40	W	5·44	12·7	21·3	30·5	41·7	—	—	—
						β	60	60	56	52	46	—	—	—
6	Nitrogen	21·0	3	0·544	1·79	W	—	6·8	10·9	16·3	22·2	28·6	—	—
						β	—	29	31	32	32	30	—	—
6	Nitrogen	13·3	3	1·033	2·30	W	6·8	15	23·1	31·8	41·8	—	—	—
						β	60	52	50	46	43	—	—	—
6	Nitrogen	21·0	3	0·340	2·86	W	1·82	4·54	8·61	13·2	18·2	23·6	—	—
						β	16	16	21	22	23	21	—	—
6	Nitrogen	21·0	3	0·204	4·75	W	—	3·18	5·44	8·62	12·3	16·8	—	—
						β	—	10	10	12	13	12	—	—
6	Hydrogen	40·7	3	1·033	0·127	W	—	—	—	—	—	10·9	15	23·6
						β	—	—	—	—	—	81	78	70
9	Hydrogen	40·7	3	1·033	0·192	W	—	—	—	—	7·25	9·5	12·7	18·1
						β	—	—	—	—	83	81	76	66
3	Hydrogen	21·0	3	1·033	0·240	W	—	2·27	3·63	5·45	7·03	9·07	11·32	14·5
						β	—	82	81	78	74	70	65	58
6	Hydrogen	21·0	3	1·033	0·479	W	1·81	4·08	6·8	10·0	13·6	19·0	25·0	—
						β	71	72	72	72	68	60	54	—
9	Hydrogen	21·0	3	1·033	0·720	W	3·18	6·8	11·3	15·9	21·3	27·2	34·4	—
						β	60	60	60	58	55	50	45	—
6	Hydrogen	13·3	3	1·033	1·18	W	4·08	8·60	13·6	19·5	26·3	33·6	—	—
						β	70	70	66	60	56	52	—	—
3	Neon	40·7	3	1·033	0·222	W	—	2·72	4·99	7·03	9·98	13·1	17·2	23·6
						β	—	78	76	74	73	70	65	56
6	Neon	40·7	3	1·033	0·444	W	—	4·08	6·8	11·1	15·4	20·9	27·7	38·6
						β	—	70	70	70	68	62	54	46
9	Neon	40·7	3	1·033	0·666	W	—	—	9·06	15·0	21·3	30	40·4	—
						β	—	—	66	65	64	60	55	—
3	Neon	21·0	3	1·033	0·840	W	5·44	9·98	14·50	19·9	26·8	34·0	—	—
						β	72	72	66	60	54	48	—	—
6	Neon	21·0	3	1·033	1·67	W	7·25	15·4	24·0	35·4	—	—	—	—
						β	62	62	60	54	—	—	—	—
9	Neon	21·0	3	1·033	2·52	W	10·4	20·9	33·6	47·0	—	—	—	—
						β	50	46	40	36	—	—	—	—
6	Neon	13·3	3	1·033	4·12	W	8·6	17·2	27·2	40·0	—	—	—	—
						β	50	50	40	35	—	—	—	—
6	Hydrogen	17·8	2	1·033	0·664	W	—	—	5·45	8·17	11·3	15·0	21·8	—
						β	—	—	52	50	47	43	35	—
6	Nitrogen	17·8	2	1·033	1·29	W	—	5·45	9·06	14·1	19·1	26·3	36·3	—
						β	—	42	42	42	39	35	28	—
6	Neon	17·8	2	1·033	2·32	W	—	8·16	15·4	23·1	32·2	40·7	—	—
						β	—	30	30	30	28	24	—	—
6	Hydrogen	16·5	1	1·033	0·774	W	—	—	—	—	—	2·72	4·07	—
						β	—	—	—	—	—	65	56	—
6	Nitrogen	16·5	1	1·033	1·56	W	—	—	—	2·27	3·40	5·0	7·71	—
						β	—	—	—	70	60	52	44	—
6	Neon	16·5	1	1·033	2·76	W	—	—	3·18	4·54	5·9	8·16	12·7	—
						β	—	—	66	60	54	46	38	—
3	Air	20·3	4·5	1·033	0·5	W	—	6·8	12·3	17·7	23·1	29·5	—	—
						β	—	35	47	50	50	48	—	—
6	Air	20·3	4·5	1·033	1·0	W	—	12·3	22·7	32·6	42·6	—	—	—
						β	—	30	38	42	39	35	—	—
9	Air	20·3	4·5	1·033	1·5	W	—	17·7	30·8	43·5	—	—	—	—
						β	—	30	34	35	—	—	—	—

Table 2. *Results on load-capacity for plain bearings*

Speed (rev/min) × 10^3	*Lubricant*	*Radial clearance* (μ)	*Length-to-diameter ratio*	*Ambient pressure* (kg/cm^3)	λ	n =	0·1	0·2	0·3	0·4	0·5
3	Carbon dioxide	12·70	3	1·033	1·06	W	6·35	13·2	19·5	25·9	33·6
						β	54	54	53	52	52
6	Carbon dioxide	12·70	3	1·033	2·12	W	9·0	18·1	27·2	37·7	—
						β	36	36	36	36	—
9	Carbon dioxide	12·70	3	1·033	3·18	W	10·4	20·4	30·4	42·6	—
						β	27	27	27	27	—
6	Carbon dioxide	12·70	3	0·516	4·24	W	4·1	9·1	15·0	21·3	—
						β	22	23	23	23	—
7·6	Carbon dioxide	12·70	3	0·516	5·36	W	4·1	9·1	15·0	21·3	—
						β	18	19	19	19	—
3	Argon	12·70	3	1·033	1·63	W	7·26	15·0	23·6	33·6	44·5
						β	38	41	41	41	39
6	Argon	12·70	3	1·033	3·26	W	9·1	19·5	30·9	44·0	—
						β	28	28	28	28	—
9	Argon	12·70	3	1·033	4·89	W	9·1	20·4	33·0	48	—
						β	22	22	22	22	—
6	Argon	12·70	3	0·516	6·52	W	4·54	10	15·9	23·6	—
						β	19	19	19	18	—
8·6	Argon	12·70	3	0·516	9·31	W	4·54	10·4	17·3	25·0	—
						β	17	17	17	17	—

and clearance 20 μ at a specific load of 0·08 kg/cm^2. At pressures above about 3 kg/cm^2 the whirl threshold speed was constant at about 11 000 rev/min, increasing as the pressure was reduced to 11 500 rev/min at 2 kg/cm^2, 12 000 rev/min at 1 kg/cm^2, 12 700 rev/min at 0·5 kg/cm^2 and 13 700 rev/min at 0·25 kg/cm^2.

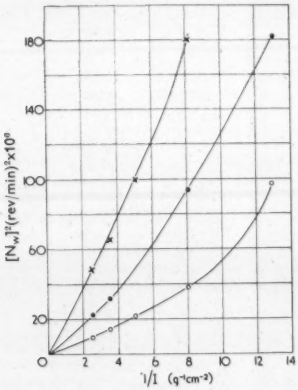

Fig. 6. Effect of transverse inertia on whirl; 5·08 cm diameter bearings

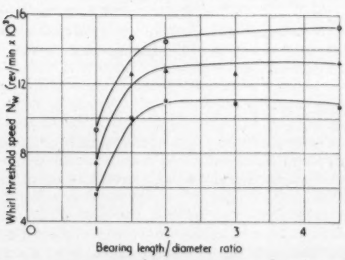

Fig. 7. Effect of length and load on whirl; 5·08 cm diameter bearings

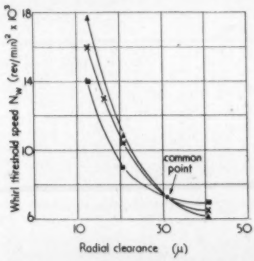

Fig. 8. Effect of clearance and viscosity on whirl; 5·08 cm diameter bearings

Table 3. *Whirl threshold speeds for varying diameter*

Diameter (cm)	*Clearance* (μ)	*Transverse moment of inertia* (kg cm^2)	*Specific load* (kg/cm^2)	*Whirl speed* (rev/min)
5·08	18	10·6	0·07	~24 000
5·08	18	10·6	0·14	~30 000
10·16	41	316	0·07	6 000
10·16	41	316	0·14	9 000
17·78	71	4890	0·07	4 500
17·78	71	4890	0·14	7 000

THEORY OF LOAD-CARRYING CAPACITY

The differential equation which determines the pressure distribution around a journal bearing of infinite length is, from the Appendix:

$$\frac{1}{\lambda p_a}\frac{\partial p}{\partial \theta} = \frac{1}{(1 + n\cos\theta)^2} + \frac{k}{\rho c(1 + n\cos\theta)^3} \qquad (1)$$

By solving this differential equation for pressure and then integrating around the bearing surface, one obtains the value for the lubricant film force and the direction in which it acts relative to the line of centres of bearing and shaft. An exact

analytical solution of this equation has been obtained by Sommerfeld for the case of an incompressible lubricant, i.e. one in which the density is independent of pressure. The final solution of Sommerfeld (quoted, e.g. by Shaw and Macks[6]) is:

$$\frac{P}{p_a} = \frac{\lambda\pi n}{(2+n^2)\sqrt{(1-n^2)}} = \frac{\lambda\pi n}{2}(1 + \tfrac{1}{8}n^4 + \tfrac{1}{4}n^6 \ldots) \quad (2)$$

$$\beta = 90° \text{ (constant independent of } \lambda \text{ and } n) \quad (3)$$

The solution of equation (1), however, is more difficult for the case of gaseous lubrication, since the density depends on the pressure and ρ must be replaced by $p^{1/K}$; here K lies between 1 and γ, depending on how closely conditions in the gas film approach to isothermal or adiabatic. An exact analytical solution of the equation has not been obtained, but approximate solutions by different methods have been obtained by Katto and Soda[3] and Ausman.[7]

The solution of Katto and Soda has been derived for isothermal conditions only, and is most accurate for large values of λ. The specific load and attitude angle are given by the two implicit equations:

$$\frac{P}{p_a} = \frac{\pi\sqrt{(1-n^2)}\{1-\sqrt{(1-n^2)}\}\sec\beta}{n(1-n^2+\tan^2\beta)} \rightarrow$$

$$\rightarrow \frac{\pi\{1-\sqrt{(1-n^2)}\}}{n\sqrt{(1-n^2)}} \text{ as } \lambda \rightarrow \infty \quad (4)$$

$$\tan\beta = \frac{(1-n^2)^{3/2}}{\lambda(1-n^2\cos\beta)} \rightarrow 0 \text{ as } \lambda \rightarrow \infty \quad (5)$$

The solution of Ausman is not restricted to isothermal conditions, and is:

$$\frac{P}{p_a} = \frac{\pi n\lambda}{2\sqrt{(1+\lambda^2/K^2)}} \rightarrow \frac{\pi nK}{2} \text{ as } \lambda \rightarrow \infty \quad (6)$$

$$\tan\beta = K/\lambda \rightarrow 0 \text{ as } \lambda \rightarrow \infty \quad (7)$$

In this solution, $K = 1$ for isothermal conditions and $K = \gamma$ for adiabatic conditions.

Since this solution is based on a series expansion of n, it is only valid in the small range of eccentricity when the load capacity is linear with eccentricity and the attitude angle independent of it. The next approximation in the series solution has been obtained by the present authors for isothermal conditions only, and can be written:

$$\frac{P}{p_a} = \frac{\pi n\lambda}{2(1+\lambda^2)}\{(1+n^2f_2)^2 + (1+n^2f_1)^2\lambda^2\}^{1/2} \rightarrow$$

$$\rightarrow \frac{\pi n}{2}(1+\tfrac{3}{4}n^2) \text{ as } \lambda \rightarrow \infty \quad (8)$$

where

$$f_1 = 0{\cdot}75 - \frac{\lambda^4 + 25\lambda^2 - 6}{4(1+\lambda^2)^2(4+\lambda^2)}$$

$$f_2 = \frac{\lambda^2(\lambda^4 + 10\lambda^2 - 24)}{4(1+\lambda^2)^2(4+\lambda^2)}$$

$$\tan\beta = \frac{(1+n^2f_2)}{\lambda(1+n^2f_1)} \rightarrow 0 \text{ as } \lambda \rightarrow \infty \quad (9)$$

The solutions for load capacity given by equations (4), (6) and (8) are plotted in Figs. 9 and 10 for typical values of eccentricity, namely 0·2, 0·4 and 0·6. As shown, at large values of λ, P/p_a approaches a constant asymptotic value. This value can be derived very simply and exactly by setting $\lambda = \infty$ in equation (1). This gives, expressing the solution as a series expansion:

$$\frac{P}{p_a} = \frac{\pi nK}{2}\left\{1 + (K+1)(K+2)\frac{n^2}{8} + \right.$$

$$\left. + (K+1)(K+2)(K+3)(K+4)\frac{n^4}{192}\ldots\right\} \quad (10)$$

$$\tan\beta = 0 \quad (11)$$

These accurate values of the asymptote have been marked on Figs. 9 and 10.

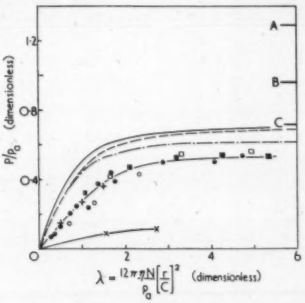

Fig. 9. Theoretical predictions for load-capacity, $n = 0{\cdot}4$

– = Katto and Soda solution
– – – = series expansion solution
– · – = Ausman solution (infinite length)
Experimental points at $n = 0{\cdot}4$, 5·08 cm diameter
○ = $l/d = 2$ slotted bearings
● = $l/d = 3$ slotted bearings
+ = $l/d = 4{\cdot}5$ slotted bearings
■ = $l/d = 3$ plain bearings in carbon dioxide
□ = $l/d = 3$ plain bearings in argon
× = $l/d = 1$ slotted bearing
A = asymptote for adiabatic conditions, $\gamma = 1{\cdot}66$ (argon)
B = asymptote for adiabatic conditions, $\gamma = 1{\cdot}30$ (carbon dioxide)
C = asymptote for isothermal conditions (independent of gas)

All of the expressions for load capacity given above {equations (2), (4), (6), (8) and (10)} refer to the case of infinitely long bearings. Ausman[5] has determined the effects of end leakage at small eccentricities, and expressed his results as end correction factors, which depend on the length/diameter ratio of the bearing and the value of the parameter λ. For example, at $\lambda = 2$, bearings of length/diameter ratios 4·5, 3, 2 and 1 should develop only 0·88, 0·85, 0·74 and 0·36 of the specific load capacity of an infinitely long bearing.

DISCUSSION OF RESULTS ON LOAD CAPACITY

Load-eccentricity ratio. The predictions of the theories summarized above are compared with each other and with experiment in Figs. 9 and 10, for eccentricity ratios of 0·2, 0·4 and 0·6.

At an eccentricity ratio of 0·4, the best solution is the series solution given by equation (8), the solution given by Katto and Soda tending to be too high at low values of λ and the solution of Ausman for isothermal conditions being too low at high values of λ. The correlation with experiment

is satisfactory, and there is no difference in the performance of bearings with and without the axial slot. There is also little fall in performance with bearing length down to $l/d = 2$, but a severe drop in performance occurs for $l/d = 1$. This is in reasonable agreement with the theory of Ausman for finite bearings, except that the shortest bearing is even poorer than predicted.

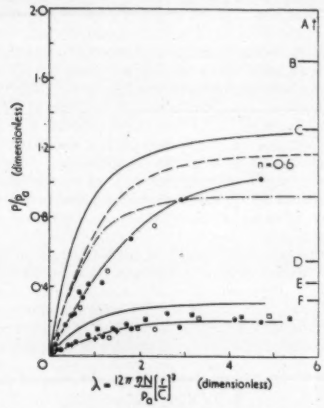

Fig. 10. Theoretical predictions for load-capacity, $n = 0{\cdot}2$ and $0{\cdot}6$

– = Katto and Soda solution
– – – = series solution
—·— = Ausman solution (infinite length)
Experimental points 5·08 cm diameter
● = $l/d = 3$ slotted bearings
○ = $l/d = 2$ slotted bearings
\+ = $l/d = 4{\cdot}5$ slotted bearings
■ = $l/d = 3$ plain bearings in carbon dioxide
□ = $l/d = 3$ plain bearings in argon

A = adiabatic asymptote for $\gamma = 1{\cdot}66$ at $\frac{P}{p_a} = 2{\cdot}52$
B = adiabatic asymptote $\gamma = 1{\cdot}30$
C = isothermal asymptote
D = adiabatic asymptote, $\gamma = 1{\cdot}66$
E = adiabatic asymptote, $\gamma = 1{\cdot}30$
F = isothermal asymptote

A most important result shown in Fig. 9 is that there is no change in load capacity, at large values of λ, between gases of varying values of γ. In particular, for the plain bearings, varying values of γ between 1·3 (carbon dioxide) and 1·67 (argon) had no effect on the load capacity within the experimental scatter of about 6%. If conditions were adiabatic, there would be a change of 33%, as shown by the asymptotes marked on Fig. 9. The results therefore indicate that conditions are isothermal. The final discrepancy of about 24% between the theoretical curve for infinitely long bearings and experiment for the longer bearings ($l/d = 2$, 3, 4·5) can be partly explained—about 12%—by the end leakage factors of Ausman, but the remaining difference is unexplained.

It is interesting to compare the present results with those published by Ford, Harris and Pentall.[4] These authors used gases having γ varying between 1·11 (dimethyl ether) and 1·67 (helium) and, in agreement with the present results, found no variation with γ, thus indicating isothermal conditions. There is, however, a significant difference between the results presented here and those presented by Ford and others. The present results nowhere exceed, or even equal, the predictions of the isothermal infinite-length theory, while those of Ford and others exceed the theory considerably at large λ; for example, at $n = 0{\cdot}4$ the results are as much as 50% higher than the ones given here.

It is worthwhile, therefore, to compare the present experimental techniques with those of Ford and others to see whether any reason exists for the differences observed. The present techniques use several large probes (0·64 cm diameter) simultaneously, and absolute capacity measurements are used. These give values of eccentricity ratio, attitude angle and clearance; the clearance obtained with the capacity bridge technique is directly checked for consistency with Solex air-gauge measurements. The capacity bridge was used without trouble because the vibrations between shaft and bearing were negligible, as shown by the vibration detection apparatus.

Ford, Harris and Pantall, who used one probe only (diameter 0·32 cm), were unable to use capacity bridge techniques because of excessive vibrations. Not only do these vibrations cause errors, but they also affect the load capacity {compare equation (17) of the Appendix}. This could well be the reason for their anomalous results. This argument is supported by the fact that the differences increase as n increases, i.e. as the vibrations become a large fraction of the minimum clearance.

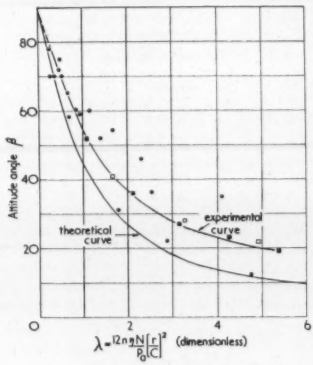

Fig. 11. Comparison of theoretical and practical attitude angles at $n = 0{\cdot}4$

● = $l/d = 3$ slotted bearings
■ = $l/d = 3$ plain bearings in carbon dioxide
□ = $l/d = 3$ plain bearings in argon

Attitude angle. As well as eccentricity ratio, the theories give predictions of the attitude angle. The comparison between theory and practice is shown in Fig. 11. Here a typical selection of results for $n = 0{\cdot}4$ is plotted, for comparison with the compressible-lubricant theoretical curve. Although there is a considerable scatter of results, the general agreement with theory is reasonable. The scatter arises because a small displacement in the apparent centre of the bearing can cause a large variation in measured angle. This is shown by the fact that, for any one bearing (e.g. the plain bearing), the results for varying speed and lubricant viscosity lie on the same curve.

THEORY OF HALF-SPEED WHIRL

The generalized form of Reynolds' equation, given in the Appendix, shows that a full journal bearing cannot sustain a load if the shaft and bearing are whirling relatively to each other at half the speed of rotation. This can be seen by setting $\partial\phi/\partial t = \omega/2$ and $\partial n/\partial t = 0$ in equation (17), giving, for isothermal conditions:

$$\frac{1}{\lambda p_a}\frac{\partial}{\partial\theta}\left\{p(1 + n\cos\theta)^3\frac{\partial p}{\partial\theta}\right\} = (1 + n\cos\theta)\frac{\partial p}{\partial\theta} \qquad (12)$$

For small or large values of λ, $\partial p/\partial\theta \to 0$, so that there can be no pressure rise in the bearing to sustain equilibrium. The experimental facts, however, are that up to a certain threshold speed a half-speed whirl is stable, while above the threshold the whirl is unstable. This means that an extra radial force, designated F_r, must exist in the gas film, even during half-speed whirling conditions, to provide the centrifugal acceleration towards the centre of the whirl. Below threshold conditions this force is greater than required, and above threshold smaller than required.

Various modes of half-speed whirl must be distinguished: either the bearing can vibrate relative to the shaft, or the shaft can vibrate within the bearings. For symmetrical systems, the centre of these whirls can be at the centre of gravity (conical whirl) or at infinity (cylindrical whirl).

For the simplest whirl, bearing cylindrical whirl, the bearing axis remains parallel to the shaft axis and the condition of stability is therefore:

$$F_r \geqslant mr(\omega/2)^2$$

or

$$\partial F_r/\partial r \geqslant m\omega^2/4 \qquad (13)$$

This condition of stability agrees with that determined by Poritsky[8] and by Boeker and Sternlicht,[9] who considered the general equation of motion of the system and showed that the motion was unstable when condition (13) obtained.

For conical vibrations of the bearing the condition is

$$\frac{l^2}{12}\cdot\frac{\partial F_r}{\partial_r} \geqslant \frac{I\omega^2}{4} \qquad (14)$$

where $\frac{1}{12}(l^2\partial F_r/\partial r)$ is the radial component of the tilt stiffness (restoring couple per unit angular displacement) of the bearing. This tilt stiffness is derived by integration, assuming that each elemental length of bearing contributes equally to the linear stiffness $\partial F_r/\partial r$, i.e. end effects are neglected.

For cylindrical vibrations of the shaft the condition is:

$$\frac{2\partial F_r}{\partial r} \geqslant \frac{M\omega^2}{4} \qquad (15)$$

and for angular motions:

$$\frac{L^2}{2}\frac{\partial F_r}{\partial r} \geqslant (I_T - I_p)\frac{\omega^2}{4} \qquad (16)$$

where $\frac{1}{2}L^2\partial F_r/\partial r$ is the tilt stiffness of two bearings and the polar inertia is introduced to allow for gyroscopic effects.

At present, because theoretical knowledge of the force F_r and its dependence on the bearing parameters is limited, these equations do not give explicit values of the whirl threshold speeds, but they do give the relationship between them and show the general laws of variation of threshold speed with bearing parameters.

DISCUSSION OF HALF-SPEED WHIRL

The criterion for bearing conical whirl, the mode of whirl measured in the present work, shows that, neglecting end effects, the whirl threshold speed is independent of bearing length (since F_r is proportional to l, and I is proportional to l^3). This is confirmed by the results plotted in Fig. 7; the drop in whirl threshold speed at low bearing lengths occurs at the same length/diameter ratio of about two as does the drop in load-carrying capacity. This is as expected, since both effects are caused by end leakage in the bearing.

Similarly, the criterion expressed by equation (14) suggests that, for a bearing of given length, the whirl threshold speed should be proportional to $1/\sqrt{I}$ if F_r were constant. Actually, since F_r will probably increase with speed, the whirl threshold speed will decrease more rapidly than as $1/\sqrt{I}$. This is confirmed by the results plotted in Fig. 6.

The main parameters not covered by the theory are bearing clearance and specific load. The clearance curves for 5·08 cm diameter bearings (Fig. 8) demonstrate that the whirl threshold speeds depend to a great extent on clearance. The smaller effect of viscosity is also apparent. It is of interest that the clearance curves for different viscosities coincide at one value of clearance, after which the direction of the effect of viscosity on whirl is reversed.

The effects of specific load and bearing diameter on whirl are shown in Table 3. No real comparison can be made between the various diameters because of differences in the relative inertias, but the trend of decreasing whirl threshold speed as diameter is increased is apparent.

It is interesting to examine the order of magnitude of the force component F_r required for stability. For example, in the case of bearing cylindrical whirl, the ratio of F_r to the stable gas film force given by equation (2) is $M\omega c^3/24l\eta\pi r^3$. For a typical bearing of length/diameter ratio 3, radius 2·54 cm and clearance 25 μ, whirling at 3000 rev/min, the ratio of the forces is only $2{\cdot}4 \times 10^{-3}$, i.e. the same order of magnitude as terms neglected in the hydrodynamic theory.

CONCLUSIONS

The experimental data have been correlated with the theory for lubrication by a compressible lubricant. The data indicate that the conditions within the gas film are isothermal, but a difference of about 24% exists between experiment and the isothermal theory of infinitely long bearings; half of this difference can be explained by means of end-leakage correction factors which were derived by Ausman,[5] but the remainder is unexplained. Comparison of the load capacities of bearings containing a slot in their upper surfaces with those without a slot has shown that the slot has no effect on the load-carrying capacity.

In the case of whirl, the theoretical discussion has shown that, when half-speed whirling conditions prevail, the main gas film forces disappear, and the force required to prevent the whirl from continuing is several orders of magnitude smaller than these. The major difficulty in the theory lies in finding the radial force which prevents whirl in the stable operating region. However, the main theoretical predictions of the effect of bearing inertia and length have been proved experimentally, and the effects of the parameters not yet covered by the theory have been determined and presented graphically.

ACKNOWLEDGEMENTS

This paper is published by permission of the Managing Director of the United Kingdom Atomic Energy Authority (Industrial Group). The experimental results were obtained by Miss P. McEwan. The earlier work on anti-whirl slots was done by Mr. J. Leicester and Mr. V. H. Brix.

REFERENCES

(1) KINGSBURY, A. J. *Amer. Soc. Naval Engrs*, **9**, p. 267 (1897).
(2) HARRISON, W. J. *Trans Camb. Phil. Soc.*, **22**, p. 39 (1913).
(3) KATTO, Y., and SODA, N. *Proceedings of 2nd Japanese National Congress on Applied Mechanics*, p. 267 (1952).
(4) FORD, G. W. K., HARRIS, D. M., and PANTALL, D. *Proc. Instn Mech. Engrs*, **171** (2), p. 93 (1957).
(5) AUSMAN, J. *Proceedings of the Conference on lubrication and wear*, Inst. Mech. Engrs, 1–3 October, 1957, p. 39 (London: Institution of Mechanical Engineers, 1957).
(6) SHAW, M. C., and MACKS, B. F. *Analysis and Lubrication of Bearings* (New York: McGraw-Hill Book Co. Inc., 1949).
(7) AUSMAN, J. *Trans Amer. Soc. Mech. Engrs*, **79** (6), p. 1218 (1957).
(8) PORITSKY, H. *Trans Amer. Soc. Mech. Engrs*, **75**, p. 1153 (1953).
(9) BOEKER, G. F., and STERNLIGHT, B. *Trans Amer. Soc. Mech. Engrs*, **78** (1), p. 13.
(10) REYNOLDS, O. *Trans Roy. Soc.*, **177**, p. 157 (1886).

APPENDIX

The generalized form of Reynolds' equation

The differential equation which determines the pressure distribution around a bearing was first derived by Reynolds.[10] The generalized form of this equation, which includes non-steady-state conditions, is given by Shaw and Macks[6] as:

$$\frac{1}{6\rho}\frac{\partial}{\partial x}\left(\frac{\rho h^3}{\eta}\frac{\partial p}{\partial x}\right)+\frac{1}{6\rho}\frac{\partial}{\partial z}\left(\frac{\rho h^3}{\eta}\frac{\partial p}{\partial z}\right)=(U_0-U_1)\frac{\partial h}{\partial x}+$$
$$+h\frac{\partial}{\partial x}(U_0+U_1)+\frac{h}{\rho}(U_0+U_1)\frac{\partial \rho}{\partial x}+2V_1$$

For the case of a bearing in which the eccentricity and attitude angle vary with time, the velocity terms on the right-hand side of this equation, relative to the bearing, become:

$$U_0=0$$
$$U_1=r\omega+(de/dt)\sin\theta-e(d\phi/dt)\cos\theta$$
$$V_1=r\omega(dh/dx)+(de/dt)\cos\theta+e(d\phi/dt)\sin\theta$$

Neglecting terms in c/r and e/r, one has:

$$\frac{1}{6\eta r^2\rho}\frac{\partial}{\partial\theta}\left(\rho h^3\frac{\partial p}{\partial\theta}\right)+\frac{1}{6\rho}\frac{\partial}{\partial z}\left(\frac{\rho h^3}{\eta}\frac{\partial p}{\partial z}\right)=\left(\omega-2\frac{\partial\phi}{\partial t}\right)\frac{\partial h}{\partial\theta}+$$
$$+\frac{\omega h}{\rho}\frac{\partial\rho}{\partial\theta}+2c\cos\theta\frac{\partial n}{\partial t}\quad(17)$$

It is required to solve this equation under steady-state conditions to obtain the theory of load capacity, and under non-steady state conditions to obtain a theory of vibration characteristics. Only the case of infinite long bearings is considered, i.e. $\partial p/\partial z$ is set equal to zero.

Setting $\partial\phi/\partial t=0$, $\partial n/\partial t=0$, the first integral of equation (17) becomes equation (1) of the paper. At half-speed whirl conditions, equation (17) becomes equation (12) of the paper.

Estimation of trace water content in a halogenated oil by means of tritiated water

By J. F. CAMERON, B.Sc., and I. S. BOYCE, B.Sc., Isotope Division, A.E.R.E., Harwell, and R. M. GLAISTER, B.Sc., Ph.D., A.Inst.P., G.V. Planer Ltd., Sunbury-on-Thames

[*Paper first received* 29 *April, and in final form* 2 *June*, 1959]

A simple but accurate method using tritiated water for determining the efficiency of a plant for drying a halogenated, hydrocarbon oil is described. By the use of tritiated water with an activity of 50 mc/ml., it is possible to measure water contents as low as 0·04 p.p.m., while, with an activity of 5 c/ml., the sensitivity may be increased to four parts in 10^{10}. An advantage of the method is that the samples may be exposed to the atmosphere for short periods without appreciably changing the labelled water content.

Poly-trifluorovinyl chloride, known as Fluorolube[1] or Fluorube,[2] is a high-density oil used in the present application as a damping fluid in rate-integrating floated gyros. The oil has been found to be slightly corrosive in the presence of water, presumably because of the formation of HCl or HF, and reduction of water content to a minimum is therefore required. To assess the efficiency of a vacuum drying plant, a reliable and accurate method was needed for estimating water contents of the order of a few p.p.m. or less. Because no standard analytical technique was sufficiently sensitive, the possibility of a radioactive-tracer method was investigated. To trace the water unambiguously throughout the drying process, it is essential to label the water molecule itself, and tritiated water (HTO) in which one of the normal hydrogen atoms is replaced by radioactive hydrogen (tritium) provides a very convenient tracer. The radioactive-tracer technique has been used to determine the solubility of water in benzene[3] by introducing the samples inside a Geiger counter, but as the soft β-radiation (maximum energy 18 keV) emitted by tritium can more conveniently be assayed in commercially available liquid scintillation counters, the latter method was chosen for this investigation. Because Fluorolube is fully halogenated and contains no hydrogen, there is no risk of substituting tritium into its molecule.

METHOD OF ASSAYING TRITIUM

Tritiated water is cheap and readily available. Stock solutions of 200 mc/ml. and 5 c/ml. activity are held at A.E.R.E., Harwell. The hazards associated with its use are small because of the rapid rate of elimination from the body and the low energy of the beta particles emitted. The maximum permissible body burden is 10 mc and the recommended maximum permissible concentrations in drinking water and in air are 0·2 μc/ml. and $0{\cdot}5\times10^{-5}$ μc/ml.[4] A radioactive half-life of 12·5 years means that only very infrequent corrections for decay need be made.

Liquid scintillation-counting equipment using both single-channel* and coincidence instruments† are commercially available. Figures for efficiency and background vary widely not only from one design to another but also with the scintillator used and the concentration of tritiated water or other quenching agents in the scintillator. However, conservative data for estimating the feasibility of determining small concentrations of tritiated water are an efficiency of 10% and background of 20 c.p.s. with a single-channel system. A coincidence apparatus was used in this investigation which gave an efficiency of 6·3% for 0·1 g of water in a 10 ml. sample of scintillator with a background of 3·3 c.p.s. at room temperature. The apparatus was used at room temperature, because the improvement obtained by cooling is only significant in single-channel equipment.

The liquid scintillator employed consisted of 80 g/l. of naphthalene, 5 g/l. of 2·5-diphenyloxazole (PPO) and 0·05 g/l. of α-napthylphenyloxazole (POPOP) dissolved in a mixture of 5 parts of xylene, 5 parts of *p*-dioxane and 3 parts of ethanol.[5] Up to 7% of water may be dissolved in this liquid, and although it is not the most efficient scintillator for assay of fluorolube which dissolves in xylene, it was conveniently available and more than sufficient for the purposes of this investigation.

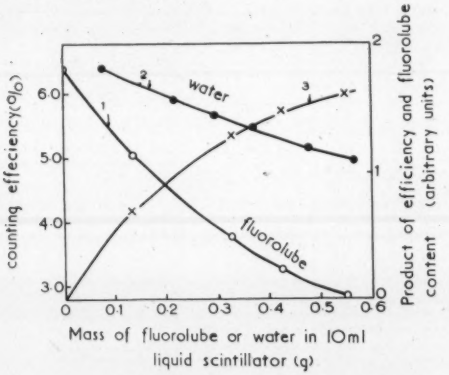

Variation of counting efficiency and the product of efficiency and Fluorolube content with mass of Fluorolube or water in 10 ml. of liquid scintillator

The degree of quenching brought about by the oil is shown by curve (1) in the figure and was determined by gradually adding inactive oil to liquid scintillator containing tritiated water. Quenching by the water itself is negligible over the concentrations obtaining, as illustrated by curve (2). Curve (3) shows that the product of the efficiency and Fluorolube content rises only slowly for quantities in excess of 0·5 g Fluorolube in 10 ml. scintillator and, as even this small amount takes about ten minutes to dissolve completely, this proportion of oil was adopted. The counting efficiency is then 3%, which means that a tritium content of 0·003 μc gives a count rate equal to that of the background. Thus, if the labelled water is of activity 50 mc/ml., this count rate will be obtained with a water content of 0·12 p.p.m. The sensitivity may be increased a hundred-fold by increasing the activity of the water to the maximum of 5 c/ml.

* Ecko Electronics Ltd., Southend-on-Sea, Essex. Nuclear Enterprises (G.B.) Ltd., Edinburgh 11. Panax Equipment Ltd., Redhill, Surrey.

† Packard Instrument Co., La Grange, Illinois, U.S.A. Technical Measurement Corps., New Haven, Conn., U.S.A. Tracerlab Inc., Houston, Texas, U.S.A.

DETERMINATION OF EFFICIENCY OF DRYING PLANT

The water was labelled using the following procedure: 500 ml. (about 1 kg) of Fluorolube was placed in a flask which was pumped until bubbling ceased, and 0·5 ml. of water containing 25 mc of tritium was then added and mixed with a high-speed stirrer to form an emulsion. The water was then allowed to separate and was removed by further evacuation. A further 1 ml. of water containing 50 mc of tritium was added, stirred and allowed to separate while the oil was held at 30° C.

By means of this two-stage process, dilution of the tritiated water by water already present in the oil was minimized. A measurement of the activity of the saturated oil indicated a saturation water content of about 60 p.p.m. at 30° C. This is in fair agreement with measurements made on a Van Slyke gas-analysis apparatus, which gave a content of 25 p.p.m. at 70° C.

The saturated oil was then passed through a vacuum drying plant where it was heated to about 100° C, and samples taken for assay. Only simple precautions were needed to prevent access of moisture to the oil after drying because the dilution of the tritium by atmospheric water vapour is slow and any absorbed moisture would consist of inactive water: the samples were merely placed in stoppered bottles. Measurements on distilled-water extracts of the pH value showed no detectable change from neutrality after this vacuum-heat treatment. Thus, no significant hydrolysis occurred at this stage.

A minimum water content of 0·04 p.p.m. has been achieved with the drying plant and measured satisfactorily by this method, which is suitable for quality control of drying plant. It is probable that this method could be extended to conventional hydrogen-containing oils.

ACCURACY

The counting time of each sample was chosen such that the relative standard deviation (coefficient of variation) never exceeded 5%. This meant that for a water content of 0·04 p.p.m., which represents a count one-third greater than background, a counting time of 25 min was necessary.[6] The extra time involved in improving statistical accuracy on counting was not deemed necessary because, especially at very low water contents, repeat measurements on samples showed deviations from the mean of up to 20%, which must result from an inhomogeneous water distribution. This inhomogeneity appears to be caused by fluctuations in the rate of flow of Fluorolube through the drying plant.

Further errors will be introduced by the large mass ratio of tritium to hydrogen which leads to differences in the chemical and physical properties of the isotopes and their compounds such as the relative solubilities and rates of vaporization of H_2O and HTO. However, the vapour pressure of HTO is only 20% less than that of H_2O at 25° C, the difference falling with increasing temperature and becoming zero above the boiling point of HTO.[7] Thus, this effect will be small at the temperature used in the drying plant and will, if present, give a pessimistic figure for the

efficiency of drying. The difference in the constants of Henry's Law is also likely to be small and certainly smaller than the inhomogeneity of the water distribution in the samples. These errors were not investigated because only approximate relative figures were required for the efficiency of the drying plant.

ACKNOWLEDGEMENTS

The authors would like to thank Mr. Milne of R.A.E., Farnborough, for suggesting the use of isotopes in connexion with this work, and Miss F. B. Follows of G.V. Planer Ltd. for her assistance. This research was carried out in association with Ferranti Ltd. under contract to the Ministry of Supply.

REFERENCES

(1) Hooker Electrochemical Company, Bulletin No. 30.
(2) I.C.I. Data Sheet for Fluorube chlorofluorocarbon lubricants.
(3) JORIS, G. G., and TAYLOR, H. S. *J. Chem. Phys.*, **16**, p. 45 (1948).
(4) Recommendations of the International Commission on Radiological Protection. Supplement No. 6, *British Journal of Radiology*, 1955.
(5) KINARD, F. E. *Rev. Sci. Instrum.*, **28**, p. 293 (1957).
(6) LOEVINGER, R., and BERMAN, M. *Nucleonics*, **9**, No. 1, p. 26 (1951).
(7) PRICE, A. H. *Nature* (*London*), **181**, p. 262 (1958).

Experimental method of investigating stresses in buttress dams

By J. R. RYDZEWSKI, Ph.D., B.Sc., A.M.I.C.E.,* Engineering Laboratory, University of Cambridge

[*Paper first received* 29 *January, and in final form* 22 *April*, 1959]

A photoelastic method is described for investigating the stress distribution in a buttress dam web of constant thickness, resting on an elastic foundation. The method is also applicable to the stress analysis of a gravity dam. The general case is considered when the elastic properties of the foundations differ from those of the material of the dam. The investigations were made by "frozen-stress" methods in which the composite model of the dam and foundations, together with its impounded liquid, was subjected to a centrifugal acceleration which amplified the body forces and liquid pressures about twenty-eight times. The model was analysed in a polariscope to obtain the difference of the principal stresses and their directions, while the sum of the principal stresses was found from measurements of the lateral extensions of the model. For the latter purpose a new technique was developed.

INTRODUCTION

Since most photoelastic materials are not stress-optically sensitive enough to produce a definite stress pattern under their own weight, photoelastic experiments on models of dams may be classified by their methods of simulating the body force effect.

Working at room temperature, and being interested in a small region within the model, Brahtz[1] and, more recently, Steinboeck[2] replaced the body forces by a number of discrete concentrated loads remote from the area under observation. A considerably more elaborate method was used by Bucky, Solakian and Baldin[3] who subjected their two-dimensional model to a centrifugal acceleration and observed the resulting stress pattern stroboscopically every time the model crossed the field of the polariscope.

Recently Locatelli, Grandiori and Moravia[4] have described two methods in which the model was given a high linear acceleration. In one case the model was mounted on a rigid frame which could slide in the vertical plane between guides. An upward acceleration was imparted to the frame by means of a stretched rubber belt, the stress pattern being recorded by means of high-speed photography. In the second method the acceleration was produced by a rapid reciprocating motion and the model was observed when it was at a dead centre of its motion.

Gelatin, being very optically sensitive to stress, does produce a stress pattern due to self-weight and has therefore been used for stress studies of dams by Plummer[5] and by Ellis and Gent.[6] This material, however, suffers from optical creep so that results have to be recorded quickly, leaving little time for determination of fractional fringe orders. The latter difficulty has forced some experimenters to use models several inches thick but the two-dimensional nature of the analysis makes such great thicknesses very undesirable. Mention is made by Gutman[7] of the successful use in Russia of agar-agar instead of gelatin.

The "frozen-stress" phenomenon in photoelasticity was made early use of for a study of dam models. Investigations were started before the war by a team under Prof. Eberhart at the University of California, but were not published until Sanks[8] completed his experiments. In these, models of Bakelite were placed in a centrifugal oven where they were allowed to cool under stress. Here, the method of separating the principal stresses is of interest; it was achieved by the determination of their sum from measurements of lateral extensions of the plane model with an apparatus similar to that recently used by Brodie.[9]

The "frozen-stress" technique was also used by Hendry[10] on a three-dimensional model of a single buttress element of the Errochty Dam. Again a centrifuge was made use of to intensity the body-force effect, but this time only the cooling part of the "stress-freezing" cycle took place in the centrifuge.

In all the above investigations separate, and often very costly, methods were used for the application of the equivalent of the water load to the model.

THE EXPERIMENTAL METHOD

The writer was interested in the effect of the elastic properties of the foundations on the stresses in the web of constant thickness of a buttress dam. Thus, in model form, the system consisted of a photoelastic model of the buttress continuously attached to a block of a different material, not necessarily itself photoelastic, representing a finite region of the foundations, as shown on Fig. 1. The object was to

* Now at Civil Engineering Department, University of Southampton.

obtain a reliable stress pattern in the lower half of the buttress when this composite model was subjected to surface and body forces. For such a "stiff" structure a dense stress pattern was not expected, and as a result the analysis had to be freed from the presence of any spurious stresses.

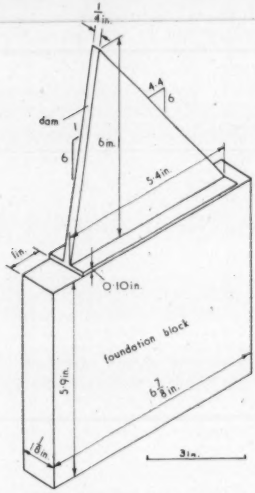

Fig. 1. Details of Araldite model of dam and foundation block

In this connexion "stress-freezing" brought with it additional difficulties. Apart from the "permanent" stresses often present in thermo-setting resins, such as the Araldite B used here, caused by uneven rates of polymeriziation in different parts of the casting, an additional source of unwanted stresses appeared in this problem. It arose from the fact that the model was composed of two materials, different not only in their elastic but also in their thermal properties, the latter causing stresses due to differential shrinkage on cooling. It was, therefore, decided to isolate all these spurious effects in a separate but identical model.

Thus two models were required for each experiment. To achieve the desired similarity the models of the triangular buttress were machined from a single block of the resin, as were also two 2 in. diameter proving disks which, when loaded diametrally, yielded the material fringe value. The buttress models were made with an integral footing which greatly facilitated the correct alinement on the foundation block, and at the same time strengthened the bond between the model and the block by increasing the area of the adhesive layer. Araldite D cold-setting resin was used as the adhesive.

Since it was impossible to reproduce on the model the actual nature of the joint between the concrete of the dam and the rock of the foundations, there appeared little objection to the departure from geometrical similarity caused by the introduction of the buttress footing. By St. Venant's principle the effect of any stresses resulting from irregularities in the plane of contact would disappear a short distance above that plane. As preliminary experiments did not reveal any stress concentrations along the glued joint, it was considered that reliable results could be obtained at a height above the foundations equal to the thickness of the model.

The two models were subjected to the same cycles of heating and cooling. When finally at room temperature, both were cut off their foundation blocks to relieve stresses set up below the "stress-freezing" temperature range. The stress system of the control model could then be subtracted from that of the loaded model in a manner similar to that described by Jessop and Stableford.[11] To test, in practice, the accuracy of the assumption about the identical nature of the two models, two such models (first thoroughly annealed) were fixed side by side on a block of aluminium, raised to 130° C and, on cooling to room temperature, were severed from their bases. The resulting stress patterns were analysed by the Senarmont method, by which fractional fringe orders can be obtained accurately to 1/100th of a fringe. This analysis was carried out along four horizontal sections of the buttress near the base. The results for the one showing the greatest discrepancy are given in Fig. 2. The maximum difference of the order of 0·15 fringes (or 0·8 lb/in.^{2}) was considered to be satisfactory.

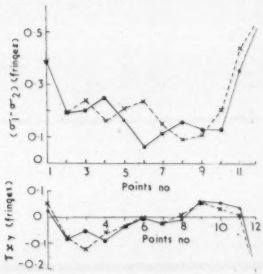

Fig. 2. Comparison of stresses in two "identical" control models for section 5·9 in. below crest. (One fringe ≃ 5·4 lb/in.^{2})

Having established the general approach to the experimental method, attention will now be turned to some of the details of its procedure. A centrifuge of the type used by Hendry was constructed. With a 66 in. radius arm and a 6 in. high model it provided an acceleration field which varied by ±5% from the mean in intensity and ±2½% in direction. Since only the cooling of the model took place on the centrifuge, the model, in its loading frame, was heated in an oven and then transferred to an insulated box at the end of the centrifuge arm. To avoid sudden cooling this box was provided with heating elements to raise it to the required temperature.

With the experiment relying on the natural cooling of the model in the centrifuge, the thickness of the model had to be such as to ensure an even rate of cooling within it. As very little information was available on this subject, an experiment was designed to obtain direct evidence. In this, stress patterns were compared in two identical models, one loaded in the centrifuge and the other under ideal conditions in a thermostatically-controlled oven. For this purpose a 2 in. wide plate with a central ⅜ in. diameter hole was loaded in tension. It was found that whereas a ⅜ in. thick plate exhibited fringes due to differential cooling, a ¼ in. thick plate did not. As a result a model thickness of ¼ in. was adopted.

In the composite model (Fig. 1) there is an appreciable

difference in thickness between the buttress and the foundation block. It was of interest, therefore, to discover the rates of cooling in different parts of the model. Four thermocouples were embedded in a model, made entirely of Araldite B, at the points shown on Fig. 3(*a*). The resulting cooling curves are presented on Fig. 3(*b*) showing a maximum time lag of about half an hour in the "stress-freezing" range.

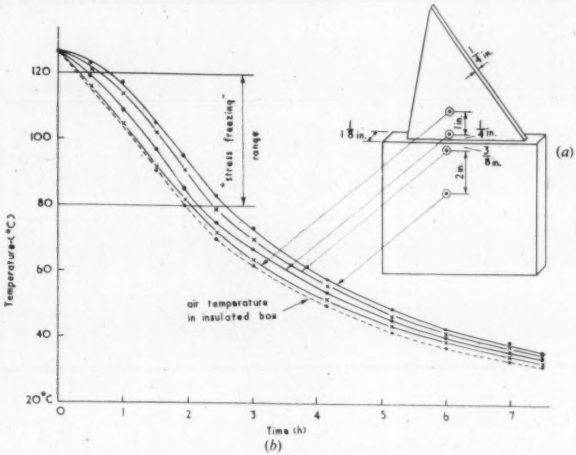

Fig. 3. (*a*) Model of dam showing position of thermocouples. (*b*)Rates of cooling obtained from thermocouples

The loading, both gravitational and hydrostatic, was simulated in the centrifuge, the speed of which was kept constant at 130·43 rev/min with the aid of a stroboscopic device. At this speed the average intensity of the acceleration field was about 28 gravities. For the model and centrifuge dimensions used, the total vertical force on various horizontal sections of the model is given in Table 1, where it is compared with that which would have been produced by a gravitational field. Likewise, a comparison is made in Table 2 between the total shear on horizontal sections, produced by the usual hydrostatic forces, and the one resulting from the pressure of a liquid acting on the model face in the centrifuge. In both cases the total force on the base of the buttress is made the same for the two systems compared.

Table 1. *Theoretical comparison of total vertical body-force load on horizontal sections of model produced centrifugally and by gravity*

	Total vertical load (lb/ϱ_M)	
Depth below crest (in.)	*Gravitational*	*Centrifugal*
1	0·113	0·108
2	0·454	0·433
3	1·022	0·987
4	1·816	1·775
5	2·838	2·806
6	4·087	4·087

ρ_M = specific gravity of model material.

Table 2. *Theoretical comparison of total shear on horizontal sections of model produced centrifugally and by gravity*

	Total shear (lb/ϱ_L)	
Depth below crest (in.	*Gravitational*	*Centrifugal*
1	0·122	0·119
2	0·489	0·477
3	1·100	1·081
4	1·956	1·933
5	3·057	3·039
6	4·402	4·402

ρ_L = specific gravity of liquid.

The actual loading was accomplished by placing the model in the loading frame, illustrated on Fig. 4, in such a way that the face of the model was in contact with a rubber bag housed in a metal cowling. This bag was filled to the required level with glycerol, which had the double advantage of a high boiling point and of chemical inertness with respect to natural rubber. The top of the bag was sealed with a "pickle bung" and an insulated cover was placed over the whole assembly, which was then heated to 130° C in an oven and transferred to the centrifuge. The latter was maintained at constant speed for five hours, at the end of which the model was removed and cut off its foundation block as previously described.

Observations of the model in the polariscope give only the difference of the principal stresses and their directions, so that additional information is required for a complete solution of the stress problem. Most of the commonly used methods involve a step-by-step integration of one of the differential equations of static equilibrium, starting with known stresses at a boundary. Often these boundary stresses cannot be determined with great accuracy and when low fringe orders are the rule, as in this case, the errors thus incurred can be substantial. What is more, these errors are carried along from point to point as the integration proceeds.

With this in mind attention was directed to techniques of obtaining the sum of the principal stresses at each point by measurement of the lateral displacement of the stressed model. However, the accuracy of measurement attained by Sanks and by Brodie made this method appear approximate com-

pared with the best results of the graphical or numerical integrations of the equations of equilibrium.

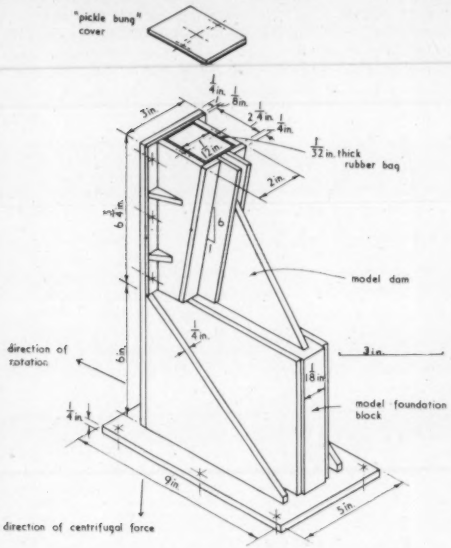

Fig. 4. Details of model loading frame, constructed throughout in Duralumin

It was found that much better accuracy in thickness measurement is generally expected of comparators used in instrument workshops for checking of surface finish. The machine available to the writer was a Sigma comparator used in conjunction with Matrix slip-gauges. The model used gave a variation of $\pm 0{\cdot}003$ in. from the slip-gauge thickness and was graduated in 0·0001 in. divisions. These were coarse enough to permit of estimation to one-tenth of a division with a certainty to one-fifth. This is five times more accurate than

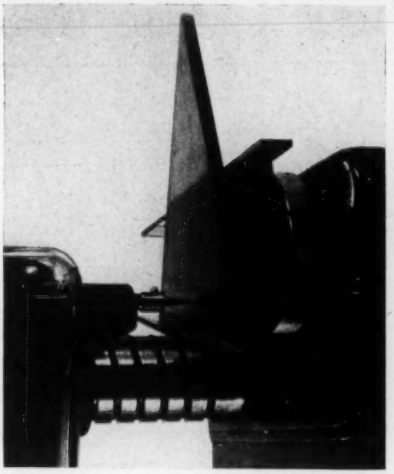

Fig. 5. Modified comparator in use as lateral extensometer

in Brodie's experiments, and in terms of a $\frac{1}{2}$ in. thick Araldite B model represents only 0·065 of a fringe.

Simple modifications to the fixed anvil and to the probe of the comparator gave a means of measuring the thickness of a model at a *point*. A detail of the modified comparator in use is given on Fig. 5.

Points on the model at which observations were made were

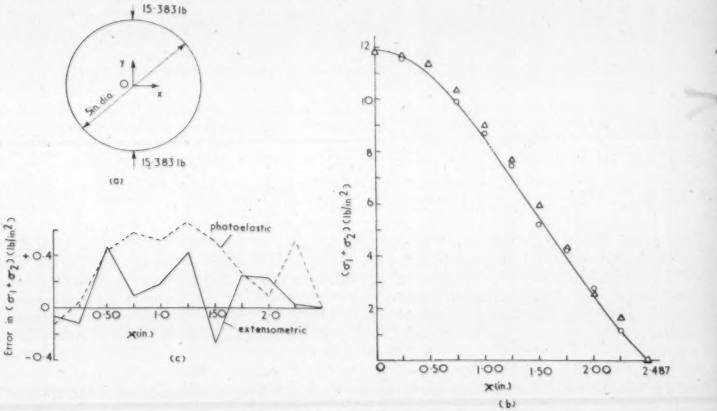

(*a*) Disk, 0·337 in. thick, under diametral loads.
(*b*) Distribution of $(\sigma_1+\sigma_2)$ on line $y = 0{\cdot}25$ in. ○ = values from lateral extension measurements. △ = values from photoelastic measurements. —— = theoretical values.
(*c*) Comparison of errors in experimental derivation of $(\sigma_1 + \sigma_2)$ on line $y = 0{\cdot}25$ in.

Fig. 6. Indication of accuracy of determining the sum of the principal stresses by measurement of lateral extension

marked by a finely scratched grid. The depressions formed at the intersections of the lines served to locate the fine point of the probe correctly, since they produced minimum readings on the comparator. Care was taken to lift the probe on moving from point to point so as not to damage the grooves. However, to assess the extent of any such damage, microscope photographs were taken of a grid intersection before probing and after probing twenty times. No widening of the grooves was observed. Also, it was found from the geometry of the groove and of the probe point that, for a strain of $2\frac{1}{2}\%$ that would accompany a stress of about 50 lb/in.^{2} in Araldite B, the resulting vertical movement of the probe would be less than 0·00001 in.

Before this method of separating the principal stresses was applied to the buttress model its accuracy was tested on a case with a known theoretical solution, shown on Fig. 6(*a*). The opportunity was taken to compare the results with those from a method relying entirely on photoelastic data; for convenience, the shear difference method was used. The results of this test, presented on Figs. 6(*b*) and (*c*), are favourable to the extensometric technique. It was also tried on a model of a locomotive bogie frame, where a dense fringe pattern and sharply defined isoclinics were of advantage to the shear difference method. Yet, here too, the extensometer gave slightly better static checks at the sections considered.

A typical set of results for a model of a buttress is given in Fig. 7. It deals with the case of an infinitely rigid foundation, which in the experiment was simulated by a block of aluminium.

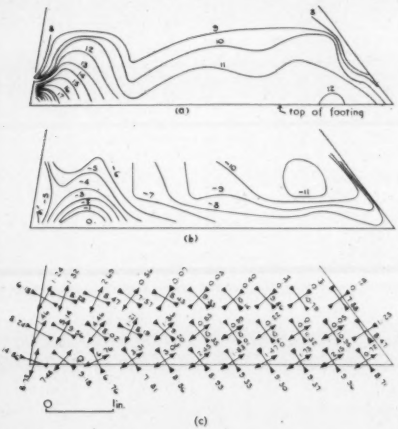

Fig. 7. Results for a model of dam on rigid foundations
(*a*) Contours of $(\sigma_1 - \sigma_2)$ (lb/in.^{2}).
(*b*) Contours of $(\sigma_1 + \sigma_2)$ (lb/in.^{2}).
(*c*) Magnitudes and directions of principal stresses. (Values given in lb/in^2).

CONCLUSION

It is hoped that the experimental work described above demonstrates sufficiently the feasibility of applying "frozen-stress" photoelasticity to models composed of more than one material. It has, also, attempted to raise the extensometric method of separating the principal stresses in plane "frozen-stress" photoelasticity to the level of accuracy considered satisfactory in other methods.

ACKNOWLEDGEMENTS

The work described in this paper has been carried out at the Engineering Laboratory of the University of Cambridge by kind permission of Prof. J. F. Baker and under the direction of Mr. E. K. Frankl. It would have been impossible without the generous assistance of the Beit Trust, the Departmental Research Fund and the Taylor Woodrow Fund.

REFERENCES

(1) BRAHTZ, J. H. *Trans Amer. Soc. Civil Eng.*, **101**, p. 1240 (1936).
(2) STEINBOECK, W. *Transactions of the 5th International Congress on Large Dams*, **4**, p. 685 (London: Lund Humphries, 1955).
(3) BUCKY, P. B., SOLAKIAN, A. G., and BALDIN, L. S. *Civil Engng*, p. 287 (1935).
(4) LOCATELLI, P., GRANDIORI, G., and MORAVIA, G. *Ricerca Sci.*, **25** (1), p. 80 (1955).
(5) PLUMMER, F. L. *Trans Amer. Soc. Civil Eng.*, **101**, p. 1281 (1936).
(6) ELLIS, J. S., and GENT, K. W. *Engng J.*, p. 1435, NOVEMBER, (1953).
(7) GUTMAN, S. G. *Transactions of the 5th International Congress on Large Dams*, **4**, p. 1387 (London: Lund Humphries, 1955).
(8) SANKS, R. L. *Proc. Amer. Soc. Civil Eng.*, **81**, Separate No. 693 (1955).
(9) BRODIE, I. *Brit. J. Appl. Phys.*, **9**, p. 201 (1958).
(10) HENDRY, A. W. *Proc. Instn Civil Engrs*, **3** (1), p. 370 (1954).
(11) JESSOP, H. T., and STABLEFORD, W. H. *Brit. J. Appl. Phys.*, **5**, p. 281 (1953).

Correspondence

Improved semiconductor-to-copper soldered contact

A major problem in the manufacture of both germanium and silicon power rectifiers is the production of an ohmic contact between the semiconducting slice and the diode base, which is capable of withstanding the stress imposed by the differential expansion of the copper and semiconductor under on-load conditions, and which should produce good wetting over the whole available area of the junction.

To ensure good heat removal from a *p–n* junction, under operating conditions, to an available heat sink, direct soldering of the semiconducting wafer to the heat sink is obviously desirable. Early production techniques employing such a connexion consisted of two steps, namely pre-tinning of the copper base with a lead base solder, using a chemical flux, followed by the subsequent firing of the diode element. Disassembled germanium units produced in this way showed extremely erratic wetting of the solder to both the copper base and the germanium wafer, and produced devices where the temperature rise on load was therefore unduly high.

Two main causes for such non-wetted areas were postulated, namely that:

(*a*) the blank areas were not wetted at the pre-tinning stage, the apparent homogeneity of the surface being produced purely by the mechanical strength of the solder film;

(*b*) the blank areas became de-wetted during firing, due to corrosion between the copper lead layer as a result of using chemical fluxes.

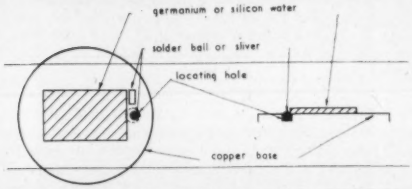

Fig. 1. Method of soldering germanium or silicon to copper

during which the solder becomes molten. At the temperature at which it alloys both with the germanium and the copper, capillary flow commences and continues until the whole area under the wafer has been filled. Owing to surface tension acting at the periphery of the waver, continued heating does not result in any further spread of the solder film. The strength of this bond is such that repeated and rapid temperature cycling of complete units showed no cracking of the germanium or silicon slices whatsoever.

In the samples of germanium soldered to copper that were examined (Fig. 2), over 90% wetting in every cell was obtained, provided that the surfaces of the germanium and copper were both flat and scrupulously cleaned before firing.

This technique is now in general use in the production of silicon and germanium semiconductor devices. It ensures not only a consistent product but also the maximum safety

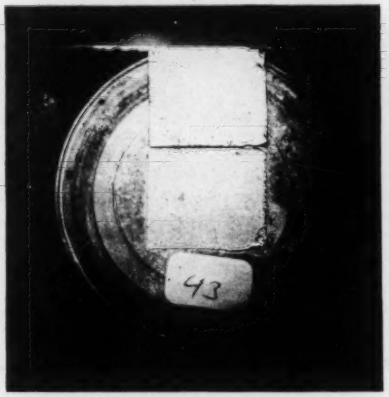

(*a*)

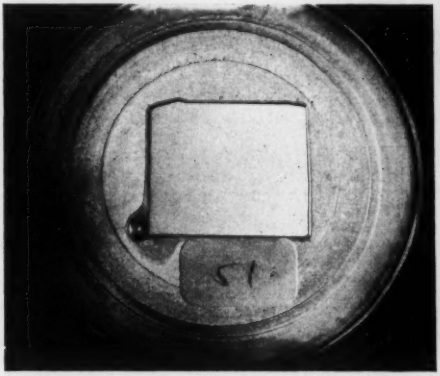

(*b*)

Fig. 2. (*a*) Showing nearly perfect alloying and wetting of base and germanium wafer. (*b*) Showing limits of solder flow

Diodes processed using organic liquids or hydrogen as fluxes gave results which left much to be desired, and a technique was therefore developed which incorporated the capillary flow of solder which is described below.

The germanium or silicon slice is etched and is placed on a similarly etched copper base. A quantity of solder, sufficient to provide a 0·002 in. layer over the diode area, is placed either in the form of a ball or a slip alongside the wafer. A small groove is usually provided to localize the solder and prevent it slipping during the subsequent manual operations (Fig. 1).

The heating cycle of the whole assembly is now commenced, of such devices under transient, overload and short circuit conditions, where a maximum and uniform heat extraction from the *p–n* junction in question is essential.

The author is indebted to the General Manager of the English Electric Valve Co. Ltd., for permission to publish this note. The contact is the subject of a provisional patent No. 33535/57.

English Electric Valve Co. Ltd.,
Chelmsford,
Essex.

G. REICHENBAUM*
[15 *April*, 1959]

*Now at Westinghouse Brake and Signal Co., London.

THIS JOURNAL is produced monthly by The Institute of Physics, in London. It deals with all branches of applied physics (including theory and technique). All rights reserved. Responsibility for the statements contained herein attaches only to the writers.
EDITORIAL MATTER. Communications concerning editorial matter should be addressed to the Editor, The Institute of Physics, 47 Belgrave Square, London, S.W.1. (*Telephone:* Belgravia 6111.) Prospective authors are invited to prepare their scripts in accordance with the *Notes for Authors*. (Price 3*s*. 6*d*. including postage.)
REPRODUCTION. The Institute of Physics is a signatory to The Royal Society's Fair Copying Declaration. Details may be obtained upon application from The Royal Society, London, W.1.
ADVERTISEMENTS. Communications concerning advertisements should be addressed to the agents, Messrs. George Jackson (Fleet St.) Ltd., Cliffords Inn, Fleet Street, London, E.C.4. (*Telephone:* Holborn 3611–2.)
CLAIMS FOR MISSING JOURNALS. Claims from regular subscribers to this *Journal* for missing numbers will only be considered if received within 60 days of the date of mailing plus normal outward time of transit and time for lodging the claim. Losses attributable to failure to notify a change of address or to similar omissions will not be considered.
SUBSCRIPTION RATES. A new volume commences each January. The charge is £6 per volume ($17 U.S.A.), including index (post paid), payable in advance. Single parts, so far as available, may be purchased at 12*s*. 6*d*. each ($1.75 U.S.A.), post paid, cash with order. Orders should be sent to The Institute of Physics, 47 Belgrave Square, London, S.W.1, or to any bookseller.

Some aspects of the design of large permanent magnets

By J. E. Cousins, B.Sc., and W. F. Nash, M.Sc., Ph.D., Physical Laboratories, The University of Nottingham

[*Paper received* 26 *March*, 1959]

This paper considers the design and construction of a large permanent magnet for use in cosmic ray studies. It is shown that there is an optimum distribution of the magnetic material in order to obtain either a maximum field, H, or a maximum line integral, $\int_{-\infty}^{+\infty} H dy$, for a given pole face area and gap size. It has been shown that a good value of the leakage factor for use in the design calculations for magnets with rectangular pole faces can be predicted theoretically. Detailed comparison between results predicted by this theory and those obtained in practice with the present magnet and other large permanent magnets suggest that these calculations can be usefully applied to magnets with pole faces of any shape. These comparisons also show, in agreement with Andrew and Rushworth, that demagnetization curves for small specimens of magnetic material are not reliable where large blocks are considered.

INTRODUCTION

Recently measurements have been made on the μ-meson spectrum underground in a laboratory beneath the Castle Rock, Nottingham. This involved the construction of a spectrograph consisting essentially of two cloud chambers and a large permanent magnet. The track of a μ-meson passing through the apparatus is recorded by the first cloud chamber placed above the magnetic field and, after deflexion, by the second chamber. This procedure allows the momentum of the particle to be calculated. In experimental work where a very uniform or very symmetrical field is required, as for example in spectrographs of this type or in nuclear resonance experiments, a double-yoke magnet is normally employed. As these magnets may weigh several hundredweights, this type of design facilitates handling during the construction and use of the magnet. The present paper treats various aspects of the design and construction of the Nottingham magnet, and the field and leakage factor obtained. Other similar designs are also discussed in order to draw conclusions on the usefulness of magnetic circuit theory.

PERMANENT MAGNET CIRCUIT THEORY

The type of magnetic circuit to be considered is illustrated in Fig. 1. Let M be the length of circuit consisting of magnetic alloy, $L - M$ the soft iron circuit (including the pole tips), and G the gap length; let A_G, A_M, A_I be the areas of cross-section of the pole faces, magnetic alloy and iron yoke sections respectively; let H_M, B_M, H_G, B_G be the corresponding magnetic field intensities and flux densities and H be the field in the air gap. For convenience the diagram shows rectangular cross-sections, although the following theory is not limited to this case.

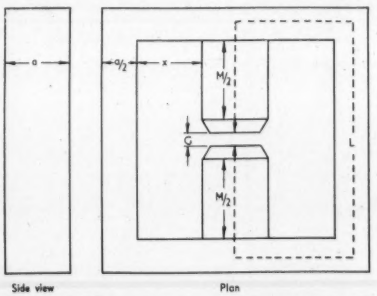

Fig. 1. Schematic diagram of Nottingham magnet

The familiar circuit equations give:

$$HG + H_m M + H_I(L - M) = 0 \quad (1)$$

$$A_m B_m = HA_G(1 + \sigma) \quad (2)$$

and

$$A_m B_m = 2A_I B_I \quad (3)$$

The factor $A_G\sigma$ in equation (2) takes into account stray flux around the air gap. Finally $B_I/H_I = \mu_I$.

Rearrangement of these equations gives:

$$B_m = -H_m\left[\epsilon\gamma\Big/\left\{1 + \frac{\epsilon\phi(\delta - \gamma)}{\mu_I}\right\}\right] \quad (4)$$

and

$$B_m = \epsilon H \quad (5)$$

where $\gamma = M/G$; $\delta = L/G$; $\epsilon = (1 + \sigma)/\eta$; $\phi = A_m/2A_I$

$$\eta = A_m/A_G$$

The quantity $\left[\epsilon\gamma\Big/\left\{1 + \frac{\epsilon\phi(\delta - \gamma)}{\mu_I}\right\}\right]$ in equation (4) contains the dimensions of the magnet and the leakage factor $(1 + \sigma)$. A reasonable value of μ_I can be obtained from the magnetization curves available for soft iron materials. The leakage factor is therefore the only unknown quantity and, if this can be determined, use of the magnetization curve, for the magnetic alloy employed and equation (4), allows the value of B_m to be computed. The value of H is then obtained from equation (5).

In order to determine the value of σ in a generally applicable form, Shutt and Whittemore[1] introduced a dimensionless variable

$$\beta^1 = Gb_G/A_G$$

where b_G is the circumference of the pole tip. The factors determining the stray flux around the air gap are then simply

β^1 and η, allowing σ to be expressed in the form of a power series:

$$\sigma = C_1\eta\,\beta^1 + C_2(\eta\beta^1)^2 + \ldots \qquad (6)$$

where C_1, C_2, ... are constants to be determined experimentally. They therefore carried out model experiments for the particular case where $\phi = 1$ and for square cross-section pole tips. The value of A_m was 4 in.^{2} and M had the values 4, 6 and 8 in. while L was 17 in.; G was varied by means of steel shims. To a good approximation it was found that only the first term in the series need be considered, and from twelve experimental arrangements it was concluded that $C_1 = 0{\cdot}95$ gave the best agreement. Further they pointed out that the use of the first term of the series is justified only if $\sigma \simeq C_1\eta\beta^1 < 1$, since σ occurs in the form $(1 + \sigma)$ in equation (2). Physically, this condition means that the stray flux shall not exceed the main flux through the air gap. The angle of taper in this case is not important and can be anywhere between 30 and 60 deg., or approximated by a step. The work involved fully-saturated magnetic material.

Calculations reported in the following section have been based on the expression for σ given in equation (6). A discussion of the validity of the result and its general applicability will be discussed later.

THE NOTTINGHAM MAGNET

(*a*) *Design considerations.* For a relativistic particle of momentum p and single electronic charge e (e.s.u.) moving in a plane perpendicular to a magnetic field H (oersteds), the equation of motion is:

$$pc = eH(ds/d\theta) \qquad (7)$$

where $ds/d\theta$ is the radius of curvature of the path (in centimetres) at the point considered, ds being the arc length along the path and θ the angle between the path and the y-axis, the direction defined for convenience in this particular case as a vertical line passing through the centres of the cloud chambers and the magnet gap. Further

$$ds = dy/\cos\theta \qquad (8)$$

Hence, if $\int_{-\infty}^{+\infty} Hdy$ is arranged to be constant in value over the whole of the region occupied by the trajectory of the particle, equation (7) can be written

$$pc = e\int_{-\infty}^{+\infty} Hdy \Big/ \int_{\theta_1}^{\theta_2} \cos\theta\, d\theta \qquad (9)$$

where $\theta_1\theta_2$ are the angles of the track of the particle above and below the field, and $\int_{-\infty}^{+\infty} Hdy$ is the vertical line integral of the field intensity measured right through the magnetic field, including the fringing field. It is obvious that pole faces of square or rectangular cross-section will be employed in this type of application.

The aim is now to design a magnet to give a maximum value of $\int_{-\infty}^{+\infty} Hdy$ for a given quantity of magnetic alloy and a given gap size. The gap size is a fixed parameter because, for square cross-section pole faces, the solid angle subtended by the magnet gap is proportional to G^2 only, and the value is determined by the size and disposition of the cloud chambers.

In formulating equation (2) it is assumed that the field acts over an effective area $(1 + \sigma)A_G$, so for square pole faces of side h, the product Hdy integrated along a line parallel to a pole face edge in the central plane of the magnet gap is $Hh(1 + \sigma)^{1/2}$. Let V be the volume of magnetic alloy to be considered. Then, by use of equation (6):

$$h(1 + \sigma)^{1/2} = \left[\frac{V}{M\eta}\left\{1 + 4C_1\eta G\left(\frac{M\eta}{V}\right)^{1/2}\right\}\right]^{1/2}$$

With V and G fixed, M and η are the only variables. The expressions for H {equations (4), (5)} contain the same two variables and also L, the total length of the iron and magnetic alloy circuit. For the purpose of calculation, and in order to simulate a typical design, the length L has been taken as

$$2M + 2G + (7/2)a \quad \text{where} \quad a = \sqrt{(V/M)}$$

This means that the cross-section of the yoke is $a^2/2$ and that the distance between the yoke and pole pieces, x in Fig. 1, is $a/2$. Also, the thickness of the iron pole tips has been arbitrarily chosen to be $G/2$.

The volume of magnetic alloy, in this case A!comax III, is 720 in.^{3}, and a gap size of about $1\frac{1}{4}$ in. was anticipated. As high fields of the order of 5000 oersteds could be expected, $\mu_I = 1000$ is used in the following computations. Finally $\phi = 1$ was chosen, i.e. total cross-section of magnetic alloy was equal to that of the iron circuit. Results of calculations of the variation of $\int_{-\infty}^{+\infty} Hdy$ with M and of H with M are shown graphically in Figs. 2 and 3. The four cases shown are for

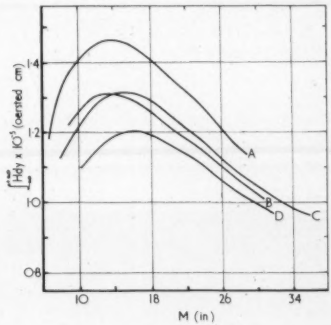

Fig. 2. Variation of $\int_{-\infty}^{+\infty} Hdy$ with 'M', the length of magnetic material, for various values of 'G', the gap size and of 'η' the ratio of the cross sectional area of the magnetic alloy to that of the pole piece

Curve A, $G = 1{\cdot}00$ in., $\eta = 1$; curve B, $G = 1{\cdot}25$ in., $\eta = 0{\cdot}75$; curve C, $G = 1{\cdot}25$ in., $\eta = 1$; curve D, $G = 1{\cdot}50$ in., $\eta = 1$.

$\eta = 1$ and $G = 1{\cdot}00$, $1{\cdot}25$ and $1{\cdot}50$ in.; also for $\eta = 0{\cdot}75$ and $G = 1{\cdot}25$ in.

Three points may be noted.

(1) The importance of maximization can be seen by considering the case $\eta = 1$, $G = 1{\cdot}25$ in. For maximum field, $M = 21$ in. is required, while for maximum $\int_{-\infty}^{+\infty} Hdy$, $M = 15$ in. The loss in $\int_{-\infty}^{+\infty} Hdy$ expected in such a magnet designed for maximum field would be close to 7%. This difference

becomes more important as the size of the gap is decreased.

(2) For a magnet designed for either maximum $\int_{-\infty}^{+\infty} Hdy$ or H for a given value of the gap size, subsequent alteration of the gap size will result in little design loss. For example, a magnet designed for maximum $\int_{-\infty}^{+\infty} Hdy$ with $G = 1{\cdot}25$ in. is still within 1% of the optimum conditions for $G = 1{\cdot}00$ or $1{\cdot}50$ in.

(3) Coning has no effect on the maximum value of $\int_{-\infty}^{+\infty} Hdy$ which may be obtained, although the disposition of the magnetic alloy is different.

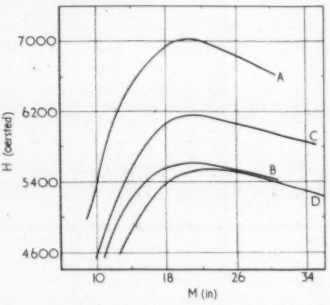

Fig. 3. Variation of the magnetic field H with 'M', the length of magnetic material, for various values of 'G', the gap size and of 'η' the ratio of the cross sectional area of the magnetic alloy to that of the pole piece

Key to curves as on Fig. 2.

(*b*) *Fabrication.* The final dimensions chosen were based on curve C of Fig. 2. The most important are given below: $L - M = 49$ in. (iron circuit); $G = 1{\cdot}27$ in.; volume of Alcomax 687 in.^{3}; $h = 6{\cdot}6$ in.; $\eta = 0{\cdot}954$; $M = 16{\cdot}8$ in. Each Alcomax pole consisted of eighteen blocks each of length $4{\cdot}2$ in. The basic cross-section of each block was $2{\cdot}2 \times 2{\cdot}2$ in., but with the central four sets of adjacent corners cut away in such a manner that four brass fixing bolts (diameter $\frac{1}{2}$ in.) could be passed symmetrically through the stack. These screwed into the $\frac{1}{2}$ in. thick pole face to a depth of about $\frac{1}{4}$ in. The other ends of the bolts passed through holes drilled in the yoke and the whole stack of Alcomax blocks was held rigid by nuts placed on the ends of the bolts and tightened on to suitable washers against the yoke. To obtain a solid stack it was found necessary to grind the faces of the stack which contacted the yoke and pole tip. This also eliminated the possibility of air gaps at these contact faces. The yoke consisted of four main arms and two short sections, one in each of the arms of the yoke parallel to the pole pieces, of such a size that the gap could be made a minimum value of $\frac{1}{2}$ in. Bolts were used to bolt the yoke at the corners and passed through these short sections. Finally it may be noted that the value of $\eta = 0{\cdot}954$ takes into account the holes left in the pole pieces to accommodate the fixing bolts. The pole tips had the same cross-sectional area as that defined by the overall dimensions of the pole pieces.

The final design values for the actual dimensions are: $H = 5760$ oersted; $1 + \sigma = 1{\cdot}70$; $\int_{-\infty}^{+\infty} Hdy = 126$ kilo-oersted cm.

(*c*) *Magnetization.* To energize the magnet, coils were placed on the poles and the air gap tightly packed with soft iron bars. Initially, 85 000 ampere turns were employed and later 128 000 ampere turns. In each case a small demagnetizing field was applied after magnetization. The observed field on removal of the keeper bars was the same for each case.

(*d*) *Field measurements.* Measurements of the variation of the field of the magnet in a plane through the centre of the gap and parallel to the pole faces were made using a search coil of small cross-sectional area and a Pye fluxmeter, calibrated by proton resonance. The basic form of the results is shown in Fig. 4 as a plot of the equipotential surfaces. Fig. 5 shows the variation of the field along the central vertical path. This is quite typical of other vertical paths. From the point of view of the cosmic-ray experiment, it is essential to know the value of $\int_{-\infty}^{+\infty} Hdy$ for vertical paths in order to determine the part of the field which may be employed if a sensibly constant value of the line integral is required over

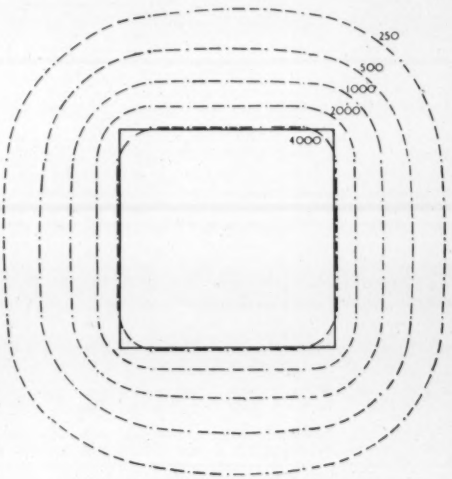

Fig. 4. Plot of the equipotential surfaces

the whole region. Over a strip 12 cm wide, the centre of the region being the vertical which passes through the centre of the magnet gap, graphical integration gave 109·0 kilo-oersted cm as the mean value, with extreme values of 109·6 and 107·8 kilo-oersted cm. Using the expression $\int_{-\infty}^{+\infty} Hdy = Hh(1 + \sigma)^{1/2}$ and a graph of $\int Hdy$, y for the mean values in this strip, the value of the leakage factor was obtained. This method gave $1 + \sigma = 1{\cdot}63$.

An investigation of the variation of the total flux flowing through the magnetic alloy, with the distance at which the readings were performed from the air gap, was made using a

single turn of wire and a fluxmeter. A further value of the leakage factor may now be presented by calculation from the ratio of the maximum value of the total flux flowing through the magnetic alloy to that flowing through the air gap, as defined by the pole faces. In this case a value of $1 + \sigma = 1 \cdot 76$ was obtained.

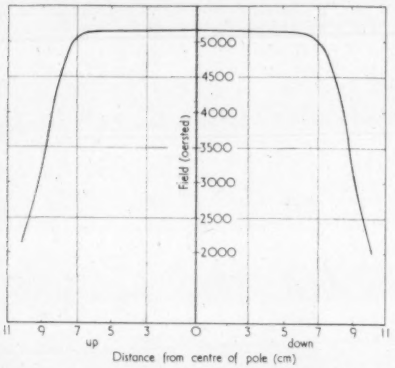

Fig. 5. Variation of the field along the central vertical path

REVIEW OF DOUBLE-YOKE MAGNET DESIGNS

Before discussing the results obtained in detail, similar designs will be discussed in cases where sufficient data could be obtained, particularly with a view to testing the results obtained by Shutt and Whittemore in their model experiments.

Table 1 shows the cases which have been considered and indicate the variety of size, shape and magnetic alloy involved. Recalling equation (4), it will be noted that one necessary piece of information is the value of μ_I. In all but one of the cases quoted, $\mu_I = 1000$ has been used, and is justified by the high flux densities involved in these designs.

Case 1. This is a single-yoke magnet built by Cockroft, Ellis and Kershaw.[2] It has been included because their observed leakage factor has frequently been used as the basis of design calculations. The magnetic material was cobalt steel. In this case the coning, occurring in the pole tips, is such that the air gap is of considerably larger cross-section than that of the poles. The experimental data recorded is that the ratio of the total flux flowing through the magnetic material at the plane where contact was made with the yoke to that crossing the end of the pole at the plane of contact with the pole tip was $1 \cdot 34$, and that the ratio of the flux through the latter to that passing through the air gap was $1 \cdot 48$, giving an overall leakage factor of $1 \cdot 98$.

By use of the preceding expression [equation (6)] a value $1 + \sigma = 1 \cdot 68$ is obtained. The agreement is not good and it should be noted that η is small for this case. In order to make an estimate of the value of the field by calculation, a value of 1700 was adopted for μ_I on account of the low flux involved. The calculated value of 2400 oersted compares favourably with the measured value of 2300 oersted.

Case 2. The value of $1 + \sigma$ guessed by Plesset, Harnwell and Seidl[3] in their design calculations was $1 \cdot 6$ following the experience of Cockroft, Ellis and Kershaw. They report that the experimental value obtained was "a little lower than this". Using the present expression, $1 + \sigma = 1 \cdot 5$ was obtained. There is no deliberate taper of the pole pieces on this design; the value $\eta = 0 \cdot 894$ taking into account fixing bolts passing through the pole pieces. Each pole face is a rectangle with sides in the ratio 2 : 1. Reasonable agreement is obtained between the calculated and observed values of the magnetic field.

Case 3. This is the magnet built by Shutt and Whittemore in the light of their model experiments. They estimated a value of $3 \cdot 5 \times 10^5$ oersted cm for $\int_{-\infty}^{+\infty} H dy$, and obtained experimentally $3 \cdot 2 \times 10^5$ oersted cm, corresponding to field values of 9050 (calculated) and 9080 (maximum field measured at the centre of the gap).

Case 4. Designed by Andrew and Rushworth[4] for use in nuclear resonance experiments, the magnet has pole pieces of circular cross-section and is tapered so that in calculations it has been necessary to use the mean cross-sectional area. This method gives $1 + \sigma = 2 \cdot 94$. Experimentally a value of $3 \cdot 0$ was obtained. It will be noted that the observed field is somewhat lower than the calculated value.

Case 5. The gap size of a magnet reported by Arnold[5] is adjustable by mechanical movement of one of the pole pieces. No comparison of leakage values was possible because of the lack of suitable information. However, Table 2 shows that a considerable discrepancy exists between calculated and observed values of the magnetic field. Further it may be noted that the discrepancy decreases as the gap size is increased.

Table 1. *Calculated and measured field values for various magnets*

Case No.	*Volume of permanent magnet material* (cm³)	A_m/A_g	A_g (cm²)	G (cm)	H (Oersted) *Calculated*	H (Oersted) *Measured*	*Magnetic material*
1	$2 \cdot 85 \times 10^4$	0·681	493	5·50	2400	2300	Cobalt Steel
2	$2 \cdot 25 \times 10^4$	0·894	824	4·00	2980	2800	"Red Dot" Alnico
3	$7 \cdot 81 \times 10^4$	1·25	824	3·18	9050	9080	Alnico V
4	$4 \cdot 29 \times 10^4$	1·85	314	5·54	5800	5500	Alcomax III
5		1·31			See Table 2		Alnico V
6	$3 \cdot 66 \times 10^2$	2·36	14·08	0·593	10700	10800	Columax
7	$3 \cdot 66 \times 10^2$	2·36	14·08	0·593	9300	8900	Alcomax III
8	$1 \cdot 96 \times 10^4$	1·84	782	3·442	7300	5900	Alcomax III

Table 2. *Comparison of calculated and measured field values for different gap sizes*

Gap size (in.)	*Calculated field* (oersted)	*Measured field* (oersted)	*Ratio of calculated to measured field values*
0·2	14700	12000	1·23
0·6	12100	10050	1·20
1·0	10200	8500	1·20
1·5	8300	7500	1·11

Cases 6, 7 *and* 8. These are examples provided by D. Hadfield.[6] Cases 6 and 7 are model experiments, again

with tapered poles of circular cross-section. A measurement of leakage gave $1+\sigma = 2{\cdot}7$, in fair agreement with a calculated value of 2·3. Case 8 is a magnet built for I.C.I. by Swift Levick and Son Ltd., and will be considered in more detail later.

CONCLUSIONS

Apart from obvious points, such as the necessity for exercising care in ascribing a value to μ_I, care in construction in order to minimize air gaps at planes of contact of the component sections and the use of a sufficiently powerful magnetizing force, four main points arise. Three relate to the expression for σ and the fourth to the relevance of the B/H curve for the magnetic material.

Conclusions related to the leakage factor. In view of the results of the magnet built by the authors and the other cases reviewed, the following extensions to the work of Shutt and Whittemore may be listed.

(i) The form $\sigma = C_1\eta\beta^1$

where $\beta^1 = Gb_G/A_G$; $\eta = A_m/A_G$ and $C_1 = 0{\cdot}95$

can be usefully applied to pole pieces of any shape, and the angle of coning is unimportant.

(ii) The magnetic material, and more significantly, the unit permeance value in the particular design does not have a great effect upon the above expression. It may however be noted that the range of unit permeance involved in the full-scale magnets reported is small, as may be expected, as optimum operating conditions will be close to the $(BM)_{max}$ condition of the demagnetization curve for the magnetic alloy.

(iii) Good results are obtained for $\sigma > 1$.

Conclusion related to the B/H curve. Reconsidering case 4, it will be recalled that the value of field obtained experimentally was somewhat lower than the calculated value. Andrew and Rushworth calculated the mean value of the product (BH) of the magnetic material from measurements of leakage and of the field in the air gap. They obtained a value of 3·25 MG-oersted which may be compared with the value of 4·75 MG-oersted expected from the demagnetization curve for the material, based on experimental determinations on comparatively small specimens.

Further evidence is obtained from cases 2, 5 and 8. Each is a large magnet, and for each there is a fairly large discrepancy between the calculated and measured field values. Certainly the difference is not accounted for by considerations of leakage. It should be noted that the reluctance of the yoke in case 5 may have been underestimated on account of the mechanical design, since small air gaps might be introduced owing to the arrangement made to allow alteration of the gap size. Also, in case 8 the designer pointed out the possibility that the soft iron pole tips may not have been fully annealed and were saturating. In the case of the Nottingham magnet the magnetic flux density in the poles was expected to be 10 200 G. The maximum measured value was 9300 G.

The effect of the choice of the value of μ_I is important. An idea of the magnitude of the effect of assuming various values of μ_I is obtained from Table 3 below.

Table 3. *Variation of expected field for various values of permeability* (μ_I)

μ_I	Expected field (oersted) Nottingham magnet	Case 4
500	5600	5600
1000	5760	5800

However, the values of μ_I chosen in the preceding work have been chosen with care and do not seem to be the source of the differences.

It may therefore be concluded, in agreement with the suggestion of Andrew and Rushworth, that the demagnetization curves for small specimens are not reliable when large blocks are to be considered, and cause a greater uncertainty in design calculations than that involved in the value of the leakage factor. However, the basic form of variation of leakage factor can be obtained from calculations of the preceding type.

ACKNOWLEDGEMENTS

We are glad to record our indebtedness to Prof. L. F. Bates, for the facilities of his laboratories and his continued interest in the work and to Dr. D. Hadfield for supplying some unpublished data on model magnets. One of us (J. E. C.) is indebted to the Department of Scientific and Industrial Research for the provision of a maintenance grant.

REFERENCES

(1) SHUTT, R. P., and WHITTEMORE, W. L. *Rev. Sci. Instrum.*, **22**, p. 73 (1951).

(2) COCKROFT, J. D., ELLIS, D. C., and KERSHAW, H. *Proc. Roy. Soc. A*, **135**, p. 628 (1932).

(3) PLESSET, E. H., HARNWELL, G. P., and SEIDL, F. G. P. *Rev. Sci. Instrum.*, **13**, p. 351 (1942).

(4) ANDREW, E. R., and RUSHWORTH, F. A. *Elect. J.* **155**, p. 1344 (1955).

(5) ARNOLD, T. J. *Phys. Rev.*, **102**, p. 136 (1956).

(6) HADFIELD, D. Private communication (1957).

Some aspects of the rheology of milk gel

By C. S. LANDAU, M.Sc., Grad.Inst.P.,* National Gas Turbine Establishment, Ministry of Supply, Farnborough, Hants

[*Paper first received* 10 *February, and in final form* 4 *June*, 1959]

Observations of the flow of milk gel have been analysed and shown to be in general agreement with Graham's theory of deformation. Individual creep curves are satisfactorily described by the sum of powers of time $t^{1/3}$, t^1 and t^3. The effect of stress on the creep of gels of various ages can be described by the sum of power terms with simple exponents. At small values of time, the strain recovered after removal of stress is proportional to the one-third power of time. There is general agreement between the predicted hysteresis loops and those observed in repeated loading tests.

LIST OF SYMBOLS

p = pressure or stress
ϵ = strain, plotted in arbitrary units
ϵ_0 = "instantaneous" strain
ϵ_R = recovered strain
t = time
w = age of gel
κ = constant (= . . . $\frac{1}{3}$, 1, 3 . . .)
β = constant (such that β/κ = 1, 2, 4, 8, . . .)
M = constant, characteristic of dimensions of specimen, etc.
D = duration of creep test
a, b, c = coefficients in the creep equation
A_1, B_1, B_2 = coefficients in the generalized creep equation
$C_1, C_2 \ldots$ = coefficients of the Nutting terms

A descriptive theory of uniaxial deformation based upon the Nutting (power-law) equation and the Boltzmann memory principle has been proposed by Graham[1, 2, 3] and shown to provide a co-ordination of results obtained in different methods of testing, for example, in creep, repeated loading, stress-relaxation, etc. Graham and Walles[3, 4] have shown that the creep and tensile behaviour of metals, particularly the Nimonic alloys, is satisfactorily described over the very broad range of stress and temperature thus far analysed. It has also been shown that certain observations made on non-metals by Scott-Blair and others[5] are generally described by the theory.

In this paper, the flow of milk gel under conditions of creep, recovery and repeated loading has been analysed in the manner suggested by Graham's theory. A broad range of age and pressure is covered. Reference is made to some of the observations reported by Scott-Blair and Burnett,[6] whose interpretation was in terms of models consisting of springs and dashpots. No attempt has been made here to refer to all of their experiments, but only to those where the stress path is comparatively simple, for example, creep and regularly repeated loading.

EXPERIMENTAL METHOD

The apparatus used is that described by Scott-Blair and Burnett.[7] In principle, a standardized sample of milk is allowed to set in a U-tube at a constant temperature of 32° C. After the desired period of ageing has elapsed, pressure is applied to one side of the column; the displacement of the meniscus at the other side is measured by the movement of an index of coloured alcohol along a narrow horizontal tube connected to the U-tube.

The process of gelling includes the formation of the bonds between the gel and the walls, so that the actual deformation of the gel occurs by a shearing mechanism. Following the treatment of Saunders and Ward,[8] the shear stress is taken to be proportional to the applied pressure and the shear strain proportional to the movement of the index. The applied pressure is measured in centimetres of kerosene and the shear strain in centimetres.

ANALYSIS OF DATA

Constant-pressure (creep) tests. According to Graham, the deformation ϵ of a material under an applied stress p (at constant temperature) can be described by the sum of a number of Nutting terms, viz.:

$$\epsilon = C_1 p^{\beta_1} t^{\kappa_1} + C_2 p^{\beta_2} t^{\kappa_2} + \ldots + \qquad (1)$$

where C, β and κ are constants. The terms can be considered to arise from the different mechanisms by which deformation proceeds. It is further postulated on experimental evidence that the constants β and κ can take on only standard values, viz., κ = . . . , $\frac{1}{3}$, 1, 3, . . . and β/κ = 1, 2, 4, 8, . . .

If deformation proceeds under constant stress, equation (1) reduces to:

$$\epsilon = \epsilon_0 + at^{1/3} + bt + ct^3 \qquad (2)$$

where ϵ_0 is a constant which takes account of the strain—both elastic and plastic—that occurs during the actual application of the load. It should be noted that a particular term in equation (2) may derive from more than one term in equation (1); this happens when the particular value of κ has associated with it more than one value of β.

Equations (1) and (2) apply directly to conditions of uniform stress while, in these tests, the stress varies with position. However, the creep curves reported by Scott-Blair and Burnett[6] appeared to be of the same form as equation (2) and therefore this analysis using Graham's equations was attempted. It has in fact been possible to describe all the creep curves by equation (2). A typical creep curve is shown

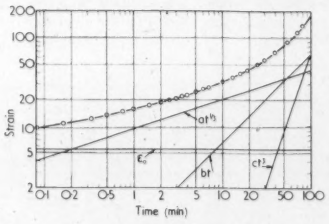

Fig. 1. A typical creep test

The curve represents equation (3), the straight lines the individual terms of that equation.

* Now at Aeronautical Research Laboratories, Department of Supply, Melbourne, Australia.

in Fig. 1, where the individual points are the experimental observations, and the full curve is the equation:

$$\epsilon = 5{\cdot}3 + 9{\cdot}2t^{1/3} + 0{\cdot}64t + 7{\cdot}7 \times 10^{-5}t^3 \qquad (3)$$

The straight lines represent the individual terms of this equation. Additional direct evidence for the existence of these standard exponents is provided in later sections.

The freedom of fitting is by no means as great as a first impression might suggest; for while the fitting to any pair of variables, say ϵ and t, might be so free as to be almost devoid of significance, the requirement of incorporating the effects of a third and fourth variable, in this instance pressure and the age of the gel, provides a very marked increase of restraint. The fitting might, according to the data, have more significance in one respect than in another.

Now equation (1) may be re-written:

$$\epsilon = (C_1p^{\beta_1} + C_2p^{\beta_2} + \ldots +)t^{\kappa_1} + (C_3p^{\beta_3} + C_4p^{\beta_4} + \\ + \ldots +)t^{\kappa_2} + \ldots + \qquad (4)$$

For one value of κ, in the simplest case, the coefficient of t^{κ_1} will be one term only, that is, Cp^{β}, where β takes its value from the series $\beta/\kappa = 1, 2, 4, 8, \ldots$ Thus, a log–log plot of coefficient against pressure (for a given age of gel) would be a straight line of slope $2^n\kappa$. It is seen that these considerations are fulfilled by the coefficient a associated with the terms with κ equal to $\frac{1}{3}$, because the plot in Fig. 2 is a family of straight lines with the standard slope $\frac{2}{3}$.

The coefficient a should also vary smoothly with age of gel at constant pressure. This is shown in Fig. 3 where a log–log plot results in a family of straight lines of slope $-\frac{1}{2}$. Thus the effect of age also can be represented by a power function, and

$$a = Aw^{-1/2}p^{2/3} \qquad (5)$$

The coefficient b (of the terms with κ equal to 1) in equation (2) is plotted logarithmically in Fig. 4 against

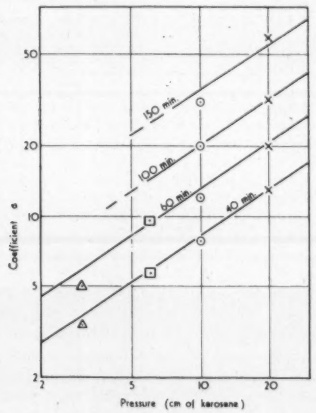

Fig. 2. Variation of the coefficient a with pressure at constant age

For clarity, the values for the gels of age 60, 100 and 150 min have been multiplied by 2, 4 and 8 respectively.

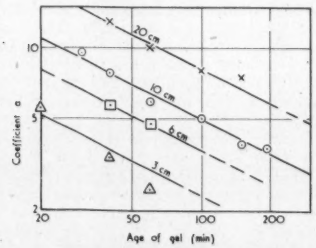

Fig. 3. Variation of the coefficient a with age of gel at constant pressure

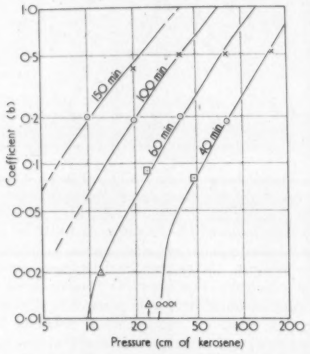

Fig. 4. Variation of the coefficient b with pressure at constant age

The pressure scale should be divided by 2, 4 or 8 for the gels of age 100, 60 and 40 min respectively.

pressure for different values of age. It is immediately obvious that, unlike the coefficient a, more than one power term is necessary to describe adequately the effect of pressure. On the evidence of metals and alloys, these terms would be summed thus:

$$b = \Sigma B'p^{\beta} \qquad (6)$$

with β taking values from the series 2^n (because now κ equals 1).

However, such a series, when plotted logarithmically, gives a graph of positive curvature (for example, curve A in Fig. 5) while the values plotted in Fig. 4 lie on a line of negative curvature. This can result if the summation of power terms is in the form

$$b^{-1} = \Sigma(B'p^{\beta})^{-1} \qquad (7)$$

(for example, curve B in Fig. 5). That is, Graham's hypothesis of power terms with standard values of exponents is retained, but the manner of summation is changed. Thus on the analogy of an electric circuit, equation (7) is similar to the parallel summation of resistances, while equation (6) corresponds to the series summation. The parallel manner of equation (7) has been used here, and the curves shown in Fig. 4 have been constructed using three terms with the standard values of β equal to 1, 2 and 16. As with the single term describing the coefficient a, each of these terms should vary in a regular manner with age (at constant pressure). It was found that, here too, the effect of age can be described

by power functions with simple exponents, and that b is given by

$$b = (B_1 w^{1/2} p^{-1} + B_2 w^{-1/2} p^{-2} + B_3 w^{-16} p^{-16})^{-1} \quad (8)$$

The exponents $\frac{1}{2}$, 1 and 2 are moderately well defined, but the exponents in the third component ($B_3 w^{-16} p^{-16}$) are the minimum values required for an adequate fit to the available data (the particular component is appreciable only for young gels at low pressure, that is, where accurate observation is particularly difficult). Equation (8) is now used for the construction of the curves in Fig. 6, where b is plotted against age. It is seen that fair agreement is obtained with the experimental values, thus providing a further check on the analysis.

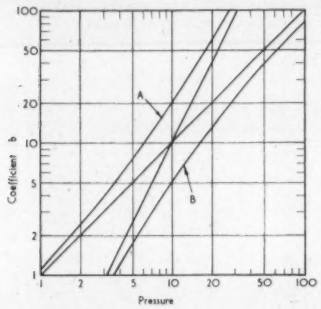

Fig. 5. Hypothetical plots of coefficient b against pressure for two component pressure terms

Several creep tests were of such duration as to provide direct evidence for the existence of a time exponent 3, but they were not sufficiently numerous to support an analysis similar to those made above for the terms with exponent $\frac{1}{2}$ and 1.

Loading modulus. In the analysis of the creep curves by equation (2), the term ϵ_0 represents the immediate deformation occurring at the application of the load. Thus p/ϵ_0 might be equivalent to an elastic modulus and should show a smooth variation with the age of the gel if the term ϵ_0 does reflect a property of the gel. That this is so is shown in Figs. 7(*a*) and 7(*b*) where Mp/ϵ_0 and log Mp/ϵ_0 respectively are plotted against the logarithm of the age. (The value of the constant M, which is characteristic of the specimen size, etc., is taken from Scott-Blair and Burnett.[6])

In the early stages of the experimental programme, the manner in which the pressure was applied sometimes introduced a slight constant error into the strain measurement, tending to make the observed ϵ_0 greater than the true ϵ_0. With this in mind, the lines in Figs. 7(*a*) and 7(*b*) are drawn to envelop the observed values of Mp/ϵ_0. The lines on each figure correspond, but these are drawn by inspection only, no attempt being made at a theoretical interpretation.

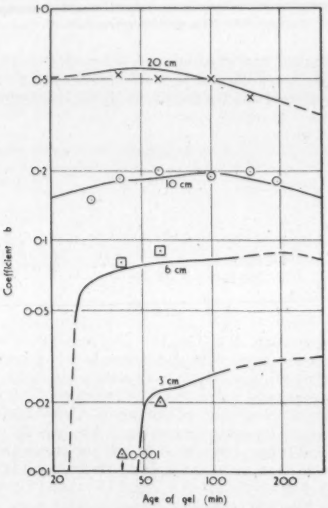

Fig. 6. Variation of the coefficient b with age of gel at constant pressure

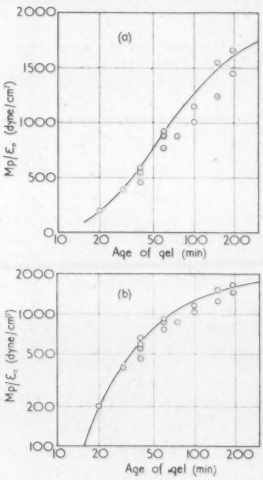

Fig. 7. Variation of loading modulus with age of gel

It should be noted that this loading modulus is not identical with that of Scott-Blair and Burnett.[7] Their use of a linearized recovery curve involves the two terms ϵ_0 and $at^{1/3}$. However, the variation found in this analysis [Fig. 7(*a*)] is similar to that found by Scott-Blair and Burnett[6] because, in this instance, ϵ_0 and $at^{1/3}$ each behave similarly with respect to age.

Recovery. After the completion of each creep test, the recovery of creep strain was observed for times up to 300 min. Now, if the conditions of constant pressure during the creep test and zero pressure after completion of test are inserted in Graham's equation [equation (14)], and integration performed for values of $\kappa \leqslant 1$, it can be shown that the recovered strain ϵ_R is given by

$$\epsilon_R = \epsilon_0 + a\{(D^{1/3} + t^{1/3}) - (D + t)^{1/3}\} \quad (9)$$

where t is time after completion of the creep test, D is duration of the creep test, and ϵ_0 and a are the same as in equation (2). If $t \ll D$, equation (9) reduces to

$$\epsilon_R = \epsilon_0 + at^{1/3} \tag{10}$$

If $t \gg D$, ϵ_R approaches a limit given by

$$\epsilon_R = \epsilon_0 + aD^{1/3} \tag{11}$$

When the observations were plotted on log–log scales (see Fig. 8) it was found in every experiment (for periods under load of between 1 and 130 min) that the initial slope

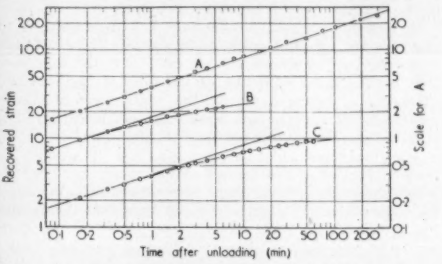

Fig. 8. Typical creep-recovery observations
The curves represent equation (12).

is $\frac{1}{3}$, with no indication of any instantaneous recovery occurring when the load is removed. Thus direct evidence is provided for the validity of the time exponent $\frac{1}{3}$, whilst the absence of any instantaneous recovery (as distinct from time-dependent recovery) indicates that the strain ϵ_0 in the creep equation [equation (2)] is not, in the present instance, recoverable and does not represent a true elastic strain. [It should be noted that in equation (2), ϵ is the total strain produced by the application of pressure.]

The whole of each recovery plot can be adequately described by equation (9) with a change in the value of the constants. That is, the equation is written:

$$\epsilon_R = a_1\{(D_1^{1/3} + t^{1/3}) - (D_1 + t)^{1/3}\} \tag{12}$$

This equation was used to draw the curves shown in Fig. 8.

Although the use made here of equation (14) has provided a very satisfactory description of the observed recovery, the equation does require modification because the inclusion, in this instance, of terms with κ greater than 1, would lead to a continually increasing strain at large values of time.

Repeated loading. A few experiments have been made by Scott-Blair and Burnett[6] on the effect of repeated loading. The pressure was raised (or lowered) in steps of about 2 cm of kerosene every 10 s, the strain being observed at the end of each period. A typical result is shown in Fig. 9(*a*). This sample of gel had an age of about 90 min, and before being tested in repeated loading, had undergone a modulus test in the course of which it was under the full test pressure for 1 min.

The stress path in these experiments is such that direct evaluation of equation (14) (as was done in the case of recovery) is difficult, while it is simpler to employ a graphical method similar to that given by Graham and Walles[3] (p. 109). Now the shape of the stress-strain loop depends on the values of both β and κ, and the analysis of the creep data forecasts that, in the above experiment, the significant term is that having β equal to $\frac{1}{3}$ and κ equal to $\frac{1}{3}$. For these values it can be shown[9] that the predicted loops have the form illustrated in Fig. 9(*b*). Comparison with Fig. 9(*a*) shows that there is excellent agreement with the experimentally observed loops:

(i) the straight line observed for increasing pressure on the first cycle becomes curved on succeeding cycles;
(ii) the average slope of this line increases with cycle number;
(iii) the unloading half-cycle has more curvature than the loading half-cycle, particularly at the start of the test.

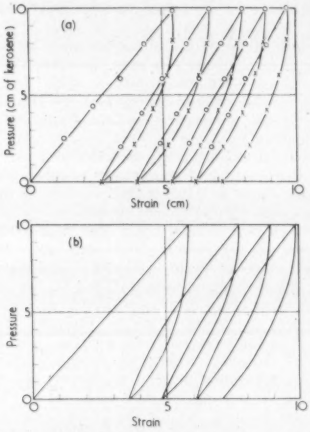

Fig. 9. Stress-strain curves for repeated loading
(*a*) Experimentally observed curve.
(*b*) Form predicted for a deformation term $p^{2/3}t^{1/3}$.

DISCUSSION

It has been usual to describe those systems which are neither truly elastic nor viscous by various groupings of elastic and viscous elements (springs and dashpots). The usefulness of this approach has decreased as the range of observations has extended, because it has been found necessary to modify the models either by the addition of further elements or by attributing complex behaviour to the existing elements.

One of the early attempts at a mathematical description of plastic behaviour is that of Nutting.[10] Scott-Blair and his co-workers[11] have shown that Nutting's equation applies to many materials, but that in some cases it does break down. They[11, 12] postulate the Principle of Intermediacy and propose the use of fractional differentials to describe those systems, the properties of which are intermediate between elastic and viscous. They suggest the equation

$$\frac{d^{\mu+\omega}\epsilon}{dt^{\mu}dp^{\omega}} = \text{const.}, \tag{13}$$

where μ and ω are generally not whole numbers. Nutting's equation, Hooke's law, etc., are special limiting cases of this equation.

An alternative approach is that of Graham,[2, 13] who pointed out that Nutting's equation expresses a unique relationship between the variables, and hence takes no account of the previous history of the material. To avoid this difficulty, Graham suggested that Nutting's equation

"was obeyed only for incremental changes, while relations between finite quantities were to be calculated by a linear superposition of Nutting elements". He tentatively chose the expression

$$\epsilon = \psi \int_0^t (t-\tau)^{\kappa} \frac{d(p^{\beta})}{d\tau} d\tau \qquad (14)$$

in which τ represents any previous instant of time and t a particular current instant of time. In principle, each term of equation (1) is of this form, and represents the evaluation of the integral when the loading path is fixed and specified. Although it seems that equation (13) may embrace equation (14), mathematical difficulties make the former less amenable to detailed analysis than the latter. In fact, the development of Graham's theory is such that graphical techniques are frequently appropriate for the analysis of behaviour under particular test conditions, for example, repeated loading.

In order to check adequately the validity of any integrative theory of deformation, it is necessary to make observations over a wide range of experimental conditions in order to reduce the probability of chance agreement. In the series of tests described here, several creep tests have extended over three cycles of logarithmic time and have entered the accelerating stage of creep. In every case, equation (2), involving the time exponents $\frac{1}{3}$, 1 and 3, has provided a satisfactory description of the strain-time variation.

Independent confirmation of the exponent $\frac{1}{3}$ has been obtained from the creep-recovery analysis. The theoretical prediction of the creep recovery involved two postulates: the principle of superposition, and an assumption [given by equation (2)] concerning the time variation of creep strain. The clear observation that the recovered strain is (initially) proportional to $t^{1/3}$ provides ample corroboration of the exponent $\frac{1}{3}$, while the large measure of configurational agreement between theory and experiment supports the use of a superposition principle, although some modification in the manner of its application is evidently necessary in order to bring the predicted magnitudes into closer agreement with those actually observed. (Scott-Blair and Burnett[6] have shown that, under limiting and simplified conditions, a principle of superposition does apply with fair accuracy to rennetted milk gel.)

The evidence for the exponents $\frac{1}{3}$ and 1 is further supported by the analysis of the families of creep curves, which showed that each of the components $at^{1/3}$ and bt varies in a smooth manner both with age of gel and with pressure.

The straight line obtained when the coefficient a was plotted against pressure (Fig. 2) is particularly significant in that it provides direct evidence for the standard value, $\beta/\kappa = 2$. Additional support for the standard values $\beta/\kappa = 2$ and $\kappa = \frac{1}{3}$, comes from the general agreement between the predicted hysteresis loops and those observed in repeated loading (Fig. 9), because the particular shape predicted depends upon the operative values of β/κ and of κ, in this instance 2 and $\frac{1}{3}$ respectively. Support is also given for the use of the superposition principle, which is directly involved in the prediction of the loops.

In the analysis of the bt component of the creep curves, three standard values of β/κ (1, 2 and 16) have provided a satisfactory description of the effect of pressure (Fig. 4) and of age (Fig. 6). A significant feature of this part of the analysis has been the manner in which the power terms are summed. In all cases of tensile creep of metals and alloys investigated by Graham and Walles,[3, 4] a series summation of the power terms has been appropriate, but in these experiments with milk gel, a parallel summation of terms has been necessary [equation (7)]. It is analogous to the series and parallel arrangements of springs and dashpots frequently employed in rheology. Thus, Scott-Blair and Burnett[6] use a Burgers model to describe the behaviour of milk gel in a region where the present analysis produces the equation

$$\epsilon = \epsilon_0 + Aw^{-1/2}p^{2/3}t^{1/3} + \frac{t}{(B_1 w^{1/2}p^{-1} + B_2 w^{-1/2}p^{-2})} \qquad (15)$$

However, the similarity between the arrangement of terms in this equation and the arrangement of springs and dashpots in the Burgers model is probably fortuitous.

In seeking a physical interpretation of the results of this analysis, the simplest guide is to suppose that each term represents an "independent" process. The first term is ϵ_0, that is, the strain occurring at the time of application of pressure. Consideration of the recovery observations indicates that it represents some kind of thixotropy[14] or static fatigue[15] which is complete within 1 min.

The time-dependent terms represent the "flowability" of the gel. The first of these terms to be effective is $Aw^{-1/2}p^{2/3}t^{1/3}$. Thus, the initial "flowability" is inversely proportional to the square-root of the age of the gel. After the deformation has proceeded for some minutes, the processes represented by the bt term become effective. That part proportional to $w^{-16}p^{-16}$ is very soon negligible, and attention may be concentrated generally on those proportional to $w^{1/2}p^{-1}$ and $w^{-1/2}p^{-2}$. It is seen that increase of age causes one term ($w^{1/2}p^{-1}$) to increase and the other ($w^{-1/2}p^{-2}$) to decrease. There is probably some co-relation between these terms and the manner in which the gel synereses, for it has been observed that an increase in age results in an increase in the quantity of syneretic liquid that appears at the end of the specimen and a decrease in that appearing on the walls of the tube.

It is noteworthy that the effect of age can be described by power functions with simple values of exponent, but the significance of this is outside the scope of this paper.

ACKNOWLEDGEMENTS

The author wishes to thank Dr. Scott-Blair and Mr. Burnett of the National Institute for Research in Dairying for giving him access to their equipment and experimental observations, and Mr. Burnett for his assistance in carrying out additional tests. He is indebted to them and to his colleagues at the National Gas Turbine Establishment for much stimulating discussion. The paper is published by permission of The Controller, Her Majesty's Stationery Office.

REFERENCES

(1) GRAHAM, A. *The Engineer*, **193,** p. 198 (1952).
(2) GRAHAM, A. *Research*, **6,** p. 92 (1953).
(3) GRAHAM, A., and WALLES, K. F. A. *J. Iron Steel Inst.*, **179,** p. 105 (1955).
(4) GRAHAM, A., and WALLES, K. F. A. *Aero. Res. Council, Current Papers*, **379** and **380**.
(5) SCOTT-BLAIR, G. W. *A Survey of General and Applied Rheology* (London: Sir Isaac Pitman and Sons Ltd., 1949).
(6) SCOTT-BLAIR, G. W., and BURNETT, J. *Brit. J. Appl. Phys.*, **10,** p. 15 (1959).
(7) SCOTT-BLAIR, G. W., and BURNETT, J. *Lab. Practice*, **6,** p. 570 (1957).
(8) SAUNDERS, P. R., and WARD, A. G. *Proc. II Internat. Congr. Rheology*, p. 284 (London: Butterworths Scientific Publications, 1953).
(9) LANDAU, C. S. Unpublished work.

(10) NUTTING, P. G. *Proc. Amer. Soc. Test. Mat.*, **21**, p. 1162 (1921).
(11) SCOTT-BLAIR, G. W., VEINOGLOU, B. C., and CAFFYN, J. E. *Proc. Roy. Soc. A*, **189**, p. 69 (1947).
(12) SCOTT-BLAIR, G. W., and CAFFYN, J. E. *Phil. Mag. (VII)*, **40**, p. 80 (1949).
(13) GRAHAM, A. Contribution to discussion on paper by McCallion and Davies, *Proc. Instn Mech. Engrs*, **169**, p. 1135 (1955).
(14) SCOTT-BLAIR, G. W., and BURNETT, J. *Brit. J. Appl. Phys.*, **10**, p. 97 (1959).
(15) REINER, M. *Rheol. Acta*. (In process of publication.)

Correction for size of cross-section of the secondary windings of mutual inductance standards of the Campbell type

By P. VIGOUREUX, D.Sc., National Physical Laboratory, Teddington, Middlesex

[*Paper received* 18 *June*, 1959]

It is shown that the mutual inductance of standards of the Campbell type can be obtained with negligible error by replacing each turn of the secondary winding by a circle at the centre of the cross-section of the wire.

The total inductance is the sum of the inductances of individual circles; this sum is expressed by a formula which is shown to agree with Searle's formula provided the length and breadth of winding used in the latter are based on the mean spacing and the mean number of wires in the rows and layers.

1. INTRODUCTION

Mutual inductance standards of the Campbell type consist of a primary made of two similar coaxial helices with a gap in between, and a coaxial secondary placed in a symmetrical position between the two halves of the primary; for reasons which will become clear later the cross-section of the secondary coil is kept small and as nearly square as possible. It is usual to calculate first the mutual inductance between the primary and a circle at the centre of the cross-section of the secondary, and then to apply a correction for the finite size of that cross-section. In the past this correction has been calculated according to a formula due to Searle and often incorrectly quoted, but given correctly by Astbury.[1] This formula applies to a secondary of rectangular cross-section of axial length $2X$ and radial depth $2Y$, and the current is assumed to be uniformly distributed; b is the radius of the circle at the centre of the cross-section, Fig. 1, M_0 the mutual

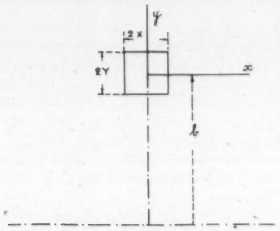

Fig. 1. Section of channel of secondary winding of mutual inductance

inductance of the primary and that circle, x is measured axially and y radially from a point on the circle. The correction is

$$M - M_0 = \frac{1}{6} \cdot \frac{X^2}{b} \cdot \frac{\partial M}{\partial y} + \frac{1}{6}(Y^2 - X^2) \frac{\partial^2 M}{\partial y^2} \qquad (1)$$

and it is kept small by making X and Y as nearly equal as possible, and choosing the radius b so that $\partial M/\partial y$ vanishes.

In practice the secondary has a large number of turns packed as uniformly as possible in a square channel, and the mutual inductance is found by multiplying M by the number of turns; but for the purpose of this paper it is convenient to refer all corrections to a single turn.

Formula (1) is, however, based on uniformity of current over the cross-section $4XY$, a condition which naturally is not fulfilled if the winding consists of a number of turns. It is therefore instructive to compare it with the result obtained by calculating the mutual inductance of each turn separately, and averaging; it will still be necessary to assume that the position of each turn is known, and in fact only if the turns are wound in a regular pattern will the final formula be of any use for comparison with (1). But in like manner formula (1) is not applicable to a multi-turn winding unless the pattern is regular.

The calculation of the mutual inductance of each turn can be broken down into two parts: first that of the mutual inductance of a circle at the centre of the cross-section of the wire, next that of the error due to the finite size of the wire. It will be shown that with any reasonable assumption for current distribution over the cross-section, this latter error is negligible for wires of the size used in the mutual inductance standards of the National Physical Laboratory. It will also be shown that the values ascribed to X and Y must be based not on the size of the channel but on the spacing of the wires.

2. RELATIONS BETWEEN DIFFERENTIAL COEFFICIENTS OF MUTUAL INDUCTANCE

For a coaxial circle half way between the two primaries

$$\frac{\partial^{m+2n+1} M}{\partial^{2n+1} x \partial^m y} = 0 \qquad (2)$$

Also for any coaxial circle

$$\frac{\partial^2 M}{\partial x^2} + \frac{\partial^2 M}{\partial y^2} = \frac{1}{b+y} \cdot \frac{\partial M}{\partial y} \qquad (3)$$

from which relations between coefficients of higher order can be obtained by differentiation.

Formulae for calculating M, $\partial M/\partial y$, $\partial^2 M/\partial y^2$, $\partial^3 M/\partial y^3$, $\partial^4 M/\partial y^4$ can be adapted from Vigoureux,[2] and all othor coefficients up to the 4th order calculated from these. Fer

the present purpose it is simpler to take a concrete example for which these coefficients have already been worked out. Dye and Hartshorn[3] give for the mutual inductance, referred to one turn, of the standard presented to the Imperial Government of Japan,

$$M - M_0 = 31{\cdot}82(x^2 - y^2) - 1{\cdot}79\,y^3 + 6{\cdot}62x^2y \qquad (4)$$

from which

$$\frac{\partial M}{\partial y} = \frac{\partial M}{\partial x} = 0$$

$$\frac{\partial^2 M}{\partial x^2} = 63{\cdot}64$$

$$\frac{\partial^2 M}{\partial y^2} = -63{\cdot}64$$

$$\frac{\partial^3 M}{\partial y^3} = -10{\cdot}74$$

$$\frac{\partial^3 M}{\partial x^2 \partial y} = 13{\cdot}24$$

For the standard in question

$$M_0 = 21\,526{\cdot}7 \text{ c.g.s. units}$$
$$b = 25{\cdot}7128 \text{ cm}$$
$$X = 0{\cdot}508 \text{ cm}$$
$$Y = 0{\cdot}521 \text{ cm}$$
$$\rho = 0{\cdot}020\,55 \text{ cm}$$

where ρ is the radius of the bare wire. There are 22 layers of 21 turns each, and the diameter of the insulated wire is 0·0477 cm. In addition to these 462 turns, there are three more required to bring the mutual inductance to the nearest possible multiple of 10, but they need not be considered in this paper.

3. ERROR DUE TO FINITE SIZE OF WIRE

First assume equal electrical resistance of all component filaments of equal area, in other words uniform current distribution, and consider a wire with its central filament at distances x, y from the neutral circle. Taking co-ordinates r, θ, evaluate

$$M = \frac{1}{\pi\rho^2}\int_0^{2\pi}\int_0^{\rho} M_{xy}(r\cos\theta, r\sin\theta)\,.\,r dr d\theta$$

$$= M_{xy} + \frac{\rho^2}{8(b+y)}\cdot\frac{\partial M_{xy}}{\partial y} + \frac{\rho^4}{192(b+y)^2}\cdot\frac{\partial^2 M_{xy}}{\partial x^2}$$

in which the differential coefficients are to be taken at the point x, y. They can, however, be referred to those at the neutral circle 0, 0; remembering that there the relations (2) hold and $\partial M/\partial y$ vanishes, we find

$$M = M_{xy} + \frac{\rho^2}{8b}\left(y\frac{\partial^2 M}{\partial y^2} + \frac{x^2}{2}\frac{\partial^3 M}{\partial x^2\partial y} + \frac{y^2}{2}\frac{\partial^3 M}{\partial y^3}\right) + \frac{\rho^4}{192b^2}\left(\frac{\partial^2 M}{\partial x^2} + y\frac{\partial^3 M}{\partial x^2\partial y}\right) \qquad (5)$$

in which y/b has been neglected compared with unity.

Inspection of this formula shows that even with the maximum values of x and y, viz. 0·508 cm and 0·521 cm, and with the values of the coefficients given above, the second and third terms of the first bracket are each less than a tenth part of the first; they also tend to cancel each other. Thus the maximum relative error is given accurately enough by inserting the maximum value of y in

$$\rho^2 y\frac{\partial^2 M}{\partial y^2}\Big/8bM$$

which has the negligible value -3×10^{-9}. The error for all the wires taken together is nothing like so large as this since the term of (5) containing the first power of y vanishes when the sum is taken.

The error has been calculated for uniform current distribution, and it is necessary to find out whether it is still negligible with other reasonable assumptions for distribution of current. One such assumption is that the resistance of a filament is proportional to its length and the current density J inversely proportional to the resistance; thus if the total current is unity we assume J equal to $k/(b + y + r\sin\theta)$ where r is the distance from the centre of the wire and θ the angle measured from the x-axis. By integration over the cross-section of the wire,

$$J = \frac{1}{\pi\rho^2}\left\{1 - \frac{\rho^2}{4(b+y)^2} - \frac{r\sin\theta}{b+y} + \frac{r^2\sin^2\theta}{(b+y)^2}\cdots\right\}$$

The mutual inductance is

$$M = \int_0^{2\pi}\int_0^{\rho} J M_{xy}(r\cos\theta, r\sin\theta)\,.\,r dr d\theta$$

which becomes

$$M = M_{xy} - \frac{\rho^2}{8(b+y)}\frac{\partial M_{xy}}{\partial y} + \frac{\rho^4}{64(b+y)^2}\left(\frac{1}{b+y}\frac{\partial M_{xy}}{\partial y} + \frac{\partial^2 M_{xy}}{\partial y^2}\right)\cdots$$

and when, as before, the coefficients are expressed in terms of those for the neutral circle, and y/b is neglected compared with unity,

$$M = M_{xy} - \frac{\rho^2}{8b}\left(y\frac{\partial^2 M}{\partial y^2} + \frac{x^2}{2}\frac{\partial^3 M}{\partial x^2\partial y} + \frac{y^2}{2}\frac{\partial^3 M}{\partial y^3}\right) + \frac{\rho^4}{64b^2}\left(\frac{\partial^2 M}{\partial y^2} + y\frac{\partial^3 M}{\partial y^3}\right) \qquad (6)$$

Comparison with (5) shows that the error with this distribution is very nearly equal in magnitude but opposite in sign to the error with uniform distribution, a property of uniform and "natural" distributions which had been indicated by Ayrton, Mather and Smith[4]. Since the actual distribution is not likely to lie outside the two above, the actual error is in the present case always negligible.

To sum up, no appreciable error is introduced by the assumption that each wire is a filament of infinitely small cross-section.

4. CORRECTION FOR FINITE SIZE OF SECONDARY WINDING

It is required to find the average of the inductances of individual turns.

When condition (2) holds the inductance of a circle at x, y referred to that of a circle at 0, 0 is

$$M(x,y) = M_0 + y\frac{\partial M}{\partial y} + \frac{1}{2}x^2\frac{\partial^2 M}{\partial x^2} + \frac{1}{2}y^2\frac{\partial^2 M}{\partial y^2} + \frac{1}{2}x^2y\frac{\partial^3 M}{\partial x^2\partial y} + \frac{1}{6}y^3\frac{\partial^3 M}{\partial y^3} + \cdots$$

Consider first the case when there are $2m$ identical rows of $2n$ turns each as in Fig. 2. The average of $2m$ turns of a row at y gives

$$M(y) = M_0 + y\frac{\partial M}{\partial y} + \frac{1}{2}y^2\frac{\partial^2 M}{\partial y^2} + \frac{1}{6}y^3\frac{\partial^3 M}{\partial y^3} + \\ + \frac{1}{2m}\sum_0^{m-1}(p+\tfrac{1}{2})^2\xi^2\left(\frac{\partial^2 M}{\partial x^2} + y\frac{\partial^3 M}{\partial x^2\partial y}\right) + \dots \\ = M_0 + y\frac{\partial M}{\partial y} + \frac{1}{2}y^2\frac{\partial^2 M}{\partial y^2} + \frac{1}{6}y^3\frac{\partial^3 M}{\partial y^3} + \\ + \frac{(4m^2-1)\xi^2}{24}\left(\frac{\partial^2 M}{\partial x^2} + y\frac{\partial^3 M}{\partial x^2\partial y}\right) + \dots$$

The average for the $2n$ layers becomes

$$M = M_0 + \frac{(4n^2-1)\eta^2}{24}\frac{\partial^2 M}{\partial y^2} + \frac{(4m^2-1)\xi^2}{24}\frac{\partial^2 M}{\partial x^2}.$$

If X and Y be defined as $m\xi$ and $n\eta$ the correction becomes

$$M - M_0 = \left(1 - \frac{1}{4n^2}\right)\frac{Y^2}{6}\frac{\partial^2 M}{\partial y^2} + \left(1 - \frac{1}{4m^2}\right)\frac{X^2}{6}\frac{\partial^2 M}{\partial x^2} \quad (7)$$

When $1 - 1/4m^2$ and $1 - 1/4n^2$ are sufficiently close to unity to have no appreciable effect on the correction, which is itself small to start with, and when account is taken of relation (3), (7) becomes identical with Searle's formula (1).

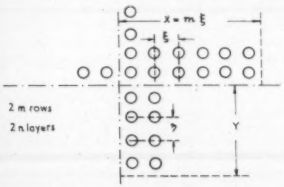

Fig. 2. Possible disposition of turns of secondary winding

If the number of rows or layers is odd, say $2m + 1$ or $2n + 1$, formula (7) still applies provided X or Y are taken to be $(m + \frac{1}{2})\xi$ or $(n + \frac{1}{2})\eta$. This is equivalent to saying that in both cases the boundary of the channel must be supposed to be at a distance from an end wire equal to half the spacing between wires.

If formula (1) is applied to the mutual inductance standard whose dimensions are given in section 2, and the values there given for X and Y are used, the relative correction $(M - M_0)/M_0$ is found to be -66×10^{-7}, whereas the more accurate formula (7) gives $-66{\cdot}4 \times 10^{-7}$; the difference is negligible.

The values of X and Y calculated from the rule above and from the diameter of the insulated wire are 0·501 and 0·525 cm, in fair agreement with the values used by Dye and Hartshorn[3] and reproduced in Section 2, indicating perhaps very slight looseness of the rows and still slighter crushing of the layers. These small changes in X and Y nevertheless cause a change of nearly 100% in the relative correction calculated from (1) or (7), which illustrates the desirability not only of arranging for X and Y to be equal, but of striving to keep the uncertainty in $X - Y$ as small as possible.

In another type of secondary winding the turns of a layer instead of being vertically above or below those of the adjacent layer, are half way between as in Fig. 3. G. H. Rayner has pointed out to the writer that if the number of layers is even, say $2n$, and the number of rows $2m + 1$ and $2m$ alternately, the correct value to take for Y is still $n\eta$, but for X it is $(m + \frac{1}{2})\xi$; the correcting factor for X^2 is then $1 - 1/16m^2$ and that for Y^2 the same as before, namely $1 - 1/4n^2$. If the rows are as before but there are $2n + 1$ layers the expressions for X and Y are a little more complicated, but always based on the density of winding. It will be found that X must be made

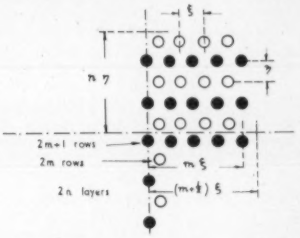

Fig. 3. Alternative disposition of turns of secondary winding

$$\frac{(n+1)(m+\frac{1}{2}) + nm}{2n+1}\xi$$

in Searle's formula, and Y made

$$\frac{(2m+1)(n+1) + 2nm}{4m+1}\eta,$$

but the correcting factors for the terms in X^2 and Y^2 are still as above, and thus the error made by making them equal to unity is in general negligible.

In formulae (1) and (7) terms of the fourth order in X and Y have been neglected. When they are included, (1) becomes

$$M - M_0 = \frac{X^2}{6}\frac{\partial^2 M}{\partial x^2} + \frac{Y^2}{6}\frac{\partial^2 M}{\partial y^2} + \\ + \frac{X^4}{120}\frac{\partial^4 M}{\partial x^4} + \frac{X^2Y^2}{36}\frac{\partial^4 M}{\partial x^2\partial y^2} + \frac{Y^4}{120}\frac{\partial^4 M}{\partial y^4} \quad (8)$$

The last three terms probably contribute only a few parts in 10^7 to the inductance, but a verification that they do not contribute a significant amount seems called for at least for one standard out of several which do not differ markedly in dimensions.

5. CONCLUSION

For wire of the size normally used in the secondary winding of a mutual inductance standard of the Campbell type, the error in the calculated mutual inductance made by replacing the wire by a circle at the centre of the cross-section is negligible.

For a secondary wound in a regular pattern, the correction for the finite size of winding is given to a sufficient accuracy by Searle's formula, provided the length and breadth used in the formula are based on the mean spacing and mean number of wires in the rows and layers.

6. REFERENCES

(1) ASTBURY, N. F. *Phil. Mag.*, **25**, p. 290 (1938).
(2) VIGOUREUX, P. *N.P.L. Coll. Res.*, **24**, p. 277 (1938).
(3) DYE, D. W., and HARTSHORN, L. *N.P.L. Coll. Res.*, **21**, p. 1 (1927).
(4) AYRTON, W. E., MATHER, T., and SMITH, F. E. *N.P.L. Coll. Res.*, **4**, p. 1 (1908).

NEW BOOKS SECTION

Contents

PAGE

Aerodynamics, flow and mechanics

Handbook of supersonic aerodynamics. Section 7: Three-dimensional airfoils (Navord Report 1488, Vol. 3) . . 485

Introduction to the theory of compressible flow . . . 485

Chemistry and the properties of materials

The determination of molecular structure 485

Electrolyte solutions 485

Electrophoresis: Theory, methods and application . . . 486

Forschung und Entwicklung auf dem Gebiete des chemischen Apparatewesens in Einzelabhandlungen. Dechema-Monographien, Band 30: Kern-wissenschaft und-technik. Band 31: Laboratoriums-technik. 486

Liquids and liquid mixtures 486

Metal fatigue 487

Molecular science and molecular engineering 487

The physical metallurgy of magnesium and its alloys . . 487

Proceedings of the third conference on carbon . . . 488

Rheology of disperse systems 488

The structure of electrolytic solutions 488

Techniques of polymer characterization 488

Heat, thermometry and low temperature physics

Cryogenic engineering 488

Einführung in der Wärme-und Stoffaustausch . . . 489

Seventh symposium (international) on combustion . . 489

Magnetic, electrical and electronic devices and properties

Conductance design of active circuits 489

Electromagnetic radiation from cylindrical structures . . 489

Fluctuation phenomena in semi-conductors 490

Introduction to monopulse 490

Noise in electron devices 490

Physik der halbleiter 491

Proceedings of conference on magnetism and magnetic materials 491

Progress in dielectrics. Vol. 1. 491

Semiconductors 491

The transistor era 491

PAGE

Mathematical theories, techniques, computers and control systems

Approximate methods of higher analysis 492

Calculateurs analogiques répétitifs 492

Conference on hyperconjugation 492

Dynamical analogies 492

Group theory and its applications to the quantum mechanics of atomic spectra 493

Les principes de la théorie électromagnétique et de la relativité 493

Matrix calculus 493

Methods based on the Wiener-Hopf technique for the solution of partial differential equations 494

Nonlinear problems in random theory 494

Programming for digital computers 494

Sampled-data control systems 494

Miscellaneous and general physics

La mesure précise du temps en fonction des exigences nouvelles de la science 495

Physikalisches Praktikum 495

Reports on progress in physics. Vol. XXII 495

Nuclear and cosmic-ray physics, apparatus, techniques and data

Nuclear electronics 495

Physics and heat technology of reactors 495

Premier colloque international de photographie corpusculaire 496

Progress in nuclear energy. Series I, Physics and mathematics 496

Progress in nuclear energy. Series VII, Medical sciences . 496

Progress in nuclear energy. Series IX, Vol. 1. Analytical Chemistry 496

Progress in nuclear physics. Vol. 7 496

Solid state physics and crystallography

Growth of crystals 496

Solid state physics. Advances in research and applications. Vol. 8 497

Structure reports. Vol. 14. Supplementary volume and cumulative index for 1940–1950 497

Reference books

Bibliography on industrial radiology, 1956–1959 . . . 497

Conversion factors and tables. Part I. Basis of tables conversion factors. (B.S. 350: Part I: 1959) 497

Glossary of terms used in vacuum technology . . . 497

Handbuch der Physik. Vol. VII/2 497

Handbook of supersonic aerodynamics. Section 7: Three-dimensional airfoils, (Navord Report 1488, Vol. 3) (Washington: U.S. Government Printing Office, for the Johns Hopkins University Applied Physics Laboratory). Pp. 88. Price $1.50.

A preface to the entire *Handbook of supersonic aerodynamics* appears in Volume 1 and includes a brief history of the project. As stated in Volume 1, "The primary criterion used in selecting material for the *Handbook* is its expected usefulness to designers of supersonic vehicles. Thus a collection of data directly useful in the design of supersonic vehicles, results of the more significant experiments and outlines of basic theory are included." This section of the handbook, dealing with three-dimensional airfoils, has the following chapter headings: Résumé of basic theory; Calculation of wing characteristics; Numerical examples; Comparison of theory and experiment; Limitations of the linearized theory.

Aerodynamics, flow and mechanics

Introduction to the theory of compressible flow. By SHIH-I PAI. (New York: D. Van Nostrand Co. Inc.; London: D. Van Nostrand Co. Ltd., 1959.) Pp. xiii + 385. Price 73*s*.

Considered as an introduction to the theory of compressible flow, this book is considerably more ambitious in the ground it covers than one might reasonably expect. My own view is that the ground it covers is too wide, and that the exposition suffers in consequence.

It is surprising, for instance, to find the author devoting some pages to introducing vector notation (with, at best, some ambiguous statements about area and volume). It is perhaps not quite so surprising to find in this day and age a chapter on magneto-gas dynamics (though I think its omission could be defended in a book with the above title), but surely the discussion of electromagnetic units is out of place here. Detonation, covered in the chapter on shock waves, is certainly more at home within these pages, but the brevity with which it is treated makes one wonder about the wisdom of including it.

On the other hand, the book would, in my opinion, have benefited from a fuller treatment of some of the basic principles, such as dynamical similarity, thermodynamics, shock wave structure (which I found misleading) and, in the chapters on viscous motion, on the stress, rate-of-strain relation and dissipation. I also think that in places the arrangement of the book could be improved; it is, for example, difficult to understand the full implications of the Prandtl–Meyer solution before the theory of characteristics.

In short I think the emphasis in an introduction should have been differently placed. In its favour one can say that many useful results are made readily accessible to the student.

L. HOWARTH

Chemistry and the properties of materials

The determination of molecular structure. By P. J. WHEATLEY. (London: Oxford University Press, 1959.) Pp. vi + 263. Price 35*s*.

There are now many experimental techniques which cast light on the arrangement of atoms in molecules, and the author has sought to provide an elementary and comprehensive introduction to them. After a discussion of symmetry the following techniques are introduced in turn:—infra-red and Raman spectroscopy; electron diffraction; X-ray diffraction; neutron diffraction; stereochemistry; electric dipole moments; magnetic susceptibility and nuclear magnetic resonance. The experimental apparatus is in each case described in only the barest outline and mathematical argument is kept to a minimum. In this way the author is able to devote a good proportion of his book to practical examples, and to a discussion of the value and limitations of each method. An outline derivation of some of the basic formulae which are quoted without proof might have aided the physical understanding of the processes and the significance of the measured quantities, but this may be asking too much of a book which covers a great deal of ground in a limited space. For the same reason one should perhaps not complain that pure quadrupole resonance and electron spin resonance find no place, though in view of its achievements high-resolution nuclear magnetic resonance might be thought to deserve more than two pages. The style is clear and misprints are rare. The book can be commended to students of both physics and chemistry as a useful comprehensive introduction to the subject.

E. R. ANDREW

Electrolyte solutions. 2nd ed. By R. A. ROBINSON and R. H. STOKES. (London: Butterworths Scientific Publications, 1959.) Pp. xv + 559. Price 63*s*.

The authors have restricted themselves to a discussion of three properties which they consider to be fundamental, viz. conductance, ionic activity, and diffusion. The interionic attraction theory of aqueous solutions and the molecular and ionic model on which it is based have now been studied sufficiently comprehensively to be included in a systematic presentation of these properties. The result is a book which is thorough and fascinating to read. The clarity of style and presentation of the subject is outstanding and will be much appreciated by the reader.

The treatment begins with the basic concepts of the influence of the solvent and solute on one another, of activity coefficients, conductance, ionic mobility and diffusion. The authors give an excellent discussion of the Debye–Hückel ionic interaction theory with its modern refinements, and the full resources of this theory are applied with a sure touch to account for the variation of conductivities with concentration.

Diffusion is given considerable space because the subject is not fully discussed in other textbooks and this contribution is particularly valuable. The ion association theory of Bjerrum is critically reviewed.

Experimental methods are described and discussed in detail, the authors' practical experience providing authentic assessment of the relative merits of different techniques. The book concludes with a chapter on the activity coefficients of ions in mixed electrolytes. Experimental data are presented in extensive tables in the appendices and there is a brief but adequate subject index. The text of this second edition has been revised to include new experimental and theoretical developments.

This admirable book provides a penetrating analysis of modern experimental and theoretical studies in the physical chemistry of electrolyte solutions and will be welcomed by students and workers in many fields.

M. G. DERIAZ

Electrophoresis: Theory, methods and application. Edited by M. BIER. (New York: Academic Press Inc.; London: Academic Books Ltd., 1959.) Pp. xx + 563. Price £5 7*s*. 6*d*.

This book comprises an Introduction by A. Tiselius and eleven articles on every possible application of electrophoresis. Two articles are theoretical, four deal with moving boundary electrophoresis, three with zone electrophoresis and one each with preparative and the microscope methods of electrophoresis. In the first two articles J. Th. G. Overbeek and J. Lijklema give a concise treatment of the charge and potential of the electrical double layer extending their analysis to curved surfaces and polyelectrolytes and K. Linderstrom-Lang and S. O. Nielson discuss the interpretation of the titration curves of proteins. L. G. Longsworth contributes two authoritative chapters on the theory and practice of moving boundary electrophoresis, the former including an invaluable section on recent developments in the field of protein-protein interaction. The more extended applications of this method are taken up by R. A. Brown and S. N. Timasheff who deal with the assessment of protein heterogeneity, the polymerization and isomerization of proteins and their behaviour at acid pHs. D. H. Moore adds a detailed review on the analysis of plasma and other body fluids.

A complete description of the procedures and materials for zone electrophoresis are given by H. G. Kunkel and R. Trautman and this article also includes an important section on theoretical principles. Ch. Wunderly discusses paper electrophoresis by reference largely to serum and incorporates much comparative information on technique and materials. The third article in this series by T. Wieland covers the analysis of substances other than proteins, e.g. sugars, amino acids, nucleotides, etc.

M. Bier writes on preparative electrophoresis without supporting media covering density gradient electrophoresis, electrodecantation, electrophoresis-convection and the newer forced-flow electrophoresis developed mainly by the author. Finally C. C. Brinton and M. A. Lauffer discuss the information that can be obtained about viruses, bacteria and cells by electrophoresis.

The authors are, without exception, authorities in the fields they review and for this reason the standard of the whole book is high. There is little doubt that it will be welcomed and used as the standard work on this subject and as such will fill a gap in current biochemical literature. Perhaps the only criticism to be made is one of scope rather than content. A number of the topics of the book, e.g. paper electrophoresis, have been extensively dealt with in recent books and monographs and it might therefore have been profitable to omit these topics and allow some expansion of the remainder. However, this must not detract from the fact that the editor deserves every praise for his efforts in producing a timely volume which can be warmly recommended to specialists and non-specialists alike.

E. M. SHOOTER

Forschung und Entwicklung auf dem Gebiete des chemischen Apparatewesens in Einzelabhandlungen. Dechema-Monographien, Band 30: Kern-wissenschaft und-technik. (Frankfurt: Dechema, 1958.) Pp. 260. Price DM 30.

This monograph contains 15 papers on nuclear chemical and engineering topics, divided roughly as follows: isotope applications (6), materials problems (4), chemical processing and waste disposal (2), counting methods (2), and reactor instrumentation (1). Reviews are included of fuel element design and testing, materials testing under irradiation, and corrosion in aqueous reactor systems, while the control and instrumentation of the Karlsruhe reactor is described in some detail. Three specialist papers of interest deal with the use of tracers to study the corrosion of metallic surfaces by H_2S, measurement of wear in Diesel- and petrol-engine cylinders, and the distribution of water flowing from rivers into lakes or the open sea.

In some cases the article presented might to advantage have been either enlarged or supplemented to give a wider review of the field in question; the reviewer would have liked to see more comprehensive coverage, for example, of chemical processing and of waste disposal. An article on the analytical problems associated with nuclear technology would have been a useful addition. These, however, are minor criticisms of a book which should prove to be a useful introductory text, particularly for Continental workers.

C. B. AMPHLETT

Forschung und Entwicklung auf dem Gebiete des chemischen Apparatewesens in Einzelabhandlungen. Dechema-Monographien, Band 31: Laboratoriums-technik. (Frankfurt: Dechema, 1959.) Pp. 297. Price DM 32.80.

This book is a collection of twenty-five papers read at a conference held in conjunction with the ACHEMA Exhibition in 1958. The papers cover a wide range of laboratory equipment and refer almost exclusively to apparatus shown at the exhibition for the first time. Subjects discussed include: application of sedimentation balances, ultracentrifuges, various titration methods, high-vacuum distillation, electrophoresis and improvements in a number of standard laboratory tests and equipment. The quality of the papers is variable. Besides excellent contributions on problems such as the sedimentation balance or high-frequency titrations, there are a number of review articles containing hardly anything new. Not unexpectedly, there is also present a certain lack of balance, e.g. developments in the field of ultra-centrifuges being followed by improvement in the method of moisture determination, which consists of introducing the vapours at the top of the condenser instead of at the bottom. The wide range of subjects discussed makes the usefulness of the book debatable. One cannot help feeling that a better purpose would have been served by having the papers published in the relevant journals.

H. SAWISTOWSKI

Liquids and liquid mixtures. By J. S. ROWLINSON. (London: Butterworths Scientific Publications, 1959.) Pp. ix + 360. Price 75*s*.

This is an advanced treatise which, in three sections, describes and interprets the behaviour of liquids in equilibrium with their vapours.

The first section discusses the thermodynamics of pure fluids from the triple point to the critical point. The second section begins with a discussion of liquid mixtures at moderate pressures in terms of the excess thermodynamic functions. This is followed by a more qualitative description of the behaviour of mixtures at high pressure. In the third section an account is given of the statistical thermodynamics of fluids and the interpretation of the experimental results in terms of intermolecular forces.

The book will appeal to two types of reader: the specialist

with a good knowledge of thermodynamics and mathematical techniques who wishes to follow the closely reasoned argument, and the physical chemist or chemical engineer who has here a vast amount of factual information in a source-book distinguished from others by its thermodynamic approach. Each will find it necessary to read selectively but both will find the book of great value.

A. E. BROWN

Metal fatigue. Edited by J. A. POPE. (London: Chapman and Hall Ltd., 1959.) Pp. xiv + 381. Price 70*s*.

This book to some extent disarms the critic since, in his foreword, Prof. Pope makes clear most of the disadvantages likely to be found in reading a volume of this kind. It is an account of a course of lectures given at Nottingham University in 1955, and inevitably there is great unevenness in presentation of the individual chapters, and some repetition is only so be expected. By its nature, therefore, this is a book which is not likely to make enjoyable reading and, for example, Cazaud's *Fatigue of Metals* even in translation by Fenner (also published by Chapman and Hall Ltd. in 1953) is a pleasanter book to consult.

Personally I cannot agree that the first five chapters dealing with engineering aspects of fatigue failure are properly described as the "Fundamentals of fatigue", necessary though they are to a complete account of the subject. Too little account generally is given of the physical and metallurgical phenomena notable associated with fatigue, both of these fields where notable advances have been made in recent years.

There are, of course, many good features in the volume. For instance, the section on crack propagation gives a very interesting account of a recent study at the Mechanical Engineering Research Laboratory, and that on corrosion fatigue and fretting corrosion is clear if not, perhaps, complete. Similarly, the chapters dealing with the effects of temperature and with the properties of materials give a comprehensive survey of existing data, perhaps the most complete to date, but they suffer, of course, since by their nature they cannot make interesting reading.

Perhaps the most readable chapter is that by Teed on the "Fatigue of aircraft". This is perhaps because it is more in the form of a literary effort and gives a survey of the change in outlook in relation to aircraft fatigue which has occurred with the passage of time. It is supplemented in technical detail by Chapter 14 on "Joints", Chapter 16 on "Aircraft structures" and in various sections of Part Three on the "Fatigue of engineering components". In this part, Chapter 17 by Cox on "Reproducibility of results" is particularly useful.

The comments in the last paragraph perhaps indicate the merits of the volume. Most readers who are interested in some aspect of fatigue can, by careful study and selection, find most of the material they need to have, except for the fundamental physics and metallurgy. The serious student of the subject will probably find the volume well worthy of study.

L. ROTHERHAM

Molecular science and molecular engineering. By A. R. VON HIPPEL. (New York: John Wiley and Sons, Inc.; London: Chapman and Hall Ltd., 1959.) Pp. xv + 446. Price £7 8*s*.

This book is the outcome of a Summer School held in 1956 at the Laboratory for Insulation Research in the Massachusetts Institute of Technology, and it forms the last part of a three-volume work on modern materials research. It consists of twenty-five chapters, written by a number of authors under the editorship of Professor von Hippel, in which a unified treatment is presented of a selection of electric, magnetic, mechanical, and chemical properties of matter, in terms of the fundamental structure of matter; and in addition there are descriptions of a number of practical applications such as gas discharge tubes and masers. The particular selection of topics, which ranges from the mechanism of thunderstorms to the synthesis of polymers, has doubtless been governed by the interests of the Laboratory for Insulation Research, and it is not one that would be chosen by the average physicist; but the presentation is stimulating, the book is beautifully produced, and the present reviewer found much to interest him, particularly in those chapters outside the range of knowledge of the ordinary physicist. However, it must be added that it is not clear to whom the book is primarily addressed, or indeed to whom it would prove sufficiently useful for its price not to be prohibitive. For it covers a wide range of topics, starting from considerations that are really too elementary (for example, even the laws of thermodynamics are discussed), so that the treatment is inevitably too highly compressed to be of use to the young student and rather too superficial to be of great use to the more mature research worker.

W. F. VINEN

The physical metallurgy of magnesium and its alloys. By G. V. RAYNOR. (London: Pergamon Press Ltd., 1959.) Pp. ix + 531. Price 75*s*.

Metallic magnesium was not isolated from its salts until about 150 years ago and, apart from its application to pyrotechnics, it was not considered a potentially useful material until the development of aircraft, where its low density made it of particular interest to engineers. Within the last thirty years, considerable progress in the technology of the metal and of its alloys has been made, and they are now accepted as standard engineering materials, particularly in the form of castings. During the same period the science of physical metallurgy has grown from a research interest to a subject of extensive practical importance for the metallurgical and engineering industries. The author's work forms a very significant part of the development of this subject, and he and his associates have made extensive studies of the alloy systems based on magnesium; it is appropriate, therefore, that he should have written this book, which he hopes may prove complementary to works dealing with the technology of the metal.

The major portion of the book deals with the binary alloys of magnesium and other elements, and correlates their alloying behaviour, both in the formation of solid solutions and of intermetallic compounds, in terms of their electronic structure and constitution. Before these aspects of alloying are described, earlier chapters deal mainly with properties of the pure metal and the influence of alloying on the lattice spacings. Only the barest outline of chemical reactivity is given in Chapter 2 and, while this is adequate for the immediate purpose, the chapter title, "The physical and chemical properties of magnesium", might be regarded as rather misleading.

The book is authoritative and exhaustive in its treatment of the fundamentals of alloy formation, and is essential for students of this aspect of magnesium technology.

W. BETTERIDGE

Proceedings of the third conference on carbon. (London: Pergamon Press Ltd., 1959.) Pp. x + 718. Price £7.

This volume contains eighty of the papers presented at the third conference on carbon, held in Buffalo, U.S.A., in June 1957, which established a meeting ground for physicists, chemists and technologists interested in carbon, its production and applications. Aspects of the subject covered are solid state physics, chemistry of solid carbon compounds and reactions, irradiation effects and studies of the properties of resulting products as a function of processing variables. The publication contains extensive reviews of recent major advances in carbon research and the proceedings represent an international survey of the fields.

Rheology of disperse systems. Edited by C. C. MILL. (London: Pergamon Press Ltd., 1959.) Pp. vii + 223. Price 60*s*.

This volume contains the proceedings of a conference sponsored by the British Society of Rheology, and held at the University College of Swansea in September 1959. The papers cover the latest experimental and theoretical work in the field, and are previously unpublished.

The papers fall into two groups; in one the dispersions studied were dilute or composed of non-interacting particles and experiments were designed to test hydrodynamic theory; in the other group, concentrated suspensions as used industrially, mainly in various forms of surface coating, were studied with the object of relating performance to rheological properties.

Disperse systems, either as emulsions or dispersions of solid particles in liquids, form a large group of materials of industrial importance, and this book should be a useful addition to the library of the many industries where this subject is of great importance.

The structure of electrolytic solutions. Edited by W. J. HAMER. (New York: John Wiley and Sons, Inc.; London: Chapman and Hall Ltd., 1959.) Pp. xii + 441. Price £7 8*s*.

This book is the outcome of a symposium held in Washington D.C. in May 1957. Its scope and purpose are not unlike those of the Faraday Society discussions in this country; the United Kingdom is, in fact, adequately represented. As the title implies, the emphasis is on structure. This means, for example, distinguishing between the strong and weak electrolytes of the physical chemist, and the physicists' (and electrochemists') more restricted meaning—merely that of a conducting solution—without all the complexities of "strong" and "weak".

Recent work on such diverse subjects as fused electrolytes, ion solvation and ion transfer is well covered, and there is a welcome section on the properties of the rare earths in electrolytic solutions. Here, the authors are on the frontiers of knowledge, since substantially more information on ion-solvent interaction will be needed before a number of observed irregularities can be explained. Decrease of ionic radius is evidently not a simple matter. There is a readable introduction; twenty-six contributions, with author and subject indexes, form the body of the volume. Altogether a useful compilation.

F. I. G. RAWLINS

Techniques of polymer characterization. Edited by P. W. ALLEN. (London: Butterworths Scientific Publications, 1959.) Pp. xiv + 256. Price 50*s*.

"Polymer characterization" is a vague but convenient phrase used by polymer chemists to describe the measurement of various properties that differentiate polymers one from another, often properties related to molecular weight. This book is intended primarily as an introduction to some of the practical techniques used in this field, and should be especially valuable to newcomers, though experienced workers will also find it well worth reading.

The eight authors discuss the following topics: the preparation of solutions; fractionation by using solubility differences; determination of number-average and weight-average molecular weights by physical means; solution viscometry; end-group analysis; and characterization of block and graft copolymers with respect to composition.

There are some omissions: melt viscosities are not mentioned; the otherwise excellent chapter on fractionation does not indicate that fractionation with respect to structure may complicate fractionation with respect to molecular weight; and the important procedure of extrapolation to zero concentration deserves more discussion than it is given. Despite this, the general standard is high, and references to the original literature are abundant. The book should fulfil its stated purpose.

P. A. SMALL

Heat thermometry and low temperature physics

Cryogenic engineering. By R. B. SCOTT. (New York: D. Van Nostrand Co. Inc.; London: D. Van Nostrand Co. Ltd., 1959.) Pp. x + 368. Price 42*s*.

Many of the engineering techniques used for low temperature processes have been described in the literature, where there is also a wealth of information on the properties of the materials processed and those used in constructing plant and equipment. Russell B. Scott, who is well known for his contributions to American cryogenic engineering, has written much of this published information and of his own wide experience into a textbook which gives a good introduction to this subject. In *Cryogenic engineering* he discusses first the liquefaction and separation of gases, then adiabatic demagnetization and low temperature thermometry. The longest chapter (73 pages) deals with the important subject of insulation and includes a good introduction to the characteristics and design of vacuum systems. Insulation is further discussed in the subsequent chapters on containers and pipe lines for liquids boiling at low temperatures. The various modes of heat transfer, conduction, convection and radiation, are discussed and the role of various insulants to reduce them is described. Concluding chapters review the properties of cryogenic fluids and of the materials used in constructing plant and equipment for processing and handling them. Thermodynamic diagrams large enough for approximate calculations have been provided.

In a book of this size it is impossible to discuss in detail all the problems peculiar to cryogenic engineering but Dr. Scott has shown where many of them lie and the means available for dealing with them. Further details may be found in the literature to which references are given. One would have expected to find an account of the opaque mixtures of silica

aerogel and metallic powders newly developed as insulants, and to Barber's platinum resistance thermometers, together with a warning against the use of helium in platinum resistance thermometer sheaths. These, however, are minor omissions in a useful and welcome textbook.

The volume is well produced, generously supplied with references and has adequate name and subject indices. It is unusually free from misprints and errors. It is one that should be in the hands of all concerned with low temperature engineering and industrial processes. A. H. COCKETT

Einführung in der Wärme-und Stoffaustausch. 2nd. ed. By E. ECKERT. (Berlin: Springer-Verlag, 1959.) Pp. xi + 295. Price DM 28.80.

This well-produced book is a second edition of a work first published in 1949. In the interim period the author has made available an English version—*Introduction to transfer of heat and mass* (New York: McGraw–Hill Book Co., 1950) —and it would appear that the present edition is also to have an American counterpart—*Heat and mass transfer*, by E. R. G. Eckert and R. M. Drake (New York: McGraw–Hill Book Co., 1959). The general arrangement is again similar but new material has been included and a good proportion of the references relate to papers published during the last decade.

The main sectional headings are: I, the fundamentals of heat exchange; II, heat conduction; III, heat transmission; IV, heat radiation; V, mass exchange, whilst an Appendix gives thermal propreties taken from recent publications.

R. W. POWELL

Seventh symposium (international) on combustion. (London: Butterworths Scientific Publications, 1959.) Pp. xlvi + 959. Price £11 4s. 0*d*.

This volume contains the proceedings of the Seventh symposium on combustion held in London and Oxford last year. There are in all 124 papers with the discussion on them and the texts of the inaugural addresses to the symposium.

The papers were divided into eleven subject groupings for presentation and this format is maintained in the book. The largest group is that of thirty-one papers on the "Mechanism of combustion reactions". Most of the papers in this group deal with the elucidation of the detailed kinetics of the reactions investigated. It is clear from the papers and the discussion that much more knowledge of the transients and intermediates occurring is necessary before prediction of the behaviour of practical combustion systems will be possible.

The second and third groups consist of five papers on "Spectroscopy of flames" and six on "Ions in flames". Seventeen papers are devoted to the "Structure and propagation of flames", which is dealt with in both theoretical and experimental studies.

There are ten papers on "Ignition and limits of inflammability" in which again both theoretical and experimental approaches to the problem are reported. The nine papers on "Interactions of flames and surfaces" deal with flame quenching, liquid drop combustion and carbon formation in flames. The eight papers on "Turbulence in flames" are all concerned with turbulent premixed flames.

"Combustion in practical flowing systems" forms a group of eleven papers covering such topics as flame stabilization by bluff bodies, combustion chamber stability and open hearth model studies amongst others. The remaining three groups consist of nine papers on "Detonation and its initiation", including several experimental and theoretical papers by Russian authors; seven papers on "Special fuels", such as diborane-hydrocarbon mixtures, alkylsilanes and metal combustion; eleven papers on "Instrumentation in combustion research" describing gas sampling and analysis methods, temperature measurement and other techniques.

M. G. PERRY

Magnetic, electrical and electronic devices and properties

Conductance design of active circuits. By K. A. PULLEN. (New York: John F. Rider, Inc.; London: Chapman and Hall Ltd., 1959.) Pp. xiii + 330. Price 80*s*.

The author, and particularly the publisher claim that here is a new approach to the design of active circuits. Many readers would not entirely agree with this as they are already used to employing the concept of conductance design in circuits employing valves and transistors, perhaps more so in the case of pentodes than for triodes.

Designers will, however, find this book of distinct value; the methods of working are clearly set out and the author stresses that for such non-linear devices the conductance parameter is not a constant and he refers throughout to small-signal behaviour. For large-signal applications a point-by-point technique is adopted.

Examples are given for the design of circuits for amplifiers, oscillators, relaxation oscillators, mixers and detectors, employing both valves and transistors.

Several instances occur where the designer must assume certain values or ratios, e.g. the ratio of anode voltage swing to anode supply; appropriate figures for these are quoted in the text but the reader is given no explanation as to why such values should be adopted. Some further notes in these cases would be helpful. A. J. MADDOCK

Electromagnetic radiation from cylindrical structures. By J. R. WAIT. (London: Pergamon Press Ltd., 1959. Pp. ix + 200. Price 50*s*.

The radiation characteristics of an aerial are affected, either by design or adventitiously, by the shape and size of the structure of which it forms part. In general, it is difficult to find a rigorous theoretical solution because of the difficult boundary conditions; designers then have to rely largely on experiment.

The author of this book derives theoretical solutions for a number of specific arrangements of dipoles or slots in association with corner reflectors, circular and elliptical cylinders and related cases. The results are expressed in the form of infinite series; some of these are very cumbersome, and their application would require a great deal of computation. It is therefore helpful to have many of the results displayed in graphical form. Rapidly convergent forms are derived for special regions of interest. There is an Appendix summarizing basic electromagnetic wave theory, and a good bibliography. The value of the book lies not only in the specific solutions given, but also in introducing the reader to methods of dealing with apparently intractable problems. But it covers a relatively

narrow field and also demands a good mathematical background; it is a book for the specialist. H. PAGE

Fluctuation phenomena in semi-conductors. By A. VAN DER ZIEL. (London: Butterworths Scientific Publications, 1959.) Pp. viii + 168. Price 35*s*.

During the last few years, many of the problems concerned with the understanding of fluctuation phenomena or noise in semiconductor materials and devices have been clarified, and the author in this book presents a survey of the present status of the theoretical and experimental work in this interesting field. Noise characterization of two- and four-terminal networks, noise measurements, and a survey of mathematical methods used in noise analysis are the subjects covered in the first three chapters, whilst Chapters 4 and 5 deal with generation-recombination noise and flicker noise in semiconductor materials. The author's classification of noise into three main headings, that is, generation-recombination, diffusion and modulation noise, is to be commended because it gives direct reference to the physical causes of the noise. The contribution and resemblances of these noise sources to the generally accepted classification of noise, that is, thermal, shot and flicker noise, are then discussed in the chapters dealing with specific devices.

Chapters 6–10 deal with noise in various semiconductor devices such as photoconductors, semiconductor resistors, semiconductor diodes and junction transistors. The last chapter covers applications and minimum-noise considerations for photocells, transistors and diodes as mixers and parametric amplifiers. There are numerous references, and as the author has attempted to give an account of what has already been accomplished and where the unsolved problems lie, this book should help in stimulating further research.

B. E. BUCKINGHAM

Introduction to monopulse. By D. R. RHODES. (New York: McGraw-Hill Book Co. Inc.; London: McGraw-Hill Publishing Co. Ltd., 1959.) Pp. x + 119. Price 46*s*. 6*d*.

This monograph is intended to provide the first general treatment of the concept of monopulse and to serve as a general introduction to the underlying principles for the use of students and practising engineers. As the author states, the word "monopulse" has been coined to describe direction finding systems which are capable of determining the angular position of a source of radiation from the reception of a single pulse. In monopulse radar, where the received pulse is an echo from the scattering target, the distance as well as the direction may be obtained, and it is in this field where most applications have been found.

The book opens with a clear introduction to the concept and a brief description of some early monopulse radar systems. It is interesting to learn that the first British and American experiments were undertaken quite independently in 1940, and furthermore that in the United States the Naval Research Laboratories and the Bell Telephone Laboratories were, unknown to each other, each developing systems based on the monopulse idea. The increased accuracy of monopulse in the field of radar arises mainly because the effect of target scintillation is substantially removed by the simultaneous comparison of the signals from two or more aerials, in contrast to the sequential nature of beam switching or conical scanning techniques.

A unified theory of monopulse is developed, based on three postulates which are used to define a concept of pure monopulse. The first and most important postulate is that angle information appears as a ratio and is therefore independent of the received signal level. The special theory, limited to the cases of either pure amplitude or pure phase sensing, is elaborated to define three classes of monopulse (complex sensing, which has received very little practical attention, is briefly alluded to in the general theory). Some techniques by which various forms may be physically realized are then considered and systems suitable for detection in both one and two planes are outlined. Three examples of pseudo-monopulse systems are given which, although having many of the characteristics of true monopulse, violate one or more of the three postulates.

Limitations on the form of the aerial aperture and pattern functions are examined for the case of simple sensing.

The last chapter gives a detailed analysis of the Class I system, which uses the sum and difference method and has the advantages of stability of cross-over indication and relative simplicity in duplexing and mechanical scanning.

There are a few minor criticisms; the use of "mil" for, presumably, milliradian (p. 19) is unfamiliar, at least in England. The statement that "half the power received by a matched antenna is reradiated" (p. 89) is not generally true. Reference 2 (p. 110) is not readily available, and may not be available at all. A more serious criticism, in the light of the classes of readers for whom the book is intended, is that the treatment, whilst very probably being fruitful for those already well versed in the field, may be too difficult for the student and too academic for the engineer. G. T. THOMPSON

Noise in electron devices. Edited by L. D. SMULLIN and H. A. HAUS. (Published jointly by The Technology Press of Massachusetts, Institute of Technology and John Wiley and Sons, Inc., New York; London: Chapman and Hall Ltd., 1959.) Pp. xvi + 413. Price 96*s*.

This volume differs from a number of recently published works on noise, in that it does not deal with the mathematics of random processes, but with the characteristics of the valves and transistors themselves. It brings together much recently published information which was previously only available in scattered papers.

The seven individual chapters are largely complete in themselves, and are each written by an expert in the particular field. The foundations of valve noise are covered in the first chapter on effects arising at the cathode, while two chapters cover respectively flicker and shot noise in grid control valves. A long contribution on noise propagation along electron beams is contributed by Haus himself, while low-noise travelling-wave tubes are as extensively covered by R. W. Peter. The last two chapters cover semiconductor and transistor noise, including a discussion on noise due to irradiation.

A high standard is maintained throughout the book and excellent bibliographies follow each chapter. No book on such a fast moving field as noise theory could be completely up to date, and the editors point out that while they were not able to include discussion of masers and reactance (parametric) amplifiers in the work, the noise mechanisms involved are no different from those that are discussed.

This is a book that can be thoroughly recommended to all who are interested in the ultimate performance of amplifiers. While much mathematics is involved in its full understanding, a great deal can be learnt from it by reading alone.

W. H. ALDOUS

Physik der halbleiter. By A. F. JOFFÉ. (Berlin: Akademie-Verlag, 1958.) Pp. x + 400. Price DM 35.

The subject-matter of this book starts with an account of ionic solids and metals, and then continues with semiconductors. After a general description of their properties the quantum theory applicable to semiconductors is outlined. This is followed by a treatment of crystal structure, vibrational properties and thermal conductivity, electron scattering, surface properties, *p–n* junctions and devices based on these. Emission processes, the effects of a magnetic field, and the thermoelectric properties and their applications are then discussed. The final section deals with the methods of measuring the most important semiconductor parameters, and the properties of the best known semiconducting materials.

The book provides a very useful general introduction to the subject, and some of the treatment is very stimulating, as would be expected from Prof. Joffé. The book appears to be a direct translation of the Russian original—the writer is not competent to judge its accuracy! As an English translation is in preparation, with some new material added since the original was written, the German translation will perhaps be of limited interest to students in this country.

D. A. WRIGHT

Proceedings of conference on magnetism and magnetic materials. (New York: American Institute of Physics.) Pp. vi + 323.

This supplement to the (American) *Journal of Applied Physics* contains the papers presented at the fourth annual Conference on "Magnetism and magnetic materials" held in Philadelphia from 17 to 20 November, 1958. It was sponsored by the Magnetics Sub-Committees of the American Institute of Electrical Engineers Committee on Basic Sciences with the co-operation of the American Physical Society, the American Institute of Mining, Metallurgical and Petroleum Engineers and the Office of Naval Research. The following sessions were held:—General session; ferrites; computer components; micromagnetics; domain walls; magnetic properties of metals and alloys; fine particles; amplifiers, microwave applications; resonance; metallurgical considerations; fundamental interactions; instrumentation; thin films; neutron diffraction and irradiation; garnets and other compounds; anisotropy, other than in thin films.

Progress in dielectrics. Vol. 1. Edited by J. B. BIRKS and J. H. SCHULMAN. (London: Heywood and Co. Ltd., 1959.) Pp. ix + 312. Price 70*s*.

This is the first volume of a series, a companion to the book *Progress in semiconductors* of the same publishers, and promises to be of an equally high standard. Every scientist must be thankful to the editors and collaborators of these modern "Progress" and "Advanced" series, which usually contain the experience of a first-class specialist, backed by an average of about a hundred references, and which will save him an otherwise prohibitive amount of reading. It might have been thought that the progress in dielectrics in recent years was less spectacular than the progress in semiconductors, but every reader of this volume will be surprised at the amount of new material collected in the last ten years. The editors, Dr. J. B. Birks of Manchester University and Dr. J. H. Schulman of the U.S. Naval Research Laboratory, deserve high credit for their work.

In the first article J. H. Mason sums up the results of recent investigations in the "Dielectric breakdown in solid insulation" in masterly and complete fashion. This is backed by J. W. Davisson's companion article on the "Directional breakdown effects in crystals". T. J. Lewis has contributed an exhaustive article on the "Electric strength of dielectric liquids" with a great amount of new experimental material. The theory is, of necessity, somewhat less satisfactory. Liao and Plump's article on "Gaseous dielectrics" is a purely engineering approach to the subject and indispensable to high-voltage engineers. One must be particularly thankful to A. D. Franklin for having given an up-to-date review of the ferro-electricity of barium titanate, this extremely important new material, and to P. Popper for his brilliant article, both theoretically and from the practical point of view, on non-oxide ceramic dielectrics, of which this is the first complete modern review, with 188 references. The closing article by J. B. Birks on the "Electrophoretic deposition of insulating materials" is an excellent summing-up of an important technique, with a very satisfactory theoretical discussion.

This series will be indispensable for all physical and engineering laboratories.

D. GABOR

Semiconductors. Edited by N. B. HANNAY. (New York: Reinhold Publishing Corporation; London: Chapman and Hall Ltd., 1959.) Pp. xxiii + 767. Price £6.

This book deals very competently with the chemical and physical properties of semiconductors, and with the relation between them. It is written from the chemical point of view and its approach differs, therefore, from that of most books on the subject; there is correspondingly much in it which is new and stimulating.

Following two survey articles there are detailed accounts of methods of crystal growing, the control of composition of solids by freezing, interactions between defects of various kinds, and diffusion processes in silicon and germanium. There is a detailed account of the chemical and physical properties of a number of divalent oxides and sulphides, a careful treatment of the transport properties in germanium and silicon and a general account of the Group III—Group V and other "covalent" compounds. A thorough discussion of infra-red absorption in semiconductors follows, which includes the magneto-optical effects. This is followed by an account of recombination and trapping processes and of experiments on these, and by a detailed treatment of imperfections in germanium and silicon which includes an account of dislocation theory of general validity. Later sections deal with the 3d transition metal oxides, organic semiconductors and semiconductor surfaces.

The book is very well written and produced and can be warmly recommended.

D. A. WRIGHT

The transistor era. Edited by C. C. GEE and C. A. MARSHALL. (London: Heywood and Co. Ltd., 1959.) Pp. 96. Price 5*s*.

The main aim of this book is to provide a source of reference to the availability of transistors and allied equipment manufactured in the United Kingdom; but in order to place the British contribution in a world setting a survey is also included of semiconductor manufacturers in other countries.

The products covered are transistors, diodes and rectifiers and photosensitive devices.

Mathematical theories, techniques, computers and control systems

Approximate methods of higher analysis. By L. V. KANTOROVICH and V. I. KRYLOV. (Groningen: P. Noordhoff Ltd., 1958.) Pp. xii + 681. Price $17.00.

The book under review is an English translation by Curtis D. Benster of the fourth edition of the Russian version. The book first appeared in 1936 with the title *Methods for the approximate solution of partial differential equations*. The authors feel that the change to the more general title is justified by the inclusion of chapters on conformal mapping and the solution of integral equations. The treatment is confined to linear equations with an occasional indication that extension to non-linear cases is possible. Only boundary value problems are dealt with to the exclusion of initial and mixed boundary conditions. The partial differential equations considered are mostly those of Poisson and Laplace and the biharmonic equations. The book is mainly about analytic methods and solutions. Approximation is involved in the numerical evaluation of some analytic expression such as the evaluation of a finite number of terms in an infinite series of the Fourier type. Little mention is made of computational details.

The first chapter contains an advanced treatment of Fourier series and their application to the solution of partial differential equations with particular emphasis on the improvement of convergence. Integral equations of the Fredholm type and their application of Dirichlet's problem in potential theory are dealt with in Chapter 2. Chapter 3 is concerned with finite-difference ratios and their use in the solution of ordinary and partial differential equation. The variational methods principally of Ritz and Galerkin are described in considerable detail in Chapter 4. The last three chapters deal with conformal transformation and its applications.

The book gives a good indication of Russian work. Most of the numerous references are to papers by Russian authors and very little is to be found about English or American work though there would probably be even less reference to Russian work in a corresponding book by English authors. The translator has done a good service in making such a readable translation of this valuable book available to English readers.

J. CRANK

Calculateurs analogiques répétitifs. By R. TOMOVIC. (Paris: Masson et Cie, 1958.) Pp. viii + 184. Price 3000 fr.

The author, who is in charge of research at the "Boris Kidrich" Institute in Belgrade, has written this monograph in French. The main attraction of the book is that it deals with the repetitive type of machine which has been somewhat neglected in books published so far.

Theoretical considerations, details of design and applications are considered in the three separate parts of the book. The first deals (*a*) with the general principles of use of this type of machine, (*b*) with a discussion of stability and (*c*) with the operation of scaling. The second part discusses in considerable detail the errors arising in the operations of addition and integration. Next we have an account of methods of performing the non-linear operations of multiplication, division and function generation. This part also contains a discussion of auxiliary equipment followed by circuit diagrams of amplifiers of various machines in Eastern Europe.

The third part contains chapters on ordinary differential equations and integral equations. Machines of very high repetition rates are discussed in the final chapter.

The author has obviously had considerable experience of computers which makes all the more astonishing the errors which occur—e.g. in Fig. 10.4 we have a sine function generator with only two amplifiers.

The book certainly helps to fill some of the gaps that exist in the literature on this type of computer.

C. C. RITCHIE

Conference on hyperconjugation. (London: Pergamon Press, Ltd., 1959.) Pp. 168. Price 35*s*.

This book contains the major papers, and discussions following them, presented at the 1958 conference on hyperconjugation held at Indiana University. The papers stress various aspects of hyperconjugation and the discussions further stress the diverse nature of the evidence pertaining to hyperconjugation, and the present flexible lines of approach to the science by workers in this field.

Dynamical analogies. 2nd ed. By H. F. OLSON. (New York: D. Van Nostrand Inc.; London: D. Van Nostrand Co. Ltd., 1958.) Pp. xi + 278. Price 51*s*.

When Mr. Olson wrote the first edition of this book in 1943 it was a most valuable introduction to a subject which was then quite new. There is no doubt that since its appearance it has helped many electrical engineers to gain a much clearer understanding of mechanical systems and many mechanical engineers a better understanding of electrical circuits. In the first edition it could be forgiven that the examples he gave were not fully worked out but in the second edition it is nothing short of exasparating to find that, throughout the book, only the most obvious analogies are given and the complete analysis is never worked out. As a result, when one has assimilated the ideas of the early chapters, the later ones do little more than indicate a number of interesting mixed systems in the analysis of which the analogies can be used to advantage. It is a very great pity indeed that he has not completed the analysis of the moving coil and moving armature transducers, which are of considerable importance in automatic control systems.

The early chapters are undoubtedly of considerable value in giving a clear picture of the dynamic behaviour of simple physical systems and his table of units and dimensions for electrical, mechanical rectilinear, mechanical rotational and acoustical systems are very useful. These tables bring out an important point in connexion with dynamical analogies, which results from the fact that to be of use they must all be represented by the same differential equation. This is, that the dimensions of electrical and acoustical quantities are complicated expressions of mass, length and time, because we define them in terms of force. This obscures the simplicity of the analogy but if it is appreciated that it is inertia resisting change of the dependent variable, not mass, which is the fundamental quantity, the analogy is immediately obvious and in terms of Q (quantity), J (inertia) and T (time), the dimensions of all the dependent quantities will be the same, no matter what the system.

Some of the definitions given in the introductory chapter are exceedingly good, particularly those of kinetic and potential energy and it is useful to have Newton's laws included. In the following chapter it is surprising that, although acoustical radiation resistance is mentioned, electrical radiation resistance has been forgotten. When it comes to the equations of motion, e^{jwt} has been introduced very suddenly and without explanation. Similarly a little later the Lagrange equation has also been introduced without proper explanation. In Fig. 5.17 on page 94 the centre fixings in the diagram of the rectilinear system are not required provided the centre member is stiff, which is a much more likely situation to meet in practice. It is useful to include the reciprocity, Thevenin's, superposition and similarity theorems but the exposition of the reciprocity theorem is not at all clear and Thevenin's theorem is extremely badly expressed. With regard to the superposition theorem, it should be pointed out that this is only applicable to linear systems. The distinction between noise and distortion in chapter 12 is good but in Fig. 12.1 and Fig. 12.2 it is confusing that distortion is shown as coming in from outside the system when, in fact, it is due to non-linearities within the system. The treatment of feedback is so elementary that it is hardly worth including and it is unfortunate that in making this addition a new set of definitions has been included, which do not conform with those generally accepted.

Summing up, the second edition adds little to the first edition that is useful and it is a pity that the opportunity has been missed of showing how the principles can be applied successfully to the solution of some of the electromechanical and electro-hydraulic problems which beset controls engineers.

J. F. COALES

Group theory and its applications to the quantum mechanics of atomic spectra. By E. P. WIGNER. Translated from the German by J. J. GRIFFIN. (New York: Academic Press Inc.; London: Academic Books Ltd., 1959.) Pp. xi + 372. Price 70*s*. 6*d*.

This book is, of course, a classic. When Wigner first published it in German in 1931, group theory was purely a toy for mathematicians, and its introduction into physics met considerable resistance. However, Wigner was right: symmetry properties are at the very basis of quantum theory, and group theory is the natural tool to deal with them, and indeed a very flexible and elegant one once you have learned to handle it.

Here then is the first English translation. It contains the complete contents of the original; in addition, Wigner has included three new chapters on Racah coefficients, on time inversion and on classical limits. Mathematical chapters in which such fundamental techniques as matrix calculus, abstract group theory and representation theory are developed alternate with chapters on the elements (not very elementary!) of quantum mechanics, perturbation theory, angular momentum and electron spin and so on. As the title indicates, the book is limited to the application to atomic spectra; the author has not found it possible to extend the scope so as to cover the all-important applications of group theory to our understanding of nuclei and fundamental particles.

The style is clear while compact, and not as abstract as the subject might suggest; a number of examples help the reader to keep his feet on the ground. It is not a book for the beginner; but a well-trained graduate student should not find it unduly difficult.

O. R. FRISCH

Les principes de la théorie électromagnétique et de la relativité. By MARIE-ANTOINETTE TONNELAT. (Paris: Masson et Cie, 1959.) Pp. 394. Price 5000 fr.

This volume will prove a valuable addition to the libraries of physicists and applied mathematicians. Its basic aim is a study of the underlying principles of electromagnetic theory, the theory of relativity and the important, though sometimes elusive, relationship between them. Professor Tonnelat begins her book with a systematic study of Maxwell's theory and its development in the hands of Lorentz. The second section deals with the special theory of relativity, its four-dimensional formulation and its consequences in kinematics, dynamics and electromagnetism. This section concludes with a chapter on the experimental evidence supporting the special theory. In the third section we find an attractive exposition of the general theory of relativity in which the geometrical nature of gravitation is lucidly expounded. The final chapter of this section provides a valuable and exhaustive survey of the various attempts which have been made to formulate a unified theory of gravitation and electromagnetism. The author wisely refrains from providing mathematical details in this chapter, though references are, of course, provided. These three sections form the book proper but a fourth section of over forty pages provides the mathematical equipment necessary for those unfamiliar with tensor calculus. This presentation of the tensor calculus is essentially geometric in character and should prove acceptable to both physicists and mathematicians.

The reviewer was impressed by the thoroughness with which this book is documented and by the lucid nature of the exposition. The implications of crucial experiments and the meanings of the more important formulae are all carefully expounded. As a reference book this work would have been of value if only an index of terms used and an index of authors cited had been included.

The format of the volume is beautiful to look upon and a pleasure to hold, but the size of fount used for tensor suffixes is such that any prospective reader over forty would be wise to consult an occulist before he begins. The only misprints detected were trivial. The author and the publishers may both be congratulated on this fine book.

D. E. RUTHERFORD

Matrix calculus. By E. BODEWIG. (Amsterdam: North-Holland Publishing Co., 1959.) Pp. xi + 452. Price 65*s*.

This is the second edition of a book which made a very favourable impression when it was first published in 1956. It has been expanded from 330 to 450 pages. The whole volume has been revised, many sections have been amplified, and some curtailed. The lay-out has been improved. Where several equalities were confined to a single line, they have now been spread over several lines. The text has been broken up into shorter chapters and altogether the appearance of the book has been greatly improved.

Lanczos' *pq*-algorithm, Rutishauser's *LR*-algorithm and Wilkinson's method are among the new results, and hitherto unpublished work is described on the deflation of complex eigen-values, the application to differential equations of the inversion of the general geodetic chain and its matricial generalization.

For those who know the first edition, enough has been said. For those not familiar with the first edition, the aim of the book is a systematic presentation of the notation developed by the author, whereby results previously expressed

in terms of individual elements, involving possibly several summation signs, are now expressed in terms of matrix products in a form usually more convenient for further development, and often more readily apprehended.

The book is neither a textbook nor a treatise. In both these one expects to start from scratch, building the subject up in the one case by easy stages, in the other in a formal logical sequence. The author of the present book although recognizing the desirability of a logical development, is too impatient of the early stages. A knowledge of determinants is assumed and some familiarity with matrices as well.

Even so, some of the early work is a trifle casual, as for example on page 55 where it is asserted that the matrix X, having the eigenvectors as columns, is orthogonal. This is not a logical deduction from the previous work in which there is no mention of normalizing the eigenvectors. Furthermore, there are too many references forward for a textbook.

It is primarily as a comprehensive reference book on numerical methods and on matrices as a branch of numerical analysis, that this book is of value, and in this field it has already established itself by the first edition as indispensable.

A. W. GILLIES

Methods based on the Wiener–Hopf technique for the solution of partial differential equations. By B. NOBLE. (London: Pergamon Press Ltd., 1958.) Pp. x + 246. Price 65*s*.

This book uses the approach of D. S. Jones, in which Fourier transforms are applied directly to the partial differential equation without formulating the intermediate integral equation, as was done in the original Wiener–Hopf technique.

The first chapter covers the complex variable theory required, and later chapters develop the method in applications to a wide range of problems. Throughout it is emphasized that the method can be used to give numerical results, and the solutions of problems are usually carried far enough to give at least one result of physical significance in simple form.

The standard of this series of monographs on pure and applied mathematics, under the general editorship of Prof. Sneddon, is well maintained.

A. W. GILLIES

Nonlinear problems in random theory. By N. WIENER. (New York: The Technology Press of The Massachusetts Institute of Technology; John Wiley and Sons, Inc.; London: Chapman and Hall Ltd., 1958.) Pp. ix + 131. Price 36*s*.

This book is the first of a new series of Research Monographs from the Massachusetts Institute of Technology. The intention is to make available important research studies, such as have been published semi-privately in the past as laboratory reports and such like.

We have here the record of a course of fifteen lectures given by Prof. Wiener to a selected group of graduate students at M.I.T., produced by means of tape-recording, photographing formulae written on the blackboard, and so on.

Starting with the discussion of a Brownian motion function, it is shown how a system of orthogonal functions may be developed and applied in a variety of different branches of physics. The whole discussion is conducted in rather abstract terms, and is in places very tentative. One suspects that in the original lecture course a lot of clarification was done in discussions after the lectures, and these have not found their way into the text. One is left feeling a great deal of sympathy with the student who asks "Can we have a numerical example please?"

A. W. GILLIES

Programming for digital computers. By J. JEENEL. (London: McGraw-Hill Publishing Co. Ltd., 1959.) Pp. viii + 517. Price 93*s*.

There are now several good and authoritiative books on digital computer programming which are relatively inexpensive and easily available; the appearance of a new and very expensive addition to the field thus requires considerable justification.

The author claims that the present book is intended for readers with no previous programming experience, but this is true of all of the previous books and, in any case, since the reviewer, who has been programming for over twelve years, found the book very difficult to understand, this particular claim does not appear to stand examination.

Previous books have been of two kinds; those which concentrated on the programming of a particular machine, and those which set up a hypothetical and universal machine specially for teaching. Jeenel's book does neither and, in fact, a complete set of machine instructions does not appear anywhere in the book, the reader being left to piece them together from various references scattered throughout the text.

To add to the general confusion there are such minor irritations as the representation of "subtract" by the code number 02 on p. 2 and by 06 on p. 9. The author's prose style, too, is turgid, for example on p. 12 we find: "The control desk . . . also enables the operator to initiate manually the automatic execution of a stored program, that is, to 'start' the machine."

It is thus not surprising that seventy-five pages elapse before a programme for adding one hundred numbers together appears, and no fewer than 227 pages before sub-routines are mentioned.

These are only a few of the faults which could be mentioned. The good portion of the book is the last two chapters (8 and 9), where operating, testing, checking and planning are mentioned. But these sixty pages do not make possible the recommendation of so expensive a book.

A. D. BOOTH

Sampled-data control systems. By E. I. JURY. (New York: John Wiley and Sons, Inc.; London: Chapman and Hall Ltd., 1958.) Pp. xv + 453. Price £6 8*s*.

Control systems based on sampled data are in some cases inevitable, and in other cases highly desirable for either economic or technological reasons. Radar tracking gives an essentially discontinuous input, data-transmission links may have to be shared for economy of space, weight or cost, and digital computation may be required for increased accuracy or versatility, at the price of finite times for individual computations; sampling as with a chopper-bar may allow more sensitive detectors, a single detector may sample like data in sequence at different stations, and a single digital computer may perform different mathematical operations as different components of the overall control process.

For those who are already thoroughly familiar with the mathematics of continuous control systems, in terms of Laplace-transform calculus and complex-variable theory, this work will provide a valuable, comprehensive and up-to-date account of extensions of these techniques to the discrete-sample field, as might be expected from an author who has *inter alia* been a consultant to Bell Telephone Laboratories.

There are extensive tables of the (modified-Laplace) transforms used, literature references about every second page, and incorporation (with acknowledgements) of current doctorate-thesis material. The emphasis throughout is on mathematical techniques of analysis and synthesis, and detailed applications receive little consideration. There is an appendix of about 90 problems, which can provide the reader with a check list of the individual procedures discussed.

This is a book written for electrical-engineering technologists at honours or post-graduate level; the mathematical content is (necessarily and properly) so high that many practical but non-mathematical engineers might scarcely recognize it had relevance to their work.

T. H. O'BEIRNE

Miscellaneous and general physics

La mesure précise du temps en fonction des exigences nouvelles de la science. By B. DECAUX. (Paris: Masson et Cie, 1959.) Pp. 126. Price 1300 F.

A neat, comprehensive and up-to-date summary of the fields of science in which very accurate time measurement is required, and of the techniques by which this accuracy can be attained.

The author, who is a chief telecommunications engineer, describes the role and importance of time-keepers in the measurement of frequencies, as required in radio transmitters; of distances, as in radio or radar navigational aids; and describes in outline the historical methods and in more detail the modern methods—the caesium clock, with ingenious modifications such as the "Atomichron", and the ammonia "Maser"—by means of which high precision is achieved. He also refers to time determination and to the units of time and their definition, and looks to the future.

F. A. B. WARD

Physikalisches Praktikum. 9th ed. By W. H. WESTPHAL. (Braunschweig: Friedr. Vieweg and Sohn, 1959.) Pp. vii + 285. Price DM 19.80.

The fact that this is the ninth edition of a work which first appeared in 1937 seems proof of its popularity, at least in Germany. The new edition has a number of new experiments, mainly in the sections on optics and electricity and magnetism. Despite this, the present volume is smaller than the older editions. This has been achieved by a considerable condensation of the detailed error calculations, which the reviewer found rather tiresome when he was a student. The book addresses itself, of course, primarily to students taking a first-year physics course at a University, but as it is in German it will be of little use to British students. This is unfortunate because I have not seen any other book on practical physics which sets out in detail not only all the measurements, evaluations and plots of the measurements on approximately fifty experiments, but also carries through an adequate error calculation in most cases. Students would find this extremely helpful. The book contains sections on mechanics, heat, optics, electricity and magnetism; the experiments deal with the basic principles, no "clever" experiments being included. There are paragraphs on units, a very good discussion on errors and error calculation; an appendix on damped oscillations, on galvanometers and a more advanced discussion of errors.

Most of the experiments are of first-year standard, but some go beyond this, e.g. coupled pendulums, polarization of light, compound lens systems, string electrometer, thermionic valves. In general, the equations governing a particular experiment are just stated, in other cases a full derivation is given. The reviewer could not find the reason for this differential treatment; in some instances the derivation was obviously given because one could not find it easily in standard textbooks, e.g. corrections to the simple pendulum, oscillations of a balance.

It would be a pleasure to recommend this book, or something like it, to our students, but someone would have to translate it first.

F. ANSBACHER

Reports on progress in physics. Vol. XXII. Edited by A. C. STICKLAND. (London: The Physical Society, 1959.) Pp. iv + 634. Price 50*s*.

These annual volumes, which are produced under the general supervision of the Papers Committee of The Physical Society, aim at presenting the results of recent work in selected fields in a form suitable for the physicist who is not a specialist in that field.

This volume contains three specially written contributions by Russian scientists which have been specially translated for publication in this edition. The full contents are: Applications of quantum mechanics in theoretical chemistry, by G. C. Hall; Progress in vacuum technology, by J. Pollard; The propagation of elastic waves in crystals and other anisotropic media, by M. J. P. Musgrave; Relativity, by H. Bondi; Double beta decay, by H. Primakoff and S. P. Rosen; Physical problems of thermoelectricity by A. F. Joffe and L. S. Stil'bans; Paramagnetic resonance data, by J. W. Orton; Experimental investigations of the ionospheric E-layer, by B. J. Robinson; Radio-frequency spectroscopy of exicited atoms, by G. W. Series; The theory of a Fermi liquid, by A. A. Abrikosov and I. M. Khalatnikov; Invariance in elementary particle physics, by N. Kemmer, J. C. Polkinghorne and D. L. Pursey; Nuclear magnetism in pure liquids, by J. G. Powles; Experimental work with ^{3}He, by V. P. Peshkov and K. N. Zinov'eva; The two-nuclear interaction, by R. J. N. Phillips

The reports published in this volume are also issued as individual articles at prices depending on their length.

Nuclear and cosmic-ray physics, apparatus, techniques and data

Nuclear electronics. (Wien: International Atomic Energy Agency, 1959.) Pp. 451. Price 24*s*.

The papers, and the discussions upon them, read during the "Colloque international sur l'electronique nucleaire" organized by the Société Française des radio-electriciens in Paris in September 1958 are given in this volume. The colloquium contained five sessions under the following titles:—Scintillation radiation detectors; Radiation detectors using ionizing methods, and gamma-ray spectrometers; Pulse technique: fast electronics; Pulse technique: classical electronics; Reactor control: measurements. Some of the papers are published in French but the majority are in English.

Physics and heat technology of reactors. Edited by F. COLEMAN. Translated from the Russian. (New York: Consultants Bureau Inc.; London: Chapman and Hall Ltd., 1958.) Pp. v + 174. Price £8 8*s*.

This volume contains nineteen papers on fundamental reactor design problems which are the original work of

several Soviet authors. The papers are conveniently divided into two groups, those in the first group dealing with reactor physics calculations and experimental work, and in the second group with problems which are more of an engineering nature, such as the analysis of heat removal and determination of optimum thermal efficiency. All the papers are of a rather specialized nature and will be of interest to scientific workers involved in the detailed design of reactors and nuclear plant.

Two papers by G. I. Marchuk deal with the solution of multigroup neutron diffusion equations. The two methods described employ widely different approaches to the problem, the first being an approximate analytical solution which the author claims adequately allows for strong absorption in the slowing-down region, while the second method presents a numerical solution technique employing finite differences, and which is therefore of a rather more conventional nature. People working on this particular problem will find the two comparative approaches of considerable interest.

An interesting paper by a group of experimenters describes the use of the neutron "pulse" method for studying neutron slowing-down in graphite and in heterogeneous uranium-graphite systems. They present information on the change in neutron spectrum obtained together with their conclusions on the basic physical reasons leading to these effects.

An important paper deals with the experimental determination of fission product yields from uranium 233, and gives data on the absorption cross-sections measured for some of these elements.

The papers on heat removal aspects of reactor design do not appear to be so satisfying as those dealing with reactor physics, probably because such problems are usually specific to particular reactor types and the subject hardly lends itself to papers of a generalized nature. Nevertheless, some interesting ideas are presented, and the subjects covered are optimum shape of fuel elements, optimum working temperatures for reactors, the use of saturated steam in atomic power stations and the characteristic features of boiling water reactor steam cycles.

This collection of papers no doubt constitutes a useful and important volume on specialized reactor problems and can be recommended as a useful asset to libraries and workers covering this field of science. D. V. WORDSWORTH

Premier colloque international de photographie corpusculaire. (Paris: Centre National de la Recherche Scientifique, 1958.) Pp. 451. Price 5300 fr.

This volume contains the proceedings of a symposium held in Strasbourg in July 1957. The 47 papers are grouped into 8 sections with the following titles:—L'image latente dans les émulsions ordinaires; L'image latente dans les émulsions corpusculaires; Préparation et propriétés des émulsions; Quelques caractéristiques des émulsions corpusculaires soviétiques; Traitement des émulsions corpusculaires; Méthodologié; Quelques applications nucléaires ayant des répercussions photographiques; Applications de la méthode dans d'autres domaines posant des problèmes photographiques.

Progress in nuclear energy. Series I, Physics and mathematics, Vol. 3. Edited by D. J. HUGHES, J. E. SANDERS and J. HOROWITZ. (London: Pergamon Press Ltd., 1958.) Pp. viii + 403. Price £5 5*s*.

Progress in nuclear energy. Series VII, Medical sciences, Vol. 2. Edited by J. C. BUGHER, J. COURSAGET and J. F. LOUITT. (London: Pergamon Press Ltd., 1958.) Pp. viii + 288. Price £5 5*s*.

Progress in nuclear energy. Series IX, Vol. 1. Analytical chemistry. Edited by M. T. KELLEY. (London: Pergamon Press Ltd., 1959.) Pp. 369. Price £5 5*s*.

These volumes comprise a selection of the papers presented at the 2nd U.N. Conference on the Peaceful Uses of Atomic Energy held in Geneva during September 1958. In each instance the selection made from the large number of papers presented is intended to give a reasonably balanced view of the work of the conference in the particular fields. (The full proceedings are being published by the United Nations.)

In the Physics and Mathematics volume there are 21 papers and a cross-section and subject index, and in the Medical Sciences volume there are 25 papers and a subject index.

The papers which have been included in the Analytical Chemistry volume are intended to give a balanced view of the work of the conference in connexion with the progress of analytical chemists and their techniques in the fields of nuclear energy. Emphasis is placed on methods of analysis as applied to reactor research, atomic energy programs, processes in the chemical and metallurgical industries and in health physics. Use of neutron activation analysis, radioactivation analysis, X-ray spectrometry and electrochemical methods for remote control analysis are discussed.

The papers are grouped under five main subject headings which are as follows:— Reactor applications; Activation analysis; Spectrographic techniques; Industrial applications; Health physics.

Progress in nuclear physics. Vol. 7. Edited by O. R. FRISCH. (London: Pergamon Press Ltd., 1959.) Pp. viii + 326. Price 84*s*.

The articles in this volume summarize recent advances in the important fields covered and there are extensive cross references. Four of the authors are at American Universities and the fifth author, like the Editor, was temporarily in America when he made his contribution. The contents are: The bubble chamber, by D. V. Bugg; Resonance fluorescence in nuclei, by F. R. Metzger; Spallation, by G. Harvey; Optical model for nuclear scattering, by A. E. Glassgold; Measurement of helicity, by Lee Grodzins; Weak interaction, by J. J. Sakurai.

Solid state physics and crystallography

Growth of crystals. Edited by A. SHUBNIKOV and N. N. SHEFTAL. (New York: Consultants Bureau, Inc.; London: Chapman and Hall Ltd., 1959.) Pp. 293. Price 120*s*.

In March 1956 the Institute of Crystallography, of the Academy of Sciences of the U.S.S.R, held its first convention on crystal growth in Moscow. Eighty-three reports were presented at the plenary and sectional meetings dealing with all aspects of crystal growth. The present book contains forty-three of the papers, most of which are devoted to the growth of single crystals, and it is hoped that these will give a picture, if a little incomplete, of the work of Soviet scientists on this topic.

Solid state physics. Advances in research and applications. Vol. 8. Edited by F. SEITZ and D. TURNBULL. (New York: Academic Press Inc.; London: Academic Books Ltd., 1959.) Pp. xiv + 519. Price 96*s*. 6*d*.

The first article in this volume, forming Part I of an account of the electronic spectra of solids, is written by D. S. McClure and deals with the spectra of molecular crystals. This represents the start of a policy of including in each volume at least one article on organic solids. The article discusses the theoretical basis and experimental results obtained, especially on the aromatic hydrocarbons, on fluorescence, and on energy transfer processes.

R. Newman and W. W. Tyler have carried out a great deal of research on photoconductivity in germanium. They present in the second article a detailed account of the status of this subject and of its contribution to the understanding of photoconductivity as a whole. This arises because of the very high degree of control which can be obtained over germanium. The article on neutron scattering by L. S. Kothari and K. S. Singwi deals very competently with the theory of the scattering of thermal neutrons in a solid, the comparison of theory with experiment in various metals and in graphite, the use of long wavelength neutrons to study lattice dynamics, and the mechanism of the slowing down of thermal neutrons. G. Heiland, E. Mollwo and F. Stöckmann in their paper on zinc-oxide discuss in great detail its physical forms, the nature and motion of defects, the optical properties, and many aspects of the conductivity processes. Finally, S. Amelinckx and W. Dekeyser have written a very thorough and valuable analysis of the structure of grain boundaries and their effects on the mechanical and electrical properties of solids.

This volume is, like the earlier ones in the series, a most important contribution to the literature on solid state physics.

D. A. WRIGHT

Structure reports. Vol. 14. Supplementary volume and cumulative index for 1940–1950. General Editor: A. J. C. WILSON. (Utrecht: N. V. A. Oosthoek's Uitgevers MIJ, for the International Union of Crystallography, 1959.) Pp. viii + 215. Price 68*s*.

This volume contains cumulative indexes for the contents of volumes 8 to 13 of *Structure reports*, covering the years 1940 to 1950 inclusive. Most important are the subject index (inorganic and organic structures), the formula index and the author index, but these are supplemented by the separate indexes for carbon compounds (according to the numbers of carbon and hydrogen atoms in the formula) and for metals (not appearing in the separate volumes where the systems are arranged in alphabetical order in the text). In the preparation of the indexes, those for certain of the earlier volumes covered have been revised and brought up to the standard of those of the more recently published volumes.

These indexes occupy altogether about 160 pages. In addition, the volume contains about 40 pages of supplementary reports on publications previously omitted, and about 15 pages of (cumulative) corrigenda. The reviewer is unable, in a brief random sample test, to detect any error, but—a very minor point—finds it strange that nowhere in this volume does there appear to be any indication of the way in which the years 1940–1950 are distributed over the volumes 8–13 with which it is associated.

W. H. TAYLOR

Reference books

Bibliography on industrial radiology, 1956–1959. By H. R. ISENBURGER. (New Jersey: St. John X-ray Laboratory, 1959.) Pp. 27. Price $4.00.

The seventh Supplement to *Industrial radiology*, the second edition of which was published by John Wiley and Sons, New York, in 1943, contains a comprehensive list of references published on the subject of industrial radiology from 1956 to 1958. The periodic publication of these supplements is intended to keep the subject-matter of *Industrial radiology* up to date.

Conversion factors and tables. Part I. Basis of tables conversion factors. (B.S. 350: Part I: 1959.) (London: British Standards Institution, 1959.) Pp. 114. Price 15*s*.

This first part of the revision of B.S. 350, Conversion factors and tables, is a fully indexed volume, giving extended basic information on units, together with the standard abbreviation for each unit or combination of units considered. A feature of the Standard is the inclusion of comprehensive tables of conversion factors, showing the relationship between any two of the British and metric units used in the measurement of a given physical quantity. Summary tables of units and conversion factors are also included, together with an appendix on thicknesses of sheets and diameters of wires.

Glossary of terms used in vacuum technology. (London: Pergamon Press Ltd., 1958.) Pp. 63. Price 10*s*.

The need for some standardization in the nomenclature of vacuum technology was recognized in America by the Committee on Vacuum Techniques (now the American Vacuum Society) in 1953. This glossary of some 400 terms represents five years of hard painstaking work and succeeds in fulfilling this need. In all important aspects it is closely related to British recommendations (see B.S. 2951: 1958). Although largely intended for American use this booklet will be useful for workers in Europe requiring a close and detailed contact with American literature on vacuum technology.

J. H. LECK

Handbuch der Physik. Vol. VII/2. Edited by S. FLÜGGE. (Berlin: Springer-Verlag, 1958.) Pp. 273. Price DM 76.

This volume of the *Handbuch der Physik* (called Kristallphysik II) contains two articles. The first of these, by Dr. A. Seeger, deals with crystal plasticity and occupies the major part of the book. The second contribution, by Prof. Dehlinger, is on "Transformations and precipitation in crystals". Seeger gives a full account of the experimental facts on the deformation of single crystals, including details of the mechanical properties and of microscopic observations of surface slip lines. This part of the article is a very useful review of previous work and includes a large number of references. The next 60 pages are devoted to an account of the theory of crystal plasticity. This part represents, in the main, a summary of the author's many papers on this subject, and is rather less critical than is desirable for this kind of review. Dehlinger's article is an interesting short account of the mechanisms of nucleation and of the kinetics of precipitation and transformation processes in crystals.

P. B. HIRSCH

Cathode work function, sparking potentials and secondary ionization coefficients for oxide-coated cathodes in hydrogen

By D. E. Davies, B.Sc., Ph.D., A.Inst.P., and B. J. Hopkins, B.A., Ph.D.,* Department of Physics, University College of North Staffordshire, Keele, Staffs.

[*Paper first received* 2 *December*, 1958, *and in final form* 8 *April*, 1959]

The Kelvin vibrating electrode technique has been applied to measure the contact potential difference between oxide-coated cathodes and a gold reference surface in the presence of hydrogen. Special high vacuum (Alpert) techniques were used to ensure high gas purity. By the use of both calcium oxide and barium oxide cathodes, in various states of activation, it was possible to obtain a range of work function from 1·4 to 3·6 eV. Paschen curves were plotted for each of these oxide cathodes at room temperature, and minimum sparking potentials and secondary ionization coefficients were determined. A linear relation was found between the cathode work function and the minimum sparking potential. The slope of this line indicated that a 1 eV change in work function corresponded to a change of 55 V in the minimum sparking potential. The slope of the line was confirmed by independent work function measurements using the graph of the Richardson thermionic equation. The curves (ω/α) v (E/p) showed a rapid increase in ω/α with decreasing values of E/p at $E/p < 100$ V/cm mm of mercury.

In the previous paper, Davies and Fitch[1] have discussed the significance of a relationship between the sparking potential and the work function of a metallic cathode in a discharge in hydrogen. Previous attempts to relate these two variables have suffered from the disadvantage that the work function of the cathode was not measured under the conditions of the discharge. In order to overcome this, Davies and Fitch adopted the Kelvin work function technique, which had the advantage that it could be applied either in a vacuum or in hydrogen. The results produced are not absolute work functions, but values based upon an assumed work function for a gold reference surface in the presence of gas. This limitation does not affect the results of Davies and Fitch, since their investigations were based upon work function differences. The conclusion from their work was that changes in the sparking potential could be correlated with changes in the cathode work function. The relatively small work function changes they observed (0·3 eV) were attributed to the formation of a layer of hydrogen positive ions on an insulating layer of oxygen permanently attached to the copper cathode.

The aim of the work reported in this paper was primarily to extend the previous measurements over a much larger work function range, and also to measure the cathode work function by some alternative method in addition to the Kelvin method. An oxide-coated cathode at room temperature was used to provide a cathode surface, the work function of which could be varied between 1 and 4 eV by a variety of treatments, and by a suitable choice of oxide. It should, therefore, be possible to extend the range of the measurements of Davies and Fitch by a factor of at least ten. The work function of the oxide cathode could also be determined under vacuum conditions by use of the Richardson thermionic equation.

APPARATUS AND TECHNIQUES

(*a*) *The tube*. Basically the tubes were similar in design to those of Davies and Fitch. Three electrodes were incorporated, one of which (the oxide cathode) was fixed while the other two were fitted to a movable glass arm. This arm could be rotated magnetically from outside the tube so that the positions of two electrodes were interchanged. In this way either a nickel button electrode or a vibrating glass electrode could be fixed parallel to the surface of the oxide cathode. The oxide cathode was prepared on an O nickel base stamped into a cylindrical button 1·9 cm in diameter. The alkaline earth carbonate was sprayed on to the button and subsequently decomposed in a vacuum to form the oxide. These large buttons were indirectly heated by means of coils of ceramic insulated tungsten wire 0·51 mm diameter. At a cathode temperature of 900° C these required about 80 W of heater power. The temperature of the cathode could be followed by means of a tungsten-nickel thermocouple, welded on to the inside of the cathode button. The vibrating glass electrode was similar to those described by Davies and Fitch, except that it was made slightly larger (1·9 cm diameter) to match the larger size cathode. The metallic anode was a button exactly the same as the cathode base, and was mounted above the cathode so as to be parallel in one fixed position. Finally, a gold bead (prepared on a tungsten filament in hydrogen) was fitted to the tube in such a position that on heating it would evaporate over the surface of the glass electrode when the nickel anode was over the cathode. The evaporation of gold on to other parts of the tube was prevented by a sheet nickel screen surrounding the bead. The whole assembly was mounted on a glass frame sealed to a seven-lead hard glass pinch (supplied by Siemens–Edison Swan Co. Ltd.). Before sealing the tube into its envelope the latter was provided with an earthed Aquadag screen painted on to the inside of the glass wall.

The tubes were built with a view to obtaining a vacuum of better than 10^{-9} mm of mercury. The metallic parts were therefore reduced to a minimum, and positioned so that they could be outgassed either by eddy currents or by direct heating. All of the materials used in the assembly of these tubes were thoroughly cleaned and, wherever possible, the metallic components were heated in an atmosphere of hydrogen and subsequently not handled.

After heating the cathode button (complete with thermocouple, heater, and support wires) in an atmosphere of hydrogen, the appropriate carbonate suspension (supplied by the General Electric Co. Ltd.) was applied to the surface by

* Now at the Physics Department, University of Southampton.

spraying. The final thickness of the carbonate layer was about 100 μ.

(*b*) *The vacuum systems.* Two vacuum systems were used; one to provide hydrogen in a good state of purity, and the other to remove air and carbon dioxide from the experimental tube. The hydrogen side of the apparatus was exactly the same as that used by Davies and Fitch and described in their paper. The second vacuum system was connected to the hydrogen supply through a pair of gold-sealed palladium osmosis tubes. This second system was a high-speed mercury train designed to achieve not only a good pumping speed (to remove the large volumes of carbon dioxide evolved during breakdown of the carbonates to oxide) but also a pressure of better than 10^{-6} mm of mercury. No stop-cocks were fitted on the high-vacuum side in order to reduce the danger of grease contamination. Two liquid air traps shielded the experimental tube from the two-stage mercury diffusion pump.

Between the two vacuum systems was built an arrangement of glass breakers and constrictions, so that the tube could be pumped out several times on the high vacuum system. The most satisfactory type of breakers were those of the "pig's-tail" variety, operated magnetically by a glass encased iron slug. The ultra-high vacuum techniques first described by Alpert were adopted to produce the low pressures (of the order of 10^{-9} mm of mercury) required, and each tube was sealed to the system together with a Bayard–Alpert type ionization gauge and a molybdenum getter.

(*c*) *Processing of the experimental tube.* After achieving a rough vacuum of the order 10^{-5} mm of mercury the whole of the glass between the palladium osmosis tube and the first liquid air trap was baked at a temperature of 420° K for about forty-eight hours. While the glassware was still hot the metal parts in the tube were given a preliminary outgassing by means of eddy currents. The cathode temperature was then raised slowly to 900° C over a period of twenty-four hours. This caused the carbonate layer on the cathode to decompose to oxide with a large evolution of carbon dioxide. When all the gas had been pumped from the cathode, liquid air was applied to the second liquid air trap, and the pressure then fell below 10^{-6} mm of mercury. Outgassing cycles were commenced; these consisted of heating all of the metallic parts in the tubes either directly or by eddy currents to above 1000° C. Large volumes of gas were evolved from the gold bead, and this had to be left for long periods at a temperature just below the evaporation point before the pressure would fall below 10^{-6} mm of mercury. After any one of these cycles, the system was rebaked for a short period to remove the carbon dioxide adsorbed during the breakdown of the carbonates. When the pressure failed to rise above 10^{-6} mm of mercury at any one of these outgassing stages, the constriction was given a preliminary heating to the softening point and finally sealed. The pressure at seal-off was usually about 5×10^{-7} mm of mercury. After seal-off the getter was fired in liquid air and this usually resulted in a fall in pressure to less than 10^{-7} mm of mercury. The inverted ion gauge was then operated as a pump and the pressure fell to well below 10^{-9} mm of mercury in about six hours. In a few instances the pressure in the assembly would not fall below 10^{-7} mm of mercury, regardless of how long the ion gauge had pumped. In these cases it was generally assumed that there was a fine leak, though no leak could ever be detected by any of the techniques available. The results from such tubes appear to be exactly the same as those from the ultra-high vacuum tubes.

When the best vacuum had been achieved, the tube was ready for investigation. Measurements were made in a vacuum or the palladium osmosis tube was heated immediately and hydrogen admitted.

(*d*) *Measurements.* The cathode temperature was measured by means of a tungsten-nickel thermocouple. The rest of the measuring circuits and apparatus have been described by Davies and Fitch.

RESULTS

Paschen curves have been plotted for cathodes of both barium and calcium oxide in various states of activity. This range of cathodes made it possible to obtain a variation in work function from 1·4 to 3·6 eV. Since the gold surface could also be used as a cathode, the range could be further extended to the assumed value for the work function of gold (Riviere 4·7 eV).[2] In general, the Paschen curves were plotted over a limited range never greater than $p \times d = 20$ mm mercury × cm, but usually just sufficient to allow the minimum (V_{sm}) to be fixed. A pair of curves for a barium oxide cathode are reproduced in Fig. 1. Very low minimum

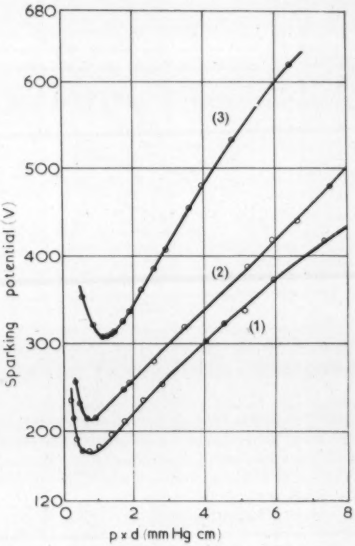

Fig. 1. Paschen curves in hydrogen for cathodes of: (1) activated barium oxide; (2) unactivated barium oxide; (3) evaporated copper film (Davies and Fitch)

sparking potentials were observed, especially for well activated cathodes. The coefficient ω/α was calculated as a function of E/p using the Townsend sparking criterion:

$$(\omega/\alpha)\{\exp(\alpha d_s) - 1\} = 1$$

where ω/α, α and d_s have their usual meanings. Davies and Milne's[3] values of α/p as a function of E/p were used in the calculation.

Typical curves, obtained with various types of oxide surface, are shown in Fig. 2. For comparison, a curve for an evaporated copper cathode is included on the same diagram. It will be noticed that throughout the range of values of E/p,

the secondary emission from all of the oxide surfaces is much greater than from a copper cathode. The curves for calcium oxide cathodes have been found to show a much higher secondary emission than similar curves for barium oxide cathodes, especially at low values of E/p. Activation always had the effect of increasing the secondary emission over all ranges of E/p. Unactivated barium oxide cathodes have not shown the rapid increase in ω/α with decreasing values of E/p observed with other oxide surfaces, and the curves for such cathodes are very similar in shape to that shown for a metal cathode. In no case has it been possible to demonstrate that the increase of ω/α reaches a peak. In spite of this, it is felt that the curves obtained so far are a good indication that the dominant secondary process in the breakdown at low values of E/p, is emission from the oxide cathode by the incidence of photons generated in the discharge.[4]

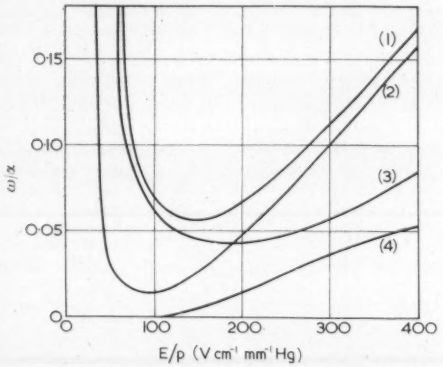

Fig. 2. Secondary emission curves in hydrogen for various cathode surfaces. (1) activated calcium oxide; (2) activated barium oxide; (3) unactivated calcium oxide; (4) evaporated copper film (Davies and Fitch)

The explanation for the greater emission from activated calcium oxide cathodes over that from activated barium oxide cathodes at low values of E/p is thought to lie in the high sensitivity of calcium oxide to irradiation. This has been found in previous work in this laboratory,[5] and is at the moment under investigation.

Of the five tubes that were constructed for this investigation three had cathodes of barium oxide and two had cathodes of calcium oxide. The work function and sparking potential results from the first four of these tubes are summarized in Table 1, together with two points due to Davies and Fitch.

TABLE 1. *Summary of work function and sparking potential results from cathodes*

Tube	*Cathode*	*Condition*	*Work function (eV)*	*Minimum sparking potential V_{sm} (V)*
2	BaO	Activated	1·4	146
3	CaO	Activated	2·6	246
4	CaO	Activated	2·7	230
1	BaO	Unactivated	3·6	285
4	Au	Clean film	4·7	335
Davies and Fitch	Cu	Oxide layer	4·34	308
	Cu	H^+ ion layer	4·00	275

All of these work functions (with the exception of that of the gold which was assumed) were measured by the Kelvin method with respect to gold.

The alternative work function technique adopted in these investigations was obtained from the graph of the Richardson thermionic equation, and this was applied in the case of two points. The Richardson graphs were, of course, made in a vacuum, and it was assumed that no change took place in the emissive work function when hydrogen gas was admitted. This appears to be a reasonable assumption, since no change was ever observed in the Kelvin work function when hydrogen was admitted. It is realized that such a result could be explained by a parallel change in the work function of the gold as hydrogen was introduced. It is, however, thought unlikely that the two changes would exactly cancel.

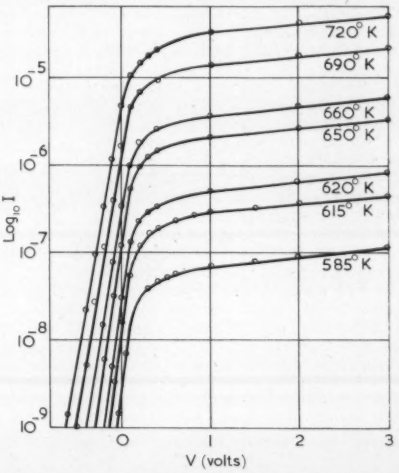

Fig. 3. Emission characteristics for tube 5 (activated barium oxide cathode)

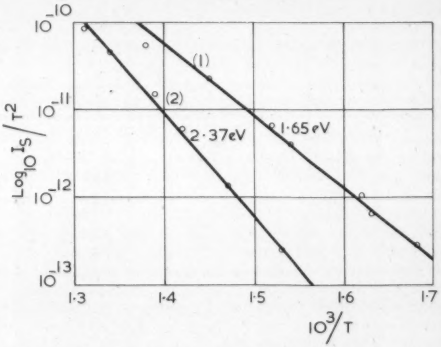

Fig. 4. Graph obtained from the Richardson thermionic equation for tube 5. (1) activated barium oxide; (2) unactivated barium oxide

The values used for the zero field emission in the Richardson graphs were obtained from plots of $\log_{10} I$ against V, the required emission being at the intersection of the two linear regions. Typical curves are shown in Figs. (3) and (4).

Both of these sets of measurements were made with one tube. In the first instance the work function was determined thermionically, hydrogen being then introduced and the minimum sparking potential measured. The tube was then re-evacuated, completely reprocessed, and finally, emission-drawn until the maximum activity was achieved. Measurements were again made of the work function and the minimum sparking potential. The results so obtained are given in Table 2.

TABLE 2. *Results of measurements of work function and sparking potential on one tube*

		Work function (Richardson) (eV)	*Minimum sparking potential V_{sm} (V)*
Tube 5	BaO (unactivated)	2·37	212
	BaO (activated)	1·65	174

When these two points are plotted on the same graph with the Kelvin results good agreement is found, Fig. 5. From a consideration of the nature of the two work function methods it is thought that such good agreement may be partly

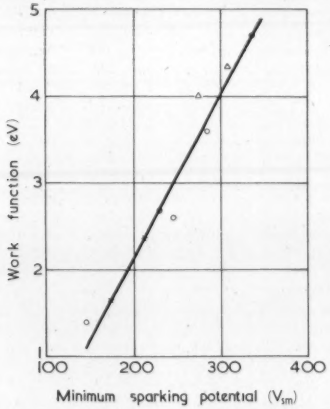

Fig. 5. Plot of work function against minimum sparking potential in hydrogen for cathodes of various work functions

○ = by the Kelvin method and for oxide-coated cathodes
× = by the Richardson method
△ = by the Kelvin method and for evaporated copper film (Davies and Fitch)

fortuitous. The slope of the graph of the Richardson equation gives the emissive work function of the cathode at absolute zero temperature, while the Kelvin method measures the average work function of the whole cathode at the temperature of the measurement. Since it is to be expected that the minimum sparking potential would be related to the emissive work function of the cathode at room temperature, neither of the two methods measures exactly what is required. In theory it should be possible to relate the two work functions by applying a correction to the emissive work function using a known value of $d\phi/dT$. In practice, however, for an oxide-coated cathode, measurements of $d\phi/dT$ have only been made over a restricted temperature range[6] and these are even conflicting as to whether $d\phi/dT$ is positive or negative. Thus, until an accurate knowledge of $d\phi/dT$ is available, it is not possible to estimate the emissive work function of the cathode in the presence of a gas at the same temperature as the measurements of the minimum sparking potential.

CONCLUSIONS

Measurements have been made using an oxide-coated cathode as a surface of known and variable work function. By a variety of treatments it has been possible to vary the work function of such a cathode over a range of several volts. A linear relation was found to exist between the cathode work function and the minimum sparking potential, the slope of which indicated that a 1 eV change in the work function of the cathode surface resulted in a change of some 55 V in the minimum sparking potential.

The advantages of the techniques described above are:

(i) the use of good vacuum conditions, usually better than 10^{-9} mm of mercury;

(ii) the work function measurements were made on the actual cathode used for the determination of the minimum sparking potential. Thus, the effect of adsorbed gas layers on the cathode was automatically accounted for;

(iii) a wide range of cathode work functions was possible using various oxide cathode surfaces;

(iv) the emissive work function of the cathode before the introduction of gas could also be determined. This made it possible to check the slope of the line relating ϕ and V_{sm}, although it was still not possible to relate V_{sm} to absolute values of the cathode work function without accurate knowledge of the temperature variation of the work function of an oxide-coated cathode;

(v) the secondary ionization coefficient ω/α could be calculated as a function of E/p for various types of cathode surfaces.

ACKNOWLEDGEMENTS

The authors wish to thank Prof. F. A. Vick for extending to them the facilities of the laboratory.

One of the authors (B. J. H.) makes acknowledgement to Metropolitan-Vickers Electrical Co. Ltd. for a scholarship which enabled him to take part in the work. Thanks are also due to the General Electric Co. Ltd. and to Siemens-Edison Swan Co. Ltd. for the gift of materials, and to Dr. A. A. Shepherd of Ferranti Ltd. for the gift of cathode buttons.

The authors also wish to thank Mr. F. Rowerth and Mr. H. Birchall of the College technical staff for assistance in the preparation of the paper.

REFERENCES

(1) DAVIES, D. E., and FITCH, R. K. *Brit J. Appl. Phys.*, **10**, p. 502 (1959).

(2) RIVIERE, J. C. *Proc. Phys. Soc. B (London)*, **70**, p. 676 (1957).

(3) DAVIES, D. E., and MILNE, J. C. *Brit. J. Appl. Phys.*, **10**, p. 301 (1959).

(4) LLEWELLYN JONES, F., and DAVIES, D. E. *Proc. Phys. Soc. B (London)*, **64**, p. 519 (1951).

(5) HOPKINS, B. J., and VICK, F. A. *Brit. J. Appl. Phys.*, **9**, p. 257 (1958).

(6) HERMAN, G. and WAGNER, S. *The Oxide-Coated Cathode*. Vol. 2 (London: Chapman and Hall Ltd., 1951).

Influence of the cathode work function on the sparking potential in hydrogen

By D. E. Davies, B.Sc., Ph.D., A.Inst.P., and R. K. Fitch, B.A., M.Sc., Grad.Inst.P.,* Department of Physics, University College of North Staffordshire, Keele, Staffs.

[*Paper first received* 2 *December*, 1958, *and in final form* 8 *April*, 1959]

The Kelvin or vibrating electrode method of measuring contact potential differences has been used to follow changes in work function of evaporated metallic films in a parallel plate electrode system in hydrogen at about 10 mm of mercury pressure. A reduction in cathode work function of the order of 0·3 eV was effected by passing a current of 10^{-7} A for 10 s. After about 30 min the cathode work function returned to its original value. Similar treatment caused a reduction in the sparking potential of 30 V, which also returned to its original pre-discharge value in times of the order of 30 min. This, together with other experimental data, is consistent with the fact that positive ions from the discharge current remained on the cathode surface for periods up to 30 min after the current was switched off. It has been possible to demonstrate that, while these positive ions are being neutralized, there is a relationship between the work function of a cathode and its sparking potential in hydrogen.

The role of the cathode in a d.c. discharge in hydrogen has been studied by previous investigators.[1, 2, 3] In some of these a relationship was assumed between the cathode work function and the sparking potential, in order to explain the observed phenomena. This assumption was easily justified in a qualitative manner as follows.[4] The Townsend criterion for a self-maintained current in hydrogen can be written as:

$$1 - A\{\exp(\alpha d_s) - 1\} = 0 \qquad (1)$$

or:

$$1 - A\left[\exp\{f(V_s/pd_s)pd_s\} - 1\right] = 0 \qquad (2)$$

where A is a measure of the cathode emission, d_s the electrode separation at which the spark passes in a gas at a pressure p for the applied sparking potential V_s; $\alpha = pf(V_s/pd_s)$ is the first Townsend ionization coefficient. Since the cathode emission is related to the cathode work function, then, from equation (2), the sparking potential should vary with the cathode work function for a given value of pd_s. This qualitative argument was confirmed experimentally by Llewellyn-Jones and Henderson[1] and by Jacobs and La Rocque,[3] using the tabulated values of work functions of the cathode materials. In view of the complex nature of the adsorbed layers of gas atoms (and/or ions) that are possible under gas discharge conditions, and their possible effect on the work function of a cathode surface, it was thought to be desirable to measure the cathode work function and the sparking potential under identical conditions.

This paper thus sets out the results of an investigation (*a*) into the feasibility of applying the Kelvin method to follow changes in the cathode work function when the gas pressures are of the order of 10 mm of mercury, and (*b*) on the preliminary experiments to establish a relationship between the sparking potential in hydrogen and the work function of the cathode.

EXPERIMENTAL APPARATUS AND PROCEDURE

The experimental tube consisted essentially of one fixed electrode—the cathode, and two movable electrodes—the anode and the reference electrode. (see Fig. 1) The electrodes were formed by melting boro-silicate glass in a carbon mould of suitable shape and inserting a tungsten rod in the glass whilst it was molten. This tungsten rod then served as an electrical connexion to the deposited film. The flat portion of each electrode (approximately 1·5 cm diameter) was ground, flame polished and the tungsten rods finally cleaned electrolytically. The electrodes were assembled within a glass frame (mounted on to a commercial pinch supplied by Siemens–Edison Swan Co. Ltd.) in such a way that two of them could be rotated by means of an external magnet into two stable positions: (*a*) with the anode and cathode parallel at a measured gap separation (usually 0·1 cm), and (*b*) with the reference electrode opposite the cathode. Sparking potential measurements were made with the electrodes in position (*a*) and contact potential differences measured in position (*b*). In the latter position the reference electrode vibrated with respect to the cathode at a frequency between 10 and 30 c/s, depending on the dimensions of the crossed tungsten strip supports. The electrode was set in vibration by simply tapping the envelope of the tube. Tungsten filaments carrying beads of the appropriate metals were mounted on the pinch so that a film of copper could be evaporated on to the cathode and on to the anode, and a film of gold on to the reference electrodes. The evaporating atoms were directed towards the appropriate electrodes by means of nickel cylinders surrounding the tungsten filaments. All of the metallic parts were heated in an atmosphere of hydrogen prior to assembly. Before sealing the completed tube into an envelope, the inside of the latter was coated with a conducting film of Aquadag which was maintained at earth potential during work function measurements.

The vacuum system consisted of two parts: (1) a conventional all-glass system with oil diffusion pump, rotary backing pump, oil manometer and a hydrogen generation set with a palladium osmosis tube; and (2) a grease-free system with two cold traps, a mercury diffusion pump, another cold trap, a water vapour trap, and a rotary backing pump. The experimental tube was connected to system (1) through a palladium osmosis tube and to system (2) through a glass seal and a constriction. The tube was initially opened to the vacuum system (2) by breaking the glass seal with a magnetically operated breaker, but only when the pressure in the system (2) was below 10^{-5} mm of mercury. It could be isolated from this system by collapsing the constriction. With the above precaution it was hoped that mercury vapour contamination of the tube would be eliminated.

The contact potential difference between the reference electrode and the cathode was determined as follows. A resistance of 10^8 Ω was connected between the two electrodes. When the reference electrode was set vibrating, the capacitance

* Now at the College of Advanced Technology, Birmingham.

between it and the cathode altered. Owing to the contact potential difference between them, charge flowed through the resistence, thereby generating an oscillating potential difference across the high resistance. This was then fed into an amplifier of high impedance input and of high gain

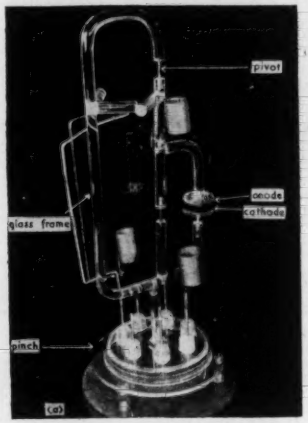

(*a*)

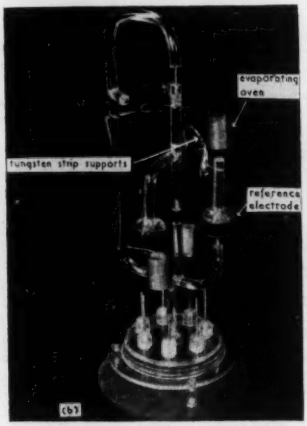

(*b*)

Fig. 1. Model of experimental tube in two stable positions (*a*) with anode and cathode parallel and (*b*) with reference electrode opposite the cathode

(10000 : 1). The amplified oscillating potential difference was displayed on an oscilloscope. By means of a backing-off potential in series with the tube and the $10^8\ \Omega$ resistance, the signal received on the oscilloscope was reduced to zero. The backing-off potential was then equal and opposite to the contact potential difference between the two electrodes. The tube and amplifier were adequately screened to increase the signal-to-noise ratio. It was possible to determine the contact potential difference to $\pm 0{\cdot}002$ V.

The sparking potential in hydrogen was determined by applying a potential (increased in steps of 1 V) to the electrodes for a fixed time (5 s). The lowest potential, at which a steady current of 10^{-8} A flowed, was taken as the sparking potential.

The tube, together with all the glass between the palladium osmosis tube and the constriction, was baked at 420° C for several hours. During this time hydrogen generated in system (1) and purified by passage through a palladium osmosis tube was admitted to the tube through a second palladium osmosis tube and pumped out through system (2). In this way it was hoped that any oxygen in the system would be removed. After this process both systems were pumped with the connecting osmosis tube hot, and the experimental tube, etc., baked for forty-eight hours to remove adsorbed hydrogen.

The tube was isolated from system (2) at a pressure less than 10^{-6} mm of mercury. The films were evaporated in the sequence, copper on to the anode, gold on to the reference electrode and finally copper on to the cathode. It was hoped that the residual gas pressure would be reduced by the gettering action of the evaporating films.

RESULTS

In the interests of simplicity the contact potential difference measurements have been converted into actual work functions of the cathode surface. This has been done by adopting Riviere's value for the work function of the gold reference surface.[5] It must be stressed at this stage, however, that the results quoted are not absolute work functions, and also that the results are still valid should the work function of gold in hydrogen prove to be different from the value published by Riviere. Thus, the only assumption made is that the work function of the gold surface remains constant throughout the measurements.

From Fig. 2(*a*) it will be seen that, during the 20 min after the copper film had been deposited, the work function fell by 0·05 eV. This can be explained in terms of the adsorption of hydrogen liberated during the evaporation of the film on

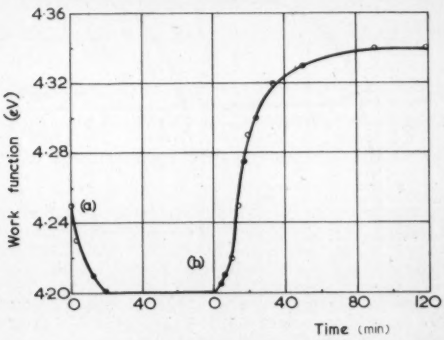

Fig. 2. Work function of a copper cathode as a function of time; (*a*) immediately after its deposition, (*b*) on admitting hydrogen through the palladium osmosis tube

to the copper surface (since the beads were formed in hydrogen). After this first 20 min the work function of the copper surface remained constant indefinitely. The effect of heating the palladium osmosis tube to admit hydrogen is shown at point (*b*) of Fig. 2. The explanation for this large increase in cathode work function could not be found until the palladium osmosis tubes were examined closely. It was then found that each tube had been sealed at one end by means of silver solder. Such a seal would, of course, allow oxygen to diffuse slowly into the experimental tube together with the hydrogen. This oxygen would be preferentially adsorbed on the cathode surface and would account for the increase in work function. Subsequent work with palladium osmosis tubes sealed with gold did not show this effect. Thus, the surface for which the following investigations are reported is not a clean metallic surface, but one which has an adsorbed oxygen or oxide layer.

The gas pressure in the tube was set at that corresponding approximately to the minimum sparking potential by adjusting the pressure in the vacuum system (1) and heating the palladium osmosis tube joining it to the experimental tube until the pressure, as indicated by an oil gauge in the system (1), no longer altered. It was then assumed that there was no pressure gradient through the palladium tube. In this manner the pressure in the tube was measured without contaminating the gas in the tube in any way.

During measurements with the early experimental tubes it was observed that, in order to produce the initial discharge, it required a higher potential difference than with subsequent discharges; i.e. it appeared that the cathode surface had been modified by the passage of the first discharge. This effect was examined in the following manner. A self-maintained current (10^{-7} A) was passed between the anode and cathode for 10 s, after which the reference surface was immediately brought above the cathode and its work function followed with time. The result is shown in Fig. 3. Immediately after the discharge it will be observed that the cathode work function fell by about 0·3 eV, but within 30 min it had returned to its previous stable value of about 4·34 eV. On repeating this sequence of operations the second part of the curve in Fig. 3 was obtained, and subsequent discharges showed that this form of curve was quite reproducible. The effect was observed in four similar tubes, although the magnitude of the change was not always the same in each case. The changes in work function for one tube were found to be independent of the magnitude of the current (over a limited range) and of its duration. The effect of these small changes in the work function of the cathode surface on the sparking potential in hydrogen were then investigated.

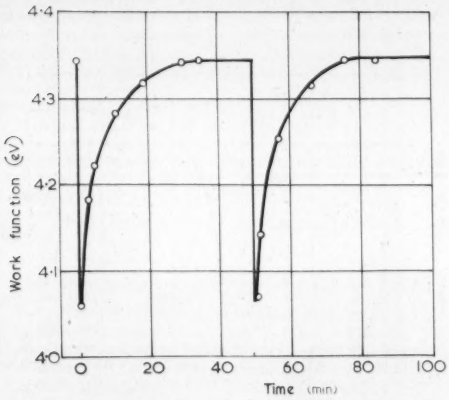

Fig. 3. Work function of a copper cathode as a function of time after a current of 10^{-7} A had passed for 10 s between anode and cathode at times of 0 and 50 min

A discharge current of 10^{-7} A was passed between anode and cathode for a period of 10 s and the sparking potential immediately redetermined. An exactly similar discharge was again passed and, after a time t, the sparking potential was again measured. This process was continued until the curve of V_s against t, shown in Fig. 4, was obtained. Again in this figure two curves are plotted to illustrate the reproducibility of the effect. Similar results were obtained from the four other tubes.

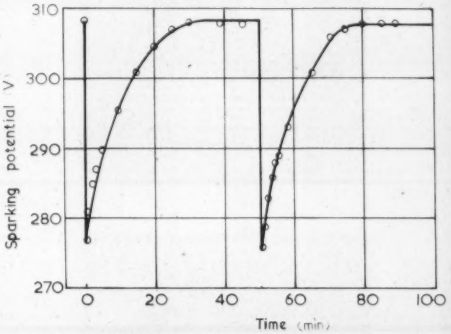

Fig. 4. The sparking potential in hydrogen of a copper cathode as a function of time after a current of 10^{-7} A had passed for 10 s between anode and cathode at times of 0 and 50 min

The effect of passing a discharge in the reverse direction, i.e. with the cathode positive, was studied next. Apart from the reversal of polarity, exactly the same discharge conditions were maintained. Work function measurements immediately after the discharge indicated an increase in the cathode work function of roughly the same magnitude as the decrease caused by the normal discharge. In an exactly analogous manner a decay took place until the normal work function was reached in about 30 min. No change in the sparking potential was recorded after the passage of a reverse discharge, in complete contrast to the effect of a normal discharge.

DISCUSSION OF THE RESULTS

There are two possible explanations for the changes in the work function of the cathode surface:

(*a*) that hydrogen positive ions produced by the current of 10^{-7} A in the forward direction are deposited on an insulating oxygen layer already on the cathode, and in this way form an electrical double layer on the cathode surface with the positive end outermost. This type of electrical double layer would reduce the work function of the cathode, which would subsequently recover slowly with time as the positive ions were neutralized;

(*b*) that the hydrogen positive ions combine with the oxygen adsorbed on the cathode surface to form water vapour, and thus expose a clean surface of lower work function. The subsequent adsorption of oxygen from the gaseous atmosphere would result in a gradual increase in work function. In order to decide between these two explanations it is necessary to consider the effect of passing a reverse current. In this case electrons would be deposited in the cathode surface, and would thus form an electrical double layer which would increase the effective work function of the cathode surface. These electrons would leak away with time giving the observed decrease in work function. On the other hand, the removal of oxygen by the bombarding electrons would result first in a decrease in ϕ and then in a slow increase in ϕ with time as the oxygen was readsorbed. This does not agree with the results presented above.

The observed changes in ϕ correspond to changes in V_s (Figs. 3 and 4), except in the case when electrons on the insulating layer of oxygen raised the work function but produced no change in V_s. However, this is not at all surprising in that any exposure of the stable, but lower, work function portion of the cathode surface (due to loss of electrons) would enable the gap to break down at the lower values of V_s corresponding to that lower work function i.e. unless the cathode surface was completely covered with electrons all the time it would be impossible to observe the higher values of V_s corresponding to the higher values of ϕ.

A similar type of argument eliminates explanation (*b*) in that this type of explanation allows only two values of V_s; i.e. that corresponding to the clean copper surface with a lower and stable work function and that corresponding to the copper surface completely covered with a monolayer of oxygen. Values of V_s between these limits would be impossible.

CONCLUSIONS

It is concluded from this investigation that the Kelvin method for determining the work function of a metal film cathode can be applied in the presence of hydrogen at a pressure of the order of 10 mm of mercury to give reproducible results. These results indicate the importance of high gas purity and good vacuum conditions if insulating films on the cathode surface are to be avoided. The effect of these insulating layers on second and subsequent discharges has been demonstrated.

Although absolute work function measurements could not be made this does not affect the results, since these are based on differences in work function and in sparking potential. However, it has been possible to measure both of these quantities under identical conditions, which has not previously been achieved. In this way a relationship has been demonstrated between the work function of the cathode surface and its sparking potential in hydrogen.

ACKNOWLEDGEMENTS

The authors wish to thank Prof. F. A. Vick for extending to them the facilities of the laboratory, and also Dr. J. W. Mitchell, of the H. H. Wills Laboratory, University of Bristol, for extremely helpful discussion on work function techniques. Thanks are also due to Siemens-Edison Swan Co. Ltd. for the gift of pinches and envelopes.

One of the authors (R. K. F.) wishes to thank the British-Thomson Houston Co. for the award of a research scholarship from September 1955 to December 1956.

The authors also wish to thank Mr. F. Rowerth and Mr. H. Birchall of the College technical staff for assistance in the preparation of the paper.

REFERENCES

(1) LLEWELLYN-JONES, F., and HENDERSON, J. P. *Phil. Mag.*, **28**, p. 185 (1939).
(2) LLEWELLYN-JONES, F., and DAVIES, D. E. *Proc. Phys. Soc. B* (*London*), **64**, p. 397 (1951).
(3) JACOBS, H., and LA ROCQUE, A. P. *Phys. Rev.*, **74**, p. 113 (1947).
(4) LLEWELLYN-JONES, F., *Phil. Mag.*, **28**, p. 192 (1939).
(5) RIVIERE, J. C. *Proc. Phys. Soc. B* (*London*), **70**, p. 676 (1957).

Efficiency of characteristic K_α X-ray production in copper between 9 and 15 kV

By N. A. DYSON, M.A., Ph.D.*

[*Paper received* 13 *May*, 1959]

Absolute measurements are described of the production of K_α characteristic X-radiation in copper, and the data are compared with existing information. The measurements (together with a single existing observation) cover a range of electron energies between 9 and 15 kV.

In the course of some measurements of the continuous X-ray spectrum, reported elsewhere,[1, 2] the characteristic *K*-radiation from copper was excited, and its intensity measured by an absolute method at several voltages. An account of these measurements is given, and they are compared with existing data. The targets consisted of copper foil, in the region of one micron in thickness, and the measurements were made in the forward direction.

* The author is at present at the Radiotherapeutic Research Unit, Hammersmith Hospital, London. This paper is based on experimental work carried out at the Cavendish Laboratory, Cambridge.

EXPERIMENTAL METHOD AND RESULTS

The apparatus and methods used for these measurements have already been described.[2] The X-ray tube consisted of a three-electrode gun, a weak magnetic lens, and a "window-type" target. For the measurements reported here, copper targets of 0·75, 1·63 and 3·0 μ thickness were used and, in all cases, these thicknesses were sufficient to bring the incident electrons to rest. The radiation was detected using a proportional counter, and pulse-height distributions of the X-ray spectra were obtained using a single-channel pulse-height analyser. The characteristic K_α- and K_β-radiation appeared as a single peak superimposed on the continuous

background. Pulse-height distributions were obtained at four different voltages above the K-excitation potential. The energy in the peak was calculated by measuring the area under it, correcting for the continuous radiation and for absorption and detection losses, and relating the result to the incident-beam current. For copper, the fraction of the total K-radiation which appears in the K_α line (strictly the $K_{\alpha 1}$ and $K_{\alpha 2}$ lines together) can be shown to be 0·88,[3] and so the efficiency for K_α-production can readily be calculated. The results, expressed as the total number of K_α-quanta leaving the point of production, per incident electron, are shown in the figure.

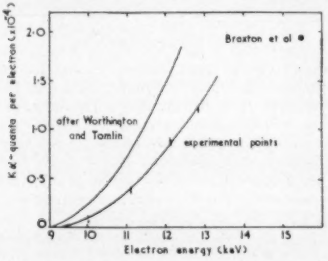

Production of characteristic K_α-radiation in copper

COMPARISON WITH EXISTING DATA

There are few measurements of the intensity of characteristic radiation, and the only measurement which can be compared directly with the present work is that by Braxton, Baez and Kirkpatrick.[4] They determined the energy efficiency for the production of characteristic K_α-radiation in a thick copper target at 15·5 kV, and found a value of 10^{-4}, corresponding to $1{\cdot}94 \times 10^{-4}$ quanta per electron. This value is shown in the figure for comparison, and is reasonably consistent with the present measurements.

The only other source for comparison is the calculated data on the intensities of characteristic radiation given by Worthington and Tomlin.[5] These authors reviewed the experimental and theoretical data for the cross-section Q_k for K-ionization as a function of electron energy. Experimental data for nickel and silver are available consisting, in each case, of a series of relative intensity measurements[6, 7] from thin targets (that is, targets which allow the transmission of electrons with negligible energy loss) standardized by single absolute determinations.[8, 9] If the electron energy is expressed in the form $U = V/V_k$, where V is the accelerating voltage, and V_k the K-excitation potential, the product $Q_k V_k^2$ appears to be approximately the same function of U for both elements. The theoretical development by Mott and Massey,[10] and its extension to smaller values of U by Worthington and Tomlin[5] show that $Q_k V_k^2$ is in fact independent of Z, but, quantitatively, the agreement between theory and experiment is not good. It is agreed that $Q_k V_k^2$ rises sharply from zero at $U = 1$ to a maximum at about $U = 2{\cdot}5$, and then falls off as U is further increased, but the experimental values reach their maximum at a higher value of U, and then fall off less rapidly, than the theory suggests.

However, the experimental data are sufficiently reliable to enable an integration (incorporating a suitable energy-loss expression) to be carried out, and this has been done by Worthington and Tomlin.[5] Under thick target conditions (that is, conditions in which the electrons are brought to rest within the target, as in the present work) they expressed the ionization as n, the number of K-ionizations per electron, from which the number of K_α-quanta per electron could be calculated simply by multiplying by the fluorescence yield and correcting for the K_β contribution.

The quantity n was evaluated for silver only. However, detailed calculations of a quantity $N_\phi(U)$ were carried out for several elements, including copper. The quantity $N_\phi(U)$ is defined in such a way that the total number (per electron) of K_α-quanta, including radiation arising by fluorescence, leaving a massive target at an angle ϕ to the target surface and within a solid angle $d\omega$ is given by $N_\phi d\omega/4\pi$. The calculations included an allowance for the variation of target absorption with ϕ and, because of the varying depth of origin of the radiation, with U, but the calculations may be related directly to the present circumstances without any recalculation of the integrals. The present measurements extend only up to $U = 1{\cdot}45$, for which the maximum depth of origin of copper K-radiation is only $0{\cdot}3\ \mu$.* The calculations of Worthington and Tomlin are mainly for very small values of ϕ, at which the absorption effects are relatively large; but at 45 deg. (the highest angle computed by them) the effective thickness of target involved is less than $0{\cdot}5\ \mu$, in which the absorption of characteristic K_α-radiation is only about 2·5%. This is negligible, so their values of N_ϕ calculated at 45 deg. are very nearly equal to the total number of K_α-quanta escaping from the atoms of the target material per incident electron, and are therefore directly comparable with the present experimental results.

Values for the number of K_α-quanta per electron calculated in this way are shown in the figure. These calculated values are higher than the experimental data by a factor of approximately 2.

DISCUSSION

Although the three sets of data shown in the diagram all represent the number of K_α-quanta leaving the atoms of a copper target, and are thus directly comparable, the effect of fluorescent radiation (arising from K-shell ionization caused by the photoelectric absorption of continuous radiation) has to be considered. In the present measurements, the amount of fluorescent radiation produced is not the same as with a massive target. In the latter case, about half the total continuous radiation will be absorbed, giving rise to fluorescence, whereas with a target consisting of a thin foil, considerably less than half the total continuous radiation is absorbed, although most of the radiation emitted at right-angles to the electron beam will be absorbed. However, Stoddard[13] found that the fluorescent contribution to the total characteristic radiation from a massive copper target amounted to only 13% (nearly constant over a wide range of values of U), so any uncertainty introduced by fluorescence effects in the comparison between the present work and the calculations of Worthington and Tomlin[5] cannot be more than this.

Braxton *et al.*[4] state that the characteristic radiation they measured was "that produced . . . by electron bombardment", and if this is taken to mean that it excludes the fluorescent contribution, their value must be increased by a factor of 1·15 (from Stoddard's data) to make it comparable with the rest of the data in the diagram.

* Calculated from the range-energy data of Lane and Zaffarano[11] with a correction derived from the Bethe–Bloch energy-loss expression[12] to convert from aluminium to copper.

Although there are no data other than that to which reference has already been made which are suitable for comparison with the present work, a number of measurements of the ratio of characteristic-to-continuous-radiation intensities has been made by Bendit,[14] extending down to 15 kV. This data however refers, to the intensities at the point of leaving the X-ray tube and cannot be related to absolute measurements without a knowledge of target and window absorption. The same author reviews a number of measurements (made by himself and others) at 30 kV. Wide discrepancies were noted by him which possibly arise from uncertainties in making measurements at very small glancing angles (2–3 deg.). For these reasons it seems unlikely that these data can be related to the absolute data already obtained.

It is noteworthy that Worthington and Tomlin[5] made an absolute observation of the K_α-characteristic radiation intensity (at a small angle to the target surface) at 30 kV. They obtained a value of approximately one-half the value predicted by them for the appropriate conditions, but attributed the discrepancy to experimental error.

It can be concluded, at least for voltages below 15 kV, that the calculations of Worthington and Tomlin[5] yield results which are high by a factor of approximately two, and that the present measurements are in moderate agreement with the single determination of Braxton *et al.*[4]

ACKNOWLEDGEMENTS

The author wishes to acknowledge the receipt of a maintenance grant from the Department of Scientific and Industrial Research during the period of the experimental work, and would like to thank Dr. V. E. Cosslett for his guidance and constructive criticism at all stages of the investigation.

REFERENCES

(1) Cosslett, V. E., and Dyson, N. A. *Contribution to "X-ray Microscopy and Microradiography"*, p. 405 (New York: Academic Press Inc., 1957).
(2) Dyson, N. A. *Proc. Phys. Soc.*, **73**, p. 924 (1959).
(3) Compton, A. H., and Allison, S. K. *X-rays in Theory and Experiment*, 2nd ed., p. 641 (New York: Van Nostrand, 1935).
(4) Braxton, W. L., Baez, A. V., and Kirkpatrick, P. *Phys. Rev.*, **68**, p. 106 (1945).
(5) Worthington, C. R., and Tomlin, S. J. *Proc. Phys. Soc.*, **69a**, p. 401 (1956).
(6) Pockman, L. T., Webster, D. L., Kirkpatrick, P., and Harworth, K. *Phys. Rev.*, **71**, p. 330 (1947).
(7) Webster, D. L., Hansen, W. V., and Duveneck, F. B. *Phys. Rev.*, **43**, p. 839 (1933).
(8) Smick, A. E., and Kirkpatrick, P. *Phys. Rev.*, **67**, p. 153 (1945).
(9) Clark, J. C. *Phys. Rev.*, **48**, p. 30 (1935).
(10) Mott, N. F., and Massey, H. S. W. *The Theory of Atomic Collisions* (London: Oxford University Press, 1949).
(11) Lane, R. O., and Zaffarano, D. J. *Phys. Rev.*, **94**, p. 960 (1954).
(12) Paul, W., and Steinwedel, H. *"β- and γ-ray Spectroscopy"*, Chap. 1 (Amsterdam: North Holland Publishing Co., 1955).
(13) Stoddard, K. B. *Phys. Rev.*, **46**, p. 837 (1934).
(14) Bendit, E. G. *Brit. J. Appl. Phys.*, **9**, p. 312 (1958).

Electrical conductivity of vitrain during carbonization

By M. I. Pope, B.Sc., Ph.D., A.R.I.C., and S. J. Gregg, D.Sc., F.R.I.C., Washington Singer Laboratories, The University, Exeter

[*Paper first received* 22 *June, and in final form* 15 *July*, 1959]

Some vitrain samples, representative of the whole coal range, have been carbonized in oxygen-free nitrogen and their electrical conductivity measured *in situ*. The results have been interpreted in terms of the known processes occurring during carbonization.

Although it has long been known that coals become electrically conducting after heating at moderate temperatures (for example, Sandor[1]), no detailed investigation of the changes in electrical conductivity with temperature of carbonization appear to have been undertaken. It was therefore decided to carry out a systematic investigation using a series of vitrains for which a considerable body of other data has already been accumulated elsewhere. Despite the complexity of the changes occurring in coals during carbonization, the recent introduction of several new techniques of investigation in this field (such as infra-red absorption, mass spectrometry and paramagnetic resonance) has made it possible to formulate a reasonable hypothesis for the results obtained.

MATERIALS

Details of the powdered vitrains are given in the table. Except for sample *H*, all experiments were carried out on compacts prepared at 60 000 lb/in.^{2} in a split mould of $\frac{1}{2}$ in. diameter, the applied pressure being maintained for three minutes by means of a hydraulic press. In the case of sample *H*, which could not be compacted, a block of the original vitrain was ground to a cube of size similar to that of the compacts, using a high-speed carborundum wheel.

Details of powered vitrain

Sample	*Origin of vitrain*	*% carbon (d.m.f.)*	*% volatile matter*	*Rank No.*
A	Nailstone, Yard Seam	78·5	43	902
B	Cannock Wood, Shallow Seam	80·0	43	802
C	Markham Main, Barnsley Seam	82·5	41	602
D	Dinnington Main, Barnsley Seam	85·0	37	502
E	Houghton Main, Parkgate Seam	87·5	32	401
F	Roddymoor, Ballarat Seam	88·5	27	301
G	Coegnant, Gellideg Seam	91·5	16·3	203
H	Blaenhirwaun, Pumpquart Seam	94·0	5·0	101

EXPERIMENTAL

Measurement of the electrical conductivity was carried out with the electrometer valve bridge circuit shown in Fig. 1. At no time was the potential gradient across the sample allowed to exceed 1 V/cm. Application of a small potential difference (E_1) across the sample causes a change in the grid potential of V_1, thus resulting in a change in the potential difference across the anode load resistance; the difference between the two anode potentials is indicated by the galvanometer. The grid potential of V_1 can then be restored to its original value by application of an opposing e.m.f. (E_2). It can then be shown that the resistance of the sample (R_x) is given by the equation:

$$R_x = R_s\left(\frac{E_1}{E_2} - 1\right).$$

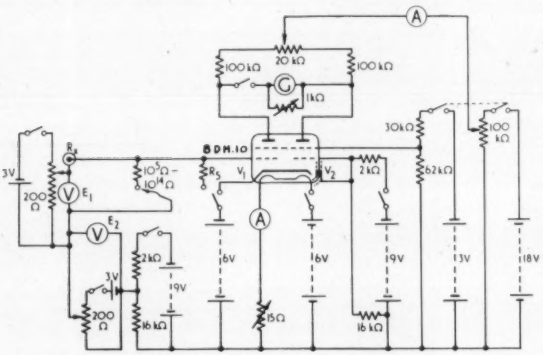

Fig. 1. Circuit of the electrometer valve bridge used for resistance measurements

The vitrain compacts were subjected to a rate of rise of temperature of 3° C/min in an atmosphere of oxygen-free nitrogen, using the apparatus shown in Fig. 2. A Mullite tube (*A*) of 15 mm internal diameter is mounted horizontally

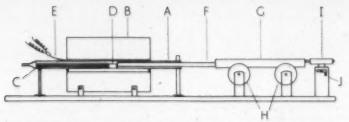

Fig. 2. The furnace in which the resistance of compacted samples can be measured in atmospheres of various gases, up to 1000° C

in a tubular electric furnace (*B*); the tube is reduced to a narrow neck at one end so that a steady flow of gas can be passed over the sample. A fluted silica spacer (*C*) keeps the compacted sample (*D*) in a fixed position near the centre of the furnace, and directly below the junction of a platinum rhodium thermocouple (*E*). A Mullite rod (*F*) of 12 mm diameter has one end inserted concentrically into the silver steel rod (*G*) which is balanced so as to move freely on two pulley wheels (*H*). The steel rod is pressed against the compact by a spring-loaded device (*I*) which exerts a pressure well in excess of that required to give constant conductivity readings. Electrical contact with the compact is made by means of two platinum-foil electrodes pressed against its opposing faces, connexion being made through 36 s.w.g. platinum wires led out through each end of the furnace tube (*A*).

RESULTS AND DISCUSSION

The variation of electrical resistance of the vitrains as a function of temperature is shown in Fig. 3. With the exception of anthracite (sample *H*), all the vitrains show a fall in resistance from about 10^{11} Ωcm at 100° C to about 1 Ωcm above 800° C; the initial resistance of the anthracite is somewhat lower because of intrinsic semiconduction. The results are replotted as the rate of change of electrical resistance as a fuuction of temperature (Fig. 4), and, as will be seen, the curves exhibit a number of common features and vary in a fairly definite manner with the rank of the vitrain. The samples having carbon contents below 91% show maxima at (1) 300–350° C and (2) 450–500° C; all show a broad maximum (3) between 600 and 700° C and minima (4) at 150° C and (5) between 500 and 600° C. Despite the complexity of the curves, repeat experiments have shown that all the peaks illustrated in Fig. 4 are reproducible.

The peaks will now be dealt with in order of increasing temperature. The minimum (4) occurring at 150° C is readily explained by loss of physically adsorbed water, which is largely responsible[2] for the electrical conduction of coals (of lower rank than anthracite) at room temperature. This peak can, in fact, be completely eliminated if the compact is first air-dried for several hours at 110° C and allowed to cool over phosphorus pentoxide. An endothermic peak in the d.t.a. curves for a range of coals has also been observed at 150° C and has been ascribed[3] to loss of water.

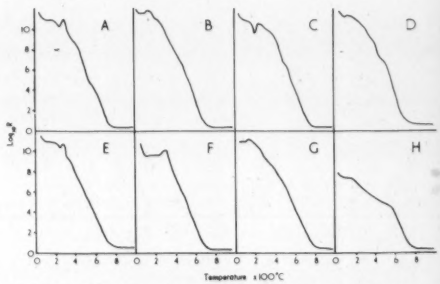

Fig. 3. The log resistivity of the vitrains plotted against temperature of carbonization, in an atmosphere of oxygen-free nitrogen

The first maximum (1) observed between 300 and 350° C occurs in a region where there is no evidence of any structural decomposition of the vitrain. However, Holden and Robb[4] have shown by mass spectrometry that between 170 and 300° C an appreciable amount of alkyl aromatic material is evolved. They have concluded that the molecules are physically adsorbed; their removal from the micropores in the vitrain would then involve an energy of activation, for reasons

similar to those advanced to account for the anomalous adsorption of nitrogen and other gases at liquid-air temperature.[5] For the large aromatic molecules in question, this energy of activation would be correspondingly larger and desorption would accordingly first occur at higher temperatures.

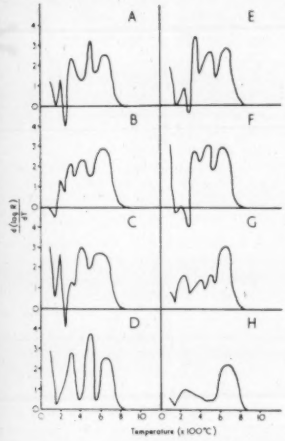

Fig. 4. The rate of change of the resistivity of the vitrains, plotted in arbitrary units, against temperature of carbonization in oxygen-free nitrogen

Removal of such adsorbed material would allow better contact between the particles of vitrain and possibly also promote a certain amount of ordering of the component aromatic layers, thus accounting for the small but definite decrease in electrical resistance occurring over this temperature range. It has already been observed[6] that desorption of *n*-butane or of ethyl chloride from previously saturated compacts of vitrain does produce an appreciable increase in the electrical conductivity.

The maximum (2) at 400–450° C appears to correspond to the primary carbonization process,[7] during which tar is formed, presumably as a result of the rupture of aliphatic bridges between aromatic groups. The evidence from X-ray analysis,[8] supported by that from infra-red adsorption,[9] strongly suggests that no appreciable growth in the mean aromatic-layer diameter occurs much below 600° C. However, when aromatic material is volatilized from a vitrain to give tar, those aromatic layers remaining in the residue will be able to achieve a relatively high degree of alinement.[8] In addition, it is known[10] that the free radical concentration in carbonized coals reaches a maximum at about 500° C. A typical example (for a coal of 81·9% initial carbon content) is illustrated in Fig. 5, curve I; thence it will be seen that the electrical conductivity (curve II) also shows a corresponding increase in the same temperature range. Now when an aliphatic group attached to an aromatic sheet is removed, an electron trap is formed; electrons from the π band can now jump into the trapping σ orbitals[11] where bond fission has occurred, leaving conducting holes in the π band. The fall in the free radical concentration above 500° C, despite a continuing increase in the electrical conductivity, is caused by growth in the mean aromatic-layer diameter which occurs during secondary carbonization. Thus, the peak at 400–450° C probably arises as a result of two related processes: (*a*) the aromatic layers taking up a preferred orientation parallel to one another, and (*b*) conduction due to positive holes created in the π band as a result of rupture of the aliphatic bridges between the aromatic layers.

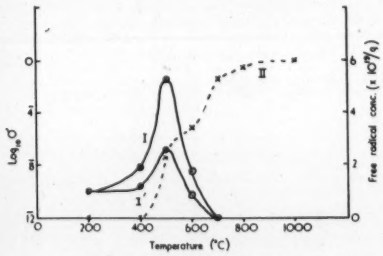

Fig. 5. Curves of free radical concentration, measured (I) in vacuum, (I′) in air and of log conductivity (II) measured in air, plotted against temperature of carbonization for a coal of 81·9% initial carbon content

The minimum (5) between 500 and 600° C probably marks the approaching completion of the primary carbonization process and the onset of secondary carbonization.

The broad maximum (3) occurring between 600 and 700° C coincides with the secondary carbonization process,[7] in which the bulk of the simple gaseous carbonization products (mainly methane and hydrogen), are formed. Removal of the peripheral alkyl groups on the ordered aromatic layers now allows considerable growth in the mean layer diameter of the aromatic sheets to occur, as is indicated by the X-ray studies of Diamond and Hirsch.[8] Confirmatory evidence for this growth in aromatic layer diameter during secondary carbonization is given by the reduction in the energy gap between the valence and conduction bands, which occurs[9] between 600 and 700° C. Inokuchi[12] has determined this energy gap for a large number of polynuclear aromatic molecules of known structure, and it has since been shown[13] from his results that a linear relation exists between the energy gap and the reciprocal of the aromatic surface area. Thus, the maximum (3) between 600 and 700° C is brought about by the growth in aromatic-layer diameter, made possible by the removal of aliphatic periphery groups.

Between 800 and 1000° C, little further change in the carbonized material appears to occur; the energy gap falls very slightly[9] (if at all) over this range of temperature, and correspondingly the electrical conductivity remains sensibly constant.

The diminution of peaks 1 and 2 for semi-anthracite in Fig. 4 *G* and their disappearance for anthracite in Fig. 4 *H* can now be understood. Anthracites already possess well-ordered aromatic sheets, in which the mean layer diameter is somewhat greater than for coals of lower rank. Consequently, primary carbonization no longer occurs, so that sample *H* exhibits intrinsic semiconductor properties up to the temperature (550° C) at which secondary carbonization begins. Calculation of the energy gap (E_g) for semiconduction from the slope of the curve of log conductivity (log σ) against the reciprocal of the absolute temperature ($1/T$) in Fig. 6, by application of the well-known relationship

$$\sigma = A \exp(-E_g/2kT)$$

gives a value of $E_g = 1{\cdot}00$ eV. From the relationship between E_g and the aromatic surface area, this energy gap

would be equivalent to an area of approximately 80 Å^2, or a mean aromatic-layer diameter of about 9 Å^2. This figure is in strikingly good agreement with the value of mean layer diameter obtained by Hirsch[14] for a vitrain of the same carbon content, 94%, by means of X-ray analysis.

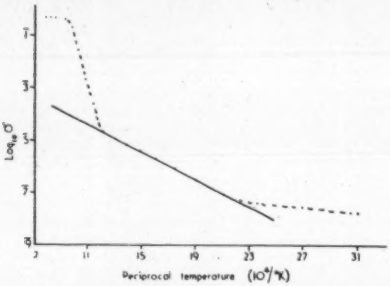

Fig. 6. The conductivity of a vitrain of 94% initial carbon content plotted against the reciprocal of the absolute temperature

CONCLUSION

The variation in the electrical conductivity of vitrains with temperature of carbonization is of much the same general form for all samples below the rank of anthracite, that is, from 78·5–91·5% carbon. As the temperature is increased, carbonization of vitrains appears to pass through the following four successive stages, each of which predominates for a definite range of temperature:

(1) loss of adsorbed water at 150° C;
(2) loss of adsorbed alkyl aromatic compounds and other volatile material between 150 and 300 or 350° C;
(3) primary carbonization, during which formation of tar occurs between 450 and 500° C;
(4) secondary carbonization, during which the bulk of the simple gaseous products are formed and growth in the mean aromatic-layer diameter occurs, between 600 and 700° C.

Between 800 and 1000° C little change in the carbonized material appears to occur.

Calculation of the mean aromatic-layer diameter in an anthracite sample, from the energy gap between the valence and conduction bands, leads to a value in good agreement with that expected from X-ray analysis of an anthracite with the same carbon content.

ACKNOWLEDGEMENTS

The authors wish to thank the National Coal Board for the supply of samples and for financial support of this work; and also Dr. D. J. E. Ingram for determination of the free radical concentration in a number of samples.

REFERENCES

(1) SANDOR, J. *Conference on the Ultra-fine Structure of Coals and Cokes, London* (1943).
(2) GREGG, S. J., and POPE, M. I. *3rd International Conference on Coal Science, Valkenburg* (1959).
(3) GLASS, H. D. *Econ. Geol.*, **49**, p. 294 (1954).
(4) HOLDEN, H. W., and ROBB, J. C. *3rd International Conference on Coal Science, Valkenburg* (1959).
(5) GREGG, S. J., and POPE, M. I. *Fuel (London)*. In the press.
(6) GREGG, S. J., and POPE, M. I. To be published.
(7) WOLFS, P. M. J., VAN KREVELEN, D. W., and WATERMAN, H. I. *3rd International Conference on Coal Science, Valkenburg* (1959).
(8) DIAMOND, R., and HIRSCH, P. B. *Conference on Industrial Carbon and Graphite, London* (1957).
(9) DURIE, R. A., and SZEWCZYK, J. *3rd International Conference on Coal Science, Valkenburg* (1959).
(10) AUSTEN, D. E. G., INGRAM, D. J. E., and TAPLEY, J. G. *Trans Faraday Soc.*, **54**, p. 400 (1958).
(11) MROZOWSKI, S. *Symposium on Properties of Carbon, Durham* (1956).
(12) INOKUCHI, H. *Bull. Chem. Soc., Japan*, **24**, p. 222 (1951).
(13) SCHUYER, J., and VAN KREVELEN, D. W. *Fuel (London)*, **34**, p. 213 (1954).
(14) HIRSCH, P. B. *Conference on Science in the Use of Coal, Sheffield* (1958).

Journal of Scientific Instruments

Contents of the November issue

ORIGINAL CONTRIBUTIONS

Papers

Semi-automatic control system for producing constant cooling rates. By W. L. Phipps.
Surge diverters using trigatrons. By T. E. Broadbent and A. Fernandez.
Apparatus for combined thermal analysis and dilatometry. By J. H. Pearce and P. G. Mardon.
Improved apparatus for floating-zone melting by electron bombardment. By E. F. Birbeck and A. Calverley.
Improved microbeam back-reflexion X-ray camera with arrangement for irradiating a preselected area. By H. M. Otte and R. W. Cahn.
Torsion-effusion apparatus for the study of vapour pressures of alloys. By J. N. Pratt and A. T. Aldred.
Direct stress machine for combined fatigue and creep testing. By A. H. Meleka.
TIM: a brushless generating magnetometer. By C. W. McCutchen.
Simple electrical analogue for the solution of linear simultaneous equations. By D. B. Dove.
Single pen, strip chart recorder for unattended long period operation. By C. J. Sumner.

Laboratory and Workshop notes

Precision pressure gauge for the range 0 to 30 mm of mercury. By E. H. Hirsch.
Linear saw-tooth time base. By J. S. Mainstone.
Thermoelectric e.m.f. of tin-cadmium alloys. By H. Charnock and S. A. Yeo.
Chemical cleaning of oxidized nickel-iron-cobalt alloys for glass-to-metal seals. By N. Rain.

NOTES AND NEWS

Notes and comments

THIS JOURNAL is produced monthly by The Institute of Physics, in London. It deals with all branches of applied physics (including theory and technique). All rights reserved. Responsibility for the statements contained herein attaches only to the writers.
EDITORIAL MATTER. Communications concerning editorial matter should be addressed to the Editor, The Institute of Physics, 47 Belgrave Square, London, S.W.1. (*Telephone:* Belgravia 6111.) Prospective authors are invited to prepare their scripts in accordance with the *Notes for Authors*. (Price 3*s*. 6*d*. including postage.)
REPRODUCTION. The Institute of Physics is a signatory to The Royal Society's Fair Copying Declaration. Details may be obtained upon application from The Royal Society, London, W.1.
ADVERTISEMENTS. Communications concerning advertisements should be addressed to the agents, Messrs. George Jackson (Fleet St.) Ltd., Cliffords Inn, Fleet Street, London, E.C.4. (*Telephone:* Holborn 3611–2.)
CLAIMS FOR MISSING JOURNALS. Claims from regular subscribers to this *Journal* for missing numbers will only be considered if received within 60 days of the date of mailing plus normal outward time of transit and time for lodging the claim. Losses attributable to failure to notify a change of address or to similar omissions will not be considered.
SUBSCRIPTION RATES. A new volume commences each January. The charge is £6 per volume ($17 U.S.A.), including index (post paid), payable in advance. Single parts, so far as available, may be purchased at 12*s*. 6*d*. each ($1.75 U.S.A.), post paid, cash with order. Orders should be sent to The Institute of Physics, 47 Belgrave Square, London, S.W.1, or to any bookseller.

Effect of crystallographic twins on the d.c. and a.c. properties of nickel-iron alloys

By J. E. THOMPSON, Ph.D., The English Electric Co. Ltd., Nelson Research Laboratories, Stafford

[*Paper received* 25 *June*, 1959]

A number of alloys of nickel-iron (equal parts) have been prepared from pure materials by powder metallurgy techniques. The degree of cold rolling and the annealing temperature have been varied in an attempt to obtain the optimum magnetic properties in the material after magnetic annealing. It has been found that crystallographic twins of varying number, length and thickness are produced during the annealing process. The effect of these twins on the coercive force and alternating total loss is discussed.

1. INTRODUCTION

Conventional magnetic materials made by the normal melting techniques contain non-magnetic impurities which have a deleterious effect on the magnetic properties, though it is difficult to obtain a precise correlation between impurities and magnetic properties. Materials are now available as very pure powders which can be sintered under controlled atmosphere conditions. A nickel-iron alloy (equal parts) was made by this method and heavily cold rolled to produce strip, which was wound into small coils and annealed at various temperatures from 1050 to 1300° C. The cores were then magnetically annealed and slowly cooled to room temperature. The d.c. coercive force and the a.c. total loss were measured accurately by the normal test methods.

On examination it was found that the alloy strip contained crystallographic twins, which, because of the high degree of preferred grain orientation (100)[001], were arranged with the twin boundaries at 45° to the rolling direction. The twins in this thickness (0·004 in.) of material pass straight through the strip and the area fraction of twins, β, and their distribution in terms of length l and width t was found to vary with degree of rolling and annealing temperature.

The d.c. coercive force can be explained in terms of the twin parameters on a model which is an extension of that used by Kersten[1] to predict the coercive force due to spherical impurities. One complication that arose was that the magnitude of the d.c. coercive force consisted of two parts, that from the twins and a second from the contribution of dislocations.

The calculation of a.c. loss of a magnetic material is an interesting problem. The actual loss experienced is considerably greater for these materials than is predicted in the well-known classical theory, which has been modified recently by Williams[2] and Lee.[3] However, this paper is concerned only with the increase in loss due to the presence of the twinned material, and the possible way in which domain movements are modified.

2. THE COERCIVE FORCE

The inclusion theory of coercive force developed in a number of papers by Kersten,[1] evaluates the change in wall area as the domain moves across a lattice of spherical inclusions. If the area of the wall associated with the inclusion is A, and the wall moves a distance dx, then the change in wall area is $e_w.dA$. For a 180° wall movement, the change in magnetization energy is $2HI_s.dv$, where H is the magnetic field, I the intensity of magnetization, dv a change in volume, and e_w the wall energy per unit area. Equating these two energies, $e_w.dA = 2HI_s.Adx$ ($dv = A.dx$). Under these conditions the field required to cause movement is the coercive force, so that

$$H_c \sim \frac{e_w}{I_s} \cdot \frac{1}{2A} \cdot \frac{dA}{dx} \qquad (1)$$

The position of minimum energy will be with the wall positioned across the centre of the sphere, and the values of A and dA/dx were worked out for spherical inclusion.

Kersten found good agreement with previous experimental results on Fe_3C.

Néel[4] has criticized the above on the grounds that the energy associated with the magnetic poles on the interface of the inclusion and magnetic material has been neglected. He developed a theory[5] to make allowances for this and for fluctuations in the direction of magnetization caused by strains. Expressions were developed for iron, where most of the energy is associated with non-magnetic inclusions, and in nickel, where most of the energy is associated with fluctuations of strain. Good agreement with theory was obtained in a number of cases.

More recently, Dijkstra and Wert[6] have obtained the contribution to the coercive force of randomly distributed non-magnetic inclusions for various cases, which included changes in wall energy and free pole effects. Experimental results were obtained using Fe_3C precipitates of various diameters.

3. THE EFFECT OF TWINS ON THE D.C. COERCIVE FORCE

In the case of twinned material, the whole material is magnetic, and compared with non-magnetic inclusions, free pole effects are very much reduced. It will be assumed that magnetization of the twins is independent of the bulk material and is not influenced by small external fields. Consequently, the energy of the wall will not be influenced by the presence of the twin, except where changes in wall area occur.

The material is sufficiently thin for the twins to pass completely through the strip, and the orientation of these twins is at 45° to the rolling direction and main crystal orientation.

In order to study the dependence of the coercive force on the twin parameters two models were adopted.

Model (*a*). Suppose the fractional area of twins to be β. The area of a twin is tl and the number per unit length of surface is $(\beta/tl)^{1/2}$. The spacing between centres is $(tl/\beta)^{1/2}$

and the average area of wall associated with a twin is $(tl/\beta)^{1/2}$ × depth of material. A change in wall area will only occur when the wall moves off the end portion and the change of area is $t\sqrt{2}$ × depth in a distance $t/\sqrt{2}$. The value of $1/A \,.\, dA/dx$ is consequently $2(\beta/tl)^{1/2}$, and equation (1) becomes

$$H_c \sim \frac{e_w}{I_s} \cdot \left(\frac{\beta}{tl}\right)^{1/2} \qquad (2)$$

So far, the concept of the particles lying on a uniform lattice has been used, which in practical cases is a limitation. The following simple calculation overcomes this difficulty.

Model (*b*). Consider a domain wall moving across a particular twin. There is no energy change until the wall begins to move off the edge, and some average area of the wall associated with this process is required. The wall can be terminated by a second twin which cuts the wall so that the wall is also moving over this end portion. If a particular twin is taken with the wall in a certain position, then the terminating twin must lie as shown in Fig. 1, with a separation of centres $t/\sqrt{2}$. The value of dA/dx is constant as the wall moves from the particular twin, and the terminating twin can be anywhere within a strip of width $2t/\sqrt{2}$.

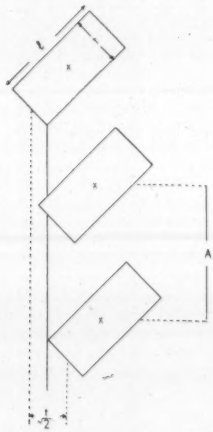

Fig. 1. Position of a terminating twin and the expected spacing A

One way of obtaining the associated distance is as follows. The terminating twin can lie above or below the fixed twin and must lie within a rectangle, length $2A$ and width $2t/\sqrt{2}$. The area containing a single twin is tl/β. The distance A can be found by equating $2A \,.\, 2t/\sqrt{2}$ and tl/β, whence $A = l\sqrt{2}/4\beta$.

An alternative proof can be obtained by using a Probability Theorem quoted in Levy and Roth.[7]

Using this value the coercive force becomes

$$H_c \sim \frac{e_w}{I_s} \cdot \frac{4\beta}{\sqrt{2}.l} \qquad (3)$$

There are then two possible expressions for H_c, depending on the assumptions, as given by equations (2) and (3).

In the materials considered, the twin distribution in terms of length, width and β were measured. Such distributions, of which Fig. 2 is a typical example, were fairly sharp. The mean value of l or of $(tl)^{1/2}$ was taken.

The results are presented graphically in Figs. 3 and 4.

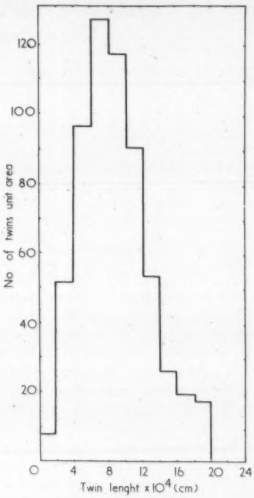

Fig. 2. Typical distribution curve for twin length

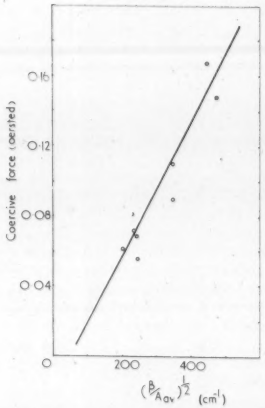

Fig. 3. Graph of the coercive force and $(\beta/A_{av})^{1/2}$ for the 50–50 Ni–Fe

4. THE CONSTANT OF PROPORTIONALITY

The theoretical slope of the $H_c.\beta/l$ or $(\beta/tl)^{1/2}$ graph is e_w/I_s. Values of e_w have been given by Kersten[8] as $e_w = 2(k\theta/a)^{1/2} \,.\, K^{1/2}$, where k is Boltzmann's constant, θ is the Curie temperature, a is the lattice spacing, and K is the first anisotropy constant.

Néel[4] has derived the value $e_w = a(2EK/3)^{1/2}$, where E is the energy of the molecular field per cubic centimetre, which if taken equal to $6k\theta/a^3$ makes the two expressions equivalent.

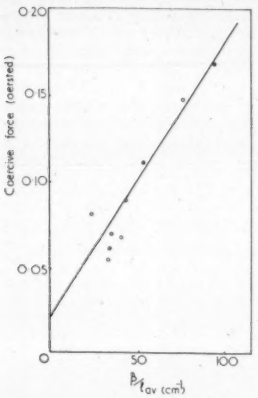

Fig. 4. Graph of the coercive force and β/l_{av} for the various samples

Taking a Curie temperature of $\sim 800°$ K, $k \sim 1{\cdot}4 \times \times 10^{-16}$ erg deg^{-1}, $a = 2{\cdot}0 \times 10^{-8}$ cm and $K = 3 \times 10^4$ erg cm^{-3}, the value of e_w is $\sim 1{\cdot}5$ erg cm^{-2}.

Now $I_s \sim 15000/4\pi$, so that the slope e_w/I_s in equation (2) is $0{\cdot}69 \times 10^{-3}$ and the slope in equation (3) is $1{\cdot}94 \times 10^{-3}$. The corresponding experimental values are $0{\cdot}40 \times 10^{-3}$ and $1{\cdot}6 \times 10^{-3}$.

5. DISCUSSION

Both these values are in fair agreement with the predicted value, though the graph of H_c plotted against β/l gives a better fit with the experimental points and is based on a more satisfactory experimental model. It is also worth pointing out that there had been a certain amount of general evidence previously that the coercive force was dependent inversely on the grain size, and this is borne out by the formula, since l, the length of the twin depends on the grain size. The problem then of making a good magnetic material of low coercive force reduced to a metallurgical one of making β/l small, i.e. have as few and as long twins as possible.

The positive intercept on the axis of H_c for $\beta/l = 0$ is worth comment, since it indicates that there is a small contribution to the coercive force due to some other cause. Vicena[9] and Kersten[10] have considered, apart from strained regions, three possible influences on the coercive force, namely—(i) dislocation lines, (ii) dislocation rings, and (iii) dislocation rings and impurity centres.

The general value quoted for 50–50 Ni–Fe (0·24 oersted) was higher than the minimum value (0·02 oersted) found here, though it should be noted that as a result of the manufacturing technique the present material is low in impurity concentration and dislocation density, and is in agreement with a value of 0·015 oersted for "dislocation-free" Ni–Fe quoted in Kersten's paper.

6. A.C. LOSSES

Experimental work. The twins have a deleterious effect on the a.c. loss and also on the magnetic amplifier characteristics of the material. The B–H loop under these conditions can be considered to have three components: hysteresis loss due to coercive force, to alternating flux conditions, and to twins (Fig. 5). It was found experimentally that the a.c. loss when plotted against the d.c. coercivity gave a straight line, as shown in Fig. 6, and the value of the intercept on the

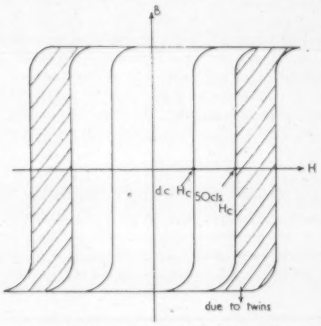

Fig. 5. The B–H loop for a material having a certain fraction twinned

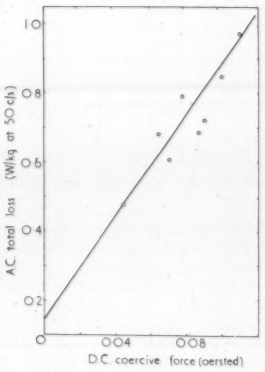

Fig. 6. Graph to find the a.c. loss for zero twinning

loss axis for zero H_c was considered to be the a.c. loss associated with a twin-free basic material. An experimental loss factor, which gives the increased ratio in the alternating frequency component of the loss with twins to that without twins, can be defined by an expression

$$\{\text{total a.c. loss} - (\text{d.c. loss} + 0{\cdot}15)\} \div 0{\cdot}15$$

values of which are given in the table. This table also gives values of β, t and l to complete the experimental data.

The presence of twinned material has a disproportionately large effect on the loss of Ni–Fe which cannot readily be explained. The misalined magnetic material essentially forms distinct grains which may have complex domain

structures around them. Williams[11] has found such structures associated with inclusions in magnetic materials, though it is doubtful if these structures exist in Ni–Fe around twin boundaries. Little is known of the loss mechanisms associated with such processes.

The measured "eddy" current loss is considerably greater than that given by the classical eddy current theory, a fact which has been the subject of a number of papers. Williams, Shockley and Kittel[2] have recently obtained a rigorous solution for the eddy current loss of plane walls in a rectangular bar. Lee[3] has considered the problem also and has derived an expression for the ratio of the actual loss to the classical eddy current loss, denoted by η in terms of the domain width and material thickness. However, the present paper is concerned only with the increase in loss due to the presence of twinned material, and so a constant ED_{50} is, therefore, taken to represent the total (a.c. loss $-$d.c. loss) at 50 c/s without twins, which is the eddy current contribution to the loss.

7. TWIN CONTRIBUTION TO A.C. LOSS

The model assumed here is that the domain walls will become curved on passing across a twin and that the curvature is determined by allowing an increase in wall length, to be equal to the reduction in length passing across a twin (Fig. 7). After this condition has been reached, the wall will move off

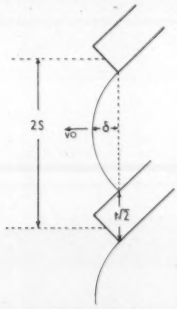

Fig. 7. Model adopted to determine the extra loss term

the twin and the "edges" will begin to catch up to the centres at an increased velocity, until the condition for minimum wall energy (straight) is reached. The increase in velocity of certain portions of the wall will give rise to an increased watts loss.

The concept of a wall curved in this manner is not based directly on experiment and a number of objections can be raised. Under d.c. conditions, complex domain structures have been noted around holes and the walls remain straight (Williams and Shockley).[11] Measurements have not been possible on boundary shape or movements, though the use of the Kerr magneto-optical method may be of assistance with the problem (Conger[12]).

However, it is worth while developing the proposed model and comparing the theoretical results with the experimental data.

From the point of view of calculating the radius of curvature, an approximation that the wall is circular can be made, though in practice the curvature at the centre is likely to be small and a maximum at the edges (Fig. 7).

The straight portion of the wall is taken to be $2S - t\sqrt{2}$ and the curved portion $2S$, so that approximately for a chord $2S$ the radius is $S^2/2m$ and the increase in length is $(4/3)\,(m^2/S)$, which is also equal to $t\sqrt{2}$. An initial value of $r^2 = S^2/3t\sqrt{2}$ is obtained with a value of $2S$ equal to (*a*) $(tl/\beta)^{1/2}$ or (*b*) $l\sqrt{2}/4\beta$. For simplicity, the wall will now be assumed to be a straight line moving with a velocity v_0 at the centre, and an increased velocity at the edges (Fig. 8).

To obtain the additional velocity term the concept of magnetic pressure as used by Galt[13] can be applied where $p = 2HI_s$ over a straight wall which is associated with a velocity v_0. An additional term is now included, e_w/r, which arises from wall curvature and is obtained from the soap bubble concept. Over a curved surface there is an additional velocity term $v_0 . e_w/2HI_s . 1/r$ normal to the surface.

8. CALCULATION OF THE WATT LOSS FACTOR

Consider an interval of time δt and Fig. 8. The small area has a depth δw and width $\delta n . w/S$, where δn is the distance moved in time δt in the direction from B towards A. Now

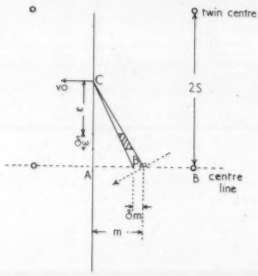

Fig. 8. Diagram used for the calculation of the additional loss due to twins

$\delta n = -\delta m$, where δm is the change in the distance the wall central line is behind the general wall measured in direction A to B. The initial value of m is given by $\frac{1}{2}(3\sqrt{2}tS)^{1/2}$ and the final value is stated later.

The area over which the wall moves in δt is

$$= 2v_0\delta t . \delta w + 2w . \delta w . \delta n/S \qquad (4)$$

It is convenient to replace δt, since δt equals δn divided by the additional velocity term in the direction of motion, or

$$\delta t = \delta n \Big/ \left\{ v_0 \cdot \frac{1}{\alpha} \cdot \frac{1}{r} \cdot S/(m^2 + S^2)^{1/2} \right\} \text{ with } \alpha = 2HI_s/e_w$$

The velocity at a distance w from the point C is

$$v_0 \left\{ 1 + \frac{1}{\alpha} \cdot \frac{1}{r} \cdot S/(m^2 + S^2)^{1/2} \cdot \frac{w}{S} \right\} \qquad (5)$$

Normally the total eddy current loss is proportional to frequency (or velocity in this case) squared and so the loss associated with the small area due to the increased speed would be increased by a factor

$$\left\{ 1 + \frac{1}{\alpha} \cdot \frac{1}{r} \cdot S/(m^2 + S^2)^{1/2} \cdot \frac{w}{S} \right\}^2 \qquad (6)$$

However, the number of transversals across a given area is constant at 50 c/s so that in spite of the speeding up process the number of excursions remains fixed, which effectively removes the square from equation (6).

The increased watts loss must be expressed per unit area and with the substitution $r = S^2/2m$ gives

$$\frac{ED\int_{w=0}^{w=S}\int_{m_1}^{m_2}\left\{1+\frac{1}{\alpha}\frac{2m}{S^2}\cdot\frac{w}{(m^2+S^2)^{1/2}}\right\}\left\{\frac{\alpha S}{2m}(m^2+S^2)^{1/2}+\frac{w}{S}\right\}dm\,.\,dw}{\int_0^S\int_{m_1}^{m_2}\left\{\frac{\alpha S}{2m}(m^2+S^2)^{1/2}+\frac{w}{S}\right\}dm\,.\,dw} \qquad (7)$$

The watts loss is thus expressed as a factor, by which the loss has to be increased to allow for the presence of the twins, over the loss of untwinned material.

The limit for the curved edge to move a distance dn is obtained by dividing δn by the additional velocity term; and the total time for the wall to change from $n = 0$ to $m_1 - m_2$, or in terms of m from m_1 to m_2, is equal to the time integral between these points. This also equals the time taken for the general wall moving with a velocity v_0 to move a distance $2S - (m_1 - m_2)$,

whence

$$\int_{m_1}^{m_2} -\frac{dm}{v_0}\cdot\frac{\alpha S^2}{2m}\left(1+\frac{m^2}{S^2}\right)^{1/2} = \frac{2S-(m_1-m_2)}{v_0} \qquad (8)$$

The initial value of m is $m_1 = \frac{1}{2}(3\sqrt{2}\,.\,tS)^{1/2}$ and so the final value of m can be found.

The process is repetitive over a distance $2S$ so that the centre will move a distance $2S - (m_1 - m_2)$, whilst the edge moves a distance $2S$. To complete the process the wall must pivot with the edges fixed and the centre moving a distance $m_1 - m_2$ at a velocity v_0. There is, therefore, an addition to be made to the numerator of equation (7) to allow for the additional loss, and for areas in the denominator, which now becomes $2S^2$ (half width only considered).

The integrations involved for the complete form of equations (7) and (8) can be evaluated by suitable expansion and subsequent integration. Values of the loss factor obtained this way were checked using an integration programme on the DEUCE computer, and are given in the table.

Table

Sample No.	β	$t\,.\,10^4$	*(a)* $(\beta/t)^{1/2}$	*(b)* β/l	*Experimental loss factor*	*Theoretical loss factor* (a)	(b)
34A	0·0510	1·34	833	262	2·48	1·58	1·10
30A	0·0131	2·48	222	34·8	1·25	1·12	1·02
32A	0·0222	1·14	585	110	2·60	1·28	1·03
37B	0·0362	1·75	544	146	3·04	1·35	1·06
35B	0·0196	1·49	400	67·6	1·73	1·19	1·03
35A	0·0170	1·12	512	82·9	1·86	1·22	1·03

9. COMPARISON WITH EXPERIMENTAL RESULTS

The theoretical loss ratios can be compared with the experimental values in the table. These results are plotted in Fig. 9, which shows that whilst a reasonable linear relationship is obtained, the slope is under-estimated. Model (*a*) gives the nearest fit, though previously in the d.c. coercivity work it had been model (*b*). The difference is essentially one of deciding what is the effective spacing of the twins.

10. THE PARAMETERS TO USE IN THE FORMULA

Two values have been obtained for $2S$, making different assumptions for the d.c. loss, and these values were also used for the a.c. loss. For the numbers taken, the bending of the wall, as represented by m, is about three times the width of the strip taken for the evaluation of the expected distance in model (*b*). Consequently the wall will be disturbed and the expected distance probably reduced, though the precise effect is difficult to evaluate.

The magnitude of H required for substitution into these expressions presents a problem. Under d.c. conditions, and for a square loop material, the d.c. coercive force would be the appropriate value to take, since the loss does not depend on the applied field. With the present model, under alternating conditions with no twins present, the appropriate value would be that of the coercive force. Since the strip consists of a matrix of material having a basic a.c. loss of this value, plus the variable effect of twins, the value of H_c taken is the basic a.c. coercive force $\sim$0·05 oersted which is constant for all specimens.

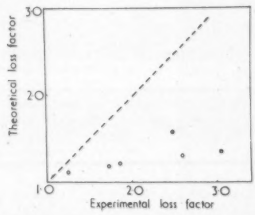

Fig. 9. Experimental loss factor plotted against theoretical loss factor for twinned Ni–Fe, using model (*a*)

11. CONCLUSION

It has been found that twins formed in 50–50 Ni–Fe have a deleterious effect on the magnetic properties of the material. It has been shown that the d.c. coercivity of the Ni–Fe is related simply to the fraction of twinned material and to the length of these crystallographic twins. The control and purity of the material seems to be sufficiently good for a low coercivity to be obtained in the absence of twinned regions.

A model to describe an additional loss process during a.c. magnetization has been developed, the basic concept of which has been that parts of the wall are accelerated and retarded, with a resulting increase in loss due to passing over twins. The variation of loss with twin parameters has been predicted reasonably well, though the model has not been completely satisfactory and some more complicated oscillating and retardation process may be responsible for the large increase in watts loss. Other twin-dependent loss processes are probably occurring, for which no account can be given.

ACKNOWLEDGEMENTS

The author is indebted to Mr. V. A. Hughes, Mr. T. B. Burnett, and other colleagues for many helpful suggestions. Thanks are also due to Mr. J. K. Brown, Director of Research, for his interest and for permission to publish this work.

REFERENCES

(1) KERSTEN, M. *Z. Phys.*, **44**, p. 63 (1943); **124**, p. 714 (1948).
(2) WILLIAMS, H. J., *et al. Phys. Rev.*, **80**, p. 1090 (1950).
(3) LEE. E. W. I.E.E. Monograph 284 M.
(4) NÉEL, L. *Cahiers de Phys.*, **25**, p. 1 (1944).
(5) NÉEL, L. *Ann. Inst. Fourier*, **22**, p. 299 (1946).
(6) DIJKSTRA, L. J., and WERT, C. *Phys. Rev.*, **79**, p. 979 (1950).
(7) LEVY, H., and ROTH, L. *Elements of Probability* (London: Oxford University Press, 1936), p. 80.
(8) KERSTEN, M. *Probleme der Technischen Magnetizieringskurve* (Berlin: Springer-Verlag, 1938), p. 42.
(9) VICENA, F. *Czech J. Phys.*, **5**, p. 480 (1955).
(10) KERSTEN, M. *Z. angew. Phys.*, **8**, p. 496 (1956).
(11) WILLIAMS, H. J., and SHOCKLEY, W. *Phys. Rev.*, **75**, p. 178 (1949).
(12) CONGER, R. W. *Proceedings Non-linear Magnetics and Magnetic Amplifier Conference*, A.I.E.E. (August 1958), p. 444.
(13) GALT, J. K. *Bell Syst. tech. J.*, **34**, p. 439 (1955).

Thermal transients in graphite-copper contacts

By W. DAVIES, B.Sc., Ph.D., A.M.I.E.E., Engineering Department, University College of South Wales and Monmouthshire, Cardiff

[*Paper first received* 22 *December*, 1958, *and in final form* 15 *May*, 1959]

Calculation of the transient temperature distribution in a current-carrying electric contact is important in those cases in which the contact members make actual contact for only a comparatively short time. Special reference is made here to the contact of graphite and copper, and consideration is given firstly to the case in which the metal is clean, and secondly to that in which the metal is covered with a film of oxide. Finally, the decay of the temperature at a contact spot following the separation of the contact members is discussed. The analysis treats of a single circular contact spot of very small radius.

LIST OF PRINCIPAL SYMBOLS

θ = temperature at any point above that of parts of the contact members remote from the contact spot
λ = thermal conductivity
c = heat capacity per unit volume
ρ = resistivity
I = contact current
b = radius of contact spot
Q = rate of generation of heat in oxide disk

INTRODUCTION

In sliding contacts of graphite and copper the duration of actual contact of the graphite and an asperity on the metal may be as short as 10^{-4} s. In such circumstances the temperature distribution in the current-carrying contact does not attain its steady state value, and it is of some interest to calculate the transient distribution for a single contact spot.

Under certain conditions the higher asperities—the contact asperities—on the metal are free of any overlying film, but in contacts operating in normal atmospheres these asperities are covered by a film of cuprous oxide.[1] In what follows the development of the temperature in a current-carrying constrictive contact of graphite and copper is calculated for both clean and oxide-coated metal.

For the sake of simplicity it will be supposed that the contact members make actual contact at a number of small circular spots, which are so dispersed that they do not interact with one another either thermally or electrically. The abutting surfaces of these contact members will be assumed to be plane, except, of course, in the immediate vicinity of the actual contact areas. This paper is concerned then with the temperature distribution arising from one contact spot of the type illustrated by Fig. 1.

The resistivities, thermal conductivities and heat capacities per unit volume of the contact materials will be assumed to be independent of temperature.

It is assumed that the main bodies of the contact members are thermally and electrically insulated from one another in all parts, except for the actual circular disk of contact. This assumption implies that the transfer of heat through any gas in the gap between the contact members will be disregarded, as will any absorption of heat by this gas. This assumption is a reasonable one because the sliding

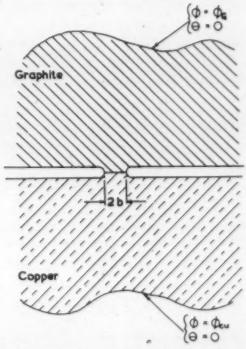

Fig. 1. Single-spot contact of graphite and copper

motion of most practical contacts is of the familiar "stick–slip" type, and the stick-phase corresponds with by far the greater part of the period of contact of two asperities. During the stick-phase, when the contact members are not in relative motion, the velocity of any gas present is probably too low for heat transfer and absorption to be of much account, and these, incidentally, become progressively less important as the gas pressure is reduced.

For a contact carrying a steady current I, the electrical potential function ϕ at any point in the contact satisfies the equation

$$\nabla^2\phi = 0 \tag{1}$$

Likewise at any point in the contact the temperature function θ satisfies the equation

$$\nabla^2\theta + A = k(\partial\theta/\partial t)$$

where A involves I^2 as a factor.

If the contact materials are assumed to be both linear and isotropic, it follows that the *nature* of the temperature distribution at any instant is not dependent on the magnitude of the current (so long as it is not zero), although the actual temperature at any point is, of course, dependent on this current. Consequently the nature of the temperature distribution, that is the shapes of the isothermal surfaces and the streamlines of heat flow, are determined by a solution of the equation

$$\nabla^2\theta = k(\partial\theta/\partial t) \tag{2}$$

consistent with the prescribed initial and boundary conditions.

The solution for θ in equation (2) can be taken as

$$\theta = \psi(x, y, z), \sigma(t)$$

Substituting this solution in equation (2), it is found that $\sigma(t)$ must be of the form $K\exp(-t/\tau)$ and that $\psi(x, y, z)$ is to be a function satisfying the equation

$$\nabla^2\psi + k\psi = 0 \tag{3}$$

This latter equation is of the wave type, and the wave-front has a shape determined in part by the equation

$$\nabla^2\psi = 0$$

and in part by the prescribed boundary conditions.

(The initial condition, namely $\theta = 0$ for $t \leqslant 0$, has to be considered in determining θ finally.)

For the electrical and thermal fields within the contact one has then,

$$\left.\begin{aligned}\nabla^2\phi &= 0\\ \nabla^2\psi &= 0\end{aligned}\right\}\ \text{at all points}$$

and thence

$$\left.\begin{aligned}\partial\phi/\partial u &= 0\\ \partial\theta/\partial u &= 0\\ \partial\psi/\partial u &= 0\end{aligned}\right\}\ \text{at the electrically and thermally insulating mantle surface}$$

and thence

$$\left.\begin{aligned}\phi &= \phi_G\\ \theta &= 0\\ \psi &= 0\end{aligned}\right\}\ \text{at a far surface in the graphite}$$

and thence

$$\left.\begin{aligned}\phi &= \phi_{Cu}\\ \theta &= 0\\ \psi &= 0\end{aligned}\right\}\ \text{at a far surface in the copper}$$

It follows from these equations and boundary conditions that, within the contact members, the surfaces of equipotential are likewise isothermal, and the streamlines of current are coincident with those of heat flow.

If the contact is axially symmetrical, as it is in Fig. 1 with the axis of symmetry normal to the plane contact area, then this plane surface is evidently equipotential and isothermal. The shapes of other equipotential and isothermal surfaces within the contact members are then determined by the configuration of the contact area. If this contact area is circular, the equipotential and isothermal surfaces are confocal oblate ellipsoids of revolution. The axis of symmetry of this family of ellipsoids corresponds with the axis of the circular contact area, and their foci lie on its perimeter (see Fig. 2).

If, in the case of the symmetrical contact, the contact members have identical thermal and electrical characteristics, then the surface of maximum temperature is the contact disk itself. However, graphite is less well conducting than copper, and in a contact of these materials the surface of maximum temperature is in the graphite. This case is illustrated by Fig. 2. It will be observed that in this figure the two halves of a given oblate ellipsoid of revolution (one half in the graphite, the other in the copper) are not, of course, at the same potential, and they are not at the same temperature. These semi-ellipsoids would be at the same temperature only if the contact members had identical characteristics.

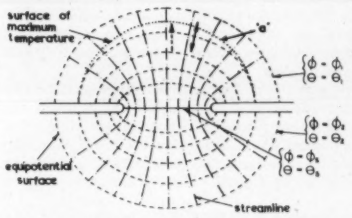

Fig. 2. Equipotential surfaces and streamlines in actual contact

– – – – → = current
——— → = heat flow
"a" = spherical surface of radius $2b$

If one assumes that copper, when compared with graphite, is perfectly conducting to heat and electricity, then temperature and potential gradients within the metal are negligible and the temperature at the contact disk is virtually the same as that in all parts of this contact member.

Physical constants of natural graphite and copper

	Thermal conductivity ($J\,cm^{-1}\,s^{-1}/deg\,C^{-1}$)	*Thermal capacity* ($J\,cm^{-1}/deg\,C^{-1}$)	*Resistivity* ($\Omega\,cm$)
Graphite	0·315	0·96	2×10^{-3}
Copper	3·9	3·4	$1{\cdot}7 \times 10^{-6}$

It should be noted that whereas there is continuity in the direction of the electric current through the contact, heat flow along the common streamlines is in opposite directions on either side of the surface of maximum temperature. In the graphite then, the isothermal surfaces, although identical in form with the surfaces of equipotential, are more closely grouped near the surface of maximum temperature if they are drawn for a common interval of temperature, than are the equipotential surfaces drawn for a common interval of potential.

CALCULATION OF THE TEMPERATURE DISTRIBUTION

Development of the temperature distribution in a film-free contact. Typical values of the relevant physical constants of copper and natural graphite are given in the table, and because of the very much greater conductivities of the metal it is assumed below that the copper is perfectly conducting.

In these circumstances, if the contact spot is circular, the type of thermal and electrical fields within the graphite, which have already been described and which are illustrated

by Fig. 2, are obtained. Suppose that at some instant $t = 0$ the current through a contact spot rises suddenly from zero to the value I amperes, and remains at this value thereafter. It is required now to find how the temperature distribution develops with time.

The mathematical difficulty of dealing with thermal transients in the ellipsoidal thermal and electrical fields described here is considerable. The problem becomes tractable, however, and an approximate solution is obtained if the confocal ellipsoidal surfaces referred to are replaced by concentric spheres with their common centre at the centre of the contact disk.

If such a model of the thermal and electrical fields within the contact members is chosen, then one of the equipotential and isothermal surfaces has a diametral section corresponding with the contact area. It follows, therefore, that this surface in the model must be at the same potential and temperature as the contact area itself. This implies that the volume of material within this particular spherical surface is effectively perfectly conducting to heat and electricity, and this surface thereby constitutes one boundary of the thermal and electrical fields within the contact members; actually then, in this case, a boundary in the graphite.

Consider a thin hemispherical shell of material, the boundary surfaces of which coincide with surfaces which are equipotential and isothermal; let the radius of the shell be r and its thickness δr. Noting then that the difference between the heat inflow at one boundary surface and the heat outflow at the other, in some interval of time δt, must be equal to the difference between the heat generated in the shell due to its electrical resistance and the heat absorbed by the shell in this interval of time, and ignoring the Thomson effect, one has:

$$\left\{-2\pi(r+\delta r)^2 \,.\, \lambda \,.\, \left[\frac{\partial\theta}{\partial r}\right]_{r+\delta r} + 2\pi r^2\lambda\left[\frac{\partial\theta}{\partial r}\right]_r\right\} . \,\delta t = I^2\frac{\rho \,.\, \delta r}{2\pi r^2} \,.\, \delta t - 2\pi r^2 \,.\, \delta r \,.\, C \,.\, \delta\theta \quad (4)$$

where θ is the temperature of the shell, and $\delta\theta$ is the increase in θ in the interval of time δt.

Neglecting terms involving small quantities of the second and higher orders, equation (4) reduces to the form:

$$\frac{\partial^2\theta}{\partial r^2} + \frac{2}{r}\cdot\frac{\partial\theta}{\partial r} + \frac{\gamma}{r^4} = \frac{C}{\lambda}\cdot\frac{\partial\theta}{\partial t} \quad (5)$$

where $$\gamma = I^2\rho/4\pi^2\lambda$$

Assuming that for all values of $t \leqslant 0$, the temperatures of the contact members are everywhere the same at some value which is here taken to be zero, the solution of equation (5) must satisfy the initial condition:

$$\theta = 0 \quad \text{for} \quad t \leqslant 0$$

Again, if it be assumed that the thermal conductivity of the metal is so much greater than that of the graphite that temperature gradients in the metal can be neglected, then the latter may be supposed to remain at a constant temperature ($\theta = 0$). In such circumstances, only the temperature development in the graphite is of concern and it must be noted that the solution of equation (2) must satisfy the boundary conditions

$$\theta = 0 \quad \text{at} \quad r = b$$

and $$\text{at} \quad r = \infty$$

for all values of t.

In order to simplify equation (5), make a transformation of variables in accordance with the equations:

$$\theta = \frac{1}{r}\left\{v + \frac{\gamma}{2}\left(\frac{1}{b} - \frac{1}{r}\right)\right\} \quad (6)$$

and $$r = b(1 + x) \quad (7)$$

This transformation leads, after some reduction, to the result

$$k(\partial^2 v/\partial x^2) = (\partial v/\partial t) \quad (8)$$

where $k = \lambda/b^2c$.

The initial and boundary conditions to be satisfied by the solution of equation (8) are such that

$$v = -(\gamma/2b)\phi(x) \quad \text{at} \quad t = 0$$

where $$\phi(x) = x/(1 + x)$$

and $v = 0$ at $x = 0$, for all values of t.

Equation (8) is identical in form with the classical equation of the linear flow of heat in an isotropic and homogeneous medium, and the conditions imposed on the solution of equation (8) correspond with an initial distribution of temperature, with the plane at $x = 0$ held at zero temperature for all values of t in the heat conduction problem. The solution of this particular problem for an initial distribution of temperature $f(x)$ is well known,[2] and it is

$$v = \frac{1}{2\sqrt{(\pi kt)}}\int_0^\infty f(x')\cdot\left[\exp\left\{\frac{-(x-x')^2}{4kt}\right\} - \exp\left\{\frac{-(x+x')^2}{4kt}\right\}\right]\cdot dx'$$

The solution of equation (8) is then

$$v = -\frac{1}{2\sqrt{(\pi kt)}}\int_0^\infty \frac{\gamma}{2b}\cdot\phi(x')\cdot\left[\exp\left\{\frac{-(x-x')^2}{4kt}\right\} - \exp\left\{\frac{-(x+x')^2}{4kt}\right\}\right]\cdot dx'$$

If now one puts

$$\beta^2 = (x - x')^2/4kt$$

then the integral

$$-\frac{1}{2\sqrt{(\pi kt)}}\int_0^\infty \frac{\gamma}{2b}\cdot\phi(x')\cdot\exp\left\{\frac{-(x-x')^2}{4kt}\right\}\cdot dx'$$

becomes

$$\frac{1}{\sqrt{\pi}}\int_{\frac{x}{2\sqrt{(kt)}}}^{-\infty}\frac{\gamma}{2b}\cdot\phi\{x - 2\beta\sqrt{(kt)}\}\cdot\exp(-\beta^2)\cdot d\beta$$

Again, if one puts

$$\beta^2 = (x + x')^2/4kt$$

the integral

$$\frac{1}{2\sqrt{(\pi kt)}}\int_0^\infty \frac{\gamma}{2b}\cdot\phi(x')\cdot\exp\left\{\frac{-(x+x')^2}{4kt}\right\}\cdot dx'$$

becomes

$$\frac{1}{\sqrt{\pi}}\int_{\frac{x}{2\sqrt{(kt)}}}^{\infty}\frac{\gamma}{2b}\cdot\phi\{2\beta\sqrt{(kt)} - x\}\cdot\exp(-\beta^2)\cdot d\beta$$

Thus

$$v = \frac{\gamma}{2b\sqrt{\pi}}\left[\int_{\frac{x}{2\sqrt{(kt)}}}^{\infty} \phi\{2\beta\sqrt{(kt)} - x\} \cdot \exp(-\beta^2) \cdot d\beta + \right.$$
$$\left. + \int_{\frac{x}{2\sqrt{(kt)}}}^{-\infty} \phi\{x - 2\beta\sqrt{(kt)}\} \cdot \exp(-\beta^2) \cdot d\beta\right]$$

If in the second of these integrals one puts

$$\beta = -\alpha$$

then this integral becomes

$$-\int_{\frac{-x}{2\sqrt{(kt)}}}^{\infty} \phi\{2\alpha\sqrt{(kt)} + x\} \cdot \exp(-\alpha^2) \cdot d\alpha$$

Replacing α by β in order to preserve the notation, one finally obtains

$$v = \frac{\gamma}{2b\sqrt{\pi}}\left[\int_{\frac{x}{2\sqrt{(kt)}}}^{\infty} \phi\{2\beta\sqrt{(kt)} - x\} \cdot \exp(-\beta^2) \cdot d\beta - \right.$$
$$\left. - \int_{\frac{x}{2\sqrt{(kt)}}}^{\infty} \phi\{2\beta\sqrt{(kt)} + x\} \cdot \exp(-\beta^2) \cdot d\beta\right]$$

The function $\phi(u)$ is, by definition, $u/(1+u)$.

Reverting now to the temperature at a point a distance $r(>b)$ from the centre of the contact area, t seconds after the establishment of the steady current, one has:

$$\theta = \frac{1}{r}\left(\frac{\gamma}{2b\sqrt{\pi}}\left[\int_{\left(\frac{r}{b}-1\right)/2\sqrt{(kt)}}^{\infty} \phi\left\{2\beta\sqrt{(kt)} - \left(\frac{r}{b}-1\right)\right\} \cdot \exp(-\beta^2) \cdot d\beta - \right.\right.$$
$$\left. - \int_{-\left(\frac{r}{b}-1\right)/2\sqrt{(kt)}}^{\infty} \phi\left\{2\beta\sqrt{(kt)} + \left(\frac{r}{b}-1\right)\right\} \cdot \exp(-\beta^2) \cdot d\beta\right] +$$
$$\left. + \frac{\gamma}{2}\left(\frac{1}{b} - \frac{1}{r}\right)\right) \quad (9)$$

The development of the temperature at the warmest section of the constriction resistance (in the graphite) is of special interest.

It follows from the assumption that ρ, λ and c are independent of temperature that the position of the warmest section is independent of time. This being so one can readily determine the position of this section by considering the distribution of temperature in the steady state ($t \to \infty$).

For the instants $t \to \infty$ it is clear from equation (9) that

$$\left[\theta\right]_{t\to\infty} = \frac{\gamma}{2r}\left(\frac{1}{b} - \frac{1}{r}\right) \quad (10)$$

for any finite $r \geqslant b$.

It is easy then to see that the warmest section is the hemispherical surface corresponding with $r = 2b$ in the graphite.

The temperature at the warmest section at any instant is thus

$$\theta_M = \frac{\gamma}{4b^2\sqrt{\pi}}\left[\int_{\frac{1}{2\sqrt{(kt)}}}^{\infty} \phi\{2\beta\sqrt{(kt)} - 1\} \cdot \exp(-\beta^2) \cdot d\beta - \right.$$
$$\left. - \int_{\frac{1}{-2\sqrt{(kt)}}}^{\infty} \phi\{2\beta\sqrt{(kt)} + 1\} \cdot \exp(-\beta^2) \cdot d\beta\right] + \frac{\gamma}{8b^2} \quad (11)$$

and its steady-state value is

$$\left[\theta_M\right]_{t\to\infty} = \frac{\gamma}{8b^2} \quad (12)$$

At any isothermal surface then, the temperature at any instant is given by the expression

$$\theta = \left[\theta\right]_{t\to\infty} \cdot \{1 - \chi(kt, r)\} \quad (13)$$

where

$$\chi(kt,r) = \frac{r}{(r-b)\sqrt{\pi}}\left[\int_{-\left(\frac{r}{b}-1\right)/2\sqrt{(kt)}}^{\infty} \phi\left\{2\beta\sqrt{(kt)} + \left(\frac{r}{b}-1\right)\right\} \cdot \exp(-\beta^2) d\beta \right.$$
$$\left. - \int_{\left(\frac{r}{b}-1\right)/2\sqrt{(kt)}}^{\infty} \phi\left\{2\beta\sqrt{(kt)} - \left(\frac{r}{b}-1\right)\right\} \cdot \exp(-\beta^2) \cdot d\beta\right]$$

For the warmest section in particular

$$\theta = (\gamma/8b^2)\{1 - \chi(kt)\} \quad (14)$$

where

$$\chi(kt) = \frac{2}{\sqrt{\pi}}\left[\int_{\frac{1}{-2\sqrt{(kt)}}}^{\infty} \phi\{2\beta\sqrt{(kt)} + 1\} \cdot \exp(-\beta^2) \cdot d\beta - \right.$$
$$\left. - \int_{\frac{1}{2\sqrt{(kt)}}}^{\infty} \phi\{2\beta\sqrt{(kt)} - 1\} \cdot \exp(-\beta^2) \cdot d\beta\right]$$

Values of the function $\{1 - \chi(kt)\}$ are given in Fig. 3.

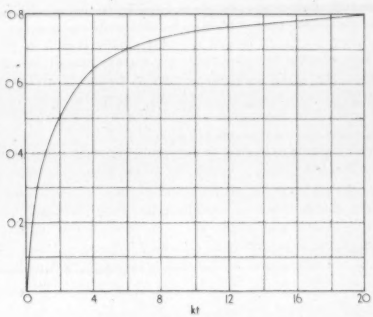

Fig. 3. Values of the function $\{1 - \chi(kt)\}$

It is of some interest to calculate the temperature rise in the case of a brush of natural graphite sliding on a clean copper disk. Approximate values of the relevant physical constants of natural graphite are as follows:

thermal conductivity (λ) = 0·315 J cm^{-1} s^{-1} °C^{-1}
thermal capacity (c) = 0·958 J cm^{-1} °C^{-1}
resistivity (ρ) = 2×10^{-3} Ω cm

Assuming that the total current is 150 A, and that contact takes place at three identical spots each having a radius of

0·01 cm (brush load 1 kg; brush Brinell hardness $0·25 \times 10^6$ g/cm^2) one obtains:

$$\gamma = I^2\rho/4\pi^2\lambda = 0·403$$
$$k = \lambda/b^2c = 3290$$

The steady-state value of the temperature at the warmest region is then

$$\left[\theta_M\right]_{t\to\infty} = \frac{\gamma}{8b^2} = 500° \text{ C}$$

The relative motion of the brush and the disk follows the familiar pattern of stick-slip sliding. In this type of sliding actual static contact at a contact spot is maintained, and the brush moves along with the disk until the restraining force on the brush reaches a value equal to the tangential force of adhesion at the contact area. At this point true sliding begins, with a relative velocity of the two members very much greater than the apparent or average velocity. The actual duration of the first stage, called the stick-phase, and the sliding speed during the second stage, called the slip-phase, are dependent on the mechanical characteristics of the brush-holder and the values of the coefficients of static and kinetic friction. The duration of the stick-phase is ordinarily very much longer than that of the slip-phase, and appreciably longer than a time interval based on the diameter of a contact spot and the average speed of sliding (the speed of the disk surface).

If the speed of the disk surface is 500 cm/s, then the temperature at the warmest region can be calculated very approximately by taking a value of t of the order of 10^{-4} s, which is two to three times the time interval $2b/500$ s.

For this case then

$$kt = 3290 \times 10^{-4}$$

and the corresponding value of $\{1 - \chi(kt)\}$ is 0·1. The temperature rise at the warmest region—in the graphite—is then of the order of $0·1 \times 500°$ C, that is 50° C.

The special interest which attaches to the region of maximum temperature requires that one should assess the extent to which the spherically symmetrical fields of the model depart from the axially symmetrical ellipsoidal fields of the actual contact in the region $r = 2b$, where, in the model, the temperature has its maximum value.

If the axis of symmetry of the contact is taken to be the Y-axis of the Cartesian system of co-ordinates, so that the circular contact spot of radius b lies in the $Z - X$ plane with its centre at the origin of co-ordinates, then the equation to the family of confocal ellipsoidal equipotential and isothermal surfaces of the exact fields is

$$\frac{x^2}{b^2+\lambda} + \frac{y^2}{\lambda} + \frac{z^2}{b^2+\lambda} = 1$$

where λ is a parameter.

The contact spot itself corresponds with $\lambda = 0$. For a semi-ellipsoid of base radius $2b$, it is readily seen that

$$2b = \sqrt{(b^2 + \lambda)}$$

so that

$$\lambda = 3b^2$$

The height of this ellipsoid at the axis of symmetry is

$$y = \sqrt{\lambda} = \sqrt{3} \,.\, b$$

The spherical surface of radius $r = 2b$, and the ellipsoidal surface of base radius $2b$ are shown in Fig. 2. These two surfaces, one referring to the model, and the other to the actual contact, diverge from one another to the greatest extent at the axis of symmetry. At this axis the height of the spherical surface is $2b$, and that of the ellipsoid is $\sqrt{3} \,.\, b$; the ratio of these heights is 1 : 0·866.

It appears, therefore, that in the region of maximum temperature in the model, the fields of the model do not differ very radically from the exact fields of the actual contact.

Development of the temperature distribution in a contact with oxide-coated metal. If the surface of the copper is covered, as it is in normal practice, with a film of cuprous oxide, then the oxide caps on the summits of the contact asperities on the metal can account for 70 to 80% of the contact resistance.[1] This means that in such a case the electrical heating takes place almost entirely in the film at the surface of the contact spots on the metal. The heat generated in this way diffuses into both contact members, and the problem is to determine the transient distribution of temperature which results from this form of heating.

The model of the single-spot contact already described will be used, and in the present case, the development of heat due to ohmic resistance of the contact members themselves will be neglected, the whole of the heat being assumed to be generated in the circular disk of cuprous oxide which separates them.

If the rates at which heat passes into the contact members are q_1 and q_2 watts respectively, then one has:

$$q_1 + q_2 = Q = VI \text{ watts}$$

where V is the potential difference across the oxide disk.

The current I will be assumed constant as in the previous case, and the heat capacity of the oxide disk neglected.

Write:

$$q_1 = \alpha Q$$

and

$$q_2 = (1 - \alpha) \,.\, Q$$

and for the sake of simplicity assume that the fraction α is constant or that, or worst, it varies comparatively slowly with the development of the temperature distribution. The value of this fraction can be determined eventually by making use of the fact that the temperature at the contact interface is necessarily the same for both contact members.

In accordance with the simplified model, spherical symmetry of heat flow is assumed in each of the contact members; consequently the equation of heat conduction in the present case is

$$\frac{\partial^2\theta}{\partial r^2} + \frac{2}{r}\frac{\partial\theta}{\partial r} = \frac{c}{\lambda}\cdot\frac{\partial\theta}{\partial t} \qquad (15)$$

where θ is the temperature at a radial distance r from the centre of the contact spot ($r > b$).

Equation (15) follows easily from equation (5) by putting $\rho = 0$ in that equation. The initial condition to be satisfied by the solution of equation (15) is that

$$\theta = 0 \quad \text{for} \quad t \leqslant 0$$

for all values of r, and the boundary conditions are such that:

(*a*) the flux of heat across the hemispherical surface of radius b in one contact member is αQ, while the flux of heat across a corresponding surface in the other member is $(1 - \alpha)Q$. watts;

(*b*) the temperature tends to the arbitrary datum value (zero) as r approaches infinity in either member.

For the first contact member one has:

$$\frac{\partial^2\theta_1}{\partial r_1^2} + \frac{2}{r_1}\frac{\partial\theta_1}{\partial r_1} = \frac{c_1}{\lambda_1}\cdot\frac{\partial\theta_1}{\partial t} \qquad (16)$$

with the conditions:

$$\theta_1 = 0 \quad \text{at} \quad t \leqslant 0$$

for all values of r_1

$$\left.\begin{aligned}\left[\frac{\partial\theta_1}{\partial r_1}\right]_{r_1=b} &= -\frac{\alpha Q}{\lambda_1 2\pi b^2}\\ \theta_1 &\to 0 \quad \text{for} \quad r_1 \to \infty\end{aligned}\right\} \text{for all values of } t$$

Introducing a new variable v such that

$$v = r_1\theta_1$$

equation (16) reduces to the form

$$k_1(\partial^2 v/\partial r_1^2) = \partial v/\partial t \tag{17}$$

where the diffusivity $k_1 = \lambda_1/c_1$.

The conditions imposed on the solution of equation (17) are:

$$v = 0 \quad \text{at} \quad t \leqslant 0 \text{ for all values of } r_1 \geqslant b;$$

$$\left(-\frac{v}{r_1^2} + \frac{1}{r_1}\frac{\partial v}{\partial r_1}\right)_{r_1=b} = -\frac{\alpha Q}{\lambda_1 \cdot 2\pi b^2}$$

Using the technique of the Laplace transform calculus, and taking t as the variable of integration, the subsidiary equation corresponding with equation (17) is

$$k_1(\partial^2\bar{v}/\partial r_1^2) = p\bar{v} \tag{18}$$

while

$$\left(-\frac{\bar{v}}{r_1^2} + \frac{1}{r_1}\frac{\partial\bar{v}}{\partial r_1}\right)_{r_1=b} = -\frac{1}{p}\frac{\alpha Q}{\lambda_1 \cdot 2\pi b^2} \tag{19}$$

The general solution of equation (18) is

$$\bar{v} = A\exp\{-\sqrt{(p/k_1)}r_1\} + B\exp\{-\sqrt{(p/k_1)}r_1\}$$

However, since v, and then $\bar{v}$, tends to zero as r_1 approaches infinity, one has simply

$$\bar{v} = A\exp\{-\sqrt{(p/k_1)}r_1\} \tag{20}$$

From equations (19) and (20) it is found that

$$A = \frac{\alpha Q}{2\pi\lambda_1 b}\cdot\frac{\exp\{\sqrt{(p/k_1)}b\}}{p\{(1/b) + \sqrt{(p/k_1)}\}}$$

Thus

$$\bar{v} = \frac{\alpha Q}{2\pi\lambda_1 b}\cdot\frac{\exp\{-\sqrt{(p/k_1)}\cdot(r_1 - b)\}}{p\{(1/b) + \sqrt{(p/k_1)}\}} \tag{21}$$

$$\ldots r \geqslant b$$

Inversion of this equation gives

$$v(r_1, t) = \frac{\alpha Q}{2\pi\lambda_1 b}\cdot\frac{1}{2\pi i}\int_{\Gamma-i\infty}^{\Gamma+i\infty}\frac{\exp(pt)}{p\{(1/b) + \sqrt{(p/k_1)}\}}\cdot\frac{\exp\{-\sqrt{(p/k_1)}\cdot(r_1 - b)\}}{p\{(1/b) + \sqrt{(p/k_1)}\}}\cdot dp =$$

$$= \frac{\alpha Q}{2\pi\lambda_1}\left[\operatorname{erfc}\left\{\frac{r_1 - b}{2\sqrt{(k_1 t)}}\right\} - \exp\left(\frac{(r_1 - b)}{b} + \frac{k_1 t}{b^2}\right)\cdot\operatorname{erfc}\left\{\frac{r_1 - b}{2\sqrt{(k_1 t)}} + \frac{1}{b}\sqrt{(k_1 t)}\right\}\right]$$

$$\ldots r_1 \geqslant b$$

so that

$$\theta_1(r_1, t) = \frac{\alpha Q}{2\pi\lambda_1 r_1}\left[\operatorname{erfc}\left\{\frac{r_1 - b}{2\sqrt{(k_1 t)}}\right\} - \exp\left\{\frac{(r_1 - b)}{b} + \frac{k_1 t}{b^2}\right\}\cdot\operatorname{erfc}\left\{\frac{r_1 - b}{2\sqrt{(k_1 t)}} + \frac{1}{b}\sqrt{(k_1 t)}\right\}\right] \tag{22}$$

$$\ldots r_1 \geqslant b$$

It is obvious then that for the other contact member one has:

$$\theta_2(r_2, t) = \frac{(1-\alpha)Q}{2\pi\lambda_2 r_2}\left[\operatorname{erfc}\left\{\frac{r_2 - b}{2\sqrt{(k_2 t)}}\right\} - \exp\left(\frac{r_2 - b}{b} + \frac{k_2 t}{b^2}\right)\operatorname{erfc}\left\{\frac{r_2 - b}{2\sqrt{(k_2 t)}} + \frac{1}{b}\sqrt{(k_2 t)}\right\}\right] \tag{23}$$

$$\ldots r_2 \geqslant b$$

At the spherical surface for which $r_1 = r_2 = b$, and thence at the contact spot itself one has

$$\theta = \theta_M = \frac{\alpha Q}{2\pi\lambda_1 b}\{1 - \exp(\eta_1^2)\cdot\operatorname{erfc}(\eta_1)\} \tag{24}$$

from equation (22) and

$$= \frac{(1-\alpha)Q}{2\pi\lambda_2 b}\{1 - \exp(\eta_2^2)\cdot\operatorname{erfc}(\eta_2)\} \tag{25}$$

from equation (23) where

$$\eta_1 = (1/b)\sqrt{(k_1 t)} \quad \text{and} \quad \eta_2 = (1/b)\sqrt{(k_2 t)}$$

Values of the function $\{\exp(\eta^2)\operatorname{erfc}(\eta)\}$ are given in Fig. 4.

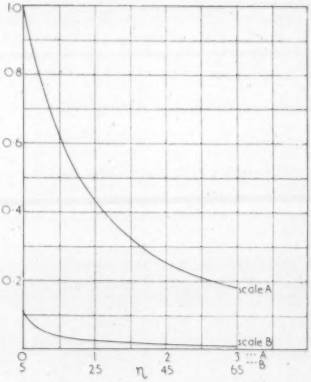

Fig. 4. Values of the function $\exp\eta^2\operatorname{erfc}(\eta)$

An expression for the fraction α can be obtained from equations (24) and (25).

Thus

$$\alpha = \frac{\lambda_1\{1 - \exp(\eta_2^2)\cdot\operatorname{erfc}(\eta_2)\}}{\lambda_1\{1 - \exp(\eta_2^2)\cdot\operatorname{erfc}(\eta_2)\} + \lambda_2\{1 - \exp(\eta_1^2)\operatorname{erfc}(\eta_1)\}} \tag{26}$$

On the basis of the much simplified analysis, the fraction α appears to be time-varying.

For small values of the time t, that is for small values of η, it is seen that

$$\alpha = \frac{\lambda_1\sqrt{k_2}}{\lambda_1\sqrt{k_2} + \lambda_2\sqrt{k_1}} \tag{27}$$

so that the heat flux Q is shared by the contact members in the very earliest stages in the ratio

$$(\lambda_1\sqrt{k_2})/(\lambda_2\sqrt{k_1}) \quad \text{or} \quad \sqrt{(\lambda_1 c_1)}/\sqrt{(\lambda_2 c_2)}$$

For large values of the time t, it is seen that

$$\alpha = \lambda_1/(\lambda_1 + \lambda_2) \tag{28}$$

so that the heat flux is shared in the later stages ($t \to \infty$) in the ratio λ_1/λ_2.

Noting that for copper $k = 1{\cdot}14$ and $\lambda = 3{\cdot}9$, while for natural graphite $k = 0{\cdot}33$ and $\lambda = 0{\cdot}315$, it is seen that with $b = 0{\cdot}01$ cm and t of the order of 10^{-4} s, η_{cu} and η_{gr} are of the order of $1{\cdot}07$ and $0{\cdot}58$ respectively. For such small values of η, the function $\{1 - \exp(\eta^2)\text{erfc}(\eta)\}$ is almost directly proportional to η, and the fraction α is then constant and independent of time t.

It is readily seen that the steady-state distribution of temperature is the same in both contact members, and one has, in fact,

$$\left[\theta(r, t)\right]_{t\to\infty} = \frac{Q}{2\pi r(\lambda_1 + \lambda_2)} \tag{29}$$

At the contact spot itself the steady-state temperature rise is

$$\left[\theta_M(t)\right]_{t\to\infty} = \frac{Q}{2\pi b(\lambda_1 + \lambda_2)} \tag{30}$$

It is instructive to calculate the temperature rise at the contact spots in a practical case. Assuming that the total current is 150 A and that the contact interface potential difference is $0{\cdot}8$ V, and assuming as before that actual contact takes place at three identical circular spots each of a radius of $0{\cdot}01$ cm, it is seen that

$$Q = (150/3) \times 0{\cdot}8 = 40 \text{ watts}$$

If the duration of contact is of the order of 10^{-4} s then

$$\alpha_{Cu} = \frac{\lambda_{Cu}\sqrt{k_{gr}}}{\lambda_{Cu}\sqrt{k_{gr}} + \lambda_{gr}\sqrt{k_{Cu}}} = 0{\cdot}78$$

The heat flux into the copper is therefore

$$40 \times 0{\cdot}78 = 31{\cdot}2 \text{ watts}$$

For $t = 10^{-4}$ s, $b = 0{\cdot}01$ cm and $k_{Cu} = 1{\cdot}14$, one has $\eta_{Cu} = 1{\cdot}07$

Using equation (24) and Fig. 4 it is found then that θ_M is of the order of 75° C. This is, of course, the temperature rise at the contact spot above the temperature of the main masses of the contact members.

In the foregoing calculation any heating in the contact members themselves has been ignored. A more accurate estimate of the temperature rise in the graphite can be made by superposing the temperature distributions in this member for the film-free and the oxide-coated contacts.

The temperature rise in the region $r = 2b$ in the graphite under film-free conditions was found to be 50° C; using equation (23) it is found that the temperature rise in this region due to heat developed in the oxide layer only is about 18° C. Consequently the total temperature rise in this region is of the order of 70° C. However, there is a complication here; the oxide may tend to act as a thermal barrier between the graphite and the copper and the conditions of the present analysis for the film-free contact cannot then be met. The result is that the temperature rise would exceed 70° C.

Decay of the temperature at a contact spot following the separation of the contact members. Consider only the practical case of a film-covered contact. When contact ceases, the electrical generation of heat at the contact spot ceases. If it is assumed that no heat is thereafter radiated into the surrounding atmosphere, then the temperatures can be calculated fairly readily by regarding the cessation of heat generation at a spot as being equivalent to a continuance of the electrical heating with a superposed abstraction of heat from the spot at the same rate.

Heat generation in the oxide film begins at the instant $t = 0$, and the temperature at the contact spot on the metal due to this heat generation is given by equation (24).

If contact ceases at the instant $t = T$, the cessation of electrical heating can be simulated by a superposed abstraction of heat at the rate of αQ watts.

Writing

$$t_1 = t - T$$

it is seen that the temperature at a contact spot due to this abstraction of heat is

$$-\frac{\alpha Q}{2\pi\lambda_1 b}\left[1 - \exp\{(1/b^2)k_1 t_1\} \cdot \text{erfc}\left\{\frac{1}{b}\sqrt{(k_1 t_1)}\right\}\right] \quad \ldots t_1 > 0$$

Thus, for all values of t greater than T, the temperature at a contact spot is

$$\theta_M = \frac{\alpha Q}{2\pi\lambda_1 b}\left\{\left(1 - \exp\{(1/b^2)k_1(t_1 + T)\} \cdot \text{erfc}\left[\frac{1}{b}\sqrt{\{k_1(t_1 + T)\}}\right]\right) - \left[1 - \exp\{(1/b^2)k_1 t_1\} \cdot \text{erfc}\left\{\frac{1}{b}\sqrt{(k_1 t_1)}\right\}\right]\right\}$$

$$= \frac{\alpha Q}{2\pi\lambda_1 b}\left(\exp\{(1/b^2)k_1 t_1\} \cdot \text{erfc}\left\{\frac{1}{b}\sqrt{(k_1 t_1)}\right\} - \exp\{(1/b^2)k_1(t + T)\} \cdot \text{erfc}\left[\frac{1}{b}\sqrt{\{k_1(t_1 + T)\}}\right]\right) \quad \ldots t_1 > 0 \tag{31}$$

If T is large so that virtually steady-state conditions prevail prior to the cessation of contact, then the second term within the brackets becomes negligibly small, and the temperature at a contact spot on the metal is given by the expression

$$\theta_M = \frac{\alpha Q}{2\pi\lambda_1 b}\left[\exp\{(1/b^2)k_1 t_1\} \cdot \text{erfc}\left\{\frac{1}{b}\sqrt{(k_1 t_1)}\right\}\right] \tag{32}$$

For a contact spot on the graphite the temperature is

$$\theta_M = \frac{(1 - \alpha)Q}{2\pi\lambda_2 b}\left[\exp\{(1/b^2)k_2 t_1\} \cdot \text{erfc}\left\{\frac{1}{b}\sqrt{(k_2 t_1)}\right\}\right] \tag{33}$$

The appropriate value of α must be used in equations (31), (32) and (33). Actual calculation of θ_M can be simplified by using Fig. 4.

REFERENCES

(1) Davies, W. *Proc. Instn Elect. Engrs*, Monograph 271 U (December 1957).

(2) Carslaw, H. S., and Jaeger, J. C. *Conduction of Heat in Solids* (Oxford: University Press, 1947).

Glow discharge characteristics of helium-neon mixtures

By G. F. Weston, M.Sc., Mullard Research Laboratories, Salfords, Nr. Redhill, Surrey

[*Paper received* 14 *May*, 1959]

The maintaining and breakdown potentials for a number of helium–neon mixtures have been determined over a pressure × distance (*pd*) range of 1 to 75 cm mm of mercury. The normal cathode fall and the minimum breakdown potential were higher for mixtures containing from 1 to 5% neon, than for either of the pure gases. At higher *pd* values the breakdown potential was lower for mixtures of the order of 50% helium–50% neon than for the pure gases. These results suggest reactions between the two gases affecting the ionization coefficients. Charge exchange processes, detected by Oskam in the afterglow of such mixtures, are consistent with the emission spectra of the glow discharges, and are the probable cause of the variations.

Although various inert gas mixtures are used in commercial glow-discharge tubes, the neon–argon system of mixtures is the only one which has been studied in any detail.[1–3] These mixtures show the well-known "Penning" effect, i.e. a large increase in the first Townsend coefficient α when a small percentage of argon is added to the neon, due to the high probability of ionization of the argon atoms by the neon metastables. In helium–neon mixtures such a reaction is energetically impossible, and one might expect a gradual change in the d.c. breakdown and maintaining potentials from the values obtained in helium to those obtained in neon, as the percentage of neon in helium is increased. However, Acton[4] found that the maintaining potential for mixtures containing a small concentration of neon (of the order of 5%) was some 20% higher than for either of the pure gases. These measurements were made at a constant pressure, electrode separation and current, with nickel electrodes. This paper gives the results of measurements made of the breakdown and maintaining potential under uniform field conditions for a number of helium–neon mixtures. The variations obtained are discussed in the light of the work of Oskam,[5] who has studied the decay of electron densities in the afterglow of similar mixtures.

EXPERIMENTAL TUBES

Simple parallel plate diodes were used in the investigation, with molybdenum disk electrodes, 0·5 mm thick and 15 mm diameter. In some tubes the gap was fixed at 3 to 5 mm, whilst in others one of the electrodes was free to slide perpendicular to its plane by a side arm arrangement, so that the gap could be varied by an external magnet. By altering either the pressure or the gap distance, a pressure × distance (*pd*) range of from 1 to 75 cm mm of mercury could be obtained. The two types of tubes are shown in Fig. 1.

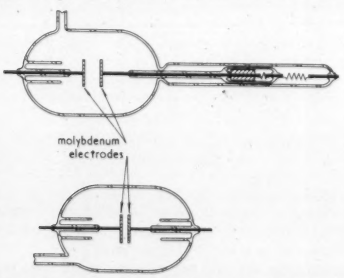

Fig. 1. Experimental tubes for gas discharge characteristics

Molybdenum electrodes were selected because of the good reproducibility and stability of the breakdown and maintaining characteristics, which can be achieved when the cathode is heavily sputtered in the way described by Penning and Moubis[6] in 1944. The method is efficient for removing active gas contamination, and no further cleaning of the gas is required. Results comparable to values obtained on sealed-off tubes could be obtained on the pump, if the sputtering was carried out at each pressure with the diode isolated by a bakeable metal tap. In the case of helium very little sputtering occurred, although consistent results were obtained up to a *pd* value of the order of 50 cm mm of mercury. A mercury diffusion pump and mercury manometer were used on the pump system, but these were isolated from the tube by two liquid air traps which were kept cold throughout the experiments. The spectrographically pure gases were obtained mixed from the British Oxygen Co., and for each mixture values of breakdown and maintaining potential were measured on at least four tubes, one of which had a variable gap. The breakdown statistical delay was eliminated by radioactive priming from a small source outside the tube.

RESULTS

Breakdown potential. The Paschen curves of breakdown potential V_S against *pd* are given in Fig. 2 for helium and neon gas. The spread of average values at any particular value of *pd* for the various tubes was less than 2%, although individual measurements showed slightly wider variations. The curves have slopes similar to the earlier curves of Penning and Addink[1] for neon using iron electrodes, and of Townsend and McCallum[7] for helium with nickel electrodes, but the whole of each respective curve is lower. This is expected from consideration of the second Townsend coefficient γ, which is higher for molybdenum than for iron or nickel.

The curves are very similar for the two gases, and no large variations in the breakdown potential were found when the two gases were mixed. This is illustrated in Fig. 3, where the breakdown potential V_S has been plotted against the percentage of neon for different *pd* values. At the higher *pd* values there is a lowering of V_S over the range 10 to 90% neon. This is not large in comparison with the effects in neon–argon, and decreases as *pd* is decreased. The Paschen minimum shows a maximum value at about 1 to 5% neon, and although the difference is small it is significant, as will be explained later.

MAINTAINING POTENTIAL

Since the maintaining potential is a function of the tube current as well as pressure and distance, the minimum in

the $i - V$ curve has been taken in comparing the characteristics of the various mixtures. A plot of these minimum values V_M against pd gives a curve similar to that shown in Fig. 4(*a*) for helium. The centre portion represents the

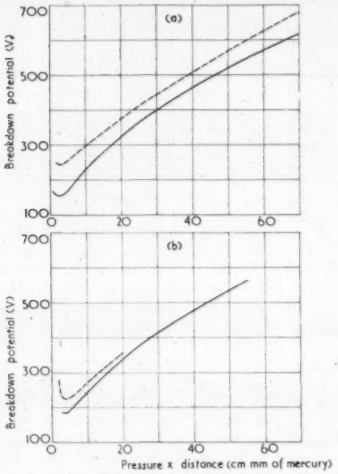

Fig. 2. Paschen curves for neon and helium with molybdenum electrodes

(*a*) neon — — — — = results obtained by Penning and Addink.[1]

(*b*) helium - - - - = results obtained by Townsend and McCallum.[7]

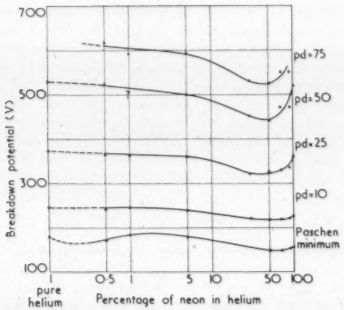

Fig. 3. The variation of breakdown potential with neon concentration in helium–neon mixtures

Values of pd are given in cm mm of mercury.

normal cathode fall; the increase in V_M at the lower value of pd is due to the glow being restricted, whilst at the higher value of pd it is due to the formation of an anode fall. In the case of helium the curve appeared to follow the similarity law, and the same curve is obtained by varying either the pressure or the distance.

The equivalent V_M pd curve for neon is rather different, and two effects are seen; firstly, the anode fall occurs at very much higher values of pd than for helium, and secondly, the normal cathode fall does not obey the similarity principle, but decreases with increasing pressure at any given value of pd. This is shown in Fig. 4(*b*). The variation of the normal cathode fall V_N with pressure was first reported by Jurriaanse[8] in 1946, who found similar effects in argon, and

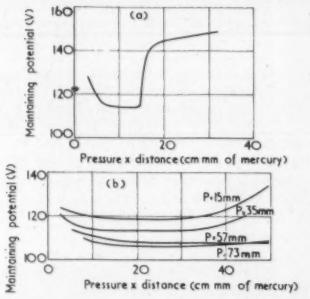

Fig. 4. The minimum maintaining potential as a function of pd for neon and helium

(*a*) helium; (*b*) neon.

mixtures of argon with neon and helium. Although such a variation was particularly looked for, it was not found in helium or the helium–neon mixtures until the helium concentration in neon was less than 10%. The mixtures showed similar curves to the helium with the anode fall occurring at relatively low pd values. The pd value at the onset of the anode fall depended on the amount of neon present, varying from 10 cm mm of mercury for 5% neon to 18 cm mm of mercury for 90% neon. The variation of the normal cathode fall V_N with the percentage of neon is shown in Fig. 5. This shows a maximum at about 1 to 5% neon which is similar

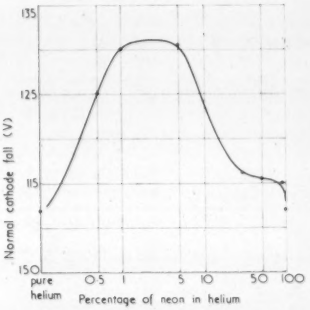

Fig. 5. Variation of normal cathode fall with neon concentration

to the results obtained by Acton. However, since Acton was working at a value of pd of about 12, the rather larger effects that he obtained may have been due to the introduction of an anode fall in some of the mixtures.

Comparing the cathode fall with the breakdown potential (Fig. 3), one sees that although there is little correlation with V_S at high pd values, the V_S curve at the Paschen minimum

shows a similar maximum at 1 to 5% neon. Approximate theory suggests that the cathode fall and the minimum breakdown potential are similar functions of the Townsend coefficients, although there is no complete theory linking the two. It was considered worth seeing if an empirical correlation could be obtained by plotting V_N against the breakdown minimum V_B. With the exception of helium the points lie on a straight line, and further, if values for other gases and electrode materials taken from the literature are also plotted, the points obtained lie approximately on the same line. This is shown in Fig. 6.

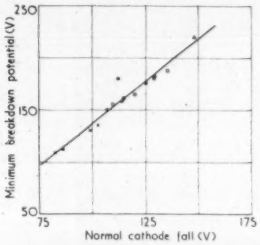

Fig. 6. Relation between minimum breakdown potential and normal cathode fall

● = helium with molybdenum cathode
○ = helium–neon mixtures with molybdenum cathode
× = neon–argon mixture with molybdenum cathode (V_B, Frouws[10]; V_N, Jurriaanse, Penning and Moubis[9])
△ = neon with copper cathode (V_B, Kruithof[12]; V_N, Penning and Moubis[11])
□ = neon with nickel cathode (V_B, Townsend and McCallum[7]); V_N, Penning and Moubis[11])

Over the range $V_N = 80$ to 150 V the line can be expressed by the equation

$$V_N = 0{\cdot}58\ V_B + 22 \qquad (1)$$

where V_N and V_B are in volts.

DISCUSSION

The variation of the breakdown and maintaining potential with percentage of neon in helium can only be explained by assuming that there is a reacton between the two gases which affects the ionization coefficients α and/or γ.

Although helium metastable atoms cannot ionize the neon atoms, they can excite them according to the reacton

$$He^* + Ne \rightarrow He + Ne' \rightarrow He + Ne + h\nu \qquad (2)$$

Such a reaction, however, is only likely to affect γ if the helium metastables play a significant part at the cathode surface, whereas at the pressures used in the experiments it is more likely that positive ion bombardment of the cathode is the chief cause of secondary electrons. Recently Oskam,[5] measuring processes in the afterglow of helium–neon mixtures, has shown that other reactions can take place based on charge transfer processes between the helium molecular ion and neon. The presence of helium molecular ions in a helium discharge by a three-body process is now well known.

$$He^+ + 2He \rightarrow He_2^+ + He \qquad (3)$$

At pressures above a few millimetres of mercury the probability of this reaction is very great, and Oskam found only molecular ions present in his tubes filled to 5 and 23 mm of mercury pressure.

Since the "internal" energy of the helium ion is close to the ionization potential of neon, charge exchange can take place in the mixture according to the equation

$$He_2^+ + Ne \rightarrow Ne^+ + 2He \qquad (4)$$

It is likely that the charge exchange reaction takes place in the tubes used in view of the emission spectra which has been obtained. Pure helium shows strong helium molecular bands, which are absent when a small percentage (of the order of 0·5%) of neon is added (see Fig. 7).

At higher pressures and higher neon concentrations, Oskam found that the neon ion could take part in a further three-body reaction to produce molecular ions with their subsequent dissociative recombination.

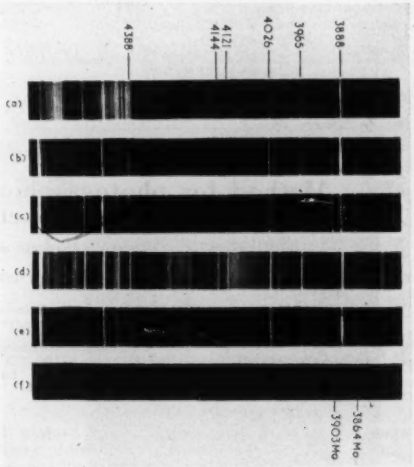

Fig. 7. Spectrographs of neon–helium mixtures

(*a*) helium; (*b*) 99·5% helium, 0·5% neon; (*c*) 70% helium, 30% neon; (*d*) 50% helium, 50% neon; (*e*) 10% helium, 90% neon; (*f*) neon.

From measurements of the recombination coefficient, Oskam believes that the molecular ion formed is a neon–helium one according to the equation

$$Ne^+ + Ne + He \rightarrow (NeHe)^+ + Ne \qquad (5)$$

Evidence for the existence of such a molecular ion has been given by Druyvesteyn[13] in 1931 when he discovered two unidentified bands in the discharge emission spectra of a 50% neon–50% helium mixture; one between the helium lines 4026 and 4121 Å, and the other between 4219 and 4276 Å. This has recently been confirmed by Jongerius[14] in Utrecht, who found the bands present in the negative glow but not in the positive column. The bands were looked for in the laboratory: they were not present in mixtures containing up to 30% neon, but were very strong in 50% neon–50% helium and could still be detected in mixtures containing only 10% of helium. This is shown in Fig. 7.

Both the charge exchange process and the formation of the

$(NeHe)^+$ ion will alter the mobility and energy of the positive charge carrier, thus at least affecting the second Townsend coefficient γ. The cross-section for charge exchange is very high according to Oskam, of the order of $1{\cdot}5 \times 10^{-15}$ cm^2, and therefore will be nearly as effective as the Penning reaction in neon–argon mixtures. The increase in V_B and V_N at small concentrations of neon in helium may be due, therefore, to this charge exchange process, whereas the drop in V_S at higher values of pd and neon concentrations might be explained by the formation of the $(NeHe)^+$ ion. Unfortunately there is not enough information available on the values of α and γ to be able to assess the results of these reactions in terms of the breakdown and maintaining characteristics.

ACKNOWLEDGEMENTS

The author wishes to thank the Director of Mullard Research Laboratories and the Directors of Mullard Ltd. for permission to publish this paper.

REFERENCES

(1) PENNING, F. M., and ADDINK, C. C. J. *Physica*, **1**, p. 1007 (1934).
(2) KRUITHOF, A. A., and PENNING, F. M. *Physica*, **4**, p. 430 (1937).
(3) KRUITHOF, A. A., and DRUYVESTEYN, N. J. *Physica*, **4**, p. 450 (1937).
(4) ACTON, J. R. British Patent No. 734,611: 1955.
(5) OSKAM, H. J. Thesis (University of Utrecht: November 1957).
(6) PENNING, F. M., and MOUBIS, J. H. A. *Philips Res. Rep.*, **1**, p. 119 (1946).
(7) TOWNSEND, J. S., and MCCALLUM, S. P. *Phil. Mag.*, **17**, p. 678 (1934).
(8) JURRIAANSE, T. *Philips Res. Rep.*, **1**, p. 407 (1946).
(9) JURRIAANSE, T., PENNING, F. M., and MOUBIS, J. H. A. *Philips Res. Rep.*, **1**, p. 225 (1946).
(10) FROUWS, S. M. Paper read at 3rd International Conference on Ionization Phenomena in Gases, Venice, 1957.
(11) PENNING, F. M., and MOUBIS, J. H. A. *Physica*, **15**, p. 721 (1949).
(12) KRUITHOF, A. A. *Physica*, **7**, p. 519 (1940).
(13) DRUYVESTEYN, M. J. *Nature* (*London*), **128**, p. 1076 (1931).
(14) OSKAM, H. J., and JONGERIUS, H. M. *Physica*, **24**, p. 1092 (1958).

Method for photographic identification of microscopic radioactive particles

By J. SISEFSKY, Research Institute of National Defence, Dept. 4, Stockholm 80

[*Paper received* 8 *June*, 1959]

A method is described for identification and microscopy of small radioactive particles mixed with a large amount of inactive ones. The particles are prepared on a celluloid coating on a glass plate. The plate is coated with nuclear emulsion in gel form which is reversal developed *in situ* leaving the active particles visible, in the centres of clear circular spots against a brown transparent background.

INTRODUCTION

In examining radioactive aerosols it sometimes happens that the active particles cannot be extracted without being mixed with a much greater number of inactive particles. A method to determine which particles are radioactive is therefore desirable. The problem is particularly evident in the examination of air-borne nuclear weapon dust, and this paper describes a method for identifying individual particles in such dust.

PRELIMINARY SELECTION OF ACTIVE PARTICLES

In the cases here described the particles were collected on glass-fibre paper through which air was filtered in an air sampler, either on the ground or in an aircraft at heights up to 15 000 m. The filter-paper was first autoradiographed with a fast X-ray film (Ilford "Ilfex") for 1 to 7 days. By suitable marking of the filter and the film they can, after developing, be matched together again practically as they were during the exposure, although the film may be slightly deformed under processing.

The blackening, which is mainly caused by the beta-radiation, appears as circular, dense spots with diffuse edges. The smallest spots, visible to the naked eye, are due to particles which have given some thousands of beta-disintegrations during the exposure period. The biggest spots observed (due to about 10^8 beta-disintegrations obtained by exposures for one week) were several millimetres in diameter. Weaker activities than some thousands of disintegrations give diffuse spots, which are usually masked by the background of development fog.

The sizes of the spots thus give a rough measure of the particle activities. However, they cannot be immediately used for accurate activity measurements, as the beta-sensitivity of the X-ray film depends on the beta-energy, and the mean beta-energy from nuclear weapon dust is a function of the age of the dust, bomb-type, etc. The spot sizes are only to a minor degree dependent upon the distance between the particle and the film as long as this is not so great that the spot becomes fully diffuse even at its centre.

After matching filter and film it is possible to punch out small filter cores containing the radioactive particles by means of a 4 mm hollow punch. The filter cores must then be prepared for microscopy, for which purpose the following procedure is used.

Clean glass plates 10×10 cm, $1{\cdot}7$ mm thick, with rounded edges and corners, are dipped in a highly viscous solution of celluloid in acetone, the surplus of which is allowed to run off. After drying, the glass disk is entirely coated by a thin (some ten microns thick) clear film of celluloid. Any "blush" spots that may occur are cleared up with acetone vapour. The process is repeated two or three times. By allowing the film of celluloid to surround the plate completely, it is prevented from loosening during the subsequent photographic treatment.

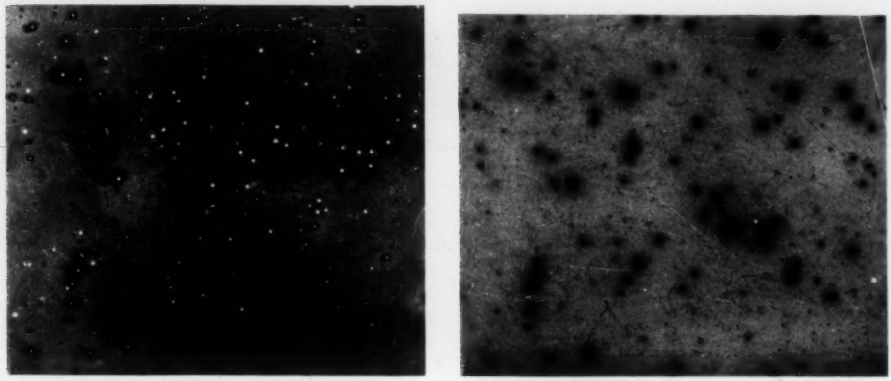

(*a*) (*b*)

Fig. 1. (*a*) Part of an emulsion-coated plate showing several clear spots surrounded by rings caused by active particles, and false spots without rings caused by air bubbles. Magnification × 2. (*b*) By means of the corresponding X-ray film autoradiograph the true spots can be distinguished from the false ones

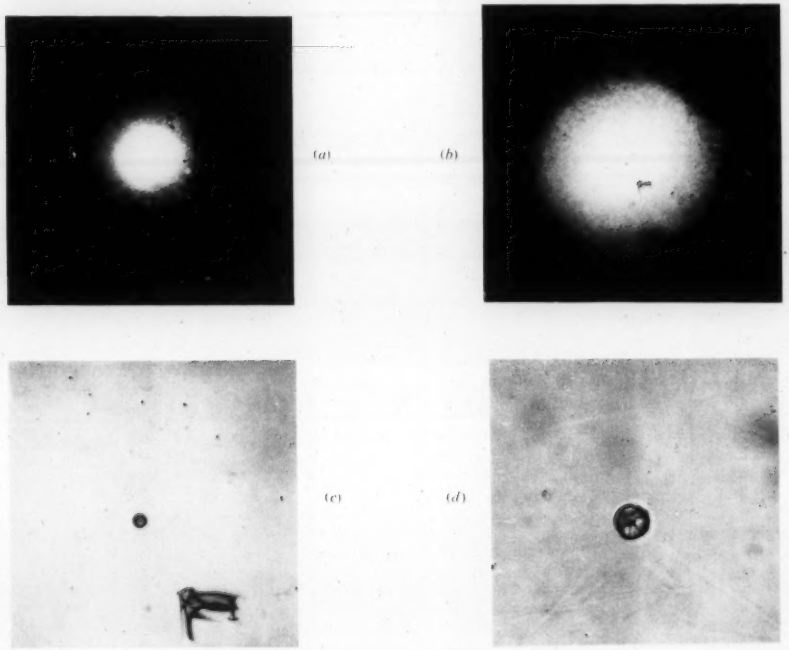

(*a*) (*b*) (*c*) (*d*)

Fig. 2. Identification of a 5 μ particle

(*a*) Magnification × 50; (*b*) × 125; (*c*) × 500, and (*d*) × 1250.

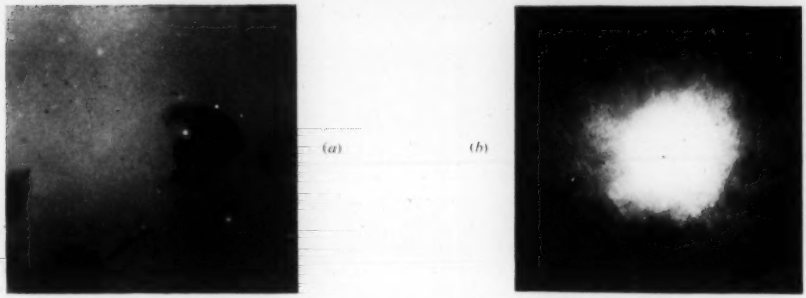

Fig. 3. Identification of a 0·5 μ particle
(*a*) Magnification × 50, and (*b*) × 1250.

The filter cores are stirred up in a little syrupy celluloid solution until they are torn apart into individual fibres. The paste obtained is then spread out with a spatula on the prepared plate as thinly as possible, or is alternatively diluted with acetone and filtered through fine metal gauze (mesh size, about 200 μ) on to the plate. The latter method gives a better transparency, but there is a risk of losing some particles, especially the smaller ones, which may stick to the glass fibres remaining on the gauze.

When the plate has dried, the particles are embedded in the celluloud film close to the surface, and are thus protected from chemical attack during the subsequent treatment. Moreover, the glass-fibres are nearly invisible, since they have roughly the same refractive index as the celluloid. In a microscope numerous particles are now visible, though the overwhelming majority are dust particles of no interest which have accompanied the filter cores. If the number of these particles is very large, the condition can be bettered by a repetition of the whole process mentioned above (the celluloid film is easily cut up and removed from the glass plate). This repeated treatment may be necessary when processing air samples taken at ground level, where there is often a thick layer of dust on the filters.

CLOSE SELECTION OF ACTIVE PARTICLES

It is difficult or impossible, however, to bring down the number of irrelevant particles to such an extent that none of them is likely to be situated at the place where an autoradiograph indicates the presence of a radioactive particle. This is especially the case when the particle size is close to the resolving limit of the microscope (0·2 μ). Thus it is necessary to indicate the positions of the active particles more accurately.

This can be done by using beta-sensitive nuclear emulsion in gel form, which is poured over the plate and then developed *in situ*. If the development is carried out according to the directions for use, the active particles will give black circular spots, surrounded by beta-tracks. These spots, of course, completely hide the particles that have caused them. This difficulty is overcome by reversal-development of the emulsion, leaving the exposed spots clear against a dark background. The procedure is briefly as follows (a detailed description is given in the Appendix). In order to make the emulsion stick to the celluloid, the coated plate is first prepared with a substratum. The nuclear emulsion for beta-particles is poured on to the plate in a thin layer and dried.

During exposure, the plate is also autoradiographed on an X-ray film, which is later used as an aid for microscopy and activity determination (see below).

After a suitable exposure time the X-ray film is developed as usual (ID 42, 4 min) and the plate with the beta-emulsion is reversal-developed. In order to make microscopy possible, the opaque black background is converted to a transparent brown one by a second bleaching process.

The plate is now ready for microscopical examination. The particles are observed in the centres of clear circular spots, sometimes surrounded by brown, diffuse rings against a yellowish-brown fine-grain background. The positions of the particles are defined within some ten microns. These clear areas are smaller than the corresponding spots on the X-ray film, and usually not visible to the naked eye. Therefore the X-ray film is used for a coarse orientation of the situation of the clear spots, as well as for eliminating false spots which can arise from air bubbles in the emulsion or the blackening of the film due to chemical attack by dust particles, etc.

As mentioned before, the autoradiograph spot diameters do not give accurate measurements of the activity strengths of the corresponding particles. However, if it can be supposed that all particles in a sample originate in the same explosion, calibration by means of the stronger particles which are measurable with ordinary activity counters ($\sim 10^{-10}$ curie), makes possible an estimation of the activity of the weaker ones, which cannot be measured in any other way.

The accompanying photographs give some examples of the use of the method.

ACKNOWLEDGEMENT

The author wishes to thank Professor H. Bäckström for valuable discussions.

REFERENCES

(1) THORNE BAKER, T. *Photographic Emulsion Technique*, 2nd ed. p. 227 (Boston: American Photographic Publishing Co., 1948).

(2) BÄCKSTRÖM, H. *Fotografisk handbolk*, 2nd ed. p. 450 (Stockholm: Bokförlaget Natur och Kultur, 1942).

APPENDIX

Procedure and Formulae

Substratum treatment. 0·5 g pyroxyline (or celluloid) and 0·5 g photographic gelatine are dissolved into 33 ml. hot

glacial acetic acid and the solution diluted with 1000 ml. methanol. The plate is dipped into this solution, surplus fluid is allowed to run off and the plate is then thoroughly dried. (Substratum layers seemingly dry may cause coagulation in the liquid emulsion by their content of acetic acid.)

For the emulsion coating, a few millilitres of Ilford Nuclear Emulsion in gel form (type G 5) is heated to 50° C, according to the directions for use, poured on to the plate, spread with plastic spatula and the surplus allowed to run off so as to form a thin uniform layer, which is dried by a stream of hot air.

As the method described does not make use of the ability of the beta-sensitive emulsion to give visible beta-tracks, it is not necessary to use the emulsion within a month after manufacture as is stated in the maker's directions for use; emulsion a year old, kept in an ordinary refrigerator, has given good results.

To expose the plate, it is placed particle-side down on an X-ray film (Ilfex) and its position marked with a pencil. The package is placed under pressure during the exposure period which must be long enough for the weakest sources to give at least some thousands of disintegrations.

Reversal Development. This procedure is a modification of the usual one in order to make the exposed spots completely clear and to prevent the emulsion from loosening. There is a tendency to such loosening in spite of the substratum treatment, more so, it seems, in basic and neutral baths than in acid. Therefore 2% acetic acid in distilled water is used for all rinsings and the bath immersions are made as short as possible.

The first development should be carried out from 10 to 15 min in undiluted ID.19 and the plate should be rinsed for a further 5 min; it should then be bleached for 5 min in a bath consisting of sodium dichromate 10 g, conc. sulphuric acid 10 ml, and distilled water 1000 ml. The clearing up should take 5 min in a bath consisting of sodium sulphite 100 g and distilled water 1000 ml. The plate should then be rinsed for 10 min and then exposed by illuminating from the back for several minutes.

For the second development the plate should be placed in ID.42 for 5 min and fixed in a fast acid fix (ammonium thiosulphate) for 10 min or more if necessary. All baths following the fixing must be chloride-free (distilled water). After fixing, the plate should be rinsed for 10 min and the final bleaching is carried out in the same bleaching bath as above in double concentration, followed by a double concentrated clearing bath. This time the black silver is, in a few minutes, bleached into red-yellow, which, in the following clearing bath, is converted into a brown, transparent colour, that appears granulated at large magnification.

After bleaching the plate should be rinsed for a further 10 min and then dried by means of a hot air stream.

Study of cadmium sulphide crystals grown from the vapour phase in a stream of argon

By J. Woods, B.Sc., Ph.D., A.Inst.P., Research Laboratories, The General Electric Co. Ltd., Wembley, England

[*Paper first received* 27 *April, and in final form* 28 *August*, 1959]

Crystals of cadmium sulphide have been grown by reacting a stream of argon containing cadmium vapour with a stream of hydrogen sulphide. The variations in crystal habit which occur are very similar to those reported for ice crystals by Hallett and Mason.[1] Growth features were studied using a metallurgical microscope. Although growth occurs in layers, spirals were only observed on rare occasions. The evidence indicates that ordinary two-dimensional nucleation over a plateau is more common, and is affected by the impurities added. Nucleation also occurs at sites on the edge of a crystal face or at the apexes of re-entrant angles between growth steps from neighbouring sources. Various types of cavity have also been observed in the volume of some crystals, and possible methods of formation are discussed.

During the past decade considerable interest in cadmium sulphide has been excited by the large photoconductive effect which it displays. In consequence the electrical and optical properties of single crystals have been investigated extensively and various methods of crystal preparation have been described, see Kröger, Vink and van den Boomgaard.[2] In essence there are two basic crystal growth techniques. In one of these (Frerichs[3]), CdS vapour is synthesized at 1050–1200° C and then condensed at a lower temperature. In the other (Reynolds and Czyzak[4]) a charge of CdS powder is heated in a sealed tube in an atmosphere of hydrogen sulphide or an inert gas, so that prismatic crystals grow on the charge. A variation of this method is to maintain a temperature gradient along the sealed tube so that the charge vapourizes and crystals grow at the cooler end of the tube.

Crystals prepared by the various methods differ in size, colour, crystal habit and degree of perfection. Often some pieces of crystal which appear to be optically perfect are found to be polycrystalline on X-ray examination. This applies particularly to crystals grown by the sealed-tube technique. Despite these variations, few authors give more than a cursory description of the type of crystal used in their work, and the possible effects of the various crystalline imperfections are rarely considered. However, it has often been found that the diffusion of impurities into a CdS crystal depends on the manner in which the crystal was prepared. It seems likely that this may be partly or wholly attributable to the presence of structural imperfections. With this in mind, a study has been started of the growth and dissolution mechanisms operative in CdS crystals grown from the vapour phase. This paper is confined to effects in crystals prepared using the Frerichs[3] technique and is mainly concerned with the microscopic examination of growth features. An account of the etch pits and patterns which can be produced in these crystals will be given later.[5]

PREPARATION OF CRYSTALS

The crystals were prepared by reacting streams of cadmium vapour and H_2S at temperatures from 1050–1200° C and allowing the CdS vapour to condense on the walls of the

containing silica tube at 900° C. The supply of cadmium vapour was obtained by passing argon over a silica boat containing about 10 g of molten cadmium. The cadmium boat was contained in a 3 ft long clear silica tube in which the whole process was carried out. The stream of argon and cadmium vapour was passed to the reaction zone where it encountered a stream of H_2S supplied *via* a smaller silica tube. The H_2S stream was washed, purified, dried and monitored with a flow-meter before entering the reaction zone. Various rates of gas flow were used during the course of the work but were usually of the order of 100 ml/min. The exhaust gases were burned off and the colour of the flame gave an indication of the presence or absence of cadmium vapour in the gas flow. The cadmium was consumed in two to four hours depending on the rate at which it was carried over. When the cadmium was exhausted, the power to the furnace was gradually reduced. When the temperature of the crystal growth region fell to 300–400° C, the H_2S flow was stopped and the tube was continuously flushed with argon until it reached room temperature.

When required, various impurities were grown into the crystals. Chlorine was incorporated by adding hydrogen chloride to the hydrogen sulphide. Gallium or indium was added by passing argon over a boat containing the molten metal at temperatures near 1000° C. The quantities of chlorine, gallium or indium grown into the crystals were in the range 0·01 to 0·1% as determined from measurements of the electrical conductivity and Hall affect (Kröger, Vink and Volger[6]).

CRYSTAL HABIT

The crystals grew by the hundred in a thick crust on the inner wall of the containing silica tube. All the crystals prepared, with and without deliberate impurity additive, had the hexagonal wurtzite structure. The principal crystal forms obtained were as follows: (1) Rectangular plates up to 2 cm^2 in area and between 0·01 and 0·1 mm thick. These plates were usually, but not always, striated, with the striations parallel to the *c*-axis, which was in the plane of the plate lying parallel, perpendicular or at 60° to the longer axis of the plate. (2) Hexagonal rods and needles up to 3 cm long with diameters up to 1 mm. (3) Scrolls and hollow hexagonal columns which appeared to have been formed from rectangular plates wrapping themselves about the *c*-axis. (4) Hexagonal plates with the *c*-axis perpendicular to the plane of the plate; these plates were about 1 cm^2 in area and 0·1 mm thick. (5) Large crystals in which a flat hexagonal face 1–2 cm^2 in area formed the base of a hexagonal pyramid 1–5 mm high. The pyramid was terraced on each of its six sides, and it terminated at the top in a smaller plateau about one-quarter the area of the base. (6) Dendritic crystals, either formed by branching from a central prismatic rod, or from a hexagonal plate showing ribs and sprouting new branches from the corners.

The crystal habit was determined by the cadmium vapour pressure, the growth temperature and the impurity added. The dependence of the crystal habit on these growth conditions is summarized in the table. When 10% HCl gas was added to the H_2S flow, the crystals grew to a considerably larger size compared with the purest crystals, and some showed signs of having melted partially. The dependence of the crystal habit on the supply of cadmium vapour and the growth temperature was relatively unaffected by the presence of HCl. The only difference detected was that the range of temperature over which growth occurred was extended downwards to 850° C. The largest crystals were obtained when gallium or indium was used as an impurity additive; the colour of the resultant crystals ranged from yellow to red to dark brown as the impurity concentration increased from 0·01% to 0·1%.

Dependence of crystal habit on growth conditions

Impurity added	*Cadmium temperature* (° C)	*Growth temperature* (° C)	*Crystal habit*
Nil	500	900–1000	Rectangular plates ~0·01 mm thick
Nil	650	1000	Rectangular plates ~0·05 mm thick
Nil	650	900	Hexagonal rods and needles
10% HCl added to H_2S	500	900–1000	Rectangular plates ~0·02 mm thick
10% HCl added to H_2S	650	1000	Rectangular plates ~1 mm thick
10% HCl added to H_2S	650	900	Rods, needles, scrolls
10% HCl added to H_2S	650	850	Dendrites formed on a central column
Ga or In (0·1%)	500	950–1000	Hexagonal plates and pyramids
Ga or In (0·1%)	650	950–1000	Rectangular plates and scrolls
Ga or In (0·1%)	650	900–950	Scrolls, hollow rods, rods and needles
Ga or In (0·1%)	650	850–900	Dendrites formed on central column, and dendrites formed on a hexagonal plate

The various forms of CdS crystals described above bear a remarkable similarity to the various habits in which ice crystallizes. Hallett and Mason[1] who grew ice from the vapour in conditions of controlled supersaturation and temperature have shown that, above a certain supersaturation, the habit is almost entirely dependent on the temperature. In the range 0 to −30° C the following transitions in habit occurred: plates → needles → hollow prismatic columns → plates → dendritic crystals → plates → rods. At low supersaturations, plates were formed over the whole temperature range. It seems likely that the growth habit of CdS crystals follows a somewhat similar pattern, and although it was not possible to determine the composition of the vapour and the temperature profile in the growth region, the following points of similarity have nevertheless been noted. At low supersaturations the principal crystal form is a platelet, no matter what the growth temperature. With no impurities, or with chlorine added, the *c*-axis lies in the plane of the plate and defines a direction of rapid growth. When gallium or indium is present, rapid growth occurs in all the a-directions and hexagonal plates are formed. At higher supersaturations, plates are formed at the highest temperatures, followed by needles, hollow columns and dendritic crystals at decreasing temperatures.

GROWTH FEATURES ON BASAL PLANES

A large number of crystals of all types has been examined using a metallurgical microscope with bright field illumination, and selected crystals have been studied using multiple-beam

Fizeau fringes. Few growth steps or markings could be observed on the basal planes of the hexagonal rods or the thin rectangular plates. However, numerous features were readily observed on the basal planes of the hexagonal plates and pyramids where the *c*-axis was along the smallest dimension.

Etching experiments (Woods[5]) show that cadmium sulphide displays polarity effects. Thus hexagonal pits can be etched chemically on one basal plane, arbitrary designated (0001), but not on the other (000$\bar{1}$). The present investigation shows that the growth mechanism also is different on opposite basal planes. Growth spirals have been observed on the crystals, but only on about one crystal in fifty. The spirals on (000$\bar{1}$) were regular hexagonal, originating from one or more screw dislocations of the same sign. A typical multiple spiral is shown in Fig. 1. The estimated step height of these

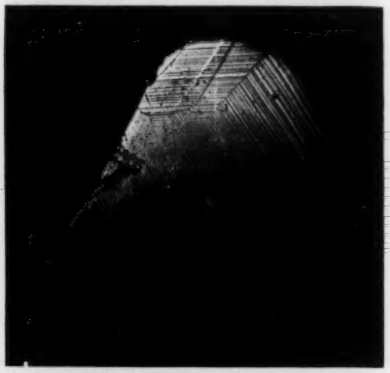

Fig. 1. Multiple spiral growth hill on (000$\bar{1}$) ($\times$150)

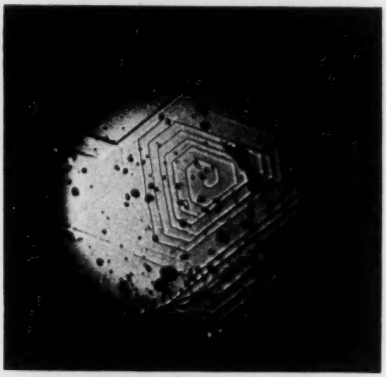

Fig. 2. Spiral growth hill on (0001) ($\times$150)

hexagonal spirals was at least ten times the height of a unit cell, indicating that the spirals were not elementary. An example of the spiral growth found on (0001) is shown in Fig. 2 where the first few turns have a trigonal symmetry. The step height of such growth hills could not be measured by multiple-beam interferometry because of the irregular shape of crystals on which they occurred. However, the high visibility of the steps under bright field illumination indicates that they were several multiples of a unit cell in height. Rounded spirals of the type reported by Reynolds and Greene[7] for CdS crystals grown on a charge of powder were not observed on our specimens.

No terraced hills of the type expected to grow from two closely spaced screw dislocations of opposite sign have been observed, but a terraced hexagonal hill with a perfectly flat top was by far the most frequently observed growth feature. An example is shown in Fig. 3. Here again the steps were of

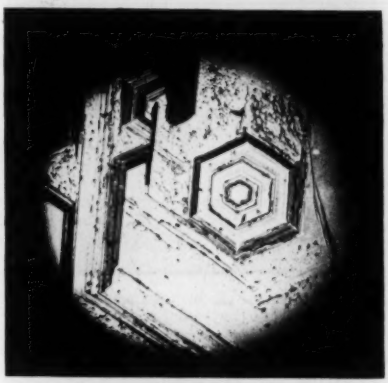

Fig. 3. Terraced hexagonal growth hill on (000$\bar{1}$) ($\times$60)

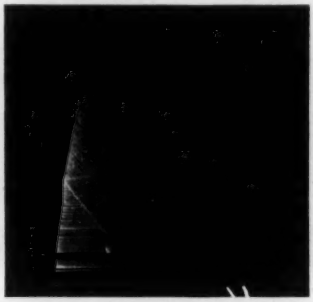

Fig. 4. Hexagonal growth hill with nucleation point at crystal edge ($\times$60)

irregular width and the step height was many multiples of a unit cell. Growth hills of this type were found mainly on (000$\bar{1}$) faces. Fig. 4 illustrates another growth feature often found on (000$\bar{1}$) faces, that is, a hill formed by nucleation and layer growth starting at a point on the extreme edge of the crystal face.

So far, mainly growth features on (000$\bar{1}$) planes have been discussed, where the growth steps were usually polygonal and straight over considerable lengths. Thus all the features

observed on (000$\bar{1}$) planes showed well-developed hexagonal symmetry. In contrast, the growth markings on the (0001) planes were often highly irregular. A typical example of such irregularities is shown in Fig. 5 where, in addition, the highest level contains a number of small triangular depressions. A second example of growth on a (0001) plane is shown in Fig. 6 where it can be seen that the steep steps were formed

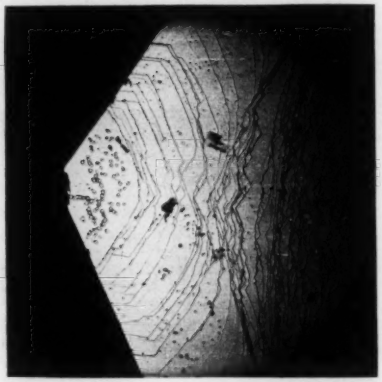

Fig. 5. Irregular growth steps on (0001) ($\times 60$)

Fig. 6. Another (0001) face showing a multitude of small hexagonal growth features ($\times 60$)

by the amalgamation of numerous small, cylindrical hexagonal hills. With this type of growth, many cavities are left when expanding hexagons meet. After examining large numbers of crystals, it was concluded that nucleation occurs much more readily on (0001) than on (000$\bar{1}$) faces. Spirals such as that shown in Fig. 2 were the only large area prominences with well-developed symmetry which were observed on (0001) faces. However, on faces smoother than those shown in Figs. 5 and 6 it was not uncommon to find shallow hexagonal depressions. These depressions were bounded by regular hexagons and had perfectly flat bottoms. They were quite unlike the thermal etch pits described by Woods.[5] Chemical etching improved the visibility of these shallow depressions which suggests that they were formed at the site of some singularity, possibly in the manner proposed by Tolansky[8] for the formation of trigons on diamond.

VOIDS

At room temperature, the optical absorption edge of cadmium sulphide is near 0·51 μ. Crystals are therefore transparent to visible light and their interiors can be examined with an ordinary microscope using transmitted light. When crystals were examined in this manner, various types of void and inclusion could be distinguished. A micrograph of some of the most common voids is shown in Fig. 7. The voids

Fig. 7. Oval-shaped voids parallel to c-axis ($\times 150$)

were oval-shaped, and were often interconnected by narrow channels. The major axis of the oval was parallel to the c-axis. This type of void was frequently found in crystals

Fig. 8. Collapse of large sheet-like void leading to formation of oval-shaped voids ($\times 60$)

grown in the presence of HCl. Some of these cavities contain a high concentration of chlorine, probably in the form of cadmium chloride. This has been shown by cleaving across a set of these cavities and observing the partially orientated crystallization of needles of cadmium chloride on the (0001) cleavage face.

Some indication of the way in which the voids are formed can be inferred from the micrograph shown in Fig. 8. This shows the interior of a rectangular platelet. Across the centre of the photograph a large void can be seen. This was presumably formed between two separate crystalline sheets. As the large void collapsed, smaller oval-shaped cavities were generated and left in a trail behind the main collapsing vacant sheet.

Another common bulk imperfection, which is triangular in shape, is shown in Fig. 9. This imperfection, which is

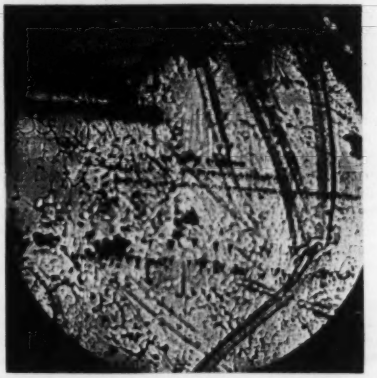

Fig. 9. Grouping of triangular voids into bands perpendicular to *c*-axis (×60)

usually an empty cavity appears, in some crystals, to contain segregated impurity. All triangular voids in one crystal had the same orientation along the *c*-axis with the apex directed towards the (000$\bar{1}$) face. Occasionally isolated triangular imperfections were observed, but usually they were grouped together to form bands which were either parallel or perpendicular to the *c*-axis as in Fig. 9. These imperfections in the body of a crystal were often found in company with triangular pits on a parallel crystal surface. It would appear that the bulk imperfections and the surface pits are of common origin.

DISCUSSION OF GROWTH FEATURES

The concept of spiral growth round a screw dislocation was originally proposed by Frank[9] to explain crystal growth at low supersaturation. Spirals have since been observed on numerous different crystals. The present work shows that the spiral growth mechanism can operate in CdS crystals condensed from a vapour stream. So far no elementary spirals have been observed but they may have escaped observation.

The evidence so far suggests that although spiral growth round dislocations of multiple strength does occur on some CdS crystals, this does not form the principal growth mechanism. Spiral growth probably occurs when the supply of cadmium is becoming exhausted and the effective supersaturation drops to a low value. The principal growth process at the higher supersaturations where the major part of growth occurs, appears to be a straightforward two-dimensional nucleation near the centre of a plateau, leading to the formation of hexagonal terraced hills. No evidence has been obtained, even using phase-contrast microscopy, that the closed hexagonal steps are generated from a pair of screw dislocations of opposite sign. Nucleation, which is much more profuse on (0001) than on (000$\bar{1}$), can, however, occur at other singularities on a face. Thus, often a point on the edge of the crystal is favoured, possibly because of contact with another crystal. Sometimes, layer growth was observed which originated from a re-entrant angle between two growth steps from separate sources. The bunching of steps to produce multiple step heights can be explained by the mechanism proposed by Elbaum and Chalmers.[10]

The origin of the oval-shaped voids is well demonstrated in Fig. 8, but the origin of the triangular shaped cavities is not so obvious. However, observation showed that in some platelets, additional crystalline sheets grow in the *c*-direction over the underlying platelets rather in the manner suggested by Chalmers and Martius,[11] that is, the end of the advancing sheet is sawtoothed in shape and kink sites are provided with no dislocations present. If, for some reason, such a layer is overtaken by another layer, the subsequent collapse of the lattice would lead to a band of triangular voids.

It is clearly not possible at the moment to offer a convincing explanation of the various modes of growth of CdS crystals. Further work is required in which crystals are grown in known, variable supersaturations in conditions in which the effects of vapour composition, temperature and impurities can be studied.

REFERENCES

(1) Hallett, J., and Mason, B. J. *Proc. Roy. Soc. A*, **247**, p. 440 (1958).

(2) Kröger, F. A., Vink, H. J., and van den Boomgaard, J. *Z. Phys. Chem.*, **203**, p. 1 (1954).

(3) Frerichs, R. *Phys. Rev.*, **72**, p. 594 (1947).

(4) Reynolds, D. C., and Czyzak, S. J. *Phys. Rev.*, **79**, p. 543 (1950).

(5) Woods, J. To be published.

(6) Kröger, F. A., Vink, H. J., and Volger, J. *Philips Res. Rpts*, **10**, p. 39 (1955).

(7) Reynolds, D. C., and Greene, L. C. *J. Appl. Phys.*, **29**, p. 559 (1958).

(8) Tolansky, S., and Wilcock, W. L. *Nature (London)*, **157**, p. 583 (1946).

(9) Frank, F. C. *Disc. Faraday Soc.*, **5**, p. 74 (1949).

(10) Elbaum, C., and Chalmers, B. *Canadian J. Phys.*, **33**, p. 196 (1955).

(11) Chalmers, B., and Martius, U. M. *Phil. Mag.*, **43**, p. 686 (1952).

Torsion balance measurements with molecular beams

By D. W. Bassett, B.Sc., Ph.D., and A. J. B. Robertson, M.A., Ph.D., Department of Chemistry, King's College, London, W.C.2

[*Paper first received* 1 *June, and in final form* 27 *August*, 1959]

A torsion balance is described for measuring the momentum carried by the molecules in a molecular beam with an intensity of about 10^{12} mol./s or more. The beam struck a vane suspended on a platinum fibre 3 μ in diameter. The balance could be used at elevated temperatures. At room temperature, measurements of the balance deflexion were made to 1 part in 500, under favourable conditions. An investigation was made of the intensity of a molecular beam of carbon dioxide formed by a fairly simple molecular-beam generator, which is described. Deviations of gas flow from molecular flow and attenuation of the beam by scattering were important factors.

For a direct experimental investigation of the efficiency of the exchange of translational energy in collisions between cold gas molecules and a hot surface, a simple but sensitive torsion balance was developed which measured the force exerted on a surface by the collision of a molecular beam. As a detector of molecular beams, the torsion balance is relatively insensitive and, because of the difficulties of its construction and operation, has seldom been used for this purpose.[1] Such balances have usually consisted of a light metal vane suspended on a fine fibre and may be used satisfactorily for the measurements of forces greater than 10^{-6} dyn. In the work described here it was necessary to heat the balance *in vacuo*, and measure forces of 10^{-6}–10^{-4} dyn to better than 1 part in 500, if possible.

PRINCIPLES

The force exerted on a surface by the collision of a molecular beam of a non-condensing gas is calculated by assuming that the molecules of gas collide with the surface, are adsorbed, and subsequently evaporate according to the cosine law. It is assumed that the distribution of velocities in the molecular beam is Maxwellian so that the number of molecules with velocities in the range c striking the surface in unit time is proportional to $c^3 \exp(-mc^2/2kT_1)dc$, where T_1 is the temperature of the beam molecules, m their mass and k is Boltzmann's constant. When the beam is incident on the surface at an angle ϕ to the normal, the total force acting normally on the surface is:

$$F = \tfrac{3}{4}n(2\pi mkT_1)^{1/2}\cos\phi + \tfrac{1}{2}n(2\pi mkT_3)^{1/2}.$$

The first term is the force resulting from the adsorption of the molecular beam (of n mol./s) on the surface, and the second term is the force resulting from the subsequent evaporation of the molecules with a Maxwellian velocity distribution corresponding to a temperature T_3.

Measurements of this force made with the surface temperature T_2 both equal to and different from the beam temperature T_1 may be used to deduce the temperature T_3 of the evaporating molecules. Since the force is determined only by the translational energy of the molecules, the value of T_3 obtained is characteristic of the translational energy of the evaporating molecules. Values of the translational-energy accommodation coefficient a_t, given by:

$$a_t = (T_3 - T_1)/(T_2 - T_1),$$

may thus be obtained.[2] Calculation shows that the difference between the forces to be measured for the two extreme cases; $T_3 = T_1$ and $T_3 = T_2$, is very small unless large differences of temperature between the beam and the surface are used.

If a molecular beam strikes the surface of a vane suspended on a torsion fibre at a distance d from the fibre, the angle of twist θ of the vane is given by $\tau\theta = dF$. The torsional constant τ of the fibre may be determined from measurements of the periodic time of torsional oscillations of the vane (T) and the calculated moment of inertia of the suspended system (I), because:

$$T = 2\pi(I/\tau)^{1/2}$$

It is thus possible to obtain the beam intensity n in terms of the balance deflexion and other measurable quantities. In such experiments T_2 is made equal to T_1. A knowledge of a_t is not needed. The torsion balance may thus be used for absolute determinations of beam intensities, provided the Maxwellian velocity distribution holds. The torsion balance can always be used to investigate the momentum of particles in a beam.

The force F acting normally on a surface due to the collision at normal incidence of a molecular beam of 10^{12} mol./s of carbon dioxide at 300° K, is $5{\cdot}43 \times 10^{-6}$ dyn. This force is of the same order as the forces measured by Copley and Deitz,[3] who used a torsion balance with a fibre 6 cm long and about 3 μ in diameter. They showed that the balance must be screened from electrostatic charge and isolated from mechanical vibration for satisfactory performance.

APPARATUS

The isolation of the torsion balance from mechanical vibration was of great importance. The section of the apparatus containing the balance and the molecular beam generator was therefore constructed on its own rigid steel frame cemented to a firm floor. The pumping and gas-handling systems were constructed on entirely separate frames. Connexions between the various parts were kept to a minimum and were made with flexible stainless steel bellows clamped at each end so that they did not contract when evacuated. The mechanical vacuum pumps were serious vibration sources, but their effects were removed by placing the pumps in an adjoining room and making connexions to them through the wall.

The molecular beam was produced by effusion of gas through the circular source hole A of the beam generator (Fig. 1). The beam was defined by the circular holes A and C. The hole B served to shorten the path length of the beam in the region A to B of highest pressure just outside the source where scattering would be greatest. The large circular hole D served to reduce background effusion into the tube E containing the torsion balance. Gas passing through A but not through B was pumped away by pump 1, since the right-hand end of the tube T was completely closed except for the hole B. But the diaphragm containing the hole C was fixed to the end of T only by small bolts (not shown in Fig. 1) so that gas flowed through the spaces between the bolts and was

pumped away by pump 2. This arrangement was rigid enough to give a molecular beam of reproducible intensity, and was not difficult to aline. When carbon dioxide was used as the experimental gas, the regions between the holes were pumped by traps immersed in liquid air. The pumping speeds were about 10 l./s. The holes were made by boring

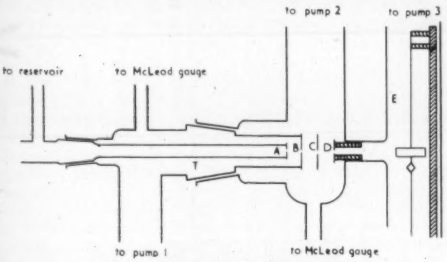

Fig. 1. Molecular beam generator

circular holes in thin copper foil and their diameters were *A*, 0·107 mm; *B*, 0·212 mm; *C*, 0·333 mm; *D*, 1·3 mm. The distance from *A* to *C* was 1·8 cm. Alinement of the holes was carried out optically using a low-power microscope. The torsion balance was housed in the tube *E*, Fig. 1, which, for electrostatic screening, was coated internally with platinum by vacuum evaporation. Windows in *E* for observation of the alinement of the molecular beam and the torsion balance were left clear. The platinum layer was connected to earth.

In some initial experiments, a gilded silica fibre was used for the torsion balance, but the sensitivity was unexpectedly low and very variable. This was the result of the build-up of electrostatic charge on the balance vane following breakdown of the electrical conduction of the gold layer on the fibre, presumably as a result of attack by mercury vapour. Similar changes in sensitivity were noted by Copley and Deitz[3] who used a metallized silica fibre. This difficulty was overcome by the use of a metal fibre for the balance shown in Fig. 2.

This balance consisted of a platinum vane 1·7 cm long, 0·45 cm wide, 0·0006 cm thick, attached to a small mirror with a fine rigid wire, and the whole suspended at the centre of a platinum fibre about 3 μ in diameter and 13 cm long. The frame of the balance was constructed in steel, so that the whole instrument could be heated *in vacuo*. Adjustment of the position of the vane could be made in two ways: by using a magnet outside the apparatus to rotate the fibre frame about the bearing *GG'*; and by screwing the whole balance up or down through the threaded bearing *H* by turning the threaded rod *J*. The bearing *H* was prevented from rotating in the glass envelope by a small lug fitting into its supporting tube *L*. Thus the vane could be adjusted to intercept completely the molecular beam when the torsion balance was in the apparatus. This was of great importance because it was found not practical to remove the balance from the apparatus without breaking the very fine platinum fibre. All bearing surfaces were lubricated with dry colloidal graphite to give good electrical contacts. The complete balance could be connected to earth through the terminal *T*.

The fibre was attached to the balance both above and below the vane. The joints, like those of the vane to the fibre and to the wire supporting the mirror, were made with electro-deposited copper.[4] The fibre, a platinum wire 3 μ in diameter, was obtained by desilvering Wollaston wire. Before use, the platinum fibre was annealed by repeatedly passing a small flame beneath its length so that it was heated to redness. The fixing of the fibre and the vane and mirror assembly to the balance was carried out with the balance in a horizontal position, using a jig attached to the fibre frame to support the weight of the vane and mirror assembly. It was necessary to move the balance with the jig from the construction bench to a position beneath its final containing tube (*E*, Fig. 1) before rotating the balance into a vertical position, because of the fragile nature of the platinum fibre. When vertical, the jig could be removed but, to avoid breaking

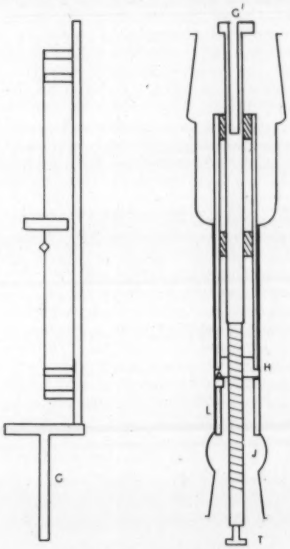

Fig. 2. Torsion balance

G fits into *G'* and can be rotated in it. Threaded part of the rod *J* fits into threaded part of bearing *H*.

the fibre, the balance had to be raised into position in the apparatus mechanically with a screw device. Very slight jerks at this stage usually broke the fibre. Before evacuation of the apparatus, the position of the balance was adjusted so that the molecular beam was incident normally on the vane and was completely intercepted by it.

During experiments the position of the balance vane was observed by means of a lamp and a scale at 1 m. At pressures below 10^{-5} mm of mercury, the vane oscillated continuously. The amplitude of the oscillations depended on the extent of the mechanical disturbance of the balance, but was often less than 10 mm on the scale in quiet external conditions. The mean position of the vane was determined from the scale positions of the extremes of the oscillations. Observation showed that, if the fibre was not taut, the mean position also oscillated slowly. This slow oscillation probably resulted from interaction of the torsional oscillation with the simple-pendulum motion of the vane. Measurement of the periodic time for torsional oscillations showed that the balance

sensitivity remained constant to within 1% during the life of a given fibre. The zero position of the vane also remained nearly constant. The balance sensitivity was reduced by placing a magnet near the vane. Correct choice of the magnet and its position allowed any desired lowering of the sensitivity to be obtained. The moment of inertia of the suspended system was about $2{\cdot}7 \times 10^{-3}$ g cm^2 and the periodic time of free torsional oscillations was between 20 and 25 s, depending on the fibre being used.

To determine the deflexion of the torsion balance by a molecular beam, the balance zero was first obtained from the mean positions of a number of oscillations. The beam was turned on by letting gas at a measured pressure into the beam source (behind A in Fig. 1). This was done carefully as sudden changes in the force acting on the torsion balance caused excessively large increase in the amplitude of its oscillations. The mean deflected position was determined and the sensitivity deduced by measuring the period of torsional oscillations. After closing the gas reservoir and pumping out the beam source to remove the molecular beam, the balance zero was re-determined. As random changes in the zero of about 1 or 2 mm on the scale often occurred, the balance deflexions were calculated from the mean of the initial and final zeros. Under favourable operating conditions, with a balance period of 15 s, deflexions of 150–200 mm on the scale could be measured to better than 1 part in 500.

Some experiments were carried out with the balance at elevated temperatures by winding a heater on the tube E containing the balance. Under these conditions the room temperature performance was seldom obtained and changes in both sensitivity and zero occurred. Out-gassing of the glass, instability of the balance temperature, and the tension in the fibre appeared to be important factors determining the balance behaviour. The measurements of the force exerted on the vane by a molecular beam made with the balance heated were not sufficiently accurate to allow a reliable deduction of the translational-energy accommodation coefficient.

SOME EXPERIMENTAL RESULTS

Quantitative measurements of molecular beams were only made when the beam intensity for a given source pressure had reached a steady value. Because of changes in the vacuum, this condition was generally not achieved until several days after the initial evacuation. The variation of the balance deflexion δ was measured as a function of the pressure p in the beam source (behind A in Fig. 1), to examine the characteristics of the apparatus. For source pressures less than 0·5 mm of mercury the measured deflexions were small and liable to serious error as the result of changes in the balance zero. Some typical results obtained with a molecular beam of carbon dioxide at 293° K are shown in Fig. 3. The deflexions plotted have been corrected by the factor $1/T^2$ to remove the effect of slight variations in the balance sensitivity. Calculation shows that the measured deflexions correspond to beam strengths of the same order as those calculated from the source pressure and the dimensions of the hole system. For example, with a reservoir pressure of 0·725 mm the observed and calculated beam strengths were both $1{\cdot}7 \times 10^{12}$ mol./s. The agreement happens to be exact at this pressure because of a cancellation of opposing factors, as shown below (see Fig. 4).

According to the laws of molecular flow, the intensity of a molecular beam (n) should vary linearly with the source pressure p. The presence of the maximum in the plot of Fig. 3 indicates that the intensity was increasingly reduced by scattering as p increased. If this scattering occurs in a region of length L in which the mean free path is λ, the beam attenuation is described by the factor $\exp(-L/\lambda)$. Most of the scattering presumably occurred in the region between the source A and the hole B (Fig. 1, $L = 0{\cdot}8$ cm). For molecular flow from the source, the beam intensity should

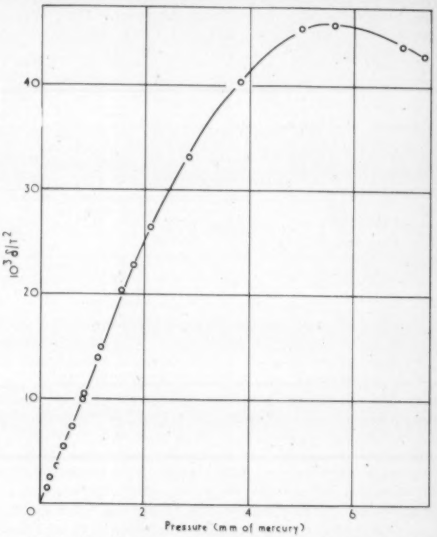

Fig. 3. Variation of observed balance deflexion δ with pressure p of gas in molecular beam source. Deflexion δ is in cm at 1 m

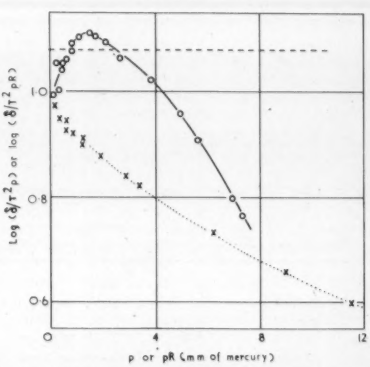

Fig. 4. Interpretation of measurements with molecular beams

——— log (δ/T^2p) against p.
– – – – theoretical value.
· · · · · log (δ/T^2pR) against pR.

be proportional to p and the mean free path in the scattering region inversely proportional to p, so that a plot of log (n/p) or log (δ/T^2p) against p should give a straight line. The solid curve of Fig. 4 shows the results of Fig. 3 plotted in this way. The experimental values can be compared with a theoretical value of log (δ/T^2p) calculated from the dimensions of the apparatus and the sizes of the two holes (A and C, Fig. 1) defining the beam, and for a molecular beam which is not attenuated by scattering. This theoretical value is shown in Fig. 4, and was calculated assuming the flow of gas through the first hole A to be molecular flow through a hole in an infinitely thin diaphragm. The theoretical value neglects scattering of the beam and is therefore directly comparable with the observed value extrapolated to zero source pressure. The agreement shown in Fig. 4 is quite good; the slight discrepancy could arise from mis-alinement of the holes of the beam generator. The increase of log (δ/T^2p) with p for values of p below 1·5 mm of mercury indicates that the beam intensity did not change linearly with source pressure in this region. To examine this effect, the relation between the rate at which molecules flowed from the source and p was studied by measuring the rate of fall of pressure in the reservoir, using carbon dioxide. Although rather inaccurate because of the limitations of the apparatus, the results obtained showed that the relationship was non-linear; the rate of flow increased more rapidly. Fig. 5 shows this effect.

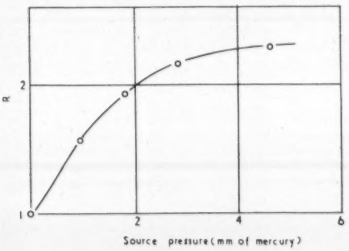

Fig. 5. Flow of carbon dioxide through a small hole in a thin diaphragm. Gas pressure on one side of diaphragm is source pressure, and on other side is very nearly zero

R is the ratio of the measured flow rate at a given pressure and the flow rate calculated at this pressure from the measured flow rate at the lowest pressure studied, 0·02 mm of mercury, by assuming a linear relationship between flow rate and pressure. This ratio should of course be unity at all pressures for molecular flow from the source. At 0·02 mm of mercury, the flow must be molecular.

Because the ratio R measures the extent of the deviation from molecular flow at any source pressure, the unscattered beam intensity should be proportional to pR and the mean free path in the scattering region inversely proportional to pR. The dotted curve of Fig. 4 shows a plot of log (δ/T^2pR) against pR using the values of Figs. 3 and 5. In spite of the uncertainty in the exact values of R, an almost linear plot is obtained. The slope of this line may be used to deduce a value for the mean free path of carbon dioxide in the scattering region when the pressure in this region is known. If it is assumed that scattering only occurred between the source hole A and hole B, the mean free path at a pressure of $1{\cdot}5 \times 10^{-3}$ mm of mercury was 0·5 cm.

DISCUSSION

Both the beam intensities measured with the torsion balance and the pressure variation of the flow rate indicate that the gas flow from the source ceased to be truly molecular at a source pressure less than 0·5 mm of mercury. This is not unexpected because the mean free path of carbon dioxide in the source, as deduced from measurements of the beam attenuation by scattering, would equal the source-hole radius at a carbon-dioxide pressure of 0·15 mm of mercury: this is the usual criterion for the upper limit of molecular flow. However, the ratio of the beam intensity to source pressure increases with increasing source pressure above this limit. Other workers have observed this ratio to decrease at pressures above the limit of molecular flow.[5] It has been assumed that collisions cause the formation of a "cloud" of molecules just in front of the source slit, and the surface of this cloud, rather than the slit, acts as the beam source. Increase of the source pressure is assumed to enlarge the cloud rather than increase its intensity. This explains the fall in the ratio of beam intensity to source pressure observed in experiments with narrow-slit systems in which the source slit does not define the beam. In the experiments described here, the beam detector could "see" an area at the source larger than the hole so that, if cloud formation occurred and caused an apparent increase in the source area, this would not necessarily affect the rate of increase of the beam intensity. The measured beam intensities therefore probably reflect the change in the number of molecules flowing from the source, and indeed the curves of Fig. 4 show that the pressure variation of the beam intensity parallels the variation of the flow rate as determined by measurements of the rate of fall of pressure in the reservoir. A more complete interpretation of the results is not justified because the breakdown of molecular flow is probably accompanied by fairly marked changes in the velocity distribution in the molecular beam. Such a change would invalidate the calculation of beam intensities from deflexions of the torsion balance using the equations developed above. The pressure dependence of flow rates in the transition region between molecular and hydrodynamic flow depends considerably on the aperture profile. It is probable that the pressure dependence observed in Fig. 5 reflects the profile of the source hole, but this was not determined.

The value of the mean free path of carbon dioxide obtained indicates that the collision diameter of the molecules in scattering collisions was larger than the diameter effective in the measurement of viscosity. This is normally found in molecular beam experiments, although in the experiments described here the scattering angle of about 1° is comparatively large.

Published results with which the performance of the torsion balance may be compared are those of Copley and Deitz[3] who noted a variable sensitivity. The use of both metallized silica and platinum fibres in the work described here shows that the most important factor giving a variable sensitivity is probably the build up of electrostatic charge on the balance vane. In the experiments described here with gilded silica fibres, this was probably caused by breakdown of the electrical conduction of the metal layer in the presence of mercury vapour. The use of platinum fibres removed this effect, but further increased the difficulty of constructing the balance. The use of tungsten fibres would probably be preferable, because these are reported to be stronger than silica fibres.[6] With the vane of the torsion balance connected to earth, metallizing and earthing the inside of the containing vessel provided suitable screening from external electrical effects.

The methods described for isolation of the torsion balance from electrical and mechanical disturbances permitted a very simple but sensitive balance to be used for the measurement of forces of 10^{-5} dyn to 1 part in 500. The smallest force which could be measured experimentally was limited by the need to separate its effect from random fluctuations of the vane position caused by mechanical disturbance. With such a sensitive, long-period instrument, operated *in vacuo*, the effects of mechanical disturbance are damped only slowly. It seems possible that considerable improvement in performance could be obtained without spoiling the simplicity of the torsion balance by using automatic feedback control. With balances of the sensitivity used here, the rapid damping of mechanical disturbances would permit the measurement of smaller forces because more sensitive methods of observation than the lamp and scale could be used.

These experiments indicate that the torsion balance is suitable for use in physico-chemical experiments when comparative or absolute measurements of the intensities or momenta of molecular beams of gases are required, as long as the intensities are greater than about 10^{12} mol./s. This instrument may also be used for the study of the exchange of energy in gas-solid collisions and, with the balance described, operation at high temperature is permitted by the method of construction adopted.

ACKNOWLEDGEMENTS

The authors thank Mr. E. Sherwood for the construction of the frame of the torsion balance, the Institute of Petroleum for a grant towards the cost of the apparatus, and the Ministry of Education for a grant to D. W. Bassett.

REFERENCES

(1) SMITH, K. F. *Molecular Beams*, Chapter 1 (London: Methuen and Co. Ltd., 1955).
(2) SASAKI, N., TAKU, K., and MITANI, K. *Mem. Coll. Sci. Kyoto (A)*, **25**, p. 75 (1949).
(3) COPLEY, M. J., and DEITZ, V. *Rev. Sci. Instrum.*, **8**, p. 314 (1937).
(4) BASSETT, D. W., and ROBERTSON, A. J. B. *J. Sci. Instrum.*, **36**, p. 321 (1959).
(5) KNAUER, F., and STERN, O. *Z. Phys.*, **39**, p. 764 (1926).
(6) BOCKRIS, J. O'M., and PARSONS, D. F. *J. Sci. Instrum.*, **30**, p. 340 (1953).

Steady-state temperature distribution in solids undergoing certain change of property

By T. J. MIRSEPASSI, B.Sc., M.Sc., Ph.D., A.S.M.E., Sigma Xi, Heat and Mass Flow Laboratory, Aerojet-General Corporation, Azusa, California, U.S.A.

[*Paper first received* 29 *June, and in final form* 10 *August*, 1959]

In the design of high-temperature equipment, two problems are often encountered: (1) determining the effect of slow changes of the thermal conductivity (which can occur as a result of chemical and/or mechanical factors) on the thermal behaviour of the equipment, and (2) finding the most efficient combination of materials for the design of the equipment when several materials are available. Both of these problems are customarily solved by trial-and-error techniques. In this paper, it is first shown that the temperatures before and after such changes of the thermal conductivity are related by simple linear equations. It is demonstrated that the process of trial-and-error in the solution of the above problems can be entirely eliminated by the use of these simple equations.

When determining steady-state temperature distribution in a solid, it is often necessary to take into account changes of thermal conductivities of materials. Such changes can be caused by one or a combination of the following: (*a*) temperature dependence of thermal conductivities, (*b*) slow changes in chemical composition, and (*c*) diffusion of a material with a different thermal conductivity through the boundaries.

By way of example, the bottom of a blast furnace where molten iron gradually diffuses into the pores of the refractory, and the penetration continues until the moving front reaches the solidification temperature of the iron,[1, 2, 3] is considered. Knowledge of the final location of the penetration front is vital to the design of the required cooling system and to the resulting safety of the operation. Mathematically, the problem consists of determining the shape of the boundary between two materials in a composite solid such that it becomes an isothermal surface of specified temperature for a given set of conditions along the external boundaries. Problems of this nature, being too complex for analytical solution, are usually solved numerically or on computers (for example, resistive-network analogue); even then the operations are lengthy and many tedious trial-and-error operations are required. When one such problem was under study for a possible analytical solution,[1] a very useful fact was found about steady-state heat conduction—and, for that matter, about field distributions in general—which revealed a simple relationship between temperature distributions before and after such change of thermal conductivities. This relationship eliminates entirely the trial-and-error operations in numerical or computer solution; it can also be utilized to solve the problem analytically when the temperature function before change of materials is known.

In thermal-design criteria (for example, high-temperature rocket engines, flame deflectors, furnace walls, etc.), where it is necessary to use an insulating material most efficiently—that is, in the range of temperatures for which it is best suited—this finding also has numerous applications.[1]

After stating and proving this finding as a theorem, the case of temperature-dependent thermal conductivity and the case of regions containing sources and sinks are discussed; then, by means of a numerical example, one application of the theorem to practical problems is shown.

THEOREM

Statement. In Fig. 1, M is a composite solid with no heat sources or sinks inside and with the following

conditions along the boundaries: C_A receiving heat from a medium at uniform temperature T_A, C_B losing heat to a medium at uniform temperature T_B, and perfect insulation along the remaining boundaries. C_1 (at temperature T_1) and C_2 (at temperature T_2) represent two isothermal surfaces entirely situated in one material and not intersecting C_A or C_B. If the material filling the space between C_1 and C_2 is replaced by a material with a different thermal conductivity, the resulting temperature distribution in M is linearly related to the temperature distribution before the replacement.

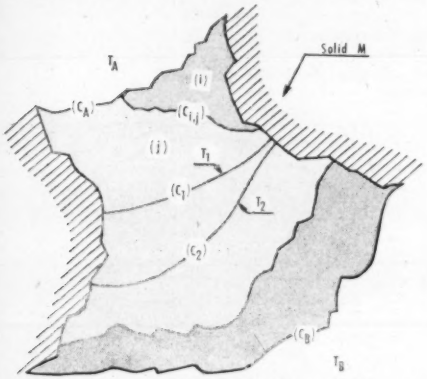

Fig. 1. Composite solid without heat source or sink inside boundaries

Proof. If $t(x, y, z)$ denotes the temperature function in M before the replacement, then, because no sources or sinks exist in M, the temperature and the flux are both continuous through M[4], and the following equations are satisfied:

(*a*) The differential equation of steady-state temperature distribution in M:

$$\nabla^2 t(x, y, z) = 0. \tag{1}$$

(*b*) The boundary conditions:

(i) along C_A,

$$\partial t/\partial n + h(t - T_A) = 0, \tag{2}$$

where $\partial/\partial n$ denotes differentiation in the direction of the outward normal to the surface, and h represents (exterior conductivity)/(conductivity of substance),[4] and is assumed a function of location x, y, z along C_A,

(ii) along C_B,

$$\partial t/\partial n + h'(t - T_B) = 0, \tag{3}$$

where h', similar to h, is a function of position along C_B,

(iii) along the rest of the boundary,

$$\partial t/\partial n = 0 \tag{4}$$

(*c*) The conditions along separation surfaces:[4] if perfect contact between adjacent materials is assumed, these conditions, written for the separation surface $C_{i,j}$ for example, are:

$$t(x, y, z)|_{(i)\to} = t(x, y, z)|_{(j)\to} \tag{5}$$

and

$$K_i(\partial t/\partial n)|_{(i)\to} = K_j(\partial t/\partial n)|_{(j)\to} \tag{6}$$

where K_i and K_j are the thermal conductivities, of (*i*) and (*j*) respectively, and the subscripts $(i)\to$ and $(j)\to$, referring to materials (*i*) and (*j*), denote the directions of approach to the separation surface.

If it is supposed that the material in the region C_1, C_2, having an original thermal conductivity of K_j, is replaced by a new material with thermal conductivity K_j', and if $\theta_1(x, y, z)$, θ_2 (x, y, z) and $\theta_3(x, y, z)$ denote the new temperature distributions in the regions C_A, C_1; C_1, C_2; and C_2, C_B respectively. Then, assuming the theorem proved, θ_1, θ_2 and θ_3 are linear functions of $t(x, y, z)$. That is:

$$\theta_1 = \alpha_1 t + \beta_1, \tag{7}$$

$$\theta_2 = \alpha_2 t + \beta_2, \tag{8}$$

$$\theta_3 = \alpha_3 t + \beta_3, \tag{9}$$

where α_1, β_1, α_2, β_2, α_3, and β_3 are constants.

Since, by virtue of the uniqueness theorem,[5] only one solution exists for the steady-state temperature distribution in a composite solid with specified boundary conditions, therefore θ_1, θ_2 and θ_3 constitute the unique solution if they satisfy:

(*a*) Laplace's equation, that is, equation (1);

(*b*) Boundary conditions, that is, equations (2), (3) and (4); and

(*c*) Conditions along separation surfaces, that is, equations similar to equations (5) and (6).

By virtue of linear relationships expressed by equations (7)–(9), equations (1) and (4) are obviously satisfied. This is also true for equations of the type of equations (5) and (6) when written for separation surfaces inside the regions C_A, C_1 and C_2, C_B.

The boundary condition along C_A is satisfied if:

$$\partial\theta_1/\partial n + h(\theta_1 - T_A) = 0,$$

or, after replacing θ_1 by equation (7):

$$\alpha_1\{\partial t/\partial n + h(t - T_A)\} + h\{\beta_1 - (1 - \alpha_1)T_A\} = 0. \tag{10}$$

Because t satisfies equation (2), the first term of the above equation is zero. Therefore θ_1 satisfies the condition along this boundary if:

$$\beta_1 - (1 - \alpha_1)T_A = 0. \tag{11}$$

Similarly, θ_3 satisfies the boundary condition along C_B if:

$$\beta_3 - (1 - \alpha_3)T_B = 0. \tag{12}$$

The condition of continuity of temperature function written for the separation surface C_1, is satisfied if:

$$\theta_1(x, y, z)|_{(C_1)} = \theta_2(x, y, z)|_{(C_1)},$$

or:

$$(\alpha_1 t + \beta_1)|_{(C_1)} = (\alpha_2 t + \beta_2)|_{(C_1)},$$

and finally:

$$\alpha_1 T_1 + \beta_1 = \alpha_2 T_1 + \beta_2. \tag{13}$$

The condition of continuity of flux across the separation surface C_1 requires that:

$$K_j(\partial\theta_1/\partial n) = K_j'(\partial\theta_2/\partial n),$$

or, after replacing θ_1 and θ_2 by equations (7) and (8):

$$K_j\alpha_1 = K_j'\alpha_2. \tag{14}$$

Similarly, it is shown that θ_2 and θ_3 satisfy the conditions of continuity of temperature and flux along C_2 if:

$$\alpha_2 T_2 + \beta_2 = \alpha_3 T_2 + \beta_3, \tag{15}$$

and:

$$K_j'\alpha_2 = K_j\alpha_3. \tag{16}$$

By solving the system of simultaneous algebraic equations (11)–(16), all the coefficients in equations (7)–(9), are found. Because the functions θ_1, θ_2, and θ_3 thus defined satisfy all the required conditions, the theorem is proved and equations (7)–(9) constitute the new temperature distribution in M.

It can be easily shown[1] that the system of equations (11)–(16) has always a unique solution.

NOTES

(1) The equations (7)–(9) show that the isothermal surfaces throughout M remain isothermal after the replacement. Therefore, the temperatures inside the regions C_A, C_1; C_1, C_2; and C_2, C_B can be expressed in dimensionless form by temperature-difference ratios, leading to the following equations:

$$\frac{\theta_1(x, y, z) - \Theta_1}{T_A - \Theta_1} = \frac{t(x, y, z) - T_1}{T_A - T_1} \tag{17}$$

$$\frac{\theta_2(x, y, z) - \Theta_2}{\Theta_1 - \Theta_2} = \frac{t(x, y, z) - T_2}{T_1 - T_2} \tag{18}$$

$$\frac{\theta_3(x, y, z) - T_B}{\Theta_2 - T_B} = \frac{t(x, y, z) - T_B}{T_2 - T_B} \tag{19}$$

where Θ_1 and Θ_2 denote the temperatures along C_1 and C_2 after the replacement. Since θ_1, θ_2 and θ_3 in the above expressions satisfy equations (11), (12), (13) and (15), the remaining equations to be satisfied are (14) and (16) which become, respectively,

$$\frac{K_j(T_A - \Theta_1)}{T_A - T_1} = \frac{K_j'(\Theta_1 - \Theta_2)}{T_1 - T_2} \tag{20}$$

$$\frac{K_j'(\Theta_1 - \Theta_2)}{T_1 - T_2} = \frac{K_j(\Theta_2 - T_B)}{T_2 - T_B} \tag{21}$$

Thus by solving equations (20) and (21), any two unknown temperatures (for example, Θ_1 and Θ_2) can be found in terms of the known values.

(2) It can easily be shown that, if the materials in several between-isothermal regions—regions like C_1, C_2—are replaced, the theorem still holds,[1] namely, the temperature distributions before and after the change of materials are linearly related. Furthermore, if, in the above theorem, K_j' is a function of temperature—

$$K_j' = K_0\phi(\theta) \tag{22}$$

where K_0 is a constant and $\phi(\theta)$ is a known function of θ—it can be shown[1] that equations (17) and (19) remain unchanged. At the same time, equations (18), (20) and (21) become,[1] respectively:

$$\frac{\int_{\Theta_2}^{\theta_2(x,y,z)} \phi(\theta')d\theta'}{\int_{\Theta_2}^{\Theta_1} \phi(\theta')d\theta'} = \frac{t(x, y, z) - T_2}{T_1 - T_2} \tag{23}$$

$$\frac{K_j(T_A - \Theta_1)}{T_A - T_1} = \frac{K_0 \int_{\Theta_2}^{\Theta_1} \phi(\theta')d\theta'}{T_1 - T_2} \tag{24}$$

$$\frac{K_0 \int_{\Theta_2}^{\Theta_1} \phi(\theta')d\theta'}{T_1 - T_2} = \frac{K_j(\Theta_2 - T_B)}{T_2 - T_B} \tag{25}$$

where θ' denotes the variable of integration. Because $\phi(\theta)$, and therefore $\int\phi(\theta')d\theta'$, are known, by solving the system of simultaneous equations (24) and (25) the new temperatures along C_1 and C_2, namely Θ_1 and Θ_2, can be determined.

(3) The theorem can also be applied to the general case in which C_A and C_B are surface source and sink. For example, in the special case where C_A is a point source (Fig. 2), and C_B is as specified in the theorem, equations (17) and (20) are replaced respectively by:

$$\frac{\theta_1(x, y, z) - \Theta_1}{\Theta_A - \Theta_1} = \frac{t(x, y, z) - T_1}{T_A - T_1} \tag{26}$$

$$\frac{K_j(\Theta_A - \Theta_1)}{T_A - T_1} = \frac{K_j'(\Theta_1 - \Theta_2)}{T_1 - T_2} \tag{27}$$

where Θ_A is the new temperature at the source, and equations (18), (19) and (21) remain unchanged.

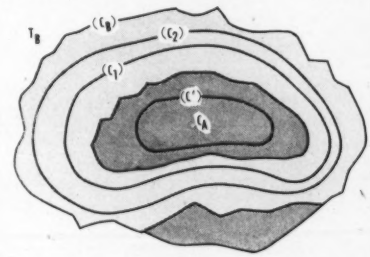

Fig. 2. Composite solid: C_A is a point heat source.

The condition at the source C_A, satisfied by $t(x, y, z)$, is[4]:

$$K_j(4\pi r^2)\partial t/\partial n|_r = Q, \tag{28}$$

where K_j is the thermal conductivity of material containing the source, r is the radius of a small sphere around the source, and Q is the rate of heat generation at the source.

Because θ_1 must also satisfy the above condition, therefore:

$$K_j(4\pi r^2)\partial\theta_1/\partial n|_r = Q \tag{29}$$

If θ_1 is replaced by its value from equation (26), then from a comparison of the result with equation (28), it follows that:

$$\Theta_A - \Theta_1 = T_A - T_1 \tag{30}$$

Equations (21), (27) and (30) form a system of simultaneous equations by means of which three unknowns (for example, Θ_A, Θ_1 and Θ_2) can be determined.

If, instead of replacing the material in the region C_1, C_2, the material inside the isothermal surface C' which contains the source C_A, is replaced, then the two temperature functions θ_1 for the region inside C', and θ_2 for the region outside C' are related to $t(x, y, z)$ by the following equations:

$$\frac{\theta_1(x, y, z) - \Theta_1}{\Theta_A - \Theta_1} = \frac{t(x, y, z) - T_1}{T_A - T_1},$$

$$\frac{\theta_2(x, y, z) - T_B}{\Theta_1 - T_B} = \frac{t(x, y, z) - T_B}{T_1 - T_B}.$$

The condition at the source and the condition of continuity of flux across C', lead, respectively, to the following equations:

$$K_j'(\Theta_A - \Theta_1) = K_j(T_A - T_1),$$

$$\frac{K_j'(\Theta_A - \Theta_1)}{T_A - T_1} = \frac{K_j(\Theta_1 - T_B)}{T_1 - T_B},$$

where K_i' denotes the thermal conductivity of the new material. The above system of equations serves to obtain Θ_A and Θ_1, for example, in terms of the known values.

EXAMPLE

Determining depth of iron penetration in blast furnace bottom. It was mentioned on p. 538 that, in blast furnaces, molten iron diffuses into the refractory bottom, and that the problem of determining the maximum penetration in a given design is of great technical importance.[2, 3, 6] This problem can be readily solved by means of the above theorem.

Because penetration takes place only as long as the diffusion front is in a molten state, the final contour of penetration, C_S in Fig. 3, is uniformly at the solidification temperature of

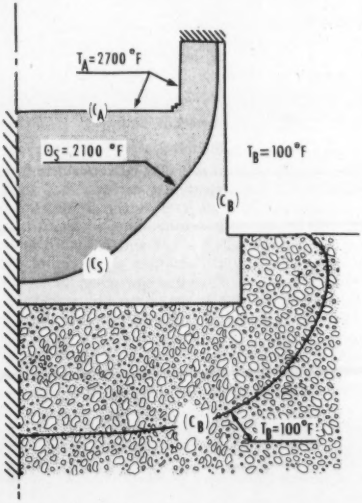

Fig. 3. Bottom of blast furnace after iron penetration

iron. Because the coefficient h between the molten iron and the refractory bottom of the furnace is very large, in equation (2) h tends to infinity, and the ambient temperature T_A prevails along C_A as surface temperature. Consequently, the region C_A, C_S becomes a between-isothermal region similar to C_1, C_2 in the theorem, and the iron-impregnated refractory can be considered as a replacement of the original refractory material in C_A, C_S. Thus, the temperature distributions in C_A, C_S and C_S, C_B are:

$$\frac{\theta_1(x, y, z) - \Theta_S}{T_A - \Theta_S} = \frac{t(x, y, z) - T_S}{T_A - T_S},$$

$$\frac{\theta_2(x, y, z) - T_B}{\Theta_S - T_B} = \frac{t(x, y, z) - T_B}{T_S - T_B}$$

where:

t = temperature distribution in C_A, C_B before penetration,
θ_1 = temperature distribution in C_A, C_S after penetration,
θ_2 = temperature distribution in C_S, C_B after penetration,
T_S = temperature of C_S before penetration,
Θ_S = temperature of C_S after penetration,
T_A = temperature along C_A,
T_B = outside ambient temperature.

The condition of continuity of flux across C_S becomes:

$$\frac{K_i(T_A - \Theta_S)}{T_A - T_S} = \frac{K_r(\Theta_S - T_B)}{T_S - T_B} \tag{31}$$

in which K_r and K_i denote the thermal conductivities of original refractory and iron-impregnated refractory respectively. Equation (31), when solved for T_S, determines the before-penetration temperature of the isothermal surface C_S. Then, using the known temperature distribution before penetration (Fig. 4, which is usually obtained by resistive-network analogue technique[7, 8, 9]) the location of C_S is determined. Numerically, if:

T_A = 1480° C
T_B = 37·8° C
Θ_S = 1150° C
K_r = 0·0023 Wcm^{-1}deg C^{-1} (0·005 cal.cm^{-1}s^{-1}deg C)
K_i = 0·159 Wcm^{-1}deg C^{-1} (0·038 cal.cm^{-1}s^{-1}deg C)

the value for T_S becomes 507·48° C, and the location of C_S is the isotherm representing 507·48° C (945·47° F in Fig. 4).

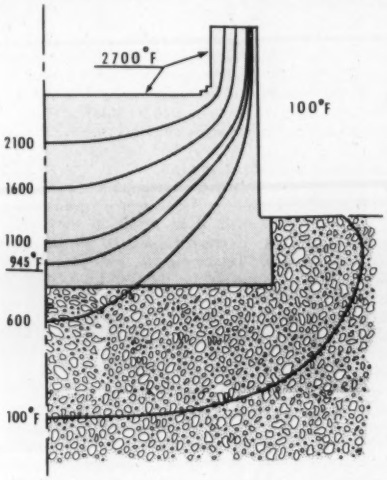

Fig. 4. Temperature distribution in bottom of blast furnace before iron penetration

The increase in heat loss through the bottom of the furnace because of this penetration of iron can be readily obtained. In fact, the thermal resistance of C_S, C_B has remained unchanged, and the temperature difference $(T_S - T_B)$ is increased to $(\Theta_S - T_B)$. Therefore, the new rate of heat loss, Q_S, is:

$$Q_S = \frac{\Theta_S - T_B}{T_S - T_B} \cdot Q_0,$$

where Q_0 denotes the rate of heat loss before penetration takes place.

REFERENCES

(1) MIRSEPASSI, T. J., Ph.D. Thesis (Columbia University, 1955) (Microfilm).
(2) ELLIOT, G. D., and staff. *The Iron and Steel Institute*, Special Report No. 30, Section X, p. 232 (1944).
(3) PASCHKIS, V., and MIRSEPASSI, T. *Iron and Steel Engineer*, February, 1954.
(4) CARSLAW, H. S., and JAEGER, J. C. *Conduction of Heat in Solids* (Oxford: The Clarendon Press, 1959).
(5) BERGMAN, S., and SCHIFFER, M. *Kernel functions and elliptic differential equations*, p. 15 (New York: Academic Press, 1953).
(6) PASCHKIS, V., and MIRSEPASSI, T. *Iron and Steel Engineer*, June 1956.
(7) LIEBMANN, G. *Brit. J. Appl. Phys.*, **1**, p. 92 (1950).
(8) MIRSEPASSI, T. J., and KALISKI, E. J. *Columbia Engineering Quarterly*, March, 1953.
(9) LIEBMANN, G. *Brit. J. Appl. Phys.*, **4**, p. 193 (1953).

Correspondence

Use of an electronic analogue computer with resistance network analogues

It is interesting to see that Mr. Korthals Altes, in his paper published on p. 176 of the April issue of this *Journal*, makes use of memory elements in open-loop configuration in applying a single analogue function generator to control the currents fed to a resistance network.

Although this arrangement requires only two-pole switching as opposed to three-pole in the feedback method,* it does demand, as the author mentions, that each memory element should have a constant and accurately known output/input characteristic over the full operating range. It would therefore be valuable if we could be told what linearity has in fact been achieved by the elements described, what is the spread in gain from one to another, and how small is the offset between input and output voltages.

The rate of loss of memory is given as 0·2 V/min in 60 V, which is 1/180% per second. This seems to be rather better than is actually required, even assuming that eighty-one elements are in use, if scanning can be performed at 20 elements per second. To achieve this low drift rate, the grid current has been reduced to 10^{-10}A, and this implies that the stepping switch insulation and the capacitor leakage resistance are each better than about $10^{12}\,\Omega$. Presumably the capacitors are of the plastic film type, but it would be interesting to know if any special steps were found necessary to obtain this high value in the switch.

Both the feedback and the open-loop method† can be arranged either to control the feed-in currents directly or, alternatively, to set up voltages which are applied to fixed resistors connected to the network nodes. Current control requires either many separate h.t. supplies, or else some device such as a capacity-coupled system with periodic "zeroing", to take out the common h.t. voltage. By adopting voltage control, the author has avoided this complication, but at the expense of having to generate a voltage $\phi - f(\phi)$ instead of merely $f(\phi)$ in solving $d^2\phi/dx^2 = f(\phi)$. The writer is now inclined to favour this choice of voltage control, but within a feed-back system the accuracy of which is virtually independent of all memory element characteristics except the drift rate.

This arrangement has, in fact, been used in a twenty-element computer built recently for the analysis of problems arising in the course of combustion research carried out under Prof. D. B. Spalding of Imperial College. Up to twenty simultaneous equations can be solved of the type

$$\mu\, Tn = a_{n1}\phi_1 + a_{n2}\phi_2 + \ldots a_{nm}\phi_m$$

where $\phi = f(T)$, μ is a constant, and

$$n, m = 1, 2, \ldots 20$$

Each memory element is a plug-in transistorized unit and controls 0 to 10 V, representing ϕ, across a 25 Ω load. The high current available (0·4 A) permits each load to comprise twenty 500 Ω coefficient-setting potentiometers in parallel (400 in all) each of which is not unduly loaded by a 50 kΩ summing resistor. Four transistors give each unit a current gain exceeding about 10^6, so that changes in the input current are almost entirely due to varying collector leakage in the first transistor. By using a low-leakage type transistor and an adjustable bias current, the actual input current is held to plus or minus a few microamperes at ambient temperatures up to about 40° C, giving a drift rate below ±0·2% per second in a cycle duration of 3 seconds with a memory capacity of 250μF. A chopper-stabilized amplifier is used in a feedback loop to set the ϕ voltages precisely equal to the sequential outputs of a single function generator.

G. Kent Ltd.,
Luton,
Beds.

I. C. HUTCHEON
[13 *May*, 1959]

* HUTCHEON, I. C. *Brit J. Appl. Phys.*, **8**, p. 370 (1957).
† Brit. Pat. Application No. 348/57.

We shall try below to give satisfactory answers to the questions which Mr. Hutcheon poses in his letter.

(1) The data given on the rate of loss of memory of the elements only concern these elements without any wiring or switching mechanism.

(2) The maximum spread of the average gain caused by non-linearity is about 0·5% (Fig. 1).

(3) The maximum spread in gain caused by unequality of the elements is about 0·25% (Fig. 2).

(4) The elements can be balanced; with input voltage zero the output voltage is less than 10 mV.

(5) If we assume a statistical distribution of the errors, Liebmann states one may assume they will not accrue and accumulate in the iterating process, but on the contrary reduce and diminish each others influence.

(6) The size of these errors are in no way alarming if we take into account the errors caused by inaccuracy in measuring, distinction of finite difference and differential equation, leakage and faults in the analogue computer.

(7) The current is 10^{-10}A. To achieve a leakage current

of the same rate the total leakage resistance of the stepping switch, wiring, etc., has to be $10^{12}\ \Omega$ when $V_{output} = 60$ V and $C = 47\ \mu$F. It was difficult to fulfil this in a simple way in the two-dimensional machine with its eighty-one elements. The leakage resistance obtained is about $4 \times 10^9\ \Omega$. Since the original paper was published the capacitors have been substituted by large ones ($C = 1\ \mu$F), to reduce leakage errors. The loss of memory caused now by total leakage in machine and element is about 0·9 V/min.

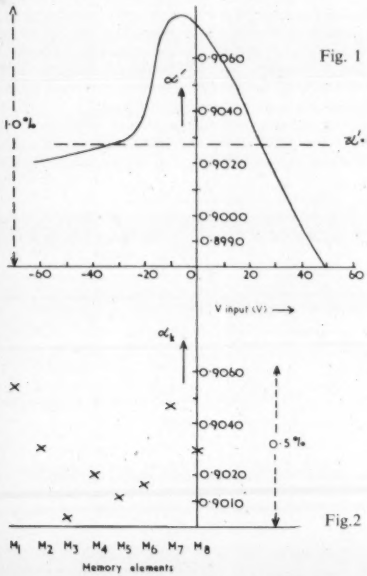

Fig. 1

Fig.2

Fig. 1. α' is the average gain of the memory elements at a constant input voltage

Fig. 2. α_k is the average gain of memory element M_k at an input voltage between $+60$ and -60 V

(8) Memory elements of special quality are being studied to be used with resistance networks for the solution of the equation:

$$\Delta^2\phi + \left(\frac{\delta\phi}{dt}\right) = f(x, y, \phi, t)$$

Delft University of Technology, The Netherlands.

J. PH. KORTHALS ALTES
L. DEKKER
H. P. J. GILISSEN

[16 *June*, 1959]

Single-etch extraction replica method adapted for carbon films

The single-etch extraction replica method[1] for isolating included material from steels possesses a number of advantages over double-etch methods[2, 3] in which the second etch is performed through the replica film. Thus, the method is not restricted to small particles, gives unweakened replica films free from etching debris, enables a wider range of materials to be satisfactorily isolated and permits a single extraction replica film to be obtained from the whole of the specimen. The resolution of the particles thus isolated has been shown by the recent work of Schrader[4] to be extremely high.

The single-etch method was originally described for use with plastic films but some investigators prefer to use carbon films because of their greater strength and better behaviour when examined in the electron microscope at high beam intensity. Therefore, in order to make use of these further advantages, the single-etch method has now been adapted for use with carbon films in the following manner.

The metal specimen is given the optimum extraction etch, carefully rinsed with alcohol, carbon evaporated directly on to it, coated with a thick collodion film, dry-stripped and the collodion dissolved. By using thick (0·003 to 0·004 in.) collodion backing films, the whole carbon film is often completely stripped, and in those instances where the carbon film is only partially stripped, sufficiently large areas for electron microscope and electron diffraction studies usually result. The extraction replicas thus obtained are of particularly high quality.

In some investigations it is necessary to examine the included materials present in particular areas of a specimen. This can be readily performed with the single-etch extraction replica method using plastic films since the replica film corresponding to the whole of the specimen is removed in one piece, and hence marked areas can be located by a preliminary optical microscope survey and suitably mounted on electron microscope grids. When carbon extraction replica films are made either as described above or by the method of Smith and Nutting,[3] particular areas may not be stripped or may be difficult to locate. To overcome this limitation a further variation of the single-etch method using carbon films has been devised which ensures that at each application a complete carbon extraction replica film corresponding to the whole of the specimen is obtained. The details of this procedure are as follows.

After etching and rinsing the metal specimen, a thick collodion film is applied, dry-stripped in one piece, carbon evaporated on to the side originally in contact with the metal surface, and the collodion dissolved. Although this is a two-stage process and relies on transference of the particles from the metal to the collodion and then to the carbon, excellent results are obtained.

ACKNOWLEDGMENTS

Thanks are due to Mr. R. A. Hacking, Director of Research, for permission to publish this letter.

Physics Department,
Central Research Laboratories,
Richard Thomas and Baldwins Ltd.,
Whitechurch,
Aylesbury, Bucks.

G. R. BOOKER
J. NORBURY

[6 *March*, 1959]

REFERENCES

(1) BOOKER, G. R., and NORBURY, J. *Brit. J. Appl. Phys.*, **8**, p. 109 (1957).
(2) FISHER, R. M., A.S.T.M. Special Tech. Publication No. 155, p. 49 (1953).
(3) SMITH, E., and NUTTING, J. *Brit. J. Appl. Phys.*, **7**, p. 214 (1956).
(4) SCHRADER, A. *Archiv. für das Eisenhüttenwesen*, **29**, p. 793 (1958).

Notes and comments

BINDING ORDERS

Orders and enquiries about the binding of back-numbers of this *Journal* should be sent direct to Messrs. E. A. Weeks and Son, 168 Gower Street, London, N.W.1. (EUSton 4674), and *not* to the Institute. The price for binding has been reduced and will in future be 22*s.* post free (standard case). Separate cases are also available at a reduced rate of 13*s.* 6*d.* The indexes and title-pages will be issued with the March, 1960 issue of this *Journal*.

The Physical Society's annual exhibition of scientific instruments and apparatus

The Physical Society announces that its forty-fourth annual exhibition will be held at the Royal Horticultural Society's Old and New Halls, Westminster, London, S.W.1, from 18–22 January, 1960 (inclusive).

Entrance to the exhibition is by ticket only and these may be obtained, free of charge, from the offices of the Society, 1 Lowther Gardens, Prince Consort Road, London, S.W.1. Members of The Institute of Physics may obtain tickets from the Institute. The handbook of scientific instruments and apparatus published in connexion with the exhibition is available from the Society, price 6*s.*, by post 8*s.*

Proceedings of Comité Consultatif de Thermométrie

It has been announced that the proceedings of the 1958 meeting of the Comité Consultatif de Thermométrie of the Comité International des Poids et Mesures have now been published by Gauthier–Villars of Paris. The 230-page book comprises the minutes and report of the meeting, together with reprints of the documents which were considered. These include accounts of the international intercomparisons which have been made to verify the agreement between the scales realized by the different national laboratories and show an agreement of about 0·001 deg C at 100° C and of two or three degrees at 2200° C. An account is also given of work with platinum resistance thermometers in the range 11° to 90° K, whereby it is hoped to extend the international scale into this region. Resistance thermometer measurements of the freezing-point of zinc made at the National Research Council in Canada, the Mendeleev Institute of Metrology in Leningrad and the National Physical Laboratory agree on a figure of 419·505° C (Int. 1948) to within ±0·001 deg C.

New periodicals

The Pergamon Press Ltd. have announced the publication of a further three periodicals entitled *Reactor technology*, *Planetary and space science* and *The annals of occupational hygiene*.

The first of these is issued quarterly and forms Part (B) of the *Journal of Nuclear Energy*. Published under the general Editorship of Dr. J. V. Dunworth, of the United Kingdom Atomic Energy Authority, the Journal is stated to have been "founded to provide an international medium for publication of papers on technological subjects drawn from all scientific disciplines which contribute to the development of nuclear energy for peaceful purposes."

The aim of *Planetary and space science* is to serve as a medium for the publication of original work on the upper regions of the earth's atmosphere, the interplanetary space and all related problems. The Editor-in-chief is Mr. M. Greenberg and the periodical is published bi-monthly.

The *Annals of occupational hygiene* is produced quarterly under the Editorship of Dr. C. N. Davies. The first issues contain papers devoted to different aspects of "Noise in Industry".

British Standards Yearbook 1959

The latest issue of the *British Standards Yearbook* contains information about the Institution and the services it offers. It lists the British Standards current at 1 January, 1959, and gives a brief description of each. It is available from the British Standards Institution, 2 Park Street, London, W.1. The price is 15*s.* (including postage).

Journal of Scientific Instruments

Contents of the December issue

ORIGINAL CONTRIBUTIONS

Papers

Nuclear resonance absorption circuit. Part 1. Sensitivity considerations; Part 2. Practical design. By F. N. H. Robinson.

Compact calorimeter for measuring the overall thermal efficiency of freestanding fires and stoves for room warming. By M. W. Thring.

Multi-channel photoelectric scanning instrument for sizing microscopic particles. By B. B. Morgan and E. W. Meyer.

A method of measuring displacement using optical gratings. By D. L. A. Barber and M. P. Atkinson.

Stabilized torque magnetometer. By W. F. Archenhold, A. C. Brown and J. E. Thompson.

Laboratory and workship notes

Simple bleeder valve for critical adjustment of air pressure. By D. K. Edwards.

Tunable wave-guide cell cavity for an electron spin resonance spectrometer. By J. E. Bennett, and E. H. Morgan.

Sensitive method for the measurement of small rotations. By R. J. King and J. W. Gates.

Simple method for the control of the liquid level in a manometer. By J. G. Cunningham.

Device for graduating test-tubes and similar glassware. By J. W. Porteous.

Correspondence

Cryostat for reactor irradiation in liquid nitrogen. From G. Bortels.

NOTES AND NEWS

New books

THIS JOURNAL is produced monthly by The Institute of Physics, in London. It deals with all branches of applied physics (including theory and technique). All rights reserved. Responsibility for the statements contained herein attaches only to the writers.

EDITORIAL MATTER. Communications concerning editorial matter should be addressed to the Editor, The Institute of Physics, 47 Belgrave Square, London, S.W.1. (*Telephone:* Belgravia 6111.) Prospective authors are invited to prepare their scripts in accordance with the *Notes for Authors*. (Price 3*s.* 6*d.* including postage.)

REPRODUCTION. The Institute of Physics is a signatory to The Royal Society's Fair Copying Declaration. Details may be obtained upon application from The Royal Society, London, W.1.

ADVERTISEMENTS. Communications concerning advertisements should be addressed to the agents, Messrs. George Jackson (Fleet St.) Ltd., Cliffords Inn, Fleet Street, London, E.C.4. (*Telephone:* Holborn 3611–2.)

CLAIMS FOR MISSING JOURNALS. Claims from regular subscribers to this *Journal* for missing numbers will only be considered if received within 60 days of the date of mailing plus normal outward time of transit and time for lodging the claim. Losses attributable to failure to notify a change of address or to similar omissions will not be considered.

SUBSCRIPTION RATES. A new volume commences each January. The charge is £6 per volume ($17 U.S.A.), including index (post paid), payable in advance. Single parts, so far as available, may be purchased at 12*s.* 6*d.* each ($1.75 U.S.A.), post paid, cash with order. Orders should be sent to The Institute of Physics, 47 Belgrave Square, London, S.W.1, or to any bookseller.